

UC San Diego

UC San Diego Electronic Theses and Dissertations

Title

Marine-Derived Heterocycles from Porifera (Sponges) of the Bahamas and Western Australia: Synthetic and Structural Studies Enhanced by Chiroptical Methodologies

Permalink

<https://escholarship.org/uc/item/7xz787gh>

Author

Salib, Mariam Nader

Publication Date

2022

Peer reviewed|Thesis/dissertation

UNIVERSITY OF CALIFORNIA SAN DIEGO

Marine-Derived Heterocycles from Porifera (Sponges) of the Bahamas and Western Australia:

Synthetic and Structural Studies Enhanced by Chiroptical Methodologies

A dissertation submitted in partial satisfaction of the requirements
for the degree Doctor of Philosophy

in

Chemistry

by

Mariam Nader Salib

Committee in charge:

Professor Tadeusz F. Molinski, Chair
Professor Carlo Ballatore
Professor Thomas Hermann
Professor Dionicio R. Siegel
Professor Michael Tauber

2022

The dissertation of Mariam Nader Salib is approved, and it is acceptable in quality and form for publication on microfilm and electronically.

University of California San Diego

2022

DEDICATION

This dissertation is dedicated to my amazing parents Nader and Nabila for encouraging me to pursue my own passion in chemistry, and to my wonderful siblings Nancy, Basim, Sarra and Peter for cheering me up when I'm down. I wouldn't have succeeded in my life without your love, support, and encouragement.

Thank you.

TABLE OF CONTENTS

Dissertation Approval Page.....	iii
Dedication	iv
Table of Contents	v
List of Abbreviations	viii
List of Figures	xv
List of Schemes	xxix
List of Tables	xxxii
Acknowledgments	xxxiv
Vita	xxxvii
Abstract of the Dissertation	xxxix
Chapter One. Introduction	1
1.1 Marine Natural Products as a Source of Drug Leads	1
1.2 Bromotyrosine-Derived Alkaloids from Verongida Sponges	4
1.3 Cholinesterase Inhibitory Activity of Marine Natural Products	9
1.3.1 Alzheimer’s Disease	9
1.3.2 FDA Approved Cholinesterase Inhibitors	13
1.3.3 Cholinesterase Enzymes	15
1.3.4 Cholinesterase Inhibitors from Marine Sponges	18
1.4 Conclusions	24
1.5 References	26
Chapter Two. Bromo-spiroisoxazoline Alkaloids, Including an Isoserine Peptide, from the Caribbean Marine Sponge <i>Aplysina lacunose</i>	36
2.1 Introduction	37
2.2 Isolation and Structural Elucidation of Lacunosins A–B and Desaminopurealin	37
2.3 Conclusions	52
2.4 Acknowledgments	53
2.5 Experimental Section	54
2.6 Appendix	58
2.7 References and Notes	76
Chapter Three. Discovery Of Spiroisoxazoline Inhibitors of Acetylcholinesterase from <i>Pseudoceratina verrucosa</i>	80
3.1 Introduction	81

3.2 Isolation and Structure Determination of Methyl Purpuroceratates A and B and Purpuroceratic Acid C	82
3.3 Structure Determination of Ningalamides A and B	84
3.4 Chiroptical Analysis of Configurational Heterogeneity	91
3.5 Biological Activities	97
3.6 Conclusions	98
3.7 Acknowledgments	99
3.8 Experimental	99
3.9 Appendix	104
3.10 References and Notes	138
 Chapter Four. Discovery of Bioactive Bromotyrosine Alkaloids from the Bahamian Marine Sponge <i>Aiolochoxia crassa</i>	141
4.1 Introduction	142
4.2 Isolation and Structure Determination of Debromoianthelline, Pseudoceratinic Acid, Methyl Pseudoceratinate, and 13-Oxo-ianthelline	143
4.3 Structure Determination of Aiolochoxiaramides A–D and Proposed Biogenesis	149
4.4 Relative Stereochemistry of Aiolochoxiaramides A–D by DFT Calculations	156
4.5 Structure Determination and Proposed Biosynthesis of 7-Hydroxy-purealidin J ...	158
4.6 Proposed Biogenesis of 3-Oxo-ianthelline and Configurational Heterogeneity of BTAs	160
4.7 Biological Activities	165
4.8 Conclusions	166
4.9 Acknowledgments	167
4.10 Experimental	167
4.11 Appendix	173
4.12 References and Notes	255
 Chapter Five. Absolute Stereostructure of Axinoside-1, A Complex Glycolipid from a Western Australian Axinellid Sponge	260
5.1 Introduction	261
5.2 Isolation and Structure Determination of Axinoside-1	262
5.3 Determination of the Absolute Configuration at C-13 and C-23	270
5.4 Synthesis of Models 5.9a,b and Determination of the Absolute Configuration at C-17	273
5.5 Isolation, Structure Determination and Biological Activity of Oceanapins A–G	279
5.6 Conclusions	285
5.7 Acknowledgments	286
5.8 Experimental	286
5.9 Appendix	312
5.10 References	406
 Chapter Six. Progress Towards the Total Synthesis of Lepadin I	409
6.1 Introduction to Lepadins A–L	409
6.2 Select Total Synthesis	413
6.2.1 Toyooka's Approach to (–)-Lepadin B	413

6.2.2 Kibayashi's Approach to (-)-Lepadins A–C	415
6.2.3 Pu and Ma's Approach to (-)-Lepadins A–E and H	419
6.2.4 Blechert's Approach to <i>ent</i> -Lepadins F and G	420
6.2.5 Tong's Approach to Lepadins A–E, H, and <i>ent</i> -I	423
6.2.6 Other Synthetic Routes Towards Lepadins A–H	424
6.3 Retrosynthesis of Lepadin I	426
6.4 Synthesis of Lepadin I	427
6.4.1 Synthesis of β -Ketoester 6.74	427
6.4.2 Synthesis of Aldehydes 6.75a–e	430
6.4.3 Synthesis of C5 Alkyl Chain	431
6.4.4 Assembly of <i>cis</i> -DHQ Core and Installation of C5 Alkyl Chain	432
6.4.5 Attempts to Install the C-5 Sidechain	438
6.4.6 Future Directions and Completion of the Total Synthesis of Lepadin I ...	440
6.5 Conclusions	442
6.6 Experimental	442
6.7 Appendix	462
6.8 References	533

LIST OF ABBREVIATIONS

AA:	Amino acid
A β :	Amyloid β -protein
AC:	Absolute configuration
Ac ₂ O:	Acetic anhydride
ACh:	Acetylcholine
AChE:	Acetylcholinesterase
AD:	Alzheimer's disease
ADC:	Antibody drug conjugate
Ag ₂ O:	Silver oxide
AIBN:	Azobisisobutyronitrile
Ala:	Alanine
APP:	A β precursor protein
APT:	Attached Proton Test
Aq:	Aqueous
Bn:	Benzyl
Boc:	<i>tert</i> -Butyloxycarbonyl
(Boc) ₂ O:	Di- <i>tert</i> -butyl dicarbonate
BrTyr:	Bromotyrosine
Br _x Tyr:	3,5-Br ₂ Tyr and 3-BrTyr
BSTFA:	<i>N,O</i> -Bis(trimethylsilyl)acetamide
BTAs:	Bromotyrosine alkaloids
Bu ₂ Mg:	Di- <i>n</i> -butyl magnesium

Bu ₄ NI:	Tetra- <i>n</i> -butylammonium iodide
BuCh:	Butyrylcholine
BuChE:	Butyrylcholinesterase
CDA:	Chiral derivatizing agent
CDI:	1,1'-Carbonyldiimidazole
CEs:	Cotton effects
CH ₂ N ₂ :	Diazomethane
ChAT:	Choline acetyltransferase
ChE:	Cholinesterase
CNS:	Central nervous system
COSY:	Correlation Spectroscopy
CP HPLC:	Chiral-phase HPLC
CYP:	Cytochrome P ₄₅₀
Dab:	1,4-diaminobutanoic acid
DABCO:	1,4-Diazabicyclo[2.2.2]octane
DBU:	1,8-Diazabicyclo[5.4.0]undec-7-ene
DCC:	N,N'-Dicyclohexylcarbodiimide
DCM:	Dichloromethane
DFT:	Density Functional Theory
DH:	Dehydratase Domain
DHQ:	Decahydroquinoline
DMAP:	4-Dimethylaminopyridine
DME:	Dimethoxyethane

DMF:	Dimethylformamide
DMP:	Dess-Martin Periodinane
DMSO:	Dimethyl sulfoxide
dppp:	1,3-bis(diphenylphosphino)propane
DQF-COSY:	Double quantum-filtered COSY
DTNB:	Ellman's reagent or 5,5'-dithiobis-(2-nitrobenzoic acid)
ECCD:	Exciton-coupled circular dichroism
ECD:	Electronic circular dichroism
ER:	Enoyl reductase Domain
ESIMS:	Electrospray ionization mass spectrometry
Et ₂ O:	Diethyl ether
Et ₃ N:	Triethylamine
EtOAc:	Ethyl acetate
FDAA:	1-Fluoro-2,4-dinitrophenyl-5-L-alaninamide
FDTA:	1-Fluoro-2,4-dinitrophenyl-5-L-tryptophanamide
FTIR:	Fourier-transform infrared spectroscopy
GABA:	γ -aminobutyric acid
GC-EI-MS:	Gas chromatography electron impact mass spectrometry
GIAO:	Gauge-Independent Atomic Orbital
Glu:	Glucose or glutamic acid
Gly:	Glycine
His:	Histidine
HMBC:	Heteronuclear Multiple-Bond Correlation Spectroscopy

HMPA:	Hexamethylphosphoramide
HPLC:	High-performance liquid chromatography
HR-ESI-MS:	High-resolution electrospray ionization mass spectrometry
HSer:	Homoserine
HSQC-TOCSY:	Heteronuclear Single Quantum Coherence-Total Correlation Spectroscopy
HSQC:	Heteronuclear Single-Quantum Correlation Spectroscopy
HWE:	Horner-Wadsworth-Emmons
IC:	Inhibitory Concentration
<i>i</i> Pr:	Isopropyl
<i>iso</i> Ser:	Isoserine
KHMDS:	Potassium hexamethyldisilazide
K_i :	Inhibitory constant
KR:	Keto-reductase Domain
KS:	Keto-synthase Domain
L-Selectride:	Lithium tri- <i>sec</i> -butylborohydride
LC-MS:	Liquid chromatography-mass spectrometry
Leu:	Leucine
LiHMDS:	Lithium hexamethyldisilazide
Lys:	Lysine
Me:	Methyl
MeCN:	Acetonitrile
MeOH:	Methanol

MIC:	Minimum Inhibitory Concentration
MMFF:	Molecular modeling force field
MnO ₂ :	Manganese dioxide
MNPs:	Marine natural products
MPA:	α -Methoxyphenylacetic acid
nAChRs:	Nicotinic acetylcholine receptors
<i>n</i> -Bu:	<i>n</i> -Butyllithium
N-Troc-Cl:	N-trichloroethyl chloroformate
N-Troc	N-trichloroethyloxycarbonyl
N-Ts:	N-tosyl
NaH:	Sodium hydride
NaHMDS:	Sodium hexamethyldisilazide
NaIO ₄ :	Sodium periodate
NFTs:	Neurofibrillary tangles
NMA:	2-methoxy-2-(naphth-1-yl)acetic acid
NMDA:	<i>N</i> -methyl D-aspartate
NMR:	Nuclear Magnetic Resonance
NOE:	Nuclear Overhauser Effect
NOESY:	Nuclear Overhauser Effect Spectroscopy
Orn:	Ornithine
OsO ₄ :	Osmium tetroxide
<i>p</i> -TsOH:	<i>p</i> -Toluenesulfonic acid
PAS:	Peripheral anionic site

PCC:	Pyridinium chlorochromate
PDC:	Pyridinium dichromate
Ph:	Phenyl
Phe:	Phenylalanine
PhMe ₂ SiCl:	Phenyldimethylsilyl chloride
PKS:	Polyketide synthase
PMB:	<i>p</i> -Methoxybenzyl
PPTS:	Pyridinium <i>p</i> -toluenesulfonate
PR-PKS:	Partially reducing PKS
Py/Pyr:	Pyridine
<i>R</i> -MTPA-Cl:	(<i>R</i>)-(-)- α -Methoxy- α -(trifluoromethyl)phenylacetyl chloride
RC:	Relative configuration
Red-Al:	Sodium bis(2-methoxyethoxy)aluminum hydride
RMSD:	Root-mean-square deviation
RP-HPLC:	Reverse-phased HPLC
scrF:	Self-Consistent Reaction Field
SAM:	<i>S</i> -Adenosyl methionine
SAR:	Structure-Activity Relationship
Ser:	Serine
SIO:	Spiroisoxazoline or spirocyclohexadienyl-isoxazoline
SmI ₂ :	Samarium iodide
TBAF:	Tetra- <i>n</i> -butylammonium fluoride
TBDMS:	<i>tert</i> -Butyldimethylsilyl

TBDPS:	<i>tert</i> -Butyldiphenylsilyl
TBS:	<i>tert</i> -Butyldimethylsilyl
TE:	Transesterification Domain
TES:	Triethylsilyl
TFA:	Trifluoroacetic acid
TfOH:	Triflic acid
THF:	Tetrahydrofuran
THP:	Tetrahydropyran
TIPS:	Triisopropylsilyl
TIPSOTf:	Triisopropylsilyl trifluoromethanesulfonate
TLC:	Thin layer chromatography
TMS:	Trimethylsilyl
TNF- α :	Tumor necrosis factor α
TOCSY:	Total Correlation Spectroscopy
UV:	Ultraviolet
Val:	Valine
Xyl:	Xylose

LIST OF FIGURES

- Figure 1.1: (a) Number and proportional distribution of bioactive MNPs from various marine organisms. PN/NT** and PVHD refer to “protection of neurons/neurotoxicity” and “prevention of heart and vascular disease,” respectively. Remaining bioactivities that cannot be classified in the above groups are categorized under “other activity.” (b) Distribution of chemical classes in *Porifera* and *Cnidaria*. Figures (a) and (b) were taken directly from reference 2..... 2
- Figure 1.2: The structures of approved marine drugs: (a) the amino acid sequence and 3D structure of ω -conotoxin MVIIA (ziconotide/Prialt[®]), (b) trabectedin (Yondelis[®]), and (c) the drug load monomethyl auristatin E (brentuximab-vedotin/Adcetris[®]). The 3D structure of ziconotide was adopted directly from Wikipedia; see reference 13..... 3
- Figure 1.3: The three basic *Porifera* body structures, adopted from Wikimedia Commons. The figure was adopted directly from reference 14..... 3
- Figure 1.4: Representative structures of the four subclasses of bromotyrosine-derived alkaloids.. 5
- Figure 1.5: Anatomic locations of the limbic system that plays an important role in learning and memory functions. Figure was taken from reference 50..... 10
- Figure 1.6: Brain atrophy in advanced Alzheimer’s disease. Image taken from reference 57..... 11
- Figure 1.7: (a) Sequential proteolytic processing of APP to A β 42: APP cleavage by β -secretase and γ -secretase to A β 42 monomers, and subsequent aggregation to A β 42- oligomers and plaques. (b) Destabilization (dissociation) of microtubules upon loss of tau binding, hyperphosphorylation, and aggregation of tau into neurofibrillary tangles (NFTs). Images taken from reference 60..... 12
- Figure 1.8: Structures of cholinesterase inhibitors..... 14
- Figure 1.9: Differences in active site gorges of human (a) AChE (hAChE) and (b) BuChE (hBuChE, see reference 76). The transition state of ACh or butyrylcholine (BuCh) is modeled in the active site and represented in ball and stick. The gorge (gray), acyl-binding pocket (magenta), catalytic triad (sticks in cyan), and key aromatic residues (yellow) are depicted..... 16
- Figure 1.10: Structures of brominated ChE inhibitors from Verongida sponges..... 19
- Figure 1.11: The active site of AChE showing the PAS region and the hydrolysis of ACh in the active site. Figure taken from reference 70..... 19
- Figure 1.12: Structures of brominated ChE inhibitors from different sponge classes..... 21
- Figure 1.13: Structures of galantamine (**1.18**), petrosamine (**1.42**), and 2-bromoamphimedine (**1.43**)..... 22
- Figure 1.14: Structures of ChE inhibitors from different sponge classes..... 23

Figure 2.1: The structures of lacunosins A (2.1), B (2.2), desaminopurealin (2.3), verongidoic acid methyl ester (2.4a), (+)-purealidin-R (2.4b), and verongidoic acid (2.4c).....	38
Figure 2.2: α -Chymotrypsin inhibition by fractions from size-exclusion chromatography (Sephadex LH-20, MeOH elution) of <i>Aplysina lacunosa</i> solvent-partitioned extract. See Experimental Section.....	39
Figure 2.3: COSY and HMBC correlations of (–)- 2.3 (600 MHz, CD ₃ OD).....	40
Figure 2.4: (a) ¹ H NMR spectra of the diastereotopic 10-CH ₂ of 2.2 (600 MHz, CD ₃ OD) and (b) simulated spectrum of ABX. Line width, 1.15 Hz, δ_A 3.589, $J = 13.0, 6.0, 4.8$ Hz; δ_B 3.644, $J = 13.0, 6.0, 4.8$ Hz. Epimer: δ_A 3.600, $J = 13.0, 6.0, 4.8$ Hz; δ_B 3.652, $J = 13.0, 6.0, 4.8$ Hz (δ_X is not shown). Ref. 20.....	42
Figure 2.5: Energy-minimized conformers (MMFF) of (1 <i>S</i> ,6 <i>R</i>)-verongidoic acid methyl ester (2.4a). (a) The six lowest <i>E</i> conformers. (b) Model of the Lowest <i>E</i> conformer (iSpartan).....	47
Figure 2.6: UV-vis and ECD spectra (c 2.49 x 10 ⁻⁵ M, MeOH, 23 °C) of 6'-methoxy-2'-naphthoate ester (–)- 2.7 derived from (+)- 2.4a	47
Figure 2.7: Structures of Dibromo-cyclohexa-1,3-dienyl Natural Products from Verongid Sponges.....	59
Figure 2.8: ¹ H NMR of Compound 2.1 (500 MHz, CD ₃ OD).....	60
Figure 2.9: ¹³ C NMR of Compound 2.1 (125 MHz, (CD ₃) ₂ CO).....	61
Figure 2.10: HSQC of Compound 2.1 (600 MHz, CD ₃ OD).....	62
Figure 2.11: HMBC of Compound 2.1 (600 MHz, CD ₃ OD).....	63
Figure 2.12: ¹ H NMR of Compound 2.2 (600 MHz, CD ₃ OD).....	64
Figure 2.13: DQF-COSY of Compound 2.2 (600 MHz, CD ₃ OD).....	65
Figure 2.14: HSQC of Compound 2.2 (600 MHz, CD ₃ OD).....	66
Figure 2.15: HMBC of Compound 2.2 (600 MHz, CD ₃ OD).....	67
Figure 2.16: ¹ H NMR of Compound 2.3 (600 MHz, CD ₃ OD).....	68
Figure 2.17: ¹ H NMR Expansion of Compound 2.3 (600 MHz, CD ₃ OD).....	69
Figure 2.18: DQF-COSY of Compound 2.3 (600 MHz, CD ₃ OD).....	70

Figure 2.19: HSQC of Compound 2.3 (600 MHz, CD ₃ OD).....	71
Figure 2.20: HMBC of Compound 2.3 (600 MHz, CD ₃ OD).....	72
Figure 2.21: (a) UV-vis and (b) CD of Compounds 2.1 ($c = 3.93 \times 10^{-4}$ M), 2.2 (3.56×10^{-4} M) and 2.3 (4.63×10^{-4} M) (MeOH, 23 °C).....	73
Figure 2.22: (a) UV-vis and (b) CD of Compounds 2.3 ($c = 5.06 \times 10^{-4}$ M), 2.4a (1.07×10^{-3} M), 2.S6 (1.80×10^{-4} M) and 2.S18 (9.17×10^{-4} M) (MeOH, 23 °C).....	74
Figure 2.23: ¹ H NMR of Ester 2.7 (CDCl ₃ , 600 MHz).....	75
Figure 3.1: The structures of purpuroceratic acid methyl esters A (3.1b) and B (3.2b), purpuroceratic acid C (3.3a), ningalamide A (3.4), and ningalamide B (3.5), in addition to other known compounds.....	83
Figure 3.2: Key COSY (blue, bold) and HMBC (black, arrow) correlations of ningalamide A (3.4).....	86
Figure 3.3: Key COSY (blue, bold) and HMBC (black, arrow) correlations of 3.5	89
Figure 3.4: ECD of Compounds (a) 3.1a–3.1b ($c = 1.85 \times 10^{-4}$ M), 3.2a–3.2b (9.23×10^{-4} M), 3.3a–3.3b (9.23×10^{-4} M), and (b) 3.4–3.5 ($c = 1.25 \times 10^{-4}$ M) (CH ₃ OH, 23 °C).....	92
Figure 3.5: Chiral-phase HPLC chromatogram (λ 280 nm) (a) UV-vis detection and (b) ECD of purealidin-R (3.6) (Amylose-1, 4% <i>i</i> PrOH-hexanes, 1 mL.min ⁻¹). Peak 1: (+)- 3.6a : $t_R = 63.14$ min, area = 92.19. Peak 2: (-)- 3.6b : $t_R = 76.47$ min, area = 7.81.....	93
Figure 3.6: Structures of Dibromo-cyclohexa-1,3-dienyl Natural Products from Verongid Sponges.....	105
Figure 3.7: ¹ H NMR of Compound 3.1b (500 MHz, CD ₃ OD).....	106
Figure 3.8: ¹³ C NMR of Compound 3.1b (125 MHz, CD ₃ OD).....	107
Figure 3.9: ¹ H NMR of Compound 3.2b (500 MHz, CD ₃ OD).....	108
Figure 3.10: ¹³ C NMR of Compound 3.2b (125 MHz, CD ₃ OD).....	109
Figure 3.11: ¹ H NMR of Compound 3.3a (600 MHz, CD ₃ OD).....	110
Figure 3.12: ¹³ C NMR of Compound 3.3a (125 MHz, CD ₃ OD).....	111
Figure 3.13: Clip-COSY of Compound 3.3a (600 MHz, CD ₃ OD).....	112
Figure 3.14: HSQC of Compound 3.3a (600 MHz, CD ₃ OD).....	113

Figure 3.15: ^1H NMR of Compound 3.4 (600 MHz, CD_3OD).....	114
Figure 3.16: ^1H NMR Expansion of Compound 3.4 (600 MHz, CD_3OD).....	115
Figure 3.17: DQF-COSY of Compound 3.4 (600 MHz, CD_3OD).....	116
Figure 3.18: HSQC of Compound 3.4 (600 MHz, CD_3OD).....	117
Figure 3.19: HMBC of Compound 3.4 (600 MHz, CD_3OD).....	118
Figure 3.20: ^1H NMR of Compound 3.5 (600 MHz, CD_3OD).....	119
Figure 3.21: ^1H NMR Expansion of Compound 3.5 (600 MHz, CD_3OD).....	120
Figure 3.22: APT of Compound 3.5 (150 MHz, CD_3OD).....	121
Figure 3.23: DQF-COSY of Compound 3.5 (500 MHz, CD_3OD).....	122
Figure 3.24: HSQC of Compound 3.5 (600 MHz, CD_3OD).....	123
Figure 3.25: HMBC of Compound 3.5 (500 MHz, CD_3OD , $^1J_{\text{CH}}$ 8 Hz).....	124
Figure 3.26: HMBC of Compound 3.5 (500 MHz, CD_3OD , $^1J_{\text{CH}}$ 4 Hz).....	125
Figure 3.27: ^1H NMR of Compound 3.5 (600 MHz, DMSO-d_6).....	126
Figure 3.28: ^1H NMR Expansion of Compound 3.5 (600 MHz, DMSO-d_6).....	127
Figure 3.29: DQF-COSY of Compound 3.5 (600 MHz, DMSO-d_6).....	128
Figure 3.30: HSQC-ASAP of Compound 3.5 (600 MHz, DMSO-d_6).....	129
Figure 3.31: HMBC of Compound 3.5 (600 MHz, DMSO-d_6 , $^1J_{\text{CH}}$ 8 Hz).....	130
Figure 3.32: (a) UV-vis and (b) CD Chiral-Phase HPLC Traces of Compound 3.1b (Amylose-1 10% IPA-hexanes, $1 \text{ mL}\cdot\text{min}^{-1}$, (+)- 3.1b : $t_{\text{R}} = 29.68 \text{ min}$, area = 74.31; (–)- 3.1b : $t_{\text{R}} = 34.20 \text{ min}$, area = 25.69; 48.6 %ee).....	131
Figure 3.33: (a) UV-vis and (b) CD Chiral-Phase HPLC Traces of Compound 3.2b (Amylose-1 10% IPA-hexanes, $1 \text{ mL}\cdot\text{min}^{-1}$, (+)- 3.2b : $t_{\text{R}} = 26.99 \text{ min}$, area = 73.12; (–)- 3.2b : $t_{\text{R}} = 32.47 \text{ min}$, area = 26.88; 46.2 %ee).....	132
Figure 3.34: (a) UV-vis and (b) CD Chiral-Phase HPLC Traces of Compound 3.3b (Amylose-1 10% IPA-hexanes, $1 \text{ mL}\cdot\text{min}^{-1}$, (+)- 3.3b : $t_{\text{R}} = 26.37 \text{ min}$, area = 74.66; (–)- 3.3b : $t_{\text{R}} = 29.50 \text{ min}$, area = 25.34; 49.3 %ee).....	133

Figure 3.35: CD of Compounds 3.1a ($c = 1.85 \times 10^{-4}$ M), and 3.1b (1.85×10^{-4} M) in CH ₃ OH (dotted, 23 °C) or CH ₃ CN.....	134
Figure 3.36: CD of Compounds (a) S3.1 ($c = 3.12 \times 10^{-4}$ M), S3.2 (3.12×10^{-4} M), S3.3 (1.39×10^{-4} M), (b) S3.4 ($c = 3.12 \times 10^{-4}$ M), S3.5 (1.04×10^{-4} M), and S3.6 (1.04×10^{-4} M) (MeOH, 23 °C).....	135
Figure 3.37: CD of Compounds (a) 3.6 ($c = 6.25 \times 10^{-4}$ M), 3.7 (1.25×10^{-4} M), S3.7 (3.12×10^{-4} M), (b) S3.8 ($c = 2.08 \times 10^{-4}$ M), S3.9 (3.75×10^{-4} M), and S3.10 (2.08×10^{-4} M) (MeOH, 23 °C).....	136
Figure 4.1: The structures of new bromotyrosine alkaloids 4.1–4.5 , and key relevant BTAs.....	144
Figure 4.2: Key COSY (bold) and HMBC (arrow) correlations of compounds 4.3–4.5	148
Figure 4.3: Proposed biogenesis of aiolochroiamides A and B (4.4a and 4.4b).....	151
Figure 4.4: Proposed biosynthesis of alkaloids 4.5a and 4.5b	155
Figure 4.5: Global minimal energy structures of (a) (12 <i>R</i> *,14 <i>R</i> *)- 4.4 , (b) (12 <i>R</i> *,14 <i>S</i> *)- 4.4 , (c) (8 <i>S</i> *,7' <i>S</i> *,8' <i>R</i> *)- 4.5a , and (d) (8 <i>S</i> *,7' <i>R</i> *,8' <i>R</i> *)- 4.5b optimized at the B3LYP/6-31G(d,p) level using Gaussian 16.....	157
Figure 4.6: Key COSY (bold –) and HMBC (arrow) correlations of 7-hydroxy-purealidin J (4.6).....	158
Figure 4.7: Putative biosynthesis of 7-hydroxypurealidin (4.6) through free-radical autoxidation.....	160
Figure 4.8: Putative biogenesis of 4.3	161
Figure 4.9: ¹ H NMR of Compound 4.1 (500 MHz, CD ₃ OD).....	174
Figure 4.10: ¹³ C NMR of Compound 4.1 (125 MHz, CD ₃ OD).....	175
Figure 4.11: ¹ H NMR of Compound 4.2a (500 MHz, CD ₃ OD).....	176
Figure 4.12: ¹³ C NMR of Compound 4.2a (125 MHz, CD ₃ OD).....	177
Figure 4.13: ¹ H NMR of Compound 4.2b (500 MHz, CD ₃ OD).....	178
Figure 4.14: ¹³ C NMR of Compound 4.2b (125 MHz, CD ₃ OD).....	179
Figure 4.15: ¹ H NMR of Compound 4.3 (500 MHz, CD ₃ OD).....	180

Figure 4.16: ^{13}C NMR of Compound 4.3 (125 MHz, CD_3OD).....	181
Figure 4.17: DQF-COSY of Compound 4.3 (500 MHz, CD_3OD).....	182
Figure 4.18: HSQC of Compound 4.3 (500 MHz, CD_3OD).....	183
Figure 4.19: HMBC of Compound 4.3 (500 MHz, CD_3OD).....	184
Figure 4.20: ^1H NMR of Compound 4.4a,b (600 MHz, CD_3OD).....	185
Figure 4.21: ^1H NMR Expansion of Compound 4.4a,b (600 MHz, CD_3OD).....	186
Figure 4.22: ^{13}C NMR of Compound 4.4a,b (125 MHz, CD_3OD).....	187
Figure 4.23: DQF-COSY of Compound 4.4a,b (600 MHz, CD_3OD).....	188
Figure 4.24: HSQC-ASAP of Compound 4.4a,b (600 MHz, CD_3OD).....	189
Figure 4.25: ^{13}C -Coupled HSQC of Compound 4.4a,b (600 MHz, CD_3OD).....	190
Figure 4.26: HMBC of Compound 4.4a,b (600 MHz, CD_3OD).....	191
Figure 4.27: ^1H NMR of Compound 4.5a (500 MHz, CD_3OD).....	192
Figure 4.28: ^1H NMR Expansion of Compound 4.5a (500 MHz, CD_3OD).....	193
Figure 4.29: ^{13}C NMR of Compound 4.5a (125 MHz, CD_3OD).....	194
Figure 4.30: DQF-COSY of Compound 4.5a (500 MHz, CD_3OD).....	195
Figure 4.31: gHSQC of Compound 4.5a (500 MHz, CD_3OD).....	196
Figure 4.32: gHMBC of Compound 4.5a (500 MHz, CD_3OD).....	197
Figure 4.33: ^1H NMR of Compound 4.5b (600 MHz, CD_3OD).....	198
Figure 4.34: ^1H NMR Expansion of Compound 4.5b (600 MHz, CD_3OD).....	199
Figure 4.35: DQF-COSY of Compound 4.5b (600 MHz, CD_3OD).....	200
Figure 4.36: HSQC-ASAP of Compound 4.5b (600 MHz, CD_3OD).....	201
Figure 4.37: HMBC of Compound 4.5b (600 MHz, CD_3OD).....	202
Figure 4.38: ^1H NMR of Compound 4.6 (600 MHz, CD_3OD).....	203

Figure 4.39: DQF-COSY of Compound 4.6 (600 MHz, CD ₃ OD).....	204
Figure 4.40: HSQC of Compound 4.6 (600 MHz, CD ₃ OD).....	205
Figure 4.41: HMBC of Compound 4.6 (600 MHz, CD ₃ OD).....	206
Figure 4.42: Antifungal Activity of Chromatography Subfractions (SF) against <i>Candida</i> and <i>Cryptococcus</i> spp.....	208
Figure 4.43: Inhibitory activity of Chromatography Subfractions (SF) against BuChE.....	210
Figure 4.44: The structures of (12 <i>R</i> *,14 <i>R</i> *)- and (12 <i>R</i> *,14 <i>S</i> *)- 4.4	212
Figure 4.45: The structures of the four diastereoisomers of compound 4.5	214
Figure 5.1: Structures of axinoside-1 (5.1), axinoside-1 peracetate (5.2), and ceramides 5.3a–g	262
Figure 5.2: ¹ H and ¹³ C assignments, ¹ J _{CH} coupling constants of anomeric carbons, and key TOCSY (blue arrows) and NOESY (red arrows) correlations of the monosaccharides of axinoside-1 peracetate (5.2). See reference 12.....	265
Figure 5.3: ESIMS fragmentation of 5.1 after primary loss of –2H ₂ O to <i>i</i>	270
Figure 5.4: Differential ¹ H NMR anisotropy ($\Delta\Delta\delta^{RS} = \Delta\delta^R(\mathbf{5.8}) - \Delta\delta^S(\mathbf{5.19}$ or $\mathbf{5.20})$) of the <i>tris</i> -(1-NMA)-esters 5.8 , 5.19 (blue bars) and 5.20 (orange bars) of aglycone 5.4 and model compounds 5.9a and 5.9b , respectively. Horizontal scale is C locant number.....	277
Figure 5.5: COSY (bold) and HMBC (arrows, blue) correlations of 5.3a–g	279
Figure 5.6: ECD spectrum of 5.26 (CH ₃ CN).....	284
Figure 5.7: Differential cytokine release—IL-10 and IL-12p40—from dendritic cells stimulated by oceanapins A–G (5.3a–g).....	284
Figure 5.8: SEM Images of Spicules of Axinellid Sponge 93-07-067. Scale bars (10 μM and 20 μM) at bottom.....	313
Figure 5.9: ¹ H NMR of Compound 5.1 (600 MHz, CDCl ₃).....	314
Figure 5.10: MS ⁿ Analysis (Positive Ion Mode) of Compound 5.1	315
Figure 5.11: MS ⁿ Analysis (Negative Ion Mode) of Compound 5.1	319
Figure 5.12: ¹ H NMR of Compound 5.2 (600 MHz, CDCl ₃).....	324

Figure 5.13: ^1H NMR Expansion of Compound 5.2 (600 MHz, CDCl_3).....	325
Figure 5.14: ^{13}C NMR of Compound 5.2 (125 MHz, CDCl_3).....	326
Figure 5.15: DQF-COSY of Compound 5.2 (600 MHz, CDCl_3).....	327
Figure 5.16: HSQC of Compound 5.2 (600 MHz, CDCl_3).....	328
Figure 5.17: ^{13}C -Coupled HSQC of Compound 5.2 (600 MHz, CDCl_3).....	329
Figure 5.18: HMBC of Compound 5.2 (600 MHz, CDCl_3).....	330
Figure 5.19: TOCSY of Compound 5.2 (600 MHz, CDCl_3 , 40 mS).....	331
Figure 5.20: TOCSY Expansion of Compound 5.2 (600 MHz, CDCl_3 , 40 mS).....	332
Figure 5.21: Long-range TOCSY of Compound 5.2 (600 MHz, CDCl_3 , 120 mS).....	333
Figure 5.22: Long-range TOCSY Expansion of Compound 5.2 (600 MHz, CDCl_3 , 120 mS)....	334
Figure 5.23: HSQC-TOCSY of Compound 5.2 (600 MHz, CDCl_3).....	335
Figure 5.24: MS^n Analysis (Positive Ion Mode) of Compound 5.2	336
Figure 5.25: ^1H NMR of Compound 5.4 (500 MHz, CDCl_3).....	343
Figure 5.26: ^1H NMR of Compound 5.8a (600 MHz, CDCl_3).....	344
Figure 5.27: DQF-COSY of Compound 5.8a (600 MHz, CDCl_3).....	345
Figure 5.28: HSQC of Compound 5.8a (600 MHz, CDCl_3).....	346
Figure 5.29: HMBC of Compound 5.8a (600 MHz, CDCl_3).....	347
Figure 5.30: TOCSY of Compound 5.8a (600 MHz, CDCl_3).....	348
Figure 5.31: ^1H NMR of Compound 5.8b (600 MHz, CDCl_3).....	349
Figure 5.32: DQF-COSY of Compound 5.8b (600 MHz, CDCl_3).....	350
Figure 5.33: HSQC of Compound 5.8b (600 MHz, CDCl_3).....	351
Figure 5.34: HMBC of Compound 5.8b (600 MHz, CDCl_3).....	352
Figure 5.35: TOCSY of Compound 5.8b (600 MHz, CDCl_3).....	353

Figure 5.36: ^1H NMR of Compound (<i>R</i>)- 5.15 (400 MHz, CDCl_3).....	354
Figure 5.37: ^{13}C NMR of Compound (<i>R</i>)- 5.15 (100 MHz, CDCl_3).....	355
Figure 5.38: ^1H NMR of Compound (<i>S</i>)- 5.15 (400 MHz, CDCl_3).....	356
Figure 5.39: ^{13}C NMR of Compound (<i>S</i>)- 5.15 (100 MHz, CDCl_3).....	357
Figure 5.40: ^1H NMR of Compound (<i>R</i>)- 5.11 (500 MHz, CDCl_3).....	358
Figure 5.41: ^{13}C NMR of Compound (<i>R</i>)- 5.11 (100 MHz, CDCl_3).....	359
Figure 5.42: ^1H NMR of Compound (<i>S</i>)- 5.11 (400 MHz, CDCl_3).....	360
Figure 5.43: ^{13}C NMR of Compound (<i>S</i>)- 5.11 (100 MHz, CDCl_3).....	361
Figure 5.44: ^1H NMR of Compound 5.S7a (400 MHz, CDCl_3).....	362
Figure 5.45: ^{13}C NMR of Compound 5.S7a (125 MHz, CDCl_3).....	363
Figure 5.46: ^1H NMR of Compound 5.S7b (400 MHz, CDCl_3).....	364
Figure 5.47: ^{13}C NMR of Compound 5.S7b (100 MHz, CDCl_3).....	365
Figure 5.48: ^1H NMR of Compound 5.16a (400 MHz, CDCl_3).....	366
Figure 5.49: ^{13}C NMR of Compound 5.16a (100 MHz, CDCl_3).....	367
Figure 5.50: ^1H NMR of Compound 5.16b (400 MHz, CDCl_3).....	368
Figure 5.51: ^{13}C NMR of Compound 5.16b (100 MHz, CDCl_3).....	369
Figure 5.52: ^1H NMR of Compound 5.17a (400 MHz, CDCl_3).....	370
Figure 5.53: ^{13}C NMR of Compound 5.17a (100 MHz, CDCl_3).....	371
Figure 5.54: ^1H NMR of Compound 5.17b (400 MHz, CDCl_3).....	372
Figure 5.55: ^{13}C NMR of Compound 5.17b (100 MHz, CDCl_3).....	373
Figure 5.56: ^1H NMR of Compound 5.18a (400 MHz, CDCl_3).....	374
Figure 5.57: ^{13}C NMR of Compound 5.18a (100 MHz, CDCl_3).....	375
Figure 5.58: ^1H NMR of Compound 5.18b (400 MHz, CDCl_3).....	376

Figure 5.59: ^{13}C NMR of Compound 5.18b (100 MHz, CDCl_3).....	377
Figure 5.60: ^1H NMR of Compound 5.S8a (500 MHz, CDCl_3).....	378
Figure 5.61: ^{13}C NMR of Compound 5.S8a (125 MHz, CDCl_3).....	379
Figure 5.62: ^1H NMR of Compound 5.S8b (400 MHz, CDCl_3).....	380
Figure 5.63: ^{13}C NMR of Compound 5.S8b (125 MHz, CDCl_3).....	381
Figure 5.64: ^1H NMR of Compound 5.9a (400 MHz, CDCl_3).....	382
Figure 5.65: ^{13}C NMR of Compound 5.9a (100 MHz, CDCl_3).....	383
Figure 5.66: ^1H NMR of Compound 5.9b (400 MHz, CDCl_3).....	384
Figure 5.67: ^{13}C NMR of Compound 5.9b (100 MHz, CDCl_3).....	385
Figure 5.68: ^1H NMR of Compound 5.19a (400 MHz, CDCl_3).....	386
Figure 5.69: ^{13}C NMR of Compound 5.19a (125 MHz, CDCl_3).....	387
Figure 5.70: DQF-COSY of Compound 5.19a (400 MHz, CDCl_3).....	388
Figure 5.71: HSQC of Compound 5.19a (400 MHz, CDCl_3).....	389
Figure 5.72: HMBC of Compound 5.19a (400 MHz, CDCl_3).....	390
Figure 5.73: ^1H NMR of Compound 5.19b (400 MHz, CDCl_3).....	391
Figure 5.74: ^{13}C NMR of Compound 5.19b (125 MHz, CDCl_3).....	392
Figure 5.75: DQF-COSY of Compound 5.19b (400 MHz, CDCl_3).....	393
Figure 5.76: HSQC of Compound 5.19b (400 MHz, CDCl_3).....	394
Figure 5.77: HMBC of Compound 5.19b (400 MHz, CDCl_3).....	395
Figure 5.78: ^1H NMR of Compound 5.20a (400 MHz, CDCl_3).....	396
Figure 5.79: ^{13}C NMR of Compound 5.20a (125 MHz, CDCl_3).....	397
Figure 5.80: DQF-COSY of Compound 5.20a (400 MHz, CDCl_3).....	398
Figure 5.81: HSQC of Compound 5.20a (400 MHz, CDCl_3).....	399

Figure 5.82: HMBC of Compound 5.20a (400 MHz, CDCl ₃).....	400
Figure 5.83: ¹ H NMR of Compound 5.20b (400 MHz, CDCl ₃).....	401
Figure 5.84: ¹³ C NMR of Compound 5.20b (125 MHz, CDCl ₃).....	402
Figure 5.85: DQF-COSY of Compound 5.20b (400 MHz, CDCl ₃).....	403
Figure 5.86: HSQC of Compound 5.20b (400 MHz, CDCl ₃).....	404
Figure 5.87: HMBC of Compound 5.20b (400 MHz, CDCl ₃).....	405
Figure 6.1: Structures of lepadins A–L.....	410
Figure 6.2: NOE-correlations (600 MHz, CD ₃ OD) of 4a <i>S</i> ,7 <i>S</i> ,8a <i>S</i> - 6.84	430
Figure 6.3: NOE-correlations (600 MHz, CDCl ₃) of 4a <i>S</i> ,8a <i>S</i> - 6.96b and 6.98	433
Figure 6.4: Numbering assignment of 4a <i>S</i> ,8a <i>S</i> - 6.96b and 6.98	437
Figure 6.5: ¹ H NMR of Compound 6.79 (400 MHz, CDCl ₃).....	463
Figure 6.6: ¹ H NMR of Compound 6.80a (400 MHz, CDCl ₃).....	464
Figure 6.7: ¹³ C NMR of Compound 6.80a (125 MHz, CDCl ₃).....	465
Figure 6.8: ¹ H NMR of Compound 6.81b (400 MHz, CDCl ₃).....	466
Figure 6.9: ¹³ C NMR of Compound 6.81b (125 MHz, CDCl ₃).....	467
Figure 6.10: ¹ H NMR of Compound 6.76 (500 MHz, CDCl ₃).....	468
Figure 6.11: ¹³ C NMR of Compound 6.76 (125 MHz, CDCl ₃).....	469
Figure 6.12: ¹ H NMR of Compound 6.74 (500 MHz, CDCl ₃).....	470
Figure 6.13: ¹³ C NMR of Compound 6.74 (125 MHz, CDCl ₃).....	471
Figure 6.14: ¹ H NMR of Compound 6.84 (500 MHz, CDCl ₃).....	472
Figure 6.15: ¹³ C NMR of Compound 6.84 (125 MHz, CDCl ₃).....	473
Figure 6.16: ¹ H NMR of Compound 6.86a (500 MHz, CDCl ₃).....	474
Figure 6.17: ¹ H NMR of Compound 6.86b (500 MHz, CDCl ₃).....	475

Figure 6.18: ^{13}C NMR of Compound 6.86b (125 MHz, CDCl_3).....	476
Figure 6.19: ^1H NMR of Compound 6.86c (400 MHz, CDCl_3).....	477
Figure 6.20: ^{13}C NMR of Compound 6.86c (125 MHz, CDCl_3).....	478
Figure 6.21: ^1H NMR of Compound 6.86d (500 MHz, CDCl_3).....	479
Figure 6.22: ^{13}C NMR of Compound 6.86d (125 MHz, CDCl_3).....	480
Figure 6.23: ^1H NMR of Compound 6.87a (500 MHz, CDCl_3).....	481
Figure 6.24: ^1H NMR of Compound 6.87b (500 MHz, CDCl_3).....	482
Figure 6.25: ^1H NMR of Compound 6.87c (400 MHz, CDCl_3).....	483
Figure 6.26: ^{13}C NMR of Compound 6.87c (125 MHz, CDCl_3).....	484
Figure 6.27: ^1H NMR of Compound 6.87d (400 MHz, CDCl_3).....	485
Figure 6.28: ^1H NMR of Compound 6.88a (500 MHz, CDCl_3).....	486
Figure 6.29: ^1H NMR of Compound 6.88b (500 MHz, CDCl_3).....	487
Figure 6.30: ^1H NMR of Compound 6.88c (400 MHz, CDCl_3).....	488
Figure 6.31: ^1H NMR of Compound 6.88d (400 MHz, CDCl_3).....	489
Figure 6.32: ^{13}C NMR of Compound 6.88d (125 MHz, CDCl_3).....	490
Figure 6.33: ^1H NMR of Compound 6.75a (400 MHz, CDCl_3).....	491
Figure 6.34: ^{13}C NMR of Compound 6.75a (125 MHz, CDCl_3).....	492
Figure 6.35: ^1H NMR of Compound 6.75b (400 MHz, CDCl_3).....	493
Figure 6.36: ^1H NMR of Compound 6.75c (400 MHz, CDCl_3).....	494
Figure 6.37: ^1H NMR of Compound 6.75d (400 MHz, CDCl_3).....	495
Figure 6.38: ^1H NMR of Compound 6.90 (400 MHz, CDCl_3).....	496
Figure 6.39: ^{13}C NMR of Compound 6.90 (125 MHz, CDCl_3).....	497
Figure 6.40: ^1H NMR of Compound 6.91 (500 MHz, CDCl_3).....	498

Figure 6.41: ^{13}C NMR of Compound 6.91 (125 MHz, CDCl_3).....	499
Figure 6.42: ^1H NMR of Compound 6.92 (500 MHz, CDCl_3).....	500
Figure 6.43: ^{13}C NMR of Compound 6.92 (125 MHz, CDCl_3).....	501
Figure 6.44: ^1H NMR of Compound 6.93 (400 MHz, CDCl_3).....	502
Figure 6.45: ^{13}C NMR of Compound 6.93 (100 MHz, CDCl_3).....	503
Figure 6.46: ^1H NMR of Compound 6.96b (500 MHz, CDCl_3).....	504
Figure 6.47: ^{13}C NMR of Compound 6.96b (125 MHz, CDCl_3).....	505
Figure 6.48: COSY of Compound 6.96b (500 MHz, CDCl_3).....	506
Figure 6.49: gHSQC of Compound 6.96b (500 MHz, CDCl_3).....	507
Figure 6.50: HMBC of Compound 6.96b (500 MHz, CDCl_3).....	508
Figure 6.51: 1D NOE of Compound 6.96b : {H-2} (δ_{H} 4.18, 600 MHz, CDCl_3).....	509
Figure 6.52: 1D NOE of Compound 6.96b : { H-3} (δ_{H} 2.81, 600 MHz, CDCl_3)	510
Figure 6.53: 1D NOE of Compound 6.96b : {H-4a} (δ_{H} 1.82, 600 MHz, CDCl_3).....	511
Figure 6.54: 1D NOE of Compound 6.96b : {H-8a} (δ_{H} 4.04, 600 MHz, CDCl_3).....	512
Figure 6.55: 1D NOE of Compound 6.96b : {H ₃ -14(Me)} (δ_{H} 1.28, 600 MHz, CDCl_3).....	513
Figure 6.56: ^1H NMR of Compound 6.96c (500 MHz, CDCl_3).....	514
Figure 6.57: ^{13}C NMR of Compound 6.96c (125 MHz, CDCl_3).....	515
Figure 6.58: ^1H NMR of Compound 6.98 (500 MHz, CDCl_3).....	516
Figure 6.59: ^{13}C NMR of Compound 6.98 (125 MHz, CDCl_3).....	517
Figure 6.60: DQF-COSY of Compound 6.98 (500 MHz, CDCl_3).....	518
Figure 6.61: gHSQC of Compound 6.98 (500 MHz, CDCl_3).....	519
Figure 6.62: gHMBC of Compound 6.98 (500 MHz, CDCl_3).....	520
Figure 6.63: 1D NOE of Compound 6.98 : {H-4a} (δ_{H} 1.98, 600 MHz, CDCl_3).....	521

Figure 6.64: 1D NOE of Compound 6.98 : {H-8a} (δ_{H} 4.25, 600 MHz, CDCl ₃).....	522
Figure 6.65: ¹ H NMR of Compound 6.71 (400 MHz, CDCl ₃).....	523
Figure 6.66: ¹³ C NMR of Compound 6.71 (100 MHz, CDCl ₃).....	524
Figure 6.67: DQF-COSY of Compound 6.71 (400 MHz, CDCl ₃).....	525
Figure 6.68: HSQC-NUS of Compound 6.71 (400 MHz, CDCl ₃).....	526
Figure 6.69: HMBC-NUS of Compound 6.71 (400 MHz, CDCl ₃).....	527
Figure 6.70: NOESY of Compound 6.71 (400 MHz, CDCl ₃).....	528
Figure 6.71: ¹ H NMR of Compound 6.100 (400 MHz, CDCl ₃).....	529
Figure 6.72: ¹³ C NMR of Compound 6.100 (100 MHz, CDCl ₃).....	530
Figure 6.73: ¹ H NMR of Compound 6.106 (400 MHz, CDCl ₃).....	531
Figure 6.74: ¹³ C NMR of Compound 6.106 (100 MHz, CDCl ₃).....	532

LIST OF SCHEMES

Scheme 1.1: Proposed biogenesis of oxime bromotyrosines and spiroisoxazolines.....	6
Scheme 1.2: Proposed biogenesis of spirooxepinisoxazolines.....	7
Scheme 2.1: Hydrolysis of 2.2 and derivatization of isoSer by L-FDTA (2.5).....	46
Scheme 2.2: Naphthoate ester (–)- 2.7 from acylation of (+)- 2.4a	46
Scheme 2.3: Biosynthetic hypothesis for 2.1 , 2.2 and 2.4b	52
Scheme 3.1: Hydrolysis of 3.4 and derivatization of homoserine residue with L-FDTA (3.8) to 3.9	87
Scheme 3.2: Total Synthesis of (+)- 3.7a , (–)- 3.7b , and Methyl Purpuroceratate C (±)- 3.3b . See Table 3.3 for ECD.....	94
Scheme 4.1: Hydrolysis of 4.3 and derivatization of 2,4-diaminobutanoic acid with L-FDTA (4.8).....	149
Scheme 5.1: Methanolysis of 5.2 , persilylation of OMe-glycosides with Pierce’s reagent (BSTFA), and MS fragmentation analysis of the aglycone (5.4) and persilylated <i>O</i> -Me glycosides.....	264
Scheme 5.2: (a) Enantioselective reduction of ethyl levulinate (5.5) and lactonization to 5.6 , and (b) ECD spectra of 5.4 (1.49 mM, MeOH) and 5.6 (8.99 mM, MeOH).....	269
Scheme 5.3: (a) Yamaguchi esterification of 5.4 to 5.8a and 5.8b , and (b) $\Delta\delta^{RS}$ ($\delta^R - \delta^S$) values. See Ref. 20-21.....	271
Scheme 5.4: Proposed retrosynthesis of models 5.9a and 5.9b	273
Scheme 5.5: Preparation of enantioenriched (<i>R</i>)- and (<i>S</i>)- 5.11	274
Scheme 5.6: Synthesis of Model Compounds 5.9a and 5.9b , and the corresponding triesters 19a,b and 20a,b	276
Scheme 5.7: Methanolysis of 5.3a–g under acidic conditions.....	280
Scheme 5.8: Degradation of 5.3a–g under acidic and basic conditions.....	282
Scheme 5.9: Naphthyl and acetyl derivatization of 5.21i–l	283
Scheme 5.10: Synthesis of (<i>R</i>)- and (<i>S</i>)-1-NMA.....	291
Scheme 5.11: Synthesis of tris-NMA derivatives 8a,b	293

Scheme 5.12: Synthesis of alcohol (–)- 5.10	294
Scheme 5.13: Synthesis of (<i>R</i>)- and (<i>S</i>)- 5.11	295
Scheme 5.14: Synthesis of (<i>R</i>)- 5.12	300
Scheme 5.15: Synthesis of models 5.9a,b	301
Scheme 5.16: Synthesis of tris-NMA derivatives 5.19a,b and 5.20a,b	309
Scheme 6.1: Toyooka and co-workers' total synthesis of lepadin B. See reference 6.....	414
Scheme 6.2: Kibayashi's synthesis of the keto aldehyde intermediate 6.27 . See reference 7.....	416
Scheme 6.3: Kibayashi's synthesis of lepadin B (6.2). See reference 7.....	417
Scheme 6.4: Pu and Ma's synthesis of lepadin B. See reference 8.....	419
Scheme 6.5: Blechert's synthesis of common intermediate 6.51 . See reference 9.....	421
Scheme 6.6: Tong's synthesis of common intermediates 6.62a,b	423
Scheme 6.7: Retrosynthetic approaches to the lepadins.....	425
Scheme 6.8: Proposed retrosynthesis of lepadin I.....	426
Scheme 6.9: Synthesis of the amino alcohol 6.80a	427
Scheme 6.10: (a) Selective benzyl-protection of 6.80a , and (b) oxidative cleavage of 6.81b to 6.76	428
Scheme 6.11: Preparation of 6.74 and tandem Robinson annulation–aza-Michael cyclization with acrolein or crotonaldehyde.....	429
Scheme 6.12: Preparation of aldehydes 6.75a–d from 2-propyn-1-ol.....	430
Scheme 6.13: Preparation of aldehyde 6.75e from propiolic acid.....	431
Scheme 6.14: Synthesis of the C-5 sidechain.....	431
Scheme 6.15: Robinson–aza-Michael sequence with β -ketoester 6.74 and aldehydes 6.75a–e ...	432
Scheme 6.16: Robinson–aza-Michael sequence with β -ketoester 6.97 and aldehyde 6.75b	434
Scheme 6.17: Robinson–aza-Michael sequence with β -ketoester 6.74 and aldehyde 6.75b	436

Scheme 6.18: <i>t</i> -BuO-deprotection and decarboxylation of 6.96b and Wittig olefination with 6.71	439
Scheme 6.19: <i>t</i> -BuO-deprotection and decarboxylation of 6.102 and HWE olefination with 6.103	440
Scheme 6.20: Proposed route to complete the total synthesis of lepadin I.....	441

LIST OF TABLES

Table 2.1: ^1H and ^{13}C NMR Data for 2.1–2.3 in CD_3OD	43
Table 2.2: Chiroptical Data ($[\alpha]_D$, ECD) for Three Chemotypes (<i>A-C</i>) of Dibromocyclohexa-1,3-dienes.....	48
Table 3.1: ^1H and ^{13}C NMR data for 3.1b–3.2b , and 3.3a (CD_3OD).....	85
Table 3.2: ^1H and ^{13}C NMR data for 3.4 (CD_3OD) and 3.5 (DMSO-d_6).....	88
Table 3.3: Specific Rotation $[\alpha]_D$ and ECD Data of Spiroisoxazolines (CH_3OH). ^a	95
Table 3.4: Homologous SIO Carboxylic Acids and Proposed ‘Origin’ AA of the Second Module.....	97
Table 3.5: In vitro Inhibition (IC_{50} , μM) of AChE and BuChE by SIO Alkaloids.....	98
Table 3.6: ^1H and ^{13}C NMR data of Compound 3.5 (CD_3OD).....	137
Table 4.1: ^{13}C NMR data for 4.1–4.4 and 4.6 in CD_3OD	146
Table 4.2: ^1H NMR data for 4.1–4.4 and 4.6 in CD_3OD	147
Table 4.3: ^1H and ^{13}C NMR data for 4.5a and 4.5b (CD_3OD).....	154
Table 4.4: Physical and chiroptical properties of key spiroisoxazolines 4.13–4.16	164
Table 4.5: Antifungal activities (MIC_{90} (μM) of Aiolochochromides C (4.5a), D (4.5b), Ianthelline (4.7), and Ningalamide B (4.9) against <i>Candida</i> and <i>Cryptococcus</i> spp.....	166
Table 4.6: Antifungal Activities (Disk-Diffusion Assay) of ‘Layers A-D’ and Chromatography Subfractions (SF) against <i>Candida</i> and <i>Cryptococcus</i> spp.....	207
Table 4.7: BuChE Inhibitory Activity of ‘Layers B and C’ Sephadex LH-20 Subfractions (SF).....	209
Table 4.8: Calculated (GIAO) ^{13}C and ^1H Chemical Shifts of 4.4a,b in MeOH.....	213
Table 4.9: Calculated ^{13}C Chemical Shifts of 4.5a and 4.5b in MeOH.....	215
Table 4.10: Calculated ^1H Chemical Shifts of 4.5a and 4.5b in MeOH.....	216
Table 4.11: Cartesian Coordinates and Relative Energies of Optimized Conformers of 4.4a,b ($\Delta E < 2 \text{ kJ/mol}$).....	217

Table 4.12: Cartesian Coordinates and Relative Energies of Optimized Conformers of 4.5a and 4.5b ($\Delta E < 8$ kJ/mol).....	225
Table 5.1: 1D and 2D NMR data for 5.2	266
Table 5.2: HR-ESI-MS of Oceanapins A–G (5.3a–g).....	279
Table 5.3: HR-ESI-MS of sphingosine base 5.21 , 5.24 , triacetate 5.25 , and <i>N,O</i> -derivative 5.26	281
Table 5.4: GCMS analysis of 5.23	283
Table 6.1: The sources and biological activities of lepadins A–L.....	412
Table 6.2: Literature syntheses of lepadins A–I.....	413
Table 6.3: Reductive conditions of 6.79 to 6.80a,b	427
Table 6.4: Attempted conditions for <i>O</i> -selective benzylation and oxidative cleavage.....	428
Table 6.5: Conditions for the Robinson–aza-Michael reaction with 6.74 and 6.75a–e	432
Table 6.6: Step <i>i</i> reaction conditions and % yields of 6.98 or 6.96b (see Scheme 6.16).....	435
Table 6.7: ¹ H and ¹³ C NMR data for 4a <i>S</i> ,8a <i>S</i> - 6.96b and 6.98 (CDCl ₃).....	438

ACKNOWLEDGMENTS

First and foremost, I would like to thank my advisor and mentor Dr. Ted Molinski for his mentorship, support, and guidance throughout graduate school. Ted's infectious enthusiasm and curiosity have had a tremendous influence on me as a scientist. He encouraged me to think independently and critically and taught me to be thorough and analytical when solving scientific problems. Ted, your leadership and mentorship inspired me as a doctoral student and will stay with me for the rest of my career.

I would also like to thank my former lab colleagues Dr. Matthew Jamison, and Dr. Christopher Gartshore for introducing me to the Molinski lab, and for their guidance and mentorship on the isolation, structural elucidation, and synthesis of marine natural products. Thank you for your kind and encouraging words and for sharing your chemistry knowledge with me. I enjoyed working with both of you. I also wish to thank Dr. Rudi Hendra, a former visiting Fulbright Fellow from the University of Riau, Indonesia, for our collaboration on the bromotyrosine alkaloids projects from *Pseudoceratina verrucosa* and *Aiolochoia crassa*. I enjoyed our invigorating scientific discussions as well as our personal conversations and getting to know one another. It was wonderful to work and collaborate with you.

I am deeply grateful to Dr. Carlo Ballatore, Dr. Thomas Hermann, Dr. Dionicio Siegel, and Dr. Michael Tauber for serving on my doctoral committee and for reading my dissertation. I am appreciative of your invaluable support during my graduate studies, helpful feedback and stimulating discussions.

I am incredibly thankful to Dr. Brendan Duggan, Dr. Anthony Mrse, and Dr. Xuemei Huang for maintaining the Skaggs School of Pharmacy and Pharmaceutical Sciences, and the Chemistry and Biochemistry NMR facilities. I am greatly indebted to you for your assistance with

setting up NMR experiments, aid in interpreting NMR data, and helpful suggestions to address challenging structural elucidations of novel marine natural products. Most importantly, thank you for answering my many NMR questions. I am also grateful to Dr. Yongxuan Su, the manager of the Molecular Mass Spectrometry Facility in the Department of Chemistry and Biochemistry at UCSD, for his assistance with all MS analysis needs.

I would also like to thank the Bertrand group for being wonderful neighbors for all these years, and for making my doctoral experience a positive one. Thank you for your friendliness, welcoming nature and for your unwavering encouragement. I am so glad that I met every single one of you. I would also like to thank Victor Wang and Melinda Serrato with whom I developed friendships that will stay with me for the rest of my life. Victor, I am so thankful that you did a rotation in the Molinski group because it gave me a chance to meet and get to know you. I cherish our chemistry talks, and our discussions on everything that was happening in our lives. Melinda, I enjoyed our honest conversations, and in you, I found a confidante. Thank you for listening to me and for being supportive and understanding.

I wish to also thank my dear friend Bashayer Althufairi. I am so glad that you initiated our first conversation because it brought you into my life. Thank you for helping me cope with my problems and, instead, of making me laugh and forget everything. I would also like to thank Nicole Daneshvar for being an amazing housemate, incredible friend and for her encouragements as I wrote my dissertation.

Last but not least, this dissertation wouldn't be possible without the support of my parents and siblings. I would like to thank my parents, Nader and Nabila, for giving me the opportunity to pursue my own passions and education in chemistry, and for being so supportive of my decisions and choices. I would also like to thank my siblings Peter, Basim, Nancy and Sarra for keeping me

grounded and making me laugh. I would especially like to thank my sister Sarra, my best friend and travel companion through life, and my mother Bila for their unwavering loyalty, unfailing presence, empathy and understanding. Thank you all for being a part of my life.

Chapter 2, in total, is a reprint of the material, “Bromo-spiroisoxazoline Alkaloids, Including an Isoleucine Peptide, from the Caribbean Marine Sponge *Aplysina lacunosa*” *J. Nat. Prod.* **2020**, 83, 1532-1540. The dissertation author was the primary author of this paper and gratefully acknowledges the contributions of coauthors Matthew T. Jamison, and Tadeusz F. Molinski.

Chapter 3, in total, is a reprint of the material, “Spiroisoxazoline Inhibitors of Acetylcholinesterase from *Pseudoceratina verrucosa*. Quantitative Chiroptical Analysis of Configurational Heterogeneity and Total Synthesis of (±)-Methyl Purpuroceratate C” *J. Nat. Prod.* **2022**, Submitted. The dissertation author was the primary author of this paper and gratefully acknowledges the contributions of coauthors Rudi Hendra, and Tadeusz F. Molinski.

Chapter 4, in total, is a reprint of the material, “Bioactive Bromotyrosine Alkaloids from the Bahamian Marine Sponge *Aiolochoxia crassa*. New Dimerization and Oxidative Motifs.” *J. Org. Chem.* **2022**, Submitted. The dissertation author was the primary author of this paper and gratefully acknowledges the contributions of coauthors Rudi Hendra, and Tadeusz F. Molinski.

Chapter 5, in part, is a reprint of the material, “Colossal NMR Anisotropy Relays Remote Stereoconfiguration. The Absolute Stereostructure of the Complex Glycolipid, Axinoside-1, from a Western Australian Axinellid Sponge.” In preparation for submission to *J. Am. Chem. Soc.* The dissertation author was the primary author of this paper and gratefully acknowledges the contributions of coauthor Tadeusz F. Molinski.

Vita

Education

- 2013 University of California San Diego
Bachelor of Science, Chemistry
- 2018 University of California San Diego
Master of Science, Chemistry
- 2022 University of California San Diego
Doctor of Philosophy, Chemistry

Publications

1. **Salib, M. N.**; Molinski, T. F. “Cyclic Hexapeptide Dimers, Antatollamides A and B, from the Ascidian *Didemnum molle*. A Tryptophan-Derived Auxiliary for L- and D-Amino Acid Assignments.” *J. Org. Chem.* **2017**, *82*, 10181-10187.
2. **Salib, M. N.**; Molinski, T. F. “Six Trikentrin-like Cyclopentanoindoles from *Trikentrion flabelliforme*. Absolute Structural Assignment by NMR and ECD.” *J. Org. Chem.* **2018**, *83*, 1278-1286.
3. Gartshore, C. J.; **Salib, M. N.**; Renshaw, A. A.; Molinski, T. F. “Isolation of bastadin-6-*O*-sulfate and expedient purifications of bastadins-4, -5 and -6 from extracts of *Ianthella basta*.” *Fitoterapia* **2018**, *126*, 16-21.
4. Molinski, T. F.; **Salib, M. N.**; Pearce, A. N.; Copp, B. R. “The Configuration of Distaminolyne A is *S*: Quantitative Evaluation of Exciton Coupling Circular Dichroism of *N,O*-Bis-arenoyl-1-amino-2-alkanols.” *J. Nat. Prod.* **2019**, *82*, 1183-1189.
5. **Salib, M. N.**; Jamison, M. T.; Molinski, T. F. “Bromo-spiroisoxazoline Alkaloids, Including an Isoserine Peptide, from the Caribbean Marine Sponge *Aplysina lacunosa*.” *J. Nat. Prod.* **2020**, *83*, 1532-1540.
6. Hendra, R.; **Salib, M. N.**; Molinski, T. F. “Spiroisoxazoline Inhibitors of Acetylcholinesterase from *Pseudoceratina verrucosa*. Quantitative Chiroptical Analysis of Configurational Heterogeneity and Total Synthesis of (±)-Methyl Purpuroceratate C.” *J. Nat. Prod.* Submitted.
7. **Salib, M. N.**; Hendra, R.; Molinski, T. F. “Bioactive Bromotyrosine Alkaloids from the Bahamian Marine Sponge *Aiolochoia crassa*. New Dimerization and Oxidative Motifs.” *J. Org. Chem.* Submitted.

8. **Salib, M. N.**; Molinski, T. F. “Colossal NMR Anisotropy Relays Remote Stereoconfiguration. The Absolute Stereostructure of the Complex Glycolipid, Axinoside-1, from a Western Australian Axinellid Sponge.” *J. Am. Chem. Soc.* In preparation.

Awards

- | | |
|-------------|--|
| 2019 | ACS Poster Award at American Society of Pharmacognosy’s Annual Meeting |
| 2019 | Distinguished Graduate Student Fellowship – UCSD |
| 2020 – 2021 | Teddy Traylor Award – UCSD |
| 2020 – 2021 | Carol and George Lattimer Award for Graduate Excellence – UCSD |
| 2021 – 2022 | Oceanids Memorial Fellowship – UCSD |
| 2021 – 2022 | Sigma Delta Epsilon Tau Chapter Fellowship – UCSD |

ABSTRACT OF THE DISSERTATION

Marine-Derived Heterocycles from Porifera (Sponges) of the Bahamas and Western Australia:
Synthetic and Structural Studies Enhanced by Chiroptical Methodologies

by

Mariam Nader Salib

Doctor of Philosophy in Chemistry

University of California San Diego, 2022

Professor Tadeusz F. Molinski, Chair

This dissertation discusses the structural elucidation and total synthesis of bioactive marine natural products. Separation of the MeOH extracts of three Verongida sponges provided novel bromotyrosine alkaloids (BTAs), the structures of which revealed oxidative and non-oxidative dimerization and other unprecedented structural motifs. The Caribbean *Aplysina lacunosa* and Western Australian *Pseudoceratina verrucosa* furnished eight novel BTAs characterized by a spirocyclohexadienyl-isoxazoline (SIO) ring system. Evaluation of the MeOH extract of the Bahamian *Pseudoceratina crassa* revealed the presence of nine new BTAs embodied by an *O*-

methyl-2,6-dibromotyrosyl ketoxime. The planar structures of the 17 alkaloids were determined by interpretation of MS, 1D and 2D NMR data, and the absolute configuration of the SIO unit was ascertained by ECD. Analysis of the compounds by specific rotation, Cotton effects and chiral-phase HPLC revealed that BTAs are configurationally heterogeneous. Extracts from *A. lacunosa* showed inhibitory activity against α -chymotrypsin. Alkaloids from *P. verrucosa* and *P. crassa* selectively inhibited acetylcholinesterase and butyrylcholinesterase, respectively.

The structure of the unusually complex glycolipid axinoside-1 was elucidated by integrated spectroscopic analysis, MS, degradation, and derivatization to reveal a tetrasaccharide, comprising three D-xylose units and one D-glucose, linked to a C₂₈-aglycone. The identities of the sugar units were established after acidic methanolysis, conversion to persilylated ethers and GCMS analysis with comparison to authentic standards. Linkage analysis was performed by HMBC, and anomeric configurations were established from interpretation of ¹J_{CH} coupling constants. The location of the 2° OH groups in the aglycone and the site of glycosylation were ascertained through MS fragmentation. The absolute configuration of the terminal γ -butyrolactone in the aglycone was determined by ECD. Configurational assignment of the three free 2° OH groups was achieved from interpretation of the colossal ¹H NMR anisotropy induced in the δ values of their corresponding tri-(naphth-1-yl)methoxyacetic acid (NMA) esters, and comparative analysis of $\Delta\delta$ values of the corresponding tri-NMA derivatives of two stereodefined synthetic models, prepared by multistep synthesis.

Lastly, extensive efforts towards the total synthesis of lepadin I, a selective butyrylcholinesterase inhibitor, were carried out leading to an advanced intermediate through tandem Robinson annulation–aza-Michael cyclization, setting the stage for the end-game and completion of the natural product.

CHAPTER ONE. INTRODUCTION

1.1 Marine Natural Products as a Source of Potential Drug Leads

The world's oceans cover more than 70% of the earth's surface and are home to about one million species of animals and over a billion species of microbes, with many yet to be discovered. Of the 35 animal phyla currently identified, only one phylum, the *Onychophora* or velvet worms, is completely absent from aquatic life.¹ *Mollusca*, *Porifera*, *Cnidaria*, *Platyhelminthes*, *Nematoda*, *Annelida*, *Arthropoda*, *Echinodermata*, and *Chordata* comprise the nine major and best-known animal phyla. The latter phyla are predominately marine, with *Arthropoda*, *Nematoda* and *Mollusca* encompassing the most diverse marine species. Marine invertebrates are well-known sources of diverse natural products, with the *Porifera* (sponges) and *Cnidaria* (corals, hydras, jellyfish, sea anemones, etc.) phyla accounting for ~54% of the total number of bioactive marine natural products (MNPs, Figure 1.1).² Marine organisms, along with associated-symbiotic microorganisms (such as dinoflagellates and colonizing bacteria), produce and release secondary metabolites or 'toxins'³ as a mechanism of chemical defense.⁴ Many of these unique and complex molecules display profound biological activities and show remarkably high hit rates in biological screenings compared to terrestrial natural products.⁵ Subsequently, MNPs have presented a significant source of drug leads for the pharmaceutical industry (Figure 1.1).

The potential of new drug candidates has encouraged the search for bioactive MNPs in the hopes of treating life-threatening illnesses. Several technological advances and research methods have facilitated the discovery of new MNPs. Developments in automated extraction, prefractionation, mass spectrometry, NMR and dereplication methodologies have tremendously reduced the time in identifying known and new natural products. Although, over 38,000 MNPs

have been identified as of June 2022,⁶ only a small subset of marine organisms has been examined for bioactive natural products.⁷

Currently, seven MNPs are marketed drugs, primarily as cancer therapeutics (Figure 1.2).¹ The peptide ziconotide (**1.1**, trade name Prialt[®]), originally isolated from the tropical cone snail *Conus magus*, is the first MNP to receive drug approval in the United States in 2004 for the treatment of severe, chronic pain in spinal cord injury.^{1,8} Trabectedin (**1.2**, Yondelis[®]) – a second drug isolated from the tropical sea squirt *Ecteinascidia turbinata* – received approval in Europe in 2007 for the treatment of soft tissue sarcoma and ovarian cancer, and in the United States in 2015 for the treatment of metastatic liposarcoma.^{1,9} A third example is the antibody-drug conjugate (ADC) brentuximab-vedotin (Adcetris[®]) developed by Seattle Genetics. Brentuximab-vedotin was approved by the FDA in 2011 and EU in 2015 for the treatment of patients with stage 3 or 4 Hodgkin lymphoma.¹⁰ The ADC drug is composed of an antibody against the CD30 antigen, a cleavable linker, and the cytotoxic drug monomethyl auristatin E (**1.3**), an analog of the marine pentapeptide dolastatin 10. Pettit’s group first prepared monomethyl auristatin E to explore the cytotoxic structure-activity relationship (SAR) of dolastatin 10,¹¹ originally isolated from the marine sea hare *Dolabella auricularia*.¹²

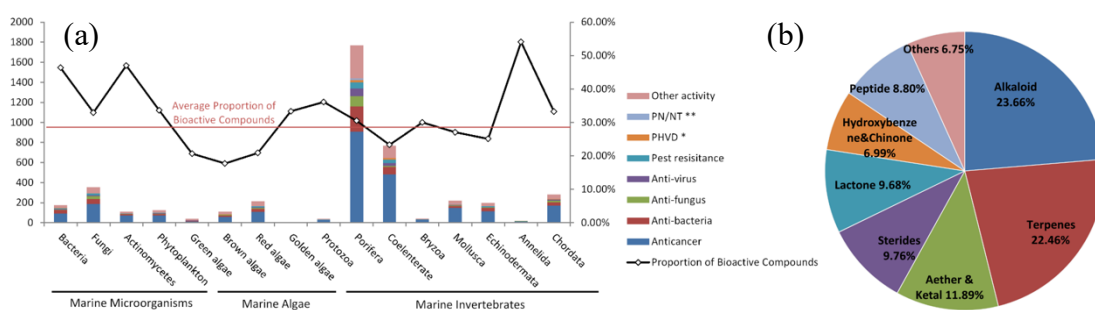


Figure 1.1: (a) Number and proportional distribution of bioactive MNPs from various marine organisms. PN/NT** and PVHD refer to “protection of neurons/neurotoxicity” and “prevention of heart and vascular disease,” respectively. Remaining bioactivities that cannot be classified in the above groups are categorized under “other activity.” (b) Distribution of chemical classes in *Porifera* and *Cnidaria*. Figures (a) and (b) were taken directly from reference 2.

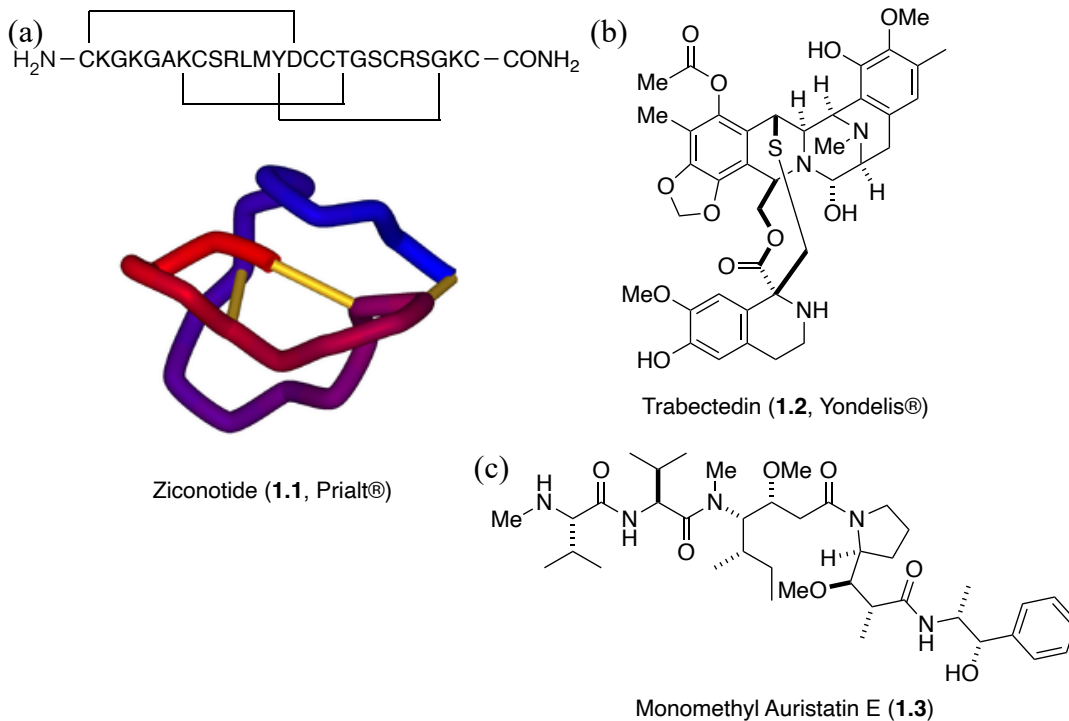


Figure 1.2: The structures of approved marine drugs: (a) the amino acid sequence and 3D structure of ω -conotoxin MVIIA (ziconotide/Prialt®), (b) trabectedin (Yondelis®), and (c) the drug load monomethyl auristatin E (brentuximab-vedotin/Adcetris®). The 3D structure of ziconotide was adopted directly from Wikipedia; see reference 13.

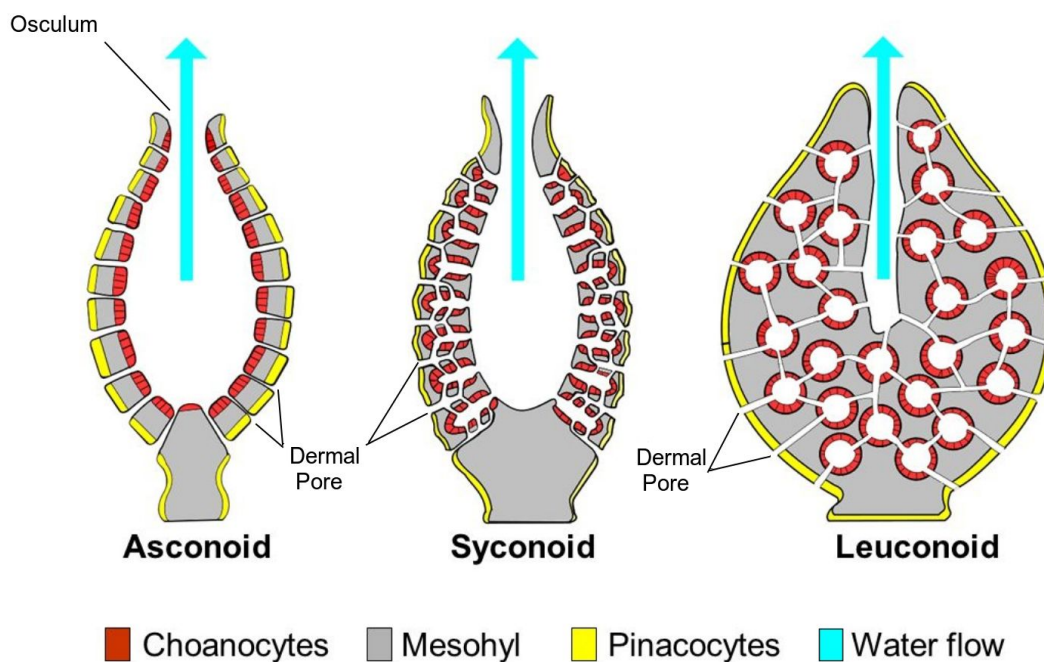


Figure 1.3: The three basic *Porifera* body structures, adopted from Wikimedia Commons. The figure was adopted directly from reference 14.

1.2 Bromotyrosine-Derived Alkaloids from Verongida Sponges

Sponges (phylum *Porifera*) are primitive multicellular organisms consisting of mainly asymmetrical bodies made of complex networks of canals and chambers.¹⁵ These simple invertebrates adopt three basic morphologies: asconoid, syconoid and leuconoid (Figure 1.3).¹⁵ The simplest – asconoid – have small vase-like porous structures, an osculum (opening at the top), and a spongocoel (exposed inner chamber) lined with choanocytes (collar cells lined with flagella). Similar in structure, syconoid sponges possess folds within their thickened body wall along with ostia (elongated pores) that form canals, increasing the surface area and enabling sponges to capture more nutrients including bacteria, plankton, and detritus. Leuconoid sponges, with their intricate interconnected canal systems, are the biggest of all three sponge types and enjoy the largest surface area of all.

Approximately 90–95% of the species *Porifera* belongs to the class *Demospongiae*. Demosponges possess the leuconoid body form in a variety of asymmetrical shapes with skeletons consisting of soft spongin or hard spicules made of calcium carbonate or silicon dioxide (silica). Marine demosponges emerged over 635 million years ago in the second geologic period of the Neoproterozoic Era. Abundant sedimentary concentrations of 24-isopropylcholestanes, geologically stable biomarkers of 24-isopropylcholesten-3-ols,¹⁶ detected in formations of the Huqf Supergroup of the South Oman Salt Basin, revealed that demosponges emerged in the Cryogenian period and represent the oldest Metazoa (multicellular animals) in the fossil record.¹⁷

Marine sponges are an extraordinary source of biologically relevant secondary metabolites with unique chemical diversity in their complex structures and broad range of biological activities. Among marine microorganisms, marine algae and marine invertebrates, the largest number of MNPs of most diverse structures have been isolated from marine sponges.² Sponges are sessile

benthic organisms adept at forming mutualistic relationships with microbial species, thus, forming a diverse microbial community within sponges that contribute to their ample chemical diversity. It is no coincidence that MNPs from sponges differ significantly from the well-known canonical structures of natural products from the plant Kingdom where the origin of folkloric medicines and the basis of modern pharmacopeias lie.

Among these are sponges of the order Verongida; abundant producers of chemically diverse bromotyrosine alkaloids (BTAs) that provide the sessile organisms with chemical defenses against predation¹⁸⁻¹⁹ and fouling.²⁰⁻²¹

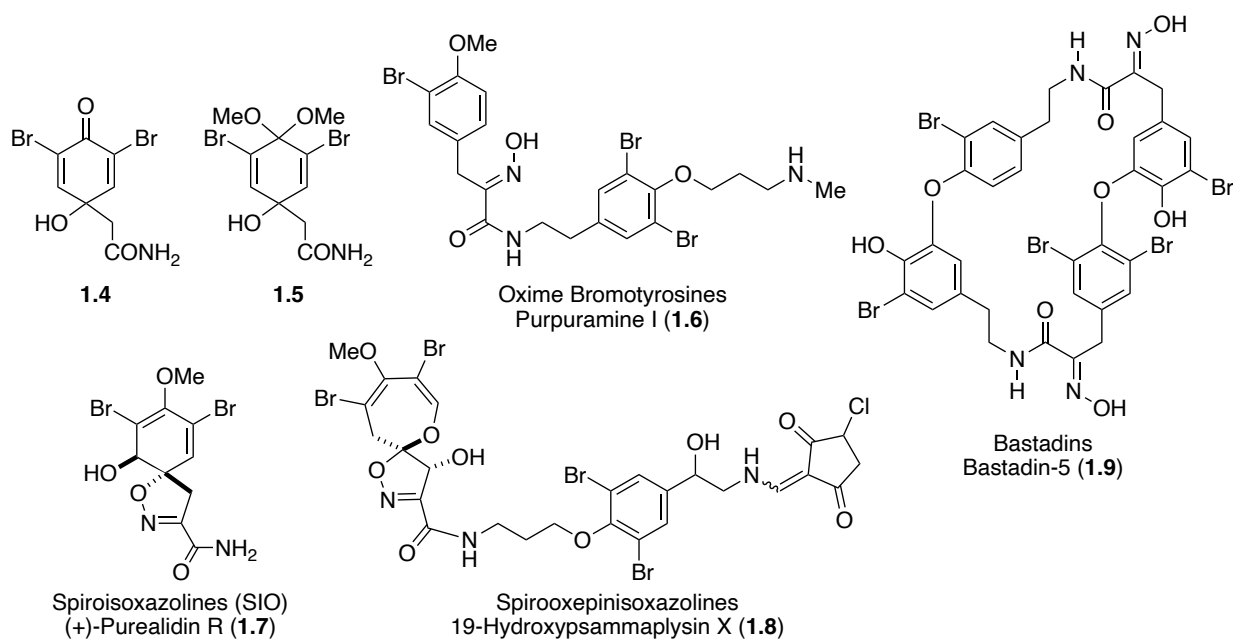
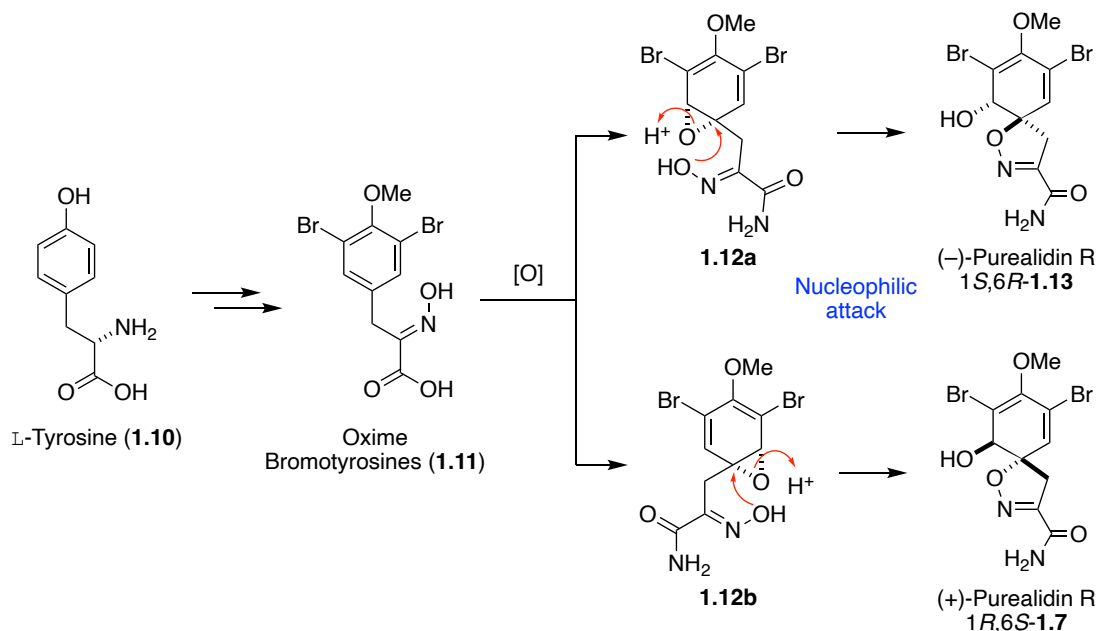


Figure 1.4: Representative structures of the four subclasses of bromotyrosine-derived alkaloids.

Bromotyrosine alkaloids (BTAs) represent one of the most abundant and structurally diverse class of marine-derived natural products with over 800 congeners now identified.^{22,23} The first report of these secondary metabolites occurred in 1967 when Sharma and Burkholder related the isolation of the broad-spectrum antibiotic **1.4** and dimethoxyketal **1.5** from the marine sponges *Verongia cauliformis* and *V. fistularis*, respectively.²⁴⁻²⁵ Since then, additional bromotyrosine-

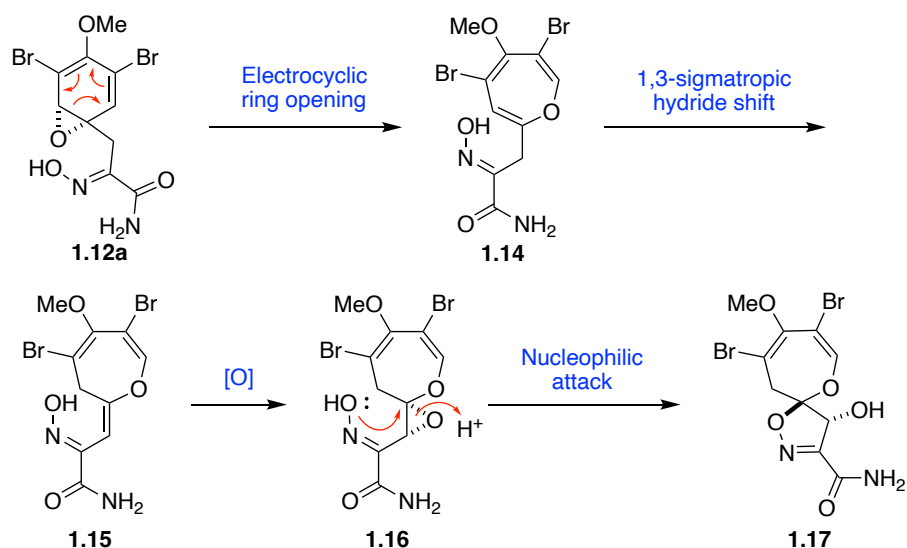
derived MNPs exhibiting diverse biological activities including antimicrobial, antifungal, antibacterial, cytotoxicity, antifouling, antiviral, enzyme inhibition, and calcium channel regulation have been reported.²²⁻²³ The highly modular nature of the BTAs along with chemical modifications in the aromatic rings, linkers and terminal coupling partners gives rise to an array of biosynthetically related alkaloids. The chemical diversity of this class of compounds can be epitomized by a single unifying postulate: the condensation of a bromotyrosyl ketoxime or bromooxepine with short-chain amines derived from decarboxylated proteinogenic or non-proteinogenic amino acids. Subsequently, BTAs can be divided into four subclasses including the oxime bromotyrosines, spiro-cyclohexadienyl-isoxazoline or spiroisoxazoline (SIO), spirooxepinisoxazoline, and bastadins exemplified by purpuramine I (**1.6**),²⁶ (+)-puralidin R (**1.7**),²⁷ 19-hydroxypsammamplysin X (**1.8**),²⁸ and bastadin-5 (**1.9**),²⁹ respectively (Figure 1.4).



Scheme 1.1: Proposed biogenesis of oxime bromotyrosines and spiroisoxazoles.

Biogenetically, the spiroisoxazoles (SIOs) and related spirooxepinisoxazoles are derived from the same arene oxide precursor, **1.12** (Scheme 1.1 and 1.2).^{30,31,32} The oxime

bromotyrosines are biosynthesized from tyrosine in a four step sequence (arbitrary order): deamination (aminotransferase) to the α -ketoacid, methylation (methylase, SAM) of the phenol, bromination (bromoperoxidase), and transformation to the α -ketoxime (oximinotransferase, Scheme 1.1).³² Subsequent nucleophilic attack of the oxime HO onto the arene oxide with C–O bond cleavage and protonation gives the SIO skeleton with the hydroxyl group at C-1. The majority of the SIOs exhibit a positive optical rotation ($[\alpha]_D$) and positive Cotton effects ($\Delta\epsilon$) consistent with the 1*R*,6*S*-configuration; fewer are of the antipodal 1*S*,6*R*-configuration. For example, (–)-purealin³³ and (–)-purealidin R³⁴ (**1.13**) were isolated from the Okinawan sponge *Psammaphysilla porea*, while (+)-purealin³⁴ and (+)-purealidin R²⁷ (**1.7**) were obtained from the Southern Australian sponge *Pseudoceratina* spp. suggesting that the biosynthesis of the SIO alkaloids is enantiodivergent. The enantiodivergent desymmetrization occurs during the monooxygenase-promoted epoxidation of the arene thus providing two antipodes **1.12a** and **1.12b** that give rise to the 1*S*,6*R*- and 1*R*,6*S*-absolute configuration.³²



Scheme 1.2: Proposed biogenesis of spirooxepinisoxazolines.

To date, 45 spirooxepinisoxazoline alkaloids have been identified including psammaphysins A-Z and their 19-hydroxy derivatives,^{28,30} ceratinamides A-B,³⁵ psammaceratin A,³⁶ ceratinadin A-F,^{37,38,39} and frondophysin A-B.⁴⁰ All the spirooxepinisoxazolines are characterized by a distinctive HO in the isoxazoline ring, and some of the derivatives are acylated by a terminal fatty acyl sidechain. The oxepin of the spirooxepinisoxazoline skeleton may be biosynthesized from the arene oxide **1.12** through a disrotatory electrocyclic ring opening (Scheme 1.2).³² A subsequent 1,3-sigmatropic hydride shift furnishes olefin **1.15**, which gives epoxide **1.16** upon oxidation.³² Nucleophilic attack by the oxime HO upon epoxide **1.16** provides the dihydrooxepin **1.17**.³² Although, the relationship between optical rotations, Cotton effects, and absolute configuration of the SIO alkaloids is well understood, the corresponding correlations for members of the spirooxepinisoxazoline subclass remain unclear due to the greater conformational flexibility of the dihydrooxepin compared to the spirocyclohexadienes.^{30a}

Marine sponges belonging to the genus *Ianthella*, of the order Verongida, are characteristic producers of brominated metabolites including the bromobenzofurans exemplified by the iantherans,⁴¹ and BTAs represented by aerophysinin-1,⁴² fistularin-3,⁴³ and the bastadins. Kazlauskas and colleagues reported the isolation of the first seven bastadins in 1980-81,^{29,44} and numerous studies have been published since regarding the identification, biological activity, and synthesis of this family of 28 compounds. The acyclic or macrocyclic metabolites are derived from four units of tyrosine that have undergone extensive aryl ring hydroxylation and bromination, decarboxylation to a tyramine, and oxidation of the 2-amino group to a distinct ketoxime unit. Bastadins 1–3 are characterized by one oxidative phenolic coupling of two tyramine tyrosine subunits whereas the remaining bastadins, including bastadin-5 (**1.9**, Figure 1.4), are bis-biaryl ether tetrapeptides with a parent *bastarane*²⁹ skeleton or the isomeric *isobastarane* ring.

The biogenetic origin of BTAs remains contentious due to contradictory evidence suggesting that BTAs arise from the host and associated symbiont organisms. Brominated alkaloids, found localized within the spherulous cells of the gelatinous mesohyl of *Aplysina* sponges, suggest that spherulous cells of the sponge host may be the biogenetic producers of these brominated metabolites.^{45,46,47} This is contrary to the findings of Berlinck and coworkers who isolated several BTAs from cultures of the marine bacterium *Pseudovibrio denitrificans* Ab134, obtained from specimens of the sponge *Arenosclera brasiliensis*. The findings indicate that the marine bacterium *Pseudovibrio denitrificans* Ab134 may be responsible for the biosynthesis of some brominated alkaloids.⁴⁸ Recently, Agarwal and colleagues utilized a multi-omic approach to examine the microbiome and natural product chemistry of geographically (Guam, Solomon Islands, Florida Keys, and Puerto Rico) and phylogenetically distinct Verongida sponges.⁴⁹ The presence of bromotyrosine alkaloids in phylogenetically and geographically distinct marine sponges is independent of the associated microbiome signifying that the sponge host itself may be the biosynthetic source of these alkaloids.⁴⁹ Still, the authors discovered a significant correlation between the disparate microbiome and disparate metabolome of the oxime bromotyrosines, SIOs, and bastadins suggesting that the microbiome plays a crucial role in shaping the metabolome.⁴⁹

1.3 Cholinesterase Inhibitory Activity of Marine Natural Products

1.3.1 Alzheimer's Disease

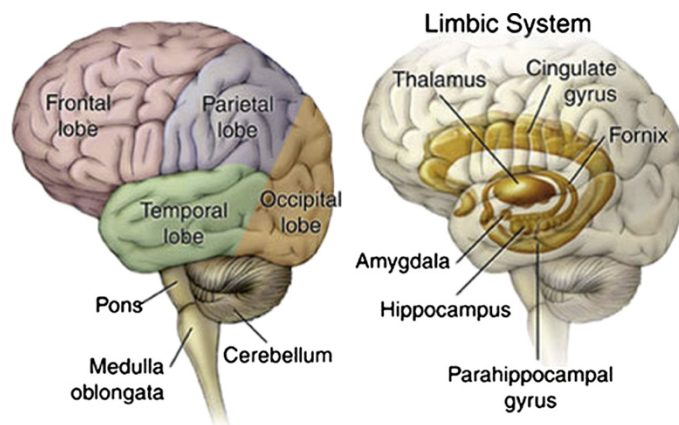


Figure 1.5: Anatomic locations of the limbic system that plays an important role in learning and memory functions. Figure was taken from reference 50.

Alzheimer’s disease (AD) is a progressive neurodegenerative disorder associated with severe synaptic loss and substantial brain atrophy in the frontal (intelligence, reasoning, and social behavior) and parietal lobes (language) as well as the entorhinal cortex, hippocampus, and amygdala in the temporal lobe (memory) (Figures 1.5 – 1.6). AD was the sixth leading cause of death in the US in 2019, and the seventh leading cause of death in 2020 and 2021 after the emergence of COVID-19 and its addition to the list of “top 10 causes of death.”⁵¹⁻⁵² Currently, an estimated 6.1 – 6.4 million Americans, age 65 or older, are living with the disease, and 73% of those individuals are age 75 or older.⁵³ By 2060, it’s anticipated that the number of Americans age 65 and older in the United States (US) suffering from AD will increase to 13.9 million. Furthermore, by 2050, AD is expected to place a financial burden of \$1 trillion on the United States economy, tripling from the \$305 billion spent in 2020.⁵⁴ According to the World Alzheimer Report 2021, over 55 million individuals worldwide were living with dementia in 2021, and that number is anticipated to reach 78 million by 2030.⁵⁵ Worldwide, the estimated cost of dementia in 2019 amounted to \$1.3 trillion, and is anticipated to surpass \$2.8 trillion by 2030.⁵⁶ Although, the financial burden of AD is quite extensive, the long duration of the illness, much of which is spent

in a state of severe disability, has significantly burdened dementia patients along with their caregivers and families.

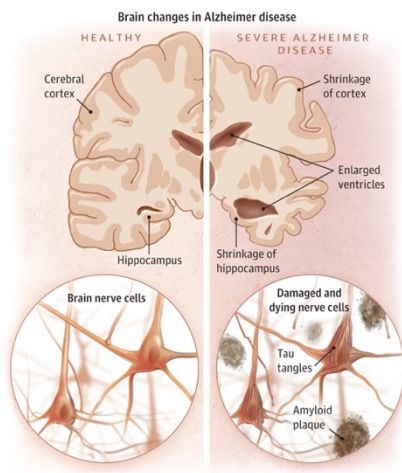


Figure 1.6: Brain atrophy in advanced Alzheimer’s disease. Image taken from reference 57.

Age is the greatest risk factor for AD along with lifestyle and preexisting health problems such as diabetes, cardiovascular disease, and neurological disorders.⁵⁸ Presently, the baby-boomer generation, born from 1946 – 1964, has already begun to reach age 65 with the oldest members of this generation turning age 75 in 2021. The prevalence of AD related dementia increases considerably after age 65 with the risk of developing the disease doubling every five years. An estimated 40% of individuals age 85 and older are living with AD today.⁵⁵

Clinically, AD slowly develops and progressively deteriorates from preclinical and mild cognitive impairment to severe dementia over the span of years and possibly decades.⁵⁹ AD patients experience memory loss, confusion, incoherent communication, personality and behavioral changes, and cognitive impairment,⁶⁰ and they require significant assistance with daily activities including eating, bathing, clothing, and other routine self-care tasks.⁵⁹ Neuronally, AD is primarily characterized by neuronal and synaptic loss correlated with the depletion of the human cholinergic neuronal markers choline acetyltransferase (ChAT) and acetylcholinesterase (AChE) in the basal forebrain and hippocampus.⁶¹⁻⁶² Moreover, as AD advances from mild to severe

dementia, the ratio of human butyrylcholinesterase (BuChE) to AChE increases significantly from 0.6 to 0.9 in the frontal cortex and 0.6 to 11 in the entorhinal cortex.⁶³ Subsequently, the cholinergic pool in an AD brain is substantially depleted, giving rise to the cholinergic hypothesis, and significantly affecting cognition and memory processing.⁶⁴ The progressive decline of the neurotransmitter acetylcholine (ACh) is strongly correlated with cognitive deterioration, memory impairment and behavioral dysfunction observed in AD patients.⁶⁰

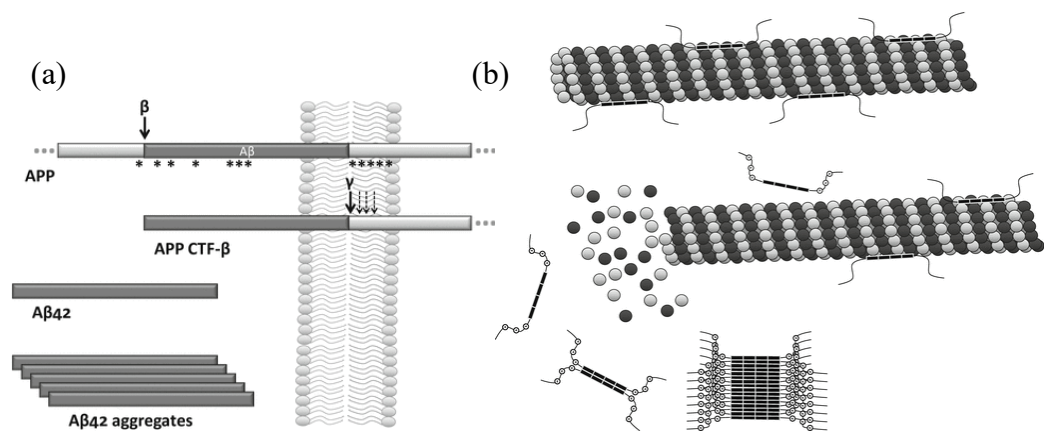


Figure 1.7: (a) Sequential proteolytic processing of APP to A β 42: APP cleavage by β -secretase and γ -secretase to A β 42 monomers, and subsequent aggregation to A β 42- oligomers and plaques. (b) Destabilization (dissociation) of microtubules upon loss of tau binding, hyperphosphorylation, and aggregation of tau into neurofibrillary tangles (NFTs). Images taken from reference 60.

Pathologically, an AD brain features the accumulation of extraneuronal amyloid plaques and intraneuronal neurofibrillary tangles along with neuroinflammation of glia cells including microglia and astrocytes (Figure 1.6). Amyloid plaques consist of amyloid β -proteins (A β) that are secreted proteolytic products of the type 1 transmembrane A β precursor protein (APP, Figure 1.7).⁶⁰ APP is successively proteolyzed by two membrane-bound aspartate proteases to the A β -40 and A β -42 peptides.⁶⁰ Initial cleavage of APP by β -secretase (BACE-1) at the β -site provides a C-terminal fragment (APP CTF- β) that is further processed by the promiscuous γ -secretase at the ϵ cleavage site to liberate two APP intracellular domains (AICD), A β 48 and A β 49. Sequential

trimming of A β 49 and A β 48 by a carboxypeptidase function of γ -secretase (presenilin 1 and 2) delivers A β 40 and A β 42, respectively. The minor variant (A β 42) is particularly predisposed to the formation of soluble oligomers and aggregates.⁶⁰

The downstream neurofibrillary tangles (NFTs) are comprised of hyperphosphorylated aggregates of the microtubule-associated tau protein.⁶⁰ In healthy individuals, tau binds to microtubules and promotes their self-assembly, formation and stabilization. In contrast, hyperphosphorylated tau forms NFTs that disrupt intracellular functions, through the disintegration of cytoskeletal microtubules and associated tubulin proteins, leading to the collapse of neurite extension and stabilization followed by synaptic loss and cognitive decline. Evidence suggests that pathological NFT formation is well correlated with neurodegeneration, more than amyloid pathology, in AD pathogenesis.⁶⁰

Neuroinflammation or chronic immune activation of microglial and astrocytes, mediated by the clearance of A β plaques, exacerbates neuronal degeneration.⁶⁵ Overactivation of microglial cells and reactive astrocytes promotes the production of high concentrations of pro-inflammatory cytokines (the tumor necrosis factor (TNF- α), interferon- γ and interleukin-1) and chemokines that stimulate chronic neuroinflammation.⁶⁵ Additionally, reactive astrocytes release high levels of reactive oxygen species (ROS) that cause oxidative stress, and in turn, induce nitrosative stress (overproduction of nitric oxide, NO).⁶⁶ Chronic inflammation plays a central role in the onset of AD and contributes significantly to the progression and severity of the disease.

1.3.2 FDA Approved Cholinesterase Inhibitors

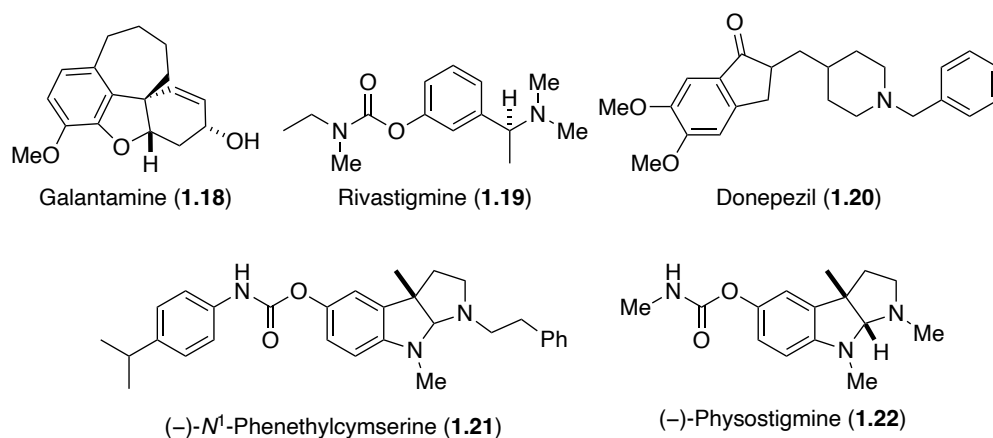


Figure 1.8: Structures of cholinesterase inhibitors.

Current AD therapeutics target either the clearance of β -amyloid plaques or maintenance of the ACh neurotransmitter pool by inhibition of the cholinesterase (ChEs) enzymes. Drugs targeting β -amyloid have suffered colossal disappointments in recent years with one exception.⁶⁷ Biogen's aducanumab (Aduhelm[®])—a human monoclonal antibody involved in the clearance of brain β -amyloid ($A\beta$ -plaques)—received controversial FDA approval in June 2021 after it showed “incomplete and contradictory” data in two concurrent phase III clinical trials.⁶⁷⁻⁶⁸ Although, aducanumab is the first disease-modifying therapy to receive accelerated approval for the treatment of the underlying cause of AD, additional clinical studies are needed to confirm the drug's benefits (slow progression of AD symptoms or enhance cognition). Conversely, Pfizer's antibody bapineuzumab, Eli Lilly's solanezumab, Merck's BACE (β -secretase) inhibitor verubecestat, and Johnson & Johnson's BACE inhibitor atabecestat are among several amyloid targeting drugs to fail in late-stage clinical trials in patients with moderate to advanced AD due to their inability to slow cognitive decline.⁶⁷

In contrast, ChE inhibitors including Janssen's galantamine (1.18, Razadyne[®]), Novartis's rivastigmine (1.19, Exelon[®]), and Pfizer's donepezil (1.20, Aricept[®]) were developed and approved by the FDA based on the cholinergic hypothesis of AD (Figure 1.8).⁶⁹⁻⁷⁰ The alkaloid

galantamine hydrobromide, originally isolated from the snowdrop *Galanthus nivalis*, is a reversible competitive inhibitor of AChE and an allosteric modulator of nicotinic acetylcholine receptors (nAChRs).⁷¹ The pseudo-irreversible inhibitor rivastigmine is a simplified analog of the naturally occurring physostigmine (**1.22**) isolated from the Manchineel tree and Calabar bean.⁷⁰ Compared to physostigmine, rivastigmine is a potent *in vivo* inhibitor of AChE and BuChE due to its improved bioavailability and increased lipophilicity enhancing its ability to cross the blood-brain barrier into the central nervous system (CNS).⁷² The synthetic piperidine derivative donepezil, approved in 1996 for the treatment of AD, is a highly selective noncompetitive reversible inhibitor of AChE.⁷³ ChE inhibitors are typically prescribed in combination with the *N*-methyl D-aspartate (NMDA) antagonist memantine (Namenda) to alleviate the neurotoxic effects of excess glutamate arising from the over-activation of glutamate receptors.⁷⁴ ChE inhibitors delay the progression of AD symptoms and improve memory, thinking, reasoning, language comprehension and communication, and activities of daily living by increasing the concentration of the neurotransmitter ACh in the CNS. The aforementioned inhibitors are largely selective towards AChE except for rivastigmine, which selectively inhibits hBuChE with an IC₅₀ of 0.037 μM (hAChE, IC₅₀ = 4.15 μM).⁷⁵

1.3.3 Cholinesterase Enzymes

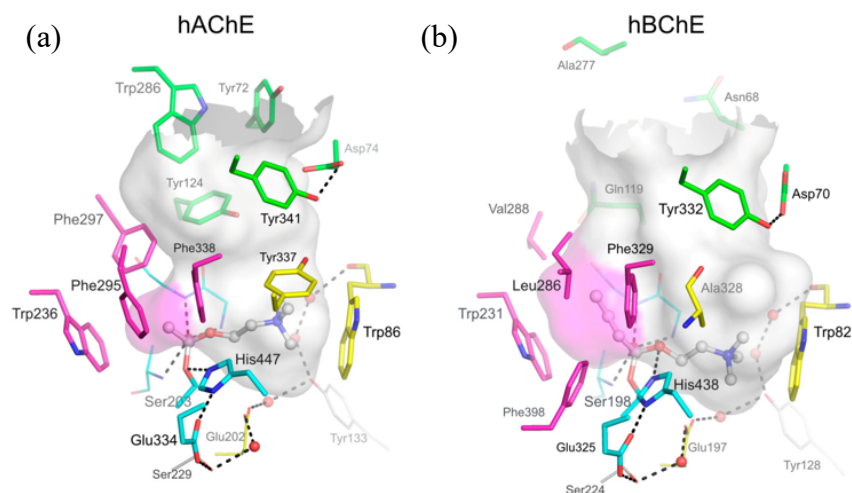


Figure 1.9: Differences in active site gorges of human (a) AChE (hAChE) and (b) BuChE (hBuChE, see reference 76). The transition state of ACh or butyrylcholine (BuCh) is modeled in the active site and represented in ball and stick. The gorge (gray), acyl-binding pocket (magenta), catalytic triad (sticks in cyan), and key aromatic residues (yellow) are depicted.

The structurally and functionally related serine hydrolases, hAChE and hBuChE, catalyze the hydrolysis of choline esters (Figure 1.9).⁷⁷ Both ChEs belong to the α/β -hydrolyse fold superfamily of enzymes that are characterized by a central β -sheet surrounded by α -helices.⁷⁷ X-ray crystallography of hAChE and hBuChE established that the active site, located at the bottom of an essentially hydrophobic 20 Å gorge, consists of a catalytic triad of Ser, His and Glu.⁷⁸ In hBuChE, the gorge is lined with six aromatic amino acid residues, in contrast with the 14 aromatic amino acid residues found interacting with ligands in hAChE. Moreover, the acyl pocket of hBuChE is lined with two small hydrophobic amino acids, Val288 and Leu286, that are replaced with two larger phenylalanine residues (Phe295 and Phe297) in hAChE.⁷⁶⁻⁷⁸ The acyl binding pocket (Figure 1.9, magenta), located in the active site gorge, orients and holds the acyl group of the respective substrate (acetyl for ACh; butyryl for butyrylcholine or BuCh) in place during hydrolysis. The aromatic rings of the two Phe residues protrude into the active site gorge in hAChE and tightly accommodate the acetyl chain of ACh. In contrast, the relatively smaller sidechains of

Val and Leu effect a conformational change onto the active site of the enzyme and enable it to accommodate the binding of bulkier substrates and inhibitors.

Both ChEs catalyze the hydrolysis of ACh though BuChE also hydrolyzes butyrylcholine (BuCh) and succinylcholine. AChE is highly efficient at the hydrolysis of ACh at low concentrations, but is substrate inhibited at higher levels.⁷⁹ Conversely, the non-specific BuChE is substrate activated at the concentrations of substrate inhibition in AChE.⁷⁹ The phenomenon of substrate inhibition in AChE likely arises because of the binding of a second ACh substrate at the P-site (located at the lip of the gorge, labeled in green, Figure 1.9) which then blocks the release of the hydrolysis products.⁷⁶ In BuChE, substrate activation is mediated by the binding of a second substrate at the P-site of the enzyme-substrate complex that further stabilizes hydrolysis intermediates.⁷⁶ Additionally, BuChE is capable of compensating for some of the functions of AChE. Experiments with AChE knockout mice – which survive to maturity – show that BuChE can supersede AChE in sustaining the structural and functional integrity of the cholinergic system.⁸⁰ Furthermore, knockout mice are highly susceptible to the toxic effects of selective BuChE inhibitors such as organophosphates.⁸¹

Evidence suggests that BuChE may participate in the transformation of diffuse A β -amyloid plaques (benign form) to the compact and pathogenic structures associated with neurodegeneration and dementia.⁸²⁻⁸³ Histofluorescence staining with the fluorescent dye thioflavin S—which binds to β -pleated sheets and helical filaments in amyloid deposits and neurofibrillary tangles, respectively—revealed the presence of three types of plaques: (1) diffuse non-neuritic plaques (thioflavine S-negative) and (2) compact but non-neuritic plaques (thioflavine S-positive) associated with non-demented individuals, and (3) compact neuritic plaques found in AD patients.⁸³ Computed densitometry revealed a fivefold to sixfold increase in the BuChE reactivity

in amyloid plaques of patients with AD.⁸² In demented AD patients, BuChE correlates positively with the generation of neocortical neuritic β -amyloid plaques, neurofibrillary tangles, dystrophic neurites and neuropil threads, when compared with non-demented controls.⁸²⁻⁸³

Lahiri and colleagues demonstrated that the potent and selective BuChE inhibitor (–)-*N*¹-phenethylcymserine (**1.21**, Figure 1.8) improved cognitive function in aged rats.⁸⁴ Carbamate **1.21** is an analog of the alkaloid (–)-physostigmine (**1.22**), a reversible ChE inhibitor isolated from the Calabar bean *Physostigma venenosum* of tropical West Africa and fruit of the Manchineel tree *Hippomane mancinella* of the wetlands of North and South America.⁷⁰ Phenethylcymserine possesses 5000-fold selectivity towards BuChE and induces a dose-dependent increase in the extracellular levels of ACh in rat cortex as measured by microdialysis methods, improves cognitive performance and memory processing in aged rats as assessed in a maze model, and reduces the levels of secreted A β -40, A β -42 and APP in rat brain.⁸⁴ The findings support the hypothesis that BuChE inhibitors, along with AChE inhibitors, remain a valid target for treatment of AD as they enhance ACh concentrations in the brain and improve cognition.

1.3.4 Cholinesterase Inhibitors from Marine Sponges

Numerous cholinesterase (ChE) inhibitors have been isolated from marine organisms. The marine environment is an exceptional source of new and potent bioactive MNP, including selective ChE inhibitors, that may serve as natural pharmacophores to inspire the development of clinically relevant drugs. Marine sponges, particularly of the order Verongida, are prolific producers of brominated ChE inhibitors, the inhibitory potencies of which are measured in the archetypal Ellman protocol developed in 1961.⁸⁵ A few of these metabolites from marine sponges have been selected for further discussion.

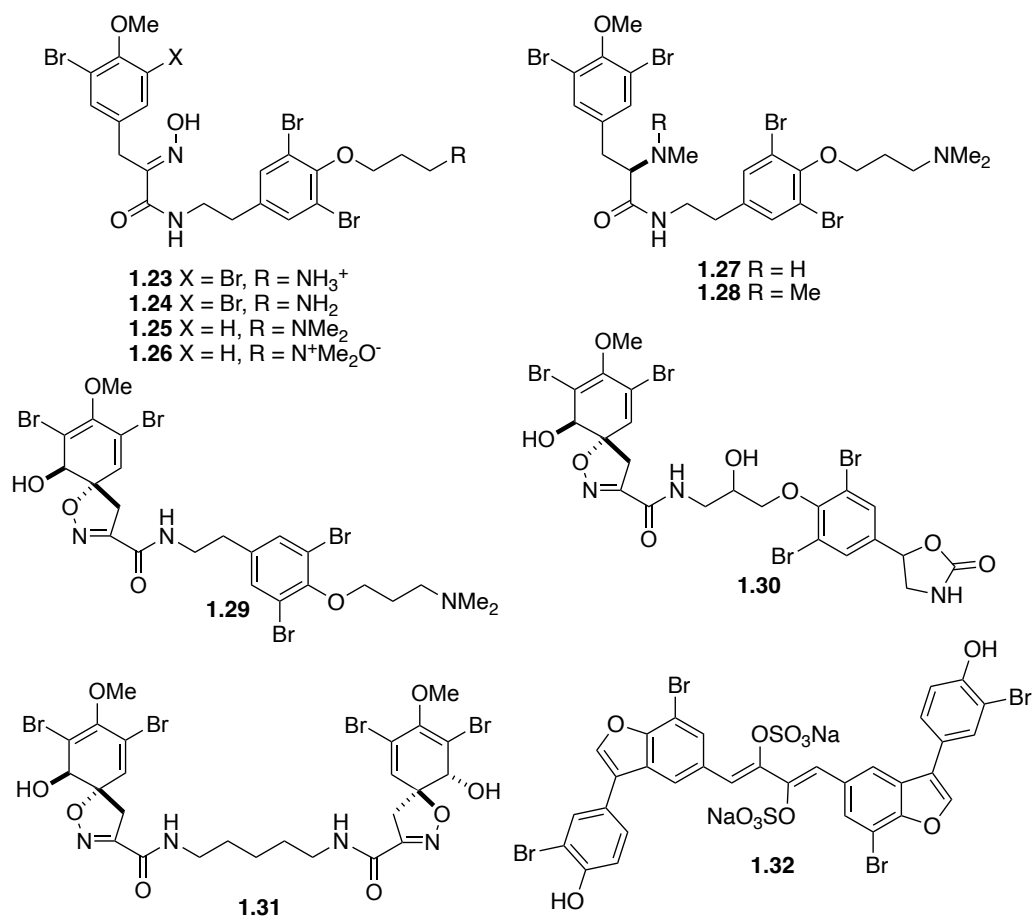


Figure 1.10: Structures of brominated ChE inhibitors from Verongida sponges.

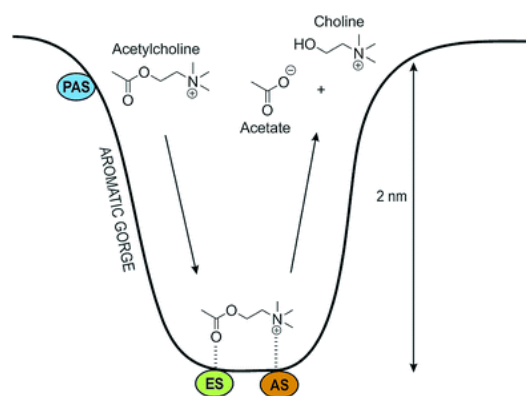


Figure 1.11: The active site of AChE showing the PAS region and the hydrolysis of ACh in the active site. Figure taken from reference 70.

Aplysamine-4 (**1.23**), originally isolated from the Hawaiian sponge *Psammaphysilla purpurea*,⁸⁶ is a non-competitive reversible inhibitor of insect AChE with a K_i of 2 μM (Figure 1.10).⁸⁷ The corresponding free amine **1.24**, obtained from alkaline treatment of **1.23**, is significantly less active against insect AChE ($K_i = 22 \mu\text{M}$). Similarly, aplysamine-2 (**1.25**), isolated from extracts of the Australian marine sponge *Aplysina* sp.,⁸⁸ inhibited AChE through non-competitive binding with an IC_{50} of 1.3 μM .⁸⁹ In contrast, purpuramine J (**1.26**),⁹⁰ which only differs from **1.25** in its terminal N-oxide motif, is not active against AChE.⁸⁹ The activities of aplysamine-4 and aplysamine-2 reflect the importance of the terminal ammonium and dimethylamine functionalities for the inhibitory activity against AChE. The ammonium and dimethylamino moieties are expected to form π -cation interactions with the peripheral anionic site (PAS) of AChE in a similar manner as the quaternary ammonium group of ACh (Figure 1.11).⁷⁰ The PAS region is located at the gorge entrance of the enzyme and is lined with aromatic residues that form π -cation interactions and guide ACh towards the active site at the bottom of the gorge.⁷⁰

Additionally, the presence of the oxime group in the bromotyrosine-derived metabolites appears critical for the inhibition of AChE. In contrast to oximes **1.23** and **1.25**, amines **1.27** and **1.28** weakly inhibited AChE with IC_{50} 's of 70 and 107 μM , respectively (Figure 1.10).⁸⁹ Puralidin Q (**1.29**), a spiro-cyclohexadienyl-isoxazoline alkaloid from the Okinawan sponge *Psammaphysilla purpurea*,²⁷ is a potent non-competitive inhibitor of AChE with an IC_{50} of 1.2 μM . Analogously, homoaerothioin (**1.31**)⁹¹ is a potent competitive inhibitor of electric eel AChE (eeAChE, $\text{IC}_{50} = 2.9 \mu\text{M}$), hAChE ($\text{IC}_{50} = 4.5 \mu\text{M}$), and BuChE ($\text{IC}_{50} = 6.2 \mu\text{M}$), while fistularin 1 (**1.30**)⁴³ moderately inhibited hAChE ($\text{IC}_{50} = 47.5 \mu\text{M}$).⁹² Unique iantheran A (**1.32**), a dimeric tetrabrominated benzofuran containing a rare 2,3-dihydroxy-1,3-butadiene disulfate moiety, was isolated from extracts of *Ianthella* sp. collected in the Great Barrier Reef, Australia.⁹³ Compound

1.32 was evaluated against a panel of enzymes, and was identified as a potent inhibitor of several enzymes including AChE ($IC_{50} = 0.42 \mu\text{M}$).⁹³

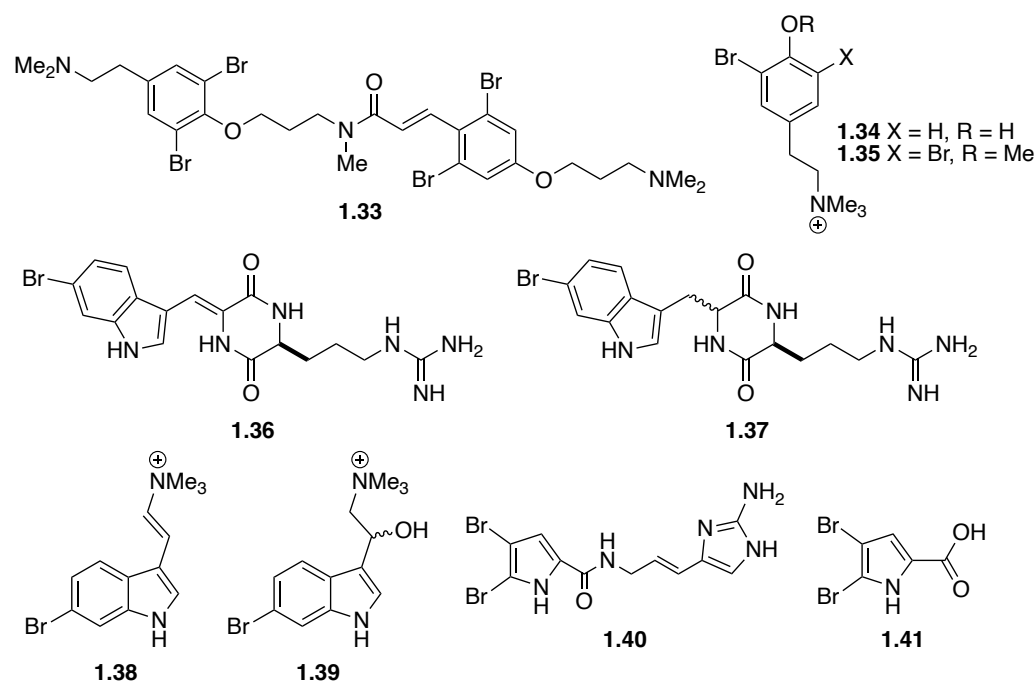


Figure 1.12: Structures of brominated ChE inhibitors from different sponge classes.

Additional brominated secondary metabolites and ChE inhibitors have been isolated from different orders of the Demospongiae class (Figure 1.12). Psammaplysene D, isolated from extracts of the marine sponge *Psammoclemma* sp.⁹⁴ and Polynesian sponge *Suberea ianthelliformis*,⁹⁵ is a potent mixed competitive/non-competitive inhibitor of AChE (IC_{50} of 1.3 μM) that binds to both the free enzyme and enzyme-substrate complex.⁹⁵ Interestingly, the *N,N*-dimethyl-3-phenoxypropan-1-amine terminus and *trans*-cinnamoyl moiety were crucial for the inhibitory activity against AChE. Moodie and co-workers isolated the tyramine metabolite stryphnusin (**1.34**) from the Norwegian boreal sponge *Stryphnus fortis* and evaluated its inhibitory activity against eeAChE ($IC_{50} = 232 \mu\text{M}$) and equine serum BuChE (eqBuChE, inactive).⁹⁶ Subsequently, the authors prepared a library of analogs to investigate the structure-activity relationship (SAR) of **1.34**. The synthetic analog **1.35** showed significantly enhanced inhibition of

eeAChE ($IC_{50} = 57 \mu\text{M}$) and eqBuChE ($IC_{50} = 20 \mu\text{M}$) implying that the additional bromination and methylation of the phenol were sufficient to increase the bioactivity.⁹⁶

In 2016, Anderson and colleagues evaluated compounds **1.36-1.39**, isolated from the deep water boreal sponge *Geodia barretti* collected off the Norwegian coast, as inhibitors of eeAChE and eqBuChE (Figure 1.12).⁹⁷ The 2,5-diketopiperazines baretin (**1.36**) and 8,9-dihydrobaretin (**1.37**) showed significant inhibition of eeAChE with K_i values of 29 and 19 μM , respectively, while indoles **1.38** and **1.39** were essentially inactive with $K_i > 200 \mu\text{M}$.⁹⁷ Although, alkaloid **1.39** showed weak inhibition of eqBuChE ($IC_{50} = 222 \mu\text{M}$), 6-bromoconicamin (**1.38**, $IC_{50} = 14 \mu\text{M}$) was more potent than the two diketopiperazines.⁹⁷ Additionally, the authors prepared a library of analogs based on the scaffold of indoles **1.38-1.39** to investigate their SAR against AChE and concluded that the brominated indole motif is not sufficiently responsible for the pronounced bioactivity observed with baretin and 8,9-dihydrobaretin.⁹⁷

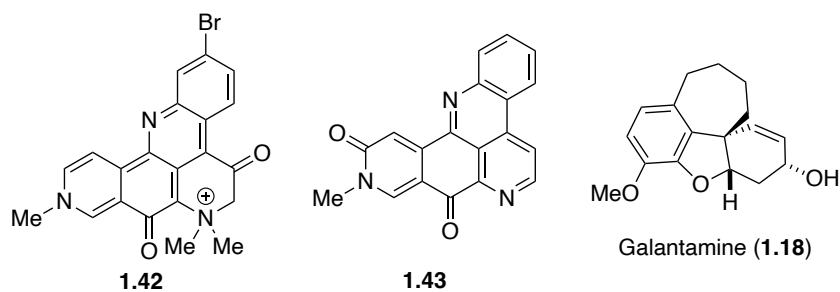


Figure 1.13: Structures of galantamine (**1.18**), petrosamine (**1.42**), and 2-bromoamphimedine (**1.43**).

Oroidin (**1.40**) and 4,5-dibromopyrrole-2-carboxylic acid (**1.41**) were originally isolated by Fattorusso and coworkers from extracts of *Agelas oroides* collected in the Gulf of Naples (Figure 1.12).⁹⁸ The two compounds were evaluated for their ability to inhibit eeAChE in a concentration-dependent manner.⁹⁹ Oroidin (**1.40**) moderately inhibited eeAChE by 18.95, 26.24 and 55.21% at 50, 100 and 200 $\mu\text{g/mL}$, respectively.⁹⁹ In contrast, the simplified pyrrole **1.41** was inactive at concentrations up to 200 $\mu\text{g/mL}$ suggesting that the 2-aminoimidazole functional group

is essential for oroidin's bioactivity. This is particularly significant as many BTAs contain the 2-aminoimidazole moiety and may potentially inhibit AChE.

The pentacyclic, pyridoacridine petrosamine (**1.42**) was isolated from the marine sponge *Petrosia* sp. collected at Carrie Bow Cay, Belize (Figure 1.13).¹⁰⁰ Petrosamine strongly inhibited eeAChE, by approximately six-fold higher potency, in comparison to the positive control galantamine (**1.18**).¹⁰¹ Petrosamine and galantamine exhibited IC₅₀ values of 91 and 590 nM, respectively. In contrast, the pyridoacridine 2-bromoamphimedine (**1.43**), obtained from extracts of the Thai sponge *Petrosia* n. sp., showed weak inhibitory activity at 300 μM.¹⁰¹ Molecular docking studies showed that the quaternary ammonium group of petrosamine formed strong interactions with key residues in the active site gorge of electric eel *Torpedo californica* AChE; thus, explaining the observed bioactivities.¹⁰¹

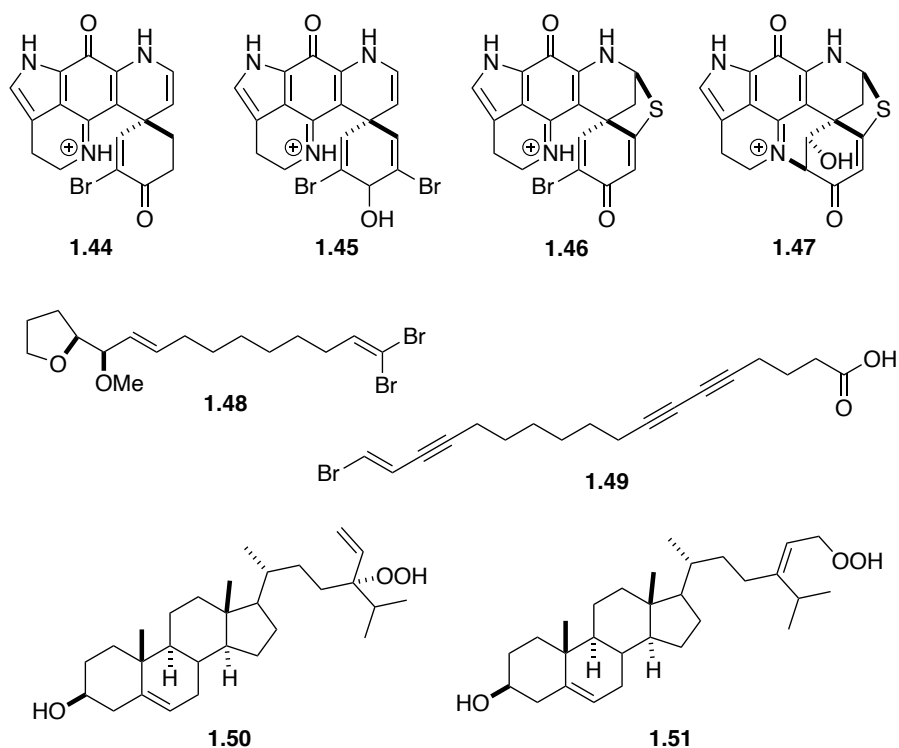


Figure 1.14: Structures of ChE inhibitors from different sponge classes.

The pyrroloiminoquinone alkaloids discorhabdins B (**1.46**), L (**1.47**), G (**1.44**), and 3-dihydro-7,8-dehydrodiscorhabdin C (**1.45**) were isolated from the methanol extracts of *Latrunculia cf. lendenfeldi* and *L. cf. bocagei* collected near the Antarctic Peninsula (Figure 1.14).¹⁰² Alkaloids **1.44-1.47** are reversible competitive inhibitors of eeAChE ($K_i = 1.6 - 15.0 \mu\text{M}$), hAChE ($K_i = 22.8 - 98.0 \mu\text{M}$), and eqBuChE ($K_i = 5.0 - 76.0 \mu\text{M}$).¹⁰³ Favorably, electrophysiological studies of discorhabdin G (**1.44**) at $8.43 \mu\text{M}$ (80% inhibition of eeAChE) showed that it lacked undesirable effects on skeletal muscle function and neurotransmission, particularly muscle twitches and tetanic contractions.¹⁰³

Liu and colleagues evaluated the alcohol extract of the South China Sea sponge *Xestospongia testudinaria* for anti-acetylcholinesterase activity and isolated several lipids and sterols including **1.48-1.51**.¹⁰⁴ Mutafuran H (**1.48**), a brominated ene-tetrahydrofuran, potently inhibited AChE at equivalent potency as the positive control tacrine with IC_{50} values of 0.64 and $0.41 \mu\text{M}$, respectively.¹⁰⁴ Additionally, xestospongic acid (**1.49**)¹⁰⁵ and the hydroperoxy sterols **1.50**¹⁰⁶ and **1.51**¹⁰⁷ moderately inhibited AChE ($\text{IC}_{50} = 12.65, 11.45$ and $14.51 \mu\text{M}$, respectively).

Marine sponges continue to deliver bioactive natural products, many of which are cholinesterase inhibitors. Some cholinesterase inhibitors were highlighted and discussed to showcase their wide chemodiversity and formidable potential for pharmacognostic studies.

1.4 Conclusions

The marine environment is a wellspring for structurally diverse and bioactive natural products. The highly diversified structural scaffolds of MNPs are a source of inspiration for drug development. Alkaloids, including decahydroquinolines and bromotyrosine-derived metabolites, constitute the largest class of marine natural products, however, the formulas of most marine

natural products lack nitrogen; chemical classes of non-nitrogenous secondary metabolites include terpenoids, polyketides, peptides, steroids, and lipids. Glycolipids, such as caminoside A and axinoside-1, comprise a rare subset of glycosylated lipids, the structures of which depart from more conventional glycosphingolipids. These structurally complex molecules often display novel, potent, and selective biological activities that complement well-known motifs of synthetic drugs. The following dissertation explores the structural determination and total synthesis of bioactive heterocycles – both alkaloids and glycolipids – from marine sponges.

1.5 References

- (1) (a) Altmann, K.-H. Drugs from the Oceans: Marine Natural Products as Leads for Drug Discovery. *Chimia* **2017**, *71*, 646–652. (b) Molinski, T. F.; Dalisay, D. S.; Lievens, S. L.; Saludes, J. P. Drug development from marine natural products. *Nat. Rev. Drug Discov.* **2009**, *8*, 69-85.
- (2) Hu, Y.; Chen, J.; Hu, G.; Yu, J.; Zhu, X.; Lin, Y.; Chen, S.; Yuan, J. Statistical Research on the Bioactivity of New Marine Natural Products Discovered during the 28 Years from 1985 to 2012. *Mar. Drugs* **2015**, *13*, 202-221.
- (3) Flam, F. Chemical Prospectors Scour the Seas for Promising Drugs. *Science* **1994**, *266*, 1324-1325.
- (4) Kelman, D.; Kashman, Y.; Hill, R. T.; Rosenberg, E.; Loya, Y. Chemical warfare in the sea: The search for antibiotics from Red Sea corals and sponges. *Pure Appl. Chem.* **2009**, *81*, 1113-1121.
- (5) Romano, G.; Costantini, M.; Sansone, C.; Lauritano, C.; Ruocco, N.; Ianora, A. Marine microorganisms as a promising and sustainable source of bioactive molecules. *Mar. Environ. Res.* **2017**, *128*, 58–69.
- (6) <http://pubs.rsc.org/marinlit>, accessed June 2022.
- (7) Blunt, J. W.; Copp, B. R.; Keyzers, R. A.; Munro, M. H. G.; Prinsep, M. R. Marine natural products. *Nat. Prod. Rep.* **2017**, *34*, 235-294.
- (8) (a) Olivera, B. M.; Gray, W. R.; Zeikus, R.; Mcintosh, J. M.; Varga, J.; de Santos, V.; Cruz, L. J. Peptide Neurotoxins from Fish-Hunting Cone Snails. *Science* **1985**, *230*, 1338-1343. (b) Terlau, H.; Olivera, B. M. *Conus* venoms: a rich source of novel ion channel-targeted peptides. *Physiol. Rev.* **2004**, *84*, 41-68.
- (9) (a) Wright, A. E.; Forleo, D. A.; Gunawardana, G. P.; Gunasekera, S. P.; Koehn, F. E.; McConnell, O. J. Antitumor tetrahydroisoquinoline alkaloids from the colonial ascidian *Ecteinascidia turbinata*. *J. Org. Chem.* **1990**, *55*, 4508-4512. (b) Rinehart, K. L.; Holt, T. G.; Fregeau, N. L.; Stroh, J. G.; Keifer, P. A.; Sun, F.; Li, L. H.; Martin, D. G. Ecteinascidins 729, 743, 745, 759A, 759B, and 770: potent antitumor agents from the Caribbean tunicate *Ecteinascidia turbinata*. *J. Org. Chem.* **1990**, *55*, 4512-4515. (c) D'Incalci, M.; Badri, N.; Galmarini, C. M.; Allavena, P. Trabectedin, a drug acting on both cancer cells and the tumour microenvironment. *Br J Cancer.* **2014**, *111*, 646-650.
- (10) Senter, P. D.; Sievers, E. L. The discovery and development of brentuximab vedotin for use in relapsed Hodgkin lymphoma and systematic anaplastic large cell lymphoma. *Nat. Biotechnol.* **2012**, *30*, 631-637.

-
- (11) Pettit, G.R.; Srirangam, J. K.; Barkoczy, J.; Williams, M. D.; Boyd, M. R.; Hamel, E.; Pettit, R. K.; Hogan, F.; Bai, R.; Chapuis, J. C.; McAllister, S. C.; Schmidt, J. M. Antineoplastic agents 365. Dolastatin 10 SAR probes. *Anticancer Drug Des.* **1998**, *13*, 243-277.
- (12) Pettit, G. R.; Kamano, Y.; Herald, C. L.; Fujii, Y.; Kizu, H.; Boyd, M. R.; Boettner, F. E.; Doubek, D. L.; Schmidt, J. M.; Chapuis, J.-C.; Michel, C. *Tetrahedron* **1993**, *49*, 9151–9170.
- (13) <https://en.wikipedia.org/wiki/Ziconotide>.
- (14) https://commons.wikimedia.org/wiki/File:Porifera_body_structures_01.png.
- (15) Bailey, Regina. "Parazoa of the Animal Kingdom." ThoughtCo. <https://www.thoughtco.com/parazoa-of-the-animal-kingdom-4148041> (accessed June 30, 2022).
- (16) Gold, D. A.; Grabenstatter, J.; de Mendoza, A.; Riesgo, A.; Ruiz-Trillo, I.; Summons, R. E. Sterol and genomic analyses validate the sponge biomarker hypothesis. *Proc. Natl. Acad. Sci.* **2016**, *113*, 2684-2689.
- (17) Love, G.D.; Grosjean, E.; Stalvies, C.; Fike, D.A.; Grotzinger, J.P.; Bradley, A.S.; Kelly, A.E.; Bhatia, M.; Meredith, W.; Snape, C.E.; Bowring, S.A.; Condon, D.J.; Summons, R.E. Fossil steroids record the appearance of Demospongiae during the Cryogenian period. *Nature* **2009**, *457*, 718-722.
- (18) Thoms, C.; Schupp, P. J. Activated Chemical Defense in Marine Sponges—a Case Study on *Aplysinella rhax*. *J. Chem. Ecol.* **2008**, *34*, 1242-1252.
- (19) Thoms, C.; Wolff, M.; Padmakumar, K.; Ebel, R.; Proksch, P. Chemical Defense of Mediterranean Sponges *Aplysina cavernicola* and *Aplysina aerophoba*. *Z. Naturforsch. C* **2004**, *59*, 113-122.
- (20) Ortlepp, S.; Sjögren, M.; Dahlström, M.; Weber, H.; Ebel, R.; Edrada, R.; Thoms, C.; Schupp, P.; Bohlin, L.; Proksch, P. Antifouling Activity of Bromotyrosine-Derived Sponge Metabolites and Synthetic Analogues. *Mar. Biotechnol.* **2007**, *9*, 776-785.
- (21) Teeyapant, R.; Woerdenbag, H. J.; Kreis, P.; Hacker, J.; Wray, V.; Witte, L.; Proksch, P. Antibiotic and Cytotoxic Activity of Brominated Compounds from the Marine Sponge *Verongia aerophoba*. *Z. Naturforsch. C* **1993**, *48*, 939-945.
- (22) Peng, J.; Li, J.; Hamann, M. T. The marine bromotyrosine derivatives. *Alkaloids Chem. Biol.* **2005**, *61*, 59-262.

-
- (23) Niemann, H.; Marmann, A.; Lin, W.; Proksch, P. Sponge derived bromotyrosines: structural diversity through natural product combinatorial chemistry. *Nat. Prod. Commun.* **2015**, *10*, 219-231.
- (24) Sharma, G. M.; Burkholder, P. R. Studies on the antimicrobial substances of sponges II. Structure and Synthesis of a bromine-containing antibacterial compound from a marine sponge. *Tetrahedron Lett.* **1967**, *8*, 4147-4150.
- (25) Sharma, G. M.; Burkholder, P. R. Antimicrobial substances of sponges IV. Structure of a bromine-containing compound from a marine sponge. *J. Org. Chem.* **1970**, *35*, 2823-2826.
- (26) Yagi, H.; Matsunaga, S.; Fusetani, N. Purpuramines A-I, new bromotyrosine-derived metabolites from the marine sponge *Psammaplysilla purpurea*. *Tetrahedron* **1993**, *49*, 3749-3754.
- (27) Kobayashi, J.; Honma, K.; Sasaki, T.; Tsuda, M. Puralidins J-R, new bromotyrosine alkaloids from the Okinawan marine sponge *Psammaplysilla purea*. *Chem. Pharm. Bull.* **1995**, *43*, 403-407.
- (28) Lee, Y.-J.; Han, S.; Lee, H.-S.; Kang, J. S.; Yun, J.; Sim, C. J.; Shin, H. J.; Lee, J. S. Cytotoxic psammaplysin analogues from a *Suberea* sp. marine sponge and the role of the spirooxepinisoxazoline in their activity. *J. Nat. Prod.* **2013**, *76*, 1731-1736.
- (29) Kazlauskas, R.; Lidgard, R. O.; Murphy, P. T.; Wells, R. J.; Blount, J. F., Brominated tyrosine-derived metabolites from the sponge *Ianthella basta*. *Aust. J. Chem.* **1981**, *34*, 765-786.
- (30) (a) Mudianta, I. W.; Skinner-Adams, T.; Andrews, K. T.; Davis, R. A.; Hadi, T. A.; Hayes, P. Y.; Garson, M. J. Psammaplysin derivatives from the Balinese marine sponge *Aplysinella strongylata*. *J. Nat. Prod.* **2012**, *75*, 2132-2143. (b) Roll, D. M.; Chang, C. W. J.; Scheuer, P. J.; Gray, G. A.; Shoolery, J. N.; Matsumoto, G. K.; Duyne, G. D. V.; Clardy, J. Structures of the psammaplysin. *J. Am. Chem. Soc.* **1985**, *107*, 2916-2920.
- (31) Finefield, J. M.; Sherman, D. H.; Kreitman, M.; Williams, R. M. Enantiomeric Natural Products: Occurrence and Biogenesis. *Angew. Chem. Int. Ed.* **2012**, *51*, 4802-4836.
- (32) Ragini, K.; Fromont, J.; Piggott, A. M.; Karuso, P. Enantiodivergence in the biosynthesis of bromotyrosine alkaloids from sponges? *J. Nat. Prod.* **2017**, *80*, 215-219.
- (33) Nakamura, H.; Wu, H.; Kobayashi, J.; Nakamura, Y.; Ohizumi, Y.; Hirata, Y. Puralin, a novel enzyme activator from the Okinawan marine sponge *Psammaplysilla purea*. *Tetrahedron Lett.* **1985**, *26*, 4517-4520.
- (34) Salim, A. A.; Khalil, Z. G.; Capon, R. J. Structural and stereochemical investigations into bromotyrosine-derived metabolites from southern Australian marine sponges, *Pseudoceratina* spp. *Tetrahedron* **2012**, *68*, 9802-9807.

-
- (35) Tsukamoto, S.; Kato, H.; Hirota, H.; Fusetani, N. Ceratinamides A and B: a fouling dibromotyrosine derivatives from the marine sponge *Pseudoceratina purpurea*. *Tetrahedron* **1996**, *52*, 8181-8186.
- (36) Youssef, D. T. A.; Asfour, H. Z.; Shaala, L. A. Psammaceratin A: a cytotoxic psammaplysin dimer featuring an unprecedented (2Z,3Z)-2,3-bis(aminomethylene)succinimide backbone from the Red Sea sponge *Pseudoceratina arabica*. *Mar. Drugs* **2021**, *19*, 433.
- (37) Kon, Y.; Kubota, T.; Shibazaki, A.; Gono, T.; Kobayashi, J. Ceratinadins A-C, new bromotyrosine alkaloids from an Okinawan marine sponge *Pseudoceratina* sp. *Bioorg. Med. Chem. Lett.* **2010**, *20*, 4569-4572.
- (38) Gotsbacher, M. P.; Karuso, P. New antimicrobial bromotyrosine analogues from the sponge *Pseudoceratina purpurea* and its predator *Tylodina corticalis*. *Mar. Drugs* **2015**, *13*, 1389-1409.
- (39) Kurimoto, S.-i.; Ohno, T.; Hokari, R.; Ishiyama, A.; Iwatsuki, M.; Omura, S.; Kobayashi, J.; Kubota, T. Ceratinadins E and F, new bromotyrosine alkaloids from an Okinawan marine sponge *Pseudoceratina* sp. *Mar. Drugs* **2018**, *16*, 463.
- (40) Jiao, W.-H.; Li, J.; Zhang, M.-M.; Cui, J.; Gui, Y.-H.; Zhang, Y.; Li, J.-Y.; Liu, K.-C.; Lin, H.-W. Frondoplysin A and B, unprecedented terpene-alkaloid bioconjugates from *Dysidea frondosa*. *Org. Lett.* **2019**, *21*, 6190-6193.
- (41) (a) Okamoto, Y.; Ojika, M.; Sakagami, Y. Iantheran A, a dimeric polybrominated benzofuran as a Na,K-ATPase inhibitor from a marine sponge *Ianthella* sp. *Tetrahedron Lett.* **1999**, *40*, 507-510. (b) Okamoto, Y.; Ojika, M.; Suzuki, S.; Murakami, M.; Sakagami, Y. Iantherans A and B, unique dimeric polybrominated benzofurans as Na,K-ATPase inhibitors from a marine sponge *Ianthella* sp. *Bioorg. Med. Chem.* **2001**, *9*, 179-183. (c) Greve, H.; Meis, S.; Kassack, M. U.; Kehraus, S.; Krick, A.; Wright, A. D.; König, G. M. New Iantherans from the Marine Sponge *Ianthella quadrangulata*: Novel Agonists of the P2Y₁₁ Receptor. *J. Med. Chem.* **2007**, *50*, 5600-5607.
- (42) Fattorusso, E.; Minale, L.; Sodano, G. Aeroplysinin-1, an antibacterial bromo-compound from the sponge *Verongia aerophoba*. *J. Chem. Soc., Perkin trans. 1* **1972**, *1*, 16-18.
- (43) Gopichand, Y.; Schmitz, F. J. Marine natural products: fistularin-1, -2 and -3 from the sponge *Aplysina fistularis* forma *fulva*. *Tetrahedron Letters* **1979**, *20*, 3921-3924.
- (44) Kazlauskas, R.; Lidgard, R. O.; Murphy, P. T.; Wells, R. J. Brominated tyrosine-derived metabolites from the sponge *Ianthella basta*. *Tetrahedron Lett.* **1980**, *21*, 2277-2280.

-
- (45) Thompson, J.E.; Barrow, K.D.; Faulkner, D.J. Localization of two brominated metabolites, aerothionin and homoaerothionin, in spherulous cells of the marine sponge *Aplysina fistularis* (= *Verongia thiona*). *Acta Zool* **1983**, *64*, 199-210.
- (46) Turon, X.; Becerro, M. A.; Uriz, M. J. Distribution of brominated compounds within the sponge *Aplysina aerophoba*: coupling of X-ray microanalysis with cryofixation techniques. *Cell Tissue Res.* **2000**, *301*, 311-322.
- (47) Wu, Y.-C.; García-Altres, M.; Pintó, B.; Ribes, M.; Hentschel, U.; Pita, L. Opisthobranch grazing results in mobilisation of spherulous cells and re-allocation of secondary metabolites in the sponge *Aplysina aerophoba*. *Sci. Rep.* **2020**, *10*, 21934.
- (48) Nicacio, K. J.; Ióca, L. P.; Fróes, A. M.; Leomil, L.; Appolinario, L. R.; Thompson, C. C.; Thompson, F. L.; Ferreira, A. G.; Williams, D. E.; Andersen, R. J.; Eustaquio, A. S.; Berlinck, R. G. S. Cultures of the Marine Bacterium *Pseudovibrio denitrificans* Ab134 Produce Bromotyrosine-Derived Alkaloids Previously Only Isolated from Marine Sponges. *J. Nat. Prod.* **2017**, *80*, 235-240.
- (49) Mohanty, I.; Tapadar, S.; Moore, S. G.; Biggs, J. S.; Freeman, C. J.; Gaul, D. A.; Garg, N.; Agarwal, V.; Traxler, M. F. Presence of Bromotyrosine Alkaloids in Marine Sponges Is Independent of Metabolomic and Microbiome Architectures. *mSystems* **2021**, *6*, 1-17.
- (50) Braun, K. The prefrontal-limbic system: development, neuroanatomy, function, and implications for socioemotional development. *Clin. Perinatol.* **2011**, *38*, 685-702.
- (51) (a) Heron, M. Deaths: Leading Causes for 2019. National Vital Statistics Reports. Vol. 70, No. 9. Hyattsville, MD: National Center for Health Statistics. 2021. (b) Murphy, S. L.; Kochanek, K. D.; Xu, J.; Arias, E. Mortality in the United States, 2020. NCHS Data Brief; No. 427. Hyattsville, MD: National Center for Health Statistics. 2021.
- (52) Ortaliza, J.; Orgera, K.; Amin, K.; Cox, C. COVID-19 Continues to be a Leading Cause of Death in the U.S. in August 2021. Accessed July 22, 2021. Available at: [https://www.healthsystemtracker.org/brief/covid-19-continues-to-be-a-leading-cause-of-death-in-the-u-s-in-august-2021/#Average%20daily%20deaths%20in%20the%20United%20States%20from%20COVID-19%20\(August%202021\)%20and%20other%20leading%20causes%20\(2021\)](https://www.healthsystemtracker.org/brief/covid-19-continues-to-be-a-leading-cause-of-death-in-the-u-s-in-august-2021/#Average%20daily%20deaths%20in%20the%20United%20States%20from%20COVID-19%20(August%202021)%20and%20other%20leading%20causes%20(2021))
- (53) Rajan, K. B.; Weuve, J.; Barnes, L. L.; McAninch, E. A. Wilson, R. S.; Evans, D. A. Population Estimate of People with Clinical Alzheimer's Disease and Mild Cognitive Impairment in the United States (2020-2060). *Alzheimer's Dement.* **2021**, *17*, 1966-1975.
- (54) Wong, W. Economic Burden of Alzheimer Disease and Managed Care Considerations. *Am. J. Manag. Care.* **2020**, *26*, S177-S183.

-
- (55) Gauthier, S.; Rosa-Neto, P.; Morais, J. A.; Webster, C. World Alzheimer Report 2021: Journey through the diagnosis of dementia. *Alzheimer's Disease International, London*, **2021**, 1-314.
- (56) <https://www.who.int/news-room/fact-sheets/detail/dementia>.
- (57) Jin, J. Alzheimer Disease. *JAMA* **2015**, *313*, 1488.
- (58) <https://www.alzheimers.org.uk/about-dementia/types-dementia/who-gets-alzheimers-disease>.
- (59) <https://www.mayoclinic.org/diseases-conditions/alzheimers-disease/in-depth/alzheimers-stages/art-20048448>.
- (60) Wolfe, M. S. Targets and Strategies Toward the Development of Alzheimer Therapeutics. In *Alzheimer's Disease II. Topics in Medicinal Chemistry*; Wolfe, M. S., Eds.; Springer, Cham: Switzerland, 2016, *24*, 1-25.
- (61) Perry, E. K.; Perry, R. H.; Blessed, G.; Tomlinson, B. E. Changes in brain cholinesterases in senile dementia of Alzheimer type. *Neuropathol. Appl. Neurobiol.* **1978**, *4*, 273-277.
- (62) Perry, E. K.; Perry, R. H.; Blessed, G.; Tomlinson, B. E. Necropsy evidence of central cholinergic deficits in senile dementia. *Lancet.*, **1977**, *1*, 189.
- (63) Geula, C.; Mesulam, M. M. Cholinesterases and the pathology of Alzheimer disease. *Alz. Dis. Assoc. Dis.* **1995**, *9*, 23-28.
- (64) Lahiri, D. K.; Farlow, M. R.; Hintz, N.; Utsuki, T.; Greig, N. H.; Cholinesterase inhibitors, β -amyloid precursor protein and amyloid b-peptides in Alzheimer's disease. *Acta Neurol. Scand.* **2000**, Supplement *176*, 60-67.
- (65) Heneka, M. T.; Carson, M. J.; El Khoury, J.; Landreth, G. E.; Brosseron, F.; Feinstein, D. L.; Jacobs, A. H.; Wyss-Coray, T.; Vitorica, J.; Ransohoff, R. M.; Herrup, K.; Frautschy, S. A.; Finsen, B.; Brown, G. C.; Verkhratsky, A.; Yamanaka, K.; Koistinaho, J.; Latz, E.; Halle, A.; Petzold, G.C.; Town, T.; Morgan, D.; Shinohara, M. L.; Perry, V. H.; Holmes, C.; Bazan, N. G.; Brooks, D. J.; Hunot, S.; Joseph, B.; Deigendesch, N.; Garaschuk, O.; Boddeke, E.; Dinarello, C. A.; Breitner, J. C.; Cole, G. M.; Golenbock, D. T.; Kummer, M. P. Neuroinflammation in Alzheimer's disease. *Lancet Neurol* **2015**, *14*, 388-405.
- (66) Chun, H.; Lee, C. J. Reactive astrocytes in Alzheimer's disease: A double-edged sword. *Neurosci. Res.* **2018**, *126*, 44-52.
- (67) <https://www.cnn.com/2019/03/21/health/alzheimers-drug-trial-failure-aducanumab-bn/index.html>

-
- (68) <https://alzheimersnewstoday.com/aducanumab/>
- (69) <https://www.nia.nih.gov/health/how-alzheimers-disease-treated>
- (70) Moodie, L. W. K.; Sepčić, K.; Turk, T.; Frangež, R.; Svenson, J. Natural cholinesterase inhibitors from marine organisms. *Nat. Prod. Rep.* **2019**, *36*, 1053-1092.
- (71) Lilienfeld, S. Galantamine – a novel cholinergic drug with a unique dual mode of action for the treatment of patients with Alzheimer’s disease. *CNS Drug Rev.* **2002**, *8*, 159-176.
- (72) Polinsky, R. J. Clinical pharmacology of rivastigmine: a new-generation acetylcholinesterase inhibitor for the treatment of Alzheimer’s disease. *Clin. Ther.* **1998**, *20*, 634-647.
- (73) Wilkinson, D. G. The Pharmacology of donepezil: a new treatment for Alzheimer’s disease. *Expert Opin. Pharmacother.* **1999**, *1*, 121-135.
- (74) Kuns, B.; Rosani, A.; Varghese, D. Memantine. In: StatPearls [Internet]. Treasure Island (FL): StatPearls Publishing. Accessed July 22, 2022. Available at: <https://www.ncbi.nlm.nih.gov/books/NBK500025/>.
- (75) Soukup, O.; Winder, M.; Killi, U. K.; Wsol, V.; Jun, D.; Kuca, K.; Tobin, G. Acetylcholinesterase inhibitors and drugs acting on muscarinic receptors-potential crosstalk of cholinergic mechanisms during pharmacological treatment. *Curr. Neuropharmacol.* **2017**, *15*, 637-653.
- (76) Rosenberry, T. L.; Brazzolotto, X.; Macdonald, I. R.; Wandhammer, M.; Trovaslet-Leroy, M.; Darvesh, S.; Nachon, F. Comparison of the binding of reversible inhibitors to human butyrylcholinesterase: A crystallographic, kinetic and calorimetric study. *Molecules* **2017**, *22*, 2098-2119.
- (77) Darvesh, S.; Hopkins, D. A.; Geula, C. Neurobiology of butyrylcholinesterase. *Nat. Rev. Neurosci.* **2003**, *4*, 131-138.
- (78) Nicolet, Y.; Lockridge, O.; Masson, P.; Fontecilla-Camps, J. C.; Nachon, F. Crystal structure of human butyrylcholinesterase and of its complexes with substrate and products. *J. Biol. Chem.* **2003**, *278*, 41141-41147.
- (79) Mushtaq, G.; Greig, N. H.; Khan, J. A.; Kamal, M. A. Status of acetylcholinesterase and butyrylcholinesterase in Alzheimer’s disease and type 2 Diabetes Mellitus. *CNS Neurol. Disord. Drug Targets* **2014**, *13*, 1432-1439.
- (80) Mesulam, M.-M.; Guillozet, A.; Shaw, P.; Levey, A.; Duysen, E. G.; Lockridge, O. Acetylcholinesterase knockouts establish central cholinergic pathways and can use butyrylcholinesterase to hydrolyze acetylcholine. *Neuroscience* **2002**, *110*, 627-639.

-
- (81) Xie, W.; Stribley, J. A.; Chatonnet, A.; Wilder, P. J.; Rizzino, A.; McComb, R. D.; Taylor, P.; Hinrichs, S. H.; Lockridge, O. Postnatal developmental delay and supersensitivity to organophosphate in gene-targeted mice lacking acetylcholinesterase. *J. Pharmacol. Exp. Ther.* **2000**, *293*, 896-902.
- (82) Mesulam, M.-M.; Geula, C. Butyrylcholinesterase reactivity differentiates the amyloid plaques of aging from those of dementia. *Ann. Neurol.* **1994**, *36*, 722-727.
- (83) Guillozet, A. L.; Smiley, J. F.; Mash, D. C.; Mesulam, M.-M. Butyrylcholinesterase in the life cycle of amyloid plaques. *Ann. Neurol.* **1997**, *42*, 909-918.
- (84) Greig, N. H.; Utsuki, T.; Ingram, D. K.; Wang, Y.; Pepeu, G.; Scali, C.; Yu, Q.-S.; Mameczarz, J.; Holloway, H. W.; Giordano, T.; Chen, D.; Furukawa, K.; Sambamurti, K.; Brossi, A.; Lahiri, D. K. Selective butyrylcholinesterase inhibition elevates brain acetylcholine, augments learning and lowers Alzheimer β -amyloid peptide in rodent. *PNAS* **2005**, *102*, 17213-17218.
- (85) Ellman, G. L.; Courtney, K. D.; Andres, Jr., V.; Featherstone, R. M. A New and Rapid Colorimetric Determination of Acetylcholinesterase Activity. *Biochem. Pharmacol.* **1961**, *7*, 88-95.
- (86) Jurek, J.; Yoshida, W. Y.; Scheuer, P. J.; Kelly-Borges, M. Three New Bromotyrosine-Derived Metabolites of the Sponge *Psammaphysilla purpurea*. *J. Nat. Prod.* **1993**, *56*, 1609-1612.
- (87) Sepčić, K.; Mancini, I.; Vidic, I.; Franssanito, R.; Pietra, F.; Macek, P.; Turk, T. Antibacterial and anticholinesterase activities of aplysamine-4, a bromotyrosine-derived metabolite of a Red Sea marine sponge. *J. Nat. Toxins* **2001**, *10*, 181-191.
- (88) Xynas, R.; Capon, R. J. Two new bromotyrosine-derived metabolites from an Australian marine sponge, *Aplysina* sp. *Aust. J. Chem.* **1989**, *42*, 1427-1433.
- (89) Olatunji, O. J.; Ogundajo, A. L.; Oladosu, I. A.; Changwichit, K.; Ingkaninan, K.; Yuenyongsawad, S.; Plubrukarn, A. Non-Competitive Inhibition of Acetylcholinesterase by Bromotyrosine Alkaloids. *Nat. Prod. Commun.* **2014**, *9*, 1559-1561.
- (90) Tabudravu, J. N.; Jaspars, M. Puralidin S and Purpuramine J, Bromotyrosine Alkaloids from the Fijian Marine Sponge *Druinella* sp. *J. Nat. Prod.* **2002**, *65*, 1798-1801.
- (91) Moody, K.; Thomson, R. H.; Fattorusso, E.; Minale, L.; Sodano, G. Aerothionin and homoaerothionin: two tetrabromo spirocyclohexadienylisoxazoles from *Verongia* sponges. *J. Chem. Soc., Perkin Trans. 1* **1972**, *0*, 18-24.
- (92) Sirimangkalakitti, N.; Olatunji, O. J.; Changwichit, K.; Saesong, T.; Chamni, S.; Chanvorachote, P.; Ingkaninan, K.; Plubrukarn, A.; Suwanborirux, K., Bromotyrosine

-
- Alkaloids with Acetylcholinesterase Inhibitory Activity from the Thai Sponge *Acanthodendrilla* sp. *Nat. Prod. Commun.* **2015**, *10*, 1945-1949.
- (93) Okamoto, Y.; Ojika, M.; Suzuki, S.; Murakami, M.; Sakagami, Y. Iantherans A and B, unique dimeric polybrominated benzofurans as Na,K-ATPase inhibitors from a marine sponge, *Ianthella* sp. *Bioorg. Med. Chem.* **2001**, *9*, 179-183.
- (94) Buchanan, M. S.; Carroll, A. R.; Addepalli, R.; Avery, V. M.; Hooper, J. N. A.; Quinn, R. J. Psammaplysenes C and D, Cytotoxic Alkaloids from *Psammoclemma* sp. *J. Nat. Prod.* **2007**, *70*, 1827-1829.
- (95) El-Demerdash, A.; Moriou, C.; Toullec, J.; Besson, M.; Soulet, S.; Schmitt, N.; Petek, S.; Lecchini, D.; Debitus, C.; Al-Mourabit, A. Bioactive Bromotyrosine-Derived Alkaloids from the Polynesian Sponge *Suberea ianthelliformis*. *Mar. Drugs* **2018**, *16*, 146.
- (96) Moodie, L. W. K.; Žužek, M. C.; Frangež, R.; Andersen, J. H.; Hansen, E.; Olsen, E. K.; Cergolj, M.; Sepčić, K.; Hansen, K. Ø.; Svenson, J. Synthetic analogs of stryphnusin isolated from the marine sponge *Stryphnus fortis* inhibit acetylcholinesterase with no effect on muscle function or neuromuscular transmission. *Org. Biomol. Chem.* **2016**, *14*, 11220-11229.
- (97) Olsen, E. K.; Hansen, E.; W. K. Moodie, L.; Isaksson, J.; Sepčić, K.; Cergolj, M.; Svenson, J.; Andersen, J. H. Marine AChE inhibitors isolated from *Geodia barretti*: natural compounds and their synthetic analogs. *Org. Biomol. Chem.* **2016**, *14*, 1629-1640.
- (98) Forenza, S.; Minale, L.; Riccio, R.; Fattorusso, E. New bromo-pyrrole derivatives from the sponge *Agelas oroides*. *J. Chem. Soc. D: Chem. Commun.* **1971**, 1129-1130.
- (99) Orhan, I. E.; Ozcelik, B.; Konuklugil, B.; Putz, A.; Kaban, U. G.; Proksch, P. Bioactivity screening of the selected Turkish marine sponge and three compounds from *Agelas oroides*. *Rec. Nat. Prod.* **2012**, *6*, 356-367.
- (100) Molinski, T. F.; Fahy, E.; Faulkner, D. J.; Van Duyne, G. D.; Clardy, J. Petrosamine, a novel pigment from the marine sponge *Petrosia* sp. *J. Org. Chem.* **1988**, *53*, 1340-1341.
- (101) Nukoolkarn, V.; Saen-oon, S.; Rungrotmongkol, T.; Hannongbua, S.; Ingkaninan, K.; Suwanborirux, K. Petrosamine, a potent anticholinesterase pyridoacridine alkaloid from a Thai marine sponge *Petrosia* n. sp. *Bioorg. Med. Chem.* **2008**, *16*, 6560-6567.
- (102) Hu, J.-F.; Fan, H.; Xiong, J.; Wu, S.-B. Discorhabdins and Pyrroloiminoquinone-Related Alkaloids. *Chem. Rev.* **2011**, *111*, 5465-5491.
- (103) Botić, T.; Defant, A.; Zanini, P.; Žužek, M. C.; Frangež, R.; Janussen, D.; Kersken, D.; Knez, Ž.; Mancini, I.; Sepčić, K. Discorhabdin alkaloids from Antarctic *Latrunculia* spp. sponges as a new class of cholinesterase inhibitors. *Eur. J. Med. Chem.* **2017**, *136*, 294-304.

-
- (104) Zhou, X.; Lu, Y.; Lin, X.; Yang, B.; Yang, X.; Liu, Y. Brominated aliphatic hydrocarbons and sterols from the sponge *Xestospongia testudinaria* with their bioactivities. *Chem. Phys. Lipids* **2011**, *164*, 703-706.
- (105) Bourguet-Kondracki, M. L.; Rakotoarisoa, M. T.; Martin, M. T.; Guyot, M. Bioactive bromopolyacetylenes from the marine sponge *Xestospongia testudinaria*. *Tetrahedron Lett.* **1992**, *33*, 225-226.
- (106) Guyot, M.; Davoust, D.; Belaud, C. Hydroperoxy-24 vinyl-24 cholesterol, nouvel hydroperoxyde naturel isole de deux tuniciers : *Phallusia mamillata* et *Ciona intestinalis*. *Tetrahedron Lett.* **1982**, *23*, 1905-1906.
- (107) Sheu, J.-H.; Wang, G.-H.; Sung, P.-J.; Chiu, Y.-H.; Duh, C.-Y. Cytotoxic sterols from the Formosan Brown Alga *Turbinaria ornate*. *Planta Med.* **1997**, *63*, 571-572.

CHAPTER TWO. DISCOVERY OF BROMO-SPIROISOXAZOLINE ALKALOIDS FROM
THE CARIBBEAN MARINE SPONGE *APLYSINA LACUNOSA*

Abstract: Three new bromotyrosine spiroisoxazoline alkaloids, lacunosins A and B (**2.1–2.2**) and desaminopurealin (**2.3**), were isolated from a MeOH extract of the marine sponge *Aplysina lacunosa* that showed modest α -chymotrypsin inhibitory activity. The structures of **2.1–2.3** share the spirocyclohexadienyl-isoxazoline ring system found in purealidin-R and several other Verongid sponge secondary metabolites. Compounds **2.1** and **2.2** are coupled to a glycine and an isoserine methyl ester, respectively. Alkaloid **2.3** is linked, contiguously, to an *O*-1-aminopropyl 3,5-dibromotyrosyl ether and finally, to histamine through an amide bond. The planar structures of all three compounds were obtained from analysis of MS and 1D and 2D NMR data. The absolute configuration of the SIO unit of **2.1–2.3** was assigned by electronic circular dichroism (ECD). The isoserine amino acid residue in **2.2** was found to be a 1:1 mixture of epimers using a new Marfey's type reagent, derived from Trp-NH₂. Allylic *O*-naphthoylation of the SIO subunit enhances the ECD spectrum of SIOs and improves discrimination of enantiomorphs. A unifying hypothesis is proposed that links the biosynthesis of several of the new compounds with previously reported analogues.

2.1 Introduction

Among the earliest marine natural products reported are alkaloids and peptides containing modified bromotyrosine residues from marine sponges (Porifera), mainly in the order Verongida. Approximately 300 bromotyrosine alkaloids of marine origin have been reported in the literature to date.^{1,2} The formidable oxidative brominating capacity of Verongid sponges is manifested in not only secondary metabolites, but also high-levels of bromotyrosine amino acid residues in the structural proteins (chitin) of *Ianthella basta*³ and *Aplysina cavernicola*.⁴ Bromotyrosine secondary metabolites from marine sponges show a variety of biological properties, including antibacterial,⁵ anti-inflammatory,⁶ antineoplastic,⁷ and antifungal activities that clearly demonstrate bio- and chemodiverse repertoires. A remarkable report by Berlinck and coworkers shows that several bromotyrosine-derived natural products, conventionally associated with Verongid sponges, are produced by fermentation of a Verongid sponge-derived bacterium, *Pseudovibrio denitrificans* Ab134.⁸

In screening for protease inhibitors, we found the MeOH extract of the marine sponge *Aplysina lacunosa* from the Bahamas exhibited significant inhibition of α -chymotrypsin activity. Here we report the structures of three new brominated spiroisoxazoline (SIO) alkaloidal peptides, lacunosins A (**2.1**) and B (**2.2**) and des-aminopurealin (**2.3**), from an assay-guided survey of extracts with α -chymotrypsin inhibitory activity. The structure of alkaloid **2.2** includes a rare isoserine residue.

2.2 Isolation and Structural Elucidation of Lacunosins A–B and Desaminopurealin

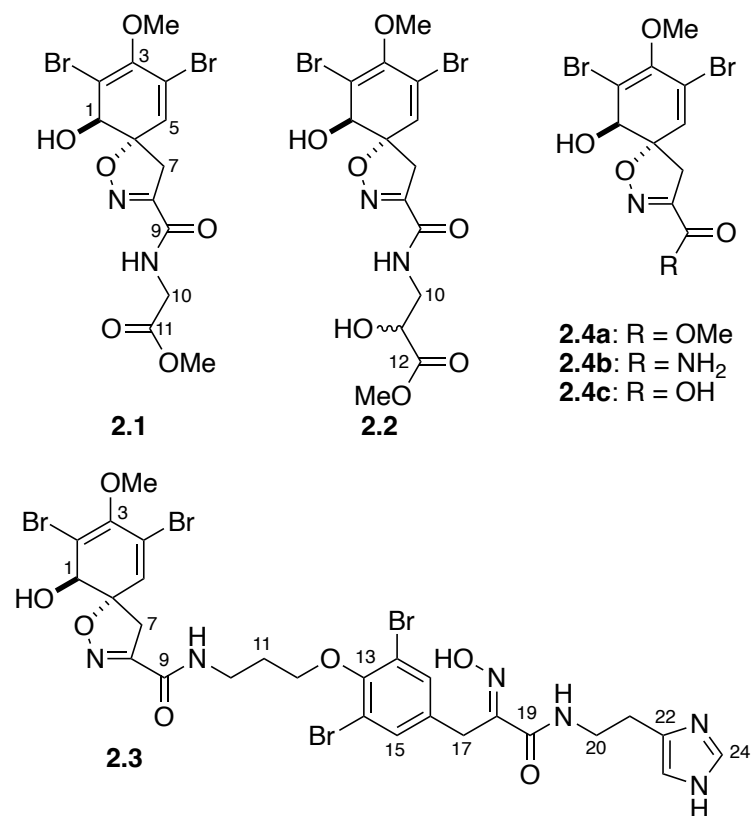


Figure 2.1: The structures of lacunosins A (**2.1**), B (**2.2**), desaminopurealin (**2.3**), verongidoic acid methyl ester (**2.4a**), (+)-purealidin-R (**2.4b**), and verongidoic acid (**2.4c**).

Extracts of the sponge *A. lacunosa* were found to induce 100% inhibition of α -chymotrypsin at 50 $\mu\text{g}\cdot\text{mL}^{-1}$. The total MeOH extract of *A. lacunosa* was separated by progressive solvent partitioning into four fractions A–D, and α -chymotrypsin inhibitory activity was found to partition into the $\text{CH}_2\text{Cl}_2/\text{MeOH}$ -soluble “B fraction”. Further purification of the latter by size exclusion chromatography further segregated activity into mid-eluting and late-eluting fractions (Figure 2.2). HPLC and examination by LCMS and ^1H NMR delivered three new bromotyrosine-derived metabolites (**2.1–2.3**) in addition to the known compounds aeropylsinin-1,⁹ aerophobin-1,¹⁰ aerophobin-2,¹¹ purealidin-N,¹² purealin,¹³ methyl ester **2.4a**,¹⁴ and aplysinin-B^{7a} (for structures, see Appendix). MS analysis of **2.1** and **2.2** showed $[\text{M}+\text{Na}]^+$ of 474.9113 and 504.9215 corresponding to molecular formulas of $\text{C}_{13}\text{H}_{14}\text{Br}_2\text{N}_2\text{O}_6$ and $\text{C}_{14}\text{H}_{16}\text{Br}_2\text{N}_2\text{O}_7$, respectively. The

isotopic patterns of the sodium adduct ions confirmed the presence of two Br atoms in each of **2.1** and **2.2**. Additionally, FTIR absorptions at ~ 3400 and $1680\text{--}1670\text{ cm}^{-1}$ revealed the presence of OH/NH and amide carbonyl groups, respectively. Comparison of the ^1H and ^{13}C NMR data of **2.1** and **2.2** (Table 2.1) with reported literature values for (+)-puralidin-R¹² (**2.4b**, Figure 2.1) demonstrated that both **2.1** and **2.2** contained the SIO moiety with different side chains attached to the amide NH.

The ^1H and ^{13}C NMR spectra of **2.1** showed the characteristic features of the *O*-Me-spiroisoxazoline ring system common to puralidin-R (**2.4b**) and many other bromotyrosine-derived natural products from Verongid sponges. Additionally, the ^1H and HSQC spectra of **2.1** revealed an extra C-11 OMe group (δ_{H} 3.72, s; δ_{C} 52.3) and the deshielded methylene CH₂-10 (δ_{H} 4.01, 2H, s; δ_{C} 41.3). The C-9 signal (δ_{C} 170.4) in **2.1** was assigned to a carboxamide which was linked, sequentially by HMBC correlations, to the deshielded CH₂-10 (δ_{H} 4.02, 2H) and the terminal methyl ester group at δ_{H} 3.72, therefore, constituting a Gly-OMe residue. Compound **2.1** is the *N*-Gly-OMe-extended derivative of **2.4b**.

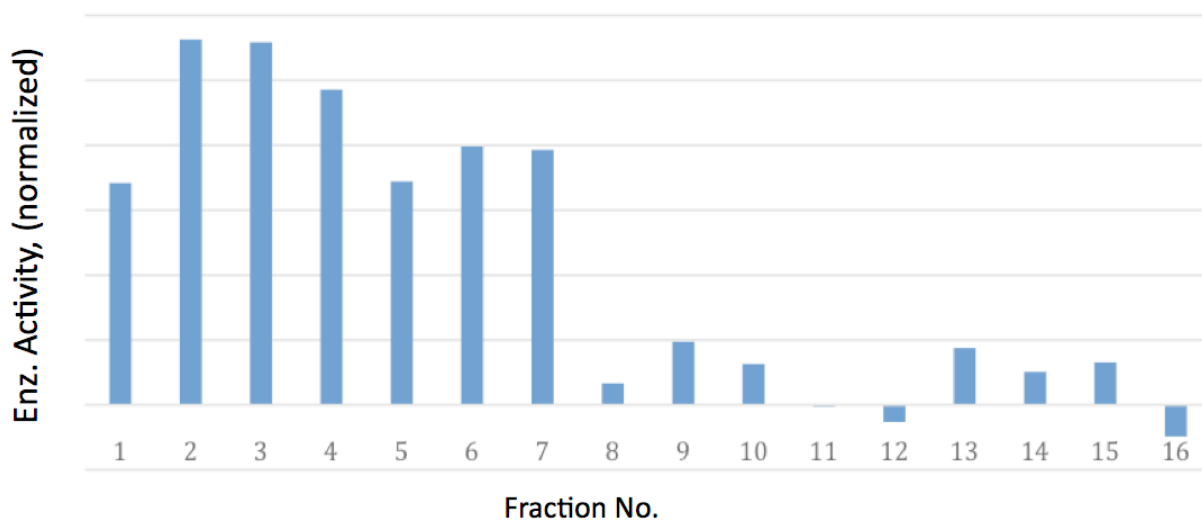


Figure 2.2: α -Chymotrypsin inhibition by fractions from size-exclusion chromatography (Sephadex LH-20, MeOH elution) of *Aplysina lacunosa* solvent-partitioned extract. See Experimental Section.

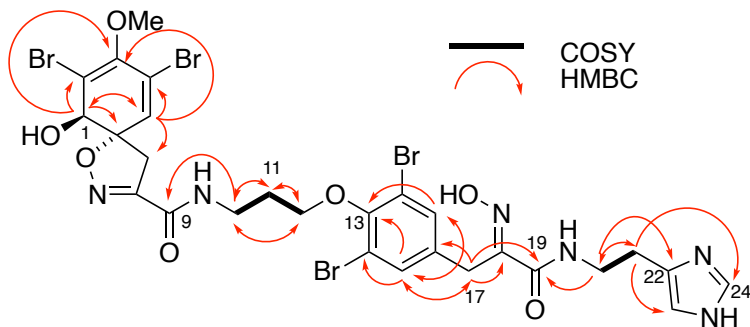


Figure 2.3: COSY and HMBC correlations of (–)-**2.3** (600 MHz, CD₃OD).

The ¹H and HSQC spectra of **2.2** indicated a diastereotopic CH₂ group (δ_{H} 3.64, m and 3.60, m) with a complex multiplet structure (see Figure 2.4 and discussion, below), an *O*-CH-11 (δ_{H} 4.34, dd, 6.0, 4.8), and the 13-MeO signal (δ_{H} 3.75, s; δ_{C} 58.9) in addition to the anticipated SIO ring. A COSY cross-peak between the CH₂-10 and the CH-11 signals, together with HMBC correlations between CH₂-10 and C-9/C-11/C-12, between CH-11 and C-11/C-12, and between C-13-MeO and the carbonyl C-12 (δ_{C} 172.8) suggests **2.2** comprises an SIO joined to an isoserine (*isoSer*) methyl ester residue through an amide bond.

Compound (–)-**2.3**, with the formula C₂₇H₂₈Br₄N₆O₇, is the desamino analog of purealin, a potent inhibitor of myosin and dynein ATPase isolated from an Okinawan specimen of *Psammaphysilla purea*.^{13,14b} The ¹H and ¹³C NMR spectrum of **2.3** were almost identical with those of purealin;¹³ the major differences were the presence of an imidazolyl ¹H NMR signal H-23 (δ_{H} 8.77, s, ¹J_{CH} = 218 Hz) and other minor chemical shift changes near the histamine group. Full ¹H and ¹³C NMR assignment of **2.3** was secured through DQF-COSY, HSQC and HMBC (Figure 2.3). HMBC correlations were observed from H-21 (δ_{H} 2.93, 2H, t, 6.7) to C-23 (δ_{C} 116.1) and C-24 (δ_{C} 133.3). As with almost all natural products containing α -ketoxime-bromotyrosine amides, (–)-**3** has the *E*-oxime configuration.¹⁵ The low specific rotation ($[\alpha]_{\text{D}} -11$) and weak Cotton effect [λ 253 ($\Delta\epsilon$ +0.8), 284 (+0.8)] of (–)-**2.3** suggests this sample is nearly racemic (see below).

The configuration of the *iso*Ser in **2.2** was addressed by a variant of Marfey's method.¹⁶ Total hydrolysis of **2.2** (6 M HCl, 110 °C, 16 h), followed by treatment of the residue with our newly described L-FDTA reagent (**2.5**, Scheme 2.1)¹⁷ gave DTA derivatives with superior resolutions on reversed-phase HPLC.¹⁸ Unexpectedly, two peaks corresponding to L-*iso*Ser-L-DTA ($t_R = 13.63$ min) and D-*iso*Ser-L-DTA ($t_R = 13.94$ min) were observed, suggesting the *iso*Ser residue in **2.2** was a mixture of epimers. When the hydrolysis was repeated under milder conditions (4 M HCl, 110 °C, 12 h), followed by derivatization by L-FDTA, HPLC revealed the same mixture. To exclude the possibility of epimerization during acid hydrolysis of **2.2**, authentic L-*iso*Ser was subjected to the latter conditions of hydrolysis, and upon L-FDTA derivatization and HPLC analysis, a single peak was obtained corresponding to L-*iso*Ser-L-DTA. Consequently, the above results confirm that **2.2** is a mixture of C-11 epimers (1:1).

Given the results above, the complexity of the ¹H NMR spectrum of **2.2**, particularly the 10-CH₂ multiplet structure, could now be interpreted in a different, consistent manner. From inspection of the structure of **2.2**, the expected multiplet pattern of NH-CH₂-CH(OH)- (Figure 2.4a) should be that of an ABX system (the couplings of OH and NH signals are absent due to deuterium exchange in CD₃OD: see DQF-COSY, 600 MHz, Figure 2.12). The CH₂-10 signal should, therefore, consist of a maximum of 8 lines; yet clearly 16 lines are present. The most likely interpretation is that the ¹H NMR signals for CH₂-10 of the epimeric mixture **2.2** are two overlapping eight-line spin systems—the AB parts of two ABX spin systems—with virtually the same vicinal and geminal *J* values, but each slightly offset in chemical shift by different amounts (on average, $\Delta\delta \sim 0.01$, or 6.6 Hz at 600 MHz).¹⁹ Because the nearest stereocenter C-6 is 6-bonds away, the 10-CH₂ *J*-splitting pattern would be expected to be similar for each epimer, dictated only by local torsional parameters, solvation and hydrogen bonding. The simulated ¹H NMR

spectrum²⁰ (Figure 2.4b) supports these conclusions. In short, the deceptive spectral complexity of the 10-CH₂ ¹H NMR signal of **2.2** arises from overlapping spin systems of diastereomers.²¹

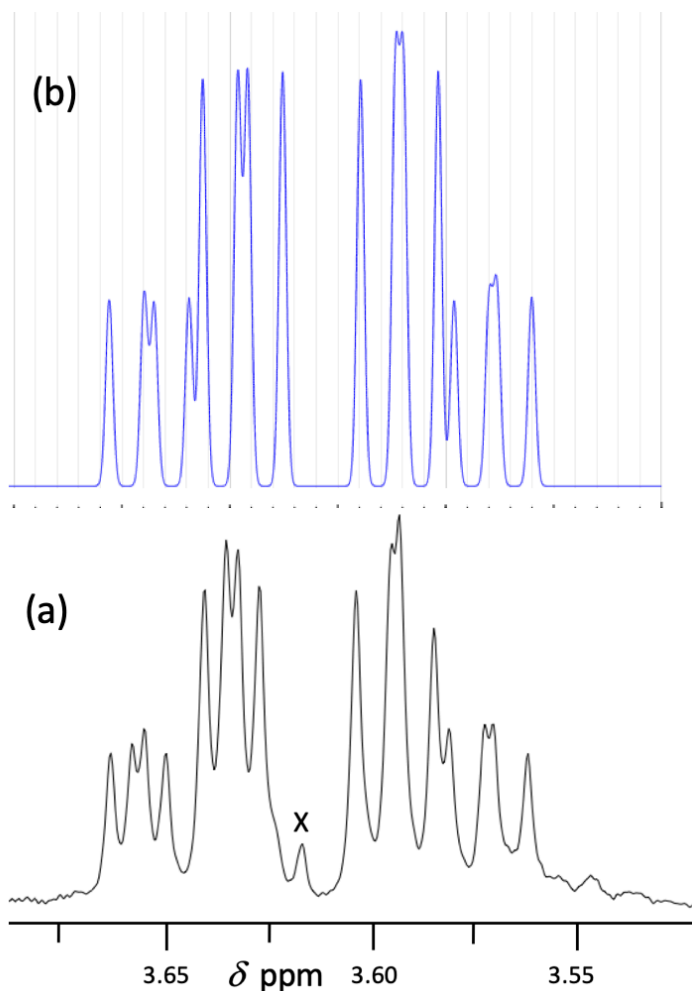


Figure 2.4: (a) ¹H NMR spectra of the diastereotopic 10-CH₂ of **2.2** (600 MHz, CD₃OD) and (b) simulated spectrum of ABX. Line width, 1.15 Hz, δ_A 3.589, $J = 13.0, 6.0, 4.8$ Hz; δ_B 3.644, $J = 13.0, 6.0, 4.8$ Hz. Epimer: δ_A 3.600, $J = 13.0, 6.0, 4.8$ Hz; δ_B 3.652, $J = 13.0, 6.0, 4.8$ Hz (δ_X is not shown). Ref. 20.

Table 2.1: ^1H and ^{13}C NMR Data for **2.1–2.3** in CD_3OD .

#	δ_{C} , type			δ_{H} (int., mult, J , Hz)		
	2.1 ^{a,b}	2.2 ^a	2.3 ^a	2.1 ^c	2.2 ^d	2.3 ^d
1	75.2, CH	74.0, CH	74.1, CH	4.08, s	4.11, s	4.08, s
2	113.9, C	112.6, C	112.9, C			
3	148.7, C	147.8, C	147.7, C			
4	122.1, C	121.3, C	121.3, C			
5	132.3, CH	130.6, CH	130.8, CH	6.41, s	6.443 [6.437 ^e], s	6.42, s
6	91.9, C	91.0, C	90.9, C			
7	39.9, CH ₂	38.7, CH ₂	38.7, CH ₂	3.76, d (18.0) 3.09, d (18.0)	3.79, d (18.6) 3.11, d (18.6)	3.78, d (18.6) 3.10, d (18.6)
8	154.7, C	153.4, C	153.8, C			
9	160.3, C	160.2, C	160.2, C			
10	41.3, CH ₂	42.5, CH ₂	36.6, CH ₂	4.01, s	3.644 [3.652 ^e], ddd (13.0, 6.0, 4.8) 3.600 [3.589 ^e], ddd (13.0, 6.0, 4.8)	3.58, t (6.9)
11	170.4, C	69.1, CH	29.2, CH ₂		4.34, dd (6.0, 4.8)	2.10, pent (6.6)
12		172.8	70.8, CH ₂			4.04, t (6.0)
13			151.2, C			
14			117.5, C			
14'			117.5, C			
15			133.1, CH			7.46, s
15'			133.1, CH			7.46, s
16			136.2, C			
17			27.4, CH ₂			3.81, s
18			150.6, C			
19			164.2, C			
20			37.6, CH ₂			3.56, t (6.7)
21			24.4, CH ₂			2.93, t (6.7)
22			133.1, C			
23			116.1, CH			7.30, s
24			133.3, CH			8.77, s ($^1J_{\text{CH}} = 218$ Hz)
3-OMe	60.2, CH ₃	58.9, CH ₃	59.0, CH ₃	3.71, s	3.75, s	3.72, s
11-OMe	52.3, CH ₃			3.72, s		
12-OMe		51.3, CH ₃			3.77, s	

^a ^{13}C chemical shifts were obtained indirectly from HSQC and HMBC data. ^b125 MHz, $(\text{CD}_3)_2\text{CO}$. ^c500 MHz. ^d600 MHz. ^eSignal for C-11 epimer. See text for discussion of multiplet complexity and Figure 2.4b for NMR simulation. ^fFrom ^{13}C "satellite" measurements.

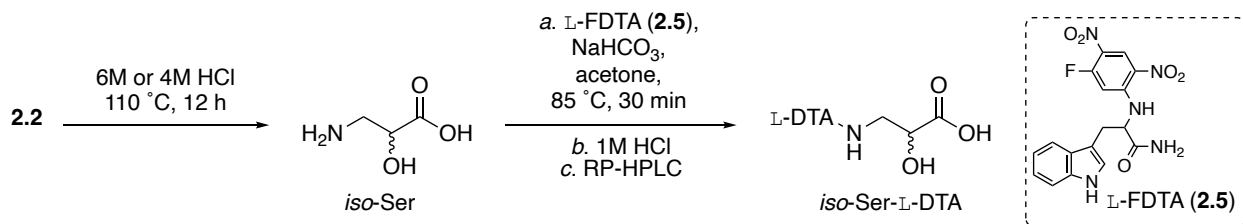
The absolute configurations of the brominated cyclohexadienyl-SIOs were originally assigned by Rinehart and coworkers, who correlated the ECD spectrum and X-ray crystal structure of the degenerate skewed 1,3-dienes in (+)-aerothionin,^{22,23} based on earlier studies of aeroplysinin-1 by Fulmor and coworkers²⁴ and pioneering chiroptical studies of skewed dienes by Moscowitz²⁵ and others.²⁶ The 1,3-diene in the canonical SIO structure, verongidoic acid (**2.4c**) deviates from planarity by approximately +17°²⁷ (Figure 2.5) and is expected to manifest a positive Cotton effect (CE). In fact, two positive CEs are observed in the C₂ dimer, (+)-aerothionin (Table 2.2): λ 245 nm ($\Delta\epsilon$ +23.7) and 284 (+21.4).²² The optical rotations of the commonly-configured (1*R*,6*S*)-SIOs are also consistently dextrorotatory (Table 2.2). Similar trends are observed in other brominated skewed 1,3-cyclohexadienes, (-)-aeroplysinin-1 (**2.S5**) and aplysinin-1 (**2.S8**), which lack an SIO ring system. The ECD spectra of **2.1–2.3** (Figure 2.20) each showed the same positive CEs, albeit of lower magnitudes than (+)-aerothionin. The strongest CEs were those of **2.1** [λ 253 ($\Delta\epsilon$ +5.2), 284 (+3.6)] and the weakest, those of **2.3**. It can be concluded that the dominant chirality of the SIO ring in **2.1–2.3** is (1*R*,6*S*), as depicted, but **2.3** is nearly racemic. Further chiroptical determination of the %ee of **2.1–2.3** is impeded by lack of reliable standard SIOs of known %ee.²⁸

Concern was raised about the relatively lower magnitude CEs observed in **2.1–2.3**. Given that $\Delta\epsilon$ is a molar quantity, the magnitude of the CE should be relatively invariant across all similar SIOs that lack additional stereogenic centers,²⁹ yet this is not the case. For example, the magnitudes of the CE at λ ~250 nm observed in samples of fistularin-3 (**2.S2**) range from $\Delta\epsilon$ +16 to +32.1 (Table 2.2). We were left to consider the possibility that **2.1–2.3** are not homochiral; that is, the SIO ring system is formed with imperfect stereofidelity.³⁰ There is precedence for this phenomenon; for example, ianthesine-A (**2.S14**), -B–D, from an Australian *Ianthella* sp.,³¹

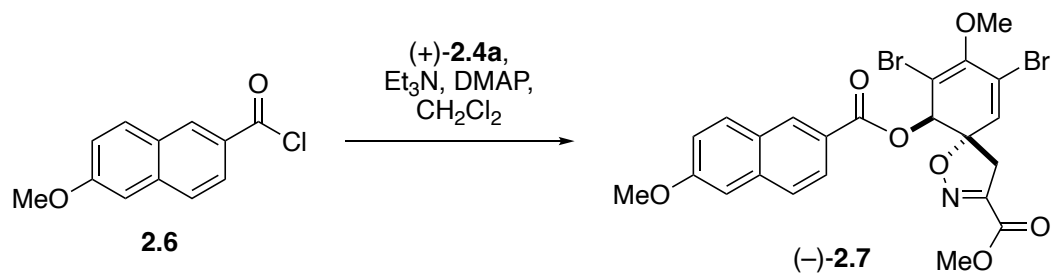
purealidin B (**2.S15**) from an Okinawan *Psammaphysilla purea*,³² and pseudoceratinines A and C (**2.S16** and **2.S17**) from *P. verrucosa*³³ have SIO rings of the antipodal (1*S*,6*R*) configuration. Capon and co-workers isolated (±)-purealin (**2.S18**) from Southern Australian specimens of *Pseudoceratina* spp. and convincingly demonstrated that coisolated (–)-pseudoceratinine A (**2.S16**) and (–)-aerophobin-2 were partial racemates after conversion (*R*-MTPA, DCC) to a mixture of their respective diastereomeric *R*-Mosher's esters (dr 2:1).³⁴ From a sample of *P. verrucosa* collected in Dampier, Western Australia, Karuso and coworkers found the (–)-enantiomer of (+)-purpuroceratic acid B (**2.8b**)^{35,36} along with other antipodal SIO compounds.³⁷ Finally, the curious case of **2.4c** offers an even more interesting study: The EC of **2.4c** (Table 2.2) is of lower magnitude and *opposite in sign* to that of fistularin-3 (**2.S2**), both isolated from the *same specimen* of *Pseudoceratina* sp. from the Bahamas.³⁸

The 1,3-diene twist of SIOs gives rise to a modest CE, which becomes difficult to detect in “near racemic” samples. In order to enhance the ECD signal in SIOs and provide an independent indicator of chirality we exploited the useful cyclic allylic benzoate method developed by Nakanishi and coworkers.³⁹ The exciton coupling (EC) observed between the two nondegenerate chromophores—a benzyloxy group and the adjacent C=C bond—gives rise to a split Cotton effect of which the sign of longer wavelength component is determined reliably from the helicity. When extended to acyclic 1,3-dienyl naphthoate esters, the magnitude of the EC is enhanced significantly. From energy minimized models of **2.4a** (Figure 2.5), it is apparent the diene helicity ($\theta(\text{H-1-C-1-C-6-H6}) = 17.2^\circ$) and allylic helicity ($\theta(\text{H-1-C-1-C-6-H6}) = 102.2^\circ$) are of the same sign. We reasoned that the superposition of CEs arising from helicities of the 1,3-diene and 1,3-dienyl naphthoate moieties would reinforce the magnitude of the CE.

Treatment of synthetic (+)-**2.4a**^{14c} with 6-methoxy-2-naphthoyl chloride (**2.6**)⁴⁰ (Et₃N, DMAP, CH₂Cl₂, Scheme 2.2) gave naphthoate ester (–)-**2.7**. The ECD spectrum of naphthoate ester (–)-**2.7**, (Figure 2.6) showed additional complexity not seen in the ECD spectrum of the parent SIO including a red-shifted positive Cotton effect (λ 310 nm, $\Delta\epsilon$ +7.6) corresponding to the forbidden *R*-band ($n \rightarrow \pi^*$) of the naphthoate chromophore. Although the magnitude of the CE in (–)-**2.7** is no greater than native SIOs, the “fingerprint” CE of similar 6-methoxy-2-naphthoate esters may be useful for fine-scale chiroptical analyses where longer wavelength features are preferable.



Scheme 2.1: Hydrolysis of **2.2** and derivatization of *iso*Ser by L-FDTA (**2.5**).



Scheme 2.2: Naphthoate ester (–)-**2.7** from acylation of (+)-**2.4a**.

(a)

#Conf.	Energy, E (kJ.mol ⁻¹)	Torsional Angle, θ^a (deg°)
6	6.6	8.9
5	6.4	7.3
4	5.7	8.0
3	1.4	-13.9
2	1.1	17.6
1	0.0	17.2 ^b

a. θ (H-1-C-1-C-6-H6). b. θ' (H-1-C-1-C-6-H6) = 102.2

(b)

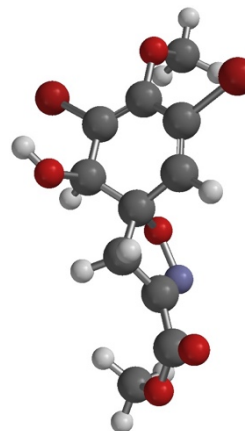


Figure 2.5: Energy-minimized conformers (MMFF) of (1*S*,6*R*)-verongidoic acid methyl ester (**2.4a**). (a) The six lowest E conformers. (b) Model of the Lowest E conformer (iSpartan).

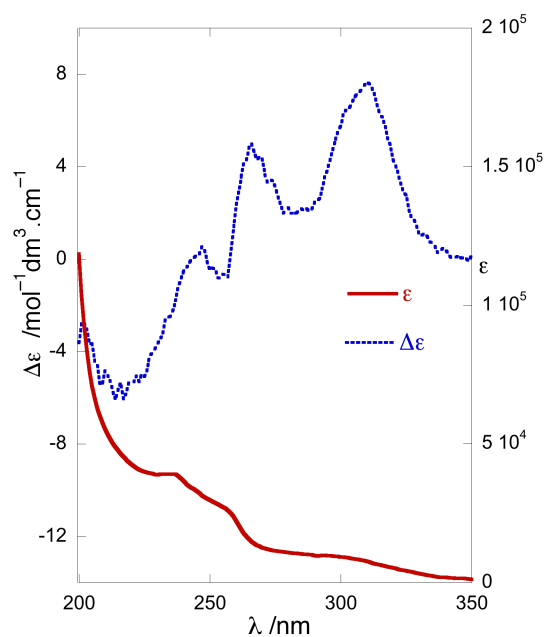
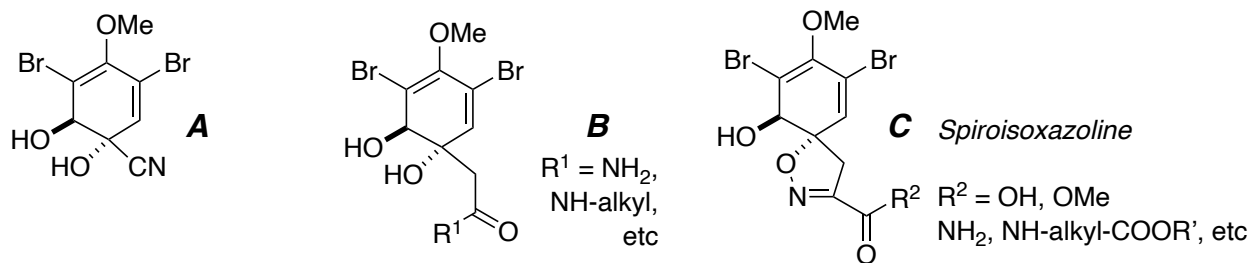


Figure 2.6: UV-vis and ECD spectra (c 2.49 x 10⁻⁵ M, MeOH, 23 °C) of 6'-methoxy-2'-naphthoate ester (–)-**2.7** derived from (+)-**2.4a**.

Table 2.2: Chiroptical Data ($[\alpha]_D$, ECD) for Three Chemotypes (A-C) of Dibromocyclohexa-1,3-dienes.



Compound	Type	Origin	Species	$[\alpha]_D$	$\lambda / \text{nm} (\Delta\epsilon)^a$	$\lambda / \text{nm} (\Delta\epsilon)^a$	Ref
2.1	C	Bahamas	<i>Ap. lacunosa</i> ^b	+71.8	253 (+5.2)	284 (+3.6)	^c
2.2	C	Bahamas	<i>Ap. lacunosa</i> ^b	+32	253 (+3.1)	284 (+2.8)	^c
2.3	C	Bahamas	<i>Ap. lacunosa</i> ^b	-11	253 (+0.8)	289 (+0.8)	^c
(+)-Aerotherionin (2.S1)	C	Mexico	<i>Ap. fistularis</i> ^d	+210 ^e	245 (+23.7)	284 (+21.4)	22
Fistularin-3 (2.S2)	C	Belize	<i>Ai. crassa</i> ^f		273 (+32.1)	287 (+27.6)	5c
Araplysellin III (2.S3b)	C	Belize	<i>Ai. crassa</i> ^f	+96.3 ^g			5c
Hexadellin C (2.S4)	C	Belize	<i>Ai. crassa</i> ^f	+102 ^h			5c
(-)-Aeropylsinin-1 (2.S5)	A	Caribbean	<i>Ia. ardis</i> ^{i,j}	-198 ^k	282 (-15)		24
(+)-Aeropylsinin-1 (2.S6)	A	Bahamas	<i>Ia. sp.</i>	+182 ^k			24
'Verongidoic acid' (2.4c)	C	Bahamas	<i>Ps. crassa</i> ^{l,i}		245 (-9.1)	284 (-6.4)	48
2.S2	C	Virgin Islands	<i>Ap. f. fulva</i> ^m	+104.2 ^p			41
2.S2	C	Bahamas	<i>Ps. crassa</i> ^{l,i}		245 (+16)	284 (+15)	48
2.S2	C	Brazil	<i>Ap. cauliformis</i> ^o		252 (+19.7)	286 (+19.7)	52
2.S2	C	Bahamas	' <i>Ap. fulva</i> ' ^p		251 (+19.0)	285 (+17.8)	52
'11- <i>epi</i> -Fistularin-3' ^q (2.S7)	C	Australia	<i>Ag. oroides</i> ^r	+65.2 ^s	248 (+23.7)	284 (+20.6)	42

a. MeOH. Literature values of molar ellipticities, $[\theta]$, are normalized: $\Delta\epsilon = 3300[\theta]$. See Appendix for the structures **2.S1–2.S19b**. b. *Aplysina lacunosa*. c. This work. See Experimental. d. *Aplysina fistularis*. e. (c 1.0, MeOH). f. *Aiolochoxia crassa*. g. (c 0.19, MeOH). h. (c 0.067, MeOH). i. renamed *Aiolochoxia crassa*. j. *Ianthella ardis*. k. (c 0.5, acetone). l. *Pseudoceratina crassa*. m. *Pseudovibrio denitrificans* Ab134 isolated from sponge *Arenosciera braziliensis*. n. *Aplysina* forma *fulva*. o. *Aplysina cauliformis*. p. Originally identified as *Aplysina fulva*, but upon review, it is more likely *Aplysina fistularis*. q. The configuration at C-11 is variable.⁵² r. *Agelas oroides*. s. (c 1.04, acetone). t. *Aplysina fulva*. u. (c 0.002, MeOH). v. *Aplysina caissara*. w. (c 0.0014, MeOH). x. (c 0.0021, MeOH). y. (c 0.06, MeOH). z. (c 0.04, MeOH). aa. *Pseudoceratina verrucosa*. ab. (c 0.4, MeOH). ac. Less common (1*S*,6*R*) configuration. ad. (c 1.02, MeOH). ae *Psammaphysilla purea* (likely *P. purpurea*). af. (c 1.3, MeOH). ag. (c 1, MeOH). ah. (c 2.1, MeOH). ai. no chiroptical data; presumably "0". aj. (c 0.55, MeOH). ak. (c 6.25, CH₂Cl₂).

Table 2.2: Chiroptical Data ($[\alpha]_D$, ECD) for Three Chemotypes (A-C) of Dibromocyclohexa-1,3-dienes continued.

Compound	Type	Origin	Species	$[\alpha]_D$	λ /nm ($\Delta\epsilon$) ^a	λ /nm ($\Delta\epsilon$) ^a	Ref
Aplysinafulvin (2.S8)	B	Brazil	<i>Ap. fulva</i> ^t	+130 ^u	251 (+1.63)	285 (+0.79)	43
(12 <i>S</i>)-Hydroxy-11-oxo-aerothionin (2.S9)	C	Bahamas	<i>Ap. fistularis</i> ^d	+152.5	250 (+18.2)	288 (+15.2)	44
(12 <i>R</i>)-Hydroxy-11-oxo-aerothionin (2.S10)	C	Bahamas	<i>Ap. fistularis</i> ^d	+162.7	251 (+18.3)	288 (+15.0)	44
11-Hydroxyaerothionin (2.S11)	C	Brazil	<i>Ap. caissara</i> ^v	+178 ^w	248 (+24)	284 (+24)	45
Caissarine C (2.S12)	C	Brazil	<i>Ap. caissara</i> ^v	+175 ^x	248 (+26)	290 (+27)	45
<i>N</i> -sulfatoaplysillin I (2.S13)	C	Bahamas	' <i>Ap. fulva</i> ' ^t	+100 ^y	244 (+8.3)	285 (+8.0)	50
(+)-Purpuroceratic acid B (2.8b)	C	Bahamas	' <i>Ap. fulva</i> ' ^t	+140 ^z	243 (+7.0)	289 (+5.2)	50
(-)-Purpuroceratic acid B (2.8b)		Australia	<i>Ps. verr</i> ^{aa}	-9 ^{ab}			37
Ianthesine A (2.S14) ^{ac}	C	Australia	<i>Ianthella</i> sp.	-118 ^{ad}	248 (-10.2)	285 (-9.94)	31
Purealdin B (2.S15) ^{ac}	C	Japan	<i>Psa. pur.</i> ^{ae}	-4.5 ^{af}	252 (-2.5)	290 (-2.4)	32
Pseudoceratinine A (2.S16) ^z	C	New Caledonia	<i>Ps. verr.</i> ^{aa}	-158 ^{ag}	248 (-9.66)	290 (-8.48)	33
(-)-Purealin (2.S18) ^z	C	Japan	<i>Psa. pur.</i> ^{ae}	-85 ^{ah}	245 (-9.51)	284 (-9.15)	13
(±)-Purealin (2.S18)	C	Australia	<i>Ps. sp</i>	^{ai}			34
Subereamolline A (2.S19a)	C	Egypt	<i>Suberea mollis</i>	+156.5 ^{aj}			46
Subereamolline A (2.S19a)	C	Egypt	<i>Suberea mollis</i>	+22.9 ^{ak}			46

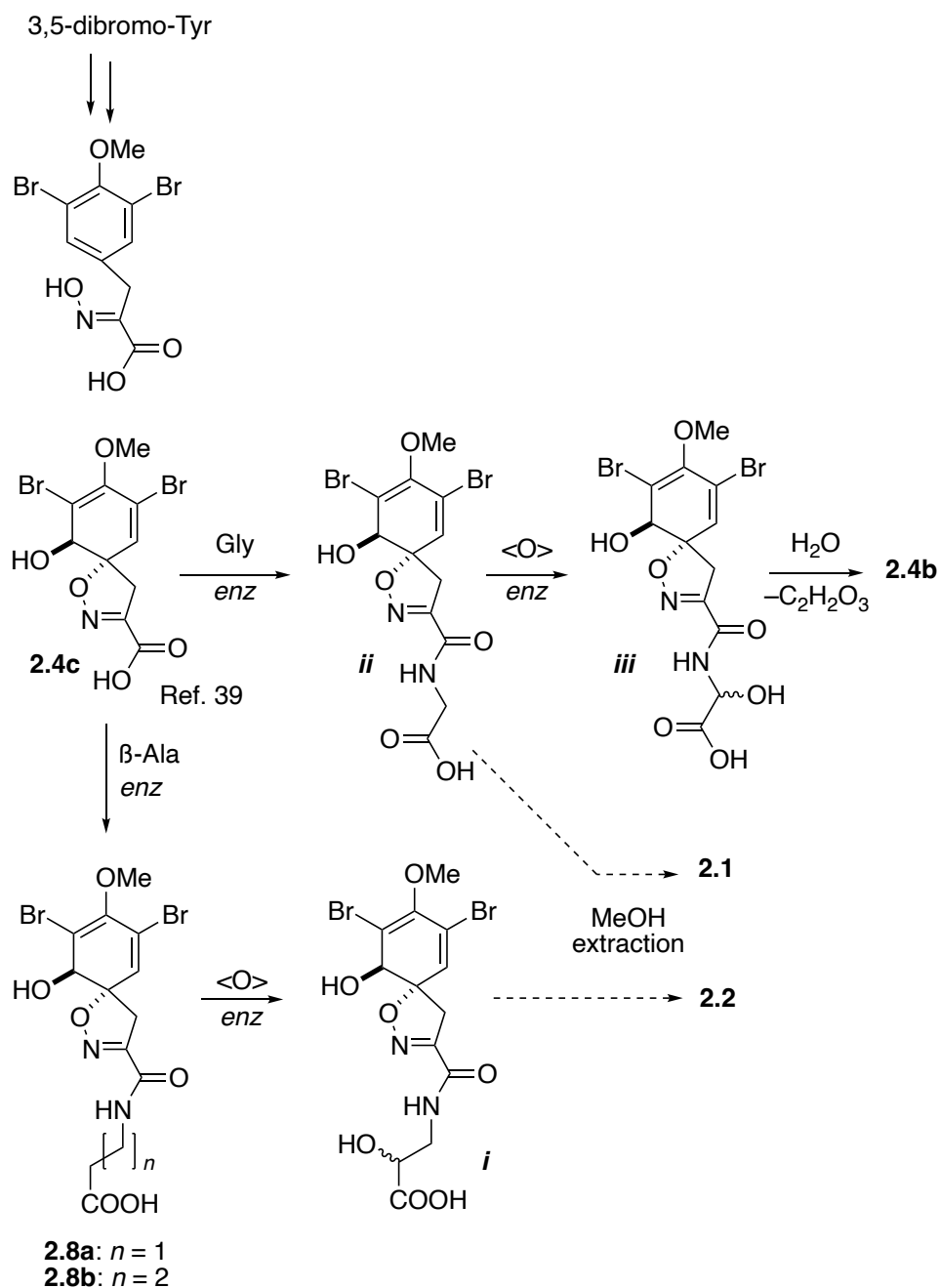
a. MeOH. Literature values of molar ellipticities, $[\theta]$, are normalized: $\Delta\epsilon = 3300[\theta]$. See Appendix for the structures **2.S1–2.S19b**. b. *Aplysina lacunosa*. c. This work. See Experimental. d. *Aplysina fistularis*. e. (c 1.0, MeOH). f. *Aiolochoiria crassa*. g. (c 0.19, MeOH). h. (c 0.067, MeOH). i. renamed *Aiolochoiria crassa*. j. *Ianthella ardis*. k. (c 0.5, acetone). l. *Pseudoceratina crassa*. m. *Pseudovibrio denitrificans* Ab134 isolated from sponge *Arenosclera braziliensis*. n. *Aplysina* forma *fulva*. o. *Aplysina cauliformis*. p. Originally identified as *Aplysina fulva*, but upon review, it is more likely *Aplysina fistularis*. q. The configuration at C-11 is variable.⁵² r. *Agelas oroides*. s. (c 1.04, acetone). t. *Aplysina fulva*. u. (c 0.002, MeOH). v. *Aplysina caissara*. w. (c 0.0014, MeOH). x. (c 0.0021, MeOH). y. (c 0.06, MeOH). z. (c 0.04, MeOH). aa. *Pseudoceratina verrucosa*. ab. (c 0.4, MeOH). ac. Less common (1*S*,6*R*) configuration. ad. (c 1.02, MeOH). ae *Psammaphysilla purea* (likely *P. purpurea*). af. (c 1.3, MeOH). ag. (c 1, MeOH). ah. (c 2.1, MeOH). ai. no chiroptical data; presumably "0". aj. (c 0.55, MeOH). ak. (c 6.25, CH₂Cl₂).

Brominated SIOs arise from bromination–oxidation of tyrosine, as shown by Rinehart and co-workers using ^{14}C -labeling.⁴⁷ Much speculation has appeared on the biosynthesis of the SIO and subsequent transformation, the consensus being that the SIO ring system arises from oxidation of a 3,5-Br₂Tyr- α -ketoxime to an 1,2-arene epoxide followed by intramolecular $S_{\text{N}}2$ attack-ring opening by the C=NOH group. The dominance of (+)-(1*R*,6*S*)-SIO stereoisomers in Nature attest to *re*-facial selectivity of the putative arene epoxidase, with the less common (–)-(1*S*,6*R*) enantiomorphs arising from variant enzymes exhibiting preferential *si*-facial selectivity, or even nonselectivity in the cases of near-racemic SIOs. Another way to view this outcome is imperfect desymmetrization by O atom addition to the aryl ring of the 3,5-Br₂Tyr- α -ketoxime precursor.

In this report, our interest was on the origin of *isoSer*, a rare nonproteinogenic amino acid observed in **2.2** and the first time in an SIO. Although it is possible that *isoSer* derives from an independent, discrete biosynthetic pathway like most other AAs, the *rac*-modification seen in **2.2** suggests an alternative explanation: a post-assembly oxidation of the SIO-containing compound (Scheme 2.3). Condensation of **2.4c** (reported from *Pseudoceratina* sp.⁴⁸ and as a fermentation product of *Pseudovibrio denitrificans* Ab1348⁴⁹ and given the name ‘verongidoic acid’) with β -alanine would give purpuroceratic acid A (**2.8a**),³⁶ a likely intermediate also found with homologues (e.g. purpuroceratic acid B, **2.8b**), in at least two other Verongid sponges.^{14a,50} Compound **2.8a** would then suffer stereorandom α -hydroxylation by a monooxygenase enzyme (Scheme 2.3) giving carboxylic acid **i**; the corresponding methyl ester **2.2** arises as an artifact of adventitious Fischer–Speier esterification during extraction with MeOH.⁵¹ Earlier observations of non-specific hydroxylation of spiroisoxazolines from *Aplysina* sp. support the notion that such “biotransformations” may be commonplace in the biosyntheses of brominated SIOs.⁵² Finally, a unifying hypothesis comes to mind. The structure of purealidin-R (**2.4b**), itself, may arise from a

well-known pathway to C-terminal primary amides.⁵³ α -hydroxylation of the terminal Gly residue of **ii** (again, **2.1** arises from **ii** by adventitious methylation of **ii**) to give the carbinolamine **iii** followed by hydrolytic loss of glyoxylic acid to give **2.4b**.

Several peptides with *iso*Ser residues have been shown to be protease inhibitors. For example, a series of synthetic *iso*Ser-containing peptides showed significant inhibition of aminopeptidase-N.⁵⁴ Upon assay, none of the new compounds **2.1–2.3**, or the other seven known secondary metabolites from the active extract of *A. lacunosa* showed inhibition of α -chymotrypsin at concentrations up to 25 $\mu\text{g}\cdot\text{mL}^{-1}$, suggesting the chemical entity responsible for inhibitory activity is a very minor, potent congener that escaped detection, or decomposed during purification.



Scheme 2.3: Biosynthetic hypothesis for **2.1**, **2.2** and **2.4b**.

2.3 Conclusions

In conclusion, three new brominated spiroisoxazoline alkaloids **2.1–2.3** were isolated from extracts of *Aplysina lacunosa*, and their structures determined by integrated analysis of MS, NMR and ECD data. The rare amino acid (±)-*iso*Ser was found as a residue in **2.2**, a 1:1 mixture of

epimers. Configurational heterogeneity is noted in spiroisoxazolines, both in ECD and the range of magnitude of the Cotton effects ($\Delta\varepsilon$) and preparation of diastereomeric amides from **2.4c**. None of the new or known compounds were responsible for activity in the α -chymotrypsin inhibition assay.

Chapter 2, in total, is a reprint of the material, “Bromo-spiroisoxazoline Alkaloids, Including an Isoleucine Peptide, from the Caribbean Marine Sponge *Aplysina lacunosa*” *J. Nat. Prod.* **2020**, *83*, 1532-1540. The dissertation author was the primary author of this paper and gratefully acknowledges the contributions of coauthors Matthew T. Jamison, and Tadeusz F. Molinski.

2.4 Acknowledgements

We thank M. Cabrera-Abad, K. Planck and R. Hendra for assistance in HPLC purification of **2.1–2.4a** and (–)-**2.7**, and E. P. Stout for assistance with collection of marine sponge samples, A. Mrse and B. Duggan for NMR support, X. Su for HRMS measurements, and J. Pawlik (UNC Wilmington) and the crew of the *R.V. Walton Smith* for the logistics of sample collection in the Bahamas. M. C-A and K. P. were supported by the STARS summer research program, UC San Diego. Acquisitions of the Agilent TOF mass spectrometer and the 500 MHz NMR spectrometer were made possible with funds from the NIH Shared Instrument Grant program (S10RR025636) and the NSF Chemical Research Instrument Fund (CHE0741968), respectively. We are grateful for support for this research from the NIH (AI100776, AT009783).

2.5 Experimental Section

General Experimental Procedures. Optical rotations were measured on a JASCO P-2000 polarimeter at the D-double emission line of Na. UV-Vis spectra were measured on a JASCO V-630 spectrometer. ECD spectra were measured on a JASCO J-810 spectropolarimeter at 23 °C in quartz cells of 1, 2 or 5 mm pathlength. FTIR spectra were collected from thin film samples using a JASCO FTIR-4100 fitted with an ATR ZnSe plate. 1D and 2D NMR spectra were measured on a JEOL ECA (500 MHz) spectrometer, equipped with a 5 mm $^1\text{H}\{^{13}\text{C}\}$ room temperature probe, or a Bruker Avance III (600 MHz) NMR spectrometer with a 1.7 mm $^1\text{H}\{^{13}\text{C}/^{15}\text{N}\}$ microcryoprobe (23 °C). Chemical shifts were referenced to internal solvent or residual ^1H signals (CDCl_3 , δ_{H} 7.26 ppm; δ_{C} 77.16. CD_3OD , δ_{H} 3.31; δ_{C} 49.00). LC-MS measurements were performed with a Thermoelectron Surveyor UHPLC coupled to an MSD single-quadrupole detector. HR-ESI-TOF mass spectroscopy analyses were conducted on an Agilent 1200 HPLC connected to an Agilent 6350 TOF-MS at the Small Molecule Mass Spectrometry Facility at the Department of Chemistry and Biochemistry at UCSD. Preparative, semi-preparative and analytical HPLC purifications were carried out on a JASCO system consisting of a UV-VIS detector (UV-2075), dual-pumps (PU-2086 Plus), and a dynamic mixer (MX-2080-32).

Biological Material. The sponge *Aplysina lacunosa* (11-14-018) was collected in 2011 from Little San Salvador Island in the Bahamas (lat. 24° 35.242'N, long. 75° 58.495'W) at a depth of -23 m using scuba and kept frozen (-20 °C) until needed. A type sample (MeOH) is archived in the Department of Chemistry and Biochemistry, UCSD.

Extraction and Isolation. A sample of *A. lacunosa* (11-14-018) was lyophilized (dry wt. 24.0 g) and extracted twice with MeOH (2 x 400 mL). The combined, filtered extracts were concentrated under reduced pressure to yield an extract (5.17 g), which was dissolved in

MeOH/H₂O (9:1, 400 mL) before repeated partitioning against hexanes (3 x 400 mL) to provide the hexane-soluble 'A' fraction (0.2517 g). The MeOH/H₂O solution (6:4, 600 mL) was adjusted to 40% v/v H₂O, and the mixture repeatedly partitioned against CH₂Cl₂ (2 x 400 mL). The combined CH₂Cl₂ layers were concentrated to deliver the CH₂Cl₂-soluble 'B-fraction' (0.8412 g) after removal of volatiles. The MeOH/H₂O layer was concentrated under reduced pressure and the residual aqueous layer extracted with *n*-BuOH (2 x 300 mL) to yield the *n*-BuOH-soluble 'C' layer (1.2460 g) and H₂O-soluble 'D' layer (2.8300 g) after removal of volatiles.

The 'B-fraction' (0.7342 g) was separated by size-exclusion chromatography (Sephadex LH-20, MeOH) and the eluate grouped into 16 fractions by TLC profiling (9:1 of CH₂Cl₂/MeOH, UV-activity, *p*-anisaldehyde stain). The tenth fraction (18.5 mg) was further purified by reversed-phase preparative HPLC (Phenomenex C₁₈ column, 150 x 21.2 mm, 5 μm, under gradient elution: initial conditions 10% CH₃CN/H₂O-0.1% TFA for 3 min to 60% CH₃CN/H₂O-0.1% TFA over 20 min, 13 mL.min⁻¹ flow rate) to yield lacunosin A (**2.1**, 3.2 mg) eluting at $t_R = 17.19$ min. The eleventh fraction (10.0 mg) was also purified by reversed-phase semi-preparative HPLC (Phenomenex C₁₈ column, 250 x 10 mm, 5 μm, step gradients, initial conditions: 30% CH₃CN/H₂O-0.1% TFA for 5 min to 75% CH₃CN/H₂O-0.1% TFA for an additional 25 min, 2.5 mL.min⁻¹ flow rate) to yield 13 fractions. Fraction 6 (0.3 mg) contained lacunosin B (**2.2**) eluting at $t_R = 18.95$ min. Fraction 9 (0.2 mg) which eluted at $t_R = 21.38$ min was further purified by reverse-phase analytical HPLC (Synergi Hydro-RP column, 150 x 4.6 mm, 4 μm, step gradients, initial conditions 20% CH₃CN/H₂O-0.1% TFA for 3 min to 70% CH₃CN/H₂O-0.1% TFA for 32 min, 0.7 mL.min⁻¹ flow rate) to yield desaminopurealin (**2.3**, 0.1 mg) that eluted at $t_R = 24.50$ min. An additional 0.7 mg of compound **2.3** was purified from the twelfth fraction (11.7 mg) of the LH-20 column under similar semi-preparative HPLC conditions as the eleventh fraction. Additional

HPLC separations delivered aeroplysinin-1,⁹ aerophobin-1,¹⁰ aerophobin-2,¹¹ purealidin-N,¹² methyl ester **2.4a**,^{14a,b} and aplysinin-B^{7a} and whose identities were confirmed by MS and ¹H NMR.

Lacunosin A (2.1): pale yellow solid; $[\alpha]^{23.8}_D +71.8$ (*c* 1.00, MeOH); ECD (*c* 3.93 x10⁻⁴M, MeOH) λ_{\max} ($\Delta\epsilon$) 214 (-1.8), 227 (0), 253 (+5.08), 282 (+3.7) nm; UV (MeOH) λ_{\max} (log ϵ) 194 (3.48), 230 (3.37), and 282 (3.09); FTIR (ATR, film, ZnSe) ν 3353, 1744, 1671, 1599, 1541, 1438, 1205, 1133, 1047, 1025, 988, 916, 837, 801, 766 and 722 cm⁻¹; ¹H and ¹³C NMR data, Table 2.1; HRMS (ESI-TOF) *m/z* 474.9113 [M+Na⁺] (calcd for C₁₃H₁₄Br₂N₂O₆Na⁺, 474.9111).

Lacunosin B (2.2): white solid; $[\alpha]^{23.9}_D +31.8$ (*c* 0.15, MeOH); UV (MeOH) λ_{\max} (log ϵ) 194 (3.68), 225 (3.48), and 281 (3.15) nm; ECD (*c* 3.56 x10⁻⁴M, MeOH) λ_{\max} 214 ($\Delta\epsilon$ -1.4), 227 (0), 251 (+3.1) and 282 (+2.7) nm; FTIR (ATR, film, ZnSe) ν 3427, 1685, 1207, 1141, 805, and 724 cm⁻¹; ¹H and ¹³C NMR data, Table 2.1; HRMS (ESI-TOF) *m/z* 504.9215 [M+Na]⁺ (calcd for C₁₄H₁₆Br₂N₂O₇Na⁺, 504.9216).

Desaminopurealin (2.3): white solid; $[\alpha]^{23.5}_D -10.5$ (*c* 0.13, MeOH); UV (MeOH) λ_{\max} (log ϵ) 205 (3.88), 221 (4.56) and 275 (3.04) nm; ECD (*c* 4.63 x10⁻⁴M, MeOH) λ_{\max} ($\Delta\epsilon$) 214 (-0.34), 227 (0), 251 (+0.8) and 282 (+0.7); FTIR (ATR, film, ZnSe) ν 3405, 1684, 1207, 1142, 804, and 722 cm⁻¹; ¹H and ¹³C NMR data, Table 2.1; HRMS (ESI-TOF) *m/z* 864.8828 [M+H]⁺ (calcd for C₂₇H₂₉Br₄N₆O₇⁺, 864.8826).

Compound (2.4a): white solid; $[\alpha]^{21.4}_D +145$ (*c* 0.44, MeOH), lit.^{14c} $[\alpha]^{27.9}_D +165.5$ (*c* 0.325, C₆H₆); ECD (1.07 x10⁻³M, MeOH) λ ($\Delta\epsilon$) 222 (4.48), 252 (12.58) and 289 (-4.83) nm; ¹H NMR and HRMS of **2.4a** were consistent with literature values.^{14b,c}

Acid Hydrolysis of 2.2. A sample of **2.2** (0.1 mg, 0.2 μ mol) was dissolved in 4 M HCl (100 μ L, 400 μ mol) and stirred in a sealed vial at 110 °C for 12 h. The solution was cooled to room

temperature, dried under a stream of N₂, and derivatized with L-FDTA (**2.5**)¹⁷ to yield the *iso*Ser-DLT derivatives of **2.2** for LC-MS analysis (see below).

Absolute Configuration of iso-Ser in Compound 2.2. To the acid hydrolysate of **2.2** in H₂O (50 μL) was added 1 M NaHCO₃ (50 μL, 50 μmol) and L-FDTA¹⁷ (**2.5**, 0.25 mg, 0.65 μmol) in acetone (75 μL). The reaction was stirred at 85 °C for 30 min, cooled and neutralized with 1 M HCl (50 μL, 50 μmol). The derivatized hydrolysate (20 μL) was diluted with MeOH (80 μL), centrifuged and analyzed by LC-MS (Hypersil Gold, C₁₈ column, 50 x 2.1 mm, 1.9 μm, linear gradient, initial conditions 15%-45% CH₃CN/H₂O-0.1% HCOOH over 25 min, 0.5 mL·min⁻¹ flow rate). L-DTA derivatives of authentic standards of L- and DL-*iso*Ser eluted gave peaks at *t*_R = 13.63 min and 13.94 min, respectively. The LC-MS analysis of L-DTA derivative of the acid hydrolysate of **2.2** gave both L-*iso*Ser-L-DTA and D-*iso*Ser-L-DTA (ratio ~1:1).

6'-Methoxy-2'-naphthoate Ester ((±)-2.7). A solution of (±)-**2.4a**^{14c} (1.0 mg, 2.5 μmol) in CH₂Cl₂ (0.2 mL) was treated sequentially with 6-methoxy-2-naphthoyl chloride (**2.6**, 0.55 mg, 10 μmol, prepared from the corresponding carboxylic acid and oxalyl chloride), Et₃N (1.0 mg, 10 μmol) and DMAP (~0.5 mg) at 0 °C, then stirred for 16 h at 23 °C. The mixture was concentrated, applied to a preparative TLC plate (silica, 20 x 20 x 0.1 cm) and the plate eluted (40:60 EtOAc-hexanes) to give a non-polar UV-active fraction (1.4 mg) containing (±)-**2.7** (*R*_f = 0.26, 35:65 EtOAc-hexanes). The latter was further purified by HPLC (normal phase, Rainin Dynamax 10 x 250 mm, 5μ, 35% EtOAc-hexanes, 4.0 mL·min⁻¹) to give (±)-**2.7** as a straw-yellow solid (0.73 mg, 49%). UV-vis (MeOH) λ_{max} 209 nm (log₁₀ ε 4.16), 241 (4.17), 255 (4.18), 310 (3.48); ¹H NMR (500 MHz, CDCl₃) δ_H 8.49 (1H, s), 7.97 (1H, dd, *J* = 8.4, 1.2 Hz), 7.85 (1H, d, *J* = 9.0 Hz), 7.77 (1H d, *J* = 8.4 Hz), 7.21 (1H, dd, *J* = 9.0, 2.4 Hz), 7.16 (1H, d, *J* = 2.4 Hz), 6.40 (1H, s), 6.18 (1H, s), 3.96 (3H, s, 6'-OMe), 3.85* (3H, s, 3-OMe), 3.82* (3H, s, COOMe), 3.61 (1H, d, *J* = 18.6 Hz,

H-7b), 3.10 (1H, d, $J = 18.6$ Hz, H-7a); HRMS (ESI-TOF) m/z 601.9418 $[M+Na]^+$ (calcd for $C_{14}H_{16}Br_2N_2O_7Na^+$, 601.9420).

(1*R*,6*S*)-6'-Methoxy-2'-naphthoate Ester (1*R*,6*S*)-**2.7**). A sample of (\pm)-**2.4a** (4.2 mg) was separated by semi-preparative chiral-phase HPLC (Phenomenex, Amylose-2, 10 x 250 mm, 30:70 CH_3CN-H_2O , 4.0 mL.min⁻¹) to give pure (+)-**2.4a** ($t_R = 18.2$ min, 1.5 mg) and (-)-**2.4a** ($t_R = 30.6$ min, 1.5 mg). A sample of (+)-**2.4a** (0.78 mg, 2.0 μ mol) was acylated with freshly prepared 6-methoxy-2-naphthoyl chloride (**6**, 7.9 μ mol) and Et₃N (7.9 μ mol) in CH_2Cl_2 (80 μ L) to give (1*R*,6*S*)-**2.7a** (0.29 mg) after purification by HPLC (normal phase, Rainin Dynamax 10 x 250 mm, 5 μ , 35% EtOAc-hexanes, 4.0 mL.min⁻¹ $t_R = 7.4$ min). (1*R*,6*S*)-**2.7**: colorless solid; $[\alpha]_D^{23} -21$ (c 0.058, MeOH); UV-vis (MeOH) λ_{max} ($\log_{10} \epsilon$) 210 (4.11), 237 (4.37), 253 (4.20) and 310 (3.82) nm; ECD (2.49 x 10⁻⁵ M, MeOH) λ ($\Delta\epsilon$) 217 (-5.7), 267 (+4.7) and 310 (+7.6) nm; ¹H NMR (600 MHz), identical with that of (\pm)-**2.7**; HRMS (ESI-TOF) m/z 596.9860 $[M+NH_4]^+$ (calcd for $C_{27}H_{19}Br_2N_2O_7^+$, 596.9867).

2.6. Appendix

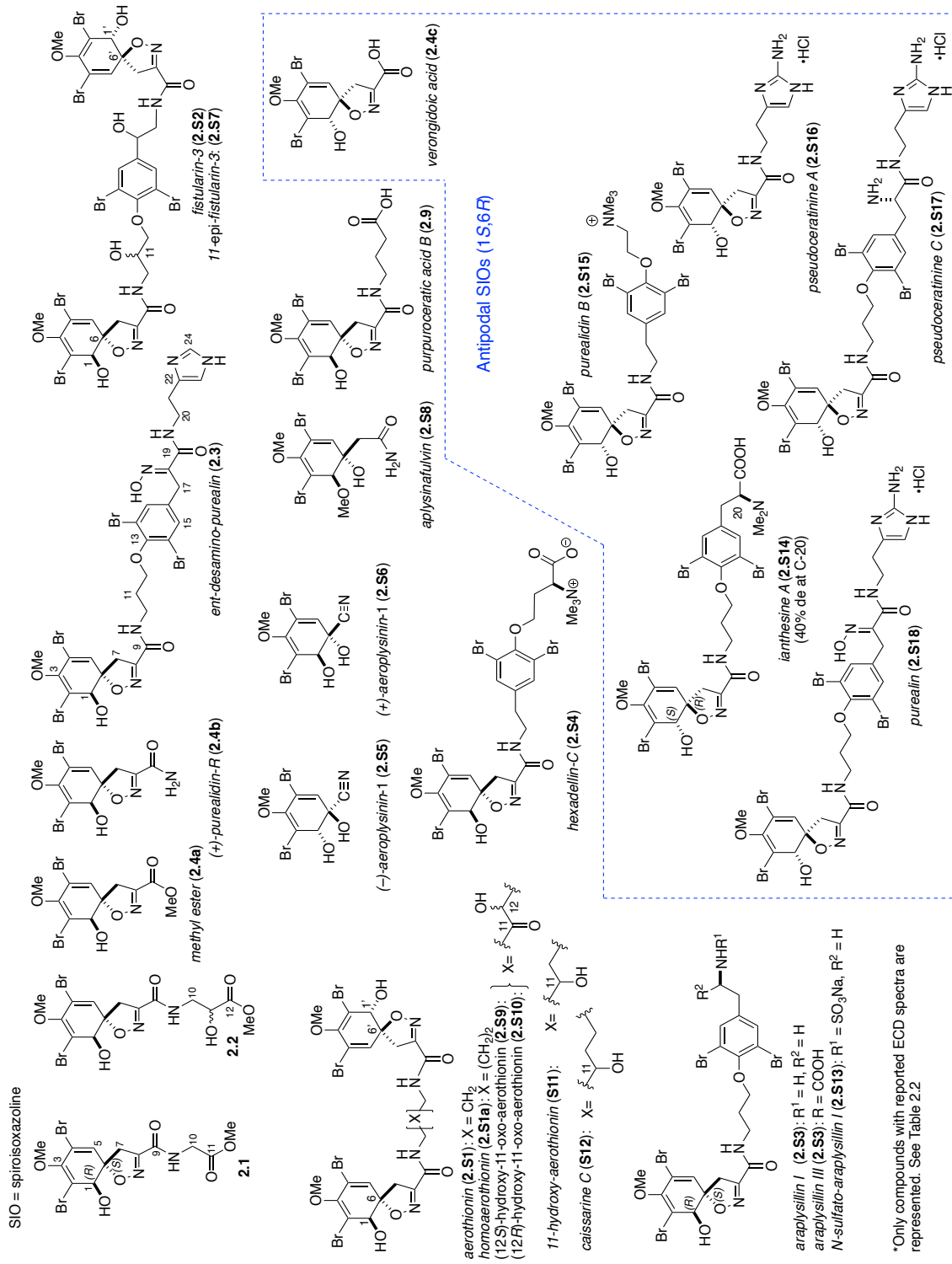
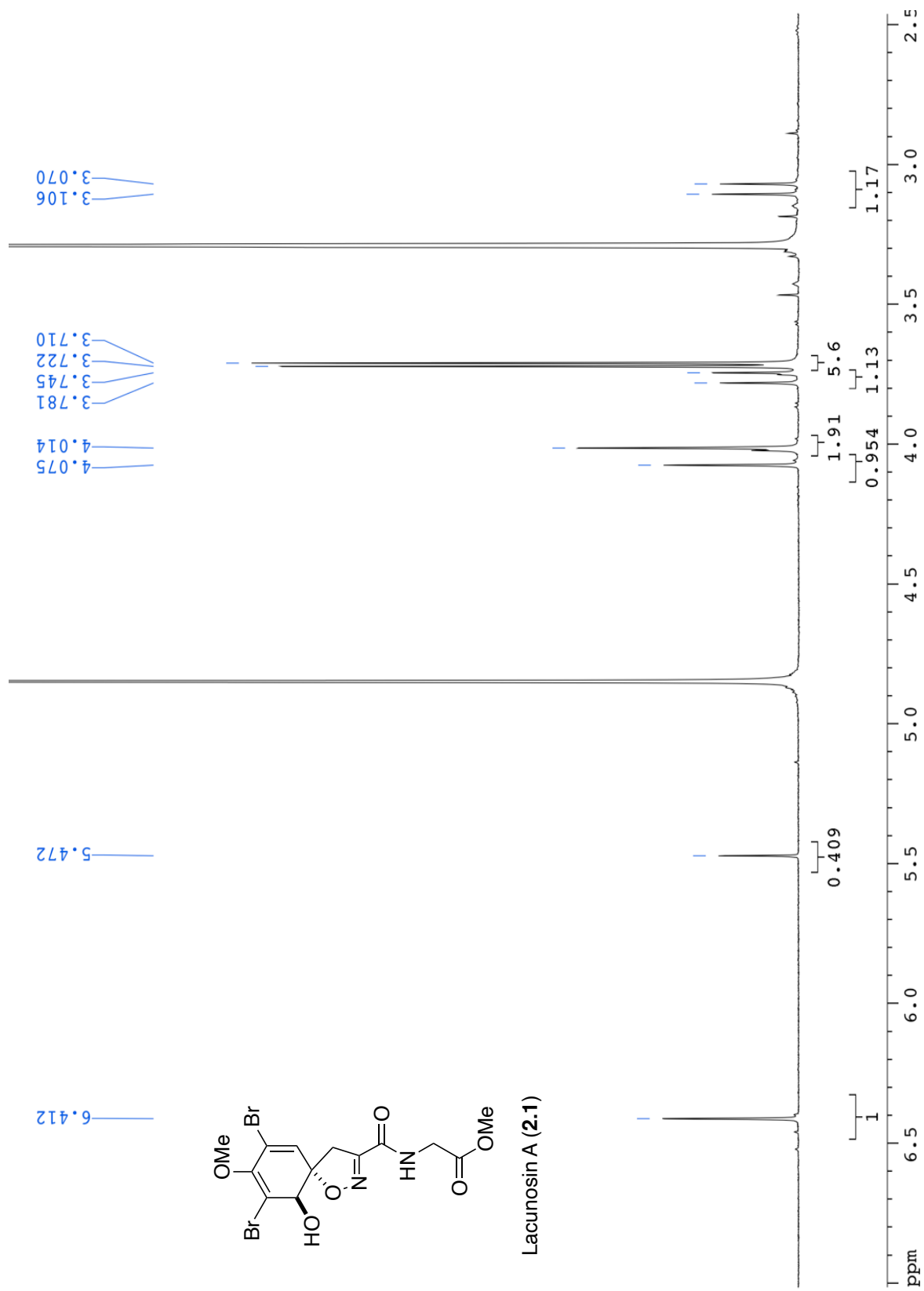


Figure 2.7: Structures of Dibromo-cyclohexa-1,3-dienyl Natural Products from Verongid Sponges



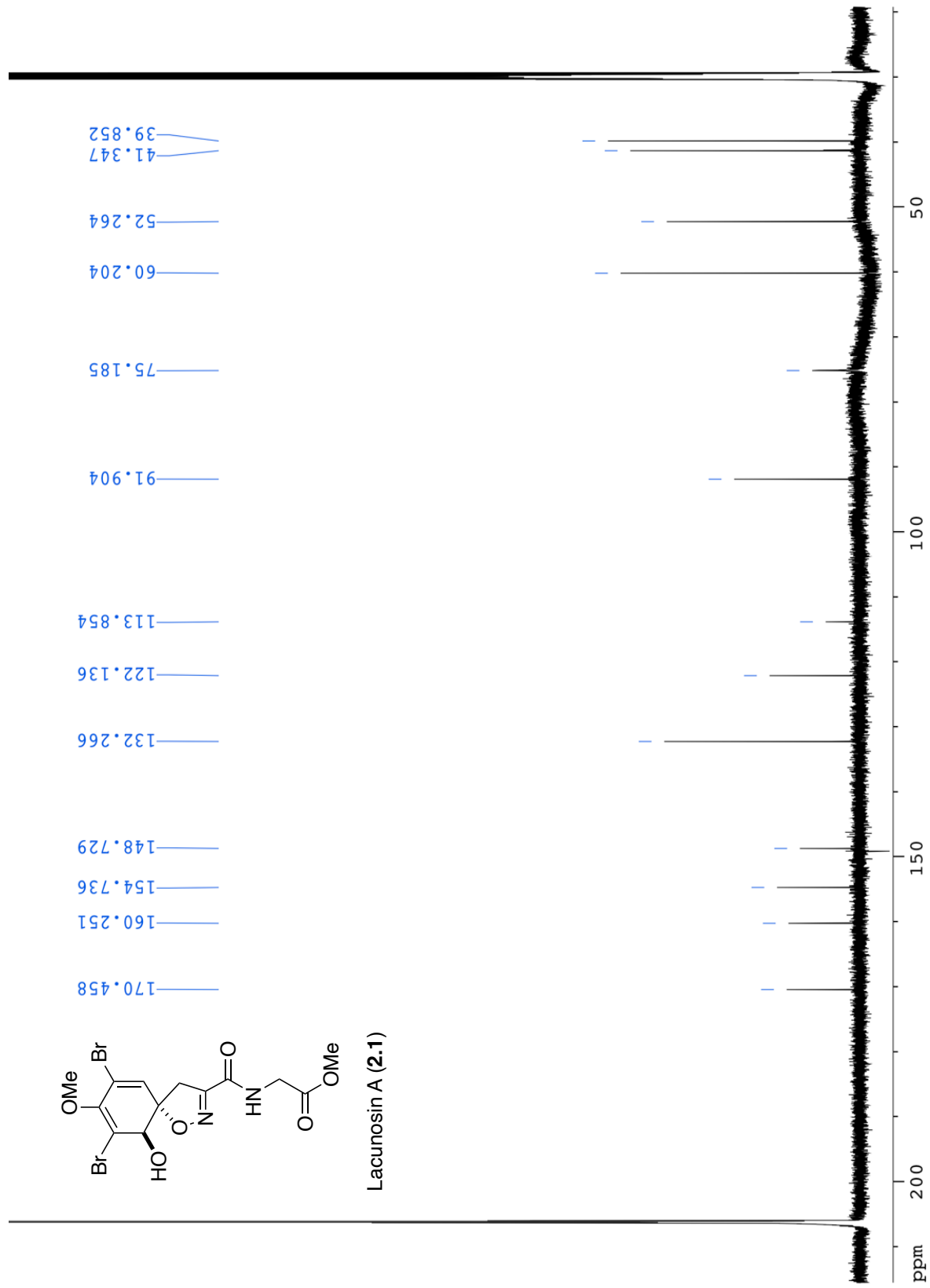


Figure 2.9: ^{13}C NMR of Compound 2.1 (125 MHz, $(\text{CD}_3)_2\text{CO}$).

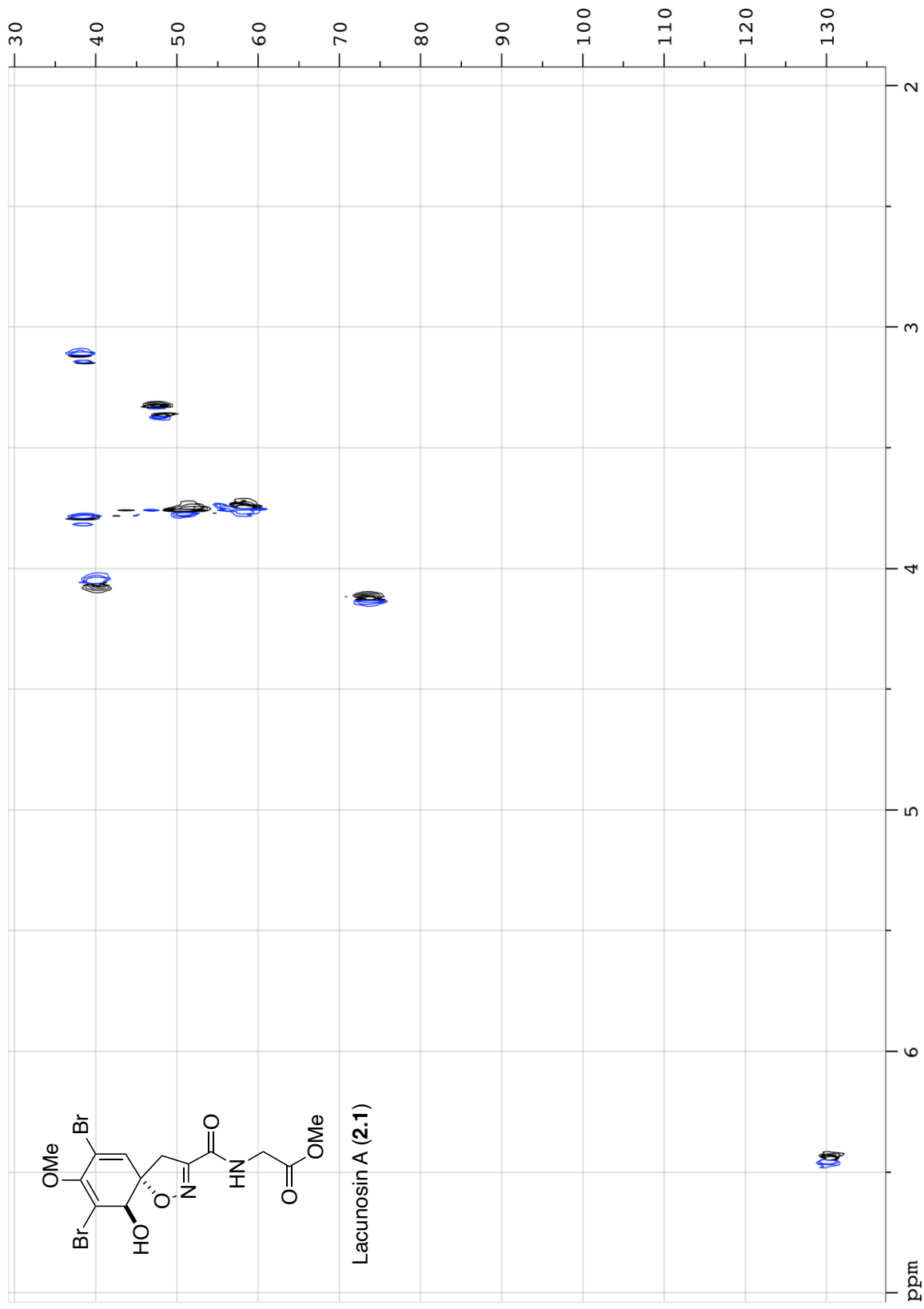
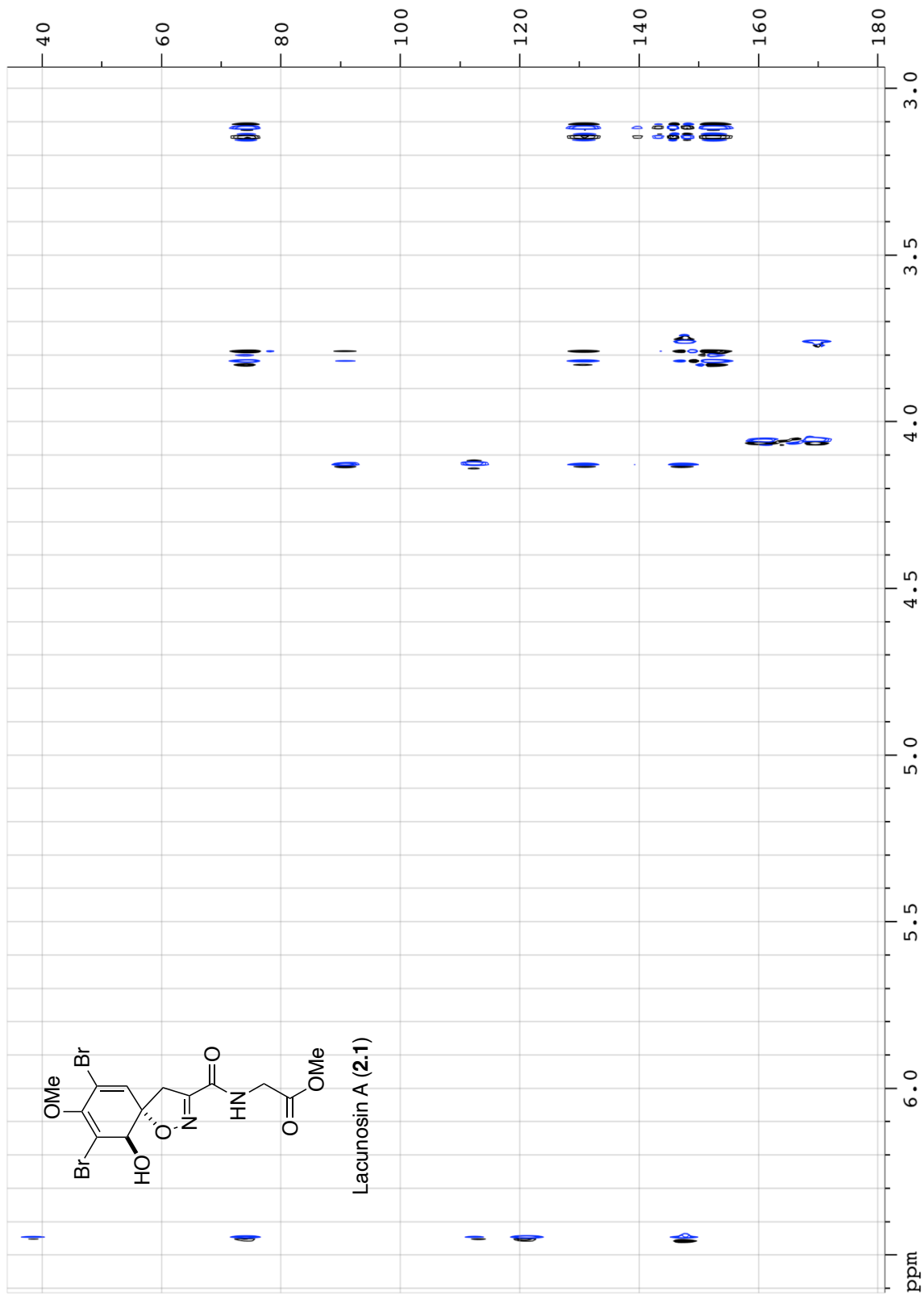


Figure 2.10: HSQC of Compound 2.1 (600 MHz, CD₃OD).



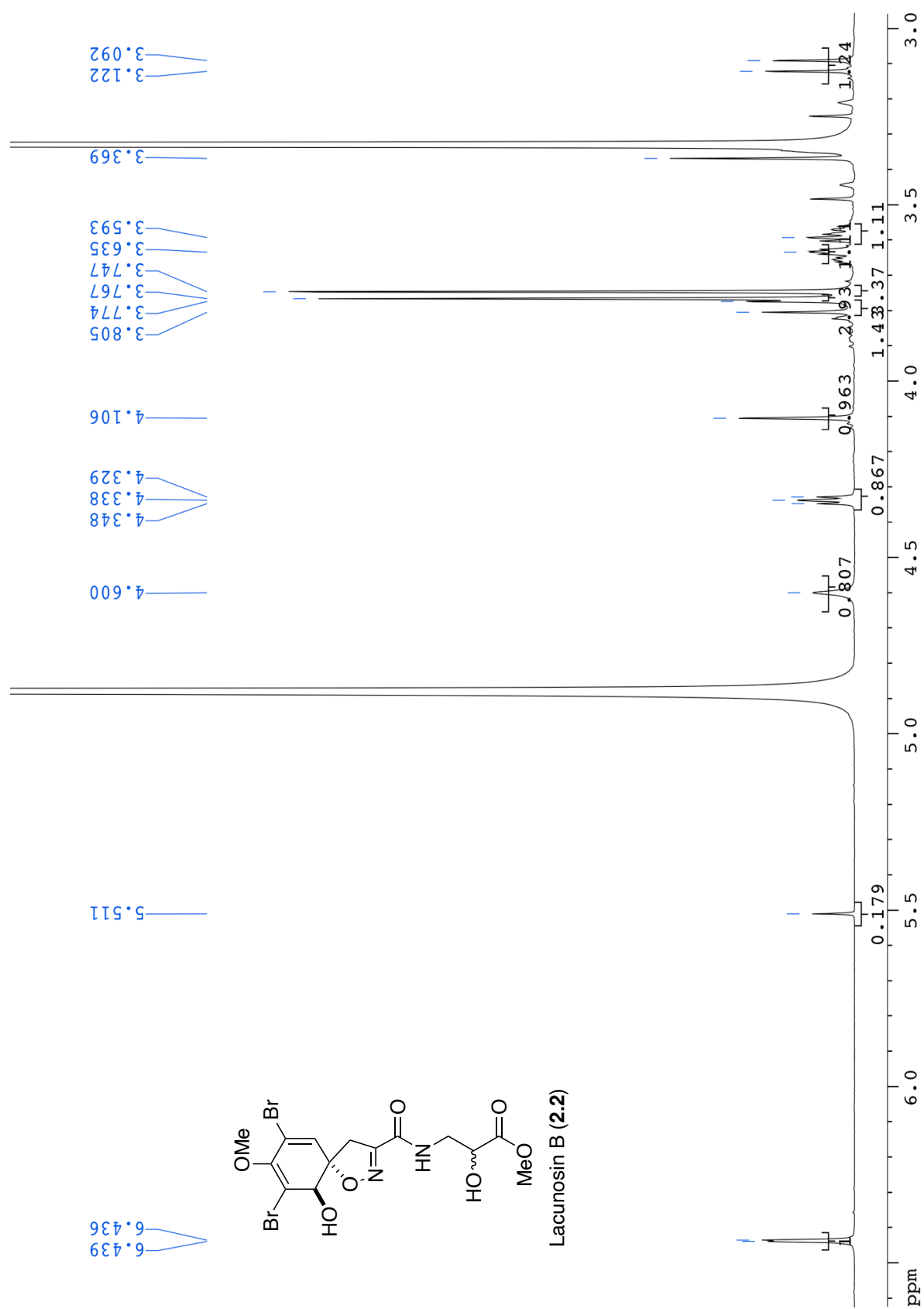




Figure 2.13: DQF-COSY of Compound 2.2 (600 MHz, CD₃OD).

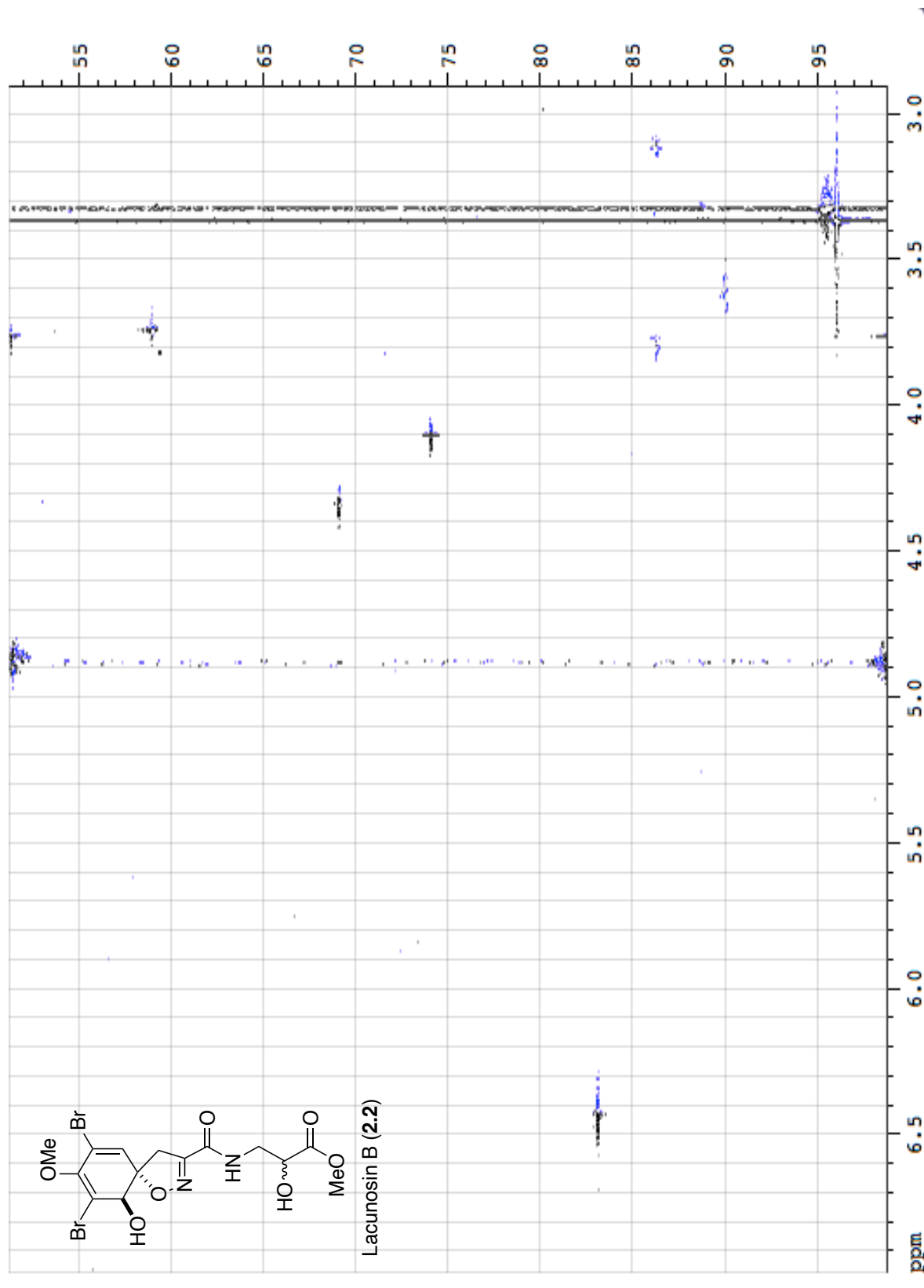


Figure 2.14: HSQC of Compound 2.2 (600 MHz, CD₃OD).

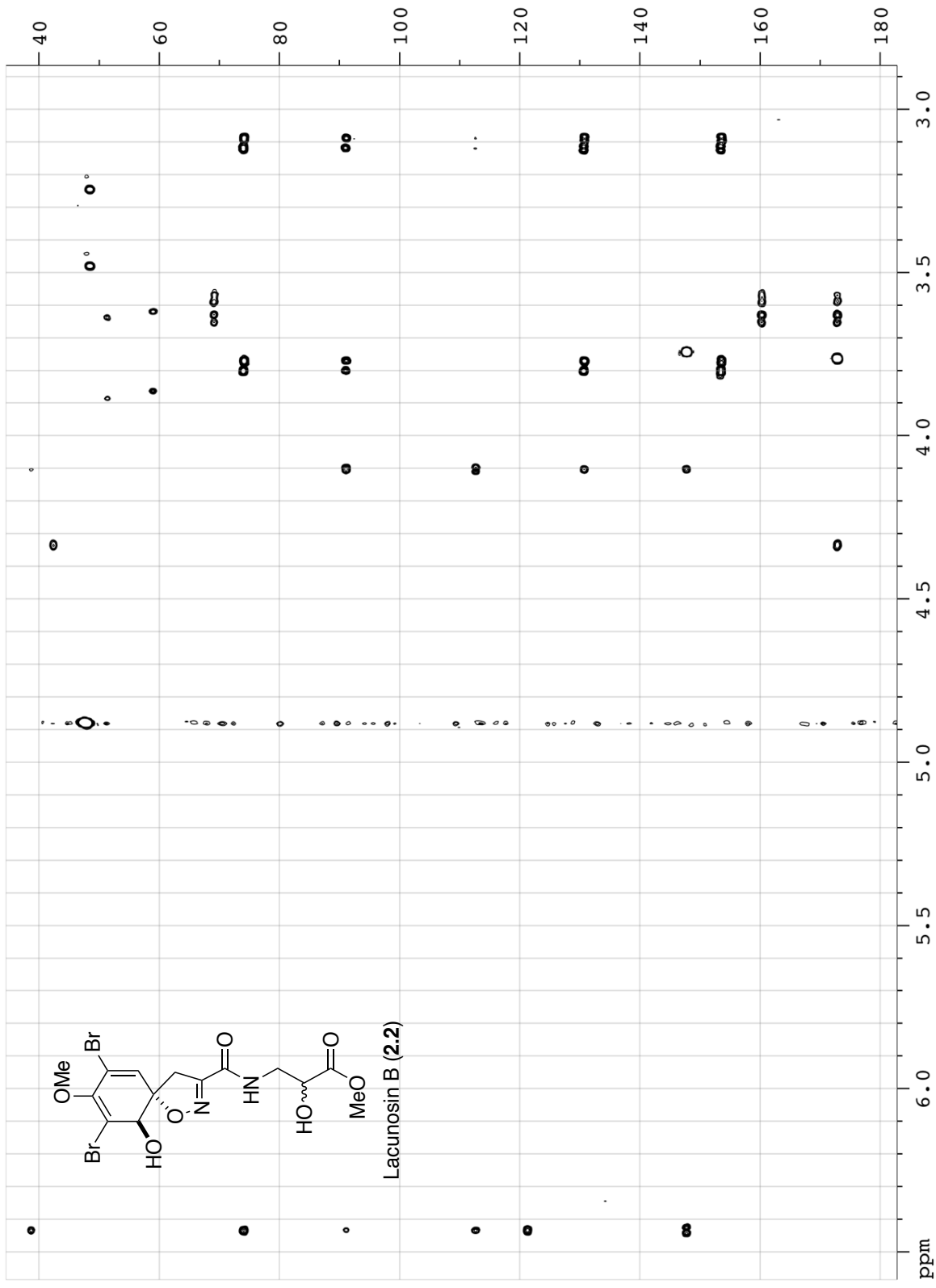


Figure 2.15: HMBC of Compound 2.2 (600 MHz, CD₃OD).

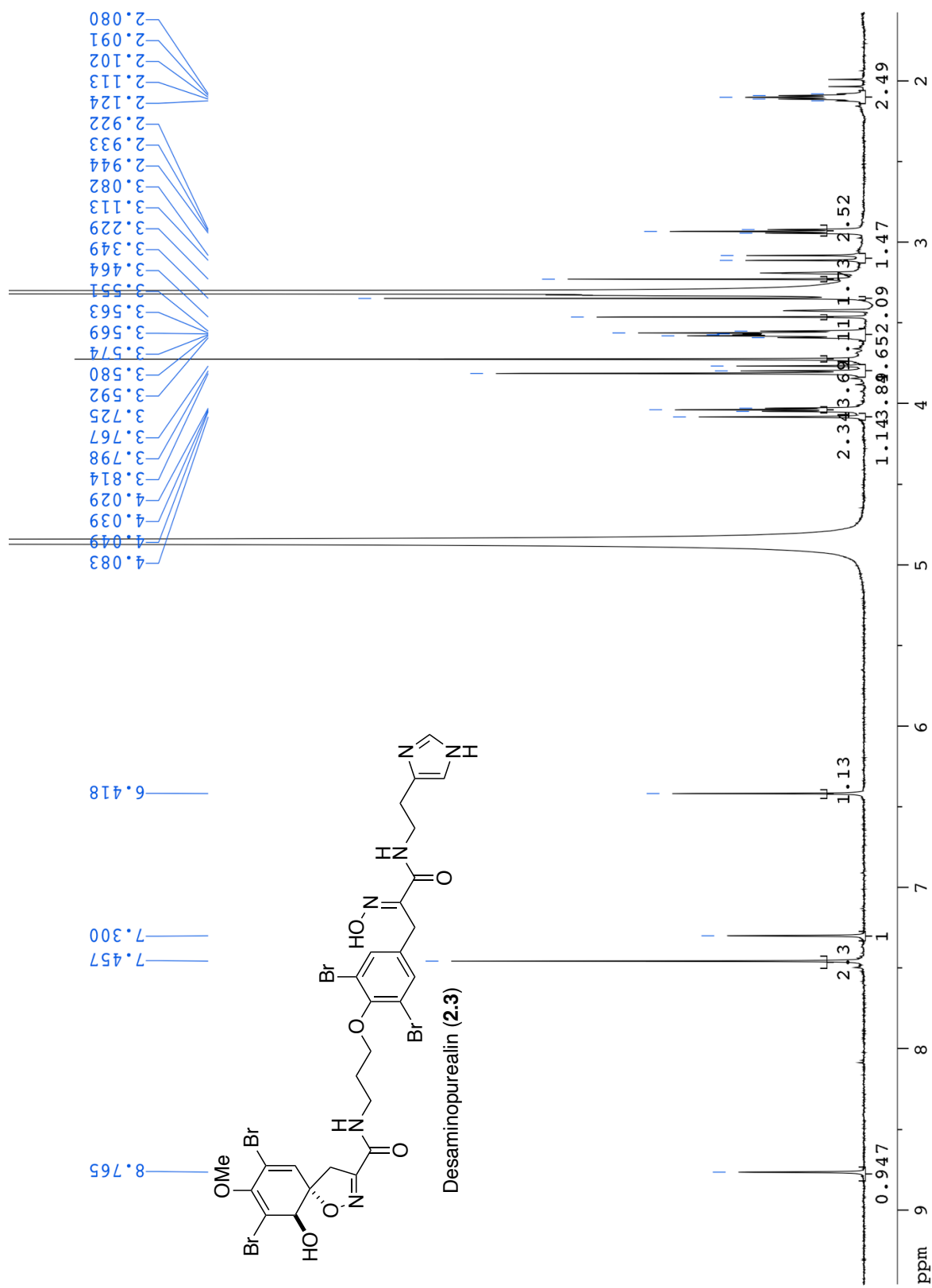


Figure 2.16: ¹H NMR of Compound 2.3 (600 MHz, CD₃OD).

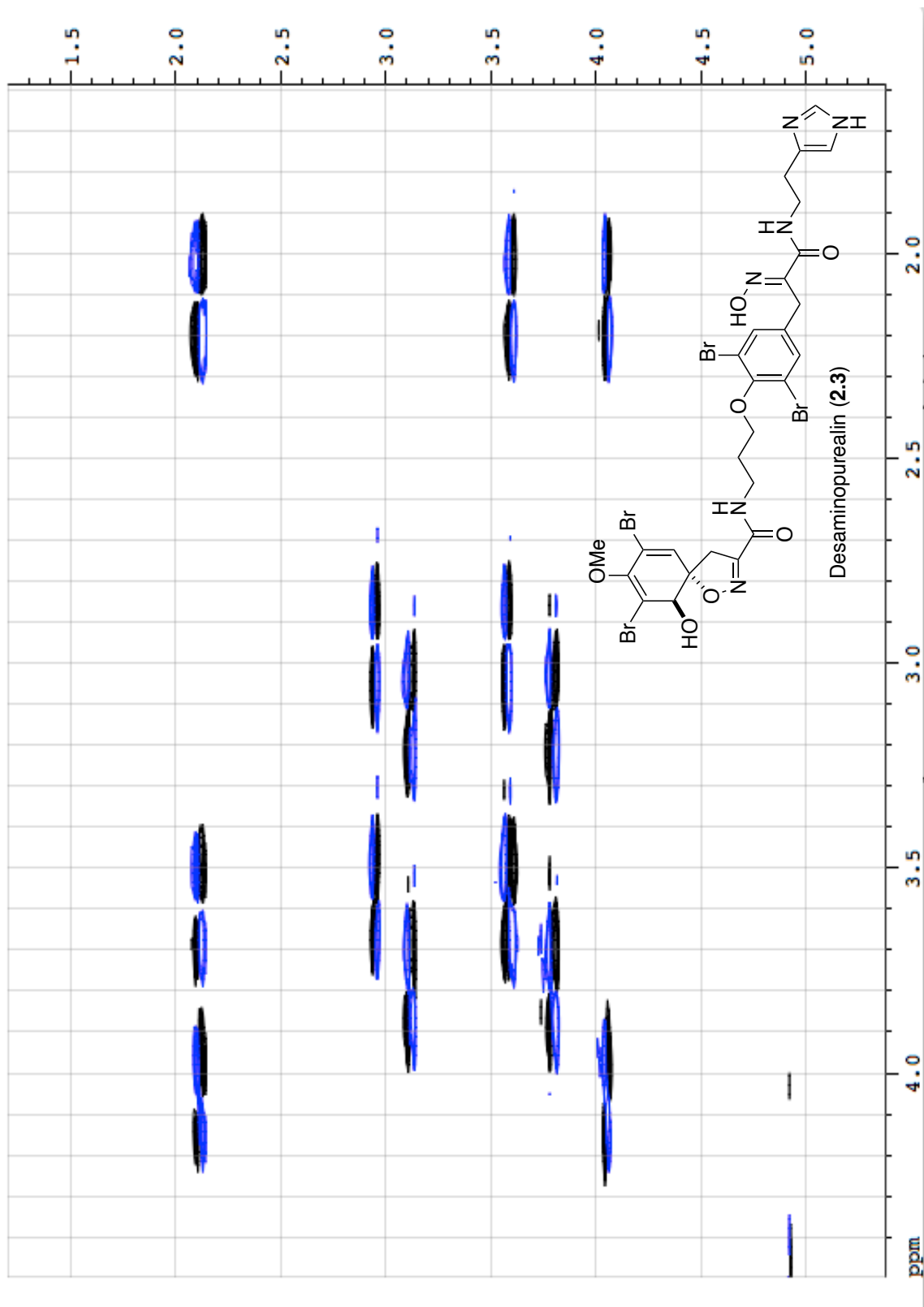
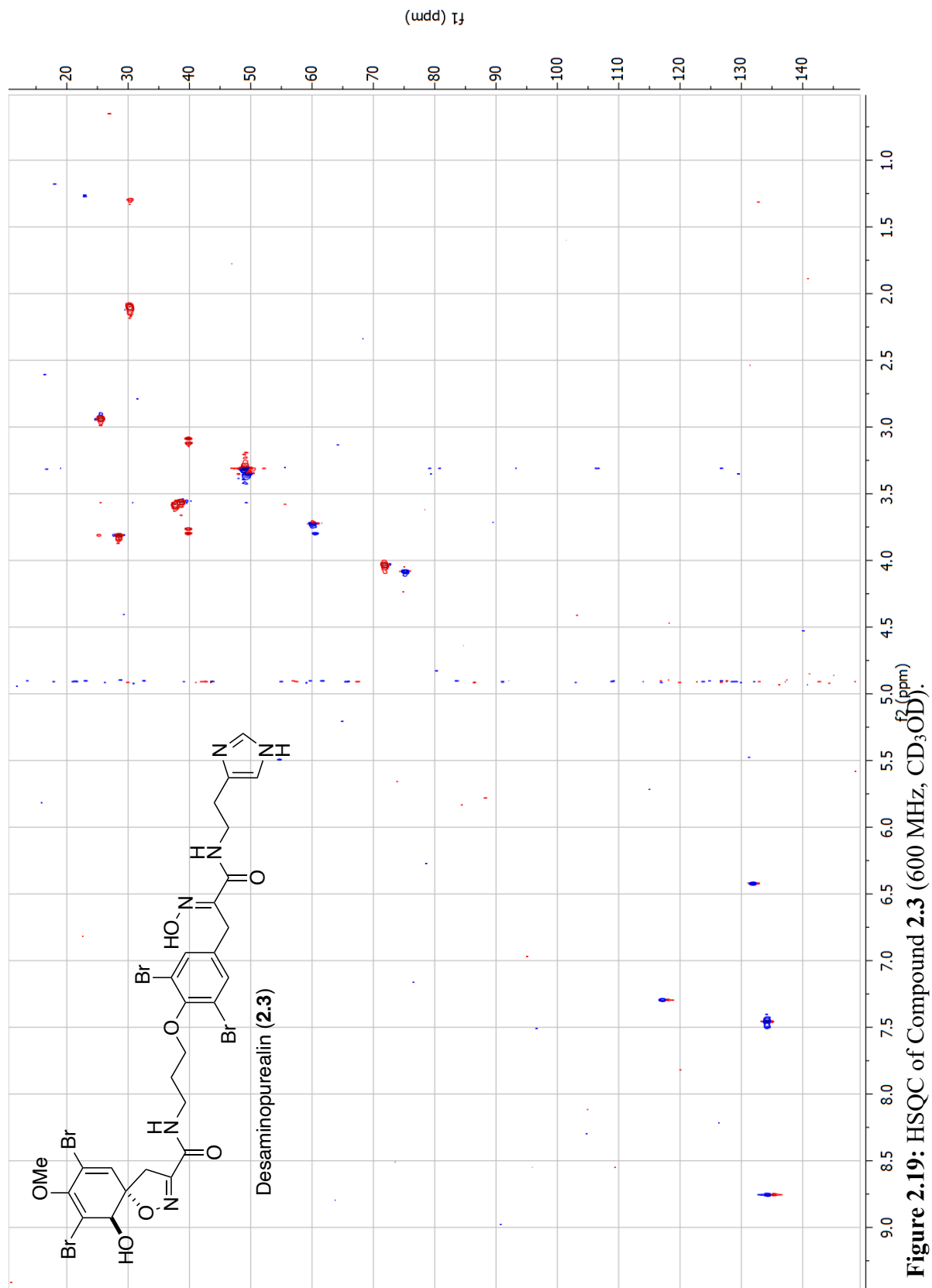
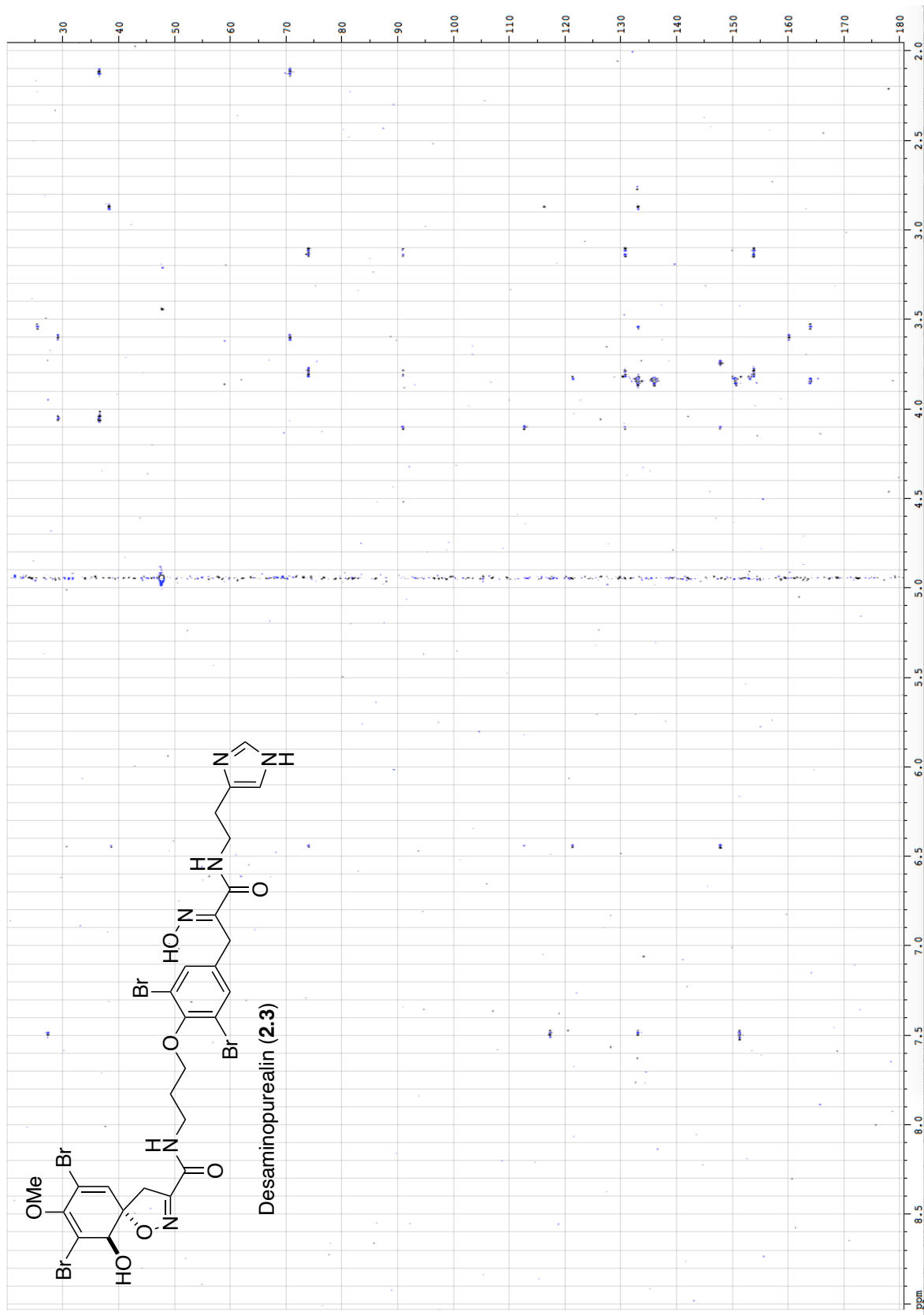


Figure 2.18: DQF-COSY of Compound **2.3** (600 MHz, CD₃OD).





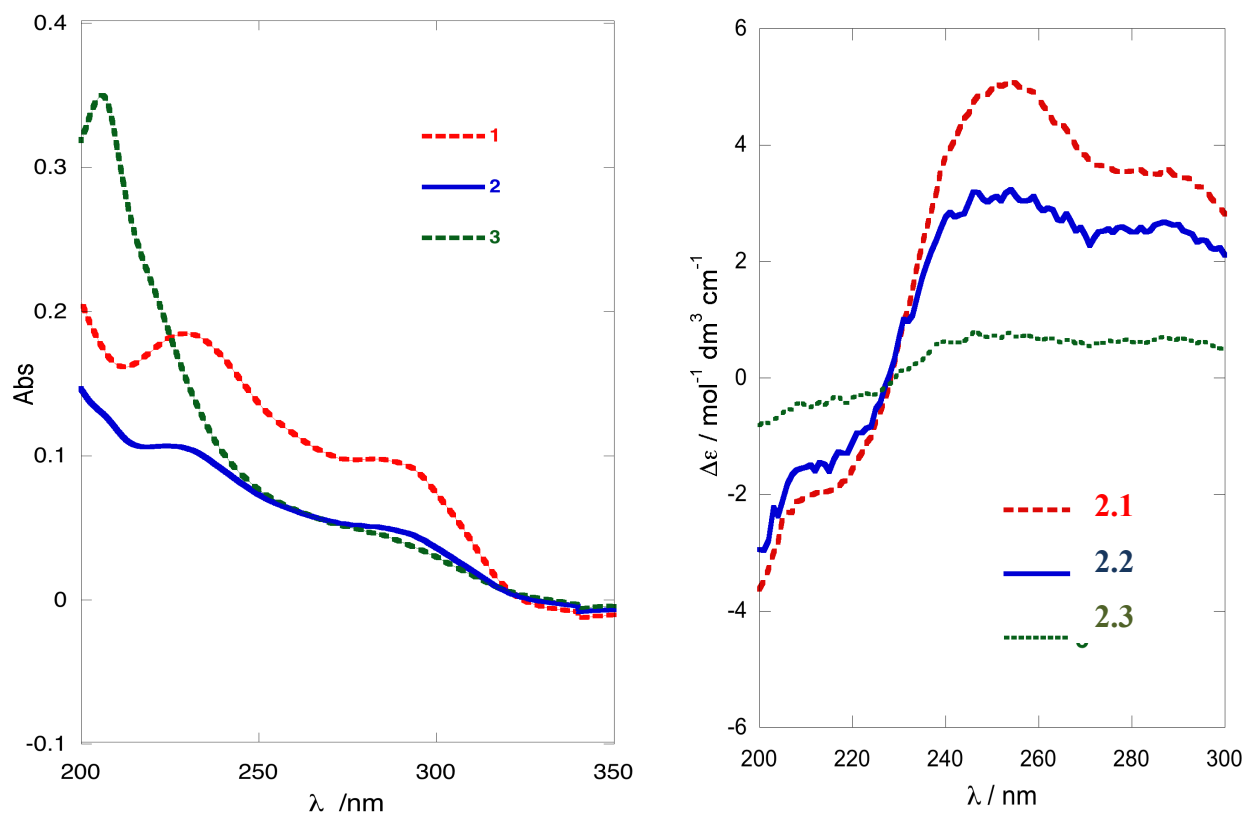


Figure 2.21: (a) UV-vis and (b) CD of Compounds **2.1** ($c = 3.93 \times 10^{-4}$ M), **2.2** (3.56×10^{-4} M) and **2.3** (4.63×10^{-4} M) (MeOH, 23 °C).

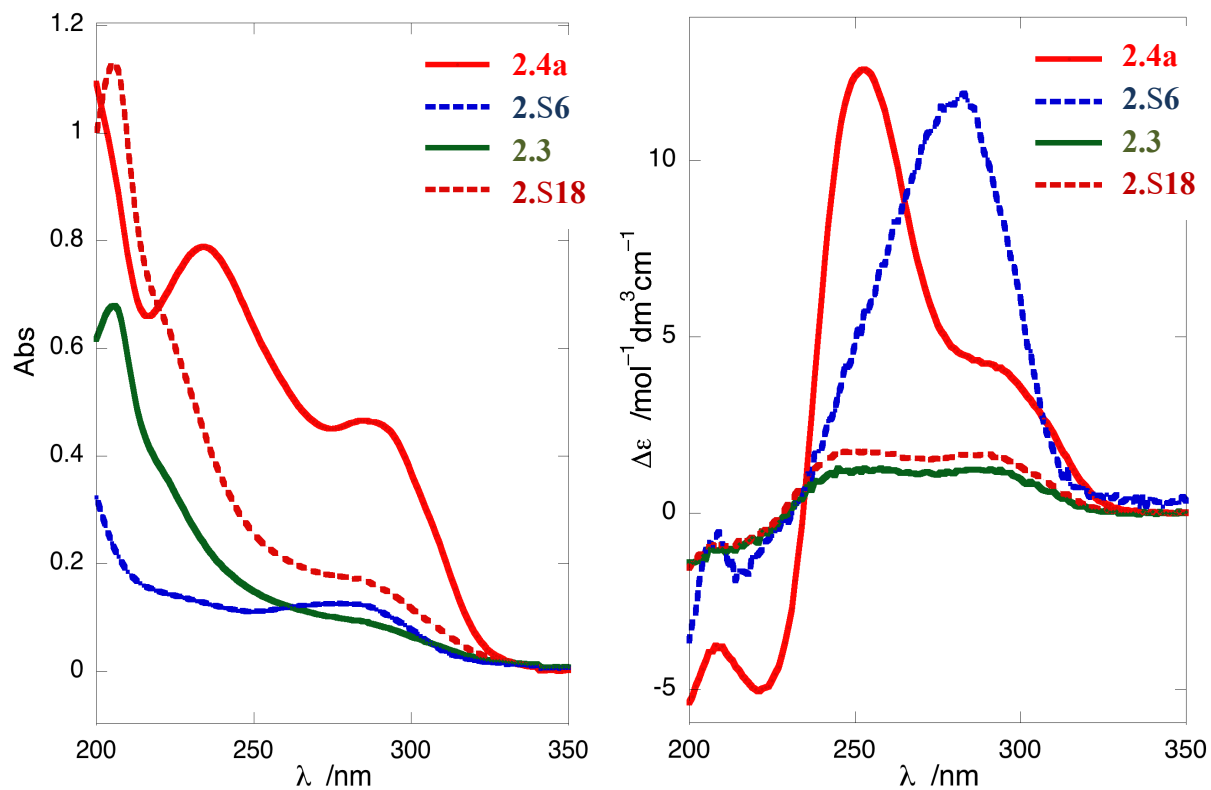
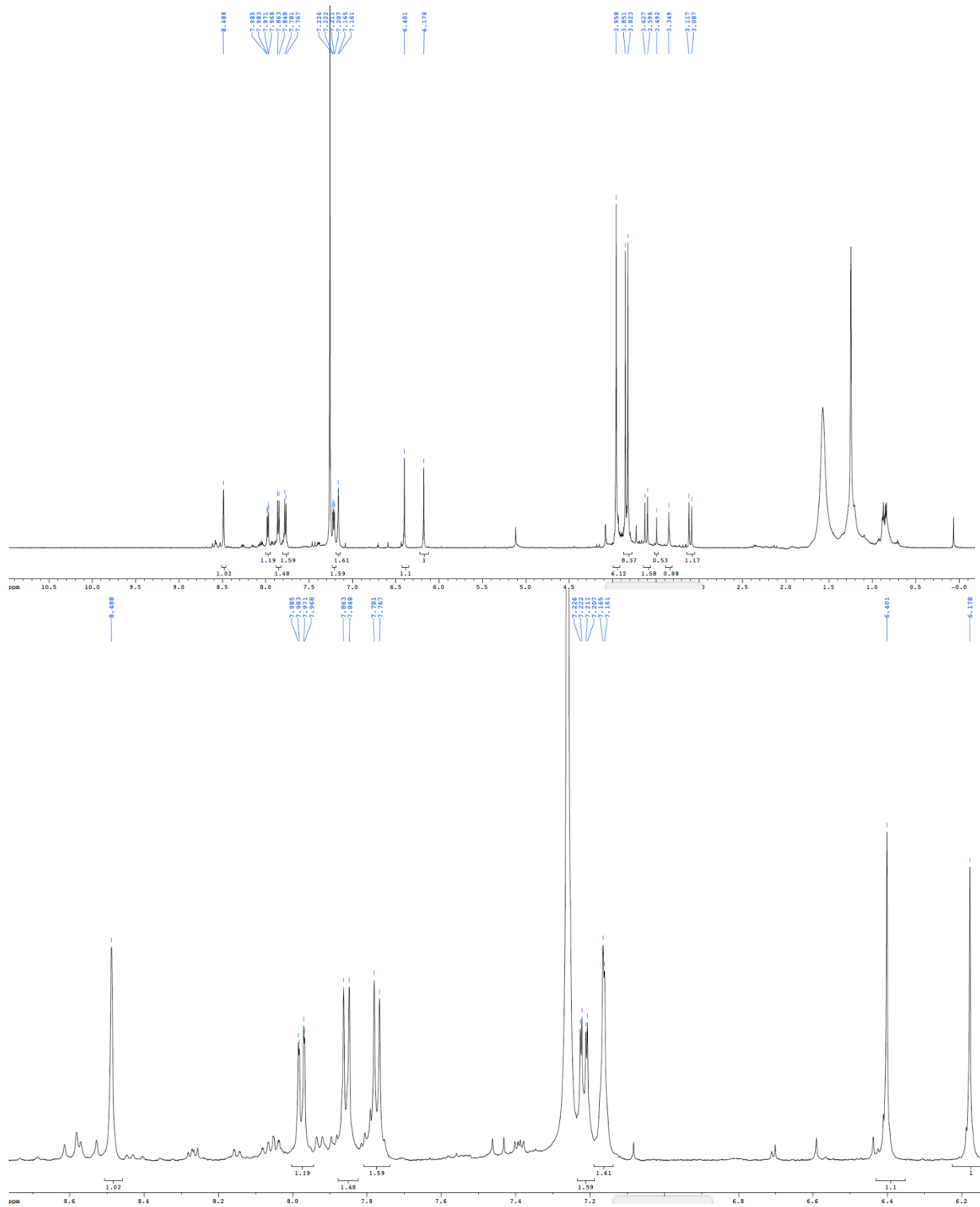


Figure 2.22: (a) UV-vis and (b) CD of Compounds **2.3** ($c = 5.06 \times 10^{-4}$ M), **2.4a** (1.07×10^{-3} M), **2.S6** (1.80×10^{-4} M) and **2.S18** (9.17×10^{-4} M) (MeOH, 23 °C).



2.7 References and Notes

- (1) Peng, J.; Li, J.; Hamann, M. T. *Alkaloids Chem. Biol.* **2005**, *61*, 59-262.
- (2) Lira, N. S.; Montes, R. C.; Tavares, J. F.; da Silva, M. S.; da Cunha, E. V.; de Athayde-Filho, P. F.; Rodrigues, L. C.; da Silva Dias, C.; Barbosa-Filho, J. M. *Mar. Drugs* **2011**, *9*, 2316-2368.
- (3) Ueberlein, S.; Machill, S.; Schupp, P. J.; Brunner, E. *Mar. Drugs* **2017**, *15*, 34-49.
- (4) Ueberlein, S.; Machill, S.; Niemann, H.; Proksch, P.; Brunner, E. *Mar. Drugs* **2014**, *12*, 4417-4438.
- (5) (a) Kobayashi, J.; Tsuda, M.; Agemi, K.; Shigemori, H.; Ishibashi, M.; Sasaki, T.; Mikami, Y. *Tetrahedron* **1991**, *47*, 6617-6622. (b) Andersen, R. J.; Faulkner, D. J. *Tetrahedron Lett.* **1973**, *14*, 1175-1178. (c) Gao, H.; Kelly, M.; Hamann, M. T. *Tetrahedron* **1999**, *55*, 9717-9726.
- (6) De Medeiros, A.; Gandolfi, R. C.; Secatto, A.; Falcucci, R. M.; Faccioli, L. H.; Hajdu, E.; Peixinho, S.; Berlinck, R. G. S. *Immunopharmacol. Immunotoxicol.* **2012**, *34*, 919-924.
- (7) (a) Shaala, L. A.; Youssef, D. T. A.; Badr, J. M.; Sulaiman, M.; Khedr, A. *Mar. Drugs*. **2015**, *13*, 1621-1631. (b) Göthel, Q.; Sirirak, T.; Köck, M. *Beilstein J. Org. Chem.* **2015**, *11*, 2334-2342.
- (8) Nicacio, K. J.; Ióca, L. P.; Fróes, A. M.; Leomil, L.; Appolinario, L. R.; Thompson, C. C.; Thompson, F. L.; Ferreira, A. G.; Williams, D. E.; Andersen, R. J.; Eustaquio, A. S.; Berlinck, R. G. S. *J. Nat. Prod.* **2017**, *80*, 235-240.
- (9) Fattorusso, E.; Minale, L.; Sodano, G. *Chem. Commun.* **1970**, 751-752.
- (10) Gunasekera, M.; Gunasekera, S. P. *J. Nat. Prod.* **1989**, *52*, 753-756.
- (11) Cimino, G.; De Rosa, S.; De Stefano, S.; Self, R.; Sodano, G. *Tetrahedron Lett.* **1983**, *24*, 3029-3032.
- (12) Kobayashi, J.; Honma, K.; Sasaki, T.; Tsuda, M. *Chem. Pharm. Bull.* **1995**, *43*, 403-407.
- (13) (a) Nakamura, H.; Wu, H.; Kobayashi, J. i.; Nakamura, Y.; Ohizumi, Y.; Hirata, Y. *Tetrahedron Lett.* **1985**, *26*, 4517-4520. (b) Nakamura, Y.; Kobayashi, M.; Nakamura, H.; Wu, H.; Kobayashi, J.; Ohizumi, Y. *Eur. J. Biochem.* **1987**, *167*, 1-6.
- (14) (a) Ciminiello, P.; Fattorusso, E.; Magno, S.; Pansini, M. *J. Nat. Prod.* **1994**, *57*, 1564-1569. (b) Zhu, G.; Yang, F.; Balachandran, R.; Höök, P.; Vallee, R. B.; Curran, D. P.; Day, B. W. *J. Med. Chem.* **2006**, *49*, 2063-2076. (c) Shearman, J. W.; Myers, R. M.; Brenton, J.

-
- D.; Ley, S. V. *Org. Biomol. Chem.* **2011**, *9*, 62-65.
- (15) Two lines of evidence to support the presence of thermodynamically more stable *E*-geometry include the C-17 chemical shift (δ_c 27.4; c.f. *E,E*-psammaplyin A, δ 27.1. (a) Arabshahi, L.; Schmitz, F. J. *J. Org. Chem.* **1987**, *52*, 3584-3586), and the consistent presence of a hydrogen bond between the oxime N and the amide NH observed in X-ray structures (b) Kazlauskas, R.; Lidgard, R. O.; Murphy, P. T.; Wells, R. J.; Blount, J. F. *Aust. J. Chem.* **1981**, *34*, 765-786. Natural products with the rare less-stable *Z*-geometry (viz. bastadin isomers) have been documented. (c) Calcul, L.; Inman, W. D.; Morris, A. A.; Tenney, K.; Ratnam, J.; McKerrow, J. H.; Valeriote, F. A.; Crews, P. *J. Nat. Prod.* **2010**, *73*, 365-372.
- (16) Marfey, P. *Carlsberg Res. Commun.* **1984**, *49*, 591-196.
- (17) Salib, M. N.; Molinski, T. F. *J. Org. Chem.* **2017**, *82*, 10181–10187.
- (18) The Marfey's derivatives L- and D-*iso*Ser-L-DAA (Ref. 16), prepared from standard *iso*Ser samples and L-FDAA, failed to separate under the same reversed phase HPLC conditions.
- (19) Duplication of the H-5 vinyl ^1H NMR signal ($\Delta\delta = 0.003$; Table 2.1) is also observed.
- (20) Castillo, A. M.; Patiny, L.; Wist, J. *J. Magn. Reson.* **2011**, *209*, 123-130.
- (21) This is not contradictory to our independent findings that the epimer ratio of *iso*Ser in **2.2** is 1:1 but 67:33 of the SIO heterocycle (see Note 27, below and discussion in the text). For simplicity of argument, if the latter ratio is approximated to 2:1 and the components permuted, the four outcomes are two enantiomeric pairs of diastereomers: (1*S*,6*R*,11*S*), (1*S*,6*R*,11*R*), (1*R*,6*S*,11*R*) and (1*R*,6*S*,11*S*) in the proportions 3:3:2:2. The NMR-distinguishable diastereomers, therefore, are present in the ratio of 5:5 or 1:1
- (22) McMillan, J. A.; Paul, I. C.; Goo, Y. M.; Rinehart, K. L.; Krueger, W. C.; Pschigoda, L. M. *Tetrahedron Lett.* **1981**, *22*, 39-42.
- (23) Fattorusso, E.; Minale, L.; Sodano, G. *Chem. Commun.* **1970**, 752-753.
- (24) Fulmor, W.; Van Lear, G. E.; Morton, G. O.; Mills, R. D. *Tetrahedron Lett.* **1970**, *11*, 4551-4552.
- (25) Moscowitz, A.; Charney, E.; Weiss, U.; Ziffer, H. *J. Am. Chem. Soc.* **1961**, *83*, 4661-4663.
- (26) Burgstahler, A. W.; Ziffer, H.; Weiss, U. *J. Am. Chem. Soc.* **1961**, *83*, 4660-4661.
- (27) MMFF. Molecular modeling of aeroplysillin-1 shows the diene has similar helicity (this work, MMFF, dihedral $\theta = \pm 17.6^\circ$), in good correspondence with the X-ray crystal structure assignments of both (+)- and (-)-aeroplysillin-1 ($\theta = 17.3 \pm 1^\circ$). Cosulich, D. B.; Lovell, F. M. *Chem. Commun.* **1971**, 397-398.

-
- (28) If one assumes, for example, highly dichroic (+)-aerothionin (**S2**, Table 2.2) is optically pure (“100% ee”, also see Note 38), the ratio of CE magnitudes of **S2** and **2.2** implies the latter is only 19.3% ee (er = 63:37). Lack of precision of ECD measurements on sub-milligram sample of **2.2** limits the accuracy of this conclusion.
- (29) We have found the effects of more distal stereocenters in SIOs upon the net ECD spectrum, e.g. fistularin-3 and 11-hydroxyfistularin-3, to be negligible.
- (30) Another possibility we considered is that **2.4c** is formed as a racemic or near-racemic modification and kinetically resolved in downstream enzymatic coupling reactions. This possibility would explain enantiomeric **2.4c** and fistularin-3 in the same sample. Ref. 48.
- (31) Okamoto, Y.; Ojika, M.; Kato, S.; Sakagami, Y. *Tetrahedron* **2000**, *56*, 5813-5818.
- (32) Kobayashi, J. i.; Tsuda, M.; Agemi, K.; Shigemori, H.; Ishibashi, M.; Sasaki, T.; Mikami, Y. *Tetrahedron* **1991**, *47*, 6617-6622.
- (33) Benharref, A.; Païs, M.; Debitus, C. *J. Nat. Prod.* **1996**, *59*, 177-180.
- (34) Salim, A. A.; Khalil, Z. G.; Capon, R. J. *Tetrahedron* **2012**, *68*, 9802-9807.
- (35) Kijjoa, A.; Bessa, J.; Wattanadilok, R.; Sawangwong, P.; Nascimento, M. S. J.; Pedro, M.; Silva, A. M. S.; Eato, G.; van Soest, R.; Herz, W. *Z. Naturforsch., B: Chem. Sci.* **2005**, *60*, 904-908.
- (36) From values of $[\alpha]_D$, we estimate the Karuso sample of (–)-**8b** from NW Australia to be only 7% ee – rather than a different ionization state, as speculated by the authors – to our sample of (+)-**8b** from the Bahamas (Ref. 50).
- (37) Ragini, K.; Fromont, J.; Piggott, A. M.; Karuso, P. *J. Nat. Prod.* **2017**, *80*, 215-219.
- (38) It is perhaps no coincidence that earlier-reported SIOs, purified by crystallization (e.g. (+)-aerothionin, Ref. 22), are optically enriched through the process and have the highest values.
- (39) (a) Gonnella, N. C.; Nakanishi, K.; Martin, V. S.; Sharpless, K. B. *J. Am. Chem. Soc.* **1982**, *104*, 3775-3776. (b) Harada, N.; Iwahuchi, J. Yokota, Y.; Uda, H. A. *J. Am. Chem. Soc.* **1981**, *103*, 5590-5591
- (40) The 6-methoxy-substituted naphthoic acid was chosen for its stronger electronic transition dipole moment (donor-acceptor effect).
- (41) Gopichand, Y.; Schmitz, F. J. *Tetrahedron Lett.* **1979**, *20*, 3921-3924.

-
- (42) König, G. M.; Wright, A. D. *Heterocycles* **1993**, *36*, 1351-1358.
- (43) Nuñez, C. V.; de Almeida, E. V. R.; Granato, A. C.; Marques, S. O.; Santos, K. O.; Pereira, F. R.; Macedo, M. L.; Ferreira, A. G.; Hajdu, E.; Pinheiro, U. S.; Muricy, G.; Peixinho, S.; Freeman, C. J.; Gleason, D. F.; Berlinck, R. G. S. *Biochem. Syst. Ecol.* **2008**, *36*, 283-296.
- (44) Ciminiello, P.; Costantino, V.; Fattorusso, E.; Magno, S.; Mangoni, A.; Pansini, M. *J. Nat. Prod.* **1994**, *57*, 705-712.
- (45) Lira, T. O. d.; Berlinck, R. G. S.; Nascimento, G. G. F.; Hajdu, E. *J. Braz. Chem. Soc.* **2006**, *17*, 1233-1240.
- (46) Abou-Shoer, M. I.; Shaala, L. A.; Youssef, D. T. A.; Badr, J. M.; Habib, A.-A. M. *J. Nat. Prod.* **2008**, *71*, 1464-1467.
- (47) Carney, J. R.; Rinehart, K. L. *J. Nat. Prod.* **1995**, *58*, 971-985.
- (48) Aiello, A.; Fattorusso, E.; Menna, M.; Pansini, M. *Biochem. Syst. Ecol.* **1995**, *23*, 377-281.
- (49) Compound **2.4c** is likely the precursor to all SIOs.
- (50) Rogers, E. W.; Molinski, T. F. *J. Nat. Prod.* **2007**, *70*, 1191-1194.
- (51) Counter examples of biosynthesized carboxylic acid methyl esters have been described. (a) Molinski, T. F.; Ireland, C. J. *J. Org. Chem.* **1988**, *53*, 2103-2105. (b) Ferreira, E.L.F.; Williams, D.E.; Ióca, L.P.; Morais-Urano, R.P.; Santos, M.F.C.; Patrick, B.O.; Elias, L.M.; Lira, S.P.; Ferreira, A.G.; Passarini, M.R.Z.; Sette, L.D.; Andersen, R.J.; Berlinck, R.G.S. *Org. Lett.* **2015**, *17*, 5152-5155.
- (52) Rogers, E. W.; Fernanda de Oliveira, M.; Berlinck, R. G. S.; König, G. M.; Molinski, T. F. *J. Nat. Prod.* **2005**, *68*, 891-896.
- (53) Owen, T. C.; Merkler, D. J. *Medical Hypotheses* **2004**, *62*, 392-400.
- (54) Yang, K.; Fen, J.; Fang, H.; Zhang, L.; Gong, J.; Xu, W. *J. Enzym. Inhib. Med. Chem.* **2012**, *27*, 302-310.

CHAPTER THREE. DISCOVERY OF SPIROISOXAZOLINE INHIBITORS OF
ACETYLCHOLINESTERASE FROM *PSEUDOCERATINA VERRUCOSA*

Abstract: Examination of the MeOH extract of the Western Australian sponge, *Pseudoceratina verrucosa*, collected near Ningaloo Reef, for selective acetylcholinesterase (AChE) inhibitors, yielded five new bromotyrosine alkaloids, methyl purpuroceratates A and B (**3.1b** and **3.2b**), purpuroceratic acid C (**3.3a**) and ningalamides A and B (**3.4** and **3.5**). The structures of **3.1–3.4** share the dibromo-spirocyclohexadienyl-isoxazoline (SIO) ring system found in purealidin-R while ketoxime **3.5** is analogous to ianthelline and purpurealidin I. The planar structures of all five compounds were obtained from analysis of MS, 1D and 2D NMR data, and the absolute configuration of the spiroisoxazoline (SIO) unit was assigned by electronic circular dichroism (ECD) and comparison with standards prepared by total synthesis of methyl purpuroceratate C, (\pm)-**3.3b**. Compound **3.4** is the most complex SIO described, to date. The configuration of the homoserine subunit (C) in **3.4** was ascertained, after acid hydrolysis, with an L-tryptophanamide derivative based on Marfey's method. Chiral-phase HPLC, with comparison to synthetic standards, revealed that most SIOs isolated from *P. verrucosa* were configurationally heterogeneous; some, essentially racemic. Chiral-phase HPLC, with UV-ECD detection is demonstrated as a superlative method for configurational assignment and quantitation of the enantiomeric composition of SIOs. Two SIOs – aerophobin-1 and aplysinamisine II – emerged as selective inhibitors of AChE over butyrylcholinesterase (BuChE, IC₅₀ ratio >10) while aplysamine-2 moderately inhibited both cholinesterase (ChEs, IC_{50, AChE} 0.46 μ M, IC_{50, BuChE} 1.03 μ M). SIO alkaloids represent a potentially new structural manifold for lead-discovery of new therapeutics for treatment of Alzheimer's disease.

3.1 Introduction

Marine sponges (Porifera), mainly in the order Verongida, are prolific producers of bromotyrosine (BrTyr) alkaloids. Over 300 bromotyrosine alkaloids of marine origin have been reported in the literature to date.^{1,2} These natural products have modular structures comprising subunits linked by amide bonds or *O*-arylethers between component derived from extensive modifications of the parent amino acids (AAs) 3,5-Br₂Tyr and 3-BrTyr (collectively, Br_xTyr), connected through other AA-derived linkers. Here, the common structural themes of the subunits include decarboxylation of Br_xTyr to brominated phenethylamines, and oxidation of the α -amino group to the corresponding α -ketoximine; a functional group that often suffers further oxidative cyclization to bicyclic spiroisoxazolines (SIOs). Many SIOs have been shown to possess significant bioactivity including antibacterial activity; a subject that has been extensively reviewed.^{3,4} A significant recent finding by Berlinck and coworkers shows that several bromotyrosine-derived natural products, previously known from Verongid sponges, are expressed by a Verongid sponge-derived bacterium, *Pseudovibrio denitrificans* Ab134 under fermentation conditions; a discovery that supports the hypothesis that most, if not all, sponge-associated SIOs are of microbial origin.³ Contemporary drugs for treatment of Alzheimer's disease (AD) address neurotransmitter insufficiency by blocking acetylcholinesterase (AChE) to ameliorate loss of cognitive function. The standard of care is currently the plant alkaloid, galantamine from *Galanthus* spp. and other species. The SIOs, with their unique modular structural motif, were attractive targets for exploring alternatives to galantamine as possible leads for development of AD therapeutics.

In a survey for selective inhibitors of acetylcholinesterase (AChE) over butyrylcholinesterase (BuChE) from marine invertebrates, extracts of a sample of *Pseudoceratina*

verrucosa from Exmouth Gulf, Indian Ocean, Western Australia, were examined. Here we report the structures of five new Br_xTyr alkaloids: purpuroceratic acid methyl esters A and B (**3.1b**, **3.2b**),^{5,6} purpuroceratic acid C (**3.3a**), ningalamide A (**3.4**), and ningalamide B (**3.5**), in addition to the known compounds purealidin-R (**3.6**),⁴ verongidoic acid methyl ester (+)-**3.7b**,⁷ and other Br_xTyr secondary metabolites (see Experimental). The total synthesis of methyl purpuroceratate C (±)-**3.3b** is described in service as a standard for quantitative analytical methodology to determine %ee of SIOs based on chiral phase-HPLC coupled with electronic circular dichroism (ECD) detection. The structure of compound **3.4** is the most complex SIO reported to date; all compounds exhibit heterogeneous enantiomeric compositions.

3.2 Isolation and Structure Determination of Methyl Purpuroceratates A and B and Purpuroceratic Acid C

The MeOH extract of *Pseudoceratina verrucosa* was progressively solvent-partitioned against hexane, CH₂Cl₂, *n*-BuOH, and H₂O to provide four partitions, A–D. Partition B was separated into 11 fractions by size-exclusion chromatography (Sephadex LH-20, CH₃OH). Fractions 3-5 were further purified by reversed-phase HPLC (C₁₈) to deliver **3.1–3.5** in addition to known compounds purpuroceratic acids A (**3.1a**)⁶ and B (**3.2a**),^{6,8} purealidin R (**3.6**),⁴ verongidoic acid methyl ester (**3.7b**),⁷ aerophobin-1 (**S3.1**, for structures, see Appendix),⁹ aerophobin-2 (**S3.2**),^{9b} *N*-methyl-aerophobin-2 (**S3.3**),¹⁰ purealidin J (**S3.4**), and K (**S3.5**),⁴ 14-oxo-aerophobin-2 (**S3.6**),¹¹ aplysinamisine II (**S3.7**),¹² pseudoceratinamide A (**S3.8**),¹³ purpurealidin J (**S3.9**),¹⁴ hexadellin C (**S3.10**),¹⁵ purpuramine I (**S3.12**),¹⁶ and araplysillin-III (**S3.13**).¹⁵

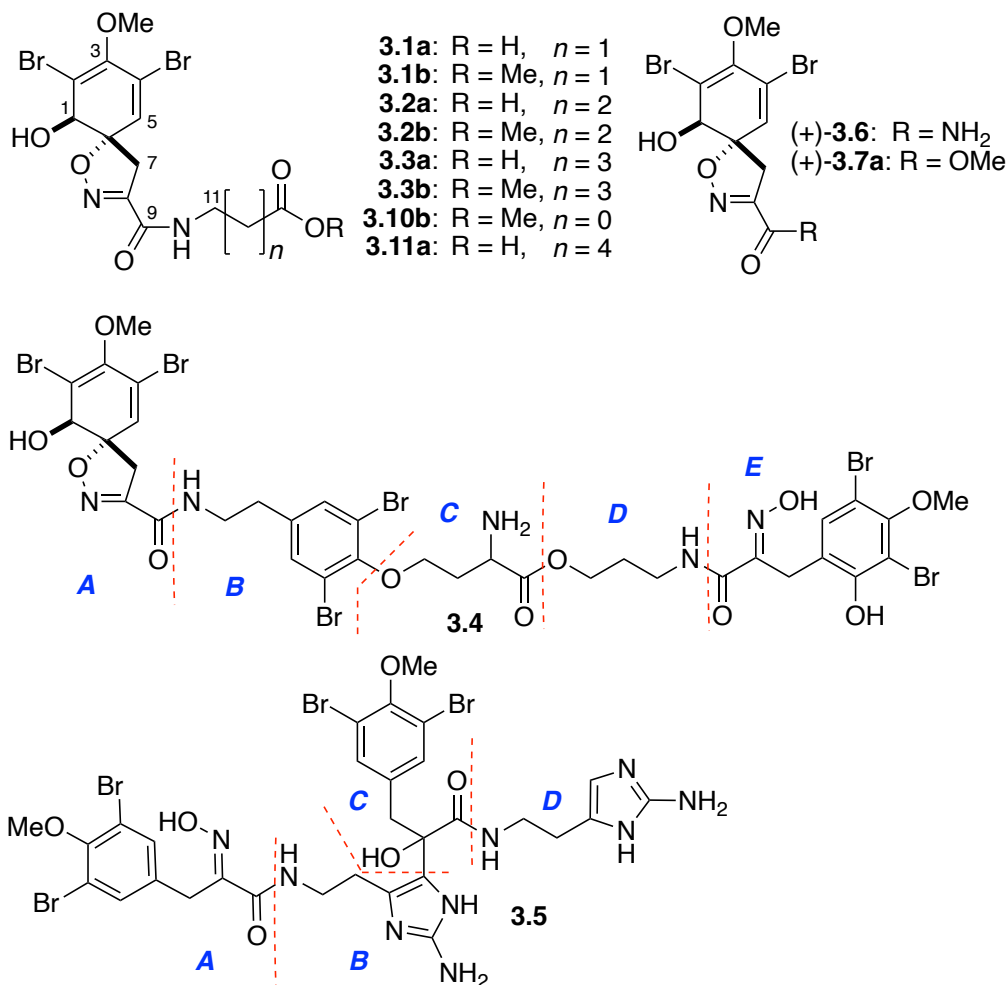


Figure 3.1: The structures of purpuroceratic acid methyl esters A (**3.1b**) and B (**3.2b**), purpuroceratic acid C (**3.3a**), ningalamide A (**3.4**), and ningalamide B (**3.5**), in addition to other known compounds.

The HRMS of **3.1b** and **3.2b** confirmed their molecular formulas of C₁₄H₁₆Br₂N₂O₄ (m/z 488.9254; calcd 488.9254 for C₁₄H₁₆Br₂N₂O₄Na⁺) and C₁₅H₁₈Br₂N₂O₆ (m/z 502.9416; calcd 488.9254 for C₁₅H₁₈Br₂N₂O₆Na⁺), respectively; the isotopic patterns of both ions indicated the presence of two Br atoms. The ¹H and ¹³C NMR spectra of **3.1b** and **3.2b** (Table 3.1) were similar to the reported data for purpuroceratic acids A (**3.1a**) and B (**3.2a**),^{6,8} respectively, except for the presence of extra signals due to a methoxyl group at δ_{H} 3.68 (3H, s) and 3.66 (3H, s), and δ_{C} 52.3 ppm, suggesting the corresponding homologous esters, methyl purpuroceratates A and B (**3.1b**–

3.2b). Methyl esters **3.1b–3.2b** could have arisen as artifacts of purification from acid-promoted Fischer-type esterification while standing in CH₃OH solvent, although evidence is lacking.⁵

HRMS of purpuroceratic acid C (**3.3a**) showed an [M+H]⁺ peak at 479.9527 (calcd 479.9532) corresponding to a molecular formula of C₁₅H₁₈Br₂N₂O₆. The isotopic pattern of the protonated molecular ion confirmed two Br atoms. FTIR absorptions at ~3400 and 1680-1670 cm⁻¹ revealed the presence of OH or NH and amide carbonyl groups, respectively. ¹H and ¹³C NMR spectra of **3.3a** were similar with those reported for (+)-purealidin-R (**3.6**)⁴ which suggests the structure of **3.3a** consists of an SIO amide linked to a different side chain as evidenced by ¹H NMR and 2D spectroscopic data: δ_H 6.42 (1H, s), 4.34 (1H, dd, 6.0, 4.8), 3.76 (1H, d, 18.0), 3.09 (1H, d, 18.0), and 3.77 (3H, s) corresponding to the *O*-Me-spiroisoxazoline unit and δ_H 3.35 – 3.32 (2H, m), 2.38 (2H, t, 7.3), and 1.62 (4H, ddt, 13.8, 10.4, 7.2) belonging to the alkyl sidechain. A contiguous ¹H spin system, comprising δ_H 1.62 (4H, ddt, 13.8, 10.4, 7.2) with δ_C 39.2, 34.4, 29.8, and 23.3, along with a carboxyl group signal at δ_C 177.4, correlated to a 4-aminobutanoic acid side chain (Table 3.1). COSY correlations confirmed the spin system and defined the structure as purpuroceratic acid C (homopurpuroceratic acid B, **3.3a**). Treatment of **3.3a** with diazomethane gave the corresponding methyl ester **3.3b** (quantitative). A structure **3.3a**, previously proposed by Nicacio and coworkers, who coined the name ‘homopurpuroceratic acid B’,³ was based on limited LC HRMS and MS-MS data. Here, compound **3.3a**, renamed purpuroceratic acid C for consistency of nomenclature, is fully characterized for the first time.

3.3 Structure Determination of Ningalamides A and B

Ningalamide A (**3.4**) was isolated as a colorless solid with a molecular formula of C₃₅H₃₇Br₆N₅O₁₁ (*m/z* 1176.7582; calcd 1176.7590); the presence of six Br atoms was supported

by the observation of the expected heptet isotopomer cluster in the HRMS spectrum. FTIR absorptions at ~3400 and 1680-1670 cm⁻¹ were consistent with OH or NH and a 2° amide group, respectively.

Table 3.1: ¹H and ¹³C NMR data for **3.1b–3.2b**, and **3.3a** (CD₃OD).

Position	δ_{H} (int., mult, <i>J</i> , Hz) ^a			δ_{C}^b		
	3.1b	3.2b	3.3a	3.1b	3.2b	3.3a
1	4.07 (1H, s)	4.07 (1H, s)	4.07 (1H, s)	75.5	75.5	75.5
2				114.1	114.2	114.6
3				149.3	149.3	149.2
4				122.7	122.7	122.7
5	6.42 (1H, s)	6.42 (1H, s)	6.42 (1H, s)	132.5	132.3	132.2
6				92.4	92.3	92.2
7a	3.76 (1H, d, 18.0)	3.76 (1H, d, 18.0)	3.76 (1H, d, 18.0)	40.1	40.1	40.0
7b	3.09 (1H, d, 18.0)	3.09 (1H, d, 18.0)	3.09 (1H, d, 18.0)	40.1	40.1	40.0
8				155.1	155.2	155.8
9				161.6	161.7	161.5
10	3.52 (2H, t, 6.8)	3.35 – 3.32 (2H, m)	3.35 – 3.32 (2H, m)	36.4	39.7	39.2
11	2.60 (2H, t, 6.8)	2.38 (2H, t, 7.3)	1.62 (2H, ddt, 13.8, 10.4, 7.2)	34.4	25.6	29.8
12		1.85 (2H, q, 7.1)	1.62 (2H, ddt, 13.8, 10.4, 7.2)	173.7	32.0	23.3
13			2.38 (2H, t, 7.3)		175.4	34.4
14						177.4
13-OCH ₃	3.68 (3H, s)			52.3		
14-OCH ₃		3.66 (3H, s)			52.3	
OCH ₃	3.72 (3H, s)	3.73 (3H, s)	3.73 (3H, s)	60.3	60.3	60.3

^a500 MHz. ^b125 MHz.

The ¹H NMR of **3.4** shows more complexity than that of fistularin-3,¹⁷ and revealed the presence of five subunits, A-E, as described below. A terminal SIO (subunit A) was acylated to a 2,6-dibromotyramine (subunit B) that was in turn ether-linked to a homoserine residue (subunit

C). The amino acid was esterified to a 3-amino-1-propanol linker (subunit D) and terminated with an *O*-methyl-2',6'-dibromo-3'-hydroxytyrosyl ketoxime (subunit E).

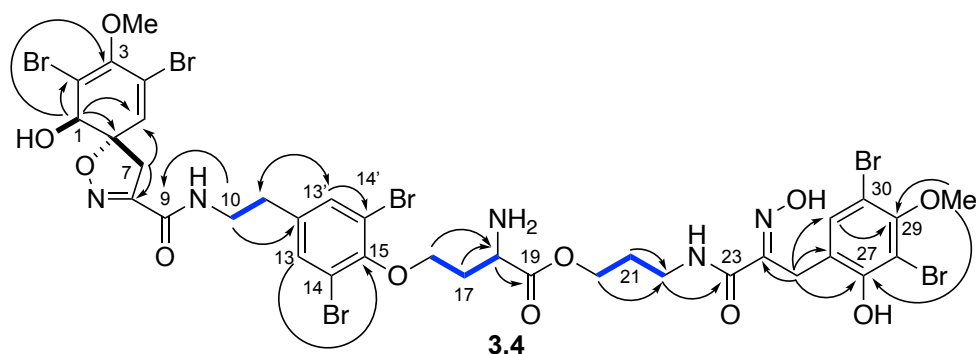


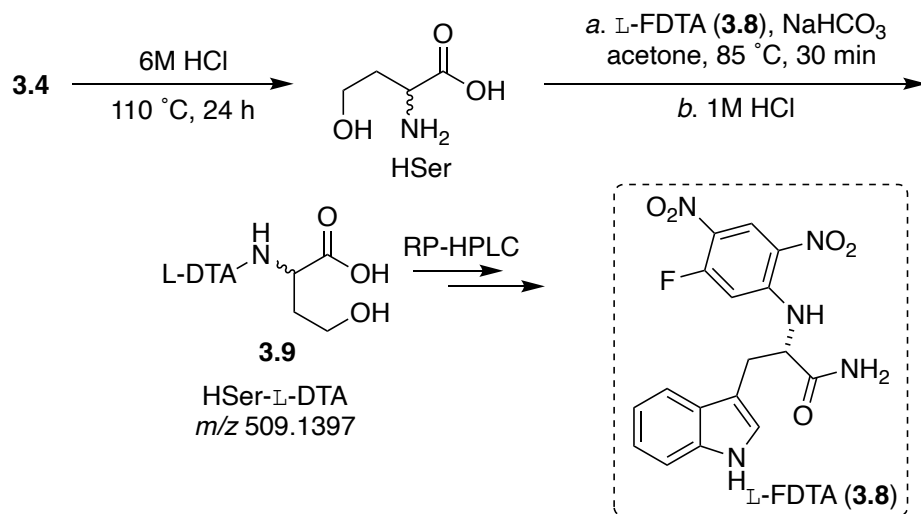
Figure 3.2: Key COSY (blue, bold) and HMBC (black, arrow) correlations of ningalamide A (3.4).

COSY correlations observed between signals δ_{H} 3.49 (2H, t, 7.2) and δ_{H} 2.79 (2H, t, 7.2), attached to C-10 and C-11, respectively, in addition to HMBC correlations between C-10 methylene to the amide δ_{C} 160.7 and quaternary carbon at C-12 (δ_{C} 139.0), C-11 methylene to the aromatic CH's at δ_{C} 133.7, and aromatic CH's at δ_{H} 7.45 (2H, s) to δ_{C} 118.2 and 152.0 clearly showed an SIO amide linked to an *O*-methyl 2,6-dibromotyramine (Table 3.2). COSY cross-peaks comprised a contiguous spin system of diastereotopic CH₂ at C-17 (δ_{H} 2.37 (1H, m), 2.56 (1H, m)), CH₂ at C-16 (δ_{H} 4.20, 2H, m) and CH at C-18 (δ_{H} 4.02, 2H, m). HMBC correlations were also observed from H-16 and H-17 to α -carbon at C-18 (δ_{C} 53.8) as well as from H-18 to the carbonyl at δ_{C} 172.5 consistent with a homoserine residue ether linked to the aforementioned tyramine subunit. Although, no HMBC correlations were observed between H-16 and C-15, the chemical shifts (δ_{H} 4.20 and δ_{C} 71.4) are in agreement with a primary aryl ether.

COSY correlations were also detected between the methylene H-21 (δ_{H} 2.06, 2H, p, 6.0) and two other methylenes at δ_{H} 3.54 (2H, t, 6.6) and 3.99 (2H, t, 6.0) positioned at C-20 and C-22, respectively. The HMBC correlation detected between H-22 and the 2-ketoximo amide signal (δ_{C}

164.8), along with the presence of the C-20 (δ_C 71.7), are compatible with subunit D in structure **3.4**. Terminal subunit E is also found in purpuramine M,¹⁸ and is formally the intramolecular elimination product (ring opened SIO) of subunit A. Thus, ningalamide A (**3.4**), is composed of five modules A-E, is the most complex SIO reported to date (all known SIOs consist of no more than 4 modules).

The absolute configuration of the homoserine residue in **3.4** was addressed using our recently reported variant of the Marfey's method.¹⁹ The L-tryptophanamide analog of Marfey's reagent (L-FDTA, **3.8**) gave derivatives of standard DL-homoserine (DL-DTA-HSer, **3.9**) that showed peaks on RP-HPLC ($t_R = 15.92$ min, $t_R = 16.28$ min) (C₁₈) with comparable separation to adducts prepared from L-FDAA (Scheme 3.1).²⁰ Total hydrolysis of **3.4** (6 M HCl, 110 °C, 24 h) followed by derivatization of the residue with reagent **3.8** (NaHCO₃, acetone, 85 °C, 30 min) and reversed phase HPLC revealed **3.9** as a 1:1 mixture ($t_R = 15.81$ min, $t_R = 16.17$ min).²¹ Consequently, **3.4** is ~1:1 diastereomeric mixture.

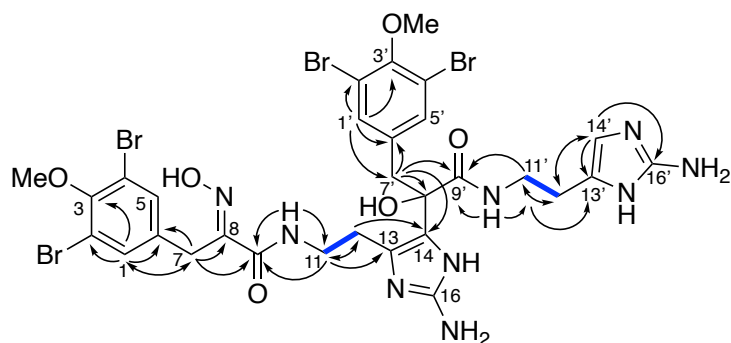


Scheme 3.1: Hydrolysis of **3.4** and derivatization of homoserine residue with L-FDTA (**3.8**) to **3.9**.

Table 3.2: ¹H and ¹³C NMR data for **3.4** (CD₃OD) and **3.5** (DMSO-*d*₆).

Position	δ_{H} (int., mult, <i>J</i> , Hz)	δ_{C}	Position	δ_{H} (int., mult, <i>J</i> , Hz)	δ_{C}
	3.4^a	3.4^b		3.5^a	3.5^b
1	4.08 (1H, s)	74.7	1	7.46 (1H, s)	132.7
2		113.4	2		117.3
3		148.4	3		151.8
4		122.1	4		117.3
5	6.41 (1H, s)	131.4	5	7.46 (1H, s)	132.7
6		91.6	6		136.4
7a	3.75 (1H, d, 18.6)	39.5	7	3.75 (2H, s)	29.6
7b	3.06 (1H, d, 18.6)				
8		154.5	8		150.8
9		160.7	9		163.0
10	3.49 (2H, t, 7.2)	40.8	10-NH	8.12 (1H, t, 5.4)	
11	2.79 (2H, t, 7.2)	34.5	11	3.22 (2H, m)	38.3
12		139.0	12a	2.70 (1H, m)	23.7
			12b	2.75 (1H, m)	
13/13'	7.45 (2H, s)	133.7	13		120.6
14/14'		118.2	14		122.9
15		152.0	15-NH	^c	
16	4.20 (2H, m)	71.41	16		^d
17a	2.56(1H, m)	31.6	17-NH ₂	^c	
17b	2.37 (1H, m)				
18	4.02 (1H, m)	53.8	1'	7.42 (1H, s)	134.6
19		172.51	2'		116.5
20	3.99 (2H, t, 6.0)	71.7	3'		152.0
21	2.05 (2H, p, 6.0)	29.8	4'		116.5
22	3.54 (2H, t, 6.6)	37.2	5'	7.42 (1H, s)	134.4
23		164.8	6'		134.6
24		151.7	7a'	3.04 (1H, d, 13.2)	41.8
			7b'	3.34 (1H, d, 13.8)	
25	3.99 (2H, s)	23.6	8'		74.8
26		128.3	9'		171.1
27		154.5	10'-NH	8.11 (1H, t, 6.6)	
28		114.4	11a'	3.11 (1H, m)	37.3
			11b'	3.30 (1H, m)	
29		152.0	12a'	2.36 (1H, m)	24.5
			12b'	2.46 (1H, m)	
30		113.2	13'		124.1
31	7.39 (1H, s)	133.1	14'	6.44 (1H, s)	108.8
3-OMe	3.72 (3H, s)	59.8	15'-NH	^c	
29-OMe	3.82 (3H, s)	60.31	16'		146.9
			17'-NH ₂	^c	
			3-OMe	3.73 (3H, s) ^e	60.1
			3'-OMe	3.74 (3H, s) ^e	60.1

^a600 MHz. ^bObtained from the indirect dimension of HSQC and HMBC (600 MHz). ^cCould not be assigned due to lack of HMBC correlations. ^dNot detected by HMBC (600 MHz, DMSO-*d*₆). C-16 was assigned a δ_{C} 147.7 through APT (150 MHz, CD₃OD). See SI Table S1 for complete assignment of **5** in CD₃OD. ^eAssignment of δ_{H} of the two MeO groups may be interchanged.



3.5

Figure 3.3: Key COSY (blue, bold) and HMBC (black, arrow) correlations of **3.5**.

Ningalamide B (**3.5**) was purified as a colorless solid with a molecular formula of $C_{30}H_{33}Br_4N_9O_6$ (m/z 930.9282; calcd 930.9287 for $[M+H]^+$) corroborating the presence of four Br atoms. FTIR absorptions at ~ 3200 and 1680 - 1670 cm^{-1} were indicative of a hydroxy, NH and an amide carbonyl group, respectively. Compound **3.5** is a new structural motif in the Br_x Tyr alkaloid family: an oxidized pseudo-dimer of four subunits; an *O*-methyl-2,6-dibromotyrosine ketoxime (subunit A) amide linked to a fully oxidized 2-aminohistamine unit (at C-13, subunit B) that is α -alkylated (at C-14) to an *O*-methyl-2',6'-dibromophenyl lactate (subunit C), in turn, contiguously esterified to a 2'-aminohistamine residue (subunit D).

HMBC correlations observed from the aromatic CH's at δ_H 7.46 (2H, s), attached to C-1 and C-5, to δ_C 117.3 (C-2 and C-4), 151.8 (C-3), 136.4 (C-6) and 29.6 (C-7) as well as correlations between the H-7 methylene at δ_H 3.75 (2H, s) and the aromatic quaternary carbons at δ_C 132.7 (C-1 and C-5) and 136.4 (C-6), ketoxime at δ_C 150.8 located at C-8 and the ketoxime amide at δ_C 163.0 positioned at C-9 were indicative of an *O*-methyl-2,6-dibromotyrosine ketoxime (subunit A). COSY correlations were seen between signals at δ_H 3.22 (2H, m) and δ_H 2.70 (1H, m) and 2.75 (1H, m), attached to C-11 and C-12, respectively, in addition to HMBC correlations between the NH at δ_H 8.12 (1H, t, 5.4) and the ketoxime amide at δ_C 163.0 (C-9) and the methylene at δ_C 38.3 (C-11). Additional HMBC correlations between the methylene at C-11 and the amide at C-9 and

the quaternary carbon at δ_C 120.6 (C-13), as well as the methylene at C-12 and the quaternary carbons at δ_C 120.6 (C-13) and 122.9 (C-14) were consistent with a fully oxidized 2-aminohistamine unit (subunit B) amide linked to the aforementioned *O*-methyl-2,6-dibromotyrosine ketoxime subunit at C-13 and alkylated at C-14. Although, no HMBC correlations were observed between H-12 and C-16 in the HMBC (600 MHz, DMSO- d_6 , $^1J_{CH} = 8$ Hz or 500 MHz, CD $_3$ OD, $^1J_{CH} = 4$ Hz), a quaternary carbon at δ_C 147.7 observed in the APT (150 MHz, CD $_3$ OD) is consistent with the imidazole of the 2-aminohistamine subunit.

HMBC correlations of **3.5** were also seen between the aromatic CH's at δ_H 7.42 (2H, s), attached to C-1' and C-5', and the aromatic quaternary carbons at δ_C 116.5 (C-2' and C-4'), 152.0 (C-3') and 134.6 (C-6') as well as the diastereotopic methylene at δ_C 41.8 (C-7'). Additional HMBC correlations were observed between the methylene at δ_H 3.04 (1H, d, 13.2) and δ_H 3.34 (1H, d, 13.8) at H-7' and δ_C 122.9 (C-14), the aromatic CH's at δ_C 134.4 (C-1' and C-5'), the quaternary carbons at δ_C 134.6 (C-6') and 74.8 (C-8'), and the amide carbonyl at δ_C 171.1 (C-9'). The quaternary carbon at δ_C 74.8 is compatible with a tertiary alcohol. MS fragmentation of **3.5** revealed a protonated ion at m/z 444.38 consistent with cleavage of the C–C bond between the carbon bearing the tertiary alcohol (C-8') and C-14 of the 2-aminohistamine subunit followed by loss of H $_2$ O. Furthermore, HMBC correlations were seen from the OH at δ_H 6.70 (1H, br s) and the amide at δ_C 171.1 (C-9'), methylene at δ_C 41.8 (C-7'), and the quaternary carbons at δ_C 74.8 (C-8') and 122.9 (C-14) arriving at subunit C: a 2-(4'-methoxy-2',6'-dibromophenyl)lactate that is α -alkylated at C-14 of the 2-aminohistamine of subunit B.

COSY correlations were also detected between the diastereotopic methylenes at δ_H 3.11 (1H, m), 3.30 (1H, m), 2.36 (1H, m) and 2.46 (1H, m) positioned at C-11' and C-12', respectively, in addition to HMBC correlations from H-11' to the amide at C-9' and the quaternary carbon at

C-13' (δ_C 124.1), correlations between H-12' methylene and H-14' (δ_H 6.44, 1H, s, $^1J_{CH} = 198$ Hz, 600 MHz, CD_3OD), and correlations between H-14' and C-16' (δ_C 146.9) are compatible with a second 2-aminohistamine unit (subunit D) in compound **3.5**.

3.4 Chiroptical Analysis of Configurational Heterogeneity

The absolute configurations of compounds **3.1–3.5** were addressed using a combination of chiroptical methods ($[\alpha]_D$, ECD) and chiral-phase HPLC. The ECD spectra of **3.1–3.3** showed two positive Cotton effects at λ_{max} 253 and 286 nm (Figure 3.4a) with similar magnitude and sign as aerothionin, isolated from *Aplysina fistularis*,²² in congruence with the (1*R*,6*S*)-**3.1–3.3** configuration as depicted. Unexpectedly, the free carboxylic acids **3.1a–3.3a** displayed stronger Cotton effects (CEs) compared to corresponding methyl esters **3.1b–3.3b** (Figure 3.4a). The origin of the higher intensity CEs for the free carboxylic acids compared to their esters may be associated with the common head-to-tail dimerization of free carboxylic acids, leading to a higher effective concentration. Simple additivity of $\Delta\epsilon$ has been observed in covalently linked dimeric SIOs, e.g. the C_2 symmetric aerothionin [λ 245 (+23.7), 284 (+21.4)].²²

Molar ECD, $\Delta\epsilon$, should be relatively invariant in SIO natural products that contain only one SIO unit, yet we observed relatively low $\Delta\epsilon$ values (**3.1b–3.3b**) compared to known SIO natural products, suggesting **3.1b–3.3b** are partially racemic compounds. This was confirmed by chiral-phase HPLC (CP HPLC, Cellulose-1 or Amylose-2 columns), which produced baseline-separations of enantiomers and revealed that **3.1b–3.3b** are each approximately 5-50% ee (Figures 3, S26–28). The configuration of the dominant enantiomer of natural product (+)-**3.3b** was confirmed by co-injection with authentic standard, prepared by total synthesis from (+)-**3.7a** (Scheme 3.2).

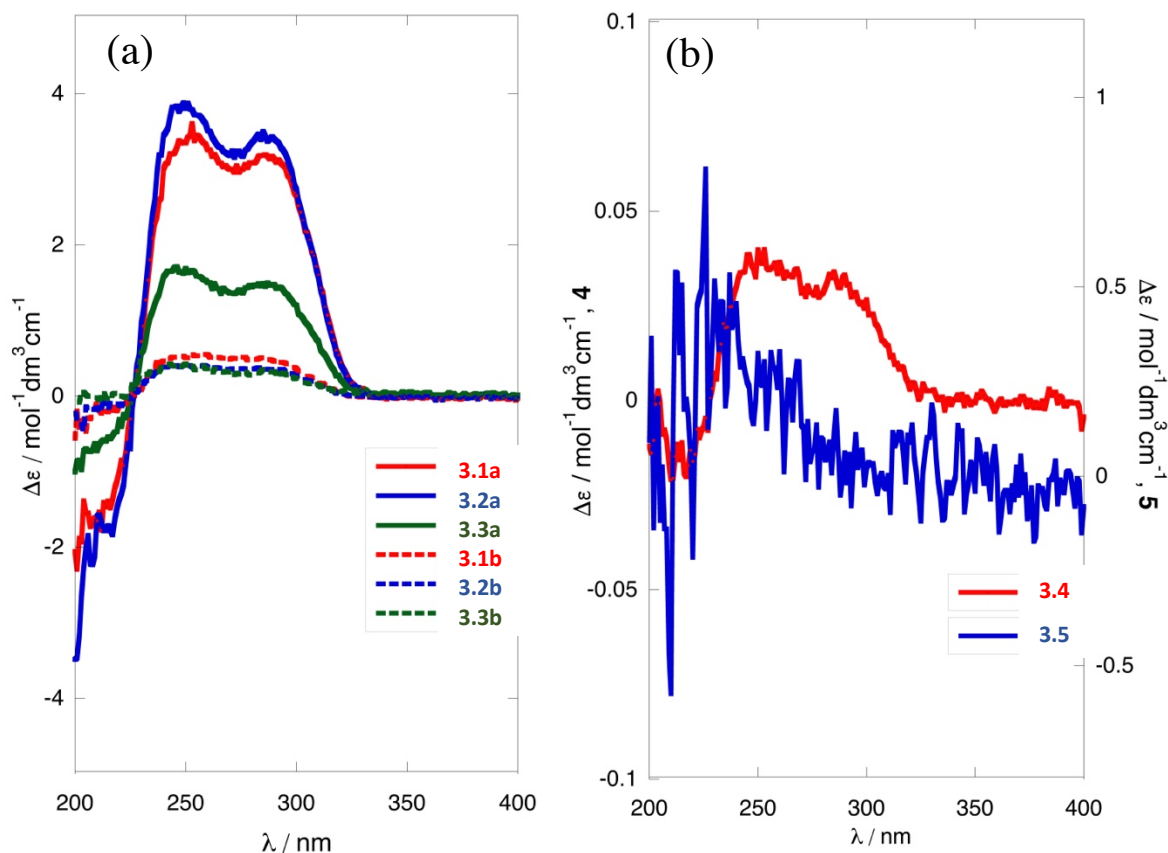


Figure 3.4: ECD of Compounds (a) **3.1a–3.1b** ($c = 1.85 \times 10^{-4}$ M), **3.2a–3.2b** (9.23×10^{-4} M), **3.3a–3.3b** (9.23×10^{-4} M), and (b) **3.4–3.5** ($c = 1.25 \times 10^{-4}$ M) (CH₃OH, 23 °C).

Previous reports have alluded to the chiroptical data of SIOs with lower CEs than expected, for example aerotionin,²² but *quantitative* standardization of SIOs has been lacking. In order to quantitate CEs in neutral SIO natural products, the parent SIO methyl ester (\pm)-**3.7** was synthesized in six steps from 2-hydroxy-4-methoxybenzaldehyde according to the procedure of Ley and coworkers²³ (Scheme 3.2) and resolved by CP HPLC to give optically pure (+)-1*R*,6*S*-**3.7a** and (–)-1*S*,6*R*-**3.7b** (>95% ee) which were used to standardize chiral-phase HPLC with ECD detection (see below).

Each enantiomer (+)-**3.7a** and (–)-**3.7b** exhibited a CE due to the dibromocyclohexadiene chromophore with a sign that conformed to the ‘skewed diene’ rule described by Moskowitz and

others,²⁴ and their magnitude of the CEs were much larger than those measured for **3.1–3.3** (Table 3.3), suggesting the latter were partially racemic. Compound **3.4** showed two weak positive CEs at approximately λ 255 and 283 nm, consistent with the dominant (1*R*,6*S*) enantiomer, while near-zero CEs for **3.5** are consistent with the absence of optical activity. We suspected the relatively low $\Delta\epsilon$ values (Table 3.3) measured for the known compounds **S3.1–S3.10** are also likely due to near-racemic modifications. For example, chiral-phase HPLC (Amylose-1), with dual UV-ECD detection, of **3.6** gave two peaks ($t_R = 63.14$ min and $t_R = 76.47$ min) with positive and negative CEs (λ 280 nm), respectively, corresponding to 84.4% ee.

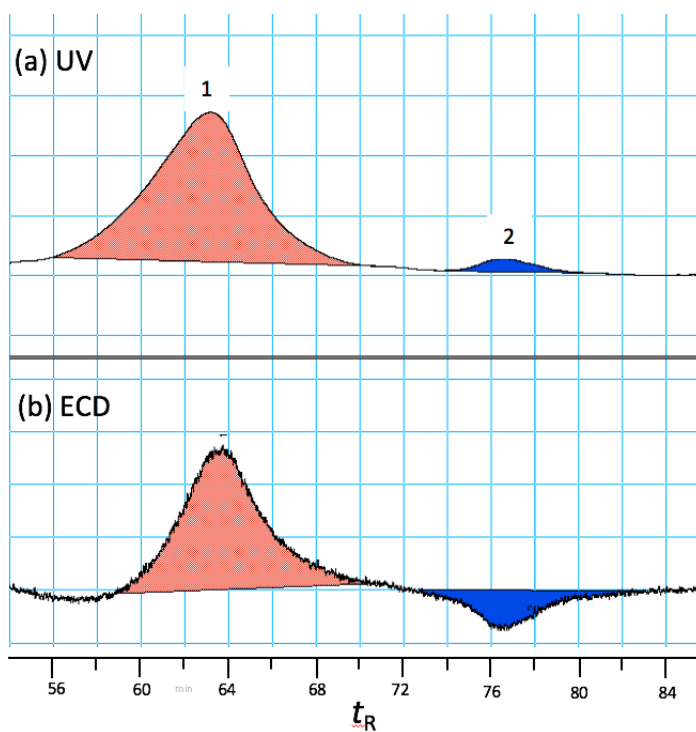
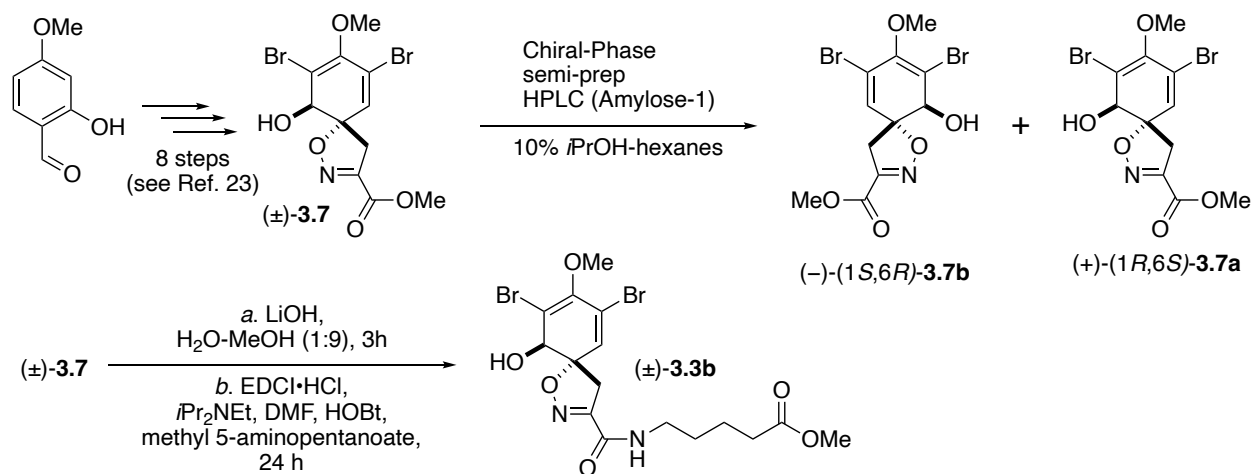


Figure 3.5: Chiral-phase HPLC chromatogram (λ 280 nm) (a) UV-vis detection and (b) ECD of purealidin-R (**3.6**) (Amylose-1, 4% *i*PrOH-hexanes, 1 mL.min⁻¹). Peak 1: (+)-**3.6a**: $t_R = 63.14$ min, area = 92.19. Peak 2: (-)-**3.6b**: $t_R = 76.47$ min, area = 7.81.



Scheme 3.2: Total Synthesis of $(+)$ -**3.7a**, $(-)$ -**3.7b**, and Methyl Purpuroceratate C (\pm) -**3.3b**. See Table 3.3 for ECD.

Table 3.3: Specific Rotation $[\alpha]_D$ and ECD Data of Spiroisoxazolines (CH₃OH).^a

Compound	$[\alpha]_D$ (c g.100 mL ⁻¹)	λ_2 /nm ($\Delta\varepsilon$)	λ_2 /nm ($\Delta\varepsilon$)	Ref.
3.1a	+128 (c 0.52)	253 (+3.65)	284 (+3.13)	6
3.2a	+139 (c 0.80)	251 (+3.87)	285 (+3.49)	6,8
3.3a	+116 (c 0.52)	253 (+1.67)	287 (+1.49)	<i>b</i>
3.1b	+40.0 (c 0.42)	253 (+0.56)	284 (+0.50)	<i>b</i>
3.2b	+58.2 (c 0.33)	251 (+0.41)	285 (+0.37)	<i>b</i>
3.3b	+41.6 (c 0.48)	253 (+0.42)	284 (+0.35)	<i>b</i>
3.4	~0 (c 0.4)	253 (+0.039)	285 (+0.034)	<i>b</i>
3.5	~0 (c 1.2)	0	0	<i>b</i>
3.6	+86.4 (c 0.48)	254 (+7.78)	284 (+5.62)	4
3.7	+97.5 (c 0.43)	254 (+0.59)	285 (+0.54)	7
(+)- 3.7a ^{b,c}	+163 (c 0.1)	254 (+27.84)	285 (+9.68)	<i>b</i>
(-)- 3.7b ^{b,c}	-163 (c 0.1)	254 (-31.87)	285 (-11.13)	<i>b</i>
Aerophobin-1 (S3.1)	+135.1 (c 0.86)	252 (+4.74)	285 (+4.11)	9
Purealidin J (S3.2)	+88.6 (c 0.44)	253 (+2.17)	283 (+1.86)	4
<i>N</i> -Methyl-aerophobin-2 (S3.3)	+95.2 (c 0.16)	253 (+3.34)	286 (+2.85)	10
Aerophobin-2 (S3.4)	+127.7 (c 0.66)	253 (+2.17)	290 (+1.88)	9b
Purealidin K (S3.5)	+25.9 (c 0.44)	253 (+1.52)	286 (+1.17)	4
14-Oxo-aerophobin-2 (S3.6)	+45.4 (c 0.76)	253 (+1.84)	283 (+1.52)	11
Aplysinamisine II (S3.7)	+51.7 (c 0.91)	253 (+4.51)	285 (+4.11)	12
Pseudoceratinamide A (S3.8)	+156.1 (c 0.52)	253 (+2.00)	286 (+1.77)	13
Purpurealidin J (S3.9)	+13.4 (c 0.50)	253 (+0.73)	286 (+0.57)	14
Hexadellin C (S3.10)	+102.6 (c 0.64)	253 (+1.66)	284 (+1.13)	15

^aMeasurements made on compounds in this study. ^bThis work. ^c>95% ee. For total synthesis of (+)-**3.7a** and (-)-**3.7b**, and (±)-**3.3b**, see Scheme 3.2.

Our foregoing results lend rigor to a quantitative analysis of stereochemical heterogeneity among the Br_xTyr SIO metabolites and contributes data to the ongoing discussion on ‘enantiodivergence’ in their biosynthesis, most recently expanded by Karuso and coworkers.¹³

Finally, a comment on the homologous series purpuroceratic acids A-C (**3.1a–3.3a**) is in order to clarify and inform future investigations of Br_xTyr secondary metabolites from Verongid sponges. The three homologous carboxylic acids, together with the hypothetical **3.10a** (‘*nor*-purpuroceratic acid A’), the parent of our recently reported methyl ester, lacunosin A, **3.10b** from *Aplysina lacunosa*,²⁵ constitute two core modules also found in many other SIOs. The biosynthesis of β-alanine and 4-aminobutyric acid (GABA) in bacteria originate from well-known pathways, including reductive-transamination of Asp, but the provenance of 5-aminopentanoic acid in **3.3a**, is less obvious. One hypothesis is that the latter arises from a radical-mediated α-deamination of a basic ‘origin’ AA (Table 3.4).²⁶ Support for radical-promoted biosynthesis is suggested by the structure of **5**: a dimerization that appears to be the result of an α-radical, derived from a brominated α-hydroxyphenyllactic acid, and radical aromatic substitution (e.g. S_{RN}1) upon the 2-aminohistamine module. If so, the structures **3.1a–3.3a** and **3.10a** links the common Br₂Tyr-derived α-ketoxime with ω-aminoalkanoic acids β-alanine and GABA through radical-deamination products of 1,4-diaminobutanoic acid (Dab) (in **3.2a**) and Orn (in **3.3a**), respectively. The rather uniform pattern of **3.1a–3.3a**, and **3.10a** suggests that another, as yet unreported secondary metabolite, corresponding to the hypothetical ‘purpuroceratic acid D’ (**3.11a**), derived from Lys, may be found in related sponges.

Table 3.4: Homologous SIO Carboxylic Acids and Proposed ‘Origin’ AA of the Second Module.

Entry	Cmpd	Formula	‘Origin’ AA	Ref.
1	3.10a^a	C ₁₂ H ₁₂ Br ₂ N ₂ O ₆	Gly	25
2	3.1a	C ₁₃ H ₁₄ Br ₂ N ₂ O ₆	β-Ala	6
3	3.2a	C ₁₄ H ₁₆ Br ₂ N ₂ O ₆	Dab ^b	6
4	3.3a	C ₁₅ H ₁₈ Br ₂ N ₂ O ₆	Orn ^c	3, <i>d</i>
5	3.11a^e	C ₁₆ H ₂₀ Br ₂ N ₂ O ₆	Lys ^f	–

a. Hypothetical parent carboxylic acid of Me ester, lacunosin A (**3.10b**). *b.* 2,4-diaminobutanoic acid. *c.* 2,5-diaminopentanoic acid. *d.* This work. *e.* Hypothetical ‘purpuroceratic acid D’. *f.* 2,6-diaminohexanoic acid.

3.5 Biological Activities

Alkaloids from *P. verrucosa* were evaluated by in vitro inhibition of acetylcholinesterase (AChE) and butyrylcholinesterase (BuChE) (Table 3.5). Of the 10 compounds tested, two emerged with significant selectivity towards AChE (ratio IC₅₀'s (BuChE/AChE) >10): aerophobin-1 (**S3.1**) and aplysinamisine II (**S3.7**). Compound **S3.7** was a more potent inhibitor of AChE (IC₅₀ 0.77 μM) than the standard, galantamine•HBr (IC₅₀ 1.18 μM).

Table 3.5: In vitro Inhibition (IC₅₀, μM) of AChE and BuChE by SIO Alkaloids.

Compound	IC ₅₀ μM		Ratio IC ₅₀ s (BuChE /AChE)
	AChE	BuChE	
3.5	>100	14.0	<0.14
Purealidin-R (3.6)	3.32	15.4	4.6
Aerophobin-1 (S3.1)	5.74	>100	>17
Aplysinamisine II (S3.7)	0.77	10.3	13
Pseudoceratinamide A (S3.8)	5.80	10.7	1.9
Hexadellin C (S3.10)	4.79	10.0	2.1
Aplysamine-2 (S3.11)	0.46	1.03	2.2
Purpuramine I (S3.12)	5.40	2.71	0.50
Araplysillin III (S3.13)	19.9	>100	>5.0
Galantamine• HBr	1.18	19.6	17

^aFor assay conditions, see Experimental.

3.6 Conclusions

In summary, five new brominated spiroisoxazoline alkaloids **3.1b–3.2b**, **3.3a**, **3.4** and the oxidatively dimerized OMe-2,6-dibromo-1,3-cyclohexadiene ketoxime amide, **3.5**, were isolated from extracts of *Pseudoceratina verrucosa* and their structures determined by integrated analysis of MS, NMR and ECD data. Compound **3.4** is a 1:1 mixture of diastereomers; the homoserine residue in **3.4** is essentially racemic. Variability in stereochemical homogeneity is again observed in new and known spiroisoxazolines, both in the range of magnitudes of $\Delta\varepsilon$ in ECD as measured by chiral-phase HPLC (dual UV-vis and ECD detection). Quantitation of optical purity in SIOs was standardized by synthesis of (+)-(1*R*,6*S*)-**3.7a** and (–)-(1*S*,6*R*)-**3.7b** followed by their resolution and characterization by ECD-detected chiral phase HPLC.

The identification of selective AChE inhibitors from SIOs, including one more potent than galantamine, are promising results that reveal the modular SIO alkaloid architecture to be a potentially useful platform for development of selective cholinesterase inhibitors. Expanded investigation of SIO natural products, and the synthesis of enantiopure natural and non-natural products based on their structures, may open new avenues for development of AD therapeutics.

Chapter 3, in total, is a reprint of the material, “Spiroisoxazoline Inhibitors of Acetylcholinesterase from *Pseudoceratina verrucosa*. Quantitative Chiroptical Analysis of Configurational Heterogeneity and Total Synthesis of (\pm)-Methyl Purpuroceratate C” *J. Nat. Prod.* **2022**, Submitted. The dissertation author was the primary author of this paper and gratefully acknowledges the contributions of coauthors Rudi Hendra, and Tadeusz F. Molinski.

3.7 Acknowledgements

We thank S. Taylor and D. Manker for assistance with sample collection, A. Mrse and B. Duggan for NMR support, and X. Su for HRMS measurements. The purchases of the Agilent TOF mass spectrometer and the 500 MHz NMR spectrometer were made possible with funds from the NIH Shared Instrument Grant program (S10RR025636) and the NSF Chemical Research Instrument Fund (CHE0741968), respectively. MS is grateful for support from a Graduate Research Fellowship, Department of Chemistry, UCSD. RH thanks the Fulbright Foundation for the support of a Fellowship while on leave at UCSD. This research was supported by grants (TFM) from the NIH (AI100776, AT009783).

3.8 Experimental

General Experimental Procedures. UV-vis spectra were measured on a JASCO V-630 double beam spectrometer. FTIR spectra were collected on thin film samples using a JASCO FTIR-4100 fitted with an ATR accessory (ZnSe plate). Optical rotations were measured on a JASCO P-2000 polarimeter at the D-double emission line of Na°. ECD spectrum were measured on a JASCO J-810 spectropolarimeter at 23 °C in quartz cells of 1, 2 or 5 mm pathlength. 1D and 2D NMR spectrum were measured at 23 °C on a JEOL ECA spectrometer (500 MHz), equipped with a 5 mm $^1\text{H}\{^{13}\text{C}\}$ room temperature probe, or a Bruker Avance III (600 MHz) NMR spectrometer with a 1.7 mm $^1\text{H}\{^{13}\text{C}/^{15}\text{N}\}$ microcryoprobe. HR-ESI-TOF mass spectroscopic analyses were carried out on an Agilent 1200 HPLC coupled to an Agilent 6350 TOF-MS at the Small Molecule Mass Spectrometry Facility, Department of Chemistry and Biochemistry (UCSD). Preparative, semi-preparative and analytical HPLC were completed on a JASCO system consisting of a UV-vis detector (UV-2075), dual-pumps (PU-2086 Plus), and a dynamic mixer (MX-2080-32). Chiral phase HPLC was carried out, with specified columns and solvent systems, using the above JASCO dual pump system coupled to a JASCO CD-2095 Plus detector with dual-channel detectors (UV-vis and ECD), outputted to a PowerChrom 280 ADC (16 bit). Chromatograms were processed and integrated with native software. LC-MS measurements were performed with a Thermoelectron Surveyor UHPLC coupled to an MSD single-quadrupole detector. Electric eel acetylcholinesterase (EC 3.1.1.7, Type VI-S), equine butyrylcholinesterase (EC 3.1.1.8), and galantamine hydrobromide were purchased from Sigma-Aldrich. *S*-Butyrylthiocholine iodide, *S*-acetylthiocholine iodide and 5,5'-dithio-bis-nitrobenzoic acid (DTNB) were purchased from Fisher Scientific.

Biological Material. The sponge *Pseudoceratina verrucosa* (93-07-101) was collected in January 1993 from Exmouth Gulf, near Ningaloo Reef, Western Australia by hand, using scuba,

at a depth of -9 m and kept frozen (-20 °C) until needed. A type sample (MeOH) is archived in the Department of Chemistry and Biochemistry, UCSD.

Extraction and Isolation. A sample of *P. verrucosa* was lyophilized (dry wt. 235 g) and extracted with CH₃OH (2 x 500 mL, 12 h) and the combined CH₃OH extracts were concentrated and the water content adjusted to approximately 1:9 (H₂O/CH₃OH, 500 mL). The extract was partitioned with hexane (2 x 500 mL) to give fraction A (0.506 g). The aqueous-CH₃OH layer was adjusted with water (2:3 H₂O/CH₃OH) and extracted with CH₂Cl₂ (2 x 500 mL) to yield fraction B (2.61 g). The CH₃OH was evaporated and the resultant aqueous layer was partitioned against *n*-BuOH (2 x 500 mL) to provide fraction C (2.54 g) and fraction D (3.51 g).

Fraction B (1.5 g) was further purified by size-exclusion chromatography (Sephadex LH-20, CH₃OH) to yield 11 fractions, which were pooled according to TLC and *p*-anisaldehyde staining. Fractions 4 and 5 were combined (165 mg) and purified by flash chromatography (silica, 2:8 CH₃OH/CH₂Cl₂) to yield 6 subfractions, combined according to TLC and *p*-anisaldehyde staining. Subfraction 1 (20.6 mg) was re-purified by reversed phase HPLC (Phenomenex Luna C₁₈, 5 μ, 250 x 10 mm, 70:30 to 30:70 of 0.1% TFA-H₂O/CH₃CN over 30 min, 2.5 mL.min⁻¹, λ = 254 nm) to yield purpuroceratic acid A methyl ester (**3.1b**, 1.9 mg, *t_R* = 17.37 min), and purpuroceratic acid B methyl ester (**3.2b**, 1.6 mg, *t_R* = 18.44 min). The second and fourth subfractions (34.4 mg and 8.7 mg) were purified under similar conditions to give purpuroceratic acid C (**3.3a**, 1.7 mg, *t_R* = 17.52 min), and ningalamide A (**3.4**, 1.6 mg, *t_R* = 20.65 min). Ningalamide B (**3.5**, 0.8 mg, *t_R* = 18.35 min) was purified by RP-HPLC (Phenomenex Luna C₁₈, 5 μ, 250 x 10 mm, 70:30 to 20:80 of 0.1% TFA-H₂O/CH₃CN over 40 min, 2.5 mL.min⁻¹, λ = 254 nm). In addition, 14 known bromotyrosine alkaloids were isolated; their HRMS and ¹H NMR data matched reported literature values (see text).

Purpuroceratic Acid A Methyl Ester (3.1b). A pale yellow solid; $[\alpha]^{23.8}_{\text{D}} +128$ (c 0.52, CH₃OH); For the ECD spectrum, see Figure 3.4; UV (CH₃OH) λ_{max} 194 nm (ϵ log₁₀ 3.51), 230 (3.53), and 283 (3.93); For the ¹H and ¹³C NMR data, see Table 3.1; HRMS (ESI-TOF) m/z 488.9254 [M+Na]⁺ (calcd for C₁₄H₁₆⁷⁹Br₂N₂O₄Na⁺ 488.9267).

Purpuroceratic Acid B Methyl Ester (3.2b). A pale yellow solid; $[\alpha]^{23.8}_{\text{D}} +139.2$ (c 0.8, CH₃OH); For the ECD spectrum, see Figure 3.4; UV (CH₃OH) λ_{max} 194 nm (ϵ log₁₀ 3.33), 230 (3.37), and 282 (3.09); FTIR (film) ν 3353, 1744, 1671, 1599, 1541, 1438, 1205, 1133, 1047, 1025, 988, 916, 837, 801, 766 and 722 cm⁻¹; For the ¹H and ¹³C NMR data, see Table 3.1; HRMS (ESI-TOF) m/z 502.9416 [M+Na]⁺ (calcd for C₁₅H₁₈⁷⁹Br₂N₂O₆Na⁺ 502.9424).

Purpuroceratic Acid C (3.3a). A pale yellow solid; $[\alpha]^{23.8}_{\text{D}} +116.4$ (c 0.52, CH₃OH); For the ECD spectrum, see Figure 3.4; UV (CH₃OH) λ_{max} 194 nm (ϵ log₁₀ 3.81), 230 (4.36), and 280 (4.04); FTIR (film) ν 3405, 2923, 1682, 1446, 1207, 1185, and 1136 cm⁻¹; For the ¹H and ¹³C NMR data, see Table 3.1; HRMS (ESI-TOF) m/z 480.9600 [M+H]⁺ (calcd for C₁₅H₁₉⁷⁹Br₂N₂O₆⁺ 480.9604).

Purpuroceratic Acid C Methyl Ester (3.3b). A solution of CH₂N₂ in Et₂O (~0.2 M) was added dropwise to a solution of **3.3a** in CH₃OH (1 mL) at 0 °C until a permanent yellow color remained. After 10 min, excess CH₂N₂ and solvent were evaporated under a stream of N₂ gas, and the residue of **3.3b** analyzed by HPLC.

Chiral-Phase HPLC Analysis of 3.1b–3.3b. Samples of methyl esters, **3.1b–3.3b**, were dissolved in *i*PrOH-hexane (10%) and separated on a chiral-phase HPLC column (Luna Amylose-1, 5 μm , 250 x 4.6 mm, 10% *i*PrOH-hexane, isocratic, 1.0 mL.min⁻¹) coupled to a dual-channel, in-line UV-vis-ECD detector (Jasco, CD-2095 Plus, λ = 280 nm): (+)-**3.1b** (t_{R} = 29.68 min), (-)-

3.1b ($t_R = 34.20$ min), (+)-**3.2b** ($t_R = 26.99$ min), (-)-**3.2b** ($t_R = 32.47$ min), (+)-**3.3b** ($t_R = 26.37$ min), and (-)-**3.3b** ($t_R = 29.50$ min).

Ningalamide A (3.4). A colorless solid; $[\alpha]^{23.8}_D 0$ (c 0.4, CH₃OH); For the ECD spectrum, see Figure 3.4; UV (CH₃OH) λ_{\max} 194 nm (ϵ log₁₀ 3.38), 230 (3.73), and 282 (3.17); FTIR (film) ν 3410, 2927, 1683, 1442, 1200, and 1142 cm⁻¹; For the ¹H and ¹³C NMR data, see Table 3.2; HRMS (ESI-TOF) m/z 1177.7655 [M+H]⁺ (calcd for C₃₅H₃₈⁷⁹Br₆N₅O₁₁⁺ 1177.7663).

Acid Hydrolysis of Compound 3.4 and DTA-Derivatives. A sample of **3.4** (0.6 mg, 0.51 μ mol) was dissolved in HCl (6 M, 1 mL) and stirred in a sealed vial at 110 °C for 24 h. The solution was cooled to rt, dried under a stream of N₂, and derivatized with 2-((5'-fluoro-2',4'-dinitrophenyl)-*N* ^{α} -L-tryptophanamide (L-FDTA, **3.8**) at 85 °C (30 min), and quenched according to the published protocol,²⁷ to yield the homoserine-L-DTA derivatives of **3.4** for HPLC analysis. DTA derivatives of authentic L- and DL-homoserine were prepared in a similar manner.

Ningalamide B (3.5). A colorless solid; $[\alpha]^{23.8}_D 0$ (c 1.2, CH₃OH); For the ECD spectrum, see Figure 3.4; UV (CH₃OH) λ_{\max} 194 nm (ϵ log₁₀ 4.95), 227 (5.58), and 275 (4.37); FTIR (film) ν 3252, 1675, 1540, 1476, 1421, 1259, 1202, 1142 and 999 cm⁻¹; For the ¹H and ¹³C NMR data, See Table 3.2; HRMS (ESI-TOF) m/z 931.9355 [M+H]⁺ (calcd for C₃₀H₃₄⁷⁹Br₄N₉O₆⁺ 931.9360).

Total Synthesis of Methyl Purpuroceratate C (3.3b). Racemic verongidoic acid methyl ester, (\pm)-**3.7**, was prepared from 2-hydroxy-4-methoxybenzaldehyde in 8 steps according to the method of Ley and co-workers.²³ A solution of (\pm)-**3.7** (3.2 mg, 8.1 μ mol) in H₂O-MeOH (1:9, 300 μ L) was treated with LiOH (1M, 1:9 H₂O-MeOH, 81 μ L, 10 equiv). After stirring for 3 h, the mixture was quenched with a few drops of 1 M HCl to pH 3 and concentrated under a stream of N₂ to give (\pm)-**3.6**, which dissolved in DMF-CH₂Cl₂ and used directly in the next step. To the solution of (\pm)-**3.6**, was added DCC (1M CH₂Cl₂, 25 μ L, 24 μ mol, 3.0 equiv), HOBt, (1M DMF,

25 μL , 24 μmol , 3.0 equiv) and *iPr*₂NEt (5 μL , 24 μmol , 3.0 equiv) and the mixture stirred for 30 min before addition of methyl 5-aminobutyrate•HCl (3.73 mg, 22 μmol). The mixture was stirred at rt for 24 h, before dilution with CH₂Cl₂, and the solution washed sequentially with 0.1M HCl and NaHCO₃ (satd. aq.), dried (MgSO₄) and concentrated to give a pale-yellow residue which was purified by HPLC (40:60 H₂O/CH₃CN) to give ester (\pm)-**3.3b** as a colorless glass (1.1 mg) that was identical by HRMS, ¹H NMR and HPLC retention time with a sample of (+)-**3.3b** prepared from purpuroceratic acid C (**3.3a**), as described above. See SI for chiral phase HPLC (UV-vis, ECD detection).

Acetylcholinesterase and Butyrylcholinesterase Inhibition Assays. Assays of cholinesterase activity were carried out using procedures, reagents and conditions the same as previously described.²⁸ Cholinesterase inhibition was determined spectrophotometrically according to a modified protocol of that reported by Ellman.²⁹ In this assay, 150 μL of 0.1 M sodium phosphate buffer (pH 8.0), 20 μL enzyme mixture (1.25 Units/mL in dI-H₂O), and 10 μL test sample consisting of galantamine hydrobromide (1 mg/mL in MeOH, positive control), MeOH (negative control) or purified compounds dissolved in MeOH, were preincubated at rt for 30 min. 10 μL DTNB (5 mM, 10 mL of 0.1 M sodium phosphate buffer, pH 7.0, containing 15 mg NaHCO₃) was added followed by 10 μL acetylthiocholine or butyrythiocholine (10 mM, 0.1 M sodium phosphate buffer, pH 8.0). The absorbances were measured immediately at λ 410 nm in a microplate reader.

3.9 Appendix

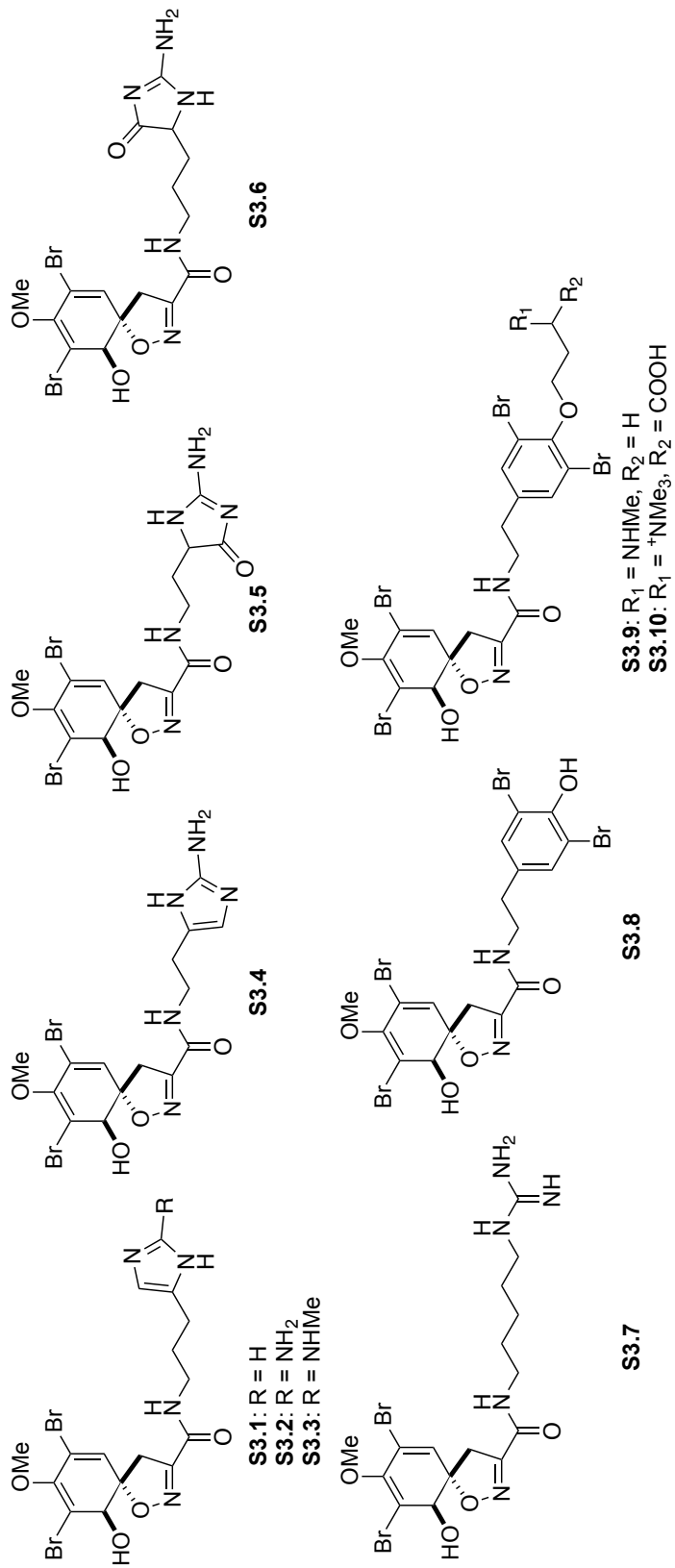


Figure 3.6: Structures of Dibromo-cyclohexa-1,3-dienyl Natural Products from Verongid Sponges.



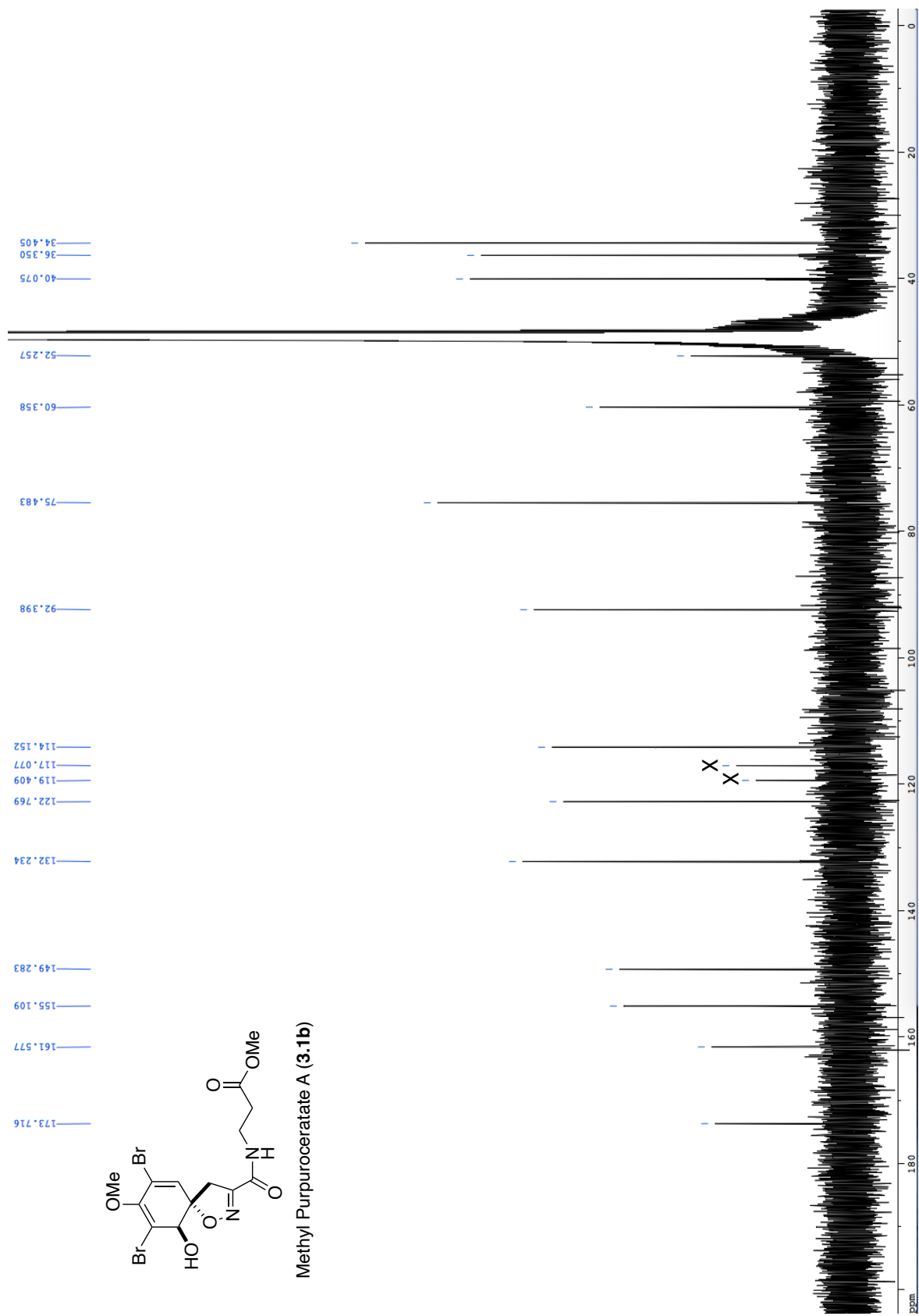
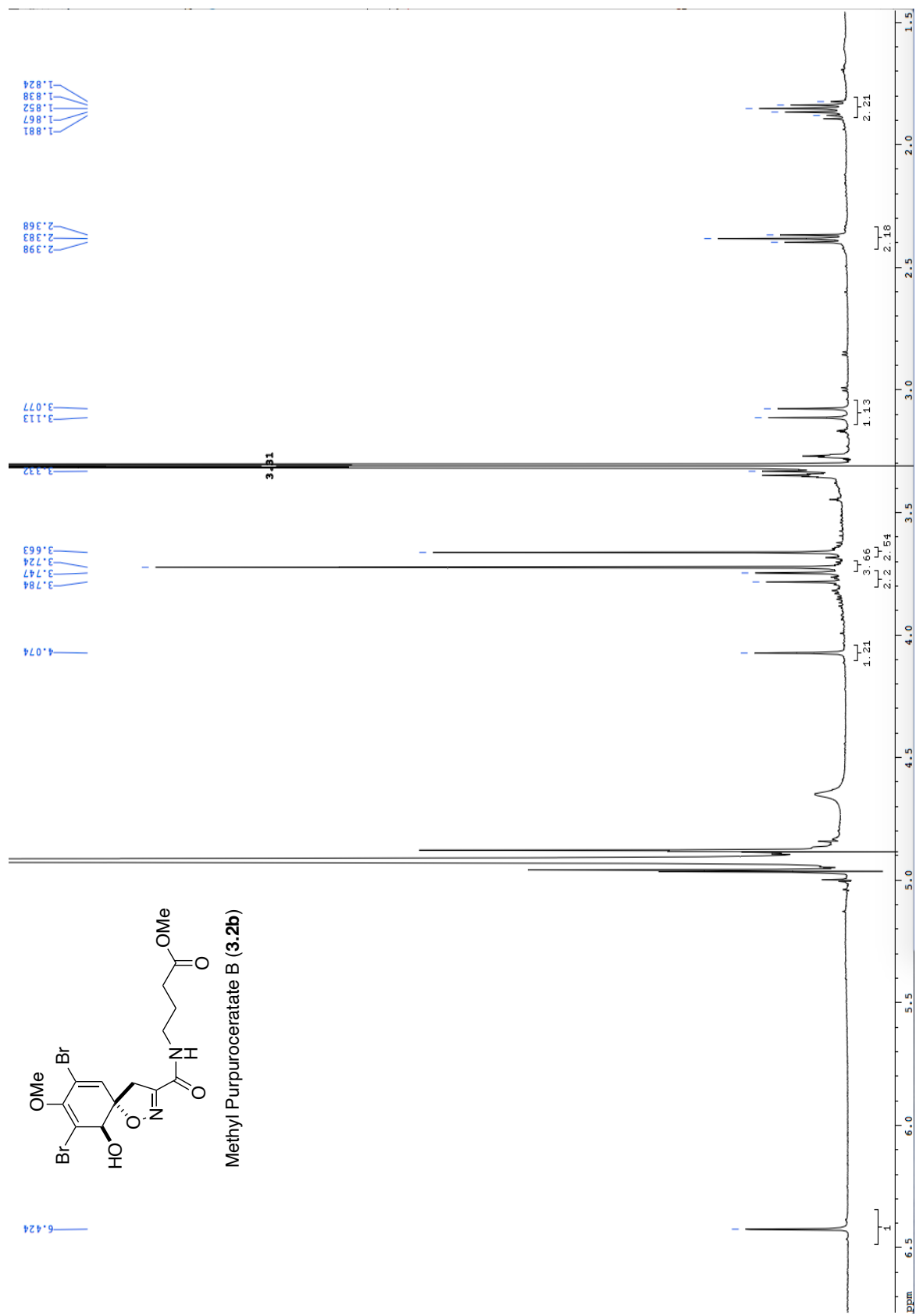


Figure 3.8: ^{13}C NMR of Compound **3.1b** (125 MHz, CD_3OD).



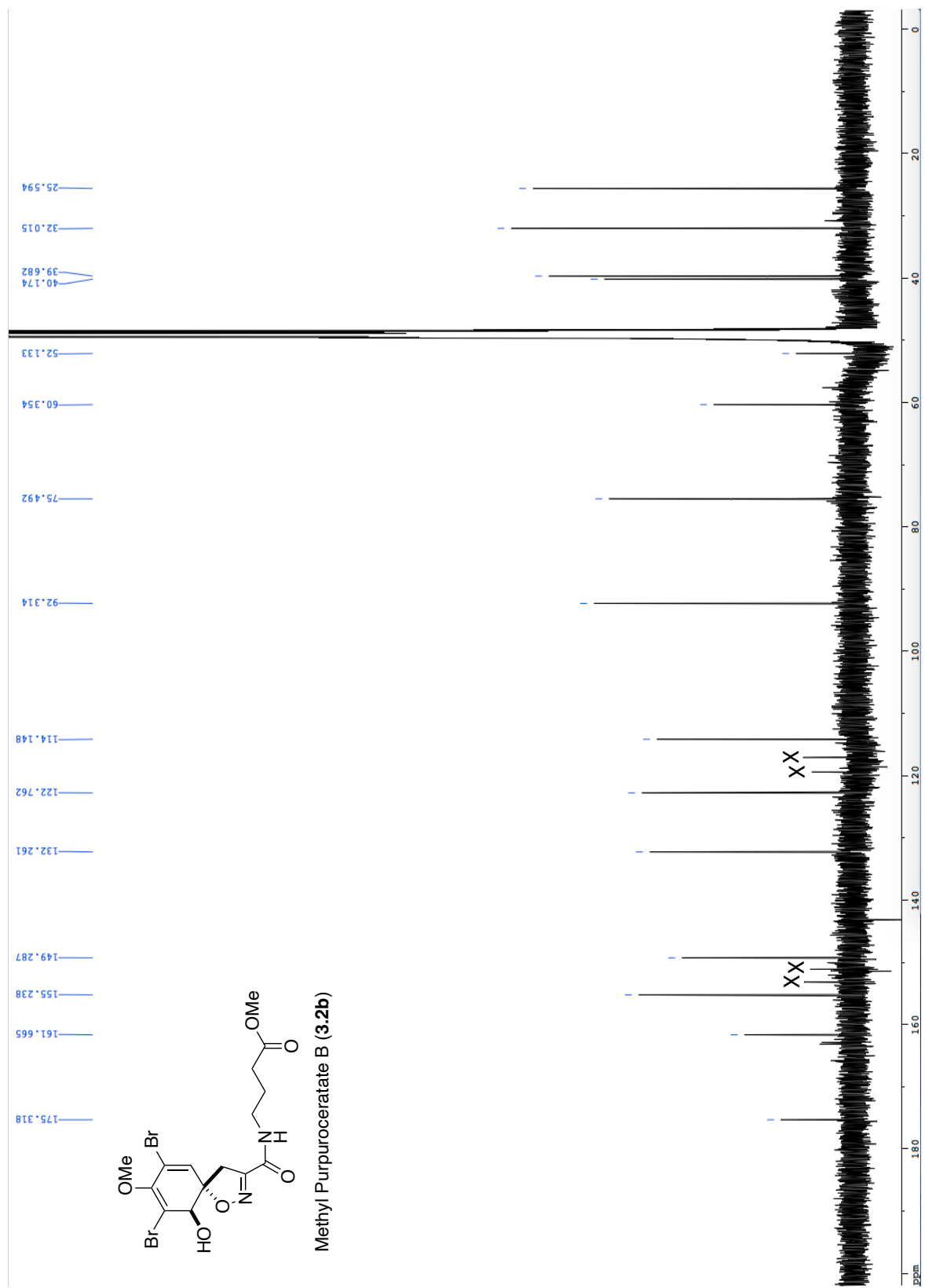


Figure 3.10: ¹³C NMR of Compound **3.2b** (125 MHz, CD₃OD).

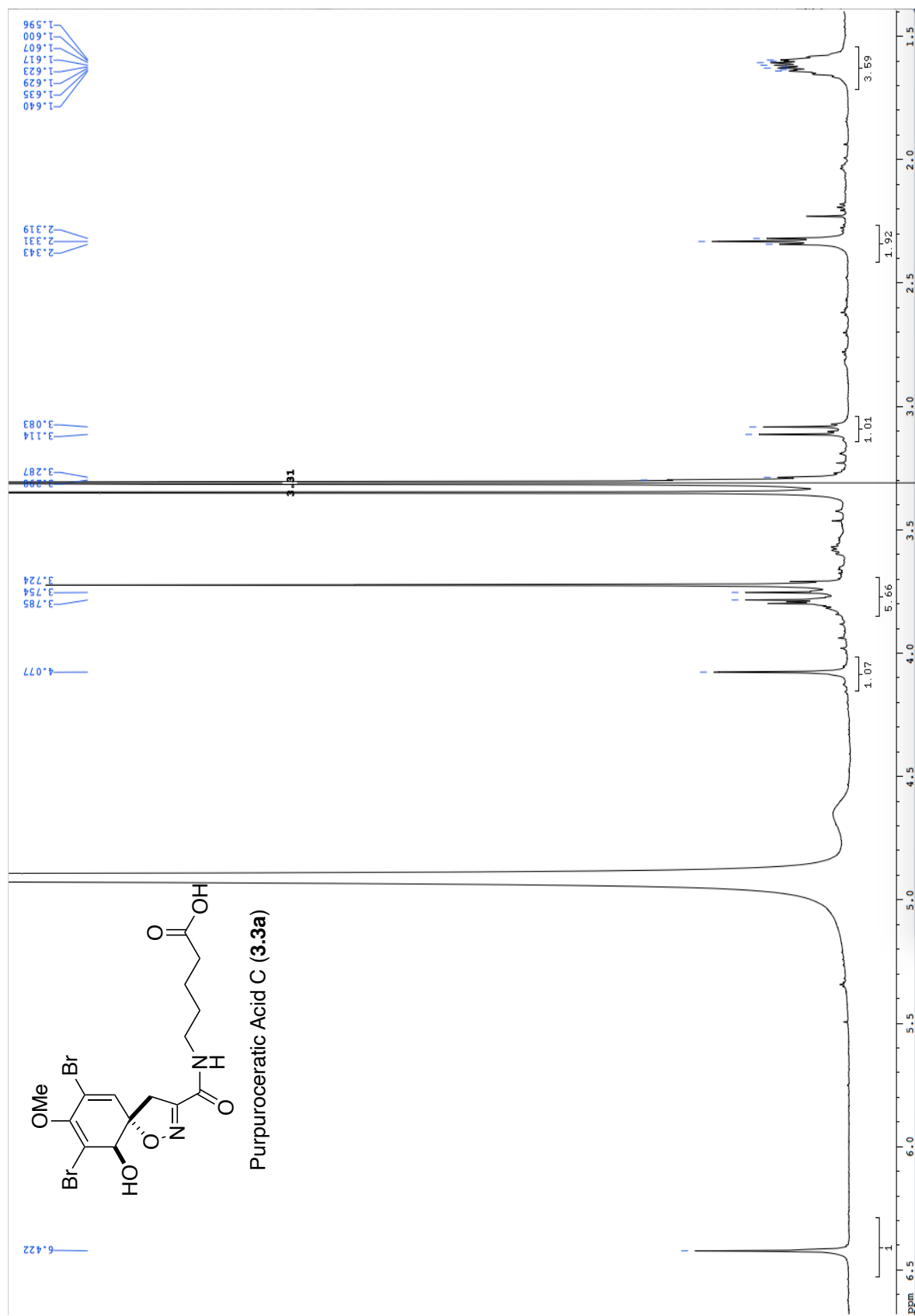


Figure 3.11: ¹H NMR of Compound **3.3a** (600 MHz, CD₃OD).

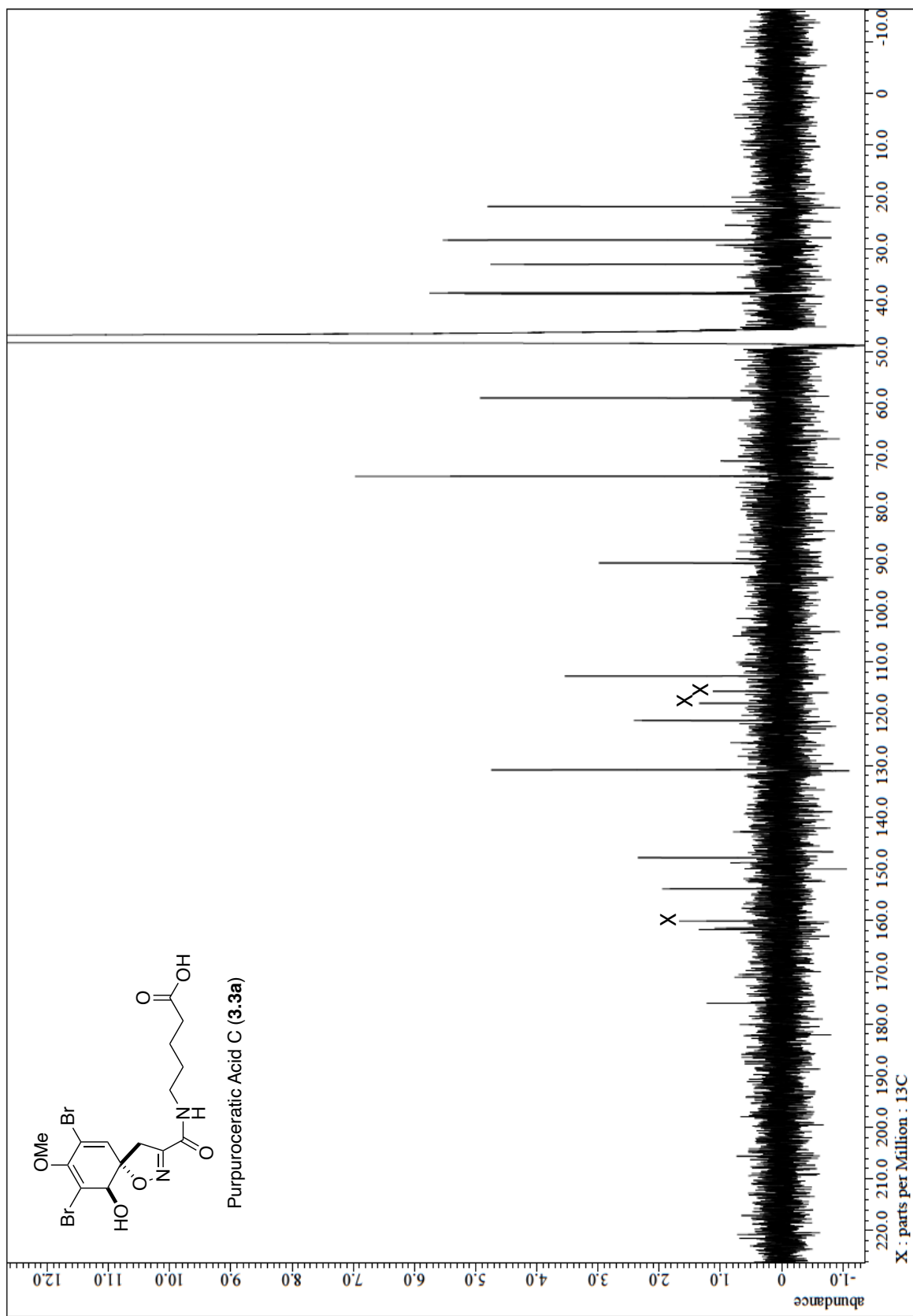


Figure 3.12: ^{13}C NMR of Compound 3.3a (125 MHz, CD_3OD).

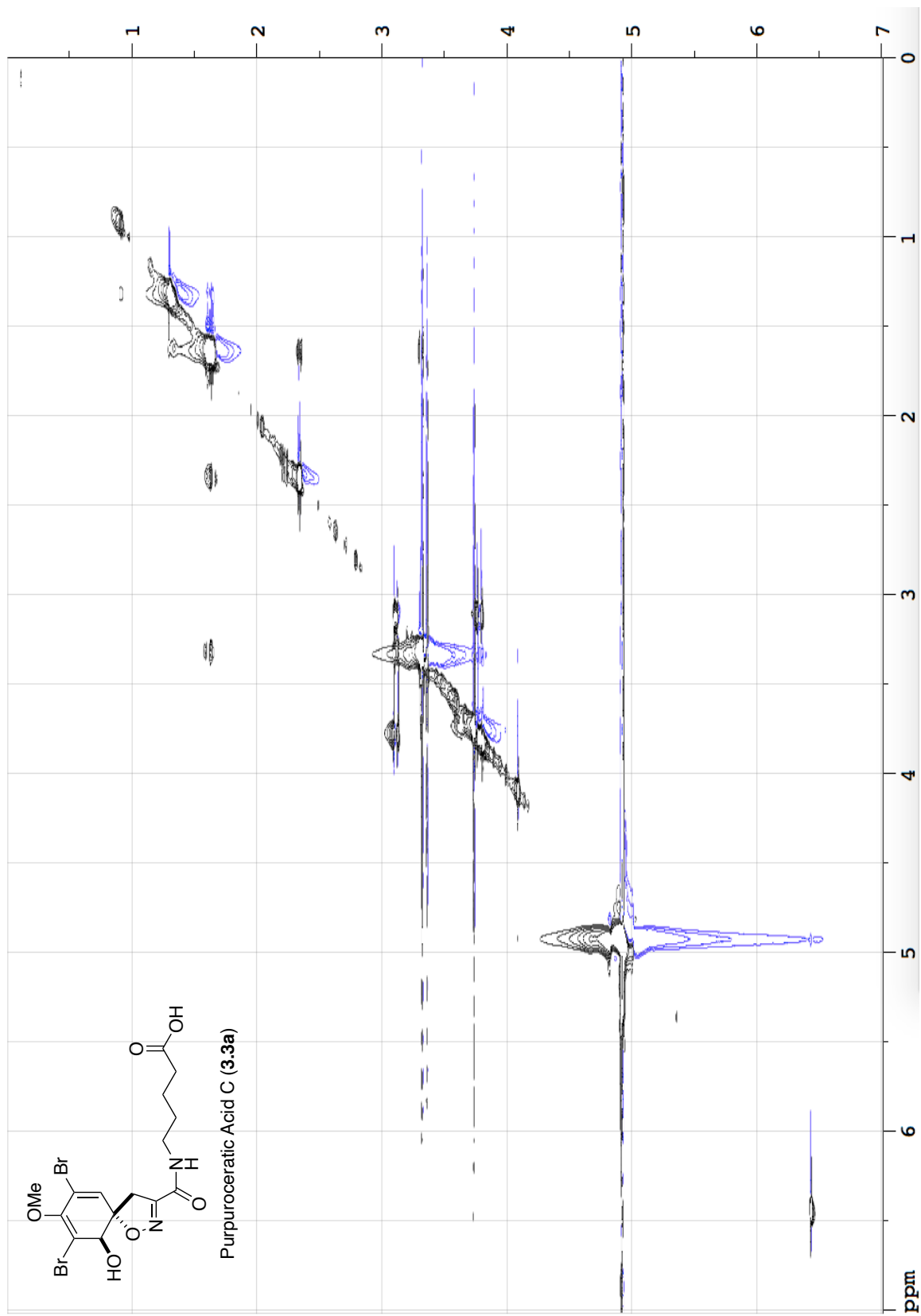


Figure 3.13: Clip-COSY of Compound 3.3a (600 MHz, CD₃OD).

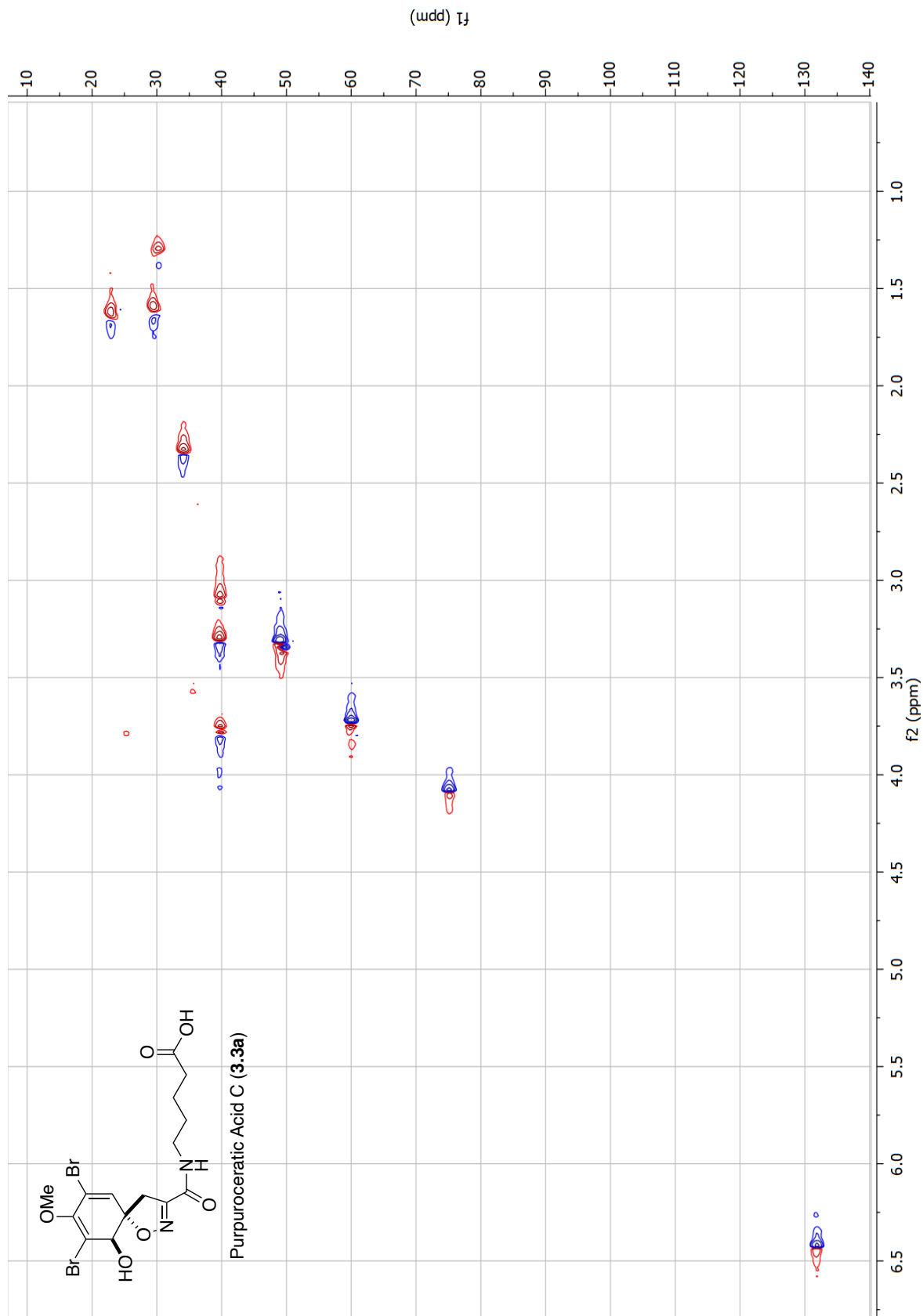


Figure 3.14: HSQC of Compound **3.3a** (600 MHz, CD_3OD).

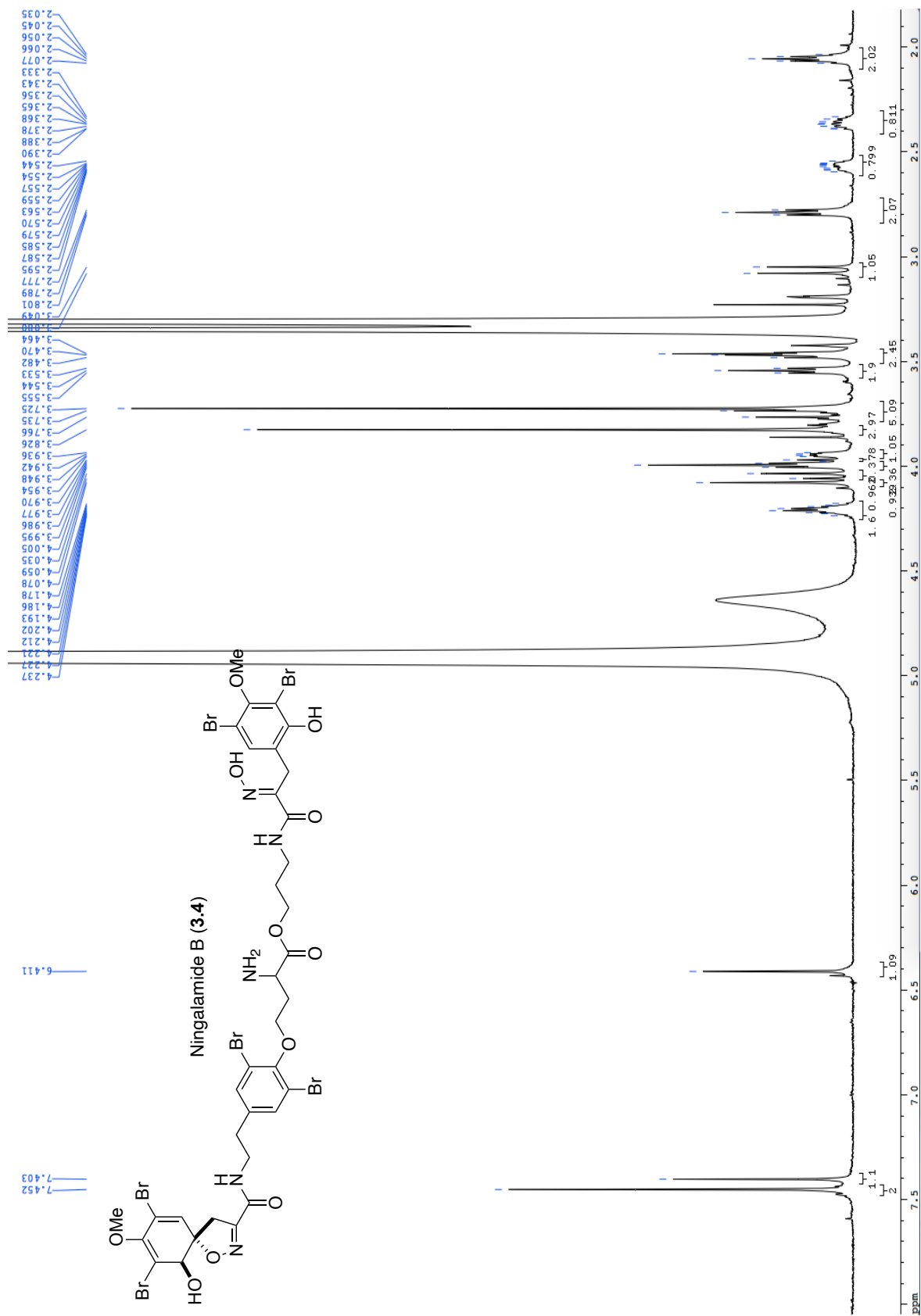


Figure 3.15: ¹H NMR of Compound **3.4** (600 MHz, CD₃OD).

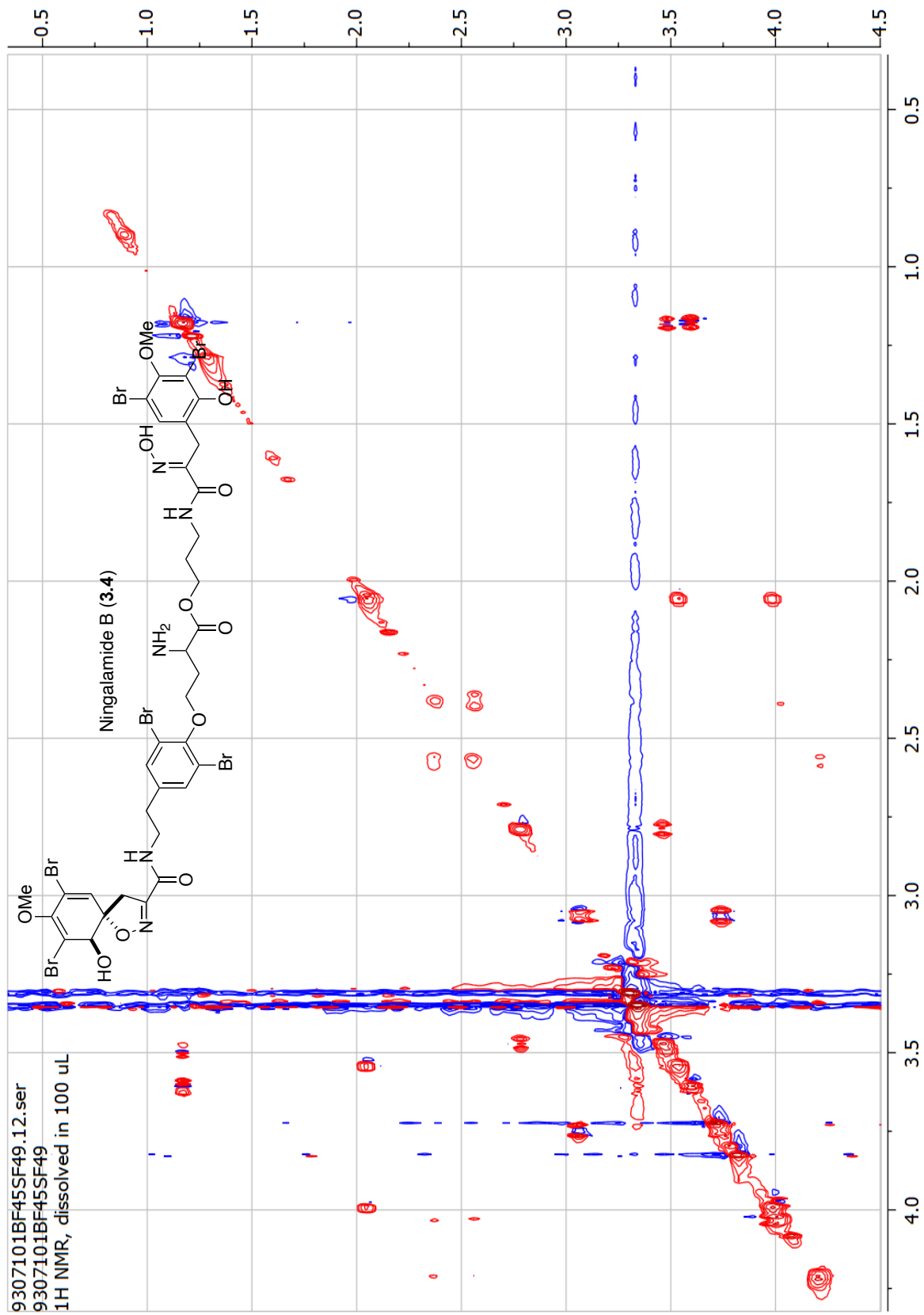


Figure 3.17: DQF-COSY of Compound 3.4 (600 MHz, CD₃OD).

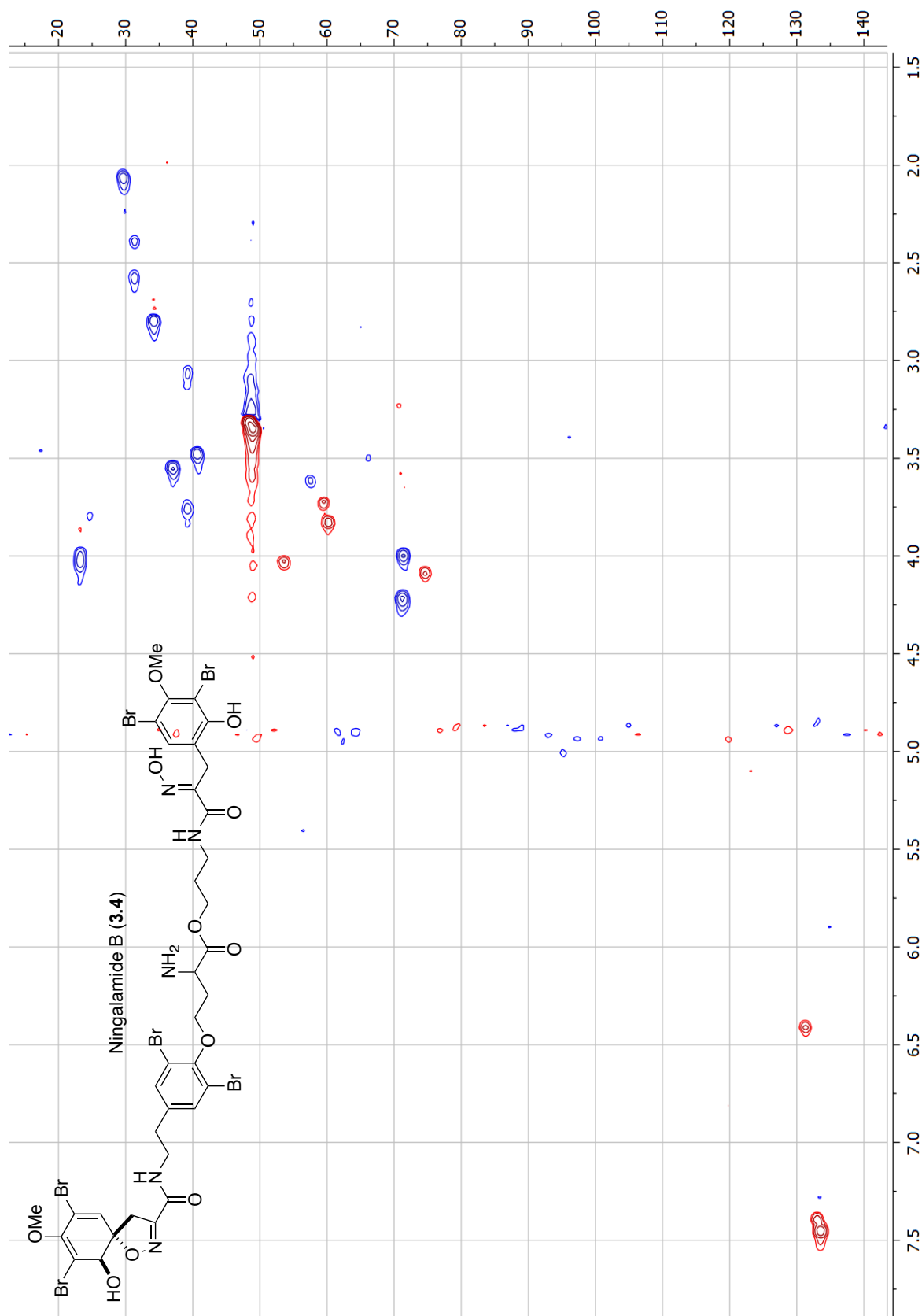


Figure 3.18: HSQC of Compound **3.4** (600 MHz, CD₃OD).

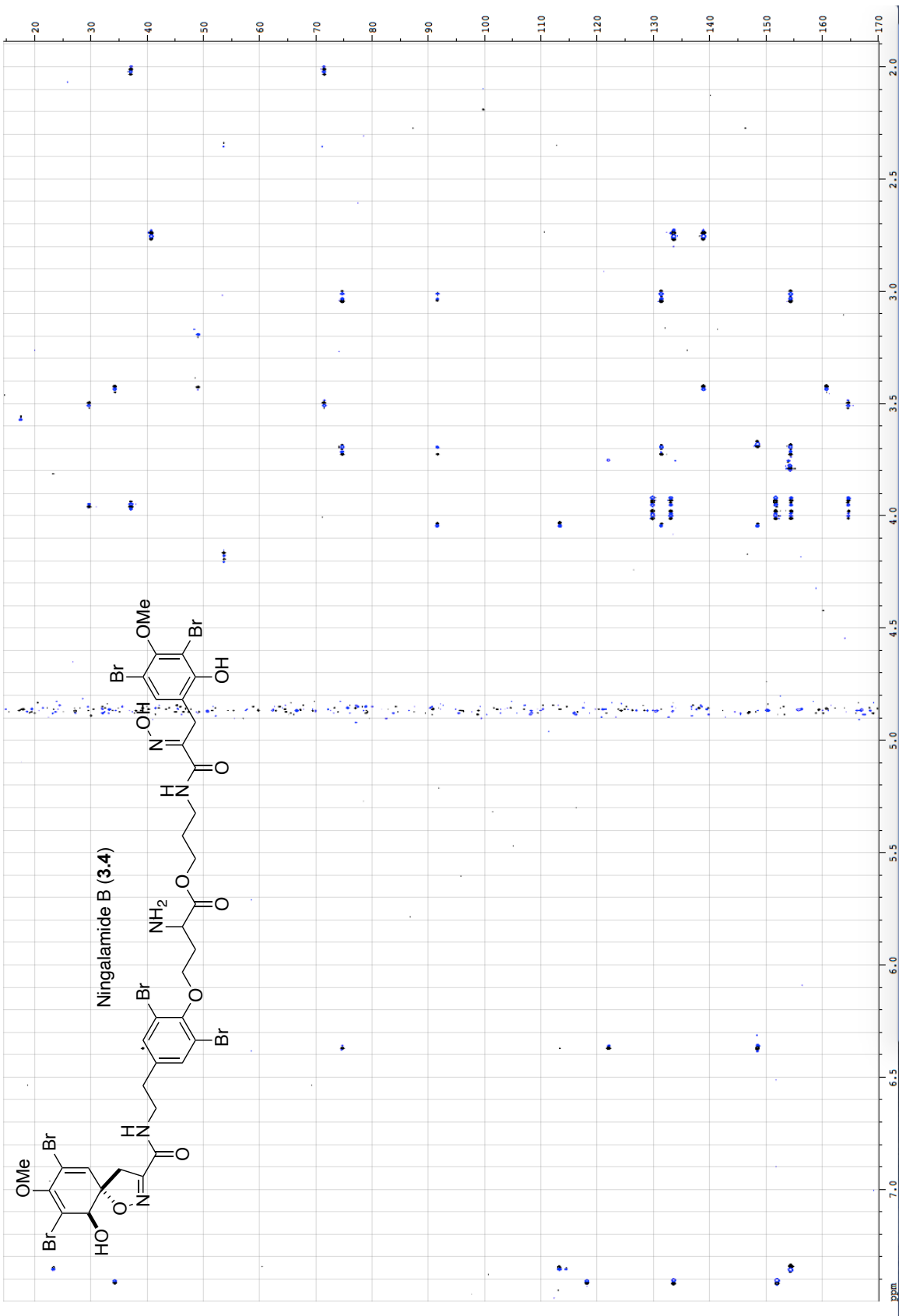
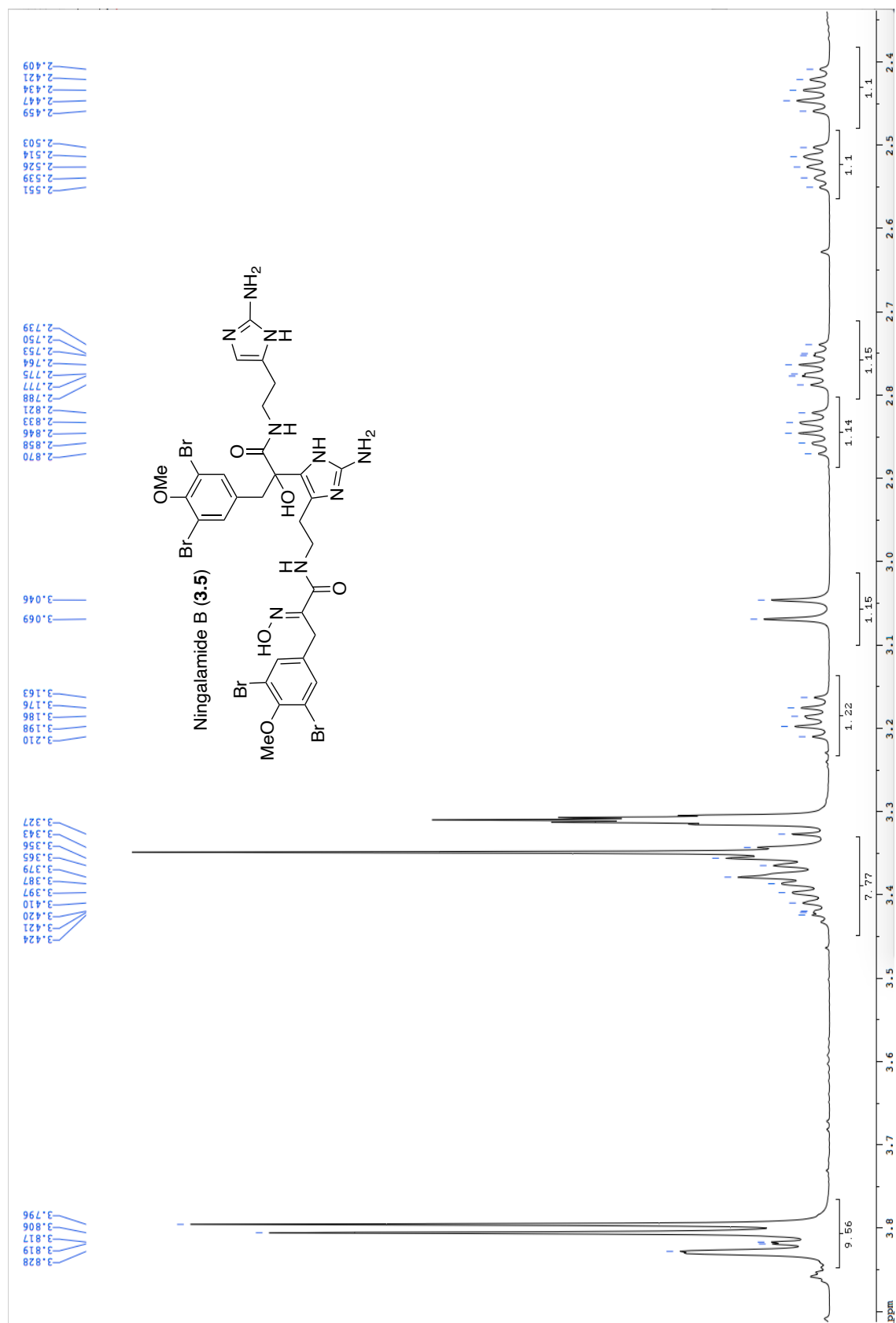


Figure 3.19: HMBC of Compound **3.4** (600 MHz, CD₃OD).



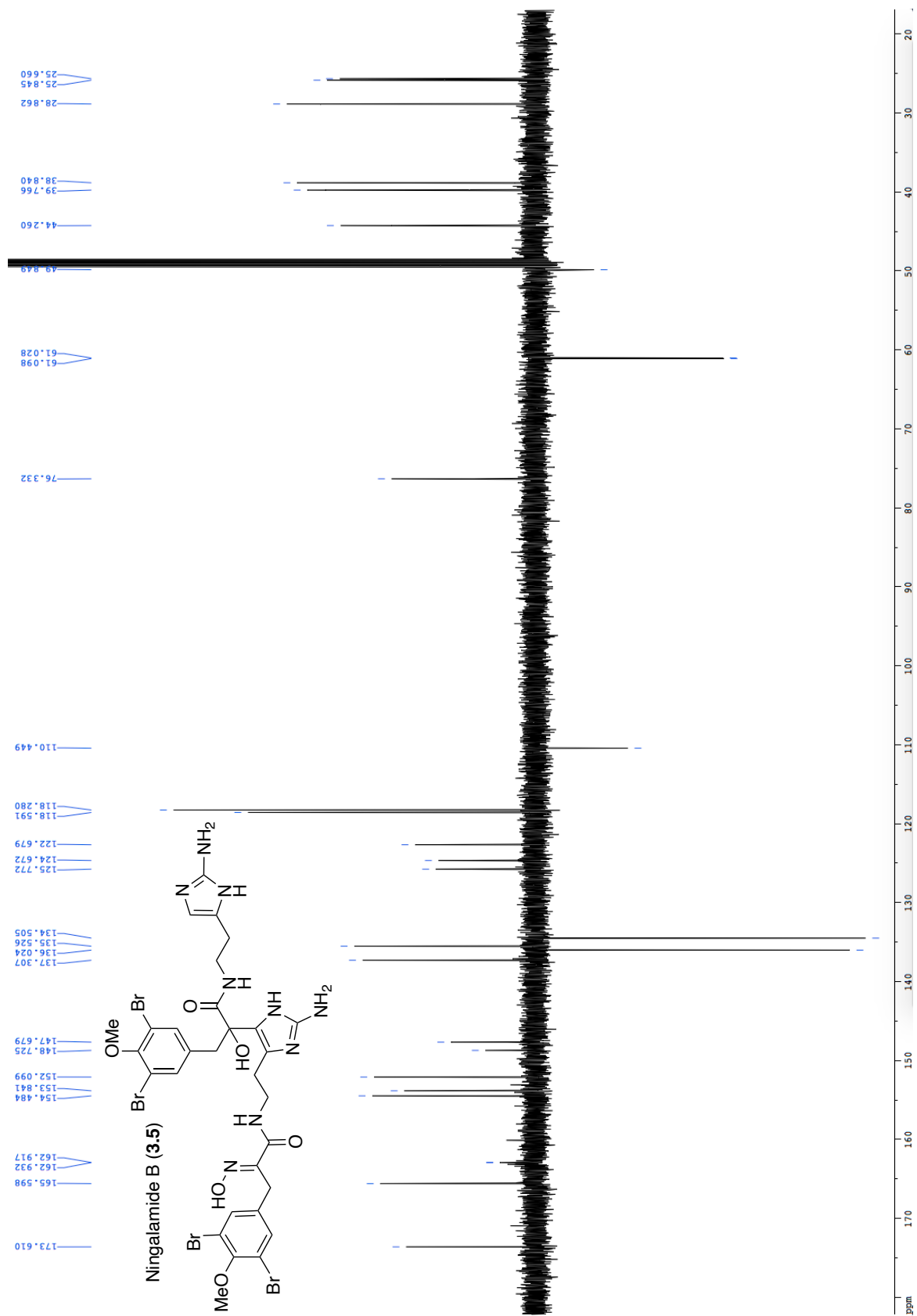


Figure 3.22: APT of Compound 3.5 (150 MHz, CD₃OD).

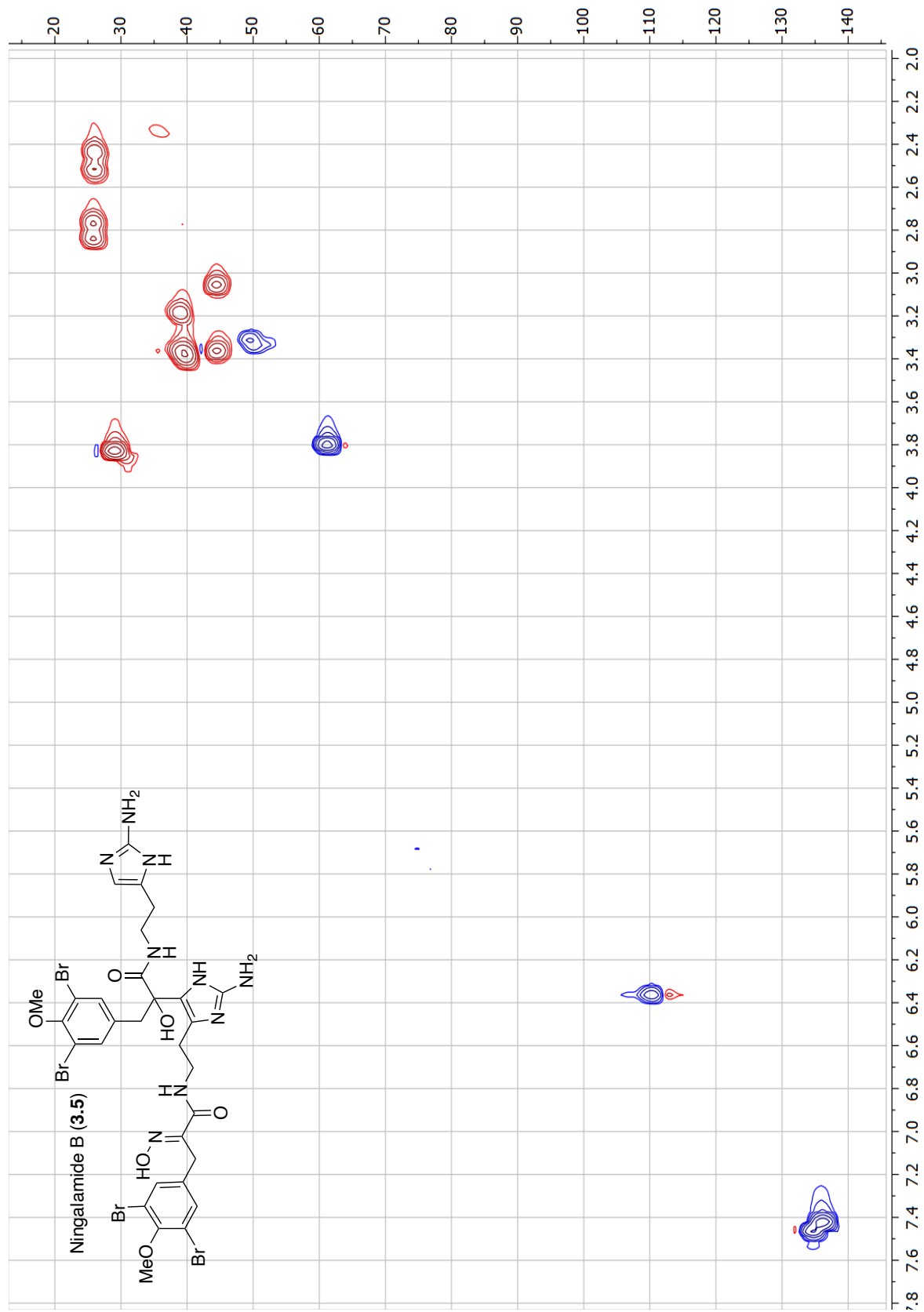
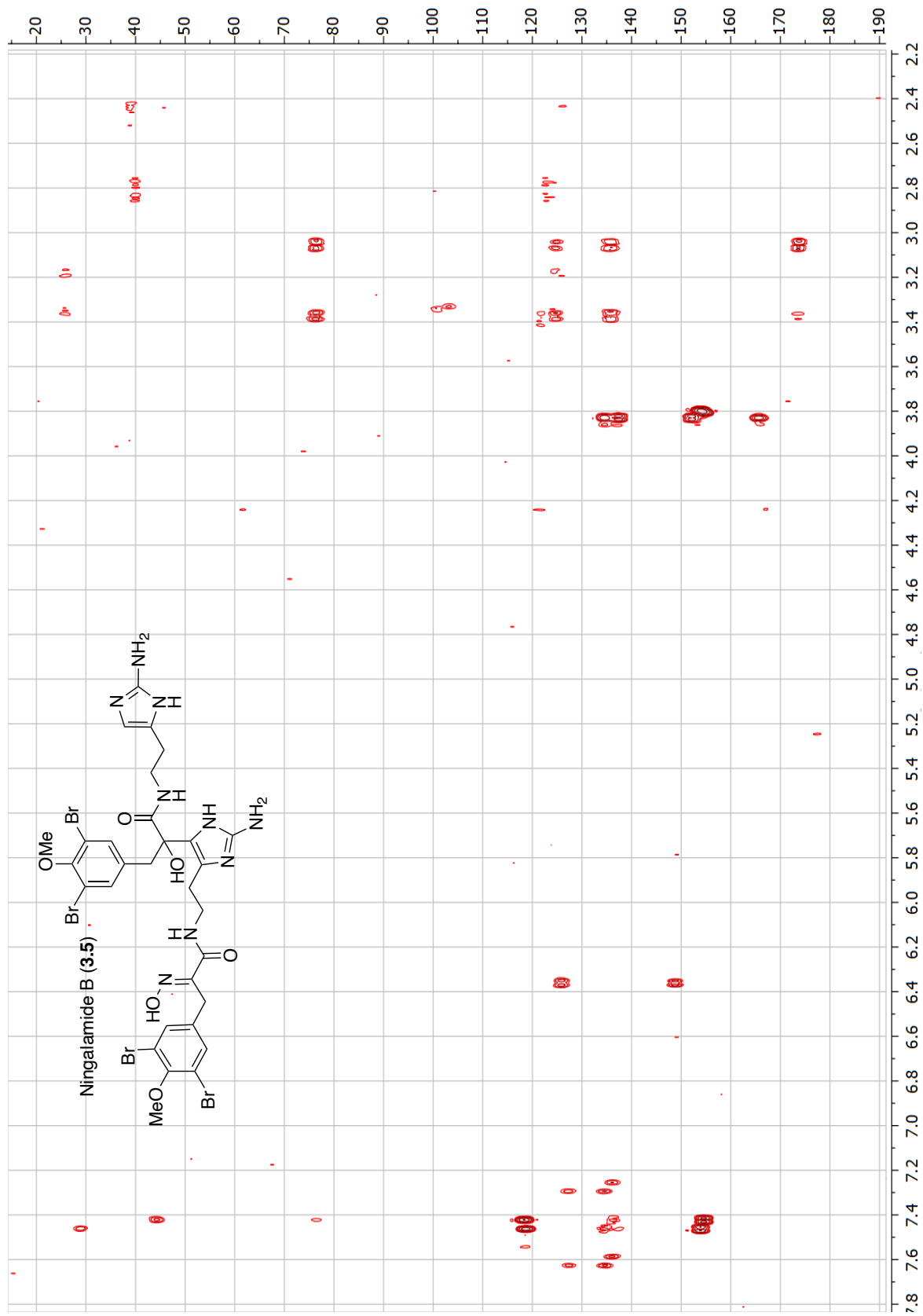
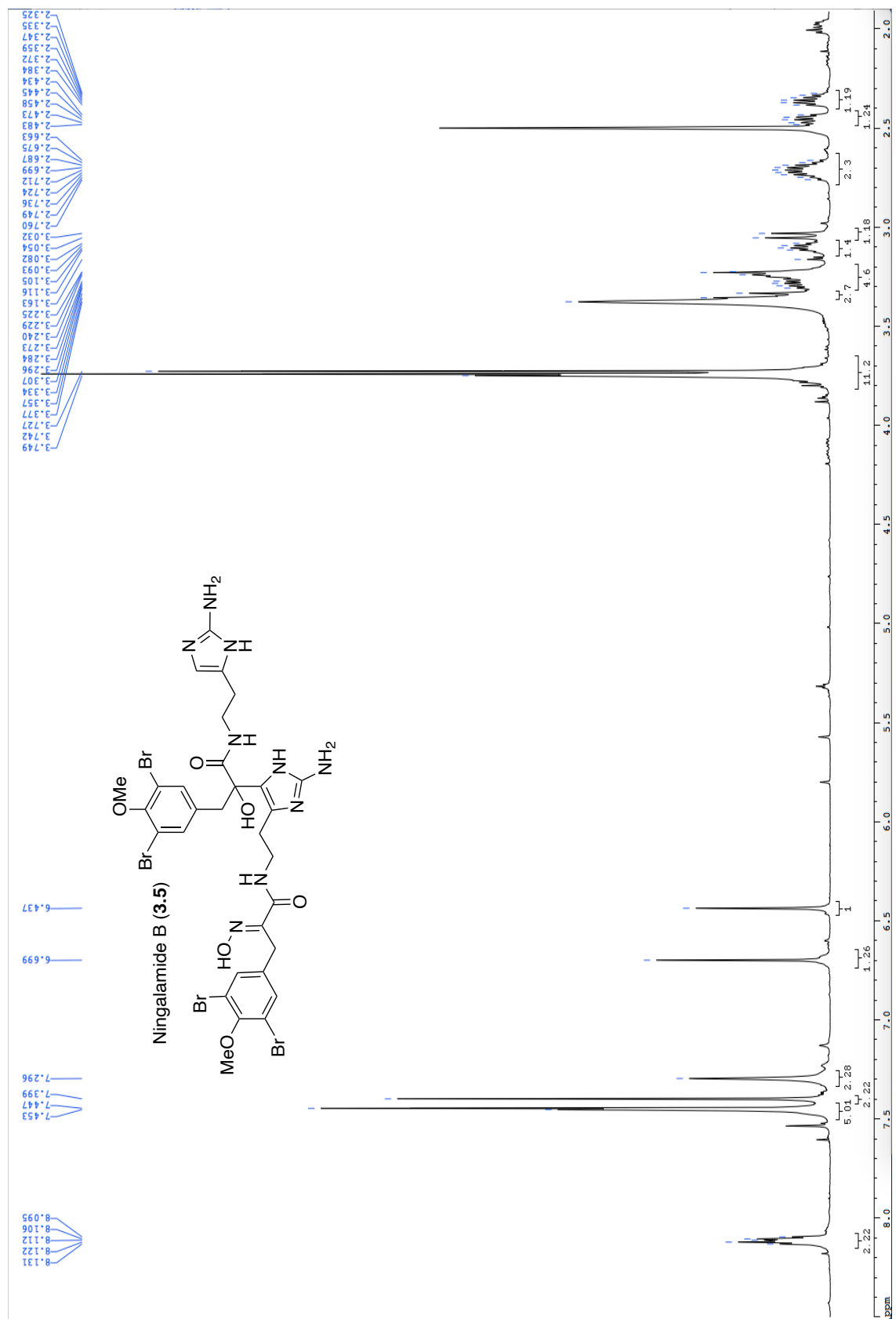


Figure 3.24: HSQC of Compound 3.5 (600 MHz, CD₃OD).





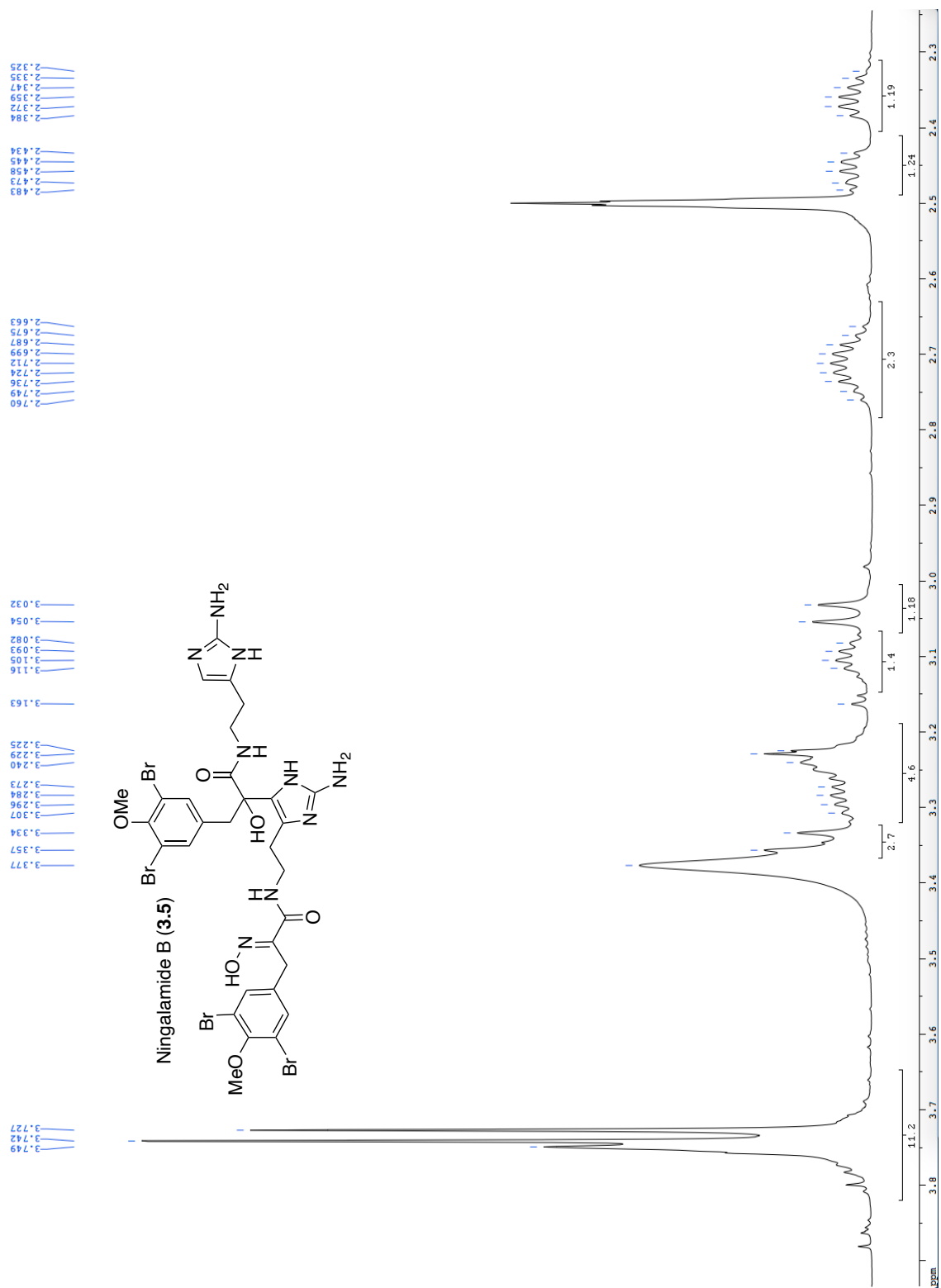
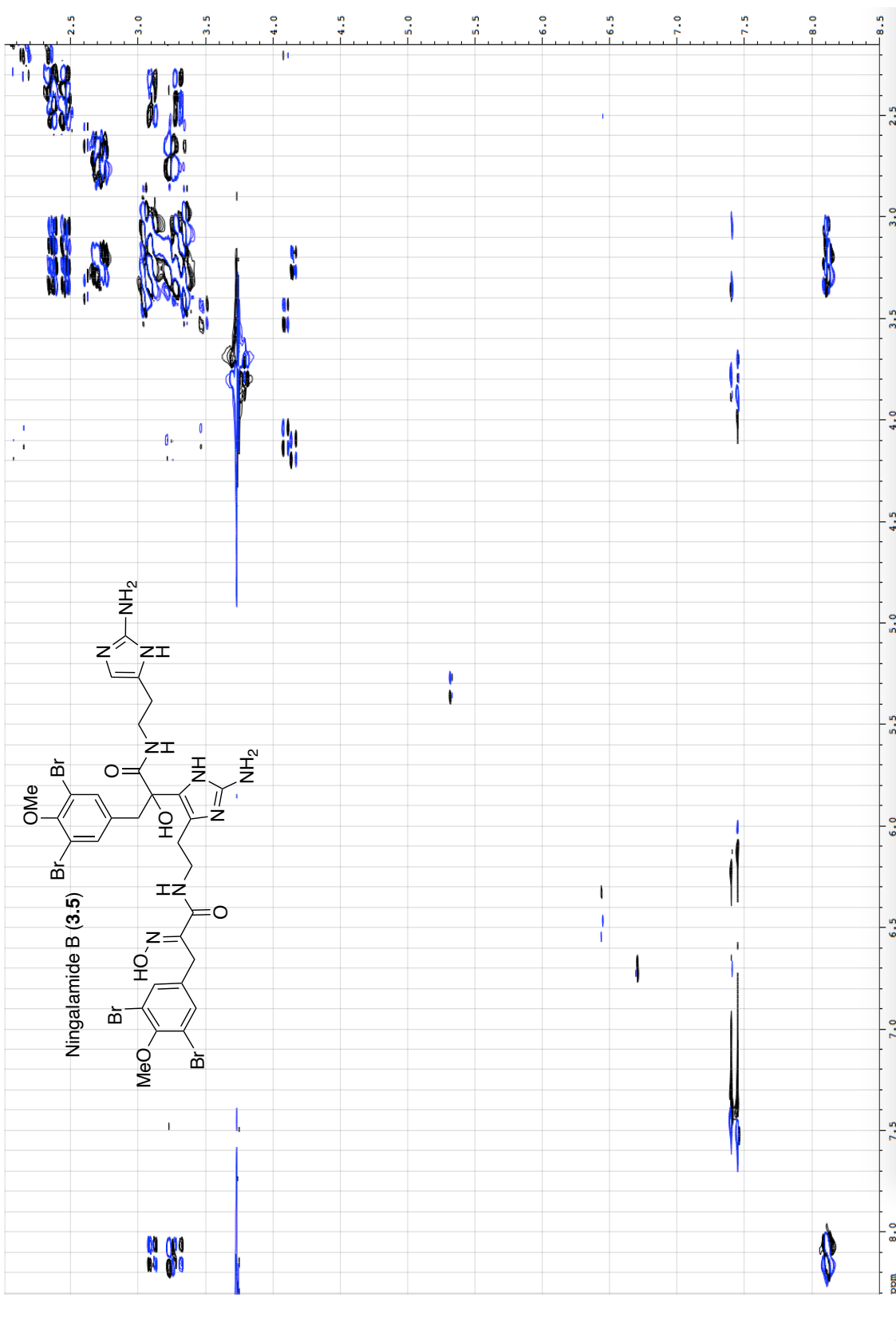


Figure 3.28: ¹H NMR Expansion of Compound **3.5** (600 MHz, DMSO-d₆).



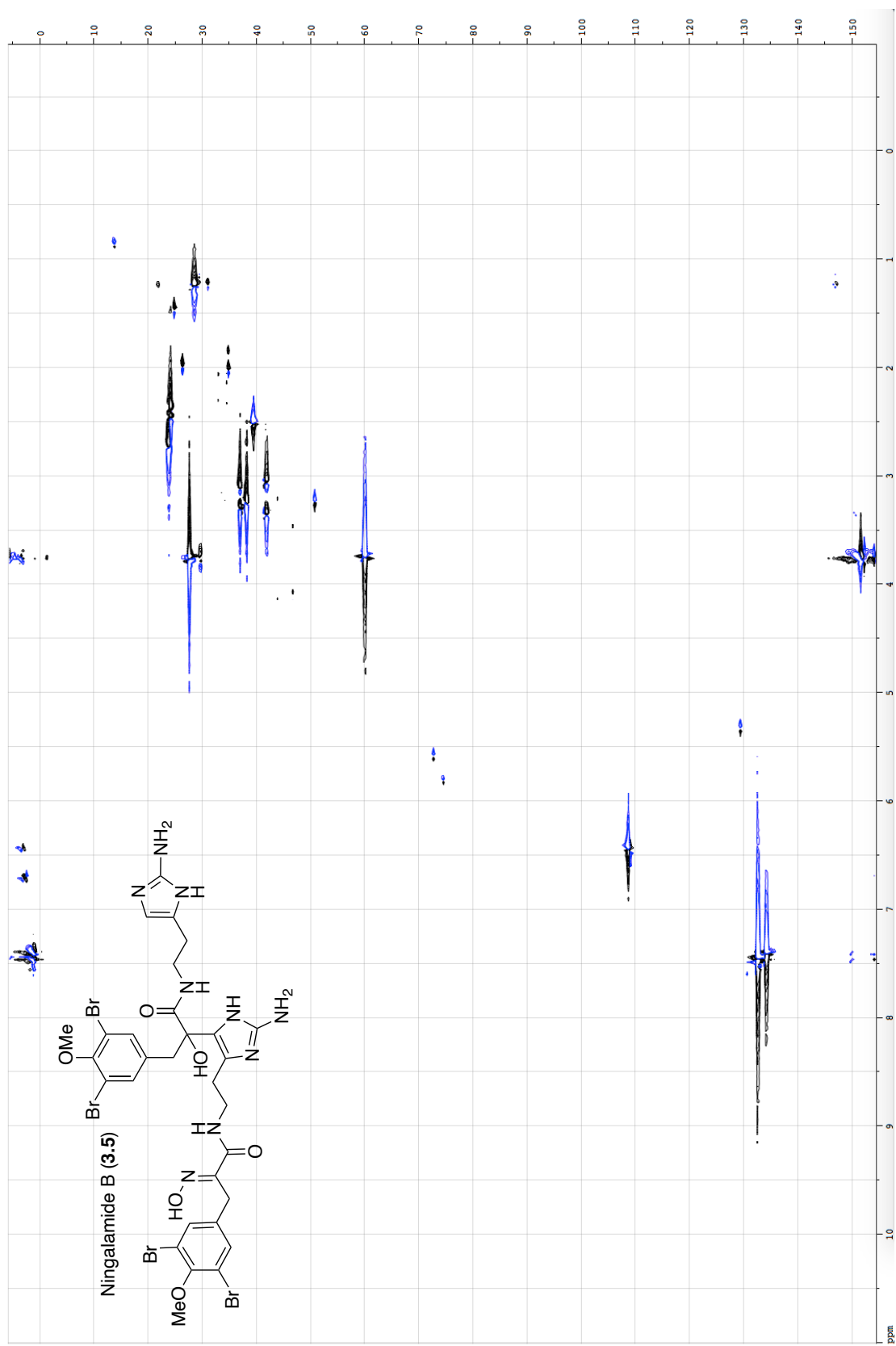
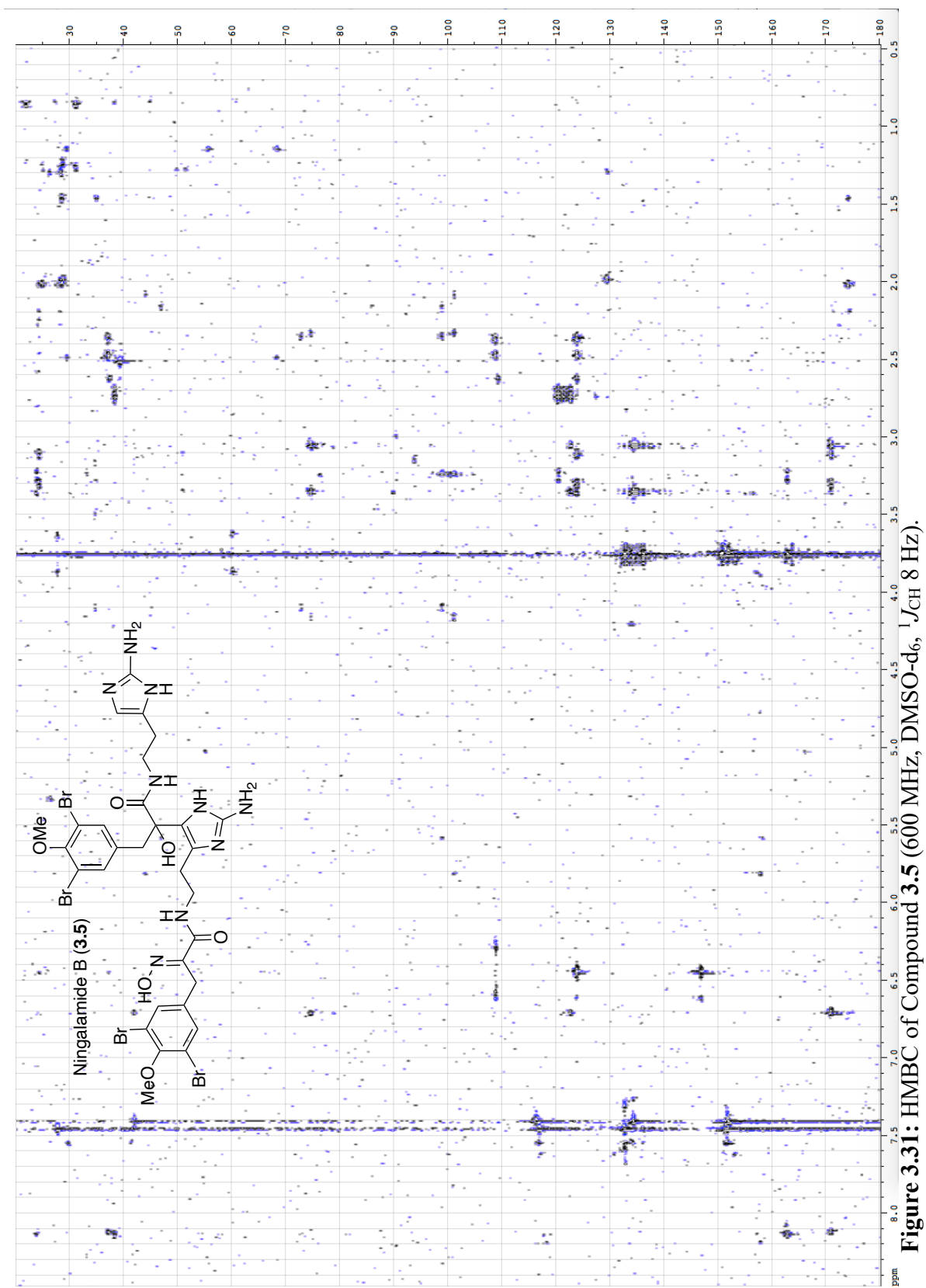


Figure 3.30: HSQC-ASAP of Compound 3.5 (600 MHz, DMSO-d₆).



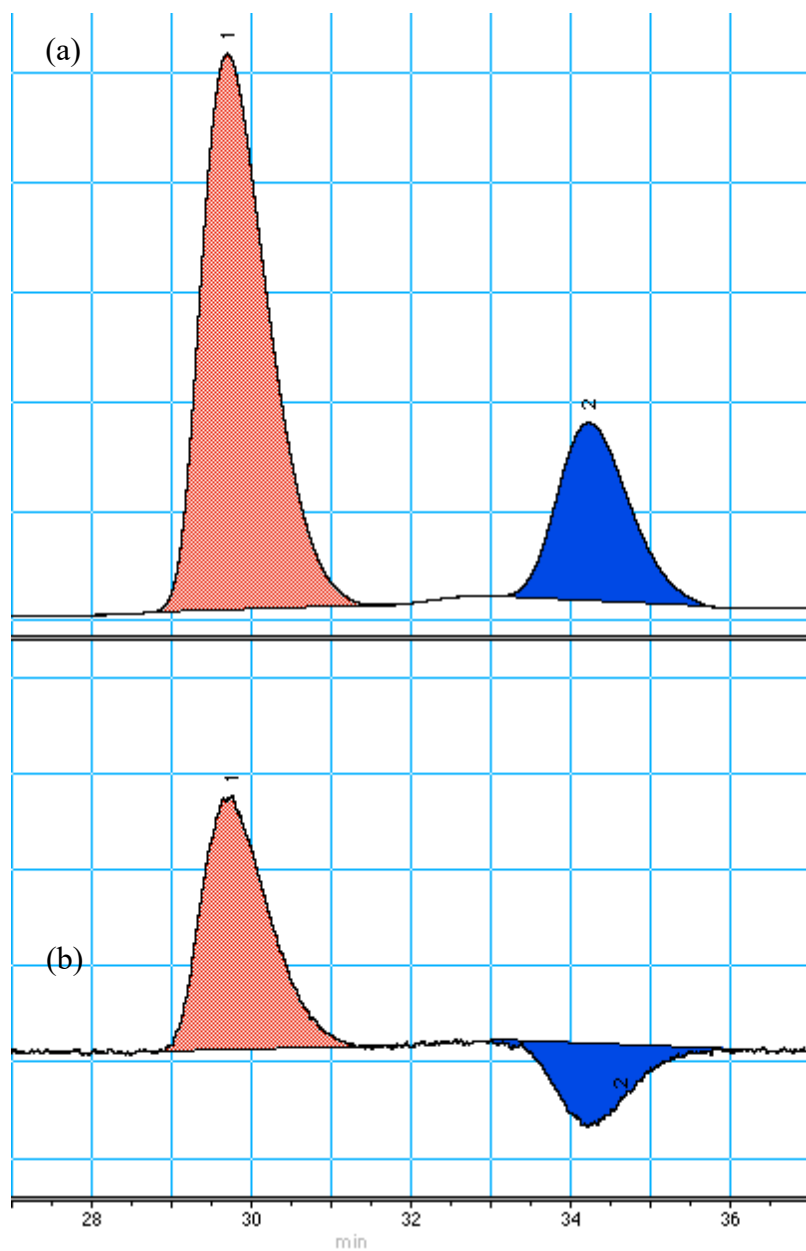


Figure 3.32: (a) UV-vis and (b) CD Chiral-Phase HPLC Traces of Compound **3.1b** (Amylose-1 10% IPA-hexanes, 1 mL.min⁻¹, (+)-**3.1b**: t_R = 29.68 min, area = 74.31; (-)-**3.1b**: t_R = 34.20 min, area = 25.69; 48.6 %ee).

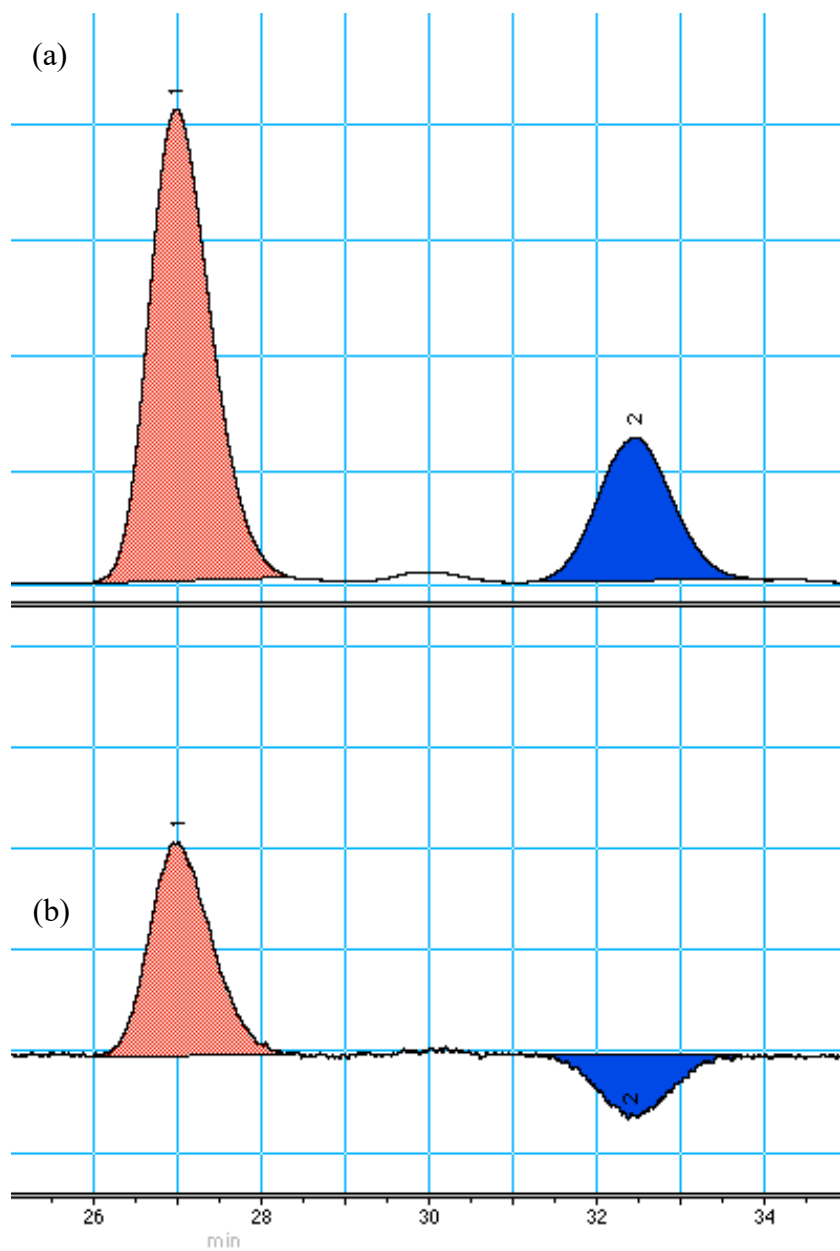


Figure 3.33: (a) UV-vis and (b) CD Chiral-Phase HPLC Traces of Compound **3.2b** (Amylose-1 10% IPA-hexanes, 1 mL.min⁻¹, (+)-**3.2b**: $t_R = 26.99$ min, area = 73.12; (-)-**3.2b**: $t_R = 32.47$ min, area = 26.88; 46.2 %ee).

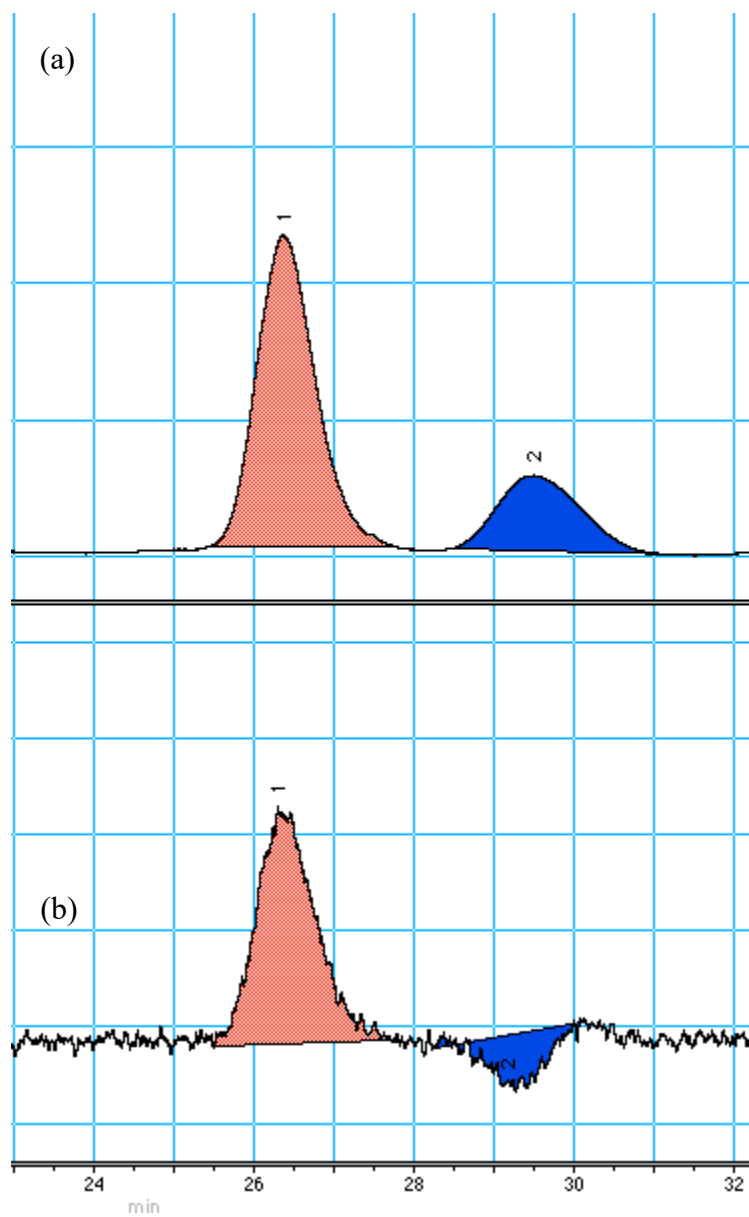


Figure 3.34: (a) UV-vis and (b) CD Chiral-Phase HPLC Traces of Compound **3.3b** (Amylose-1 10% IPA-hexanes, 1 mL.min⁻¹, (+)-**3.3b**: t_R = 26.37 min, area = 74.66; (-)-**3.3b**: t_R = 29.50 min, area = 25.34; 49.3 %ee).

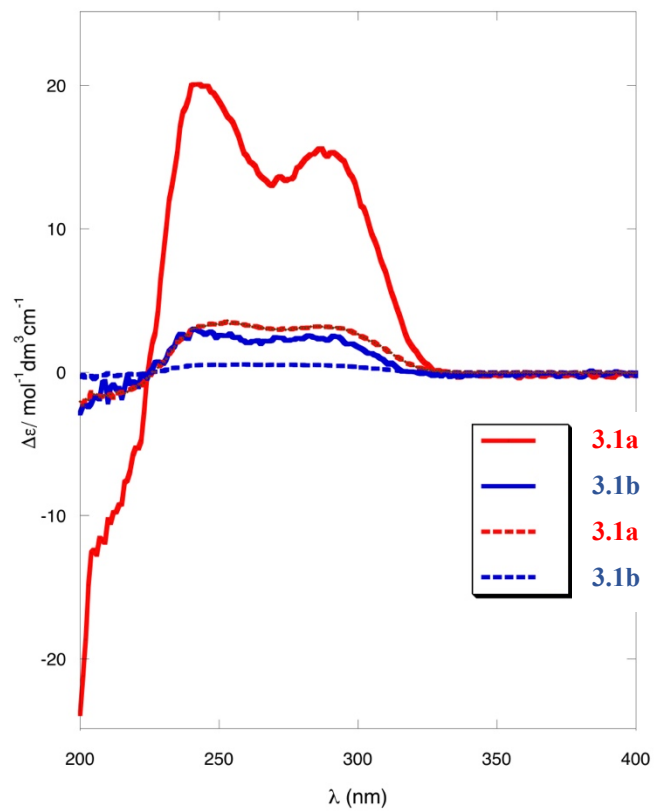


Figure 3.35: CD of Compounds **3.1a** ($c = 1.85 \times 10^{-4}$ M), and **3.1b** (1.85×10^{-4} M) in CH₃OH (dotted, 23 °C) or CH₃CN.

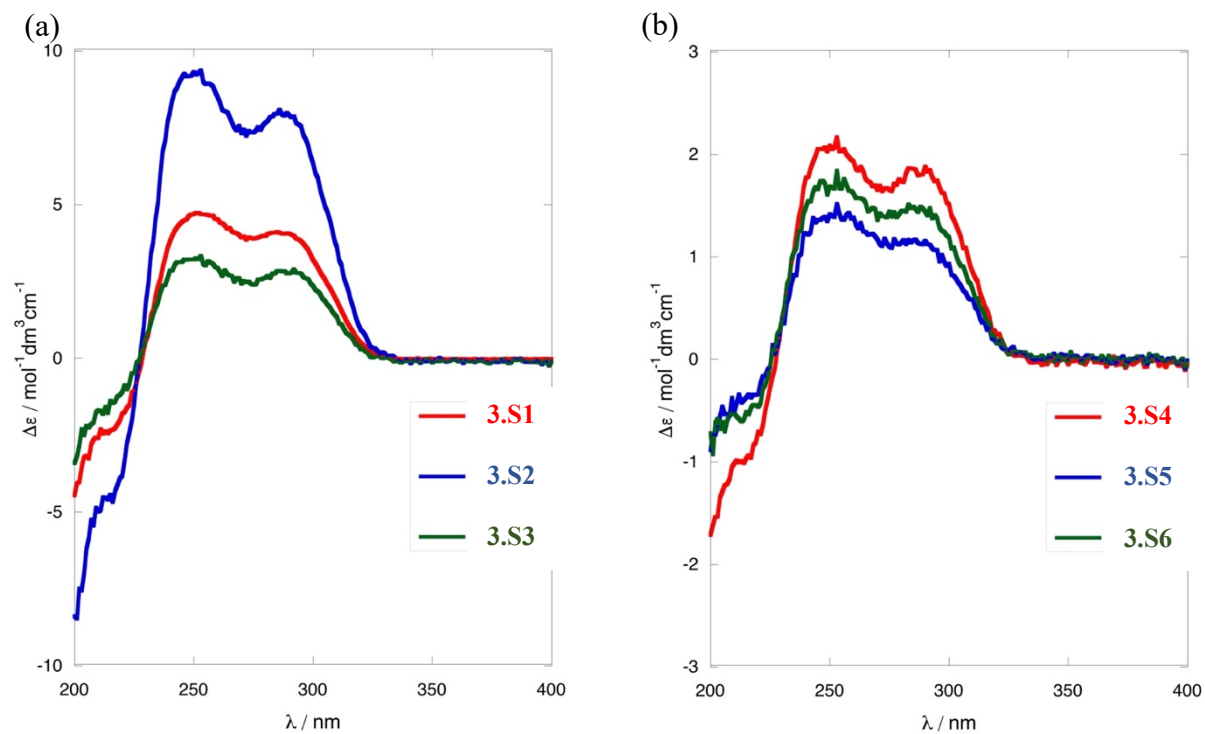


Figure 3.36: CD of Compounds (a) S3.1 ($c = 3.12 \times 10^{-4} \text{ M}$), S3.2 ($3.12 \times 10^{-4} \text{ M}$), S3.3 ($1.39 \times 10^{-4} \text{ M}$), (b) S3.4 ($c = 3.12 \times 10^{-4} \text{ M}$), S3.5 ($1.04 \times 10^{-4} \text{ M}$), and S3.6 ($1.04 \times 10^{-4} \text{ M}$) (MeOH, 23 °C).

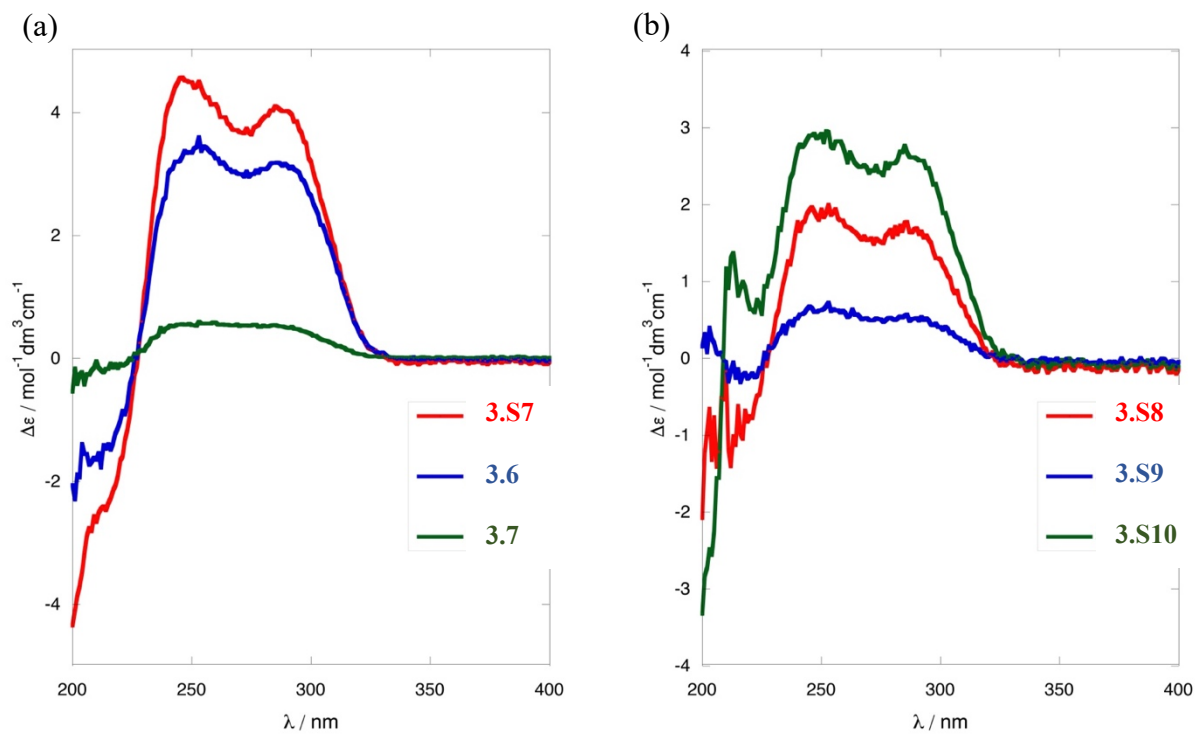


Figure 3.37: CD of Compounds (a) **3.6** ($c = 6.25 \times 10^{-4} \text{ M}$), **3.7** ($1.25 \times 10^{-4} \text{ M}$), **S3.7** ($3.12 \times 10^{-4} \text{ M}$), (b) **S3.8** ($c = 2.08 \times 10^{-4} \text{ M}$), **S3.9** ($3.75 \times 10^{-4} \text{ M}$), and **S3.10** ($2.08 \times 10^{-4} \text{ M}$) (MeOH, 23 °C).

Table 3.6: ^1H and ^{13}C NMR data of Compound **3.5** (CD_3OD).

Position	δ_{H} (int., mult, J , Hz)	δ_{C}
	3.5^a	3.5^b
1	7.46 (1H, s)	134.5
2		118.6
3		153.8
4		118.6
5	7.46 (1H, s)	134.5
6		137.3
7	3.83 (2H, d, 1.7)	28.9
8		152.1
9		165.6
11	3.37 (2H, m)	39.7
12a	2.76 (1H, m)	25.7
12b	2.83 (1H, m)	
13		122.7
14		124.7
16		147.7
1'	7.42 (1H, s)	136.0
2'		118.3
3'		154.5
4'		118.3
5'	7.42 (1H, s)	136.0
6'		135.5
7a'	3.06 (1H, d, 13.8)	44.3
7b'	3.38 (1H, d, 13.8)	
8'		76.3
9'		173.6
11a'	3.19 (1H, m)	38.8
11b'	3.40 (1H, m)	
12a'	2.43 (1H, m)	25.8
12b'	2.52 (1H, m)	
13'		125.8
14'	6.37 (1H, s, $^1J_{\text{CH}} = 198$ Hz)	110.4
16'		148.7
3-OMe	3.80 (3H, s) ^c	60.1
3'-OMe	3.81 (3H, s) ^c	60.0

^a600 MHz. ^bAcquired from APT (150 MHz). ^cAssignment of the two methoxy's may be interchanged.

3.10 References and Notes

- (1) Peng, J.; Li, J.; Hamann, M. T. The Marine Bromotyrosine Derivatives. *Alkaloids Chem. Biol.* **2005**, *61*, 59-262.
- (2) Lira, N. S.; Montes, R. C.; Tavares, J. F.; Silva, M. S. d.; De Cunha, E. V.; Athayde-Filho, P. F. d.; Rodrigues, L. C.; Dias, C. d. S.; Barbosa-Filho, J. M. Brominated Compounds from Marine Sponges of the Genus *Aplysina* and a Compilation of Their ¹³C NMR Spectral Data. *Mar. Drugs* **2011**, *9*, 2316-2368.
- (3) Nicacio, K. J.; Ióca, L. P.; Fróes, A. M.; Leomil, L.; Appolinario, L. R.; Thompson, C. C.; Thompson, F. L.; Ferreira, A. G.; Williams, D. E.; Andersen, R. J. Cultures of the Marine Bacterium *Pseudovibrio denitrificans* Ab134 Produce Bromotyrosine-Derived Alkaloids Previously Only Isolated from Marine Sponges. *J. Nat. Prod.* **2017**, *80*, 235-240.
- (4) Kobayashi, J.; Honma, K.; Sasaki, T.; Tsuda, M. Puralidins J-R, New Bromotyrosine Alkaloids from the Okinawan Marine Sponge *Psammaphysilla purea*. *Chem. Pharm. Bull.* **1995**, *43*, 403-407.
- (5) In spite of isolation of free acid **3a**, we were unable to detect, by LCMS, the homologous free acids **1a-2a** (Ref. 6) nor the homologous methyl ester **3b** in our unseparated extracts of *P. crassa*. Consequently, we choose to remain agnostic regarding whether the **1b** and **2b** are artefacts of extraction-isolation or 'true' natural products.
- (6) Kijjoa, A.; Bessa, J.; Wattanadilok, R.; Sawangwong, P.; Nascimento, M. S. J.; Pedro, M.; Silva, A. M. S.; Eaton, G. Dibromotyrosine Derivatives, A Maleimide, Aplysamine-2 and Other Constituents of the Marine Sponge *Pseudoceratina purpurea*. *Z. Naturforsch. B* **2005**, *60*, 904-908.
- (7) Original isolation article: (a) Ciminiello, P.; Fattorusso, E.; Magno, S.; Pansini, M. Chemistry of Verongida Sponges, III. Constituents of a Caribbean *Verongula* Sp. *J. Nat. Prod.* **1994**, *57*, 1564-1569. For complete NMR data of **7**, see (b) Zhu, G.; Yang, F.; Balachandran, R.; Höök, P.; Vallee, R. B.; Curran, D. P.; Day, B. W. Synthesis and Biological Evaluation of Puralin and Analogues as Cytoplasmic Dynein Heavy Chain Inhibitors. *J. Med. Chem.* **2006**, *49*, 2063-2076.
- (8) Rogers, E. W.; Molinski, T. F. Highly Polar Spiroisoxazolines from the Sponge *Aplysina fulva*. *J. Nat. Prod.* **2007**, *70*, 1191-1194.
- (9) (a) Gunasekara, M.; Gunasekara, S. P. Dihydroxyaerothiiniin and Aerophobin 1. Two Brominated Tyrosine Metabolites from the Deep-Water Marine Sponge *Verongula rigida*. *J. Nat. Prod.* **1989**, *52*, 753-756. (b) Cimino, G.; De Rosa S.; De Stefano, S.; Self, R.; Sodano, G. The Bromo-compounds of the True Sponge *Verongia aerophoba*. *Tetrahedron Lett.* **1983**, *24*, 3029-3032.
- (10) Assmann, M.; Wray, V.; Vansoest, R. W. M.; Proksch, P. A New Bromotyrosine Alkaloid from the Caribbean Sponge *Aiolochoxia crassa*. *Z. Naturforsch. C* **1998**, *53*, 398-401.

-
- (11) Fendert, T.; Wray, V. Bromoisoxazoline Alkaloids from the Caribbean Sponge *Aplysina insularis*. *Z. Naturforsch. C* **1999**, *54*, 246-252.
- (12) Rodríguez, A.; Piña, I. C. The Structures of Aplysinamisines I, II, and III: New Bromotyrosine-Derived Alkaloids from the Caribbean Sponge *Aplysina cauliformis*. *J. Nat. Prod.* **1993**, *56*, 907-914.
- (13) Ragini, K.; Fromont, J.; Piggott, A. M.; Karuso, P. Enantiodivergence in the Biosynthesis of Bromotyrosine Alkaloids from Sponges? *J. Nat. Prod.* **2017**, *80*, 215-219.
- (14) Tilvi, S. Identifying the Related Compounds Using Electrospray Ionization Tandem Mass Spectrometry: Bromotyrosine Alkaloids from Marine Sponge *Psammaphysilla purpurea*. *Eur. J. Mass Spec.* **2012**, *18*, 333-343.
- (15) Gao, H.; Kelly, M.; Hamann, M. T. Bromotyrosine-Derived Metabolites from the Sponge *Aiolochoira crassa*. *Tetrahedron* **1999**, *55*, 9717-9726.
- (16) Yagi, H.; Matsunaga, S.; Fusetani, N. Purpuramines A-I, New Bromotyrosine-Derived Metabolites from the Marine Sponge *Psammaphysilla purpurea*. *Tetrahedron* **1993**, *49*, 3749-3754.
- (17) Rogers, E.W.; de Olivera, M. F.; Berlinck, R. G. S.; König, G. M.; Molinski, T. F. Stereochemical Heterogeneity in Verongid Sponge Metabolites. Absolute Stereochemistry of (+)-Fistularin-3 and (+)-11-*epi*-Fistularin-3 by Microscale LCMS-Marfey's Analysis. *J. Nat. Prod.* **2005**, *68*, 891-896.
- (18) Dai, J.; Parrish, S. M.; Yoshida, W. Y.; Richard Yip, M. L.; Turkson, J.; Kelly, M.; Williams, P. Bromotyrosine-Derived Metabolites from an Indonesian Marine Sponge in the Family Aplysinellidae (Order Verongiida). *Bioorg. Med. Chem. Lett.* **2016**, *26*, 499-504.
- (19) Marfey, P. Determination of D-Amino Acids. II. Use of a Bifunctional Reagent, 1,5-Difluoro-2,4-Dinitrobenzene. *Carlsberg Res. Commun.* **1984**, *49*, 591-596.
- (20) DL-Homoserine-L-DAA derivatives eluted at $t_R = 14.00$ min and $t_R = 14.37$ min for L- and D-DAA derivatives, respectively. (a) Morita, H.; Shishido, A.; Matsumoto, T.; Itokawa, H.; Takeya, K. Cyclolinopeptides B-E, New Cyclic Peptides from *Linum usitatissimum*. *Tetrahedron* **1999**, *55*, 967-976.
- (21) Aside from compound **9**, the sample also showed a sodiated molecular ion of the corresponding homoserine lactone [HRMS (ESI-TOF) m/z 491.1288 $[M+Na]^+$ (calcd for $C_{21}H_{20}N_6O_7Na^+$ 491.1286)], the most likely structure given the acidic conditions of hydrolysis.

-
- (22) McMillan, J. A.; Paul, I. C.; Goo, Y. M.; Rinehart Jr., K. L.; Krueger, W. C.; Pschigoda, L. M. An X-Ray Study of Aerothionin from *Aplysina fistularis* (Pallas). *Tetrahedron Lett.* **1981**, *22*, 39-42.
- (23) Shearman, J. W.; Myers, R. M.; Brenton, J. D.; Ley, S. V. Total Syntheses of Subereamollines A and B. *Org. Biomol. Chem.* **2011**, *9*, 62-65.
- (24) (a) Moscowitz, A.; Charney, E.; Weiss, U.; Ziffer, J. Optical Activity in Skewed Dienes. *J. Am. Chem. Soc.* **1961**, *83*, 4661-4663. (b) Burgstahler, A. W.; Ziffer, H.; Weiss, U. The Configurations of Levopimaric Acid and α -Phellandrene; Interpretation of their Rotatory Dispersions. *J. Am. Chem. Soc.* **1961**, *83*, 4660-4661.
- (25) Salib, M. N.; Jamison, M. T.; Molinski, T. F. Bromo-spiroisoxazoline Alkaloids, Including an Iserine Peptide, from the Caribbean Marine Sponge *Aplysina lacunosa*. *J. Nat. Prod.* **2020**, *83*, 1532-1540.
- (26) The origin of β -alanine in primary and secondary metabolism is more complex.
- (27) Salib, M. N.; Molinski, T. F. Cyclic Hexapeptide Dimer, Antatollamides A and B, from the Ascidian *Didemnum molle*. A Tryptophan-Derived Auxiliary for L- and D-Amino Acid Assignments. *J. Org. Chem.* **2017**, *82*, 10181-18187.
- (28) Orhan, I.; Sener, B.; Choudhary, M. I.; Khalid, A. Acetylcholinesterase and Butyrylcholinesterase Inhibitory Activity of Some Turkish Medicinal Plants. *J. Ethnopharmacol.* **2004**, *91*, 57-60.
- (29) Ellman, G. L.; Courtney, K. D.; Andres, Jr., V.; Featherstone, R. M. A New and Rapid Colorimetric Determination of Acetylcholinesterase Activity. *Biochem. Pharmacol.* **1961**, *7*, 88-95.

CHAPTER FOUR. DISCOVERY OF BIOACTIVE BROMOTYROSINE ALKALOIDS FROM
THE BAHAMIAN MARINE SPONGE *AIOLOCHROIA CRASSA*

Abstract: Nine bromotyrosine alkaloids (BTAs), including debromoianthelline (**4.1**), pseudoceratinic acid (**4.2a**), methyl pseudoceratinate (**4.2b**), 13-oxo-ianthelline (**4.3**), aiolochroiamides A-D (**4.4a,b** and **4.5a,b**) and 7-hydroxypurealidin J (**4.6**), were isolated from a specimen of *Aiolochoxia crassa* (Hyatt; previously, *Pseudoceratina crassa*) collected in the Bahamas. The planar structures of **4.1–4.6** were established from analysis of ^1H , ^{13}C and 2D NMR spectra, IR, and mass spectrometry data. The structures of **4.2–4.4** consist of an *O*-methyl-2,6-dibromotyrosyl ketoxime (subunit A) amide linked to various groups (subunit B). Compound **4.1** is debromoianthelline, and alkaloids **4.2a** and **4.2b** are amides of 3-aminopropanoic acid and methyl 3-aminopropanoate, respectively. BTAs **4.3** and **4.4** are linked to 5-(2-aminoethyl)-2-iminoimidazolidin-4-one, and a hexahydropyrrolo[2,3-*d*]imidazol-2(1*H*)-imine nucleus, respectively, whereas **4.5** is a new oxidative motif in the family: it's a dimer of two units of *O*-methyl-2,6-dibromotyrosine 2-oxopropanamide linked to 2-aminohistamine through a five-membered lactam. Alkaloid **4.6** contains a spirocyclohexadienyl-isoxazoline ring system, amide-coupled to 2-aminohistamine similar to that found in purealidin J and aerophobin-1, but with an unprecedented hydroxylation at C-7. The configuration of the 2,4-diaminobutanoic acid residue in **4.3** was determined, after acid hydrolysis under microwave conditions and derivatization with L-FDTA (a tryptophan-derived reagent deployed in Marfey's method), to be a 2:1 mixture of the L- and D- enantiomers. Alkaloids, **4.4a,b** and **4.5a,b**, were racemic but isolated as diastereomeric pairs. The relative configurations of **4.4a**, **4.4b**, **4.5a** and **4.5b** were assigned by comparison of ^1H and ^{13}C chemical shifts, calculated by DFT (APFD/aug-cc-pVDZ level, GIAO, scrf), with

experimental values. Compounds **4.5a,b**, ningalamide B (**4.9**), and ianthelline (**4.7**) moderately inhibited butyrylcholinesterase, and *Candida* and *Cryptococcus* spp.

4.1 Introduction

Marine sponges of the order Verongida are prolific producers of brominated tyrosine alkaloids (BTAs) biogenetically derived from the amino acid Tyr.¹⁻² Chemical modifications in the aromatic rings and side chains give rise to a broad range of biosynthetically related compounds exhibiting diverse biological activities including antifouling (5-bromoverongamine,³ ceratinamides A–B⁴), antimicrobial (pseudoceramines A–D,⁵ araplysillins I–II⁶), antiviral (psammaplysin D,⁷ moloka'iamine⁸), antimalarial (psammaplysin H⁹), and cytotoxic (ma'edamines A–B,¹⁰ fistularin-3,¹¹ psammaplysin C¹² and E⁷). Recently, Berlinck and coworkers reported the isolation of several BTAs from cultures of the marine bacterium *Pseudovibrio denitrificans* Ab134, obtained from tissues of the sponge *Arenosclera brasiliensis*, showing that the origin of BTAs may be marine bacteria associated with Verongid sponges.¹³

Antipodal forms of BTAs, possibly arising from “enantiodivergent”¹⁴ or “enantiomeric”¹⁵⁻¹⁶ biosyntheses, have been isolated from closely associated sponges. For example, (+)-puralidin R was isolated from the Okinawan sponge *Psammaplysilla purea*,¹⁷ while Capon and coworkers obtained (–)-puralidin R from a southern Australian specimen of *Pseudoceratina* sp.¹⁸ Independently, (–)-purpuroceratic acid B was isolated by Karuso and coworkers from a Western Australian *P. cf. verrucosa*,¹⁹ and by Kijjoa et al. from *P. purpurea* from the Gulf of Thailand,²⁰ and shown to be antipodal to the (+)-enantiomer obtained by Molinski and Rogers from a Caribbean *Aplysina fulva*.^{21,22} Although most chiral marine natural products are biosynthesized in

one enantiomeric form, a rare number are produced in both forms; racemic or optically enriched over a wide range of %ee. We have compiled and reviewed chiroptical properties of spiroisoxazoline BTAs from a variety of sources.²³

In our search for inhibitors of butyrylcholinesterase (BuChE) and antifungal compounds active against azole-resistant strains of *Candida* and *Cryptococcus* spp., we examined a MeOH extract of *Aiolochoia crassa* (previously, *Pseudoceratina crassa*, Hyatt, 1875) collected in the Bahamas. Here we report the structures of nine new BTAs: debromoianthelline (**4.1**), pseudoceratinic acid (**4.2a**), methyl pseudoceratinate (**4.2b**), 13-oxo-ianthelline (**4.3**), aiolochoiamides A (**4.4a**), B (**4.4b**), C (**4.5a**), D (**4.5b**), and 7-hydroxy-purealidin J (**4.6**), in addition to the known alkaloids: ianthelline (**4.7**),²⁴ ningalamide B (**4.9**, previously isolated from a Western Australian *Pseudoceratina verrucosa*),²⁵ verongamine,²⁶ aerophobin-1,²⁷ *N,N,N*-trimethyl dibromotyrosine, and *O*-methyl-*N,N,N*-tetramethyl-bromotyrosine.²⁸ The structures of diastereomeric alkaloids **4.4a,b** and **4.5a,b** are of high-complexity; formed through pathways of pseudo-dimerization; both oxidative and tandem aldol-addition/aminal formation, not seen before among BTAs, leading to two new asymmetric quaternary centers in each.

4.2 Isolation and Structure Determination of Debromoianthelline, Pseudoceratinic Acid, Methyl Pseudoceratinate, and 13-Oxo-ianthelline

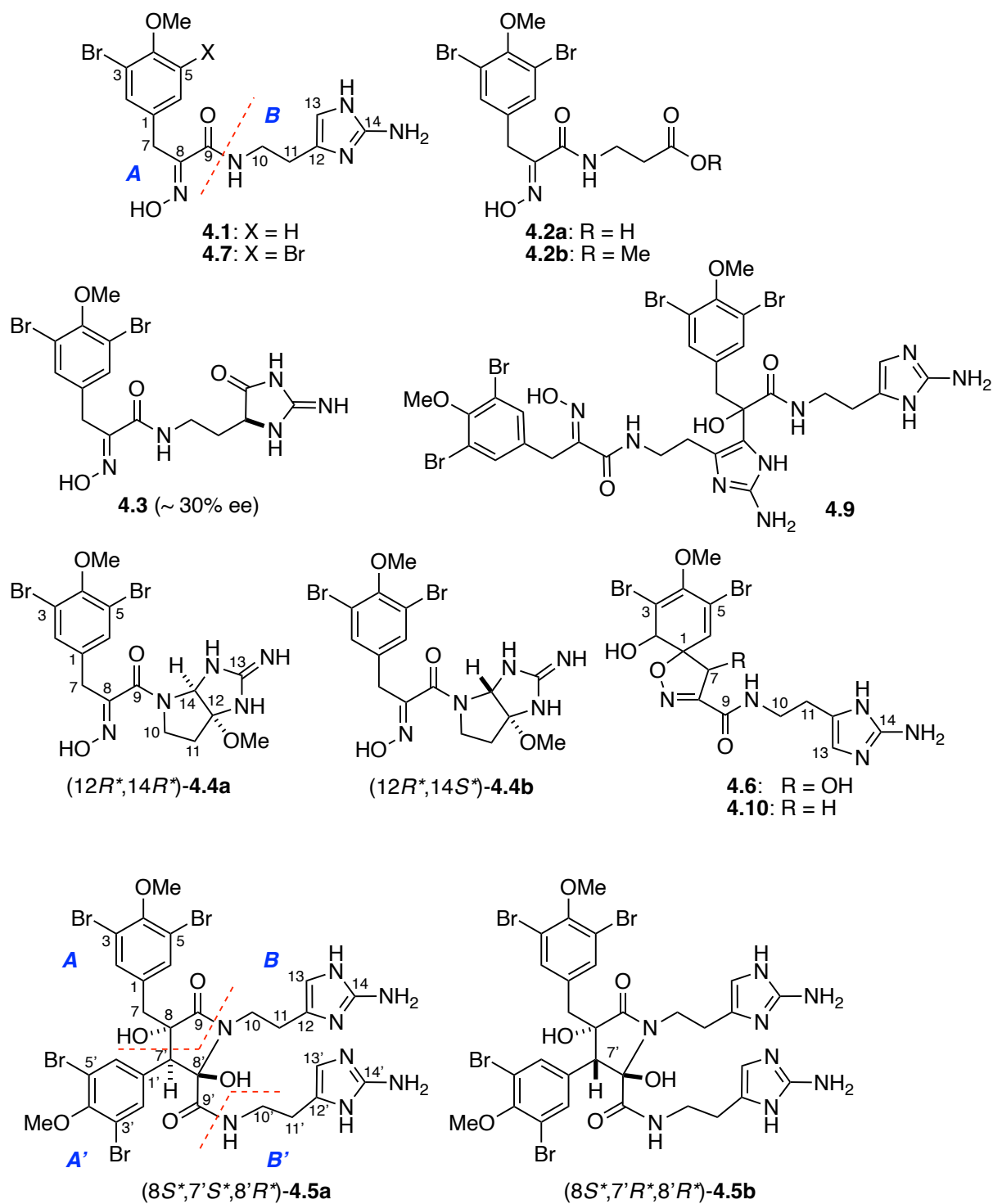


Figure 4.1: The structures of new bromotyrosine alkaloids **4.1**–**4.5**, and key relevant BTAs.

Methanol extracts *A. crassa*, collected by hand using scuba near Sweetings Cay in the Bahamas in 2007, were combined and solvent-partitioned (with progressive additions of H₂O)

against hexane, CH₂Cl₂, *n*-BuOH, and H₂O to provide ‘layers A–D’, respectively. Layer B was purified by size exclusion chromatography (Sephadex LH-20, MeOH) and reversed-phase HPLC to deliver **4.1–4.6**.

HRMS analysis of **4.1** showed [M+H]⁺ of 396.0662 corresponding to a molecular formula of C₁₅H₁₈BrN₅O₃ (calcd 396.0660 for C₁₅H₁₈BrN₅O₃); the isotopic pattern indicated the presence of one Br atom. FTIR absorptions at ~3200 and 1668 cm⁻¹ revealed the presence of OH or NH and amide carbonyl groups, respectively. ¹H and ¹³C NMR spectra of **4.1** were similar with those reported for ianthelline (**4.7**),²⁴ except **4.7** possessed a symmetrical tetrasubstituted benzene ring while the aromatic region of **1** revealed the presence of a 2,4-disubstituted anisole with ¹H NMR signals at δ_H 7.42 (1H, d, *J* = 2.2), 6.91 (1H, d, *J* = 8.5), and 7.20 (1H, dd, *J* = 8.5, 2.2), and δ_C 131.7, 134.6, 130.43, 155.8, and 113.0 consistent with debromoianthelline (**4.1**). The oxime moiety in **4.1–4.4** was assigned the *E*-geometry based on the carbon chemical shifts of the C-7 methylene (δ_C 28.7-30.8).²⁹

Table 4.1: ^{13}C NMR data for **4.1**–**4.4** and **4.6** in CD_3OD .

Position	δ_{C}						
	4.1 ^a	4.2a ^a	4.2b ^a	4.3 ^a	4.4a ^a	4.4b ^a	4.6 ^b
1	131.7	137.4	137.4	137.4	137.17 ^c	137.18 ^c	93.2
2	134.6	134.5	134.5	134.5	134.6 ^d	134.7 ^d	74.4
3	130.43	118.6	118.6	118.6	118.6 ^e	118.7 ^e	113.5
4	155.8	153.8	153.8	153.9	153.94 ^f	153.96 ^f	149.5
5	113.0	118.6	118.6	118.6	118.6 ^e	118.7 ^e	123.5
6	134.6	134.5	134.5	134.5	134.6 ^d	134.7 ^d	124.2
7	28.7	28.7	28.7	28.9	30.7	30.8	74.7
8	152.9	151.9	151.9	152.0	152.7	153.8	156.4
9	165.9	165.3	164.3	166.0	165.9	164.4	160.8
10	38.8	36.2	36.2	36.1	48.3	45.5	38.7
11	25.8	34.5	34.6	32.1	36.5	34.9	25.2
12	126.01	175.4	173.9	58.4	100.7	103.4	125.5
13	112.1			176.0	160.2	160.0	110.4
14	151.4			160.2	74.8	76.6	148.4
4-OCH ₃	56.6	61.0	61.0	61.0	61.0	61.0	60.0
12-OCH ₃			52.2		51.96	52.00	

^a125 MHz. ^b150 MHz. ^cMay be interchangeable.

The HRMS of **4.2a** and **4.2b** confirmed their molecular formulas of $\text{C}_{13}\text{H}_{14}\text{Br}_2\text{N}_2\text{O}_5$ (m/z 436.9342 $[\text{M}]^+$; calcd 436.9342 for $\text{C}_{13}\text{H}_{15}\text{Br}_2\text{N}_2\text{O}_5^+$) and $\text{C}_{14}\text{H}_{16}\text{Br}_2\text{N}_2\text{O}_5$ (m/z 450.9490 $[\text{M}]^+$; calcd 450.9499 for $\text{C}_{14}\text{H}_{16}\text{Br}_2\text{N}_2\text{O}_5^+$), respectively. The isotopic patterns of both ions indicated the presence of two Br atoms, and FTIR absorptions at ~ 3400 – 3300 and 1670 – 1650 cm^{-1} were consistent with OH or NH and amide carbonyl or carboxylic acid, respectively. The ^1H and ^{13}C NMR spectra of **4.2a** and **4.2b** (Table 4.1) are congruent with those of **4.7**²⁴ except for the replacement of the 2-aminohistamine signals with those of 3-amino propanoic acid (δ_{H} 3.50 (H₂-10, t, 6.9) and 2.53 (H₂-11, t, 6.9), and δ_{C} 36.2, 34.5 and 175.4) and methyl 3-aminopropanoate (δ_{H} 3.51 (H₂-10, t, 6.5), 2.55 (H₂-11, t, 6.5) and 3.65 (3H, s), and δ_{C} 36.2, 34.6, 173.9 and 52.2), respectively. Pseudoceratinic acid (**4.2a**) reacted with diazomethane (CH_2N_2), and furnished the corresponding methyl ester **4.2b**. Methyl pseudoceratinate (**4.2b**) may be an artefact from adventitious Fischer esterification of **4.2a** during purification of MeOH extracts.

Table 4.2: ¹H NMR data for **4.1**–**4.4** and **4.6** in CD₃OD.

Pos.	δ_{H} (int., mult, <i>J</i> , Hz)						
	4.1^a	4.2a^a	4.2b^a	4.3^a	4.4a^b	4.4b^b	4.6^b
2	7.42 (1H, d, <i>J</i> = 2.2)	7.48 (1H, s)	7.48 (1H, s)	7.49 (2H, s)	7.52 (2H, s)	7.55 (1H, s)	3.77 (1H, d, 0.6)
5	6.91 (1H, d, <i>J</i> = 8.5)						
6	7.20 (1H, dd, <i>J</i> = 8.5, 2.2)	7.48 (1H, s)	7.48 (1H, s)	7.49 (2H, s)	7.52 (2H, s)	7.55 (1H, s)	6.57 (1H, d, 0.6)
7	3.81 (2H, s)	3.83 (2H, s)	3.83 (2H, s)	3.88 (1H, d, 13.0)	3.81 (2H, s)	3.86 (2H, s)	5.57 (1H, s)
10	3.46 (2H, t, <i>J</i> = 6.9)	3.50 (2H, t, <i>J</i> = 6.9)	3.51 (2H, t, <i>J</i> = 6.5)	3.49 (1H, m)	3.40 (1H, m)	4.20 (1H, dd, 12.5, 7.5)	3.54 (2H, dt, 6.6, 1.8)
11	2.73 (2H, t, <i>J</i> = 6.9)	2.53 (2H, t, <i>J</i> = 6.9)	2.55 (2H, t, <i>J</i> = 6.5)	2.08 (1H, m)	1.96 (1H, m)	2.35 (1H, dd, 7.5, 5.0)	2.76 (2H, t, 6.6)
12				4.20 (1H, dd, 8.0, 5.0)	2.28 (1H, td, 13.0, 8.0)	2.34 (1H, dd, 7.0, 5.0)	
13	6.48 (1H, s)						6.56 (1H, s)
14					5.69 (1H, s)	5.82 (1H, s)	
4-OCH ₃	3.83 (3H, s)	3.83 (3H, s)	3.81 (3H, s)	3.81 (3H, s)	3.81 (3H, s)	3.82 (3H, s)	3.74 (3H, s)
12-OCH ₃			3.65 (3H, s)		3.34 (3H, s)	3.33 (3H, s)	

^a500 MHz. ^b600 MHz.

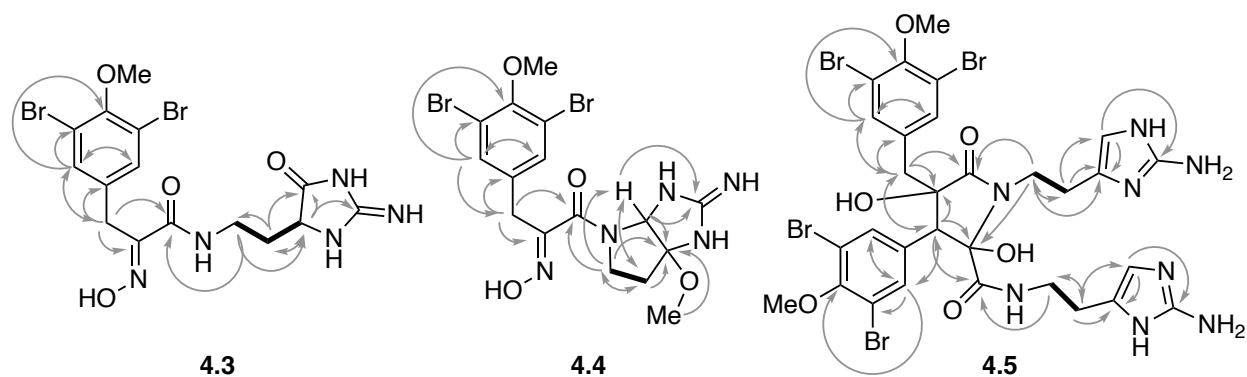
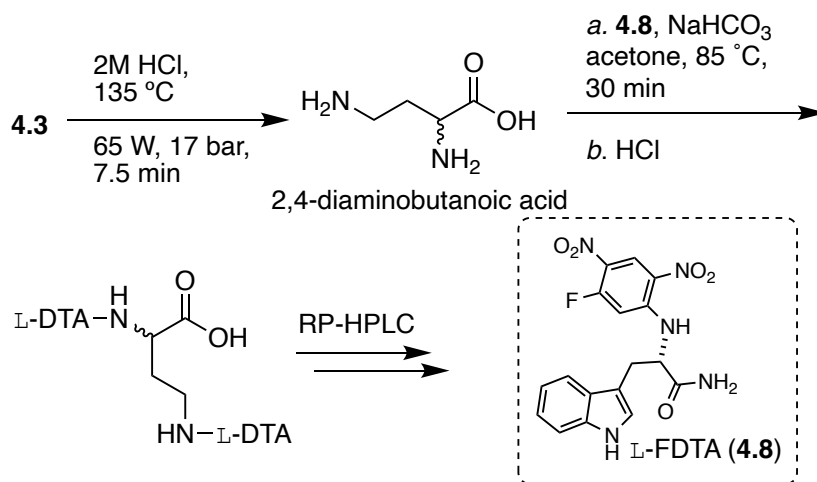


Figure 4.2: Key COSY (bold) and HMBC (arrow) correlations of compounds **4.3–4.5**.

HRMS of 13-oxo-ianthelline (**4.3**) showed an $[M+H]^+$ peak at 489.9712 corresponding to a molecular formula of $C_{15}H_{17}Br_2N_5O_4$ (m/z 489.9712 $[M]^+$; calcd 489.9720 for $C_{15}H_{18}Br_2N_5O_4^+$); the isotopic pattern of the ion revealed the presence of two Br atoms. Although the 1H and ^{13}C NMR spectra of **4.3** were similar to those of ianthelline (**4.7**), differences were observed in the 2-aminohistamine ring (C-12–C-14); a methine and an additional amide carbonyl were observed and positioned at C-12 and C-13, respectively, based on COSY and HMBC correlations. COSY correlations were observed between diastereotopic methylenes at C-10 (δ_H 3.49 (1H, m) and 3.40 (1H, m)) and C-11 (δ_H 2.08 (1H, m) and 1.96 (1H, m)), and C-11 and the methine at C-12 (δ_H 4.20 (1H, dd, 8.0, 5.0)), in addition to HMBC correlations between C-10/C-9, C-10/C-12, C-11/C-12, C-11/C-13, C-12/C-13 and C-12/C-14. The chemical shifts of C-12, C-13, and C-14 (δ_H 4.20 (1H, dd, 8.0, 5.0), δ_C 58.4, 176.0, and 160.2) in **4.3** are comparable to those of the aminoimidazolone ring in purealidin K¹⁷ and oxysceptrin.³⁰

Conventional acid hydrolysis of **4.3** (6M HCl, 110 °C, 12 h) failed to provide 2,4-diaminobutanoic acid. Subsequent acid hydrolysis under microwave conditions (2M HCl, 135 °C, 65 W, 17 bar, 7.5 min, Scheme 4.1) followed by derivatization of the hydrolysate (L-FDTA,²³ **4.8**, acetone, 85 °C, 35 min) and LC analysis of the resultant DTA-aa derivatives by RP-HPLC (C_{18} ,

0.1% TFA-H₂O-MeCN) revealed the presence of L- and D- 2,4-diaminobutanoic acid in a 2:1 ratio ($t_R = 29.48$ min, $t_R = 28.93$ min), respectively.³¹ Similar partial racemization was observed with an authentic enantiopure sample of L-2,4-diaminobutanoic acid that was subjected to hydrolysis under similar microwave conditions (ratio ~2:1). As we reported earlier,²³ use of FDTA lead to superior separations of the corresponding DTA derivatives compared to FDAA.³²



Scheme 4.1: Hydrolysis of **4.3** and derivatization of 2,4-diaminobutanoic acid with L-FDTA (**4.8**).

4.3 Structure Determination of Aiolochoiamides A–D and Proposed Biogenesis

Aiolochoiamides A (**4.4a**) and B (**4.4b**) were isolated as an inseparable mixture of two diastereoisomers (1:1 ratio by ¹H NMR integration). HRMS of **4.4a** and **4.4b** confirmed a single protonated ion: each had the molecular formula C₁₆H₁₉Br₂N₅O₄ (m/z 503.9874 [M+H]⁺; calcd 503.9877 for C₁₆H₂₀Br₂N₅O₄⁺) and the isotopic pattern of the [M+H]⁺ ion showed the presence of two Br atoms. Like most BTAs, the molecular structure of **4.4** is a fusion of molecular modules; here designated as subunits A and B. Analysis of the ¹H and ¹³C NMR spectra of **4.4a** supported the presence of an *O*-methyl-2,6-dibromotyrosyl ketoxime (subunit A) amide linked to hexahydropyrrolo[2,3-*d*]imidazol-2(1*H*)-imine (subunit B) HMBC correlations, observed for

4.4a, between the aryl methines at δ_{H} 7.52 (2H, s) and the quaternary carbons at δ_{C} 118.6 (C-3 and C-5) and 153.94 (C-4), and aryl methylene at 30.7 (C-7), in addition to correlations between the C-7 methylene (δ_{H} 3.81 (2H, s)) and C-1 quaternary carbon (δ_{C} 137.17), aryl CH's (δ_{C} 134.6), C-8 ketoxime (δ_{C} 152.7), and C-9 amide (δ_{C} 165.9), clearly indicated an *O*-methyl-3,5-dibromotyrosyl ketoxime (subunit A). COSY correlations were also observed between diastereotopic methylene signals at δ_{H} 4.20 (1H, dd, 12.5, 7.5) and 3.60 (1H, td, 12.0, 6.0) and δ_{H} 2.35 (1H, dd, 7.5, 5.0) and 2.28 (1H, td, 13.0, 8.0) attached at C-10 and C-11, respectively. Furthermore, HMBC correlations detected from H-10 and the carbonyl at C-9 (δ_{C} 165.9), as well as from H-10 and H-11 to quaternary hemiacetal at C-12 (δ_{C} 100.7) and aminal at C-12 (δ_{C} 74.8), from H-14 to the hemiacetal at C-12 and guanidine at C-13 (δ_{C} 160.2), and from the methoxy observed at δ_{H} 3.34 (3H, s) to C-12, are consistent with subunit B: a hexahydropyrrolo[2,3-*d*]imidazol-2(1*H*)-imine. The structure of **4.4b** was determined from an analysis of NMR along similar lines (Table 4.1 and 4.2).

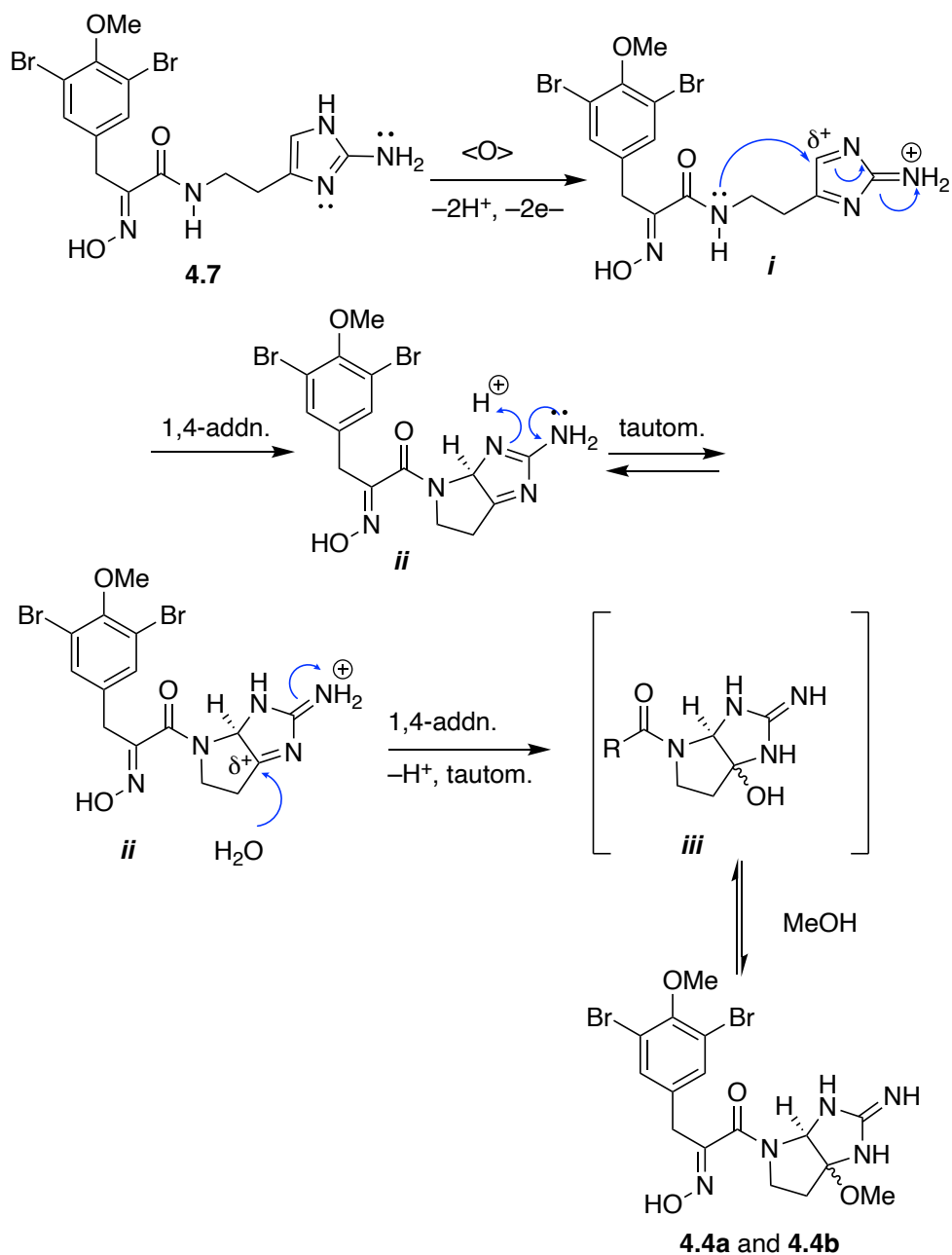


Figure 4.3: Proposed biogenesis of aiolochroiamides A and B (**4.4a** and **4.4b**).

The fused heteronucleus in aiolochroiamides A and B (**4.4a,b**) is likely formed from ianthelline (**4.7**) through a multistep sequence initiated by a 2e⁻ oxidation of the 2-aminoimidazole moiety. The triazafulvene *i* undergoes an intramolecular 1,4-addition of the amide N, tautomerization to give electrophilic *ii* followed by a second 1,4-addition to give *iii*. Intermediate *iii* is likely the authentic natural product which, during workup, suffers exchange with MeOH to

deliver **4.4a** and **4.4b**. Interestingly, epimeric **4.4a,b** did not undergo exchange with CD₃OD during the timeframe of NMR measurements, or storage (4 °C). Attempted equilibration of **4.4a,b** in the presence of stoichiometric Brønsted acid (*p*-TsOH, MeOH, 30–50 °C) lead to no observable change, suggesting the epimeric mixture exists at the thermodynamic ratio.

Aiolochroiamides C (**4.5a**) and D (**4.5b**) were purified as colorless oils (ratio 2.2:1) with isomeric molecular formulas: C₃₀H₃₂Br₄N₈O₆ (*m/z* 916.9241 [M⁺]⁺; calcd 916.9251 for C₃₀H₃₃Br₄N₈O₆⁺) and C₃₀H₃₂Br₄N₈O₆ (*m/z* 916.9232 [M⁺]⁺; calcd 916.9251 for C₃₀H₃₃Br₄N₈O₆⁺), respectively, confirming the presence of four Br atoms. From spectroscopic data (below), it became apparent that each isomer **4.5a** and **4.5b** was a pseudodimeric compound, conjoined at two bonds: a C–C and a C–N sigma bond. Each structure comprises two molecules of aryl pyruvamides of 2-aminohistamine (**4.11**) that are cyclized into a 2,4-dihydroxypyrrolidinone as supported by the following NMR evidence. HMBC correlations observed in **4.5a**, from the aromatic CH's at δ_H 7.33 (2H, s), attached to C-2 and C-6, to δ_C 118.1 (C-3 and C-5), 153.9 (C-4), and 41.6 (C-7), along with correlations between the H-7 methylene at δ_H 3.11 (1H, d, 14.5) and 2.77 (1H, d, 14.0) and the aromatic quaternary carbon at δ_C 136.1 (C-1), tertiary alcohol at 77.9 (C-8), and amide at 177.4 (C-9) supported a 3-(*O*-methyl-3,5-dibromotyrosine)-2-hydroxypropanamide (subunit A, Figure 4.2). COSY correlations were seen between signals at δ_H 3.54 (1H, m) and 3.41 (1H, m), and δ_H 2.78 (1H, m) and 2.75 (1H, m), attached to C-10 and C-11, respectively, in addition to HMBC correlations between the H-10 methylene and the amide at δ_C 177.4 (C-9), methylene at 24.7 (C-11), and quaternary carbon at 125.72 (C-12). Additional HMBC correlations between H-11 methylene and quaternary carbon at δ_C 125.72 (C-12) and the methine at 111.1 (C-13), as well as H-13 methine at δ_H 6.62 (1H, s) and the quaternary carbons at 125.72 (C-12) and 148.6 (C-14)

were consistent with a 2-aminohistamine (subunit B), amide linked through C-9 to the above-described subunit A.

HMBC correlations of **4.5a** also seen from the aryl CH's at δ_{H} 7.43 (2H, s), attached to C-1' and C-6', and the aryl quaternary carbons at δ_{C} 117.8 (C-3' and C-5') and 154.1 (C-4') and benzylic methine at 54.9 (C-7'), and from H-7' (δ_{H} 3.52 (1H, s)) to the aryl methine's at δ_{C} 136.9 (C-2' and C-6'), quaternary carbon at 133.9 (C-1'), hemiacetal at 92.5 (C-8'), and amide at 171.1 (C-9'), were indicative of a second 3'-(*O*-methyl-3',5'-dibromotyrosine)-2'-hydroxypropanamide (subunit A'). Subunit A' is amide-linked to a second 2'-aminohistamine (subunit B') through C-9'. COSY correlations were observed between signals at d_{H} 3.51 (1H, m) and 3.27 (1H, m) and d_{H} 2.60 (1H, m) and 2.56 (1H, m), attached to C-10' and C-11', respectively, in addition to HMBC correlations between the H-10' methylene and amide at δ_{C} 171.1 (C-9') and methylene at 25.8 (C-11'). Further HMBC correlations were seen between the H-11' methylene and the H-13' methine, at δ_{H} 6.37 (1H, s) and δ_{C} 110.4, to one another and to the quaternary carbon at 125.75 (C-12'), and from H-13' to the quaternary carbon at 148.7 (C-14').

Table 4.3: ¹H and ¹³C NMR data for **4.5a** and **4.5b** (CD₃OD).

Pos.	δ_{H} (int., mult, <i>J</i> , Hz)		δ_{C}	δ_{H} (int., mult, <i>J</i> , Hz)		δ_{C}
	4.5a^a	4.5a^b		4.5b^c	4.5b^d	
1	-	136.1	-	-	135.6	
2/6	7.33 (2H, s)	135.8	7.30 (2H, s)	-	135.4	
3/5	-	118.1	-	-	117.8	
4	-	153.9	-	-	153.7	
7	3.11 (1H, d, 14.5) 2.77 (1H, d, 14.0)	41.6	3.16 (1H, d, 13.8) 2.76 (1H, d, 13.8)	-	40.9	
8	-	77.9	-	-	78.6	
9	-	177.4	-	-	175.9	
10	3.54 (1H, m) 3.41 (1H, m)	40.5	3.53 (1H, m) 3.47 (1H, m)	-	38.9	
11	2.78 (1H, m) 2.74 (1H, m)	24.7	2.72 (1H, m) 2.65 (1H, m)	-	23.9	
12	-	125.72	-	-	125.2	
13	6.62 (1H, s)	111.1	6.57 (1H, s)	-	110.4	
14	-	148.6	-	-	148.5	
4-OMe	3.73 (3H, s)	61.0	3.73 (3H, s)	-	60.6	
1'	-	133.9	-	-	132.9	
2'/6'	7.43 (2H, s)	136.9	7.44 (2H, s)	-	135.4	
3'/5'	-	117.8	-	-	117.9	
4'	-	154.1	-	-	154.2	
7'	3.52 (1H, s)	54.9	3.26 (1H, ^e)	-	57.1	
8'	-	92.5	-	-	92.4	
9'	-	171.1	-	-	172.3	
10'	3.51 (1H, m) 3.27 (1H, m)	39.2	3.35 (1H, m) 3.15 (1H, m)	-	39.0	
11'	2.60 (1H, m) 2.56 (1H, m)	25.8	2.40 (1H, m) 2.30 (1H, m)	-	24.9	
12'	-	125.75	-	-	125.2	
13'	6.37 (1H, s)	110.4	6.27 (1H, s)	-	109.7	
14'	-	148.7	-	-	148.4	
4'-OMe	3.80 (3H, s)	61.1	3.79 (3H, s)	-	60.6	

^a500 MHz. ^b125 MHz. ^c600 MHz. ^dObtained from the indirect dimension of HSQC and HMBC (600 MHz). ^eObscured by solvent signal.

HMBC correlations of **4.5a**, from the H-7' at δ_{H} 3.52 (1H, s) to the methylene at δ_{C} 41.6 (C-7) and the tertiary alcohol at 77.9 (C-8), and from H-10 at δ_{H} 3.54 (1H, m) and 3.41 (1H, m) to the hemiacetal at δ_{C} 92.5 (C-8'), revealed that subunit A is C-alkylated, at C-8 and C-7', and N-

alkylated, at the amide and C-8', to subunit B. Analysis of the 1D and 2D NMR data of **4.5b** (Table 4.3) revealed that **4.5a** and **4.5b** are diastereoisomers.

Epimeric **4.5a,b** are likely formed by dimerization of the aryl pyruvamide **4.12** (Figure 4.4) through tandem reactions: aldol addition (arbitrarily depicted here as base-promoted) at the electrophilic C-8 keto group, and ring closure through aminal formation. Compounds **4.5a,b** represents a structural motif not seen before in BTAs, but preceded in the marine natural products literature by the *N*-coumaroyl-Ala-derived pyrrolidinones, anchinopeptolides A,³³ B-D³⁴ and E³⁵, from the sponge *Anchinoe tenacior*, and Br-Trp-derived pyrrolidinones from two ascidians of the genus *Eusynstyela*.^{36,37}

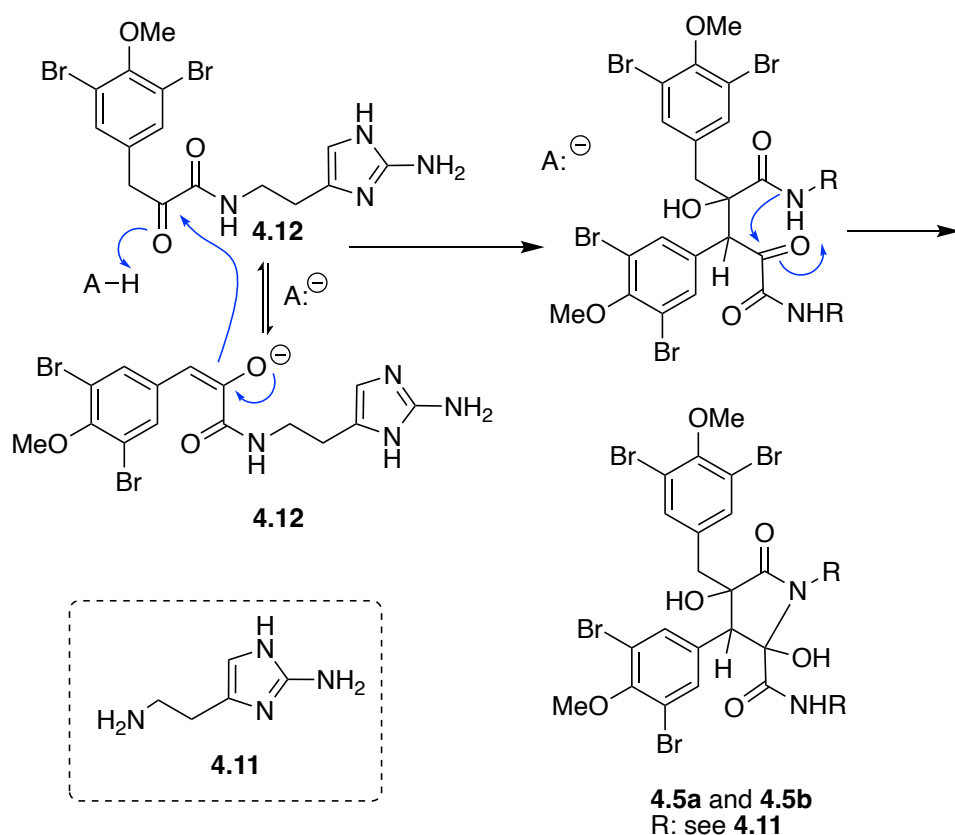


Figure 4.4: Proposed biosynthesis of alkaloids **4.5a** and **4.5b**.

4.4 Relative Stereochemistry of Aiolochoiamides A–D by DFT Calculations

Alkaloids **4.4a,b** and **4.5a,b** were essentially racemic. It was not obvious, from early considerations of the measured spectroscopic data of **4.4a,b** and **4.5a,b** how the relative configurations of the new stereocenters in each compound could be assigned. Preliminary attempts to equilibrate and capture the 1,3-diol in **4.5a,b** as rigid cyclic acetals (2,2-dimethoxypropane or $\text{CH}_2(\text{OMe})_2$, 1 equiv. *p*-TsOH) returned starting material. Consequently, we turned to DFT calculations of the ^1H and ^{13}C NMR chemical shifts of **4.4a,b**, and all four diastereomers of **4.5a,b**. It was understood that the configurations of C-8 and C-7' would be set by thermodynamic or kinetic factors of the aldol reaction – something we had no easy way of ascertaining – but the configuration of C-8' would be set by reversible amination ring closing and equilibration to the thermodynamically more favorable epimer. In any case, calculation of the chemical shifts of each diastereomer and comparison with those of the natural products lent itself as an agnostic approach for solving the stereochemistry.

The relative configurations at C12 and C14 in **4.4** and C8, C7' and C8' in **4.5** were assigned based on comparison of experimental ^1H and ^{13}C NMR chemical shifts (δ) with DFT-calculated theoretical values. A conformational search at the MMFF level in Spartan Student V8³⁸ generated 27 and 123 unique conformers, within 15 $\text{kJ}\cdot\text{mol}^{-1}$ of the global minimum, for the diastereoisomers of **4.4** and **4.5**, respectively. The geometry of the lowest energy conformers was optimized at the B3LYP/6-31G(d,p) level using Gaussian 16 (Figure 4.5).³⁹ Subsequent frequency calculations performed at the same level provided the Gibbs free energies of all conformers. Those conformers with Boltzmann-weighted averages representing more than 1.5% were subjected to additional calculations at the APFD/aug-cc-pVDZ level (GIAO,⁴⁰ scrf, MeOH) to obtain the NMR shielding tensors. Theoretical ^1H and ^{13}C chemical shifts were referenced to TMS and Boltzmann averaged

to furnish the predicated chemical shifts for (12*R**,14*R**)-4.4, (12*R**,14*S**)-4.4, (8*R**,7'*R**,8'*R**)-5, (8*S**,7'*S**,8'*R**)-4.5, (8*R**,7'*S**,8'*R**)-4.5, and (8*S**,7'*R**,8'*R**)-4.5 (See Tables S1–S3).⁴¹

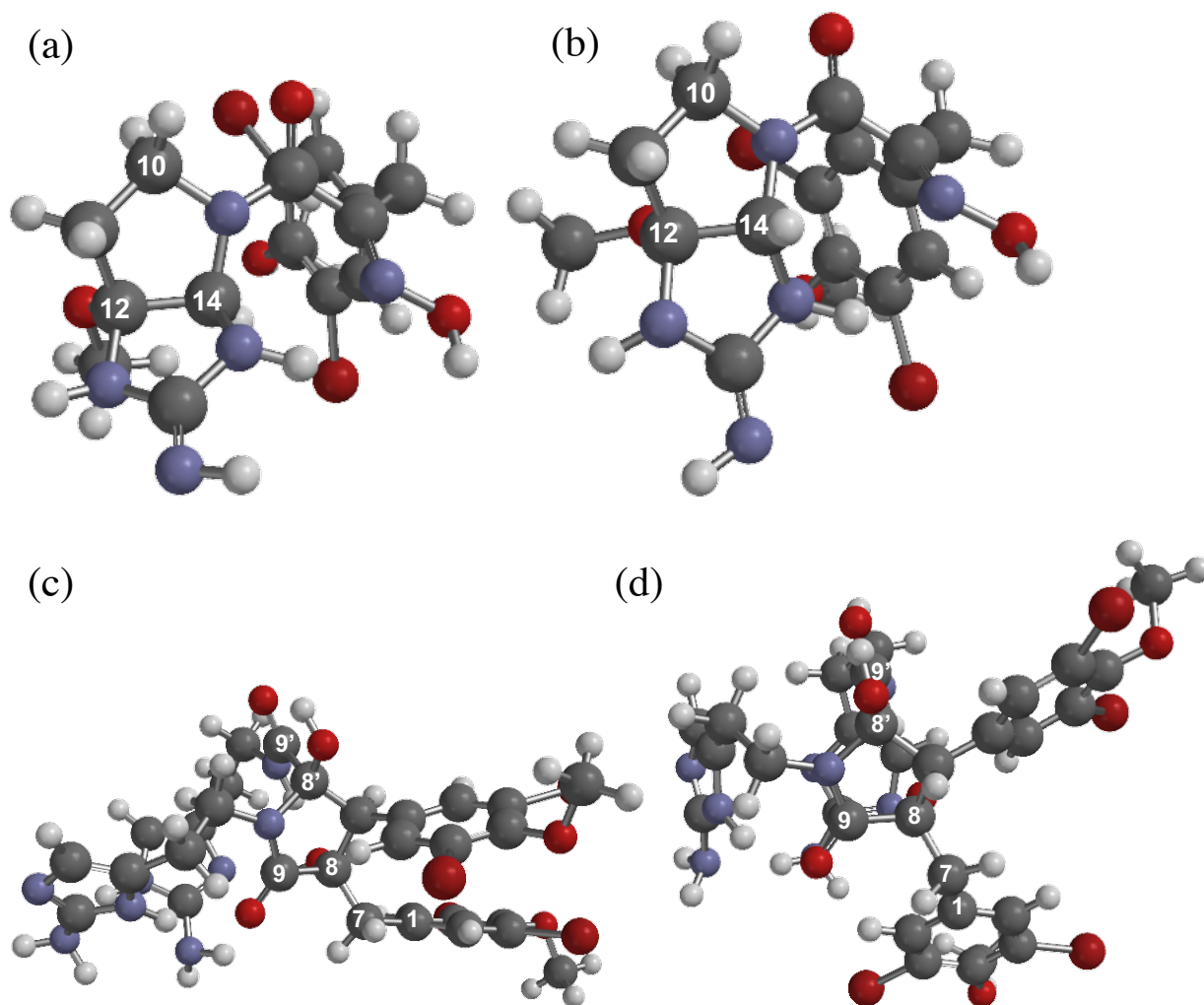


Figure 4.5: Global minimal energy structures of (a) (12*R**,14*R**)-4.4, (b) (12*R**,14*S**)-4.4, (c) (8*S**,7'*S**,8'*R**)-4.5a, and (d) (8*S**,7'*R**,8'*R**)-4.5b optimized at the B3LYP/6-31G(d,p) level using Gaussian 16.

The results showed that the δ_{H} and δ_{C} values predicated for (12*R**,14*R**)-4.4 (RMSD of 2.55 ppm for δ_{C} and 0.192 ppm for δ_{H}) and (12*R**,14*S**)-4.4 (RMSD of 4.45 ppm for δ_{C} and 0.317 ppm for δ_{H}) best matched the experimental chemical shifts of 4.4a and 4.4b, respectively. Similarly, diastereoisomers (8*S**,7'*S**,8'*R**)-4.5 (RMSD of 4.70 ppm for δ_{C} and 0.270 ppm for δ_{H})

and (8*S**,7'*R**,8'*R**)-**4.5** (RMSD of 4.33 ppm for δ_C and 0.282 ppm for δ_H) were the closest match with the experimental values of **4.5a** and **4.5b**, respectively. Importantly, the calculations show that intermolecular cyclization favors the diastereomer with *trans*-hydroxyl substituents at C-8 and C-8', respectively, in both **4.5a,b**.⁴²

4.5 Structure Determination and Proposed Biosynthesis of 7-Hydroxy-purealidin J

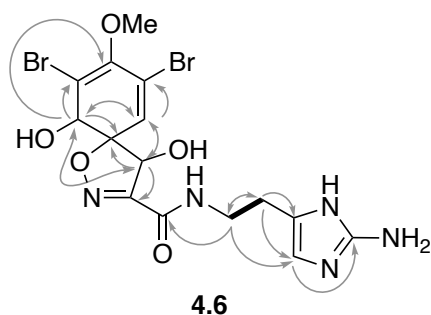


Figure 4.6: Key COSY (bold –) and HMBC (arrow) correlations of 7-hydroxy-purealidin J (**4.6**).

7-Hydroxy-purealidin J (**4.6**) was purified as a white solid with a molecular formula of $C_{15}H_{17}Br_2N_5O_5$ (m/z 505.9656 $[M+H]^+$; calcd 505.9669 for $C_{15}H_{18}Br_2N_5O_5^+$); the isotopic pattern of the pseudomolecular ion indicated the presence of two Br atoms. IR absorptions at 3365 and ~2950–2800, and 1683 cm^{-1} were attributed to NH, OH, and amide carbonyl groups, respectively. The 1H and ^{13}C NMR data of **4.6** were comparable to those of purealidin J (**4.10**)¹⁷ indicating that **4.6** possessed the common spiro-cyclohexadienylisoxazole (SIO) subunit amide-linked to 2-aminohistamine; the major differences were the replacement of the H-7 methylene (δ_H 3.19 (1H, d, 18.6) and 3.61 (1H, d, 18.6), and δ_C 39.2, DMSO- d_6) in purealidin J¹⁷ with a methine (δ_H 5.57 (1H, s), and δ_C 74.7, CD₃OD) that was shifted to a lower field, and other minor chemical shift changes in the SIO unit. HMBC correlations (Figure 4.6) observed from H-7 at δ_H 5.57 (1H, s) to

C-1 (93.2), C-2 (74.4), C-6 (124.2), and C-8 (156.4), in addition to the downfield resonances of H-7 suggested an unusual hydroxylation at C-7.

The biosynthesis of **4.6** – evidently a late-stage hydroxylation event – presents a dilemma. It is known that formation of spiroisoxazoline rings in BTAs can be stereochemically promiscuous – and both **4.6** and **4.10** from this sponge are racemic. However, enzymatic hydroxylation of the C-7 position of the putative precursor (\pm)-**4.10**, for example, by a cytochrome P₄₅₀ (CYP) and O₂, would be expected to be diastereoselective with respect to abstraction of one of the diastereotopic CH₂ hydrogen atoms. Attendant enzymatic kinetic resolution would give rise to an optically active product. In order to resolve this paradox, we propose an enzyme-independent autoxidation which is diastereoselective, but non-enantioselective. Free-radical initiated H-abstraction of (\pm)-**4.10** at C-7 (Figure 4.7) gives the C-centered radical *i* which is captured by triplet O₂ to give hydroperoxide *ii*. Diastereoselectivity would arise from exclusive attack of O₂ from the least hindered face of the spiro-ring, opposite the C-2 hydroxyl group. Although we have no experimental proof, as yet, a consequence of this hypothesis predicts the relative configuration of C-7 in *ii* should be *S*^{*},⁴³ and completion of the sequence (subsequent reduction or disproportionation of *ii*) would give (\pm)-(1*R*^{*},2*R*^{*},7*R*^{*})-**4.6**.

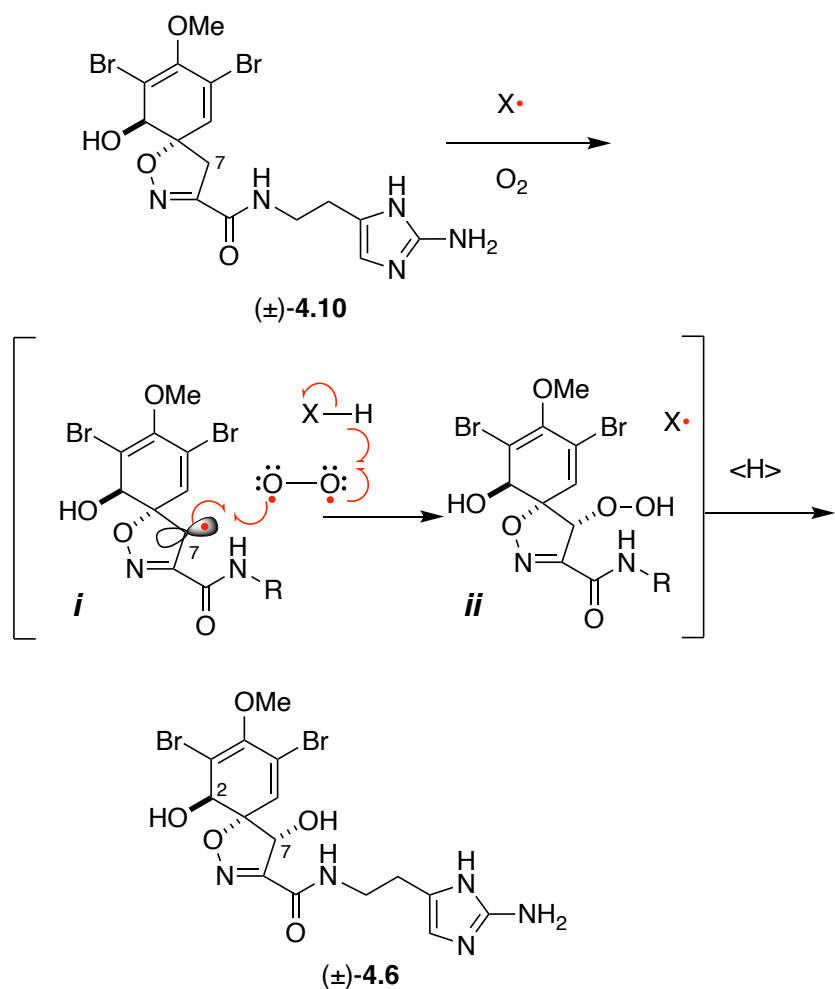


Figure 4.7: Putative biosynthesis of 7-hydroxypurealidin (**4.6**) through free-radical autoxidation.

4.6 Proposed Biogenesis of 3-Oxo-ianthelline and Configurational Heterogeneity of BTAs

In the context of the complex oxidative manifolds that tailor the structures of BTAs, revealed here and in earlier reports, it is instructive to consider possible origins of **4.3**. The guanidine-fused amino acid (AA) embedded in **4.3** is not proteinogenic; it appears to have been biosynthesized *de novo* by post-assembly modification of a precursor BTA, most likely ianthelline (**4.7**). We hypothesize **4.7** undergoes epoxidation of the 2-aminoimidazole ring (Figure 4.8) – possibly by O₂-CYP-mediated oxidation – to give bicyclic *iv* followed by a 1,2-hydride shift

(analogous to an ‘NIH shift’) to give imidazolone **4.3**. As a consequence of *syn*-facial migration of H, the configuration of the α -stereocenter in the AA is conserved. If a CYP is responsible for the new heterocyclic AA, the absolute configuration established for the 2,4-diaminobutyric acid embedded within **4.3** (*S*, albeit eroded to ~30% ee during microwave-promoted acid hydrolysis and AA analysis⁴⁴) reveals *re* facial enantioselectivity in the preceding epoxidation event. It is worth recalling that a consensus of thought supports the involvement of CYP-mediated arene epoxidation during construction of the spiroisoxazoline ring system common to many BTAs from Verongid sponges (e.g. **4.6** and **4.10**).⁴⁵

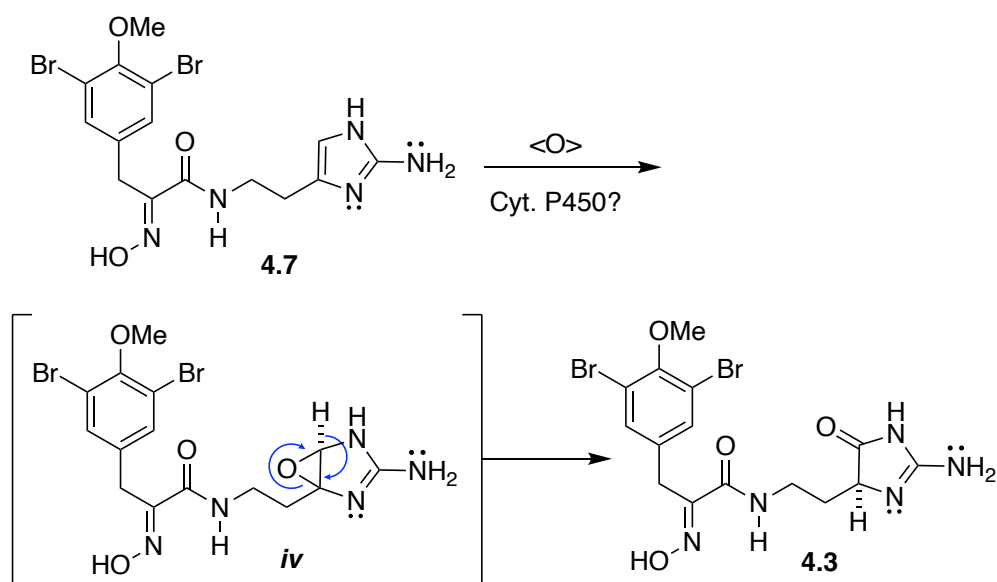


Figure 4.8: Putative biogenesis of **4.3**.

The configuration of SIO compounds such as **4.6** and **4.10** with respect to optical purity of the cyclohexadienyl-spiroisoxazoline ring system, deserves comment. Since we disclosed, from careful measurements of SIO samples by *optimized* chiral-phase HPLC coupled with an online ECD detector,²⁵ that many SIOs are partially racemic, with variable optical purities depending upon sample source and structure of the SIO, it appears that a homochiral cyclohexadienyl-SIO

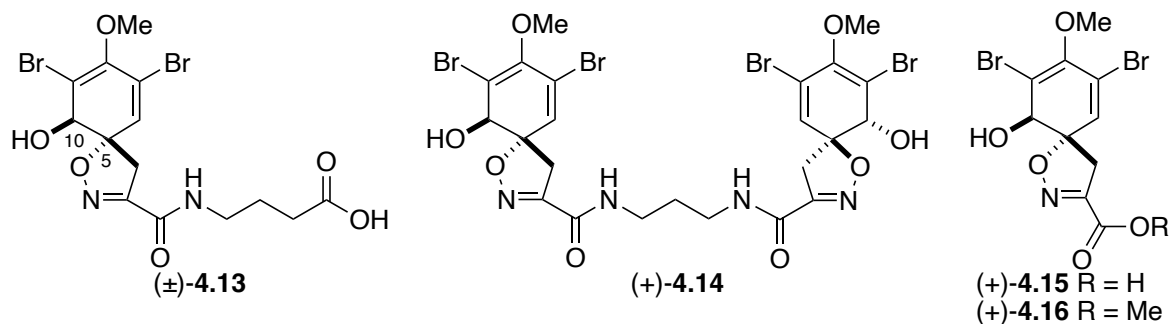
ring system in Nature is the exception rather than the rule. For example, the specific rotations of samples of purpuroceratic acid B (**4.13**, Table 4.4) differ depending upon the source of the sample. Samples of **4.13** from the Molinski and Karuso labs had $[\alpha]_{\text{D}} +140$ and -9 , respectively (Kijjoa did not report chiroptical data for their **4.13** however the lower homolog, purpuroceratic acid A, had $[\alpha]_{\text{D}} -27.7^{20}$). Karuso argued that their (–)-**4.13** was “enantiopure” from observation of a single peak in chiral phase HPLC, and that the optical differences are due to other factors (e.g. salt forms with different counterions), but we find this less convincing than the simpler explanation: their sample of (–)-**4.13** from a Western Australian *P. verrucosa* was less optically pure than (+)-**4.13** from the Caribbean, and the conditions of their chiral-phase HPLC conditions failed to separate the enantiomers.

These discrepancies in magnitudes of specific rotations compelled us to investigate further the optical purities of **4.13** and quantitatively estimate %ee from magnitudes of the Cotton effect in published ECD spectra. Units for ECD, ($\Delta\epsilon$), or $[\theta]$, being molar quantities that follows the Beer-Lambert law, are better suited for this purpose than $[\alpha]_{\text{D}}$, for this reason and others, yet it still begs a question: what is a reliable enantiopure standard for chiroptical comparison? We propose that a suitable interim standard for SIO chiroptical analysis is (+)-aerothionin (**4.14**, Table 4.4), first described by the Fattorusso and coworkers from *Verongia thiona* and *Aplysina aerophoba*,⁴⁶ and later by the Rinehart group in 1981.⁴⁷ Alkaloid (+)-**4.14** is mostly likely to be ~100% ee for two reasons: the final purification was carried out by recrystallization (m.p. $134-7$ °C⁴⁶), and the magnitude of the Cotton effects (CEs) are nearly maximal compared to those of all natural SIOs.²³ Conveniently, the absolute configuration of (+)-**4.14** was established reliably by X-ray crystallography and ECD,⁴⁷ so the CEs of (+)-**4.14** (Table 4.4: $\Delta\epsilon-1 +23.7$ (λ 245 nm), ($\Delta\epsilon-1 +21.4$ (λ 284 nm)) can be compared with those of our reported values of (+)-**4.13** to establish the

%ee of the latter. From a simple linear scaling of the shorter wavelength CE of (+)-**4.13** (λ 243 nm) and (+)-**4.14** (λ 245 nm), (+)-**4.13** is shown to be 59% ee. Subsequently, a scaling of specific rotations for natural (-)-**4.13**¹⁹ gives 15% ee.⁴⁸

Finally, Fattorusso and coworkers characterized the simplest natural canonical SIO, verongidoic acid (**4.15**),⁴⁹ by ECD (Table 4.4), but the $[\alpha]_D$ was not reported. Later Ley and coworkers using stereodefined synthesis, prepared samples of (+)- and (-)-**4.15** (~100% ee) along with their corresponding methyl esters (+)- and (-)-**4.16**,⁵⁰ but their rotations were recorded in CHCl₃ or benzene – solvents which clearly influenced the magnitudes – and cannot be used for comparisons of natural samples recorded in MeOH. Independently, using ECD scaling we could ‘back-estimate’ Fattorusso’s natural sample to be levorotatory (-)-**4.15** ($[\alpha]_D$ -33.4). Berlinck later obtained (+)-**4.15** from a cultured *Pseudovibrio denitrificans* Ab134¹³ with an $[\alpha]_D$ +140. Using similar ECD scalings, we estimated the optical purities of natural (-)-**4.15** and (+)-**4.15** samples to be 76% ee and 79% ee, respectively.

Table 4.4: Physical and chiroptical properties of key spiroisoxazolines **4.13**–**4.16**.



Cmpd.	m.p. (°C)	$[\alpha]_D$ (c g/100 mL, solv.)	ECD		%ee ^b	Ref.
			1 nm ($\Delta\epsilon_1$)	1 nm ($\Delta\epsilon_2$)		
$(-)$ - 4.13	–	–9 (0.4, MeOH)	–	–	15	19
$(+)$ - 4.13	–	+140 (0.04, MeOH)	243 (+7.0)	289 (+5.2)	59	21
$(+)$ - 4.14	134–7	+252 (acetone)	–	–	~100	46
$(+)$ - 4.14 ^b	–	+210 (1.7, MeOH)	245 (+23.7)	284 (+21.4)	~100	47
$(-)$ - 4.15 ^c	–	–	245 (–9.1)	284 (–6.4)	76	49
$(+)$ - 4.15	–	+140 (1.1, MeOH)	249 (+9.4)	292 (+5.3)	79	13
$(+)$ - 4.15	–	+44.0 (0.42, CHCl ₃)	–	–	~100	50
$(-)$ - 4.15	–	–31.3 (0.84, CHCl ₃)	–	–	~100	50
$(+)$ - 4.16 ^d	134–6	+165.5 (0.325, PhH)	–	–	~100	50
$(-)$ - 4.16	–	–150.9 (0.43, PhH)	–	–	~100	50

a. Solvent not reported. *b.* Cryst. MeOH-benzene, no m.p. reported. *b.* From scaling to $\Delta\epsilon_1$ (**4.14**) (normalized by 0.5) then scaling of $[\alpha]_D$. *c.* Sign of rotation is implied. *d.* Cryst. Et₂O.

4.7 Biological Activities

Bioactivity of the components of *Aiolochoiria crassa* were monitored by antifungal and acetylcholinesterase enzyme inhibition assays. The ‘B’ and ‘C’ layers from extraction of *A. crassa* (see Experimental and Appendix, Figures 4.42, 4.43 and Tables 4.6 and 4.7) were assayed for cholinesterase (ChE) inhibition and in vitro antifungal susceptibility (MIC₉₀, Table 4.5) against *Candida* spp. and *Cryptococcus* spp. Ianthelline (**4.7**) and ningalamide B (**4.9**), isolated from the ‘B layer’, were responsible for the antifungal activity. Compound **4.7** exhibited moderate antifungal activity against *Cryptococcus* strains and was essentially inactive against *Candida* spp. (MIC₉₀ >100 μM). This is consistent with the findings of Litaudon and co-workers,²⁴ who showed **4.7** had weak activity against *Candida albicans*. Ningalamide B (**4.9**) moderately inhibited *Candida glabrata*, *Candida krusei*, but were more potent inhibitors of *Cryptococcus neoformans* var. *gattii*, and *Cryptococcus neoformans* var. *grubii*. Additionally, no observable inhibition against acetylcholinesterase at 300 μg/mL was detected in the ‘B layer’; in contrast, both pure **4.7** and **4.11** inhibited butyrylcholinesterase (BuChE) by more than 50% at 25 μg/mL.

Aiolochoiriamides C (**4.5a**) and D (**4.5b**), procured from the ‘C layer’, displayed moderate antifungal activity against *Candida* and *Cryptococcus* strains (Table 4.5), and inhibited BuChE by approximately 70% at 25 μg/mL in a 96-well plate.

Table 4.5: Antifungal activities (MIC₉₀ (μM) of Aiolochoiamides C (**4.5a**), D (**4.5b**), Ianthelline (**4.7**), and Ningalamide B (**4.9**) against *Candida* and *Cryptococcus* spp.

Compd.	<i>C.^a albicans</i> ATCC 14503	<i>C.^a albicans</i> UCD-FRI ^c	<i>C.^a</i> <i>glabrata</i>	<i>C.^a</i> <i>krusei</i>	<i>Cry.^b</i> <i>gattii</i>	<i>Cry.^b</i> <i>grubii</i>
4.5a	>50	>50	>50	>50	50	50
4.5b	>50	>50	>50	>50	>50	>50
4.7	>100	>100	>100	>100		
4.9	43	43	12	20	6	5

a. Candida. *b. Cryptococcus.* *c.* Fluconazole-resistant strain, selected by repeated passage of *C. albicans* in Fluconazole-Sabouraud media.⁵¹

4.8 Conclusion

Nine new bromotyrosine alkaloids, including dimeric compounds **4.4a,b** and **4.5a,b**, were purified from a sample of the sponge *Aiolochoia crassa* and characterized by integrated spectroscopic measurements. The relative configurations of near-racemic aiolochoiamides A–D were determined as (12*R**,14*R**)-**4.4a**, (12*R**,14*S**)-**4.4b**, (8*S**,7'*S**,8'*R**)-**4.5a**, and (8*S**,7'*R**,8'*R**)-**4.5b** based on comparisons of the RMSD values of calculated proton and carbon chemical shifts with experimental values. Novel oxidative motifs for bromotyrosine alkaloids are evident in most of these compounds. Close examination of the alkaloid structures uncovered putative biogenesis suggestive of a manifold of both non-oxidative and oxidative mechanisms for dimerization. Circumstantial evidence is presented for an enantioselective heteroaromatic epoxidation in the elaboration of the amino acid residue in **4.3** in addition to adventitious autoxidation in the formation of **4.6**. Extended investigations of chiroptical properties of purpuroceratic acid B (**4.10**), from different sources, reveals an origin in enantiomeric biosynthesis¹⁵ with heterogeneous optical purities. Modest in vitro antifungal activity was observed for **4.9** and **4.5a,b**, while the latter dimers also weakly-inhibited butyrylcholinesterase.

Chapter 4, in total, is a reprint of the material, “Bioactive Bromotyrosine Alkaloids from the Bahamian Marine Sponge *Aiolochoxia crassa*. New Dimerization and Oxidative Motifs.” *J. Org. Chem.* **2022**, Submitted. The dissertation author was the primary author of this paper and gratefully acknowledges the contributions of coauthors Rudi Hendra, and Tadeusz F. Molinski.

4.9 Acknowledgements

We thank E. Rogers and C. Skepper for assistance with sample collection during the ‘2007 Bahamas’ expedition, J. Pawlik (UNC Wilmington), together with the captain and crew of the *RV Seward Johnson* for logistical support during collecting expeditions, and to the Government of the Bahamas for permission to collect in territorial waters. We are thankful to Tara Zand (Jeff Reinhart Group at UCSD) for her assistance with SEM image collection. We are grateful to A. Mrse and B. Duggan for NMR support and X. Su for HRMS measurements. The purchases of the Agilent TOF mass spectrometer and the 500 MHz NMR spectrometer were made possible with funds from the NIH Shared Instrument Grant program (S10RR025636) and the NSF Chemical Research Instrument Fund (CHE0741968), respectively. MS is grateful for support from a Graduate Research Fellowship, Department of Chemistry, UCSD. RH thanks the Fulbright Foundation for support while on leave at UCSD. TFM is grateful for the 2020 ACS Ernest Guenther Award for natural product chemistry. This research was supported by grants from the NIH to TFM from the NIH (AI100776, AT009783). This research was also supported in part by W. M. Keck Foundation through computing resources at the W. M. Keck Laboratory for Integrated Biology.

4.10 Experimental

General Experimental Procedures. Preparative, semi-preparative and analytical HPLC were carried out on a JASCO system comprising dual-pumps (PU-2086 Plus), a dynamic mixer (MX-2080-32) and UV-vis detector (UV-2075). Retention times and peak integrations were measured using native software. LC-MS measurements were performed with a Thermoelectron Surveyor UHPLC coupled to an MSD single-quadrupole detector. HR-ESI-TOF mass spectroscopic analyses were conducted on an Agilent 1200 HPLC coupled to an Agilent 6350 TOF-MS at the Small Molecule Mass Spectrometry Facility in the Department of Chemistry and Biochemistry at UCSD. UV-vis spectra were measured on a JASCO V-630 double beam spectrometer. FTIR spectra were collected from thin film samples using a JASCO FTIR-4100 fitted with an ATR plate (ZnSe). Optical rotations were measured on a JASCO P-2000 polarimeter at the D-double emission line of Na. CD spectrum were measured on a JASCO J-810 spectropolarimeter at 23 °C in quartz cells of 1, 2 or 5 mm pathlength. 1D and 2D NMR spectra were measured on a JEOL ECA (500 MHz) spectrometer, equipped with a 5 mm $^1\text{H}\{^{13}\text{C}\}$ room temperature probe, or a Bruker Avance III (600 MHz) NMR spectrometer fitted with a 1.7 mm $^1\text{H}\{^{13}\text{C}/^{15}\text{N}\}$ microcryoprobe (23 °C). ^{13}C NMR spectra were collected on a Varian NMR spectrometer (125 MHz) equipped with a 5 mm XSENS $^{13}\text{C}\{^1\text{H}\}$ cryoprobe. All NMR spectra were referenced to residual solvent signals (CHD_2OD , δ_{H} 3.31, CD_3OD δ_{C} 49.00 ppm).

Biological Material. The sponge *Aiolochoxia crassa* (07-36-220A) was collected in June 2007 from Sweetings Cay, the Bahamas (lat. 26° 34.752' N long. 77° 53.871' W) by hand at a depth of 15 m using scuba, and kept frozen (-20 °C) until needed. A type sample (MeOH) is archived in the Department of Chemistry and Biochemistry, UCSD.

Extraction and Isolation. A sample of *A. crassa* was lyophilized (dry wt. 127 g) and extracted with MeOH (2 x 500 mL, 12 h) and the combined MeOH extracts were concentrated,

and the water content adjusted to approximately 1:9 (500 mL, H₂O/MeOH v/v). The extract was partitioned with hexane (2 x 500 mL) to give hexane-soluble 'fraction A' (0.506 g). The aqueous MeOH layer was adjusted with water (2:3 H₂O/MeOH) and extracted with CH₂Cl₂ (2 x 500 mL) to yield CH₂Cl₂-soluble 'fraction B' (2.84 g). The remaining aqueous methanol phase was concentrated, and the resultant aqueous layer was partitioned against *n*-BuOH (2 x 500 mL) to provide the *n*-BuOH-soluble 'C layer' (4.12 g) and the H₂O-soluble 'D layer' (3.72 g).

Fraction B (1.2 g) was purified by size exclusion chromatography (Sephadex LH-20, elution with MeOH) to yield seven fractions, which were combined according to TLC profiles of *p*-anisaldehyde and ninhydrin staining. Fraction 3 (410 mg) was re-purified on RP-HPLC (Phenomenex Luna Phenyl-Hexyl 100 A, 5 μ, 250 x 21.20 mm, 85:15 to 40:60 of 0.1% TFA-H₂O/CH₃CN over 30 min, 10 mL.min⁻¹, λ = 254 nm) to yield **4.1** (3.2 mg, *t_R* = 24.37 min), and **4.2a** (0.8 mg, *t_R* = 28.14 min). The fourth fraction (64.5 mg) was purified on RP-HPLC (Phenomenex Luna C₁₈, 5 μ, 250 x 10 mm, 70:30 to 45:55 of 0.1% TFA-H₂O/MeCN over 40 min, 2.5 mL.min⁻¹, λ = 254 nm) to give **4.4a,b** (2.7 mg, *t_R* = 23.62 min). Fraction 6 (39.7 mg) was purified by reversed phase HPLC (Phenomenex Luna C₁₈, 5 μ, 150 x 21.2 mm, step-gradient, 80:20 for 3 min to 40:60 of 0.1% TFA-H₂O/CH₃CN until 33 min, 12 mL.min⁻¹, λ = 254 nm) to yield **4.2b** (1.0 mg, *t_R* = 28.05 min) and **4.3** (6.1 mg, *t_R* = 16.73 min).

Layer C (3.0 g) was separated by size-exclusion chromatography (Sephadex LH-20, MeOH) to yield eight fractions that were pooled according to TLC profiles by *p*-anisaldehyde and ninhydrin staining. Fraction 4 (0.598 g) was separated by passage through SPE C₁₈ cartridge (Strata, 10 g, step-gradient, 20:80 CH₃CN-H₂O to CH₃CN) into two fractions. Fraction 1 (0.507 g) was further purified by RP-HPLC (Phenomenex Luna C₁₈, 5 μ, 150 x 21.2 mm, step-gradient, 80:20 for 3 min to 40:60 of 0.1% TFA-H₂O/CH₃CN until 33 min, 12 mL.min⁻¹, λ = 254 nm) to

give 26 subfractions. Subfraction 7 (2.5 mg) was purified by RP-HPLC (Phenomenex Luna Phenyl-Hexyl, 5 μ , 250 x 10 mm, 80:20 for 3 min to 55:45 of 0.1% TFA-H₂O/CH₃CN until 35 min, 2.5 mL.min⁻¹, λ = 254 nm) to give **4.6** (1.5 mg, t_R = 21.48 min). Subfraction 19 (4.1 mg) was purified by RP-HPLC (Phenomenex Luna Phenyl-Hexyl, 5 μ , 250 x 10 mm, 80:20 for 3 min to 30:70 of 0.1% TFA-H₂O/CH₃CN until 45 min, 2.5 mL.min⁻¹, λ = 254 nm) to give **4.5a** (2.2 mg, t_R = 26.792 min). Subfraction 20 (3.0 mg) were purified by RP-HPLC (Phenomenex Luna Phenyl-Hexyl, 5 μ , 250 x 10 mm, 75:25 for 3 min to 30:70 of 0.1% TFA-H₂O/CH₃CN until 35 min, 2.5 mL.min⁻¹, λ = 254 nm) to give **4.5b** (1.0 mg, t_R = 21.13 min). Subfraction 21 contained pure ningalamide B (**9**, 55.1 mg, t_R = 20.35 min). Other known bromotyrosine alkaloids were isolated and identified by comparison of their HRMS and ¹H NMR data with literature values (see text).

Debromioanthelline (**4.1**): pale white solid; UV (CH₃OH) λ_{\max} 204 nm (ϵ log₁₀ 4.29), and 218 (4.02); FTIR (film) ν 3181, 1668, 1541, 1496, 1472, 1258, 1201, 1139, 1000, 801, 723 and 611 cm⁻¹; See Tables 4.1 and 4.2 for the ¹H and ¹³C NMR data of **4.1**; HRMS (ESI-TOF) m/z 396.0662 [M+H]⁺, calcd for C₁₅H₁₉BrN₅O₃⁺ 396.0666).

Pseudoceratinic Acid (**4.2a**): pale white solid; UV (CH₃OH) λ_{\max} 206 nm (ϵ log₁₀ 4.51), and 219 (4.18); FTIR (film) ν 3363, 1654, 1541, 1471, 1420, 1259, 1202, 991, 738, and 623 cm⁻¹; See Tables 4.1 and 4.2 for the ¹H and ¹³C NMR data of **4.2a**; HRMS (ESI-TOF) m/z 436.9342 [M+H]⁺, calcd for C₁₃H₁₅Br₂N₂O₅⁺ 436.9342).

Methyl Pseudoceratinate (**4.2b**): pale white solid; UV (CH₃OH) λ_{\max} 206 nm (ϵ log₁₀ 4.49), and 218 (4.18); FTIR (film) ν 3311, 1670, 1541, 1472, 1427, 1259, 1204, 1136, 1000, 726, 644, 625, and 610 cm⁻¹; See Tables 4.1 and 4.2 for the ¹H and ¹³C NMR data of **4.2b**; HRMS (ESI-TOF) m/z 450.9490 [M+H]⁺, calcd for C₁₄H₁₇Br₂N₂O₅⁺ 450.9499).

13-Oxo-Ianthelline (4.3): pale white solid; $[\alpha]^{21.3}_D 0$ (*c* 0.45, CH₃OH); UV (CH₃OH) λ_{\max} 206 nm ($\epsilon \log_{10}$ 4.65), and 221 (4.30); FTIR (film) ν 3351, 1714, 1670, 1545, 1202, 1142, 636, 609, and 603 cm⁻¹; See Tables 4.1 and 4.2 for the ¹H and ¹³C NMR data of **4.3**; HRMS (ESI-TOF) *m/z* 489.9712 [M+H]⁺ (calcd for C₁₅H₁₈Br₂N₅O₄⁺ 489.9720).

Aiolochoiamides A (4.4a) and B (4.4b): colourless oil; $[\alpha]^{21.3}_D 0$ (*c* 0.34, CH₃OH); UV (CH₃OH) λ_{\max} 206 nm ($\epsilon \log_{10}$ 4.08), and 218 (3.79); FTIR (film) ν 3248, 1683, 1451, 1204, 1138, 999, 725, and 613 cm⁻¹; See Tables 4.1 and 4.2 for the ¹H and ¹³C NMR data of **4.4a** and **4.4b**; HRMS (ESI-TOF) *m/z* 503.9874 [M+H]⁺ (calcd for C₁₆H₂₀Br₂N₅O₄⁺ 503.9877).

Aiolochoiamide C (4.5a): colourless oil; $[\alpha]^{21.3}_D 0$ (*c* 0.12, CH₃OH); UV (CH₃OH) λ_{\max} 205 nm ($\epsilon \log_{10}$ 4.85), and 218 (4.53); FTIR (film) ν 3252, 1683, 1545, 1427, 1202, 1142, 993, 841 and 723 cm⁻¹; See Table 4.3 for the ¹H and ¹³C NMR data of **4.5a**; HRMS (ESI-TOF) *m/z* 916.9241 [M+H]⁺ (calcd for C₃₀H₃₃Br₄N₈O₆⁺ 916.9251).

Aiolochoiamide D (4.5b): colourless oil; $[\alpha]^{21.3}_D 0$ (*c* 0.2, CH₃OH); UV (CH₃OH) λ_{\max} 205 nm ($\epsilon \log_{10}$ 4.50), and 218 (4.19); FTIR (film) ν 3272, 1683, 1545, 1421, 1201, 1137, 993, 846, and 723 cm⁻¹; See Table 4.3 for the ¹H and ¹³C NMR data of **4.5b**; HRMS (ESI-TOF) *m/z* 916.9232 [M+H]⁺ (calcd for C₃₀H₃₃Br₄N₈O₆⁺ 916.9251).

7-Hydroxypurealidin J (4.6): pale white solid; $[\alpha]^{21.3}_D 0$ (*c* 0.14, CH₃OH); UV (CH₃OH) λ_{\max} 194 nm ($\epsilon \log_{10}$ 3.63), 203 (3.45) and 217 (3.33); FTIR (film) ν 3365, 2923, 2848, 1683, 1204, 1139, 845, 803, 724, and 621 cm⁻¹; See Tables 4.1 and 4.2 for the ¹H and ¹³C NMR data of **6**; HRMS (ESI-TOF) *m/z* 505.9656 [M+H]⁺ (calcd for C₁₅H₁₈Br₂N₅O₅⁺ 505.9669).

Acid Hydrolysis 4.3 and Derivatization. Aqueous HCl (250 μ L, 2M, aq.) was added to **4.3** (100 μ g), and the mixture was stirred in a microwave reactor (65 W, 135 $^{\circ}$ C, 17 bar, 7.5 min). The

reaction mixture was cooled to rt and dried under a stream of N₂. The hydrolysate was dissolved in H₂O (125 μ L), and *N*-L-(5-fluoro-2,4-dinitrophenyl)tryptophanamide²³ (L-FDTA, 100 μ L, 10 mg/mL, acetone), acetone (50 μ L), and NaHCO₃ (20 μ L, 1M, aq.) were added. The reaction was stirred at 85 °C for 30 min., cooled to rt and quenched by addition of HCl (20 μ L, 1M, aq.). The derivative was analyzed by analytical-RP-HPLC (Phenomenex Luna C₁₈, 5 μ , 250 x 4.60 mm, step-gradient, 80:20 for 3 min to 30:70 of 0.1% TFA-H₂O/CH₃CN till 30 min, 1.0 mL.min⁻¹, λ = 254 nm). L- and D-DTA derivatives of authentic L-2,4-diaminobutanoic acid (L-DAB) were similarly prepared, and gave peaks at t_R = 29.63 min and 28.90 min (ratio ~3:1), respectively. The HPLC analysis of the L-DTA derivative of the acid hydrolysate of **4.3** gave both L-DAB-L-DTA and D-DAB-L-DTA at t_R = 29.47 min and 28.93 min (ratio ~2:1), respectively.

Antifungal Activity. Antifungal activity of crude samples was measured at 300 μ g/disk (6.5 mm, 12 μ L, 25 mg/mL, MeOH) using the disk diffusion method on Sabouraud dextrose (SB) agar. Antifungal activity of semi-pure samples was completed in 96-well plates using 1.25 or 2.5 mg/mL samples in MeOH. *Candida* strains were grown overnight at 37 °C in SB media while *Cryptococcus* strains were grown for 48 h at 37 °C in antibiotic medium #3. Fungal strains were diluted with the corresponding fresh media to an OD₅₉₀ of 0.02. Samples were added to final concentrations of 50 or 100 μ g/mL. Inoculated and sterile media were grown with MeOH, DMSO, and Clotrimazole (15 μ g/mL or 30 μ g/mL, DMSO) as positive and negative controls. The 96-well plates were incubated at 37 °C for 24 h for *Candida* strains and 48 h for *Cryptococcus* strains, and each well OD₅₉₀ was recorded at 590 nm. Antifungal activities of aiolochroiamides C and D (**4.5a,b**), ianthelline (**4.7**), and ningalamide B (**4.9**) were measured in triplicate in 96-well plates after 2-fold dilutions. Compounds **4.5a,b**, **4.7**, and **4.9** (2.5 mM, MeOH) was added to final concentrations of 0.10, 0.20, 0.39, 0.78, 1.56, 3.13, 6.25, 12.5, 25.0, 50.0, 100, and 150 μ M. The

plates were incubated at 37 °C (24 or 48 h), and ODs were recorded at 590 nm (SpectraMax, Model 384 Plus), and MIC₅₀ and MIC₉₀ were obtained from fitted inhibition curves (SpectraMax native software). See Appendix for more detailed data.

Cholinesterase Inhibition Assay. Electric eel acetylcholinesterase (EC 3.1.1.7, Type VI-S), equine butyrylcholinesterase (EC 3.1.1.8), and galantamine hydrobromide were purchased from Sigma-Aldrich. *S*-Butyrylthiocholine iodide, *S*-acetylthiocholine iodide and 5,5'-dithio-bis-nitrobenzoic acid (DTNB) were purchased from Fisher Sci. All reagents and conditions were the same as previously described.⁵² Cholinesterase inhibition was determined spectrophotometrically according to a modified protocol of that reported by Ellman.⁵³ In this assay, sodium phosphate buffer (150 µL, 0.1 M, pH 8.0), enzyme mixture (20 µL in dI-H₂O, 1.25 Units/mL), and test sample (10 µL) consisting of galantamine hydrobromide (1 mg/mL, positive control), or MeOH (negative control) or purified compounds dissolved in MeOH, were preincubated at rt for 30 min. A solution of DTNB (10 µL, 5 mM, of a stock solution of 10 mL of 0.1 M sodium phosphate buffer, pH 7.0, containing 15 mg NaHCO₃) was added followed by acetylthiocholine or butyrylthiocholine (10 µL, 10 mM in 0.1 M sodium phosphate buffer, pH 8.0). The absorbances were immediately measured at 410 nm. See Appendix for more detailed bioassay data.

4.11 Appendix

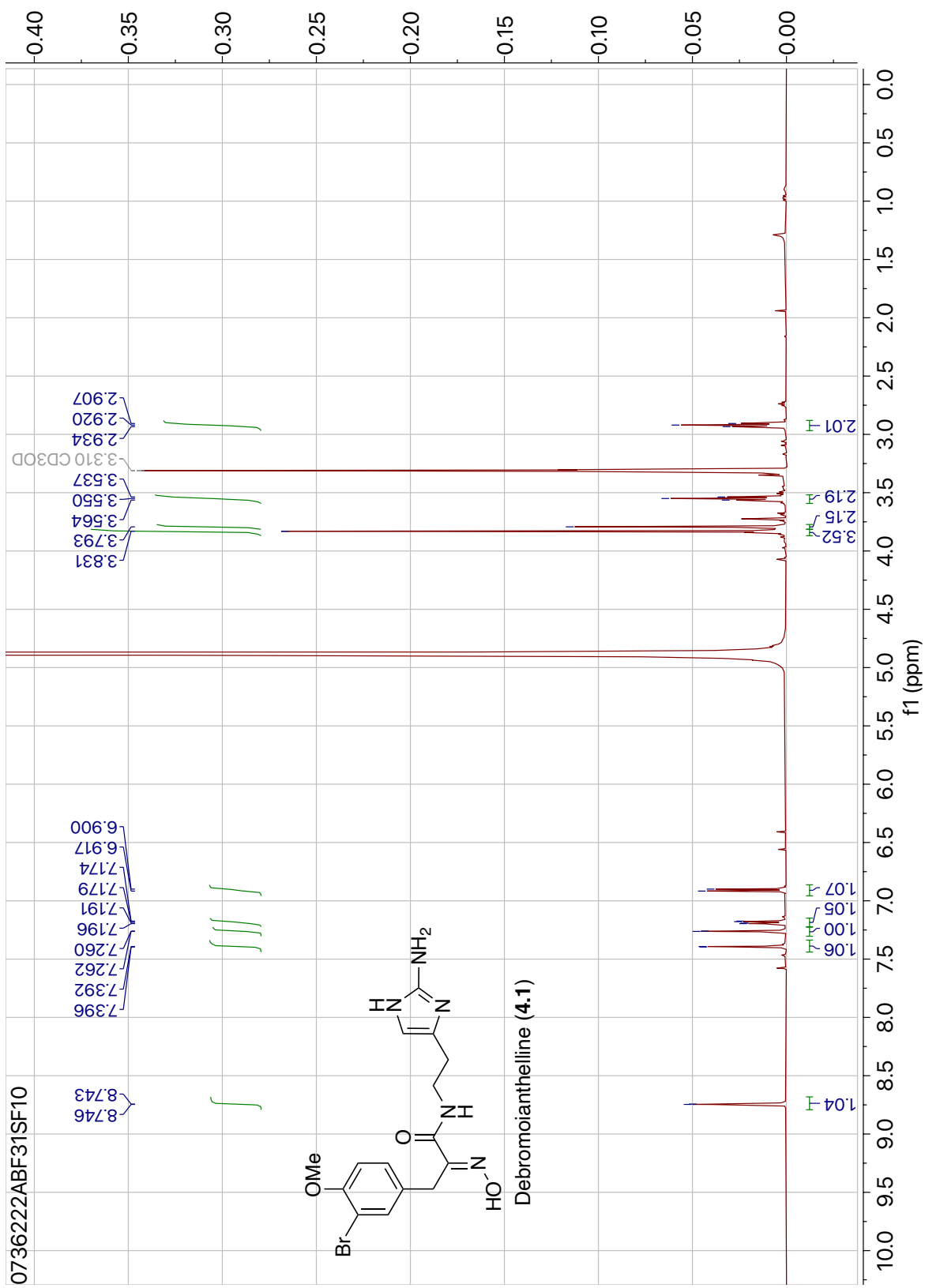
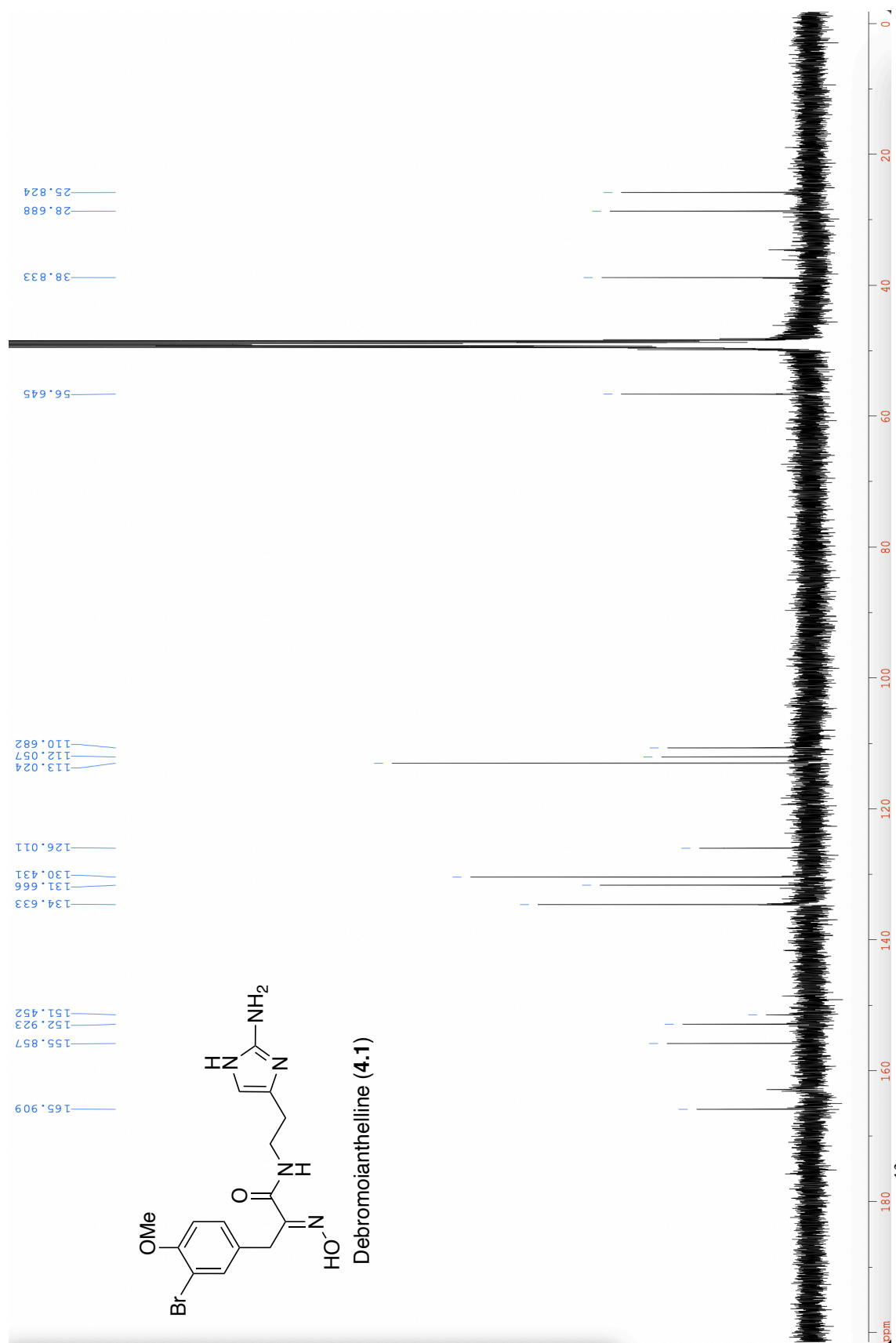


Figure 4.9: ^1H NMR of Compound 4.1 (500 MHz, CD_3OD).



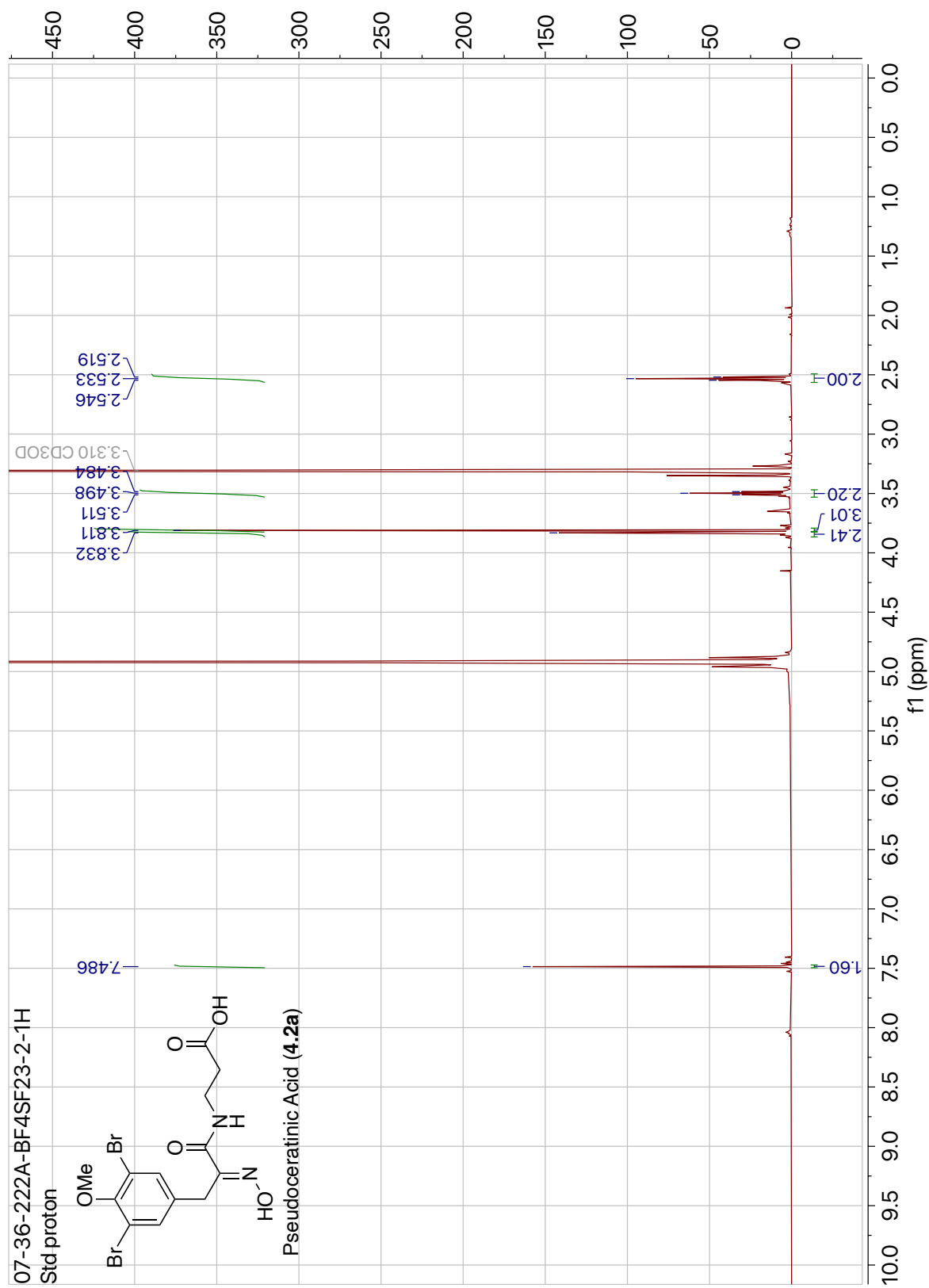


Figure 4.11: ¹H NMR of Compound 4.2a (500 MHz, CD₃OD).

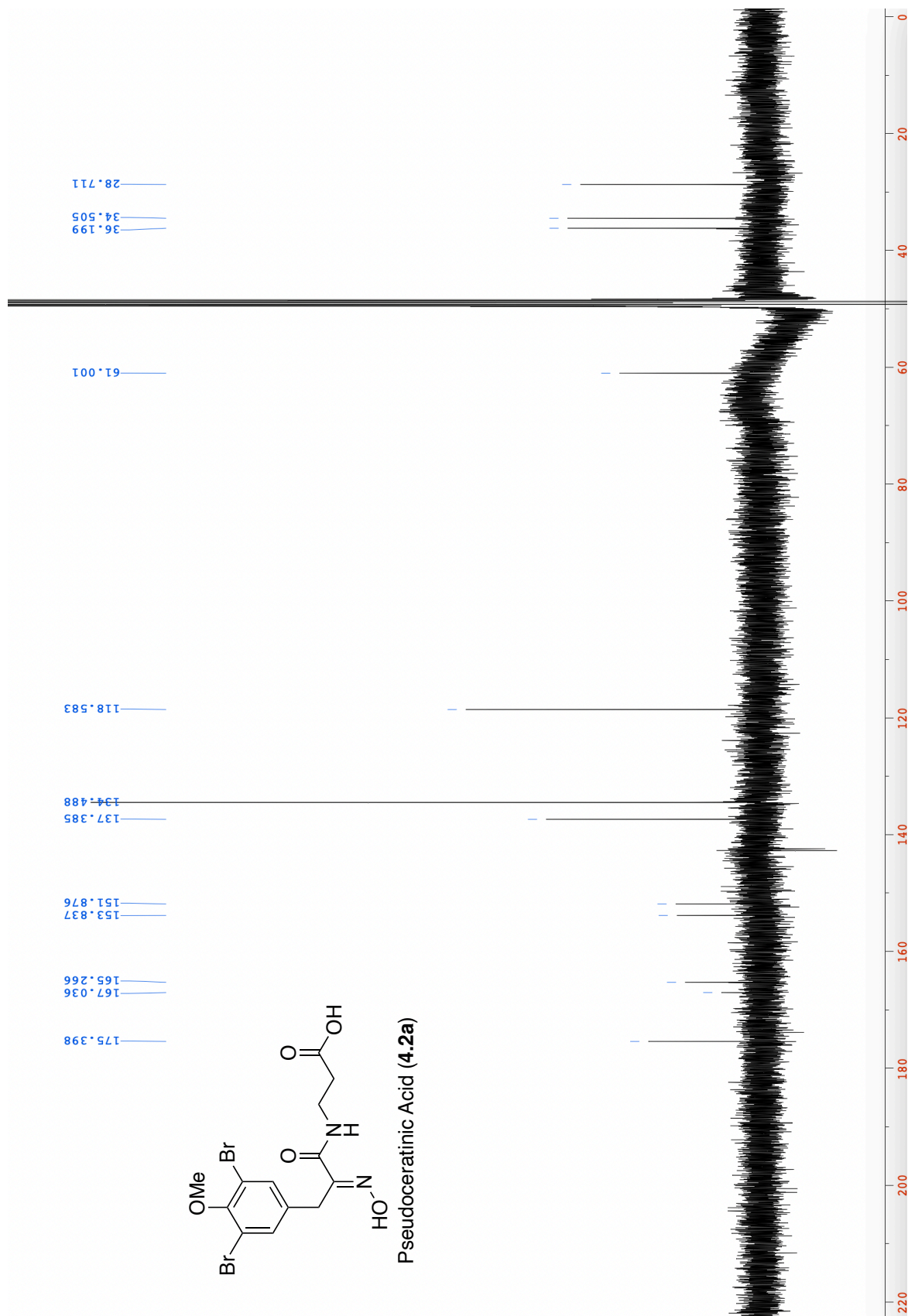


Figure 4.12: ¹³C NMR of Compound 4.2a (125 MHz, CD₃OD).

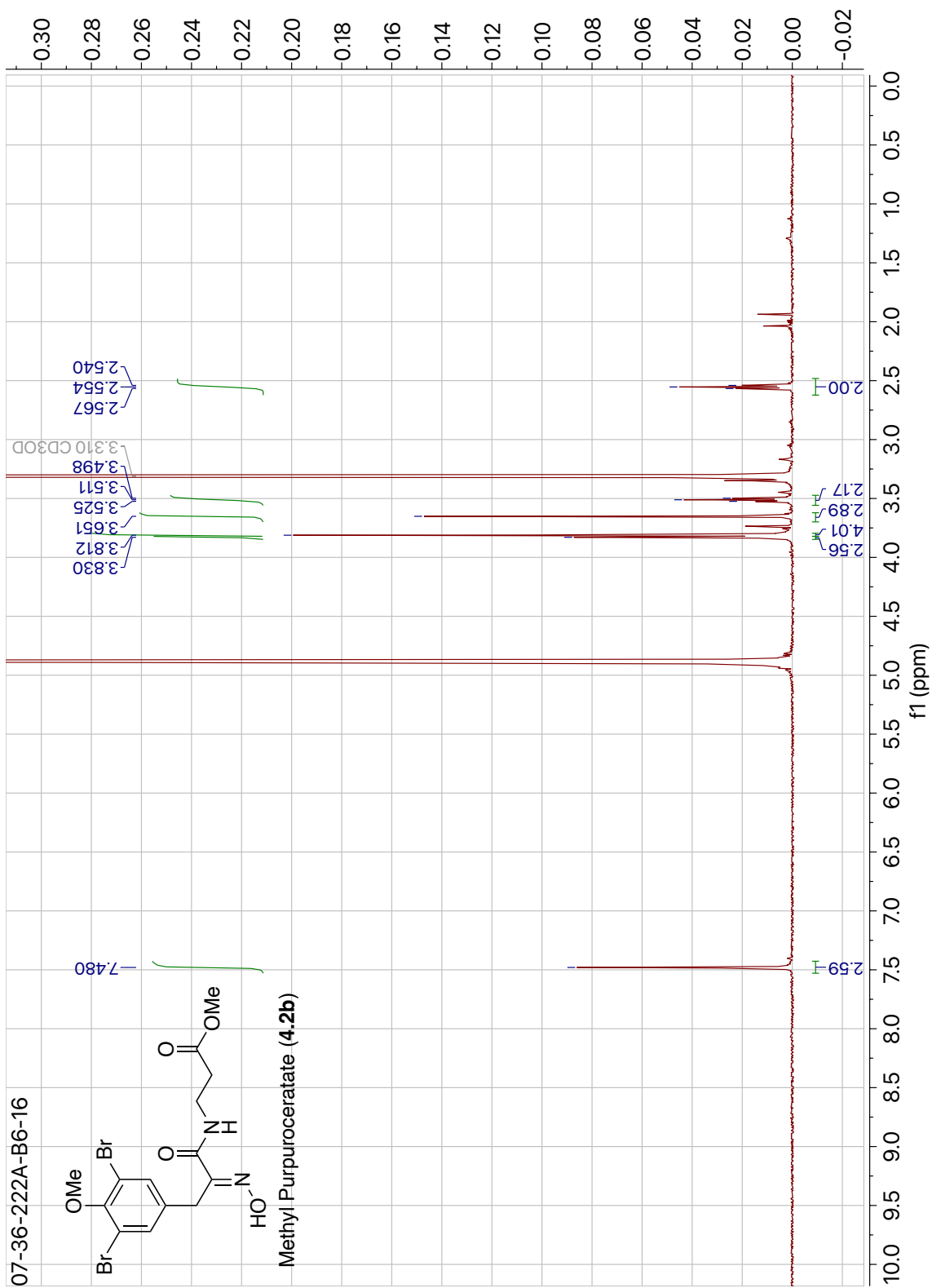


Figure 4.13: ¹H NMR of Compound 4.2b (500 MHz, CD₃OD).

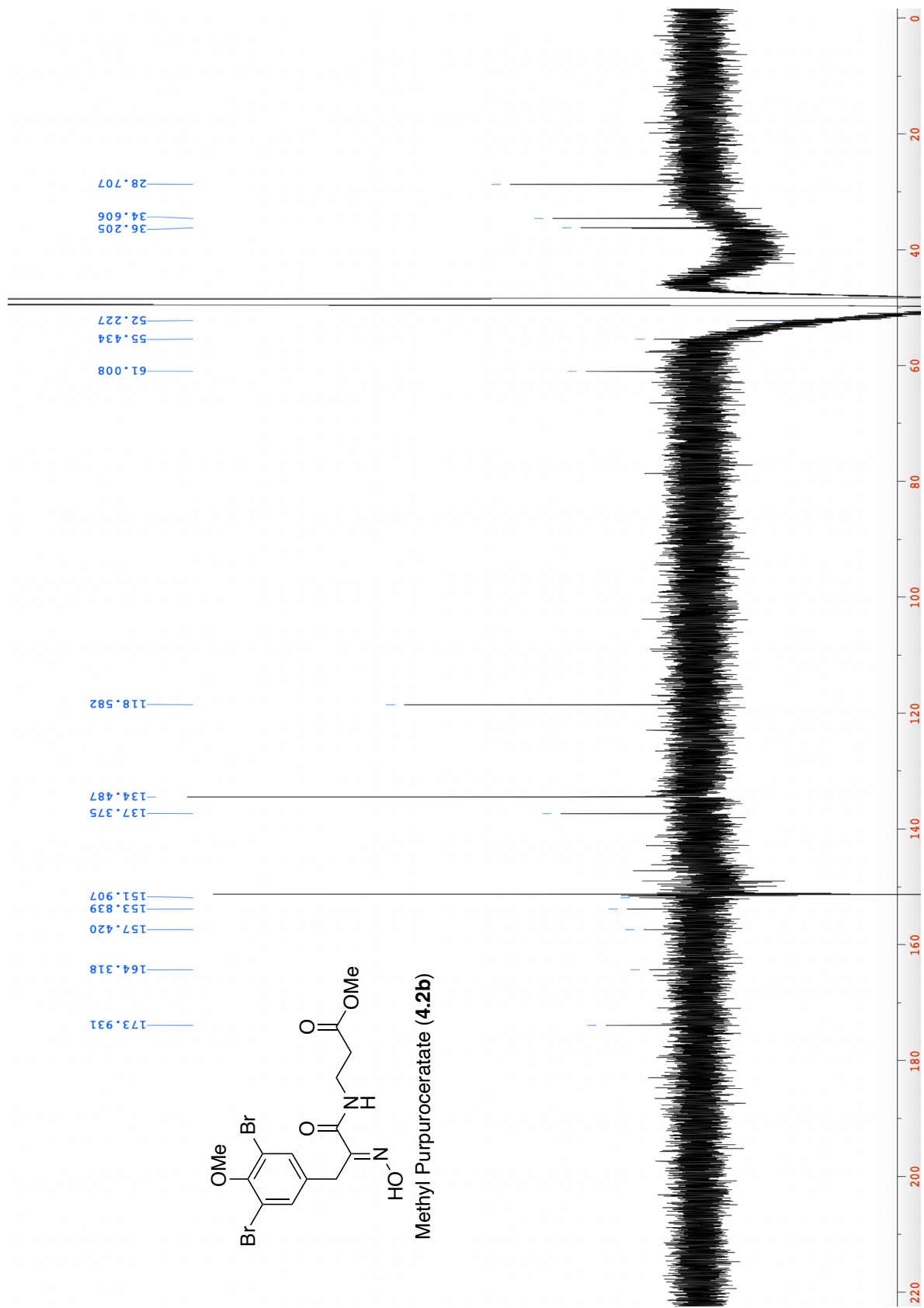


Figure 4.14: ¹³C NMR of Compound 4.2b (125 MHz, CD₃OD).

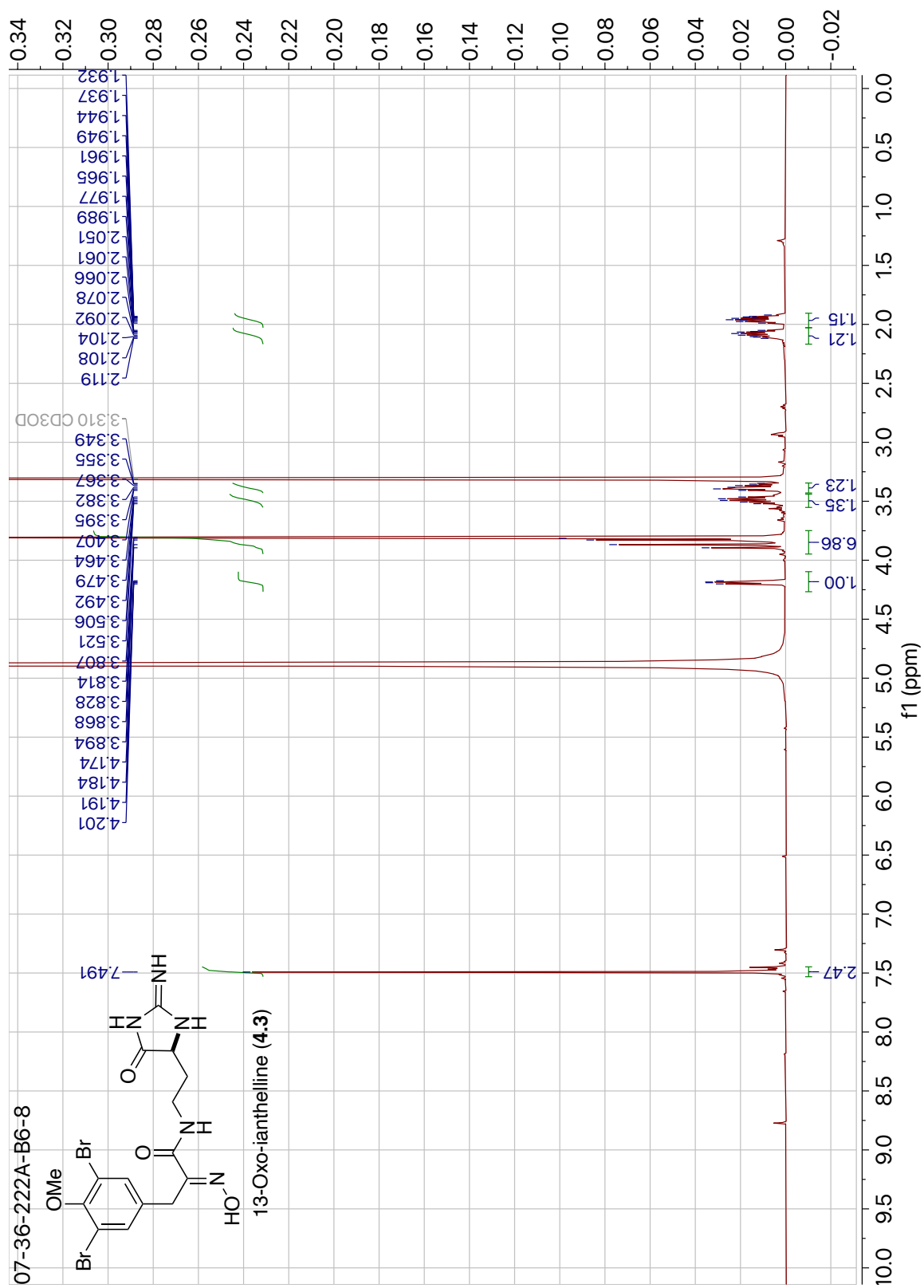


Figure 4.15: ¹H NMR of Compound 4.3 (500 MHz, CD₃OD).

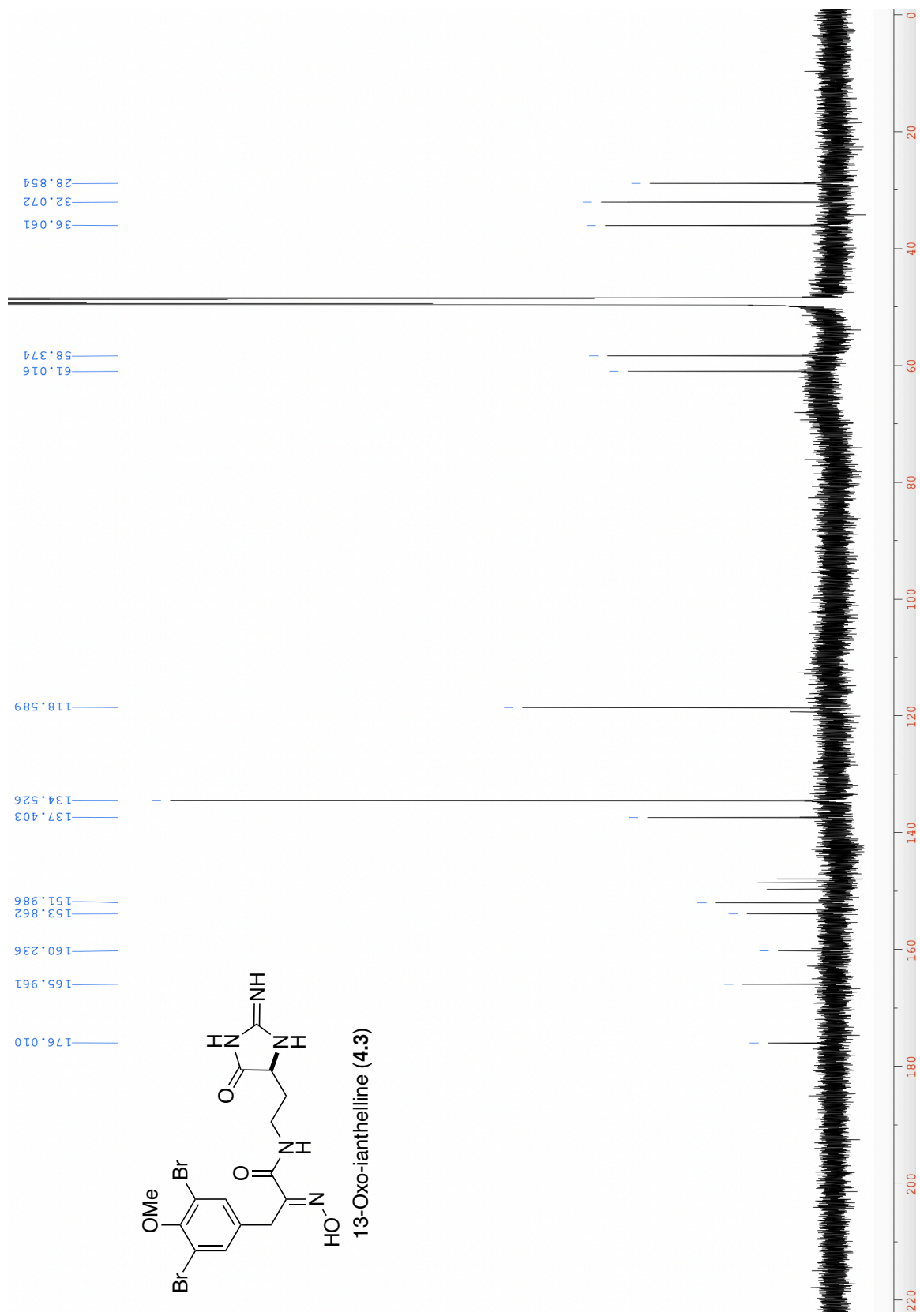
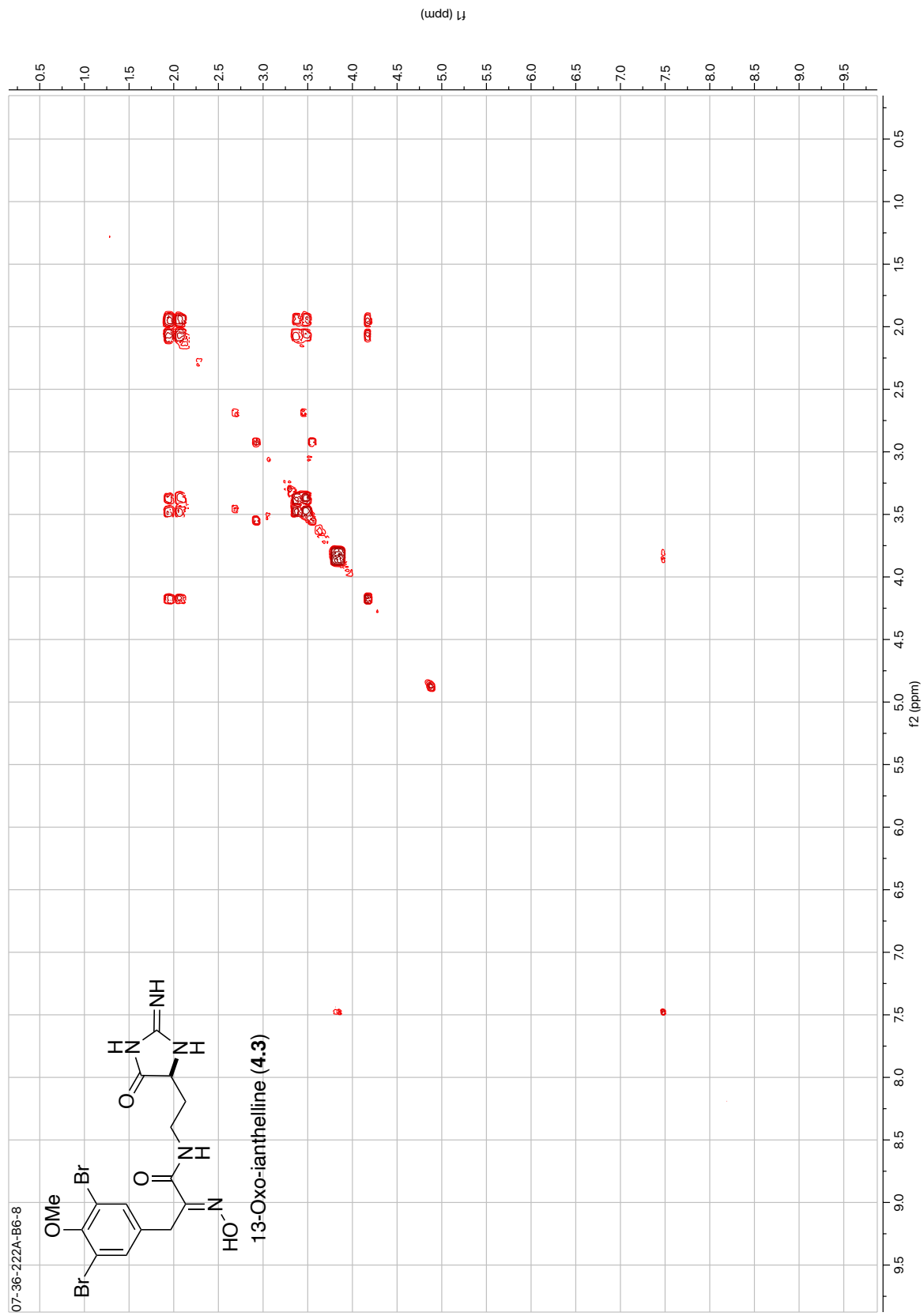
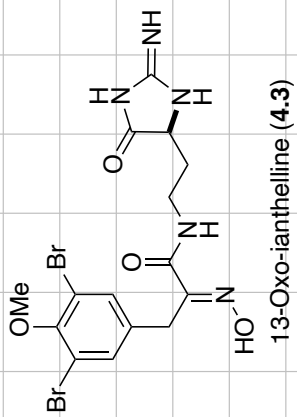


Figure 4.16: ¹³C NMR of Compound 4.3 (125 MHz, CD₃OD).

07-36-222A-B6-8



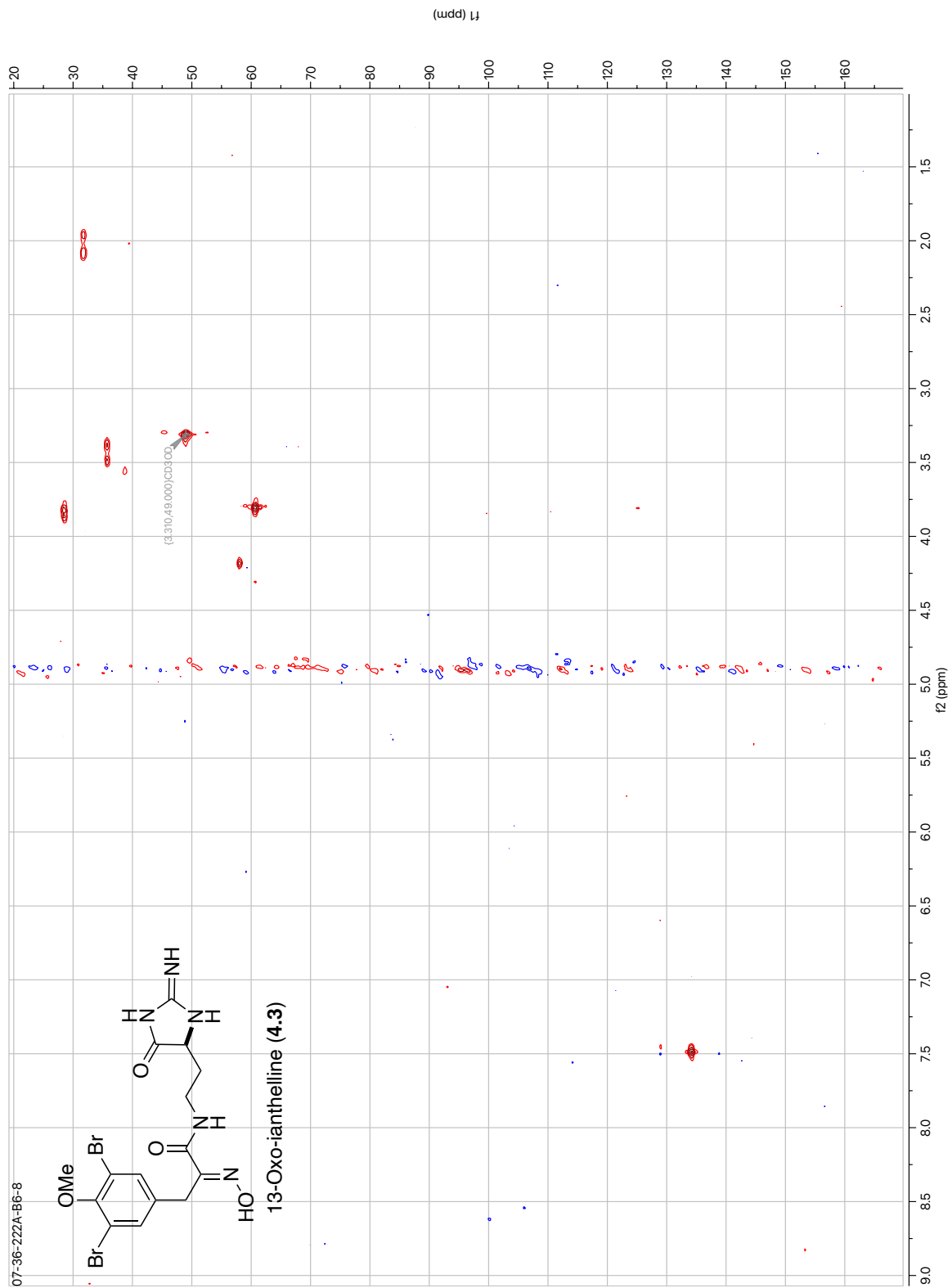


Figure 4.18: HSQC of Compound 4.3 (500 MHz, CD₃OD).

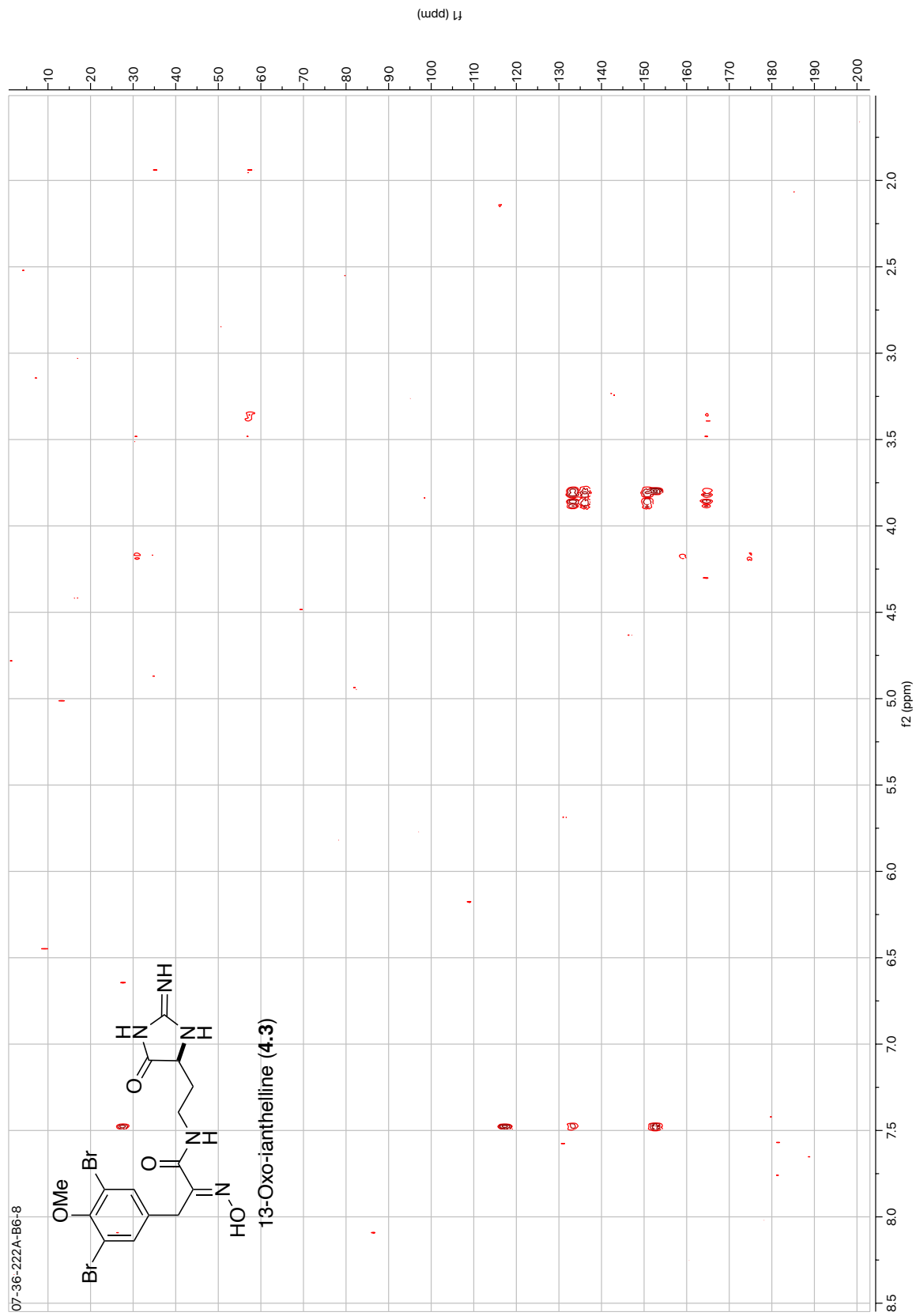
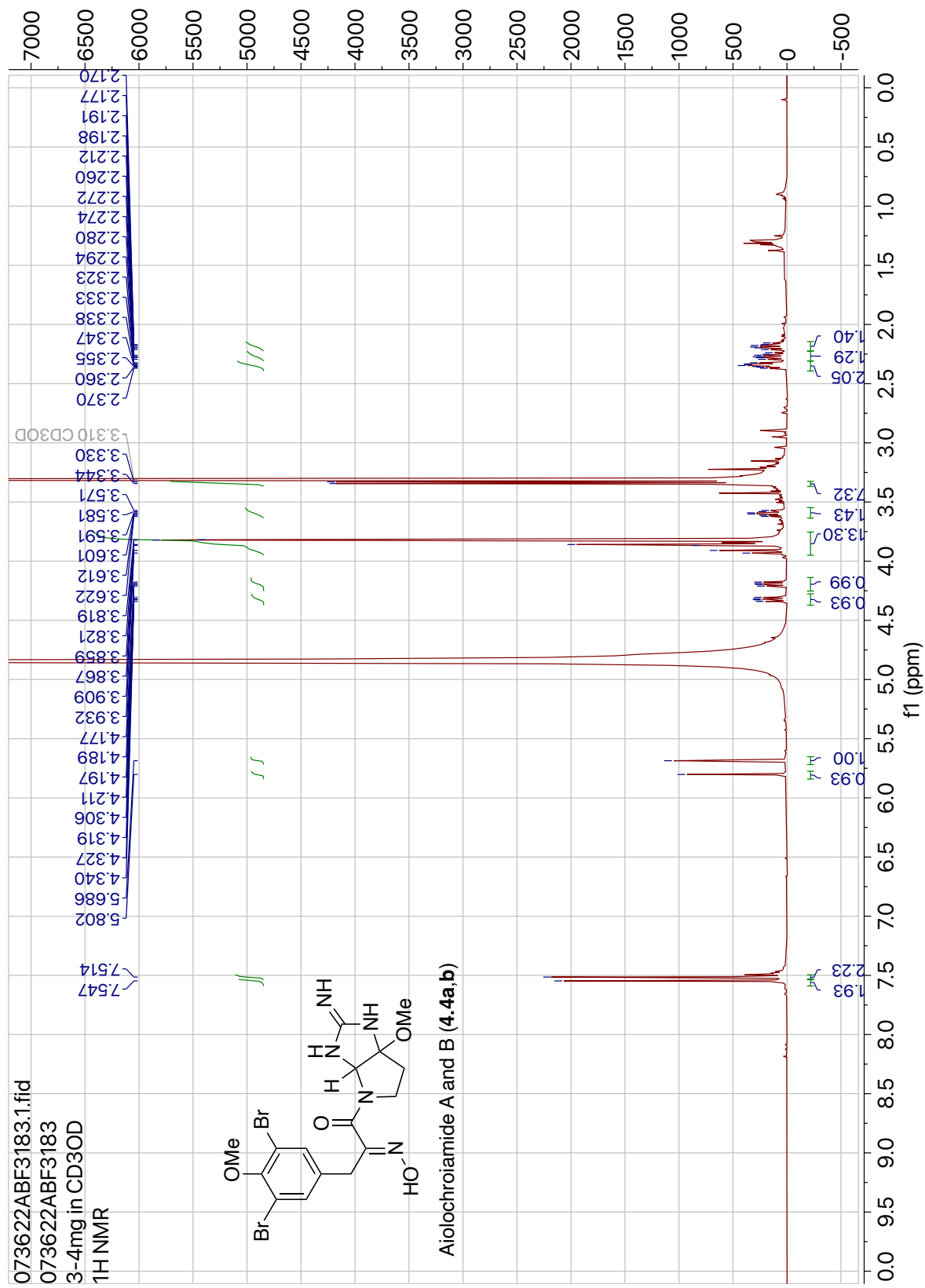


Figure 4.19: HMBC of Compound 4.3 (500 MHz, CD₃OD).



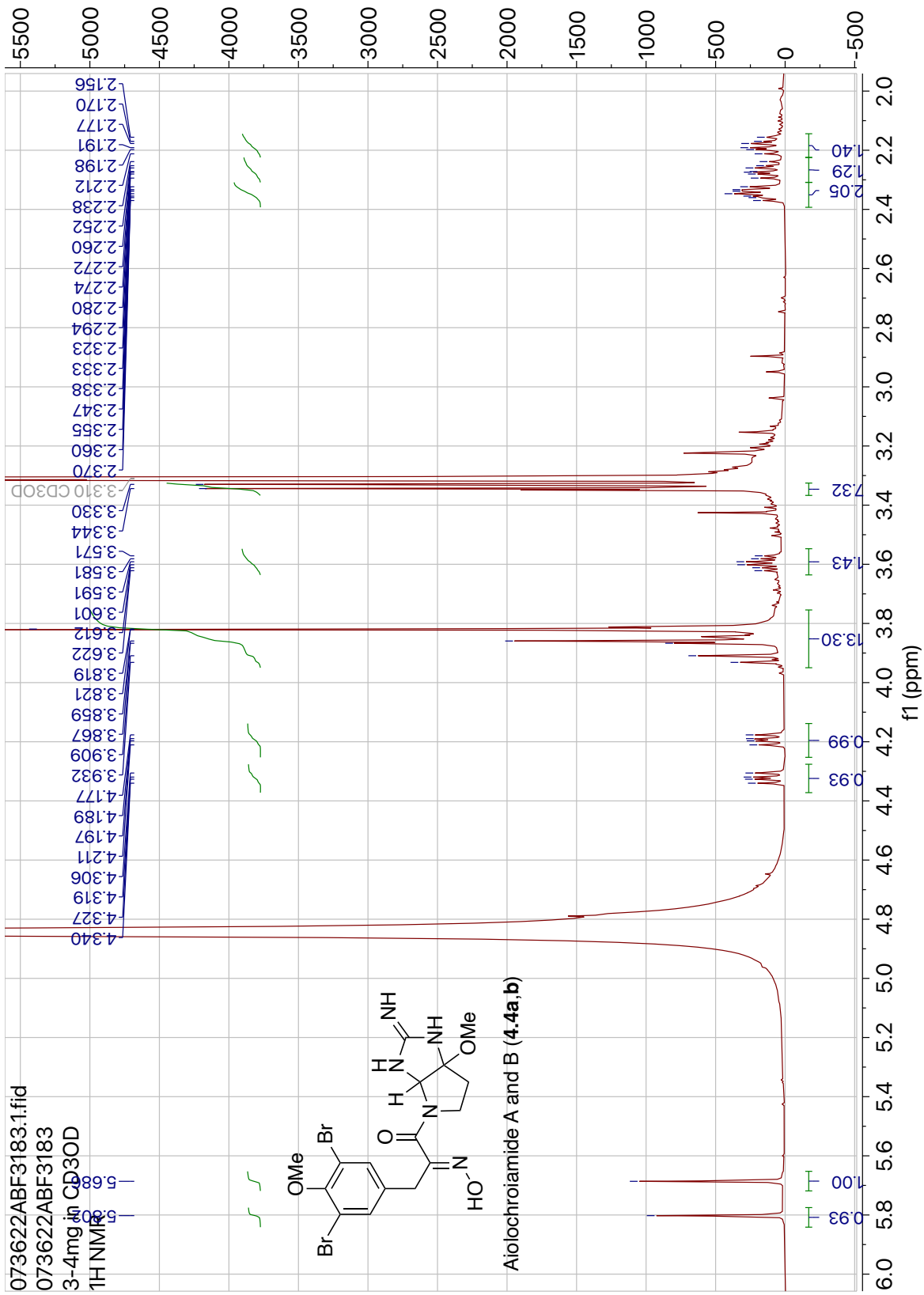


Figure 4.21: ¹H NMR Expansion of Compound 4.4a,b (600 MHz, CD₃OD).

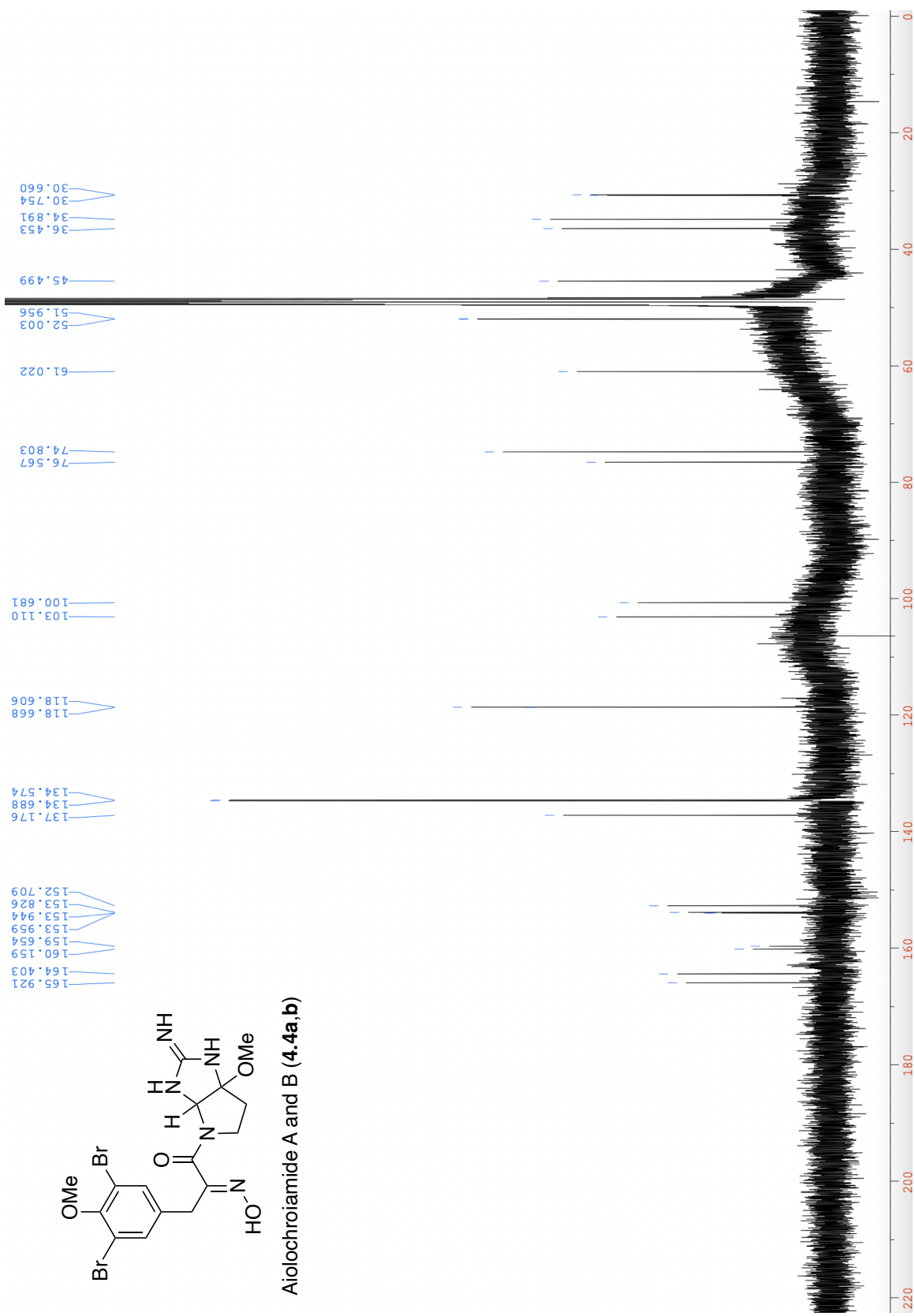


Figure 4.22: ¹³C NMR of Compound 4.4a,b (125 MHz, CD₃OD).

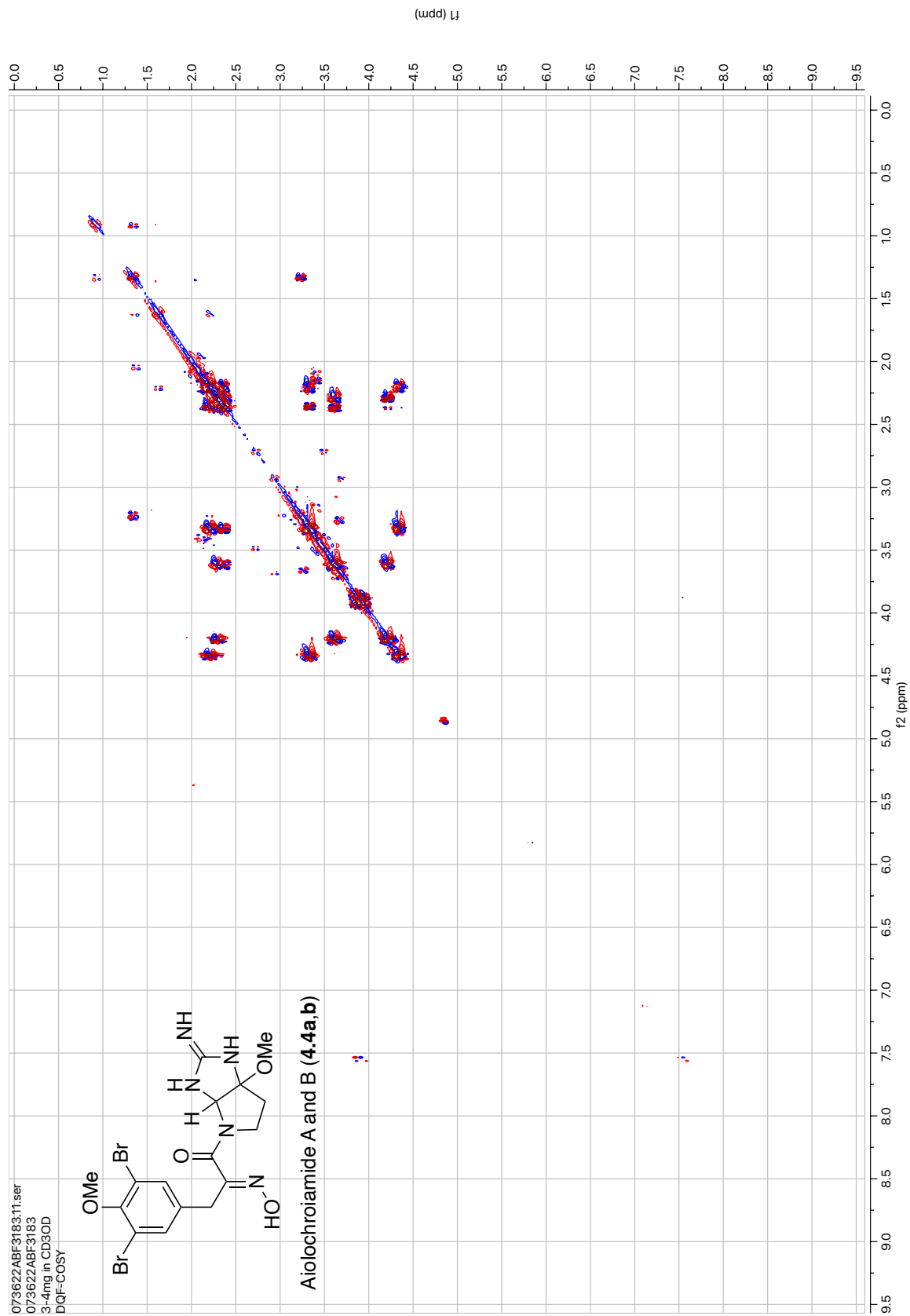


Figure 4.23: DQF-COSY of Compound 4.4a,b (600 MHz, CD₃OD).

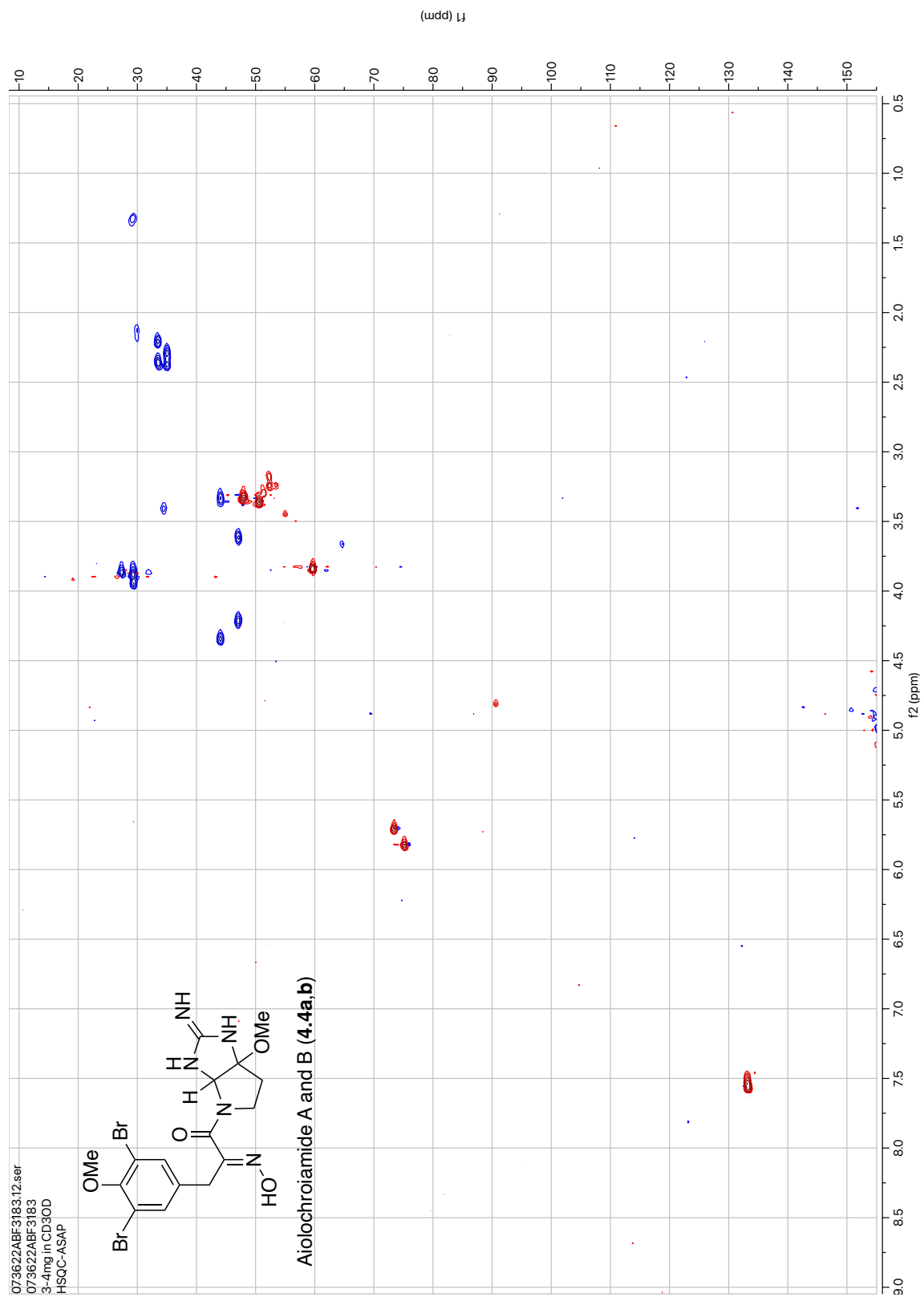
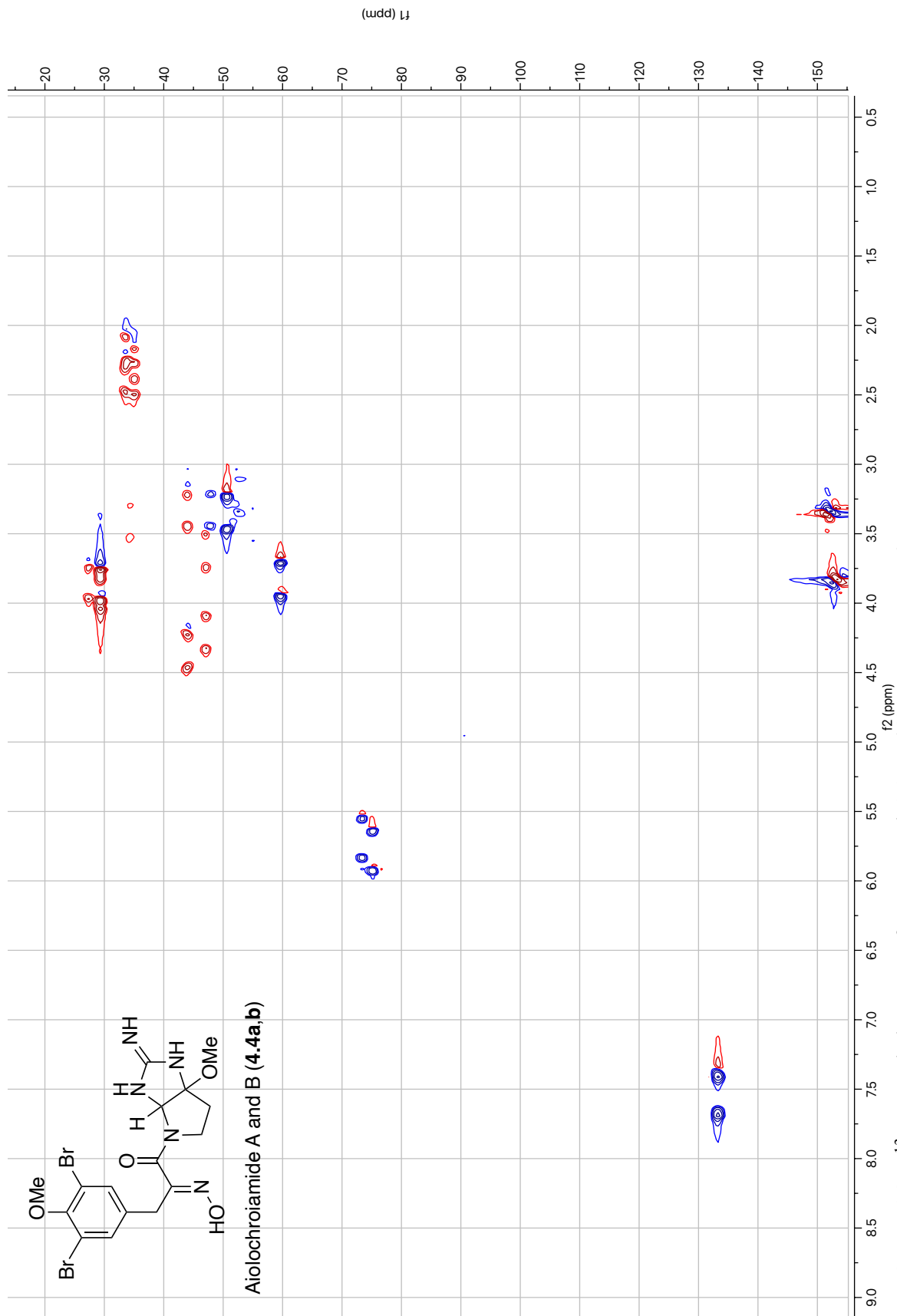
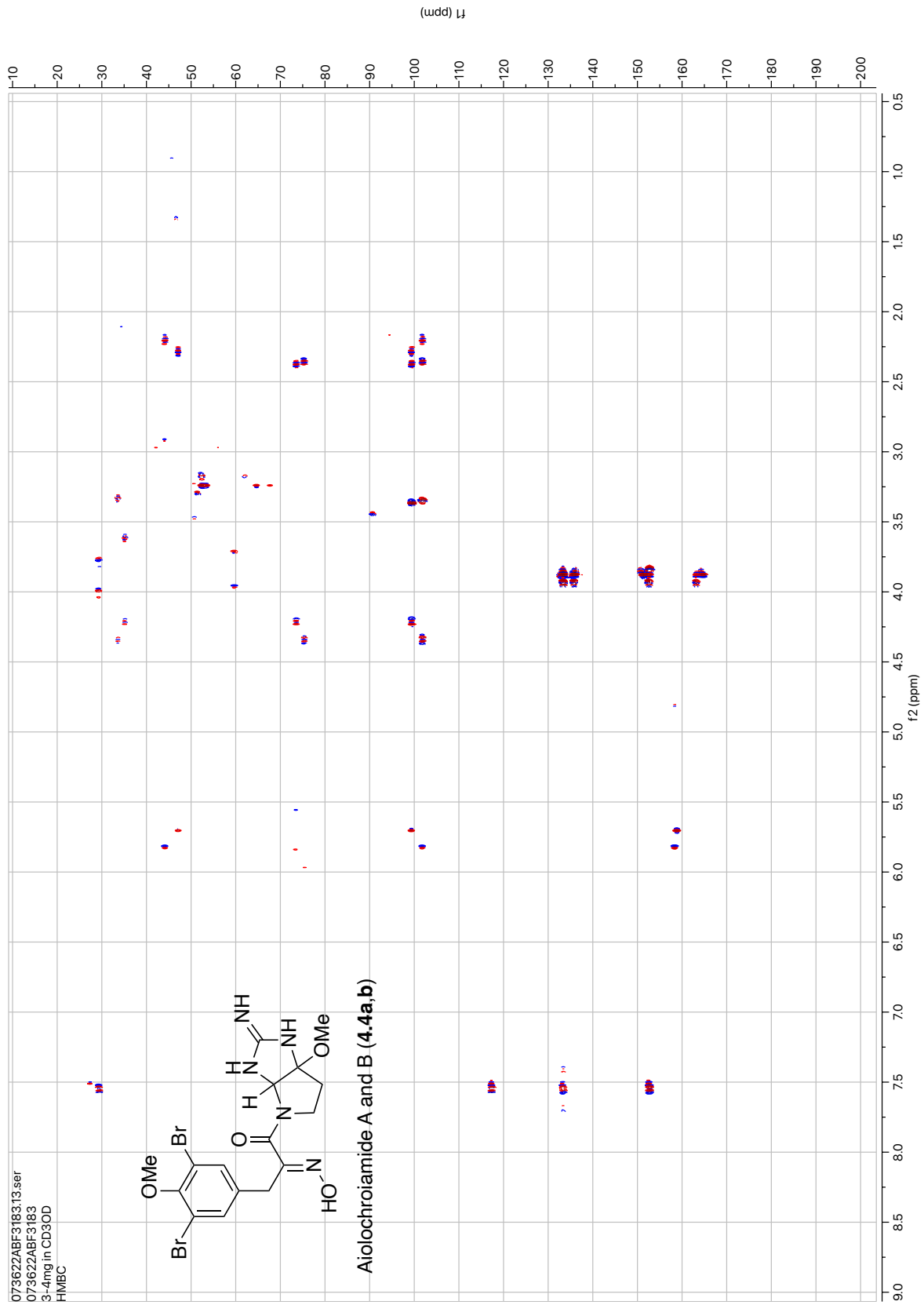


Figure 4.24: HSQC-ASAP of Compound **4.4a,b** (600 MHz, CD₃OD).





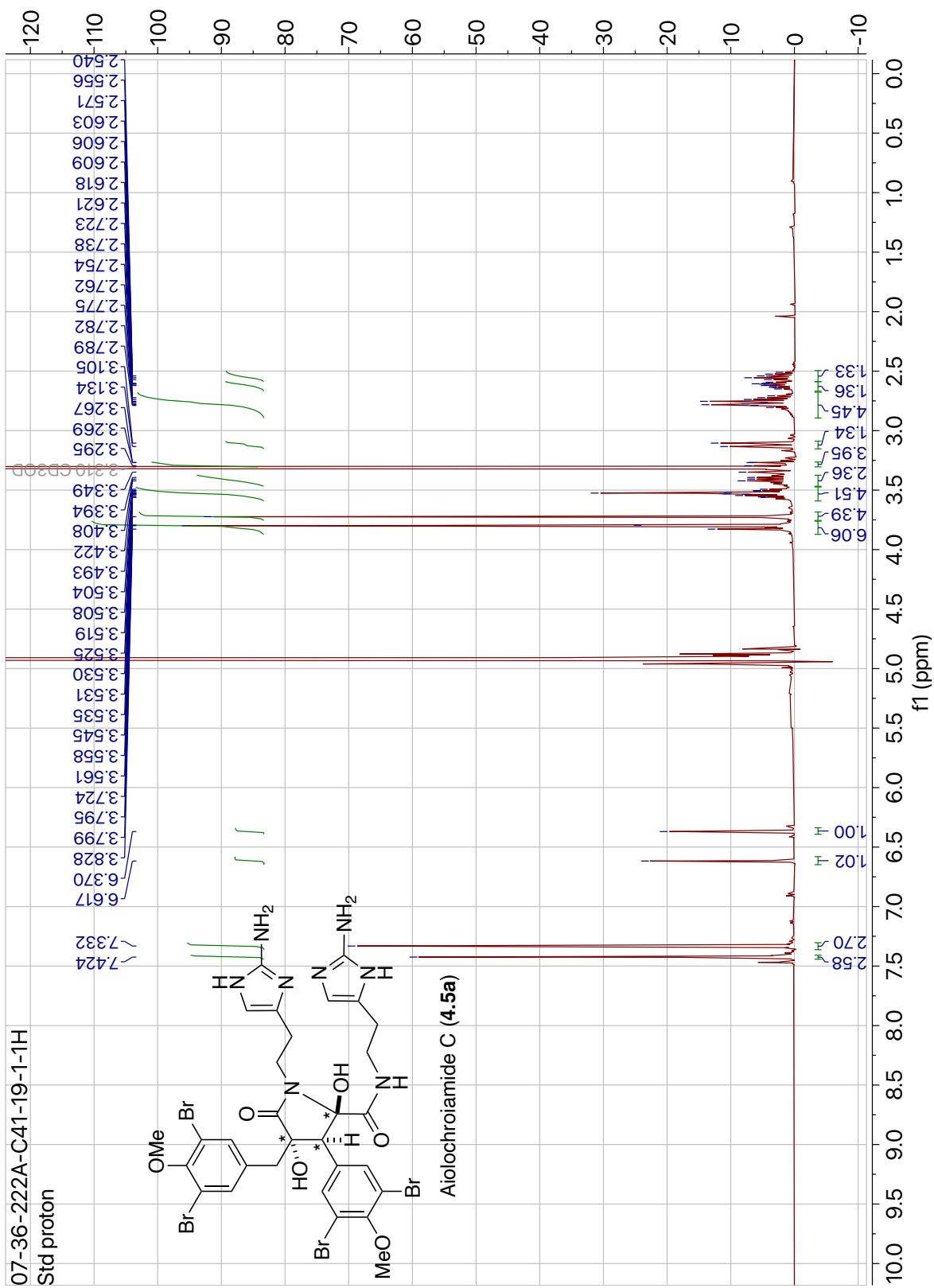


Figure 4.27: ^1H NMR of Compound 4.5a (500 MHz, CD_3OD).

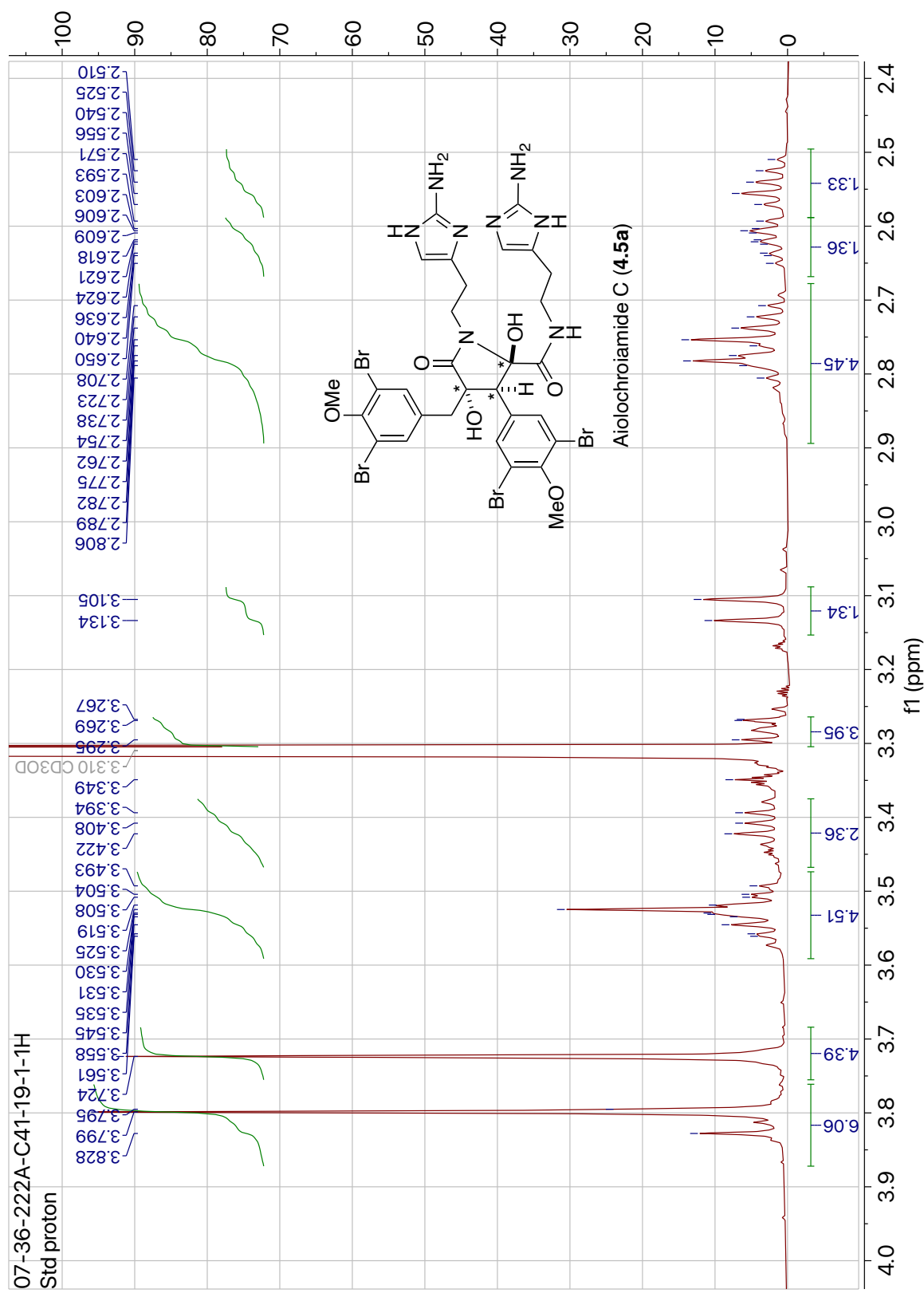
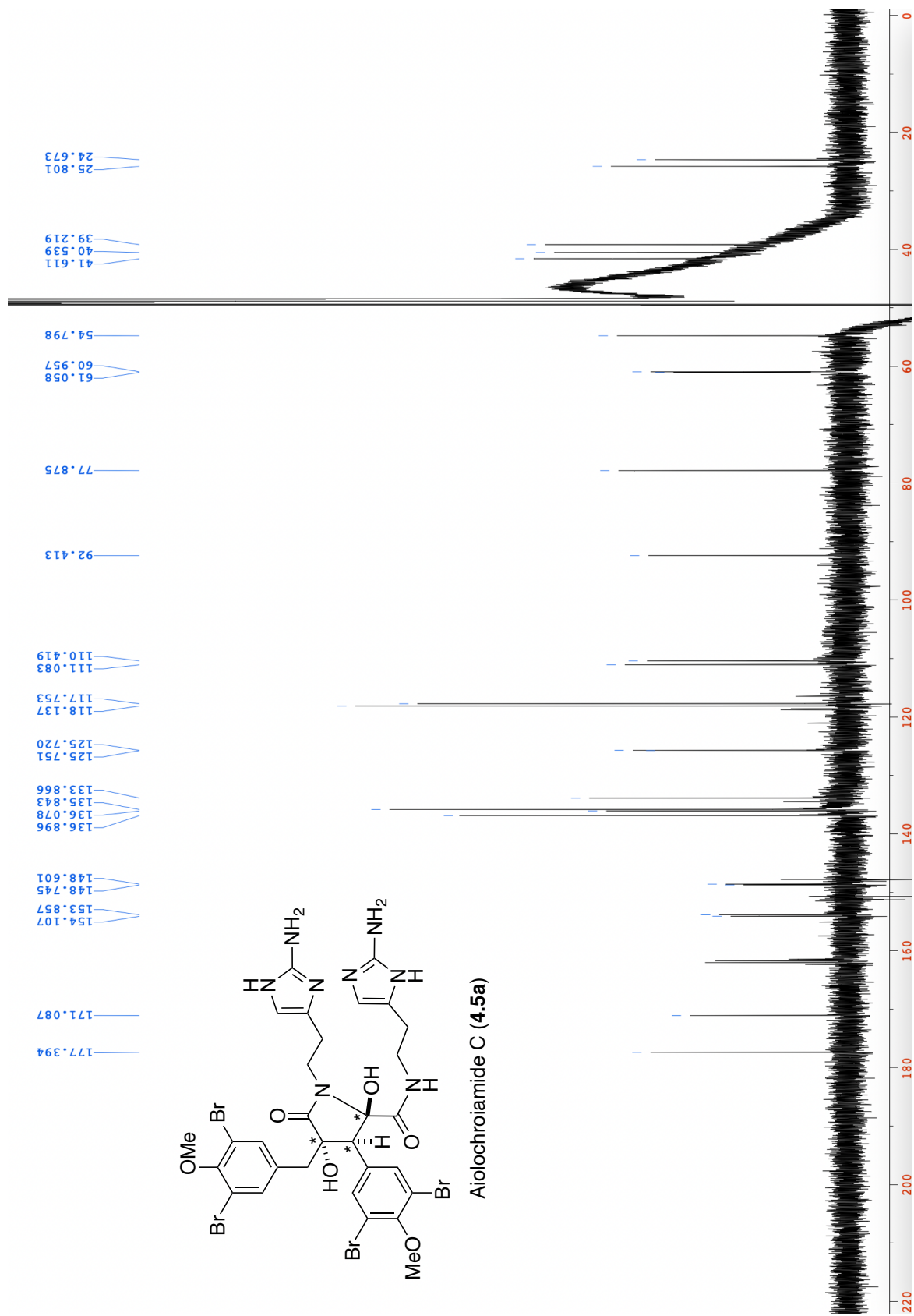


Figure 4.28: ¹H NMR Expansion of Compound 4.5a (500 MHz, CD₃OD).



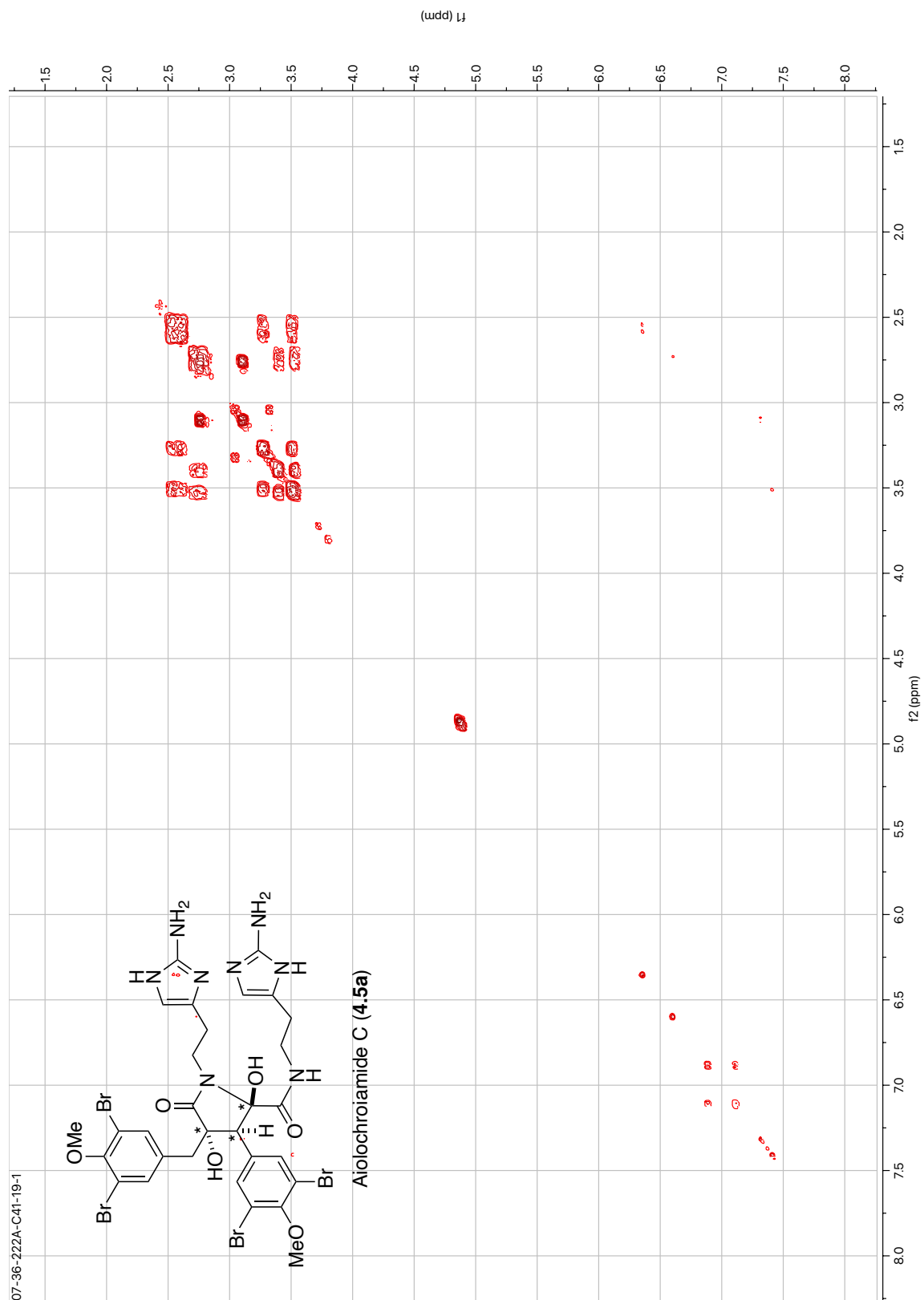


Figure 4.30: DQF-COSY of Compound **4.5a** (500 MHz, CD₃OD).

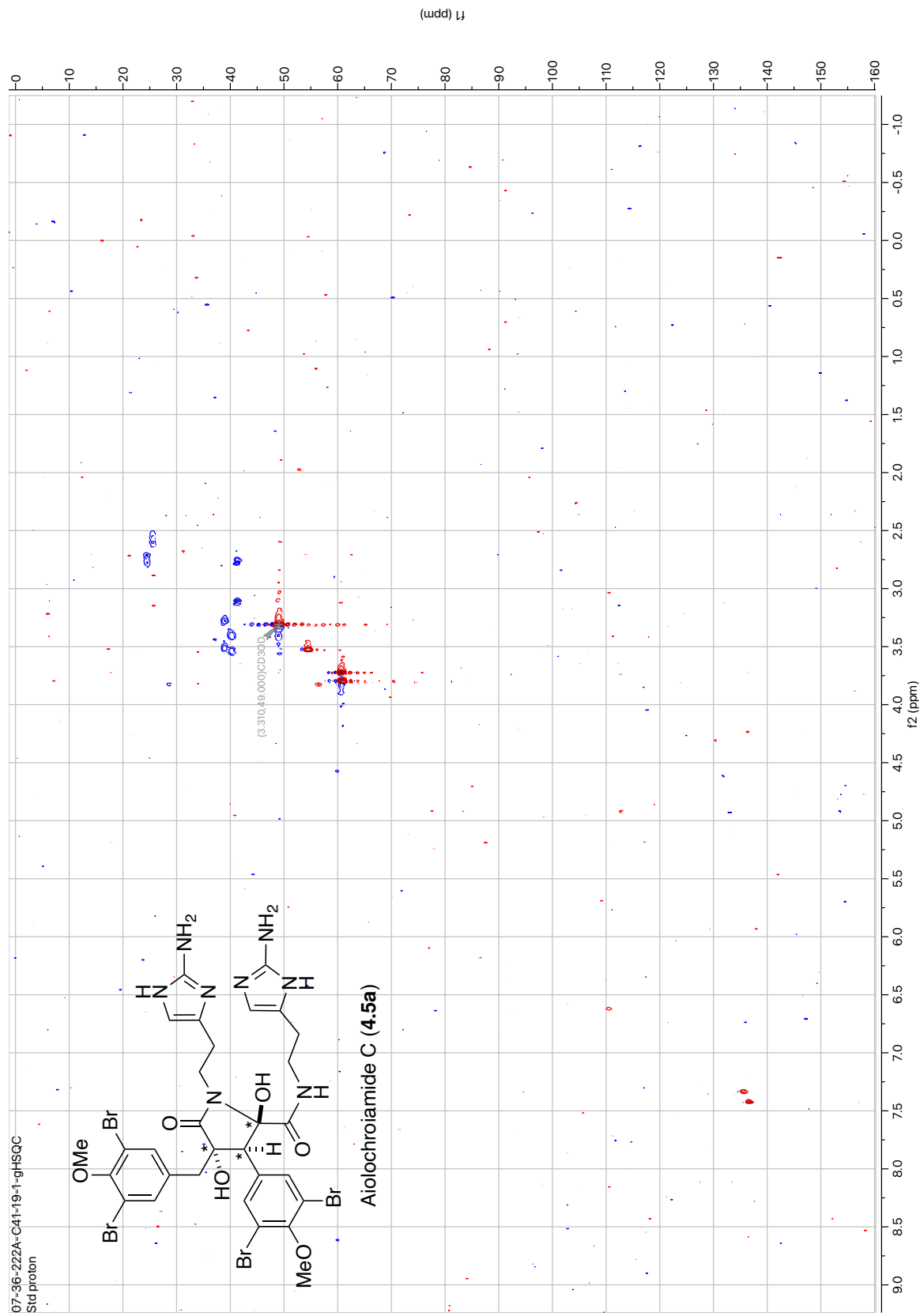


Figure 4.31: gHSQC of Compound 4.5a (500 MHz, CD₃OD).

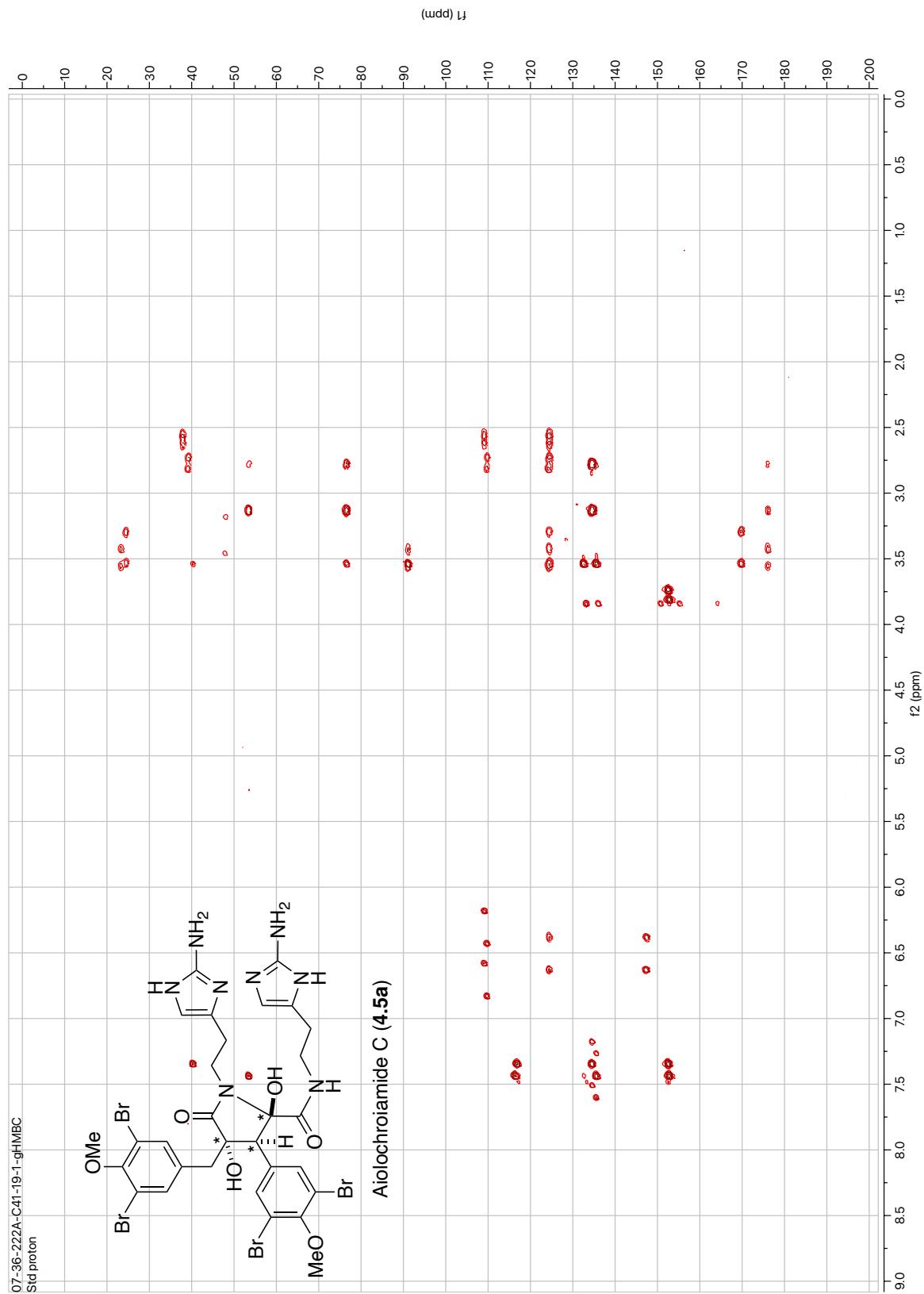


Figure 4.32: gHMBC of Compound 4.5a (500 MHz, CD₃OD).

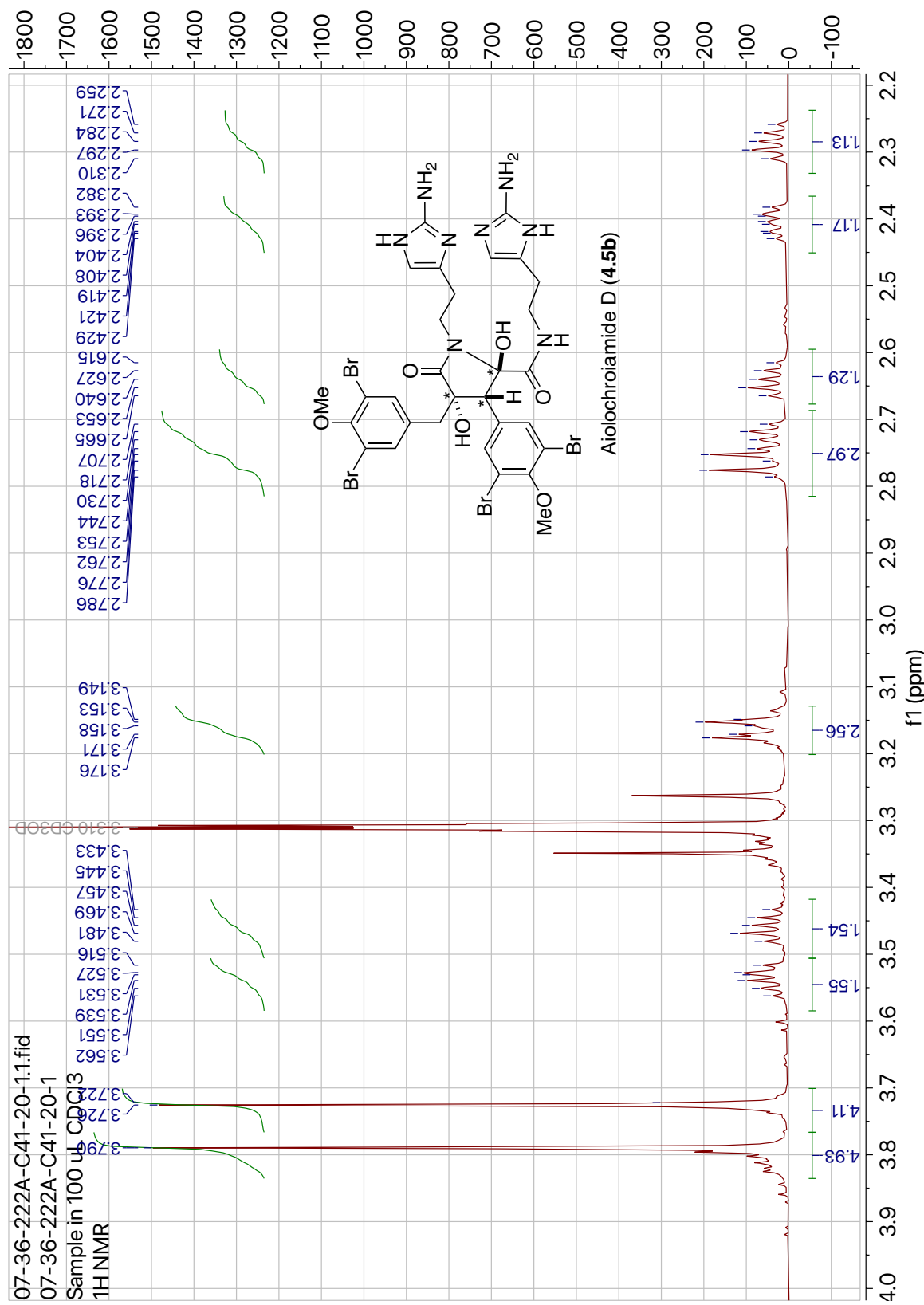


Figure 4.34: ¹H NMR Expansion of Compound 4.5b (600 MHz, CD₃OD).

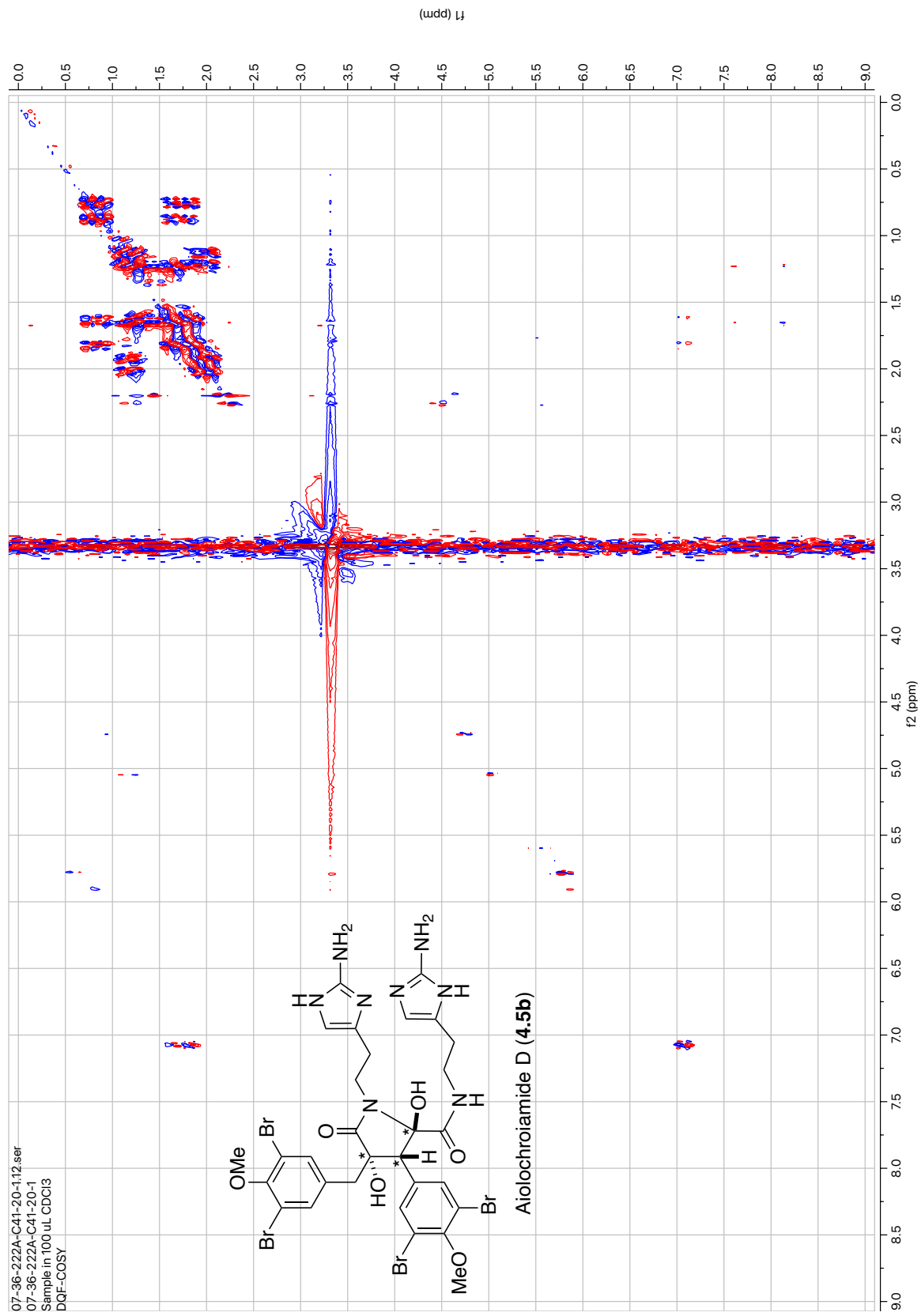


Figure 4.35: DQF-COSY of Compound **4.5b** (600 MHz, CD₃OD).

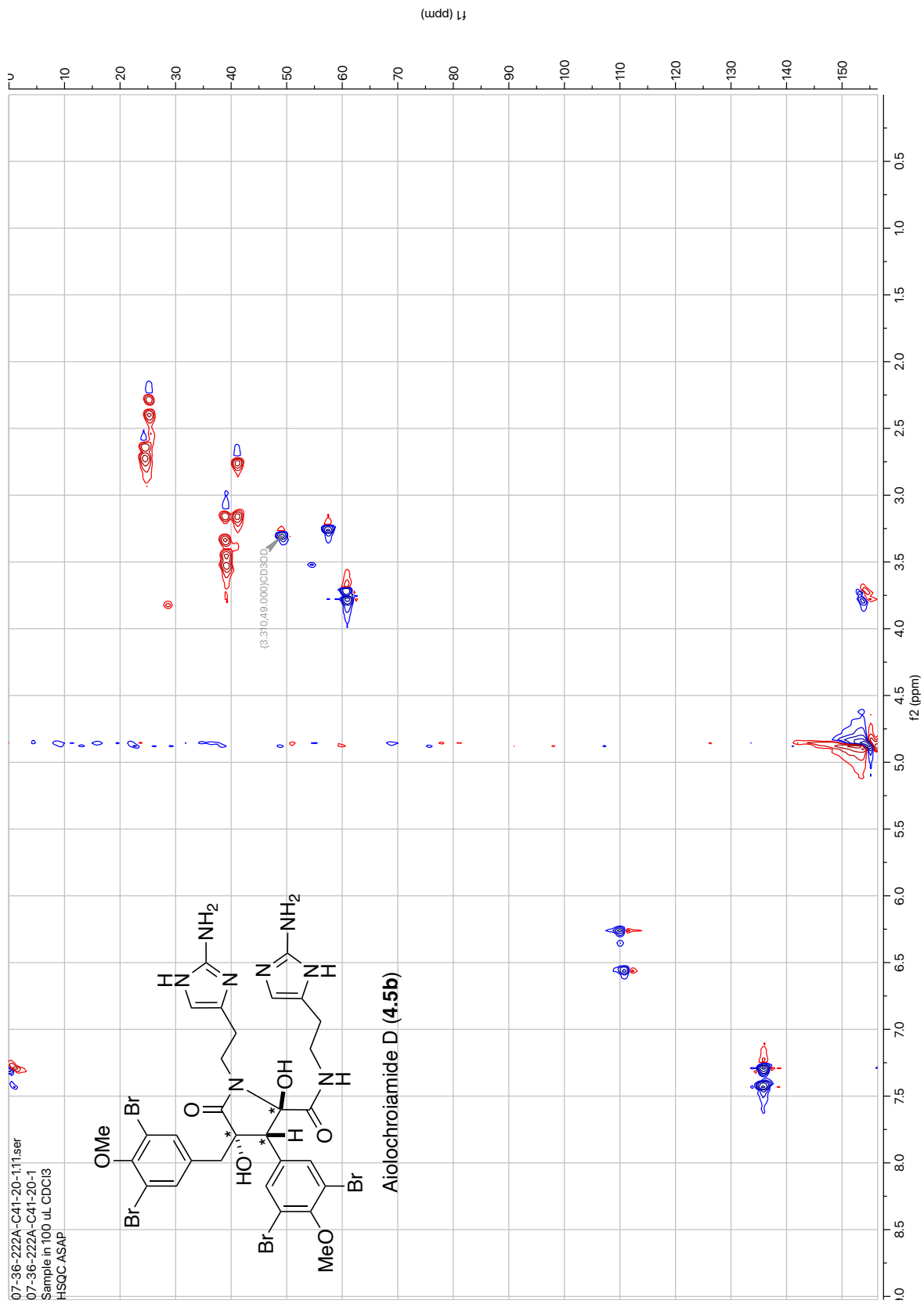


Figure 4.36: HSQC-ASAP of Compound **4.5b** (600 MHz, CD₃OD).

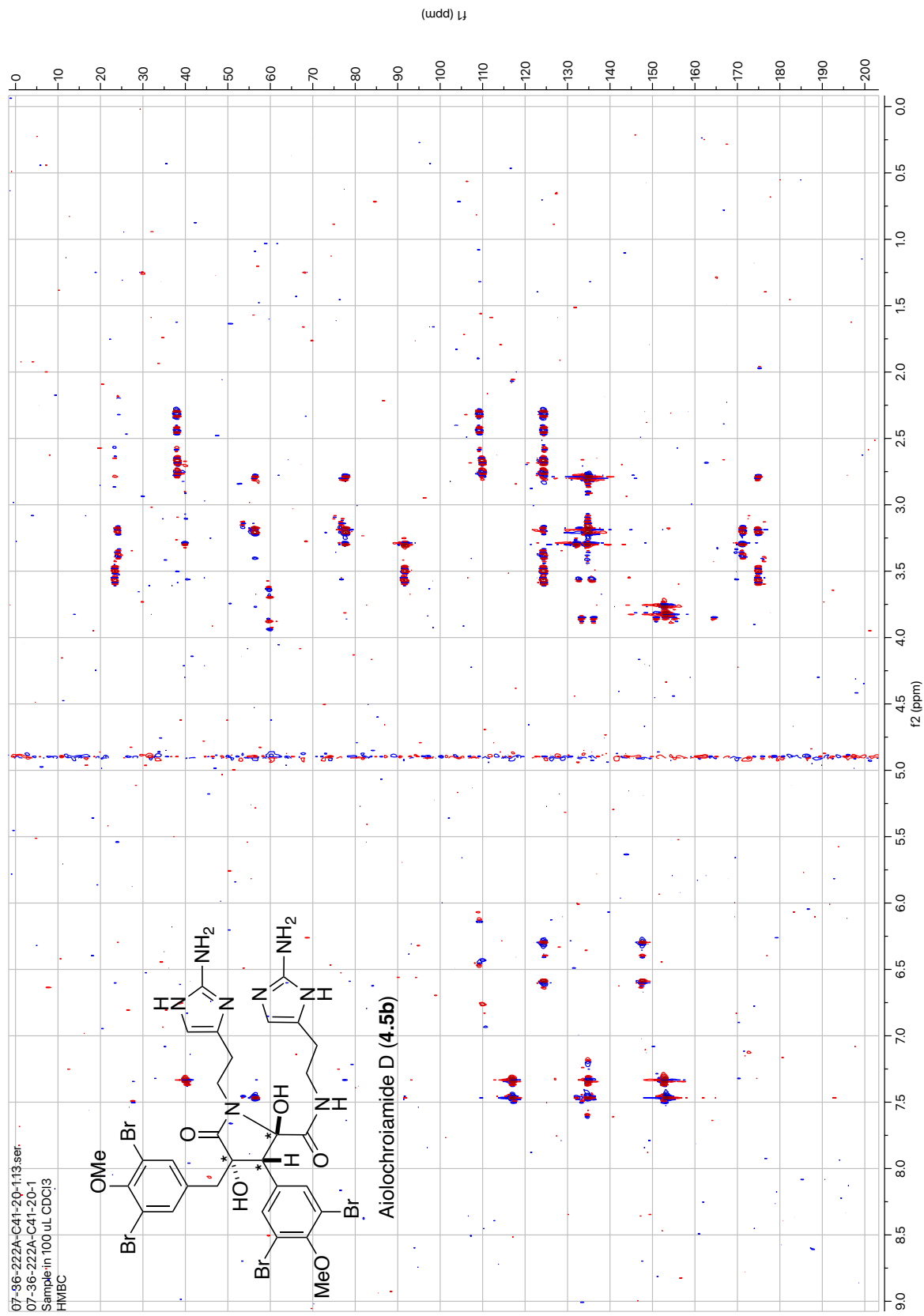


Figure 4.37: HMBBC of Compound 4.5b (600 MHz, CD₃OD).

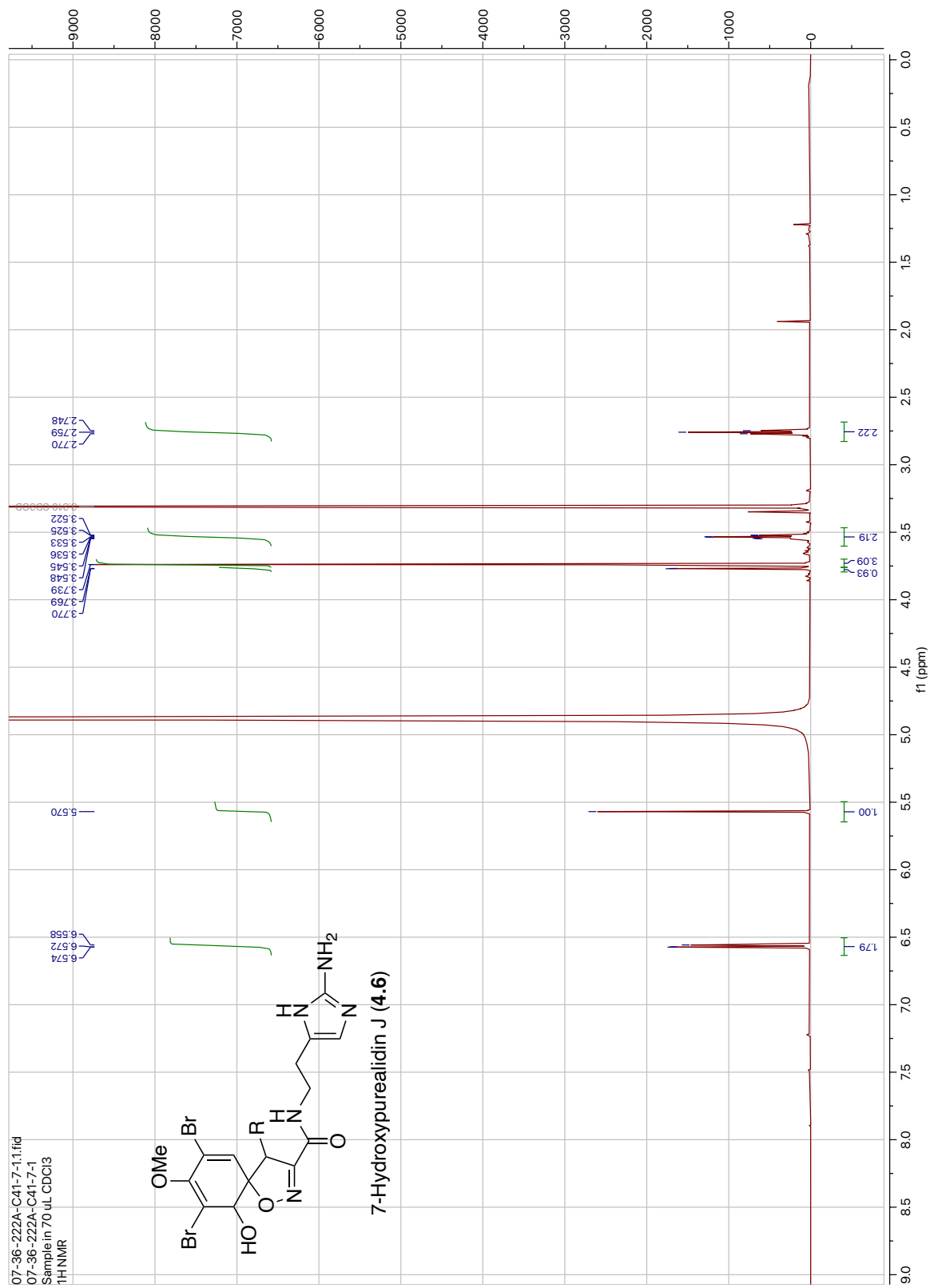


Figure 4.38: ¹H NMR of Compound 4.6 (600 MHz, CD₃OD).

07-36-222A-C41-7-114.ser
07-36-222A-C41-7-1
Sample in 70 uL CDCl3
DQF-COSY

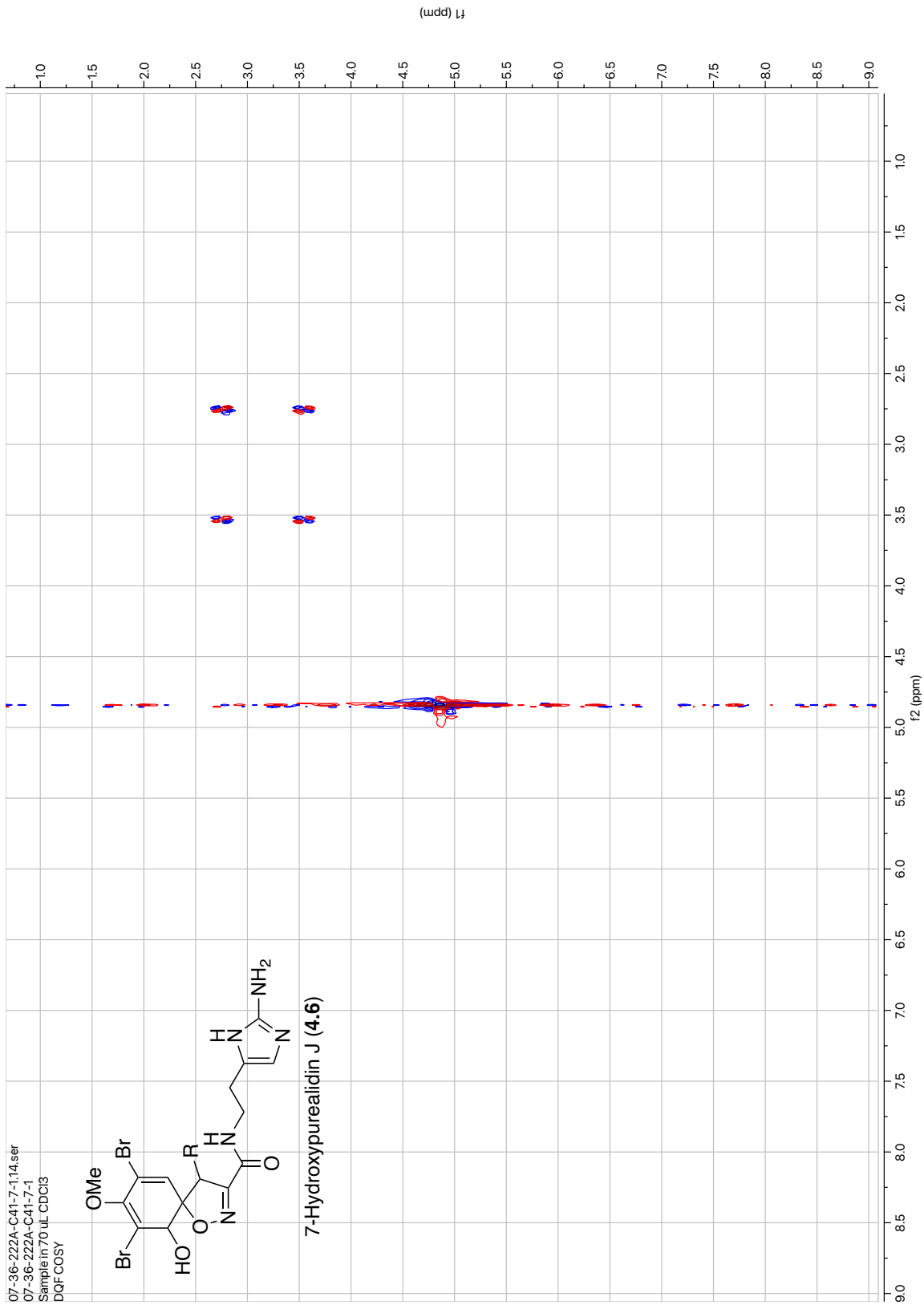
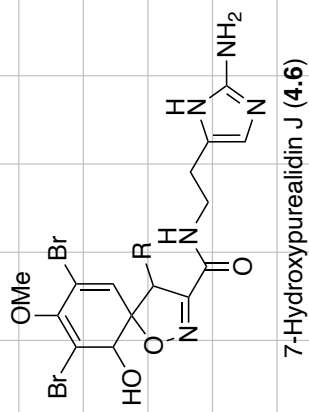


Figure 4.39: DQF-COSY of Compound **4.6** (600 MHz, CD3OD).

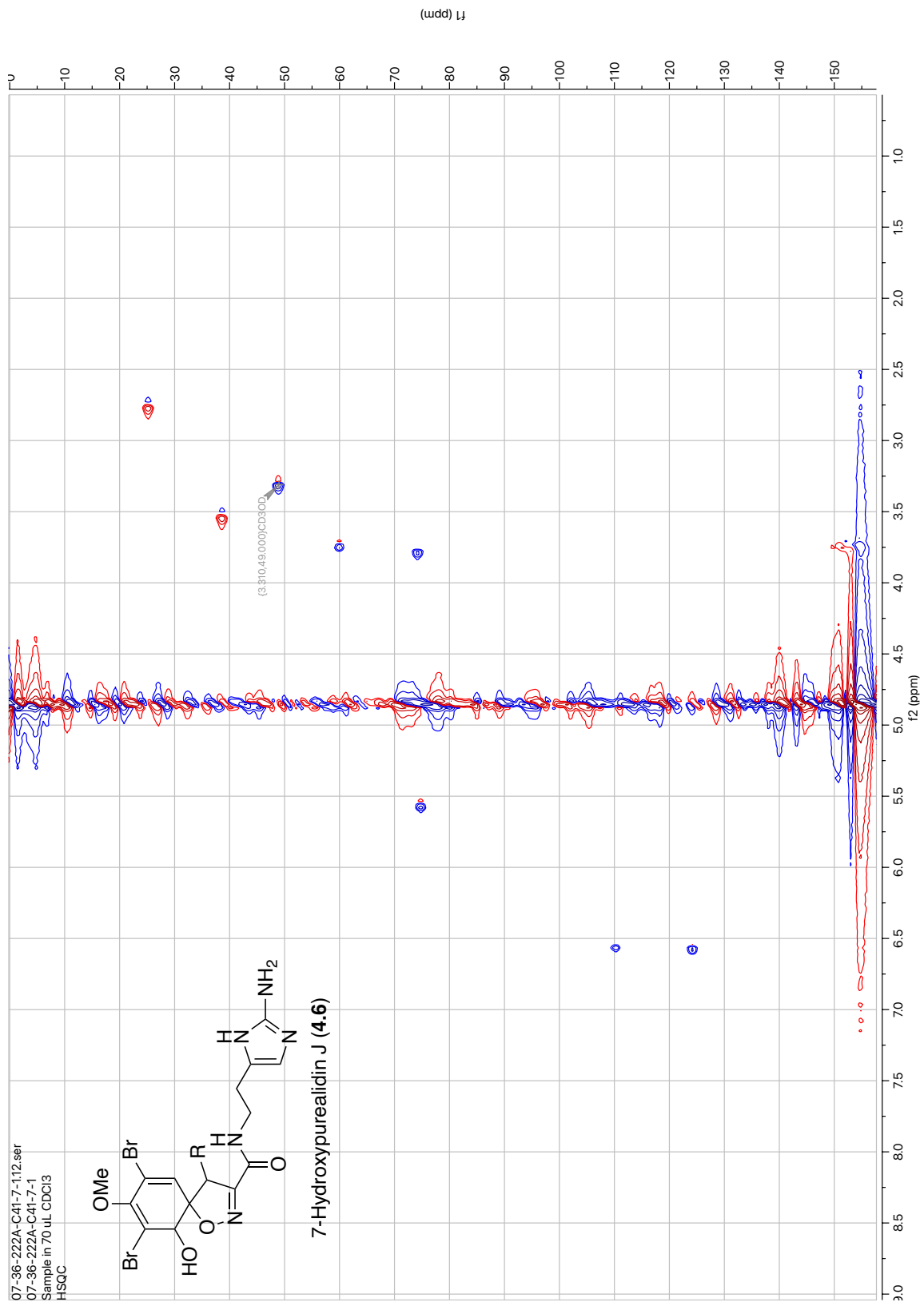


Figure 4.40: HSQC of Compound **4.6** (600 MHz, CD₃OD).

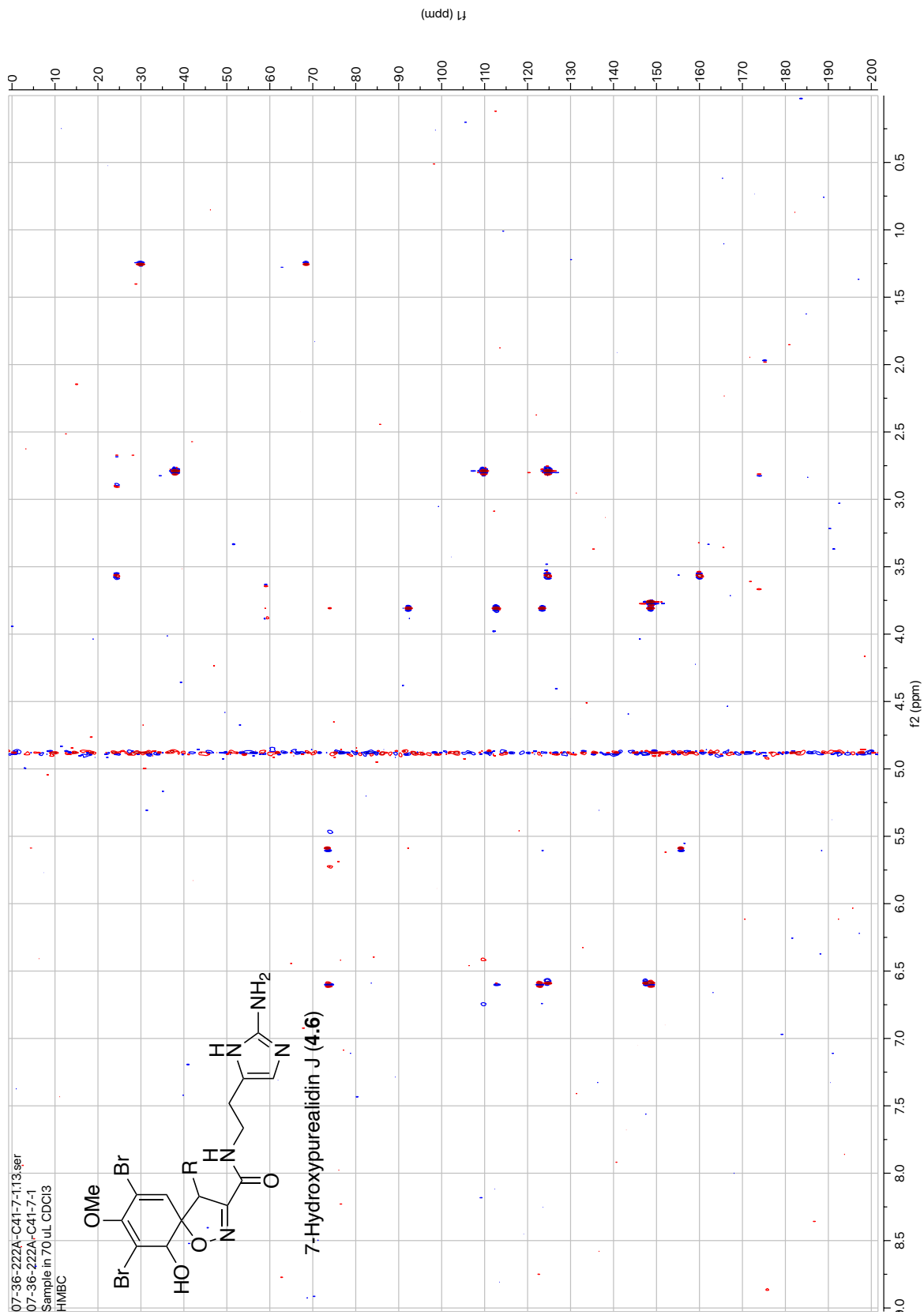


Figure 4.41: HMBc of Compound 4.6 (600 MHz, CD3OD).

Table 4.6: Antifungal Activities (Disk-Diffusion Assay) of ‘Layers A-D’ and Chromatography Subfractions (SF) against *Candida* and *Cryptococcus* spp.

Sample	<i>C. albicans</i>	<i>C. albicans</i>	<i>C.</i>	<i>C.</i>	<i>Cry. var.</i>	<i>Cry. var.</i>
	<i>ATCC 14503</i> ^e	<i>UCD-FR1</i> ^e	<i>krusei</i> ^e	<i>glabrata</i> ^e	<i>grubii</i> ^f	<i>gattii</i> ^g
Zones of inhibition (mm)						
‘Layer A’ ^a	-	-	-	-	-	-
‘Layer B’ ^a	13	12	14	12	21	10
‘Layer C’ ^a	-	-	12	10	12	8
‘Layer D’ ^a	-	-	10	11	17	10
SF1 ^{a,b}	14	12	11	13		
SF2 ^{a,b}	16	10	8	8	9	11
SF3 ^{a,b}	20	15	18	14	28	35
SF4 ^{a,b}	8	14	10	12	7	15
SF5 ^{a,c}	12	9	9	12	-	-
SF6 ^{a,c}	10	11	-	11	-	-
SF7 ^{a,b}	-	10	10	9	-	-
Ianthelline (4.7) ^a	13.5	8.5	14	12	20	18
Clotrimazole ^d	28	28	33	25	28	35

^aTested at 300 µg/disk. ^bSubfractions of the ‘B layer’ obtained from Sephadex LH-20 fractionation. ^cTested at 150 µg/disk. ^dTested at 30 µg/disk. ^e*Candida* sp. ^f*Cryptococcus neoformans* var. *grubii*. ^g*Cryptococcus neoformans* var. *gattii*.

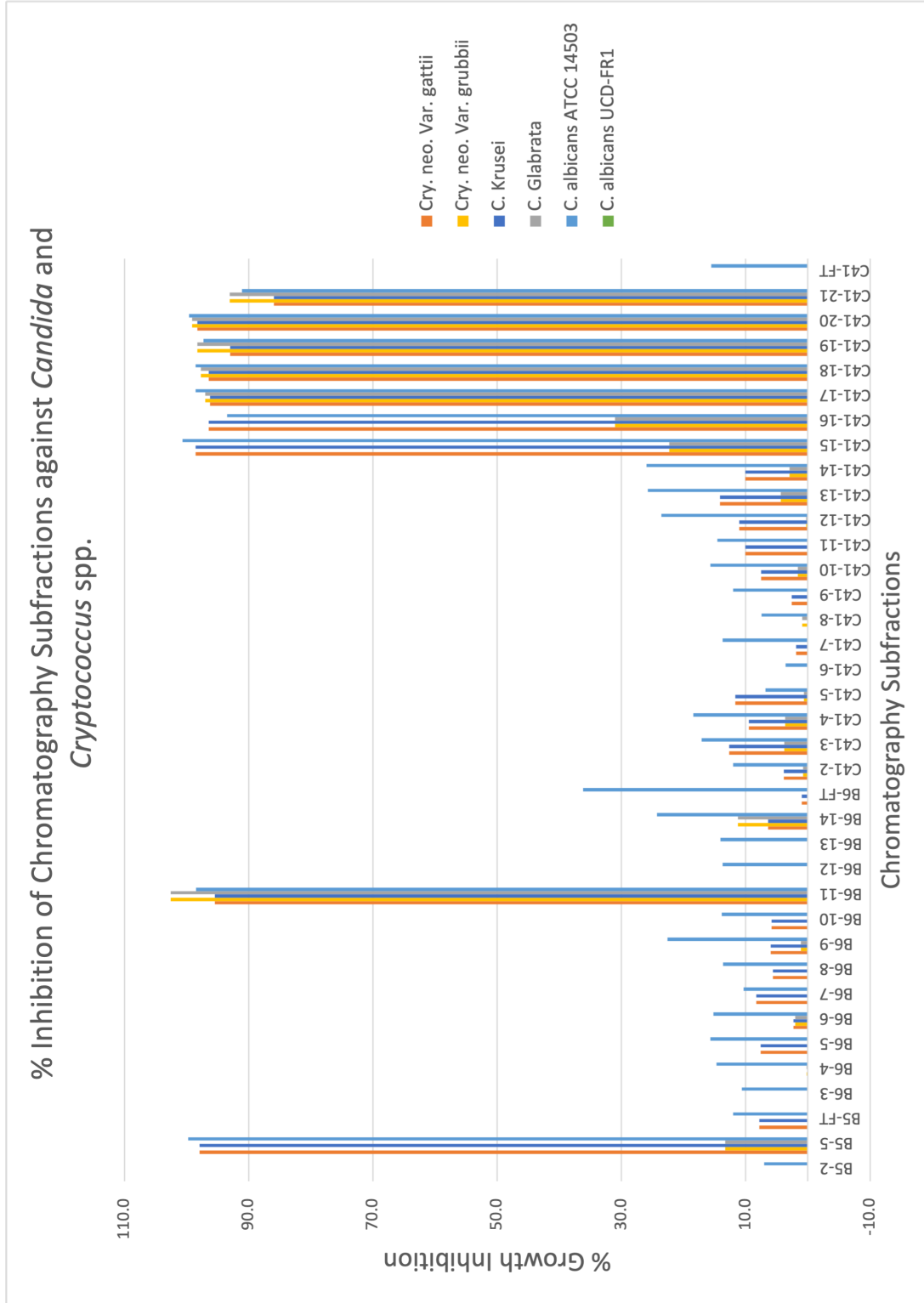


Figure 4.42: Antifungal Activity of Chromatography Subfractions (SF) against *Candida* and *Cryptococcus* spp.^a
^aSamples B5-5, B5-FT, B6-10, B6-FT, C41-4, C41-15, C41-21, and C41-FT were tested at 100 µg/mL. Remaining samples were tested at 50 µg/mL. Fractions B5-5 and C41-15 contained ianthelline (4.7). Fractions B6-11 and C41-21 contained ningalamide B (4.9). Fractions C41-19 and C41-20 contained aiolochroiamides C (4.5a) and D (4.5b), respectively.

Table 4.7: BuChE Inhibitory Activity of ‘Layers B and C’ Sephadex LH-20 Subfractions (SF).

Sample	‘Layer B’	‘Layer C’
	% Inhibition ^a	% Inhibition ^b
SF1	-5.0	41.7
SF2	19.0	39.8
SF3	68.2	63.0
SF4	75.3	56.4
SF5	75.3	56.9
SF6	59.8	50.4
SF7	58.3	34.7
SF8	63.6	41.6

^aTested at 100 µg/mL. ^bTested at 300 µg/mL.

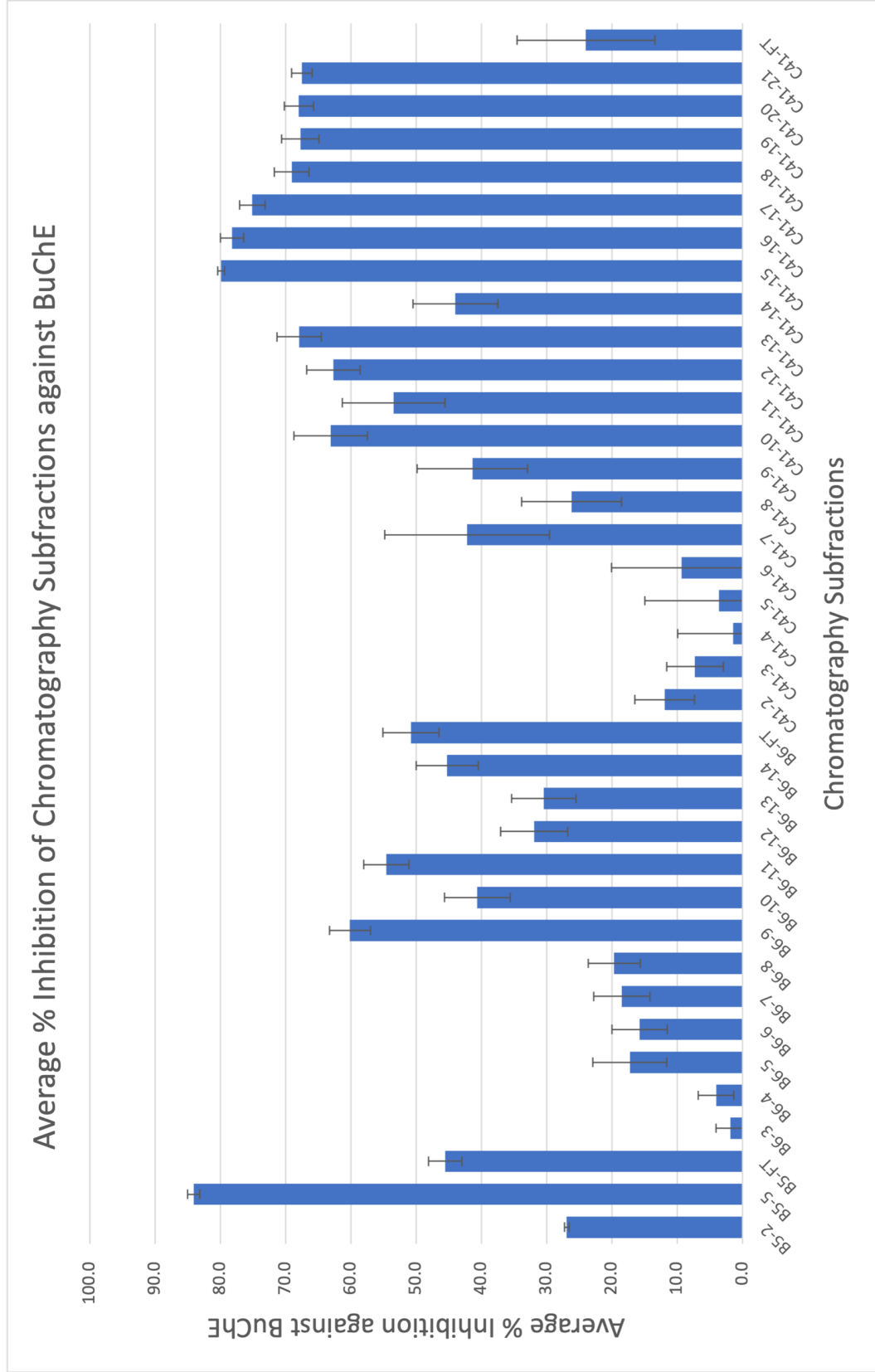


Figure 4.43: Inhibitory activity of Chromatography Subfractions (SF) against BuChE.^a
^aSamples B5-5, B5-FT, B6-10, B6-FT, C41-4, C41-15, C41-21 and C41-FT were tested at 50 µg/mL. Remaining samples were tested at 25 µg/mL.
 Fractions B5-5 and C41-15 contained ianthelline (4.7). Fractions B6-11 and C41-21 contained ningalamide B (4.9). Fractions C41-19 and C41-20
 contained aiolochroiamides C (4.5a) and D (4.5b), respectively. Inhibitory activities were measured in triplicates in 96-well plates according to the
 protocol reported by Ellman (see text reference 53).

General Procedure for DFT Calculations of the Chemical Shifts of 4.4a,b, 4.5a, and 4.5b.

The conformational search was carried out in Spartan Student V8¹ at the MMFF level, and the lowest energy conformers within 15 kJ.mol⁻¹ of the global minimum were optimized at the B3LYP/6-31G(d,p) level using Gaussian 16.²⁻³ Frequency calculations were performed at the B3LYP/6-31G(d,p) level to obtain the minimum energy conformers and computed Gibbs free energies. NMR shielding tensors were calculated at the APFD/aug-cc-pVDZ level (GIAO,⁴ scrf, MeOH) on the low energy conformers within 8 kJ.mol⁻¹ of the global minimum, and the ¹H and ¹³C chemical shifts (δ) were referenced to TMS and reported as Boltzmann-weighted averages.

1. Spartan Student V8, Wavefunction Inc., Irvine, California.
2. Gaussian 16, Revision B.01, M. J. Frisch, G. W. Trucks, H. B. Schlegel, G. E. Scuseria, M. A. Robb, J. R. Cheeseman, G. Scalmani, V. Barone, G. A. Petersson, H. Nakatsuji, X. Li, M. Caricato, A. V. Marenich, J. Bloino, B. G. Janesko, R. Gomperts, B. Mennucci, H. P. Hratchian, J. V. Ortiz, A. F. Izmaylov, J. L. Sonnenberg, D. Williams-Young, F. Ding, F. Lipparini, F. Egidi, J. Goings, B. Peng, A. Petrone, T. Henderson, D. Ranasinghe, V. G. Zakrzewski, J. Gao, N. Rega, G. Zheng, W. Liang, M. Hada, M. Ehara, K. Toyota, R. Fukuda, J. Hasegawa, M. Ishida, T. Nakajima, Y. Honda, O. Kitao, H. Nakai, T. Vreven, K. Throssell, J. A. Montgomery, Jr., J. E. Peralta, F. Ogliaro, M. J. Bearpark, J. J. Heyd, E. N. Brothers, K. N. Kudin, V. N. Staroverov, T. A. Keith, R. Kobayashi, J. Normand, K. Raghavachari, A. P. Rendell, J. C. Burant, S. S. Iyengar, J. Tomasi, M. Cossi, J. M. Millam, M. Klene, C. Adamo, R. Cammi, J. W. Ochterski, R. L. Martin, K. Morokuma, O. Farkas, J. B. Foresman, and D. J. Fox, Gaussian, Inc., Wallingford CT, 2016.
3. J. B. Foresman and Æ Frisch, *Exploring Chemistry with Electronic Structure Methods*, 3rd ed., Gaussian, Inc.: Wallingford, CT, 2015. ISBN: 978-1-935522-03-4
4. Willoughby, P. H.; Jansma, M. J.; Hoye, T. R. A guide to Small-Molecule Structure Assignment through Comutation of (¹H and ¹³C) NMR Chemical Shifts. *Nat. Prot.* 2014, 9, 643-660.

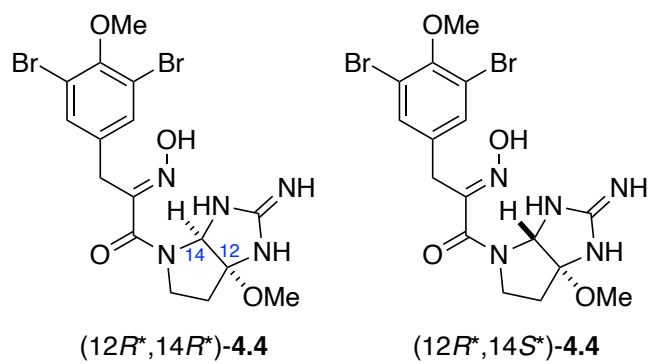


Figure 4.44: The structures of (12*R*^{*},14*R*^{*})- and (12*R*^{*},14*S*^{*})- 4.4.

Table 4.8: Calculated (GIAO) ^{13}C and ^1H Chemical Shifts of **4.4a,b** in MeOH.^a

Position	Experimental δ_{C}		Calculated δ_{C}		Experimental δ_{H}		Calculated δ_{H}	
	4.4a	4.4b	(12 <i>R</i> *,14 <i>R</i> *)- 4.4	(12 <i>R</i> *,14 <i>S</i> *)- 4.4	4.4a	4.4b	(12 <i>R</i> *,14 <i>R</i> *)- 4.4	(12 <i>R</i> *,14 <i>S</i> *)- 4.4
1	137.17	137.18	137.9	137.1	-	-	-	-
2/6	134.6	134.7	134.4	133.7	7.52	7.55	8.05	7.81
3/5	118.6	118.7	136.3	136.7	-	-	-	-
4	153.94	153.96	153.3	153.5	-	-	-	-
7	30.7	30.8	34.0	32.4	3.81	3.86	4.13	4.27
8	152.7	153.8	159.4	159.3	-	-	-	-
9	165.9	164.4	167.9	164.9	-	-	-	-
10	74.8	76.6	73.6	81.9	5.69	5.82	5.52	5.24
11	100.7	103.4	102.3	97.5	-	-	-	-
12	36.5	34.9	39.0	29.7	2.35, 2.28	2.34, 2.18	2.28, 2.27	2.41, 1.91
13	48.3	45.5	49.7	54.2	4.20, 3.60	4.32, 3.32	3.88, 3.75	4.22, 3.75
14	160.2	160.0	159.2	166.1	-	-	-	-
4-OMe	61.0	61.0	59.2	59.1	3.81	3.82	3.98	3.97
11-OMe	51.96	52.00	49.2	47.9	3.34	3.33	3.30	3.25
RMSD (4.4a) ^b	-	-	2.55	4.34	-	-	0.192	0.276
RMSD (4.4b) ^b	-	-	2.92	4.45	-	-	0.270	0.317

a. Geometry optimizations and single point energies of **4.4a,b** were calculated at the B3LYP/6-31G(d,p) level. The NMR shielding tensors of the conformers whose energies were less than 2 kJ/mole for (12*R**,14*R**)-**4.4** or 7 kJ/mole for (12*R**,14*S**)-**4.4** higher than the global minimum were calculated in MeOH (PCM model) at the APFD/aug-cc-pVDZ level, referenced to TMS and Boltzmann averaged. *B.* Brominated carbons (red) were excluded from RMSD calculations due to large deviations in calculated δ values because of poor fit due to spin-orbit coupling of the heavy Br substituent.

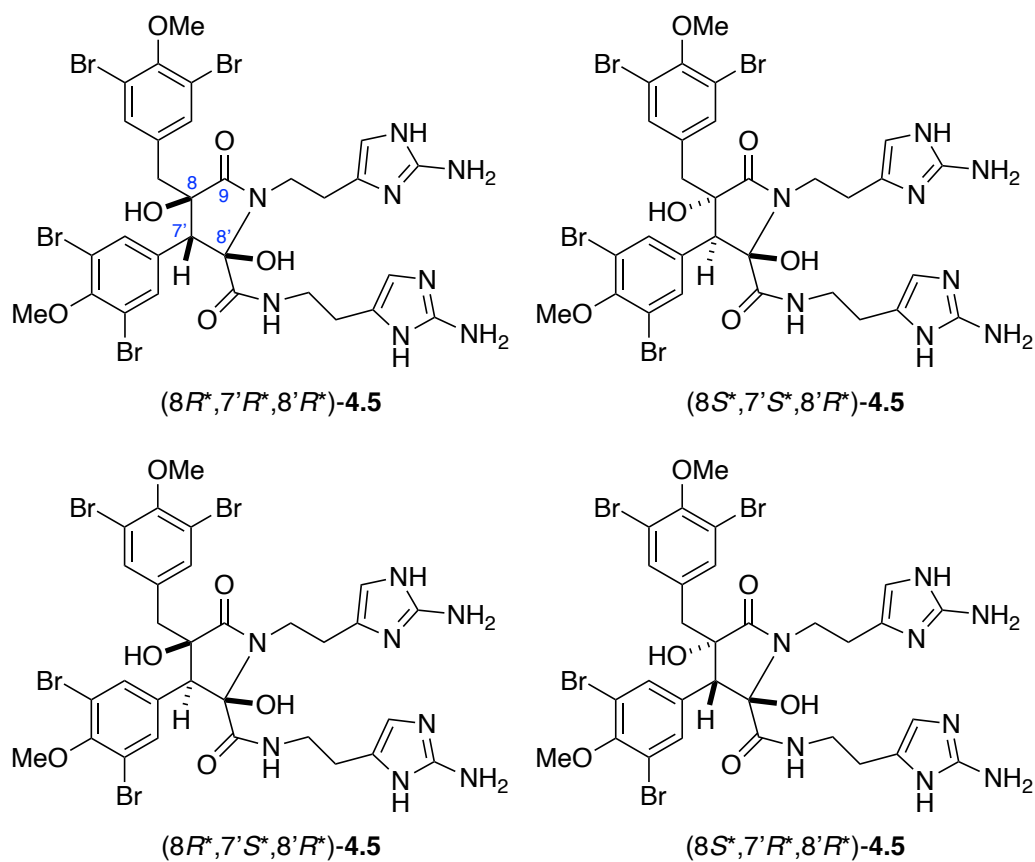


Figure 4.45: The structures of the four diastereoisomers of compound 4.5.

Table 4.9: Calculated ^{13}C Chemical Shifts of **4.5a** and **4.5b** in MeOH.^a

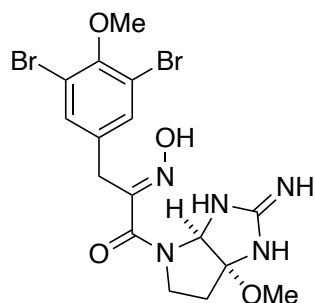
Position	Experimental δ		Calculated δ			
	4.5a	4.5b	(8 <i>R</i> *,7' <i>R</i> *,8' <i>R</i> *)- 4.5	(8 <i>S</i> *,7' <i>S</i> *,8' <i>R</i> *)- 4.5	(8 <i>R</i> *,7' <i>S</i> *,8' <i>R</i> *)- 4.5	(8 <i>S</i> *,7' <i>R</i> *,8' <i>R</i> *)- 4.5
1	136.1	135.6	137.45	138.36	137.04	136.85
2/6	135.8	135.4	134.70	135.21	136.54	135.65
3/5	118.1	117.8	135.57	135.38	135.36	136.49
4	153.9	153.7	153.61	153.50	153.58	153.91
7	41.6	40.9	39.64	42.85	39.91	42.95
8	77.9	78.6	83.47	83.92	86.16	82.33
9	177.4	175.9	182.41	179.04	183.37	178.48
10	40.5	38.9	47.03	45.61	48.99	38.16
11	24.7	23.9	28.14	24.67	26.29	26.98
12	125.72	125.2	126.75	129.52	126.18	127.13
13	111.1	110.4	123.72	122.81	124.19	124.32
14	148.6	148.5	149.12	147.77	147.21	149.79
4-OMe	61.0	60.6	58.94	58.87	59.19	59.08
1'	133.9	132.9	135.65	136.32	133.12	133.57
2'/6'	136.9	135.4	133.98	135.98	135.39	135.63
3'/5'	117.8	117.9	137.71	136.14	136.16	135.78
4'	154.1	154.2	155.72	154.68	154.81	154.00
7'	54.9	57.1	66.29	63.24	58.03	61.14
8'	92.5	92.4	96.35	93.47	96.49	92.41
9'	171.1	172.3	171.13	173.36	169.96	170.94
10'	39.2	39	41.05	45.65	45.56	41.85
11'	25.8	24.9	28.26	30.07	25.45	27.31
12'	125.75	125.2	124.22	138.12	122.99	124.44
13'	110.4	109.7	123.60	111.06	123.70	125.45
14'	148.7	148.4	152.22	149.40	149.19	149.97
4'-OMe	61.1	60.6	59.86	58.94	58.84	58.93
RMSD (5a) ^b	-	-	5.17	4.70	5.08	4.56
RMSD (5b) ^b	-	-	5.31	5.37	4.67	4.33

a. Geometry optimizations and single point energies of **5a** and **5b** were calculated at the B3LYP/6-31G(d,p) level. The NMR shielding tensors of the conformers whose energies were less than 9 kJ/mole higher than the global minimum were calculated in MeOH (PCM model) at the APFD/aug-cc-pVDZ level, referenced to TMS and Boltzmann averaged. *b.* Brominated carbons (red) were excluded from RMSD calculations due to large deviations in calculated δ values because of poor fit due to spin-orbit coupling of the heavy Br substituent.

Table 4.10: Calculated ^1H Chemical Shifts of **4.5a** and **4.5b** in MeOH.

Position	Experimental δ_{H}		Calculated δ_{H}			
	4.5a	4.5b	(8 <i>R</i> *,7' <i>R</i> *,8' <i>R</i> *)- 4.5	(8 <i>S</i> *,7' <i>S</i> *,8' <i>R</i> *)- 4.5	(8 <i>R</i> *,7' <i>S</i> *,8' <i>R</i> *)- 4.5	(8 <i>S</i> *,7' <i>R</i> *,8' <i>R</i> *)- 4.5
2/6	7.33	7.30	7.28	7.51	7.86	7.93
7	3.11, 2.77	3.16, 2.76	3.19, 2.45	3.45, 2.56	3.25, 2.69	3.43, 2.82
10	3.54, 3.41	3.53, 3.47	3.54, 2.64	3.41, 2.94	3.57, 2.83	3.85, 3.96
11	2.78, 2.74	2.72, 2.65	2.84, 2.83	3.16, 3.05	3.98, 2.93	2.83, 2.85
13	6.62	6.57	6.68	6.63	6.76	6.69
4-OMe	3.73	3.73	3.99	4.04	4.06	4.06
2'/6'	7.43	7.44	7.15	7.52	7.94	8.10
7'	3.52	3.26	2.90	3.43	2.47	3.45
10'	3.51, 3.27	3.35, 3.15	3.80, 2.77	3.65, 3.20	3.54, 3.30	3.77, 3.08
11'	2.60, 2.56	2.40, 2.30	3.12, 2.65	2.80, 2.79	3.17, 2.73	2.80, 2.47
13'	6.37	6.27	6.66	6.78	7.07	6.64
4'-OMe	3.80	3.79	4.22	4.06	4.04	4.01
RMSD (4.5a)	-	-	0.372	0.270	0.516	0.246
RMSD (4.5b)	-	-	0.405	0.339	0.543	0.282

Table 4.11: Cartesian Coordinates and Relative Energies of Optimized Conformers of **4.4a,b** ($\Delta E < 2$ kJ/mol).



(12*R*^{*},14*R*^{*})-4.4

Conf. 3

ΔG (298 K) = -6338.895328 Hartree

O	-4.19086	-0.28285	-1.28897
C	-3.24593	-0.07763	-0.32588
C	-1.20343	0.34652	1.59197
C	-2.61136	-1.14898	0.31811
C	-2.82218	1.21329	0.02071
C	-1.81826	1.43253	0.95832
C	-1.60539	-0.95174	1.25874
C	-5.54631	-0.34284	-0.80002
Br	-3.14781	-2.92958	-0.11859
Br	-3.65144	2.70942	-0.82991
C	-0.09765	0.57181	2.61113
C	1.26797	0.62424	1.96044
C	1.95660	-0.70629	1.74459
N	1.88971	1.69857	1.63120
O	1.15738	2.85102	1.89831
O	1.56641	-1.67930	2.40164
N	2.98156	-0.82912	0.85844
C	3.40891	0.12602	-0.16298
C	4.19807	-0.73742	-1.19716
C	4.68025	-1.94268	-0.36458
C	3.57390	-2.17074	0.66638
N	4.41998	1.07919	0.25489
C	5.43588	1.18720	-0.69003
N	5.22689	0.18482	-1.63652
N	6.42128	2.00745	-0.74760
O	3.41958	-1.26337	-2.24527
C	2.82767	-0.32843	-3.14901
H	2.53463	0.61939	-0.59208
H	-1.50981	2.44435	1.19372
H	-1.12834	-1.80358	1.72910
H	-5.82400	0.60047	-0.32025

H	-6.17461	-0.50826	-1.67568
H	-5.66545	-1.17421	-0.09878
H	-0.26761	1.50609	3.14746
H	-0.08422	-0.25201	3.32594
H	1.75957	3.56324	1.63496
H	5.61660	-1.67833	0.13296
H	4.85189	-2.81400	-0.99864
H	3.94579	-2.55893	1.61679
H	2.80381	-2.85968	0.30352
H	4.09854	1.90729	0.73860
H	6.05290	-0.18614	-2.08899
H	6.37911	2.65157	0.04310
H	3.57516	0.35312	-3.56509
H	2.38731	-0.92436	-3.95005
H	2.03396	0.25992	-2.67212

Conf. 8

ΔG (298 K) = -6338.895218 Hartree

O	-4.35150	-0.32249	-1.03302
C	-3.30509	-0.09205	-0.18771
C	-1.22412	0.39338	1.67353
C	-2.64483	-1.14303	0.46406
C	-2.88311	1.20990	0.11731
C	-1.86229	1.45920	1.02885
C	-1.62185	-0.91559	1.37921
C	-3.98228	-0.48908	-2.41706
Br	-3.18100	-2.93713	0.08667
Br	-3.74984	2.67962	-0.74183
C	-0.10098	0.65142	2.66561
C	1.25167	0.69170	1.98756
C	1.94689	-0.64005	1.80281
N	1.85940	1.75870	1.61155
O	1.12400	2.91431	1.85552
O	1.58273	-1.59173	2.50439
N	2.95023	-0.78568	0.89560
C	3.33637	0.13379	-0.17380
C	4.10138	-0.76121	-1.19908
C	4.62187	-1.92916	-0.33688
C	3.55021	-2.12816	0.73590
N	4.35058	1.11061	0.17572
C	5.33555	1.19155	-0.80389
N	5.10629	0.15288	-1.70581
N	6.31134	2.01664	-0.92269
O	3.29563	-1.33415	-2.20095

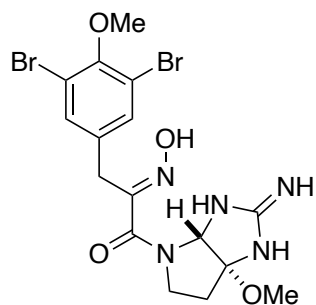
Table 4.11: Cartesian Coordinates and Relative Energies of Optimized Conformers of **4.4a,b** ($\Delta E < 2$ kJ/mol) Continued.

				C	5.56863	0.30295	0.11920
Conf. 8				C	5.35740	1.81434	-0.10735
ΔG (298 K) = -6338.895218 Hartree				C	3.97472	2.10817	0.47725
C	2.66577	-0.44028	-3.12040	N	4.10279	-0.69725	-1.39804
H	2.44426	0.60297	-0.59324	C	5.38893	-0.87491	-1.89851
H	-1.55982	2.47889	1.23628	N	6.27600	-0.40439	-0.93040
H	-1.12972	-1.75235	1.86107	N	5.77519	-1.35288	-3.02515
H	-3.32028	-1.35190	-2.53705	O	6.15449	0.16861	1.39161
H	-4.91316	-0.66268	-2.95765	C	6.42676	-1.15834	1.84594
H	-3.49876	0.41575	-2.79734	H	3.94312	-1.12289	0.67077
H	-0.26542	1.59938	3.17920	H	-2.02819	-2.41878	1.09785
H	-0.06992	-0.15231	3.40241	H	-0.95207	1.72393	0.73926
H	1.71628	3.62172	1.55882	H	-6.33322	-0.04478	0.74979
H	5.57019	-1.63702	0.12083	H	-5.88693	1.68764	0.59757
H	4.78319	-2.82243	-0.94248	H	-6.98647	0.93601	-0.59210
H	3.95518	-2.47670	1.68816	H	0.15161	0.03521	2.49094
H	2.77649	-2.83736	0.42321	H	0.00247	-1.67804	2.05754
H	4.03724	1.95285	0.63993	H	1.01869	-3.05181	-0.87104
H	5.92152	-0.22816	-2.16938	H	5.36849	2.01708	-1.18105
H	6.28847	2.68923	-0.15525	H	6.14821	2.39599	0.36903
H	3.39257	0.23132	-3.58627	H	3.44505	2.90324	-0.05166
H	2.20635	-1.07074	-3.88342	H	4.02153	2.38543	1.53560
H	1.88161	0.15899	-2.64122	H	3.36307	-1.32711	-1.67955
				H	7.15046	-0.02365	-1.26971
Conf. 10				H	4.96373	-1.63390	-3.57682
ΔG (298 K) = -6338.894781 Hartree				H	7.02348	-1.71531	1.11790
O	-5.03564	0.41256	-0.82873	H	6.98937	-1.04708	2.77427
C	-3.85088	0.16315	-0.19793	H	5.50743	-1.71843	2.05736
C	-1.34000	-0.37673	1.00110				
C	-2.90346	1.17615	0.01084	Conf. 2			
C	-3.49821	-1.12828	0.21501	ΔG (298 K) = -6338.894683 Hartree			
C	-2.26623	-1.40408	0.80147	O	-5.14023	0.49671	-0.47798
C	-1.66848	0.92308	0.59617	C	-3.89238	0.20852	-0.00518
C	-6.12129	0.76957	0.05039	C	-1.34628	-0.36826	1.09837
Br	-3.33245	2.95718	-0.53468	C	-2.92964	1.21083	0.18415
Br	-4.74818	-2.54962	-0.04730	C	-3.53423	-1.09256	0.37110
C	0.00244	-0.65924	1.66232	C	-2.28614	-1.38594	0.91336
C	1.17953	-0.52074	0.71927	C	-1.67840	0.94012	0.72534
C	1.96549	0.76708	0.78487	C	-5.27317	0.41840	-1.91156
N	1.50676	-1.39006	-0.16883	Br	-3.36609	3.00494	-0.31054
O	0.66218	-2.49241	-0.16450	Br	-4.80537	-2.49954	0.13405
O	1.40521	1.76859	1.24972	C	0.01323	-0.66956	1.71496
N	3.24757	0.82766	0.33793	C	1.16381	-0.52138	0.74115
C	4.12867	-0.28678	-0.00669	C	1.96047	0.75980	0.80696

Table 4.11: Cartesian Coordinates and Relative Energies of Optimized Conformers of **4.4a,b** ($\Delta E < 2$ kJ/mol) Continued.

Conf. 2				C	-2.28610	-1.38599	0.91323
ΔG (298 K) = -6338.894683 Hartree				C	-1.67837	0.94007	0.72520
N	1.45990	-1.37613	-0.17167	C	-5.27344	0.41842	-1.91134
O	0.60743	-2.47256	-0.16418	Br	-3.36615	3.00492	-0.31048
O	1.41792	1.75906	1.29687	Br	-4.80543	-2.49955	0.13415
N	3.23305	0.81645	0.33331	C	0.01334	-0.66967	1.71462
C	4.09798	-0.30108	-0.04094	C	1.16392	-0.52131	0.74083
C	5.54507	0.27480	0.06588	C	1.96057	0.75986	0.80683
C	5.34286	1.79056	-0.13876	N	1.45996	-1.37584	-0.17221
C	3.97372	2.08896	0.47470	O	0.60745	-2.47224	-0.16496
N	4.04342	-0.69406	-1.43650	O	1.41787	1.75911	1.29660
C	5.31873	-0.87670	-1.96225	N	3.23325	0.81650	0.33348
N	6.22719	-0.42580	-1.00473	C	4.09808	-0.30105	-0.04093
N	5.68060	-1.34391	-3.10143	C	5.54521	0.27467	0.06611
O	6.15240	0.12023	1.32580	C	5.34320	1.79050	-0.13828
C	6.42151	-1.21431	1.75930	C	3.97394	2.08898	0.47492
H	3.91741	-1.14386	0.62960	N	4.04354	-0.69375	-1.43658
H	-2.04675	-2.40644	1.18793	C	5.31887	-0.87647	-1.96227
H	-0.95271	1.73409	0.85970	N	6.22734	-0.42585	-1.00459
H	-4.60747	1.13680	-2.39932	N	5.68077	-1.34354	-3.10151
H	-5.05905	-0.59558	-2.26259	O	6.15251	0.11982	1.32598
H	-6.31072	0.67146	-2.13178	C	6.42072	-1.21486	1.75961
H	0.19043	0.00924	2.55099	H	3.91737	-1.14394	0.62942
H	0.01858	-1.69510	2.09238	H	-2.04669	-2.40650	1.18775
H	0.94050	-3.02135	-0.89020	H	-0.95265	1.73403	0.85949
H	5.33605	2.00617	-1.20998	H	-4.60781	1.13684	-2.39916
H	6.14724	2.35973	0.32992	H	-5.05934	-0.59554	-2.26243
H	3.44146	2.89499	-0.03467	H	-6.31103	0.67147	-2.13143
H	4.04229	2.35267	1.53533	H	0.19056	0.00895	2.55080
H	3.29267	-1.31316	-1.71271	H	0.01874	-1.69529	2.09183
H	7.09865	-0.04839	-1.35531	H	0.94052	-3.02089	-0.89109
H	4.85710	-1.61145	-3.64179	H	5.33670	2.00635	-1.20946
H	7.00204	-1.76675	1.01491	H	6.14755	2.35943	0.33072
H	6.99981	-1.11888	2.67971	H	3.44181	2.89499	-0.03462
H	5.50135	-1.76997	1.97865	H	4.04231	2.35279	1.53554
Conf. 1				H	3.29282	-1.31289	-1.71283
ΔG (298 K) = -6338.894681 Hartree				H	7.09880	-0.04837	-1.35509
O	-5.14033	0.49669	-0.47777	H	4.85726	-1.61088	-3.64196
C	-3.89242	0.20849	-0.00511	H	6.99949	-1.76825	1.01456
C	-1.34621	-0.36831	1.09816	H	7.00053	-1.11976	2.67910
C	-2.92966	1.21080	0.18414	H	5.50021	-1.76930	1.98059
C	-3.53424	-1.09259	0.37111				

Table 4.11: Cartesian Coordinates and Relative Energies of Optimized Conformers of **4.4a,b** ($\Delta E < 2$ kJ/mol) Continued.



(12*R*^{*},14*S*^{*})-4.4

Conf. 14

ΔG (298 K) = -6338.860225 Hartree

O	3.83696	-0.49662	1.34290
C	2.96670	-0.24853	0.32130
C	1.07490	0.27362	-1.72220
C	2.67358	1.05984	-0.08956
C	2.28010	-1.28641	-0.32390
C	1.34727	-1.04040	-1.32661
C	1.74397	1.32726	-1.08901
C	5.20730	-0.68391	0.93464
Br	2.64045	-3.08805	0.19786
Br	3.58022	2.51185	0.75797
C	0.04684	0.55295	-2.80639
C	-1.33555	0.75940	-2.22929
C	-2.17379	-0.47870	-2.00473
N	-1.89785	1.89053	-2.00582
O	-1.07363	2.97537	-2.30609
O	-1.96229	-1.47157	-2.71376
N	-3.13985	-0.47963	-1.05972
C	-3.59076	0.52199	-0.10182
C	-4.19593	-0.36810	0.99264
C	-5.10396	-1.25974	0.14938
C	-4.11587	-1.61175	-1.00614
N	-2.76456	1.39085	0.70757
C	-3.53416	1.63602	1.87001
N	-4.57735	0.67622	1.91201
N	-3.28432	2.60060	2.66882
O	-3.13531	-1.18187	1.51850
C	-3.47887	-1.96349	2.65620
H	-4.40226	1.09619	-0.57265
H	0.82910	-1.86782	-1.79766
H	1.53515	2.35210	-1.37303
H	5.29468	-1.54524	0.26562

H	5.58889	0.21695	0.44480
H	5.77058	-0.87093	1.84933
H	0.32984	1.44055	-3.37362
H	-0.01288	-0.29869	-3.48623
H	-1.64664	3.73961	-2.14272
H	-5.97024	-0.70381	-0.21632
H	-5.45697	-2.15755	0.65780
H	-4.61946	-1.71326	-1.97051
H	-3.57443	-2.53689	-0.80178
H	-2.42012	2.23108	0.25985
H	-4.93726	0.43699	2.82793
H	-3.94340	2.59835	3.44791
H	-4.31525	-2.64703	2.46234
H	-2.59432	-2.55484	2.89926
H	-3.72750	-1.34134	3.52604

Conf. 1

ΔG (298 K) = -6338.858457 Hartree

O	-3.52275	-0.93510	-1.05319
C	-2.67545	-0.41516	-0.11851
C	-0.81979	0.68095	1.72228
C	-2.61924	0.96278	0.13309
C	-1.77503	-1.22685	0.58610
C	-0.86544	-0.70041	1.49689
C	-1.70524	1.51167	1.02795
C	-4.80823	-1.34219	-0.54171
Br	-1.78214	-3.10747	0.25594
Br	-3.82687	2.11379	-0.79613
C	0.21174	1.26959	2.67129
C	1.56575	1.37960	2.00464
C	2.41749	0.13113	1.99160
N	2.09709	2.44527	1.52852
O	1.26569	3.56179	1.63918
O	2.33808	-0.64827	2.95121
N	3.24573	-0.10195	0.95243
C	3.45156	0.54657	-0.33582
C	3.65873	-0.68831	-1.24464
C	4.76938	-1.38364	-0.45839
C	4.18689	-1.26547	0.98760
N	2.50042	1.30296	-1.11357
C	2.91329	1.12735	-2.45766
N	3.76616	0.00177	-2.50350
N	2.54592	1.91396	-3.39475
O	2.61865	-1.66382	-1.20492

Table 4.11: Cartesian Coordinates and Relative Energies of Optimized Conformers of **4.4a,b** ($\Delta E < 2$ kJ/mol) Continued.

Conf. 1				C	-3.18011	-0.75074	1.32084
ΔG (298 K) = -6338.858457 Hartree				C	-4.47425	-1.27774	0.70696
C	1.30417	-1.36734	-1.68273	C	-4.31693	-0.73557	-0.75257
H	4.40521	1.09269	-0.27018	N	-1.99164	1.20225	1.39637
H	-0.18308	-1.35959	2.02135	C	-2.00588	0.64896	2.69860
H	-1.67953	2.58441	1.18085	N	-2.92860	-0.42688	2.70334
H	-4.69161	-2.12881	0.20980	N	-1.30205	1.12276	3.65288
H	-5.34043	-0.48649	-0.11552	O	-2.07404	-1.43390	0.71593
H	-5.36246	-1.73054	-1.39663	C	-1.81478	-2.74841	1.19408
H	-0.10392	2.25613	3.01058	H	-4.07422	1.19762	1.10905
H	0.33332	0.61756	3.53934	H	1.68589	2.72926	-0.85975
H	1.82147	4.28143	1.30460	H	-0.12817	-0.90210	-2.28291
H	5.71647	-0.85015	-0.55842	H	3.05523	-0.75210	2.36616
H	4.90709	-2.42570	-0.74820	H	2.34456	-2.28069	1.74663
H	4.96345	-1.09038	1.73699	H	4.09088	-2.18398	2.10667
H	3.62619	-2.15632	1.27160	H	-0.00360	2.82737	-2.61907
H	2.35399	2.26961	-0.84932	H	-0.61803	1.33840	-3.36613
H	3.79504	-0.52726	-3.36692	H	-1.62407	4.67441	-0.44842
H	2.93969	1.61246	-4.28662	H	-5.34620	-0.84839	1.20534
H	1.30741	-1.08940	-2.74281	H	-4.56911	-2.36414	0.71805
H	0.73321	-2.29015	-1.56109	H	-5.27066	-0.40297	-1.17041
H	0.82569	-0.57324	-1.10688	H	-3.88745	-1.48152	-1.42189
Conf. 5				H	-1.85248	2.20462	1.37195
ΔG (298 K) = -6338.858448 Hartree				H	-2.75854	-1.16761	3.37280
O	3.54999	-1.23782	0.39014	H	-1.44187	0.57761	4.50407
C	2.58351	-0.50889	-0.24011	H	-2.65019	-3.43646	1.01162
C	0.66394	1.01018	-1.66839	H	-0.94020	-3.09420	0.64075
C	1.57545	-1.12424	-0.99560	H	-1.57681	-2.76018	2.26618
C	2.59137	0.89258	-0.21433	Conf. 15			
C	1.65110	1.64710	-0.90955	ΔG (298 K) = -6338.858318 Hartree			
C	0.63247	-0.38918	-1.70561	O	3.38221	-1.00007	0.86190
C	3.22538	-1.63212	1.73877	C	2.51295	-0.41245	-0.01074
Br	3.93949	1.78294	0.80400	C	0.62117	0.81071	-1.73024
Br	1.50924	-3.03274	-1.05128	C	1.61400	-1.17272	-0.77160
C	-0.37970	1.82432	-2.41703	C	2.43471	0.98129	-0.14126
C	-1.66947	1.92360	-1.63346	C	1.50489	1.59133	-0.97770
C	-2.62284	0.75747	-1.74543	C	0.68342	-0.58341	-1.62047
N	-2.07504	2.92948	-0.94907	C	4.66874	-1.33033	0.30030
O	-1.15622	3.98309	-0.94012	Br	3.63697	2.06584	0.87161
O	-2.72354	0.17481	-2.83255	Br	1.66653	-3.07665	-0.62152
N	-3.36402	0.41417	-0.66835	C	-0.42319	1.46769	-2.61854
C	-3.17267	0.67705	0.75458	C	-1.74882	1.59140	-1.90084
				C	-2.61132	0.35234	-1.85829

Table 4.11: Cartesian Coordinates and Relative Energies of Optimized Conformers of **4.4a,b** ($\Delta E < 2$ kJ/mol) Continued.

Conf. 15				C	2.31674	-1.73366	-0.27414
ΔG (298 K) = -6338.858318 Hartree				C	0.56113	-0.18411	-0.84592
N	-2.25137	2.65598	-1.39258	C	4.33363	2.25183	-0.71605
O	-1.40998	3.76584	-1.51953	Br	4.91676	-1.00751	0.67556
O	-2.63317	-0.39008	-2.84833	Br	0.76520	2.66450	-0.66961
N	-3.35759	0.11252	-0.75754	C	0.13805	-2.67689	-1.13366
C	-3.25098	0.60984	0.61068	C	-1.30271	-2.54819	-0.70167
C	-3.17996	-0.70768	1.39713	C	-1.56958	-2.22492	0.74951
C	-4.40145	-1.42710	0.83165	N	-2.33878	-2.81405	-1.41024
C	-4.21842	-1.10865	-0.68940	O	-2.02876	-3.22019	-2.71009
N	-2.14287	1.32249	1.20090	O	-0.84746	-2.73461	1.61344
C	-2.17913	0.98095	2.57394	N	-2.60072	-1.40957	1.05452
N	-3.01812	-0.15191	2.71754	C	-3.48477	-0.59683	0.23104
N	-1.56025	1.65448	3.46483	C	-3.58515	0.67873	1.07839
O	-2.00128	-1.38849	0.94648	C	-3.95681	0.07505	2.43111
C	-1.65598	-2.57310	1.65418	C	-2.94516	-1.11633	2.47728
H	-4.20386	1.10585	0.84676	N	-3.19465	-0.02566	-1.06562
H	1.46448	2.67273	-1.04027	C	-3.98606	1.15065	-1.12367
H	0.00013	-1.20513	-2.18739	N	-4.42491	1.44617	0.19034
H	4.55809	-2.04602	-0.51990	N	-4.23737	1.75146	-2.22123
H	5.17820	-0.42783	-0.05048	O	-2.26340	1.22619	1.16689
H	5.24196	-1.78458	1.10899	C	-2.15738	2.47595	1.83802
H	-0.08864	2.45663	-2.93170	H	-4.46983	-1.08619	0.22184
H	-0.59448	0.85414	-3.50627	H	2.68861	-2.74681	-0.17017
H	-1.94488	4.48573	-1.15328	H	-0.45078	0.02791	-1.17527
H	-5.32547	-0.99801	1.22539	H	5.02083	1.49138	-1.09901
H	-4.41378	-2.50258	1.01262	H	3.71493	2.64647	-1.52763
H	-5.17405	-0.92284	-1.18647	H	4.90161	3.06311	-0.25972
H	-3.70520	-1.91330	-1.21676	H	0.16114	-2.80615	-2.21862
H	-2.07894	2.31697	1.02246	H	0.54201	-3.59476	-0.69387
H	-2.82928	-0.76115	3.50416	H	-2.90086	-3.38171	-3.09968
H	-1.69970	1.23945	4.38657	H	-4.99116	-0.27588	2.43101
H	-2.43339	-3.34526	1.58866	H	-3.81928	0.74658	3.27913
H	-0.74490	-2.94374	1.18141	H	-3.37440	-2.00244	2.95200
H	-1.44351	-2.37578	2.71329	H	-2.02894	-0.85168	3.00750
Conf. 13				H	-3.30872	-0.63252	-1.86846
ΔG (298 K) = -6338.858159 Hartree				H	-4.62161	2.41857	0.39391
O	3.50709	1.70638	0.33196	H	-4.80995	2.57908	-2.05186
C	2.71282	0.66501	-0.05347	H	-2.40519	2.40398	2.90448
C	1.01467	-1.50420	-0.73071	H	-1.11673	2.78371	1.72974
C	1.40393	0.87109	-0.51045	H	-2.79151	3.24724	1.38082
C	3.14441	-0.66404	0.05160				

Table 4.11: Cartesian Coordinates and Relative Energies of Optimized Conformers of **4.4a,b** ($\Delta E < 2$ kJ/mol) Continued.

Conf. 4				H	-3.86865	0.98276	-3.20950
ΔG (298 K) = -6338.857858 Hartree				H	-2.78786	-0.81876	-4.53182
O	3.71593	1.25235	-0.57650	H	-1.43344	1.62683	-2.41938
C	2.77269	0.54224	0.10759	H	-1.01222	2.65831	-1.03158
C	0.89381	-0.92680	1.63987	H	-0.91120	0.88924	-0.88401
C	1.75763	1.18234	0.83334	Conf. 10			
C	2.81071	-0.85762	0.16894	ΔG (298 K) = -6338.857694 Hartree			
C	1.88841	-1.58818	0.91293	O	-3.57284	1.46844	-0.75361
C	0.83836	0.47201	1.59788	C	-2.77238	0.60208	-0.06791
C	3.38355	1.53198	-1.95172	C	-1.02937	-1.21752	1.23434
Br	4.17291	-1.78147	-0.79961	C	-3.03610	-0.77389	-0.03970
Br	1.63485	3.08635	0.75728	C	-1.60913	1.03801	0.58250
C	-0.13679	-1.71054	2.43656	C	-0.75297	0.15511	1.23122
C	-1.46132	-1.77630	1.70839	C	-2.18141	-1.67548	0.58906
C	-2.41931	-0.62828	1.92994	C	-4.63429	2.05421	0.02759
N	-1.88683	-2.75293	0.99394	Br	-1.17642	2.89650	0.54894
O	-0.96270	-3.79470	0.89777	Br	-4.60523	-1.42443	-0.91139
O	-2.41744	-0.06051	3.03083	C	-0.09039	-2.18827	1.92984
N	-3.25743	-0.25673	0.93984	C	1.34400	-2.00892	1.49101
C	-3.39854	-0.64639	-0.45657	C	1.65203	-2.30830	0.04158
C	-3.74318	0.71826	-1.09793	N	2.34871	-1.73885	2.24154
C	-4.91779	1.11582	-0.20493	O	2.00804	-1.57288	3.58451
C	-4.31375	0.77281	1.19545	O	1.02281	-3.21432	-0.51667
N	-2.37326	-1.11981	-1.35461	N	2.59687	-1.58930	-0.60492
C	-2.80803	-0.71848	-2.64185	C	3.50126	-0.53354	-0.17328
N	-3.78075	0.29283	-2.47290	C	3.75789	0.19224	-1.51268
N	-2.35920	-1.25105	-3.71282	C	4.18496	-1.00628	-2.35996
O	-2.81640	1.77286	-0.84437	C	3.07119	-2.02564	-1.95715
C	-1.47262	1.71355	-1.32760	N	3.20665	0.58513	0.69269
H	-4.28619	-1.29411	-0.52175	C	4.10987	1.59832	0.28154
H	1.94351	-2.67047	0.92507	N	4.58193	1.25976	-1.00660
H	0.07605	1.00387	2.15594	N	4.40426	2.59523	1.02429
H	3.24850	0.60189	-2.51173	O	2.60343	0.64689	-2.21591
H	2.47995	2.14579	-2.01060	C	1.73148	1.63451	-1.66413
H	4.23026	2.08573	-2.35837	H	4.43980	-1.01354	0.14361
H	0.22090	-2.72341	2.62319	H	0.13783	0.53693	1.71722
H	-0.32118	-1.21749	3.39372	H	-2.41407	-2.73406	0.57184
H	-1.44472	-4.46902	0.39593	H	-5.30736	1.27808	0.40406
H	-5.80158	0.51343	-0.42359	H	-4.22416	2.63595	0.85855
H	-5.17099	2.17360	-0.28103	H	-5.17700	2.71398	-0.64990
H	-5.06090	0.37183	1.88555	H	-0.14827	-2.06498	3.01296
H	-3.84691	1.64294	1.65770	H	-0.38661	-3.21245	1.68876
H	-2.12068	-2.09841	-1.28943	H	2.86465	-1.41298	4.00792

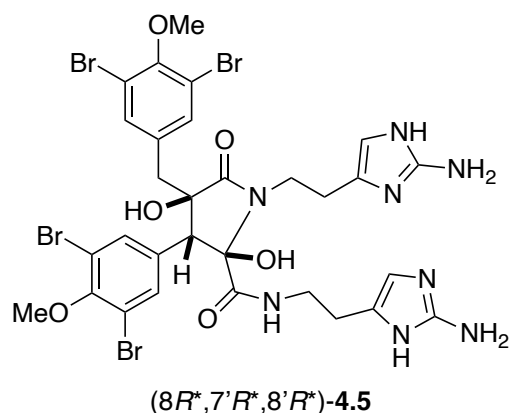
Table 4.11: Cartesian Coordinates and Relative Energies of Optimized Conformers of **4.4a,b** ($\Delta E < 2$ kJ/mol) Continued.

Conf. 10

ΔG (298 K) = -6338.857694 Hartree

H	5.17765	-1.35875	-2.07340
H	4.16793	-0.79832	-3.43011
H	3.44194	-3.05247	-1.90312
H	2.23157	-1.99774	-2.65275
H	3.22871	0.40343	1.68906
H	4.84660	2.02114	-1.62037
H	5.06172	3.21243	0.54649
H	2.27228	2.52362	-1.32331
H	1.06919	1.92562	-2.48266
H	1.13516	1.24309	-0.83781

Table 4.12: Cartesian Coordinates and Relative Energies of Optimized Conformers of **4.5a** and **4.5b** ($\Delta E < 8$ kJ/mol).



Conf. 21

ΔG (298 K) = -12338.188062 Hartree

O	6.29434	-1.73351	0.68069
C	5.09331	-1.74931	0.03524
C	2.52238	-1.73582	-1.17311
C	4.28301	-2.89491	0.01606
C	4.58245	-0.60207	-0.58472
C	3.32902	-0.59243	-1.18803
C	3.02011	-2.89796	-0.56744
C	7.42029	-2.09775	-0.13251
Br	5.62096	1.00104	-0.56178
Br	4.93899	-4.49019	0.83215
C	1.13863	-1.69329	-1.78885
C	-0.01665	-1.85149	-0.78968
C	-1.39526	-1.60160	-1.45091
N	-2.24810	-1.08618	-0.48080
O	-1.71003	-1.84506	-2.59998
C	-0.07954	-0.90429	0.44742
C	-1.60906	-1.04235	0.82128
O	0.00845	-3.21222	-0.36155
C	-3.70339	-1.15889	-0.68646
C	-4.29299	-2.57733	-0.49594
C	-5.75115	-2.65532	-0.81940
C	-6.42956	-3.26426	-1.84659
N	-7.79638	-3.07937	-1.72992
N	-6.74560	-2.06794	-0.03928
C	-7.93158	-2.35194	-0.64342
N	-9.14612	-1.81954	-0.15611
O	-1.79839	-2.27258	1.50704
C	-2.15314	0.05053	1.78683
N	-2.38542	1.28341	1.30460

O	-2.33655	-0.27735	2.96392
C	-2.84500	2.38889	2.14134
C	-4.13583	3.04318	1.62404
C	0.43938	0.50133	0.21047
C	1.58988	3.06903	-0.22178
C	1.41860	1.00762	1.07257
C	0.02596	1.30278	-0.86567
C	0.58714	2.56230	-1.06182
C	1.98885	2.25771	0.85083
O	2.12428	4.30656	-0.40015
C	3.23125	4.36147	-1.32099
Br	3.37154	2.86666	2.00087
Br	-0.02399	3.63043	-2.51911
C	-5.29024	2.09509	1.53676
C	-5.53167	0.86190	2.07339
N	-6.39522	2.33844	0.71168
N	-6.72490	0.33159	1.59953
C	-7.22260	1.25100	0.78781
N	-8.42851	1.17925	0.12556
H	0.49045	-1.34682	1.26634
H	2.97303	0.31918	-1.65356
H	2.41275	-3.79330	-0.53906
H	7.31360	-3.12176	-0.50548
H	8.29327	-2.03574	0.51861
H	7.53653	-1.39958	-0.96849
H	1.01505	-0.76319	-2.34686
H	1.00503	-2.50614	-2.50985
H	-0.59616	-3.30049	0.39664
H	-3.88495	-0.83304	-1.71348
H	-4.18059	-0.44299	-0.01251
H	-4.09422	-2.91096	0.52813
H	-3.76020	-3.26089	-1.16371
H	-6.00890	-3.84340	-2.65743
H	-6.64226	-1.38522	0.72207
H	-9.33826	-2.11913	0.79740
H	-9.89681	-2.14784	-0.75689
H	-1.98621	-2.01308	2.43537
H	-2.17054	1.46332	0.33412
H	-2.98904	1.97943	3.14217
H	-2.05723	3.14816	2.20260
H	-3.94407	3.48022	0.63288
H	-4.35452	3.89448	2.28519
H	1.77030	0.41112	1.90660
H	-0.71757	0.95224	-1.57240

Table 4.12: Cartesian Coordinates and Relative Energies of Optimized Conformers of **4.5a** and **4.5b** ($\Delta E < 8$ kJ/mol) Continued.

Conf. 21				C	-4.03596	2.39006	2.85043
ΔG (298 K) = -12338.188062 Hartree				C	0.42634	0.55180	0.13335
H	3.97580	3.59584	-1.08286	C	1.62904	3.08657	-0.33671
H	3.66856	5.35351	-1.20364	C	1.39660	1.06163	1.00346
H	2.87820	4.23238	-2.34930	C	0.04414	1.33497	-0.96625
H	-4.90453	0.30051	2.75132	C	0.63275	2.57763	-1.18316
H	-6.59821	3.20175	0.23160	C	1.99247	2.29613	0.76330
H	-8.43160	1.61390	-0.78892	O	2.19070	4.30909	-0.53688
H	-8.80065	0.22441	0.08206	C	3.31845	4.31606	-1.43310
Conf. 8				Br	3.36362	2.90960	1.92575
ΔG (298 K) = -12338.188008 Hartree				Br	0.07036	3.62036	-2.67824
O	6.21885	-1.80483	0.78081	C	-5.22199	1.62871	2.36525
C	5.03087	-1.81210	0.11149	C	-5.55598	0.31340	2.51037
C	2.48577	-1.77712	-1.14893	N	-6.19386	2.14111	1.49220
C	4.19978	-2.94280	0.09996	N	-6.68379	-0.00769	1.76925
C	4.55426	-0.66893	-0.54249	C	-7.05108	1.11894	1.17952
C	3.31348	-0.64908	-1.17113	N	-8.17252	1.29110	0.39780
C	2.94895	-2.93500	-0.50897	H	0.42303	-1.26852	1.23547
C	7.35385	-2.20648	-0.00158	H	2.98368	0.25890	-1.66227
Br	5.62185	0.91487	-0.53223	H	2.32459	-3.81843	-0.47417
Br	4.80927	-4.53214	0.96254	H	7.23575	-3.23609	-0.35524
C	1.11536	-1.72294	-1.79281	H	8.21466	-2.14647	0.66573
C	-0.06031	-1.82206	-0.81119	H	7.49975	-1.52847	-0.84941
C	-1.42126	-1.56364	-1.50210	H	1.02267	-0.80719	-2.38005
N	-2.28442	-1.02156	-0.55426	H	0.97718	-2.55410	-2.49174
O	-1.72357	-1.82352	-2.65055	H	-0.69940	-3.21257	0.41370
C	-0.12195	-0.83873	0.39299	H	-3.91806	-0.67040	-1.77808
C	-1.66011	-0.92045	0.74694	H	-4.22728	-0.44662	-0.04815
O	-0.08088	-3.16890	-0.33715	H	-4.16449	-2.93598	0.26515
C	-3.73723	-1.08789	-0.78401	H	-3.77965	-3.14246	-1.44495
C	-4.32743	-2.51747	-0.73437	H	-5.99799	-3.42453	-3.11499
C	-5.77450	-2.52978	-1.11218	H	-6.67401	-1.45945	0.56998
C	-6.42896	-2.94457	-2.24683	H	-9.41178	-1.98074	0.39203
N	-7.78732	-2.68943	-2.16710	H	-9.87424	-1.73448	-1.17407
N	-6.77351	-1.99376	-0.30461	H	-1.89695	-1.81180	2.43214
C	-7.93878	-2.11223	-0.99515	H	-2.54994	1.40814	0.05502
N	-9.13952	-1.56075	-0.49422	H	-2.03158	2.99822	2.30047
O	-1.90971	-2.10584	1.49853	H	-3.22791	3.32159	1.04342
C	-2.11895	0.25225	1.65087	H	-4.31333	3.38606	3.22136
N	-2.54943	1.38130	1.06343	H	-3.61387	1.84112	3.69357
O	-2.03299	0.08757	2.87125	H	1.72041	0.47974	1.85872
C	-2.91667	2.59298	1.79672	H	-0.69582	0.98273	-1.67544
				H	4.04459	3.54682	-1.15310
				H	3.76982	5.30425	-1.33818

Table 4.12: Cartesian Coordinates and Relative Energies of Optimized Conformers of **4.5a** and **4.5b** ($\Delta E < 8$ kJ/mol) Continued.

				C	-1.84917	-2.73808	0.00988
Conf. 8				C	-1.50217	-0.58812	1.11225
				C	-0.17839	-1.15493	-0.81476
ΔG (298 K) = -12338.188008 Hartree				C	-0.83684	-2.37957	-0.89240
H	2.98669	4.15897	-2.46467	C	-2.16336	-1.80746	1.01054
H	-5.03098	-0.43288	3.08932	O	-2.46982	-3.94607	-0.04583
H	-6.35472	3.11648	1.29175	C	-3.63079	-3.98485	-0.90023
H	-8.04826	1.90911	-0.39433	Br	-3.54969	-2.22706	2.24670
H	-8.60588	0.40459	0.11988	Br	-0.35450	-3.60664	-2.26944
				C	5.07251	-2.19860	1.69008
Conf. 19				C	5.40854	-0.95246	2.13869
ΔG (298 K) = -12338.187898 Hartree				N	6.16381	-2.59267	0.90601
O	-6.19775	1.60485	0.34126	N	6.64749	-0.55851	1.64962
C	-4.95761	1.68119	-0.21858	C	7.07748	-1.57383	0.91731
C	-2.38143	1.81920	-1.40433	N	8.29324	-1.65035	0.27434
C	-4.06281	2.71668	0.08806	H	-0.39226	1.68870	1.08805
C	-4.53418	0.73702	-1.16248	H	-2.98121	0.03130	-2.45688
C	-3.27411	0.79734	-1.74761	H	-2.13115	3.60652	-0.22714
C	-2.80099	2.79817	-0.49292	H	-5.74180	-0.09573	1.47757
C	-6.23577	0.87636	1.58064	H	-7.29144	0.73282	1.81496
Br	-5.72411	-0.68098	-1.63022	H	-5.75603	1.45412	2.37805
Br	-4.59751	4.04338	1.35110	H	-0.84416	0.91947	-2.58998
C	-0.98919	1.82854	-2.00266	H	-0.86605	2.66350	-2.70087
C	0.16100	1.97837	-0.99621	H	0.84895	3.46860	0.07719
C	1.52341	1.57481	-1.61393	H	3.94058	0.58268	-1.78511
N	2.32131	1.06233	-0.59728	H	4.18918	0.29643	-0.05618
O	1.86730	1.70692	-2.77271	H	4.30675	2.79606	0.30125
C	0.13696	1.13194	0.31313	H	4.01694	3.04649	-1.41631
C	1.67071	1.16864	0.69492	H	6.31680	3.32212	-2.91988
O	0.23123	3.36796	-0.66909	H	6.71757	1.08863	0.64599
C	3.77941	0.99778	-0.78732	H	9.46605	1.60707	0.70334
C	4.48490	2.37226	-0.69282	H	10.03559	1.46528	-0.84059
C	5.94700	2.30458	-1.00039	H	2.11332	2.22370	2.23803
C	6.68164	2.77492	-2.06122	H	2.03171	-1.40040	0.39468
N	8.02747	2.48870	-1.91100	H	2.77265	-1.77987	3.24594
N	6.88323	1.70024	-0.16331	H	1.75692	-2.93310	2.37663
C	8.09347	1.83894	-0.77020	H	3.62551	-3.53027	0.86483
N	9.25611	1.24888	-0.22590	H	3.98331	-3.85685	2.54865
O	1.95759	2.42681	1.29008	H	-1.78714	0.10285	1.89739
C	2.11206	0.10853	1.74478	H	0.57500	-0.92396	-1.55937
N	2.24703	-1.17055	1.35452	H	-4.30381	-3.15164	-0.67875
O	2.30784	0.50440	2.89868	H	-4.12568	-4.93331	-0.68905
C	2.60533	-2.24711	2.27444	H	-3.32946	-3.94941	-1.95215
C	3.84272	-3.04019	1.82549	H	4.82202	-0.29264	2.76212
C	-0.50542	-0.23624	0.19442				

Table 4.12: Cartesian Coordinates and Relative Energies of Optimized Conformers of **4.5a** and **4.5b** ($\Delta E < 8$ kJ/mol) Continued.

Conf. 19				C	-0.03138	1.34483	1.05264
ΔG (298 K) = -12338.187898 Hartree				C	-0.56792	2.60259	1.31271
H	6.30020	-3.50298	0.49402	C	-1.97921	2.42081	-0.60836
H	8.27330	-2.15452	-0.60346	O	-2.14365	4.35705	0.82367
H	8.74261	-0.73480	0.16497	C	-1.55527	5.51097	0.20452
Conf. 31				Br	-3.35474	3.11151	-1.72291
ΔG (298 K) = -12338.186897 Hartree				Br	0.05759	3.58738	2.82086
O	-6.29511	-1.85993	-0.80703	C	5.21610	1.59357	-2.30342
C	-5.10867	-1.85462	-0.13438	C	5.49673	0.27347	-2.50662
C	-2.56534	-1.80189	1.12791	N	6.21960	2.03252	-1.42597
C	-4.27887	-2.98574	-0.10381	N	6.62191	-0.12034	-1.79757
C	-4.63348	-0.70154	0.50294	C	7.04133	0.96640	-1.16902
C	-3.39305	-0.67407	1.13328	N	8.17986	1.06389	-0.39966
C	-3.02846	-2.96946	0.50535	H	-0.51347	-1.16849	-1.23446
C	-7.43482	-2.22329	-0.01346	H	-3.06818	0.24064	1.61518
Br	-5.69279	0.88360	0.47418	H	-2.40565	-3.85422	0.48479
Br	-4.89096	-4.58931	-0.93890	H	-7.32638	-3.24104	0.37631
C	-1.19481	-1.73965	1.77093	H	-8.29410	-2.17940	-0.68411
C	-0.02408	-1.81750	0.78273	H	-7.57615	-1.51444	0.80939
C	1.34566	-1.61405	1.47332	H	-1.10881	-0.82818	2.36611
N	2.21594	-1.06056	0.53709	H	-1.04647	-2.57647	2.46098
O	1.65160	-1.92301	2.60828	H	0.58370	-3.16644	-0.50467
C	0.04888	-0.78653	-0.38044	H	3.87504	-0.80911	1.75216
C	1.58252	-0.88857	-0.75193	H	4.17311	-0.53819	0.02687
O	-0.02507	-3.14412	0.25485	H	4.01757	-3.01073	-0.36917
C	3.66820	-1.18582	0.74692	H	3.64295	-3.26205	1.33731
C	4.20571	-2.63314	0.64212	H	5.86709	-3.67838	2.97227
C	5.65520	-2.71080	1.00233	H	6.57493	-1.61928	-0.65428
C	6.30611	-3.18653	2.11488	H	9.29537	-2.25105	-0.52655
N	7.67213	-2.97955	2.02675	H	9.78203	-2.06991	1.04084
N	6.66475	-2.18633	0.20021	H	1.77144	-1.71382	-2.47770
C	7.83232	-2.37057	0.87228	H	2.57709	1.36763	0.03166
N	9.04757	-1.84817	0.37475	H	2.08360	3.08213	-2.13409
O	1.79859	-2.04548	-1.55752	H	3.30819	3.30051	-0.88038
C	2.06329	0.31052	-1.60812	H	4.36393	3.41813	-3.07250
N	2.54871	1.39298	-0.97636	H	3.59868	1.92180	-3.59673
O	1.94703	0.21042	-2.83280	H	-1.79704	0.62532	-1.75578
C	2.95718	2.61938	-1.66033	H	0.70840	0.94681	1.73727
C	4.05368	2.41868	-2.73850	H	-0.51079	5.62487	0.51484
C	-0.46053	0.60704	-0.06101	H	-2.13418	6.36630	0.55463
C	-1.56281	3.16850	0.50205	H	-1.62468	5.44408	-0.88621
C	-1.43393	1.17220	-0.89328	H	4.93467	-0.42815	-3.10633
				H	6.42277	2.99217	-1.19104
				H	8.09203	1.65501	0.41747

Table 4.12: Cartesian Coordinates and Relative Energies of Optimized Conformers of **4.5a** and **4.5b** ($\Delta E < 8$ kJ/mol) Continued.

Conf. 31				C	2.04878	2.23486	0.84879
ΔG (298 K) = -12338.186897 Hartree				O	2.40747	4.29719	-0.33323
H	8.58249	0.15108	-0.16297	C	3.56321	4.28659	-1.19353
Conf. 9				Br	3.41177	2.70404	2.08535
ΔG (298 K) = -12338.186634 Hartree				Br	0.32800	3.84639	-2.57649
O	6.02942	-2.08333	0.80502	C	-5.30237	1.83897	1.91268
C	4.86855	-1.99213	0.09569	C	-6.40174	1.38681	1.23997
C	2.37709	-1.75282	-1.24738	N	-5.10043	0.90680	2.94015
C	3.97458	-3.07007	0.00552	N	-6.87611	0.20016	1.78963
C	4.48295	-0.79612	-0.52284	C	-6.05118	-0.06225	2.78549
C	3.26905	-0.67602	-1.19157	N	-6.05290	-1.21753	3.55138
C	2.74950	-2.96248	-0.64482	H	0.25203	-1.24410	1.08843
C	7.16737	-2.51969	0.04550	H	3.01055	0.26994	-1.65287
Br	5.63973	0.71924	-0.40597	H	2.07459	-3.80816	-0.67114
Br	4.45907	-4.72784	0.81718	H	7.00243	-3.52484	-0.35642
C	1.03614	-1.58994	-1.93376	H	8.00482	-2.53904	0.74419
C	-0.17927	-1.67233	-0.99963	H	7.38398	-1.81723	-0.76652
C	-1.49724	-1.30797	-1.72608	H	1.01496	-0.64255	-2.47593
N	-2.36377	-0.74809	-0.78861	H	0.87834	-2.37630	-2.67883
O	-1.76757	-1.50700	-2.89344	H	-0.94064	-3.08745	0.12376
C	-0.23256	-0.74267	0.24866	H	-3.90656	-0.37517	-2.10826
C	-1.78671	-0.75588	0.53807	H	-4.28229	0.01893	-0.42508
O	-0.28473	-3.03670	-0.59370	H	-4.44709	-2.43383	0.09413
C	-3.81035	-0.72107	-1.07660	H	-3.96741	-2.81654	-1.55621
C	-4.51518	-2.09285	-0.94487	H	-6.02560	-3.02533	-3.39962
C	-5.93016	-2.05710	-1.42583	H	-6.94028	-0.99990	0.19335
C	-6.51105	-2.50570	-2.58413	H	-9.54412	-1.17411	-0.12000
N	-7.86688	-2.23351	-2.61391	H	-10.06443	-1.42044	-1.68856
N	-6.97984	-1.46800	-0.71359	H	-2.19852	-1.72081	2.15596
C	-8.10058	-1.60666	-1.47880	H	-2.43575	1.68408	-0.07030
N	-9.32462	-1.05358	-1.10211	H	-2.58654	2.53483	2.75505
O	-2.12400	-1.96487	1.21213	H	-2.36126	3.61797	1.38368
C	-2.24558	0.38995	1.47119	H	-4.70353	3.47156	0.73242
N	-2.51668	1.58855	0.93204	H	-4.62127	3.81626	2.45154
O	-2.31763	0.14215	2.68452	H	1.63456	0.38385	1.83590
C	-2.91461	2.74183	1.73444	H	-0.62071	1.20957	-1.74417
C	-4.43248	3.03605	1.70006	H	4.23477	3.46251	-0.93429
C	0.40599	0.62251	0.07779	H	4.06591	5.24043	-1.03035
C	1.77034	3.10144	-0.21821	H	3.25755	4.20448	-2.24163
C	1.37380	1.02773	1.00374	H	-6.89998	1.84513	0.39700
C	0.11086	1.48133	-0.99190	H	-4.20114	0.74099	3.38181
C	0.77712	2.69682	-1.12298	H	-5.88283	-1.07070	4.53890
				H	-6.89504	-1.75804	3.39863

Table 4.12: Cartesian Coordinates and Relative Energies of Optimized Conformers of **4.5a** and **4.5b** ($\Delta E < 8$ kJ/mol) Continued.

Conf. 30				Br	3.41159	2.70379	2.08565
				C	-5.30224	1.83845	1.91307
ΔG (298 K) =	-12338.186633 Hartree			C	-6.40158	1.38609	1.24045
O	6.02923	-2.08334	0.80506	N	-5.10007	0.90635	2.94058
C	4.86842	-1.99213	0.09563	N	-6.87571	0.19935	1.79019
C	2.37711	-1.75275	-1.24769	C	-6.05064	-0.06289	2.78599
C	4.48292	-0.79611	-0.52294	N	-6.05214	-1.21810	3.55193
C	3.97442	-3.07005	0.00538	H	0.25205	-1.24439	1.08789
C	2.74943	-2.96242	-0.64509	H	2.07447	-3.80807	-0.67148
C	3.26909	-0.67597	-1.19180	H	3.01067	0.26999	-1.65312
C	7.16721	-2.51982	0.04566	H	7.00232	-3.52504	-0.35609
Br	4.45875	-4.72781	0.81716	H	8.00466	-2.53901	0.74436
Br	5.63973	0.71922	-0.40596	H	7.38384	-1.81750	-0.76648
C	1.03622	-1.58984	-1.93420	H	1.01508	-0.64241	-2.47629
C	-0.17925	-1.67231	-1.00020	H	0.87859	-2.37611	-2.67940
C	-1.49719	-1.30778	-1.72661	H	-0.94081	-3.08747	0.12299
N	-2.36375	-0.74813	-0.78904	H	-3.90646	-0.37505	-2.10873
O	-1.76750	-1.50657	-2.89402	H	-4.28227	0.01894	-0.42555
C	-0.23251	-0.74280	0.24820	H	-4.44703	-2.43387	0.09350
C	-1.78669	-0.75599	0.53762	H	-3.96766	-2.81645	-1.55697
O	-0.28486	-3.03671	-0.59443	H	-6.02631	-3.02418	-3.40030
C	-3.81033	-0.72103	-1.07709	H	-6.94000	-1.00012	0.19371
C	-4.51525	-2.09277	-0.94545	H	-9.54397	-1.17388	-0.11930
C	-5.93032	-2.05674	-1.42615	H	-10.06448	-1.41897	-1.68798
C	-6.51152	-2.50477	-2.58452	H	-2.19822	-1.72112	2.15547
N	-7.86730	-2.23235	-2.61391	H	-2.43606	1.68395	-0.07055
N	-6.97973	-1.46769	-0.71351	H	-2.58625	2.53471	2.75485
C	-8.10067	-1.60586	-1.47853	H	-2.36148	3.61783	1.38339
N	-9.32452	-1.05270	-1.10135	H	-4.70386	3.47120	0.73279
O	-2.12403	-1.96504	1.21158	H	-4.62126	3.81574	2.45193
C	-2.24544	0.38978	1.47086	H	-0.62055	1.20967	-1.74438
N	-2.51665	1.58841	0.93182	H	1.63451	0.38350	1.83572
O	-2.31730	0.14190	2.68419	H	4.06607	5.24058	-1.02892
C	-2.91461	2.74161	1.73432	H	3.25791	4.20524	-2.24088
C	-4.43255	3.03564	1.70032	H	4.23465	3.46262	-0.93356
C	0.40604	0.62241	0.07757	H	-6.90000	1.84426	0.39751
C	1.77026	3.10144	-0.21794	H	-4.20060	0.74059	3.38192
C	0.11095	1.48136	-0.99201	H	-5.88141	-1.07133	4.53934
C	1.37377	1.02751	1.00365	H	-6.89431	-1.75867	3.39960
C	2.04870	2.23470	0.84893				
C	0.77715	2.69690	-1.12286				
O	2.40725	4.29729	-0.33273				
C	3.56328	4.28689	-1.19267				
Br	0.32822	3.84663	-2.57629				

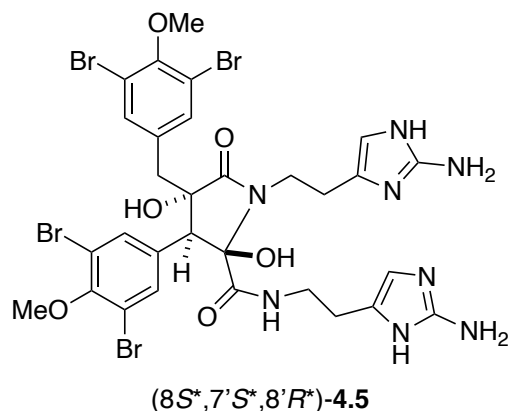
Table 4.12: Cartesian Coordinates and Relative Energies of Optimized Conformers of **4.5a** and **4.5b** ($\Delta E < 8$ kJ/mol) Continued.

Conf. 11				Br	0.70177	3.87321	-2.17417
				C	-5.12207	1.84337	2.09712
ΔG (298 K) = -12338.186381 Hartree				C	-6.25768	1.55055	1.39683
O	5.97101	-1.95991	0.39557	N	-4.98826	0.79642	3.01982
C	4.75843	-1.90282	-0.22357	N	-6.82090	0.35378	1.82774
C	2.24269	-1.76444	-1.53246	C	-6.01351	-0.07425	2.77948
C	4.46028	-0.87831	-1.13099	N	-6.10188	-1.29915	3.42243
C	3.76897	-2.87499	-0.01711	H	0.14573	-1.58066	0.86693
C	2.53562	-2.82116	-0.65922	H	1.79076	-3.58413	-0.47015
C	3.23054	-0.80333	-1.77593	H	3.03613	0.02064	-2.45339
C	6.00707	-1.30151	1.67359	H	5.59836	-0.28788	1.60271
Br	4.13052	-4.30522	1.19351	H	7.05822	-1.25802	1.96188
Br	5.78196	0.45860	-1.46278	H	5.44429	-1.87787	2.41586
C	0.88623	-1.62725	-2.19416	H	0.84545	-0.68120	-2.73810
C	-0.32079	-1.72589	-1.25081	H	0.72998	-2.41360	-2.94053
C	-1.61400	-1.18687	-1.91003	H	-1.18718	-3.19783	-0.28565
N	-2.42436	-0.66312	-0.90478	H	-3.94173	-0.02314	-2.14992
O	-1.90827	-1.23657	-3.08739	H	-4.27210	0.20776	-0.42719
C	-0.29220	-0.94465	0.09598	H	-4.63048	-2.26704	-0.18238
C	-1.84110	-0.86050	0.40390	H	-4.19466	-2.49835	-1.87273
O	-0.52186	-3.11789	-0.99201	H	-6.27469	-2.33702	-3.69455
C	-3.86630	-0.48927	-1.16490	H	-6.99993	-0.65922	0.11433
C	-4.67817	-1.80711	-1.17567	H	-9.61354	-0.59521	-0.17627
C	-6.08896	-1.60597	-1.62728	H	-10.16032	-0.61950	-1.75480
C	-6.71156	-1.87519	-2.81902	H	-2.32293	-1.95738	1.91486
N	-8.04147	-1.49585	-2.79715	H	-2.29552	1.67156	0.06361
N	-7.08343	-1.01966	-0.83768	H	-2.35303	2.23289	2.96424
C	-8.21682	-0.98340	-1.59606	H	-2.05282	3.43212	1.70875
N	-9.39025	-0.38133	-1.14150	H	-4.40426	3.53869	1.08355
O	-2.27333	-2.10331	0.94947	H	-4.28192	3.69402	2.82761
C	-2.19630	0.21297	1.45957	H	1.63122	-0.17185	1.81900
N	-2.37287	1.47938	1.05233	H	-0.47531	1.24316	-1.66567
O	-2.27713	-0.15474	2.64148	H	4.52143	2.99761	-0.45474
C	-2.67147	2.57027	1.97587	H	4.49090	4.78566	-0.36442
C	-4.16142	2.98438	1.99636	H	3.67357	3.94644	-1.71529
C	0.46468	0.36888	0.08532	H	-6.72325	2.13136	0.61273
C	2.01286	2.75482	0.10933	H	-4.10267	0.51608	3.42999
C	1.44080	0.58374	1.06544	H	-5.91862	-1.26813	4.41804
C	0.25962	1.36707	-0.87842	H	-6.98406	-1.75445	3.22444
C	1.01819	2.53417	-0.85518				
C	2.20238	1.74736	1.06556				
O	2.73269	3.90699	0.15183				
C	3.92966	3.89608	-0.65207				
Br	3.55741	1.97981	2.38369				

Table 4.12: Cartesian Coordinates and Relative Energies of Optimized Conformers of **4.5a** and **4.5b** ($\Delta E < 8$ kJ/mol) Continued.

Conf. 12				Br	1.62026	1.31948	2.74934
				C	-3.03799	2.44824	1.31578
ΔG (298 K) =	-12338.185814 Hartree			C	-2.30190	3.42534	0.68817
O	4.05232	2.34421	-1.01972	N	-4.31342	2.55420	0.75264
C	2.85169	1.75442	-1.29363	N	-3.06043	4.11574	-0.24220
C	0.37289	0.43086	-1.67632	C	-4.24490	3.55317	-0.17485
C	1.64573	2.33203	-0.87935	N	-5.33005	3.84710	-1.02005
C	2.77434	0.50305	-1.91987	H	-0.31681	-3.50126	-0.70768
C	1.56327	-0.14872	-2.13120	H	1.55165	-1.12290	-2.60066
C	0.42774	1.68992	-1.06774	H	-0.47984	2.15714	-0.70305
C	4.55074	3.19952	-2.05981	H	4.71797	2.63011	-2.98017
Br	4.39721	-0.36855	-2.41613	H	5.50091	3.59358	-1.69665
Br	1.69123	3.99821	0.04191	H	3.85730	4.02690	-2.24425
C	-0.98381	-0.25047	-1.76966	H	-1.63702	0.20559	-1.01733
C	-1.05257	-1.79082	-1.64374	H	-1.45237	-0.02161	-2.73709
C	-2.52358	-2.23491	-1.74909	H	-0.89461	-2.23273	-3.52740
N	-2.94192	-2.81240	-0.59352	H	-3.87429	-4.59980	-0.11913
O	-3.19455	-2.09230	-2.77504	H	-4.43707	-3.79703	-1.59174
C	-0.59686	-2.51002	-0.34115	H	-6.19319	-3.74623	0.03851
C	-1.90808	-2.86139	0.45791	H	-5.16343	-3.12683	1.31264
O	-0.36272	-2.40663	-2.73391	H	-6.51689	-0.68619	1.71514
C	-4.15751	-3.63623	-0.54767	H	-5.02343	-1.49737	-2.12737
C	-5.35394	-3.06300	0.23591	H	-5.76190	2.08782	-2.04495
C	-5.70931	-1.64704	-0.09035	H	-5.15527	0.85982	-3.04062
C	-6.21312	-0.63558	0.67826	H	-1.76819	-4.02181	1.94780
N	-6.31804	0.54737	-0.04242	H	-3.19602	-0.56568	0.51459
N	-5.53490	-1.07487	-1.35556	H	-4.34977	0.17874	2.49583
C	-5.88983	0.24190	-1.26175	H	-2.95520	-0.33580	3.44556
N	-5.83115	1.10747	-2.32987	H	-1.59735	1.55388	2.57847
O	-1.80762	-4.15109	0.97658	H	-3.05242	2.05459	3.41716
C	-2.26329	-1.93914	1.67502	H	1.87902	-3.57260	-0.27444
N	-2.79779	-0.72047	1.43047	H	-0.35004	-0.24087	1.28459
O	-2.00906	-2.37350	2.79817	H	4.31455	1.37902	1.49421
C	-3.25477	0.15216	2.51700	H	5.06422	0.05619	0.55630
C	-2.68923	1.58263	2.49146	H	5.77035	0.55187	2.12246
C	0.59582	-1.98537	0.43051	H	-1.27040	3.69503	0.87150
C	2.94846	-0.98547	1.67718	H	-5.09264	1.88764	0.78097
C	1.81416	-2.66399	0.31330	H	-5.10907	4.68004	-1.55671
C	0.56242	-0.81101	1.18918	H	-6.19798	3.98720	-0.51013
C	1.71556	-0.32653	1.79279				
C	2.96470	-2.16234	0.91411				
O	4.06675	-0.53693	2.30541				
C	4.84357	0.42495	1.56154				
Br	4.61758	-3.07065	0.66212				

Table 4.12: Cartesian Coordinates and Relative Energies of Optimized Conformers of **4.5a** and **4.5b** ($\Delta E < 8$ kJ/mol) Continued.



Conf. 40

ΔG (298 K) = -12338.197969 Hartree

O	4.78796	3.48285	-0.44754
C	3.62334	2.82280	-0.70720
C	1.18977	1.40813	-1.09310
C	2.37708	3.44082	-0.52998
C	3.61411	1.47885	-1.10264
C	2.42480	0.78425	-1.30109
C	1.17955	2.75744	-0.71314
Br	2.33313	5.27943	-0.01644
Br	5.26974	0.56958	-1.34448
C	5.37118	4.14435	-1.57996
C	-0.09391	0.63094	-1.31010
C	-0.98809	0.42678	-0.06940
C	-0.41956	-0.39289	1.13765
C	-2.26734	-0.34719	-0.45323
N	-2.56042	-1.25067	0.50580
C	-1.66562	-1.16405	1.69847
O	-2.92425	-0.11241	-1.47421
C	-3.81767	-2.00562	0.61224
C	-4.29588	-2.72051	-0.68902
C	-2.48320	-0.46104	2.84594
N	-2.67695	0.85804	2.75217
O	-2.97197	-1.19491	3.71246
C	-3.67479	1.58212	3.53007
O	-1.38205	1.70958	0.44436
O	-1.35382	-2.42455	2.17576
C	0.73793	-1.32846	0.82839
C	2.97453	-2.97596	0.24131
C	1.98667	-1.07180	1.40014
C	0.60782	-2.43197	-0.02529

C	1.70804	-3.23353	-0.30632
C	3.08187	-1.88024	1.10673
O	4.05997	-3.72445	-0.10065
C	4.32215	-4.83919	0.76664
Br	4.77606	-1.46706	1.86628
Br	1.50042	-4.73023	-1.47007
C	-4.16235	2.82630	2.76050
C	-4.78452	2.56567	1.41541
C	-6.11213	2.40296	1.10515
N	-6.17215	2.23004	-0.26377
C	-4.90000	2.29222	-0.73280
N	-4.03094	2.49666	0.24626
N	-4.62731	2.09904	-2.09734
C	-5.60987	-2.19739	-1.17538
C	-6.88966	-2.68976	-1.14281
N	-7.80082	-1.75122	-1.60230
C	-7.06907	-0.70022	-1.89594
N	-5.74345	-0.90297	-1.66528
N	-7.57508	0.55459	-2.29656
H	-0.06970	0.32547	1.88195
H	2.46809	-0.25569	-1.60302
H	0.24056	3.26626	-0.54276
H	5.62051	3.42256	-2.36495
H	6.28478	4.61551	-1.21475
H	4.69440	4.91207	-1.97034
H	-0.72727	1.14489	-2.04152
H	0.14392	-0.34344	-1.74472
H	-4.60470	-1.33246	0.96953
H	-3.63992	-2.74410	1.39430
H	-3.52567	-2.63680	-1.46178
H	-4.41279	-3.78733	-0.47886
H	-2.17872	1.35587	2.01053
H	-4.50284	0.89902	3.74091
H	-3.25883	1.89531	4.49634
H	-2.27756	2.01040	0.12090
H	-1.89363	-2.50800	2.99385
H	2.12144	-0.22639	2.06527
H	-0.35146	-2.68668	-0.45812
H	3.48078	-5.54017	0.76027
H	4.52418	-4.49660	1.78679
H	5.20922	-5.32950	0.36366
H	-3.32003	3.51669	2.63063
H	-4.88703	3.34178	3.39967
H	-6.99742	2.41263	1.72182

Table 4.12: Cartesian Coordinates and Relative Energies of Optimized Conformers of **4.5a** and **4.5b** ($\Delta E < 8$ kJ/mol) Continued.

Conf. 40				O	4.19883	-3.33542	0.12016
ΔG (298 K) = -12338.197969 Hartree				C	4.53556	-4.35597	1.07332
H	-6.94744	1.86787	-0.82975	Br	4.79610	-0.87114	1.85625
H	-4.71818	2.95643	-2.63587	Br	1.69042	-4.62272	-1.10520
H	-3.69365	1.71105	-2.21058	C	-4.26625	3.08026	2.44863
H	-7.21329	-3.66799	-0.81427	C	-4.90778	2.66171	1.15346
H	-4.97035	-0.26721	-1.82582	C	-6.23513	2.42227	0.89614
H	-8.54500	0.43819	-2.57418	N	-6.31839	2.10214	-0.44449
H	-7.03725	0.95335	-3.06186	C	-5.05979	2.15634	-0.94976
Conf. 24				N	-4.17751	2.49363	-0.02039
ΔG (298 K) = -12338.197558 Hartree				N	-4.81097	1.82671	-2.29271
O	4.87009	3.08995	-0.93270	C	-5.63092	-2.38278	-0.87804
C	3.64579	2.50365	-1.05368	C	-6.89332	-2.90672	-0.76226
C	1.10393	1.27157	-1.34502	N	-7.84332	-2.05105	-1.29827
C	2.45638	3.20125	-0.79753	C	-7.15183	-1.01673	-1.72075
C	3.52220	1.17589	-1.48416	N	-5.81604	-1.15368	-1.50095
C	2.27897	0.57388	-1.64296	N	-7.70560	0.17108	-2.24352
C	1.20504	2.60796	-0.93488	H	-0.13749	0.64467	1.74743
Br	2.56496	5.02311	-0.23424	H	2.23380	-0.46071	-1.96317
Br	5.09264	0.15038	-1.80191	H	0.31286	3.17261	-0.69904
C	5.43456	3.02159	0.38776	H	4.89134	3.68334	1.07102
C	-0.23050	0.56431	-1.46852	H	6.46686	3.36103	0.29174
C	-1.08291	0.48564	-0.18426	H	5.41627	1.99535	0.76860
C	-0.45945	-0.16972	1.09537	H	-0.86606	1.06362	-2.20810
C	-2.34591	-0.36190	-0.44230	H	-0.06260	-0.44726	-1.84800
N	-2.57828	-1.17232	0.61187	H	-4.60384	-1.28013	1.14924
C	-1.66084	-0.92528	1.76356	H	-3.57218	-2.60700	1.67826
O	-3.03670	-0.25693	-1.46230	H	-3.54119	-2.79348	-1.17038
C	-3.80217	-1.95697	0.83373	H	-4.37216	-3.85657	-0.04995
C	-4.29093	-2.81508	-0.37355	H	-2.26494	1.59192	1.80574
C	-2.47821	-0.12971	2.84835	H	-4.53301	1.25834	3.63178
N	-2.72574	1.16254	2.61152	H	-3.30279	2.35978	4.25165
O	-2.91613	-0.77795	3.80532	H	-2.40539	2.05215	-0.14417
C	-3.72864	1.93688	3.33263	H	-1.80459	-2.12803	3.20202
O	-1.49727	1.80987	0.19175	H	2.06872	0.22547	1.97895
O	-1.28846	-2.11418	2.36483	H	-0.27570	-2.61276	-0.25195
C	0.74312	-1.07235	0.87611	H	3.74077	-5.10688	1.13357
C	3.07152	-2.62952	0.40993	H	4.72032	-3.91844	2.06003
C	1.97944	-0.68872	1.40310	H	5.45008	-4.82086	0.70301
C	0.67103	-2.26097	0.13884	H	-3.44637	3.77443	2.22746
C	1.81629	-3.01679	-0.08486	H	-4.99195	3.64145	3.04681
C	3.11788	-1.45375	1.16862	H	-7.10655	2.46741	1.53076
				H	-7.09228	1.65544	-0.94878
				H	-4.93657	2.62000	-2.91590

Table 4.12: Cartesian Coordinates and Relative Energies of Optimized Conformers of **4.5a** and **4.5b** ($\Delta E < 8$ kJ/mol) Continued.

				Br	4.80022	-1.34358	1.90025
Conf. 24				Br	1.83614	-4.68102	-1.64790
				C	-4.09625	2.53936	2.67944
ΔG (298 K) = -12338.197558 Hartree				C	-4.79283	2.57960	1.34918
H	-3.86926	1.45339	-2.38675	C	-6.05437	2.99430	1.03768
H	-7.17844	-3.85310	-0.32329	N	-6.20450	2.76475	-0.33003
H	-5.06618	-0.51680	-1.74535	C	-5.04517	2.22078	-0.79135
H	-8.67608	-0.00385	-2.48622	N	-4.16935	2.08806	0.19748
H	-7.19444	0.50098	-3.05834	N	-4.81934	1.93156	-2.11530
				C	-5.83647	-2.03482	-0.26818
Conf. 5				C	-7.20417	-2.15703	-0.28747
ΔG (298 K) = -12338.197371 Hartree				N	-7.74940	-1.51042	-1.38250
O	4.50300	3.75345	-0.27556	C	-6.71531	-1.00100	-2.01248
C	3.40352	3.01394	-0.59979	N	-5.53373	-1.27459	-1.39066
C	1.10349	1.43204	-1.12586	N	-6.78004	-0.17851	-3.16103
C	2.10749	3.53418	-0.47112	H	-0.12924	0.20388	1.76098
C	3.51320	1.68158	-1.01775	H	2.52468	-0.12174	-1.60413
C	2.38985	0.90531	-1.28554	H	-0.00862	3.19827	-0.58504
C	0.97413	2.76829	-0.72205	H	5.42067	3.79352	-2.15406
Br	1.90370	5.35395	0.07135	H	5.94159	5.01032	-0.95591
Br	5.24250	0.90123	-1.19371	H	4.36788	5.20113	-1.77761
C	5.08314	4.47893	-1.36930	H	-0.75707	1.05788	-2.14511
C	-0.10848	0.56806	-1.41084	H	0.21710	-0.37133	-1.86569
C	-1.01866	0.27182	-0.19486	H	-2.87757	-3.52177	0.67318
C	-0.41257	-0.52846	1.00317	H	-3.38489	-2.93588	-0.91594
C	-2.19212	-0.63251	-0.64457	H	-5.13210	-3.51903	1.05884
N	-2.45983	-1.55180	0.31653	H	-4.76380	-1.89814	1.59295
C	-1.63140	-1.38376	1.52928	H	-3.52410	0.39479	1.38343
O	-2.80611	-0.51146	-1.71402	H	-5.01846	0.75806	3.52125
C	-3.36683	-2.69890	0.15097	H	-3.43487	1.12992	4.22033
C	-4.80416	-2.53639	0.70218	H	-2.43581	1.70694	0.07879
C	-2.38708	-0.65893	2.69521	H	-1.30113	-2.50743	3.00589
N	-3.35356	0.20879	2.36362	H	2.07337	-0.25836	2.03338
O	-2.04419	-0.94391	3.84566	H	-0.15520	-2.76648	-0.66637
C	-4.00972	1.12324	3.29131	H	3.77952	-5.44675	0.64372
O	-1.50529	1.48830	0.34963	H	4.72551	-4.37272	1.73149
O	-1.26182	-2.62772	2.03385	H	5.50580	-5.12918	0.31486
C	0.80017	-1.39396	0.71252	H	-3.08052	2.93458	2.56713
C	3.14668	-2.90171	0.16831	H	-4.62445	3.18458	3.38876
C	2.01146	-1.08968	1.34040	H	-6.84783	3.41204	1.63636
C	0.76616	-2.47661	-0.17695	H	-7.00312	3.00714	-0.89494
C	1.91808	-3.21027	-0.43547	H	-5.59404	1.45620	-2.58803
C	3.16031	-1.82747	1.06681	H	-3.95426	1.41239	-2.23279
O	4.28357	-3.58015	-0.15279	H	-7.83066	-2.68139	0.42121
C	4.57875	-4.69978	0.69689				

Table 4.12: Cartesian Coordinates and Relative Energies of Optimized Conformers of **4.5a** and **4.5b** ($\Delta E < 8$ kJ/mol) Continued.

			C	4.60802	3.78162	-1.91130	
Conf. 5			C	4.23817	4.24963	-0.53388	
			C	5.00174	4.98760	0.32239	
ΔG (298 K) = -12338.197371 Hartree			N	4.21668	5.18349	1.45699	
H	-4.59387	-0.97904	-1.66609	C	3.02001	4.55989	1.24438
H	-7.75932	-0.08882	-3.41833	N	2.99525	3.97440	0.05223
H	-6.28479	-0.58754	-3.95151	N	2.02597	4.52014	2.19248
			C	-1.21953	3.92792	-1.10714	
Conf. 8			C	-0.43115	4.75847	-0.36339	
ΔG (298 K) = -12338.196232 Hartree			N	-0.71695	4.64396	0.99263	
O	-6.62011	-1.04768	0.66206	C	-1.68085	3.74449	1.06440
C	-5.27007	-0.98888	0.47977	N	-2.02939	3.28283	-0.16979
C	-2.44276	-0.89590	0.19186	N	-2.23317	3.24157	2.23405
C	-4.51160	0.06594	0.99880	H	1.35486	-0.84034	-2.52742
C	-4.56269	-2.01096	-0.17132	H	-2.67173	-2.78476	-0.82256
C	-3.18018	-1.97553	-0.31444	H	-2.57155	0.92042	1.34816
C	-3.12553	0.11330	0.88049	H	-7.17598	0.57123	-0.53950
Br	-5.43365	1.48725	1.89693	H	-8.44061	-0.61951	-0.12355
Br	-5.53705	-3.49303	-0.87235	H	-7.20705	-1.03354	-1.34639
C	-7.39632	-0.49434	-0.41268	H	-0.55538	0.02911	0.61565
C	-0.93725	-0.82241	0.04556	H	-0.48608	-1.72552	0.47067
C	-0.40900	-0.72797	-1.40896	H	-0.13187	2.44480	-4.04731
C	1.13013	-0.53966	-1.49937	H	0.88223	3.25270	-2.86156
C	-0.89305	0.52071	-2.16540	H	-1.19590	4.47901	-3.17029
N	0.09889	1.44257	-2.22620	H	-2.16809	3.05727	-2.81110
C	1.31619	1.01422	-1.51680	H	3.53458	1.50734	-0.56128
O	-2.00542	0.59770	-2.68567	H	5.72148	1.96308	-1.43133
C	-0.04308	2.69155	-2.98439	H	5.03615	1.98821	-3.06811
C	-1.23798	3.57105	-2.55725	H	-1.60359	-1.58980	-2.64303
C	2.59149	1.37167	-2.33174	H	1.73278	2.46794	-0.22078
N	3.70001	1.50439	-1.55856	H	1.90881	-0.15751	1.18439
O	2.57363	1.48642	-3.55183	H	2.31812	-2.84324	-2.15109
C	4.85299	2.25982	-2.02642	H	3.26049	-5.62227	1.79793
O	-0.80914	-1.86833	-2.15524	H	3.08215	-4.50686	3.19640
O	1.38091	1.54256	-0.21330	H	4.57034	-5.47425	3.00219
C	2.00471	-1.38148	-0.59281	H	3.81298	4.04786	-2.61783
C	3.61625	-3.10873	0.99059	H	5.51244	4.30756	-2.23751
C	2.28766	-1.06940	0.74541	H	5.99536	5.39747	0.23596
C	2.52745	-2.56944	-1.12342	H	4.48566	5.68708	2.28717
C	3.31194	-3.41161	-0.34332	H	1.07057	4.45947	1.81942
C	3.07986	-1.92212	1.50808	H	2.09246	5.24426	2.89541
O	4.44412	-3.89942	1.73057	H	0.34506	5.42342	-0.71311
C	3.78310	-4.93602	2.47259	H	-2.69629	2.55215	-0.37419
Br	3.45418	-1.46555	3.32390	H	-3.23388	3.07518	2.20407
Br	4.00520	-5.01726	-1.10323				

Table 4.12: Cartesian Coordinates and Relative Energies of Optimized Conformers of **4.5a** and **4.5b** ($\Delta E < 8$ kJ/mol) Continued.

				C	4.91316	5.04724	0.21376
Conf. 8				N	4.13260	5.25661	1.34911
ΔG (298 K) =				C	2.94479	4.60884	1.15945
H	-1.96728	3.79886	3.03580	N	2.92195	3.99497	-0.01845
				N	1.95757	4.57516	2.11462
Conf. 10				C	-1.28677	3.87895	-1.16091
ΔG (298 K) =				C	-0.50681	4.73342	-0.43566
O	-6.64068	-1.10399	0.71467	N	-0.78831	4.64255	0.92305
C	-5.29120	-1.04035	0.52949	C	-1.74164	3.73346	1.01491
C	-2.46512	-0.93438	0.23571	N	-2.08716	3.24322	-0.20910
C	-4.53907	0.02940	1.02666	N	-2.28548	3.24804	2.19545
C	-4.57802	-2.07053	-0.10224	H	1.32171	-0.89475	-2.49712
C	-3.19593	-2.02879	-0.24789	H	-2.68269	-2.84498	-0.73988
C	-3.15353	0.08366	0.90539	H	-2.60406	0.90328	1.35628
Br	-5.46975	1.46188	1.89790	H	-7.22992	-1.13531	-1.29289
Br	-5.54353	-3.57231	-0.77249	H	-7.20804	0.48605	-0.51957
C	-7.42151	-0.57804	-0.37033	H	-8.46469	-0.70371	-0.07739
C	-0.96071	-0.85330	0.08334	H	-0.58191	0.00901	0.63920
C	-0.43952	-0.77711	-1.37478	H	-0.50199	-1.74715	0.51967
C	1.09786	-0.57862	-1.47349	H	-0.18942	2.34702	-4.07249
C	-0.93584	0.45481	-2.15019	H	0.81871	3.18586	-2.90292
N	0.05003	1.38205	-2.23235	H	-1.26794	4.39006	-3.23403
C	1.27229	0.97556	-1.51929	H	-2.22971	2.96836	-2.84718
O	-2.05085	0.51610	-2.66654	H	3.48257	1.53653	-0.58141
C	-0.10213	2.61487	-3.01453	H	5.66538	1.99199	-1.47391
C	-1.30334	3.49372	-2.60374	H	4.96922	1.96887	-3.10630
C	2.54204	1.32810	-2.34541	H	-1.63359	-1.67091	-2.58715
N	3.64950	1.50139	-1.57789	H	1.66764	2.46136	-0.25405
O	2.52162	1.40530	-3.56828	H	1.93206	-0.12406	1.18396
C	4.78877	2.26218	-2.07003	H	2.23843	-2.91694	-2.07328
O	-0.83210	-1.93250	-2.10167	H	5.97519	-2.76708	2.16581
O	1.33652	1.52931	-0.22568	H	6.09842	-3.93435	0.80400
C	1.97751	-1.40309	-0.55565	H	6.13175	-4.51553	2.49181
C	3.57534	-3.11535	1.05716	H	3.72092	4.02196	-2.69568
C	2.28923	-1.05482	0.76690	H	5.41890	4.31333	-2.33230
C	2.47059	-2.61584	-1.05824	H	5.89882	5.47212	0.11030
C	3.25103	-3.44899	-0.26469	H	4.39739	5.78667	2.16402
C	3.07925	-1.89811	1.54238	H	1.00047	4.49546	1.74902
O	4.28898	-3.96265	1.85162	H	2.01969	5.31294	2.80359
C	5.71095	-3.77051	1.81517	H	0.26042	5.40065	-0.80052
Br	3.50126	-1.38777	3.33329	H	-2.74596	2.50090	-0.39736
Br	3.90519	-5.08825	-0.98655	H	-2.02630	3.82487	2.98543
C	4.52378	3.78277	-1.98829	H	-3.28350	3.06549	2.17065
C	4.15594	4.27707	-0.61958				

Table 4.12: Cartesian Coordinates and Relative Energies of Optimized Conformers of **4.5a** and **4.5b** ($\Delta E < 8$ kJ/mol) Continued.

Conf. 13				N	2.05820	4.51199	2.17442
				C	-1.10974	3.96042	-1.20524
ΔG (298 K) =			-12338.195828 Hartree	C	-0.32053	4.77536	-0.44527
O	-6.70202	-0.80060	0.37385	N	-0.64669	4.67801	0.90293
C	-5.33960	-0.83540	0.32726	C	-1.63585	3.80476	0.95351
C	-2.50481	-0.81763	0.10275	N	-1.96173	3.34323	-0.28679
C	-4.64463	-1.87862	-0.30337	N	-2.23258	3.32581	2.11164
C	-4.56512	0.19891	0.86384	H	1.36425	-0.88851	-2.51621
C	-3.17625	0.21228	0.77174	H	-2.61208	1.00815	1.24650
C	-3.25887	-1.87969	-0.41611	H	-2.76078	-2.70315	-0.91149
Br	-5.64202	-3.33286	-1.02994	H	-7.02884	-2.52607	1.51051
Br	-5.46842	1.64614	1.74014	H	-8.36358	-1.34537	1.40161
C	-7.28426	-1.46152	1.50842	H	-6.95551	-0.99127	2.44164
C	-0.99466	-0.78599	-0.00773	H	-0.60297	0.05809	0.56686
C	-0.42644	-0.71675	-1.44835	H	-0.58007	-1.69851	0.43431
C	1.11972	-0.57449	-1.49668	H	0.02314	2.42465	-4.10050
C	-0.85164	0.53981	-2.22622	H	1.02292	3.21378	-2.88949
N	0.16948	1.43133	-2.26552	H	-1.00938	4.49535	-3.27013
C	1.35254	0.97266	-1.51962	H	-2.03182	3.10412	-2.93120
O	-1.94541	0.64630	-2.77840	H	3.55082	1.44334	-0.50667
C	0.08640	2.67742	-3.03715	H	5.77625	1.82581	-1.32493
C	-1.09564	3.59345	-2.65285	H	5.13228	1.84313	-2.97869
C	2.66000	1.28594	-2.30155	H	-1.61179	-1.55274	-2.70937
N	3.74815	1.41089	-1.49766	H	1.76123	2.43033	-0.22627
O	2.68152	1.37521	-3.52351	H	2.18644	-2.95036	-2.08438
C	4.92963	2.13354	-1.94572	H	1.88823	-0.17595	1.18910
O	-0.83889	-1.85006	-2.19841	H	5.79041	-2.98758	2.27050
O	1.39681	1.51050	-0.21821	H	5.90971	-4.14716	0.90182
C	1.93806	-1.44059	-0.56067	H	5.86671	-4.74365	2.58404
C	3.41476	-3.22949	1.08423	H	3.94707	3.93697	-2.58653
C	2.39836	-2.66764	-1.05967	H	5.64236	4.16221	-2.16803
C	2.22139	-1.11664	0.77442	H	6.08711	5.28496	0.29688
C	2.95209	-1.99775	1.56580	H	4.53610	5.63603	2.30744
C	3.11967	-3.53819	-0.25046	H	2.12291	5.24531	2.86795
O	4.06849	-4.11162	1.89232	H	1.11047	4.46513	1.77976
C	5.49746	-3.97655	1.90200	H	0.48228	5.41719	-0.77765
Br	3.73074	-5.19598	-0.96788	H	-2.64496	2.63218	-0.50670
Br	3.33593	-1.52112	3.37468	H	-3.23667	3.18826	2.05735
C	4.71812	3.66206	-1.85705	H	-1.97229	3.88295	2.91541
C	4.32636	4.15781	-0.49550				
C	5.08442	4.89447	0.36689				
N	4.27771	5.12217	1.48020				
C	3.07424	4.51817	1.24920				
N	3.06557	3.91481	0.06577				

Table 4.12: Cartesian Coordinates and Relative Energies of Optimized Conformers of **4.5a** and **4.5b** ($\Delta E < 8$ kJ/mol) Continued.

Conf. 14				N	2.12735	4.45209	2.24932
				C	-1.03848	4.00332	-1.15434
ΔG (298 K) =				C	-0.23928	4.79366	-0.37891
				N	-0.56967	4.67766	0.96677
O	-6.68084	-0.72410	0.31902	C	-1.57096	3.81778	1.00046
C	-5.31863	-0.77097	0.27756	N	-1.90085	3.38245	-0.24820
C	-2.48282	-0.77595	0.06380	N	-2.17681	3.32663	2.14910
C	-4.63088	-1.80977	-0.36804	H	1.39702	-0.84398	-2.54077
C	-4.53660	0.24666	0.83477	H	-2.57775	1.03087	1.23862
C	-3.14729	0.24840	0.74820	H	-2.75255	-2.64062	-0.98463
C	-3.24482	-1.82180	-0.47600	H	-7.02911	-2.46385	1.42704
Br	-5.63900	-3.24234	-1.12262	H	-8.35205	-1.26888	1.33089
Br	-5.42962	1.68740	1.73187	H	-6.94543	-0.94447	2.38243
C	-7.27437	-1.39697	1.44053	H	-0.57606	0.07743	0.54692
C	-0.97188	-0.75613	-0.03994	H	-0.56708	-1.67756	0.39275
C	-0.39580	-0.67372	-1.47677	H	0.08209	2.50797	-4.07527
C	1.15160	-0.54332	-1.51747	H	1.08858	3.26761	-2.85142
C	-0.80721	0.59726	-2.23881	H	-0.93423	4.57217	-3.21037
N	0.21964	1.48239	-2.25760	H	-1.96727	3.18357	-2.89429
C	1.39648	1.00260	-1.51467	H	3.60024	1.40486	-0.48487
O	-1.89681	0.71867	-2.79634	H	5.82996	1.78094	-1.28184
C	0.14746	2.74219	-3.00784	H	5.19820	1.84488	-2.93901
C	-1.02722	3.66088	-2.60803	H	-1.57945	-1.47915	-2.75836
C	2.70980	1.31776	-2.28551	H	1.82551	2.42884	-0.19250
N	3.79731	1.40223	-1.47637	H	1.86103	-0.21184	1.19182
O	2.73548	1.44231	-3.50444	H	2.27003	-2.88584	-2.15287
C	4.99284	2.11570	-1.90126	H	2.98661	-5.73035	1.79684
O	-0.81611	-1.79327	-2.24292	H	2.80663	-4.62107	3.19998
O	1.44029	1.51713	-0.20440	H	4.26338	-5.64134	3.04167
C	1.96490	-1.42507	-0.59210	H	4.04202	3.94732	-2.50924
C	3.45977	-3.22508	1.02445	H	5.73754	4.13759	-2.07440
C	2.21798	-1.13448	0.75692	H	6.18399	5.19368	0.41964
C	2.45793	-2.62824	-1.11690	H	4.62489	5.52469	2.42725
C	3.18543	-3.50580	-0.32076	H	2.19773	5.17155	2.95670
C	2.95289	-2.02300	1.53587	H	1.18220	4.42699	1.84687
O	4.23444	-4.05214	1.78220	H	0.57369	5.42921	-0.69841
C	3.51320	-5.06968	2.49359	H	-2.59410	2.68562	-0.48152
Br	3.28742	-1.59571	3.36668	H	-3.18291	3.20660	2.09051
Br	3.84060	-5.13073	-1.07351	H	-1.90976	3.86597	2.96279
C	4.80364	3.64499	-1.78076				
C	4.40968	4.11703	-0.41142				
C	5.17379	4.82033	0.47310				
N	4.36240	5.03801	1.58499				
C	3.15043	4.46089	1.33159				
N	3.14014	3.88468	0.13479				

Table 4.12: Cartesian Coordinates and Relative Energies of Optimized Conformers of **4.5a** and **4.5b** ($\Delta E < 8$ kJ/mol) Continued.

Conf. 41				N	3.98016	-3.26583	-2.64030
				C	4.32971	3.47155	-0.82260
ΔG (298 K) = -12338.195752 Hartree				C	4.87744	4.69887	-1.08584
O	-4.98642	-2.78927	-0.46974	N	4.10932	5.72528	-0.55913
C	-3.73318	-2.35338	-0.77589	C	3.10899	5.11489	0.03819
C	-1.13047	-1.43485	-1.45338	N	3.16406	3.75302	-0.10262
C	-2.58781	-3.10119	-0.47149	N	2.11414	5.72395	0.80188
C	-3.53571	-1.14256	-1.45278	H	0.80740	-1.10312	1.34789
C	-2.26564	-0.68627	-1.78789	H	-2.16254	0.26662	-2.29483
C	-1.30931	-2.66422	-0.80437	H	-0.45158	-3.26736	-0.53838
Br	-2.79596	-4.76967	0.43112	H	-5.27883	-1.33481	1.00940
Br	-5.06467	-0.09670	-1.90791	H	-4.91255	-2.98170	1.61014
C	-5.43788	-2.40473	0.84171	H	-6.50398	-2.63309	0.87311
C	0.24153	-0.89935	-1.81931	H	0.65209	-1.44306	-2.67976
C	1.32977	-0.95922	-0.73297	H	0.13796	0.13608	-2.15515
C	1.05621	-0.30022	0.65140	H	5.18149	0.09628	-0.60407
C	2.62661	-0.28303	-1.21737	H	4.85686	1.24038	0.71305
N	3.17549	0.42599	-0.20323	H	5.78580	2.14695	-1.55793
C	2.44307	0.32770	1.07206	H	4.19711	1.82386	-2.21046
O	3.11041	-0.44684	-2.33817	H	3.04263	-2.19455	1.01086
C	4.55577	0.93865	-0.29274	H	4.53451	-2.17466	3.58872
C	4.72419	2.10368	-1.29007	H	3.86109	-3.62697	2.82314
C	3.27356	-0.51575	2.11234	H	2.13977	-2.69288	-1.23773
N	3.41154	-1.82594	1.88635	H	2.87602	1.52639	2.47078
O	3.76811	0.10343	3.06311	H	-1.25318	-0.48551	2.05798
C	4.34660	-2.66440	2.63151	H	0.80611	2.17110	-0.63786
O	1.68376	-2.33169	-0.45565	H	-5.11213	3.94976	0.25194
O	2.30613	1.58152	1.66513	H	-4.64405	2.26924	-0.14875
C	-0.07957	0.70762	0.69525	H	-3.91935	3.64062	-1.04285
C	-2.25420	2.53175	0.82323	H	6.30894	-3.54901	2.49072
C	-1.19919	0.43359	1.48566	H	6.19836	-1.93296	1.79020
C	-0.05131	1.90535	-0.03106	H	6.27472	-5.59092	0.49907
C	-1.11683	2.79384	0.04494	H	5.29475	-5.58201	-1.86782
C	-2.26700	1.32509	1.53430	H	4.28362	-3.72423	-3.49083
O	-3.27295	3.42586	0.93446	H	3.88149	-2.25699	-2.76324
C	-4.29560	3.30307	-0.07132	H	5.77347	4.90886	-1.65525
Br	-3.79680	0.90370	2.59025	H	2.67983	3.09044	0.49745
Br	-1.02587	4.43519	-0.92673	H	1.17617	5.44278	0.53093
C	5.67931	-2.89449	1.87799	H	2.21122	6.73079	0.74069
C	5.48119	-3.49234	0.51845				
C	5.77242	-4.74584	0.05570				
N	5.28334	-4.78344	-1.25280				
C	4.71957	-3.56554	-1.50288				
N	4.83427	-2.75848	-0.46937				

Table 4.12: Cartesian Coordinates and Relative Energies of Optimized Conformers of **4.5a** and **4.5b** ($\Delta E < 8$ kJ/mol) Continued.

Conf. 3				N	3.97916	-3.26652	-2.64052
				C	4.33013	3.47121	-0.82282
ΔG (298 K) =				C	4.87779	4.69853	-1.08635
-12338.195743				N	4.10971	5.72496	-0.55963
Hartree				C	3.10950	5.11462	0.03792
O	-4.98673	-2.78851	-0.47004	N	3.16460	3.75273	-0.10273
C	-3.73337	-2.35283	-0.77603	N	2.11471	5.72375	0.80172
C	-1.13052	-1.43458	-1.45333	H	0.80772	-1.10314	1.34791
C	-2.58809	-3.10055	-0.47116	H	-2.16237	0.26662	-2.29557
C	-3.53575	-1.14223	-1.45329	H	-0.45184	-3.26679	-0.53760
C	-2.26561	-0.68608	-1.78831	H	-4.91294	-2.98104	1.60985
C	-1.30951	-2.66372	-0.80394	H	-6.50434	-2.63243	0.87276
Br	-2.79638	-4.76879	0.43187	H	-5.27920	-1.33413	1.00914
Br	-5.06459	-0.09651	-1.90906	H	0.65199	-1.44296	-2.67976
C	-5.43824	-2.40405	0.84142	H	0.13807	0.13621	-2.15509
C	0.24155	-0.89923	-1.81926	H	5.18166	0.09589	-0.60414
C	1.32989	-0.95919	-0.73302	H	4.85718	1.24001	0.71298
C	1.05646	-0.30021	0.65142	H	5.78637	2.14656	-1.55776
C	2.62669	-0.28300	-1.21749	H	4.19783	1.82346	-2.21064
N	3.17570	0.42594	-0.20335	H	3.04293	-2.19464	1.01069
C	2.44333	0.32765	1.07193	H	4.53550	-2.17414	3.58819
O	3.11043	-0.44677	-2.33831	H	3.86169	-3.62673	2.82349
C	4.55605	0.93834	-0.29283	H	2.13918	-2.69305	-1.23817
C	4.72470	2.10333	-1.29014	H	2.87642	1.52635	2.47062
C	3.27379	-0.51582	2.11219	H	-1.25277	-0.48567	2.05818
N	3.41182	-1.82601	1.88618	H	0.80618	2.17125	-0.63760
O	3.76830	0.10334	3.06299	H	-5.11187	3.94990	0.25232
C	4.34717	-2.66426	2.63126	H	-4.64372	2.26958	-0.14914
O	1.68388	-2.33164	-0.45578	H	-3.91872	3.64145	-1.04228
O	2.30648	1.58150	1.66500	H	6.30939	-3.54901	2.48997
C	-0.07935	0.70761	0.69542	H	6.19859	-1.93320	1.78889
C	-2.25408	2.53160	0.82367	H	6.27191	-5.59243	0.49954
C	-1.19889	0.43346	1.48589	H	5.29140	-5.58362	-1.86713
C	-0.05121	1.90538	-0.03081	H	4.28278	-3.72483	-3.49107
C	-1.11678	2.79381	0.04534	H	3.88092	-2.25763	-2.76350
C	-2.26675	1.32488	1.53467	H	5.77376	4.90845	-1.65589
O	-3.27293	3.42557	0.93513	H	2.68033	3.09016	0.49733
C	-4.29526	3.30337	-0.07106	H	1.17670	5.44287	0.53053
Br	-3.79644	0.90335	2.59072	H	2.21198	6.73058	0.74059
Br	-1.02585	4.43530	-0.92610				
C	5.67955	-2.89468	1.87727				
C	5.48078	-3.49295	0.51803				
C	5.77035	-4.74706	0.05588				
N	5.28092	-4.78477	-1.25245				
C	4.71865	-3.56631	-1.50310				
N	4.83453	-2.75881	-0.47006				

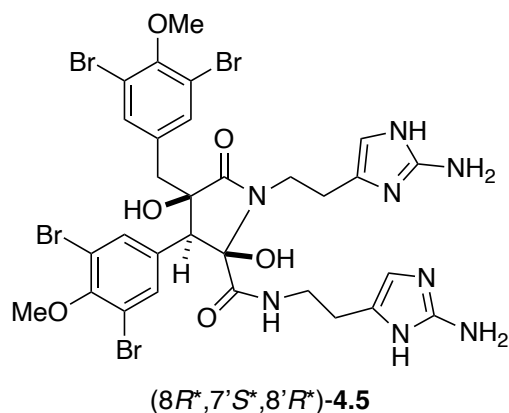
Table 4.12: Cartesian Coordinates and Relative Energies of Optimized Conformers of **4.5a** and **4.5b** ($\Delta E < 8$ kJ/mol) Continued.

Conf. 36				N	1.51582	4.48285	2.37431
				C	-1.71289	3.73203	-1.03911
ΔG (298 K) =	-12338.195680 Hartree			C	-0.76360	4.37410	-0.29831
O	-6.51445	-1.42829	0.28983	N	-1.16205	4.51418	1.02703
C	-5.15375	-1.34030	0.26736	C	-2.36786	3.98105	1.08085
C	-2.32880	-1.10211	0.10045	N	-2.75554	3.49695	-0.13657
C	-4.49970	-0.12882	0.51862	N	-3.20329	3.95923	2.18680
C	-4.34227	-2.43632	-0.06394	H	1.48313	-0.72898	-2.55948
C	-2.95777	-2.32769	-0.15105	H	-2.36583	-3.19250	-0.42537
C	-3.11881	-0.00165	0.44602	H	-2.64979	0.95506	0.64238
Br	-5.56142	1.41048	0.95176	H	-6.82070	-1.10601	2.33385
Br	-5.17418	-4.11727	-0.40851	H	-6.71815	-2.82783	1.83124
C	-7.07165	-1.83034	1.55087	H	-8.15274	-1.85296	1.40780
C	-0.82949	-0.94568	0.00136	H	-0.51799	-0.04885	0.54275
C	-0.28853	-0.86974	-1.45053	H	-0.33423	-1.80332	0.46758
C	1.21248	-0.48447	-1.52720	H	-0.47956	2.38242	-3.98446
C	-0.90172	0.28780	-2.25008	H	0.41419	3.30039	-2.78821
N	-0.07783	1.36613	-2.20490	H	-1.93710	4.08508	-3.14934
C	1.18471	1.08495	-1.49935	H	-2.54551	2.53277	-2.60099
O	-1.95816	0.18668	-2.86826	H	3.35165	1.71862	-0.51345
C	-0.41573	2.60655	-2.91535	H	5.48256	2.41835	-1.34671
C	-1.73743	3.25512	-2.45734	H	4.78985	2.50889	-2.97769
C	2.40580	1.63773	-2.28834	H	-1.34317	-1.90168	-2.67015
N	3.50437	1.81236	-1.50818	H	1.45231	2.51891	-0.13976
O	2.36569	1.85367	-3.49381	H	1.87876	-0.10555	1.18955
C	4.59071	2.68937	-1.91924	H	2.73057	-2.56589	-2.23493
O	-0.55176	-2.08094	-2.13136	H	3.97396	-5.35180	1.61978
O	1.18541	1.56830	-0.17600	H	3.60625	-4.33772	3.05782
C	2.18109	-1.22841	-0.63111	H	5.22143	-5.07462	2.86666
C	3.98558	-2.77982	0.92774	H	3.42378	4.43487	-2.38967
C	2.38904	-0.93723	0.72566	H	5.09750	4.78905	-1.97225
C	2.87728	-2.30851	-1.19232	H	5.48820	5.69374	0.60693
C	3.75588	-3.06486	-0.42492	H	3.91165	5.75985	2.62616
C	3.27626	-1.70306	1.47594	H	1.52896	5.15988	3.12563
O	4.90052	-3.47729	1.65896	H	0.57443	4.40798	1.96621
C	4.37769	-4.62981	2.33735	H	0.21255	4.71146	-0.61358
Br	3.54267	-1.27659	3.31829	H	-3.64646	3.06411	-0.33844
Br	4.68549	-4.52303	-1.22843	H	-2.69792	4.14036	3.04368
C	4.23214	4.17611	-1.69586	H	-3.79916	3.14156	2.25066
C	3.81572	4.51493	-0.29411				
C	4.51691	5.22624	0.63484				
N	3.69386	5.29770	1.75772				
C	2.53644	4.63385	1.46580				
N	2.57644	4.13284	0.23578				

Table 4.12: Cartesian Coordinates and Relative Energies of Optimized Conformers of **4.5a** and **4.5b** ($\Delta E < 8$ kJ/mol) Continued.

Conf. 23				N	3.60748	-3.88380	-2.23132
				C	4.69147	2.88226	-1.15749
ΔG (298 K) =	-12338.195018 Hartree			C	5.38501	3.99315	-1.55820
O	-5.17041	-2.67628	-0.13107	N	4.73941	5.16129	-1.18398
C	-3.93565	-2.29457	-0.56448	C	3.66740	4.75343	-0.54086
C	-1.31885	-1.47608	-1.31096	N	3.56115	3.38774	-0.50728
C	-3.65415	-0.96424	-0.90243	N	2.73801	5.56741	0.10771
C	-2.87145	-3.20526	-0.63153	H	0.61011	-0.91546	1.47929
C	-1.58559	-2.81389	-0.99022	H	-0.79230	-3.54911	-1.00418
C	-2.37723	-0.56160	-1.28037	H	-2.20742	0.47901	-1.53041
Br	-5.04153	0.33572	-0.80338	H	-6.26123	-2.24255	-1.86205
Br	-3.20636	-5.03638	-0.20917	H	-7.01011	-3.33886	-0.66847
C	-6.07906	-3.07142	-1.16997	H	-5.69206	-3.94117	-1.71178
C	0.07055	-1.01123	-1.69963	H	0.46489	-1.62087	-2.52134
C	1.14428	-1.07090	-0.59531	H	0.01663	0.00954	-2.08675
C	0.95886	-0.23091	0.70370	H	5.09973	-0.52315	-0.51488
C	2.51618	-0.62372	-1.13531	H	4.92487	0.80458	0.64903
N	3.15395	0.11706	-0.19906	H	5.98363	1.30900	-1.68127
C	2.41586	0.25583	1.06933	H	4.37718	1.10575	-2.34010
O	2.97434	-0.97739	-2.22261	H	2.64633	-2.31387	1.31363
C	4.59135	0.42641	-0.31999	H	4.12176	-2.21546	3.89858
C	4.92064	1.42942	-1.44404	H	3.29809	-3.64529	3.24570
C	3.13140	-0.56687	2.20563	H	1.77616	-2.92189	-0.87183
N	3.07763	-1.90066	2.13961	H	3.01523	1.53968	2.32318
O	3.72247	0.08414	3.07711	H	-1.32683	0.04340	2.12664
C	3.89599	-2.76650	2.98366	H	1.00324	2.09429	-0.86264
O	1.32503	-2.43517	-0.15943	H	-3.62082	5.72294	1.12894
O	2.44477	1.57612	1.51711	H	-1.84035	5.58751	1.10927
C	-0.03618	0.91459	0.63275	H	-2.79962	4.73145	2.36658
C	-1.97835	2.98528	0.53606	H	5.75218	-3.86445	2.98718
C	-1.16839	0.87633	1.45097	H	5.82952	-2.32447	2.13000
C	0.12904	2.00792	-0.22826	H	5.58679	-6.07027	1.20648
C	-0.82200	3.02096	-0.25738	H	4.67463	-6.21412	-1.18380
C	-2.12239	1.88931	1.39580	H	3.91336	-4.43677	-3.02257
O	-2.93990	3.94325	0.43396	H	3.58710	-2.88618	-2.44610
C	-2.77621	5.06076	1.32273	H	6.30528	4.02240	-2.12685
Br	-3.67590	1.77317	2.48399	H	2.99783	2.86901	0.16154
Br	-0.55405	4.51817	-1.41171	H	1.78118	5.36924	-0.17209
C	5.20806	-3.21246	2.29490	H	2.96137	6.53906	-0.07514
C	4.97727	-3.92179	0.99530				
C	5.17173	-5.23453	0.66580				
N	4.72076	-5.35984	-0.65080				
C	4.27299	-4.12964	-1.03800				
N	4.42473	-3.23699	-0.08173				

Table 4.12: Cartesian Coordinates and Relative Energies of Optimized Conformers of **4.5a** and **4.5b** ($\Delta E < 8$ kJ/mol) Continued.



Conf. 11

ΔG (298 K) = -12338.198431 Hartree

O	4.39791	-2.39544	-1.03940
C	3.35314	-1.66921	-1.53415
C	1.17932	-0.06071	-2.39935
C	2.03584	-2.14801	-1.50677
C	3.54303	-0.37382	-2.02986
C	2.49427	0.41891	-2.46996
C	0.96392	-1.35759	-1.91923
C	5.02840	-3.27357	-1.98900
Br	5.31864	0.34816	-2.08122
Br	1.71542	-3.91555	-0.88606
C	0.03754	0.81390	-2.86583
C	-0.48671	1.86278	-1.87281
C	-1.11255	1.33619	-0.55708
C	-1.09656	2.65434	0.29334
C	0.59584	2.82489	-1.30626
N	0.23887	3.15910	-0.01294
O	-1.38684	2.66058	-2.64114
C	-2.41687	0.57287	-0.56108
C	-4.83553	-0.90228	-0.37229
C	-2.53118	-0.51329	0.32000
C	-3.52022	0.91114	-1.35619
C	-4.69875	0.17742	-1.25633
C	-3.72189	-1.22427	0.41566
O	-5.97692	-1.64409	-0.32524
C	-6.95349	-1.18893	0.62525
Br	-3.84557	-2.67444	1.64725
Br	-6.18348	0.65286	-2.35496
C	-1.41430	2.41710	1.79176
O	-2.07013	3.57479	-0.15897

N	-0.53724	1.74794	2.55025
O	-2.51215	2.81019	2.20093
O	1.56244	3.26876	-1.90944
C	0.77377	4.35350	0.65227
C	2.31091	4.37482	0.79043
C	2.92576	3.19841	1.48763
C	2.98533	2.81648	2.80192
N	3.73014	1.65703	2.96241
C	4.13982	1.34695	1.74702
N	3.68029	2.23039	0.81477
N	4.88071	0.21028	1.43954
C	-0.90597	1.30294	3.89748
C	0.21926	0.48443	4.54003
C	0.65557	-0.69130	3.71626
C	0.00579	-1.77697	3.18161
N	0.87494	-2.58167	2.46638
C	2.05319	-1.99385	2.57758
N	1.98510	-0.85034	3.32432
N	3.25230	-2.47266	2.07178
H	-0.35958	0.68120	-0.10544
H	2.68166	1.41857	-2.84121
H	-0.04050	-1.76331	-1.86556
H	5.82486	-3.78179	-1.44416
H	5.45693	-2.69912	-2.81703
H	4.31204	-4.01041	-2.36438
H	0.34570	1.37842	-3.75061
H	-0.81900	0.20004	-3.15993
H	-1.82911	3.27427	-2.02671
H	-1.69182	-0.80572	0.94295
H	-3.45702	1.72129	-2.06753
H	-7.28743	-0.17507	0.38100
H	-7.79367	-1.87976	0.54495
H	-6.54773	-1.22122	1.64180
H	-2.73943	3.59123	0.56239
H	0.34345	1.43980	2.15876
H	0.31787	4.39447	1.64459
H	0.45646	5.25092	0.10746
H	2.74680	4.48027	-0.20434
H	2.55522	5.28989	1.34322
H	2.55053	3.32017	3.65433
H	3.85753	2.19649	-0.17997
H	5.54414	-0.01476	2.17128
H	5.30580	0.20438	0.51900
H	-1.14610	2.17880	4.50960

Table 4.12: Cartesian Coordinates and Relative Energies of Optimized Conformers of **4.5a** and **4.5b** ($\Delta E < 8$ kJ/mol) Continued.

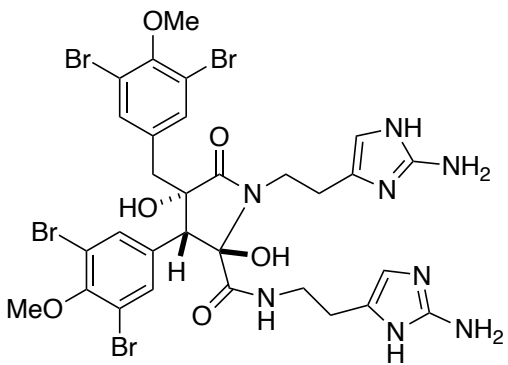
Conf. 11				C	-3.93302	0.45343	-1.30322
ΔG (298 K) = -12338.198431 Hartree				C	-2.46449	-0.73429	0.19446
H	-1.82162	0.70616	3.82439	C	-3.56653	-1.41673	0.70417
H	-0.13533	0.16983	5.52982	C	-5.01976	-0.23184	-0.77447
H	1.08247	1.13514	4.72131	O	-5.92601	-1.91274	0.69887
H	-1.04468	-2.02901	3.25399	C	-6.60787	-1.33636	1.82435
H	2.72935	-0.17316	3.48286	Br	-6.76755	0.12265	-1.44817
H	3.08270	-3.18435	1.37127	Br	-3.29772	-2.70220	2.08740
H	3.85381	-1.73788	1.70475	C	-1.75976	3.02794	0.30850
 <p style="text-align: center;">(8<i>S</i>[*], 7'<i>R</i>[*], 8'<i>R</i>[*])-4.5</p>				O	-2.45882	3.17865	-1.94837
				O	1.88979	1.92058	-2.10187
				C	0.18175	4.25354	-2.08181
				C	0.54813	5.29578	-1.01306
				C	1.81759	5.04382	-0.25467
				C	2.28884	5.55852	0.92355
				N	3.58871	5.13523	1.17522
				C	3.88963	4.37436	0.14375
				N	2.87556	4.28550	-0.76365
				N	5.07911	3.64599	0.01413
				N	-1.05669	2.44789	1.28101
				O	-2.56910	3.95578	0.44921
				C	-1.12106	2.81224	2.69205
				C	0.28371	3.09506	3.26715
				C	1.27664	2.01699	2.93428
				C	1.18926	0.65219	2.85685
				N	2.32972	0.09830	2.28978
				C	3.13066	1.13078	2.06540
				N	2.54658	2.31160	2.42996
				N	4.42526	1.05839	1.59413
H	-1.69663	0.99850	-2.54252				
H	2.99765	-0.17949	-1.88109				
H	-0.00248	-3.22702	-1.41123				
H	5.25980	-4.97191	1.37450				
H	3.55722	-4.53932	1.70034				
H	4.79768	-3.25296	1.52940				
H	0.59286	-0.27078	-3.23071				
H	-0.61524	-1.23219	-2.38683				
H	1.16918	0.04090	0.21338				
H	-4.09255	1.18625	-2.08481				
H	-1.48103	-0.94151	0.59015				
H	-5.93261	-1.24915	2.68198				
H	-7.41893	-2.02406	2.06685				
H	-7.02290	-0.35668	1.56538				
H	-2.89398	3.80036	-1.31689				
Conf. 26							
ΔG (298 K) = -12338.200246 Hartree							
O	4.27717	-4.23832	-0.24164				
C	3.32538	-3.37209	-0.68487				
C	1.37300	-1.59037	-1.71656				
C	1.98676	-3.76062	-0.82849				
C	3.65084	-2.06507	-1.07237				
C	2.70852	-1.18345	-1.59060				
C	1.02431	-2.88839	-1.32807				
C	4.47437	-4.23966	1.18380				
Br	1.48021	-5.52388	-0.31873				
Br	5.45883	-1.48665	-0.86335				
C	0.30363	-0.65547	-2.24677				
C	-0.03292	0.55533	-1.33041				
C	0.70989	1.85523	-1.73800				
N	-0.13063	2.90895	-1.60030				
C	-1.50381	2.53981	-1.16860				
C	-1.50629	1.00561	-1.46162				
O	0.24314	0.29503	0.04294				
C	-2.63584	0.21347	-0.82211				
C	-4.86727	-1.19069	0.23776				

Table 4.12: Cartesian Coordinates and Relative Energies of Optimized Conformers of **4.5a** and **4.5b** ($\Delta E < 8$ kJ/mol) Continued.

Conf. 26				C	1.56382	0.20211	1.60237
ΔG (298 K) = -12338.200246 Hartree				C	2.63236	-1.87704	1.12056
H	-0.70080	4.60056	-2.62400	O	3.74780	-0.25405	2.51542
H	0.99410	4.14365	-2.80551	C	3.68703	-0.58298	3.91276
H	0.61994	6.25433	-1.54774	Br	4.12775	-3.04246	1.27786
H	-0.28202	5.40851	-0.30845	Br	1.55224	1.90922	2.45554
H	1.78557	6.23909	1.59658	C	-2.27915	-2.25189	1.20454
H	2.76543	3.54097	-1.45552	O	-1.35561	-3.98875	-0.11202
H	5.43792	3.62222	-0.93469	O	-3.36436	-1.18617	-3.05170
H	5.77909	4.02513	0.64377	C	-3.94697	-3.46231	-1.35292
H	-0.43530	1.67630	1.03264	C	-5.12237	-3.25593	-0.36812
H	-1.76573	3.68802	2.78573	C	-5.61456	-1.84708	-0.26671
H	-1.59220	1.99130	3.24654	C	-6.02523	-1.09147	0.79478
H	0.18163	3.24492	4.35054	N	-6.28611	0.22152	0.41666
H	0.64713	4.04126	2.85168	C	-6.04561	0.24814	-0.88750
H	0.35413	0.02439	3.13779	N	-5.67687	-0.97918	-1.36076
H	2.95696	3.23567	2.34010	N	-6.18242	1.34343	-1.71402
H	4.70629	1.82813	0.98678	N	-2.57994	-0.96836	1.42279
H	4.62929	0.15794	1.17856	O	-2.38024	-3.15584	2.04432
Conf. 23				C	-3.10002	-0.48851	2.69804
ΔG (298 K) = -12338.198555 Hartree				C	-2.66380	0.95524	2.99233
O	4.41179	2.01801	-1.35002	C	-3.02651	1.97690	1.95658
C	3.23983	1.45080	-1.74230	C	-2.25731	2.94894	1.36687
C	0.80065	0.31899	-2.65760	N	-3.01816	3.77755	0.55927
C	2.04186	2.18291	-1.73957	C	-4.23679	3.29635	0.66080
C	3.17664	0.13393	-2.21989	N	-4.32566	2.21743	1.49290
C	1.98747	-0.42010	-2.68442	N	-5.35395	3.77333	-0.04927
C	0.84498	1.63923	-2.19503	H	-0.15853	-2.51534	-1.53024
C	4.76348	1.82395	0.03435	H	1.98803	-1.44614	-3.03599
Br	2.05029	3.95092	-1.03434	H	-0.05602	2.23844	-2.14723
Br	4.74262	-0.94945	-2.16622	H	5.64563	2.44290	0.20276
C	-0.51542	-0.34426	-3.00367	H	5.00455	0.77554	0.22957
C	-1.31957	-0.78182	-1.76028	H	3.95463	2.14752	0.69470
C	-2.61496	-1.52911	-2.13292	H	-1.16051	0.32128	-3.58868
N	-2.83225	-2.52095	-1.23596	H	-0.34079	-1.22571	-3.62974
C	-1.76286	-2.66628	-0.21973	H	-2.34637	0.89047	-1.55531
C	-0.61523	-1.79985	-0.83760	H	1.58204	-3.20211	-0.19134
O	-1.74403	0.36782	-1.00480	H	-0.29944	0.57837	0.63670
C	0.48411	-1.36776	0.11678	H	2.83163	-0.08989	4.38635
C	2.66222	-0.64570	1.78903	H	4.61330	-0.20858	4.35027
C	1.56184	-2.24198	0.31103	H	3.62750	-1.66751	4.05134
C	0.49520	-0.13614	0.78231	H	-1.62599	-4.24486	0.80019
				H	-3.53730	-4.46737	-1.22323
				H	-4.29856	-3.37484	-2.38422

Table 4.12: Cartesian Coordinates and Relative Energies of Optimized Conformers of **4.5a** and **4.5b** ($\Delta E < 8$ kJ/mol) Continued.

Conf. 23				O	3.64861	-0.56663	2.68265
ΔG (298 K) = -12338.198555 Hartree				C	4.72295	0.16859	2.06150
H	-5.91393	-3.94484	-0.69872	Br	1.59115	1.76285	2.51770
H	-4.82738	-3.58524	0.63280	Br	3.94460	-3.31575	1.35333
H	-6.15863	-1.41459	1.81798	C	-2.43191	-2.27458	1.14842
H	-5.21466	-1.13773	-2.25228	O	-1.52905	-3.99923	-0.19771
H	-5.66151	1.28253	-2.57910	O	-3.34370	-1.03225	-3.10219
H	-6.03901	2.23440	-1.23305	C	-4.06027	-3.33957	-1.49605
H	-2.50001	-0.30756	0.65224	C	-5.25627	-3.12108	-0.53896
H	-4.19419	-0.55792	2.69134	C	-5.69771	-1.69834	-0.40388
H	-2.73910	-1.16223	3.47822	C	-6.10793	-0.96182	0.67106
H	-1.57646	0.99596	3.12018	N	-6.30851	0.37171	0.32996
H	-3.10248	1.22521	3.96349	C	-6.03141	0.43102	-0.96562
H	-1.19574	3.10674	1.50108	N	-5.69705	-0.79385	-1.46981
H	-5.11196	1.55814	1.45578	N	-6.10323	1.55750	-1.75849
H	-6.15255	3.94738	0.55515	N	-2.67537	-0.98694	1.40802
H	-5.09359	4.63433	-0.52050	O	-2.61020	-3.20451	1.94576
Conf. 21				C	-3.21531	-0.53074	2.68370
ΔG (298 K) = -12338.198266 Hartree				C	-2.73589	0.88568	3.03642
O	4.37136	1.87816	-0.85392	C	-3.03164	1.95276	2.02538
C	3.24178	1.40198	-1.45265	C	-2.21155	2.91561	1.49211
C	0.83930	0.34432	-2.52184	N	-2.91805	3.79661	0.68995
C	2.06581	2.16357	-1.49878	C	-4.15495	3.35544	0.73860
C	3.18625	0.10374	-1.97539	N	-4.30650	2.25379	1.53058
C	2.01335	-0.41638	-2.51343	N	-5.23301	3.89515	0.01215
C	0.88393	1.65308	-2.02627	H	-0.24261	-2.52631	-1.53265
C	5.27915	2.55681	-1.73633	H	2.01158	-1.43411	-2.88773
Br	2.08124	3.91053	-0.74732	H	-0.00864	2.26610	-2.00520
Br	4.73502	-1.00047	-1.86269	H	6.11948	2.87410	-1.11757
C	-0.47283	-0.28827	-2.93565	H	4.79988	3.43507	-2.18128
C	-1.32996	-0.74376	-1.73374	H	5.63536	1.87851	-2.51883
C	-2.63701	-1.43295	-2.17239	H	-1.08460	0.40444	-3.52470
N	-2.91693	-2.44373	-1.31612	H	-0.28834	-1.15534	-3.57863
C	-1.88470	-2.65986	-0.27222	H	-2.33291	0.93846	-1.49692
C	-0.68975	-1.81703	-0.82697	H	-0.29652	0.51655	0.69876
O	-1.74142	0.39495	-0.95475	H	1.41440	-3.34066	-0.14200
C	0.40407	-1.45598	0.16287	H	5.05669	-0.32946	1.14694
C	2.60208	-0.84421	1.86022	H	5.53050	0.18683	2.79451
C	0.46577	-0.23326	0.84047	H	4.40567	1.18779	1.82482
C	1.43549	-2.38255	0.36446	H	-1.84276	-4.27658	0.69435
C	2.51410	-2.07129	1.18536	H	-3.69019	-4.36221	-1.38647
C	1.54558	0.05580	1.66585	H	-4.37734	-3.20766	-2.53382
				H	-6.06293	-3.76776	-0.91514
				H	-5.00307	-3.49373	0.45810

Table 4.12: Cartesian Coordinates and Relative Energies of Optimized Conformers of **4.5a** and **4.5b** ($\Delta E < 8$ kJ/mol) Continued.

Conf. 21				Br	2.77835	0.37458	2.29934
ΔG (298 K) = -12338.198266 Hartree				Br	4.31613	-4.17890	-0.77089
H	-6.28019	-1.31208	1.67937	C	-1.53078	-3.18899	0.47008
H	-5.21756	-0.94172	-2.35388	O	-1.12189	-4.12839	-1.66174
H	-5.56079	1.50390	-2.61074	O	-3.51129	-0.50620	-2.71778
H	-5.93761	2.42549	-1.24353	C	-3.88107	-3.21787	-1.84760
H	-2.53513	-0.30183	0.66808	C	-4.82650	-3.34916	-0.63571
H	-4.31069	-0.56074	2.64474	C	-5.24926	-2.06078	0.00229
H	-2.90049	-1.24100	3.45140	C	-5.54672	-1.75405	1.30147
H	-1.65185	0.88028	3.19411	N	-5.88916	-0.41410	1.43857
H	-3.19068	1.14123	4.00392	C	-5.80476	0.07304	0.21650
H	-1.14991	3.03043	1.66408	N	-5.44941	-0.86876	-0.70178
H	-5.11476	1.62593	1.45026	N	-5.95598	1.43136	-0.09531
H	-6.04298	4.07685	0.59902	N	-1.72915	-2.16361	1.30751
H	-4.92863	4.76254	-0.41930	O	-1.39438	-4.36822	0.82162
Conf. 7				C	-1.53090	-2.30799	2.75329
ΔG (298 K) = -12338.197991 Hartree				C	-2.30639	-1.25332	3.57425
O	2.07653	4.55916	-0.08531	C	-2.10930	0.13672	3.05266
C	1.44704	3.61605	-0.83610	C	-1.06108	1.02171	3.07412
C	0.09807	1.58860	-2.28958	N	-1.26896	2.07006	2.19070
C	2.11499	2.46633	-1.28450	C	-2.43639	1.81355	1.63811
C	0.10466	3.75196	-1.21001	N	-3.00222	0.67167	2.12275
C	-0.56032	2.76898	-1.93192	N	-2.94598	2.45524	0.50458
C	1.46075	1.46794	-1.99972	H	-0.14961	-2.16491	-2.53071
C	1.92625	4.33970	1.33538	H	-1.60857	2.90321	-2.17297
Br	3.95634	2.25000	-0.84413	H	2.00806	0.57823	-2.28766
Br	-0.85916	5.30383	-0.65547	H	2.46422	5.15543	1.81975
C	-0.70698	0.44139	-2.85657	H	2.36142	3.37735	1.62154
C	-1.23753	-0.53223	-1.76264	H	0.86941	4.35760	1.61787
C	-2.60971	-1.12786	-2.14616	H	-1.58447	0.83529	-3.37981
N	-2.70277	-2.38109	-1.64098	H	-0.12581	-0.12904	-3.58816
C	-1.44141	-2.90662	-1.07749	H	-2.00604	0.92738	-0.59230
C	-0.40641	-1.81212	-1.52577	H	0.47545	-0.07774	0.53212
O	-1.46451	0.11292	-0.51213	H	1.63076	-3.51647	-1.78800
C	0.88825	-1.78696	-0.72921	H	5.95568	-1.73479	-0.15761
C	3.36446	-1.89164	0.65989	H	6.43022	-1.24634	1.49489
C	1.17954	-0.85732	0.27970	H	5.33694	-0.20257	0.53961
C	1.83859	-2.77539	-1.02491	H	-1.12494	-4.75742	-0.90180
C	3.04797	-2.82183	-0.33950	H	-3.52950	-4.20950	-2.14307
C	2.39941	-0.91627	0.94633	H	-4.41406	-2.78449	-2.69825
O	4.53243	-1.95389	1.35705	H	-5.69872	-3.91749	-0.99058
C	5.62507	-1.23535	0.75919	H	-4.35573	-3.96784	0.13494
				H	-5.54403	-2.41872	2.15406
				H	-5.06391	-0.67779	-1.62946

Table 4.12: Cartesian Coordinates and Relative Energies of Optimized Conformers of **4.5a** and **4.5b** ($\Delta E < 8$ kJ/mol) Continued.

Conf. 7				C	-2.24334	-2.43119	0.53757
ΔG (298 K) = -12338.197991 Hartree				O	-1.50318	-3.39394	-1.49561
H	-6.30420	1.59374	-1.03402	O	-3.41859	0.56636	-2.60414
H	-6.56790	1.87049	0.58495	C	-4.03074	-2.24804	-2.23026
H	-1.75030	-1.22386	0.91303	C	-5.21674	-2.48293	-1.27905
H	-1.83133	-3.32026	3.03200	C	-5.96150	-1.25846	-0.83368
H	-0.45936	-2.21013	2.97028	C	-6.82833	-1.05023	0.20626
H	-1.96292	-1.33156	4.61125	N	-7.37630	0.22658	0.15826
H	-3.37411	-1.49855	3.57465	C	-6.83825	0.77195	-0.91279
H	-0.14092	0.94631	3.63664	N	-5.98992	-0.07000	-1.56766
H	-3.94601	0.33071	1.94726	N	-7.02479	2.10453	-1.30710
H	-3.95968	2.41930	0.40292	N	-2.44589	-1.37403	1.32563
H	-2.56495	3.39125	0.40606	O	-2.41621	-3.61642	0.85250
Conf. 2				C	-2.89386	-1.43823	2.71240
ΔG (298 K) = -12338.197785 Hartree				C	-4.09962	-0.50664	2.95834
O	4.70436	2.59368	-0.71016	C	-3.87813	0.88165	2.42685
C	3.45358	2.24757	-1.11816	C	-2.78372	1.70499	2.38573
C	0.82943	1.59226	-1.98107	N	-3.01486	2.81823	1.58810
C	3.23337	1.39068	-2.20511	C	-4.27250	2.69286	1.18951
C	2.31809	2.79106	-0.49598	N	-4.84021	1.54247	1.65893
C	1.02938	2.48835	-0.92293	N	-4.97763	3.62886	0.45757
C	1.94896	1.06005	-2.62836	H	-0.27221	-1.47004	-2.18199
C	5.32879	1.66268	0.19550	H	0.18599	2.92753	-0.40371
Br	4.73258	0.66361	-3.13175	H	1.82844	0.38165	-3.46602
Br	2.55670	3.95998	0.98592	H	6.22834	2.16091	0.55907
C	-0.56220	1.17380	-2.40240	H	5.60333	0.74242	-0.32963
C	-1.28202	0.22033	-1.42465	H	4.66932	1.42834	1.03602
C	-2.65801	-0.19601	-1.99984	H	-1.21597	2.04541	-2.52331
N	-2.90071	-1.49197	-1.69322	H	-0.52160	0.69062	-3.38436
C	-1.80022	-2.15319	-0.94803	H	-2.06462	1.64455	-0.21296
C	-0.61548	-1.15795	-1.18857	H	0.32413	0.43482	0.95356
O	-1.50744	0.84686	-0.15994	H	1.11654	-3.19148	-1.21803
C	0.56923	-1.34003	-0.25015	H	3.20310	-2.14252	3.97848
C	2.86950	-1.79703	1.35522	H	4.87190	-2.73008	3.73791
C	0.91450	-0.44951	0.77258	H	3.50184	-3.69248	3.11741
C	1.36908	-2.47691	-0.44391	H	-1.77663	-4.03006	-0.79302
C	2.48626	-2.69977	0.35338	H	-3.63373	-3.21622	-2.54411
C	2.05089	-0.67688	1.54141	H	-4.36014	-1.71799	-3.12842
O	4.02246	-1.96365	2.06304	H	-5.89858	-3.15573	-1.81963
C	3.87434	-2.67899	3.29970	H	-4.87921	-3.04305	-0.40119
Br	2.52815	0.60855	2.86735	H	-7.12168	-1.75252	0.97449
Br	3.54778	-4.25698	0.06627	H	-5.24900	0.22264	-2.21061
				H	-7.10545	2.21680	-2.31261
				H	-7.85031	2.47804	-0.84915

Table 4.12: Cartesian Coordinates and Relative Energies of Optimized Conformers of **4.5a** and **4.5b** ($\Delta E < 8$ kJ/mol) Continued.

Conf. 2				O	-3.46360	0.47067	-3.02421
ΔG (298 K) = -12338.197785 Hartree				C	-4.28092	-2.20467	-2.34488
H	-2.23688	-0.44723	0.95248	C	-5.43670	-2.25193	-1.32578
H	-3.14865	-2.47557	2.93674	C	-5.85272	-0.92942	-0.75707
H	-2.06118	-1.15176	3.36672	C	-6.37651	-0.59331	0.46124
H	-4.31487	-0.50692	4.03531	N	-6.61581	0.77339	0.54775
H	-4.97779	-0.93213	2.46095	C	-6.24185	1.24596	-0.62435
H	-1.81815	1.55049	2.84830	N	-5.79491	0.27371	-1.46714
H	-5.78385	1.21886	1.46805	N	-6.19343	2.61217	-0.94037
H	-5.58224	3.24638	-0.26990	N	-2.59859	-1.37399	1.16319
H	-4.36602	4.36216	0.12414	O	-2.50327	-3.61337	0.72383
Conf. 1				C	-2.68972	-1.50990	2.61937
ΔG (298 K) = -12338.197766 Hartree				C	-3.50032	-0.36981	3.27764
O	4.55994	2.44959	-0.68226	C	-3.09020	0.98127	2.77779
C	3.33738	2.10738	-1.17298	C	-1.98102	1.76944	2.95939
C	0.77634	1.44554	-2.20436	N	-1.93850	2.79847	2.03246
C	3.18821	1.21960	-2.24664	C	-3.01516	2.62898	1.29725
C	2.16565	2.67906	-0.65208	N	-3.76047	1.56104	1.69912
C	0.90832	2.37060	-1.16008	N	-3.24699	3.26407	0.06806
C	1.93479	0.88674	-2.75346	H	-0.38948	-1.61531	-2.32753
C	5.08206	1.55063	0.31518	H	0.03533	2.82068	-0.70415
Br	4.74479	0.44711	-3.03261	H	1.86875	0.18298	-3.57615
Br	2.30557	3.89097	0.80708	H	5.96725	2.04067	0.72271
C	-0.58617	1.02041	-2.70938	H	5.36555	0.59628	-0.14013
C	-1.39327	0.14195	-1.73112	H	4.35335	1.37973	1.11306
C	-2.75080	-0.26818	-2.33714	H	-1.21272	1.89181	-2.93301
N	-3.07501	-1.50997	-1.90268	H	-0.47788	0.47626	-3.65370
C	-2.00539	-2.18484	-1.13740	H	-2.21216	1.67474	-0.72471
C	-0.78010	-1.23244	-1.37780	H	0.95177	-3.26227	-1.21385
O	-1.70885	0.85173	-0.53490	H	0.00859	0.44355	0.76277
C	0.34033	-1.37607	-0.35791	H	2.61932	-2.02464	4.09405
C	2.50113	-1.78255	1.44122	H	4.29450	-2.63667	4.01265
C	1.14653	-2.52059	-0.44812	H	2.96736	-3.61071	3.32109
C	0.60724	-0.44853	0.65711	H	-1.97615	-4.05974	-0.93390
C	1.67500	-0.65478	1.52407	H	-3.98956	-3.22405	-2.60956
C	2.19676	-2.71745	0.44219	H	-4.60265	-1.70043	-3.26025
O	3.59191	-1.92991	2.24613	H	-6.27748	-2.73825	-1.84174
C	3.33625	-2.59401	3.49320	H	-5.16971	-2.91170	-0.49408
Br	3.27070	-4.28583	0.29473	H	-6.60888	-1.25294	1.28564
Br	2.04545	0.66924	2.84703	H	-5.20345	0.42883	-2.28792
C	-2.40340	-2.43226	0.36663	H	-6.37198	2.80409	-1.92063
O	-1.74655	-3.44404	-1.66919	H	-6.85719	3.11640	-0.36098
				H	-2.40769	-0.44803	0.78055
				H	-3.13283	-2.48402	2.83629

Table 4.12: Cartesian Coordinates and Relative Energies of Optimized Conformers of **4.5a** and **4.5b** ($\Delta E < 8$ kJ/mol) Continued.

Conf. 1				C	-5.28536	-2.81017	-0.50501
ΔG (298 K) = -12338.197766 Hartree				C	-6.00378	-1.49403	-0.44960
H	-1.67320	-1.50790	3.03385	C	-6.85348	-0.96082	0.48278
H	-3.35462	-0.44667	4.36041	N	-7.37359	0.25532	0.05445
H	-4.56871	-0.52230	3.08948	C	-6.83591	0.43928	-1.13346
H	-1.17808	1.63444	3.67124	N	-6.01447	-0.58157	-1.50774
H	-4.69101	1.30315	1.37644	N	-6.99747	1.59598	-1.90979
H	-4.22507	3.28589	-0.22687	N	-2.58445	-1.00789	1.65895
H	-2.82021	4.18369	0.05235	O	-2.44894	-3.28136	1.90843
Conf. 4				C	-2.99202	-0.65080	3.01332
ΔG (298 K) = -12338.197523 Hartree				C	-4.15135	0.36799	2.99612
O	4.55274	1.98049	-0.70579	C	-3.89847	1.52425	2.06888
C	3.34490	1.64476	-1.24455	C	-2.78987	2.28100	1.79129
C	0.79912	0.85230	-2.20481	N	-2.99887	3.10197	0.69025
C	2.20292	2.42577	-1.01734	C	-4.25549	2.87723	0.33438
C	3.17924	0.46608	-1.98237	N	-4.84446	1.93243	1.12512
C	1.93438	0.07840	-2.46710	N	-4.94125	3.55517	-0.65621
C	0.94951	2.04568	-1.48728	H	-0.35258	-2.15072	-1.63923
C	5.38430	2.78963	-1.55208	H	1.84984	-0.85183	-3.01787
Br	2.37684	4.01135	0.01893	H	0.09060	2.66354	-1.25324
Br	4.68507	-0.66915	-2.25845	H	6.30002	2.97239	-0.98829
C	-0.57152	0.34076	-2.59404	H	4.89510	3.74360	-1.77491
C	-1.34033	-0.30410	-1.42011	H	5.62436	2.25785	-2.47890
C	-2.70144	-0.87914	-1.87779	H	-1.20329	1.14707	-2.98373
N	-2.96028	-2.01377	-1.18396	H	-0.48401	-0.39524	-3.40016
C	-1.87126	-2.42519	-0.25944	H	-2.10995	1.42605	-0.69488
C	-0.68312	-1.55309	-0.78203	H	-0.01552	0.41730	1.12202
O	-1.59759	0.65450	-0.39387	H	1.40025	-3.23528	-0.65399
C	0.52318	-1.42413	0.13163	H	5.31895	-0.62953	0.72555
C	2.93533	-1.21152	1.62457	H	6.00095	-0.45933	2.37177
C	0.72168	-0.36377	1.02341	H	4.82349	0.74103	1.75617
C	1.52582	-2.39753	0.02220	H	-1.81854	-4.16542	0.45841
C	2.70629	-2.28234	0.74745	H	-3.70331	-3.91162	-1.46988
C	1.90982	-0.26303	1.73891	H	-4.41208	-2.66049	-2.49379
O	4.08478	-1.12791	2.34615	H	-5.97980	-3.60103	-0.82451
C	5.11536	-0.31252	1.75202	H	-4.96080	-3.08757	0.50300
Br	2.16030	1.25957	2.85878	H	-7.15200	-1.39092	1.42897
Br	4.08213	-3.57429	0.49612	H	-5.27807	-0.51694	-2.21595
C	-2.32439	-2.24777	1.23904	H	-7.08119	1.40273	-2.90265
O	-1.57147	-3.77107	-0.41100	H	-7.81344	2.10611	-1.58618
O	-3.44440	-0.34335	-2.70646	H	-2.39675	-0.23595	1.01884
C	-4.09262	-2.89079	-1.47345	H	-3.28123	-1.56612	3.53311
				H	-2.13048	-0.22754	3.54517
				H	-4.32612	0.70008	4.02789

Table 4.12: Cartesian Coordinates and Relative Energies of Optimized Conformers of **4.5a** and **4.5b** ($\Delta E < 8$ kJ/mol) Continued.

				C	-6.55240	-0.86722	0.69186
Conf. 4				N	-6.98671	0.40523	0.34080
ΔG (298 K) = -12338.197523 Hartree				C	-6.60157	0.54646	-0.90899
H	-5.06313	-0.14368	2.67036	N	-5.95600	-0.55284	-1.39485
H	-1.83028	2.26348	2.29080	N	-6.76301	1.71884	-1.66207
H	-5.79046	1.57508	1.02771	N	-2.74116	-0.95625	1.53140
H	-5.54187	2.97588	-1.24338	O	-2.74283	-3.21260	1.88906
H	-4.31610	4.14704	-1.18709	C	-3.45195	-0.57479	2.74753
				C	-3.09187	0.86286	3.18072
Conf. 17				C	-3.08868	1.86475	2.06798
ΔG (298 K) = -12338.197480 Hartree				C	-2.05378	2.57574	1.52223
O	4.45460	1.91534	-0.74060	N	-2.45554	3.28182	0.39948
C	3.27468	1.53036	-1.30788	C	-3.75071	3.02993	0.28624
C	0.78212	0.64417	-2.32448	N	-4.19221	2.17303	1.25956
C	2.11305	2.30296	-1.16983	N	-4.59512	3.61999	-0.63527
C	3.15650	0.31004	-1.98427	H	-0.39180	-2.34673	-1.60625
C	1.93789	-0.12494	-2.49513	H	1.88897	-1.08657	-2.99384
C	0.88577	1.87895	-1.67031	H	0.01258	2.49920	-1.50299
C	5.30563	2.69485	-1.59515	H	6.19512	2.92355	-1.00664
Br	2.21870	3.94058	-0.20824	H	4.81004	3.62676	-1.88666
Br	4.68870	-0.81324	-2.13378	H	5.59107	2.12020	-2.48270
C	-0.56398	0.08597	-2.73823	H	-1.18682	0.85355	-3.21263
C	-1.37837	-0.48423	-1.55802	H	-0.43173	-0.70343	-3.48549
C	-2.73485	-1.07057	-2.01255	H	-2.06288	1.33274	-1.00782
N	-3.01552	-2.16158	-1.25969	H	-0.20558	0.38618	1.01154
C	-1.96396	-2.51030	-0.26875	H	1.36792	-3.31457	-0.51164
C	-0.75172	-1.68664	-0.80888	H	5.17101	-0.55614	0.87814
O	-1.67447	0.53790	-0.60748	H	5.77717	-0.26706	2.53735
C	0.41810	-1.48608	0.13863	H	4.60292	0.86425	1.79735
C	2.76189	-1.13251	1.71221	H	-1.99611	-4.20245	0.55784
C	0.55604	-0.37562	0.97896	H	-3.82797	-4.04682	-1.47519
C	1.44595	-2.43843	0.12187	H	-4.51665	-2.79110	-2.51004
C	2.59269	-2.25486	0.88700	H	-6.12297	-3.55479	-0.83759
C	1.71099	-0.20560	1.73262	H	-5.03071	-3.21696	0.49132
O	3.87796	-0.98051	2.47413	H	-6.76958	-1.28031	1.66720
C	4.91638	-0.18036	1.87291	H	-5.32568	-0.56189	-2.19905
Br	1.87541	1.38585	2.77337	H	-6.96663	1.54064	-2.64020
Br	4.00529	-3.52594	0.76494	H	-7.50260	2.28087	-1.25188
C	-2.50523	-2.22327	1.18292	H	-2.52850	-0.22149	0.85685
O	-1.66899	-3.86484	-0.30823	H	-4.53127	-0.65198	2.56416
O	-3.46733	-0.56576	-2.86898	H	-3.20337	-1.28938	3.53559
C	-4.17896	-3.01182	-1.49374	H	-2.08676	0.87008	3.61482
C	-5.34217	-2.85984	-0.49474	H	-3.78476	1.14551	3.98482
C	-5.90349	-1.47809	-0.34814	H	-1.02532	2.58865	1.85863

Table 4.12: Cartesian Coordinates and Relative Energies of Optimized Conformers of **4.5a** and **4.5b** ($\Delta E < 8$ kJ/mol) Continued.

Conf. 17				C	-6.35211	0.86810	-1.00022
				N	-5.86293	-0.30634	-1.48664
ΔG (298 K) =				N	-6.30792	2.07041	-1.72305
				N	-2.69614	-1.01503	1.57466
H	-5.13997	1.82277	1.34624	O	-2.53031	-3.27575	1.85435
H	-5.25615	2.99523	-1.09962	C	-2.80455	-0.69245	3.00039
H	-4.06491	4.18251	-1.28818	C	-3.66165	0.56687	3.26386
Conf. 3				C	-3.27467	1.71283	2.38036
ΔG (298 K) =				C	-2.20160	2.56805	2.34293
				N	-2.15286	3.26178	1.14400
O	4.40388	1.87472	-0.74179	C	-3.18963	2.82512	0.46471
C	3.22574	1.50618	-1.32428	N	-3.91551	1.89942	1.15398
C	0.73439	0.65314	-2.37234	N	-3.39021	3.03955	-0.90778
C	2.07367	2.29587	-1.20292	H	-0.45746	-2.29663	-1.67600
C	3.09881	0.28651	-2.00035	H	1.82649	-1.09212	-3.02920
C	1.88185	-0.13145	-2.52922	H	-0.02520	2.50519	-1.54974
C	0.84684	1.88442	-1.71430	H	6.16196	2.85732	-0.98608
C	5.27690	2.64046	-1.58576	H	4.79874	3.57911	-1.88481
Br	2.19011	3.93811	-0.25147	H	5.56587	2.06077	-2.46900
Br	4.61688	-0.86009	-2.12553	H	-1.22014	0.89529	-3.27986
C	-0.61513	0.11691	-2.80155	H	-0.48565	-0.67402	-3.54797
C	-1.44939	-0.44175	-1.62776	H	-2.28955	1.31236	-1.13691
C	-2.79351	-1.03215	-2.09642	H	-0.24211	0.47403	0.89555
N	-3.11559	-2.08248	-1.30182	H	1.22298	-3.32440	-0.50488
C	-2.04783	-2.48278	-0.35616	H	5.07639	-0.63937	0.90384
C	-0.83093	-1.64452	-0.87846	H	5.67003	-0.36088	2.56953
O	-1.78166	0.59098	-0.70311	H	4.53825	0.80091	1.81046
C	0.32542	-1.45120	0.08776	H	-1.98884	-4.20259	0.41467
C	2.64514	-1.14731	1.70441	H	-3.99348	-3.94619	-1.46324
C	0.48478	-0.32420	0.90416	H	-4.61427	-2.70709	-2.55920
C	1.31954	-2.43877	0.11265	H	-6.29931	-3.29878	-0.91031
C	2.45704	-2.27779	0.89558	H	-5.21554	-3.01627	0.43831
C	1.62613	-0.18474	1.68690	H	-6.75378	-0.92500	1.57845
O	3.75176	-1.01934	2.48471	H	-5.24820	-0.39988	-2.29994
C	4.82044	-0.25199	1.89397	H	-6.47160	1.94675	-2.71691
Br	1.82380	1.40614	2.72039	H	-6.98697	2.71928	-1.33773
Br	3.83143	-3.59395	0.82185	H	-2.52720	-0.25021	0.92195
C	-2.45825	-2.26208	1.14825	H	-3.22079	-1.56488	3.50822
O	-1.77630	-3.84059	-0.47744	H	-1.79539	-0.52603	3.39885
O	-3.50008	-0.55104	-2.98879	H	-3.53970	0.83154	4.31947
C	-4.30376	-2.90051	-1.52868	H	-4.72079	0.32855	3.11579
C	-5.47827	-2.65555	-0.56134	H	-1.42970	2.69794	3.08899
C	-5.93099	-1.23203	-0.44134	H	-4.82898	1.52622	0.90525
C	-6.50133	-0.54772	0.59729	H	-4.35869	2.94146	-1.21979
N	-6.76119	0.77279	0.24882				

Table 4.12: Cartesian Coordinates and Relative Energies of Optimized Conformers of **4.5a** and **4.5b** ($\Delta E < 8$ kJ/mol) Continued.

Conf. 3				N	-6.72496	1.66031	-1.27399
ΔG (298 K) = -12338.197388 Hartree				N	-2.57524	-1.13592	1.39253
H	-2.98568	3.92468	-1.19261	O	-2.36013	-3.39589	1.66634
				C	-3.10477	-0.81301	2.71252
				C	-2.62240	0.57645	3.18766
Conf. 18				C	-2.74071	1.65850	2.15715
ΔG (298 K) = -12338.196930 Hartree				C	-1.78108	2.43855	1.56762
O	4.20614	2.50008	-0.86674	N	-2.30922	3.21191	0.54659
C	3.06119	1.97462	-1.38058	C	-3.60279	2.93135	0.54063
C	0.66353	0.90549	-2.45993	N	-3.92619	1.99383	1.48574
C	1.83604	2.64804	-1.25852	N	-4.54778	3.55847	-0.24968
C	3.05262	0.76270	-2.08512	H	-0.32060	-2.26215	-1.92109
C	1.88220	0.24108	-2.62802	H	1.92277	-0.70868	-3.14969
C	0.65728	2.13521	-1.78990	H	-0.26189	2.68853	-1.63368
C	4.51788	2.06202	0.47094	H	5.34230	2.69286	0.80586
Br	1.77787	4.28497	-0.28758	H	4.82912	1.01337	0.47062
Br	4.66901	-0.23344	-2.23957	H	3.65858	2.19285	1.13547
C	-0.63136	0.24412	-2.88380	H	-1.32940	0.97160	-3.31514
C	-1.36788	-0.43819	-1.71261	H	-0.44499	-0.50128	-3.66403
C	-2.72778	-1.04165	-2.13598	H	-2.02035	1.33762	-1.01144
N	-2.93882	-2.18094	-1.43107	H	1.62006	-3.08675	-1.09755
C	-1.82934	-2.55688	-0.52324	H	-0.24457	0.15726	1.02388
C	-0.66711	-1.66315	-1.07194	H	3.26874	-1.53882	4.08643
O	-1.65747	0.50142	-0.67893	H	5.03901	-1.51221	3.85100
C	0.52351	-1.48503	-0.14804	H	4.08056	-2.85734	3.17206
C	2.83850	-1.21522	1.47745	H	-1.72582	-4.28593	0.21720
C	1.63003	-2.32627	-0.32517	H	-3.73229	-4.06707	-1.71221
C	0.57523	-0.52449	0.86960	H	-4.51290	-2.76139	-2.61201
C	1.70775	-0.41139	1.66503	H	-5.98837	-3.65391	-0.88689
C	2.76686	-2.17940	0.46293	H	-4.80750	-3.39702	0.38218
O	3.98111	-1.01219	2.19337	H	-6.44896	-1.56701	1.82174
C	4.08478	-1.78637	3.39944	H	-5.33076	-0.56625	-2.09045
Br	4.28296	-3.28039	0.13363	H	-6.98842	1.55118	-2.24789
Br	1.72764	0.91248	3.04220	H	-7.44482	2.17566	-0.77665
C	-2.27410	-2.36932	0.97958	H	-2.46931	-0.36942	0.72859
O	-1.50199	-3.89781	-0.66044	H	-4.20123	-0.83469	2.66929
O	-3.52186	-0.51218	-2.91829	H	-2.79014	-1.59234	3.41017
C	-4.10006	-3.04036	-1.63886	H	-1.56506	0.52094	3.46860
C	-5.19050	-2.97475	-0.55185	H	-3.18109	0.81921	4.10227
C	-5.74865	-1.61380	-0.26547	H	-0.72353	2.45969	1.79471
C	-6.31412	-1.08413	0.86370	H	-4.85373	1.61417	1.63813
N	-6.77943	0.20574	0.64053	H	-5.22322	2.94370	-0.70683
C	-6.49626	0.43939	-0.62252	H	-4.09636	4.18923	-0.89978
N	-5.88769	-0.61688	-1.23573				

4.12 References and Notes

- (1) Peng, J.; Li, J.; Hamann, M. T. The marine bromotyrosine derivatives. *Alkaloids Chem. Biol.* **2005**, *61*, 59-262.
- (2) Lira, N. S.; Montes, R. C.; Tavares, J. F.; Silva, M. S. d.; Cunha, E. V. L. d.; Athayde-Filho, P. F. d.; Rodrigues, L. C.; Dias, C. d. S.; Barbosa-Filho, J. M. Brominated Compounds from Marine Sponges of the Genus *Aplysina* and a Compilation of their ¹³C NMR Spectral Data. *Mar. Drugs* **2011**, *9*, 2316-2368.
- (3) Thirionet, I.; Dalozé, D.; Braekman, J. C.; Willemsen, P. 5-Bromoverongamine, a novel antifouling tyrosine alkaloid from the sponge *Pseudoceratina* sp. *Nat. Prod. Lett.* **1998**, *12*, 209-214.
- (4) Tsukamoto, S.; Kato, H.; Hirota, H.; Fusetani, N. Ceratinamides A and B: New antifouling dibromotyrosine derivatives from the marine sponge *Pseudoceratina purpurea*. *Tetrahedron* **1996**, *52*, 8181-8186.
- (5) Yin, S.; Davis, R. A.; Shelper, T.; Sykes, M. L.; Avery, V. M.; Eloffson, M.; Sundin, C.; Quinn, R. J. Pseudoceramines A-D, New Antibacterial Bromotyrosine Alkaloids from the marine sponge *Pseudoceratina* sp. *Org. Biomol. Chem.* **2011**, *9*, 6755-6760.
- (6) Longeon, A.; Guyot, M.; Vacelet, J. Araplysillins-I and-II: Biologically active dibromotyrosine derivatives from the sponge *Psammaphysilla arabica*. *Experientia* **1990**, *46*, 548-550.
- (7) Ichiba, T.; Scheuer, P. J.; Kelly-Borges, M. Three bromotyrosine derivatives, one terminating in an unprecedented diketocyclopentenylidene enamine. *J. Org. Chem.* **1993**, *58*, 4149-4150.
- (8) Hamann, M. T.; Scheuer, P. J.; Kelly-Borges, M. Biogenetically diverse, bioactive constituents of a sponge, order Verongida: Bromotyramines and sesquiterpene-shikimate derived metabolites. *J. Org. Chem.* **1993**, *58*, 6565-6569.
- (9) Xu, M.; Andrews, K. T.; Birrell, G. W.; Tran, T. L.; Camp, D.; Davis, R. A.; Quinn, R. J. Psammaphysin H, a new antimalarial bromotyrosine alkaloid from a marine sponge of the genus *Pseudoceratina*. *Bioorg. Med. Chem. Lett.* **2011**, *21*, 846-848.
- (10) Hirano, K.; Kubota, T.; Tsuda, M.; Watanabe, K.; Fromont, J.; Kobayashi, J. i. Ma'edamines A and B, cytotoxic bromotyrosine alkaloids with a unique 2 (1H) pyrazinone ring from sponge *Suberea* sp. *Tetrahedron* **2000**, *56*, 8107-8110.
- (11) Gopichand, Y.; Schmitz, F. J. Marine natural products: fistularin-1, -2 and -3 from the sponge *Aplysina fistularis* forma fulva. *Tetrahedron Lett.* **1979**, *20*, 3921-3924.

-
- (12) Copp, B. R.; Ireland, C. M.; Barrows, L. R. Psammalyisin C: a new cytotoxic dibromotyrosine-derived metabolite from the marine sponge *Druinella* (= *Psammalyisilla*) *purpurea*. *J. Nat. Prod.* **1992**, *55*, 822-823.
- (13) Nicacio, K. J.; Ióca, L. P.; Fróes, A. M.; Leomil, L.; Appolinario, L. R.; Thompson, C. C.; Thompson, F. L.; Ferreira, A. G.; Williams, D. E.; Andersen, R. J.; Eustaquio, A. S.; Berlinck, R. G. S. Cultures of the Marine Bacterium *Pseudovibrio denitrificans* Ab134 Produce Bromotyrosine-Derived Alkaloids Previously Only Isolated from Marine Sponges. *J. Nat. Prod.* **2017**, *80*, 235-240.
- (14) Ma, Z.; Wang, X.; Wang, X.; Rodriguez, R. A.; Moore, C. E.; Gao, S.; Tan, X.; Ma, Y.; Rheingold, A. L.; Baran, P. S. Asymmetric syntheses of sceptrin and massadine and evidence for biosynthetic enantiodivergence. *Science* **2014**, *346*, 219-224.
- (15) Sherman, D. H.; Tsukamoto, S.; Williams, R. M. Comment on "Asymmetric syntheses of sceptrin and massadine and evidence for biosynthetic enantiodivergence". *Science* **2015**, *349*, 149-149.
- (16) Ma, Z.; Wang, X.; Wang, X.; Rodriguez, R. A.; Moore, C. E.; Gao, S.; Tan, X.; Ma, Y.; Rheingold, A. L.; Baran, P. S.; Chen, C. Response to Comment on "Asymmetric Syntheses of Sceptrin and Massadine and Evidence for Biosynthetic Enantiodivergence". *Science* **2015**, *349*, 149.
- (17) Kobayashi, J. i.; Honma, K.; Sasaki, T.; Tsuda, M. Puralidins J–R, New Bromotyrosine Alkaloids from the Okinawan Marine Sponge *Psammalyisilla purpurea*. *Chem. Pharm. Bull.* **1995**, *43*, 403–407.
- (18) Salim, A. A.; Khalil, Z. G.; Capon, R. J. Structural and stereochemical investigations into bromotyrosine-derived metabolites from southern Australian marine sponges, *Pseudoceratina* spp. *Tetrahedron* **2012**, *68*, 9802-9807.
- (19) Ragini, K.; Fromont, J.; Piggott, A. M.; Karuso, P. Enantiodivergence in the Biosynthesis of Bromotyrosine Alkaloids from Sponges? *J. Nat. Prod.* **2017**, *80*, 215-219.
- (20) Kijjoa, A.; Bessa, J.; Wattanadilok, R.; Sawangwong, P.; Nascimento, M. S. J.; Pedro, M.; Silva, A. M. S.; Eaton, G.; van Soest, R.; Herz, W. Dibromotyrosine Derivatives, A Maleimide, Aplysamine-2 and Other Constituents of the Marine Sponge *Pseudoceratina purpurea*. *Z. Naturforsch. B* **2005**, *60*, 904-908.
- (21) Rogers, E. W.; Molinski, T. F. Highly Polar Spiroisoxazolines from the Sponge *Aplysina fulva*. *J. Nat. Prod.* **2007**, *70*, 1191-1194.
- (22) In Refs. 19 and 21, the compound is un-named. For consistency, we name this carboxylic acid (+)-purpuroceratic acid C, concordant with Kijjoa's naming of the lower homologs, purpuroceratic acids A and B (Ref. 20). The numbered compound **10** in the paper by Karuso and coworkers (Ref. 19) is, therefore, *ent*(-)-purpuroceratic acid C.

-
- (23) Salib, M. N.; Jamison, M. T.; Molinski, T. F. Bromo-spiroisoxazoline Alkaloids, Including an Isoleucine Peptide, from the Caribbean Marine Sponge *Aplysina lacunosa*. *J. Nat. Prod.* **2020**, *83*, 1532-1540. See Table 4.2.
- (24) Litaudon, M.; Guyot, M. Ianthelline; derivative of 3,5-dibromotyrosine from the Sponge *Ianthella ardis* (Verongida). *Tetrahedron Lett.* **1986**, *27*, 4455-4456.
- (25) Salib, M. N.; Hendra, R.; Molinski, T. F. In submission.
- (26) Mierzwa, R.; King, A.; Conover, M. A.; Tozzi, S.; Puar, M. S.; Patel, M.; Coval, S. J.; Pomponi, S. A. Verongamine, a Novel Bromotyrosine-Derived Histamine H₃-Antagonist from the Marine Sponge *Verongula gigantea*. *J. Nat. Prod.* **1994**, *57*, 175-177.
- (27) Assmann, M.; Wray, V.; van Soest, R. W. M.; Proksch, P. A new bromotyrosine alkaloid from the Caribbean sponge *Aiolochoxia crassa*. *Z. Naturforsch., C* **1998**, *53*, 398-401.
- (28) Albrizio, S.; Ciminiello, P.; Fattorusso, E.; Magno, S.; Pansini, M. Chemistry of Verongida Sponges. I. Constituents of the Caribbean Sponge *Pseudoceratina crassa*. *Tetrahedron* **1994**, *50*, 783-788.
- (29) Arabshahi, L.; Schmitz, F. J. Brominated tyrosine metabolites from an unidentified sponge. *J. Org. Chem.* **1987**, *52*, 3584-3586.
- (30) Kobayashi, J.; Tsuda, M.; Ohizumi, Y. A potent actomyosin ATPase activator from the Okinawan marine sponge *Agelas cf. nemoechinata*. *Experientia* **1991**, *47*, 301-304.
- (31) The lack of specific rotation in **3** ($[\alpha]_D \sim 0$) is not inconsistent with the measured 30% ee optical purity. For example, eusynstyellamide B was reported, also with $[\alpha]_D \sim 0$, yet the compound displays a negative Cotton effect in the ECD spectrum.
- (32) The L- and D- DAA derivatives of L-2,4-diaminobutanoic acid eluted at 23.08 min. and 23.39 min., respectively ($\Delta t_R = 0.31$ min). The L- and D- DTA derivatives eluted at 29.68 min. and 28.98 min., respectively ($\Delta t_R = 0.82$ min).
- (33) Casapullo, A.; Finamore, E.; Minale, L.; Zollo, F. A Dimeric Peptide Alkaloid of a Completely New Type, Anchinopeptolide A, from the Marine Sponge *Anchinoe tenacior*. *Tetrahedron Lett.* **1993**, *39*, 6297-6300.
- (34) Casapullo, A.; Minale, L.; Zollo, F. Four New Dimeric Peptide Alkaloids, Anchinopeptolides B-D, and Cycloanchinopeptolide C congeners of Anchinopeptolide A, from the Mediterranean Marine Sponge *Anchinoe tenacior*. *J. Nat. Prod.* **1994**, *57*, 1227-1233.
- (35) Bastos, S.; Silva, L.; Beniddir, M. A.; Gallard, J-F.; Poupon, E.; Thomas, O. P.; Evanno, L. Chemical Insights into the Anchinopeptolide Series. *Eur. J. Org. Chem.* **2019**, 5515-5518.

-
- (36) Swersey, J. C.; Ireland, C. M.; Cornell, L. M.; Peterson, R. W. Eusynstyelamide, a Highly Modified Dimer Peptide from the Ascidian *Eusynstyela misakiensis*. *J. Nat. Prod.* **1994**, *57*, 842-845. The structure is depicted as the ring-opened α -geminal diol, but the MS and ^{13}C NMR data are more consistent with the ring-closed pyrrolidinone-aminal (Ref. 37).
- (37) Tapiolas, D. M.; Bowden, B. F.; Abou-Mansour, E.; Willis, R. H.; Doyle, J. R.; Muirhead, A. N.; Liptrot, C.; Llewellyn, L. E.; Wolff, C. W. W.; Wright, A. D.; Motti, C. A. Eusynstyelamides A, B, and C, nNOS Inhibitors, from the Ascidian *Eusynstyela latericius*. *J. Nat. Prod.* **2009**, *72*, 1115–1120.
- (38) Spartan Student V8, Wavefunction Inc., Irvine, California.
- (39) See Gaussian 16 citation in Appendix.
- (40) Willoughby, P. H.; Jansma, M. J.; Hoye, T. R. A guide to Small-Molecule Structure Assignment through Computation of (^1H and ^{13}C) NMR Chemical Shifts. *Nat. Prot.* **2014**, *9*, 643-660.
- (41) As brominated carbons are known to show considerable deviations in their calculated δ_{C} signals (spin-orbit coupling effect), they were subsequently omitted from the RMSD calculations.
- (42) This result differs from Olivier's assessment of the anchinopeptolides C and E (1:4.9 isolated yield) as anomeric *trans*- and *cis*- dihydroxypyrrolidinones, respectively, from ^1H nOe measurements of the tertiary HO group signals.³⁵ Here, we were reluctant to rely on such nOe measurements (DMSO-*d*₆) as Minale and coworkers earlier observed, with respect to anchinopeptolide A (Ref. 33) "*it is to be noted that the molecule exhibited negative NOE effects*": a phenomenon that we interpret differently as chemical exchange, not dipolar coupling.
- (43) The CIP designation changes because the priority of the hydroperoxyl group, -OOH, is higher than that of the spiro-ON group.
- (44) For the same reason, we can only estimate the *lower* limit for enantioselectivity of epoxidation to be ~30%ee.
- (45) In contrast, we have developed optimized conditions for chiral phase HPLC separations of enantiomeric spiroisoxazoline BTAs. See Ref. 25.
- (46) Fattorusso, E.; Minale, L.; Sodano, G.; Moody, K.; Thomson, R. H. Aerothionin, a Tetrabromo-compound from *Aplysina aerophoba* and *Verongia thiona*. *Chem. Commun.* **1970**, 752-753.
- (47) McMillan, J. A.; Paul, I. C.; Goo, Y. M.; Rinehart, K. L.; Krueger, W. C.; Pschigoda, L. M. An X-Ray Study of Aerothionin from *Aplysina fistularis* (Pallas). *Tetrahedron Lett.* **1981**, *22*, 39–42.

-
- (48) The underlying assumptions of quantitation, here, include a normalization (0.5) of the ECD magnitude of C_2 symmetric dimer, (+)-**14** (degenerate SIO groups), no interaction between the remote cyclohexa-1,3-dienyl SIO chromophores (i.e. no exciton coupling), and the implicit experimental accuracies of the reported $\Delta\epsilon$ and $[\alpha]_D$ values. Granted, we recognize this an imperfect quantitation, but one that is useful until an optically pure, preferably synthetic SIO standard is procured and its ECD spectrum measured.
- (49) Aiello, A.; Fattorusso, E.; Menna, M.; Pansini, M. Chemistry of Verongida Sponges – V. Brominated Metabolites from the Caribbean Sponge *Pseudoceratina* sp. *Biochem. Syst. Ecol.* **1995**, *23*, 377–281.
- (50) Shearman, J. W.; Myers, R. M.; Brenton, J. D.; Ley, S. V. Total Syntheses of Subreamollines A and B. *Org. Biomol. Chem.* **2011**, *9*, 62-65.
- (51) The parent sample of *Candida albicans* was obtained from an anonymous patient isolate (UC Davis Clinical Microbiology Laboratory, -1990).
- (52) Orhan, I.; Sener, B; Choudhary, M. I.; Khalid, A. Acetylcholinesterase and Butyrylcholinesterase Inhibitory Activity of Some Turkish Medicinal Plants. *J. Ethnopharmacol.* **2004**, *91*, 57-60.
- (53) Ellman, G. L.; Courtney, K. D.; Andres, Jr., V.; Featherstone, R. M. A New and Rapid Colorimetric Determination of Acetylcholinesterase Activity. *Biochem. Pharmacol.* **1961**, *7*, 88-95.

CHAPTER FIVE. ABSOLUTE STEREOSTRUCTURE OF AXINOSIDE-1, A COMPLEX
GLYCOLIPID FROM A WESTERN AUSTRALIAN AXINELLID SPONGE

Abstract: The absolute stereostructure of axinoside-1 (**5.1**), a complex glycolipid comprising a tetrasaccharide linked to a C₂₈ aglycone from a Western Australian Axinellid sponge, was elucidated via integrated spectroscopic MS, NMR and ECD analysis of the corresponding peracetate (**5.2**). Hydrolysis and persilylation of the sugar-containing fraction, followed by GC-EI-MS identified the tetrasaccharide components as three equivalents of D-xylose and one equivalent of D-glucose. Anomeric configurations and glycosidic linkages were secured by analysis of ¹J_{CH}, and HMBC respectively. The absolute configuration of the butyrolactone terminus of the aglycone was assigned as 4*R* by electronic circular dichroism (ECD) of the liberated aglycone against that of standard (*S*)-(-)-4-methylbutyrolactone. Acylation of the aglycone with (*R*)- and (*S*)-2-methoxy-2-(naphtha-1-yl)acetic acid (NMA) and subsequent ¹H NMR analysis of the anisotropy induced by the tris-NMA ester signals supported the 13*R*,23*R*-**5.2** configuration. The remaining stereocenter at C-17 was assigned as 17*R*-**5.2** by synthesis of two stereodefined analogs of the tris-NMA-aglycone and ¹H NMR comparison against the tris-NMA derivative of the natural aglycone.

5.1 Introduction

Glycolipids are important membrane constituents of animal and plant cells that play a vital role in cellular recognition and the immune response. They include the glyco glycerolipids and glycosphingolipids that possess a glycerol or sphingosyl backbone, respectively, and polyisoprenoid glycolipids. Glycosphingolipids consist of a sphingoid base, such as sphingosine in animals and phytosphingosine in plants, linked through an amide bond formed between the amino group of the sphingoid base and a fatty acid chain. Examples include ceramides such as oceanapins A-F isolated from the Coral Sea Haplosclerid sponge *Oceanapia* c.f. *tenuis*,¹ the anti-H5N1 metabolites isolated from the Egyptian Red Sea coral *Sinularia Candidula*,² and the weak but selective antineoplastic neritinaceramides A-E isolated from the South China Sea Bryozoan *Bugula neritina*.³ Further glycosidation of the primary alcohol of ceramides with a carbohydrate chain containing a sugar head leads predominately to neutral cerebroside and some charged gangliosides. Cerebrosides include the digalactosyl longiside isolated from the Bahamas *Agelas longissimi*,⁴ and the mixture of fatty acetylated glycolipids termed terpioside B isolated from *Terpios* sp. from Key Largo, Florida.⁵ Additional cerebroside include the biological response modifiers agelasphins, α -galactosylceramides from the sponge *Agelas mauritiana*, whose antitumor activity is a direct response of the activation of the immune system,⁶ and the *N*-acetylglucosamino glycolipids, halicylindrosides A1-4 and B1-6, from the Japanese sponge *Halichondria cylindrata*, which display antifungal and cytotoxic activity against *Mortierella remanniana* and P388 murine leukemia cells, respectively.⁷

Erylusamines,⁸ erylusamides,⁹ and simplexides¹⁰ are examples of unusual glycolipids described in the literature. The IL-6 antagonists erylusamines A-E, isolated from the Japanese sponge *Erylus placenta*, consist of a polar tetrasaccharide head glycosidically linked to a

ketodihydroxy fatty acid chain that in itself is connected through an amide to a diamine.⁸ Likewise, erylusamides A-D, indoleamine 2,3-dioxygenase inhibitors from the Atlantic *Erylus cf. deficiens*, comprise of a pentasaccharide moiety linked to dihydroxyketo amide aglycans of various length.⁹ Furthermore, the lymphocyte immunosuppressants simplexides were isolated as a mixture of homologs from the Caribbean sponge *Plakortis simplex*.¹⁰ They consist of an unusually long aglycan (34-37) chain glycosidically linked to a polar disaccharide at a mid-chain O atom.¹⁰

Here, we describe the isolation and structural elucidation of axinoside-1 (**5.1**), a complex glycolipid comprised of a tetrasaccharide glycosidically linked to a polyhydroxylated aglycone, in addition to the known ceramides oceanapins A–F (**5.3a–f**), previously isolated from the coral sea sponge *Oceanapia c.f. tenuis* by Mancini and coworkers,¹ and a seventh ceramide (**5.3g**), isolated from the gorgonian *Subergorgia suberosa* by Subrahmanyam and colleagues.¹¹

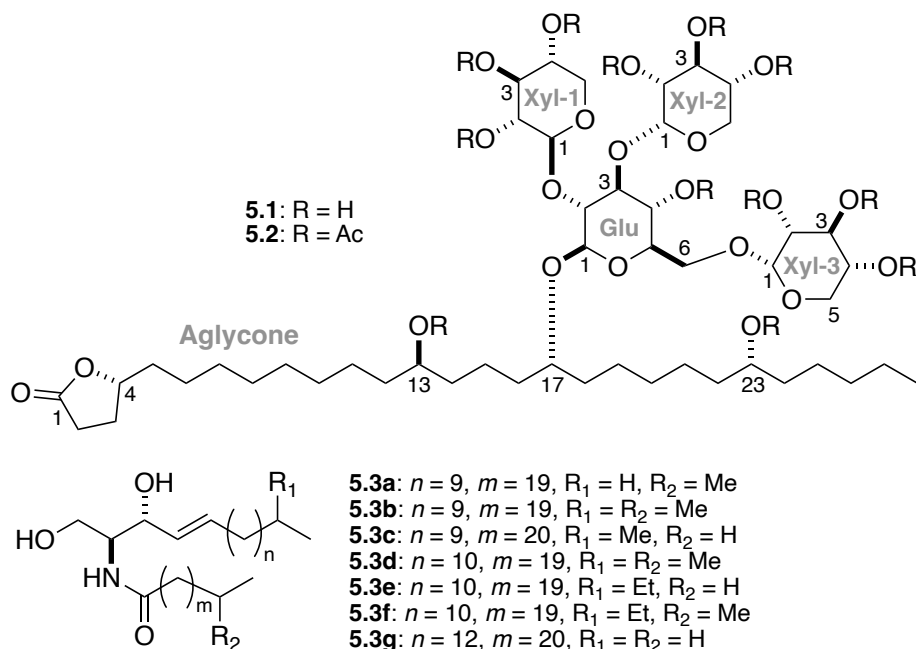


Figure 5.1: Structures of axinoside-1 (**5.1**), axinoside-1 peracetate (**5.2**), and ceramides **5.3a–g**.

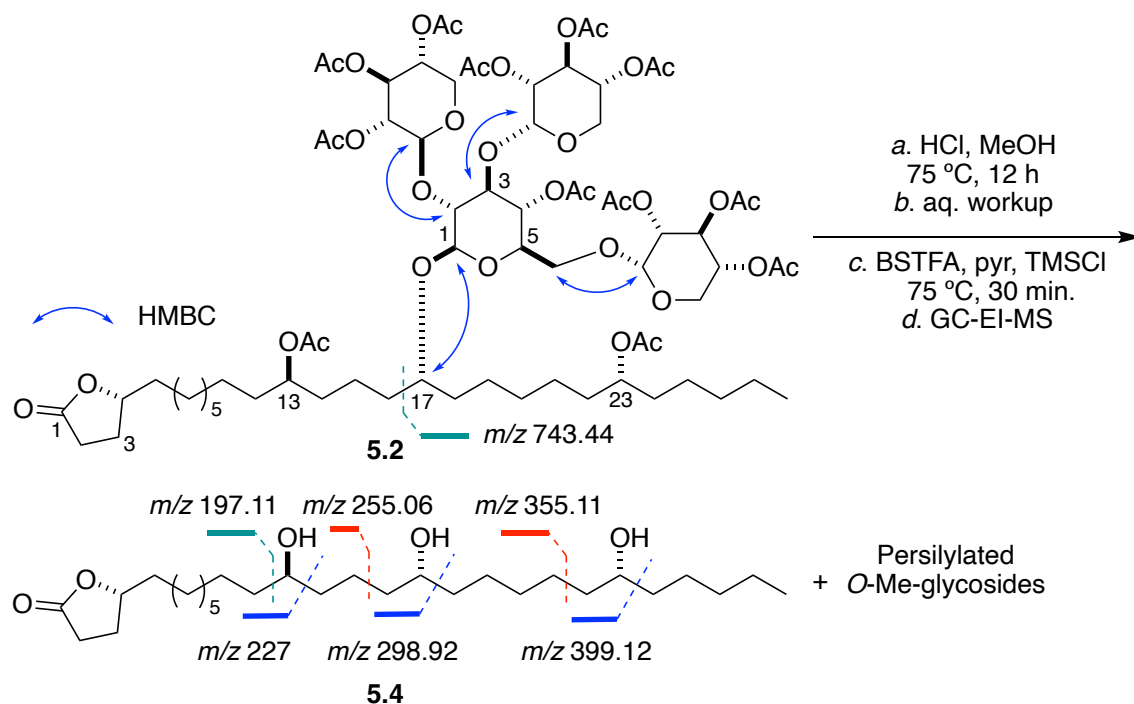
5.2 Isolation and Structure Determination of Axinoside-1

Specimens of 93-07-67 – a spectacularly brilliant red Axinellid sponge – were collected in Exmouth Gulf, Western Australia by hand using scuba in 1993 and immediately frozen. The identity of our sponge species was narrowed to the Axinellid genus based on SEM images (See Appendix, Figure 5.8) of spicules and our discussions with Dr. Mary Key Harper. A lyophilized sample of the sponge was repeatedly extracted with MeOH/CH₂Cl₂ (1:1), and the combined extract was concentrated in vacuo. The resultant crude extract was dissolved in MeOH/H₂O (9:1) and separated by progressive solvent partitioning into four fractions, ‘layers A–D’. The hexane-soluble ‘A fraction’ was purified on silica chromatography to provide an inseparable mixture of the known ceramide homologs, **5.3a–g**, as identified by analysis of NMR and mass spectrometry data. The *n*-BuOH-soluble ‘C fraction’ was chromatographed on Sephadex LH-20 (eluent: MeOH) to furnish a series of contiguous fractions containing glycolipids that were subsequently combined and concentrated. A sample of the glycolipid mixture was acetylated (Ac₂O, pyr, rt), and then purified by silica column chromatography (eluent: MeOH/CH₂Cl₂) followed by RP-HPLC (gradient elution, CH₃CN/H₂O) to provide axinoside-1 peracetate (**5.2**, Scheme 5.1) as a colorless, optically active oil ($[\alpha]_D -40.37$ (*c* 0.82, MeOH)).

HRMS analysis of **5.2** showed a prominent Na⁺ adduct molecular ion, *m/z* 1555.6927, corresponding to a formula C₇₃H₁₁₂O₃₄ (calc’d 1532.7035) for **5.2**, indicating 18 degrees of unsaturation.

Exhaustive 1D and 2D NMR analysis of **5.2** revealed the presence of multiple deshielded methine signals between δ_H 3.2 and 5.2, including four acetal and four diastereotopic methylene signals, characteristic of one hexopyranose and three pentopyranoses. The ¹H NMR also displayed two upfield-shifted diastereotopic methylenes at δ_H 1.8–2.6 and a methine at δ_H 4.88 assigned to H-4 of a γ -butyrolactone, a series of methyl resonances between δ_H 1.9 and 2.2 attributed to 12

acetate methyl signals, and resonances between δ_{H} 0.8-1.8 consistent with a long-chain unbranched hydrocarbon, terminated at the ω -end by a methyl group (δ_{H} 0.87, 3H, t, $J = 6.6$ Hz). In short, the ^1H NMR features of **5.2** were consistent with an unusually complex glycolipid.



Scheme 5.1: Methanolysis of **5.2**, persilylation of *O*Me-glycosides with Pierce's reagent (BSTFA), and MS fragmentation analysis of the aglycone (**5.4**) and persilylated *O*-Me glycosides.

Methanolysis of **5.2** under acidic conditions (MeOH, HCl, 75 °C) furnished aglycone (**5.4**) and a water-soluble glycoside mixture, which was persilylated with Pierce's reagent (BSTFA, pyr, TMSCl) to provide the corresponding persilylated *O*-Me-glycosides (Scheme 5.1). GC-EI-MS of the mixture of persilylated *O*-Me-glycosides and standards confirmed the presence of D-xylose (Xyl) and D-glucose (Glu), which eluted at the respective retention times of standards. ^{13}C and HSQC NMR data revealed the presence of four acetal signals: δ_{C} 98.9 (Glu-C-1: δ_{H} 4.34, 1H, d, $J = 7.2$ Hz), 97.6 (Xyl-1-C-1: δ_{H} 5.04, 1H, d, $J = 3.6$ Hz), 98.7 (Xyl-2-C-1: δ_{H} 4.77, 1H, m), and 100.2 (Xyl-3-C-1: δ_{H} 4.52, 1H, d, $J = 6.6$ Hz) that were assigned to the anomeric methines. The

^1H and ^{13}C NMR assignments of the four-spin systems belonging to Glu, Xyl-1, Xyl-2, and Xyl-3 were obtained from analysis of COSY, HSQC, HMBC, TOCSY, and HSQC-TOCSY spectra (Figure 5.2).

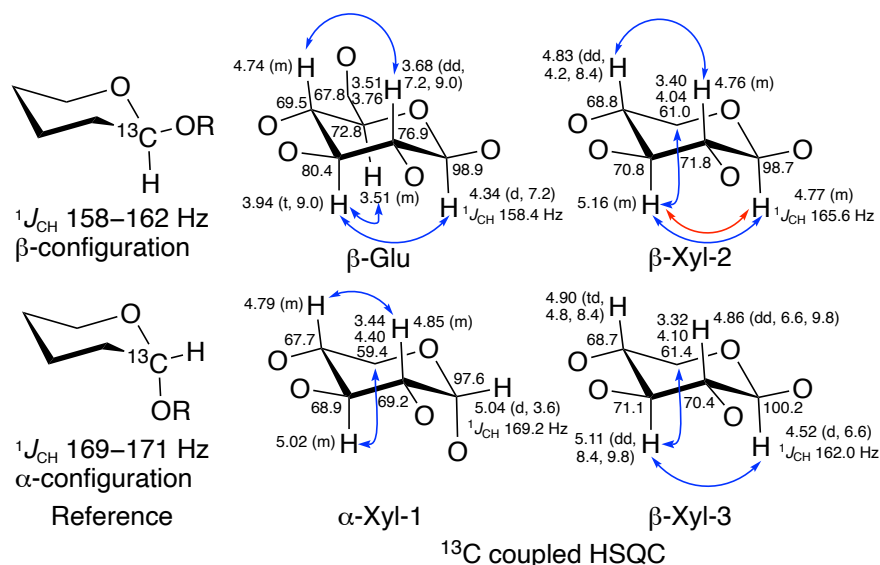


Figure 5.2: ^1H and ^{13}C assignments, $^1J_{\text{CH}}$ coupling constants of anomeric carbons, and key TOCSY (blue arrows) and NOESY (red arrows) correlations of the monosaccharides of axinoside-1 peracetate (**5.2**). See reference 12.

Sugar anomeric configurations were obtained by analysis of anomeric coupling constants (Figure 5.2).¹² The measured $^1J_{\text{CH}}$ values, obtained from coupled HSQC, were 158.4 Hz, 162.0 Hz and 169.2 Hz and supported β -D-Glu, β -D-Xyl-3, and α -D-Xyl-1, respectively. In contrast, Xyl-2, H-1–C-1 exhibited a heteronuclear coupling of equivocal magnitude ($^1J_{\text{CH}} = 165.6$ Hz,) that could not be used reliably to assign an α - or β -linkage. Fortunately, an nOe correlation between H-1 (δ_{H} 4.77, 1H, m) and H-3 (δ_{H} 5.16, 1H, m) on Xyl-2 confirmed β -Xyl-2.

Linkage analysis of **5.2** was carried out by long-range ^1H - ^{13}C NMR correlation experiments. For example, HMBC correlations between H-1 of Glu (δ_{H} 4.34, 1H, d, $J = 7.2$ Hz) and the C-17 of the aglycone (δ_{C} 78.06) established both the identity of the sugar and chain-location of the glycosidic bond. Additional HMBC correlations between H-2 of Glu at δ_{H} 3.68 (1H, dd, $J = 8.4, 7.8$ Hz) and Xyl-1–C-1 at δ_{C} 97.53, H-3 of Glu at δ_{H} 3.94 (1H, t, $J = 9.0$ Hz) and Xyl-2–C-1 at δ_{C} 98.73, and H-6 of Glu at δ_{H} 3.51 (1H, dd, $J = 14.4, 6.0$ Hz) and 3.76 (1H, dd, $J =$

14.4, 6.0 Hz) and Xyl-3-C-1 at δ_C 100.27 established α -D-Xyl-1-(1 \rightarrow 2)- β -D-Glu, β -D-Xyl-2-(1 \rightarrow 3)- β -D-Glu, and β -D-Xyl-3-(1 \rightarrow 6)- β -D-Glu linkages.

Table 5.1: 1D and 2D NMR data for **5.2**.

Position	δ_C^a	δ_H , mult (J , Hz) ^b	COSY (¹ H \rightarrow ¹ H) ^b	HMBC (¹ H \rightarrow ¹³ C) ^{b,c}	HSQC-TOCSY (¹ H \rightarrow ¹³ C) ^{b,c}
<i>aglycone</i>					
1	177.2	-	-	-	-
2	28.6	2.52, dd (1.2, 9.0) 2.53, d (9.0)	3	1, 3, 4	3, 4, 5
3	27.7	2.32, dq (6.6, 13.5) 1.85, m	2, 4	1, 2, 4, 5	2, 4
4	81.2	4.49, quint. (6.6)	3, 5	1, 2, 7	2, 3
5	35.3	1.73, m 1.59, m	4, 6	3, 4, 6, 7	4, 6
6	29.3	1.45, m 1.36, m	5	4, 5, 7	4
7	25.1	1.26-1.24			
8	^d	1.26-1.24			
9	^d	1.26-1.24			
10	^d	1.26-1.24			
11	25.2	1.26-1.24			
12	30.7	1.50, m		13	
13	73.9	4.98, m		11, 12, 14	
14	30.7	1.50, m		13	
15	25.1	1.28, m		13, 17 ^e	
16	34.3	1.53, 1.39, m		15, 17	
17	78.2	3.63, m		16, 18, 19	4-2, 4-5
18	34.3	1.53, 1.39, m		15, 16	
19	^d	1.28, m			
20	^d	1.26-1.24			
21	^d	1.26, m			
22	30.7	1.50, m		20, 21, 23	
23	73.9	4.98, m		22, 24, 25	
24	30.6	1.50, m		23, 25, 26	
25	24.7	1.26, m			
26	31.4	1.25, m			
27	22.4	1.26, m			
28	14.0	0.87, t (6.6)		26, 27	

^a125 MHz. ^b600 MHz. ^cBolded correlations refer to inter-residue connections. ^dOverlap. ^eWeak correlation.

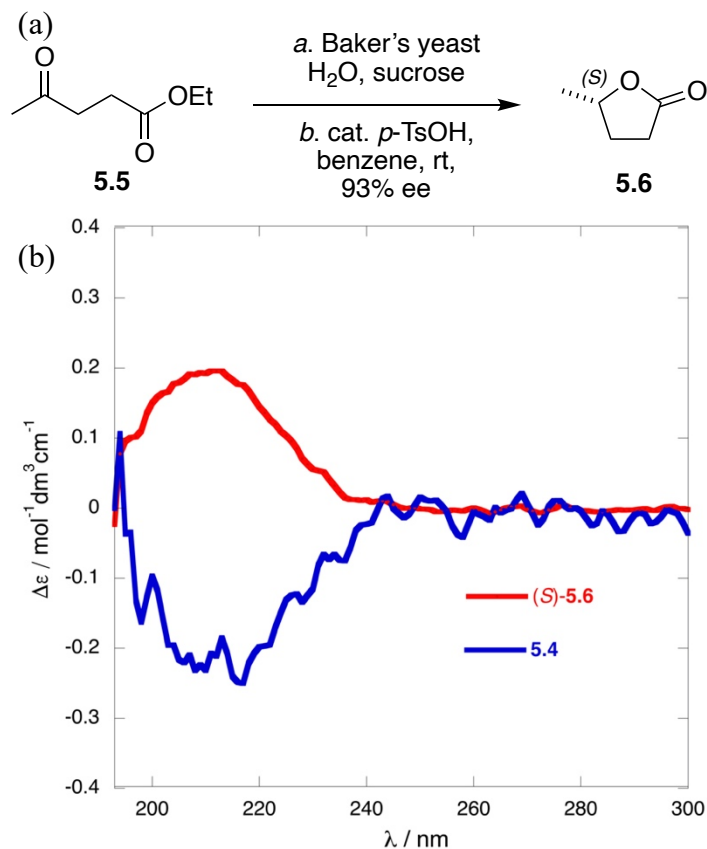
Table 5.1: 1D and 2D NMR data for **5.2** Continued.

Position	δ_C^a	δ_H , mult (J , Hz) ^b	COSY (¹ H→ ¹ H) ^b	HMBC (¹ H→ ¹³ C) ^{b,c}	HSQC-TOCSY (¹ H→ ¹³ C) ^{b,c}
<u>Xyl-1</u>					
-1	97.6	5.04, d (3.6)	<i>l</i> -2	<i>l</i> -2, <i>l</i> -4, <i>l</i> -5, 4-2	<i>l</i> -5
-2	69.2	4.85, m	<i>l</i> -1, <i>l</i> -3	<i>l</i> -1, <i>l</i> -3, <i>l</i> -4	<i>l</i> -1, <i>l</i> -3, <i>l</i> -4, <i>l</i> -5
-3	68.9	5.02, m	<i>l</i> -2, <i>l</i> -4	<i>l</i> -1, <i>l</i> -2, <i>l</i> -4, <i>l</i> -5	<i>l</i> -2, <i>l</i> -4
-4	67.7	4.79, m	<i>l</i> -3, <i>l</i> -5	<i>l</i> -2, <i>l</i> -3	<i>l</i> -3, <i>l</i> -5
-5a	59.4	3.44, dd (4.8, 12.6)	<i>l</i> -4, <i>l</i> -5b	<i>l</i> -1, <i>l</i> -3, <i>l</i> -4	<i>l</i> -3, <i>l</i> -4
-5b	-	4.40, dd (3.6, 12.6)	<i>l</i> -4, <i>l</i> -5a	<i>l</i> -1, <i>l</i> -3, <i>l</i> -4 ^e	<i>l</i> -3, <i>l</i> -4
<u>Xyl-2</u>					
-1	98.7	4.77, m	2-2	4-3 , 2-2, 2-4, 2-5a	2-3, 2-4, 2-5
-2	71.8	4.76, m	2-1, 2-3	2-1, 2-3	2-1, 2-3, 2-4
-3	70.8	5.17, m	2-2, 2-4	2-1 ^e , 2-2, 2-4, 2-5 ^e	2-1, 2-2, 2-4, 2-5
-4	68.8	4.83, dd (4.2, 8.4)	2-3, 2-5	2-3, 2-5	2-1, 2-3, 2-5
-5a	61.0	3.40, dd (8.4, 12.0)	2-4, 2-5b	2-1, 2-3, 2-4	2-3, 2-4
-5b	-	4.04, dd (4.2, 12.0)	2-4, 2-5a	2-1, 2-3, 2-4	2-3, 2-4
<u>Xyl-3</u>					
-1	100.2	4.52, d (6.6)	3-2	4-6 , 4-6' , 3-3, 3-5	3-2, 3-3, 3-4, 3-5
-2	70.4	4.86, dd (6.6, 9.8)	3-1, 3-3	3-1, 3-3, 3-4	3-1, 3-4, 3-5
-3	71.1	5.11, dd (8.4, 9.8)	3-2, 3-4	3-1 ^e , 3-2, 3-4, 3-5a ^e	3-1, 3-2, 3-4, 3-5
-4	68.7	4.90, td (4.8, 8.4)	3-3, 3-5	3-3, 3-5	3-2
-5a	61.4	3.32, dd (4.8, 12.0)	3-4, 3-5b	3-1, 3-3, 3-4	3-3, 3-4, 3-5
-5b	-	4.10, dd (4.8, 12.0)	3-4, 3-5a	3-1, 3-3, 3-4	3-3, 3-4, 3-5
<u>Glu-4</u>					
-1	98.9	4.34, d (7.2)	4-2	17 , 4-3, 4-5	4-2, 4-3, 4-4
-2	76.9	3.68, dd (7.2, 9.0)	4-1, 4-3	1-1 , 4-1, 4-3	4-1, 4-3, 4-4, 4-5
-3	80.4	3.94, t (9.0)	4-2, 4-4	2-1 , 4-2, 4-4, 4-5 ^e	4-1, 4-2, 4-4, 4-5
-4	69.5	4.74, m	4-3, 4-5	4-3, 4-5, 4-6	4-2, 4-3, 4-4, 4-5
-5	72.8	3.51, m	4-4, 4-6	4-1, 4-3, 4-4, 4-6	4-1, 4-2, 4-3, 4-4, 4-6
-6a	67.8	3.51, dd (6.0, 14.4)	4-5, 4-6b	3-1 , 4-1 ^e , 4-4, 4-5	4-4, 4-5
-6b	-	3.76, dd (6.0, 14.4)	4-5, 4-6a	3-1 , 4-1 ^e , 4-4	4-4, 4-5

^a125 MHz. ^b600 MHz. ^cBolded correlations refer to inter-residue connections. ^dOverlap. ^eWeak correlation.

HRMS analysis of the aglycone (**5.4**) presented a prominent $[M+Na]^+$ adduct at m/z 493.3865 corresponding to $C_{28}H_{54}O_5Na^+$ (calc'd 493.3863). A contiguous spin system, obtained from COSY cross-peaks in **5.2**, comprised of diastereotopic CH_2 at C-2 (δ_H 2.52, 1H, dd, $J = 9.0$, 1.2 Hz and 2.53, 1H, d, $J = 9.0$ Hz), CH_2 at C-3 (δ_H 2.32, 1H, dq, $J = 13.5$, 6.6 Hz and 1.85, 1H, m), CH at C-4 (δ_H 4.49, 1H, q, $J = 6.6$), and CH_2 at C-5 (δ_H 1.73, 1H, m and 1.59, 1H, m), in addition to HMBC correlations between the CH_2 at C-2 and the carbonyl at C-1 (δ_C 177.2), CH_2 at C-3 (δ_C 27.3), and CH at C-4 (δ_C 81.2), as well as the CH at C-4 and the C-1 carbonyl and CH_2 at C-2 (δ_C 28.6), revealed the presence of a terminal γ -butyrolactone on the aglycone. Additionally, analysis of the 1H NMR and HSQC data of **5.2** indicated the presence of two AcO groups and a glycosidic bond at δ_H 4.98 (2H, m) and 3.63 (1H, m), and δ_C 73.9 and 78.2, respectively.

The position of the three hydroxyls in aglycone **5.4** was determined through MS^n analysis (Scheme 5.1). MS fragmentation showed the successive eliminations of three H_2O molecules at m/z 453.21, 435.30 and 417.26. Fragment ions allowed placement of the three 2° HO groups at C-13, C-17, and C-23. Primary α -cleavage (blue) followed by losses of H_2O and ethylene ($CH_2=CH_2$, red, m/z 399.12 and 355.11) allowed placement of HO at C-23. A similar α -cleavage (m/z 298.92) and elimination of H_2O and $CH_2=CH_2$ (m/z 255.06) led to an allylic alcohol and located the second HO at C-17. Double H rearrangement¹³ of the allylic alcohol gave an ethyl ketone that underwent α -cleavage at the C=O and gave an acylium ion consistent with m/z 227. Subsequent loss of C=O as indicated by m/z 197.11 placed the third HO at C-13.



Scheme 5.2: (a) Enantioselective reduction of ethyl levulinate (**5.5**) and lactonization to **5.6**, and (b) ECD spectra of **5.4** (1.49 mM, MeOH) and **5.6** (8.99 mM, MeOH).

The absolute configuration of the γ -butyrolactone was determined by comparison of the ECD spectrum of **5.4** with that of standard (*S*)-(-)-4-methylbutyrolactone (**5.6**, Scheme 5.2). Enantioselective reduction of ethyl levulinate (**5.5**) with Baker's yeast (3 days) and subsequent lactonization under acidic conditions (cat. *p*-TsOH) furnished (*S*)-(-)-**5.6** (93% ee, $[\alpha]_{\text{D}} -15.4$, (*c* 1.85, CH₂Cl₂)),¹⁴ the ECD spectrum of which is antipodal to that of **5.4**. Thus, the lactone terminus has the 4*R* configuration as depicted in Scheme 5.1.

The position of the glycosidic bond in **5.2** was determined through fragmentation analysis from MSⁿ measurements of **5.1**. Zemplén deacetylation¹⁵ of **5.2** (NaOMe, anhydrous MeOH, rt) provided the natural product **5.1**. HRMS analysis of **5.1** under negative ion mode gave a prominent deprotonated molecular ion adduct at *m/z* 1027.5696 ($[\text{M}-\text{H}]^{-}$) consistent with C₄₉H₈₈O₂₂ (calc'd

1028.5767). Fragmentation of **5.1** under positive ion mode gave a protonated molecular ion adduct at m/z 743.44, corresponding to $C_{33}H_{59}O_{18}^+$ (calc'd 743.3696), consistent with water elimination and α -cleavage at C-17 (Figure 5.3, teal). A second sodiated fragment ion of strong intensity was observed at m/z 599.30, corresponding to $C_{28}H_{48}O_{12}Na^+$ (calc'd 599.3038), due to the loss of Xyl-2, Xyl-3 and α -cleavage at C-17 (depicted in red). A successive loss of Xyl-1 (depicted in blue) was detected at m/z 476.23 ($C_{23}H_{40}O_8Na^+$, calc'd 467.2615). Thus, the position of the glycosidic bond is at C-17.

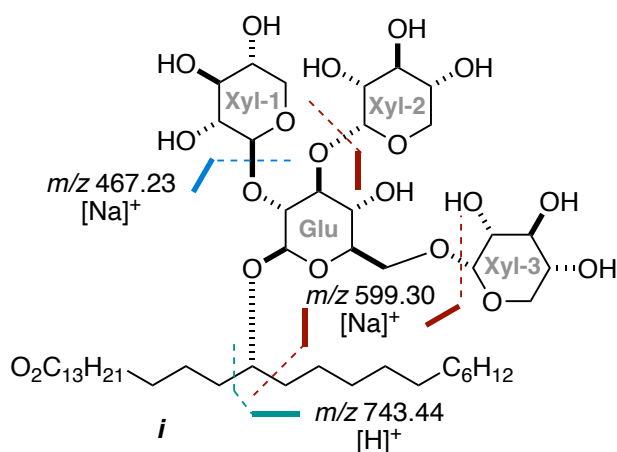
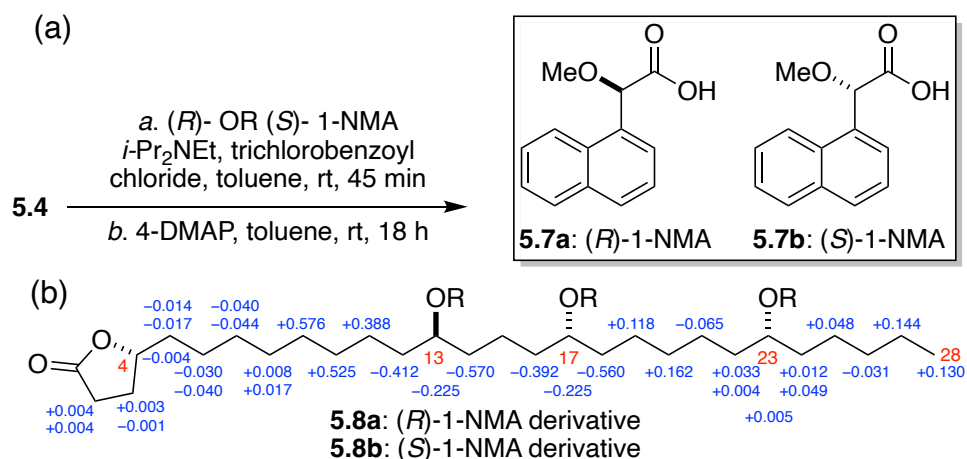


Figure 5.3: ESIMS fragmentation of **5.1** after primary loss of $-2H_2O$ to *i*.

5.3 Determination of the Absolute Configuration at C-13 and C-23



Scheme 5.3: (a) Yamaguchi esterification of **5.4** to **5.8a** and **5.8b**, and (b) $\Delta\delta^{\text{RS}}$ ($\delta^{\text{R}} - \delta^{\text{S}}$) values. See Ref. 20-21.

In order to assign configurations of C-13, C-17, and C-23 of **5.4**, we adopted a variation of the α -methoxyphenylacetic acid (MPA) ester method. MPA is employed as a chiral derivatizing agent (CDA) that introduces anisotropy in the ^1H NMR spectrum of the corresponding *R*- and *S*-MPA esters of chiral 2° alcohols, and is highly reliable for assignment of single secondary HO groups.¹⁶⁻¹⁷ The method relies upon measuring differential chemical shifts, $\Delta\delta^{\text{RS}}$, as defined in Equation 1, where δ^{R} and δ^{S} refer to the chemical shifts, at specific locants, in the *R*- and *S*-MPA esters, respectively (for simplicity, we will refer to the quantity $\Delta\delta^{\text{RS}}$ as ‘anisotropy’). Hoyer and coworkers evaluated several arylmethoxyacetic acid CDAs, after their esterification of (–)-menthol, and ascertained that (naphth-1-yl)methoxyacetic acid (1-NMA) provided the largest magnitude of $\Delta\delta$ values.¹⁸ Consequently, we selected 1-NMA as the chiral derivatizing agent (CDA) of choice over the more conventional MPA in recognition of the need to achieve maximal ^1H NMR anisotropy across the length of the long-chain in the corresponding derivatives, and link remote stereocenters with each other and the chain termini.

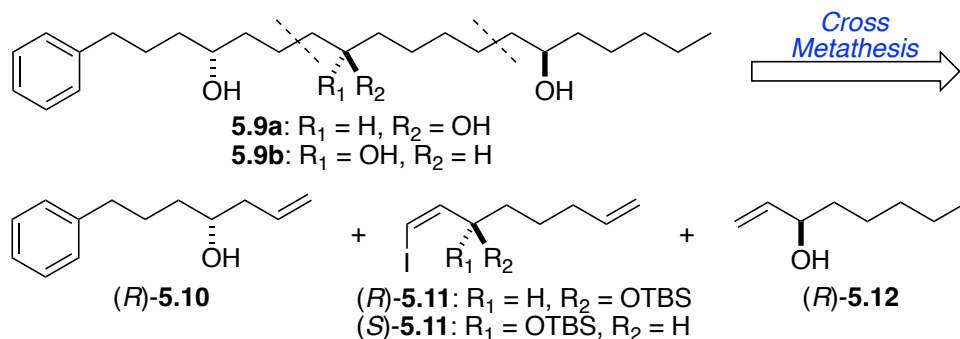
$$\Delta\delta^{\text{RS}} = \delta^{\text{R}} - \delta^{\text{S}} \quad \text{Eqn. 1}$$

The CDA, 1-NMA, was synthesized according to Kusumi and coworkers.¹⁹ Attempted triesterification of aglycone **5.4** under standard conditions (**5.7**, DCC, DMAP, CH₂Cl₂) failed, however, success was found with Yamaguchi conditions (**5.4**, **5.7a** or **5.7b**, 2,4,6-trichlorobenzoyl chloride, *i*Pr₂NEt, DMAP, toluene, rt, 18 h). Separation of the crude product by silica-HPLC provided pure **5.8a** and **5.8b**.²⁰ Scheme 5.3 depicts the colossal anisotropic shifts $\Delta\delta^{\text{RS}}$ induced by the 1-NMA group in **5.8a** and **5.8b**, in particular for the terminal methyl group which clearly showed diamagnetic shifts across six bonds ($\Delta\delta^{\text{RS}} = +0.13$ ppm) allowing a straightforward configurational assignment of C-23 in accord with the Riguera model.²¹ The ¹H NMR signals of **5.8a** and **5.8b** and, consequently reliable assignments of each $\Delta\delta^{\text{RS}}$ value, were made possible by analysis of the DQF-COSY, HSQC, HMBC and TOCSY spectra. In particular, TOCSY provided a critical relay across the largest distance – 11 bonds – from the remote C-4 in the terminal butyrolactone to the next stereocenter, C-13. Thus, in the first pass, the configurational assignment, 13*R*,23*R*-**5.4**, was made possible, but the C-17 configuration remained elusive due to opposing – and complicating – anisotropic effects ($\Delta\delta^{\text{RS}}$) of the CH₂ groups neighboring C-17.

In order to resolve these NMR ambiguities, two models, compounds **5.9a** and **5.9b**, – stereodefined analogs of aglycone **5.4** – were synthesized and converted to their corresponding (*R*)- and (*S*)- 1-NMA triesters to interrogate the C-17 configuration and verify the C-13 and C-23 assignments. Of the eight stereoisomers possible for **5.4** – four pairs of enantiomers – we ascertained only two diastereomers were necessary and sufficient for the following reasons. Having assigned C-13 and C-23 by direct inspection of unambiguous $\Delta\delta^{\text{RS}}$ values at the termini, interpretation of anisotropic effects at mid-chain would be informed by an understanding of the *relative* configuration of the remaining stereocenter with respect to C-13 and C-23. In other words, a solution to the problem would be found by answering the question, “what are the *syn*, *anti*-diol

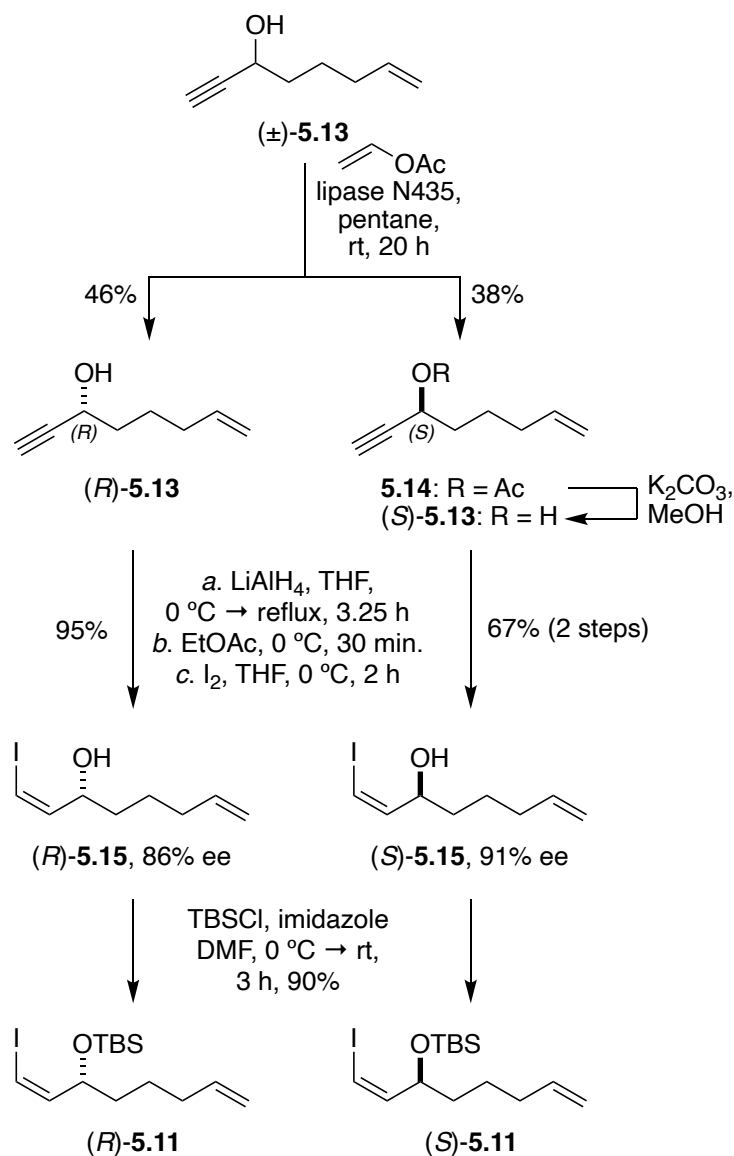
relationships of each pair, C-13–C-17 and C-17–C-23?” The answer would be found by the best-fit comparison of anisotropies of (*S*)- and (*R*)-1-NMA triesters of the natural aglycone **5.4** with triesters of only two model synthetic diastereomers.

5.4 Synthesis of Models **5.9a,b** and Determination of the Absolute Configuration at C-17



Scheme 5.4: Proposed retrosynthesis of models **5.9a** and **5.9b**.

The proposed retrosynthesis of **5.9a** and **5.9b** (Scheme 5.4) exploits the chemoselective cross metathesis of enantio-enriched **5.11** with the olefin terminus of (*R*)-**5.12** to effect carbon-carbon bond formation, followed by reductive cleavage of the C-iodine bond and a second cross metathesis of the resultant allylic alcohol with (*R*)-**5.10**. This synthetic strategy, inspired by Murata and coworkers,²² exploits **5.11** as a ‘vinyl-blocked’ linchpin; a Type III metathesis partner²³ that can be un-blocked by removal of I ($\text{Pd}(\text{PPh}_3)_4$, $n\text{-Bu}_3\text{SnH}$, benzene) for a subsequent second round of cross metathesis.

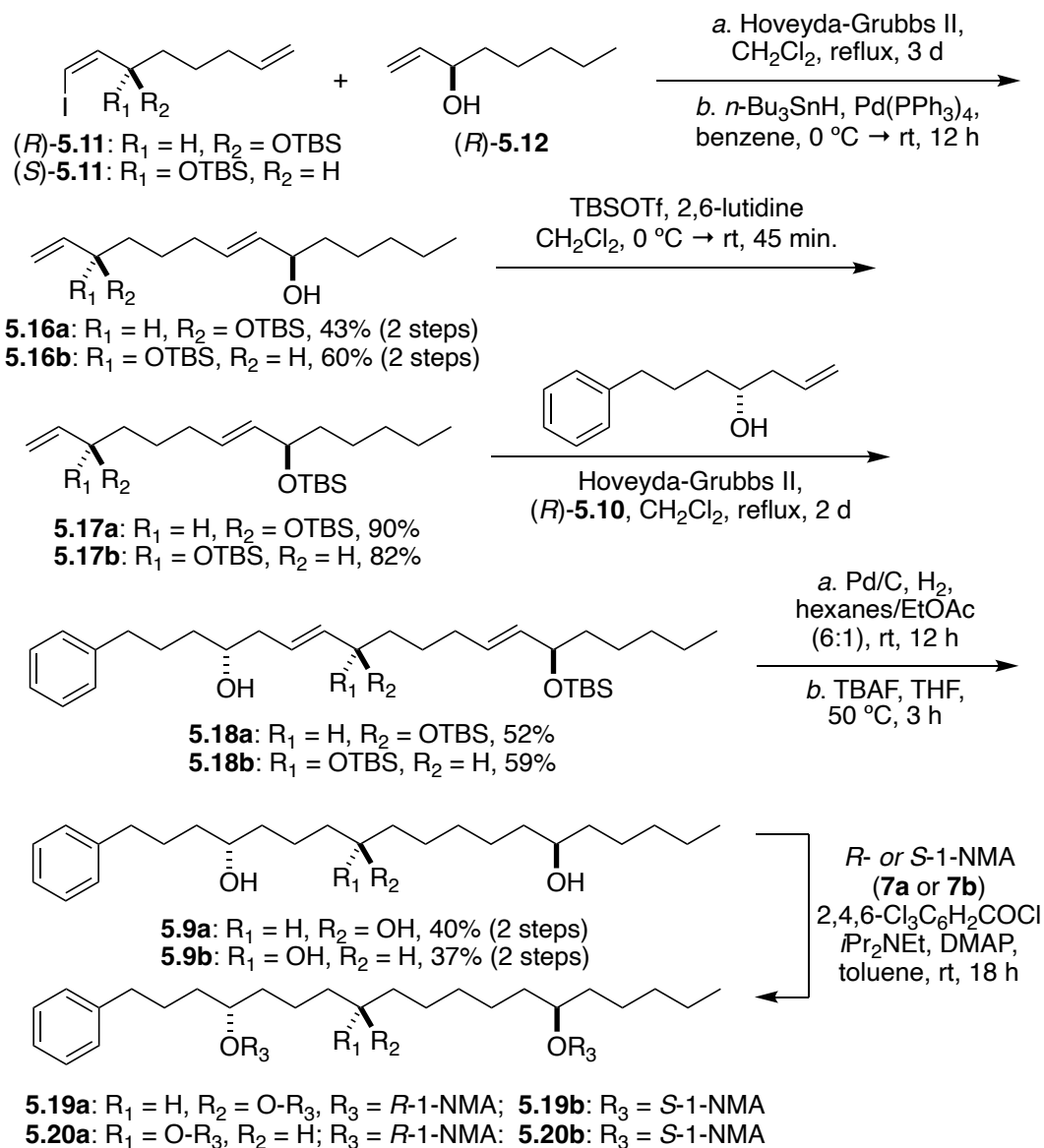


Scheme 5.5: Preparation of enantioenriched (*R*)- and (*S*)-**5.11**.

Enzymatic kinetic resolution of racemic **5.13** (Scheme 5.5) proceeded smoothly in the presence of Novozyme 435® (5% w/w, vinyl acetate-pentane, rt, 20 h) to furnish (after silica chromatographic separation) alcohol (*R*)-**5.13** (46%) and acetate **5.14** (38%). Reduction of the propargyl alcohol (*R*)-**5.13** (LiAlH_4) and capture of the intermediate vinyl-hydridoaluminate (I_2) delivered (*R*)-**5.15** (95%). The enantiomeric (*S*)-**5.15** was prepared in a similar fashion (67%, 2 steps) from (*S*)-**5.13**, the product of deacetylation of **5.14** ($\text{K}_2\text{CO}_3, \text{MeOH}$). TBS-protection of (*R*)- and (*S*)-**5.15** (TBSCl, imidazole, DMF) gave (*R*)- and (*S*)-**5.11** (~90%, each). Chiral-phase HPLC

analysis (Phenomenex Cellulose-3, 0.5% *i*PrOH/hexanes, dual UV-ECD detection, λ 280 nm), revealed the optical purities of (*R*)- and (*S*)-**5.11** were 86% and 91% ee, respectively: the absolute configuration of each enantiomer of **5.11** was secured by comparison of specific rotations with those of similar compounds in the literature.^{22,24} Analogously, (*R*)-**5.12** was synthesized (98% ee) through acetylation-kinetic resolution of (\pm)-**5.12** with lipase Novozyme 435® (vinyl acetate, Et₂O, rt, 24 h).

Synthesis of model compound **5.9a** was completed as follows (Scheme 5.6): cross metathesis of (*R*)-**5.11** and (*R*)-**5.12** mediated by the Hoveyda-Grubbs II catalyst (HG-II, CH₂Cl₂, 42 °C) followed by reductive removal of iodide (Pd(PPh₃)₄, *n*-Bu₃SnH, benzene) to give vinyl silyl ether **5.16a** in 43% (2 steps). Silylation of the latter (TBSOTf, 2,6-lutidine, CH₂Cl₂, 0 °C, 90%) gave **5.17a** and subsequent cross metathesis (HG-II, CH₂Cl₂, 42 °C) with (*R*)-**5.10** (derived from (*R*)-epichlorohydrin), delivered diene **5.18a** (45%, 2 steps). Completion of the synthesis by hydrogenation (Pd/C, hexanes/EtOAc (6:1), 1 atm H₂, rt, 12 h) followed by desilylation (TBAF, THF, 50 °C, 3 h) furnished **5.9a** (40%, 2 steps). Model compound **5.9b** was synthesized in an analogous manner from (*S*)-**5.11**.



Scheme 5.6: Synthesis of Model Compounds **5.9a** and **5.9b**, and the corresponding triesters **19a,b** and **20a,b**.

Model compounds **5.9a** and **5.9b** were converted to their 1-NMA triesters under Yamaguchi conditions (*R*- or *S*-1-NMA, 2,4,6-trichlorobenzoyl chloride, $i\text{Pr}_2\text{NEt}$, DMAP, toluene, rt, 18 h) to furnish the diastereomeric pairs **5.19a,b**, and **5.20a,b** (Scheme 5.6).²⁰ Analysis of the individual ^1H NMR signal assignments of **5.19a,b**, and **5.20a,b** and comparison of the anisotropies

with those of the aglycone-derived 1-NMA triesters ($\Delta\Delta\delta^{\text{RS}}$ values) with those of **5.8** supported a best-fit for the 17*R*-**5.4** configuration (Figure 5.4, blue bars).

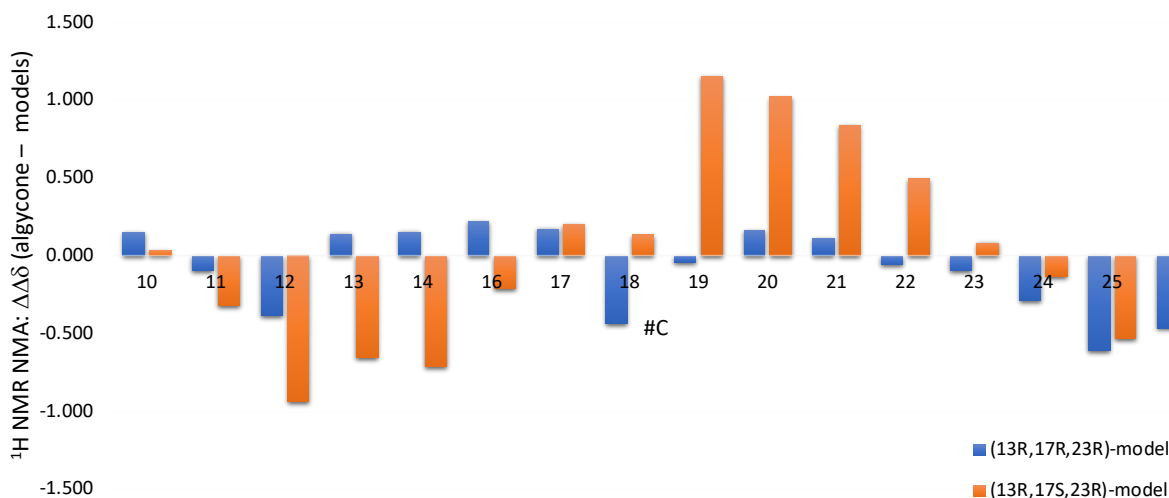


Figure 5.4: Differential ^1H NMR anisotropy ($\Delta\Delta\delta^{\text{RS}} = \Delta\delta^{\text{R}}(\mathbf{5.8}) - \Delta\delta^{\text{S}}(\mathbf{5.19}$ or $\mathbf{5.20})$) of the *tris*-(1-NMA)-esters **5.8**, **5.19** (blue bars) and **5.20** (orange bars) of aglycone **5.4** and model compounds **5.9a** and **5.9b**, respectively. Horizontal scale is C locant number.

Several interesting features of **5.4** and its 1-NMA triesters **5.8a,b** were revealed in this analysis. The ^1H NMR of each of the latter triesters showed only one set of signals and no evidence of diastereomers, revealing that **5.8a,b** and therefore, **5.4** were diastereomerically and enantiomerically pure. This evidence dispels the remote possibility that the hydroxyl groups in **5.4** were somehow introduced in a stereorandom fashion (autoxidation?) upon a linear C_{28} fatty acid precursor; rather they appear to result from directed enzyme-mediated reductions orchestrated by putative partially reducing polyketide synthase (PR-PKS). The pattern of oxidation is seen to be consistent with modular type I PKS biosynthesis for two compelling reasons: the carboxyl C-1 as an end group and alignments of oxidation sites, C-13, C-17 and C-23 with a canonical polyketide chain. Thus **5.4** is elaborated engaging 13 iterative ketide extensions (ketosynthase domains, KS) of an acetate starter unit (C-27, C-28) followed by successive rounds of partial reduction (keto-

reductase, KR with skipped rounds of dehydratase, DH, and enoyl reductase, ER). The placement of the three HO groups at C-13, C-17, and C-23 can be seen as arising from partial reduction, with many intervening CH₂ groups (e.g. C-5, C-7, C-9, C-11) developed by full reductions that engage all three modules: KR, DH and ER. Stereocenter C-4 appears to be the only oxidation site misaligned with this proposed PR PKS pattern. We postulate the oxygen at C-4 may be introduced in two possible ways through the addition of the (2*R*)-hydroxymalonyl-ACP²⁵⁻²⁶ extension unit or by a tailoring hydroxylation (CypP₄₅₀?); either post-assembly or on-assembly line followed by spontaneous or enzyme-mediated (transesterification, TE domain) cyclization to the lactone.

In the broad view, **5.1** is one of the most complex glycolipids yet described from marine invertebrates. The structure of its C₂₈ aglycone **5.4** likely reveals cryptic evidence of involvement of PR-PKS rather than traditional fatty acyl-type assembly and post-assembly oxidation as found in majority of glycolipids that comprise glycosylated long-chain 2° alcohols, or fatty acylated oligosaccharides.

In summary, the full stereostructure of the glycolipid, axinisoside-1 (**5.1**), was elucidated by a multi-pronged approach (MS, NMR, degradation) that exploited conventional analysis of the oligosaccharide segment and aglycone sub-structures. The absolute configuration of the complex C₂₈ aglycone **5.4** was solved by ECD (C-4) and exploitation of colossal NMR anisotropies of the derived 1-naphthylmethoxyacetic acid esters, **5.19a,b** and **5.20a,b** to assign the remotely-located secondary carbinols, C-13, C-17 and C-23. The oxidation pattern in **5.4** suggests a biosynthetic origin in a partially reducing polyketide synthase modular assembly line. Successful synthesis of the model compounds **9a,b** sets the stage for an informed synthesis of the aglycone, **5.4**, and, ultimately, the total synthesis of the glycolipid **5.1**.

5.5 Isolation, Structure Determination and Biological Activity of Oceanapins A–G

Additionally, an expedited protocol was developed for the identification of ceramide homologs. An inseparable mixture of ceramides (**5.3a–g**) was obtained from the ‘A layer’ of *Axinella* spp. sponge. Analysis of 1D and 2D NMR data revealed the presence of a sphingosine base connected through a peptide bond to a fatty acid chain at the amino group as depicted in Figure 5.5. Examination of the HRMS of the ceramide fraction indicated the presence of a complex mixture of homologs, differing by one methylene unit, that are consistent with the molecular formulas of oceanapins A–F, isolated previously from the sponge *Oceanapia* c.f. *tenuis* by Mancini and coworkers,¹ and a seventh homolog isolated from the gorgonian *Subergorgia suberosa* by Subrahmanyam and colleagues,¹¹ termed oceanapin G in this work (Table 5.2).

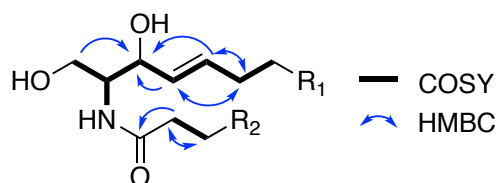
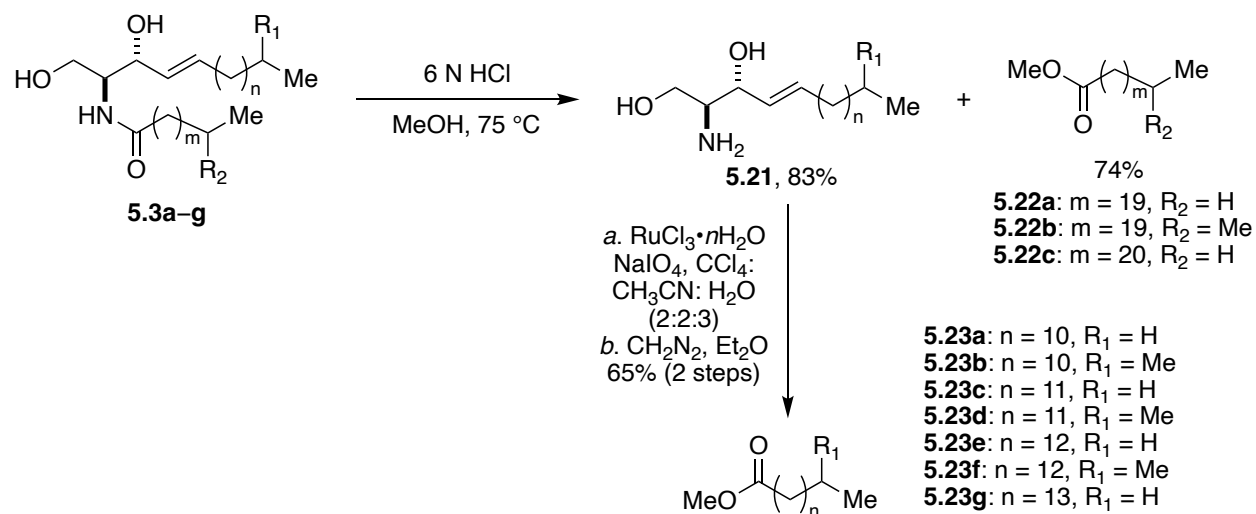


Figure 5.5: COSY (bold) and HMBC (arrows, blue) correlations of **5.3a–g**.

Table 5.2: HR-ESI-MS of Oceanapins A–G (**5.3a–g**).

Compound	[M+H] ⁺		[M+Na] ⁺		Formula
	Measured	Calc'd	Measured	Calc'd	
Oceanapin A	608.5965	608.5976	630.5787	630.5796	C ₃₉ H ₇₇ NO ₃
Oceanapin B/C			644.5944	644.5952	C ₄₀ H ₇₉ NO ₃
Oceanapin D/E	636.6279	636.6289	658.6097	658.6109	C ₄₁ H ₈₁ NO ₃
Oceanapin F	650.6435	650.6446	672.6258	672.6265	C ₄₂ H ₈₃ NO ₃
Oceanapin G	594.5818	594.5820	616.5632	616.5639	C ₃₈ H ₇₅ NO ₃



Scheme 5.7: Methanolysis of **5.3a–g** under acidic conditions.

Methanolysis (6 N HCl, MeOH, 75 °C) of **5.3a–g** yielded an aqueous layer comprising sphingosine bases (**5.21**) and a hexane-soluble layer containing the methyl esters **5.22a–c** (Scheme 5.7). GC-EI-MS of **5.22a–c** revealed the presence of three major compounds with adducts of 354 and 382 corresponding to molecular formulas of $\text{C}_{23}\text{H}_{46}\text{O}_2$ and $\text{C}_{25}\text{H}_{50}\text{O}_2$, respectively. The fragmentation patterns of the adducts supported docosanoic acid methyl ester (**5.22a**), methyl 20-methyl-heneicosanoate (**5.22b**), and tetracosanoic acid methyl ester (**5.22c**). The linear and branched fatty acid methyl esters are consistent with the oceanapins. HR-ESI-MS analysis of **5.21** revealed the presence of two sets of four homologs with $\Delta m/z$ of 14.0156 corresponding to a methylene group (Table 5.3). Interestingly, the resultant molecular formula of the major set of analogs (**5.21e–h**) corresponded to oxidized sphingosine bases that are inconsistent with those observed in the oceanapins. The molecular formula of the minor set of homologs (**5.21a–d**) matched previously observed data of the oceanapins. Consequently, two separate methanolysis reactions were completed under acidic (6 N HCl, methanol- d_4 , 75 °C) and aqueous basic (KOH, 100 °C) conditions followed by MS analysis to probe the results of the hydrolysis reaction.

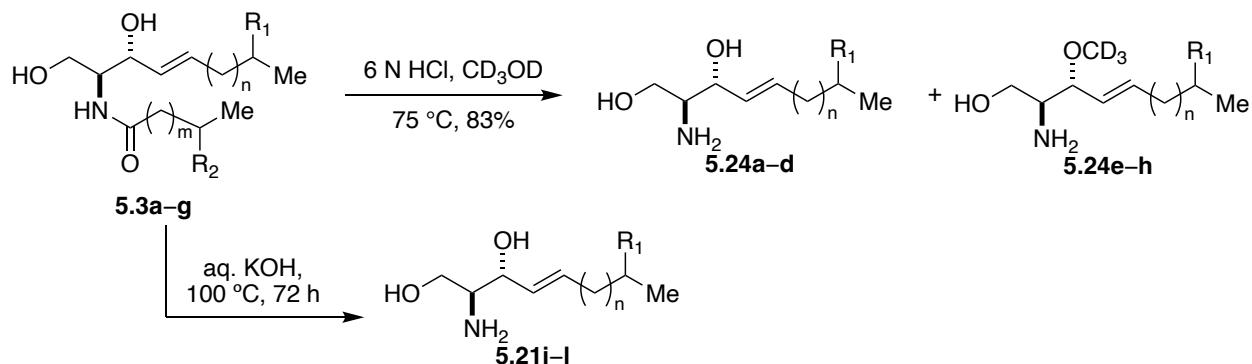
Table 5.3: HR-ESI-MS of sphingosine base **5.21**, **5.24**, triacetate **5.25**, and *N,O*-derivative **5.26**.

Homolog	Measured [M]	Calc'd [M]	Norm. %	Formula	Sphingosine Parent
5.21a	-	271.2511		C ₁₆ H ₃₃ NO ₂	C ₁₆ H ₃₃ NO ₂
5.21b	-	285.2668	21	C ₁₇ H ₃₅ NO ₂	C ₁₇ H ₃₅ NO ₂
5.21c	299.2825	299.2824	100	C ₁₈ H ₃₇ NO ₂	C ₁₈ H ₃₇ NO ₂
5.21d	313.2981	313.2981	57	C ₁₉ H ₃₉ NO ₂	C ₁₉ H ₃₉ NO ₂
5.21e	325.2982	325.2981	22	C ₂₀ H ₃₉ NO ₂	-
5.21f	339.3137	339.3137	100	C ₂₁ H ₄₁ NO ₂	-
5.21g	353.3293	353.3294	60	C ₂₂ H ₄₃ NO ₂	-
5.21h	367.3445	367.3450	5	C ₂₃ H ₄₅ NO ₂	-
5.21i	-	271.2511		C ₁₆ H ₃₃ NO ₂	C ₁₆ H ₃₃ NO ₂
5.21j	285.18 ^a	285.2668		C ₁₇ H ₃₅ NO ₂	C ₁₇ H ₃₅ NO ₂
5.21k	299.15 ^a	299.2824		C ₁₈ H ₃₇ NO ₂	C ₁₈ H ₃₇ NO ₂
5.21l	313.15 ^a	313.2981		C ₁₉ H ₃₉ NO ₂	C ₁₉ H ₃₉ NO ₂
5.24a	271.2517	271.2511		C ₁₆ H ₃₃ NO ₂	C ₁₆ H ₃₃ NO ₂
5.24b	285.2674	285.2668		C ₁₇ H ₃₅ NO ₂	C ₁₇ H ₃₅ NO ₂
5.24c	299.2829	299.2824		C ₁₈ H ₃₇ NO ₂	C ₁₈ H ₃₇ NO ₂
5.24d	313.2987	313.2981		C ₁₉ H ₃₉ NO ₂	C ₁₉ H ₃₉ NO ₂
5.24e	288.2858	288.2856		C ₁₇ H ₃₂ D ₃ NO ₂	-
5.24f	302.3013	302.3013		C ₁₈ H ₃₄ D ₃ NO ₂	-
5.24g	316.3151	316.3169		C ₁₉ H ₃₆ D ₃ NO ₂	-
5.24h	329.97 ^a	330.3326		C ₂₀ H ₃₈ D ₃ NO ₂	-
5.25a	397.3025	397.2828	7	C ₂₂ H ₃₉ NO ₅	C ₁₆ H ₃₃ NO ₂
5.25b	411.2984	411.2985	23	C ₂₃ H ₄₁ NO ₅	C ₁₇ H ₃₅ NO ₂
5.25c	425.3134	425.3141	100	C ₂₄ H ₄₃ NO ₅	C ₁₈ H ₃₇ NO ₂
5.25d	439.3291	439.3298	52	C ₂₅ H ₄₅ NO ₅	C ₁₉ H ₃₉ NO ₂
5.25e	337.2617	337.2617	5	C ₂₀ H ₃₅ NO ₃	C ₁₆ H ₃₃ NO ₂
5.25f	351.2768	351.2773	21	C ₂₁ H ₃₇ NO ₃	C ₁₇ H ₃₅ NO ₂
5.25g	365.2924	365.2930	100	C ₂₂ H ₃₉ NO ₃	C ₁₈ H ₃₇ NO ₂
5.25h	379.3080	379.3086	53	C ₂₃ H ₄₁ NO ₃	C ₁₉ H ₃₉ NO ₂
5.26a	759.3575	759.3560		C ₅₀ H ₄₉ NO ₆	C ₁₆ H ₃₃ NO ₂
5.26b	773.3711	773.3716		C ₅₁ H ₅₁ NO ₆	C ₁₇ H ₃₅ NO ₂
5.26c	787.3868	787.3873		C ₅₂ H ₅₃ NO ₆	C ₁₈ H ₃₇ NO ₂
5.26d	801.4024	801.4029		C ₅₃ H ₅₅ NO ₆	C ₁₉ H ₃₉ NO ₂

^aLR-MS.

Methanolysis of **5.3a–g** under acidic conditions in deuterated methanol resulted in two sets of four homologs. Homologs **5.24a–d** and **5.24e–h** belong to the sphingolipid base (**5.21a–d**) and deuterated *O*-methyl ethers at the 2° OH in 20-30%, respectively, signifying a significant side reaction of *O*-methyl ether formation (Scheme 5.8). *O*-methyl ether formation has previously been observed with sphingosine and dihydrosphingosine under acidic conditions; however, it can be

minimized in less concentrated acidic solutions.²⁷ In contrast, hydrolysis under aqueous basic conditions resulted only in the sphingoid base and eliminated the side reaction of *O*-methyl ether formation.²⁸ Base-promoted hydrolysis provided unambiguous results and confirmed that **5.21i-l** are the natural sphingosine bases.

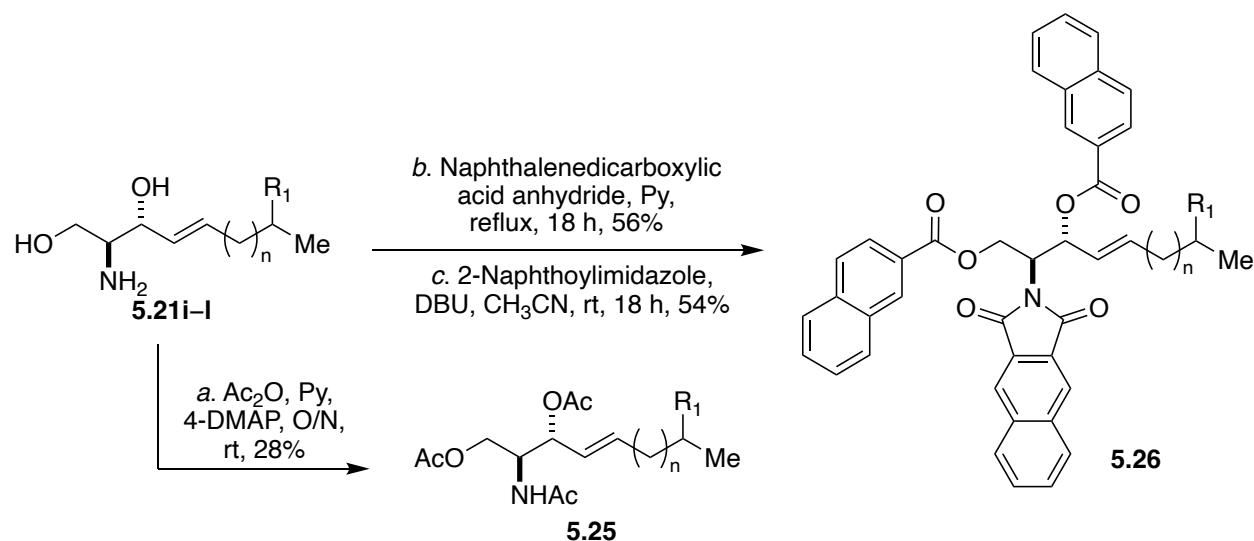


Scheme 5.8: Degradation of **5.3a-g** under acidic and basic conditions.

The sphingolipid base was further derivatized for GCMS analysis. Ruthenium oxidation (RuCl₃·*n*H₂O, NaIO₄, 2:2:3 CCl₄/CH₃CN/H₂O) followed by esterification (CH₂N₂, Et₂O) furnished the methyl esters **5.23a-g**. GCMS analysis indicated the presence of seven homologs differing by both a methylene unit and branching of the terminal chain. Moreover, acetylation (Ac₂O, Py, rt, Scheme 5.9) of **5.21i-l** gave triacetates **5.25**. HRMS analysis of **5.25** revealed the presence of four sodiated molecular adducts differing by a methylene, consistent with **5.25a-d**, in addition to the elimination product (**5.25e-h**, [M+H-Na-HOAc]⁺). The results of both GC and HR-MS are summarized in Tables 5.3 and 5.4, and are consistent with those previously observed with oceanapins A-G.

Table 5.4: GCMS analysis of **5.23**.

Homolog	Measured [M] ⁺	Matching Compound	Formula	Sphingosine Parent
5.23a	214	Dodecanoic acid	C ₁₂ H ₂₄ O ₂	C ₁₆ H ₃₃ NO ₂
5.23b	228	11-methyldodecanoic acid	C ₁₃ H ₂₆ O ₂	C ₁₇ H ₃₅ NO ₂
5.23c	228	Tridecanoic acid	C ₁₃ H ₂₆ O ₂	C ₁₇ H ₃₅ NO ₂
5.23d	242	12-methyltridecanoic acid	C ₁₄ H ₂₈ O ₂	C ₁₈ H ₃₇ NO ₂
5.23e	242	Tetradecanoic acid	C ₁₄ H ₂₈ O ₂	C ₁₈ H ₃₇ NO ₂
5.23f	256	13-methyltetradecanoic acid	C ₁₅ H ₃₀ O ₂	C ₁₉ H ₃₉ NO ₂
5.23g	256	Pentadecanoic acid	C ₁₅ H ₃₀ O ₂	C ₁₉ H ₃₉ NO ₂

**Scheme 5.9:** Naphthyl and acetyl derivatization of **5.21i-I**.

The absolute configuration of **5.21** was determined through measurement of the ECD of the *N*-naphthimide-*O*-naphthoate derivative (**5.26**) and comparison with published spectra of the four sphingosine isomers.²⁹ Kawamura and coworkers developed an *N,O*-derivatization method of sphingosine and dihydrosphingosine coupled with ECD analysis that enabled the identification of the stereochemistry of all the isomers. Reaction of **5.21i-I** with 2,3-naphthalenedicarboxylic acid anhydride in anhydrous pyridine provided the *N*-naphthimide derivative in 56% (Scheme 5.9). Subsequent esterification with 2-naphthoylimidazole and DBU in anhydrous pyridine gave **5.26** in 54%. The ECD spectrum of **5.26** in CH₃CN showed a negative cotton effect at 260 nm and a

positive cotton effect at 239 nm and revealed the absolute configuration of **5.21** to be *D*-erythro-sphingosine, which is consistent with the observed configuration of the oceanapins (Figure 5.6).

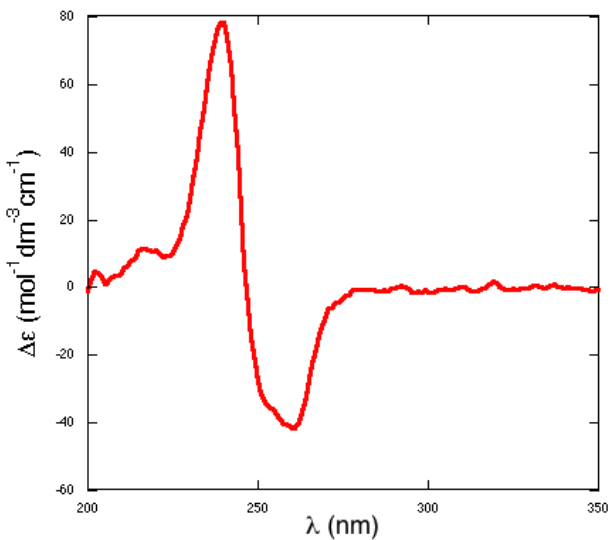


Figure 5.6: ECD spectrum of **5.26** (CH₃CN).

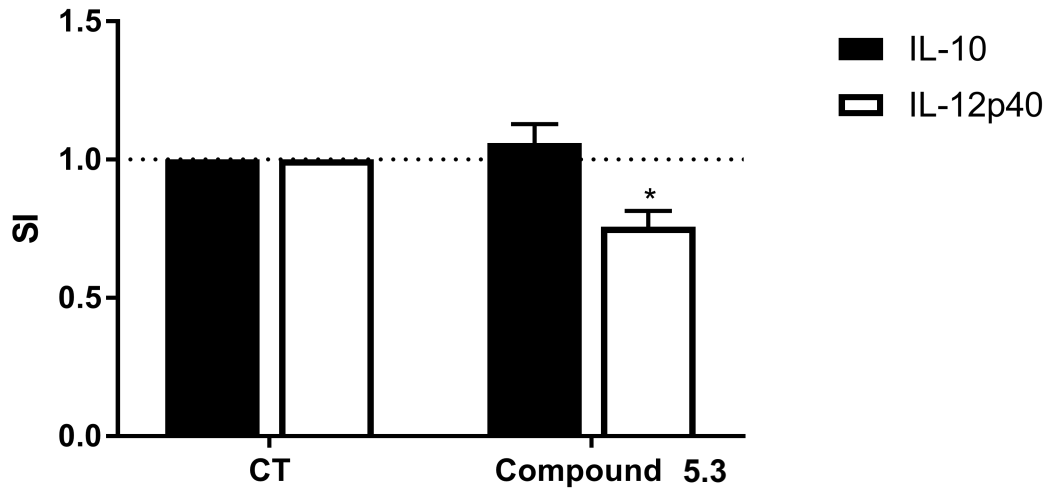


Figure 5.7: Differential cytokine release—IL-10 and IL-12p40—from dendritic cells stimulated by oceanapins A–G (**5.3a–g**).

Interestingly, oceanapins A–G (**5.3a–g**) significantly decreased the IL-12p40 secretion without impacting the production of IL-10 in dendritic cells, which suggests that **5.3a–g** possess anti-inflammatory properties.

5.6 Conclusions

In conclusion, the absolute stereostructure of axinoside-1 (**5.1**), isolated from the polar extracts of a Western Australian *Axinella* spp. sponge, was elucidated after extensive spectroscopic analysis of 1D and 2D NMR, mass spectrometry, degradation, derivatization, and synthesis. Axinoside-1 is characterized by a non-glycerol polyhydroxylated aglycone that is glycosylated at the C-17 hydroxyl by a tetrasaccharide consisting of α -D-glucose linked through a 1,2-glycosidic bond to β -D-xylose-1, 1,3-glycosidic bond to α -D-xylose-2, and 1,6-glycosidic bond to α -D-xylose-3. The configuration of the aglycone presented a challenge as the three secondary hydroxyl groups were separated from one another and the chain termini. Consequently, esterification of the aglycone with (*R*)- and (*S*)-2-methoxy-2-(naphthalen-1-yl)acetic acid (1-NMA) induced anisotropy in the ^1H NMR chemical shifts of the tri-NMA derivatives over large distances and denoted the $13R,23R$ -**5.2** configuration. Still, the configuration at C-17 remained equivocal due to the additive anisotropic effect observed in the NMR. Herein, we synthesized two stereodefined standards, and comparison against the corresponding four NMA-derivatives supported the $17R$ -**5.2** configuration. Lastly, an expedited protocol was developed to aid in the isolation and structural elucidation of the known ceramides, oceanapins A–G, which displayed anti-inflammatory properties in dendritic cells.

Chapter 5, in part, is a reprint of the material, “Colossal NMR Anisotropy Relays Remote Stereoconfiguration. The Absolute Stereostructure of the Complex Glycolipid, Axinoside-1, from

a Western Australian Axinellid Sponge.” In Preparation for submission to *J. Am. Chem. Soc.* The dissertation author was the primary author of this paper and gratefully acknowledges the contributions of coauthor Tadeusz F. Molinski.

5.7 Acknowledgements

We are thankful to Tara Zand (Jeff Reinhart Group at UCSD) for her assistance with SEM image collection and Dr. Mary Key Harper for her assistance in determining that sample 93-07-067 belongs to the Axinellid family. We are grateful to A. Mrse, B. Duggan and X. Huang for NMR support and X. Su for HRMS measurements. The purchases of the Agilent TOF mass spectrometer and the 500 MHz NMR spectrometer were made possible with funds from the NIH Shared Instrument Grant program (S10RR025636) and the NSF Chemical Research Instrument Fund (CHE0741968), respectively. MS is grateful for support from a Graduate Research Fellowship, Department of Chemistry, UCSD. TFM is grateful for the 2020 ACS Ernest Guenther Award for natural product chemistry. This research was supported by grants from the NIH to TFM from the NIH (AI100776, AT009783).

5.8 Experimental

General Experimental Procedures. Preparative, semi-preparative and analytical HPLC were completed on a JASCO system consisting of a UV-VIS detector (UV-2075), dual-pumps (PU-2086 Plus), and a dynamic mixer (MX-2080-32). LC-MS measurements were performed with a Thermoelectron Surveyor UHPLC coupled to an MSD single-quadrupole detector. GC-MS analyses were carried out on an Agilent 7820A GC equipped with an Agilent 5977B GC-MSD unit and HR-ESI-TOF mass spectroscopy analyses were conducted on an Agilent 1200 HPLC

connected to an Agilent 6350 TOF-MS at the Small Molecule Mass Spectrometry Facility at the Department of Chemistry and Biochemistry at UCSD. UV-Vis spectra were measured on a JASCO V-630 spectrometer. FTIR spectrum were collected from thin film samples using a JASCO FTIR-4100 fitted with an ATR ZnSe plate. Optical rotations were measured on a JASCO P-2000 polarimeter at the D-double emission line of Na. CD spectrum were measured on a JASCO J-810 spectropolarimeter at 23 °C in quartz cells of 1, 2 or 5 mm pathlength. 1D and 2D NMR spectra were measured on a JEOL ECA (500 MHz) or JEOL ECZ (400 MHz) spectrometer, equipped with a 5 mm $^1\text{H}\{^{13}\text{C}\}$ room temperature probe, or a Bruker Avance III (600 MHz) NMR spectrometer with a 1.7 mm $^1\text{H}\{^{13}\text{C}/^{15}\text{N}\}$ microcryoprobe (23 °C). ^{13}C NMR spectra were collected on a Varian NMR spectrometer (500 MHz) fitted with a 5 mm XSens $^{13}\text{C}\{^1\text{H}\}$ cryoprobe. NMR spectra were referenced to residual solvent signals (chloroform- d_3 , δ_{H} 7.26, δ_{C} 77.16 ppm; methanol- d_4 , δ_{H} 3.31, δ_{C} 49.00 ppm).

Biological Material. *Axinella* spp. (93-07-67) was collected in 1993 from Western Australia by hand and kept frozen (−20 °C) until needed. A type sample (MeOH) is archived in the Department of Chemistry and Biochemistry, UCSD.

Extraction and Isolation. *Axinella* spp. (wet wt. 131.30 g) was lyophilized (dry wt. 70.55 g) and extracted twice with MeOH/ CH_2Cl_2 (2 x 1000 mL, 1:1) over a period of 2 days to give the crude extract (10.3 g). The crude was dissolved in a 9:1 solution of MeOH/ H_2O (400 mL) before repeated extraction with hexanes (2 x 400 mL). The hexanes layer was dried to yield hexane-soluble ‘A layer’ (1.5465 g). H_2O was added to the aqueous MeOH layer to a final ratio of 6:4 of MeOH/ H_2O (600 mL), and then repeatedly partitioned against CH_2Cl_2 (2 x 500 mL) to provide CH_2Cl_2 -soluble ‘B layer’ (0.5226 g). The MeOH was removed, and the resultant aqueous layer was

extracted with *n*-BuOH (2 x 200mL) to furnish the *n*-BuOH-soluble 'C layer' (2.05 g) and H₂O-soluble 'D layer' (3.3042 g).

The A layer (0.9874 g) was purified by flash chromatography (SiO₂, step gradient of EtOAc in hexanes) to give six fractions. Fractions five (29.1 mg) and six (57.2 mg) were pooled and further purified on a short flash chromatography column (SiO₂, step gradient of 2 → 10% MeOH/CH₂Cl₂, stained blue with vanillin-H₂SO₄) to give ceramides **5.3a–g** (52.1 mg). The ceramides were identified by mass spectrometry, ¹H and ¹³C NMR, degradation, and derivatization.

The C layer (1.54 g) was separated by size-exclusion chromatography (Sephadex LH-20, MeOH) into ten fractions, which were pooled according to TLC (UV-activity, stains blue with cerium (IV) ammonium molybdate). The third (0.2750 g), fourth (0.3970 g) and fifth (0.4892 g) fractions contained glycolipids. A sample of fraction five (112 mg) was acetylated (Ac₂O, Py, DMAP) under N₂ at rt for 18 h. Excess reagents were removed by bulb-to-bulb distillation at 0.6 torr, and the crude product was purified by SiO₂ chromatography (0 → 2% MeOH/CH₂Cl₂) to give a clear colorless oil (89.1 mg). The oil was separated on an SPE cartridge (silica, 60 → 70% EtOAc/hexanes) to give a peracetate glycolipid mixture (48.0 mg). The mixture of peracetate esters (25 mg) was further purified by semipreparative reversed-phase HPLC (Luna C₁₈, 250 x 10.0 mm, step gradient, 25:75 H₂O-CH₃CN for 30 min to 100% CH₃CN over 5 min, 2.5 mL.min⁻¹) to give the peracetylated glycolipid **5.2** (16.0 mg, *t*_R = 41.19 min) as a clear colorless oil.

Axinoside-1 (**5.1**): colorless oil; [α]_D -26 (*c* 0.095, MeOH); FTIR (film) ν 3370, 2927, 2859, 1072, and 1043 cm⁻¹; HRMS (ESI-TOF) *m/z* 1027.5696 [M-H]⁻, calc'd for C₄₉H₈₇O₂₂⁻ 1027.5694).

Axinoside-1 Peracetate (5.2): colorless oil; $[\alpha]_D -40$ (c 0.82, CHCl_3); FTIR (film) ν 2927, 2853, 1741, 1367, 1220, 1175, 1038, and 984 cm^{-1} ; See Table 5.1 for the ^1H and ^{13}C NMR data of **5.2**; HRMS (ESI-TOF) m/z 1555.6927 $[\text{M}+\text{Na}]^+$ (calc'd 1555.6927 for $\text{C}_{73}\text{H}_{112}\text{O}_{34}\text{Na}^+$).

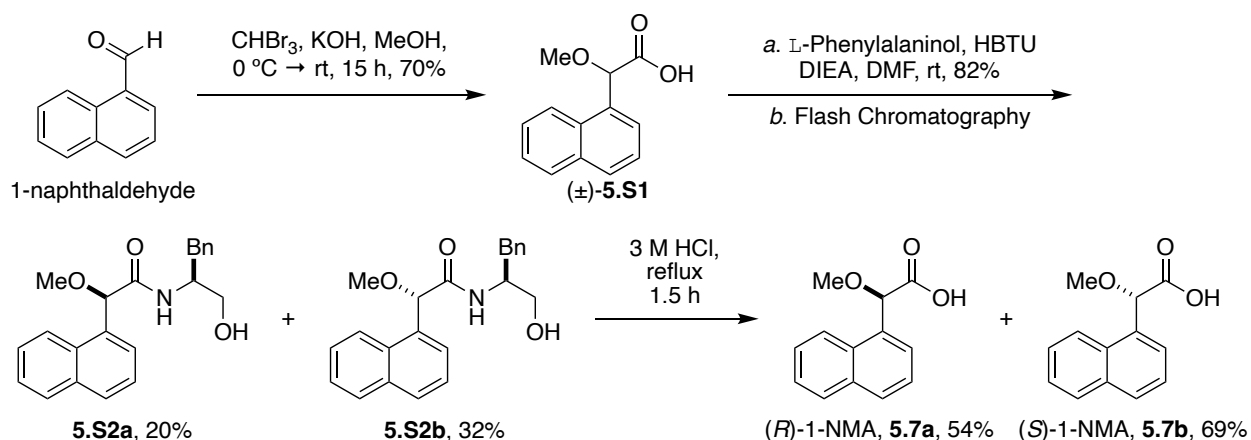
Oceanapins A–G (5.3a–g): ^1H NMR (500 MHz, CDCl_3) δ (ppm, integ., mult, J Hz) 0.86 (3H, t, 6.5), 0.88 (3H, t, 6.5), 1.14 (2H, m), 1.25 (56H, br s), 1.36 (3H, m), 1.51 (1H, septet, 6.5), 1.63 (2H, m), 2.05 (2H, q, 7.0, 14.0), 2.22 (2H, t, 7.5), 3.69 (1H, dd, 3.0, 11.0), 3.90 (1H, m), 3.94 (1H, dd, 3.5, 11.0), 4.31 (1H, t, 4.5), 5.51 (1H, dd, 6.5, 15.5), 5.78 (1H, dt, 7.0, 15.5), and 6.29 (1H, d, 7.0). ^{13}C NMR (125 MHz, CDCl_3) δ (ppm) 11.58, 14.30, 19.37, 22.82, 22.85, 25.91, 27.27, 27.36, 27.58, 28.11, 29.27, 29.39, 29.44, 29.52, 29.54, 29.64, 29.65, 29.68, 29.79, 29.81, 29.86, 30.10, 30.19, 32.08, 32.45, 34.53, 36.78, 36.98, 39.19, 54.57, 62.61, 74.76, 128.85, 134.44, and 174.15. See Table 5.2 for HR-ESI-MS data of **5.3a–g**.

Methanolysis of Compound 5.2. Concentrated HCl (2 drops) was added to a solution of **5.2** (4.0 mg) in MeOH (10 mL). The mixture was purged with N_2 , stirred at $75\text{ }^\circ\text{C}$ for 18 h, cooled to rt, and evaporated under vacuum to give a white solid. The crude was partitioned between Et_2O (3 mL) and H_2O (3 mL), and the aqueous layer was extracted with Et_2O (2 x 3 mL). The aqueous layer was concentrated under reduced pressure to give a mixture of *O*-Me-glycosides (0.5 mg). The organic layer was concentrated and purified by SiO_2 chromatography (10% MeOH/ CH_2Cl_2 , staining with cerium (IV) ammonium molybdate) to give aglycone **5.4** (1.0 mg). **5.4**: $[\alpha]^{22.2}_D +22.1$ (c 0.467, CH_2Cl_2); ECD (MeOH, c 1.49×10^{-3} M, $23\text{ }^\circ\text{C}$) λ 209 nm ($\Delta\epsilon -0.22$). ^1H NMR (500 MHz, CDCl_3) δ (ppm, integ., mult, J Hz) 0.89 (3H, d, 6.5 Hz), 1.20 – 1.60 (40H, m), 1.73 (1H, m), 1.85 (1H, m), 2.31 (1H, m), 2.53 (2H, t, 8.2 Hz), 3.40 (2H, m), 3.58 (1H, m), 4.48 (1H, m); HRMS (ESITOF) m/z 493.3865 $[\text{M}+\text{Na}]^+$ (calc'd 493.3863 for $\text{C}_{28}\text{H}_{54}\text{O}_5\text{Na}^+$).

Silylation of the O-Me-Glycoside Mixture from Methanolysis of 5.2. The interior surface of a 3.7 mL glass vial was silylated by addition of BSTFA (1 mL) and anhydrous pyridine (1 mL) at 75 °C for 30 min, then emptied and dried in an oven. BSTFA (0.9 mL), TMSCl (0.1 mL), and anhydrous pyridine (0.9 mL) were added to the *O*-Me-glycosides (0.5 mg, see above) under N₂. The solution was stirred at 75 °C for 30 min, cooled to rt, and analyzed by GC-MS (Agilent BD-5MS UI, 30 m x 0.25 mm x 0.25 μm, He, 1.2 mL·min⁻¹, 250 °C (injector temperature), 230 °C (MS source), 150 °C (MS squad), 1 μL injection). *O*-Tri-TMS-*O*-methyl D-xylopyranoside anomers eluted at 9.95 min (Peak A) and 10.16 min (Peak B), respectively. *O*-Tetra-TMS-*O*-methyl D-glucopyranoside anomers eluted at 12.48 min (Peak C) and 12.65 min (Peak D), respectively. The retention times matched those of authentic standards prepared from D-Xyl and D-Glu after methanolysis (SOCl₂, MeOH, 0 °C → 75 °C, 16 h) and silylation (Pierce's reagent (BSTFA, TMSCl, pyridine, 75 °C, 30 min). Peak A EI-MS: 217 (66), 218 (14), 206 (9), 205 (20), 204 (100), 147 (41), 133 (33), 129 (13), 75 (10), 73 (80). Peak B: 217 (61), 218 (13), 206 (8), 205 (19), 204 (100), 147 (30), 133 (27), 129 (10), 75 (9), 73 (72). Peak C: 217 (28), 218 (8), 206 (9), 205 (22), 204 (100), 147 (26), 133 (28), 129 (10), 73 (60). Peak D: 217 (24), 218 (7), 206 (9), 205 (22), 204 (100), 147 (22), 133 (24), 129 (7), 73 (55).

(-)-(S)-5-methyldihydrofuran-2(3H)-one, 5.6. Lactone (-)-**5.6** was synthesized according to a reported literature procedure.³⁰ Ethyl-levulinate (**5.5**, 1.63 g, 11.3 mmol) was added to a suspension of sucrose (12.73 g, 37.2 mmol) and yeast (50.22 g) in H₂O at rt. The mixture was placed in a shaker and agitated at 120 rpm and 25 °C for 1 d. Then the mixture was stirred at rt for 2 d. The reaction mixture was extracted with EtOAc (3 x 200 mL). The organic layer was centrifuged to separate the aqueous from the organic layer. The organic layer was washed with brine (1x), dried over MgSO₄, filtered and evaporated. The crude was purified by SiO₂

chromatography (5 → 25% EtOAc/ hexanes) to give unreacted **5.5** (0.45 g), ethyl (*S*)-4-hydroxypentanoate and **5.6** (0.93 g). The latter mixture (0.35 g) was dissolved in benzene (12 mL) and stirred at rt for 4 h with cat. *p*-TsOH. Anhydrous Na₂SO₄ and Na₂CO₃ were added to the reaction. After 30 min, the reaction mixture was filtered, and the filtrate carefully concentrated under reduced pressure to give the volatile (–)-**5.6**. [α]^{21.7}_D –15.4 (*c* 1.85, CH₂Cl₂); ECD (MeOH, *c* = 8.99 × 10^{–3} M, 23 °C) λ 210 nm (Δε +0.19). The ¹H NMR data matched the reported literatures values.³¹



Scheme 5.10: Synthesis of (*R*)- and (*S*)-1-NMA.

2-Methoxy-2-(naphth-1-yl)acetic acid, (±)-**5.S1**. Compound (±)-**5.S1** was synthesized according to a known literature procedure.³² A solution of KOH (88%, 11.5 g, 180.4 mmol) in MeOH (32.0 mL) was added to a solution of 1-naphthaldehyde (5.0 g, 32.0 mmol) and tribromomethane (4.2 mL, 46.7 mmol) in MeOH (18.0 mL), slowly over 1 h, at 0 °C in a large reaction flask (highly exothermic reaction). The solution was allowed to warm to rt over 17 h with stirring. The mixture was diluted with H₂O and extracted with CH₂Cl₂ (3 × 40 mL). The aqueous layer was acidified with concentrated HCl to pH ~ 1, extracted with EtOAc (2 × 40 mL), and the

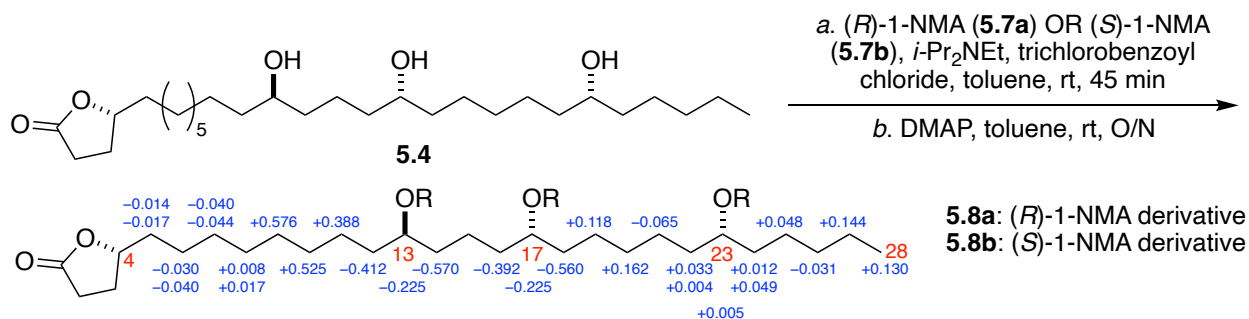
combined organic layers were dried over Na₂SO₄, filtered and evaporated. The product was crystallized from EtOAc/hexanes to give **5.S1** (4.84 g, 75%) as a pale-yellow solid.

N-((S)-1-hydroxy-3-phenylprop-2-yl)-2-methoxy-2-(naphthyl-1-yl)acetamide, **5.S2**. HBTU (0.88 g, 2.3 mmol) and DIPEA (2.0 mL, 0.12 mmol) were added to a solution of (±)-**5.S1** (0.5 g, 2.3 mmol) and L-phenylalaninol (0.35 g, 2.3 mmol) in dry DMF (6.5 mL) at rt under N₂. After 12 h, the reaction mixture was diluted with H₂O (200 mL) before repeated extraction with CH₂Cl₂ (4 x 20 mL). The combined organic layers were washed with HCl (2 x 20 mL, 1 M), H₂O (1 x 20 mL), NaHCO₃ (2 x 20 mL, 0.5 M), brine (1x), dried over Na₂SO₄, filtered and evaporated. The crude product was purified on SiO₂ chromatography (80% EtOAc/ hexanes) to give **5.S2a** and **5.S2b** in 20% and 32%, respectively, as pale-yellow oils. **5.S2a**: ¹H NMR (400 MHz, CDCl₃) δ (ppm, integ., mult, *J* Hz) 2.85 (1H, m), 2.98 (1H, dd, 6.8, 9.2), 3.32 (3H, s), 3.66 (1H, dd, 6.0, 11.2), 3.77 (1H, dd, 3.6, 10.8), 4.21 (1H, m), 5.23 (1H, s), 7.14 (1H, d, 7.2 Hz), 7.19 (2H, m), 7.23 – 7.31 (2H, m), 7.37 (1H, t, 7.2), 7.39 – 7.48 (2H, m), 7.82 (2H, m), 8.01 (1H, bs), 8.03 (1H, d, 8.4); HRMS (ESITOF) *m/z* 350.1750 [M+H]⁺ (calc'd 350.1751 for C₂₂H₂₃NO₃). **5.S2b**: ¹H NMR (400 MHz, CDCl₃) δ (ppm, integ., mult, *J* Hz) 2.05 (1H, bs), 2.94 (2H, m), 3.27 (3H, s), 3.62 (1H, m), 3.70 (1H, m), 4.17 (1H, m), 5.20 (1H, s), 7.14 (1H, d, 7.2 Hz), 7.22 (2H, m), 7.31 (2H, m), 7.42 – 7.54 (4H, m), 7.85 (2H, m), 8.19 (1H, d, 8.0); HRMS (ESITOF) *m/z* 350.1750 [M+H]⁺ (calc'd 350.1751 for C₂₂H₂₃NO₃).

(R)-2-methoxy-2-(naphthalen-1-yl)acetic acid, *(R)-1-NMA* (**5.7a**). A solution of **5.S2a** (0.16 g, 0.5 mmol) in HCl (30 mL, 30 mmol, 3 M) was refluxed at 130 °C for 1.5 h. The reaction mixture was cooled to rt and extracted with Et₂O (3x). The Et₂O layer was washed with sat'd NaHCO₃ (2x), and the base layer was acidified with HCl (1 M) and extracted with Et₂O (2x) and EtOAc (2x). The Et₂O and EtOAc were combined, washed with brine (1x), dried over Na₂SO₄,

filtered, and evaporated to give **5.7a** (53.3 mg, 54%) as an off-white solid. $[\alpha]^{21.7}_{\text{D}} -134.2$ (c 0.11, EtOH). The ^1H NMR and HRMS were consistent with reported literature values.³²

(*S*)-2-methoxy-2-(naphth-1-yl)acetic acid, (*S*)-1-NMA (**5.7b**). A solution of **5.S2b** (0.2596 g, 0.74 mmol) in HCl (3 M, 50 mL, 50 mmol) was refluxed at 140 °C for 1 h. The reaction mixture was cooled to rt, and extracted with Et₂O (3x). The Et₂O layer was washed with sat'd NaHCO₃ (2x), and the alkaline layer was acidified with concentrated HCl and extracted with EtOAc (3x). The EtOAc layer was washed with brine (1x), dried over Na₂SO₄, filtered and evaporated to give **5.S2b** (110.4 mg, 69%) as an off-white solid. $[\alpha]^{21.7}_{\text{D}} +123.3$ (c 0.115, EtOH). The ^1H NMR and HRMS were consistent with reported literature values.³²

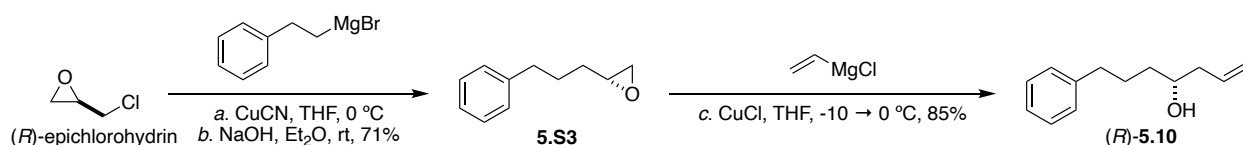


Scheme 5.11: Synthesis of tris-NMA derivatives **8a,b**.

Compound 5.8a. Compound **5.8a** was obtained by esterification of **5.4** according to a reported literature procedure.²⁰ *i*-Pr₂NEt (0.7 μL, 3.82 μmol) and 2,4,6-trichlorobenzoyl chloride (0.6 μL, 3.82 μmol) were added to a solution of **5.4** (0.2 mg, 0.42 μmol) and (*R*)-1-NMA (**5.7a**, 0.55 μL, 3.82 μmol) in dry toluene (100 μL) under Ar. After 45 min, a solution of DMAP (5 μL, 5.0 μmol, 100 mg/mL) in toluene was added. After stirring for 18 h, the reaction mixture was diluted with HCl (0.5 mL, 0.5 mmol, 1 M), and extracted with CH₂Cl₂ (3 x 0.5 mL). The organic layer was washed with H₂O (1x) and dried under N₂. The crude material was purified by semi-

preparative HPLC (SiO₂, 40% EtOAc/ hexanes, 3.0 mL·min⁻¹) to give **5.8a** (*t_R* = 10.45 min). HRMS (ESITOF) *m/z* 1087.5902 [M+Na]⁺ (calc'd 1087.5906 for C₆₇H₈₄O₁₁).

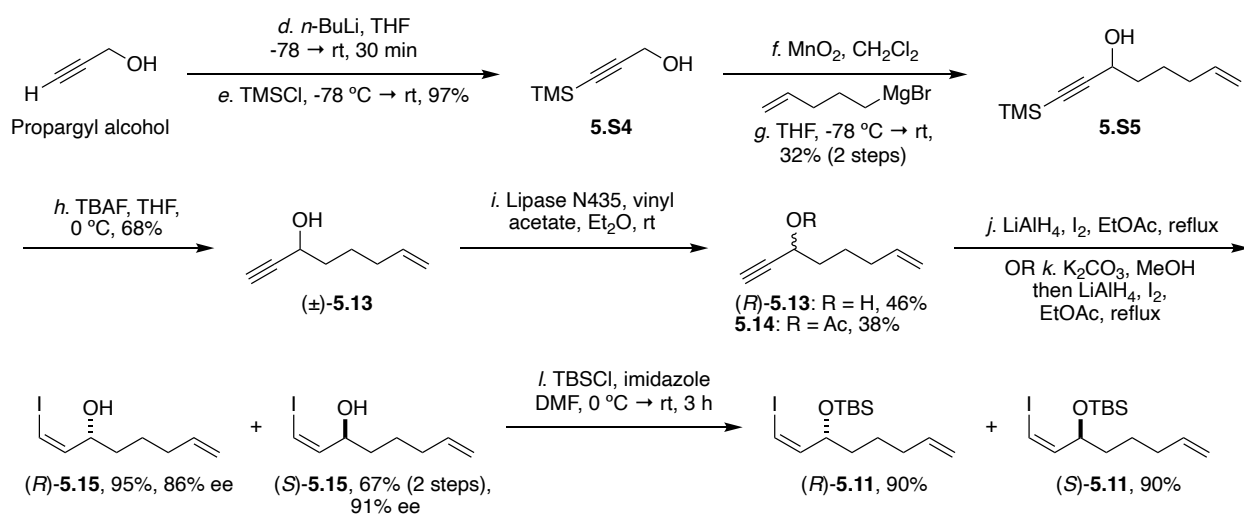
Compound 5.8b. Aglycone **5.4** (0.2 mg, 0.42 μmol) was derivatized with (*S*)-1-NMA (**5.7b**), according to the procedure described above for **5.8a**, to give **5.8b** (*t_R* = 11.63 min). HRMS (ESITOF) *m/z* 1087.5903 [M+Na]⁺ (calc'd 1087.5906 for C₆₇H₈₄O₁₁).



Scheme 5.12: Synthesis of alcohol (-)-**5.10**.

(R)-2-(3-phenylpropyl)oxirane (*(R)*-**5.10**). A solution of 2-bromoethyl benzene (2.97 mL, 21.7 mmol) in dry THF (10 mL) was added dropwise to Mg turnings (0.63 g, 26.1 mmol) coated with I₂ under N₂ in a two-necked round bottom flask equipped with a reflux condenser. The solution was refluxed for 2 h, cooled to rt, and added dropwise to a solution of *(R)*-epichlorohydrin (0.85 mL, 10.9 mmol) and CuCN (97.0 mg, 1.1 mmol) in dry THF (20 mL) at -10 °C. After stirring at -10 °C for 2h, the reaction mixture was warmed to rt and stirred for 16 h. The reaction mixture was quenched with sat'd NH₄Cl, the layers were separated, and the aqueous layer was extracted with Et₂O (3x). The combined organic layer was washed with brine (1x), dried over MgSO₄, filtered and evaporated. The crude was purified on SiO₂ (5% → 10% EtOAc/ hexanes) to give *(R)*-1-chloro-5-phenylpentan-2-ol. Crushed NaOH (2.315 g, 57.9 mmol) was added to a stirred solution of *(R)*-1-chloro-5-phenylpentan-2-ol in Et₂O (25 mL). After 18 h, the reaction mixture was filtered on Celite, and the filtrate was concentrated. The crude was purified on SiO₂ (5% → 10% EtOAc/ hexanes) to give **5.S3** (1.251 g, 71% over 2 steps) as a colorless oil. [α]_D +14.0 (*c* 2.56, CHCl₃). The ¹H NMR and HRMS matched reported literature values.³³

(*R*)-**5.10** was synthesized according to the protocol developed by Walkinshaw and colleagues.³⁴ Cu(I)Cl (30.5 mg, 0.31 mmol) was added to a flame-dried flask under N₂ and dried under vacuum at 4.2 Torr and 80 °C for 30 min before immediate use. The flask was cooled to rt and vinyl magnesium chloride (2.89 mL, 4.62 mmol, 1.6 M in THF) was added. The mixture was cooled to -10 °C, and a solution of **5.S3** (0.50 g, 3.08 mmol) in THF (2 mL) was added dropwise over 1 h. The reaction mixture was warmed to 0 °C, diluted with MeOH (0.25 mL) and subsequently quenched by addition of HCl (3.9 mL, 2 M) while maintaining the temperature between 0 – 10 °C. After 1 h, the mixture was diluted with MTBE (5 mL), the layers were separated, and the aqueous layer was extracted with MTBE (2 x 5 mL). The combined organic layer was washed with HCl (1x, 1 M), H₂O (1x), sodium thiosulfate (2x, 1 M), H₂O (1x), dried over MgSO₄, filtered and evaporated. The crude was purified on SiO₂ (10% EtOAc/hexanes) to give (*R*)-**5.10** (0.497 g, 85%) as a colorless oil. The ¹H NMR and HRMS matched reported literature values.³⁵



Scheme 5.13: Synthesis of (*R*)- and (*S*)-**5.11**.

1-(trimethylsilyl)oct-7-en-1-yn-3-ol (**5.S5**). Compounds **5.S4** were synthesized according to the reported literature procedure.³⁶ *n*-BuLi (38 mL, 94.5 mmol, 2.5 M in THF) was added

dropwise to a solution of propargyl alcohol (2.5 mL, 43 mmol) in dry THF (120 mL) at -78 °C. After stirring for 30 min at rt, the reaction mixture was cooled to -78 °C, and TMSCl (12 mL, 94.5 mmol) was added dropwise. After 5 min, the reaction mixture was warmed to rt, and stirred for 16 h. The reaction mixture was slowly quenched with HCl (100 mL, 2 M, aq.) followed by addition of sat'd aq. NaHCO₃ (50 mL). The layers were separated, and the aqueous layer was extracted with Et₂O (3 x 100 mL). The combined organic layer was dried over MgSO₄, filtered, and carefully evaporated. The crude was purified on SiO₂ (10% → 20% EtOAc/ hexanes) to give **5.S4** (5.32 g, 97%) as an orange oil.

A mixture of MnO₂ (48.4 g, 560 mmol, pre-heated at 170 °C under reduced pressure for 2-3 h) and **5.S4** (7.14 g, 55.7 mmol) in CH₂Cl₂ (280 mL) was stirred at rt for 4 d. The reaction mixture was filtered on celite, and the filtrate was carefully concentrated from an ice-bath to furnish the aldehyde. A solution of 5-bromo-1-pentene (9.2 mL, 77.9 mmol) in THF (90 mL) was added dropwise to activated Mg turnings (2.165 g, 89.1 mmol) at rt, and the suspension was refluxed for 3 h. The resultant Grignard reagent was added dropwise to the aldehyde (55.7 mmol) in THF (45 mL) at -78 °C. After stirring at rt for 18 h, the reaction mixture was quenched by slow addition of sat'd aq. NH₄Cl (30 mL), the layers were separated, and the aqueous layer was extracted with Et₂O (3 x 50 mL). The combined organic layer was washed with brine (1x), dried over MgSO₄, filtered and evaporated. The crude was purified on SiO₂ (5% → 15% EtOAc/ hexanes) to give **5.S5** (3.50 g, 32%) as a pale-yellow oil. The ¹H NMR and HRMS data are consistent with published literature values.³⁷

Oct-7-en-1-yn-3-ol ((±)-5.13). TBAF (4.3 mL, 4.3 mmol, 1 M in THF) was added to a solution of **5.12** (0.71 g, 3.6 mmol) in THF (35 mL) at 0 °C. After 1 h, the reaction mixture was quenched by addition of sat'd aq. NH₄Cl, the layers were separated, and the aqueous layer was

extracted with Et₂O (3x). The combined organic extract was washed with brine (1x), dried over MgSO₄, filtered and evaporated. The crude was purified on SiO₂ (5% → 10% EtOAc/ hexanes) to give (±)-**5.13** (0.304g, 68%). The ¹H NMR and HRMS data are consistent with the reported literature values.³⁸

(R)-Oct-7-en-1-yn-3-ol (*(R)*-**5.13**). A solution of (±)-**5.13** (1.89 g, 15.2 mmol), vinyl acetate (7.0 mL, 76 mmol) and lipase (Novozym[®] 435, 100 mg) in pentane (30 mL, 0.5 M) was agitated in an orbital shaker at rt for 20 h. The suspension was filtered through a bed of Celite, and the filtrate was carefully concentrated. The crude product was purified on SiO₂ (5% → 30% Et₂O/pentane) to give *(R)*-**5.13** (0.867 g, 46%) and **5.14** (0.97 g, 39%) as colorless oils. *(R)*-**5.13**: [α]_D +15.1 (*c* 1.00, CHCl₃). The ¹H NMR and HRMS data are consistent with the reported literature values.³⁸ **5.14**: [α]_D -73.7 (*c* 1.00, CHCl₃). The ¹H NMR and HRMS data are consistent with the reported literature values.³⁹

(S)-Oct-7-en-1-yn-3-ol (*(S)*-**5.13**). A slurry of **5.14** (0.95 g, 5.7 mmol) and K₂CO₃ (1.575 g, 11.4 mmol) in MeOH (28.5 mL, 0.2 M) was stirred at rt for 1.5 h. H₂O (50 mL) was added to dissolve the salts, and the reaction mixture was extracted with Et₂O (3 x 50 mL). The combined organic layer was washed with sat'd aq. NH₄Cl, dried over Na₂SO₄, filtered and evaporated. The crude was purified on SiO₂ (10% → 30% Et₂O/pentane) to give *(S)*-**5.13** (0.63 g, 89%) as a colorless oil. [α]_D -8.08 (*c* 1.00, CHCl₃). The ¹H NMR and HRMS data are consistent with the reported literature values.³⁸

(R,Z)-1-Iodocta-1,7-dien-3-ol (*(R)*-**5.15**). A solution of *(R)*-**5.13** (0.4169 g, 3.36 mmol) in THF (5.0 mL) was added dropwise to a suspension of LiAlH₄ (0.322 g, 8.06 mmol) in THF (35 mL) at 0 °C. The flask containing *(R)*-**5.13** was rinsed with THF (5.0 mL) and the solution was added to the reaction mixture. The reaction mixture was refluxed for 3.25 h, cooled to rt and then

0 °C, and EtOAc (3.3 mL) was added. After 30 min at 0 °C, a solution of I₂ (2.56 g, 10.1 mmol) in THF (10 mL) was added dropwise at 0 °C. After 2 h at 0 °C, the reaction mixture was quenched by addition of sat'd aq. NaHCO₃ and sat'd aq. Na₂SO₃ (50 mL, 1:1 ratio), the layers were separated, and the aqueous layer was extracted with EtOAc (3x). The combined organic layer was washed with brine (1x), dried over MgSO₄, filtered and evaporated. The crude was purified on SiO₂ (10% → 25% Et₂O/hexanes) to give (*R*)-**5.15** (0.808 g, 95%) as a colorless oil. Compounds (±)-**5.15** and (*R*)-**5.15** were dissolved in hexanes (10 mg/mL) and separated by chiral NP-HPLC (Lux Cellulose-3, 5 μm, 250 x 4.6 mm, 0.5% IPA-hexane, isocratic, 1 mL·min⁻¹, λ = 280 nm) with an in-line CD detector (Jasco, CD-2095 plus) to provide (*R*)-**5.15** (R_t = 16.67 min.), and (*S*)-**5.15** (R_t = 17.64 min.). Peak 1: (*R*)-**5.15**: t_R = 16.43 min., area = 93.09. Peak 2: (*S*)-**5.15**: t_R = 18.04 min., area = 6.91; 86%ee. [α]_D +45.7 (c 1.60, CHCl₃). ¹H NMR (500 MHz, CDCl₃) δ (ppm, integ., mult, *J* Hz) 6.34 (1H, dd, *J* = 7.6, 1.0 Hz), 6.24 (1H, t, *J* = 7.6 Hz), 5.81 (1H, ddt, *J* = 17.0, 10.2, 6.7 Hz), 5.03 (1H, dq, *J* = 17.0, 2.0 Hz), 4.97 (1H, ddt, *J* = 10.2, 2.0, 1.2 Hz), 4.41 (1H, tdd, *J* = 7.6, 5.4, 1.0 Hz), 2.16 – 2.03 (2H, m), 1.70 – 1.40 (4H, m). ¹³C NMR (125 MHz, CDCl₃) δ (ppm) 24.4, 33.7, 35.4, 74.4, 82.7, 115.0, 138.6, 143.4. HRMS (ESITOF) *m/z* 234.9973 [M–H₂O+H]⁺ (calc'd 234.9978 for C₈H₁₂I⁺).

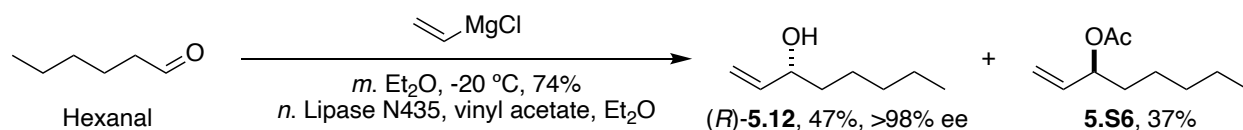
(*S,Z*)-1-Iodoocta-1,7-dien-3-ol ((*S*)-**5.13**). A solution of (*S*)-**5.13** (0.319 g, 2.57 mmol) in THF (4.0 mL) was added dropwise to a suspension of LiAlH₄ (0.246 g, 6.17 mmol) in THF (26 mL) at 0 °C. The flask containing (*S*)-**5.13** was rinsed with THF (4.0 mL) and the solution was added to the reaction mixture. The reaction mixture was refluxed for 3.25 h, cooled to rt and then 0 °C, and EtOAc (2.5 mL) was added. After 30 min at 0 °C, a solution of I₂ (1.96 g, 7.71 mmol) in THF (8 mL) was added dropwise at 0 °C. After 2 h at 0 °C, the reaction mixture was quenched by addition of sat'd aq. NaHCO₃ and sat'd aq. Na₂SO₃ (40 mL, 1:1 ratio), the layers were separated,

and the aqueous layer was extracted with EtOAc (3x). The combined organic layer was washed with brine (1x), dried over MgSO₄, filtered and evaporated. The crude was purified on SiO₂ (10% → 25% Et₂O/hexanes) to give (*S*)-**5.15** (0.593 g, 92%) as a colorless oil. Compounds (±)-**5.15** and (*S*)-**5.15** were dissolved in hexanes (10 mg/mL) and separated by chiral NP-HPLC (Lux Cellulose-3, 5 μm, 250 x 4.6 mm, 0.5% IPA-hexane, isocratic, 1 mL·min⁻¹, λ = 280 nm) with an in-line CD detector (Jasco, CD-2095 plus) to provide (*R*)-**5.15** (R_t = 16.67 min.), and (*S*)-**5.15** (R_t = 17.64 min.). Peak 1: (*R*)-**5.15**: t_R = 16.80 min., area = 2.05. Peak 2: (*S*)-**5.15**: t_R = 17.21 min., area = 97.95; 91%ee. [α]_D -30.7 (c 1.03, CHCl₃). ¹H NMR (500 MHz, CDCl₃) δ (ppm, integ., mult, *J* Hz) 6.33 (1H, dd, *J* = 7.6, 1.0 Hz), 6.23 (1H, t, *J* = 7.6 Hz), 5.80 (1H, ddt, *J* = 17.0, 10.2, 6.7 Hz), 5.02 (1H, dq, *J* = 17.0, 2.0 Hz), 4.96 (1H, ddt, *J* = 10.2, 2.0, 1.2 Hz), 4.40 (1H, tdd, *J* = 7.6, 5.4, 1.0 Hz), 2.09 (2H, tdd, *J* = 7.0, 5.4, 1.5 Hz), 1.66 – 1.38 (4H, m). ¹³C NMR (125 MHz, CDCl₃) δ (ppm) 24.4, 33.7, 35.4, 74.4, 82.6, 115.0, 138.6, and 143.4. HRMS (ESITOF) *m/z* 234.9973 [M–H₂O+H]⁺ (calc'd 234.9978 for C₈H₁₂I⁺).

(*R,Z*)-*tert*-Butyl((1-iodoocta-1,7-dien-3-yl)oxy)dimethylsilane ((*R*)-**5.11**). A solution of TBSCl (0.574 g, 3.81 mmol) and imidazole (0.303 g, 4.44 mmol) in DMF (8.0 mL) was added dropwise to a solution of (*R*)-**5.15** (0.80 g, 3.17 mmol) in DMF (4.5 mL) at 0 °C. After stirring for 3 h at rt, the reaction mixture was quenched with sat'd aq. NaHCO₃ (25 mL) and H₂O (25 mL), extracted with hexanes (3 x 30 mL), and the combined organic layer was washed with brine (1x), dried over Na₂SO₄, filtered and evaporated. The crude was purified on SiO₂ (5% Et₂O/hexanes) to give (*R*)-**5.11** (1.04 g, 90%) as a colorless oil. [α]_D -8.10 (c 1.46, CHCl₃). ¹H NMR (500 MHz, CDCl₃) δ (ppm, integ., mult, *J* Hz) 6.23 – 6.14 (2H, m), 5.81 (1H, ddt, *J* = 17.0, 10.2, 6.6 Hz), 5.02 (1H, ddt, *J* = 17.0, 2.3, 1.6 Hz), 4.96 (1H, ddt, *J* = 10.2, 2.3, 1.2 Hz), 4.40 – 4.28 (1H, m), 2.08 (2H, dddd, *J* = 7.7, 6.4, 4.8, 1.4 Hz), 1.59 – 1.37 (4H, m), 0.88 (9H, s), 0.09 (3H, s), 0.05 (3H, s).

^{13}C NMR (125 MHz, CDCl_3) δ (ppm) -4.6, -4.1, 18.2, 24.4, 26.0, 33.8, 36.4, 75.4, 79.9, 114.7, 138.9, 144.8. HRMS (ESITOF) m/z 367.0947 $[\text{M}+\text{H}]^+$ (calc'd 367.0949 for $\text{C}_{14}\text{H}_{28}\text{IOSi}^+$).

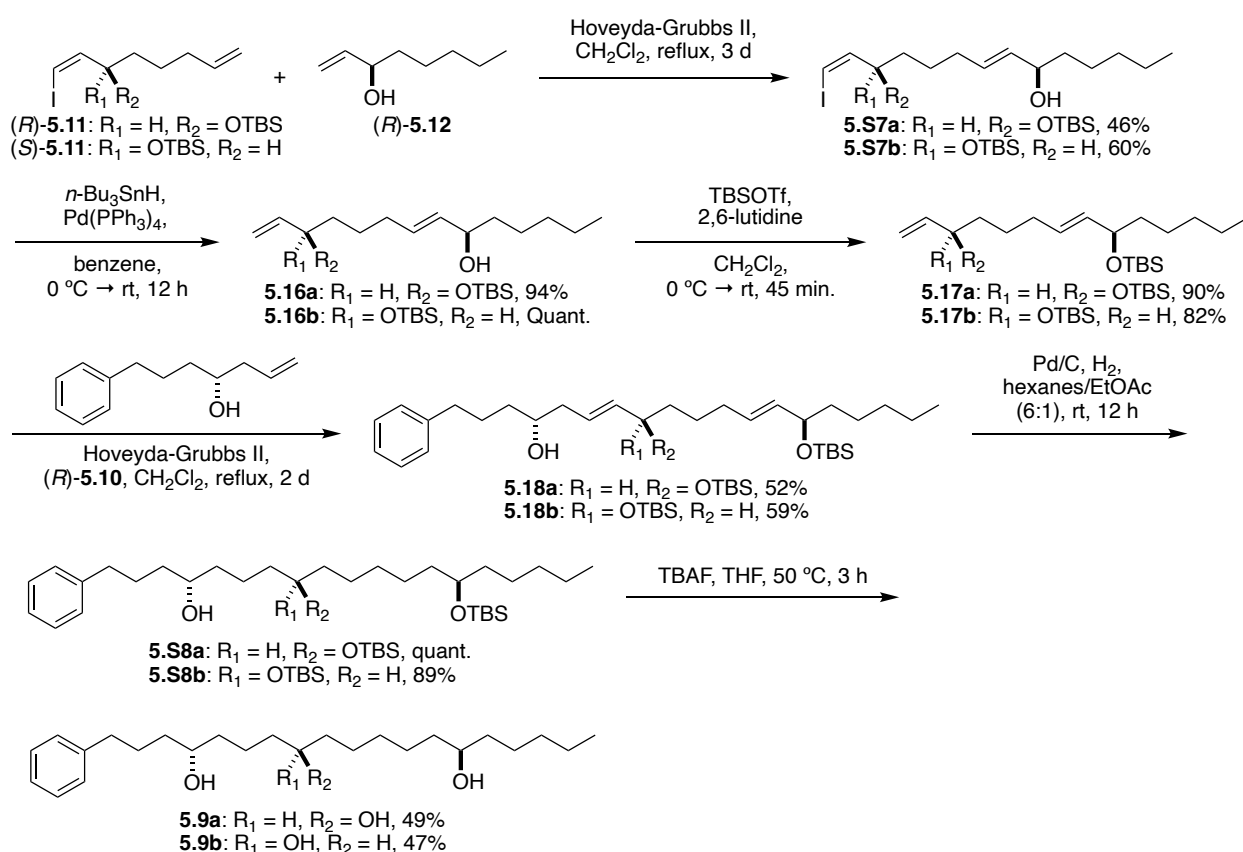
(S,Z)-*tert*-Butyl((1-iodoocta-1,7-dien-3-yl)oxy)dimethylsilane ((*S*)-**5.11**). A solution of TBSCl (0.423 g, 2.81 mmol) and imidazole (0.223 g, 3.28 mmol) in DMF (6.0 mL) was added dropwise to a solution of (*S*)-**5.15** (0.59 g, 2.34 mmol) in DMF (3.0 mL) at 0 °C. After stirring for 3 h at rt, the reaction mixture was quenched with sat'd aq. NaHCO_3 (25 mL) and H_2O (25 mL), extracted with hexanes (3 x 30 mL), and the combined organic layer was washed with brine (1x), dried over Na_2SO_4 , filtered and evaporated. The crude was purified on SiO_2 (5% EtOAc/hexanes) to give (*S*)-**5.11** (0.772 g, 90%) as a colorless oil. $[\alpha]_{\text{D}} -12.4$ (c 1.66, CHCl_3). ^1H NMR (500 MHz, CDCl_3) δ (ppm, integ., mult, J Hz) 6.24 – 6.13 (2H, m), 5.81 (1H, ddt, $J = 17.0, 10.2, 6.6$ Hz), 5.02 (1H, dq, $J = 17.0, 2.0$ Hz), 4.96 (1H, ddt, $J = 10.2, 2.0, 1.3$ Hz), 4.40 – 4.28 (1H, m), 2.08 (2H, tdd, $J = 8.1, 4.2, 2.8$ Hz), 1.54 – 1.41 (4H, m), 0.88 (9H, s), 0.09 (3H, s), 0.05 (3H, s). ^{13}C NMR (125 MHz, CDCl_3) δ (ppm) -4.6, -4.1, 24.4, 26.0, 33.8, 36.4, 75.4, 79.9, 114.7, 138.9, 144.8. HRMS (ESITOF) m/z 367.0947 $[\text{M}+\text{H}]^+$ (calc'd 367.0949 for $\text{C}_{14}\text{H}_{28}\text{IOSi}^+$).



Scheme 5.14: Synthesis of (*R*)-**5.12**.

(R)-*Oct-1-en-3-ol* ((*R*)-**5.12**). Vinylmagnesium chloride (17.2 mL, 27.5 mmol, 1.6 M in THF) was added dropwise to a solution of hexanal (3.0 mL, 25.0 mmol) in Et_2O (75 mL) at $-20\text{ }^\circ\text{C}$. After 3 h at $-20\text{ }^\circ\text{C}$, the reaction mixture was warmed to rt and stirred for 16 h. The reaction mixture was quenched by slow addition of sat'd aq. NH_4Cl , the layers were separated, and the aqueous layer was extracted with Et_2O (3 x 50 mL). The combined organic layer was washed with

brine (1x), dried over MgSO₄, filtered and evaporated. The crude was purified on SiO₂ (10% Et₂O/pentanes) to give (±)-**5.12** (2.37 g, 74%) as a colorless oil. A solution of (±)-**5.12** (2.20 g, 17.2 mmol), vinyl acetate (1.75 mL, 18.9 mmol) and lipase N435 (195 mg) in Et₂O (50 mL, 0.39 M) was shaken at rt for 24 h. The suspension was filtered, and the filtrate was carefully concentrated. The crude was purified on SiO₂ (10% → 25% Et₂O/hexanes) to give (*R*)-**5.12** (1.0242 g, 47%) and **5.S6** (1.0945 g, 37%) as colorless oils. (*R*)-**5.12**: [α]_D –5.55 (*c* 1.21, CHCl₃). The ¹H NMR and HRMS matched reported literature values.⁴⁰ **5.S6**: [α]_D –8.97 (*c* 1.79, CHCl₃). The ¹H NMR and HRMS matched reported literature values.⁴¹



Scheme 5.15: Synthesis of models **5.9a,b**.

(6*R*,7*E*,12*R*,13*Z*)-12-((*tert*-Butyldimethylsilyl)oxy)-14-iodotetradeca-7,13-dien-6-ol

(**5.S7a**). A solution of Hoveyda Grubbs II catalyst (14.9 mg, 23.7 μmol) in CH₂Cl₂ (0.5 mL) was

added dropwise to a solution of (*R*)-**5.11** (290 mg, 0.792 mmol) and (*R*)-**5.12** (304.5 mg, 2.37 mmol) in CH₂Cl₂ (2.15 mL) under N₂ at 40 °C. After 44 h, additional Hoveyda Grubbs II catalyst (14.9 mg, 23.7 μmol) in CH₂Cl₂ (0.5 mL) and (*R*)-**5.12** (101.5 mg, 0.792 mmol) were added dropwise to the reaction. After an additional 20 h, the reaction mixture was cooled to rt and purified on SiO₂ (100% hexanes → 10% Et₂O/hexanes) to give **5.S7a** (170 mg, 46%) after the recovery of unreacted (*R*)-**5.11**. [α]_D +7.17 (*c* 1.67, CHCl₃). ¹H NMR (500 MHz, CDCl₃) δ (ppm, integ., mult, *J* Hz) 6.22 – 6.13 (2H, m), 5.68 – 5.56 (1H, m), 5.47 (1H, ddt, *J* = 15.4, 7.1, 1.3 Hz), 4.39 – 4.27 (1H, m), 4.04 (1H, q, *J* = 6.7 Hz), 2.11 – 2.02 (2H, m), 1.64 – 1.20 (5H, m), 1.36 – 1.20 (7H, m), 0.88 (9H, s), 0.88 (3H, m), 0.09 (3H, s), 0.05 (3H, s). ¹³C NMR (125 MHz, CDCl₃) δ (ppm) -4.6, -4.1, 14.2, 18.2, 22.8, 24.7, 25.3, 26.0, 31.9, 32.1, 36.3, 37.4, 73.4, 75.4, 80.0, 131.9, 133.5 and 144.7. HRMS (ESITOF) *m/z* 489.1656 [M+Na]⁺ (calc'd 489.1656 for C₂₀H₃₉IO₂SiNa⁺).

(6R,7E,12S,13Z)-12-((*tert*-Butyldimethylsilyl)oxy)-14-iodotetradeca-7,13-dien-6-ol (**S7b**).

A solution of Hoveyda Grubbs II catalyst (14.9 mg, 23.7 μmol) in CH₂Cl₂ (0.5 mL) was added dropwise to a solution of (*S*)-**5.11** (292.2 mg, 0.798 mmol) and (*R*)-**5.12** (306.8 mg, 2.39 mmol) in CH₂Cl₂ (2.0 mL) under N₂ at 40 °C. After 44 h, additional Hoveyda Grubbs II catalyst (14.9 mg, 23.7 μmol) in CH₂Cl₂ (0.5 mL) and (*R*)-**5.12** (102 mg, 0.796 mmol) were added dropwise to the reaction. After an additional 20 h, the reaction mixture was cooled to rt and purified on SiO₂ (100% hexanes → 10% Et₂O/hexanes) to give **5.S7b** (223 mg, 60%) after the recovery of unreacted (*S*)-**5.11**. [α]_D +7.72 (*c* 1.35, CHCl₃). ¹H NMR (500 MHz, CDCl₃) δ (ppm, integ., mult, *J* Hz) 6.23 – 6.13 (2H, m), 5.63 (1H, dtd, *J* = 15.4, 6.7, 0.9 Hz), 5.47 (1H, ddt, *J* = 15.4, 7.1, 1.3 Hz), 4.39 – 4.27 (1H, m), 4.04 (1H, q, *J* = 6.7 Hz), 2.13 – 1.99 (2H, m), 1.63 – 1.37 (5H, m), 1.37 – 1.22 (7H, m), 0.88 (9H, s), 0.88 (3H, m), 0.09 (3H, s), 0.05 (3H, s). ¹³C NMR (125 MHz, CDCl₃) δ (ppm) -

4.6, -4.1, 14.2, 18.2, 22.8, 24.7, 25.3, 26.0, 31.9, 32.1, 36.3, 37.4, 73.4, 75.4, 80.0, 131.9, 133.6 and 144.8. HRMS (ESITOF) m/z 489.1659 $[M+Na]^+$ (calc'd 489.1656 for $C_{20}H_{39}IO_2SiNa^+$).

(*6R,12R,E*)-12-((*tert*-Butyldimethylsilyl)oxy)tetradeca-7,13-dien-6-ol (**5.16a**). *n*-Bu₃SnH (140 μ L, 0.519 mmol) was added dropwise to a solution of **5.S7a** (186 mg, 0.399 mmol) and Pd(PPh₃)₄ (46.1 mg, 39.9 μ mol) in benzene (5 mL) under N₂ at 0 °C. After stirring at rt for 18 h, the reaction mixture was quenched by addition of sat'd aq. NaHCO₃, extracted with EtOAc (3x), and the combined organic layer was washed with brine (1x), dried over Na₂SO₄, filtered and evaporated. The crude was purified on SiO₂ (5% \rightarrow 10% MTBE/hexanes) to give **5.16a** (127.4 mg, 94%) as a colorless oil. $[\alpha]_D \sim 0$ (*c* 0.90, CHCl₃). ¹H NMR (500 MHz, CDCl₃) δ (ppm, integ., mult, *J* Hz) 5.78 (1H, ddd, *J* = 16.4, 10.4, 6.0), 5.61 (1H, dt, *J* = 15.4, 6.7 Hz), 5.51 – 5.40 (1H, m), 5.12 (1H, ddt, *J* = 16.4, 2.0, 1.0 Hz), 5.01 (1H, ddt, *J* = 10.4, 2.0, 1.0 Hz), 4.08 (1H, m), 4.03 (1H, q, *J* = 6.7 Hz), 2.14 – 1.98 (2H, m), 1.68 – 1.20 (12H, m), 0.89 (9H, m), 0.88 (3H, t, 7.2), 0.04 (3H, s), 0.02 (3H, s). ¹³C NMR (125 MHz, CDCl₃) δ (ppm) -4.7, -4.2, 14.2, 18.4, 22.8, 24.9, 25.3, 26.0, 31.9, 32.3, 37.4, 37.6, 73.4, 73.8, 113.7, 132.0, 133.4 and 141.9. HRMS (ESITOF) m/z 363.2692 $[M+Na]^+$ (calc'd 363.2690 for $C_{20}H_{40}O_2SiNa^+$).

(*6R,12S,E*)-12-((*tert*-Butyldimethylsilyl)oxy)tetradeca-7,13-dien-6-ol (**5.16b**). *n*-Bu₃SnH (172 μ L, 0.638 mmol) was added dropwise to a solution of **5.S7b** (228.8 mg, 0.490 mmol) and Pd(PPh₃)₄ (57 mg, 49 μ mol) in benzene (5 mL) under N₂ at 0 °C. After stirring at rt for 18 h, the reaction mixture was quenched by addition of sat'd aq. NaHCO₃, extracted with EtOAc (3x), and the combined organic layer was washed with brine (1x), dried over Na₂SO₄, filtered and evaporated. The crude was purified on SiO₂ (5% \rightarrow 10% MTBE/hexanes) to give **5.16b** (161.5 mg, 97%) as a colorless oil. $[\alpha]_D +13$ (*c* 0.70, CHCl₃). ¹H NMR (500 MHz, CDCl₃) δ (ppm, integ., mult, *J* Hz) 5.78 (1H, ddd, *J* = 17.2, 10.4, 6.1 Hz), 5.61 (1H, dtd, *J* = 14.7, 6.8, 0.8 Hz), 5.44 (1H,

ddt, $J = 14.7, 7.1, 1.4$ Hz), 5.13 (1H, dq, $J = 17.2, 1.8$ Hz), 5.07 – 4.97 (1H, m), 4.12 – 4.06 (1H, m), 4.03 (1H, q, $J = 6.8$ Hz), 2.11 – 1.98 (2H, m), 1.72 – 1.22 (12H, m), 0.89 (9H, s), 0.88 (3H, t, 6.8), 0.04 (3H, s), 0.03 (3H, s). ^{13}C NMR (125 MHz, CDCl_3) δ (ppm) -4.7, -4.2, 14.2, 18.4, 22.8, 24.9, 25.3, 26.0, 31.9, 32.3, 37.4, 37.6, 73.4, 73.8, 113.7, 132.0, 133.4 and 141.9. HRMS (ESITOF) m/z 363.2692 $[\text{M}+\text{Na}]^+$ (calc'd 363.2690 for $\text{C}_{20}\text{H}_{40}\text{O}_2\text{SiNa}^+$).

(*5R,11R,E*)-2,2,3,3,13,13,14,14-Octamethyl-5-pentyl-11-vinyl-4,12-dioxo-3,13-disilapentadec-6-ene (**5.17a**). Freshly distilled 2,6-lutidine (89 μL , 0.762 mmol) and TBSOTf (143 μL , 0.624 mmol) were added to a solution of **5.16a** (118 mg, 0.346 mmol) in CH_2Cl_2 (3.5 mL) at 0 °C. After 45 min, the reaction mixture was quenched by addition of sat'd aq. NaHCO_3 and H_2O . The mixture was extracted with Et_2O (3x), and the combined organic layer was washed with brine (1x), dried over Na_2SO_4 , filtered and evaporated. The crude was purified on SiO_2 (100% hexanes) to give **5.17a** (141.1 mg, 90%) as a colorless oil. $[\alpha]_D^{25} +2.88$ (c 2.30, CHCl_3). ^1H NMR (500 MHz, CDCl_3) δ (ppm, integ., mult, J Hz) 5.78 (1H, ddd, $J = 17.0, 10.4, 6.0$), 5.49 (1H, dt, $J = 15.6, 6.4$), 5.37 (1H, ddt, $J = 15.6, 6.7, 1.2$ Hz), 5.12 (1H, ddd, $J = 17.0, 1.6, 1.6$), 5.01 (1H, ddd, $J = 10.4, 1.6, 1.6$), 4.10 – 4.04 (1H, m), 4.00 (1H, q, $J = 6.4$ Hz), 2.00 (2H, q, $J = 6.7$ Hz), 1.55 – 1.18 (12H, m), 0.89 (9H, s), 0.88 (9H, s), 0.88 (3H, m), 0.04 (3H, s), 0.03 (3H, s), 0.02 (3H, s), 0.01 (3H, s). ^{13}C NMR (125 MHz, CDCl_3) δ (ppm) -4.70, -4.58, -4.21, -4.00, 14.22, 18.41, 18.44, 22.81, 25.17, 25.26, 26.03, 26.09, 31.96, 32.21, 37.72, 38.61, 73.88, 73.97, 113.61, 130.12, 134.13, 142.01. HRMS (ESITOF) m/z 477.3553 $[\text{M}+\text{Na}]^+$ (calc'd 477.3555 for $\text{C}_{26}\text{H}_{54}\text{O}_2\text{Si}_2\text{Na}^+$).

(*5R,11S,E*)-2,2,3,3,13,13,14,14-Octamethyl-5-pentyl-11-vinyl-4,12-dioxo-3,13-disilapentadec-6-ene (**5.17b**). Freshly distilled 2,6-lutidine (116 μL , 0.99 mmol) and TBSOTf (187 μL , 0.813 mmol) were added to a solution of **5.16b** (153.4 mg, 0.452 mmol) in CH_2Cl_2 (4.5 mL) at 0 °C. After 45 min, the reaction mixture was quenched by addition of sat'd aq. NaHCO_3 and

H₂O. The mixture was extracted with Et₂O (3x), and the combined organic layer was washed with brine (1x), dried over Na₂SO₄, filtered and evaporated. The crude was purified on SiO₂ (100% hexanes) to give **5.17b** (169.0 mg, 82%) as a colorless oil. $[\alpha]_D +10.5$ (*c* 2.84, CHCl₃). ¹H NMR (500 MHz, CDCl₃) δ (ppm, integ., mult, *J* Hz) 5.78 (1H, ddd, *J* = 16.6, 10.4, 6.0 Hz), 5.50 (1H, dt, *J* = 15.6, 6.4 Hz), 5.37 (1H, ddt, *J* = 15.6, 6.8, 1.2 Hz), 5.12 (1H, ddd, *J* = 16.6, 1.6, 1.6 Hz), 5.01 (1H, ddd, *J* = 10.4, 1.6, 1.2 Hz), 4.11 – 4.04 (1H, m), 4.00 (1H, q, *J* = 6.4 Hz), 2.07 – 1.93 (2H, m), 1.61 – 1.16 (12H, m), 0.89 (9H, s), 0.89 (9H, s), 0.88 (3H, m), 0.04 (3H, s), 0.03 (3H, s), 0.03 (3H, s), 0.01 (3H, s). ¹³C NMR (125 MHz, CDCl₃) δ (ppm) -4.70, -4.58, -4.22, -4.01, 14.22, 18.40, 22.80, 25.13, 25.25, 26.03, 26.09, 31.95, 32.21, 37.73, 38.61, 73.87, 73.97, 113.59, 130.12, 134.14, 142.02. HRMS (ESITOF) *m/z* 477.3556 [M+Na]⁺ (calc'd 477.3555 for C₂₆H₅₄O₂Si₂Na⁺).

(*4R,6E,8R,12E,14R*)-8,14-bis((*tert*-Butyldimethylsilyl)oxy)-1-phenylnonadeca-6,12-dien-4-ol (**5.18a**). A solution of Hoveyda Grubbs II catalyst (14 mg, 22 μ mol) in CH₂Cl₂ (0.5 mL) was added dropwise to a solution of **5.17a** (100 mg, 0.22 mmol) and (*R*)-**5.10** (125.5 mg, 0.66 mmol) in CH₂Cl₂ (1.0 mL) under N₂ at 40 °C. After 18 h, additional Hoveyda Grubbs II catalyst (14 mg, 22 μ mol) in CH₂Cl₂ (0.5 mL) was added dropwise to the reaction. After an additional 18 h, the reaction mixture was cooled to rt and purified on SiO₂ (100% hexanes \rightarrow 10% Et₂O/hexanes) to give **5.18a** (70.5 mg, 52%) as a colorless oil. $[\alpha]_D +11$ (*c* 0.90, CHCl₃). ¹H NMR (500 MHz, CDCl₃) δ (ppm, integ., mult, *J* Hz) 7.32 – 7.27 (2H, m), 7.18 (3H, m), 5.57 – 5.43 (3H, m), 5.42 – 5.31 (1H, m), 4.14 – 4.03 (1H, m), 4.00 (1H, q, *J* = 6.4 Hz), 3.63 (1H, m), 2.63 (2H, t, *J* = 7.7 Hz), 2.34 – 1.60 (7H, m), 1.59 – 1.19 (13H, m), 0.884 (9H, s), 0.880 (9H, s), 0.88 (3H, m), 0.04 (6H, s), 0.01 (6H, s). ¹³C NMR (125 MHz, CDCl₃) δ (ppm) -4.61, -4.58, -4.06, -3.99, 14.22, 18.38, 18.43, 22.80, 25.25, 25.34, 26.04, 26.09, 27.64, 31.95, 32.19, 36.03, 36.46, 38.04, 38.60, 40.44,

70.94, 73.28, 73.94, 125.63, 125.88, 128.44, 128.54, 130.05, 134.17, 137.81, 142.50. HRMS (ESITOF) m/z 639.4592 $[M+Na]^+$ (calc'd 639.4599 for $C_{37}H_{68}O_3Si_2Na^+$).

(*4R,6E,8S,12E,14R*)-8,14-bis((*tert*-Butyldimethylsilyl)oxy)-1-phenylnonadeca-6,12-dien-4-ol (**5.18b**). A solution of Hoveyda Grubbs II catalyst (14 mg, 22 μ mol) in CH_2Cl_2 (0.5 mL) was added dropwise to a solution of **5.17b** (100 mg, 0.22 mmol) and (*R*)-**5.10** (125.5 mg, 0.66 mmol) in CH_2Cl_2 (1.0 mL) under N_2 at 40 $^\circ C$. After 18 h, additional Hoveyda Grubbs II catalyst (14 mg, 22 μ mol) in CH_2Cl_2 (0.5 mL) was added dropwise to the reaction. After an additional 18 h, the reaction mixture was cooled to rt and purified on SiO_2 (100% hexanes \rightarrow 10% Et_2O /hexanes) to give **5.18b** (80.1 mg, 59%) as a colorless oil. $[\alpha]_D +4.9$ (c 0.86, $CHCl_3$). 1H NMR (500 MHz, $CDCl_3$) δ (ppm, integ., mult, J Hz) 7.33 – 7.27 (2H, m), 7.24 – 7.13 (3H, m), 5.52 (2H, m), 5.47 (1H, t, $J = 6.5$ Hz), 5.37 (1H, dd, $J = 15.5, 6.7$ Hz), 4.06 (1H, m), 4.01 (1H, q, $J = 6.4$ Hz), 3.63 (1H, m), 2.64 (2H, t, $J = 7.7$ Hz), 2.49 – 2.35 (1H, m), 2.30 – 1.55 (8H, m), 1.55 – 1.17 (11H, m), 0.89 (18H, m), 0.88 (3H, m), 0.04 (6H, s), 0.02 (6H, s). ^{13}C NMR (125 MHz, $CDCl_3$) δ (ppm) - 4.61, -4.58, -4.10, -4.01, 14.22, 18.36, 18.43, 22.79, 25.24, 25.28, 26.02, 26.08, 27.64, 31.94, 32.19, 36.02, 36.42, 38.05, 38.60, 40.44, 70.97, 73.31, 73.93, 125.51, 125.86, 128.43, 128.53, 130.04, 134.16, 137.94, 142.49. HRMS (ESITOF) m/z 639.4593 $[M+Na]^+$ (calc'd 639.4599 for $C_{37}H_{68}O_3Si_2Na^+$).

(*4R,8R,14R*)-8,14-bis((*tert*-Butyldimethylsilyl)oxy)-1-phenylnonadecan-4-ol (**5.S8a**). A suspension of **5.18a** (54.9 mg, 88.9 μ mol) and Pd/C (7.5 mg) in hexanes/ $EtOAc$ (3 mL, 5/1 ratio) was stirred for 18 h under 1 atm of H_2 . The suspension was purged with N_2 and filtered on a short SiO_2 plug (50% $EtOAc$ /hexanes) to give **5.S8a** (55 mg, quant.) as a colorless oil. $[\alpha]_D +5.1$ (c 0.42, $CHCl_3$). 1H NMR (500 MHz, $CDCl_3$) δ (ppm, integ., mult, J Hz) 7.30 – 7.26 (2H, m), 7.21 – 7.14 (3H, m), 3.60 (3H, m), 2.68 – 2.56 (2H, m), 2.45 – 2.33 (1H, m), 1.97 – 1.63 (2H, m), 1.40 (11H,

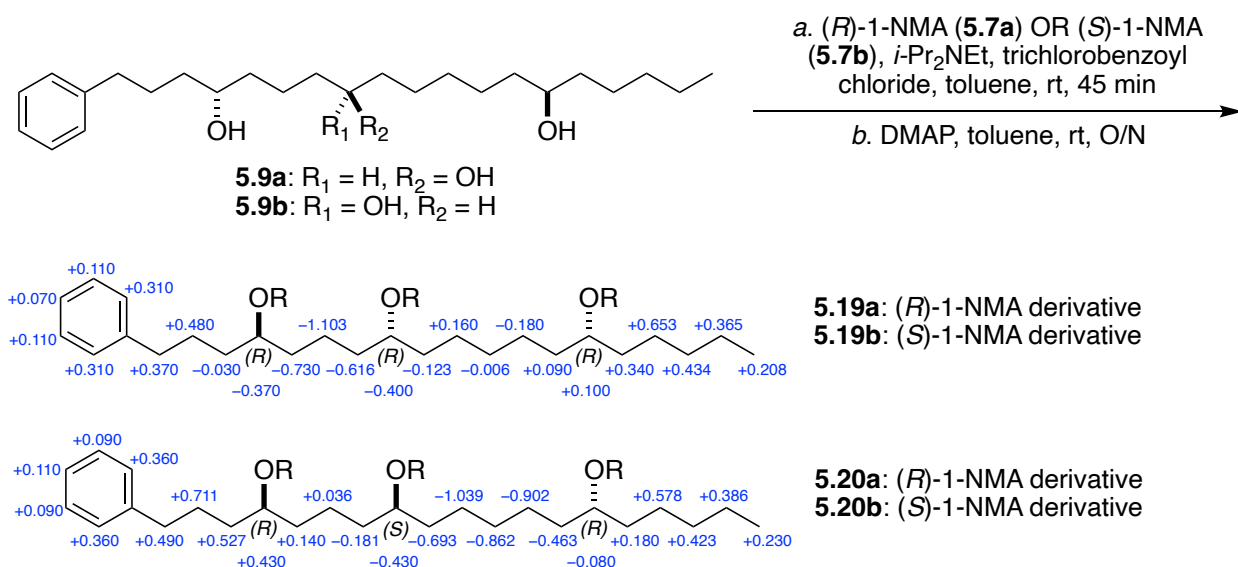
m), 1.35 – 1.17 (16H, m), 0.88 (18H, s), 0.88 (3H, m), 0.027 (3H, s), 0.029 (9H, s). ¹³C NMR (125 MHz, CDCl₃) δ (ppm) -4.39, -4.39, -4.37, -4.36, 14.12, 18.18, 18.20, 21.42, 22.71, 25.03, 25.41, 25.94, 25.96, 25.97, 27.52, 30.11, 32.10, 35.92, 36.97, 37.08, 37.11, 37.12, 37.72, 71.82, 72.26, 72.38, 125.73, 128.30, 128.41, 142.41. HRMS (ESITOF) *m/z* 621.5090 [M+H]⁺ (calc'd 621.5093 for C₃₇H₇₃O₃Si₂⁺).

(4*R*,8*S*,14*R*)-8,14-bis((*tert*-Butyldimethylsilyl)oxy)-1-phenylnonadecan-4-ol (**5.S8b**). A suspension of **5.18b** (68.4 mg, 111 μmol) and Pd/C (7.5 mg) in hexanes/EtOAc (3 mL, 5/1 ratio) was stirred for 18 h under 1 atm of H₂. The suspension was purged with N₂ and filtered on a short SiO₂ plug (50% EtOAc/hexanes) to give **5.S8b** (61.8 mg, 89%) as a colorless oil. [α]_D -5.1 (*c* 0.44, CHCl₃). ¹H NMR (500 MHz, CDCl₃) δ (ppm, integ., mult, *J* Hz) 7.32 – 7.23 (2H, m), 7.18 (3H, m), 3.61 (3H, m), 2.69 – 2.55 (3H, m), 2.38 (1H, dt, *J* = 15.8, 7.3 Hz), 1.97 – 1.12 (26H, m), 0.88 (18H, s), 0.88 (3H, m), 0.031 (9H, s), 0.028 (3H, s). ¹³C NMR (125 MHz, CDCl₃) δ (ppm) -4.27, -4.25, 14.24, 18.30, 18.32, 21.43, 22.83, 25.17, 25.53, 26.05, 26.08, 26.09, 27.65, 30.21, 32.22, 36.04, 37.09, 37.16, 37.17, 37.23, 37.25, 37.79, 71.92, 72.35, 72.51, 125.86, 128.43, 128.54, 142.53. HRMS (ESITOF) *m/z* 621.5095 [M+H]⁺ (calc'd 621.5093 for C₃₇H₇₃O₃Si₂⁺).

(4*R*,8*R*,14*R*)-1-Phenylnonadecane-4,8,14-triol (**5.9a**). A solution of **5.S8a** (45 mg, 72.5 μmol) and TBAF (0.36 mL, 362 μmol) in THF (1.0 mL) was stirred at 50 °C for 3 h. The reaction mixture was cooled to rt, quenched by addition of potassium phosphate buffer (pH 7.0), and extracted with EtOAc (3x). The combined organic layer was dried over Na₂SO₄, filtered and evaporated. The crude was purified on SiO₂ (5% → 10% MeOH/CH₂Cl₂) to give **5.9a** (13.9 mg, 49%) as a colorless oil. [α]_D -4.7 (*c* 0.44, CHCl₃). ¹H NMR (500 MHz, CDCl₃) δ (ppm, integ., mult, *J* Hz) 7.33 – 7.23 (2H, m), 7.22 – 7.13 (3H, m), 3.68 – 3.53 (3H, m), 2.63 (2H, ddd, *J* = 8.7, 6.9, 2.1 Hz), 1.85 – 1.72 (1H, m), 1.72 – 1.60 (1H, m), 1.58 – 1.20 (26H, m), 0.89 (3H, t, *J* = 6.8

Hz). ^{13}C NMR (125 MHz, CDCl_3) δ (ppm) 14.21, 21.85, 22.80, 25.47, 25.73, 25.74, 27.63, 29.80, 32.05, 36.01, 37.23, 37.33, 37.36, 37.48, 37.57, 37.62, 71.82, 71.92, 72.13, 125.89, 128.45, 128.55, 142.51. HRMS (ESITOF) m/z 437.3276 $[\text{M}+\text{HCOOH}-\text{H}]^-$ (calc'd 437.3272 for $\text{C}_{25}\text{H}_{43}\text{O}_3\cdot\text{HCOOH}^-$).

(4R,8S,14R)-1-Phenylnonadecane-4,8,14-triol (**5.9b**). A solution of **5.S8b** (55 mg, 88.5 μmol) and TBAF (0.45 mL, 443 μmol) in THF (1.0 mL) was stirred at 50 $^\circ\text{C}$ for 3 h. The reaction mixture was cooled to rt, quenched by addition of potassium phosphate buffer (pH 7.0), and extracted with EtOAc (3x). The combined organic layer was dried over Na_2SO_4 , filtered and evaporated. The crude was purified on SiO_2 (5% \rightarrow 10% MeOH/ CH_2Cl_2) to give **5.9b** (16.2 mg, 47%) as a colorless oil. $[\alpha]_{\text{D}} \sim 0$ (c 0.74, CHCl_3). ^1H NMR (500 MHz, CDCl_3) δ (ppm, integ., mult, J Hz) 7.32 – 7.23 (2H, m), 7.18 (3H, m), 3.68 – 3.53 (3H, m), 2.63 (2H, ddd, $J = 8.8, 7.0, 2.2$ Hz), 1.78 (1H, tddd, $J = 15.0, 9.0, 7.3, 3.8$ Hz), 1.72 – 1.61 (1H, m), 1.60 – 1.23 (26H, m), 0.89 (3H, t, $J = 7.2$ Hz). ^{13}C NMR (125 MHz, CDCl_3) δ (ppm) 14.21, 21.74, 22.80, 25.47, 25.71, 25.72, 27.63, 29.81, 32.05, 36.01, 37.17, 37.43, 37.46, 37.48, 37.50, 37.61, 71.89, 71.97, 72.13, 125.89, 128.45, 128.55, 142.50. HRMS (ESITOF) m/z 437.3279 $[\text{M}+\text{HCOOH}-\text{H}]^-$ (calc'd 437.3272 for $\text{C}_{25}\text{H}_{43}\text{O}_3\cdot\text{HCOOH}^-$).



Scheme 5.16: Synthesis of tris-NMA derivatives **5.19a,b** and **5.20a,b**.

Compound 5.19a. Compound **5.19a** was synthesized according to a reported literature procedure.²⁰ *i*-Pr₂NEt (8 μ L, 45.8 μ mol) and 2,4,6-trichlorobenzoyl chloride (7.2 μ L, 45.8 μ mol) were added to a solution of **5.9a** (2.0 mg, 5.1 μ mol) and (*R*)-1-NMA (**5.7a**, 6.6 mg, 30.6 μ mol) in dry toluene (400 μ L) under Ar. After 45 min, a solution of DMAP (56 μ L, 45.8 μ mol, 100 mg/mL) in toluene was added. After stirring for 18 h, the reaction mixture was diluted with a few drops of HCl (1 M), and dried under a stream of N₂. The crude was purified on SiO₂ (20% EtOAc/hexanes) to give a semi-pure crude (10.4 mg) that was further purified by semi-preparative, normal-phase HPLC (SiO₂, 60% EtOAc/hexanes, 3.0 mL·min⁻¹) to give **5.19a** (4.4 mg). HRMS (ESITOF) *m/z* 1009.5221 [M+Na]⁺ (calc'd 1009.5525 for C₆₄H₇₄O₉Na⁺).

Compound 5.19b. Aglycone **5.9a** (2.0 mg, 5.1 μ mol) was esterified with (*S*)-1-NMA (**5.7b**), according to the procedure described above for **5.19a**, to give **5.19b** (2.0 mg). HRMS (ESITOF) *m/z* 1009.5230 [M+Na]⁺ (calc'd 1009.5525 for C₆₄H₇₄O₉Na⁺).

Compound 5.20a. Aglycone **5.9b** (2.0 mg, 5.1 μ mol) was esterified with (*R*)-1-NMA (**5.7a**), according to the procedure described above for **5.19a**, to give **5.20a** (2.9 mg). HRMS (ESITOF) *m/z* 1009.5220 [M+Na]⁺ (calc'd 1009.5525 for C₆₄H₇₄O₉Na⁺).

Compound 5.20b. Aglycone **5.9b** (2.0 mg, 5.1 μmol) was esterified with (*S*)-1-NMA (**5.7b**), according to the procedure described above for **5.19a**, to give **5.20b** (4.1 mg). HRMS (ESITOF) m/z 1009.5228 $[\text{M}+\text{Na}]^+$ (calc'd 1009.5525 for $\text{C}_{64}\text{H}_{74}\text{O}_9\text{Na}^+$).

Methanolysis of 5.3a–g under Acidic Conditions in MeOH. HCl (0.45 mL, 6 N) was added to a suspension of **5.3a–g** (2.0 mg) in MeOH (2.55 mL) at rt. The suspension was purged with Ar, and stirred at 75 °C for 18 h. The reaction mixture was cooled to rt, extracted with hexanes (3 x 2 mL), and the organic layer was concentrated under a stream of N_2 to give **5.22a–c** (1.0 mg, 74%). The aqueous layer was concentrated under reduced pressure to give the sphingosine base-HCl salt (**5.21a–h**, 0.7 mg, 83%). **5.21a–h**: See Table 5.3 for HR-ESI-MS data. **5.22a–c**: ^1H NMR (500 MHz, CDCl_3) δ (ppm, integ., mult, J Hz) 0.88 (3H, t, $J = 6.5$), 1.25 (23 H, br s), 1.62 (2H, m), 2.30 (2H, t, $J = 7.5$), and 3.66 (3H, s). EIMS: 354 (40, M^+), 311 (19), 143 (30), 87 (81), 83 (15), 75 (29), 74 (100), 69 (21), 57 (27), 55 (30); 382 (39, M^+), 339 (15), 143 (29), 87 (81), 83 (16), 75 (33), 74 (100), 69 (22), 57 (31), 55 (30).

Methanolysis of 5.3a–g Under Acidic Conditions in CD_3OD . HCl (0.15 mL, 6 N) was added to a suspension of **5.3a–g** (1.2 mg) in CD_3OD (0.85 mL). The suspension was purged with Ar, and stirred at 75 °C for 16 hr. The reaction mixture was cooled to rt and extracted with hexanes (4 x 1 mL) to remove the fatty acid methyl ester. The remaining aqueous layer was concentrated under reduced pressure to give the sphingosine base-HCl salt **5.21a–d** and **5.24a–d** (1.2 mg). See Table 5.3 for HR-ESI-MS data of **5.24a–h**.

Methanolysis of 5.3a–g Under basic Conditions. The hydrolysis was performed according to the procedure by Sala and coworkers.²⁸ A suspension of **5.3a–g** (2.0 mg) in KOH (3.0 mL, 1 M aq.) was stirred at 100 °C for 3 days. The reaction mixture was cooled to rt, diluted with aqueous MeOH (0.75 mL, 8:2 $\text{H}_2\text{O}/\text{MeOH}$) and extracted with CHCl_3 (4 x 1 mL). The organic layer was

concentrated under a stream of N₂ to give the free sphingosine base **5.21i–I**. See Table 5.3 for HR-ESI-MS data of **5.21i–I**.

Ruthenium Oxidation of 5.21i–I and Methylation to 5.23a–g. RuCl₃·*n*H₂O (0.1 mL, 0.77 μmol, 2.0 mg/mL in CH₃CN) and NaIO₄ (23.0 mg, 0.11 mmol) were added to a solution of **5.21i–I** (2.3 mg, 7.7 μmol) in CCl₄/CH₃CN/H₂O (0.5/0.4/0.75 mL's). The reaction mixture was stirred vigorously for 3 h and evaporated under reduced pressure. The crude was suspended in Et₂O, centrifuged and the supernatant removed. Excess diazomethane (0.25 M, Et₂O) was added to the supernatant (2 mL) at 0 °C. The reaction mixture was stirred for 1 h and evaporated under a stream of N₂ to give **5.23a–g** (1.2 mg, 65%). See Table 5.4 for GC-EI-MS data of **5.23a–g**. EIMS for **5.23a**: 214 (5, M⁺), 183 (10), 171 (13), 143 (16), 87 (65), 75 (12), 74 (100), 69 (9), 59 (7), 55 (21); **5.23b**: 228 (6, M⁺), 197 (7), 185 (28), 143 (25), 129 (9), 87 (75), 75 (13), 74 (100), 69 (11), 55 (20); **5.23c**: 228 (7, M⁺), 185 (16), 143 (20), 129 (10), 87 (71), 75 (13), 74 (100), 69 (12), 59 (10), 57 (10), 55 (22); **5.23d**: 242 (6, M⁺), 199 (34), 143 (22), 87 (74), 83 (10), 75 (14), 74 (100), 69 (17), 59 (10), 57 (12), 55 (25); **5.23e**: 242 (9, M⁺), 199 (18), 143 (23), 87 (73), 75 (15), 74 (100), 69 (13), 59 (10), 57 (11), 55 (24); **5.23f**: 256 (11, M⁺), 213 (19), 143 (20), 87 (74), 83 (10), 75 (16), 74 (100), 69 (18), 57 (11), 55 (27); and **5.23g**: 256 (7, M⁺); 213 (15); 199 (26); 143 (26); 97 (18); 87 (77); 83 (18); 75 (17); 74 (100); 69 (25); 57 (29), 55 (38).

Acetylation of 5.21i–I to 5.25. Ac₂O (50 μL), anhydrous pyridine (50 μL) and 4-DMAP were added to **5.21i–I** (0.5 mg) under N₂. After 18 h, excess Ac₂O and pyridine were evaporated under reduced pressure, and the crude product was purified by analytical reversed-phase HPLC (Luna C₁₈, 250 x 4.60 mm, 210 nm, isocratic, MeOH, 0.7 mL·min⁻¹) to give **5.25** (0.2 mg, 28%). ¹H NMR (500 MHz, CDCl₃) δ (ppm, integ., mult, *J* Hz) 0.86 (3H, d, *J* = 6.5), 0.88 (3H, t, *J* = 6.5), 1.14 (2H, m), 1.25 (22H, br s), 1.34 (2H, m), 1.98 (3H, s), 2.02 (2H, m), 2.06 (3H, s), 2.07 (3H,

s), 4.04 (1H, dd, $J = 3.5, 11.5$), 4.30 (1H, dd, $J = 6.0, 11.5$), 4.42 (1H, m), 5.27 (1H, t, $J = 6.5$), 5.38 (1H, dd, $J = 7.5, 15.5$), 5.66 (1H, d, $J = 8.5$), and 5.79 (1H, dt, $J = 6.5, 15.0$). See Table 5.3 for HR-ESI-MS data of **5.25a–h**.

N,O-Chromophoric Derivatization of 5.21i–l to 5.26. Sphingolipid **5.21i–l** (1.0 mg) and 2,3-naphthalenedicarboxylic acid anhydride (1.5 mg) were dissolved in anhydrous pyridine (1 mL) under Ar. The mixture was purged with Ar for 5 min, stirred at 110 °C for 18 h, cooled to rt and evaporated under reduced pressure. The crude was purified by preparative TLC (Silica 60 PF₂₅₆, 1 mm, pre-washed 2x with EtOAc, developed 2x with 50% EtOAc/hexanes, R_f 0.63) to give the *N*-naphthimide (0.9 mg, 54%). 2-Naphthoylimidazole (4.0 mg) and cat. DBU were added to a solution of the *N*-naphthimide in anhydrous CH₃CN (1 mL) under Ar. After 16 h, the reaction mixture was concentrated and purified by preparative TLC (Silica 60 PF₂₅₆, 1 mm, pre-washed 2x with EtOAc, developed 2x with 25% EtOAc/hexanes) to give **5.26** (0.8 mg, 54%). The sample was further purified by semipreparative HPLC (SiO₂, isocratic, 40% EtOAc/hexanes, 3.0 mL·min⁻¹) to give **5.26** (0.2 mg). See Table 5.3 for HR-ESI-MS data of **5.26a–d**. UV (CH₃CN) λ_{\max} 237 nm (log ϵ 4.90), 260 (4.69), 280 (4.15). ECD (CH₃CN) λ 239 ($\Delta\epsilon$ +79), 260 (-41.2).

5.9 Appendix

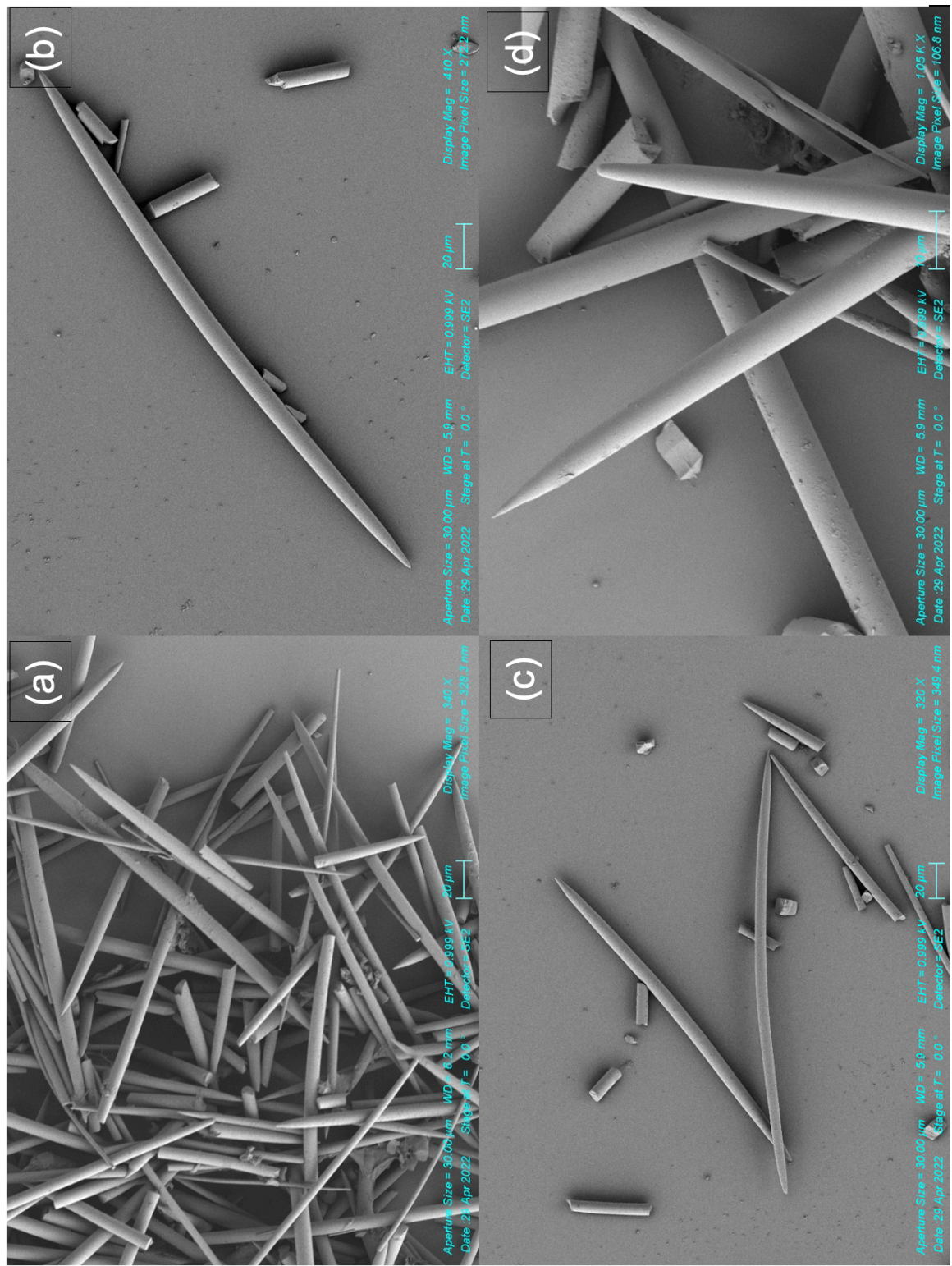
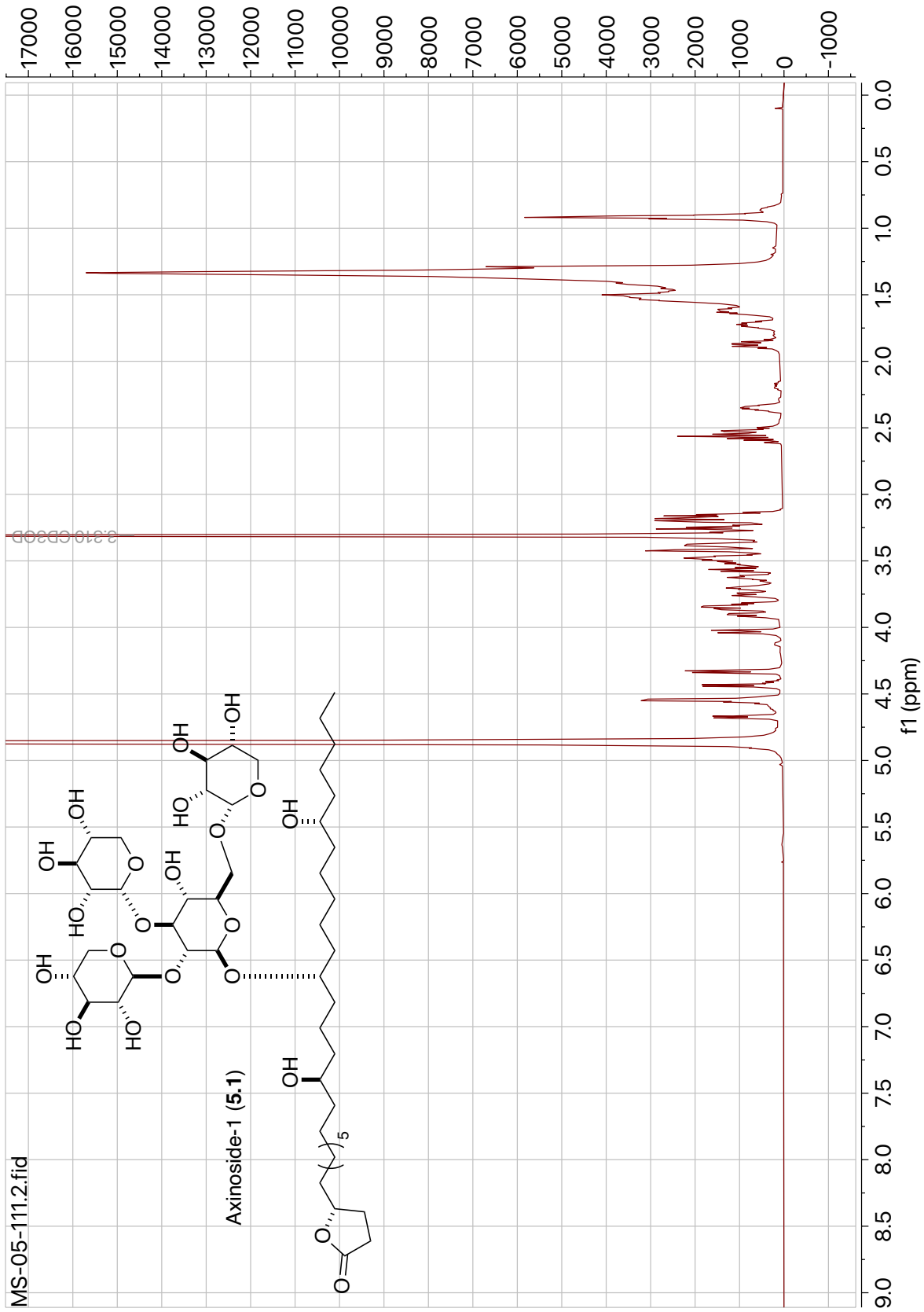


Figure 5.8: SEM Images of Spicules of Axinellid Sponge 93-07-067. Scale bars (10 μM and 20 μM) at bottom.



05111-a #18-24 RT: 0.36-0.47 AV: 7 SB: 8 0.14-0.28 NL: 7.33E7
T: + c Full ms [300.00-1600.00]

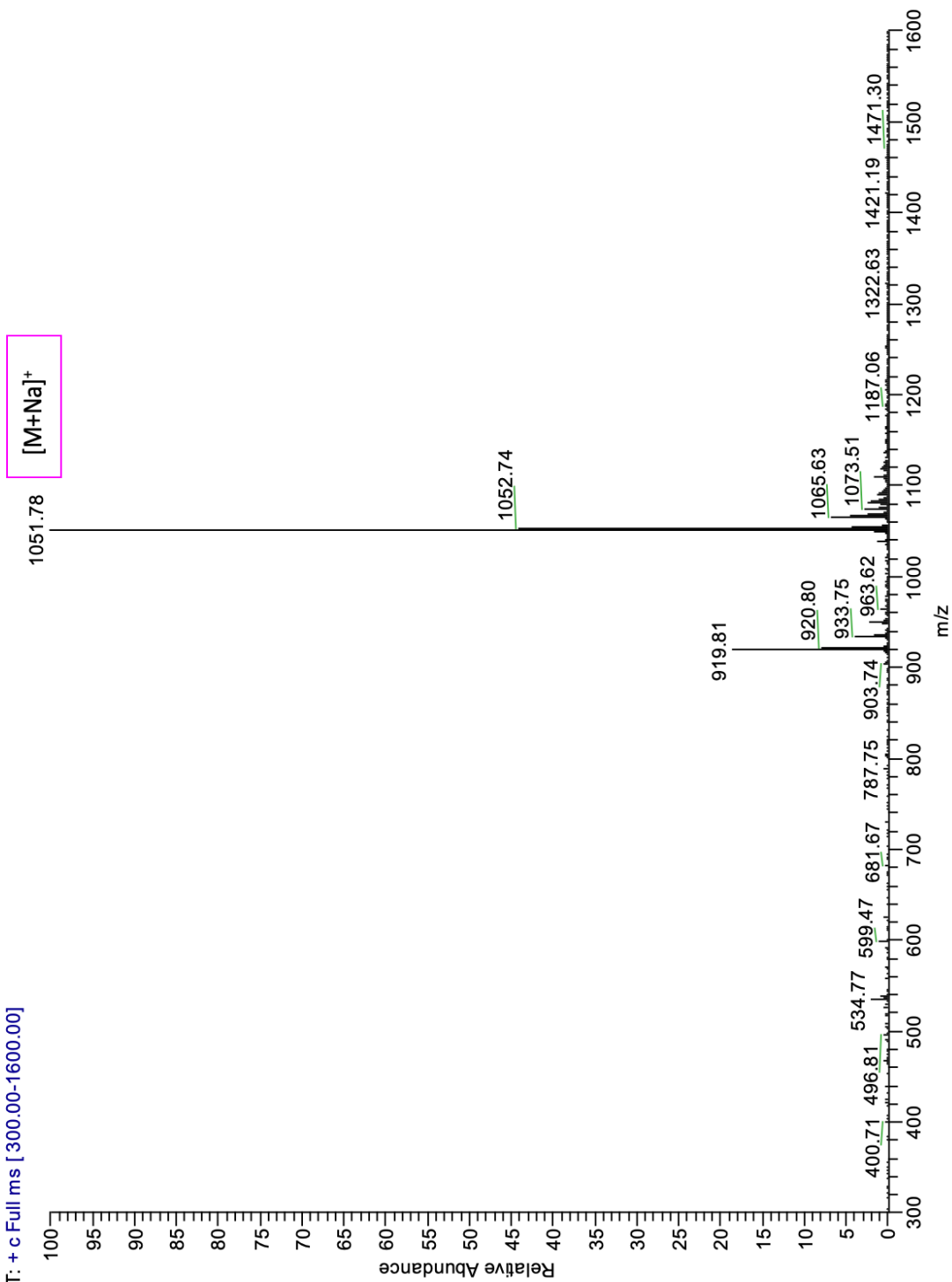


Figure 5.10: MSⁿ Analysis (Positive Ion Mode) of Compound 5.1.

05111-a #56-64 RT: 1.45-1.59 AV: 9 NL: 3.13E7
T: + c Full ms2 1052.00@40.00 [285.00-1200.00]

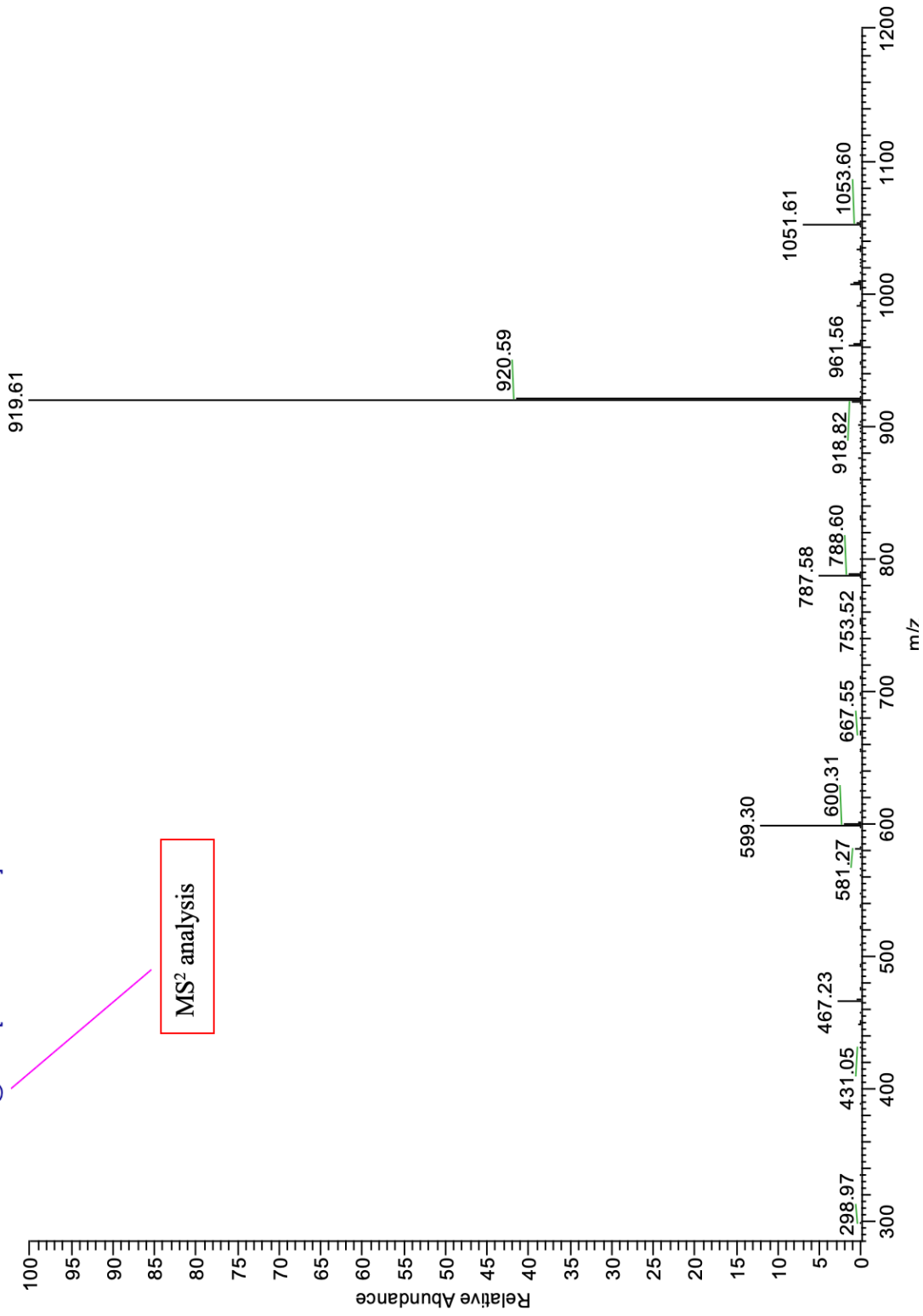


Figure 5.10: MSⁿ Analysis (Positive Ion Mode) of Compound 5.1 Continued.

05111-a #80-87 RT: 1.96-2.12 AV: 8 NL: 1.59E6
T: + c Full ms3 1052.00@40.00 920.00@40.00 [250.00-1200.00]

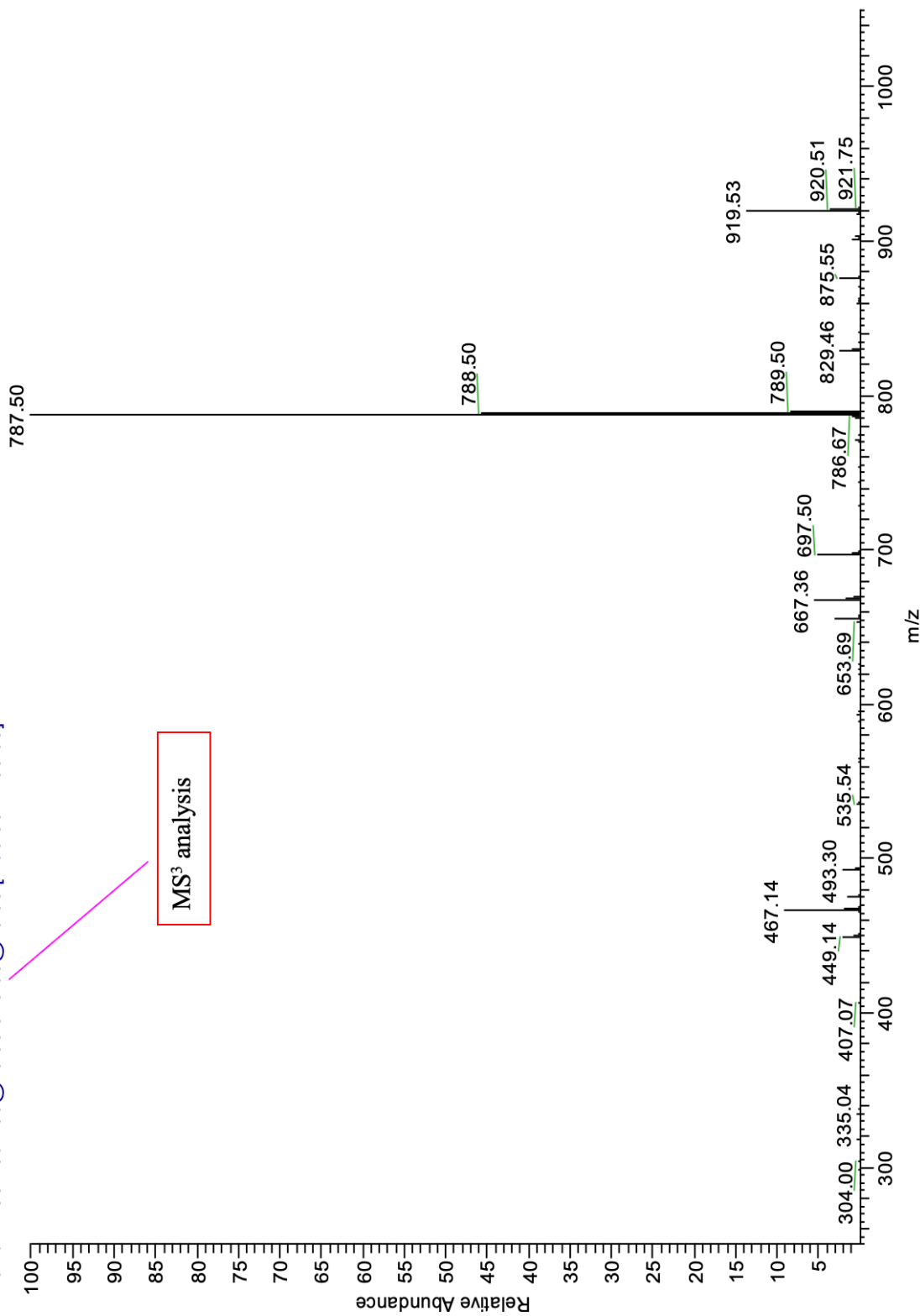


Figure 5.10: MSⁿ Analysis (Positive Ion Mode) of Compound 5.1 Continued.

05111-a #96-112 RT: 2.42-2.98 AV: 17 NL: 3.57E4
T: + c Full ms4 1052.00@40.00 920.00@40.00 788.00@40.00 [215.00-1200.00]

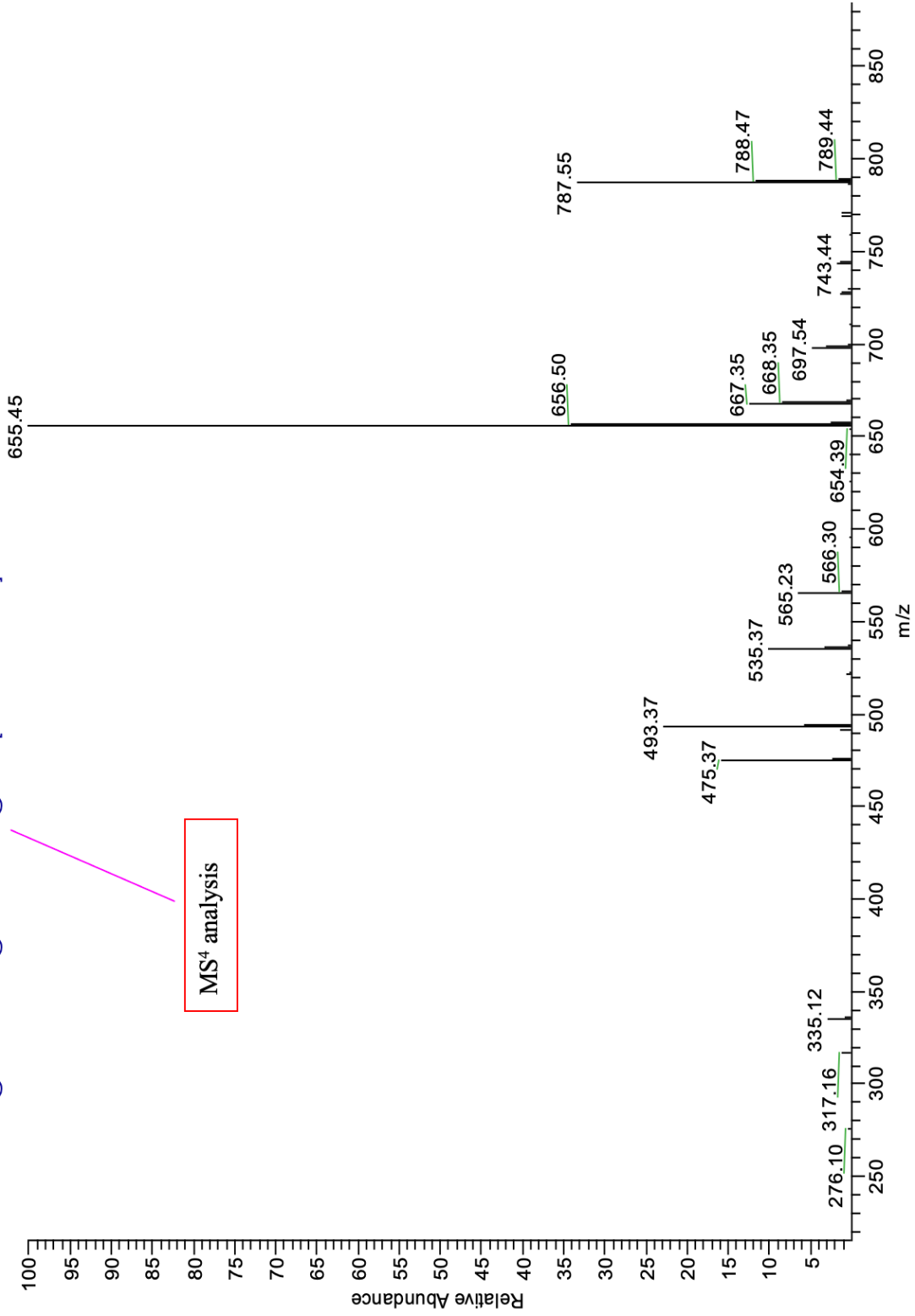


Figure 5.10: MSⁿ Analysis (Positive Ion Mode) of Compound 5.1 Continued.

05111-a #132-140 RT: 3.45-3.63 AV: 9 SB: 6 3.22-3.33 NL: 2.45E5
T: - c Full ms [215.00-1500.00]

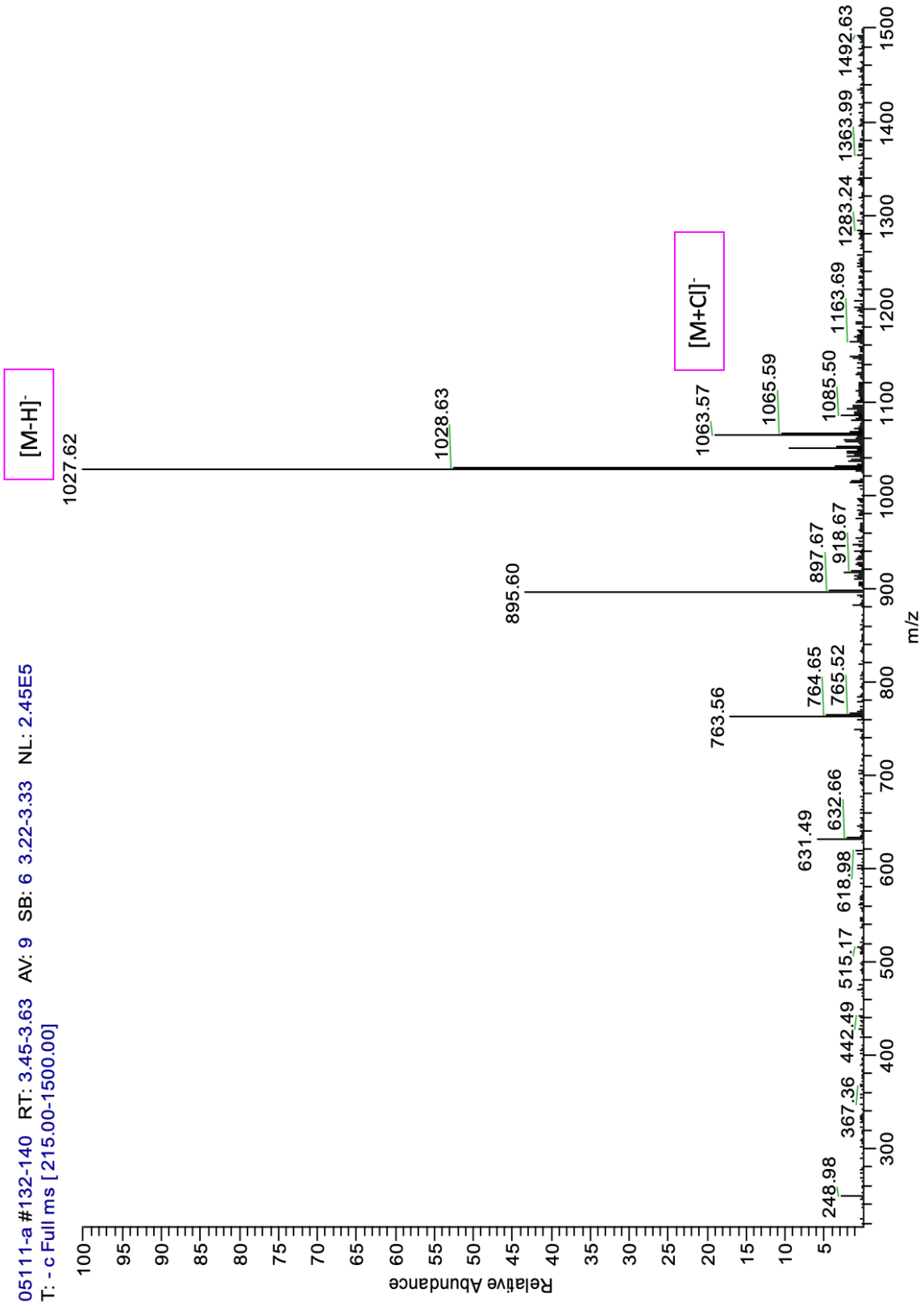


Figure 5.11: MSⁿ Analysis (Negative Ion Mode) of Compound 5.1.

05111-a #144-148 RT: 3.78-3.88 AV: 5 NL: 1.12E6
T: -c Full ms2 1028.00@40.00 [280.00-1500.00]

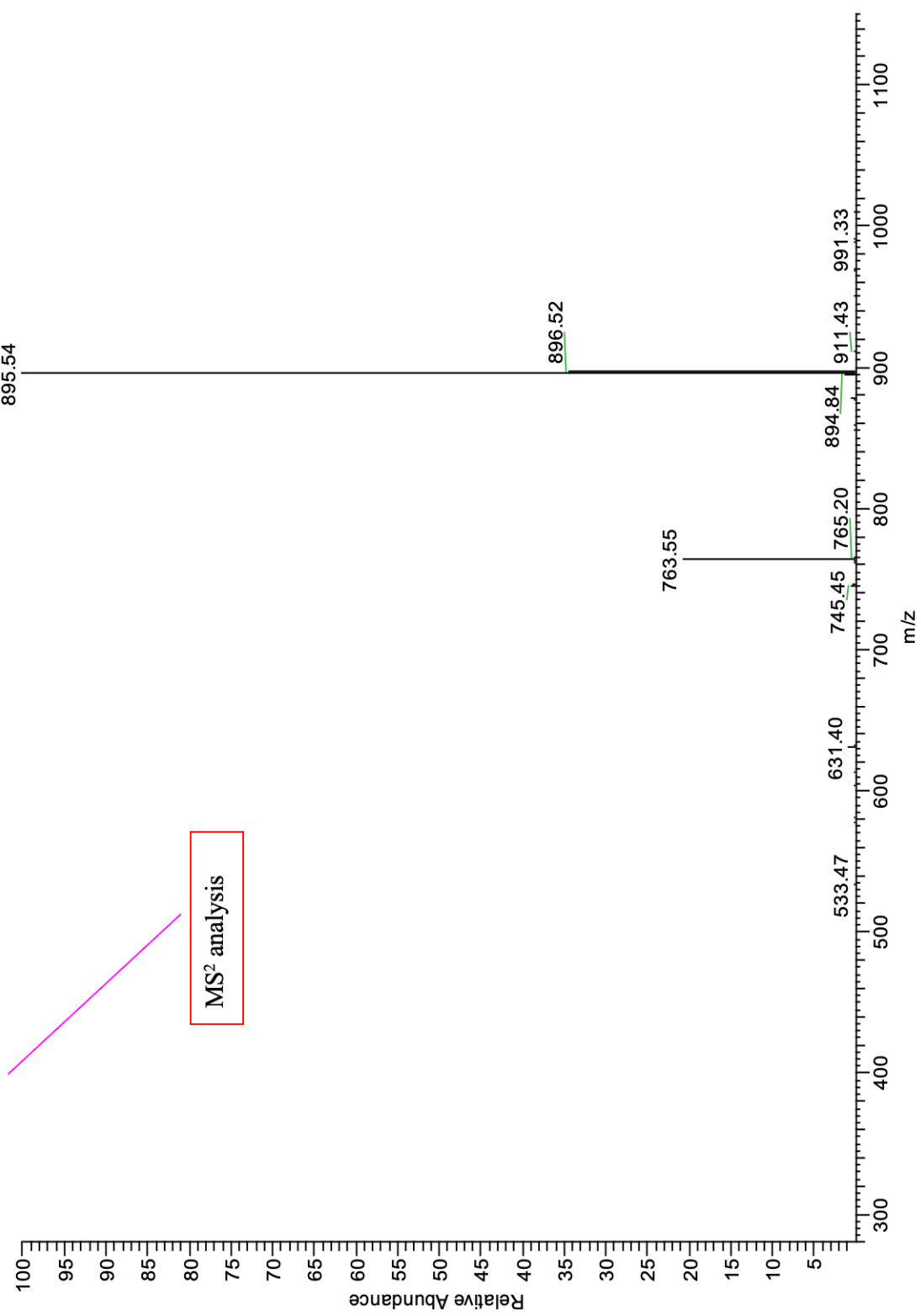


Figure 5.11: MSⁿ Analysis (Negative Ion Mode) of Compound 5.1 Continued.

05111-a #155-157 RT: 4.17-4.22 AV: 3 NL: 1.19E6
T: - c Full ms3 1028.00@40.00 895.00@40.00 [245.00-1500.00]

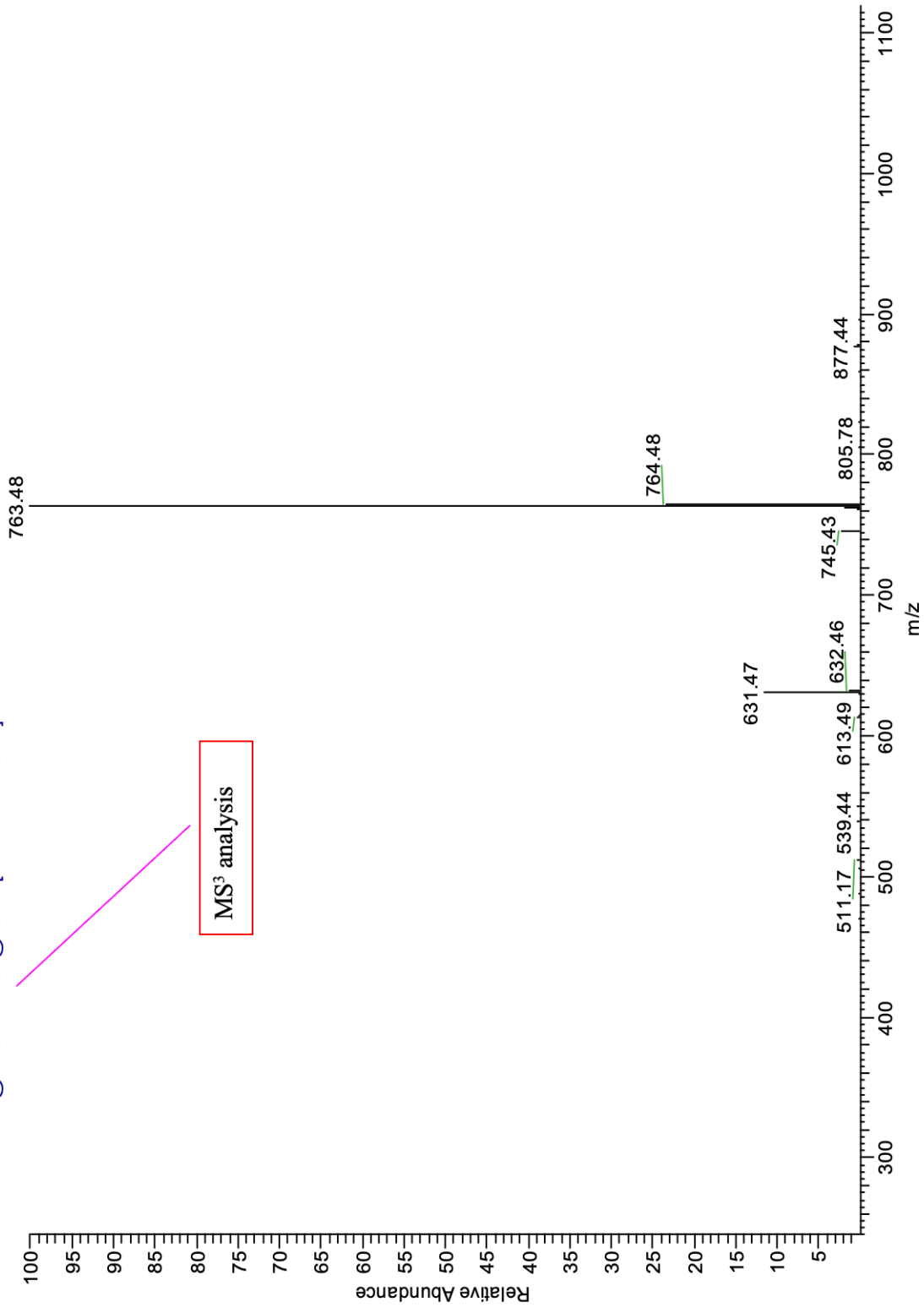


Figure 5.11: MSⁿ Analysis (Negative Ion Mode) of Compound 5.1 Continued.

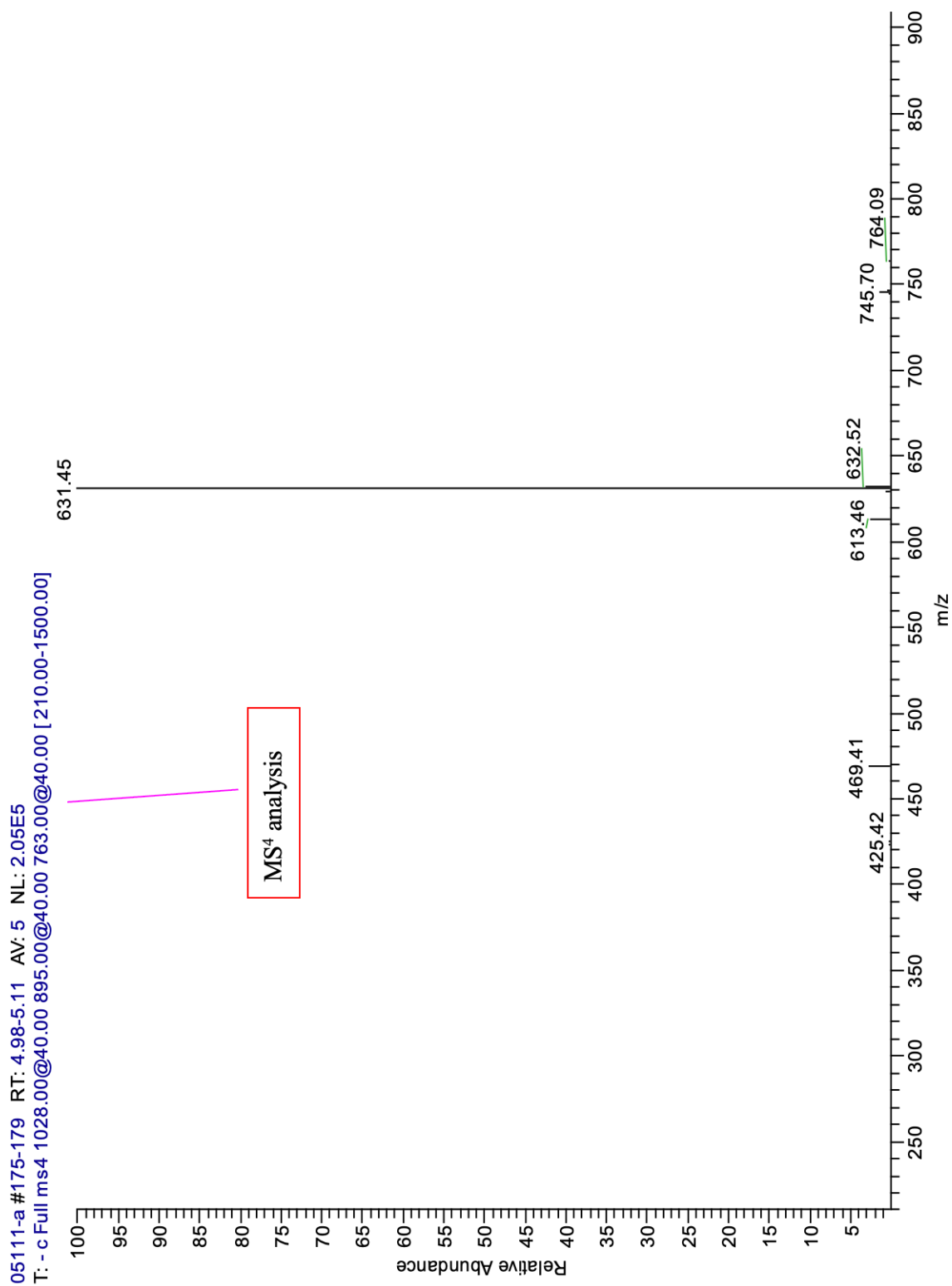


Figure 5.11: MSⁿ Analysis (Negative Ion Mode) of Compound **5.1** Continued.

05111-a #183-186 RT: 5.31-5.41 AV: 4 NL: 3.87E4
T: - c Full ms5 1028.00@40.00 895.00@40.00 763.00@40.00 631.00@40.00 [170.00-1500.00]

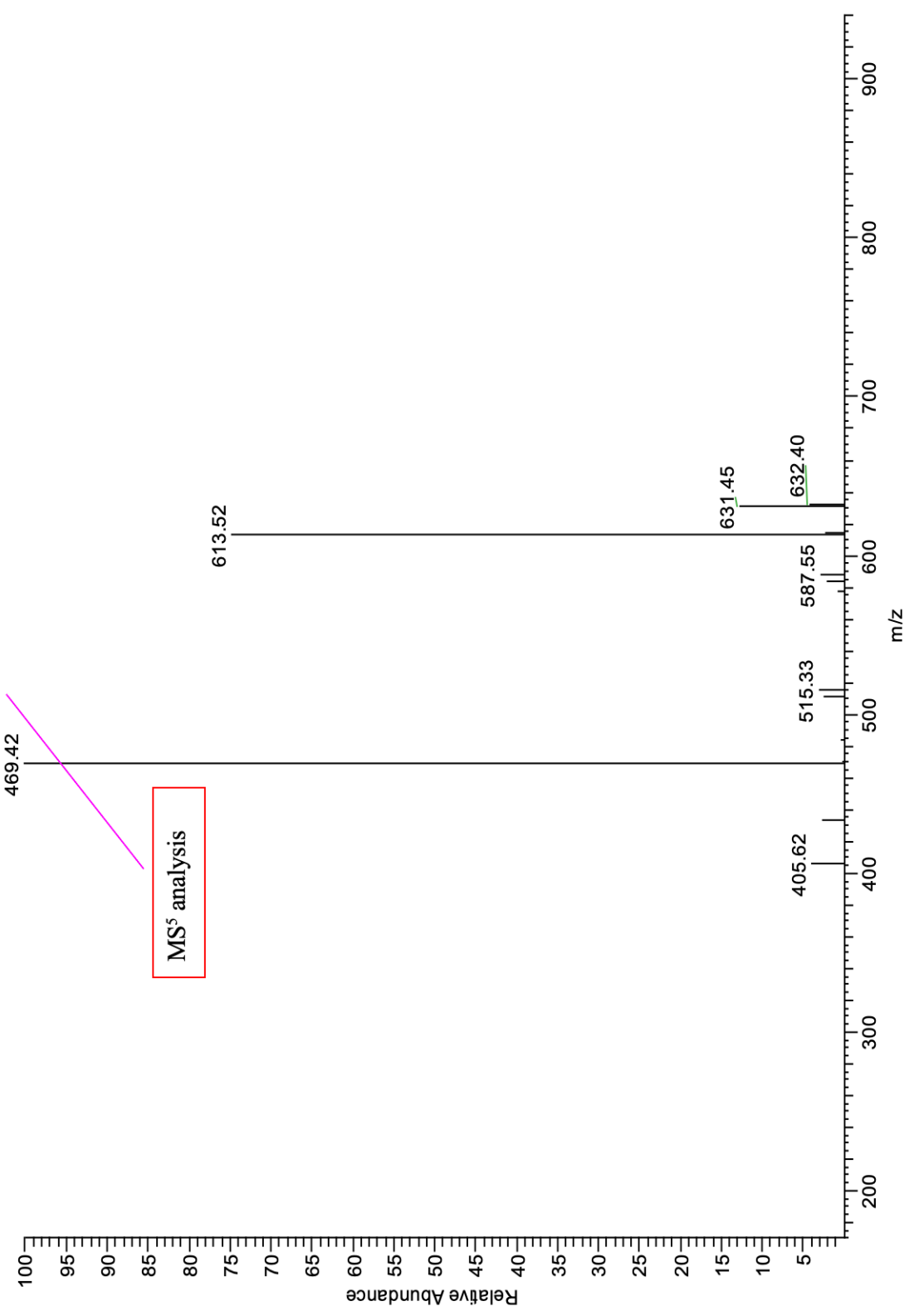


Figure 5.11: MSⁿ Analysis (Negative Ion Mode) of Compound 5.1 Continued.

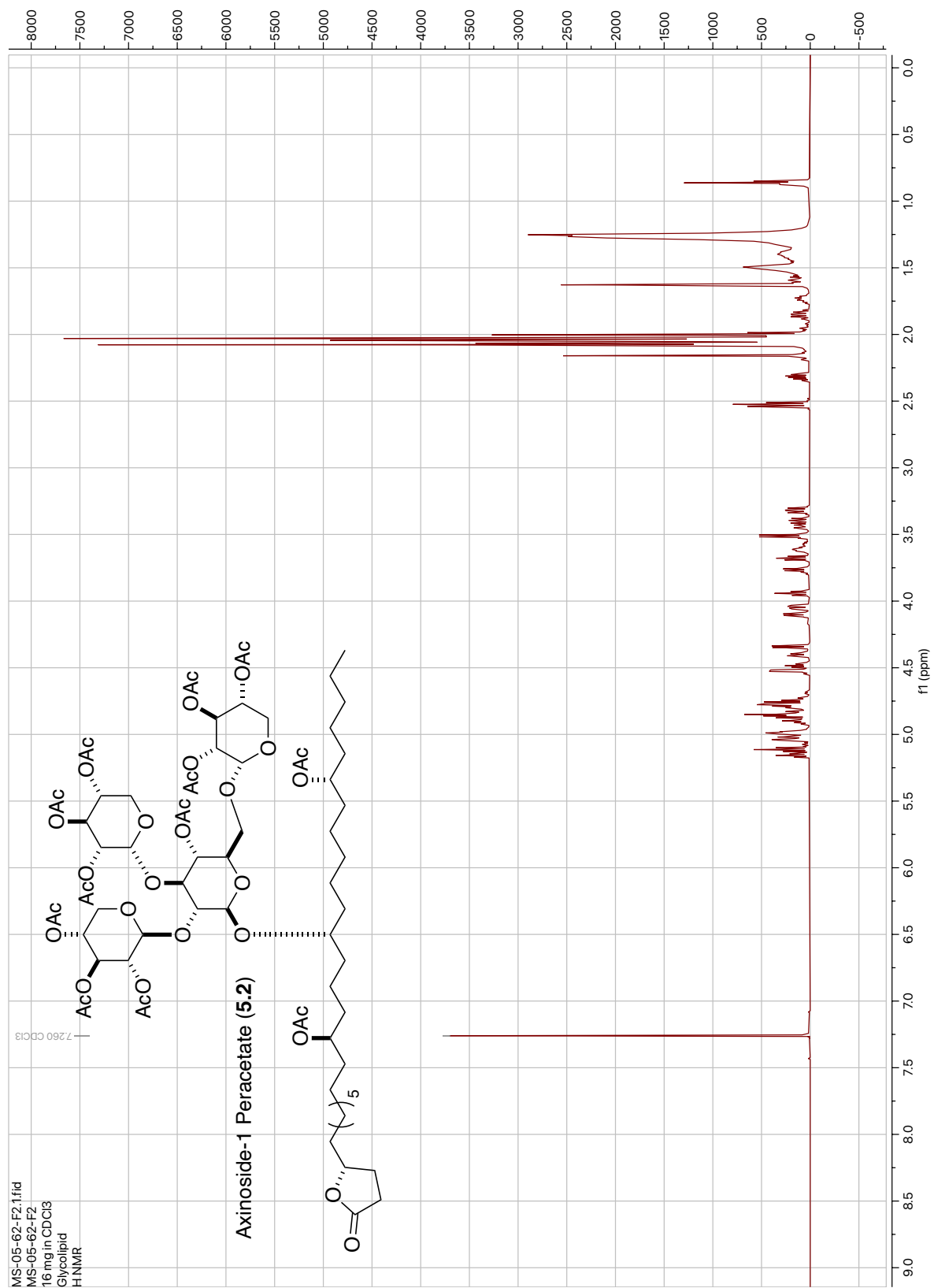


Figure 5.12: ¹H NMR of Compound 5.2 (600 MHz, CDCl₃).

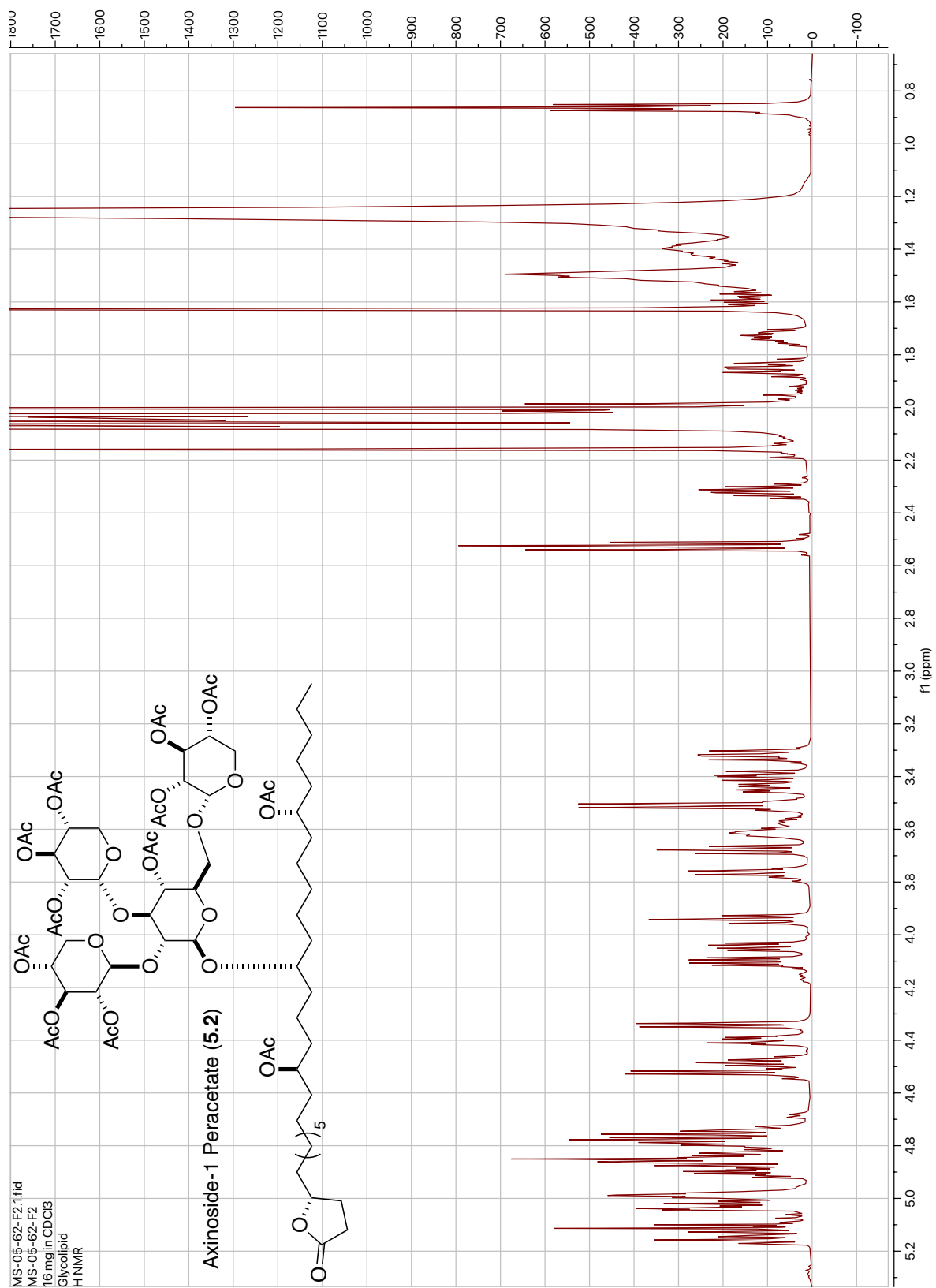


Figure 5.13: ¹H NMR Expansion of Compound 5.2 (600 MHz, CDCl₃).

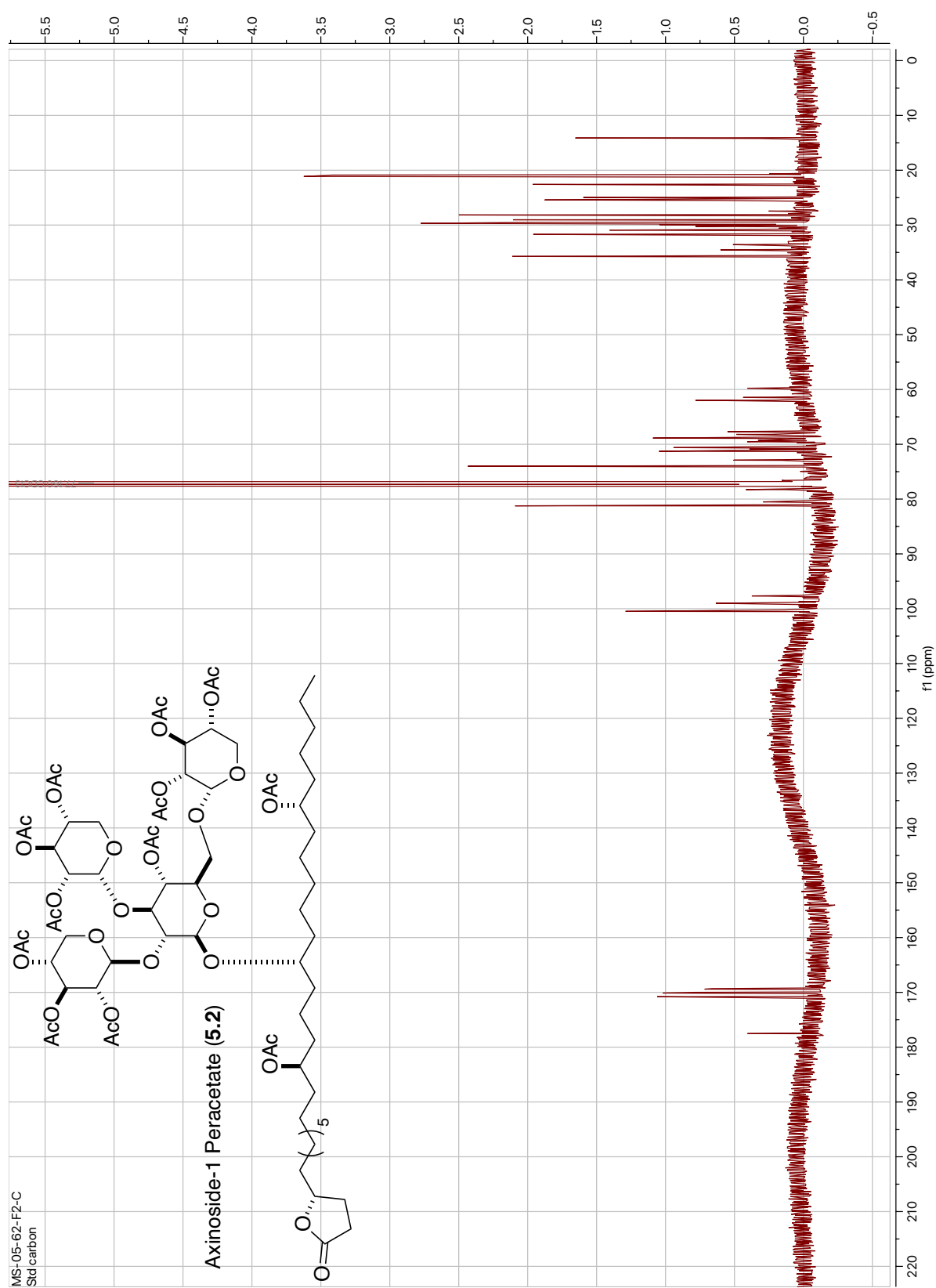


Figure 5.14: ^{13}C NMR of Compound 5.2 (125 MHz, CDCl_3).

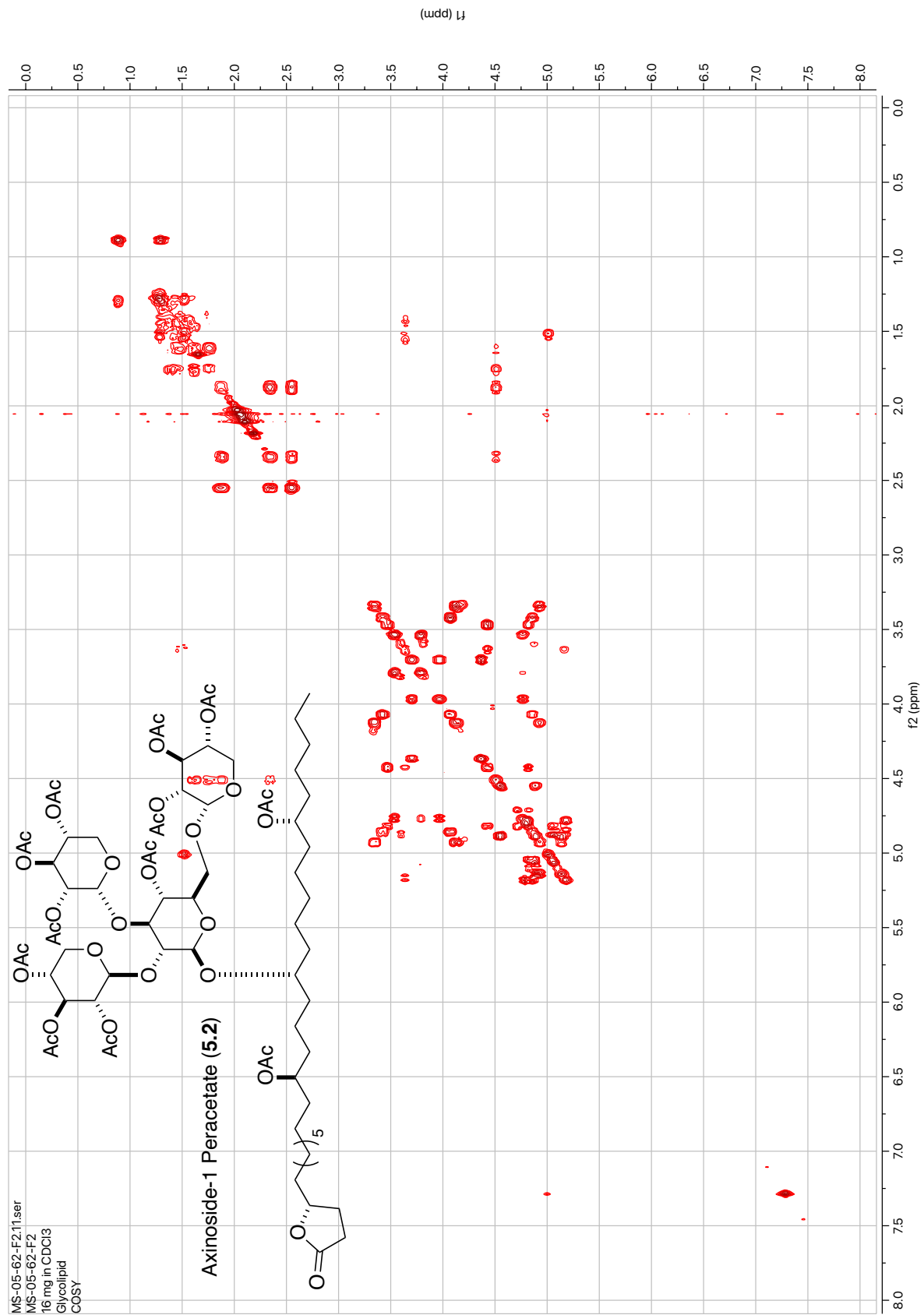


Figure 5.15: DQF-COSY of Compound 5.2 (600 MHz, CDCl₃).

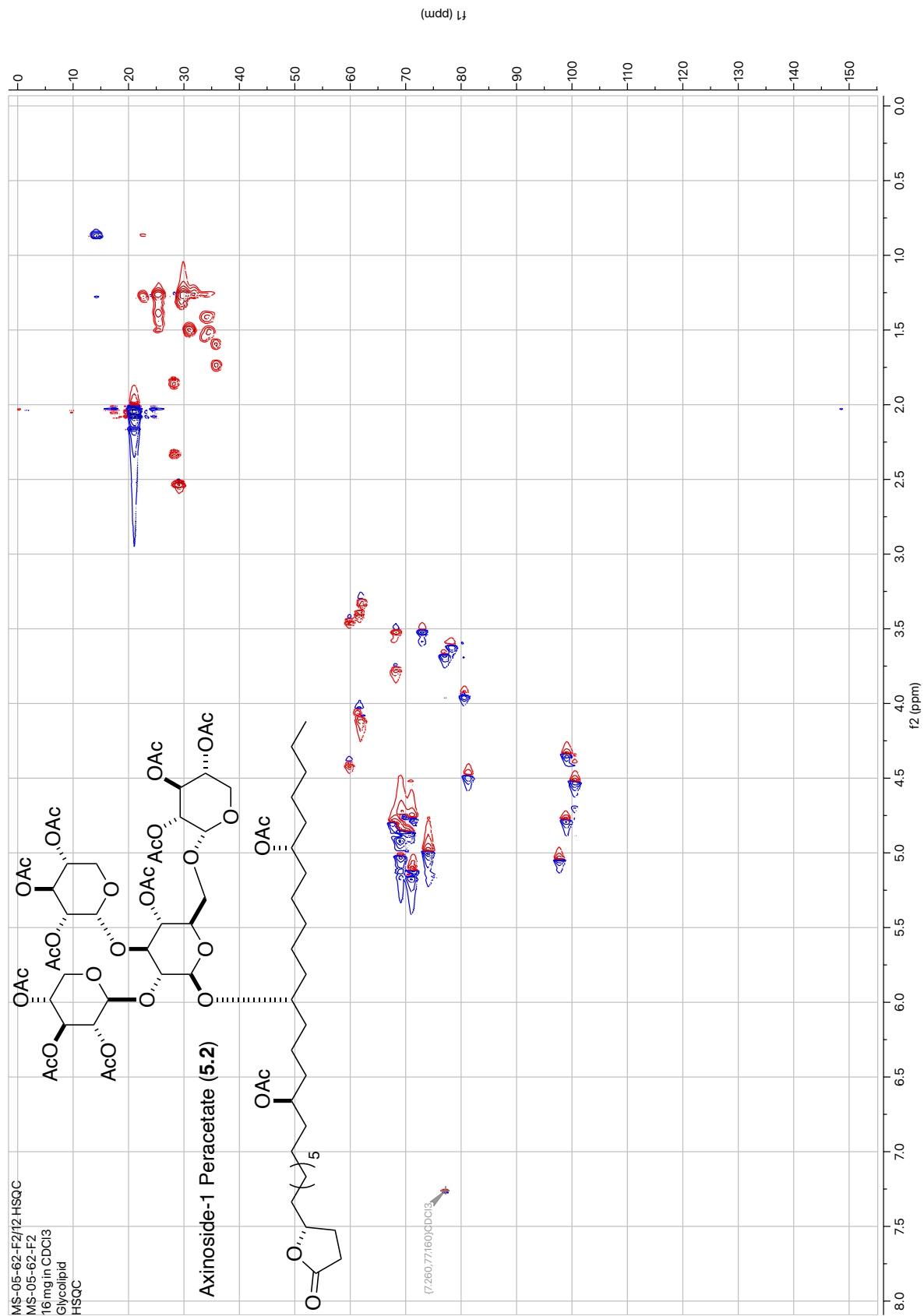


Figure 5.16: HSQC of Compound **5.2** (600 MHz, CDCl₃).

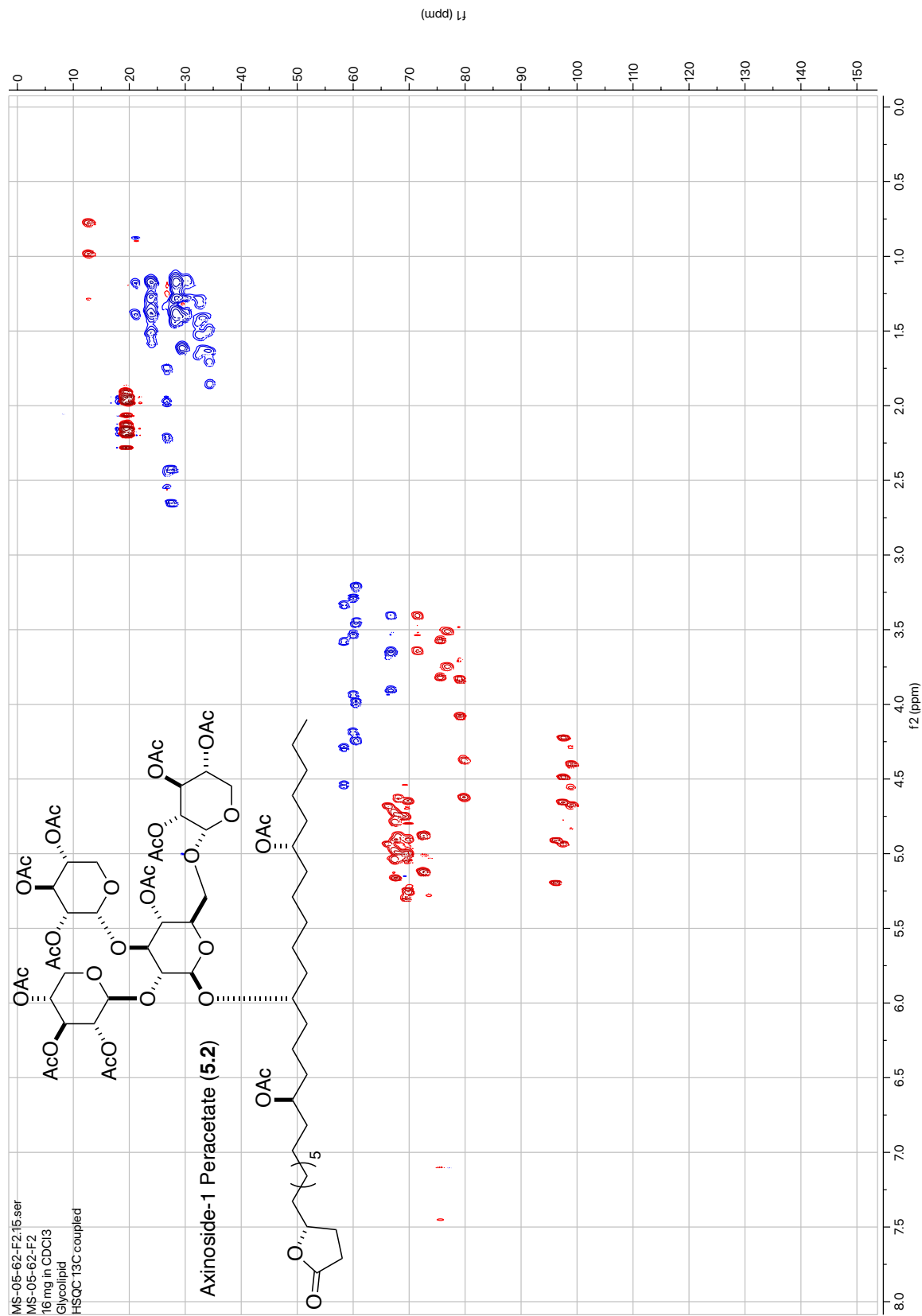
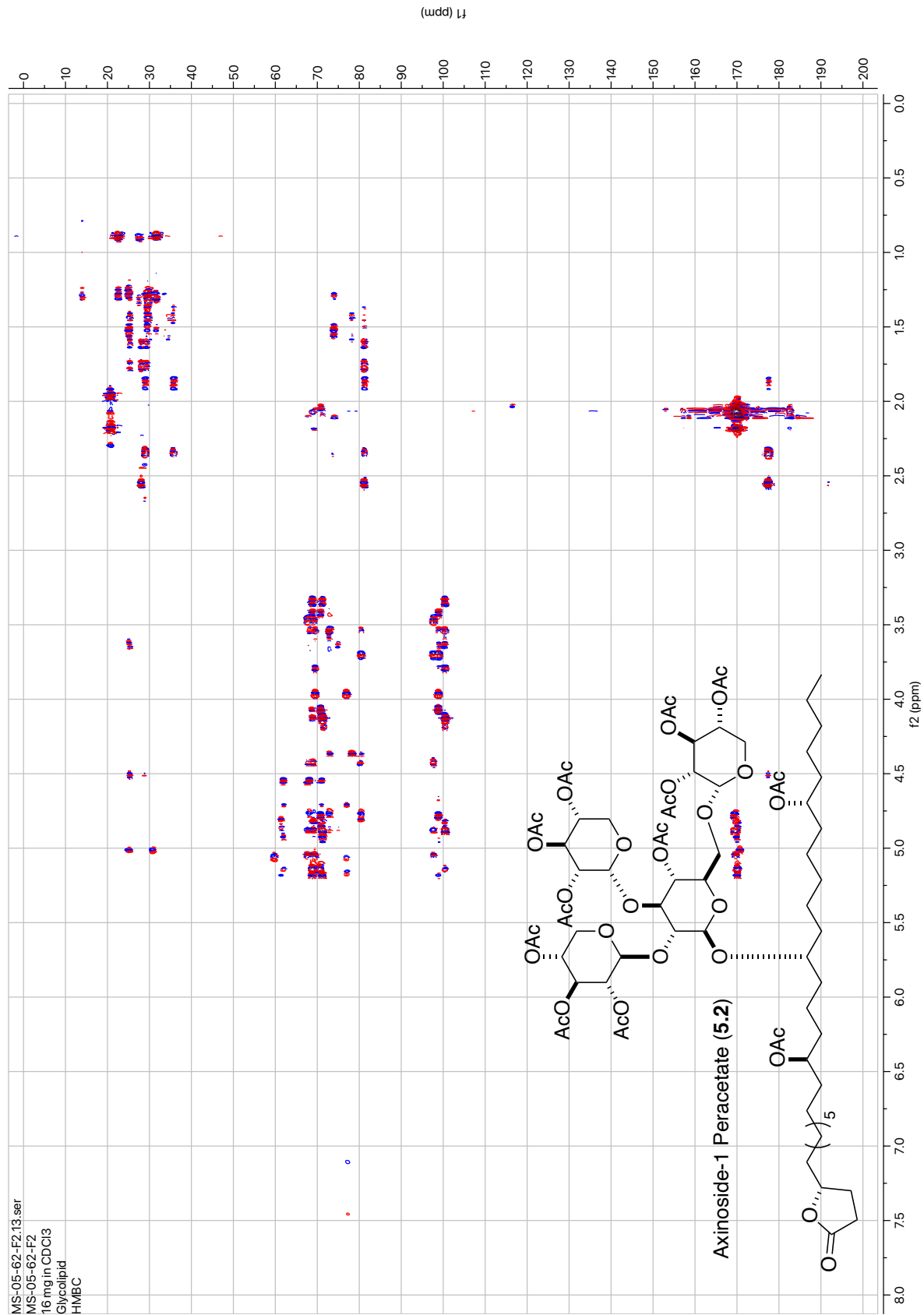


Figure 5.17: ¹³C-Coupled HSQC of Compound **5.2** (600 MHz, CDCl₃).



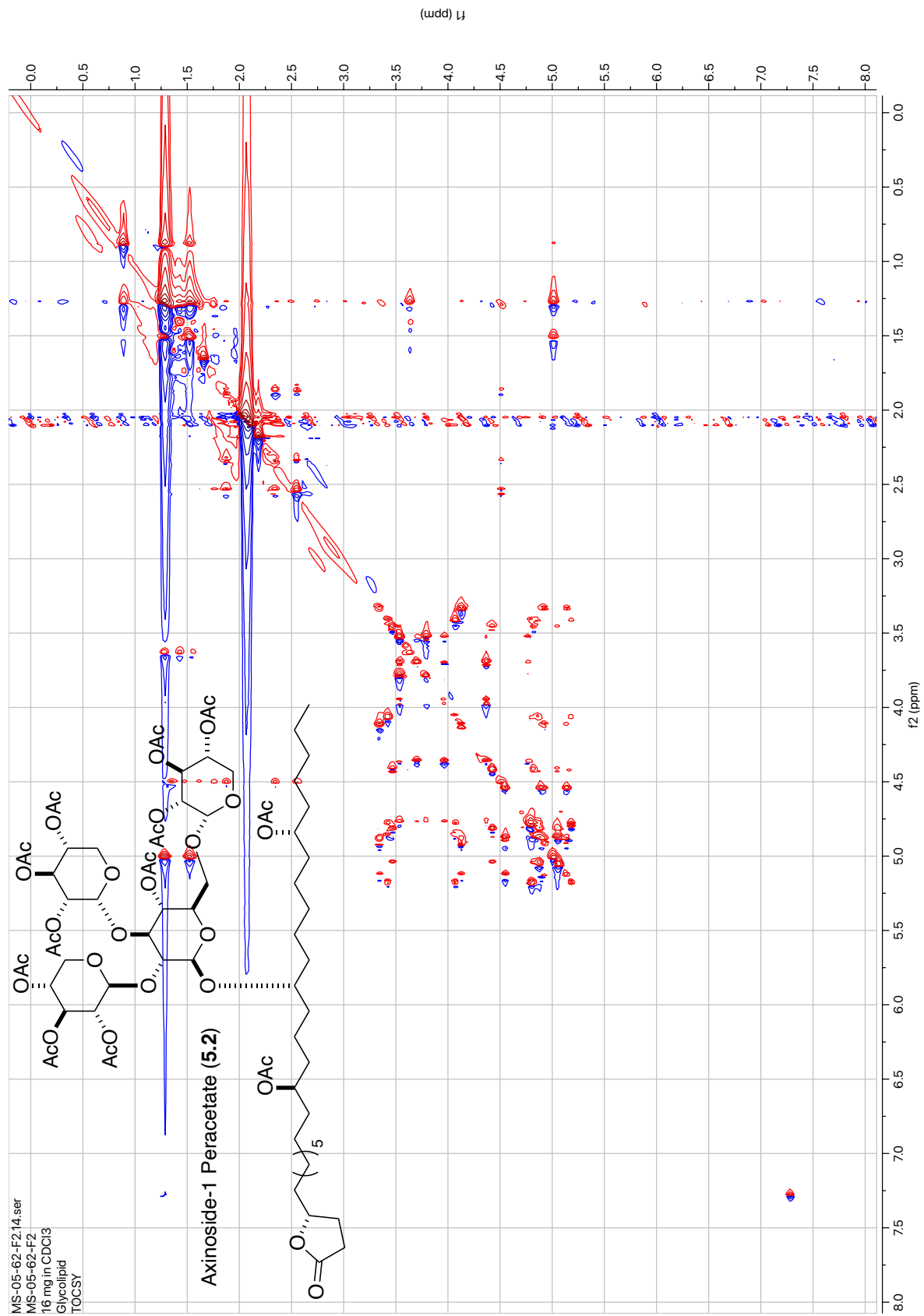


Figure 5.19: TOCSY of Compound **5.2** (600 MHz, CDCl₃, 40 mS).

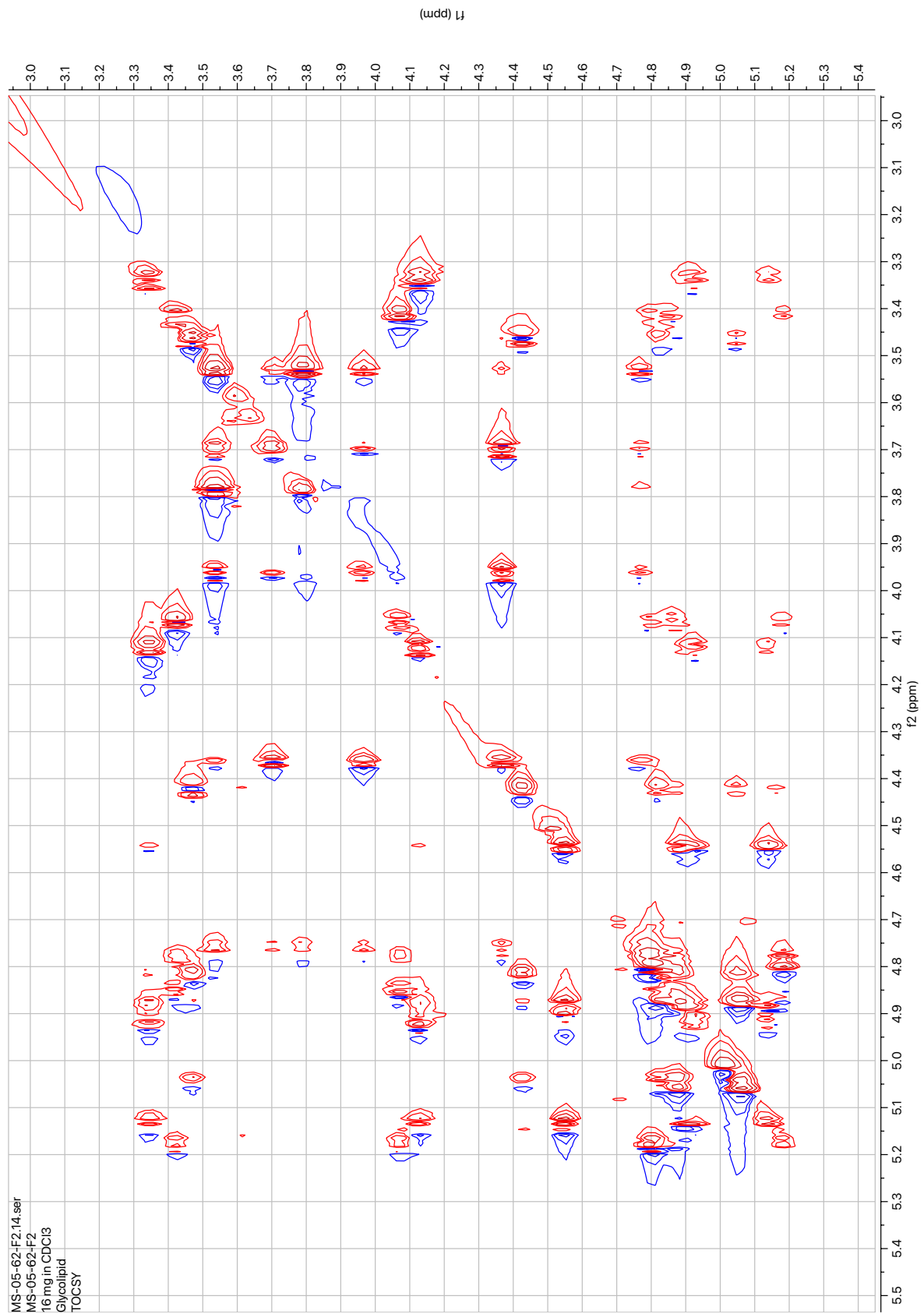


Figure 5.20: TOCSY Expansion of Compound 5.2 (600 MHz, CDCl₃, 40 mS).

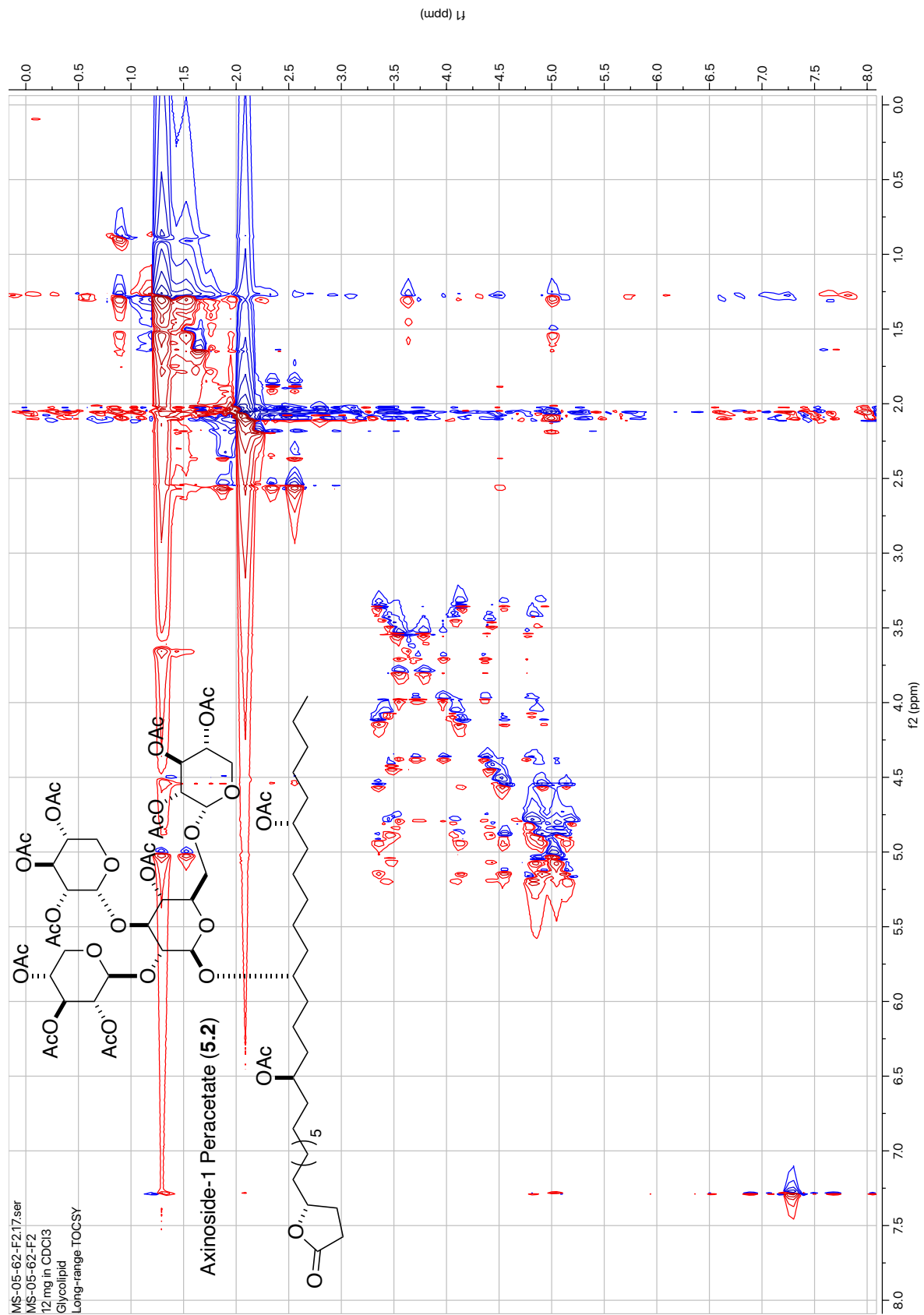


Figure 5.21: Long-range TOCSY of Compound 5.2 (600 MHz, CDCl₃, 120 mS).

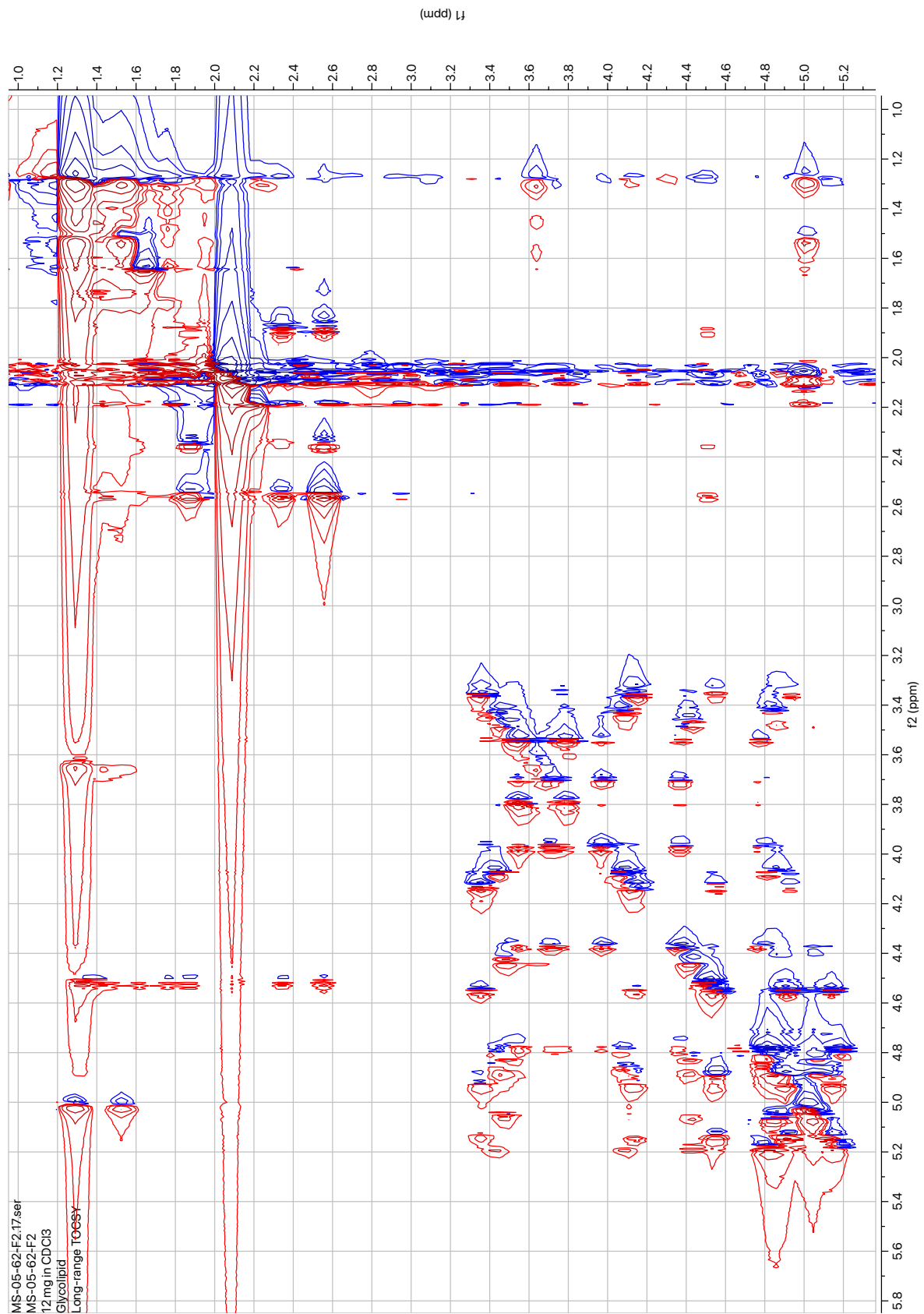


Figure 5.22: Long-range TOCSY Expansion of Compound **5.2** (600 MHz, CDCl₃, 120 mS).

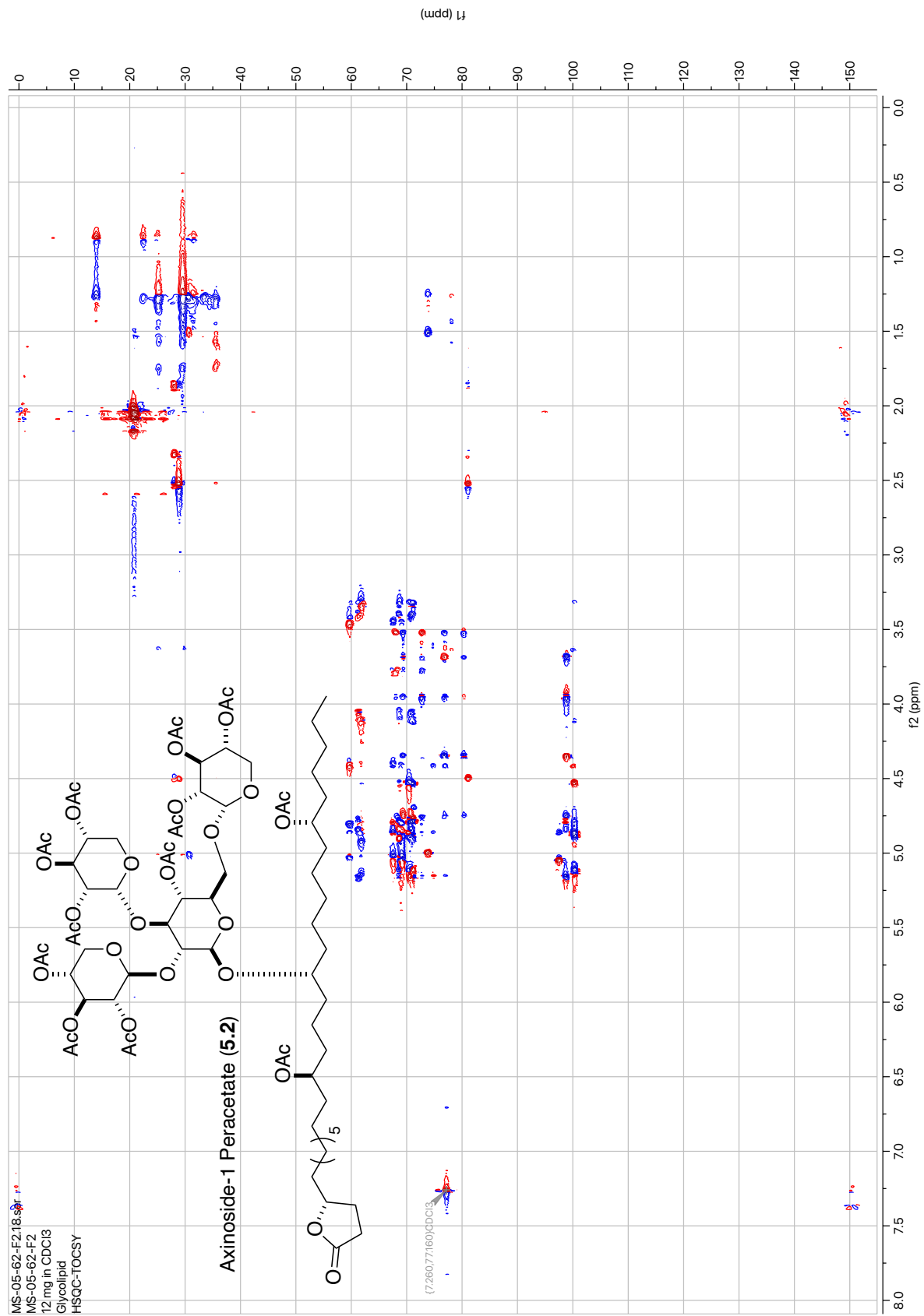


Figure 5.23: HSQC-TOCSY of Compound 5.2 (600 MHz, CDCl₃).

0562F2-a #16-20 RT: 0.33-0.42 AV: 5 SB: 7 0.10-0.23 NL: 2.33E7
T: + c Full ms [300.00-1800.00]

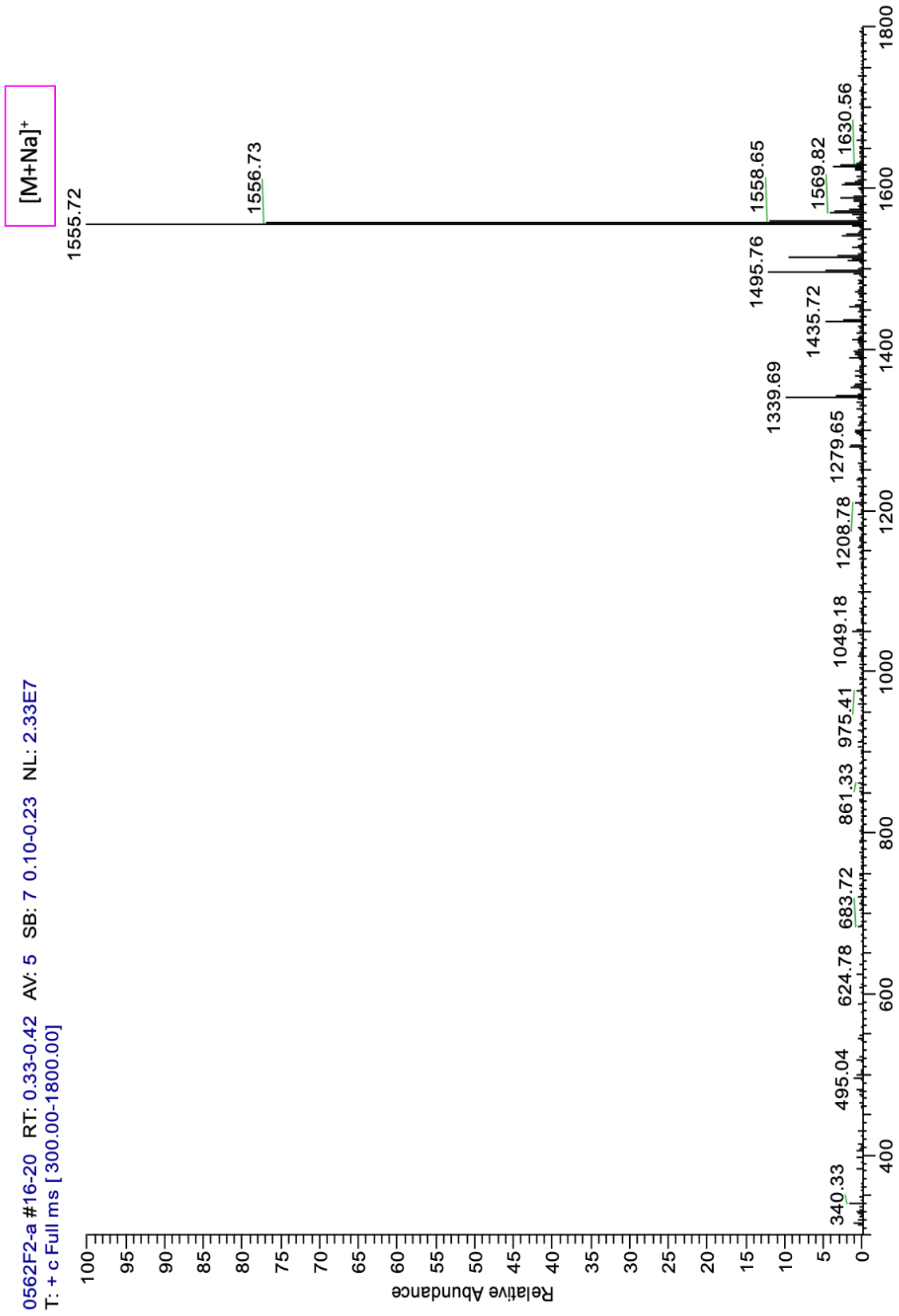


Figure 5.24: MSⁿ Analysis (Positive Ion Mode) of Compound 5.2.

0562F2-a #27-33 RT: 0.58-0.73 AV: 7 NL: 1.88E6
T: + c Full ms2 1556.00@40.00 [425.00-1800.00]

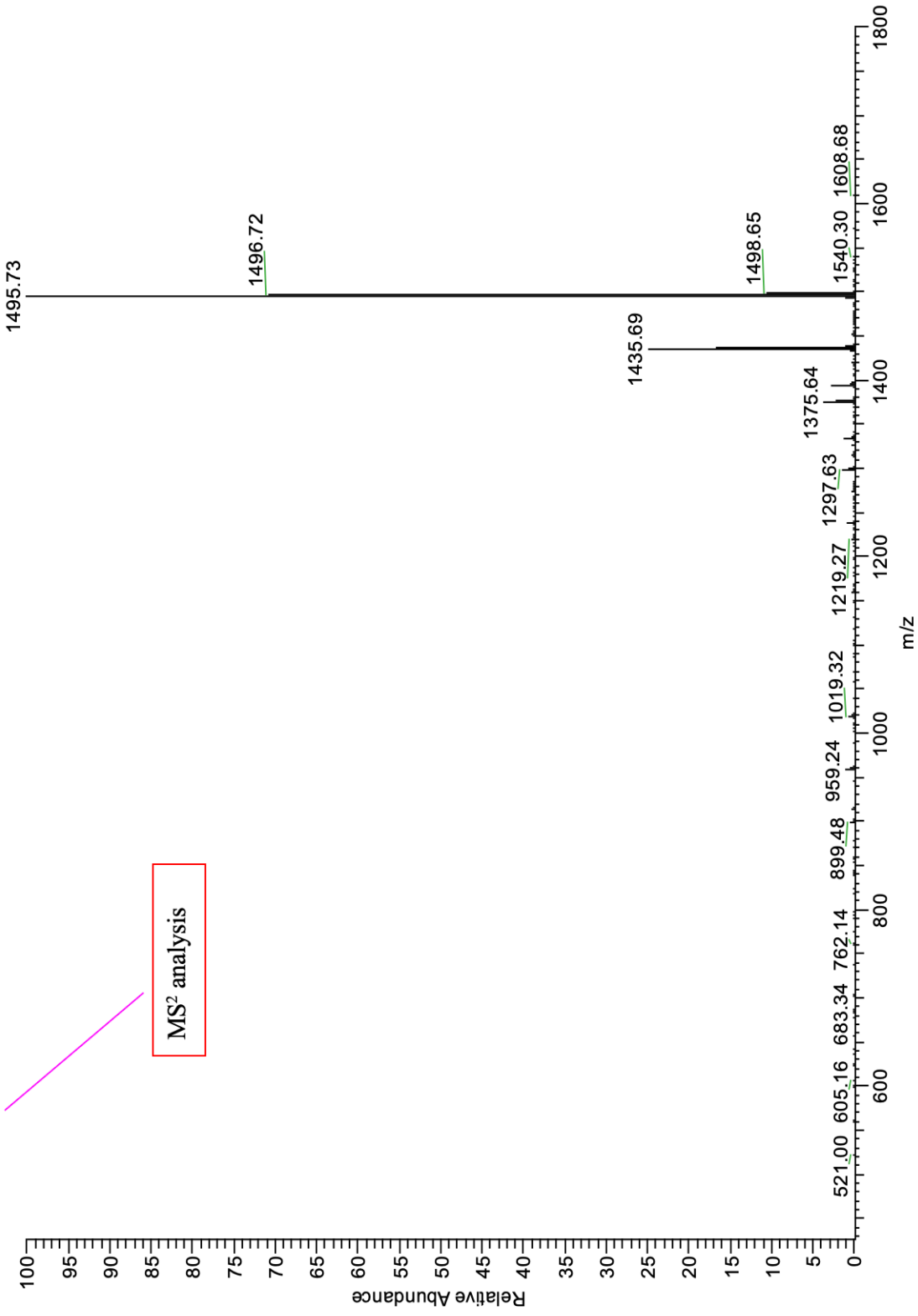


Figure 5.24: MSⁿ Analysis (Positive Ion Mode) of Compound 5.2 Continued.

0562F2-a #36-40 RT: 0.82-0.94 AV: 5 NL: 8.58E5
T: + c Full ms3 1556.00@40.00 1496.00@40.00 [410.00-1800.00]

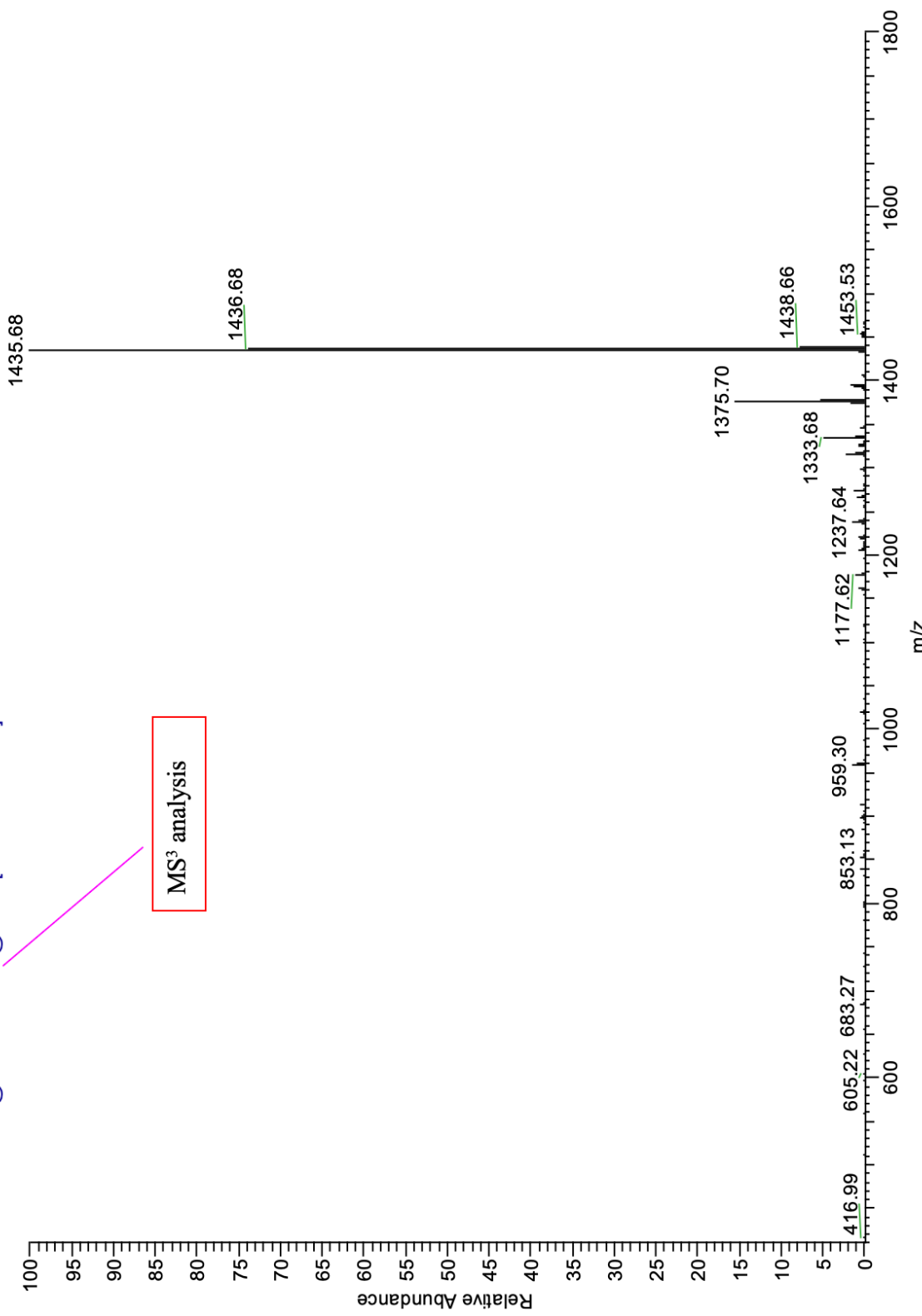


Figure 5.24: MSⁿ Analysis (Positive Ion Mode) of Compound 5.2 Continued.

0562F2-a #46-49 RT: 1.14-1.22 AV: 4 NL: 3.61E6
T: + c Full ms4 1556.00@40.00 1496.00@40.00 1436.00@40.00 [395.00-1800.00]

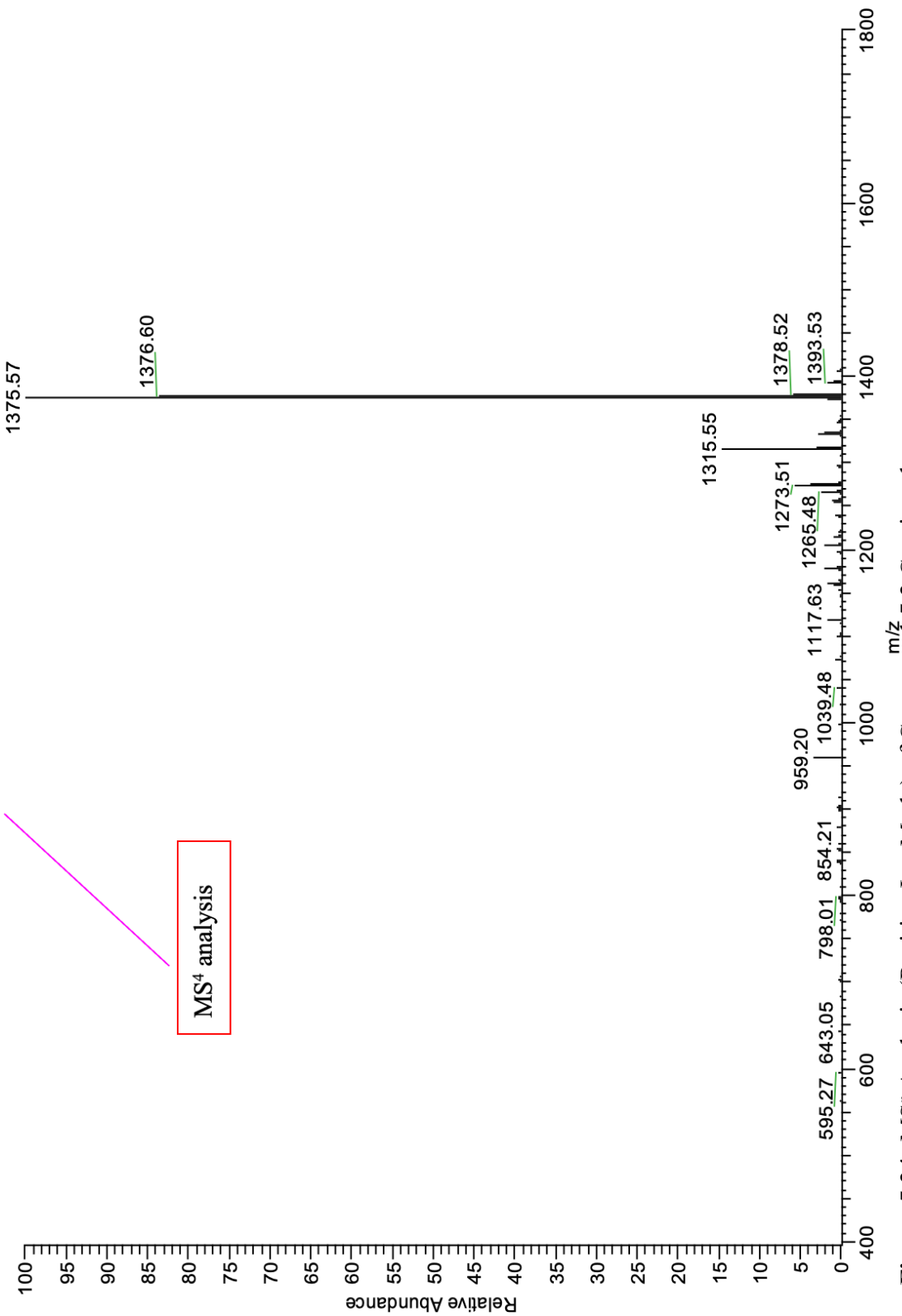


Figure 5.24: MSⁿ Analysis (Positive Ion Mode) of Compound 5.2 Continued.

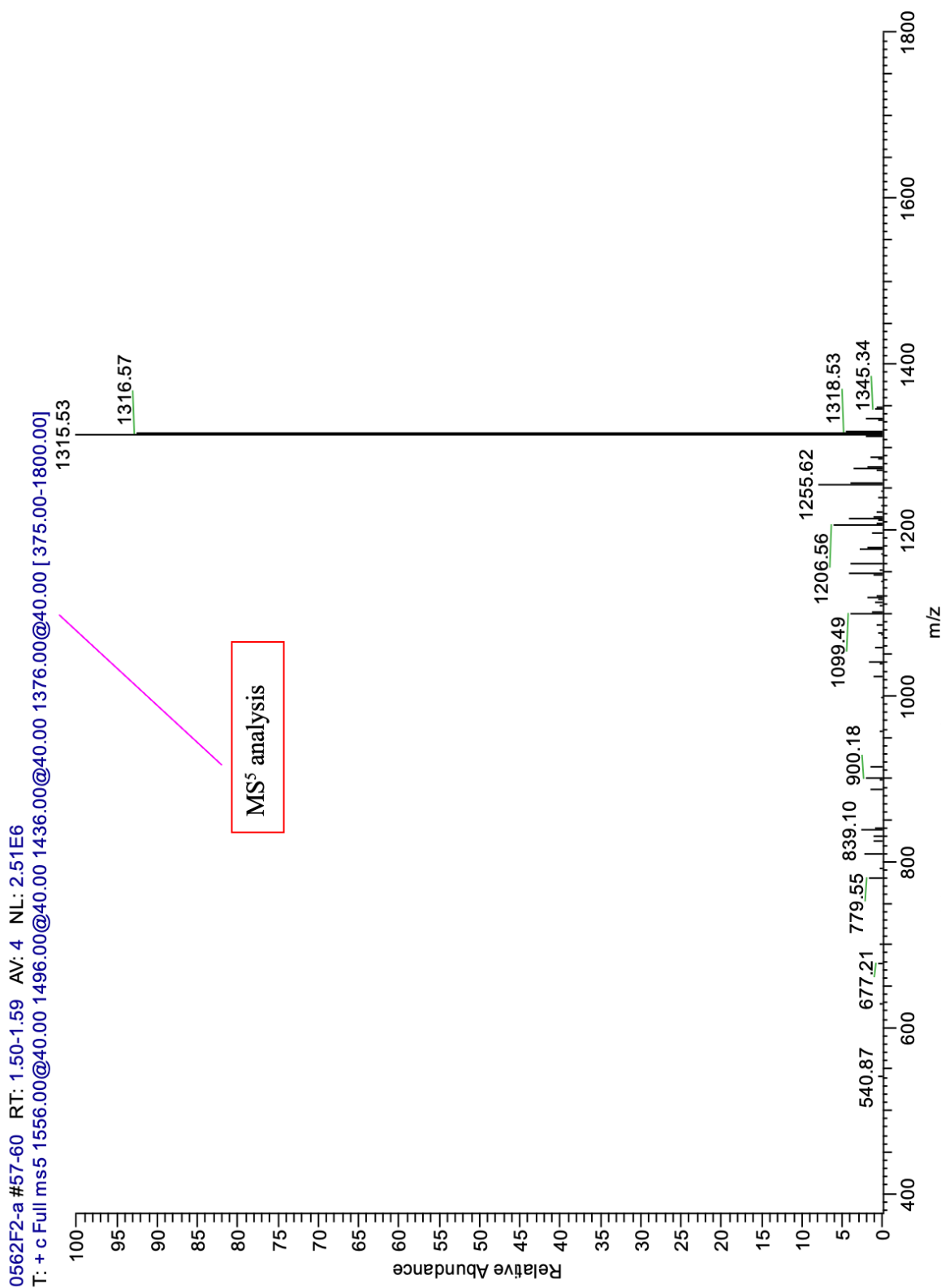


Figure 5.24: MSⁿ Analysis (Positive Ion Mode) of Compound **5.2** Continued.

0562F2-a #69-79 RT: 1.91-2.24 AV: 11 NL: 8.17E5
T: + c Full ms6 1556.00@40.00 1496.00@40.00 1436.00@40.00 1376.00@40.00 1316.00@40.00 [360.00-1800.00]

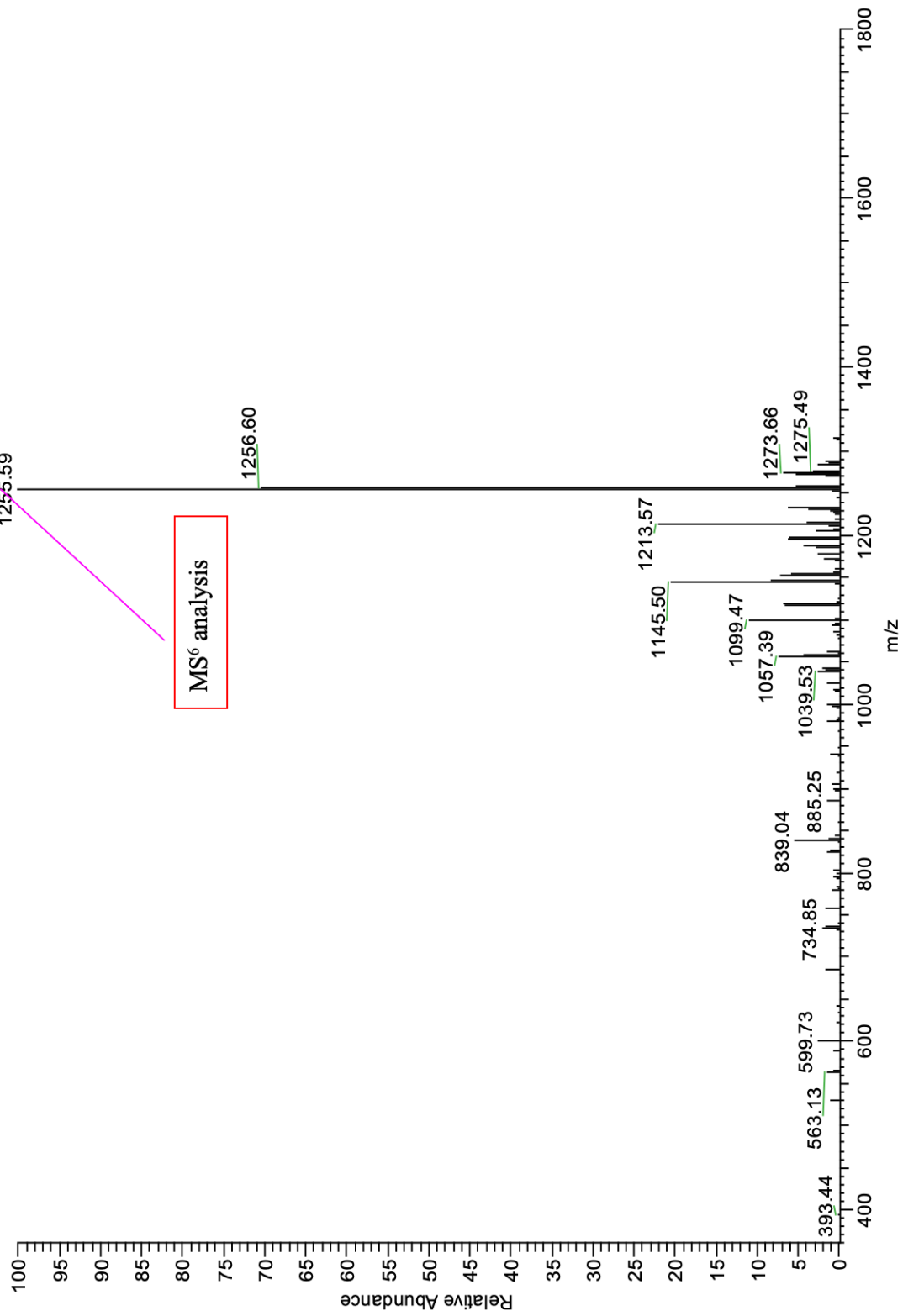


Figure 5.24: MSⁿ Analysis (Positive Ion Mode) of Compound 5.2 Continued.

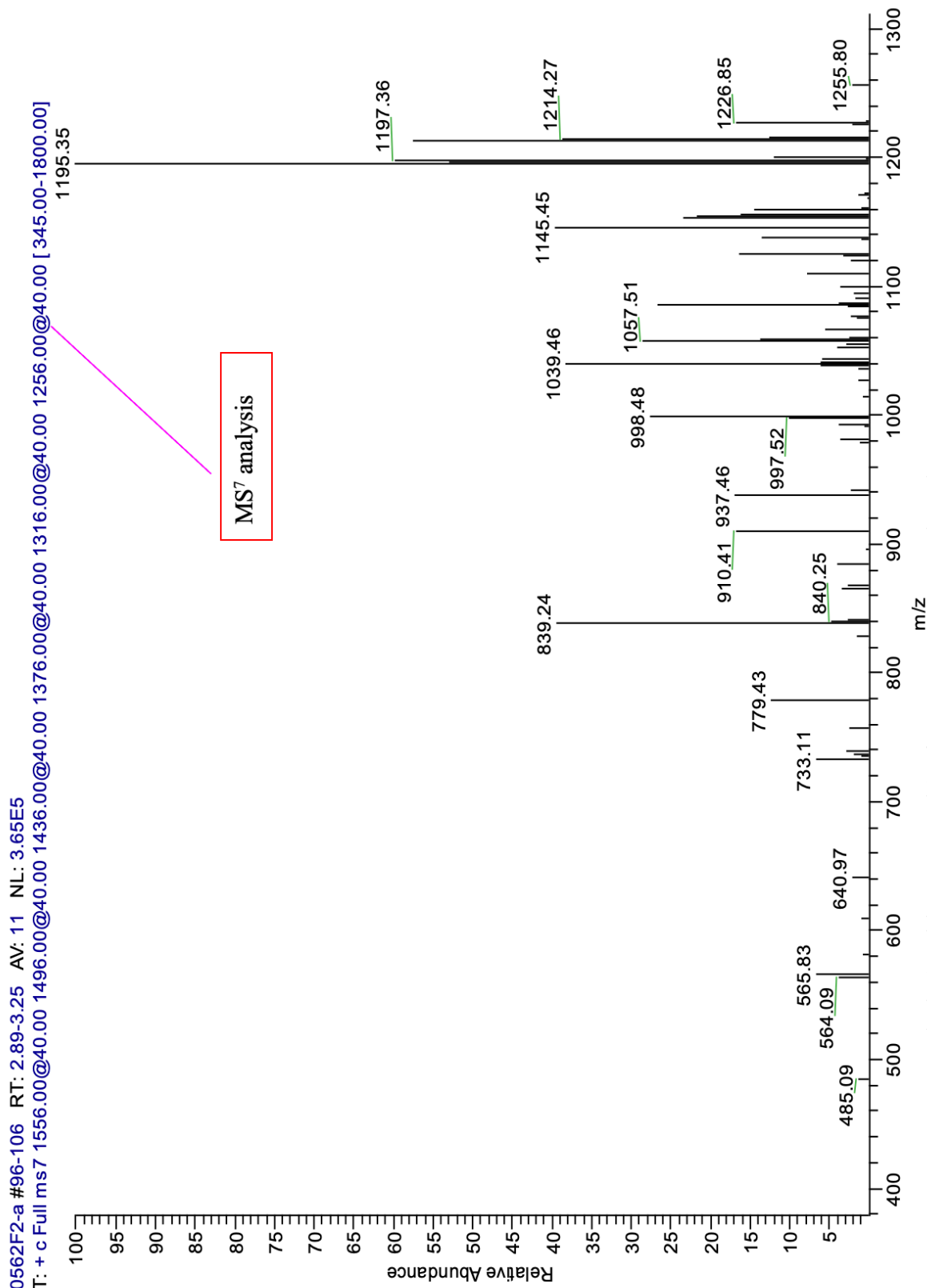
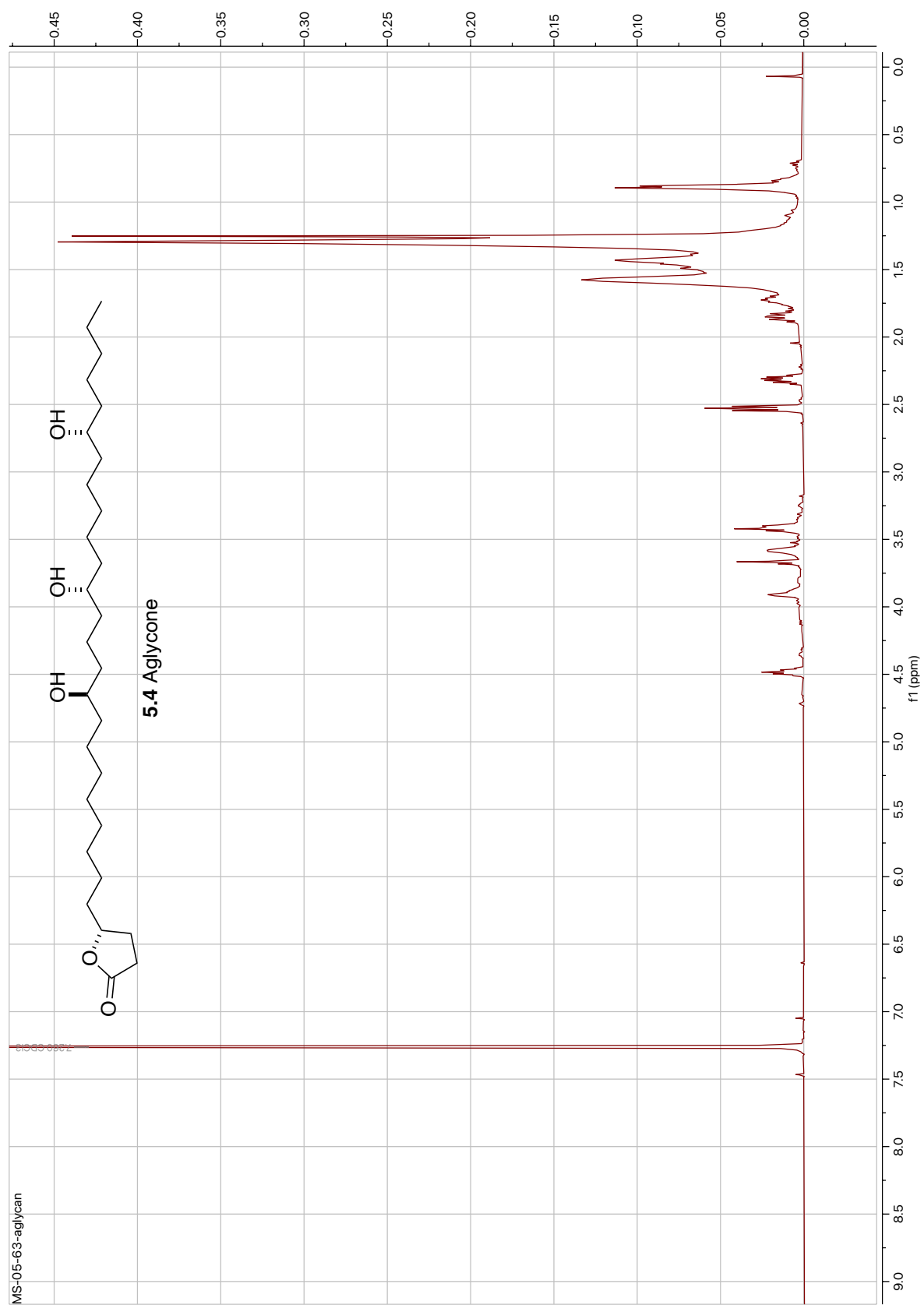


Figure 5.24: MSⁿ Analysis (Positive Ion Mode) of Compound 5.2 Continued.



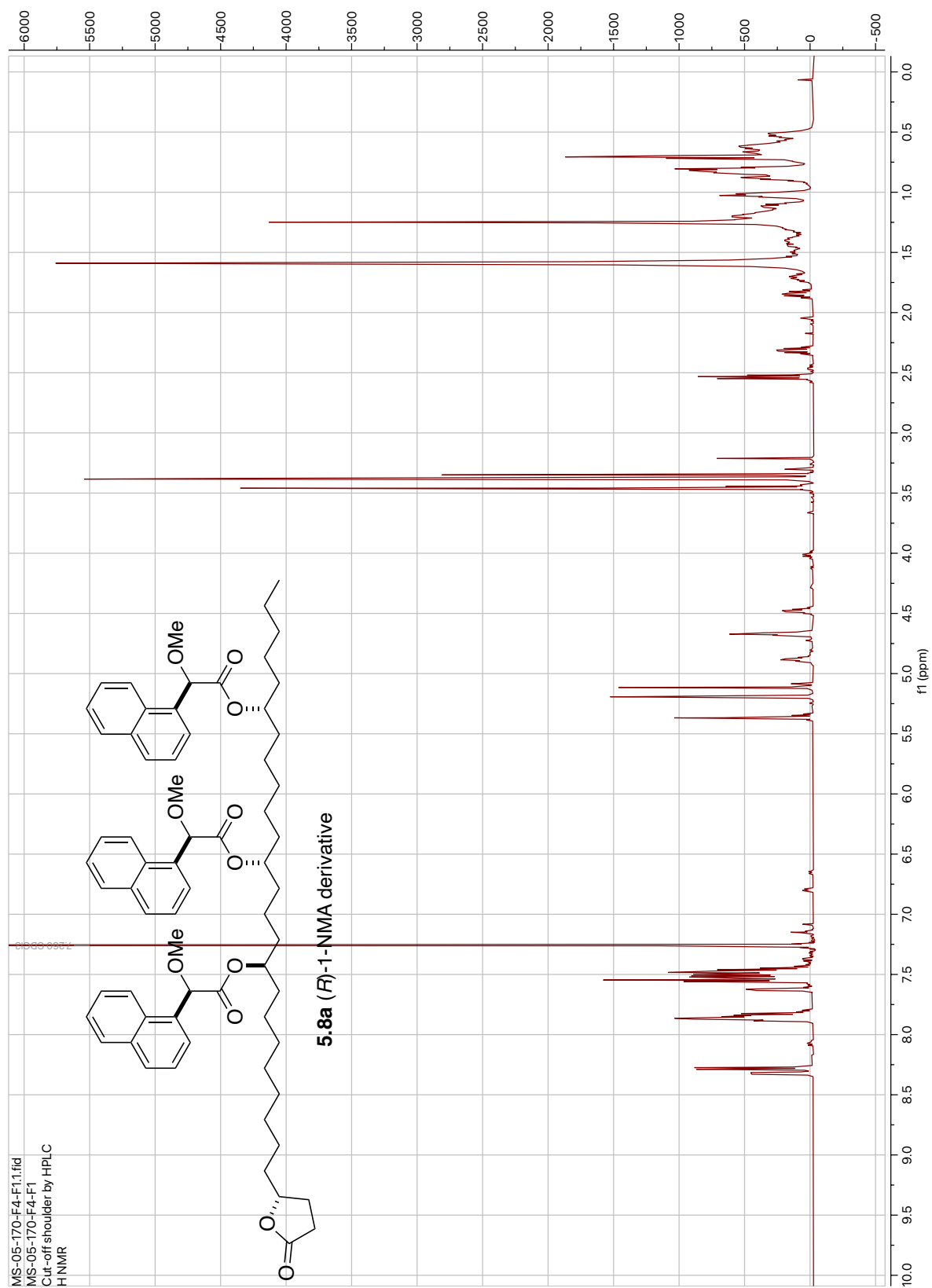
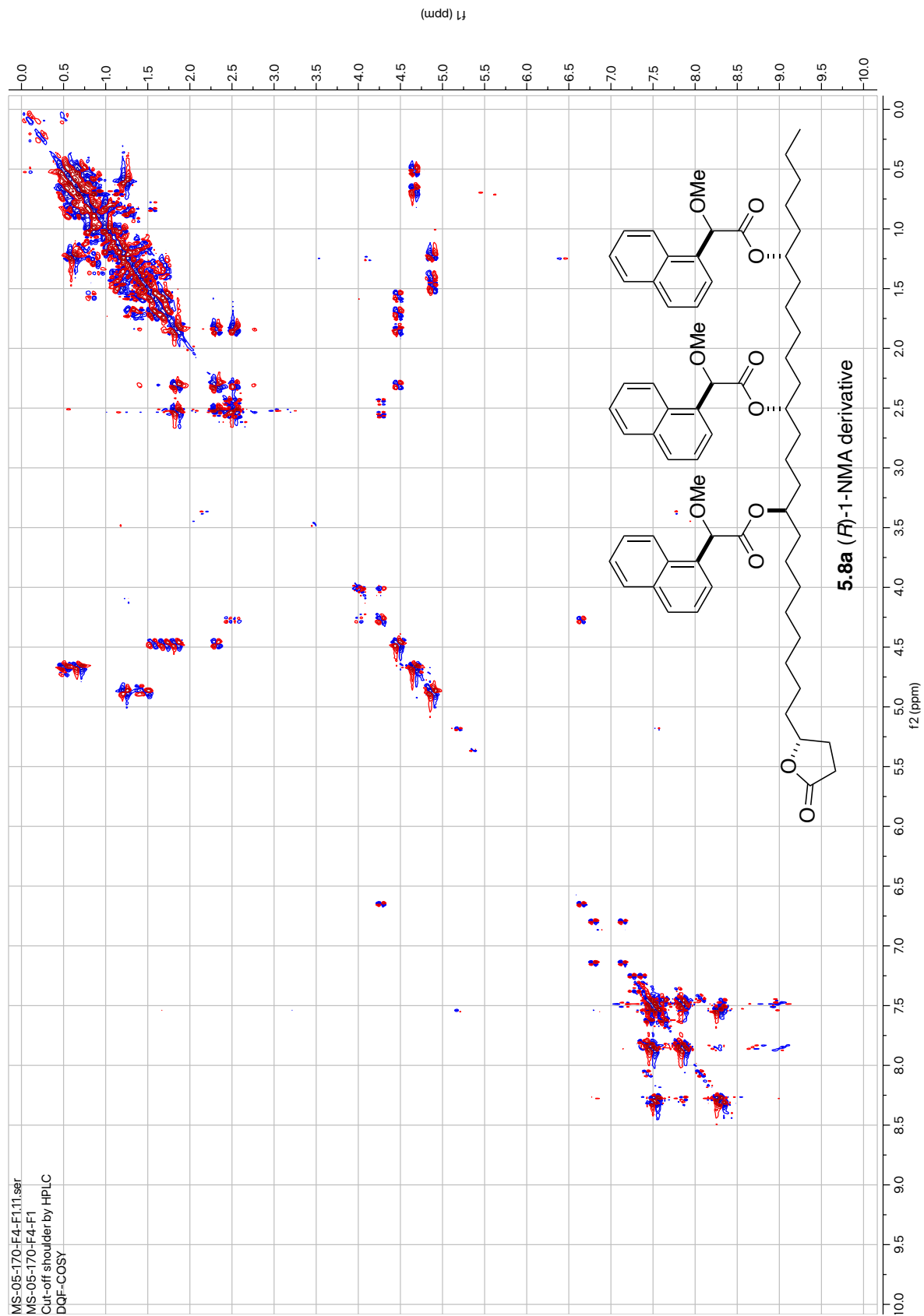


Figure 5.26: ¹H NMR of Compound **5.8a** (600 MHz, CDCl₃).



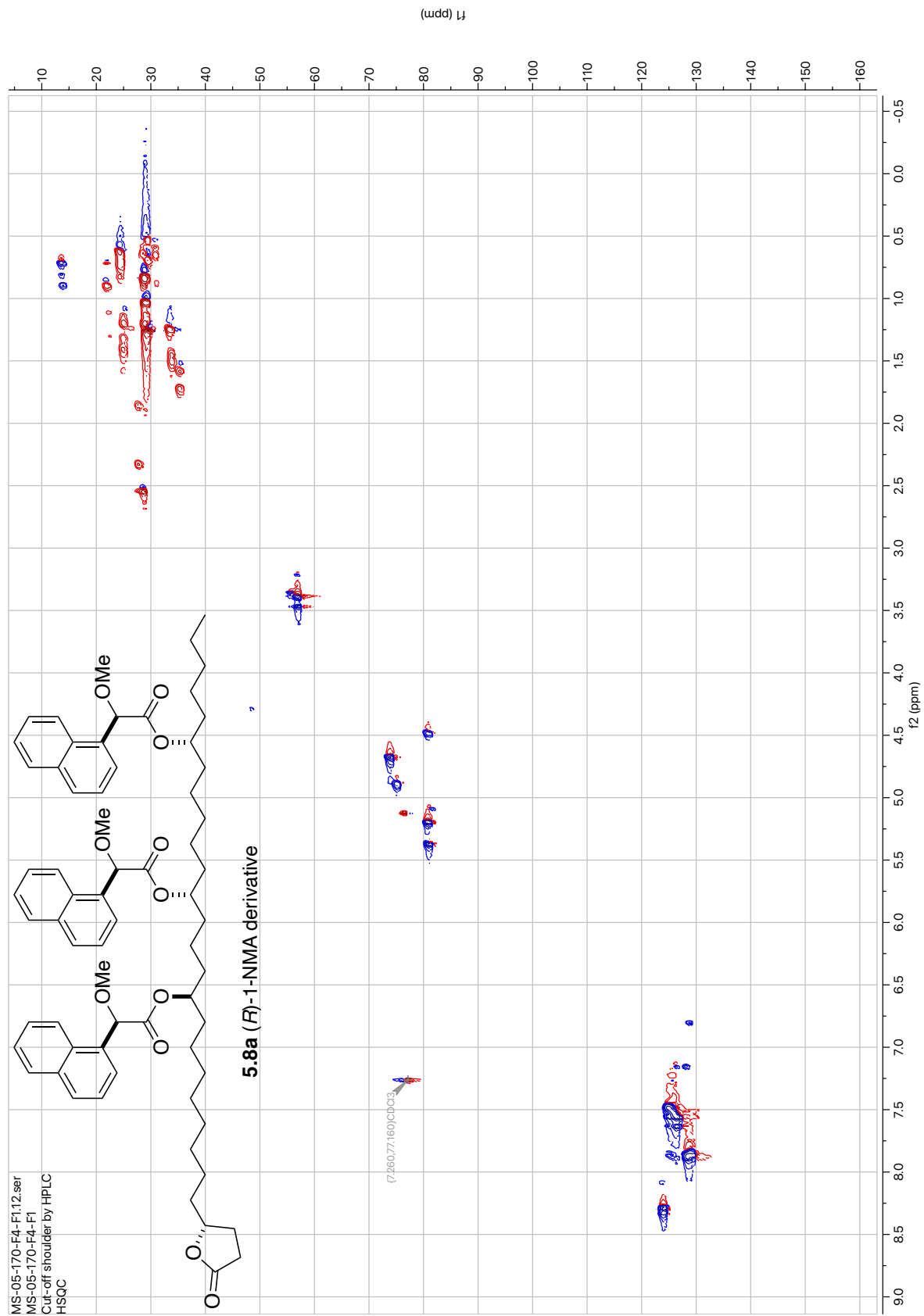


Figure 5.28: HSQC of Compound **5.8a** (600 MHz, CDCl₃).

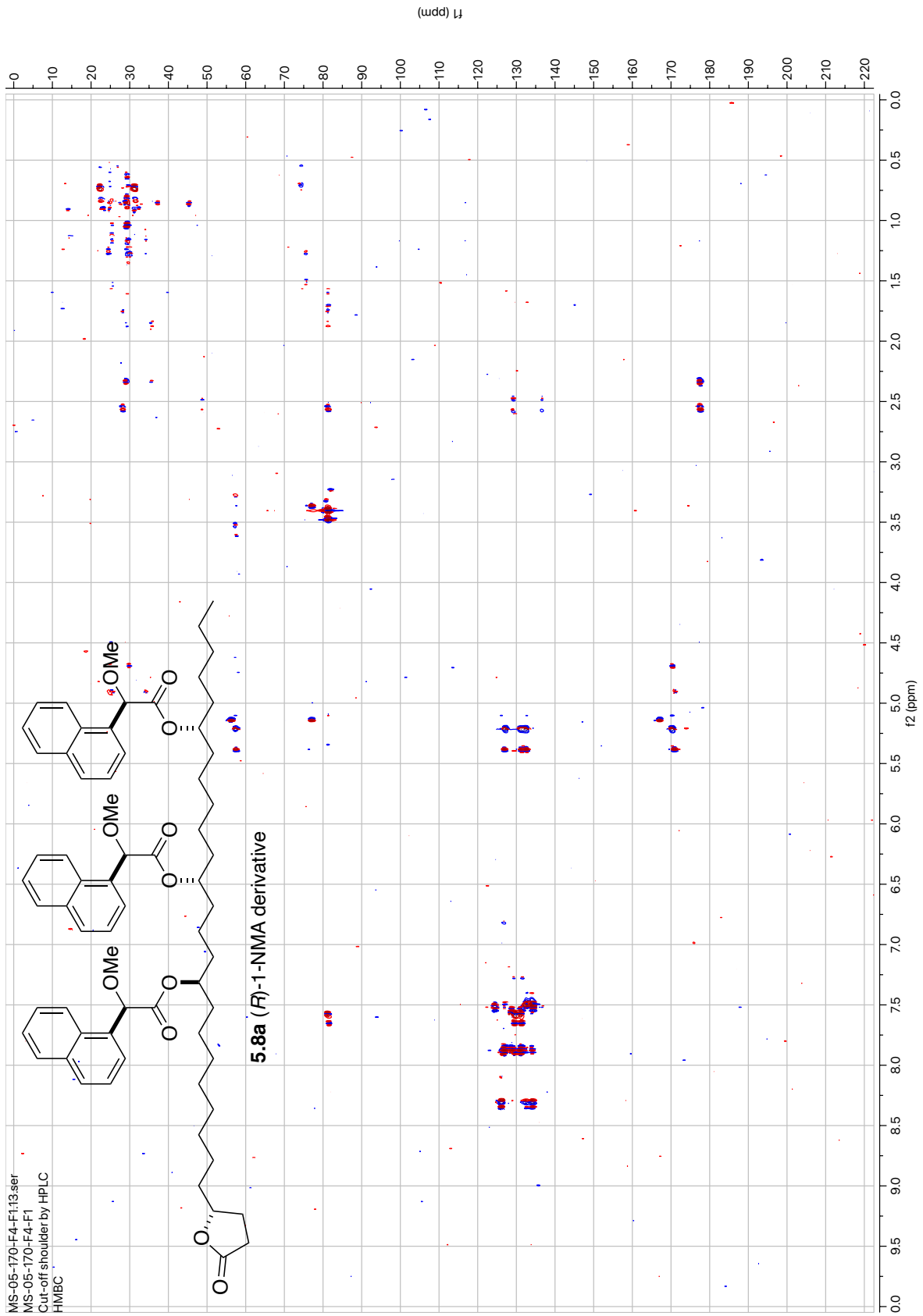


Figure 5.29: HMBC of Compound 5.8a (600 MHz, CDCl₃).

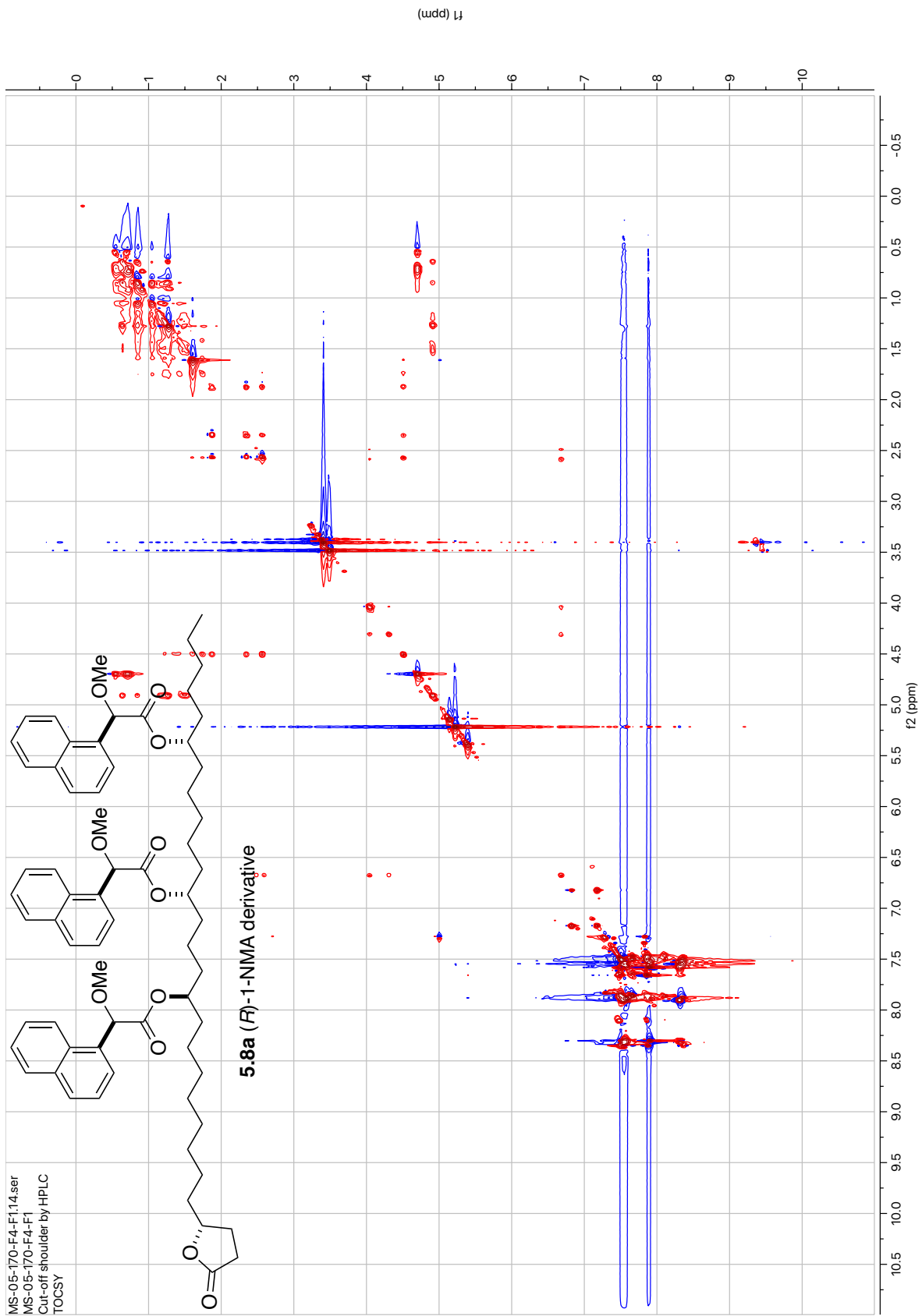


Figure 5.30: TOCSY of Compound **5.8a** (600 MHz, CDCl_3).

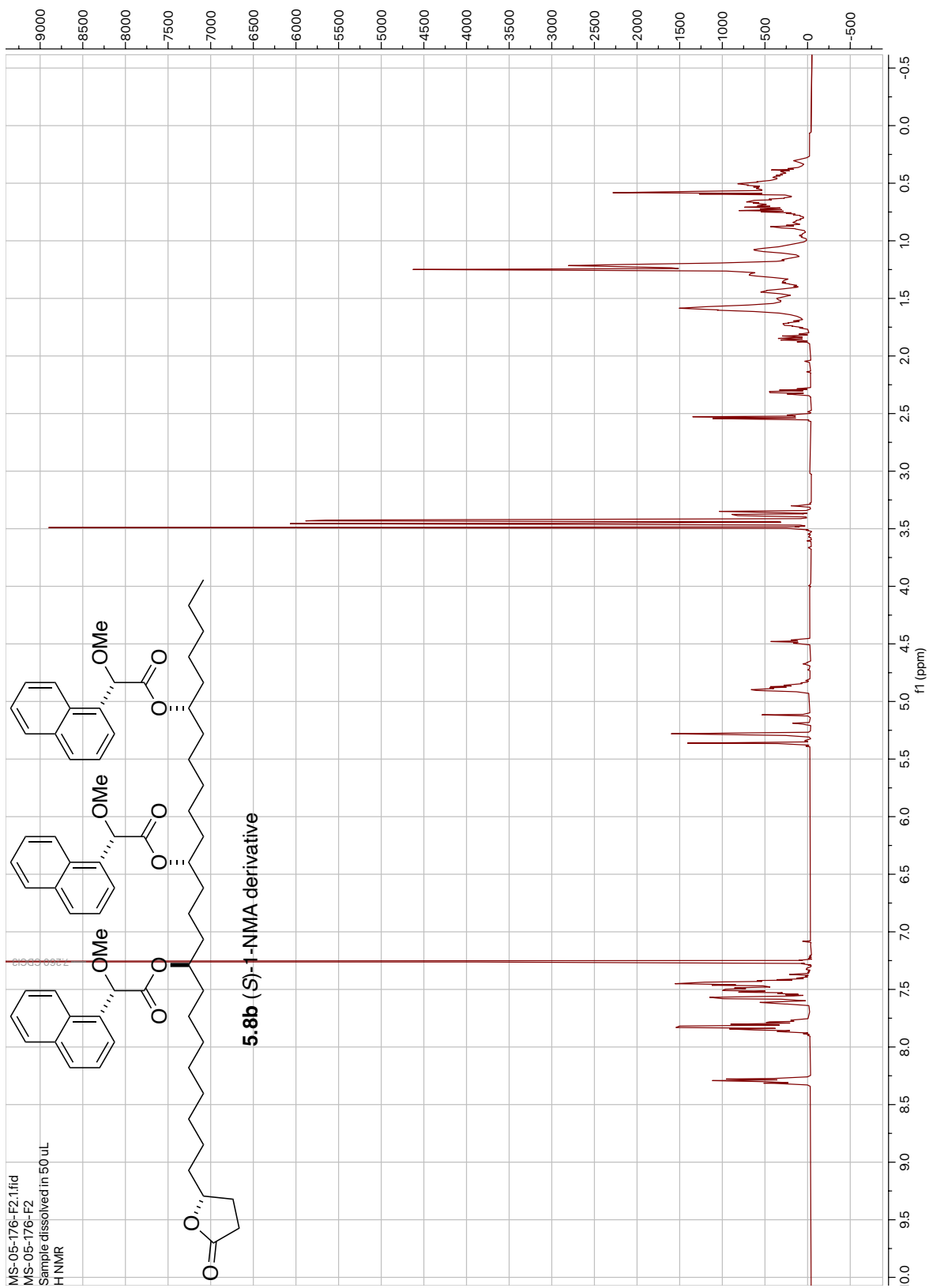


Figure 5.31: ¹H NMR of Compound **5.8b** (600 MHz, CDCl₃).

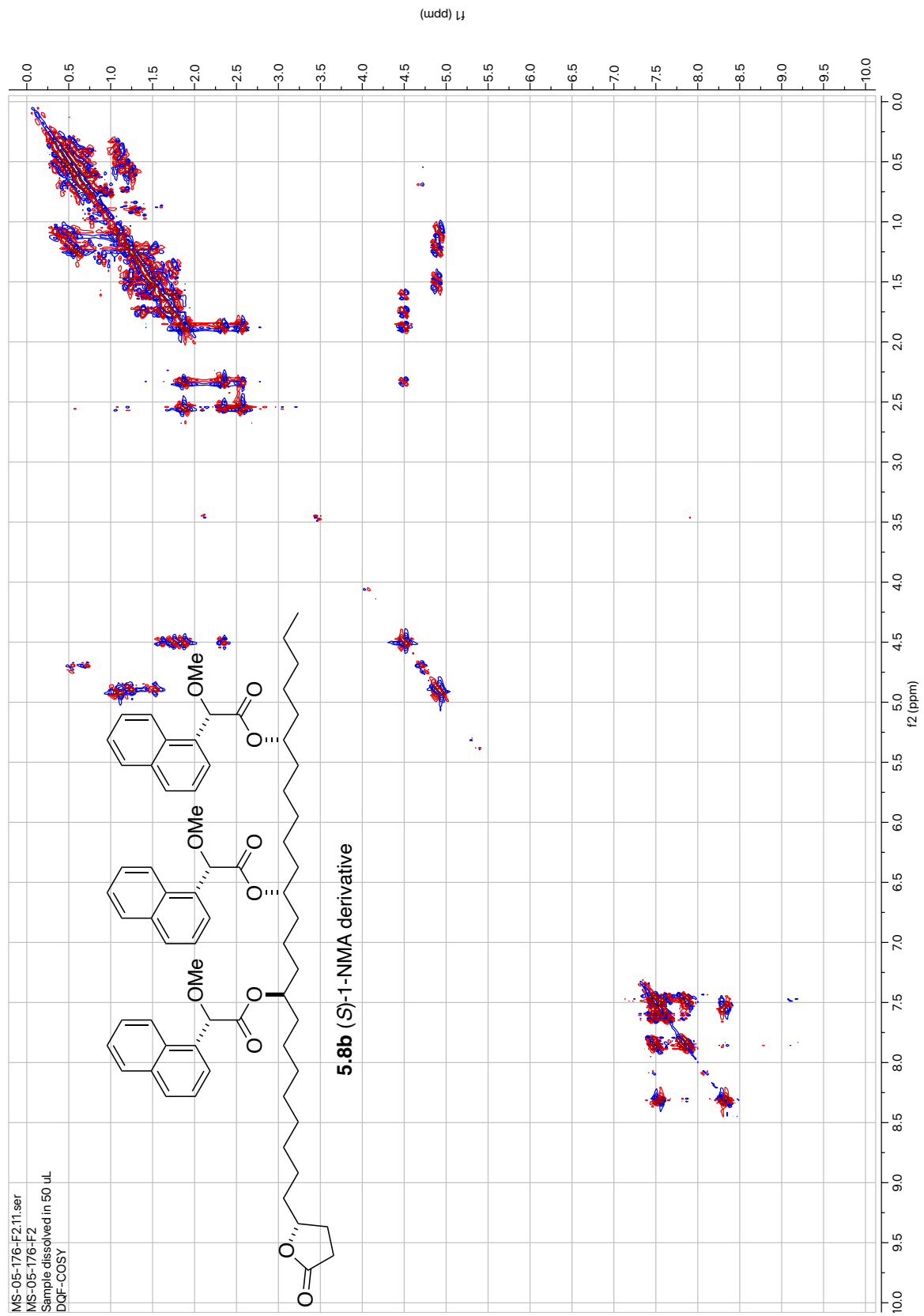
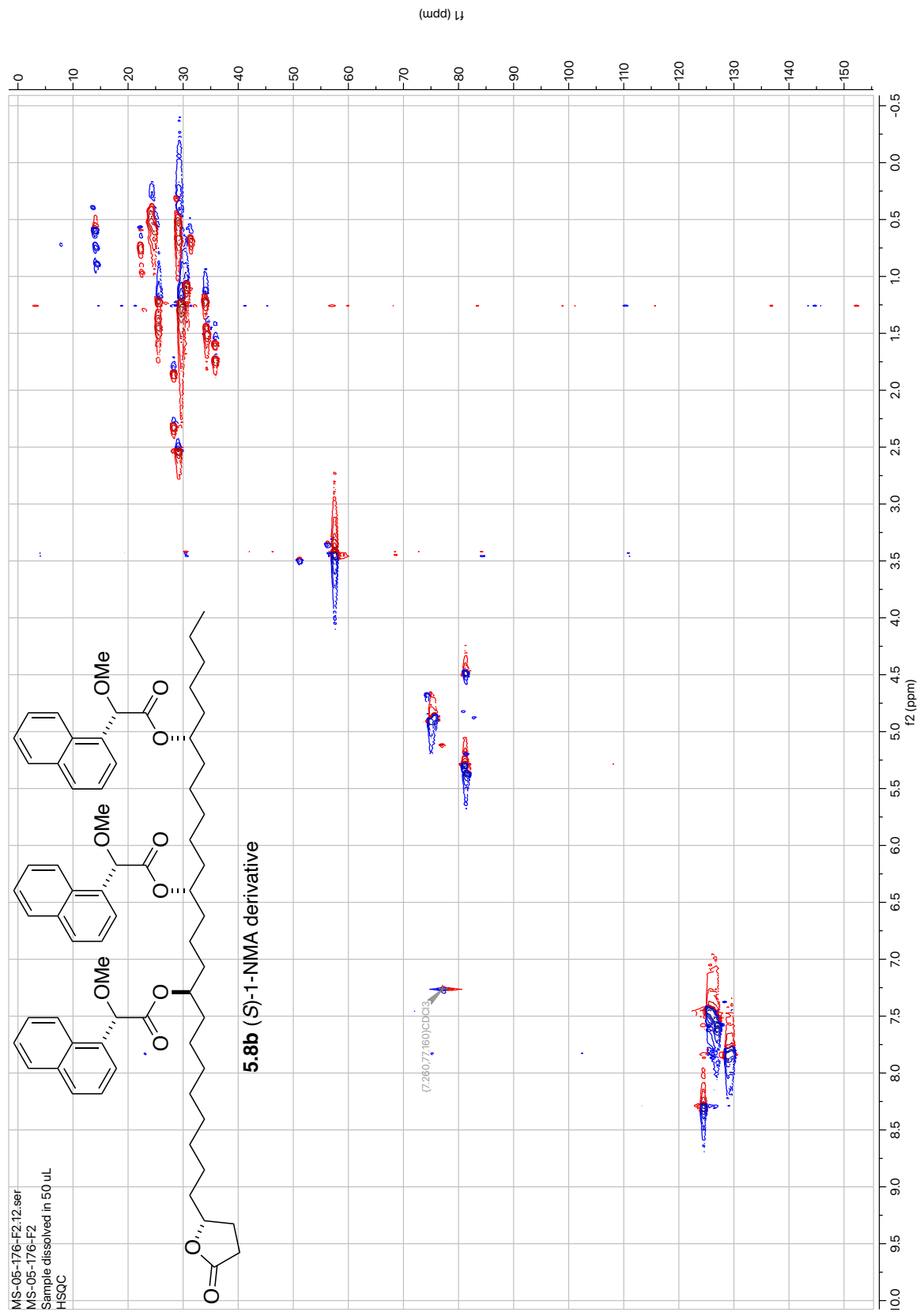


Figure 5.32: DQF-COSY of Compound **5.8b** (600 MHz, CDCl_3).



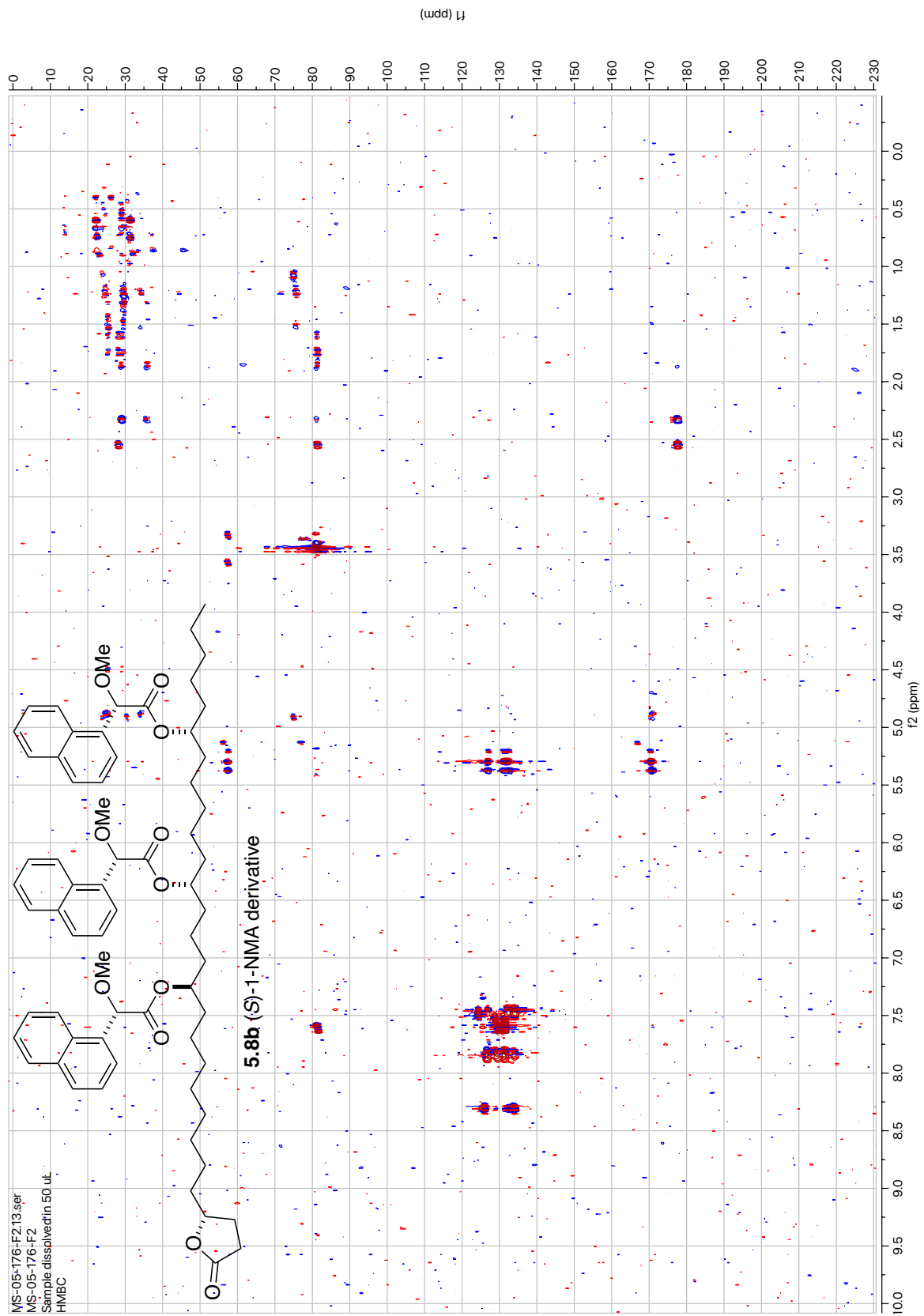


Figure 5.34: HMBC of Compound **5.8b** (600 MHz, CDCl_3).

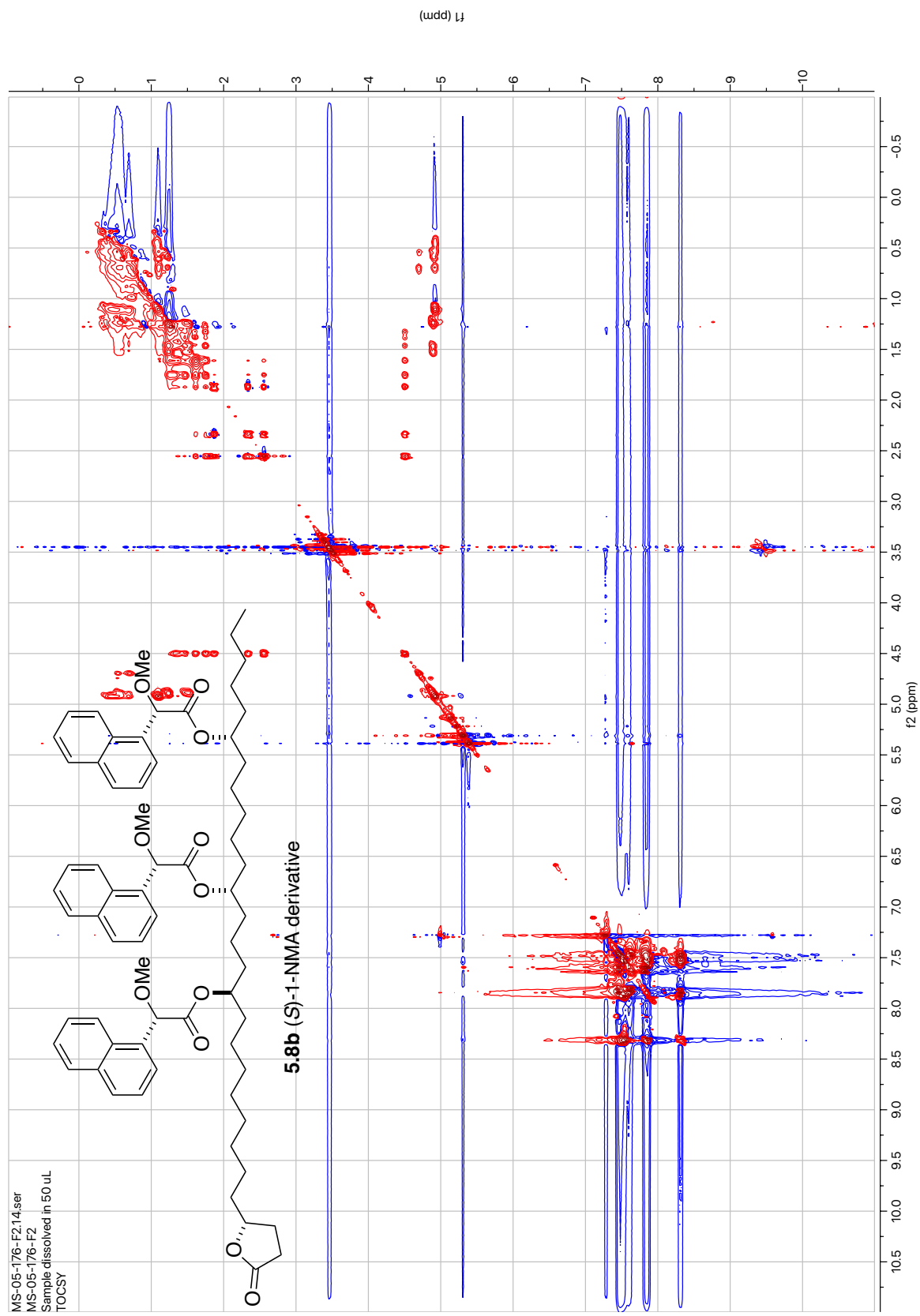


Figure 5.35: TOCSY of Compound **5.8b** (600 MHz, CDCl₃).

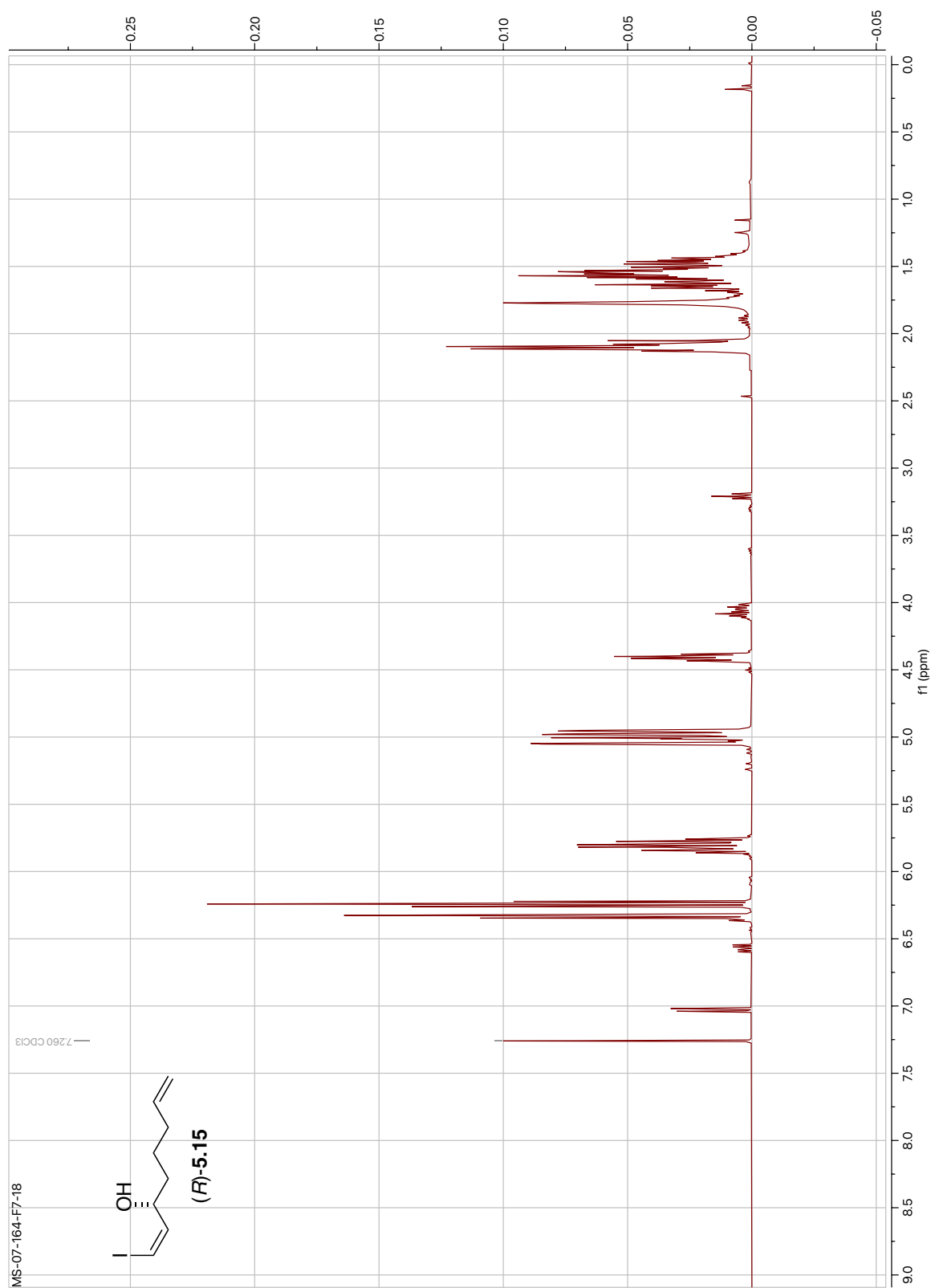


Figure 5.36: ¹H NMR of Compound **(R)-5.15** (400 MHz, CDCl₃).

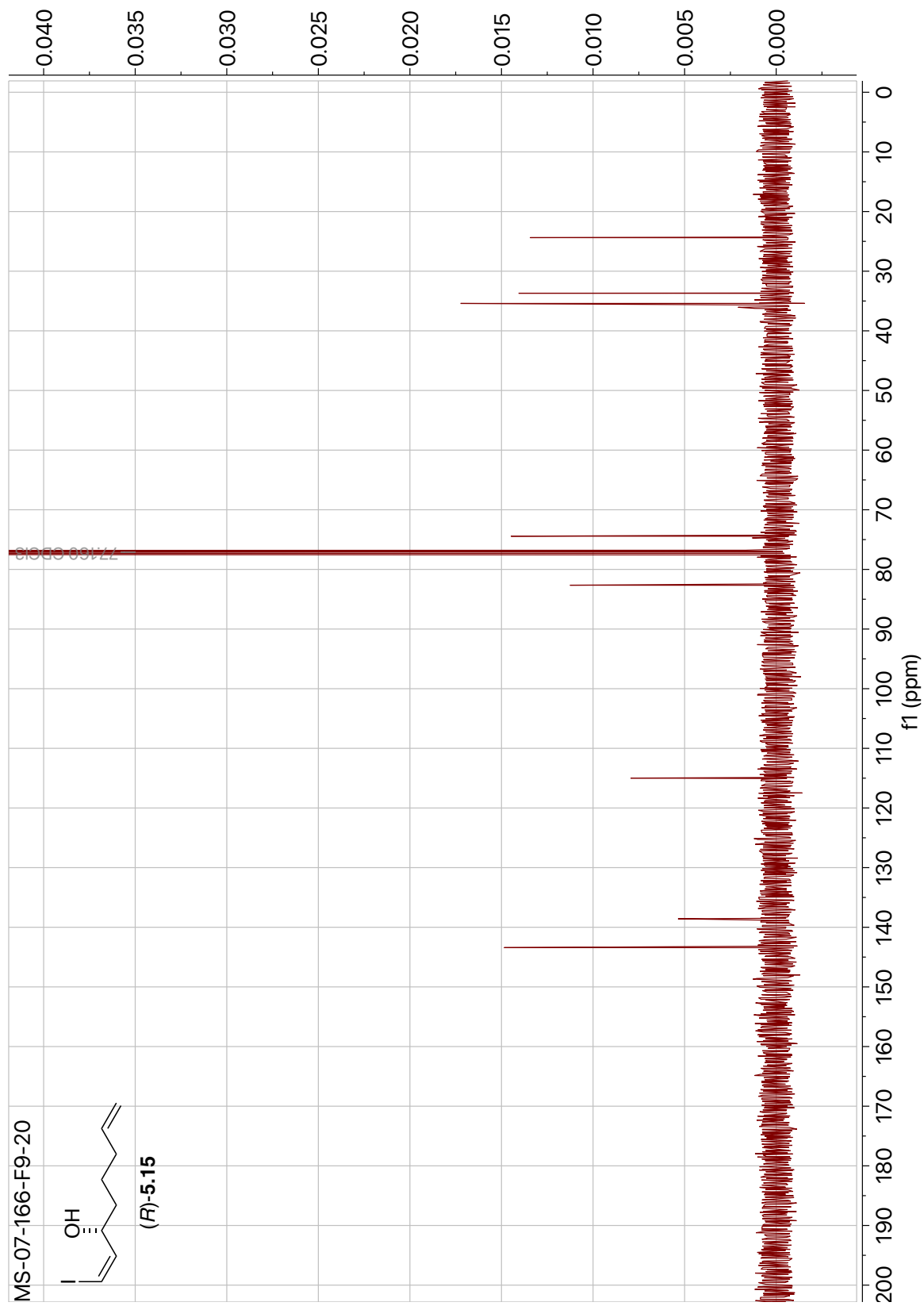


Figure 5.37: ¹³C NMR of Compound (*R*)-5.15 (100 MHz, CDCl₃).

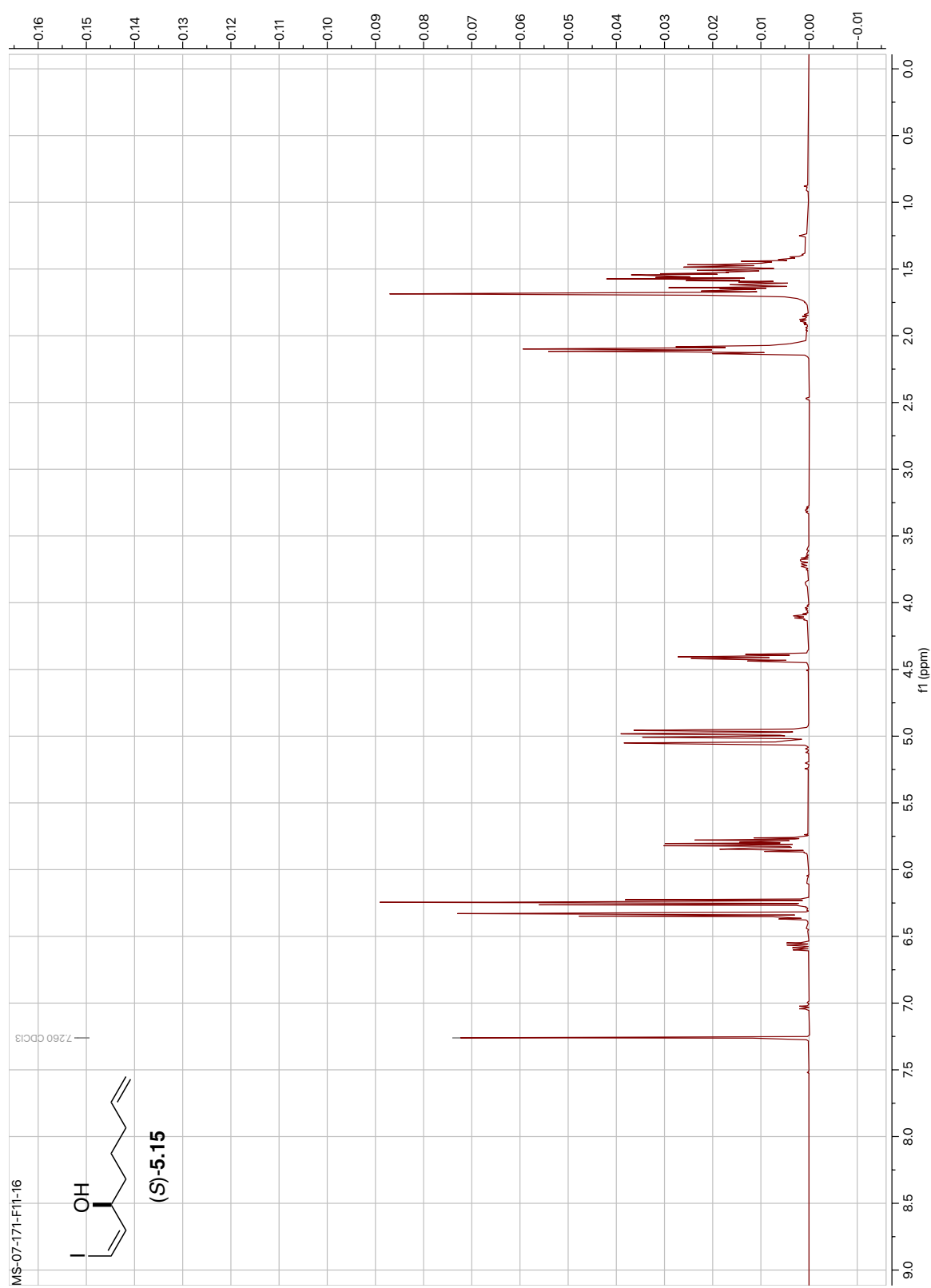


Figure 5.38: ¹H NMR of Compound (S)-5.15 (400 MHz, CDCl₃).

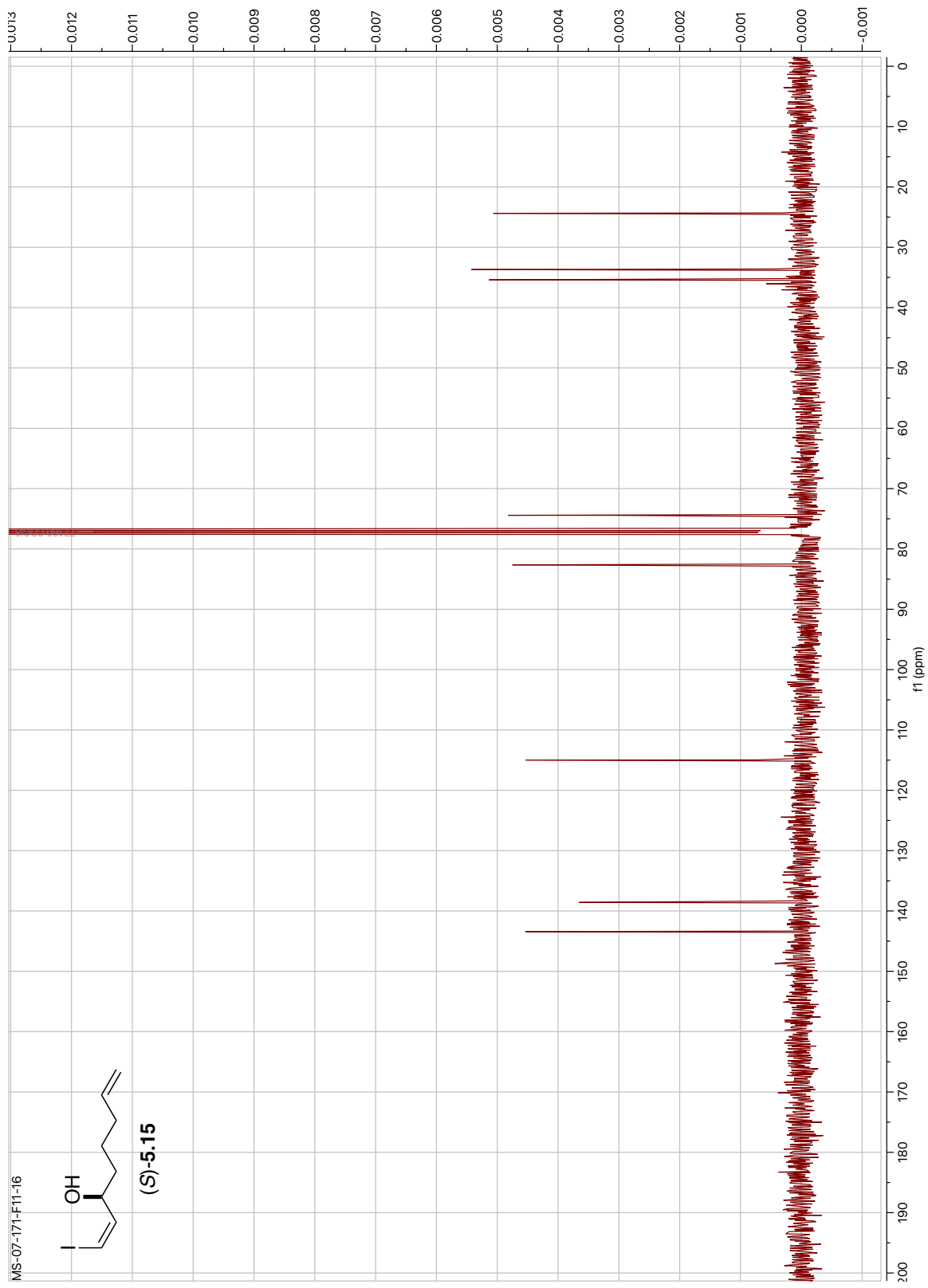


Figure 5.39: ^{13}C NMR of Compound (S)-5.15 (100 MHz, CDCl_3).

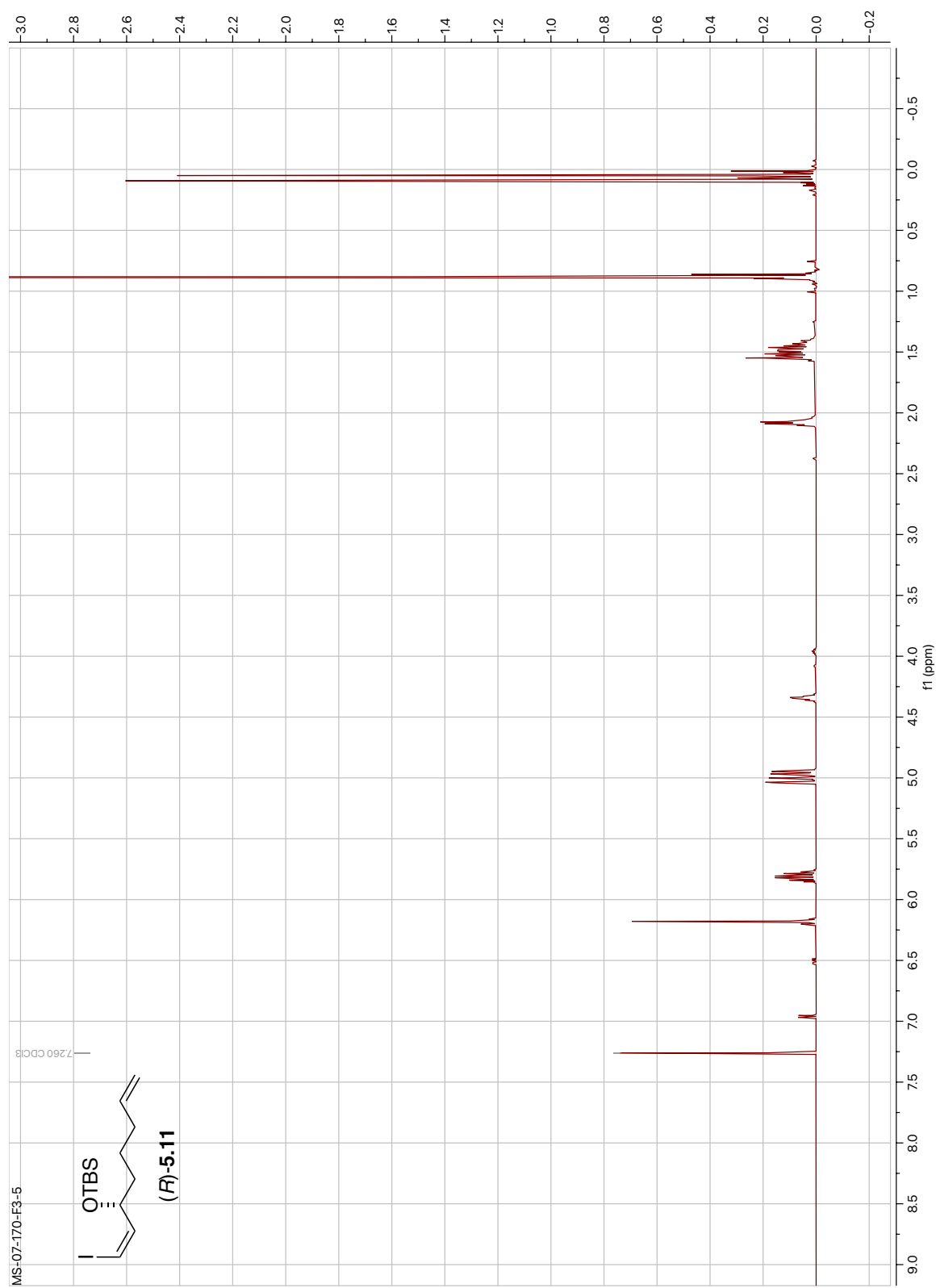


Figure 5.40: ¹H NMR of Compound (*R*)-5.11 (500 MHz, CDCl₃).

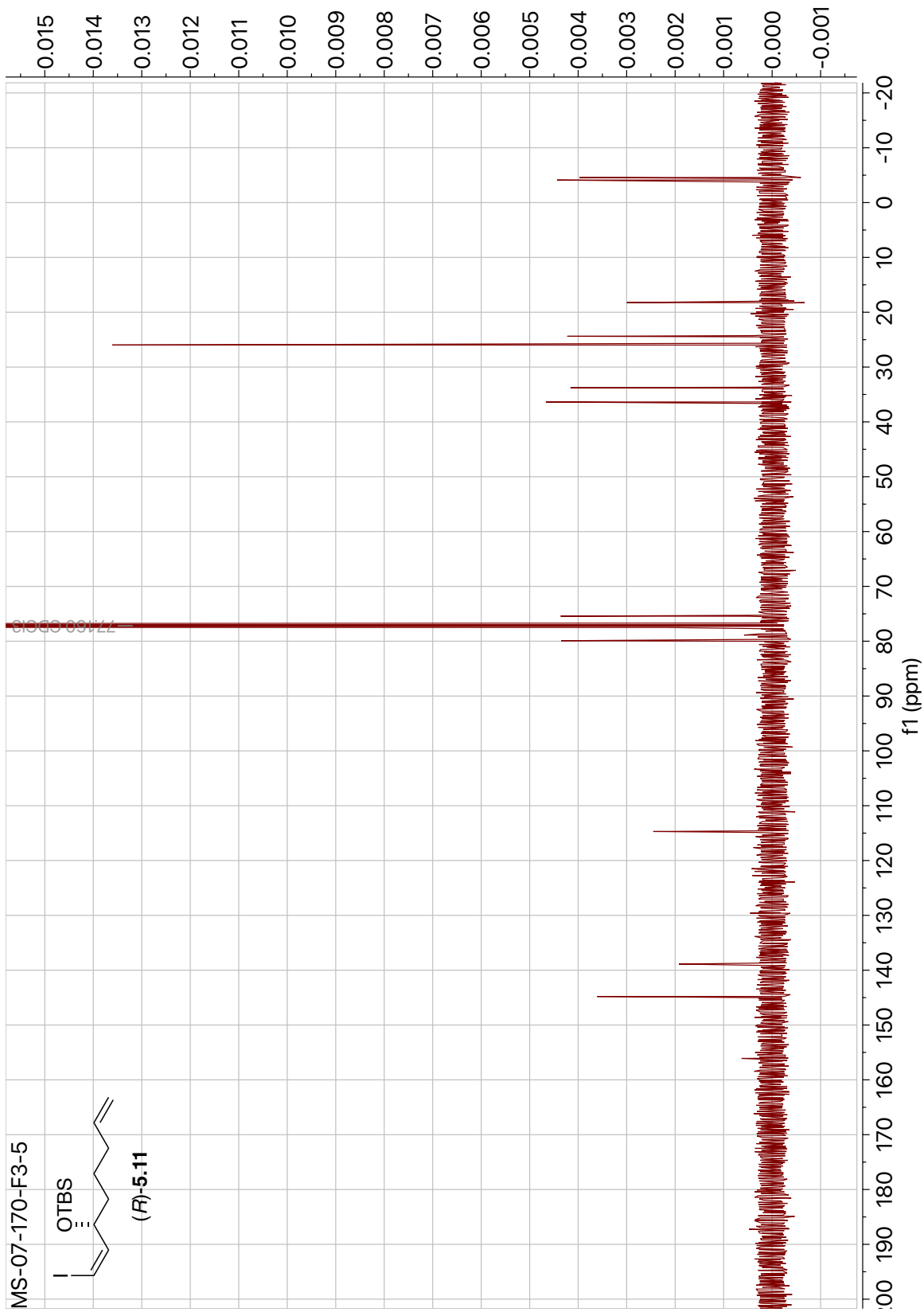


Figure 5.41: ¹³C NMR of Compound (R)-5.11 (100 MHz, CDCl₃).

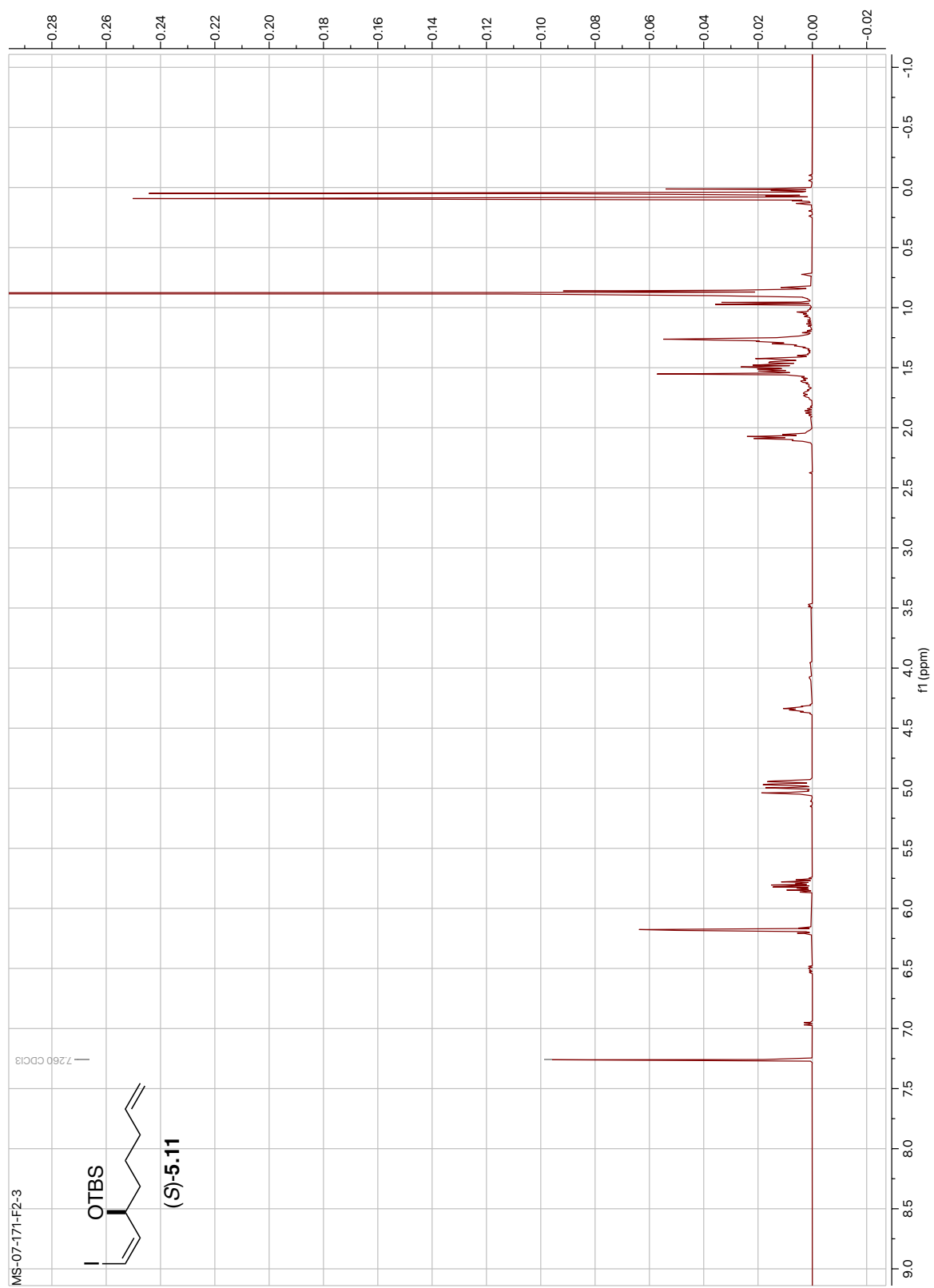


Figure 5.42: ¹H NMR of Compound (S)-5.11 (400 MHz, CDCl₃).

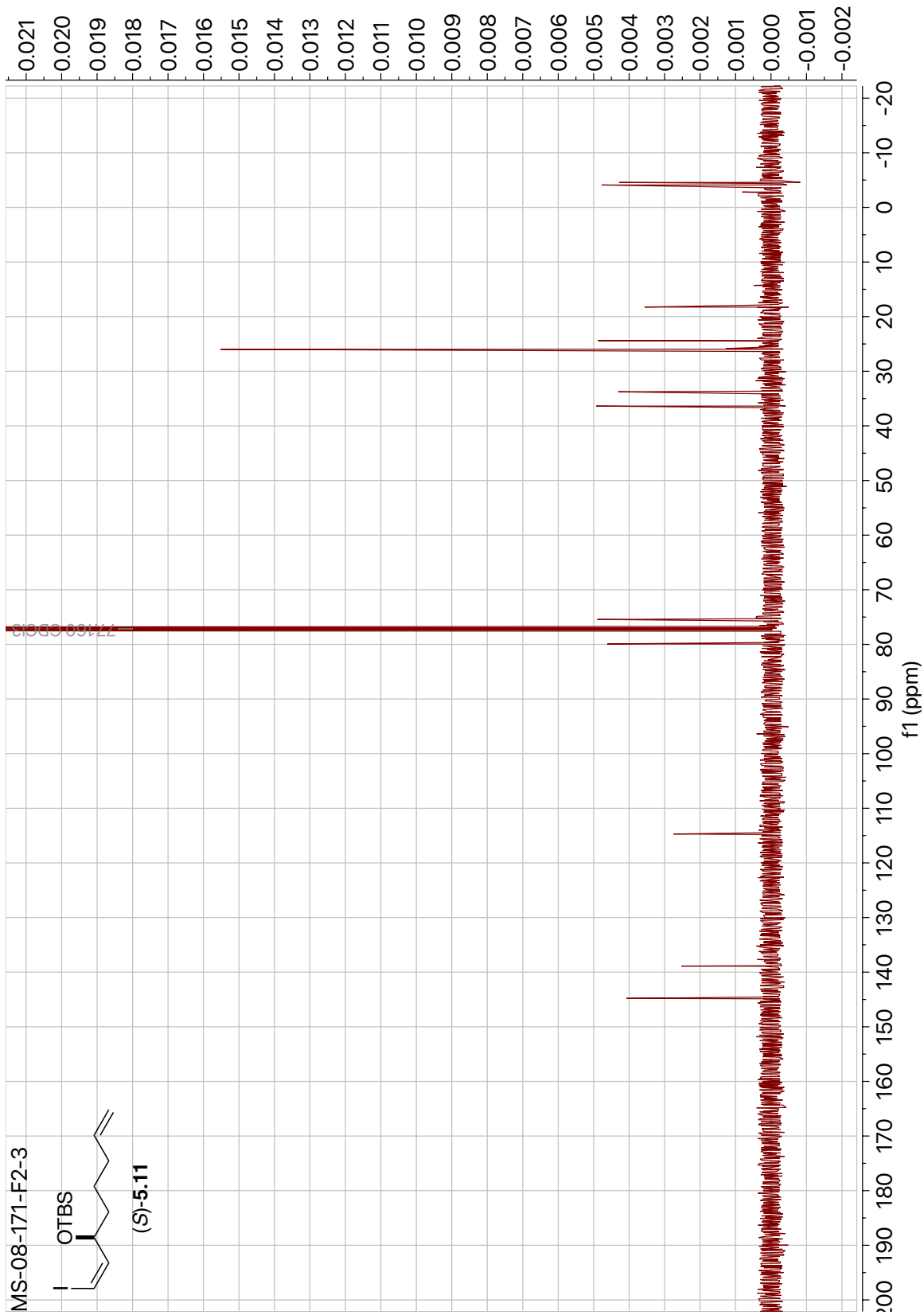
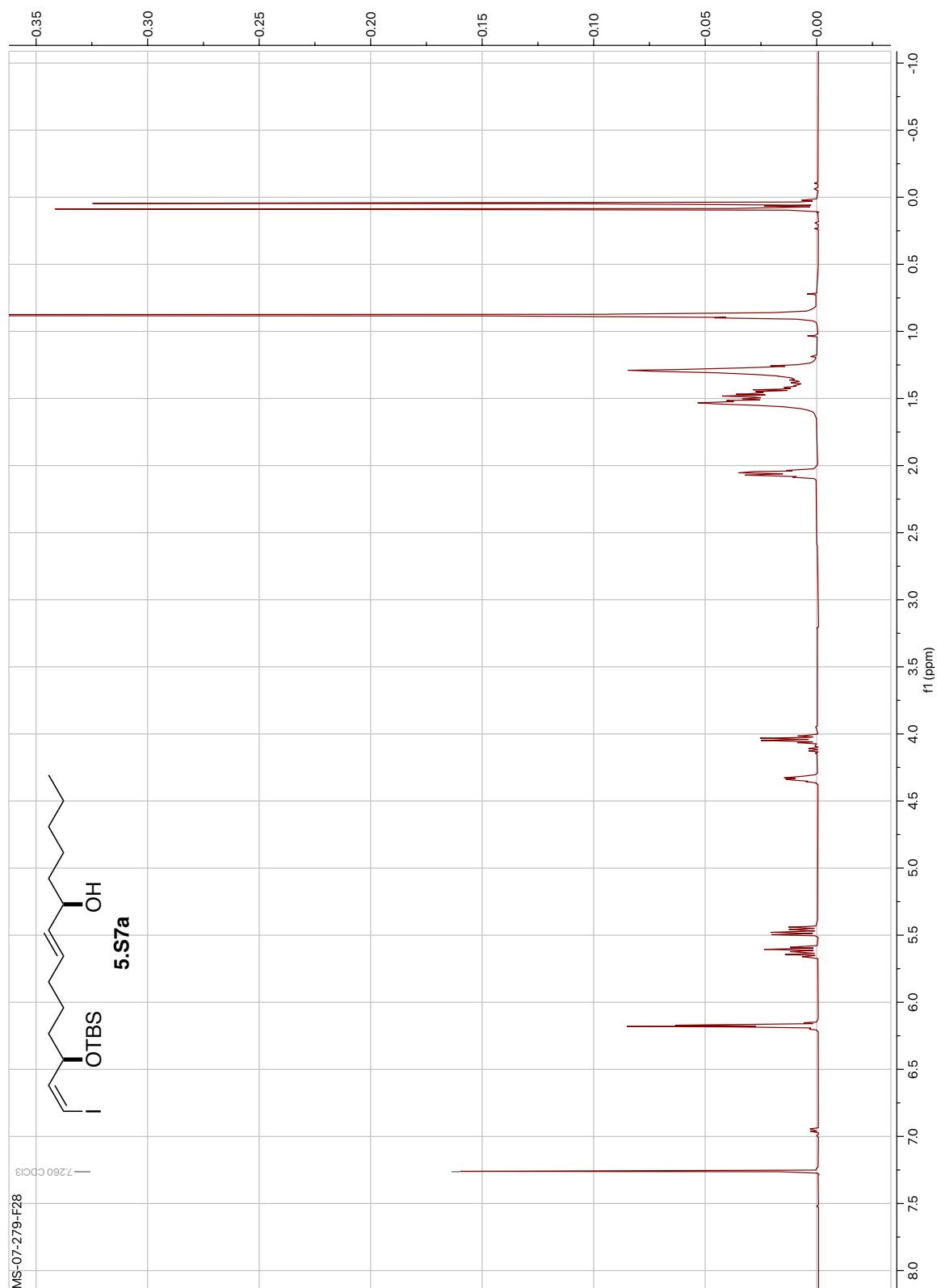


Figure 5.43: ¹³C NMR of Compound (S)-5.11 (100 MHz, CDCl₃).



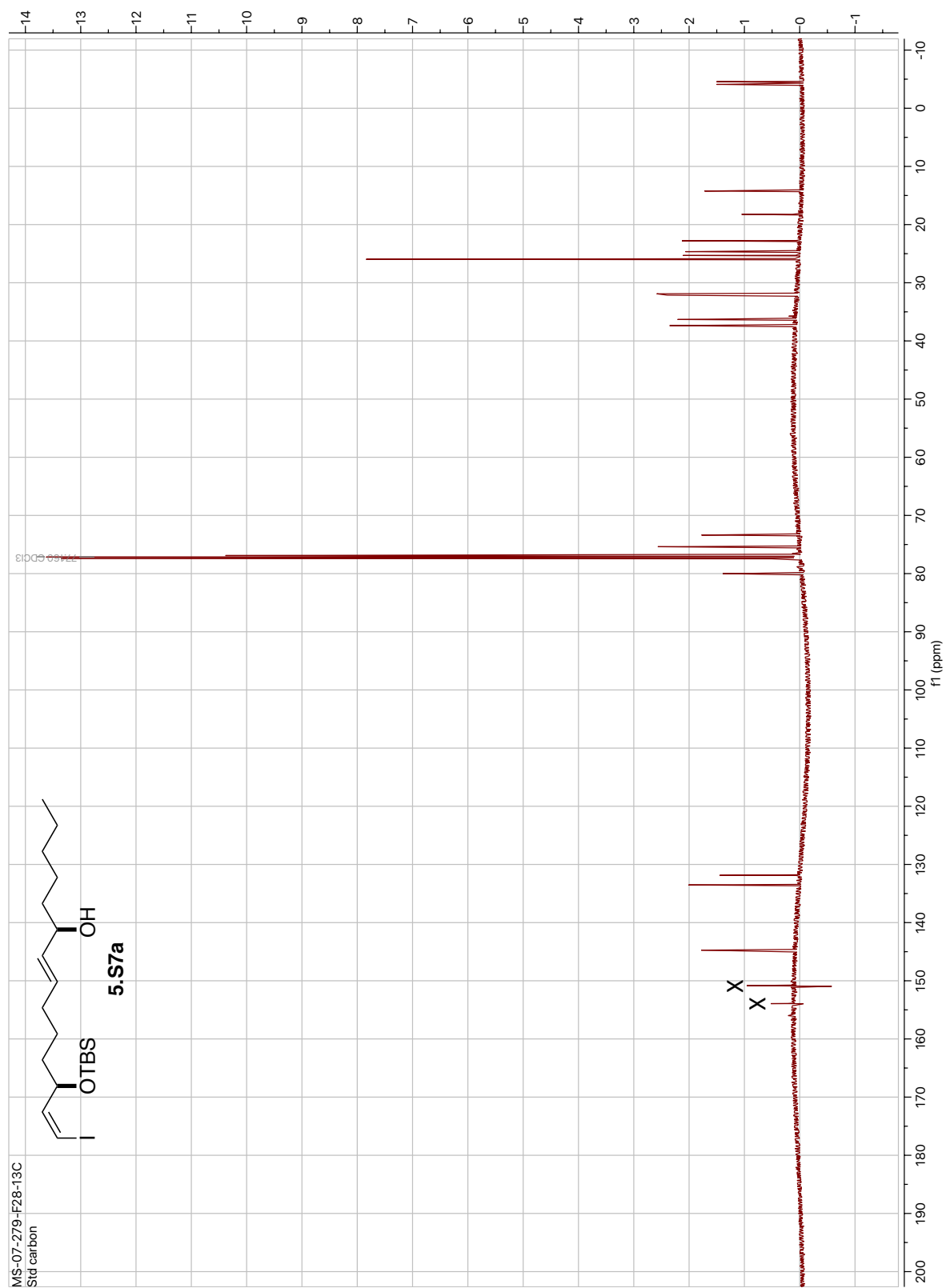


Figure 5.45: ^{13}C NMR of Compound **5.S7a** (125 MHz, CDCl_3).

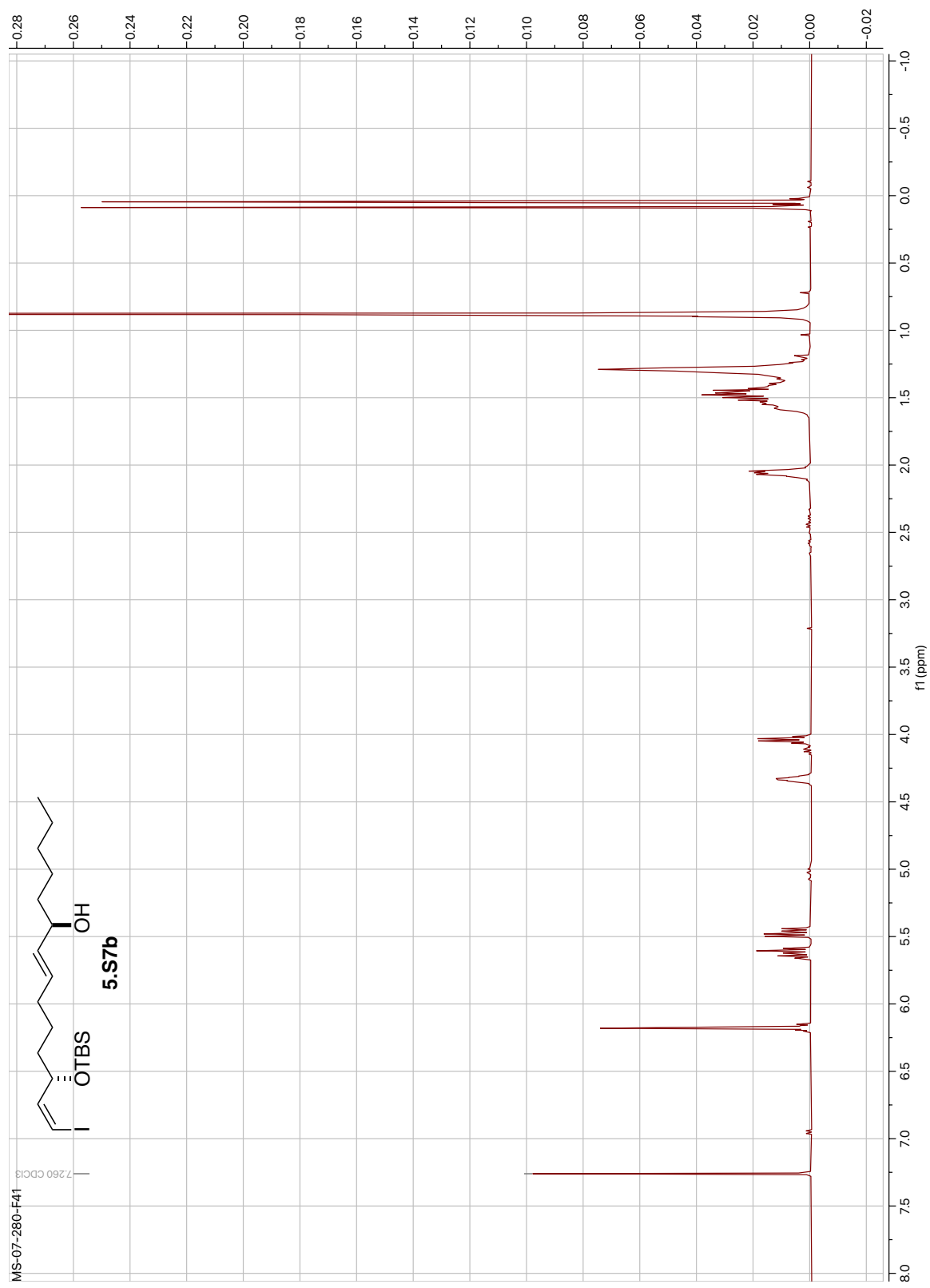


Figure 5.46: ¹H NMR of Compound **5.S7b** (400 MHz, CDCl₃).

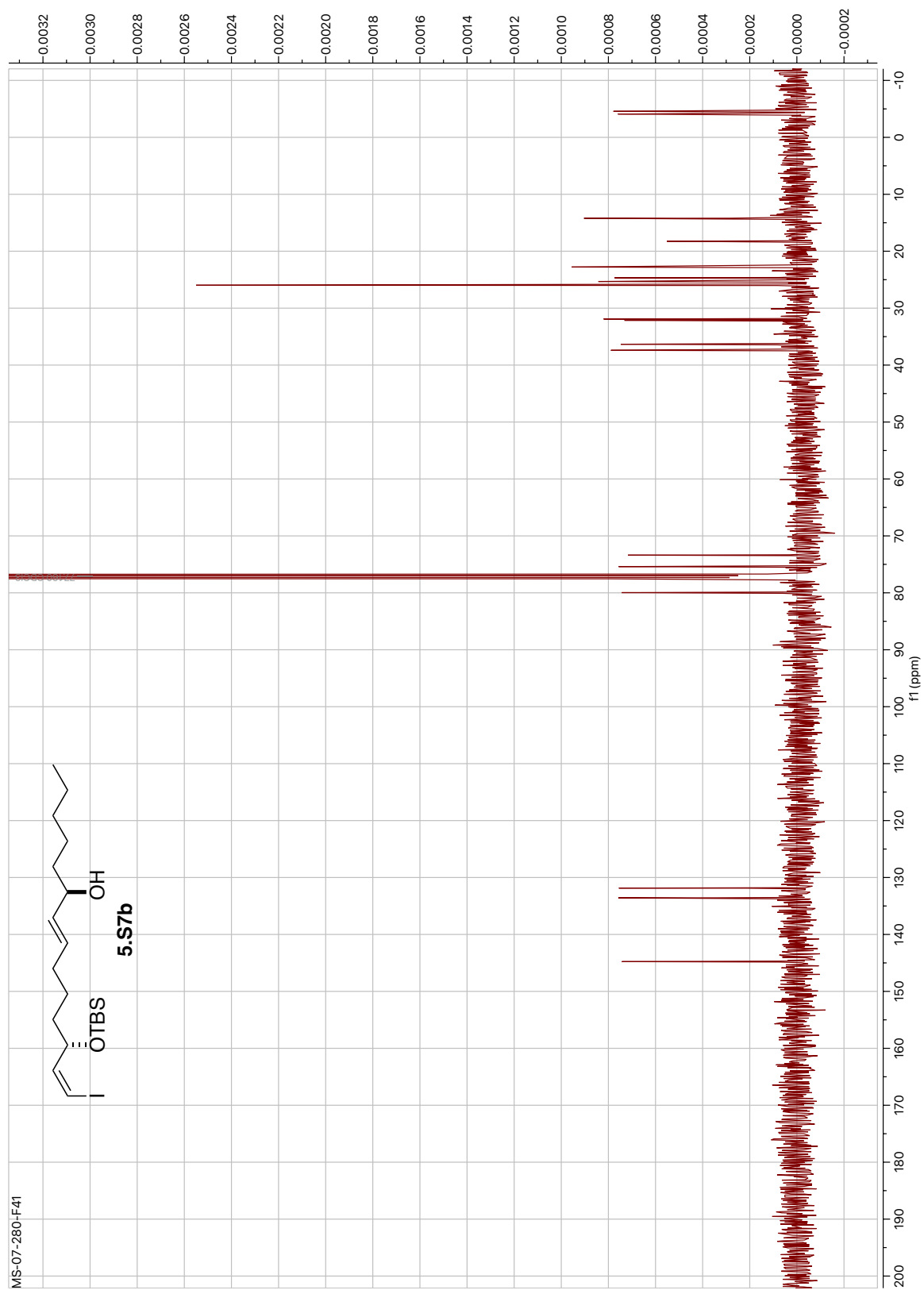


Figure 5.47: ^{13}C NMR of Compound **5.S7b** (100 MHz, CDCl_3).

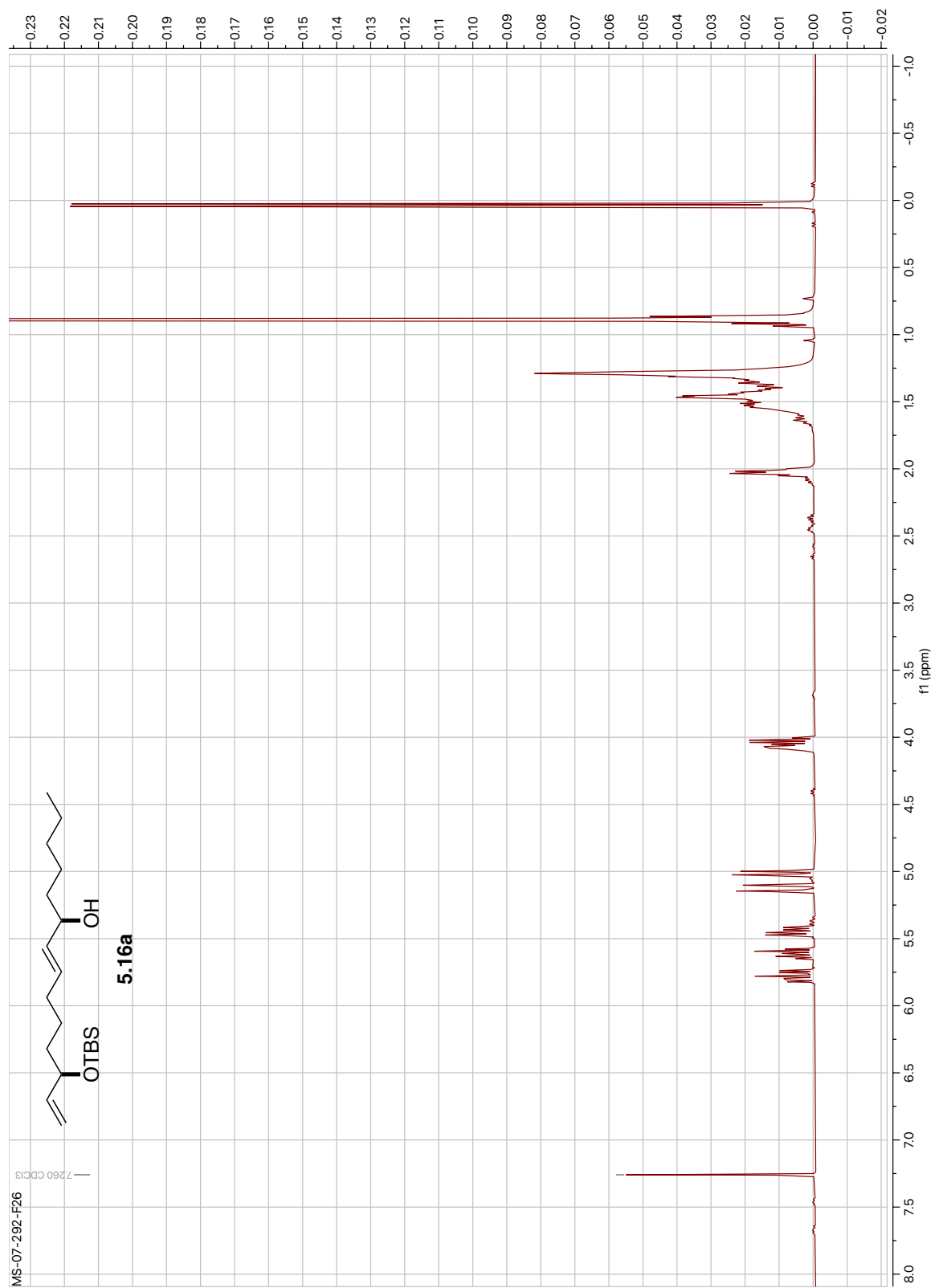


Figure 5.48: ¹H NMR of Compound **5.16a** (400 MHz, CDCl₃).

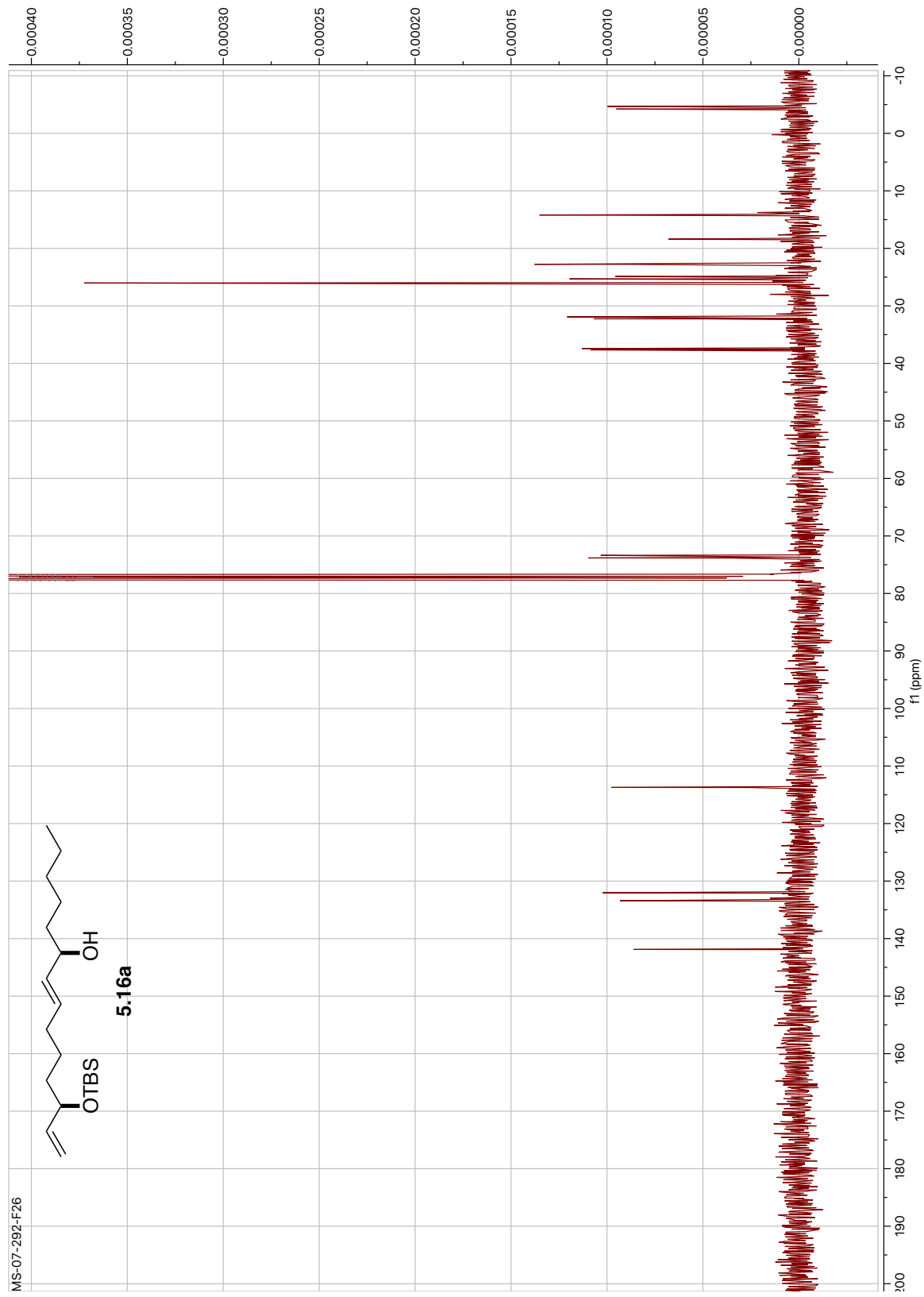


Figure 5.49: ¹³C NMR of Compound **5.16a** (100 MHz, CDCl₃).

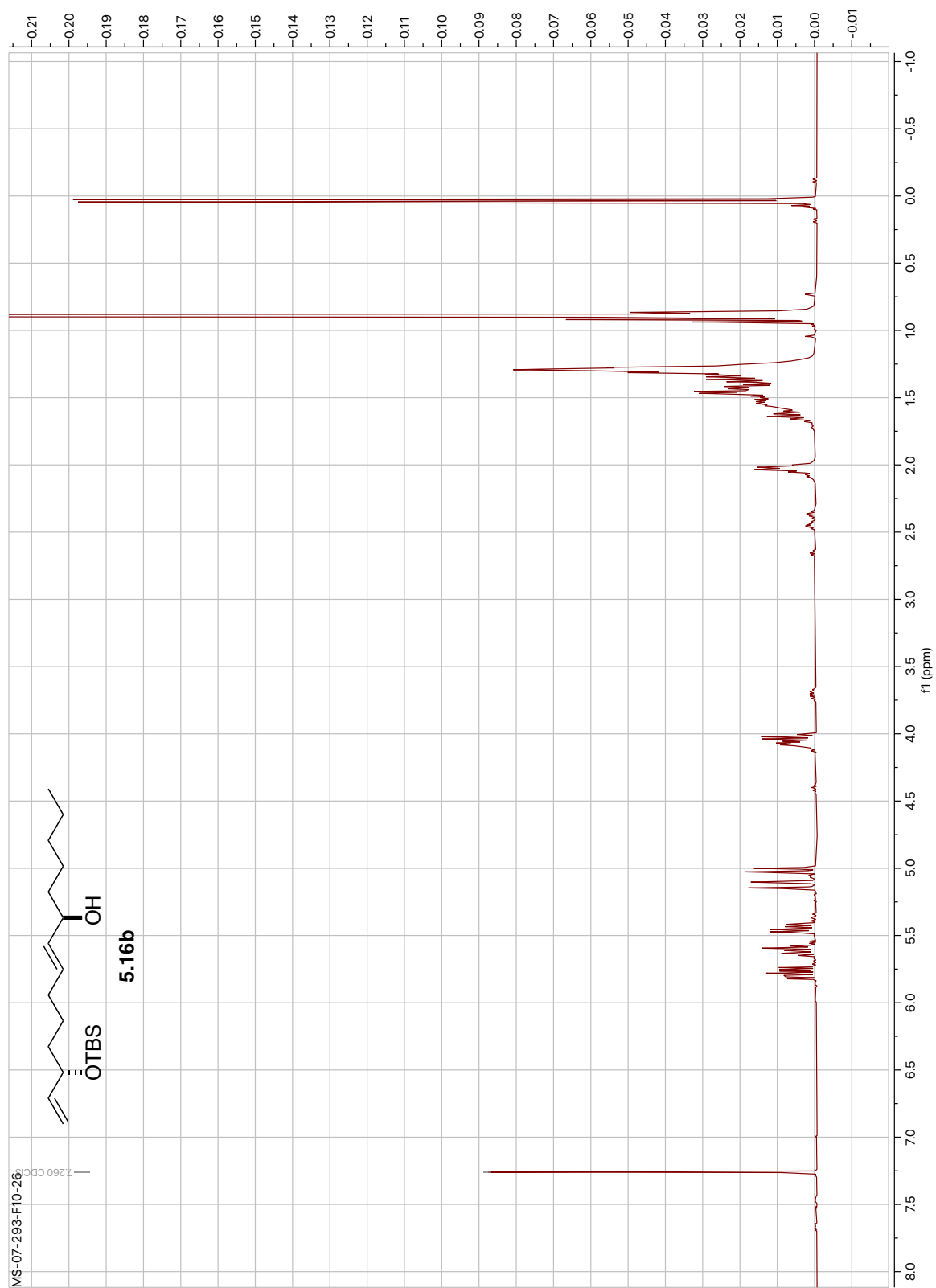


Figure 5.50: ¹H NMR of Compound **5.16b** (400 MHz, CDCl₃).

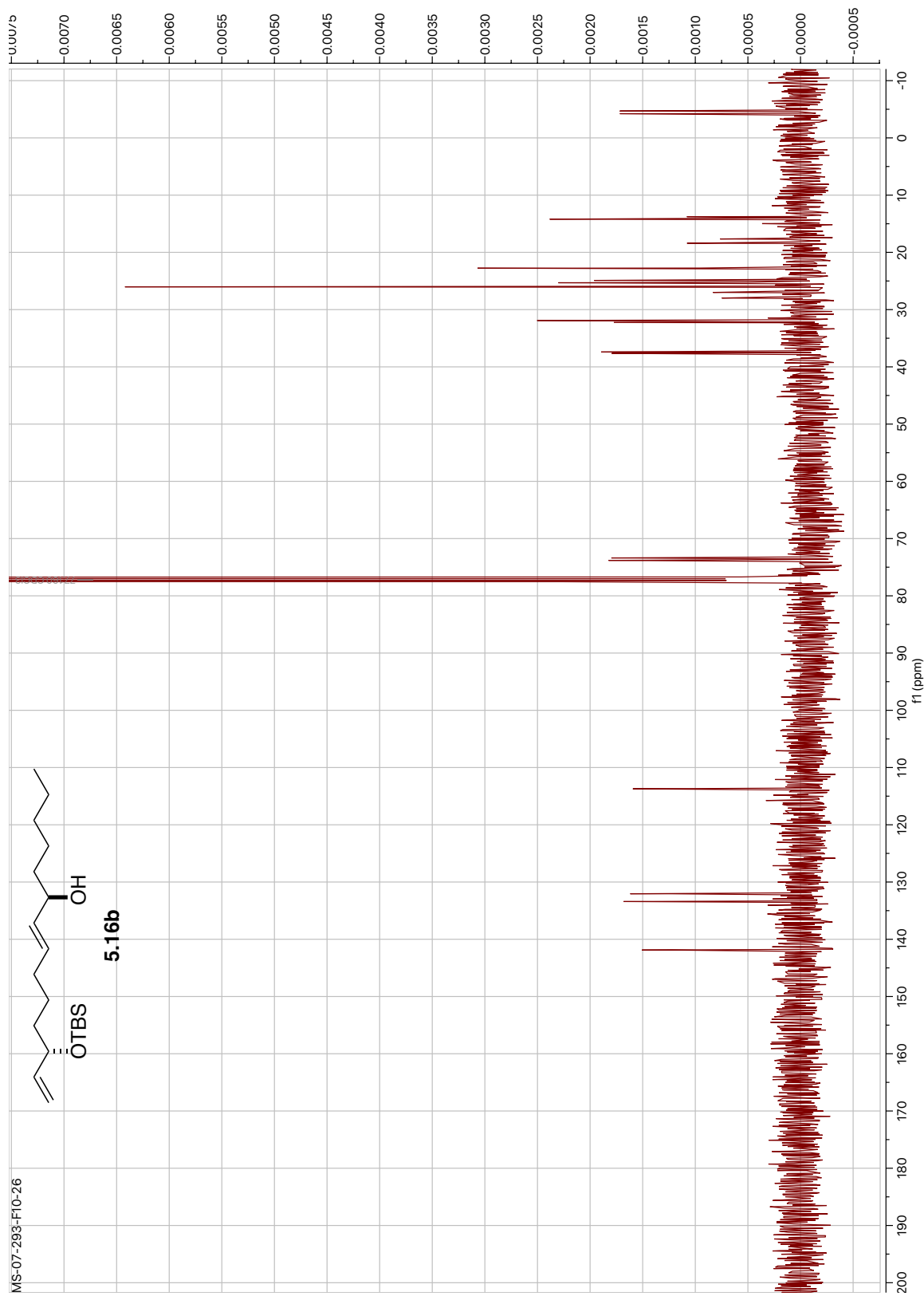


Figure 5.51: ^{13}C NMR of Compound **5.16b** (100 MHz, CDCl_3).

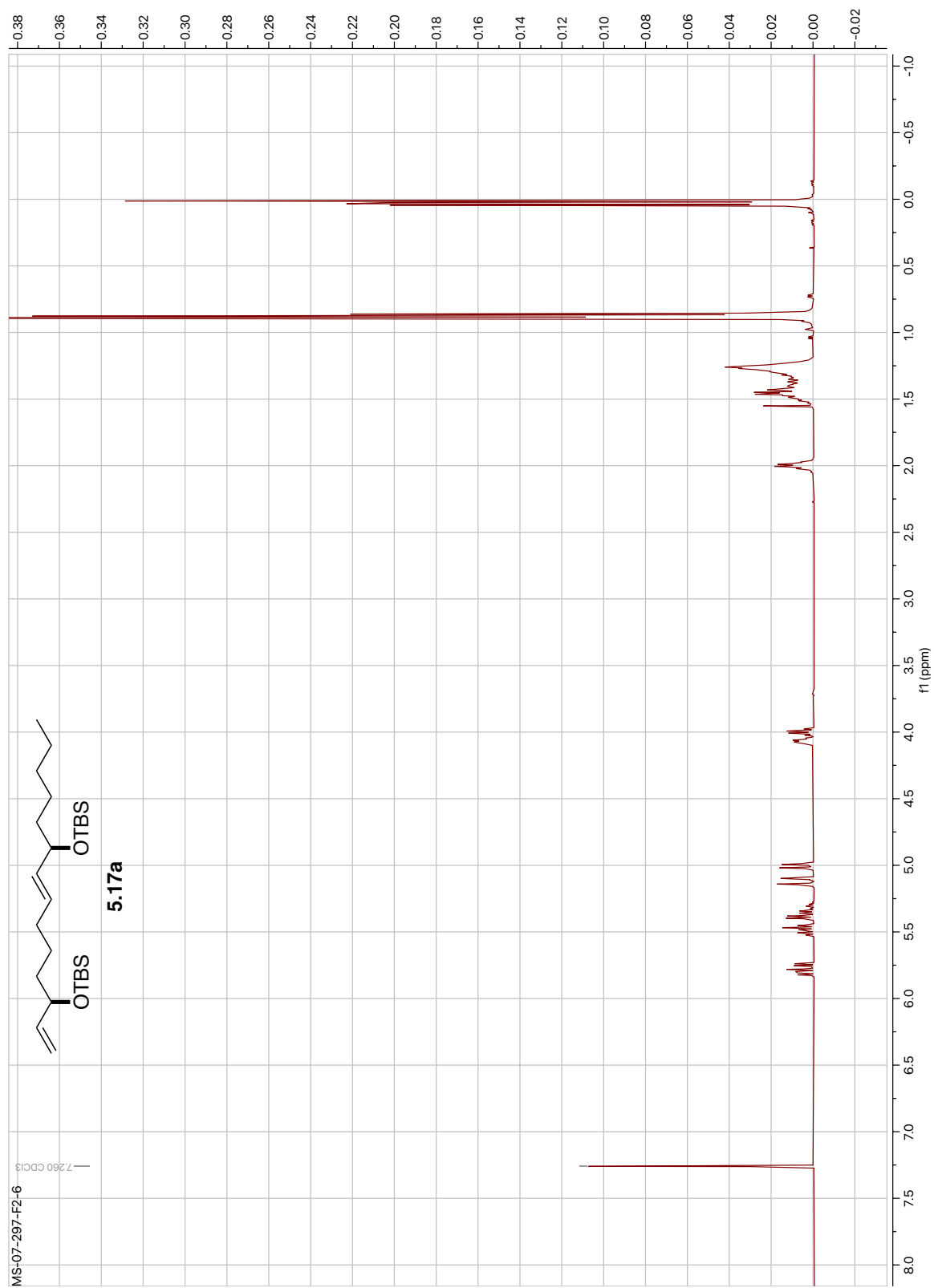


Figure 5.52: ¹H NMR of Compound **5.17a** (400 MHz, CDCl₃).

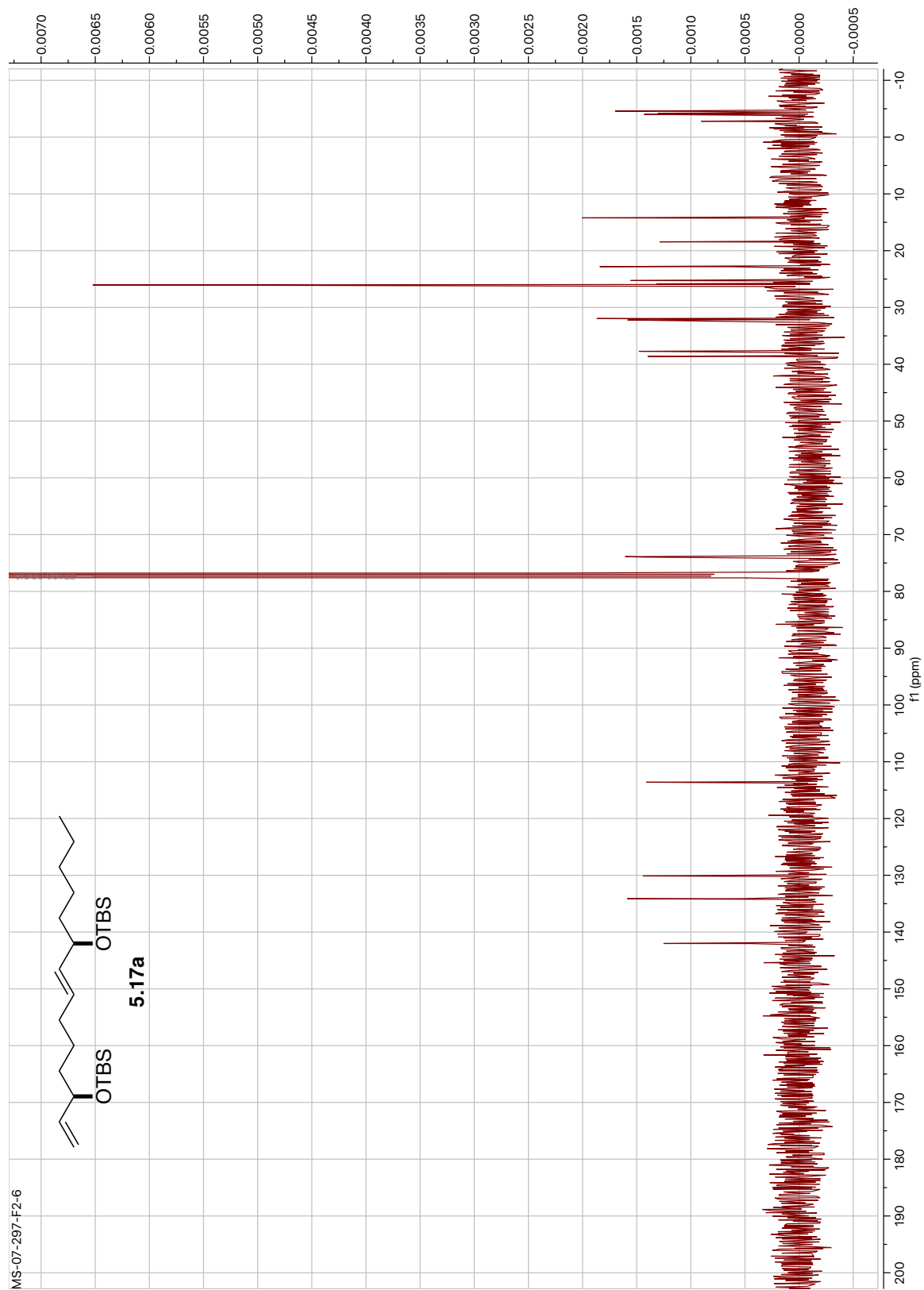


Figure 5.53: ¹³C NMR of Compound 5.17a (100 MHz, CDCl₃).

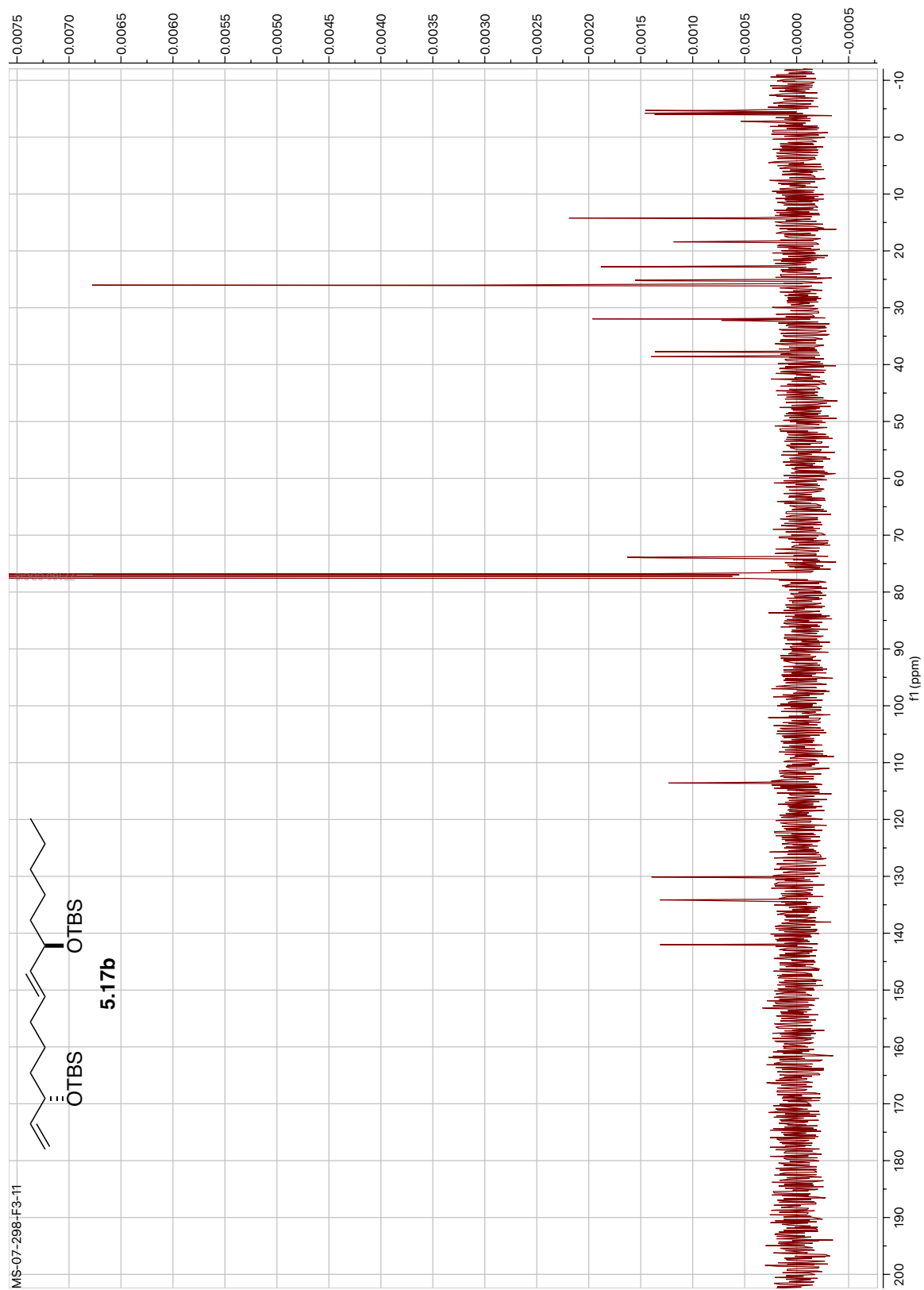


Figure 5.55: ^{13}C NMR of Compound **5.17b** (100 MHz, CDCl_3).

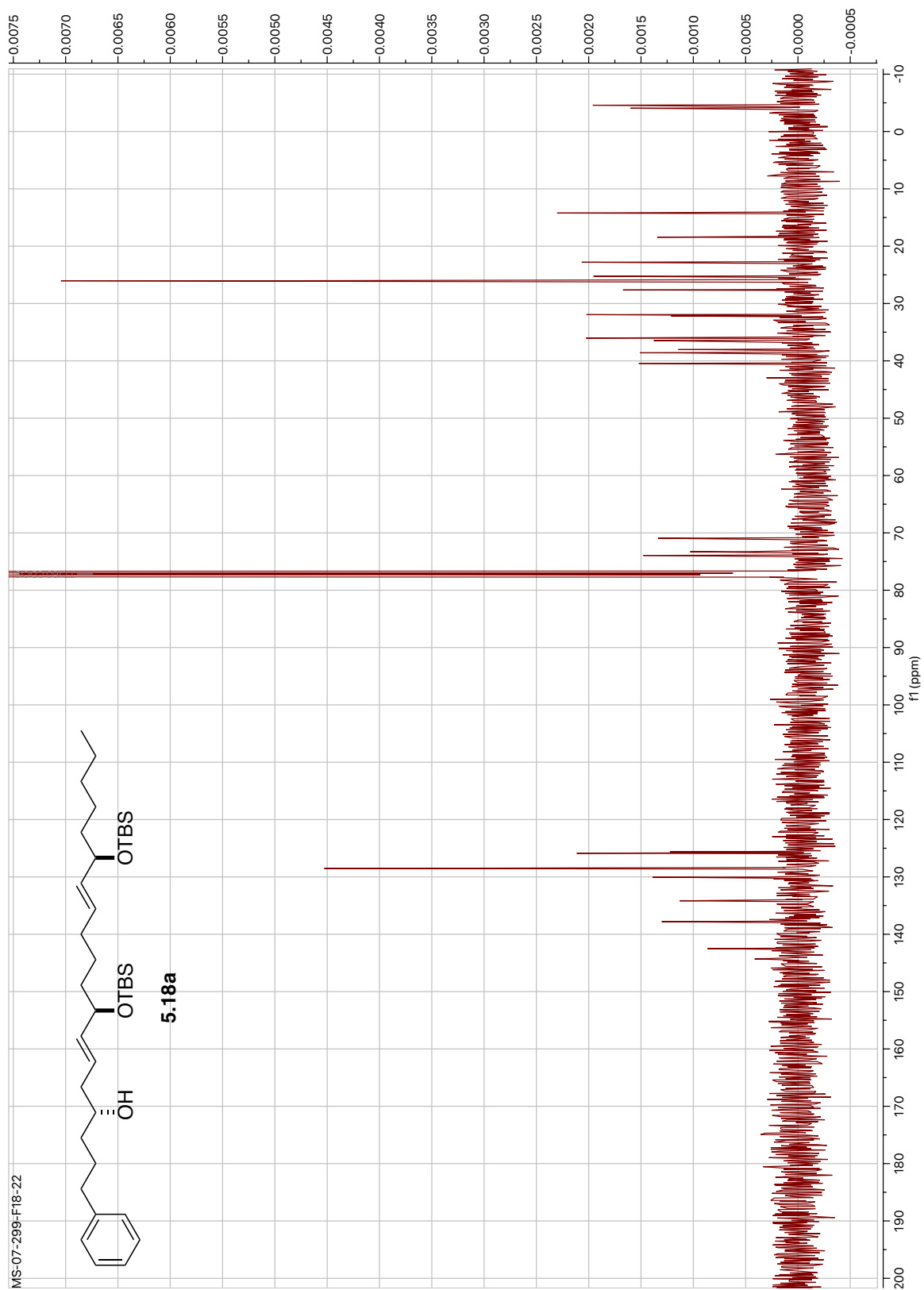


Figure 5.57: ^{13}C NMR of Compound **5.18a** (100 MHz, CDCl_3).

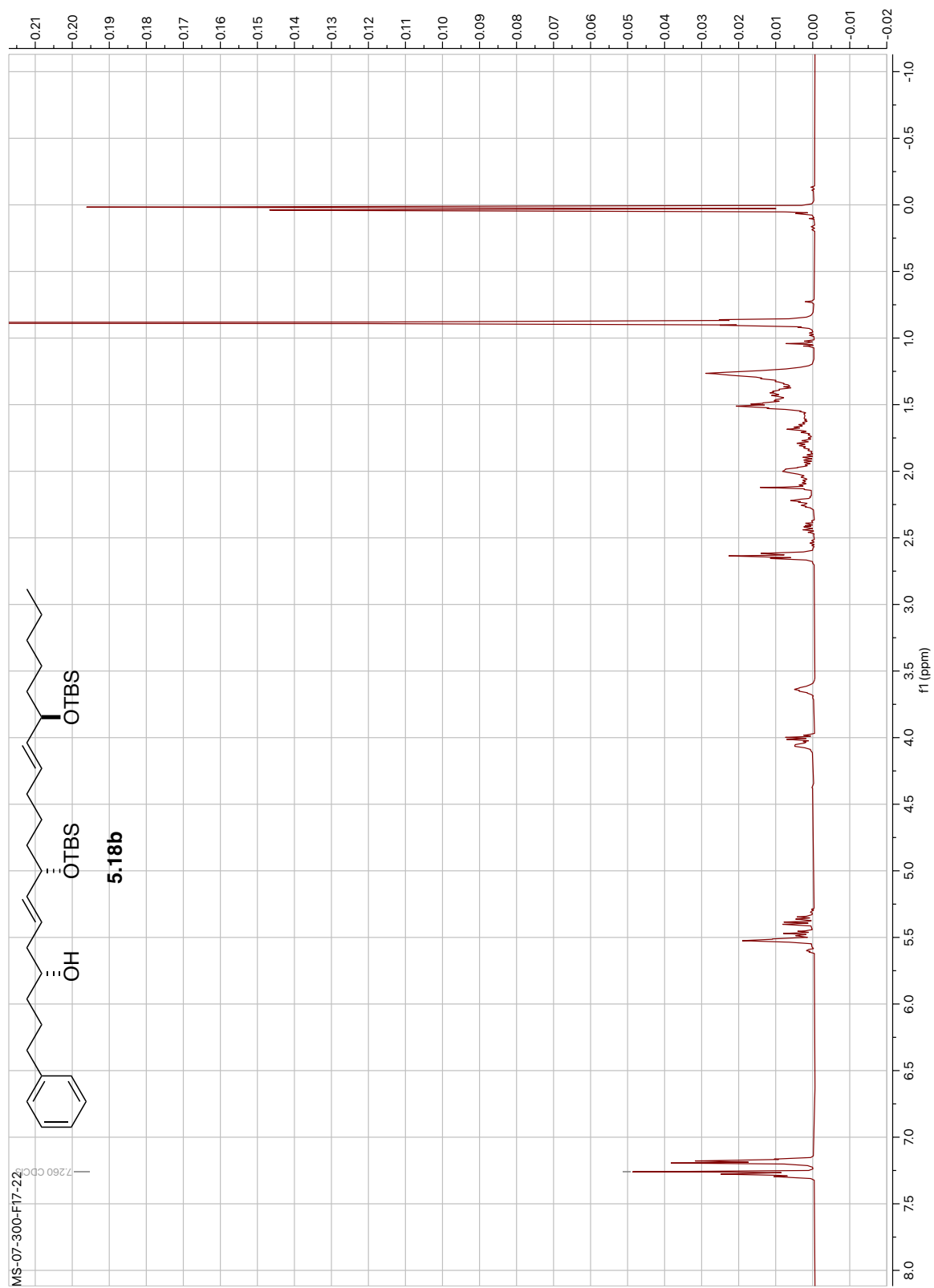


Figure 5.58: ¹H NMR of Compound **5.18b** (400 MHz, CDCl₃).

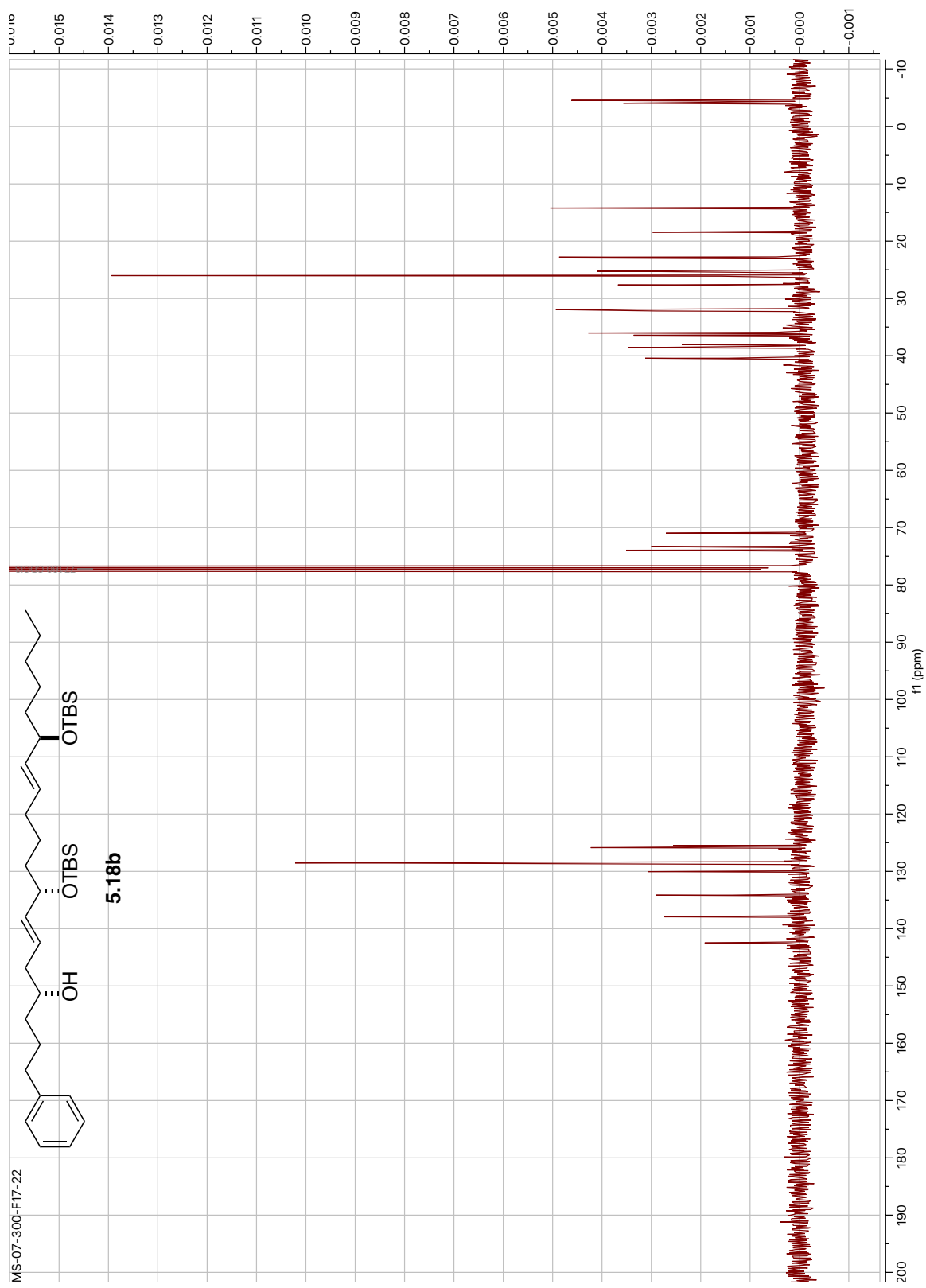


Figure 5.59: ^{13}C NMR of Compound 5.18b (100 MHz, CDCl_3).

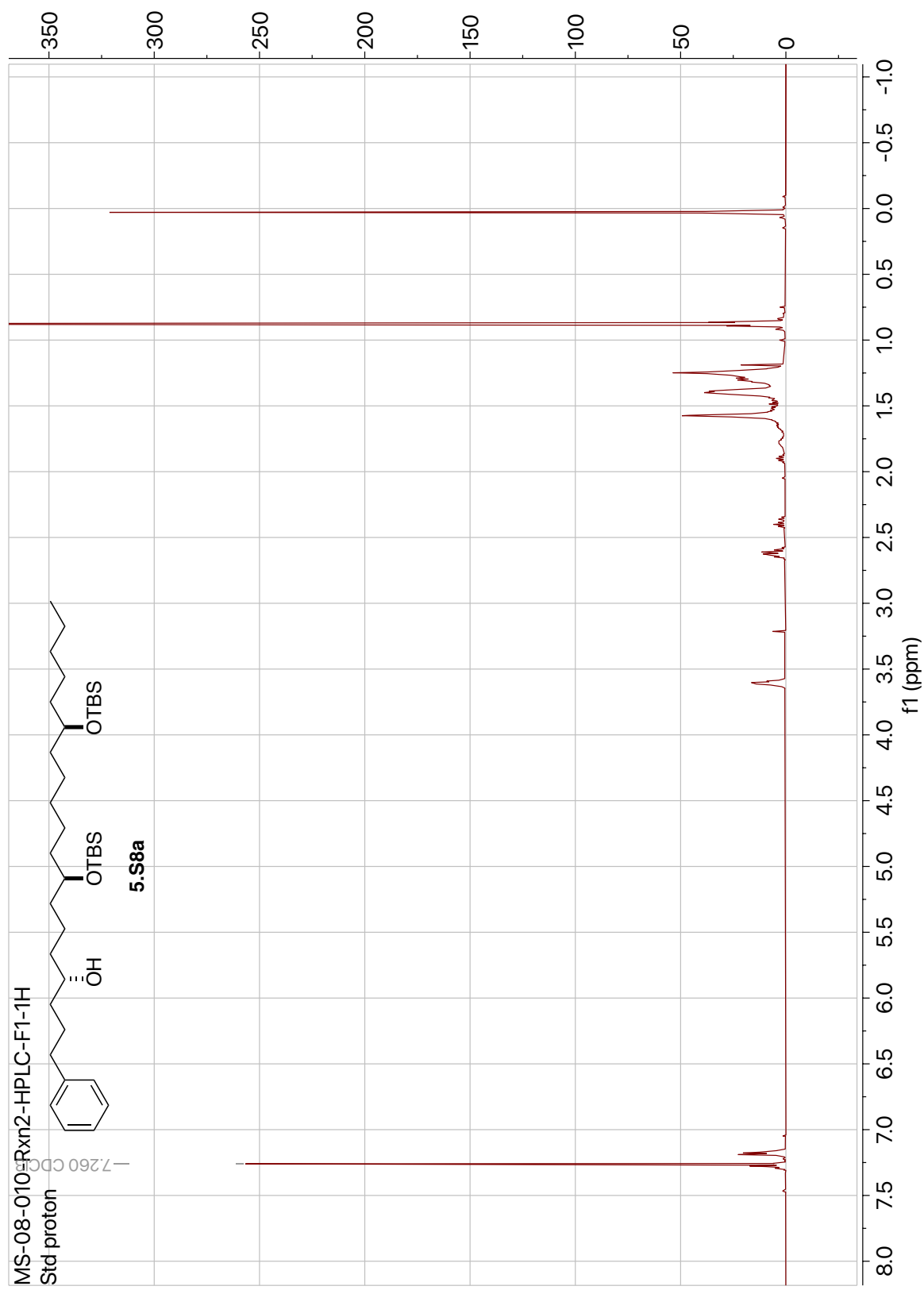


Figure 5.60: ¹H NMR of Compound **5.S8a** (500 MHz, CDCl₃).

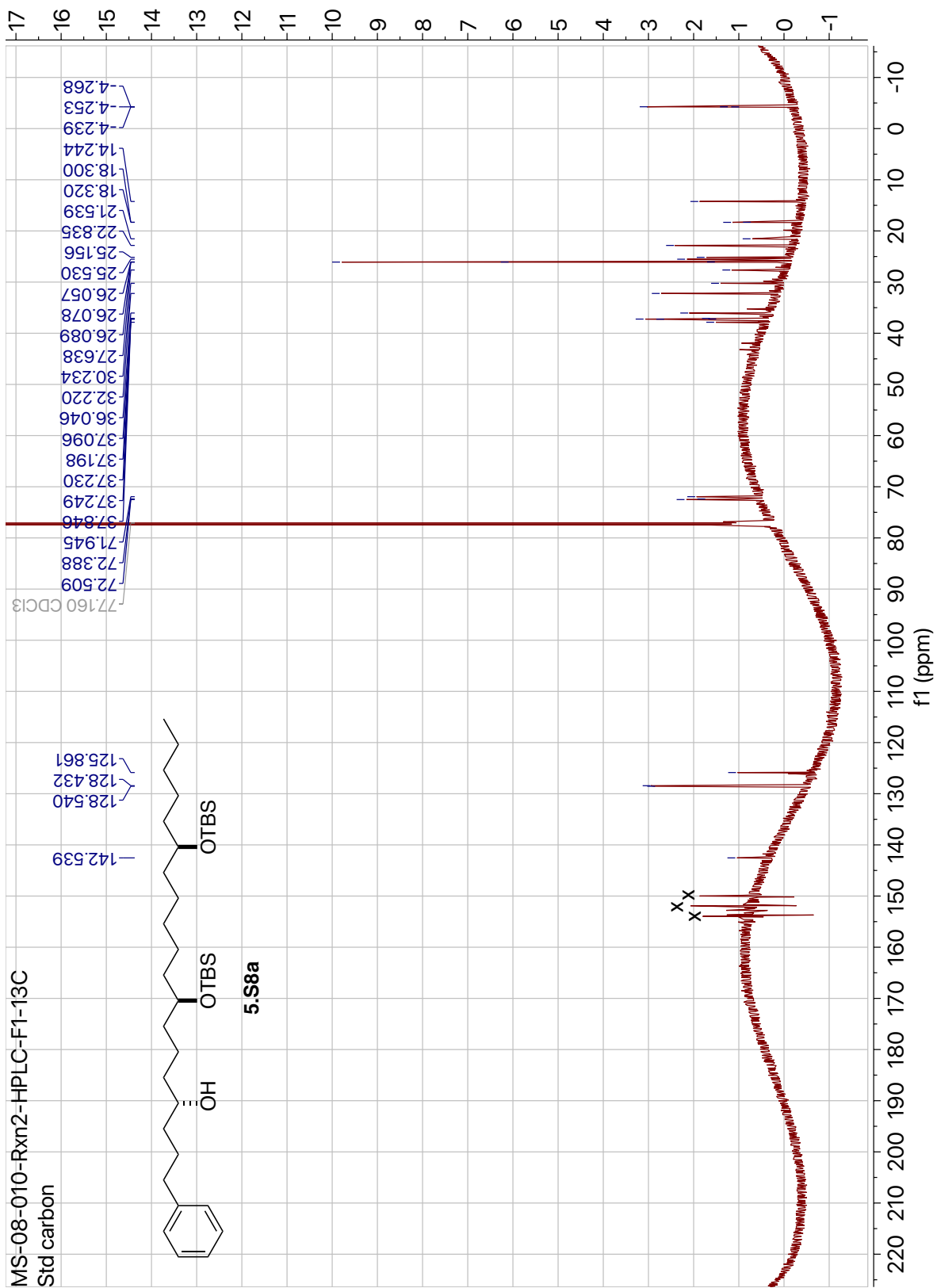


Figure 5.61: ¹³C NMR of Compound **5.S8a** (125 MHz, CDCl₃).

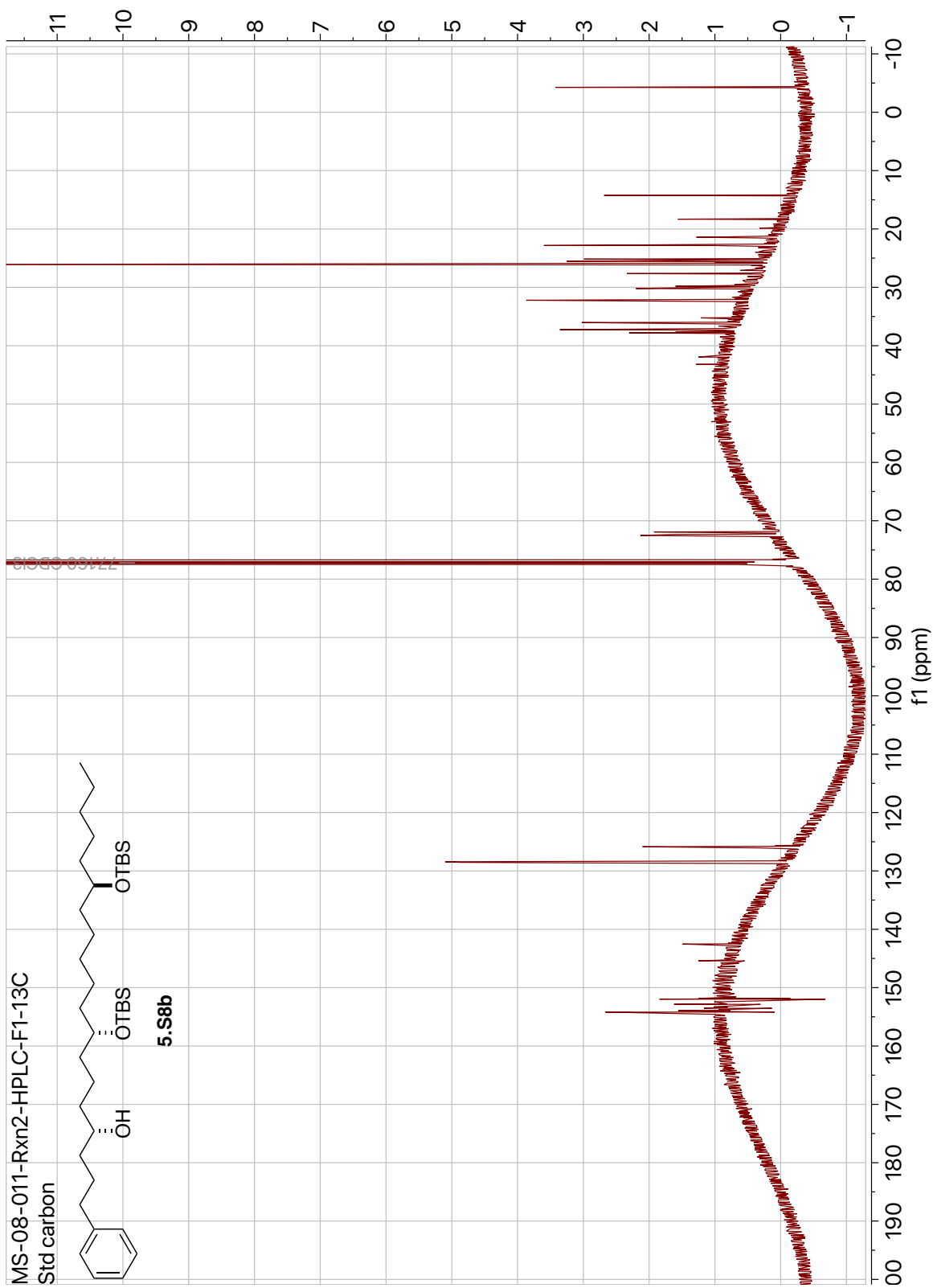


Figure 5.63: ^{13}C NMR of Compound **5.S8b** (125 MHz, CDCl_3).

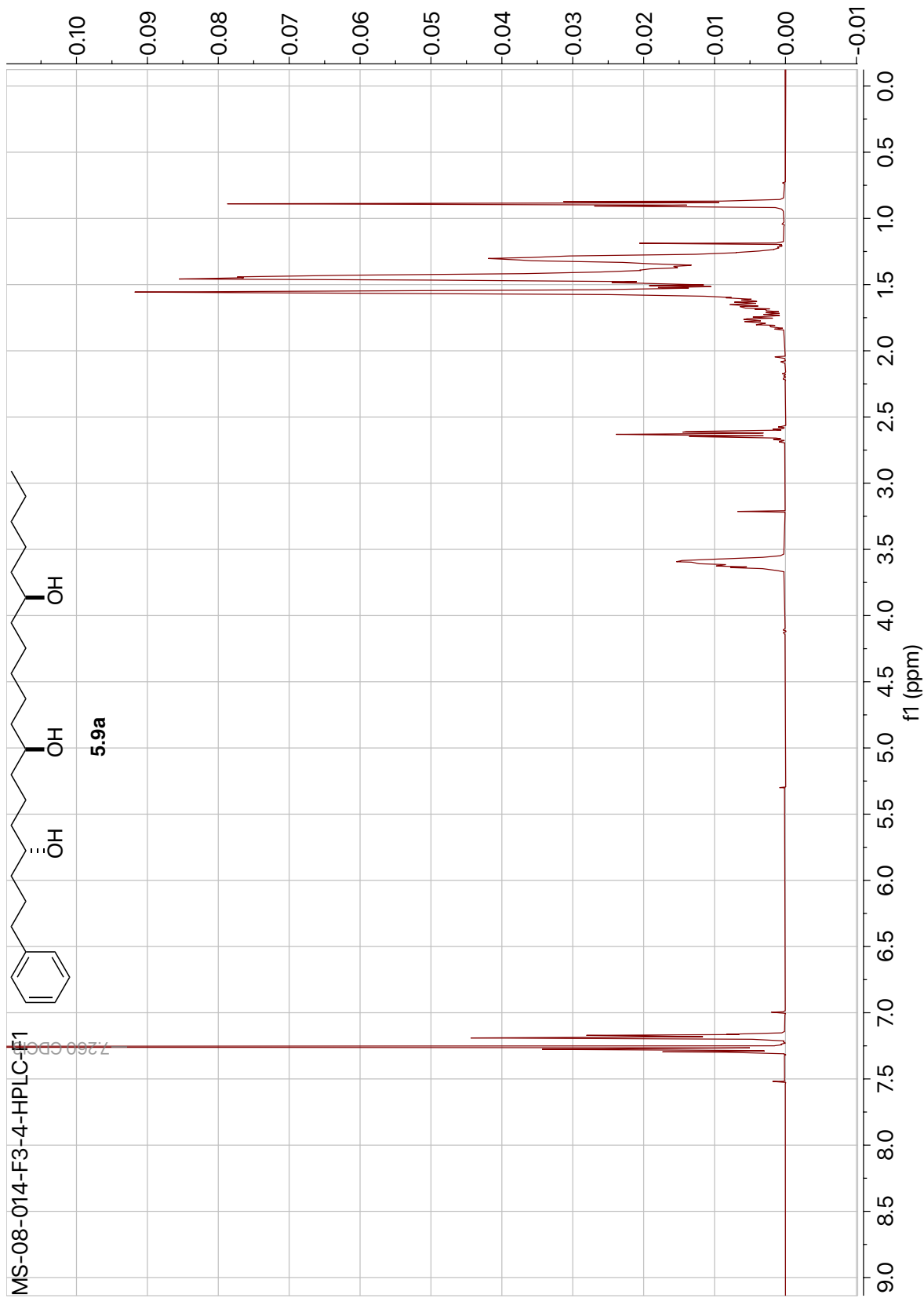
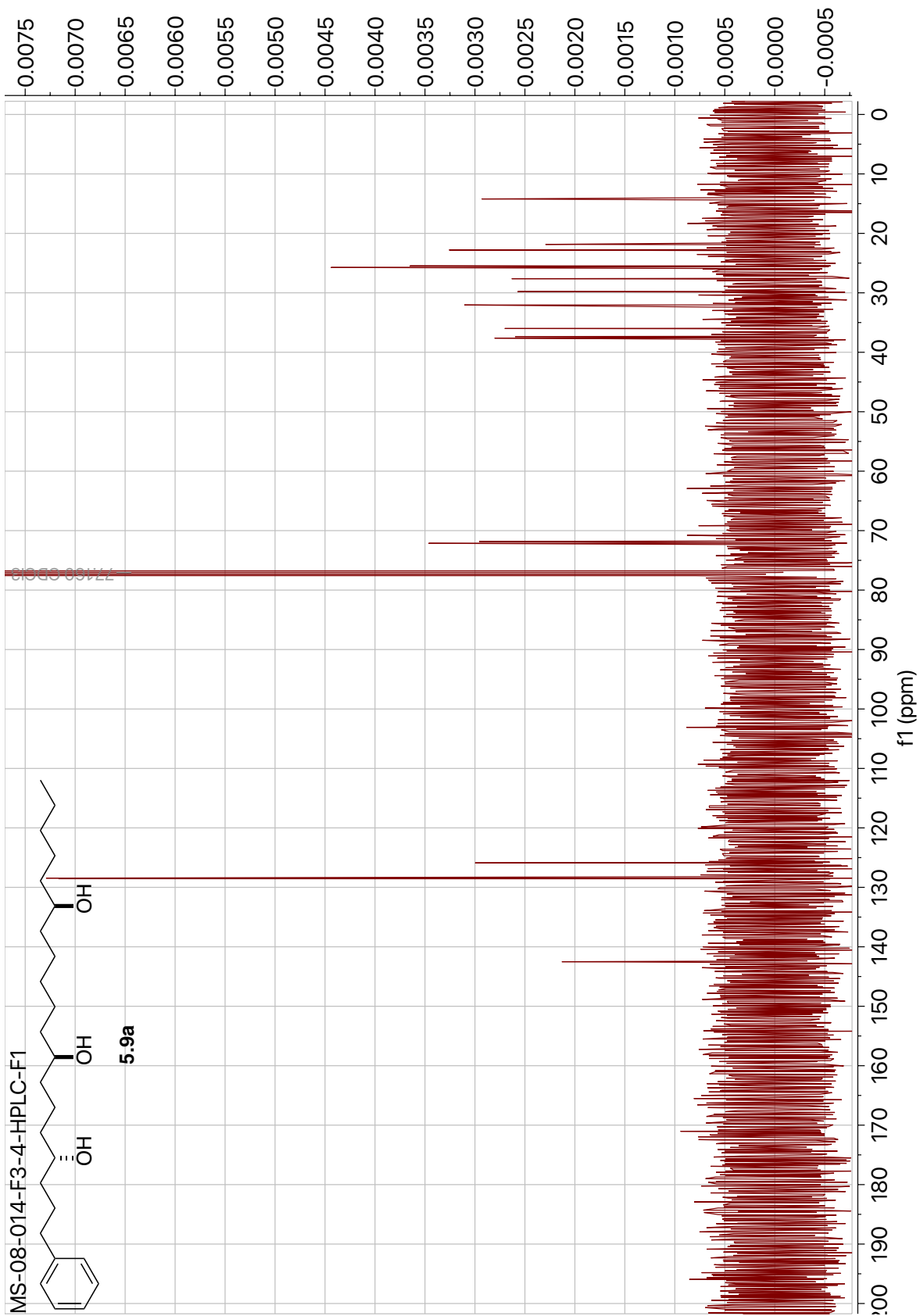


Figure 5.64: ¹H NMR of Compound **5.9a** (400 MHz, CDCl₃).



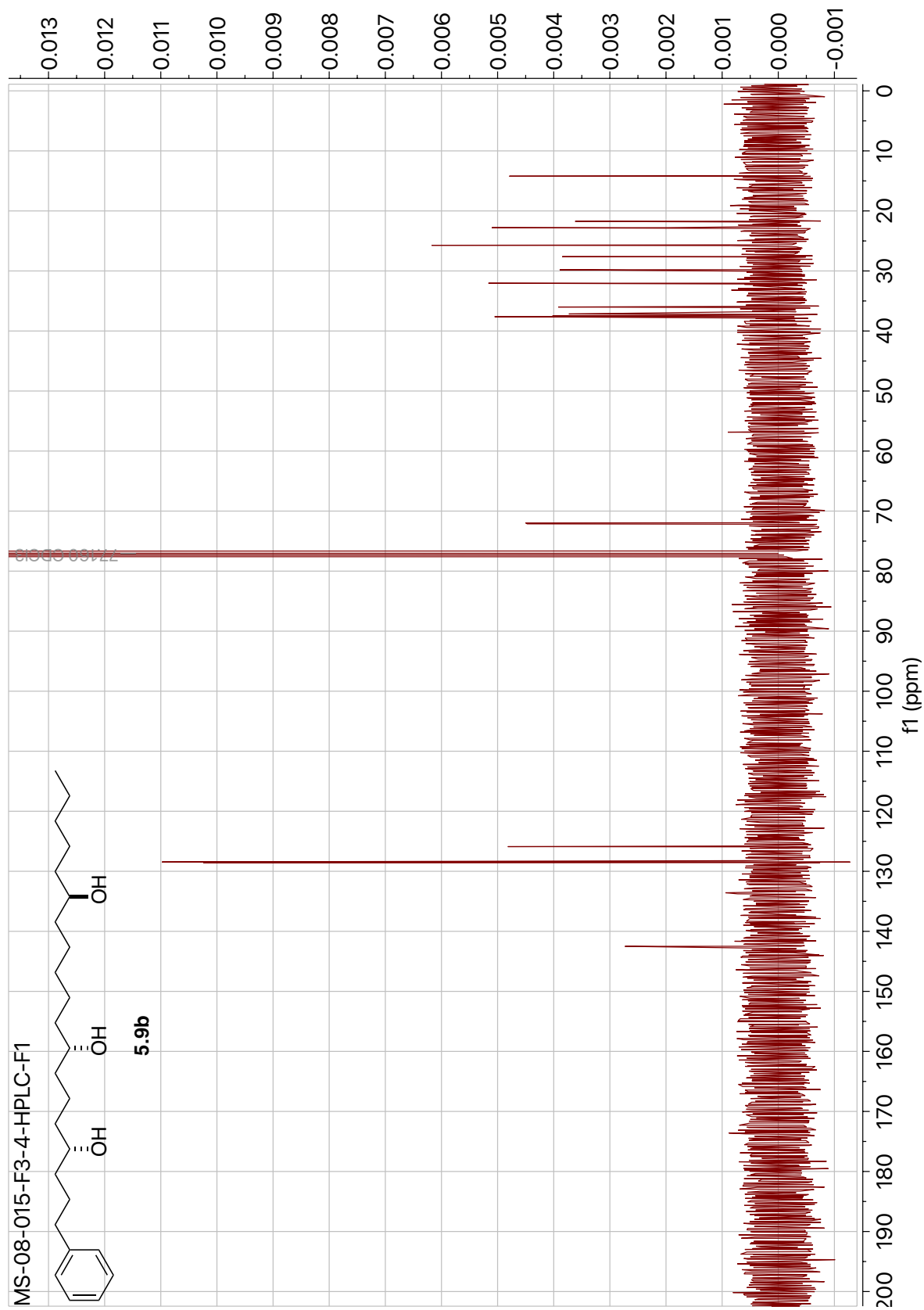


Figure 5.67: ^{13}C NMR of Compound 5.9b (100 MHz, CDCl_3).

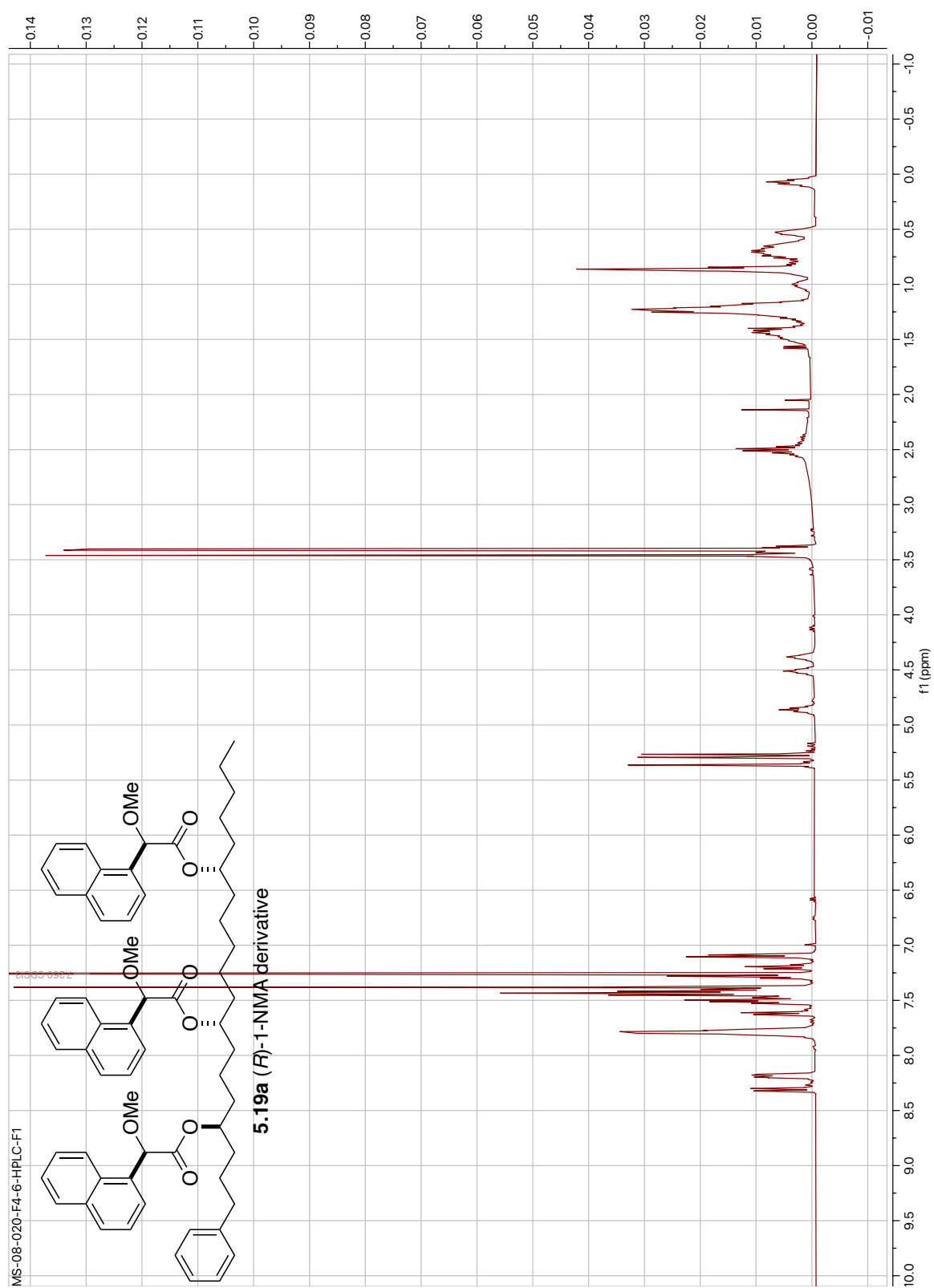
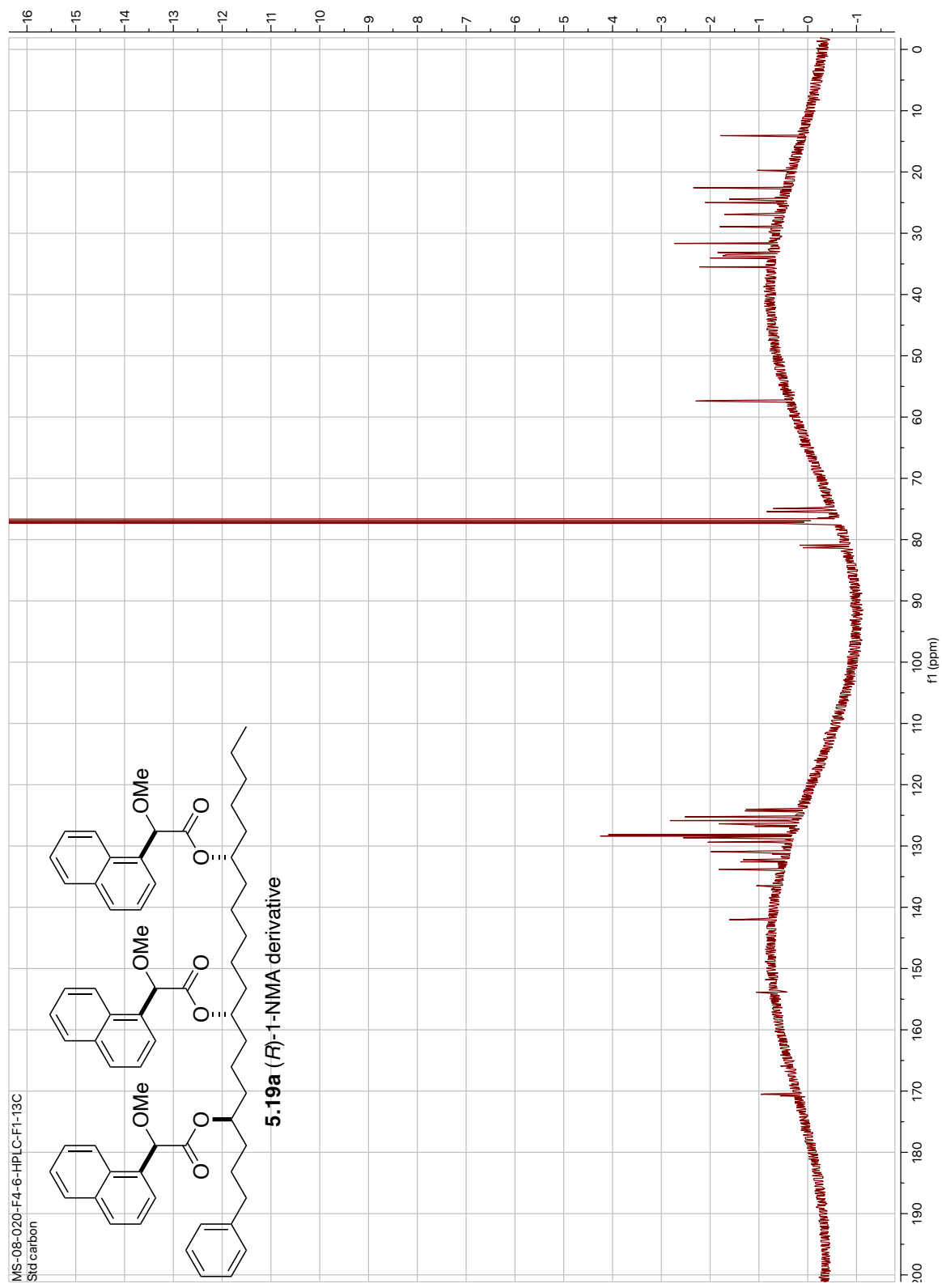


Figure 5.68: ^1H NMR of Compound **5.19a** (400 MHz, CDCl_3).



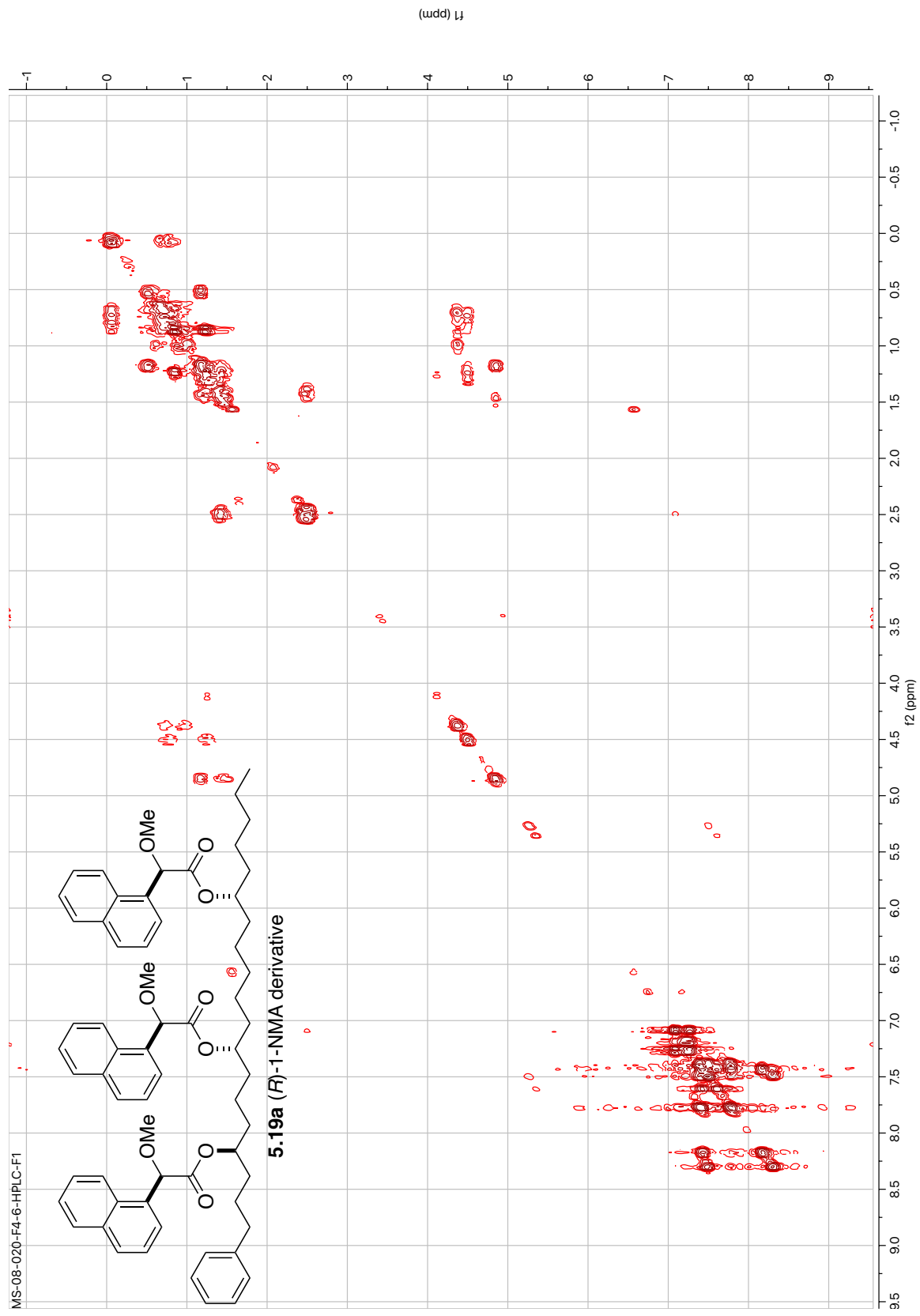


Figure 5.70: DQF-COSY of Compound **5.19a** (400 MHz, CDCl₃).

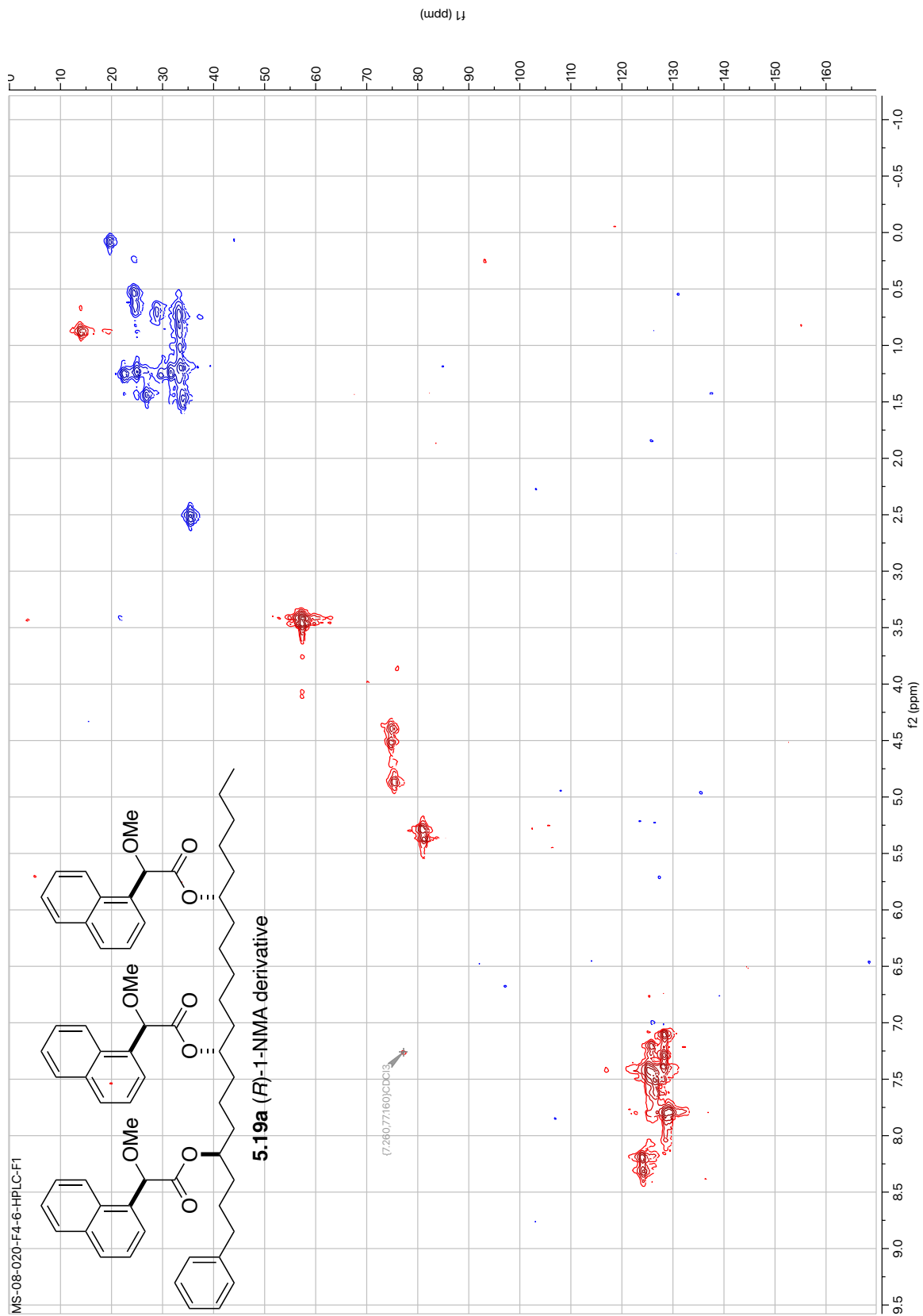


Figure 5.71: HSQC of Compound **5.19a** (400 MHz, CDCl₃).

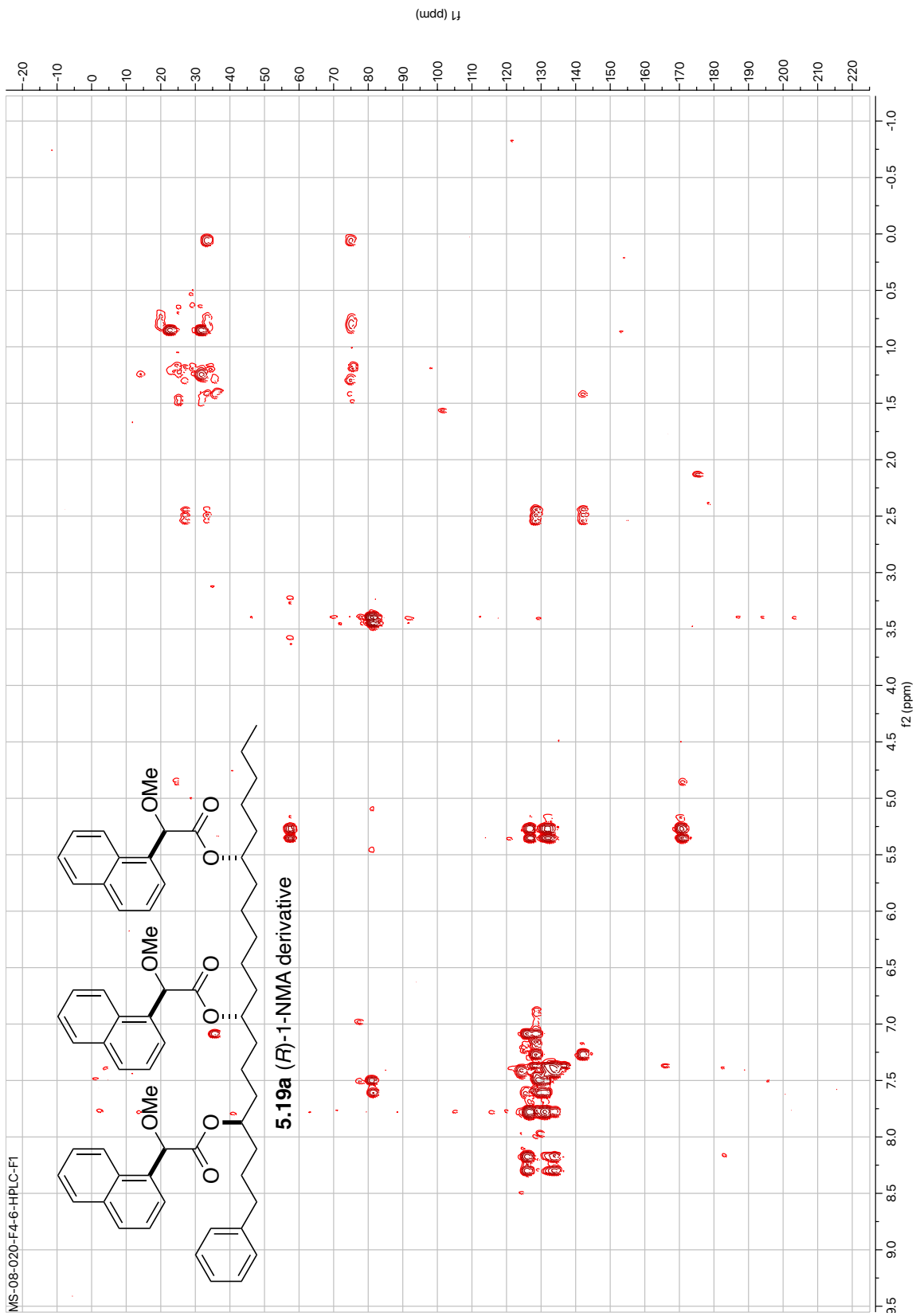


Figure 5.72: HMBC of Compound **5.19a** (400 MHz, CDCl_3).

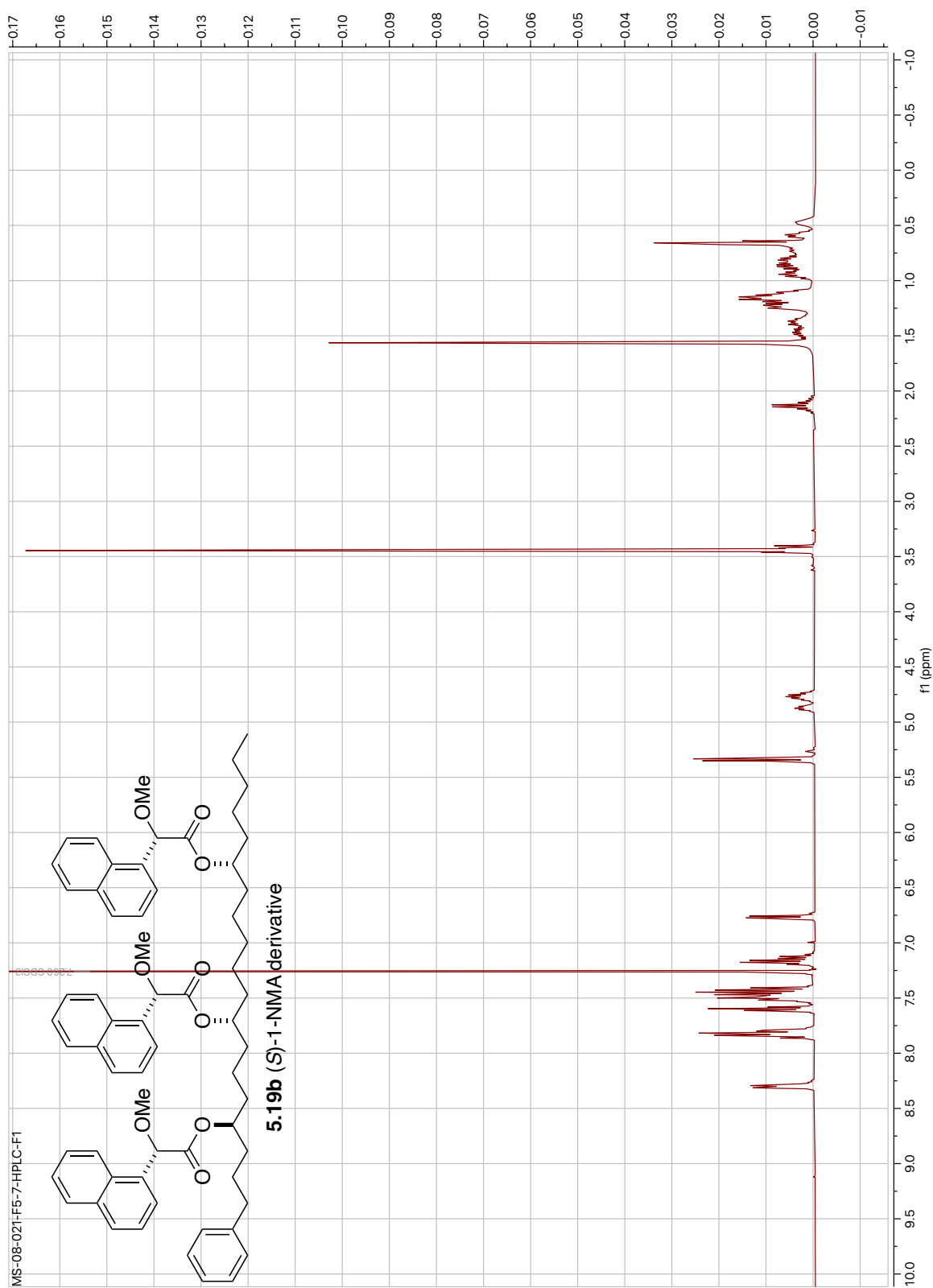
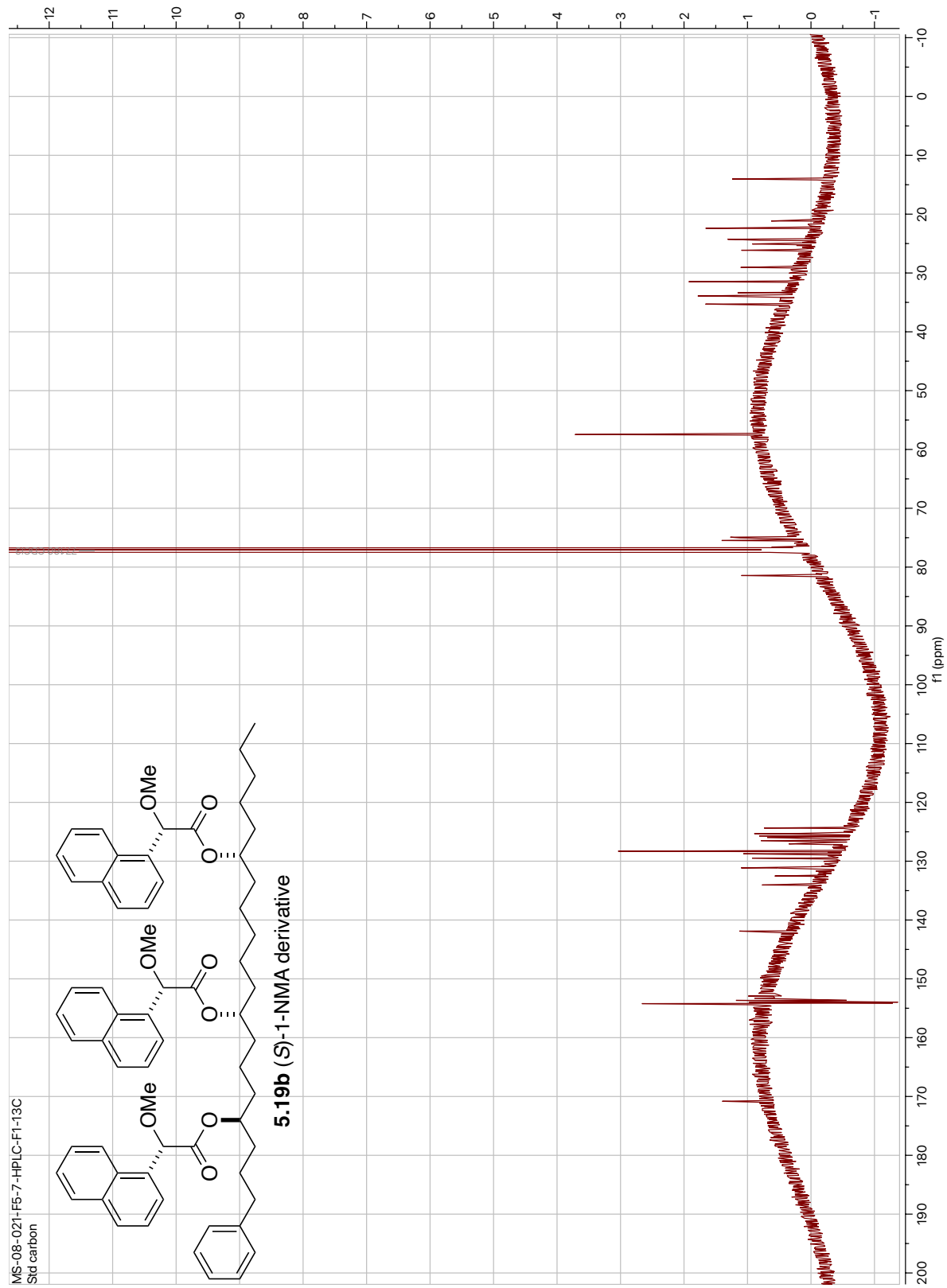


Figure 5.73: ^1H NMR of Compound **5.19b** (400 MHz, CDCl_3).



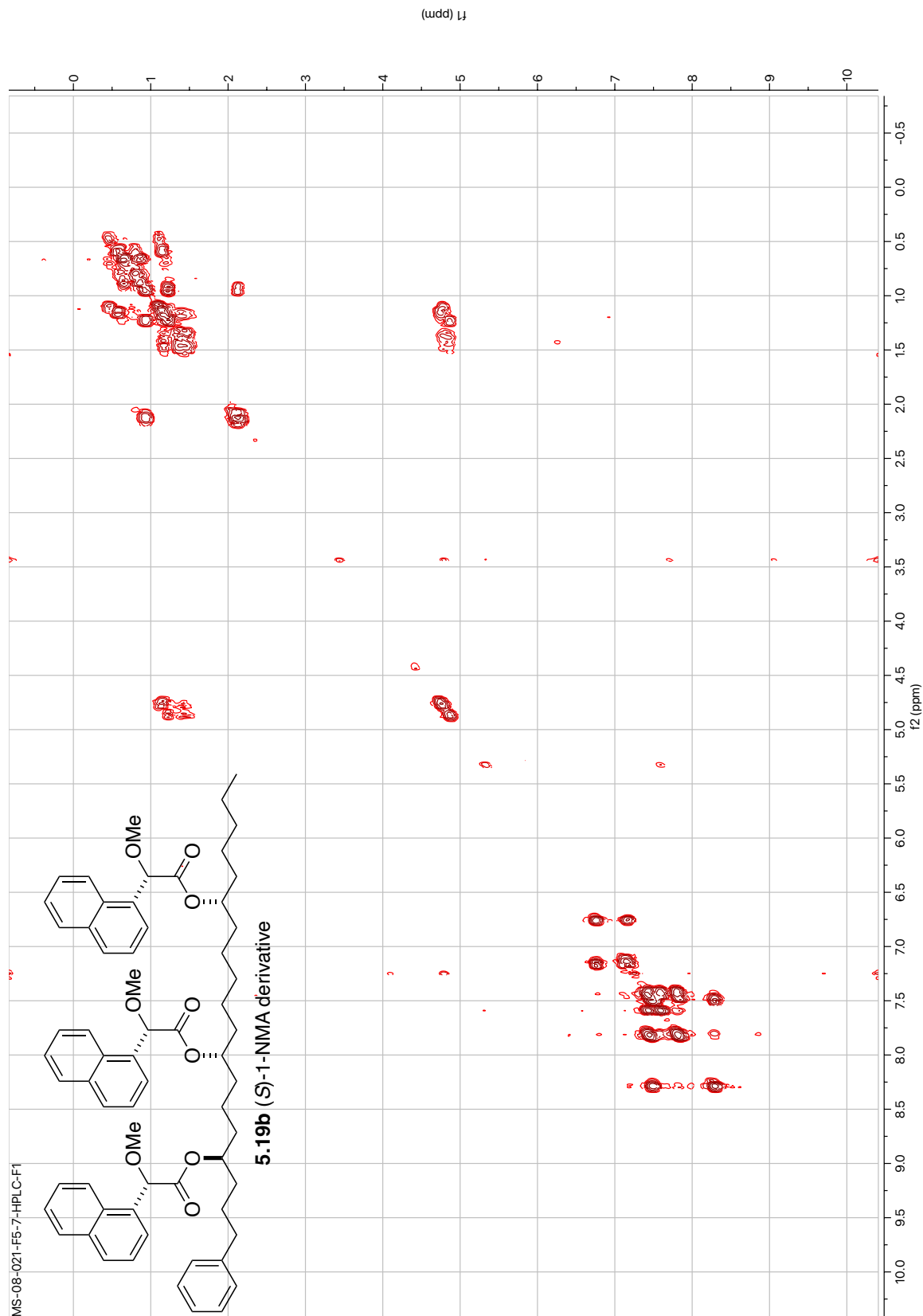


Figure 5.75: DQF-COSY of Compound **5.19b** (400 MHz, CDCl₃).

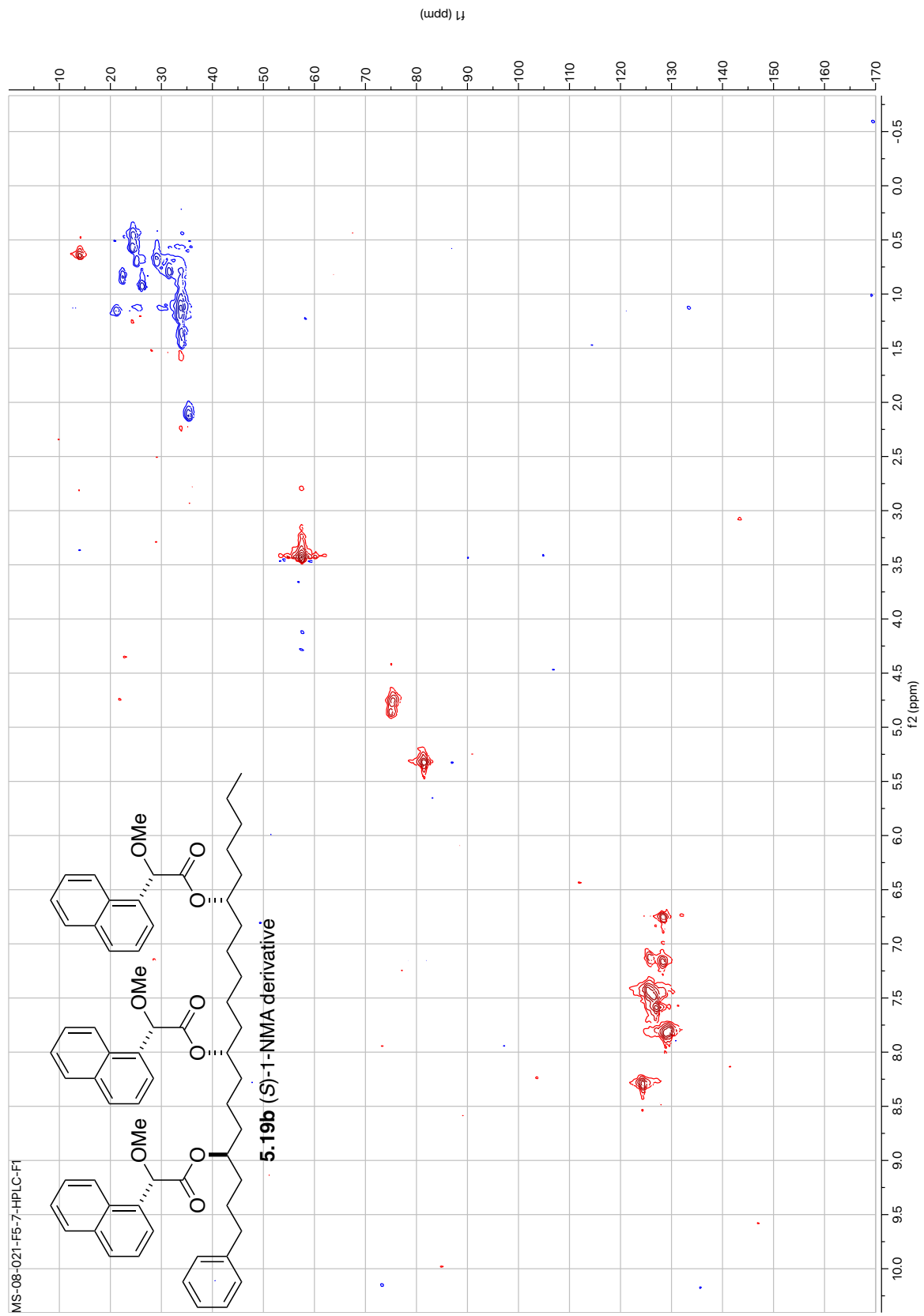


Figure 5.76: HSQC of Compound **5.19b** (400 MHz, CDCl₃).

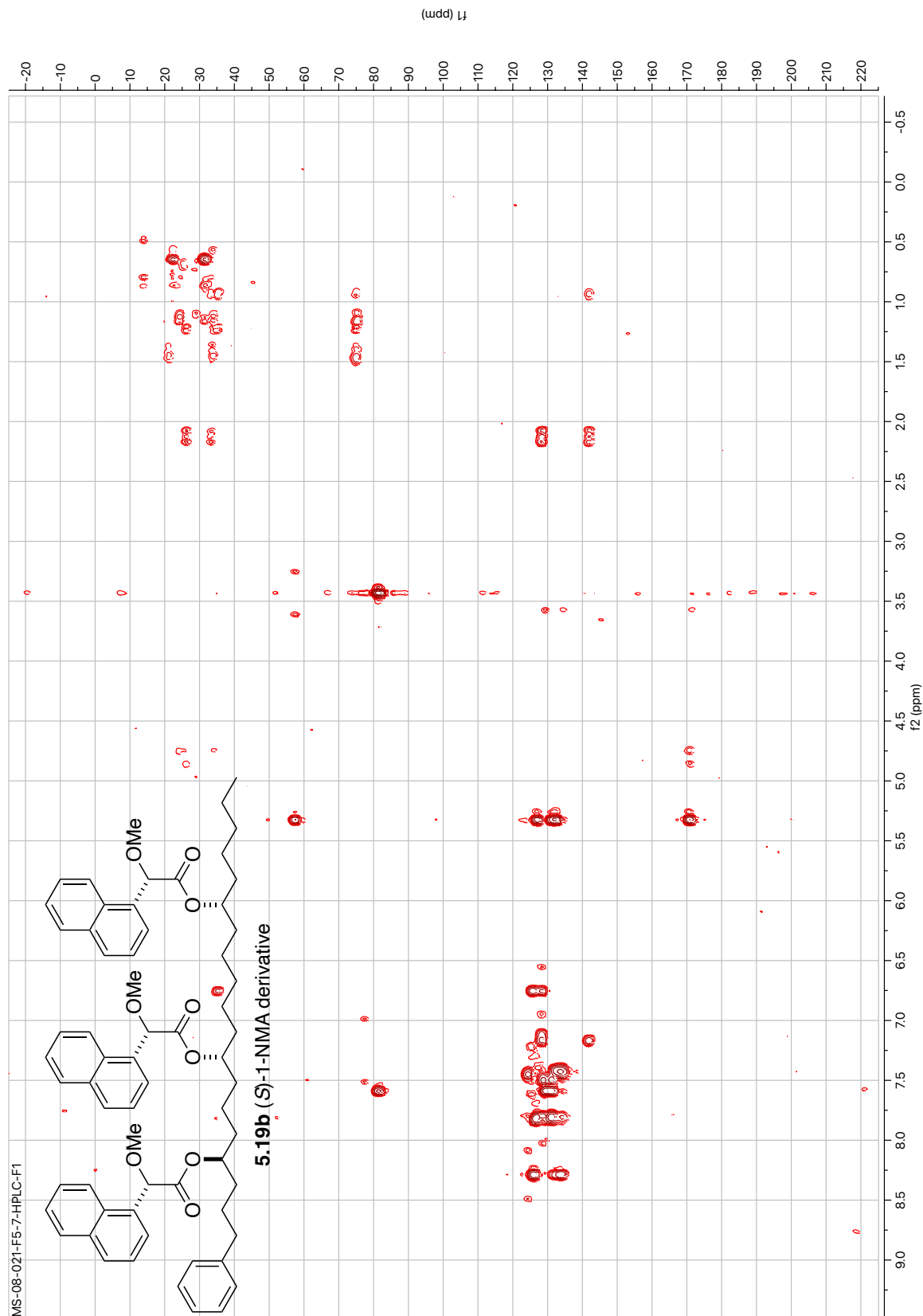


Figure 5.77: HMBC of Compound **5.19b** (400 MHz, CDCl_3).

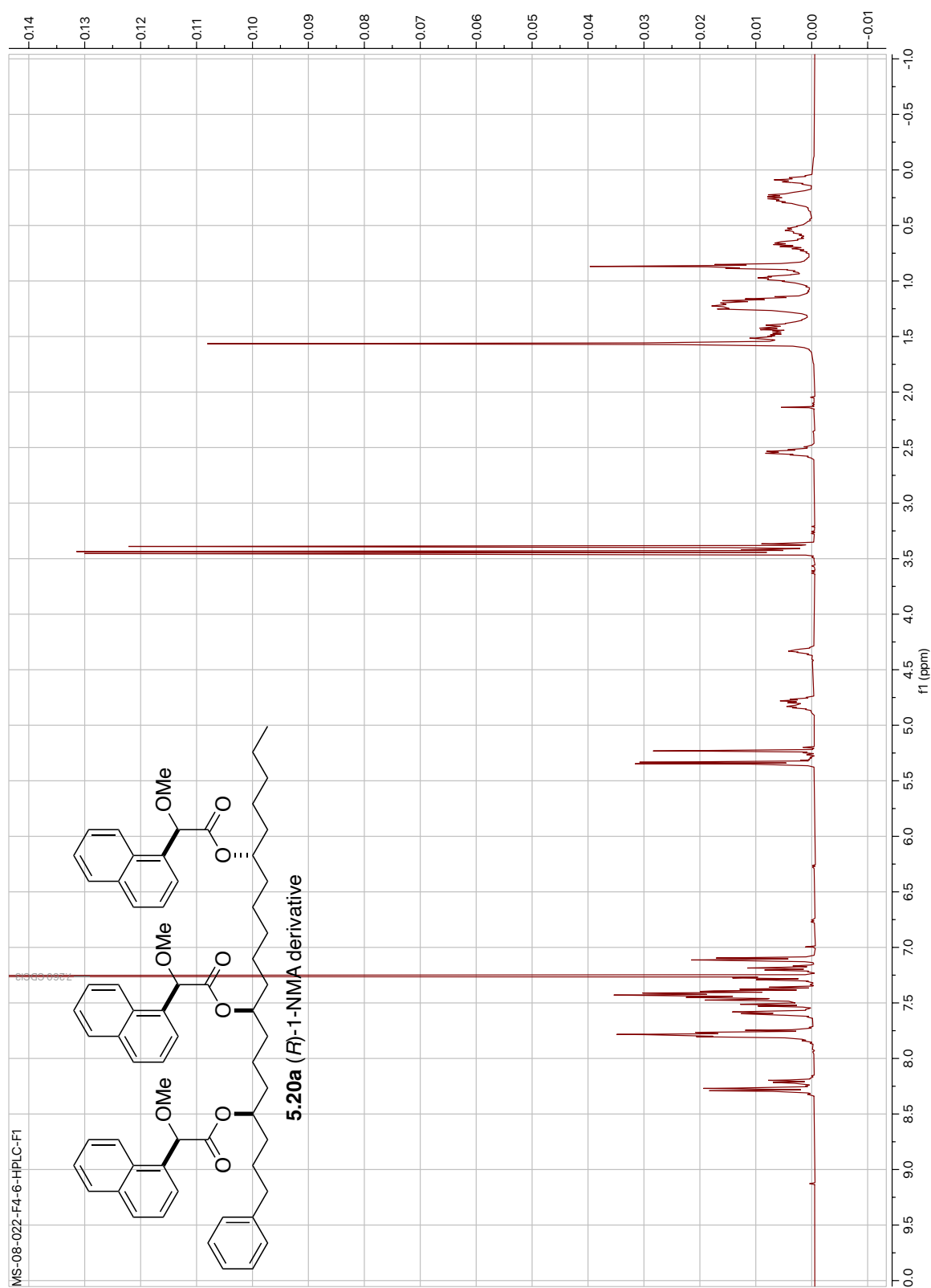


Figure 5.78: ^1H NMR of Compound **5.20a** (400 MHz, CDCl_3).

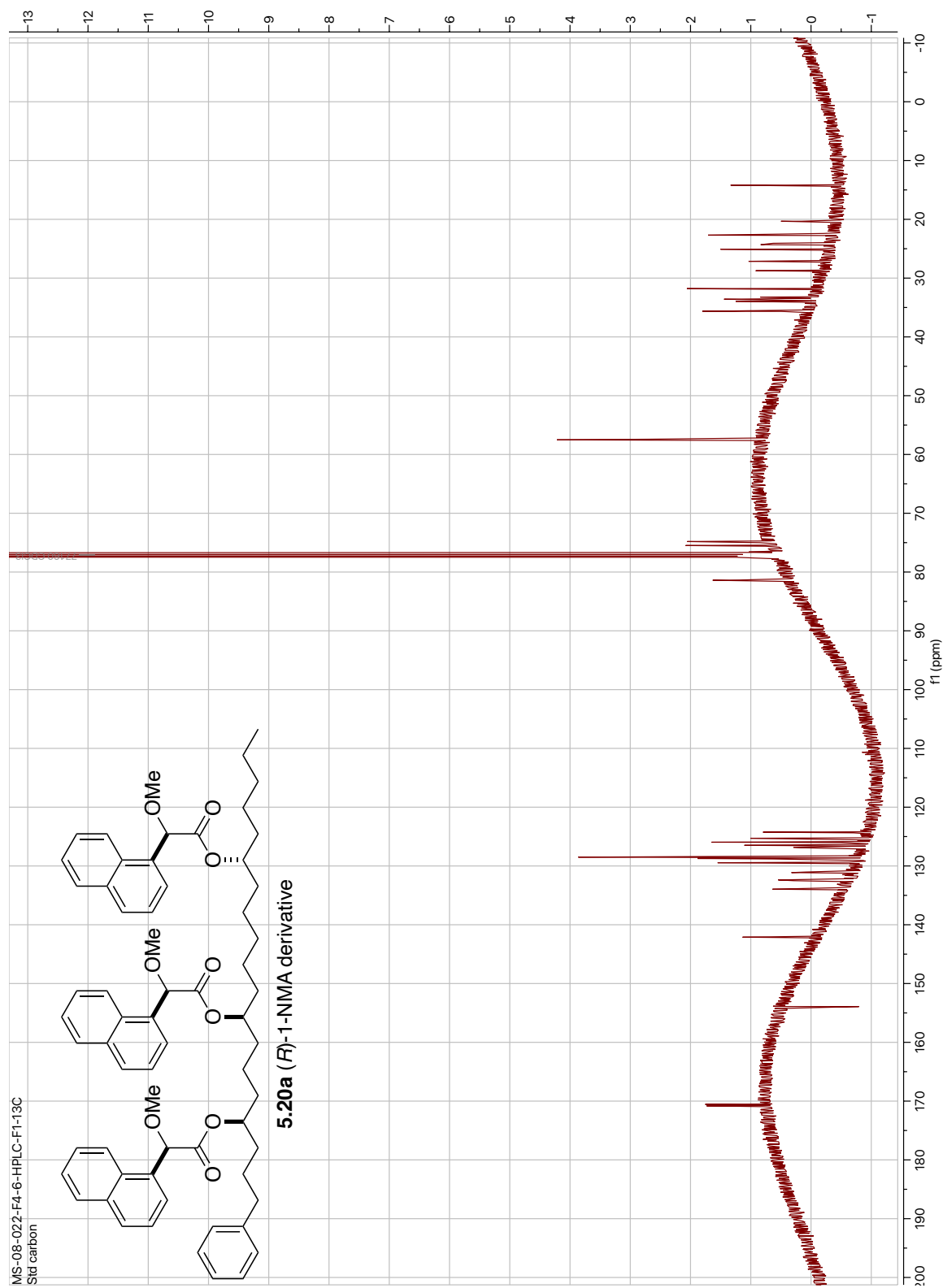


Figure 5.79: ^{13}C NMR of Compound **5.20a** (125 MHz, CDCl_3).

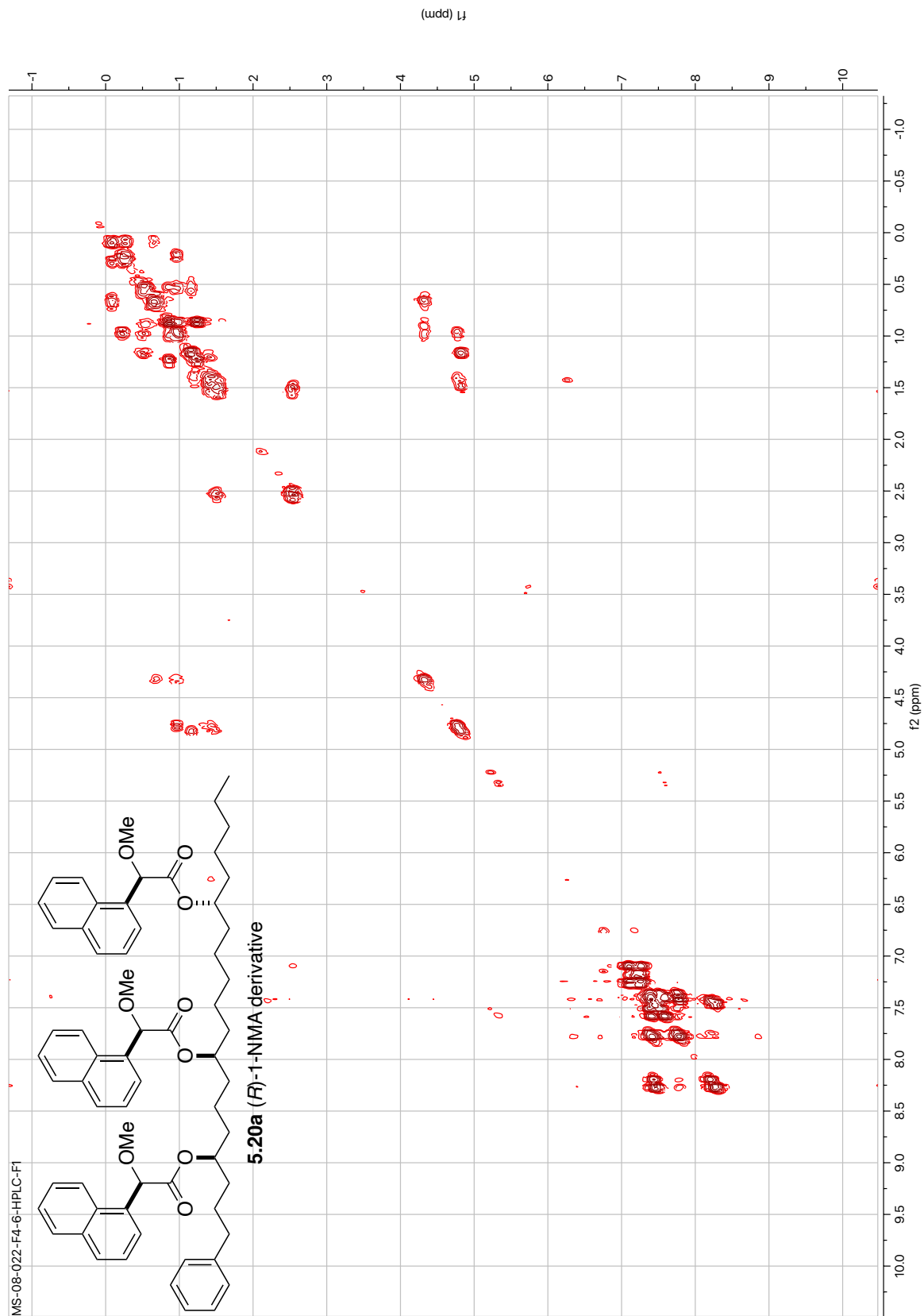


Figure 5.80: DQF-COSY of Compound **5.20a** (400 MHz, CDCl_3).

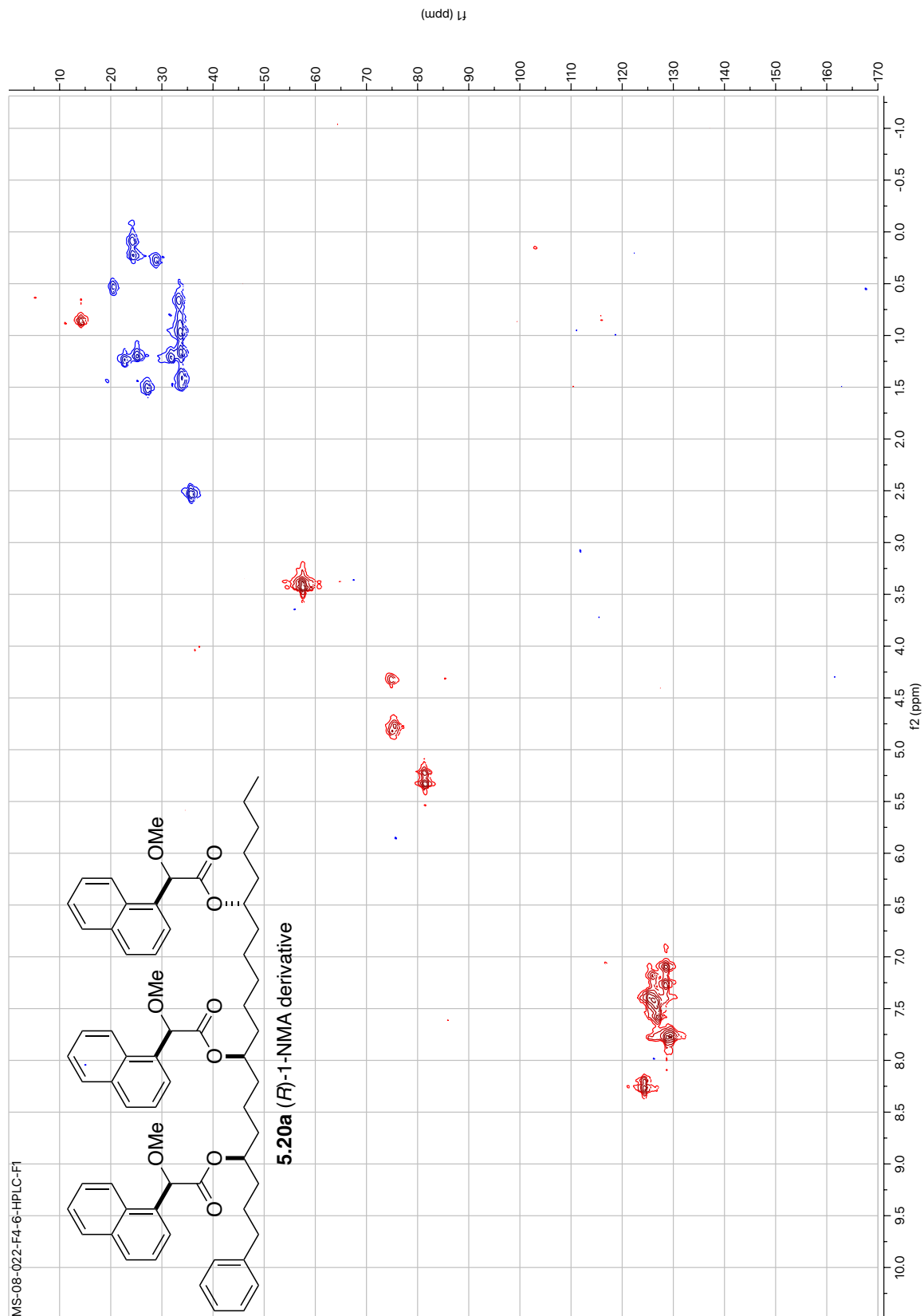


Figure 5.81: HSQC of Compound **5.20a** (400 MHz, CDCl₃).

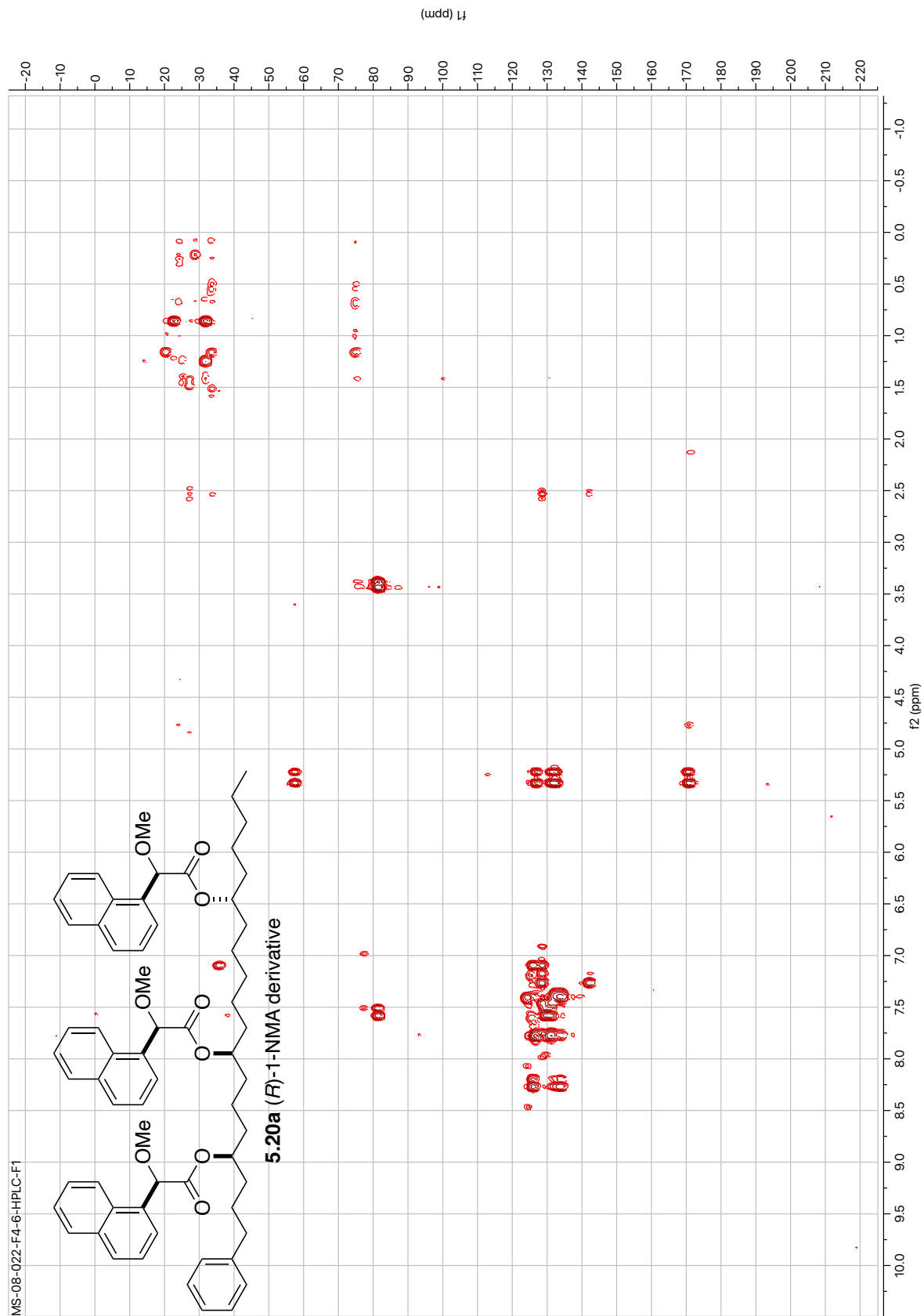
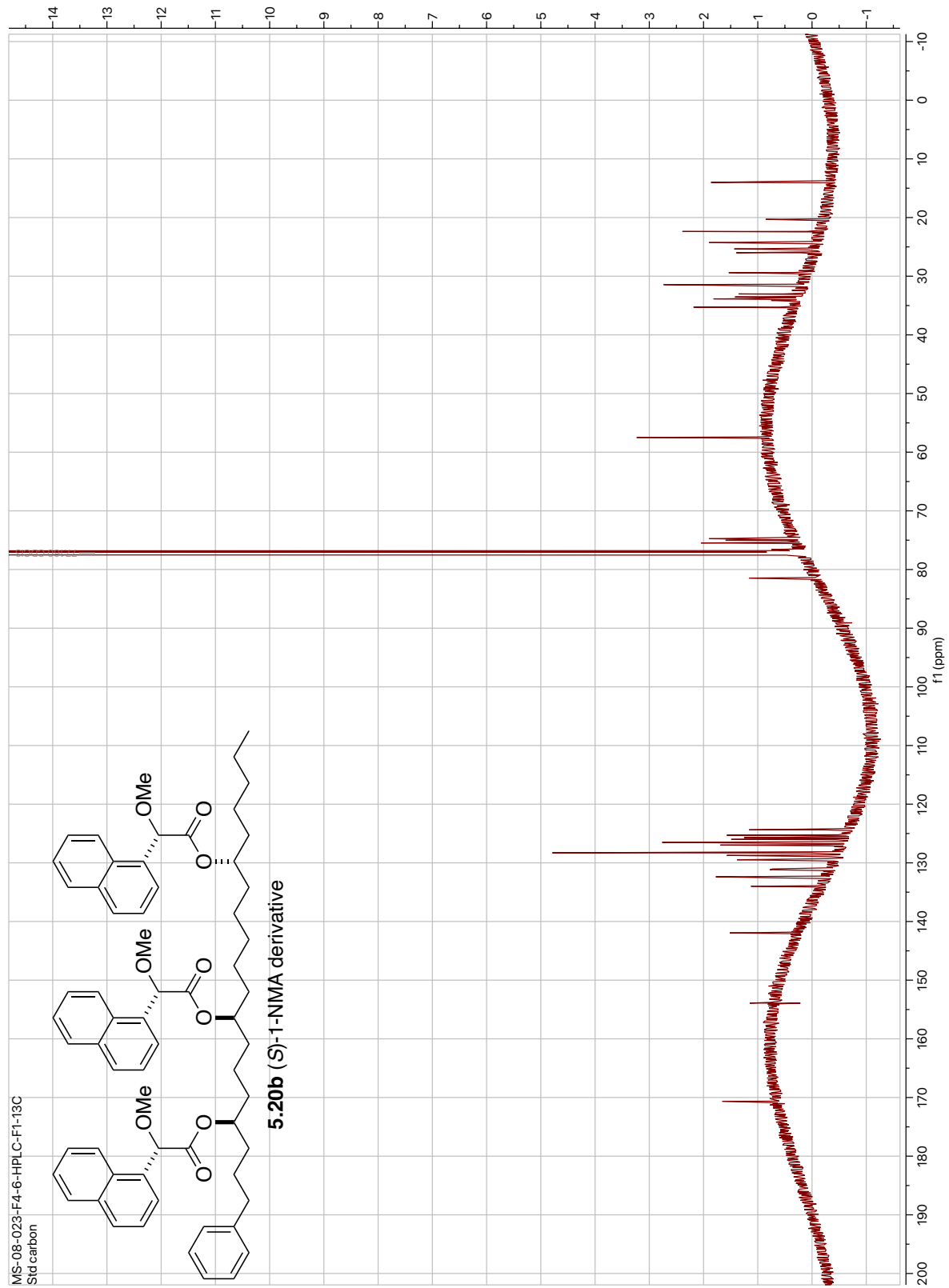


Figure 5.82: HMBC of Compound **5.20a** (400 MHz, CDCl₃).



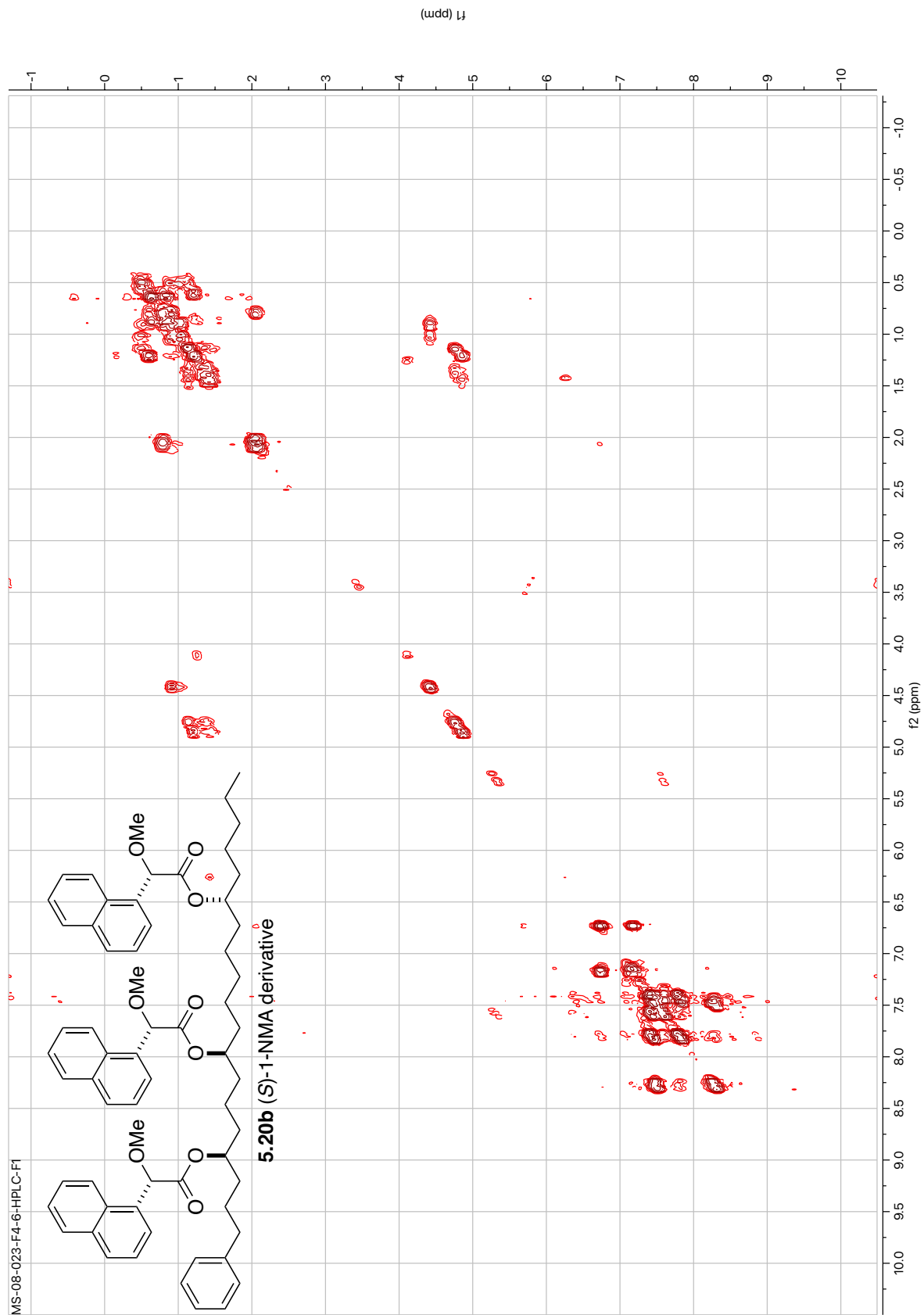
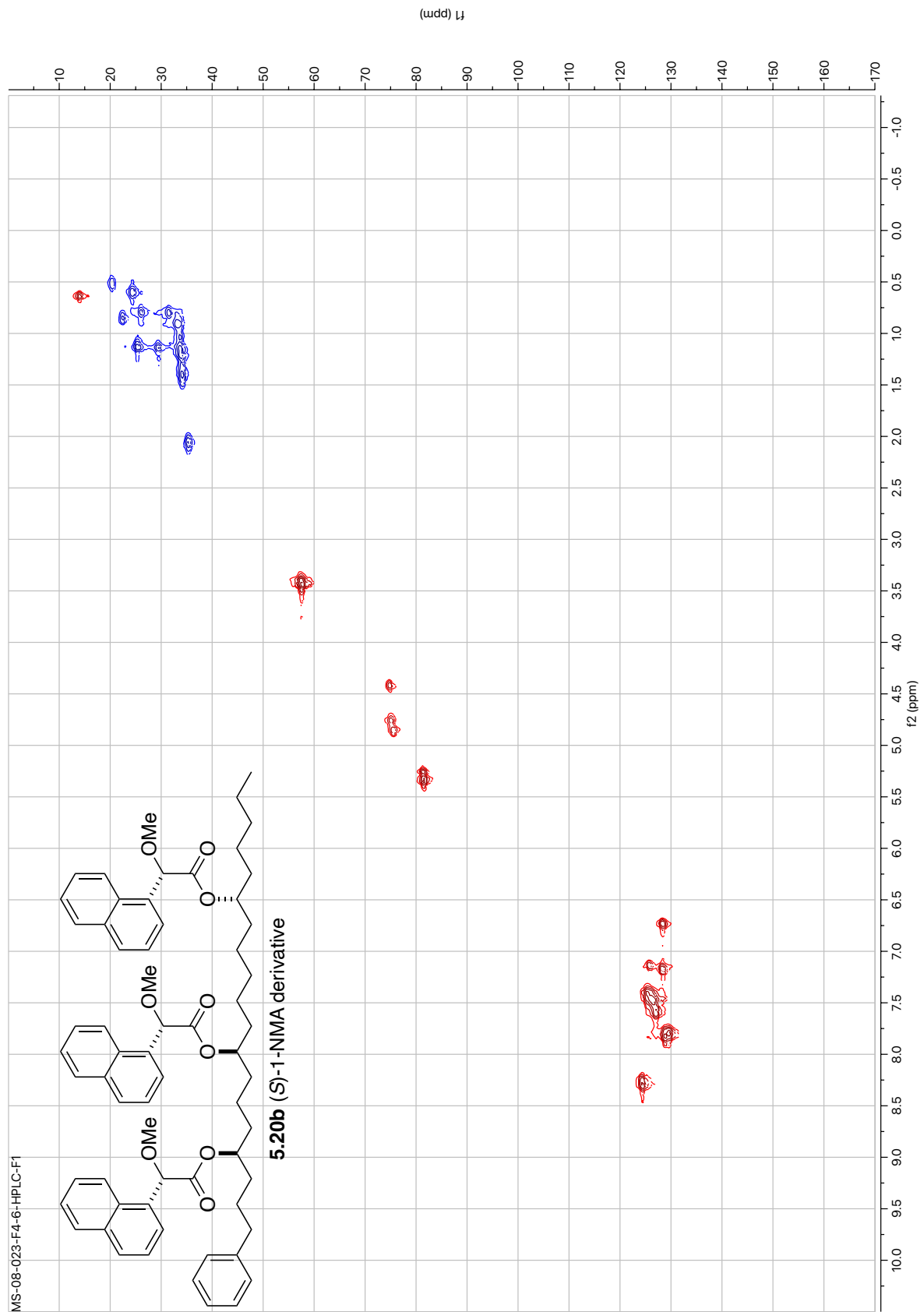


Figure 5.85: DQF-COSY of Compound **5.20b** (400 MHz, CDCl₃).



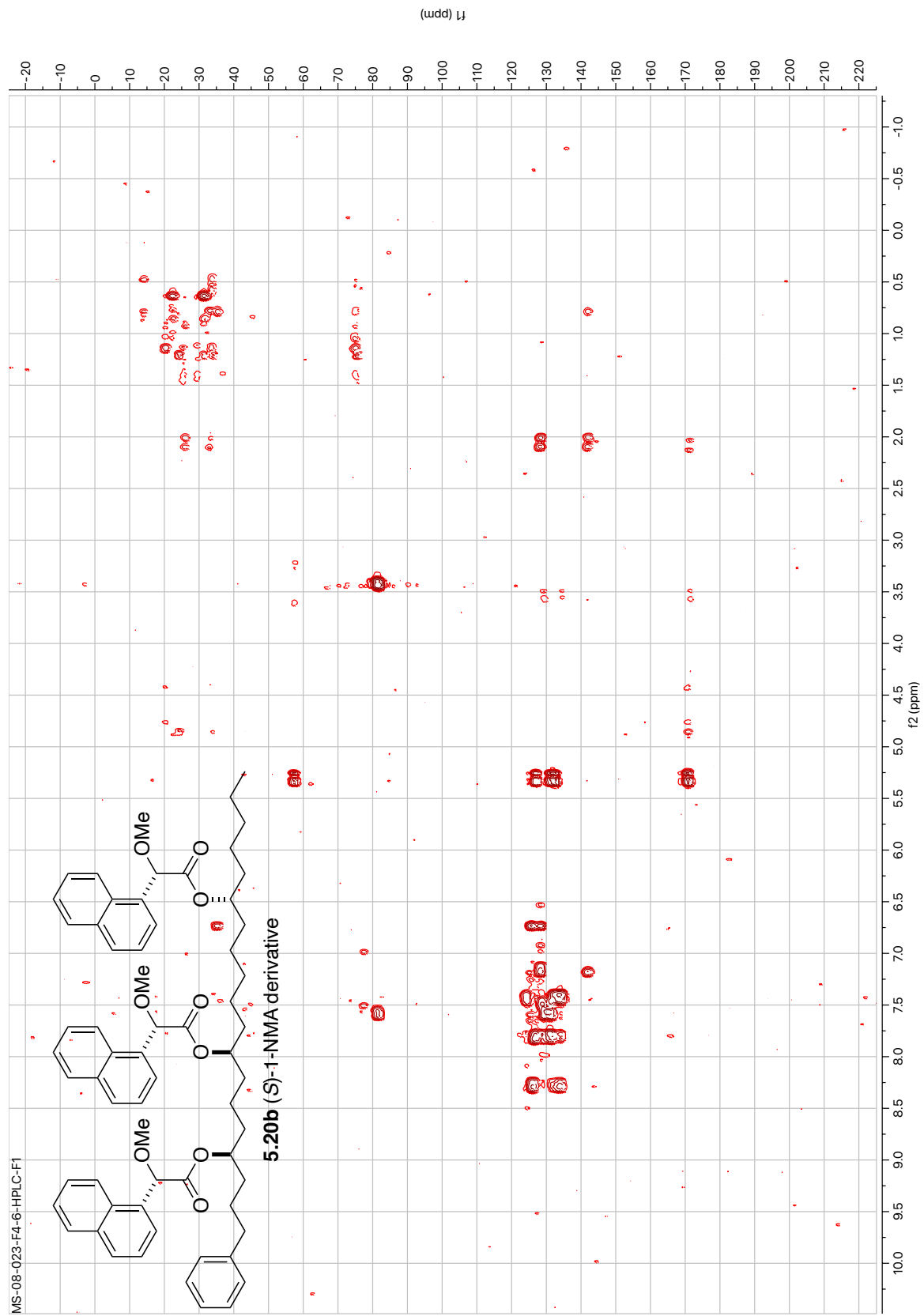


Figure 5.87: HMBC of Compound 5.20b (400 MHz, CDCl_3).

5.10 References

- (1) Mancini, I.; Guella, G.; Debitus, C.; Pietra, F. *Helv. Chim. Acta.* **1994**, *77*, 51-58.
- (2) Ahmed, S.; Ibrahim, A.; Arafa, A. S. *Tetrahedron Lett.* **2013**, *54*, 2377-2381.
- (3) Tian, X.-R.; Tang, H.-F.; Feng, J.-T.; Li, Y.-S.; Lin, H.-W.; Fan, X.-P.; Zhang, X. *Mar. Drugs* **2014**, *12*, 1987-2003.
- (4) Cafieri, F.; Fattorusso, E.; Mahajnah, Y.; Mangoni, A. *Liebigs Ann. Chem.* **1994**, 1187-1189.
- (5) Costantino, V.; Fattorusso, E.; Mangoni, A.; Teta, R.; Panza, E.; Ianaro, A. *Bioorganic Med. Chem.* **2010**, *18*, 5310-5315.
- (6) Natori, T.; Koezuka, Y.; Higa, T. *Tetrahedron Lett.* **1993**, *34*, 5591-5592.
- (7) Li, H.-Y.; Matsunaga, S.; Fusetani, N. *Tetrahedron* **1995**, *51*, 2273-2280.
- (8) (a) Fusetani, N.; Sata, N.; Asai, N.; Matsunaga, S. *Tetrahedron Lett.* **1993**, *34*, 4067-4070.
(b) Sata, N.; Asai, N.; Matsunaga, S.; Fusetani, N. *Tetrahedron* **1994**, *50*, 1105-1110.
- (9) Gaspar, H.; Cutignano, A.; Grauso, L.; Neng, N.; Cachatra, V.; Fontana, A.; Xavier, J.; Cerejo, M.; Vieira, H.; Santos, S. *Mar. Drugs* **2016**, *14*, 179-193.
- (10) Costantino, V.; Fattorusso, E.; Mangoni, A.; Di Rosa, M.; Ianaro, A. *Bioorg. Med. Chem. Lett.* **1999**, *9*, 271-276.
- (11) Subrahmanyam, C.; Kumar, S. R.; Reddy, G. D. *Indian J. Chem. Sect. B.* **2005**, *44*, 2186-2188.
- (12) Pretsch, E.; Bühlmann, P.; Badertscher, M. ¹³C NMR Spectroscopy: Coupling Constants. In *Structure Determination of Organic Compounds*; Springer-Verlag: Berlin, Heidelberg, 2009; 4th Ed.; p.149.
- (13) McLafferty, F. W.; Turecek, F. *Interpretation of Mass Spectra*, 4th ed.; University Science Books, 1993.
- (14) Jacobs, H.; Berryman, K.; Jones, J.; Gopalan, A. *Synth. Commun.* **1990**, *20*, 999-1010.
- (15) Zemplén, G.; Kuntz, A. Studien über Amygdalin, IV: Synthese des natürlichen *l*-Amygdalins. *Ber.* **1924**, *57B*, 1357-1359.
- (16) Seco, J. M.; Quiñoá, E.; Riguera, R. *Tetrahedron: Asymmetry* **2001**, *12*, 2915-2925.

-
- (17) (a) Seco, J. M.; Quiñoá, E.; Riguera, R. *Chem. Rev.* **2004**, *104*, 17-118. (b) Seco, J. M.; Quiñoá, E.; Riguera, R. *Chem. Rev.* **2012**, *112*, 4603-4641.
- (18) Hoye, T. R.; Erickson, S. E.; Erickson-Birkedahl, S. L.; Hale, C. R. H.; Izgu, E. C.; Mayer, M. J.; Notz, P. K.; Renner, M. K. *Org. Lett.* **2010**, *12*, 1768-1771.
- (19) Anita, S.; Yabuuchi, T.; Kusumi, T. *Chirality* **2003**, *15*, 609-614.
- (20) Niethe, A.; Fischer, D.; Blechert, S. *J. Org. Chem.* **2008**, *73*, 3088-3093.
- (21) Latypov, S. K.; Seco, J. M.; Quiñoá, E.; Riguera, R. *J. Org. Chem.* **1995**, *60*, 504-515.
- (22) Oishi, T.; Kanemoto, M.; Swasono, R.; Matsumori, N.; Murata, M. *Org. Lett.* **2008**, *10*, 5203-5206.
- (23) Chatterjee, A. K.; Choi, T.-L.; Sanders, D. P.; Grubbs, R. H. *J. Am. Chem. Soc.* **2003**, *125*, 37, 11360-11370.
- (24) Doi, T.; Shimizu, K.; Takahashi, T.; Tsuji, J.; Yamamoto, K. *Tetrahedron Lett.* **1990**, *31*, 3313-3316.
- (25) Chan, Y. A.; Podevels, A. M.; Kevany, B. M.; Thomas, M. G. *Nat. Prod. Rev.* **2009**, *26*, 90-114.
- (26) (a) Chan, Y. A.; Boyne, M. T. II; Podevels, A. M.; Thomas, M. G. *PNAS* **2006**, *103*, 14349-14354. (b) Chan, Y. A.; Thomas, M. G. *Biochemistry* **2010**, *49*, 3667-3677.
- (27) (a) Carter, H. E.; Nalbandov, O.; Tavormina, P. A. *J. Biol. Chem.* **1951**, *192*, 197-207. (b) Gaver, R. C.; Sweeley, C. C. *J. Am. Oil Chem. Soc.* **1965**, *42*, 294-298.
- (28) Sala, G. D.; Teta, R.; Esposito, G.; Pawlik, J. R.; Mangoni, A.; Costantino, V. *Molecules* **2017**, *22*, 1455-1465.
- (29) Kawamura, A.; Berova, N.; Dirsch, V.; Mangoni, A.; Nakanishi, K.; Schwartz, G.; Bielawska, A.; Hannun, Y.; Kitagawa, I. *Bioorg. Med. Chem.* **1996**, *4*, 1035-1043.
- (30) Jacobs, H.; Berryman, K.; Jones, J.; Gopalan, A. *Synth. Commun.* **1990**, *20*, 999-1010.
- (31) Newman-Evans, R. H.; Simon, R. J.; Carpenter, B. K. *J. Org. Chem.* **1990**, *55*, 695-711.
- (32) Anita, S.; Yabuuchi, T.; Kusumi, T. *Chirality* **2003**, *15*, 609-614.
- (33) Amatore, M.; Beeson, T. D.; Brown, S. P.; MacMillan, D. W. C. *Angew. Chem. Int. Ed.* **2009**, *48*, 5121-5124.
- (34) Alam, M.; Wise, C.; Baxter, C. A.; Cleator, E.; Walkinshaw, A. *Org. Process Res. Dev.* **2012**, *16*, 435-441.

-
- (35) Sim, I. S.; Ngai, M.-Y.; Krische, M. J. *J. Am. Chem. Soc.* **2008**, *130*, 14891-14899.
- (36) Oka, K.; Fuchi, S.; Komine, D.; Fukua, H.; Hatakeyama, S.; Ishihara, J. *Chem. Eur. J.* **2020**, *26*, 12862-12867.
- (37) Turlington, M.; Yue, Y.; Yu, X.-Q.; Pu, L. *J. Org. Chem.* **2010**, *75*, 6941-6952.
- (38) Ye, L.; He, W.; Zhang, L. *J. Am. Chem. Soc.* **2010**, *132*, 8550-8551.
- (39) Ardolino, M. J.; Morken, J. P. *J. Am. Chem. Soc.* **2012**, *134*, 8770-8773.
- (40) Sabitha, G.; Bhikshapathi, M.; Yadav, J. S. *Synthetic Communications* **2007**, *37*, 559-567.
- (41) Cluzeau, J.; Capdevielle, P.; Cossy, J. *Tetrahedron Lett.* **2005**, *46*, 6945-6948.

CHAPTER SIX. PROGRESS TOWARDS THE TOTAL SYNTHESIS OF LEPADIN I

Abstract: The following chapter details the progress made towards the total synthesis of lepadin I, a *cis*-decahydroquinoline (DHQ) alkaloid previously isolated from the ascidian *Didemnum* sp. collected in the Bahamas. Lepadin I is a selective butyrylcholinesterase (BuChE) inhibitor with an IC_{50} of 3.1 μ M and insignificant activity against acetylcholinesterase (AChE, $IC_{50} > 100 \mu$ M). The total synthesis of lepadin I proceeds through a tandem intermolecular Robinson annulation–intramolecular aza-Michael cycloaddition in the presence of the Jørgensen-Hayashi catalyst to form the *cis*-DHQ core. Extensive experiments were conducted to improve the yield of the Robinson–aza-Michael sequence, and attempts were made to install the C-5 alkyl chain by Wittig or Horner-Wadsworth-Emmons olefination. In the event, the tandem reaction stalled and the major product – that of a retro-aza-Michael reaction – was consistently isolated.

6.1 Introduction to Lepadins A–L

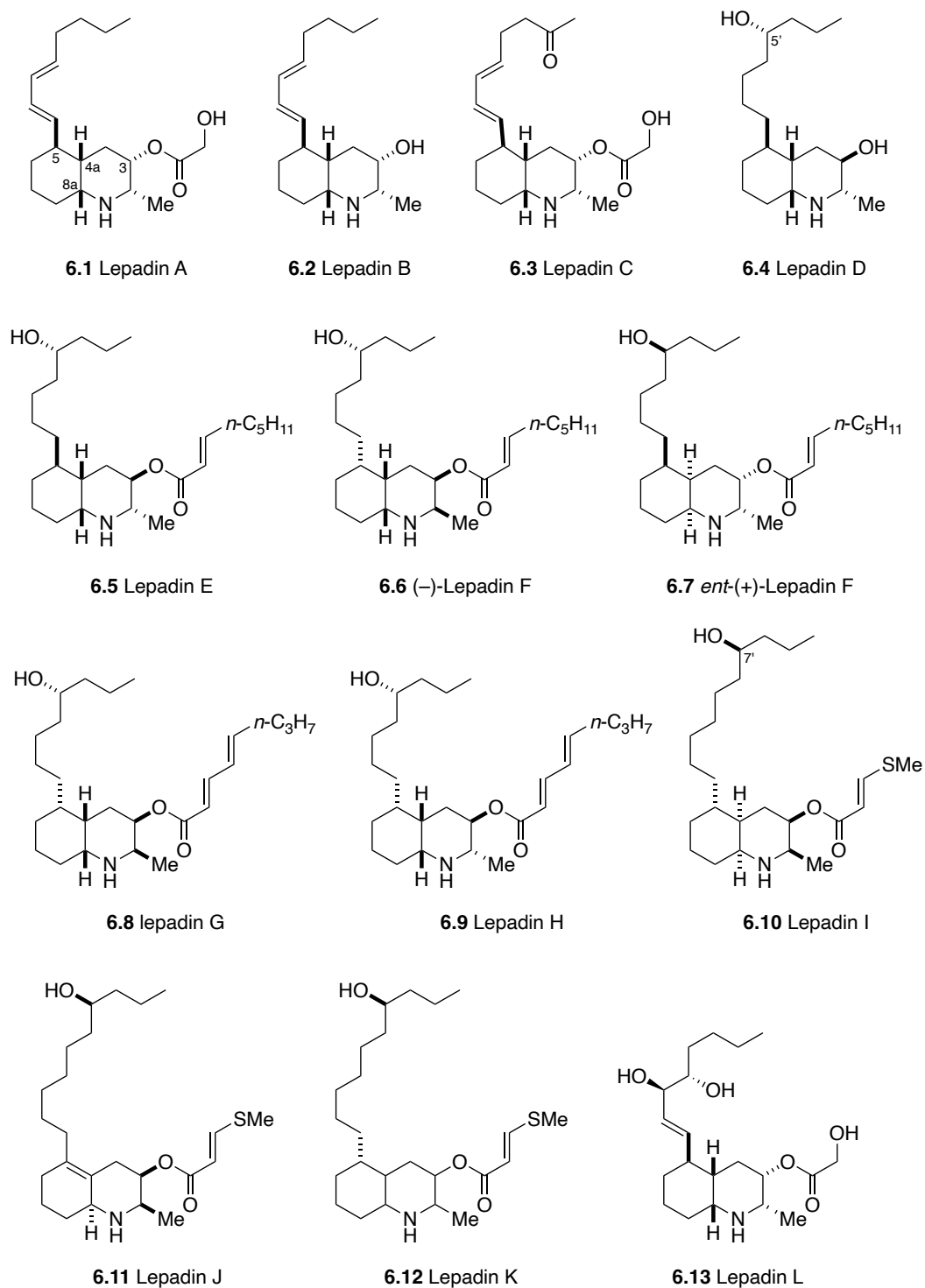


Figure 6.1: Structures of lepadins A–L.

Lepadins A–L (Figure 6.1, Table 6.1), rare DHQ alkaloids, have been isolated from ascidians including the tunicate *Clavelina lepadiformis* and its predator flatworm *Prostheceraeus*

villatus from the North Sea,¹ *C. lepadiformis* from the Mediterranean,² *Didemnum* sp. and *Aplidium tabascum* from the Great Barrier Reef,³ and *Didemnum* sp. from the Bahamas.⁴ The common core in the structures of alkaloids **6.1–6.13** comprise a *cis*-DHQ ring junction, a C-2 methyl, a C-3 hydroxyl – mostly esterified – and a functionalized 8- or 10-carbon chain pendant at C-5. Lepadins I–K are esterified as rare (*E*)-3-(methylthio)acrylates at C-3. The planar structures and relative configurations of the lepadins were determined through extensive analysis of 1D and 2D NMR spectra,^{2,4} however, all but one of the isolation reports failed to address absolute configuration (AC). This is not insignificant as the lepadins exhibit heterogeneity in both the relative configuration (RC) and AC. The ACs of lepadins A–H were assigned individually upon completion of the total syntheses by comparisons of the optical rotations of synthetic and natural products. In contrast, the absolute stereostructure of lepadin I was acquired through NOE analysis combined with exciton-coupled circular dichroism (ECCD) of the corresponding *N-p*-bromobenzamide derivative, and the advanced Mosher's analysis of the remote secondary hydroxyl in the side chain.⁴ The AC of lepadins J–L remain to be assigned, although it is likely they will be concordant with the congeneric lepadin I.

The lepadins possess a wide array of biological activities (Table 6.1). Lepadins A and B showed moderate cytotoxicity against murine leukemia P388, human breast cancer MCF7, human glioblastoma/astrocytoma U373, human ovarian carcinoma HEY, human colon LOVO, and human lung A549.^{1b} Furthermore, lepadin A exhibited potent cytotoxicity against human melanoma [A375], human colorectal carcinoma [HCT116], and mouse myoblast [C2C12], and moderate cytotoxic activity against human colon adenocarcinoma [HT29].² Investigation of lepadin A's mechanism of action on A375 cells revealed that lepadin A strongly inhibits cell migration in a wound-healing assay, induces G2/M phase cell cycle arrest by interfering with the

S phase, and impairs cell survival and reproductive integrity in a clonogenic assay.² Additionally, lepadin B is a potent blocker of $\alpha 4\beta 2$ and $\alpha 7$ neuronal nicotinic receptors expressed in *Xenopus* oocytes.⁵ Lepadins D–F exhibited antiplasmodial and antitrypanosomal activity against *Plasmodium falciparum*, and *Trypanosoma brucei rhodesiense* and *Trypanosoma cruzi*, respectively, with lepadins E and F displaying 20- and 50- fold increase in the antiplasmodial activity compared to lepadin D which correlates with the presence of the 2*E*-octenoate ester at C-3.^{3a} Lepadins E and F also showed moderate inhibitory activity of tyrosine kinase p56.³

Lepadin I (**6.10**), the focus of this work, was isolated from the ascidian *Didemnum* sp. by Molinski and coworkers.⁴ Alkaloid **6.10** is a selective BuChE inhibitor with an IC₅₀ of 3.1 μ M and negligible activity against AChE (IC₅₀ > 100 μ M).

Table 6.1: The sources and biological activities of lepadins A–L.

Compound	Species	Collection Location	Biological Activity
Lepadin A (6.1)	<i>C. lepadiformis</i> ^a	North Sea	Cytotoxic
Lepadin B (6.2)	<i>P. villatus</i> , ^b <i>C. lepadiformis</i> ^a	Bergen, Norway	Cytotoxic Blocker of $\alpha 4\beta 2$ and $\alpha 7$ neuronal nicotinic receptors
Lepadin C (6.3)	<i>P. villatus</i> , ^b <i>C. lepadiformis</i> ^a	Bergen, Norway	
Lepadin D (6.4)	<i>Didemnum</i> sp.	Queensland, Australia	Antiplasmodial Antitrypanosomal
Lepadin E (6.5)	<i>Didemnum</i> sp.	Queensland, Australia	Tyrosine kinase p56 inhibitor Antiplasmodial Antitrypanosomal
(–)-Lepadin F (6.6)	<i>Didemnum</i> sp.	Queensland, Australia	Tyrosine kinase p56 inhibitor Antiplasmodial Antitrypanosomal
ent-(+)-Lepadin F (6.7)	<i>A. tabascum</i> ^c	Queensland, Australia	
Lepadin G (6.8)	<i>A. tabascum</i>	Queensland, Australia	
Lepadin H (6.9)	<i>A. tabascum</i>	Queensland, Australia	
Lepadin I (6.10)	<i>Didemnum</i> sp.	Bahamas	BuChE inhibitor
Lepadin J (6.11)	<i>Didemnum</i> sp.	Bahamas	
Lepadin K (6.12)	<i>Didemnum</i> sp.	Bahamas	
Lepadin L (6.13)	<i>C. lepadiformis</i> ^a	Napoli, Italy	

^a*Clavelina lepadiformis*. ^b*Prostheceraeus villatus*. ^c*Aplidium tabascum*.

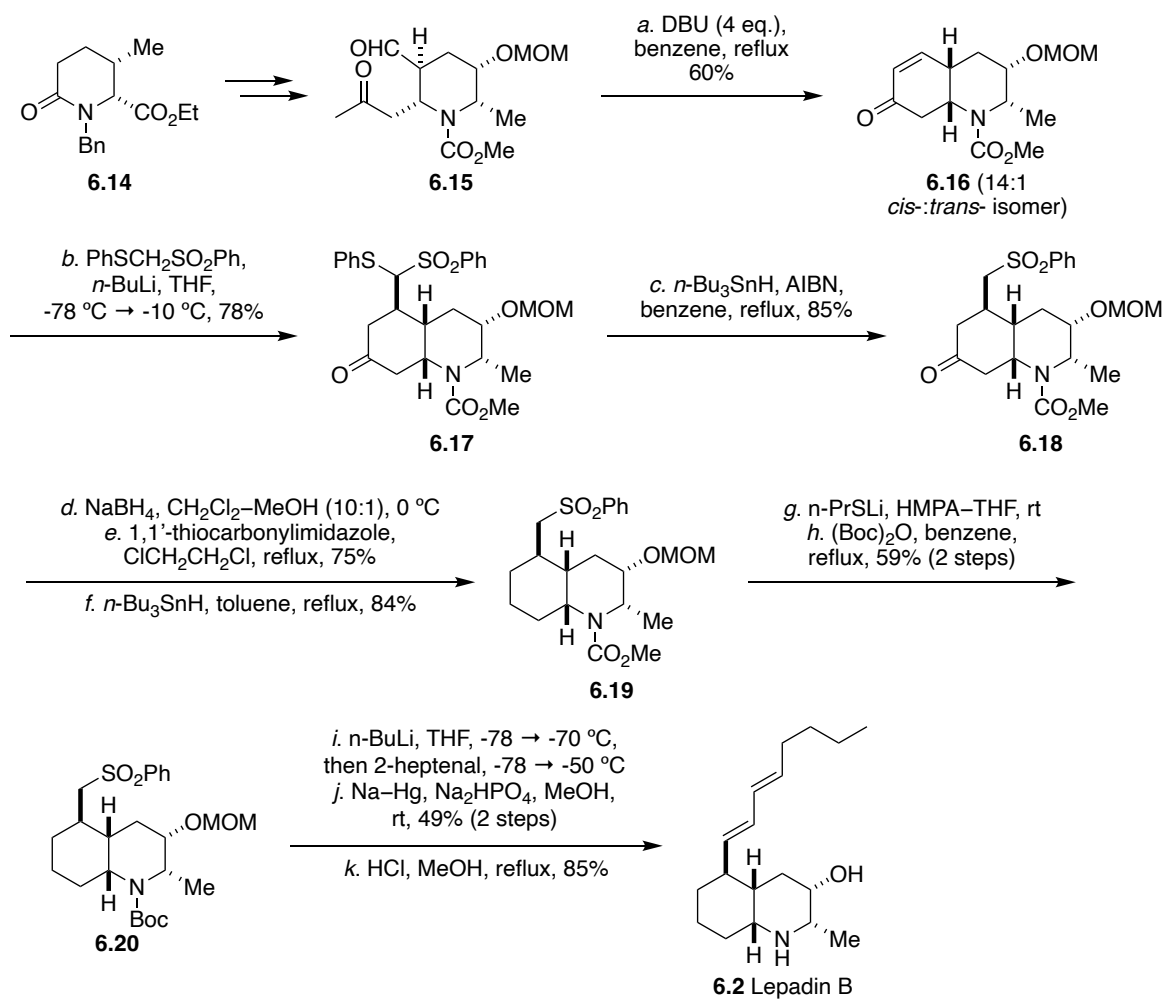
6.2 Select Total Synthesis

Several asymmetric syntheses of lepadins have been published showcasing a variety of strategies for the asymmetric construction of the *cis*-DHQ ring system (Table 6.2). Total synthesis of the lepadins enabled assignment of the AC of lepadins A–H and procured sufficient material for the evaluation of the relevant biological activities of these alkaloids. Five of these synthetic efforts have been selected for further discussion; the remaining synthetic routes will be briefly highlighted to showcase the diverse strategies to assemble the *cis*-DHQ ring system.

Table 6.2: Literature syntheses of lepadins A–I.

Author	Year	Compound	Synthetic Route	Ref.
Toyooka	1999	(–)-Lepadine B	Intramolecular Aldol Cyclization	6
Kibayashi	2000	(–)-Lepadine B	Intramolecular Diels-Alder Cyclization	7a
Kibayashi	2001	(–)-Lepadine A–C	Intramolecular Diels-Alder Cyclization	7b
Pu and Ma	2004	Lepadins A–E, H	Enamine Cyclization	8
	2006			
Charette	2008	<i>ent</i> -Lepadine B	Ring-Opening/ Ring-Closing Metathesis	12
Blechert	2008	<i>ent</i> -Lepadins F and G	Ring-Closing Metathesis	9
Hsung	2008	<i>ent</i> -Lepadins F and G	Aza-Cycloaddition	13
	2009			
Bosch	2013	(–)-Lepadins A–C,	Cyclocondensation	14
	2015	(+)-Lepadine D		
Chen	2017	Lepadins B and F	Intermolecular Diels-Alder Cyclization	15
	2021			
Tong	2021	Lepadine A–E, H, <i>ent</i> -I	Intramolecular [3+2] cycloaddition	11

6.2.1 Toyooka's Approach to (–)-Lepadine B



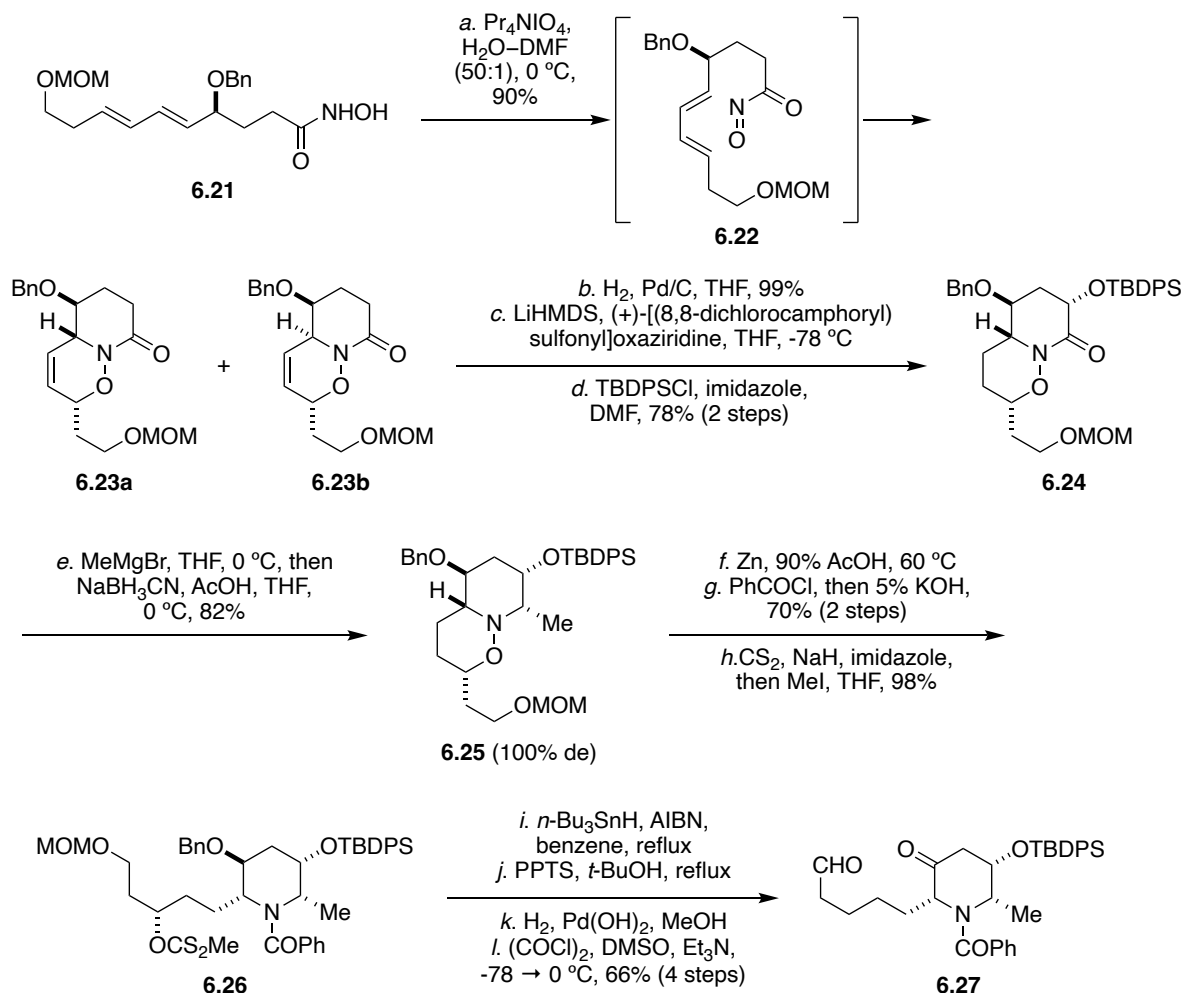
Scheme 6.1: Toyooka and co-workers' total synthesis of lepadin B. See reference 6.

The first total synthesis of (–)-lepadin B (> 30 steps, Scheme 6.1), reported in 1999 by Toyooka and colleagues, employed an intramolecular aldol cyclization of a functionalized piperidine (**6.15**), obtained from enantiopure hydroxy ester **6.14** in 13 steps, to form the desired 4a,8a-*cis*-octahydroquin-7-one core (**6.16**) in 60% as a 14:1 mixture of the *cis*-/*trans*- isomers.⁶ 1,4-Conjugate addition of the nucleophilic conjugate base of phenylthiomethyl phenyl sulfone to enone **6.16** provided a 2:1 mixture of diastereoisomers (**6.17**). Subsequent radical reduction of the phenylthio moiety gave the sulfone as a single diastereoisomer in 85%. NaBH₄ reduction of **6.18** was followed by Barton-McCombie deoxygenation of the secondary HO group. Thiocarbonylation

of the alcohol furnished the Barton's ester, which was then converted to the deoxygenated product **6.19** after radical reduction with *n*-Bu₃SnH. Protecting group swap generated the Boc-protected amine **6.20** in 59%. Lastly, Julia olefination of 2-heptenal with **6.20** under standard conditions, and subsequent MOM-deprotection of the resultant diene afforded (–)-lepadin B.

Shortly afterwards, Kibayashi's group published a second total synthesis of (–)-lepadin B that utilized an intramolecular Diels-Alder cyclization of an acylnitroso derivative to a *trans* cycloadduct followed by an intramolecular aldol reaction.⁷ Both Toyooka and Kibayashi's routes required lengthy linear reaction sequences that are greater than 30 steps.

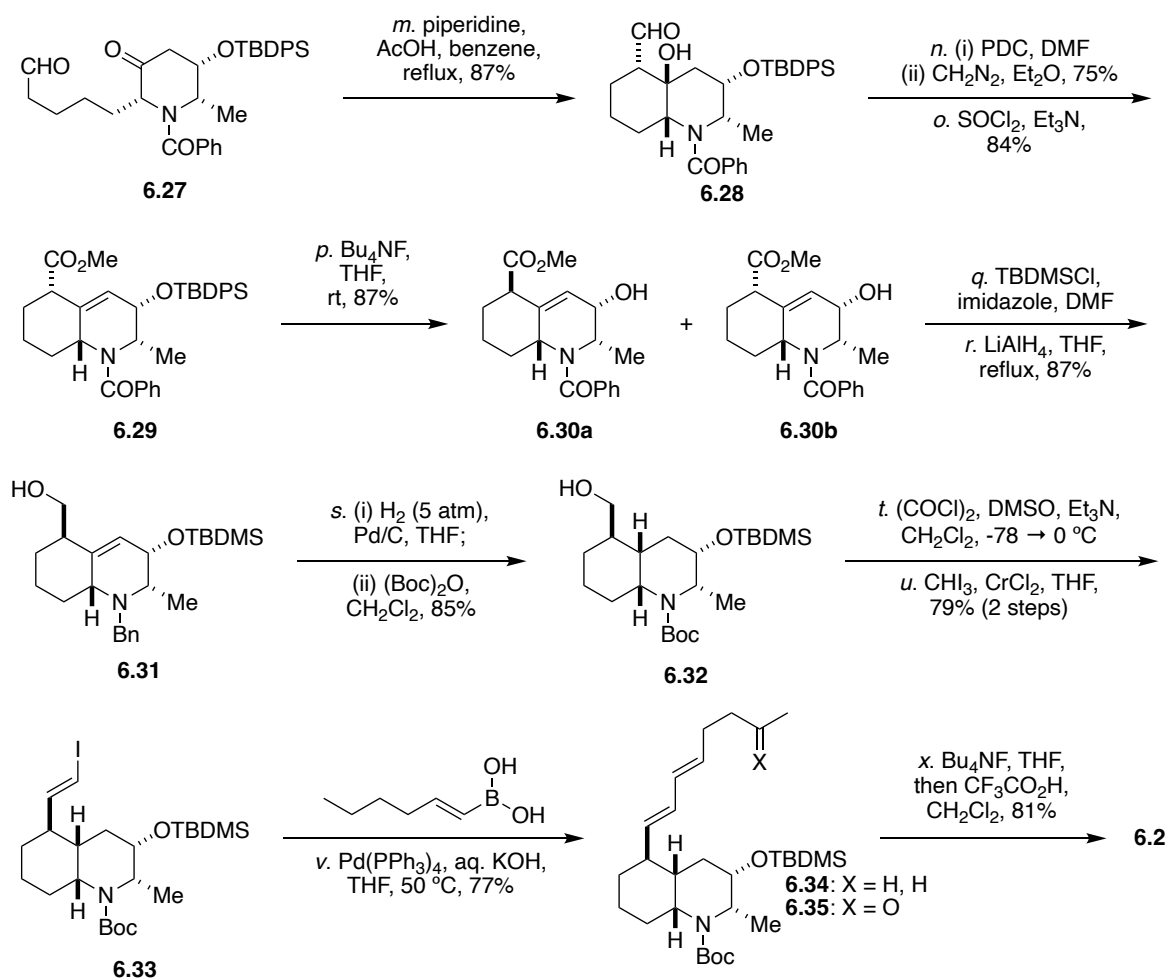
6.2.2 Kibayashi's Approach to (–)-Lepadin A–C



Scheme 6.2: Kibayashi's synthesis of the keto aldehyde intermediate **6.27**. See reference 7.

In 2000 and 2001, Kibayashi reported the total synthesis of (-)-lepadins A–C via a stereocontrolled intramolecular acylnitroso Diels–Alder reaction to access *trans*-1,2-oxazinolactam, an intramolecular aldol reaction to form the *cis*-DHQ, and a Suzuki cross-coupling to elaborate the C-5 alkyl chain.⁷ Oxidation of the hydroxamic acid **6.21**, derived from L-malic acid, gave the acylnitroso compound **6.22** which underwent cycloaddition, in aqueous media, to provide *trans*-cycloadduct (**6.23a,b**) as a 6.6:1 mixture of the *trans*-/*cis*- isomers. Hydrogenation of the vinyl bond in **6.23a** followed by oxidation of the lithium enolate with the Davis reagent, (+)-[(8,8-dichlorocamphoryl)sulfonyl]oxaziridine, and subsequent TBDPS-protection of the

resultant alcohol afforded the silyl ether with high diastereoselectivity in 78% (3 steps). A tandem Grignard addition of methylmagnesium bromide and subsequent NaBH₃CN reduction of the intermediate aminal in acidic media delivered **6.25** as a single diastereoisomer in 82% (2 steps). Zn-catalyzed reductive cleavage of the N–O bond provided the amino alcohol. *N*-benzylation of the resultant amine and successive transformation of the alcohol gave the methyl xanthate ester **6.26** in 70% (3 steps). Xanthate **6.26** was subjected to a 4-step sequence (Barton-McCombie reduction, de-benzylation, MOM-deprotection, Swern oxidation) to obtain the keto aldehyde **6.27**.



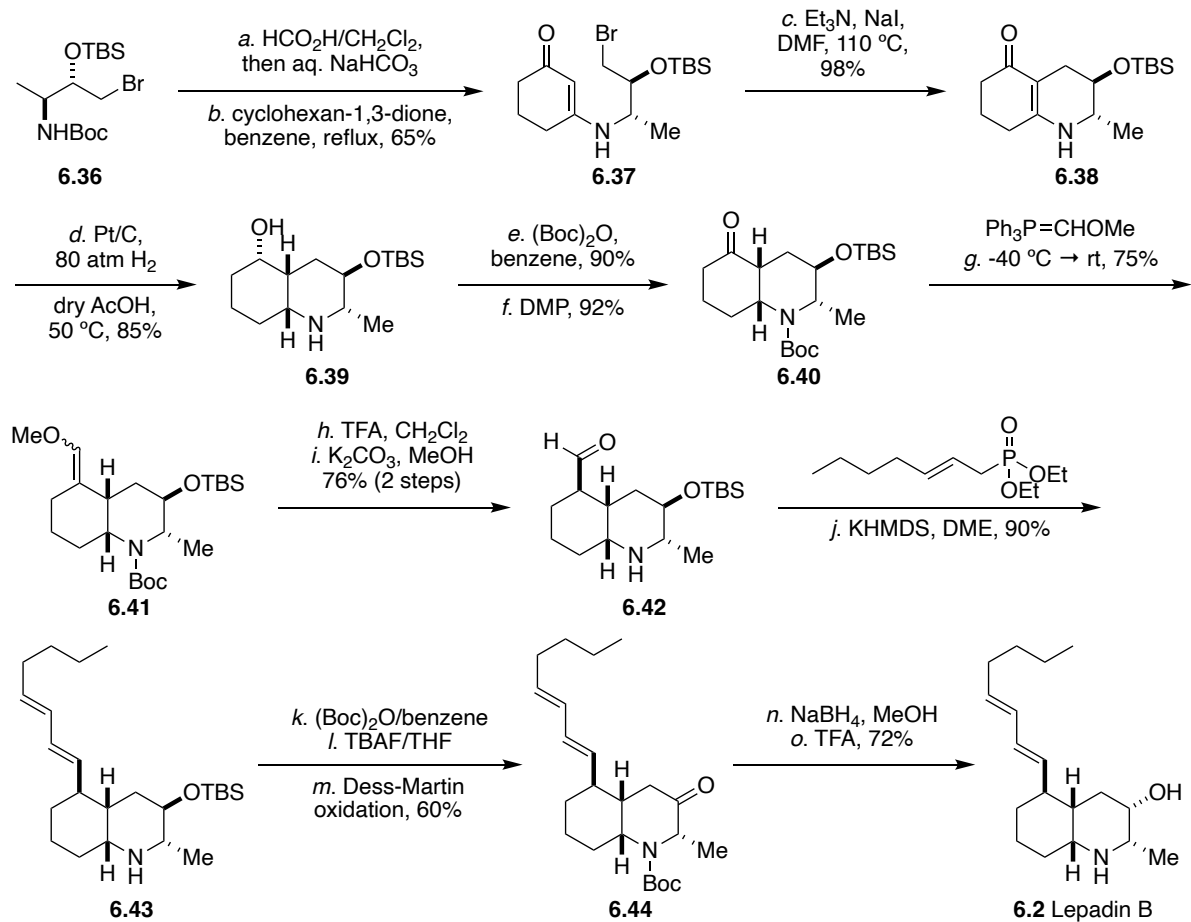
Scheme 6.3: Kibayashi's synthesis of lepadin B (**6.2**). See reference 7.

The remainder of the synthesis of lepadin B followed Scheme 6.3. Intramolecular aldol condensation of **6.27** in the presence of catalytic piperidinium acetate in refluxing benzene

furnished β -hydroxyaldehyde **6.28** as a single diastereoisomer in 87%. The octahydroquinoline **6.29** was obtained after the oxidation of aldehyde **6.28** and capture of the product carboxylic acid (diazomethane) as a methyl ester, followed by dehydration with thionyl chloride. Desilylation of the TBDPS ether in **6.29** upon treatment with TBAF also effected epimerization at C-5 and gave a 2:1 mixture of the α - and β - esters **6.30a** and **6.30b**, respectively. Silylation of the desired β -isomer (**6.30a**) followed by LiAlH₄ reduction delivered the benzyl alcohol **6.31** in 87%. The desired *cis*-DHQ was obtained in 85% upon catalytic hydrogenation of the octahydroquinoline **6.31** and subsequent N-Boc protection. Swern oxidation and Takai olefination of the resultant aldehyde gave the (*E*)-alkenyl iodide **6.33** in 79%. Palladium catalyzed Suzuki cross-coupling with (*E*)-hexen-1-ylboronic acid and subsequent global deprotection delivered the natural product (–)-lepadin B (**6.2**).

(–)-Lepadins A and C were synthesized in a procedure that paralleled the elaboration of (–)-lepadin B.^{7b} Desilylation (Bu₄NF, THF, rt, 96%) of **6.34** followed by condensation with TIPS-protected glycolic acid (DCC, cat. DMAP, CH₂Cl₂, 84%) and simultaneous Boc- and TIPS-deprotection (BF₃·Et₂O, MeCN, 0 °C, 97%) furnished (–)-lepadin A (**6.1**). (–)-Lepadins C (**6.3**) was prepared from intermediate **6.33** in a five-step sequence. Suzuki cross coupling of **6.33** with (*E*)-hexen-1-ylboronic acid followed by Swern oxidation furnished intermediate **6.35**, which was converted to lepadin C in a sequence analogous to preparation of lepadin A. The synthesis of (–)-lepadins A–C by Kibayashi and coworkers required >38 steps, most of which (like Toyooka's synthesis) were employed to build the piperidine ring; in contrast, Pu and Ma's compact preparation of the *cis*-DHQ core of lepadins A–E and H was accomplished in only eight steps through an enamine cyclization.⁸

6.2.3 Pu and Ma's Approach to (-)-Lepadin A–E and H



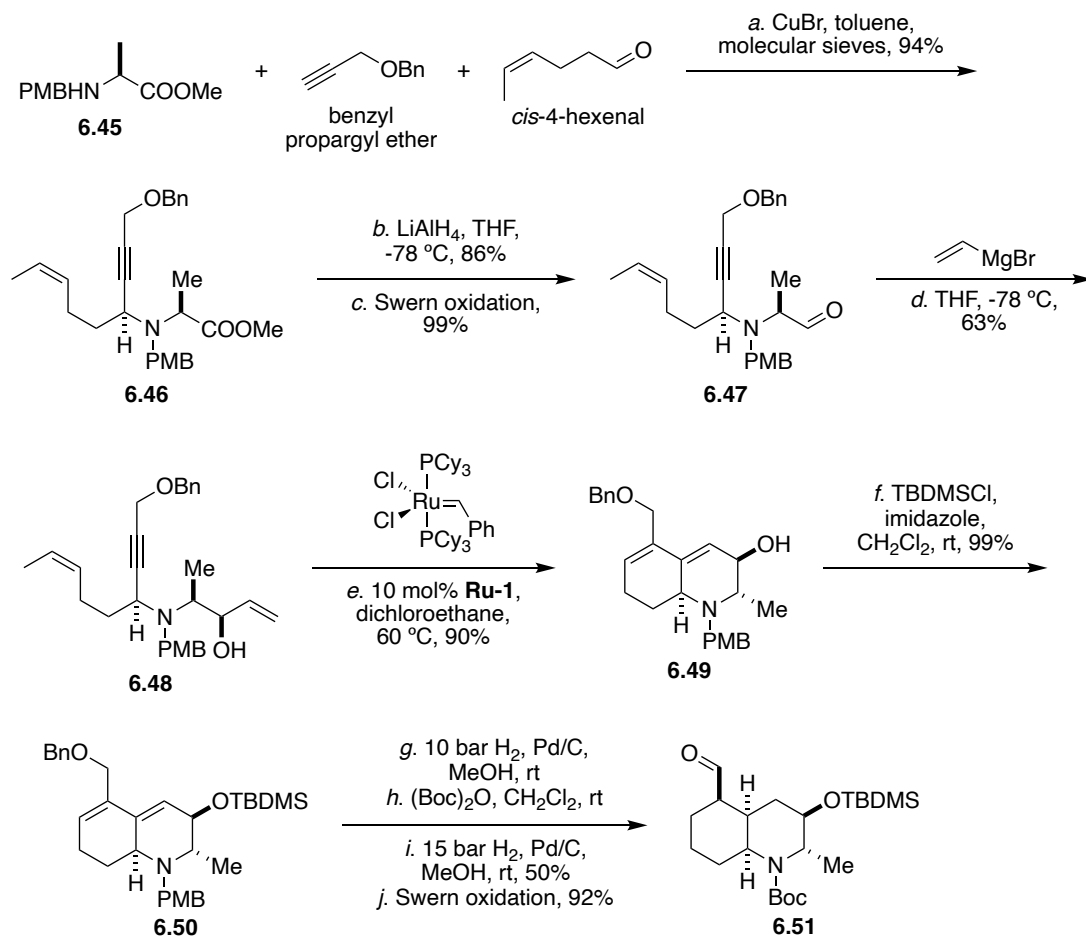
Scheme 6.4: Pu and Ma's synthesis of lepadin B. See reference 8.

Pu and Ma's total synthesis of lepadin B (Scheme 6.4) commenced with the condensation of the primary amine, obtained by Boc removal of L-alanine-derived **6.36**, with cyclohexan-1,3-dione in refluxing benzene to deliver enamine **6.37** in 65%.⁸ Subsequent alkylative cyclization of enamine **6.37** delivered enone **6.38** in excellent yield. The following challenging diastereoselective hydrogenation of the C=C bond, accompanied by ketone reduction, (Pt-C, anhydrous AcOH, 80 atm H₂, 50°) delivered H₂ from the *re* face giving 2° alcohol **6.39**. Reinstallation of the Boc-group and restoration of the ketone (Dess-Martin periodinane) furnished **6.40**, which was homologated in two steps: Wittig olefination at C-5 to methyl enol ether **6.41**, and acid hydrolysis-equilibration,

and concomitant loss of Boc, delivered aldehyde **6.42** as a single isomer with the desired β -orientation.

The assembly of lepadin B proceeded as follows. Horner-Wadsworth-Emmons (HWE) olefination gave the desired *E,E*-diene **6.43** in 90% yield and > 95% selectivity. The configuration at C-3 was re-set using an oxidation-reduction strategy. Boc-protection of **6.43** followed by TBAF-promoted cleavage of the silyl ether and subsequent DMP oxidation provided ketone **6.44** in 60% which was reduced (NaBH₄) to the corresponding α -alcohol as a single diastereoisomer. Removal of the Boc group (TFA) delivered (–)-lepadin B. Lepadins A and C were prepared, from the NaBH₄ reduction product of **6.44**, in an analogous sequence as described above.⁷

6.2.4 Blechert's Approach to *ent*-Lepadins F and G



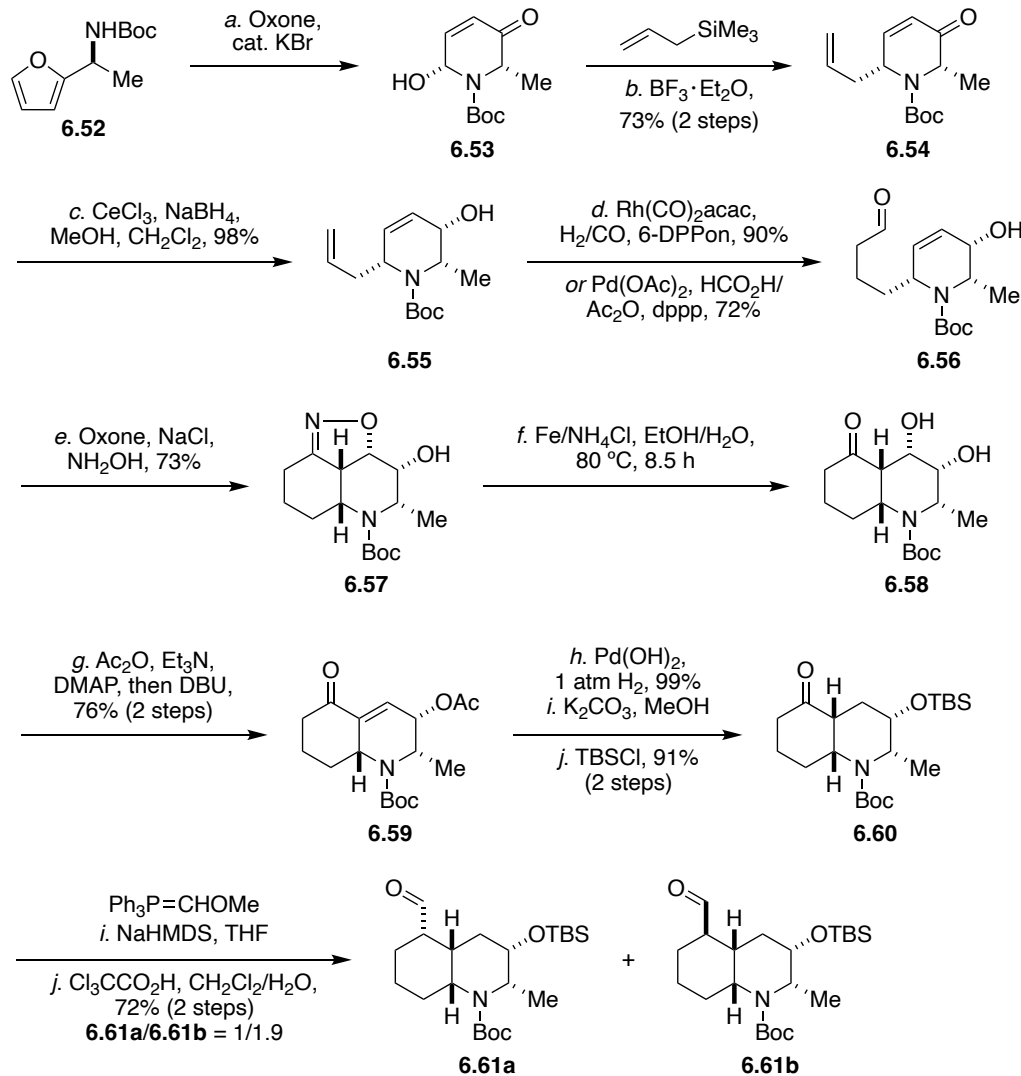
Scheme 6.5: Blechert's synthesis of common intermediate **6.51**. See reference 9.

Blechert and coworkers reported the first enantioselective syntheses of *ent*-lepadins F and G in which they employed a tandem ene-yne-ene ring closing metathesis and stereoselective hydrogenation of the resultant diene.⁹ Compound **6.45**, derived from L-alanine, was condensed with *cis*-4-hexenal, and the resultant intermediate iminium species was subjected to an in situ Cu(I)-catalyzed addition of benzyl propargyl ether to deliver an inseparable mixture of propargylamines (1:2 ratio), including the preferred **6.46**. Subsequent LiAlH₄ reduction and separation of the resultant alcohols by column chromatography followed by Swern oxidation gave aldehyde **6.47** as a single isomer. Grignard addition of vinylmagnesium chloride furnished the allylic alcohol **6.48** in 63% as a single diastereoisomer. Grubbs-mediated tandem ene-yne-ene

ring-closing metathesis of the acyclic precursor **6.48** in dichloroethane at 60 °C provided diene **6.49** in 90%. TBDMS-protection of the 2° OH gave the silyl ether **6.50**, which was transformed by a four step sequence to the key intermediate **6.51**. Concurrent catalytic diastereoselective reduction of the diene and cleavage of the *p*-methoxybenzyl group, followed by Boc-protection of the amine, subsequent removal of the benzyl group, and Swern oxidation of the resulting alcohol delivered aldehyde **6.51**.

Aldehyde **6.51** is similar to intermediate **6.42** that was prepared by Pu and Ma in their total synthesis of lepadins A–C.⁸ Blechert et. al. elaborated the alkyl chain at C-5 in a Julia-Kocienski olefination with the respective sulfone and intermediate **6.51**.⁹ Inversion of C-3 stereochemistry was accomplished by a DMP oxidation of the 2° OH at C-3 and NaBH₄ reduction of the resultant ketone. Yamaguchi esterification at the C-3 OH with 2*E*-octenoic acid and 2*E*,4*E*-octadienoic acid provided (+)-lepadins F (+8.8 (*c* = 0.25, CHCl₃); +1.5 (*c* = 0.27, CH₂Cl₂)) and (–)-G (–14.5 (*c* = 0.27, CH₂Cl₂)), respectively. Comparison of the optical rotations of the synthetic lepadins F and G with those of the natural products indicated that Blechert and coworkers synthesized the corresponding enantiomers of natural (–)-lepadin F (–1.5 (*c* = 0.1, CHCl₃)^{3a}; +5.5 (*c* = 0.12, CH₂Cl₂)^{3b}) and (+)-G (+12.5 (*c* = 0.31, CH₂Cl₂)^{3a}). While the two reported optical rotations (the magnitudes are small) of natural lepadin F are in opposition, Blechert critically concluded that they had synthesized the enantiomer of lepadin F: Kaminsky et. al. isolated lepadin F as a red oil with a positive [α]_D,^{3a} whereas Quinn and coworkers reported lepadin F as a colorless oil with a negative [α]_D.^{3b} Blechert chose to compare [α]_D based on the latter report and concluded that they had synthesized the enantiomer, but this is somewhat arbitrary as both antipodes exist in nature. The subject of rotations of small magnitudes has been addressed recently.¹⁰

6.2.5 Tong's Approach to Lepadins A-E, H, and *ent*-I

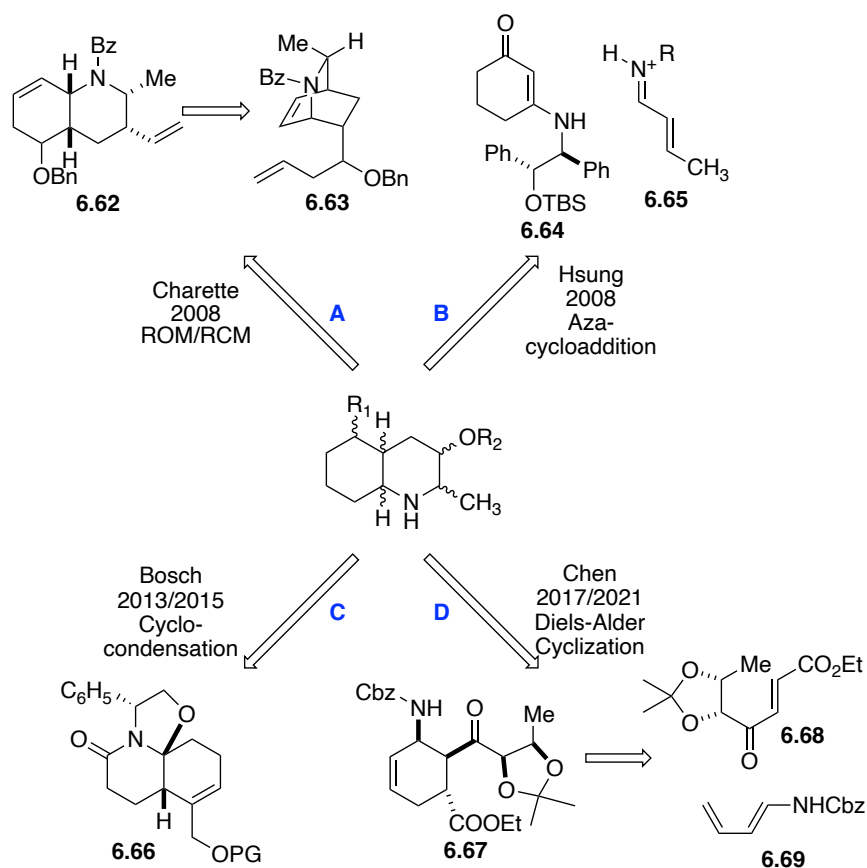


Scheme 6.6: Tong's synthesis of common intermediates **6.62a,b**.

Recently, Tong and coworkers published the total synthesis of lepadins A–E, H, and *ent*-I (Scheme 6.6).¹¹ The authors developed a five-step sequence to synthesize the DHQ core from the known *N*-Boc-1-(furan-2-yl)ethylamine (**6.52**). Aza-Achmatowicz rearrangement of **6.52**, mediated with Oxone-catalytic KBr, delivered enone **6.53**, which was allylated with allylsilane to provide **6.54** in 73% (2 steps). Luche reduction of enone **6.54** furnished the allylic alcohol **6.55**, and subsequent rhodium- or palladium-catalyzed hydroformylation gave **6.56**. Oximation of the

keto group, and oxidation to the nitrile oxide (Oxone) was followed by spontaneous intramolecular [3+2] cycloaddition to afford the tricyclic isooxazoline **6.57** in good yield. The isooxazoline was then further elaborated into the DHQ core. Reductive cleavage of the N–O bond (Fe° , NH_4Cl , hot EtOH) and subsequent acetylation-dehydration gave enone **6.59** in 76% (2 steps). Heterogeneous catalytic hydrogenation with Pearlman's catalyst ($\text{Pd}(\text{OH})_2$, H_2) followed by deacetylation-silylation delivered the 3-*O*-TBS *cis*-DHQ **6.60** in 91% (3 steps). Ketone **6.60** is functionalized similarly to intermediate **6.40** in Pu and Ma's total synthesis.⁸ Ketone homologation (Wittig reaction, acid hydrolysis) afforded a consequential mixture of diastereoisomers in a 1:1.9 ratio of **6.61a/6.61b**, respectively: 5*S*-**6.61a** was utilized in the total synthesis of lepadins D, E and H; whereas the 5*R*-**6.61b** isomer was employed in the total synthesis of lepadins A–C and *ent*-I. Notably, Pu and Ma developed a three step sequence to procure **6.61** as a single diastereoisomer (see Scheme 6.4, compound **6.42**) through a one-carbon Wittig homologation followed by simultaneous Boc-deprotection and cleavage of the methyl enol ether (TFA, CH_2Cl_2), and subsequent equilibration of the C-5 epimers (K_2CO_3 , MeOH).

6.2.6 Other Synthetic Routes Towards Lepadins A–H

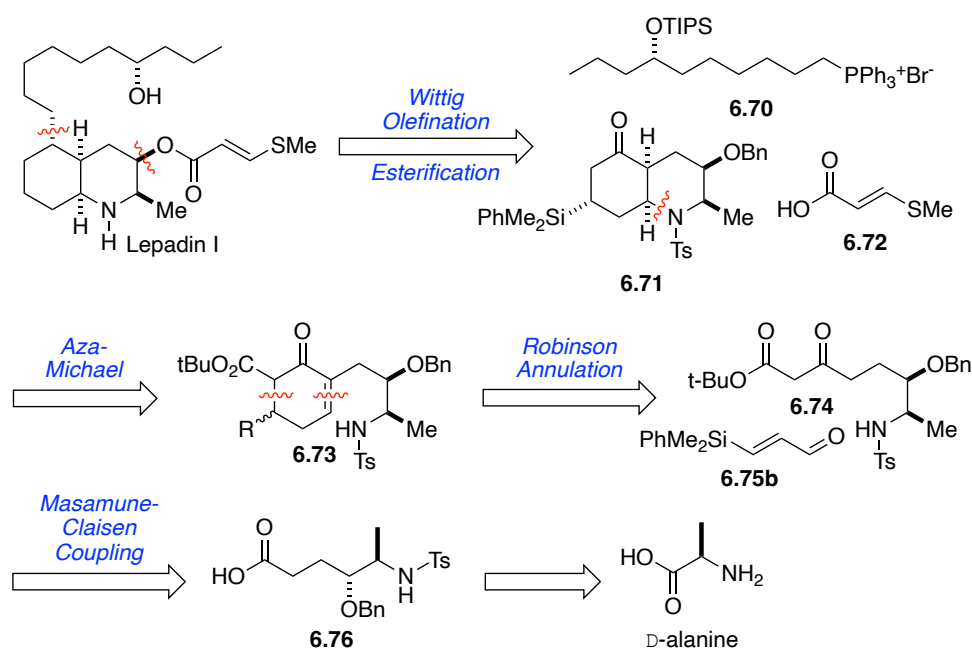


Scheme 6.7: Retrosynthetic approaches to the lepadins.

Several other routes were developed to access the *cis*-fused DHQ core. In 2008, Barbe and Charette published their synthetic route towards (+)-lepadin B, in which they built a *cis*-fused polyhydroquinoline (**6.62**) through a tandem ring-opening–ring-closing metathesis of bicyclic diene **6.63**, obtained through a regio- and diastereoselective Diels-Alder cycloaddition (Scheme 6.7).¹² Simultaneously, Hsung and colleagues utilized their own intramolecular [3+3] aza-cycloaddition of a chiral enamine (**6.64**) with a crotonaldehyde-derived iminium species (**6.65**) to build the bicyclic core of (+)-lepadin F.¹³ In 2013, Bosch and colleagues reported the total synthesis of (–)-lepadins A–C and (+)-lepadin D through a common oxazoloquinolone (**6.66**).¹⁴ Recently, Chen and coworkers published their approach towards (–)-lepadins A–C from 5-deoxy-D-ribose.¹⁵ They developed a stereocontrolled Diels-Alder cycloaddition between the chiral

dienophile **6.68** and the acylamino diene **6.69** to construct the trisubstituted cyclohexene **6.67** that was further elaborated to the *cis*-DHQ intermediate in a one-pot five step sequence of hydrogenation-cyclization. Though several elegant routes have been published to access the lepadin alkaloids, it's important nonetheless to investigate new feasible and efficient synthetic routes towards these natural products. Herein, we describe our approach to build the bicyclic core of lepadin I in a one-pot Robinson annulation–aza-Michael cycloaddition sequence.

6.3 Retrosynthesis of Lepadin I



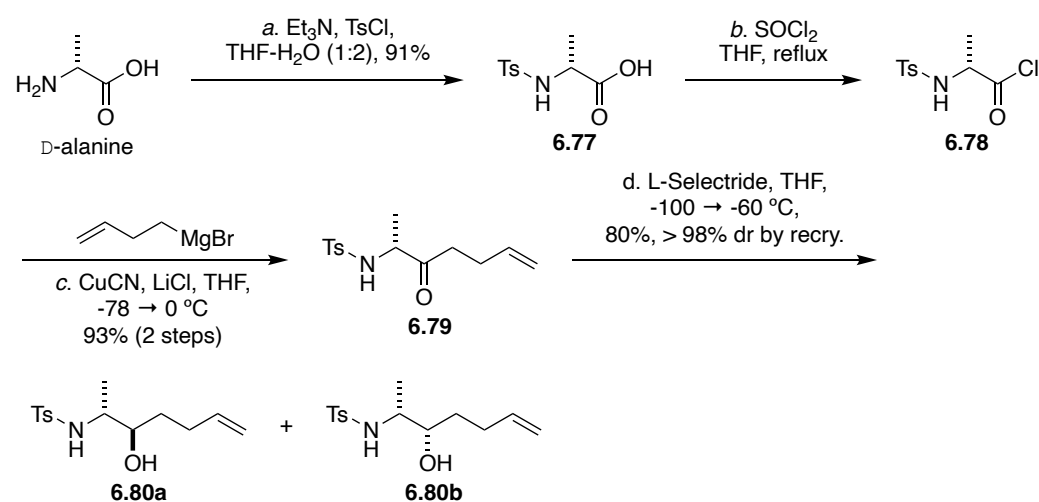
Scheme 6.8: Proposed retrosynthesis of lepadin I.

The proposed total synthesis of lepadin I proceeds through a tandem intermolecular Robinson annulation/ intramolecular aza-Michael cycloaddition of the β -ketoester **6.74** and aldehyde **6.75b** to form the *cis*-DHQ core as depicted in Scheme 6.8. The β -ketoester is obtained via a Masamune Claisen coupling of carboxylic acid **6.76**, derived from *D*-alanine, with mono-*tert*-butyl malonate. The alkyl chain at C-5 is installed by Wittig olefination followed by a stereoselective hydrogenation. The final step involves the esterification of the C-3 hydroxyl with

(*E*)-3-(methylthio)acrylic acid. The proposed synthesis exploits easily accessible building blocks including D-alanine and (*S*)-epichlorohydrin and affords a flexible route to the synthesis of other analogues of lepadin I.

6.4 Synthesis of Lepadin I

6.4.1 Synthesis of β -Ketoester 6.74



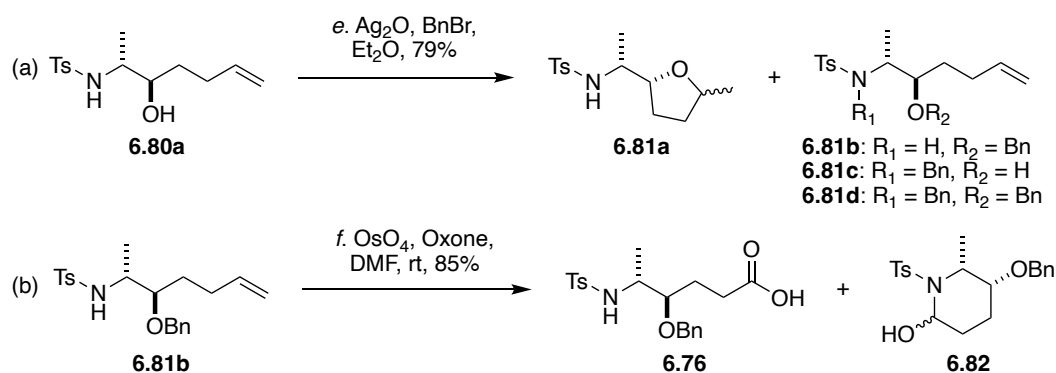
Scheme 6.9: Synthesis of the amino alcohol **6.80a**.

Table 6.3: Reductive conditions of **6.79** to **6.80a,b**.

Entry	Condition	6.80a:6.80b
1	NaBH_4 , MeOH , $0 \text{ }^\circ\text{C}$, 30 min	1:1.4
2	$\text{Zn}(\text{BH}_4)_2$, THF , $-15 \text{ }^\circ\text{C}$, 5 h	1:0.5
3	$\text{Zn}(\text{BH}_4)_2$, THF , $-78 \text{ }^\circ\text{C}$, 20 h	1:0.7
4	L-Selectride, THF , $-100 \rightarrow -60 \text{ }^\circ\text{C}$, 4 h	1:0.05

N-Tosylation of D-alanine (Scheme 6.9) and conversion to the acyl chloride **6.78** followed by addition of 4-butenylmagnesium-cuprate gave the α -methyl- β -keto product **6.79** in 93% (2 steps from **6.77**). Reduction of the ketone was surveyed under different conditions (Table 6.3). Stereoselective reduction of the product ketone with L-Selectride, under Cram selection,¹⁶ delivered the amino alcohol **6.80a** after recrystallization (>98% dr). Attempted reduction with

either NaBH₄ or Zn(BH₄)₂ in THF gave close to equimolar ratios of diastereomers. Diastereoselectivity of reduction with either the NaBH₄ or Zn(BH₄)₂ are substrate dependent. Non-chelating NaBH₄ reduction of *N,N*-dibenzyl amino ketones favors the formation of the *threo*-diastereoisomer (*anti*-2-alkyl-3-hydroxy) with high stereoselectivity (>90%).¹⁷ In contrast, chelating Zn(BH₄)₂ favors predominately the *erythro*-diastereoisomer (*syn*-2-alkyl-3-hydroxy) in the reduction of phenyl- or vinyl-conjugated α -hydroxyl β -ketones.¹⁸



Scheme 6.10: (a) Selective benzyl-protection of **6.80a**, and (b) oxidative cleavage of **6.81b** to **6.76**.

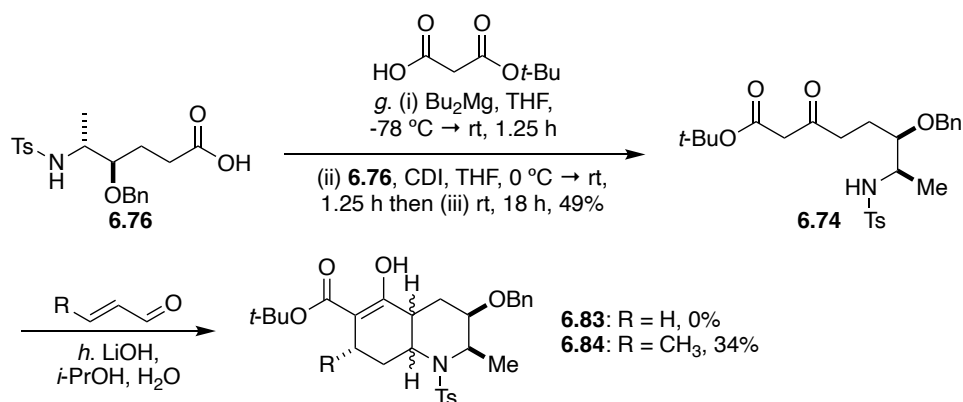
Table 6.4: Attempted conditions for *O*-selective benzylation and oxidative cleavage.

Entry	Substrate	Condition	Product (%)
1	6.80a	CCl ₃ (C=NH)OBn ^a , TfOH, <i>c</i> -C ₆ H ₁₂ -CH ₂ Cl ₂	6.81a
2	6.80a	NaH, BnBr, Bu ₄ NI, THF, 0 °C → rt	6.81c (55%), 6.81d (5%)
3	6.80a	NaH, BnBr, THF, 0 °C → rt	N.R.
4	6.80a	Ag ₂ O, BnBr, Et ₂ O, rt	6.81b (79%), 6.81d (7%)
5	6.81b	RuCl ₃ · <i>n</i> H ₂ O, NaIO ₄ , 2:2:3 CCl ₄ /MeCN/H ₂ O, rt	Complex mixture
6	6.81b	OsO ₄ , NaIO ₄ , 2,6-lutidine, 3:1 dioxane/H ₂ O, rt	6.82

a. Benzyl 2,2,2-trichloroacetimidate.

Silver-promoted *O*-selective benzylation of **6.80a** (79%) was achieved under near neutral conditions (Ag₂O, BnBr, Et₂O, Table 6.4, Scheme 6.10).¹⁹ Benzyl protection of **6.80a** under acidic conditions (entry 1) resulted in the tetrahydrofuran product **6.81a**.²⁰ In contrast, attempted selective benzylation of the secondary alcohol in the presence of the NH under basic conditions (entry 2) gave a mixture of undesired *N*- and *N,O*-benzylated products, **6.81c** and **6.81d**, in 55% and 5%,

respectively.²¹ In the absence of tetrabutylammonium iodide, the reaction returned only starting material (entry 3). Similarly, oxidative cleavage of the terminal olefin in **6.81b** to the carboxylic acid **6.76** was accomplished with OsO₄ and Oxone in DMF in 85%.²² Ruthenium (Table 6.4, entry 5) or Johnson-Lemieux²³ (Table 6.4, entry 6) oxidation of **6.81b** failed to afford the desired product. A complex mixture was observed in the per-ruthenate oxidation, whereas in the Johnson-Lemieux oxidation, the 6-membered cyclic aminal **6.82** was the sole product.



Scheme 6.11: Preparation of **6.74** and tandem Robinson annulation–aza-Michael cyclization with acrolein or crotonaldehyde.

Homologation of the carboxylic acid **6.76** to the β -ketoester **6.74** was achieved in 49% under Masamune conditions (Scheme 6.11).²⁴ Robinson annulation of the β -ketoester with acrolein was unsuccessful likely due to the polymerization of acrolein under reaction conditions. Subsequent Robinson annulation and aza-Michael cyclization with crotonaldehyde afforded a mixture of three of the four possible diastereoisomers of **6.84** in 34% yield.²⁵ NOE correlations identified the major diastereoisomer as 4a*S*,7*S*,8a*S*-**6.84** as depicted in Figure 6.2. Thus, the Robinson–aza-Michael sequence was repeated with a ‘traceless’ surrogate of acrolein in the presence of a L- or D-prolinol catalyst to improve the yield and control the configurational outcome in the same manner as crotonaldehyde. To this end, aldehydes **6.75a–d** and **6.75e** were synthesized

from 2-propyn-1-ol and propiolic acid, respectively. Protodesilylation of the *Z*-dimethyl-silyl or reductive removal of the Br-substituted analog of **6.84** would deliver an intermediate with the desired ring-junction stereochemistry for the synthesis of lepadin I.

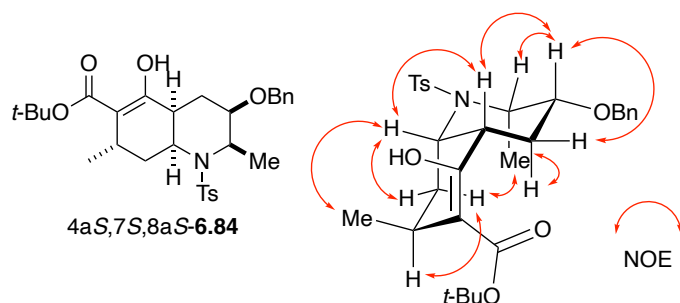
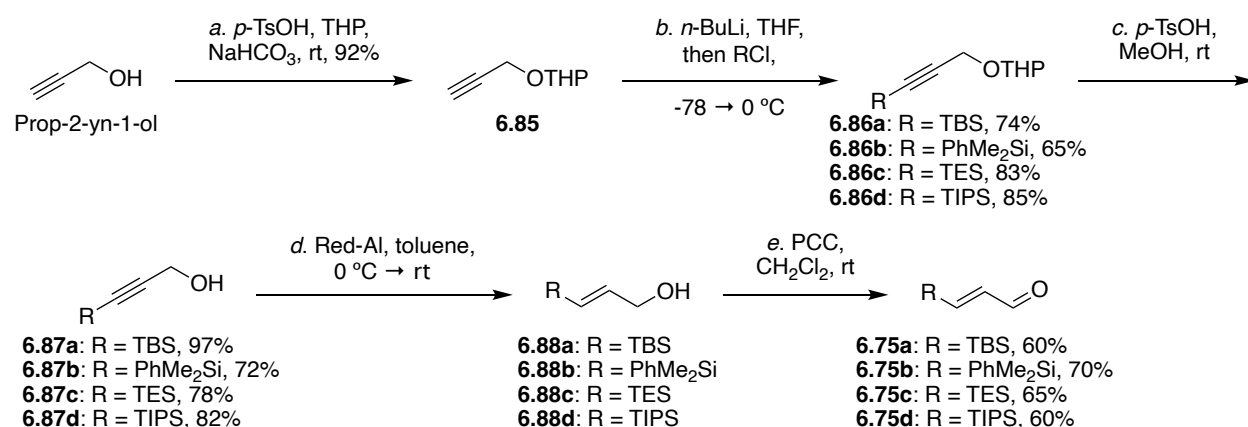


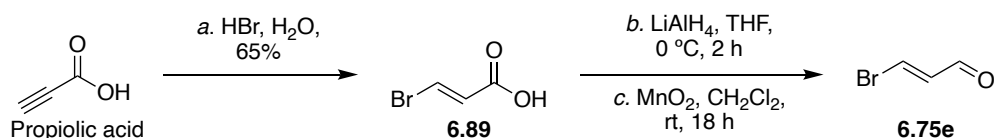
Figure 6.2: NOE-correlations (600 MHz, CD₃OD) of 4aS,7S,8aS-**6.84**.

6.4.2 Synthesis of Aldehydes **6.75a–e**



Scheme 6.12: Preparation of aldehydes **6.75a–d** from 2-propyn-1-ol.

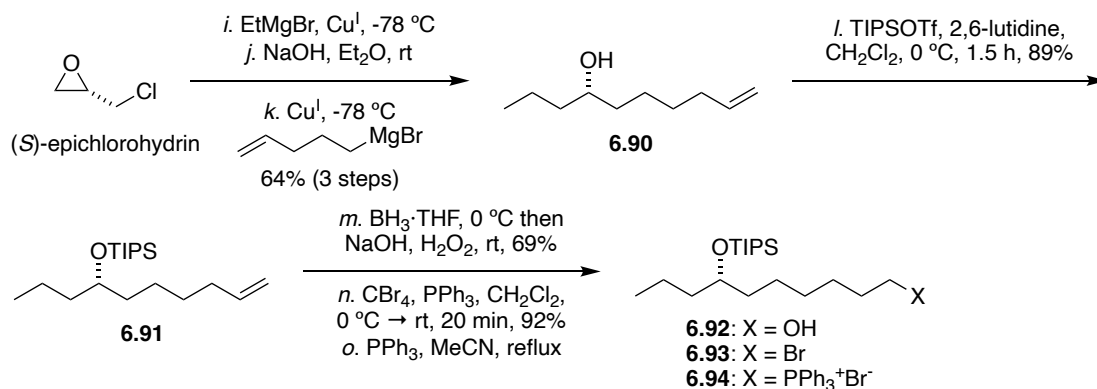
Aldehydes **6.75a–d** were synthesized from propargyl alcohol (Scheme 6.12) after protection as the THP ether **6.85** in 92%.²⁶ Deprotonation of **6.85** with *n*-BuLi followed by reaction with various chlorotrialkylsilanes gave the respective propargyl silanes **6.86a–d** in ~70–80%.²⁷ Acid-promoted removal²⁷ of the THP-group and subsequent reduction²⁸ of the propargyl alcohols **6.87a–d** with Red-Al provided the allylic alcohols **6.88a–d**, which upon PCC oxidation delivered aldehydes **6.75a–d** in moderate to good yields over 2 steps.²⁹



Scheme 6.13: Preparation of aldehyde **6.75e** from propiolic acid.

(*E*)-3-Bromoacrolein was prepared from propiolic acid in a three step sequence: aq HBr to give (*E*)-3-bromoacrylic acid (**6.89**) in 65%, reduction (LiAlH₄) to deliver the corresponding allylic alcohol, followed by MnO₂-oxidation to aldehyde **6.75e** which was used as a stock solution in CH₂Cl₂ owing to its volatility (Scheme 6.13).

6.4.3 Synthesis of C5 Alkyl Chain

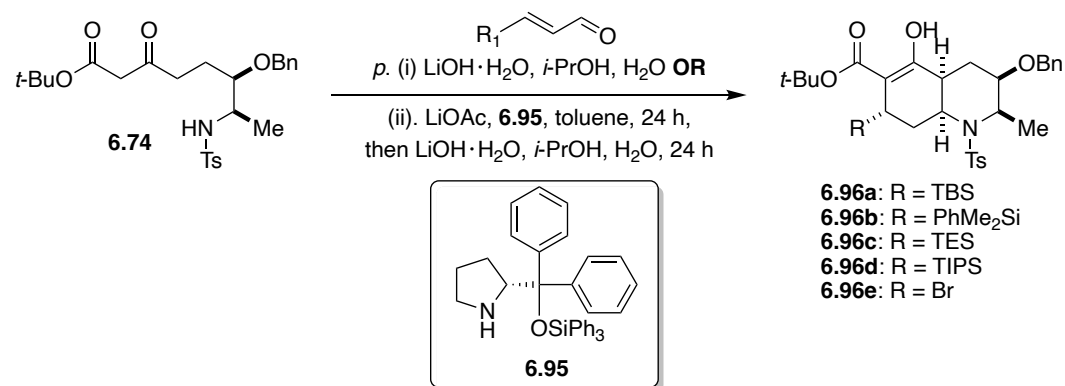


Scheme 6.14: Synthesis of the C-5 sidechain.

The precursor to the alkyl sidechain was prepared in a straightforward way modeled upon the approach by Blechert and coworkers.⁹ Cu(I)-catalyzed Grignard addition of EtMgBr to (*S*)-epichlorohydrin (Scheme 6.14), then base-promoted S_N2 ring closure to the epoxide, followed by addition of the 4-butenyl Grignard reagent, delivered alcohol **6.90** in 64% (3 steps). TIPS-protection of the 2° OH followed by hydroboration-oxidation afforded the primary alcohol **6.92** in 61% (2 steps). Subsequent conversion of **6.92** to the primary bromide **6.93** was accomplished

under standard conditions, and alkylation of **6.93** with triphenylphosphine gave the phosphonium salt **6.94** (Wittig reagent).

6.4.4 Assembly of *cis*-DHQ Core and Installation of C5 Alkyl Chain



Scheme 6.15: Robinson–aza-Michael sequence with β -ketoester **6.74** and aldehydes **6.75a–e**.

Table 6.5: Conditions for the Robinson–aza-Michael reaction with **6.74** and **6.75a–e**.

Entry	R	Product	Condition a	Condition b
			Yield	Yield
1	TBS	6.96a	N.R.	N.R.
2	SiMe ₂ Ph	6.96b	18%	21% ^a
3	TES	6.96c	N.R.	11% ^b
4	TIPS	6.96d	N.R.	N.R.
5	Br	6.96e	-	N.R.

a. Yield improved to 38% upon addition of 5 equiv of **6.75b** and catalyst **6.95**. *b.* Epimerized upon standing in CDCl₃.

The key intermediate **6.96** was accessed through Robinson annulation³⁰ followed by an intramolecular aza-Michael addition of **6.74**.³¹ The reaction conditions for the tandem Robinson-aza-Michael sequence were based upon those developed by Bonjoch and coworkers who synthesized lycoserramine Z through an intramolecular aza-Michael reaction promoted by LiOH.²⁵

The Robinson annulation–aza-Michael cyclization of β -ketoester **6.74** was attempted with five ‘traceless’ surrogates of acrolein in the absence or presence of a prolinol catalyst (**6.95**, Scheme 6.15, Table 6.5). In the absence of prolinol catalyst **6.95**, only aldehyde **6.75b**, (*E*)-3-(dimethyl(phenyl)silyl)acrylaldehyde, successfully proceeded to react with **6.74** and provide **6.96b** in 18% yield.²⁵ Similarly, in the presence of catalyst **6.95**, both aldehydes **6.75b,c** reacted with **6.74** to give **6.96b,c** in 21% and 11%, respectively. Interestingly, while the catalyst appeared to enhance the rate of the reaction, its presence was unnecessary to control the ring-junction stereochemistry as the 4*aS*,8*aS*-**6.96b** product was obtained as the sole diastereoisomer. Diastereoselection in construction of the *cis*-ring junction occurred from conjugate addition of the *N*-Ts anion from the top face. The relative configuration of the 4*aS*,8*aS*-**6.96b** isomer was identified by 1D selective NOE correlations (Figure 6.3). In contrast, while product **6.96c** was initially obtained as one diastereoisomer, it rapidly epimerized on standing (purified, stored in CDCl₃) to give ~1:1 mixture of diastereoisomers according to ¹H NMR.

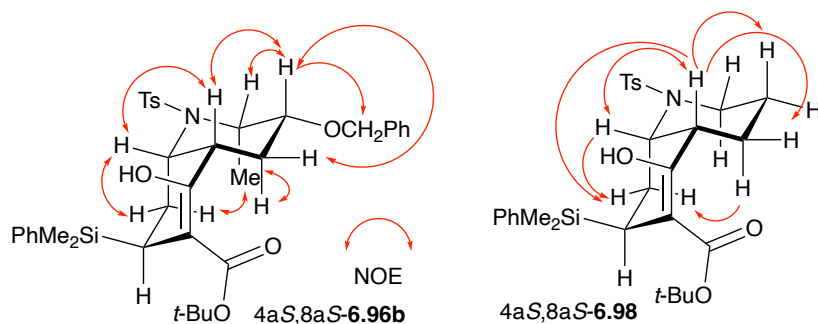
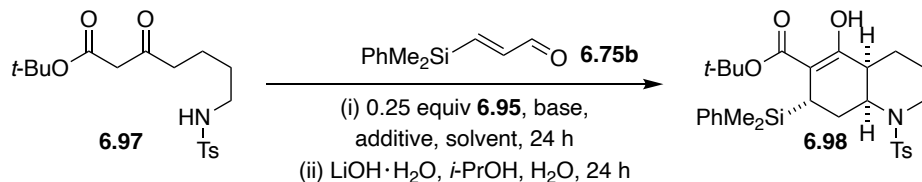


Figure 6.3: NOE-correlations (600 MHz, CDCl₃) of 4*aS*,8*aS*- **6.96b** and **6.98**.

To improve the yield of **6.96b**, the reaction was repeated in the presence of excess equivalencies of **6.75b** and purging with Ar. Although unreacted β -ketoester was observed, no remaining aldehyde was detected by TLC or ¹H NMR when 1.1 equiv of the aldehyde was used; consequently, 5.0 equivalents of **6.75b** was added to the reaction mixture, which improved the

yield of **6.96b** from 21% to 38% but only in the presence of catalyst **6.95**. Addition of excess equivalents of aldehyde appeared ineffectual in improving the yield of **6.96b** in the absence of catalyst. Furthermore, the yield of the Robinson–aza-Michael reaction decreased to 26% at higher temperatures (30 °C, **6.74**, LiOAc, 5.0 equiv **6.75b**, 0.25 equiv **6.95**, toluene, purge with Ar, rt, 22 h, then LiOH·H₂O, H₂O, *i*-PrOH, 30 °C, 20 h).



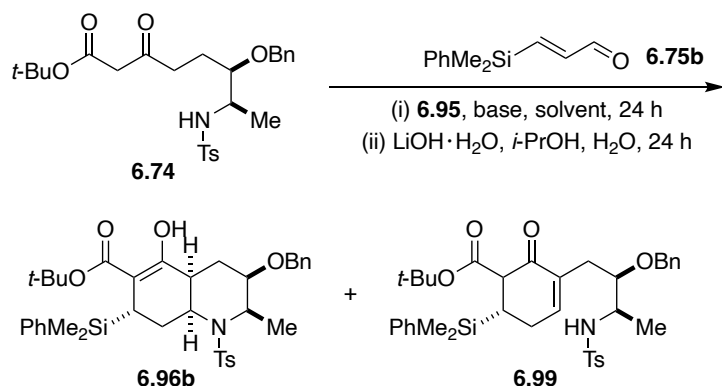
Scheme 6.16: Robinson–aza-Michael sequence with β -ketoester **6.97** and aldehyde **6.75b**.

To test the impact of conditions on the Robinson–aza-Michael reaction that might improve the yield of the *cis*-DHQ (**6.96b**), a base and solvent survey was completed with a model compound, β -ketoester **6.97**, derived in two steps from 5-aminopentanoic acid (Scheme 6.16, Table 6.6). In the cycloaddition reaction of **6.97** with **6.75b**, a notable alkali metal counterion effect was observed: $K^+ > Cs^+ > Na^+ \sim Li^+$. Bases containing K^+ or Cs^+ gave the best yields; in particular, the strong, non-nucleophilic base, $KOtBu$, and the weak alkali metal carbonate, Cs_2CO_3 , provided the highest yields at ~50%. Tertiary amines including DABCO and DBU (Table 6.6, entries 26–30) either completely failed to deliver **6.98** or delivered traces of product. In the presence of $KHCO_3$, addition of an additive such as 18-crown-6 improved the solubility of the base and the yield, slightly,³² whereas phase-transfer catalysts, such as those in entries 13–15, marginally reduced the yield of the reaction. A survey with solvents more polar than toluene, in the presence of either $KHCO_3$ or Cs_2CO_3 , decreased the yield of the product **6.98**.

Table 6.6: Step *i* reaction conditions and % yields of **6.98** or **6.96b** (see Scheme 6.16).

Entry	Condition ^a	Additive ^b	Prod.	Yield ^c
1	LiOAc, toluene, rt, 22 h		6.98	27%
2	Li ₂ CO ₃ , toluene, rt, 40 h		6.98	19%
3	Li ₂ CO ₃ , toluene, rt, 40 h	<i>d</i>	6.98	24%
4	LiOH·H ₂ O, toluene, rt, 40 h		6.98	13%
5	Na ₂ CO ₃ , toluene, rt, 40 h		6.98	29%
6	Na ₂ CO ₃ , toluene, rt, 40 h	15-crown-5	6.98	18%
7	NaOAc, toluene, rt, 40 h		6.98	30%
8	NaHCO ₃ , toluene, rt, 40 h		6.98	29%
9	K ₂ CO ₃ , toluene, rt, 40 h		6.98	27%
10	KOAc, toluene, rt, 40 h		6.98	24%
11	KHCO ₃ , toluene, rt, 40 h		6.98	29%
12	KHCO ₃ , toluene, rt, 40 h	18-crown-6	6.98	37%
13	KHCO ₃ , CH ₂ Cl ₂ , rt, 40 h	<i>e</i>	6.98	26%
14	KHCO ₃ , CH ₂ Cl ₂ , rt, 40 h	<i>f</i>	6.98	28%
15	KHCO ₃ , CH ₂ Cl ₂ , rt, 40 h	<i>g</i>	6.98	29%
16	KF, THF, rt, 40 h	18-crown-6	6.98	26%
17	KO <i>t</i> Bu, <i>t</i> -BuOH, rt, 40 h		6.98	49%
18	KO <i>t</i> Bu, THF, rt, 40 h		6.98	55%
19	KO <i>t</i> Bu, <i>t</i> -BuOH/toluene (1:1), rt, 40 h		6.98	46%
20	CsOAc, toluene, rt, 40 h		6.98	4.4%
21	CsOAc, toluene, rt, 40 h	18-crown-6	6.98	19%
22	Cs ₂ CO ₃ , toluene, rt, 40 h		6.98	38%
23	Cs ₂ CO ₃ , toluene, rt, 40 h	18-crown-6	6.98	46%
24	CsOH·H ₂ O, toluene, rt, 40 h	18-crown-6	6.98	39%
25	CsF, MeCN, rt, 40 h	18-crown-6	6.98	20%
26	pyridine, toluene, rt, 40 h		6.98	8%
27	Et ₃ N, toluene, rt, 40 h		6.98	N.R.
28	4-DMAP, toluene, rt, 40 h		6.98	N.R.
29	DABCO, toluene, rt, 40 h		6.98	4%
30	DBU, toluene, rt, 40 h		6.98	16%
31	KHCO ₃ , benzene, rt, 40 h	18-crown-6	6.98	17%
32	KHCO ₃ , CH ₂ Cl ₂ , rt, 40 h	18-crown-6	6.98	18%
33	KHCO ₃ , MeCN, rt, 40 h	18-crown-6	6.98	14%
34	Cs ₂ CO ₃ , benzene, rt, 40 h	18-crown-6	6.98	40%
35	Cs ₂ CO ₃ , CH ₂ Cl ₂ , rt, 40 h	18-crown-6	6.98	40%
35	Cs ₂ CO ₃ , MeCN, rt, 40 h	18-crown-6	6.98	34%
37	Cs ₂ CO ₃ , THF, rt, 40 h	18-crown-6	6.98	26%
38	Cs ₂ CO ₃ , MeOH, rt, 40 h	18-crown-6	6.98	32%
39	LiOAc, toluene, rt, 40 h		6.96b	38%
40	KO <i>t</i> Bu, <i>t</i> -BuOH, rt, 40 h	18-crown-6	6.96b	16%
41	Cs ₂ CO ₃ , toluene, rt, 40 h	18-crown-6	6.96b	12%
42	KHCO ₃ , toluene, rt	18-crown-6	6.96b	21%

a. In step (i), reactions were conducted with 1.0 equiv of **6.74** (entries 1 – 38) or **6.97** (entries 39 – 42), 1.0 equiv of base, 0.2 equiv of cat. **6.95**, and 2.0 equiv of aldehyde in solvent at 0.11 M concentration. After 20 – 40 h, the solvent was evaporated, and 1.0 equiv of LiOH·H₂O and 10.0 equiv of H₂O were added followed by *i*-PrOH at a final concentration of 0.11 M. *b.* Additive was added at 0.1 equiv. *c.* Yields (%) reported are isolated yields. *d.* Benzo-15-crown-5. *e.* Tetrabutylammonium hydrogen sulfate (*n*-Bu₄N⁺·HSO₄⁻). *f.* Benzyltrimethylammonium hydroxide (BnMe₃N⁺·OH⁻). *g.* Cetyltrimethylammonium hydroxide (Cetyl Me₃N⁺·HSO₄⁻).



Scheme 6.17: Robinson–aza-Michael sequence with β -ketoester **6.74** and aldehyde **6.75b**.

Regrettably, replication of the best yielding reactions with β -ketoester **6.74** (Scheme 6.17), in the presence of $\text{KO}t\text{Bu}$, KHCO_3 or Cs_2CO_3 and 18-crown-6 in *t*-BuOH or toluene (Table 6.6, entries 40–42), significantly lowered the yield of **6.96b** when compared with LiOAc and 5 equiv of **6.75b** (entry 39). A significant side product in the Robinson–aza-Michael reaction is **6.99**. Enone **6.99**, which is either the byproduct of the Robinson annulation or retro aza-Michael cycloaddition, was consistently observed and isolated in 30-40% yield, predominantly in the presence of $\text{KO}t\text{Bu}$ or Cs_2CO_3 . Attempts to induce aza-Michael cyclization after purification with either NaOH , KOH or $\text{LiOH}\cdot\text{H}_2\text{O}$ in *i*-PrOH and H_2O were nonproductive for the following reasons. In the presence of NaOH or KOH , the product was observed as the enol ether tautomer in the ^1H NMR spectrum, while in the presence of $\text{LiOH}\cdot\text{H}_2\text{O}$, the cyclization of **6.99** to **6.96b** reached equilibrium (1.5:1 of **6.99**/**6.96b** based on ratio of purified products) but failed to progress to completion. Attempts to cyclize **6.99** with $\text{LiOH}\cdot\text{H}_2\text{O}$ (1.0 equiv) and LiCl (2.0 equiv) in *i*-PrOH and H_2O led to a complex mixture of products by ^1H NMR and TLC. Additionally, an analogous substrate of **6.97** with an *N*-Troc protecting group, in place of the *N*-Ts group, failed to provide the desired *cis*-DHQ when reacted with crotonaldehyde or **6.75b**, in return, products of incomplete cyclization were obtained.

In consideration of all the above data, we conclude the tandem reaction is under thermodynamic control, attributable in part to a balance established from the property of the TsN⁻ anion as both a modest nucleophile, for the forward reaction, but also a good leaving group for the retro-aza-Michael reaction. As the forward reaction was relatively slow, we were unable to find kinetic conditions to trap the cyclized product **6.96b**. Regardless, compound **6.96b** was obtained in a best yield of 38%, based on recovered starting material, and used in the next reaction. The complete NMR assignment of compounds 4a*S*,8a*S*- **6.96b** and **6.98** is reported in Figure 6.4 and Table 6.7.

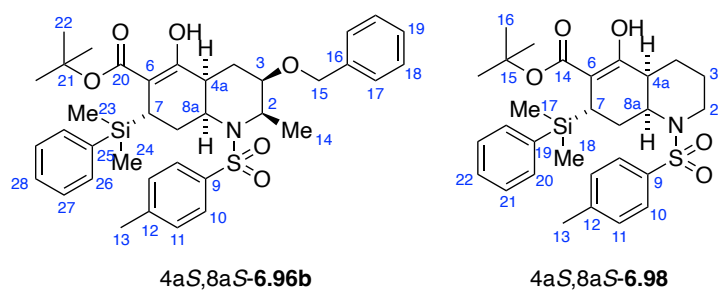


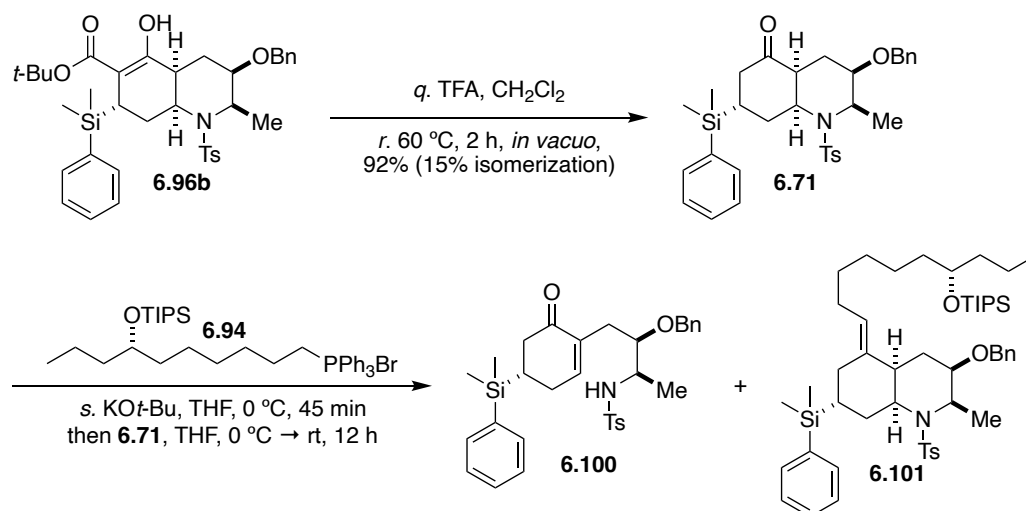
Figure 6.4: Numbering assignment of 4a*S*,8a*S*- **6.96b** and **6.98**.

Table 6.7: ^1H and ^{13}C NMR data for 4a*S*,8a*S*- **6.96b** and **6.98** (CDCl_3).

Position	δ_{H} (int., mult, <i>J</i> , Hz)	δ_{C}	Position	δ_{H} (int., mult, <i>J</i> , Hz)	δ_{C}
	4a^a	4a^b		4e^a	4e^b
1			1		
2	4.18 (1H, quintet, 6.5)	50.1	2	3.81 (1H, dt, 14.0, 2.0) 2.92 (1H, td, 13.5, 2.0)	41.0
3	2.79 (1H, dd, 4.2, 5.4, 12.0)	73.5	3	1.44 (1H, m) 1.10 (1H, qt, 13.0, 4.0)	23.8
4	2.06 (1H, m) 1.50 (1H, td, 13.2, 25.8)	26.2	4	1.36 (1H, m) 2.02 (1H, dt, 13.5, 3.0)	26.6
4a	1.80 (1H, dd, 4.8, 6.0, 13.2)	38.2	4a	1.95 (1H, dt, 12.5, 5.0)	26.6
5		169.1	5		99.2
6		100.2	6		170.7
7	2.34 (1H, m)	22.5	7	2.38 (1H, dd, 6.0, 1.0)	21.2
8	2.08 (1H, m) 2.16 (1H, td, 6.0, 13.2)	30.6	8	1.80 (1H, m) 2.20 (1H, td, 13.0, 6.5)	25.0
8a	4.03 (1H, ddd, 3.6, 6.6, 13.4)	49.7	8a	4.22 (1H, ddd, 13.2, 6.0, 3.5)	49.9
9		138.5	9		143.0
10/10'	7.17 (2H, d, 8.0)	126.0	10/10'	7.48 (2H, d, 8.0)	126.7
11/11'	7.00 (2H, d, 8.0)	129.8	11/11'	7.19 (2H, d, 8.0)	129.8
12		142.9	12		138.9
13-Me	2.35	22.5	13-Me	2.40 (3H, s)	21.6
14-Me	1.25 (3H, d, 7.0)	16.0	14		172.2
15	4.37 (2H, s)	69.9	15		82.2
16		138.1	16	1.45 (9H, s)	28.2
17/17'	7.17 (2H, d, 8.0)	127.5	17-Me	0.43 (3H, s)	0.1
18/18'	7.30 (2H, t, 8.0)	128.0	18-Me	0.43 (3H, s)	-2.2
19	7.39 (1H, m)	128.9	19		138.8
20		172.2	20/20'	7.56 (2H, m)	134.4
21		82.5	21/21'	7.40 (2H, m)	128.0
22	1.47 (9H, s)	28.3	22	7.38 (1H, m)	127.9
23-Me	0.38 (3H, s)	-0.6	23-OH	12.52 (1H, s)	
24-Me	0.49 (3H, s)	-2.9			
25		139.9			
26/26'	7.38 (2H, d, 7.0)	128.6			
27/27'	7.56 (2H, dd, 7.5, 1.5)	134.6			
28	7.39 (1H, m)	127.8			
29-OH	12.61 (1H, s)				

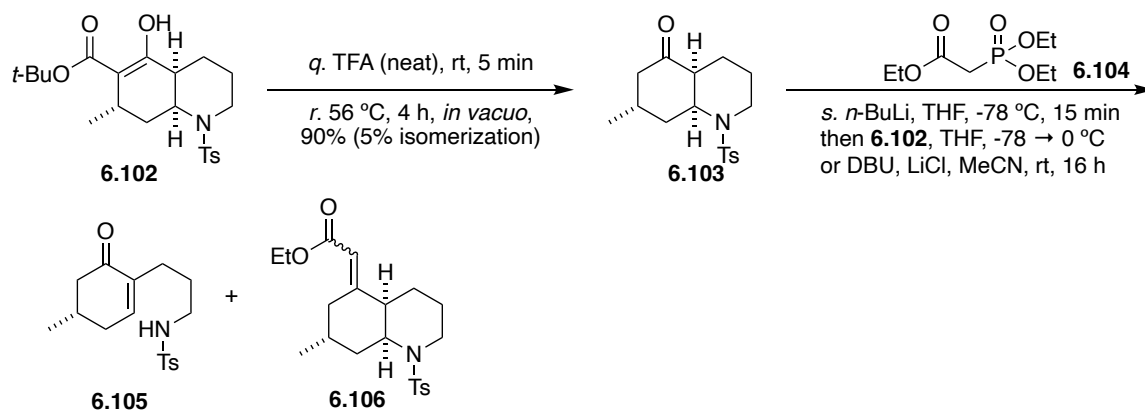
^a500 MHz. ^b125 MHz.

6.4.5 Attempts to Install the C-5 Sidechain



Scheme 6.18: *t*-BuO-deprotection and decarboxylation of **6.96b** and Wittig olefination with **6.71**.

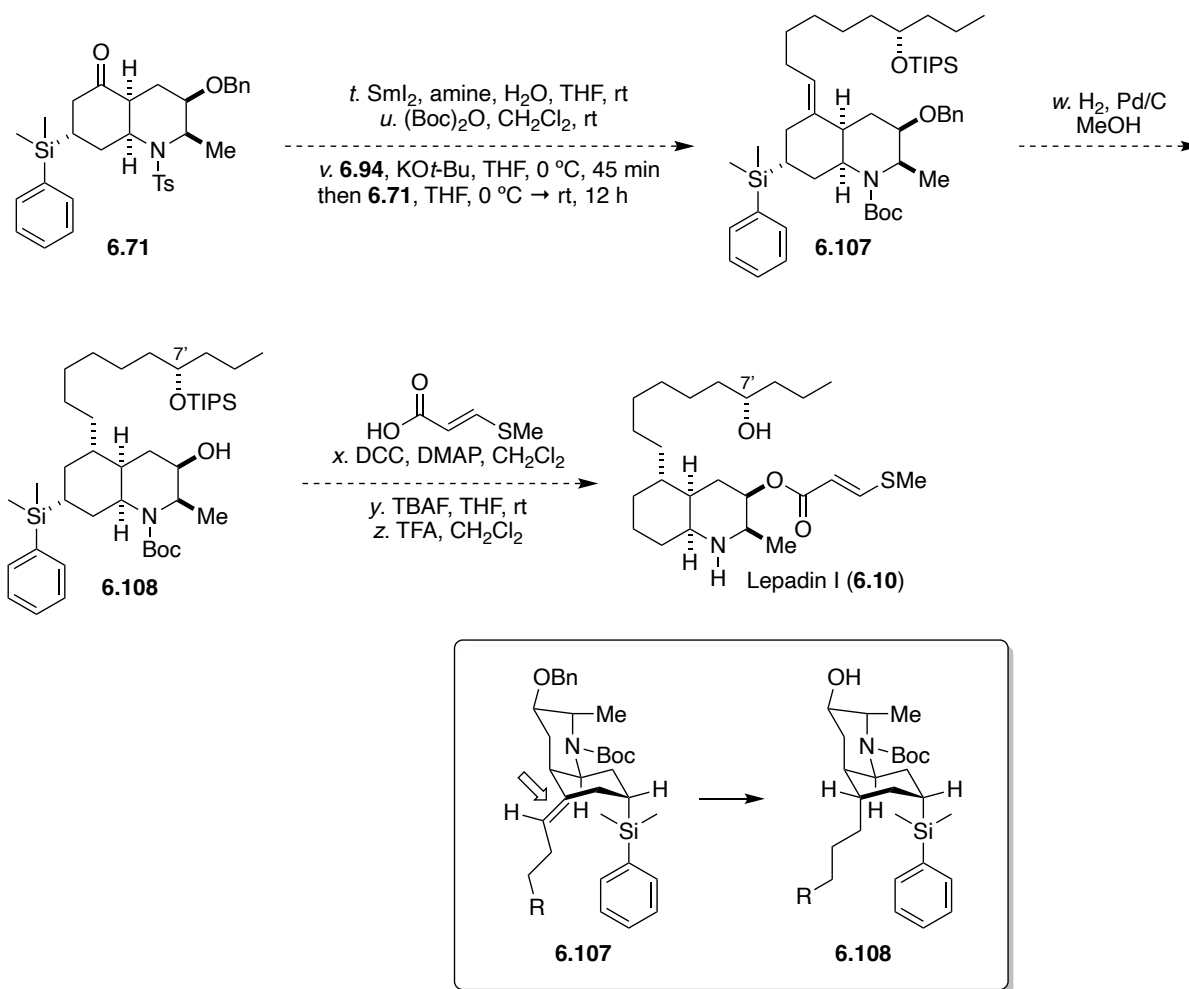
Deprotection and decarboxylation of ester **6.96b** under acidic conditions gave **6.71** in 92%. Isomerization at the C-4a center due to enolization was observed during the *t*-BuO-deprotection with TFA (5 min, rt), and it increased significantly to ~50% upon prolonged exposure to TFA (1 – 2 h, $0\text{ }^\circ\text{C}$). The Wittig reagent, derived by base treatment ($\text{KO}t\text{-Bu}$) of **6.94**, was expected to give *E*-**6.101** upon condensation with ketone **6.71** (Scheme 6.18). However, only enone **6.100**, the retro aza-Michael product, was observed and isolated. It appears that the ylide reagent is sufficiently basic to deprotonate **6.71** at C-4a, which readily undergoes retro aza-Michael ring opening – once again – due to the stability of the N-Ts anion. Subsequently, the HWE reaction with the less basic phosphonate reagent **6.104** was examined with ketone **6.103**.



Scheme 6.19: *t*-BuO-deprotection and decarboxylation of **6.102** and HWE olefination with **6.103**.

Treatment of intermediate **6.102** (Scheme 6.19), obtained from a Robinson–aza-Michael reaction of **6.97** and crotonaldehyde, with neat TFA followed by decarboxylation at 56 °C provided ketone **6.103**; gratifyingly in 90% yield and little isomerization (5% by ¹H NMR integration). Subsequent HWE condensation of **6.103** with the phosphonate carbanion, prepared from treatment of **6.104** with *n*-BuLi at -78 °C, resulted in 69% conversion in a 1:1.4:2.4 ratio of the olefin product/ketone starting material/enone (**6.106**:**6.103**:**6.105**). HWE under milder base conditions substantially decreased the ratio of desired product **6.106** compared to enone **6.105**. Condensation of **6.103** with the phosphonate carbanion, generated *in situ* from **6.104** under Masamune-Rousch conditions (DBU and LiCl in MeCN), resulted in a mixture of **6.106**:**6.103**:**6.105** (1:5:11).³³ Neither set of conditions augured well for successful progression to the desired product **6.101** with reasonable rates of conversion from the acyclic precursors and overall yield.

6.4.6 Future Directions and Completion of the Total Synthesis of Lepadin I



Scheme 6.20: Proposed route to complete the total synthesis of lepadin I.

The proposed route to accomplish the total synthesis of lepadin I (Scheme 6.20) requires retooling of several components of the linear schemes towards the goal. Clearly, the sulfonamide N-protecting group, while serving well up to the tandem-Robinson–aza-Michael reaction, became a liability in the transition towards the endgame; a protecting group swap was prescribed. Cleavage of the Ts-amide (SmI_2) followed by installation of the intact side chain, containing the *S*-C-7' stereocenter by Wittig olefination and subsequent Boc-protection would afford **6.107**. Facial-selective hydrogenation of **6.107** would provide **6.108**. Steglich esterification of the secondary

alcohol with *E*-3-(methylthio)acrylic acid followed by deprotection of the remote alcohol at C-7' (buffered TBAF) and the *N*-Boc group (anhydrous TFA) would deliver lepadin I (**6.10**).

6.5 Conclusions

In conclusion, a new synthetic route was developed for the total synthesis of lepadin I through an intermolecular Robinson annulation–intramolecular aza-Michael cyclization to form the *cis*-DHQ. Intense experimentation delivered **6.96b** in a best yield of 38% (based on recovered starting material), but severe problems with C-4a epimerization or retro-aza-Michael reaction, militated against progression to the end game in satisfactory yields. Moving forward, an *N*-protecting group swap would afford an advanced ketone, which could be subjected to Wittig or HWE olefination followed by stereoselective hydrogenation. Lastly, esterification of the C-3 hydroxyl with *E*-3-(methylthio)acrylic acid may be achieved under conventional coupling conditions (DCC) or the Yamaguchi protocol.³⁴ The proposed synthesis would provide access to useful quantities of lepadin I and a key intermediate for the exploration of SAR and the mapping of the structural elements that are responsible for selective BuChE inhibition.

6.6 Experimental

General experimental procedure. Reactions were completed in oven or flame-dried glassware with dry solvents under an inert atmosphere. Dry acetonitrile (MeCN), diethyl ether (Et₂O), tetrahydrofuran (THF), dichloromethane (CH₂Cl₂), toluene, and dimethylformamide (DMF) were degassed, dried by passage through alumina columns and stored under Argon. MeOH was dried overnight over 3Å molecular sieves. Et₃N, pyridine, DBU and 2,6-lutidine were freshly distilled from CaH₂. Reagents and solvents were purchased from MilliporeSigma, Fisher Scientific

or Alfa AesarTM, and were used as purchased without further purification unless otherwise stated. Reactions were monitored by thin layer chromatography (TLC) on MilliporeSigma precoated silica gel 60 plates (F₂₅₄). The TLC plates were visualized with UV light and stained with cerium ammonium molybdate, KMNO₄, or bromocresol green. Reaction workup was completed under standard aqueous conditions. Flash silica chromatography was performed using SiliCycle silica gel (40 – 63 μm, 60Å). 1D and 2D NMR spectra were measured on a JEOL ECA (500 MHz) or JEOL ECZ (400 MHz) spectrometer, equipped with a 5 mm ¹H{¹³C} room temperature probe, or a Bruker Avance III (600 MHz) NMR spectrometer with a 1.7 mm ¹H {¹³C/¹⁵N} microcryoprobe (23 °C), or a Varian NMR spectrometer (500 MHz) fitted with a 5 mm XSens ¹³C{¹H} cryoprobe. NMR spectra were referenced to residual solvent signals (chloroform-*d*₃, δ_H 7.26, δ_C 77.16 ppm). The following abbreviations were used in reference to NMR multiplicities: s = singlet, d = doublet, t = triplet, q = quartet, quint. = quintet, dd = doublet of doublet, dt = doublet of triplet, dq = doublet of quartet, td = triplet of doublet, ddd = doublet of doublet of doublet, ddt = doublet of doublet of triplet, tdd = triplet of doublet of doublet, m = multiplet, and br = broad. HR-ESI-TOF mass spectroscopy analyses were conducted on an Agilent 1200 HPLC connected to an Agilent 6350 TOF-MS at the Small Molecule Mass Spectrometry Facility at the Department of Chemistry and Biochemistry at UCSD. Optical rotations were measured on a JASCO P-2000 polarimeter at the D-double emission line of Na.

The concentration of *t*-BuLi was determined by titration of 2,5-dimethoxybenzyl alcohol. *t*-BuLi was added dropwise to a solution of 2,5-dimethoxybenzyl alcohol (0.17 mL, 1.19 mmol) in Et₂O (5 mL) at rt under N₂ until a permanent red-brown color persisted indicating the onset of anion formation. The concentration of *t*-BuLi was then determined based on the volume of *t*-BuLi

used in the titration, and the 1:1 molar ratio of alkyllithium reagent to 2,5-dimethoxybenzyl alcohol.

Tosyl-D-alanine (**6.77**). Compound **6.77** was synthesized according to a reported literature procedure.^{35a-b} Tosyl chloride (23.54 g, 0.123 mol) was added portion wise over 1 h to a solution of D-alanine (10.0 g, 0.112 mol) and Et₃N (47 mL, 0.337 mol) in THF (90 mL) and H₂O (180 mL) at 0 °C. The reaction was warmed to rt and stirred for 20 h. The THF was concentrated, and the aq layer was acidified with HCl (2 M) to pH ~ 2 and extracted with EtOAc (4x). The combined organic layer was washed with brine (2x), dried over Na₂SO₄, filtered, and concentrated to give **6.77** (24.34g, 89%) as a crystalline solid. ¹H NMR (400 MHz, DMSO-d₆) δ (ppm, integ., mult, *J* Hz) 1.12 (3H, d, 7.2), 2.37 (3H, s), 3.72 (1H, m), 7.36 (2H, d, 8.4), 7.66 (2H, d, 8.0), 8.04 (1H, d, 8.4). HRMS (ESITOF) *m/z* 266.0458 [M+Na]⁺ (calc'd 266.0457 for C₁₀H₁₃NO₄S). The ¹H NMR and HRMS match those reported in the literature.^{35c}

Tosyl-D-alaninoyl Chloride (**6.78**). Thionyl chloride (9.0 mL, 123 mmol) was added dropwise to a solution of **6.77** (6.0 g, 24.7 mmol) in dry THF (250 mL) at rt. After 1 h, the reaction mixture was refluxed for 4 h. The reaction was cooled to rt and concentrated to furnish the acyl chloride **6.78** as a yellow oil that was used in the next reaction without further purification.

(R)-4-Methyl-N-(3-oxohept-6-en-2-yl)benzenesulfonamide (**6.79**). The Grignard reagent but-3-en-1-ylmagnesium bromide³⁶ and compound **6.79**¹⁶ were synthesized according to reported literature procedures. A solution of 4-bromo-1-butene (5.0 mL, 49 mmol) in THF (50 mL) was added to Mg⁰ turnings (2.5 g, 103 mmol, coated with I₂ vapors) in THF (25 mL) at a rate of gentle reflux under N₂ at rt. The reaction was refluxed for 1 h, cooled to rt, and added dropwise to a suspension of LiCl (6.95 g, 164 mmol) and CuCN (7.25 g, 81 mmol) in THF (100 mL) at -40 °C that were previously dried at 0.4 Torr and 250 °C for 4 – 5 h. The suspension was cooled to -78

°C, and a solution of **6.78** (24.7 mmol) in THF (75 mL) was added dropwise to the Gilman reagent. The reaction was slowly warmed to rt and stirred for 16 h. The reaction was cooled to 0 °C and quenched by addition of sat'd aq NH₄Cl (125 mL) and H₂O to dissolve the salts. The mixture was stirred at 0 °C for 30 min and rt for another 30 min. The layers were separated, and the aq layer was extracted with MTBE (3 x 75 mL). The combined organic layer was washed with brine (1x), dried over MgSO₄, filtered and concentrated. The crude was crystallized from MTBE to give **6.79** (6.38 g, 93%) as pale-green needles. ¹H NMR (400 MHz, CDCl₃) δ (ppm, integ., mult, *J* Hz) 1.33 (3H, d, 7.2 Hz), 2.18 (2H, m), 2.33 (1H, m), 2.41 (3H, s), 2.54 (1H, m), 3.92 (1H, m), 4.89 (1H, m), 4.93 (1H, m), 5.52 (1H, d, 6.8), 5.62 (1H, m), 7.28 (2H, d, 8.4 Hz), 7.70 (2H, d, 8.4 Hz). HRMS (ESITOF) *m/z* 282.1157 [M+H]⁺ (calc'd 282.1157 for C₁₂H₁₉NO₃S). The ¹H NMR and HRMS matched the reported literature data.¹⁶

NaBH₄ Reduction of 6.79 to 6.80a,b. NaBH₄ (6.7 mg, 0.18 mmol) was added to a solution of **6.79** (25.0 mg, 0.09 mmol) in dry MeOH (2.5 mL) at 0 °C. The solution was stirred for 30 min at 0 °C, quenched with H₂O (1 mL) and a few drops of HCl (2 M). After 5 min at 0 °C, the reaction mixture was extracted with Et₂O (3x), and the combined organic layer was washed with brine (1x), dried over MgSO₄, filtered and concentrated. Based on the ¹H NMR (CDCl₃), a 1:1.4 ratio of **6.80a/6.80b** was observed.

Zn(BH₄)₂ Reduction of 6.79 to 6.80a,b. Zn(BH₄)₂ was freshly synthesized. A solution of dry ZnCl₂ (0.5 M, 16.0 mL, 16.0 mmol, THF) was added to a vigorously stirring suspension of NaBH₄ (1.09 g, 8.0 mmol) in dry THF under N₂ at room temperature. The reaction was stirred for 72 h to give a solution of Zn(BH₄)₂ (0.16 M) in THF. Zn(BH₄)₂ (1.11 mL, 0.18 mmol) was added to a solution of **6.79** (25.0 mg, 0.09 mmol) in THF (1.39 mL) at -15 °C or -78 °C. The solution was stirred at -15 °C for 5 h (Table 6.3, entry 2) and at -78 °C 16 h (Table 6.3, entry 2), quenched with

H₂O (1 mL) and a few drops of HCl (2 M). After 5 min at 0 °C, the reaction was extracted with Et₂O (3x), and the combined organic layer was washed with brine (1x), dried over MgSO₄, filtered and concentrated. Based on the ¹H NMR (CDCl₃), a mixture of **6.80a**/**6.80b** formed in 2:1 ratio at -15 °C and 1.4:1 at -78 °C, respectively.

N-((2R,3R)-3-hydroxyhept-6-en-2-yl)-4-methylbenzenesulfonamide (6.80a). Compound **6.80a** was prepared according to a reported literature procedure.¹⁶ L-Selectride (39 mL, 38.7 mmol, 1.0 M) was added dropwise over 1 h to a solution of **6.79** (5.45 g, 19.4 mmol) in dry THF (90 mL) at -100 °C. Subsequently, the reaction was stirred at -100 °C for 1h, at -78 °C for 2 h and -60 °C for 1 h before quenching with a mixture of AcOH/H₂O (180 mL, 1:1). After 3 h, the solution was concentrated, and remaining H₂O was azeotroped with toluene (3x). The crude was suspended in sat'd NaHCO₃ (100 mL) and extracted with CHCl₃/*i*-PrOH (4 x 100 mL, 4:1). The combined organic layer was washed with brine (1x), dried over MgSO₄, filtered, and concentrated to give **6.80** (5.20 g, 95%) as a mixture of 1:0.05 of **6.80a**/**6.80b** based on ¹H NMR integration. The crude was crystallized from hexanes/MTBE (24 mL, 1:2) to give **6.80a** (4.38 g, 80%) as colorless needles. The ¹H NMR and HRMS are consistent with reported literature values.¹⁶

Benzyl Protection under Acidic Conditions (Table 6.4, entry 1). The reaction was performed according to a reported literature procedure.²⁰ Trifluoromethanesulfonic acid (18 μL, 0.21 mmol) was added to a solution of **6.80a** (0.391 g, 1.38 mmol) and benzyl 2,2,2-trichloroacetimide (0.31 mL, 1.65 mmol) in dry CH₂Cl₂ (1 mL) and cyclohexane (2 mL, dried over 4 Å MS). After 6.5 h at rt, the mixture was diluted with CH₂Cl₂/cyclohexane (1:2) and filtered on a cake of Celite. The filtrate was washed with sat'd aq NaHCO₃ (1x), H₂O (1x), brine (1x), dried over Na₂SO₄, filtered and concentrated. The crude was purified on SiO₂ (20% EtOAc/hexanes) to give **6.81a** as a colorless oil.

Benzyl Protection under Basic Conditions (Table 6.4, entry 2). Compounds **6.81c,d** were prepared according to a reported literature procedure.²¹ NaH (8.5 mg, 212 μ mol, 60%) was added to a solution of **6.80a** (25.0 mg, 88 μ mol) in dry THF (0.25 mL) at 0 °C. After 30 min at rt, tetrabutylammonium iodide (3.3 mg, 9 μ mol) and benzyl bromide (12 μ L, 97 μ mol) were added to the reaction mixture. After 16 h, the reaction was quenched with sat'd aq NH₄Cl and extracted with Et₂O (3x). The combined organic layer was washed with H₂O (1x), dried over MgSO₄, filtered and concentrated. The crude was purified with SiO₂ (10% \rightarrow 50% EtOAc/hexanes) to give **6.81c** (18.1 mg, 55%) and **6.81d** (2.0 mg, 5%). **6.81c**: ¹H NMR (500 MHz, CDCl₃) δ (ppm, integ., mult, *J*Hz) 7.71 (2H, d, 8.5), 7.40 (2H, d, 7.5), 7.27-7.36 (5H, m), 5.68 (1H, m), 4.87-4.95 (2H, m), 4.66 (1H, d, 15.5), 4.09 (1H, d, 15.5), 4.74 (1H, dt, 7.0, 15.5), 3.14 (1H, td, 2.0, 9.0), 2.44 (3H, s), 2.15 (1H, m), 1.99 (1H, m), 1.42 (1H, m), 1.31 (1H, m), 0.90 (3H, d, 7.0). ¹³C NMR (125 MHz, CDCl₃) δ (ppm) 143.7, 138.3, 137.8, 130.0, 128.9, 128.3, 128.0, 127.3, 115.0, 71.6, 59.7, 48.0, 32.9, 31.7, 29.5, 21.7, and 14.6. HRMS (ESITOF) *m/z* 374.1787 [M+H]⁺ (calc'd 374.1784 for C₂₁H₂₈NO₃S⁺). **6.81d**: HRMS (ESITOF) *m/z* 464.2254 [M+H]⁺ (calc'd 464.2254 for C₂₈H₃₄NO₃S⁺).

N-((2R,3R)-3-(benzyloxy)hept-6-en-2-yl)-4-methylbenzenesulfonamide (**6.81b**).

Compound **6.81b** was synthesized according to a reported literature procedure.¹⁹ Benzyl bromide (3.15 mL, 26.5 mmol) was added to a solution of **6.80a** (2.343 g, 8.28 mmol) and Ag₂O (4.411 g, 19.0 mmol) in dry Et₂O (70 mL) at rt. After stirring for 18 h, an additional 1.0 equiv of benzyl bromide was added to the reaction. After another 40 h, the reaction was filtered, and the filtrate concentrated. The crude was purified on SiO₂ (5 \rightarrow 10% EtOAc/hexanes) to give **6.81b** (2.44 g, 79%) as a colorless oil. ¹H NMR (500 MHz, CDCl₃) δ (ppm, integ., mult, *J*Hz) 7.73 (2H, d, 6.5), 7.25-7.37 (7H, m), 5.66 (1H, m), 4.88-4.94 (2H, m), 4.69 (1H, br. d, 8.5), 4.54 (1H, d, 11.5), 4.42 (1H, d, 11.5), 3.44 (1H, m), 3.26 (1H, td, 2.5, 6.5), 2.41 (3H, s), 1.95 (2H, m), 1.57 (1H, m), 1.45

(1H, m), 1.07 (3H, d, 7.0). ¹³C NMR (125 MHz, CDCl₃) δ (ppm) 143.3, 138.4, 138.1, 138.0, 129.8, 128.6, 128.0, 127.9, 127.1, 115.1, 81.1, 72.5, 51.2, 29.7, 29.3, 21.7 and 18.8. HRMS (ESITOF) *m/z* 374.1787 [M+H]⁺ (calc'd 374.1784 for C₂₁H₂₈NO₃S⁺).

(4R,5R)-4-(benzyloxy)-5-((4-methylphenyl)sulfonamido)hexanoic acid (6.76). Compound **6.76** was synthesized according to a reported literature procedure.²² OsO₄ (0.36 mL, 35.6 μmol, 2.5% w/v in 2-methyl-2-propanol) was added to a solution of **6.81b** (1.33 g, 3.56 mmol) in DMF (17.8 mL). After 5 min, Oxone (8.76 g, 14.2 mmol) was added in one-portion. After stirring for 3 h, remaining Os^{VIII} was quenched with Na₂SO₃ (2.693 g, 21.4 mmol). After stirring for 1 h, the reaction mixture was diluted with EtOAc (50 mL) and HCl (1 M) to dissolve the salts. The layers were separated, and the aq layer was extracted with EtOAc (2 x 50 mL). The combined organic layer was washed with HCl (3x, 1 M), brine (1x), dried over Na₂SO₄, filtered, and concentrated to give **6.76** (1.19 g, 85%). ¹H NMR (500 MHz, CDCl₃) δ (ppm, integ., mult, *J* Hz) 7.74 (2H, d, 8.0), 7.25-7.39 (7H, m), 4.90 (1H, br. d, 7.5), 3.48 (1H, m), 3.36 (1H, m), 2.44 (3H, s), 2.34 (2H, m), 1.73-1.89 (2H, m), 1.05 (3H, d, 7.0). ¹³C NMR (125 MHz, CDCl₃) δ (ppm) 177.4, 143.4, 137.7, 130.1, 129.7, 128.5, 128.0, 127.8, 127.0, 80.3, 72.6, 50.8, 29.6, 24.8, 21.5, 17.8. HRMS (ESITOF) *m/z* 414.1343 [M+Na]⁺ (calc'd 414.1346 for C₂₀H₂₅NO₅SNa⁺).

tert-Butyl (6R,7R)-6-(benzyloxy)-7-((4-methylphenyl)sulfonamido)-3-oxooctanoate (6.74). Compound **6.74** was synthesized according to a reported literature procedure.²⁵ Dibutyl magnesium (3.0 mL, 3.0 mmol, 1 M in heptane) was added to a solution of mono-*tert*-butyl malonate (1.40 mL, 8.97 mmol) in dry THF (25 mL) at -78 °C under N₂. After stirring at -78 °C for 15 min, the solution was warmed to rt and stirred for 1 h. Simultaneously, in a separate flask, a solution of CDI (0.727 g, 4.48 mmol) in dry THF (12.5 mL) was added to a solution of **6.76** (1.17 g, 3.0 mmol) in dry THF (12.5 mL) at 0 °C. After stirring at 0 °C for 15 min, the solution

was warmed to rt, stirred for 1 h, and added to the above magnesium malonate solution. After 2 d, the reaction was quenched with citric acid (10% aq), the layers were separated, and the aqueous layer was extracted with Et₂O (3x). The combined organic layer was washed with sat'd NaHCO₃, brine, dried over Na₂SO₄, filtered and concentrated. The crude was purified on SiO₂ (10% → 25% EtOAc/hexanes) to provide **6.74** (0.72 g, 49%) as pale-yellow oil. A small sample was further purified by SiO₂-HPLC (40% EtOAc/hexanes, 3.0 mL/min) to give **6.74** (>95% purity). ¹H NMR (500 MHz, CDCl₃) δ (ppm, integ., mult, *J* Hz) 7.72 (2H, d, *J* = 8.3 Hz), 7.36 – 7.30 (3H, m), 7.27 (4H, m), 4.75 (1H, d, *J* = 8.7 Hz), 4.49 (1H, d, *J* = 11.6 Hz), 4.43 (1H, d, *J* = 11.6 Hz), 3.47 – 3.37 (1H, m), 3.29 (1H, td, *J* = 6.2, 2.9 Hz), 3.25 (2H, d, *J* = 8.3 Hz), 2.46 (2H, dt, *J* = 11.2, 7.3 Hz), 2.41 (3H, s), 1.80 (1H, dq, *J* = 14.0, 7.2 Hz), 1.72 (1H, ddt, *J* = 14.1, 7.7, 6.4 Hz), 1.46 (9H, s), 1.00 (3H, d, *J* = 6.7 Hz). ¹³C NMR (125 MHz, CDCl₃) δ (ppm) 203.1, 166.6, 143.4, 138.2, 138.0, 129.8, 128.6, 128.1, 128.0, 127.1, 82.1, 80.3, 72.4, 51.0, 50.5, 38.5, 28.1, 23.6, 21.7, 18.1. HRMS (ESITOF) *m/z* 512.2073 [M+Na]⁺ (calc'd 512.2077 for C₂₆H₃₅NO₆SNa⁺).

tert-Butyl (2*R*,3*R*)-3-(benzyloxy)-5-hydroxy-2-methyl-1-tosyl-1,2,3,4,4*a*,7,8,8*a*-octahydroquinoline-6-carboxylate (**6.83**). Attempted synthesis of **6.83** was completed under the conditions described by Bonjoch and coworkers.²⁵ Acrolein (3.75 μL, 56.2 μmol) and LiOH·H₂O (2.1 mg, 51.0 μmol) were sequentially added to a solution of **6.74** (25 mg, 51.0 μmol) in *i*-PrOH (0.175 mL) and H₂O (9.2 μL). After 24 h, the reaction was quenched with sat'd aq NH₄Cl and extracted with EtOAc (3x). The combined organic layer was dried over Na₂SO₄, filtered and concentrated. Based on ¹H NMR and LCMS, the reaction failed to provide **6.83**.

tert-Butyl (2*R*,3*R*)-3-(benzyloxy)-5-hydroxy-2,7-dimethyl-1-tosyl-1,2,3,4,4*a*,7,8,8*a*-octahydroquinoline-6-carboxylate (**6.84**). Compound **6.84** was synthesized according to the above-described procedure from **6.74** (29.0 mg, 59.2 μmol), crotonaldehyde (5.6 μL, 65.2 μmol,

95%) and LiOH·H₂O (2.5 mg, 59.2 μmol) in *i*-PrOH (0.205 mL) and H₂O (10.7 μL). The crude was purified on SiO₂ (25% EtOAc/hexanes) to yield **6.84** (10.9 mg, 34%). 4a*S*,7*S*,8a*S*-**6.84**: ¹H NMR (500 MHz, CDCl₃) δ (ppm, integ., mult, *J* Hz) 12.56 (1H, s), 7.58 (2H, d, 8.5), 7.24-7.38 (5H, m), 7.17 (2H, d, 8.0), 4.49 (1H, d, 12.0), 4.46 (1H, d, 12.0), 4.41 (1H, t, 6.5), 4.18 (1H, ddd, 8.5, 5.5, 2.5), 3.16 (1H, ddd, 9.0, 5.5, 3.5), 2.69 (1H, m), 2.39 (3H, s), 2.09-2.17 (2H, m), 2.05 (1H, td, 13.0, 6.0), 1.56-1.67 (2H, m), 1.50 (9H, s), 1.29 (3H, d, 7.0), 1.13 (3H, d, 7.0). ¹³C NMR (125 MHz, CDCl₃) δ (ppm) 172.4, 170.3, 143.2, 138.5, 138.0, 129.9, 128.6, 127.9, 127.6, 126.5, 103.8, 81.8, 74.5, 70.2, 49.8, 47.1, 39.1, 34.1, 28.4, 27.5, 25.2, 21.7, 20.4, and 15.8. HRMS (ESITOF) *m/z* 542.2568 [M+H]⁺ (calc'd 542.2571 for C₃₀H₄₀NO₆⁺).

2-(Prop-2-yn-1-yloxy)tetrahydro-2H-pyran (**6.85**). Compound **6.85** was prepared according to the reported procedure.²⁶ *p*-TsOH·H₂O (10 mg, 0.05 mmol) was added to 3,4-dihydro-2*H*-pyrane (16.5 g, 195 mmol). After 10 min, 2-propyn-1-ol (10 g, 180 mmol) was added dropwise over 30 min. followed by the addition of NaHCO₃ (1.12 g, 13.5 mmol) after an additional 10 min. After 16 h, the reaction was filtered to provide **1** (22.92 g, 92%) as a light-yellow oil. The ¹H NMR of **6.85** matches the reported literature values.²⁶

tert-Butyldimethyl(3-((*tetrahydro-2H-pyran-2-yl*)oxy)prop-1-yn-1-yl)silane (**6.86a**). Compound **6.86a** was prepared according to the literature procedure.²⁷ *n*-BuLi (9.84 mL, 24.6 mmol, 2.5 M in hexanes) was added dropwise to a solution of **6.85** (3.00 g, 21.4 mmol) in THF (70 mL) at -78 °C. After stirring at 0 °C for 15 min, the solution was cooled to -78 °C, and a solution of TBSCl (3.87 g, 25.7 mmol) in THF (20 mL) was added dropwise over 20 min. The mixture was warmed slowly over 12 h as the dry ice/acetone was allowed to reach rt. The reaction was quenched with the addition of sat'd aq NH₄Cl (45 mL), the layers were separated, and the aqueous layer was extracted with Et₂O (2x). The combined organic layer was washed with brine (1x), dried over

MgSO₄, filtered, and concentrated to provide a crude oil that was purified on SiO₂ (10% EtOAc/hexanes) to provide **6.86a** (4.01 g, 74%) as an oil. The ¹H NMR and HRMS of **6.86a** match the reported literature values.²⁷

Dimethyl(phenyl)(3-((tetrahydro-2H-pyran-2-yl)oxy)prop-1-yn-1-yl)silane (**6.86b**).

Compound **6.86b** was prepared according to the above-described procedure from **6.85** (3.00 g, 21.4 mmol), *n*-BuLi (9.84 mL, 24.6 mmol, 2.5 M in hexanes) and chloro(dimethyl)phenylsilane (4.3 mL, 25.7 mmol) in THF (90 mL). The obtained crude was purified on SiO₂ (1:14 of EtOAc/hexanes) to provide **6.86b** (3.79 g, 65%) as an oil. The ¹H NMR and HRMS of **6.86b** match the reported literature values.³⁷

Triethyl(3-((tetrahydro-2H-pyran-2-yl)oxy)prop-1-yn-1-yl)silane (**6.86c**). Compound **6.86c** was prepared according to the above-described procedure from **6.85** (3.00 g, 21.4 mmol), *n*-BuLi (9.84 mL, 24.6 mmol, 2.5 M in hexanes) and chlorotriethylsilane (4.31 mL, 25.7 mmol) in THF (90 mL). The obtained crude was purified on SiO₂ (1:20 of EtOAc/hexanes) to provide **6.86c** (4.54 g, 83%) as an oil. ¹H NMR (400 MHz, CDCl₃) δ (ppm, integ., mult, *J* Hz) 4.86 (1H, t, 3.0), 4.29 (2H, s), 3.85 (1H, m), 3.53 (1H, m), 1.47-1.92 (6H, m), 0.98 (9H, t, 8.0), 0.60 (6H, q, 8.0). ¹³C NMR (125 MHz, CDCl₃) δ (ppm) 102.7, 96.6, 88.4, 62.2, 54.9, 30.4, 25.5, 19.2, 7.6, and 4.4. HRMS (ESITOF) *m/z* 277.1596 [M+Na]⁺ (calc'd 277.1594 for C₁₄H₂₆O₂SiNa⁺).

Triisopropyl(3-((tetrahydro-2H-pyran-2-yl)oxy)prop-1-yn-1-yl)silane (**6.86d**). Compound **6.86d** was prepared according to the above-described procedure from **6.85** (3.00 g, 21.4 mmol), *n*-BuLi (9.84 mL, 24.6 mmol, 2.5 M in hexanes) and chlorotriisopropylsilane (5.5 mL, 25.7 mmol) in THF (90 mL). The obtained crude was purified on SiO₂ (1:20 of EtOAc/hexanes) to provide **6.86d** (5.50 g, 87%) as an oil. ¹H NMR (400 MHz, CDCl₃) δ (ppm, integ., mult, *J* Hz) 4.91 (1H, t, 3.0), 4.31 (2H, dd, 16.4, 22.4), 3.86 (1H, m), 3.52 (1H, m), 1.46-1.92 (9H, m), 1.07 (18H, s). ¹³C

NMR (125 MHz, CDCl₃) δ (ppm) 103.4, 96.4, 87.2, 62.3, 54.8, 30.5, 25.5, 19.3, 18.7 and 11.3.
HRMS (ESITOF) m/z 319.2063 [M+Na]⁺ (calc'd 319.2064 for C₁₇H₃₂O₂SiNa⁺).

3-(tert-Butyldimethylsilyl)prop-2-yn-1-ol (**6.87a**). Compound **6.87a** was prepared according to the described literature procedure.²⁷ *p*-TsOH·H₂O (0.272 g, 1.58 mmol) was added to a solution of **6.86a** (4.01 g, 15.8 mmol) in MeOH (25 mL). After 4 h, the reaction was cooled to 0 °C, neutralized with sat'd aq NaHCO₃ (35 mL) and diluted with H₂O (35 mL) to improve phase separation. The mixture was extracted with CH₂Cl₂ (3x), and the combined organic layer was dried over MgSO₄, filtered and concentrated. The crude was purified on SiO₂ (10% EtOAc/hexanes) to give **6.87a** (2.60 g, 97%) as a colorless solid. The ¹H NMR and HRMS of **6.87a** match the reported literature values.²⁷

3-(Dimethyl(phenyl)silyl)prop-2-yn-1-ol (**6.87b**). Compound **6.87b** was prepared according to the above-described procedure through the hydrolysis of **6.86b** (5.0 g, 18.2 mmol) with *p*-TsOH·H₂O (0.3137 g, 1.82 mmol) in MeOH (30 mL). The obtained crude was purified on SiO₂ (1:14 of EtOAc/hexanes) to provide **6.87b** (2.48 g, 72%) as a colorless oil. The ¹H NMR and HRMS of **6.87b** match the reported literature values.³⁸

3-(Triethylsilyl)prop-2-yn-1-ol (**6.87c**). Compound **6.87c** was prepared according to the above-described procedure through the hydrolysis of **6.86c** (4.29 g, 16.9 mmol) with *p*-TsOH·H₂O (0.290 g, 1.69 mmol) in MeOH (27 mL). The obtained crude was purified on SiO₂ (1:20 of EtOAc/hexanes) to provide **6.87c** (2.25 g, 78%) as a colorless oil. The ¹H NMR and HRMS of **6.87c** match the reported literature values.³⁹

3-(Triisopropylsilyl)prop-2-yn-1-ol (**6.87d**). Compound **6.87d** was prepared according to the above-described procedure through the hydrolysis of **6.86d** (4.95 g, 16.7 mmol) with *p*-TsOH·H₂O (0.2875 g, 1.67 mmol) in MeOH (27 mL). The obtained crude was purified on SiO₂

(1:20 of EtOAc/hexanes) to provide **6.87d** (2.91 g, 82%) as a colorless oil. The ¹H NMR and HRMS of **6.87d** match the reported literature values.⁴⁰

(E)-3-(*tert*-Butyldimethylsilyl)prop-2-en-1-ol (**6.88a**). Compound **6.88a** was prepared according to the described procedure.²⁸ Red-Al (6.54 mL, 22.9 mmol, 3.5 M in toluene) was added dropwise to a solution of **6.87a** (2.60 g, 15.3 mmol) in dry toluene (60 mL) under N₂ at 0 °C. The reaction was slowly warmed to rt, stirred for 1.5 h and quenched with the slow addition of H₂SO₄ (18 mL, 3% aq). The mixture was filtered on Celite, and the filtrate was separated. The aqueous layer was extracted with toluene (3x), and the combined organic layer was washed with brine (1x), dried over Na₂SO₄, filtered and evaporated to provide **6.88a** (2.04 g, 76%) as a colorless oil. The ¹H NMR and HRMS of **6.88a** match the reported literature values.²⁸

(E)-3-(Dimethyl(phenyl)silyl)prop-2-en-1-ol (**6.88b**). Compound **6.88b** (2.24 g, 90%) was prepared as a colorless oil according to the above-described procedure through the reduction of **6.87b** (2.46 g, 12.9 mmol) with Red-Al (5.54 mL, 19.4 mmol, 3.5 M in toluene) in toluene (50 mL). The ¹H NMR and HRMS of **6.88b** match the reported literature values.⁴¹

(E)-3-(Triethylsilyl)prop-2-en-1-ol (**6.88c**). Compound **6.88c** (2.04 g, 90%) was prepared as a colorless oil according to the above-described procedure through the reduction of **6.87c** (2.25 g, 13.2 mmol) with Red-Al (5.70 mL, 19.8 mmol, 3.5 M in toluene) in toluene (52 mL). The ¹H NMR and HRMS of **6.88c** match the reported literature values.⁴²

(E)-3-(Triisopropylsilyl)prop-2-en-1-ol (**6.88d**). Compound **6.88d** (2.76 g, 94%) was prepared as a colorless oil according to the above-described procedure through the reduction of **6.87d** (2.91 g, 13.7 mmol) with Red-Al (5.90 mL, 20.6 mmol, 3.5 M in toluene) in toluene (54 mL). ¹H NMR (400 MHz, CDCl₃) δ (ppm, integ., mult, *J* Hz) 6.25 (1H, dt, 19.2, 4.4), 5.80 (1H, dt, 19.2, 1.6), 4.21 (2H, dd, 4.4, 1.2), 1.11 (3H, m), 1.05 (18H, m). ¹³C NMR (125 MHz, CDCl₃)

δ (ppm) 146.9, 123.6, 66.1, 18.7 and 10.9. HRMS (ESITOF) m/z 213.1671 $[M+H]^+$ (calc'd 213.1669 for $C_{12}H_{25}OSi^+$).

(E)-3-(*tert*-Butyldimethylsilyl)acrylaldehyde (**6.75a**). Compound **6.75a** was prepared according to the described procedure.²⁹ PCC (5.00 g, 23.2 mmol) was added to a slurry of Celite (5.0 g) in CH_2Cl_2 (45 mL) over 10 min. A solution of **6.88a** (2.0 g, 11.6 mmol) in CH_2Cl_2 (5 mL) was added dropwise to the PCC-Celite mixture. After 90 min, the precipitate was filtered on a pad of Celite and washed with little CH_2Cl_2 . The filtrate was concentrated and purified on SiO_2 (5% \rightarrow 10% EtOAc/hexanes) to give a mixture of the *cis*- and *trans*-**6.75a** (1.54 g, 77%) as a colorless oil. 1H NMR (400 MHz, $CDCl_3$) δ (ppm, integ., mult, J Hz) 9.51 (1H, d, 7.6), 7.40 (0.44H, d, 18.8), 7.21 (1H, d, 18.8), 6.54 (1H, dd, 18.8, 7.6), 6.28 (0.47H, d, 18.8), 0.92 (9H, s), 0.91 (5.3H, s), 0.13 (6H, s), 0.11 (2.84H, s). ^{13}C NMR (125 MHz, $CDCl_3$) δ (ppm) 194.8, 169.7, 157.1, 151.0, 145.6, 134.3, 26.5, 16.7 and -6.41.

(E)-3-(Dimethyl(phenyl)silyl)acrylaldehyde (**6.75b**). Compound **6.75b** was prepared according to the above-described procedure through the oxidation of **6.88b** (2.2 g, 11.4 mmol) with PCC (4.93 g, 22.9 mmol) and Celite (5.0 g) in CH_2Cl_2 (50 mL). The crude was purified on SiO_2 (5% \rightarrow 10% EtOAc/hexanes) to give **6.75b** (1.70 g, 78%) as a colorless oil. The 1H NMR and HRMS of **6.75b** match the reported literature values.²⁹

(E)-3-(Triethylsilyl)acrylaldehyde (**6.75c**). Compound **6.75c** was prepared according to the above-described procedure through the oxidation of **6.88c** (2.04 g, 11.9 mmol) with PCC (5.11 g, 23.7 mmol) and Celite (5.0 g) in CH_2Cl_2 (45 mL). The crude was purified on SiO_2 (5% \rightarrow 10% EtOAc/hexanes) to give **6.75c** (1.454 g, 72%) as a colorless oil. Based on 1H NMR ($CDCl_3$), a mixture of 7%:93% of the *cis*-/*trans*- **6.75c** were observed. The 1H NMR and HRMS of **6.75c** match the reported literature values.²⁹

(E)-3-(*Triisopropylsilyl*)acrylaldehyde (**6.75d**). Compound **6.75d** was prepared according to the above-described procedure through the oxidation of **6.88d** (2.76 g, 12.9 mmol) with PCC (5.55 g, 25.7 mmol) and Celite (5.0 g) in CH₂Cl₂ (55 mL). The crude was purified on SiO₂ (5% → 10% EtOAc/hexanes) to give **6.75d** (1.71 g, 63%) as a colorless oil. Based on ¹H NMR (CDCl₃), only *trans*-**6.75d** was observed. The ¹H NMR and HRMS of **6.75d** match the reported literature values.²⁹

(E)-3-Bromoacrylic acid (**6.89**). A solution of propiolic acid (2.64 mL, 42.8 mmol) and HBr (17.5 mL, 48% aq) was refluxed for 1.5 h, cooled to rt, and then 0 °C. The brown crystals formed were filtered and rinsed with ice-cold water (30 mL) and dried to give **6.89** (4.19 g, 65%). The compound was used without further purification.

(E)-3-Bromoacrylaldehyde (**6.75e**). A solution of **6.89** (3.0 g, 19.9 mmol) in THF (15 mL) was added dropwise to a suspension of LiAlH₄ (0.754 g, 19.9 mmol) in THF (60 mL) at 0 °C. After stirring at 0 °C for 2 h, the reaction was quenched by the sequential addition of H₂O (0.8 mL), NaOH (2.4 mL, 20% aq), and H₂O (0.8 mL). The reaction mixture was diluted with Et₂O (100 mL), filtered, and the filtrate was washed with sat'd aq NaHCO₃, brine (1x), dried over Na₂SO₄, filtered and concentrated to give the allylic alcohol (0.7736 g). A solution of the allylic alcohol (0.7736 g, 5.65 mmol) in dry CH₂Cl₂ (8.5 mL) was added to activated MnO₂ (2.45 g, 28.2 mmol, heated at 0.4 Torr and 110 °C for 3 h). After stirring at rt for 18 h, the reaction mixture was filtered on Celite, and the Celite cake was rinsed with little CH₂Cl₂ (4 x 3 mL). Based on ¹H NMR (CDCl₃), the filtrate contained a mixture of 1:1 of the allylic alcohol/aldehyde **6.75e** in CH₂Cl₂. The filtrate was stored at -10 °C and used in the next reaction without further purification. The ¹H NMR matched reported literature values.⁴³

(S)-Dec-9-en-4-ol (**6.90**). Compound **6.90** was synthesized according to a reported literature procedure.⁹ A solution of 1-bromoethane (3.24 mL, 43.5 mmol) in THF (40 mL) was added dropwise to Mg⁰ turnings (1.32 g, 54.3 mmol) coated with I₂ under N₂ in a two-necked round bottom flask equipped with a reflux condenser. The solution was refluxed for 1.5 h, cooled to rt, and added dropwise over 1 h to a solution of *(S)*-epichlorohydrin (1.70 mL, 21.7 mmol) and CuCN (195.0 mg, 2.2 mmol) in THF (25 mL) at -78 °C under N₂. The reaction was warmed to -20 °C over 4 h, quenched with sat'd aq NH₄Cl (30 mL), the layers separated, and the aqueous layer extracted with Et₂O (4 x 30 mL). The combined organic layer was washed with brine (1x), dried over Na₂SO₄, filtered and concentrated. The crude was dissolved in Et₂O (25 mL) and stirred with crushed NaOH (4.27 g, 10.7 mmol) for 18 h. The reaction was filtered on Celite, and the filtrate was distilled on a Vigreux column at normal pressure to give the epoxide that was used as is in the next step.

A solution of 5-bromo-1-pentene (3.86 mL, 32.6 mmol) in THF (40 mL) was added dropwise to Mg⁰ turnings (1.06 g, 43.5 mmol) coated with I₂ under N₂ in a two-necked round bottom flask equipped with a reflux condenser. The solution was refluxed for 2 h, cooled to rt, and added dropwise over 1 h to a solution of the epoxide and CuCN (195.0 mg, 2.2 mmol) in THF (40 mL) at -78 °C under N₂. The reaction was warmed to 0 °C over 18 h, quenched with sat'd aq NH₄Cl (25 mL), the layers separated, and the aqueous layer extracted with Et₂O (3 x 30 mL). The combined organic layer was washed with brine (1x), dried over Na₂SO₄, filtered and concentrated. The crude was purified on SiO₂ (10% EtOAc/hexanes) to give **6.90** (2.16 g, 64% over 3 steps) as a colorless oil. ¹H NMR (500 MHz, CDCl₃) δ (ppm, integ., mult, *J* Hz) 5.81 (1H, m), 5.00 (1H, ddd, 1.2, 2.8, 13.6), 4.94 (1H, m), 3.60 (1H, m), 2.06 (2H, br q, 5.6), 1.29-1.51 (10H, m), 0.92 (3H,

t, 5.6). ¹³C NMR (125 MHz, CDCl₃) δ (ppm) 139.1, 114.5, 71.8, 39.8, 37.4, 33.9, 29.1, 25.3, 19.0, and 14.3. HRMS (ESITOF) *m/z* 157.1589 [M+H]⁺ (calc'd 157.1587 for C₁₀H₂₁O).

(S)-7-((*Dec-9-en-4-yloxy*)triisopropylsilane (**6.91**). Compound **18** was synthesized according to a reported literature procedure.⁴⁴ Freshly distilled 2,6-lutidine (0.82 mL, 7.04 mmol) and TBSOTf (1.55 mL, 5.76 mmol) were added to a solution of **6.90** (0.5 g, 3.20 mmol) in CH₂Cl₂ (32 mL) at 0 °C. After 1.5 h, the reaction mixture was quenched by addition of sat'd aq NaHCO₃ and H₂O. The mixture was extracted with Et₂O (3x), and the combined organic layer was washed with brine (1x), dried over Na₂SO₄, filtered and concentrated. The crude was purified on SiO₂ (100% hexanes) to give **6.91** (0.894 g, 89%) as a colorless oil. ¹H NMR (500 MHz, CDCl₃) δ (ppm, integ., mult, *J* Hz) 5.81 (1H, m), 4.99 (1H, m), 4.93 (1H, m), 3.80 (1H, m), 2.05 (1H, br q, 6.5), 1.26-1.53 (13H, m), 1.05 (18H, s), 0.89 (3H, t, 7.5). ¹³C NMR (125 MHz, CDCl₃) δ (ppm) 139.2, 114.4, 72.2, 39.0, 36.6, 34.0, 29.4, 24.5, 18.4, 18.3, 14.6 and 12.8.

(S)-7-((*Triisopropylsilyl*)oxy)decan-1-ol (**6.92**). BH₃·THF (9.6 mL, 9.6 mmol, 1M in THF) was added dropwise to a solution of **6.91** (0.6 g, 1.92 mmol) in THF (10 mL) at -15 °C. The solution was stirred at -15 °C for 30 min, warmed to rt and stirred for 18 h. NaOH (10 mL, 30 mmol, 3 N aq) and H₂O₂ (5 mL, 44.1 mmol, 30% aq) were added dropwise to the reaction at 0 °C. The reaction was warmed to rt, stirred for 5 h, diluted with ice-cold H₂O (60 mL) and acidified to pH ~1 with HCl (1 M). The layers were separated, and the aqueous layer was extracted with EtOAc (3x). The combined organic layers were washed with brine (1x), dried over Na₂SO₄, filtered and concentrated. The crude was purified by SiO₂ (20% EtOAc/hexanes) to give **6.92** (0.439 g, 69%) as a colorless oil. ¹H NMR (500 MHz, CDCl₃) δ (ppm, integ., mult, *J* Hz) 3.80 (1H, quint., 5.5), 3.64 (2H, t, 6.5), 1.57 (2H, quint., 7.0), 1.41-1.51 (4H, m), 1.27-1.40 (10H, m), 1.05 (18H, s), 0.89 (3H, t, 7.5). ¹³C NMR (125 MHz, CDCl₃) δ (ppm) 72.2, 63.2, 39.1, 36.7, 32.9, 29.9, 25.9, 25.0,

18.4, 18.3, 14.6, and 12.8. HRMS (ESITOF) m/z 353.2849 $[M+Na]^+$ (calc'd 353.2846 for $C_{19}H_{42}O_2SiNa^+$).

(S)-((10-Bromodecan-4-yl)oxy)triisopropylsilane (6.93). Triphenylphosphine (0.595 g, 2.27 mmol) was added in one-portion to a solution of **6.92** (0.50 g, 1.51 mmol) and carbon tetrabromide (0.627 g, 1.89 mmol) in CH_2Cl_2 (12.5 mL) at 0 °C. After stirring at 0 °C for 30 min, the reaction mixture was concentrated, and the crude was purified on SiO_2 (100% hexanes) to give **6.93** (0.55 g, 92%) as a colorless oil. 1H NMR (500 MHz, $CDCl_3$) δ (ppm, integ., mult, J Hz) 3.80 (1H, p, 5.6 Hz), 3.41 (2H, t, 6.9 Hz), 1.91 – 1.78 (2H, m), 1.53 – 1.39 (6H, m), 1.37 – 1.23 (9H, m), 1.05 (18H, s), 1.00 – 0.83 (3H, t, 7.2). ^{13}C NMR (100 MHz, $CDCl_3$) δ (ppm) 72.2, 39.1, 36.6, 34.2, 32.9, 29.3, 28.4, 24.8, 18.4, 18.3, 14.6, and 12.8.

(S)-Triphenyl(7-((triisopropylsilyl)oxy)decyl)phosphonium bromide (6.94). A solution of **6.93** (200 mg, 0.51 mmol) and triphenylphosphine (160 mg, 0.61 mmol) in MeCN (2.5 mL) was refluxed for 18 h. The reaction was cooled to rt and diluted with EtOAc and hexanes. The white precipitate formed was filtered to provide **6.94** that was used without further purification.

General Procedure for Robinson–aza-Michael Cyclization without Catalyst. Attempted synthesis of **6.96a–d** was completed under the conditions described by Bonjoch and coworkers.²⁵ Silyl derivatives **6.75a–d** (22.5 μ mol) in *i*-PrOH (70 μ L), H_2O (4 μ L, 204 μ mol) and $LiOH \cdot H_2O$ (0.9 mg, 20.4 μ mol) were sequentially added to **6.74** (10 mg, 20.4 μ mol). After 24 h, the reaction was quenched with sat'd NH_4Cl (0.5 mL) and extracted with EtOAc (3 x 0.5 mL). The combined organic layer was dried over Na_2SO_4 , filtered and evaporated. The crude was purified on SiO_2 (10% \rightarrow 20% EtOAc/Hexanes) to give the corresponding product.

General Procedure for Robinson–aza-Michael Cyclization with Catalyst. Attempted synthesis of **6.96a–e** was completed under the conditions described by Bonjoch and coworkers.²⁵

Silyl derivatives **6.75a–d** (22.5 μmol , 83 μL in toluene), **6.95** (2.1 mg, 4.1 μmol , 107 μL in toluene), and LiOAc (0.67 mg, 10.2 μmol) were added sequentially to **6.74** (10 mg, 20.4 μmol). After 24 h, the toluene was evaporated, and H_2O (4 μL , 204 μmol), $\text{LiOH}\cdot\text{H}_2\text{O}$ (0.9 mg, 20.4 μmol) and *i*-PrOH (190 μL) were added to the reaction mixture. After an additional 24 h, the reaction was quenched with sat'd NH_4Cl (0.5 mL) and extracted with EtOAc (3 x 0.5 mL). The combined organic layer was dried over Na_2SO_4 , filtered and evaporated. The crude was purified on SiO_2 (10% \rightarrow 20% EtOAc/Hexanes) to give the corresponding product.

tert-Butyl (2*R*,3*R*,4*aS*,8*aS*)-3-(benzyloxy)-7-(dimethyl(phenyl)silyl)-5-hydroxy-2-methyl-1-tosyl-1,2,3,4,4*a*,7,8,8*a*-octahydroquinoline-6-carboxylate (**6.96b**). The ^1H and ^{13}C NMR values are reported in Table 6.7. HRMS (ESITOF) m/z 684.2779 $[\text{M}+\text{Na}]^+$ (calc'd 684.2786 for $\text{C}_{37}\text{H}_{47}\text{NO}_6\text{SSiNa}^+$).

tert-Butyl (2*R*,3*R*,4*aS*,8*aS*)-3-(benzyloxy)-5-hydroxy-2-methyl-1-tosyl-7-(triethylsilyl)-1,2,3,4,4*a*,7,8,8*a*-octahydroquinoline-6-carboxylate (**6.96c**). ^1H NMR (500 MHz, CDCl_3) δ (ppm, integ., mult, J Hz) 12.53 (0.66H, s), 7.52 (2H, d, $J = 8.0$ Hz), 7.38 – 7.28 (3H, m), 7.26 – 7.23 (1H, m), 7.13 (2H, d, $J = 8.0$ Hz), 4.44 (2H, s), 4.35 (1H, quint., $J = 6.8$ Hz), 4.08 (1H, m), 3.03 (1H, m), 2.38 (3H, s), 2.23 – 2.13 (3H, m), 2.08 (1H, m), 1.95 (1H, m), 1.59 (1H, m), 1.53 (9H, s), 1.31 (3H, d, $J = 7.0$ Hz), 0.94 (9H, t, $J = 7.8$ Hz), 0.75 – 0.62 (6H, m). ^{13}C NMR (125 MHz, CDCl_3) δ (ppm) 172.3, 168.0, 143.2, 138.4, 138.1, 130.2, 130.0, 128.6, 128.4, 127.9, 127.6, 126.4, 100.9, 82.6, 73.6, 70.0, 50.3, 50.2, 38.6, 30.1, 28.4, 26.4, 21.7, 19.1, 16.1, 7.8, 3.5. HRMS (ESITOF) m/z 664.3105 $[\text{M}+\text{Na}]^+$ (calc'd 664.3099 for $\text{C}_{35}\text{H}_{51}\text{NO}_6\text{SSiNa}^+$).

tert-Butyl (4*aS*,8*aS*)-7-(dimethyl(phenyl)silyl)-5-hydroxy-1-tosyl-1,2,3,4,4*a*,7,8,8*a*-octahydroquinoline-6-carboxylate (**6.98**). The ^1H and ^{13}C NMR values are reported in Table 6.7. HRMS (ESITOF) m/z 564.2212 $[\text{M}+\text{Na}]^+$ (calc'd 564.2210 for $\text{C}_{29}\text{H}_{39}\text{NO}_5\text{SSiNa}^+$).

(2*R*,3*R*,4*aS*,8*aS*)-3-(Benzyloxy)-7-(dimethyl(phenyl)silyl)-2-methyl-1-tosyloctahydroquinolin-5(1*H*)-one (**6.71**). TFA (100 μ L) was added to a solution of **6.96b** (62.5 mg, 94.4 μ mol) at rt. After 5 min, the solvent was evaporated and traces of TFA were azeotroped off with toluene to give a brown residue. The residue was placed on the rotatory evaporator under high vacuum at 56 °C for 2 h to give ketone **6.71** (48.6 mg, 92%). ¹H NMR (500 MHz, CDCl₃) δ (ppm, integ., mult, *J* Hz) 7.62 – 7.52 (3H, m), 7.52 – 7.26 (11H, m), 7.22 (2H, td, *J* = 8.1, 2.0 Hz), 7.11 (2H, d, *J* = 8.0 Hz), 4.40 (2H, s), 4.28 (1H, q, *J* = 6.9 Hz), 4.20 (1H, dt, *J* = 12.7, 5.5 Hz), 2.95 (1H, dt, *J* = 10.4, 5.8 Hz), 2.51 – 2.40 (2H, m), 2.37 (3H, s), 2.28 (1H, dd, *J* = 13.1, 6.5 Hz), 2.23 – 2.10 (2H, m), 1.97 (1H, dt, *J* = 11.6, 6.1 Hz), 1.81 – 1.66 (3H, m), 1.51 (1H, dq, *J* = 7.6, 3.9 Hz), 1.34 (3H, d, *J* = 7.1 Hz), 0.41 (3H, s), 0.39 (3H, s). ¹³C NMR (100 MHz, CDCl₃) δ (ppm) 211.1, 143.3, 138.3, 135.2, 134.4, 130.0, 129.6, 128.6, 128.2, 128.02, 127.98, 127.6, 126.2, 73.8, 70.2, 51.4, 50.0, 49.8, 38.6, 30.1, 24.5, 21.6, 20.2, 16.4, -3.57, -3.98. HRMS (ESITOF) *m/z* 562.2444 [M+H]⁺ (calc'd 562.2442 for C₃₂H₄₀NO₄SSi⁺).

(2*R*,3*R*,4*aR*,8*aS*,*E*)-3-(Benzyloxy)-7-(dimethyl(phenyl)silyl)-2-methyl-1-tosyl-5-((*S*)-7-((triisopropylsilyl)oxy)decylidene)decahydroquinoline (**6.101**). A solution of **6.94** (95 mg, 144 μ mol) in THF (0.5 mL) was added dropwise to a suspension of KO*t*-Bu (16.2 mg, 144 μ mol) in THF (0.5 mL) at 0 °C under N₂. After 45 min at 0 °C, the ylide solution was added dropwise to a solution of **6.71** (27 mg, 48 μ mol) in THF (0.4 mL) at 0 °C. After 16 h at rt, the reaction was quenched by addition of sat'd aq NH₄Cl, diluted with Et₂O and the layers were separated. The aq layer was extracted with Et₂O (2x), and the combined organic layer was dried over Na₂SO₄, filtered and concentrated. The crude was purified on SiO₂ (5% \rightarrow 10% \rightarrow 20% EtOAc/hexanes) to give **6.100** (12.2 mg). ¹H NMR (500 MHz, CDCl₃) δ (ppm, integ., mult, *J* Hz) 7.78 – 7.61 (2H, m), 7.51 – 7.44 (2H, m), 7.42 – 7.35 (3H, m), 7.34 – 7.20 (7H, m), 6.74 (1H, t, *J* = 4.0 Hz), 4.78 (1H,

d, $J = 9.2$ Hz), 4.53 (1H, d, $J = 11.6$ Hz), 4.49 – 4.37 (1H, m), 3.42 – 3.27 (2H, m), 2.55 – 2.45 (1H, m), 2.41 (3H, s), 2.41 (1H, m) 2.26 (1H, dd, $J = 13.5, 7.1$ Hz), 2.20 – 2.12 (2H, m), 1.57 – 1.44 (1H, m), 1.14 – 0.97 (1H, m), 0.91 (3H, d, $J = 6.6$ Hz), 0.31 (6H, s). ^{13}C NMR (100 MHz, CDCl_3) δ (ppm) 200.1, 150.4, 143.2, 138.9, 138.3, 136.3, 134.9, 134.1, 129.7, 129.6, 128.4, 128.2, 128.1, 127.9, 127.1, 79.9, 72.5, 51.2, 39.1, 32.1, 27.4, 23.5, 21.7, 19.0, -5.2, -5.3. HRMS (ESITOF) m/z 562.2439 $[\text{M}+\text{H}]^+$ (calc'd 562.2442 for $\text{C}_{32}\text{H}_{40}\text{NO}_4\text{SSi}^+$).

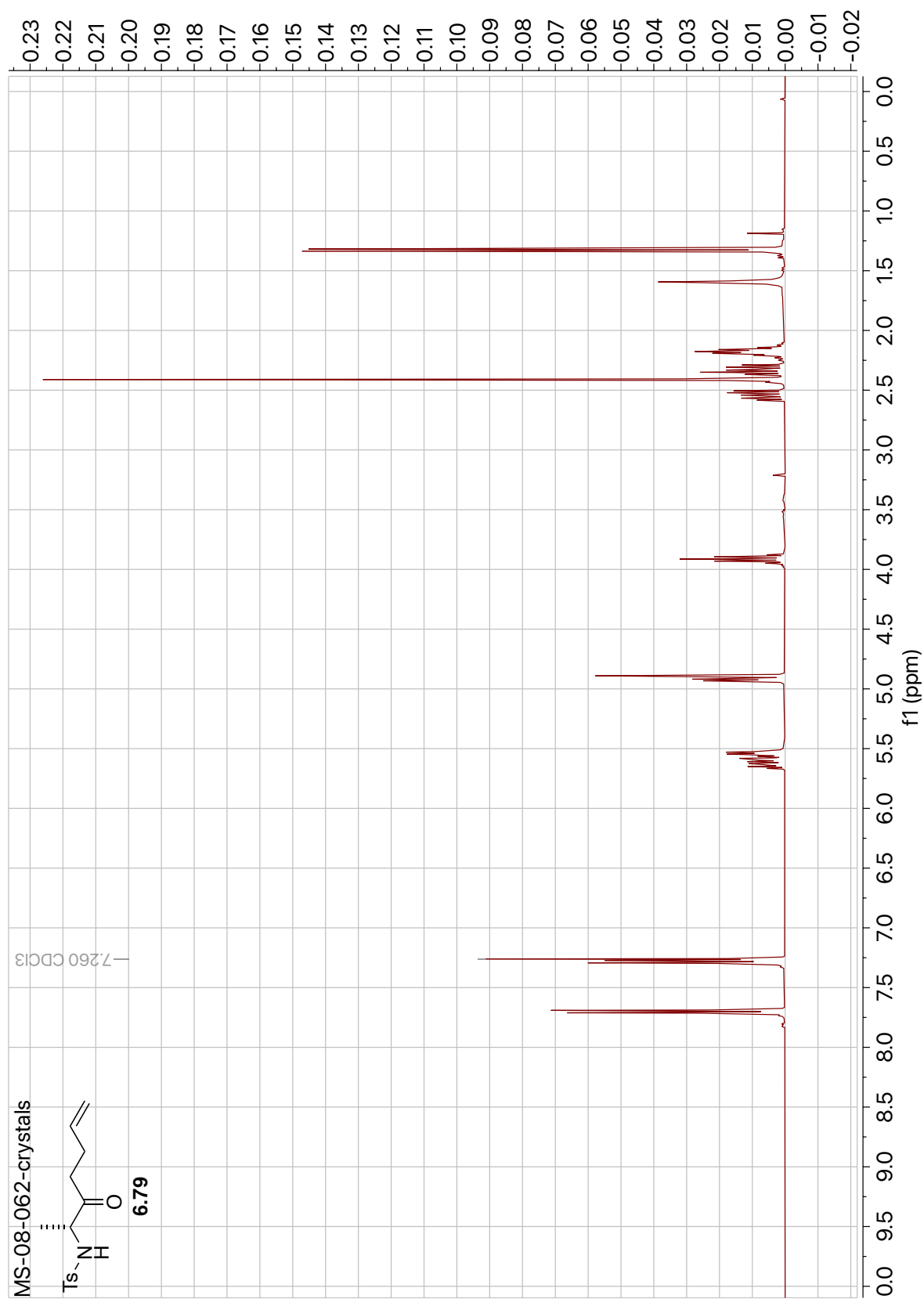
(*4aS,7S,8aS*)-7-Methyl-1-tosyloctahydroquinolin-5(1H)-one (**6.103**). TFA (400 μL) was added neat to **6.98** (96.8 mg, 230 μmol) at rt. After 5 min, the solvent was evaporated and traces of TFA were azeotroped off with toluene to give a brown residue. The residue was placed on the rotatory evaporator under high vacuum at 70 $^\circ\text{C}$ for 5 – 6 h. The crude was used in the next reaction without further purification. The ^1H NMR and HRMS matched reported literature values.²⁵

Ethyl 2-((*4aR,7R,8aS,E*)-7-methyl-1-tosyloctahydroquinolin-5(1H)-ylidene)acetate (**6.106**). *n*-BuLi (0.59 mL, 1.47 mmol, 2.5 M in THF) was added dropwise to a solution of **6.104** (292 μL , 1.47 mmol) in THF (4.25 mL) at -78 $^\circ\text{C}$. After 15 min at rt, the reaction was cooled to -78 $^\circ\text{C}$, and a solution of **6.103** (230 μmol) in THF (1.5 mL) was added dropwise to the reaction. The reaction was stirred at -78 $^\circ\text{C}$ for 40 min, -40 $^\circ\text{C}$ for 45 min, and 0 $^\circ\text{C}$ for 45 min. The reaction was quenched by addition of sat'd aq NH_4Cl and extracted with EtOAc (3x). The combined organic layer was washed with brine (1x), dried over Na_2SO_4 , filtered and concentrated. The crude was purified on SiO_2 (10% \rightarrow 20% EtOAc/hexanes) to give **6.106** (15.9 mg, 18%) and 1:2 mixture of **6.103**:**6.105** (56.4 mg). **6.106**: Based on ^1H NMR (CDCl_3), the reaction gave a 1:2 mixture of alkene isomers. The following ^1H and ^{13}C NMR characterization are of the major isomer. ^1H NMR (500 MHz, CDCl_3) δ (ppm, integ., mult, J Hz) 7.69 (2H, d, $J = 8.4$ Hz), 7.29 (2H, d, $J = 8.4$ Hz), 5.76 (1H, s), 4.26 (1H, dt, $J = 13.2, 4.9$ Hz), 4.13 (2H, q, $J = 7.2$ Hz), 3.78 (1H, m), 3.50 (1H, m),

2.96 (1H, tdd, $J = 13.0, 8.9, 2.6$ Hz), 2.43 (3H, s), 2.31 (1H, dt, $J = 12.8, 4.5$ Hz), 2.19 (1H, m), 2.06 (2H, m), 1.79 (1H, m), 1.70 – 1.48 (2H, m), 1.47 – 1.31 (2H, m), 1.27 (3H, t, 7.2), 0.92 (3H, d, 7.2). ^{13}C NMR (100 MHz, CDCl_3) δ (ppm) 166.7, 161.2, 143.2, 138.6, 129.9, 127.2, 127.0, 117.7, 117.4, 59.9, 50.9, 47.2, 39.9, 30.0, 29.1, 28.5, 25.0, 24.7, 21.7, 18.0, 14.4. HRMS (ESITOF) m/z 392.1892 $[\text{M}+\text{H}]^+$ (calc'd 392.1890 for $\text{C}_{21}\text{H}_{30}\text{NO}_4\text{S}^+$).

Separately, **6.104** (30 μL , 149 μmol), DBU (18.6 μL , 124 μmol) and **6.103** (40 mg, 124 μmol) in dry MeCN (0.5 mL) was added to a stirred solution of LiCl in MeCN (1.0 mL) under N_2 . After stirring at rt for 16 h, the reaction was quenched by addition of sat'd aq NH_4Cl and extracted with EtOAc (3x). The combined organic layer was dried over Na_2SO_4 , filtered and concentrated. Based on the ^1H NMR (CDCl_3) of the crude, the ratio of **6.106:6.103:6.105** is 1:5:11.

6.7 Appendix



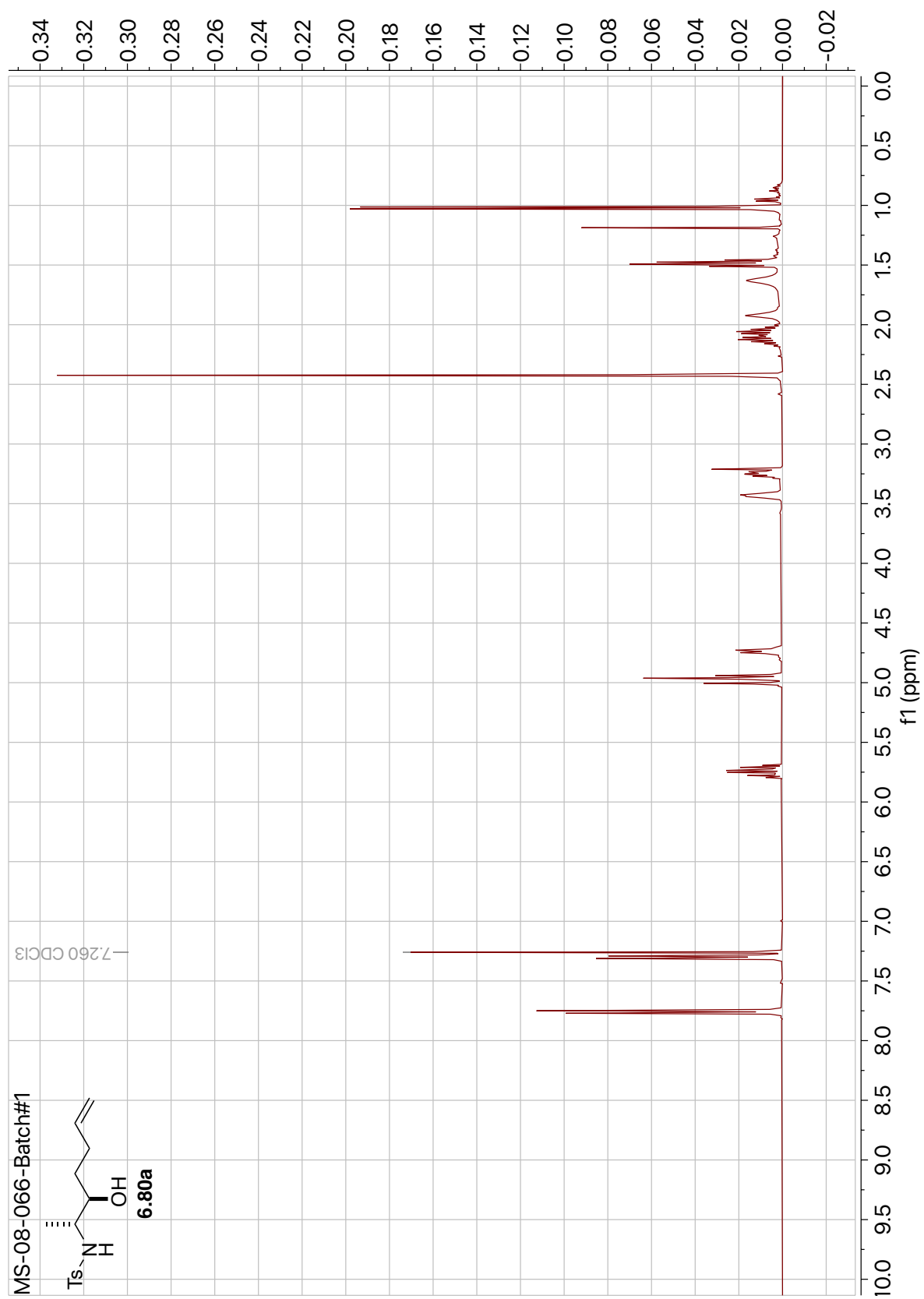


Figure 6.6: ¹H NMR of Compound 6.80a (400 MHz, CDCl₃).

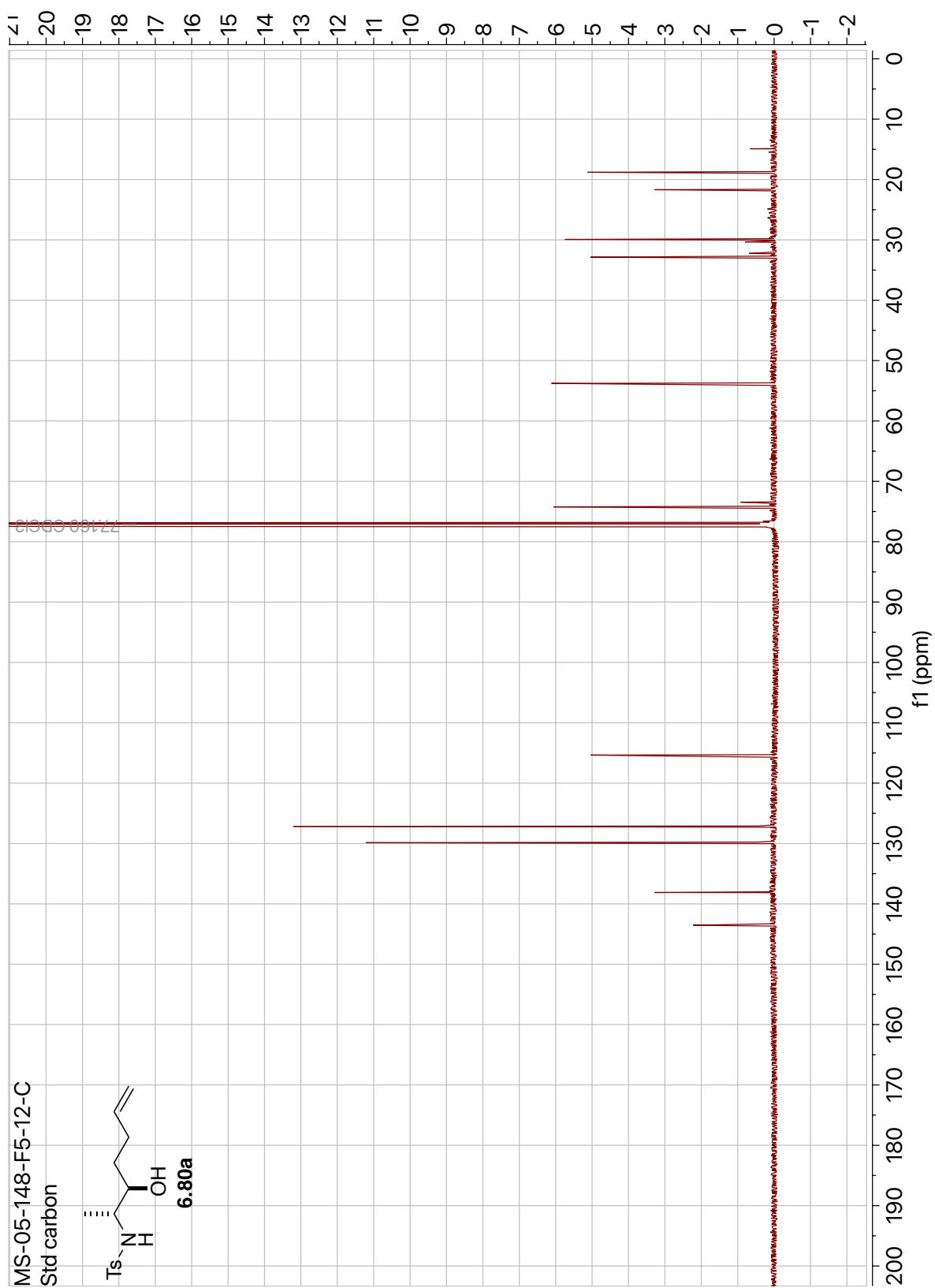


Figure 6.7: ¹³C NMR of Compound **6.80a** (125 MHz, CDCl₃).

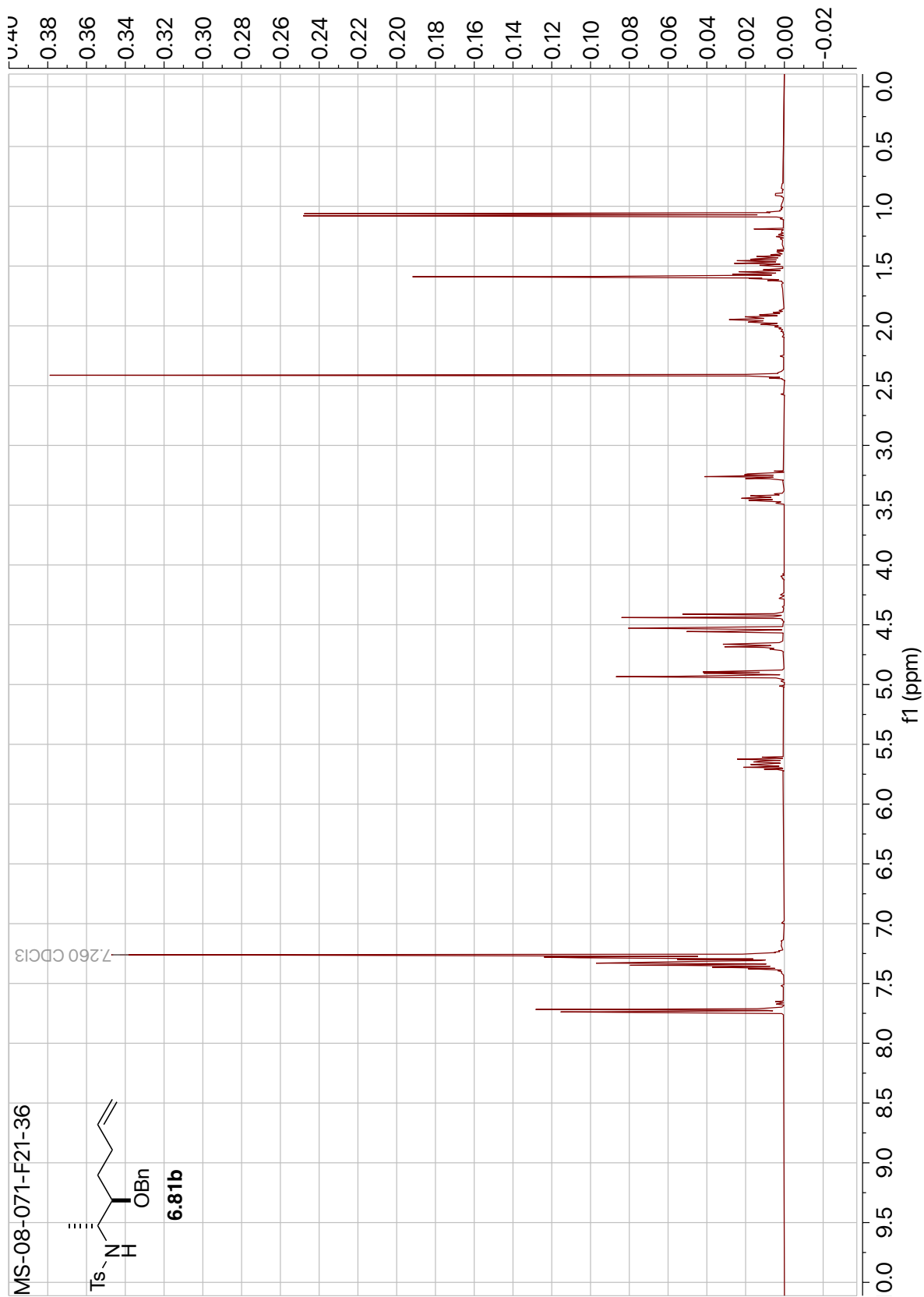


Figure 6.8: ¹H NMR of Compound **6.81b** (400 MHz, CDCl₃).

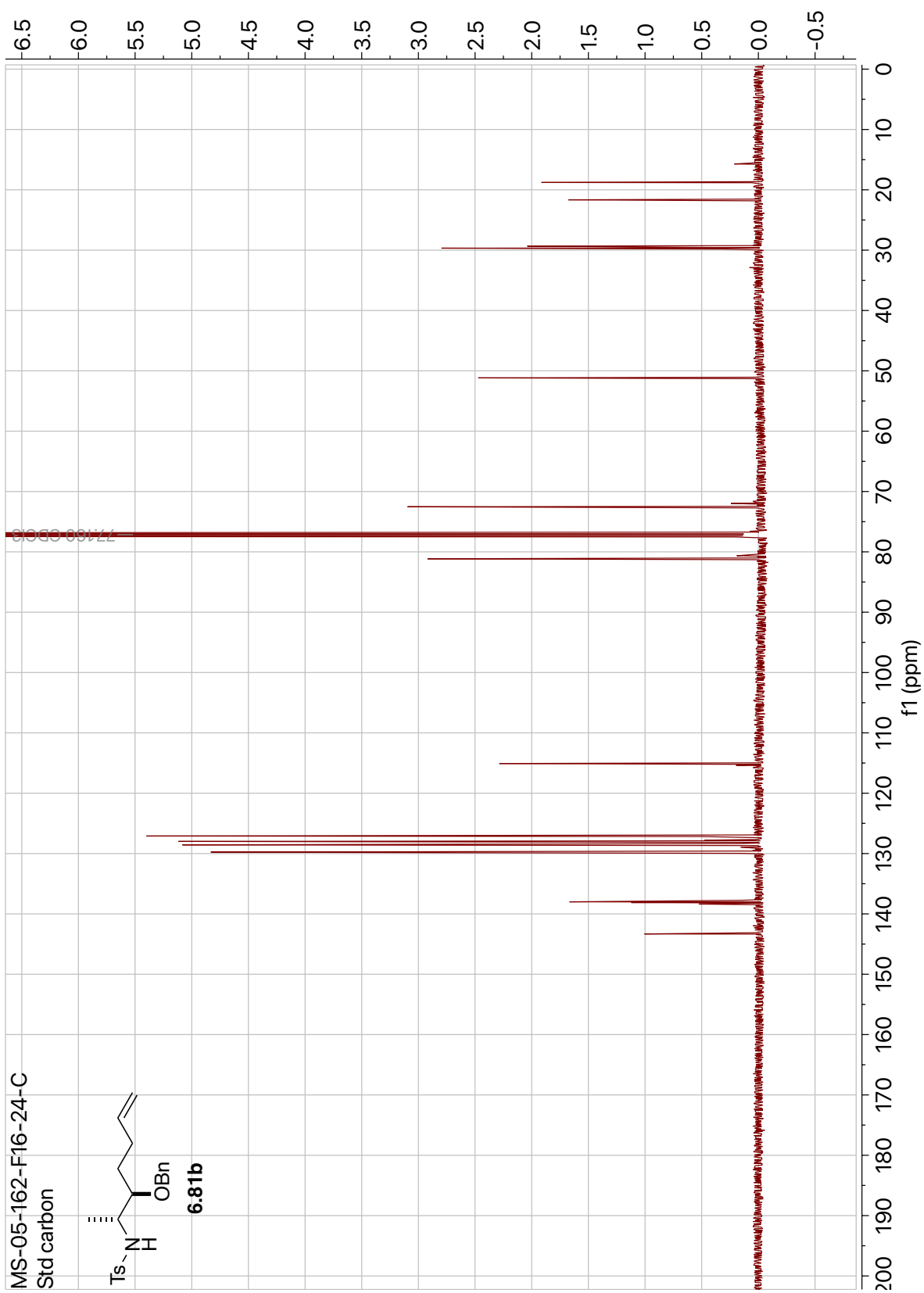


Figure 6.9: ¹³C NMR of Compound **6.81b** (125 MHz, CDCl₃).

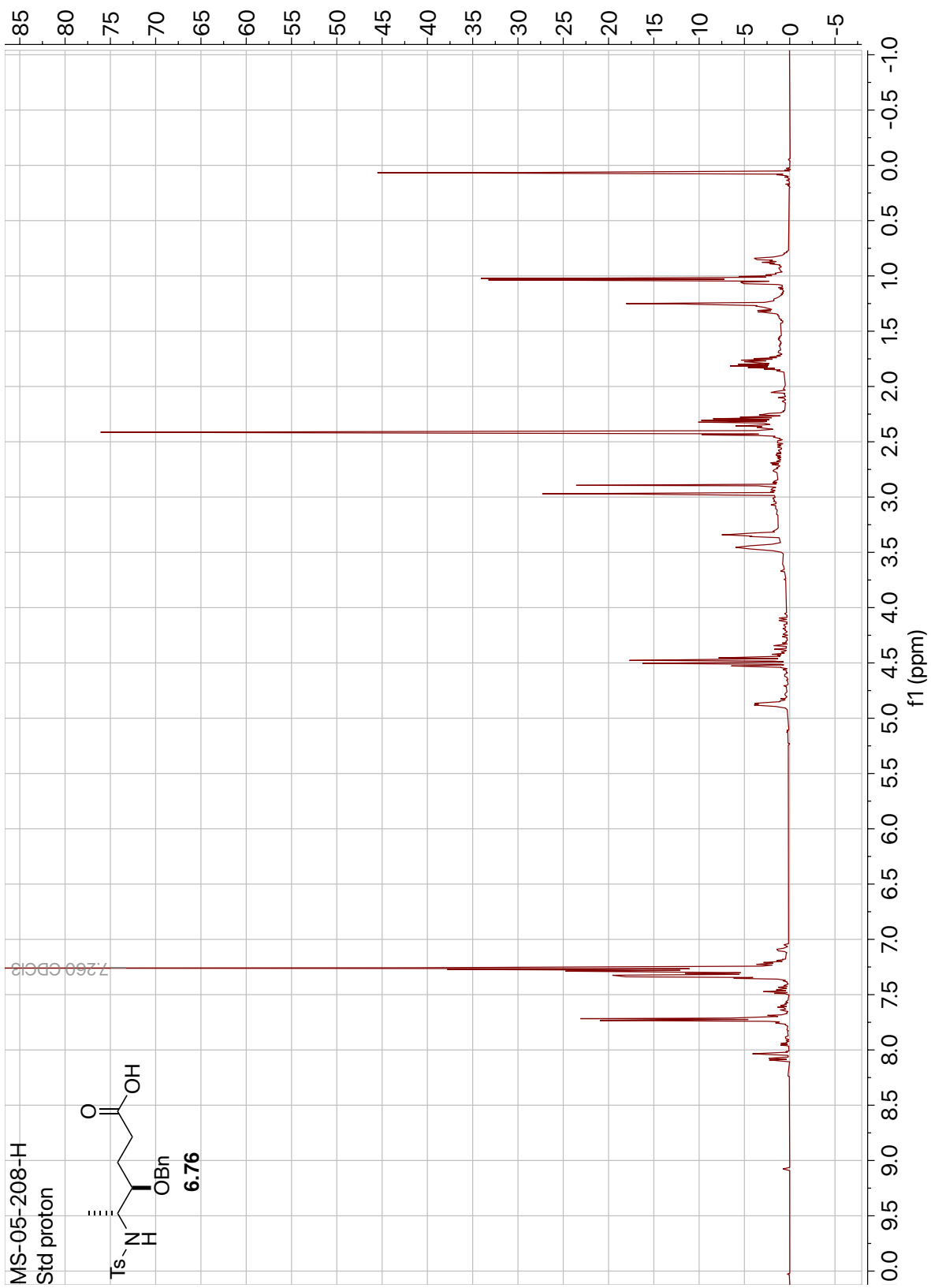


Figure 6.10: ¹H NMR of Compound 6.76 (500 MHz, CDCl₃).

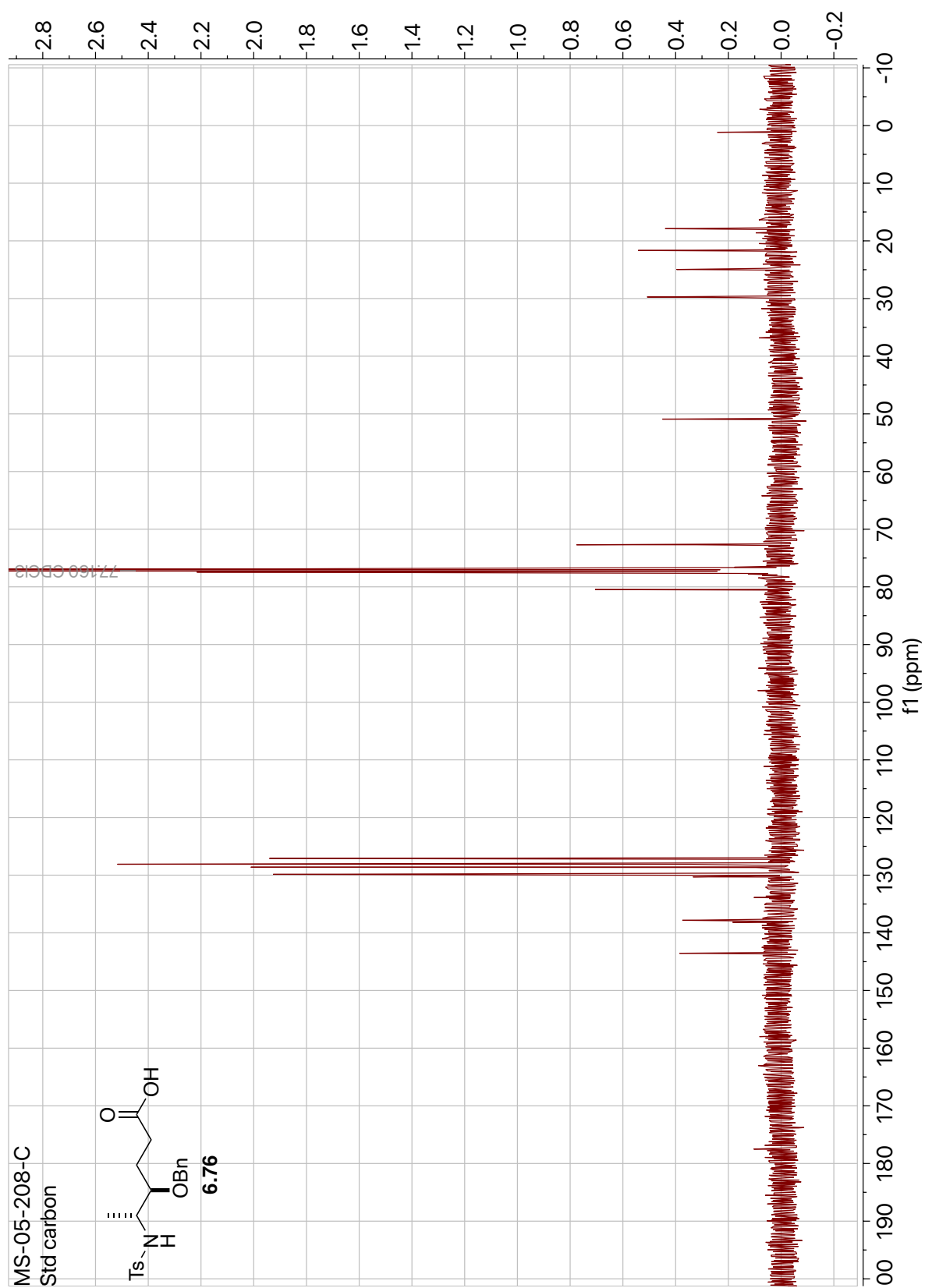


Figure 6.11: ^{13}C NMR of Compound 6.76 (125 MHz, CDCl_3).

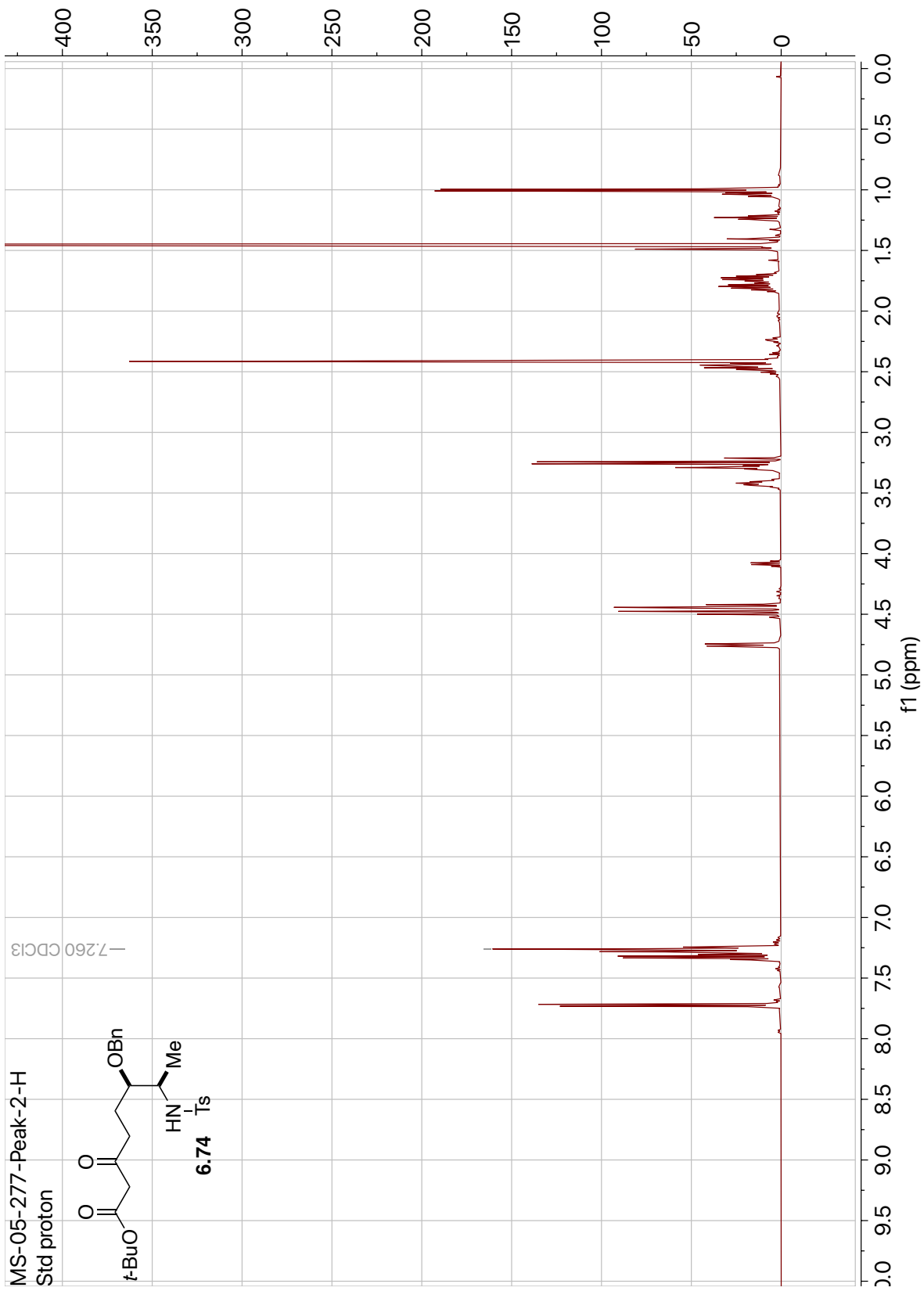


Figure 6.12: ^1H NMR of Compound 6.74 (500 MHz, CDCl_3).

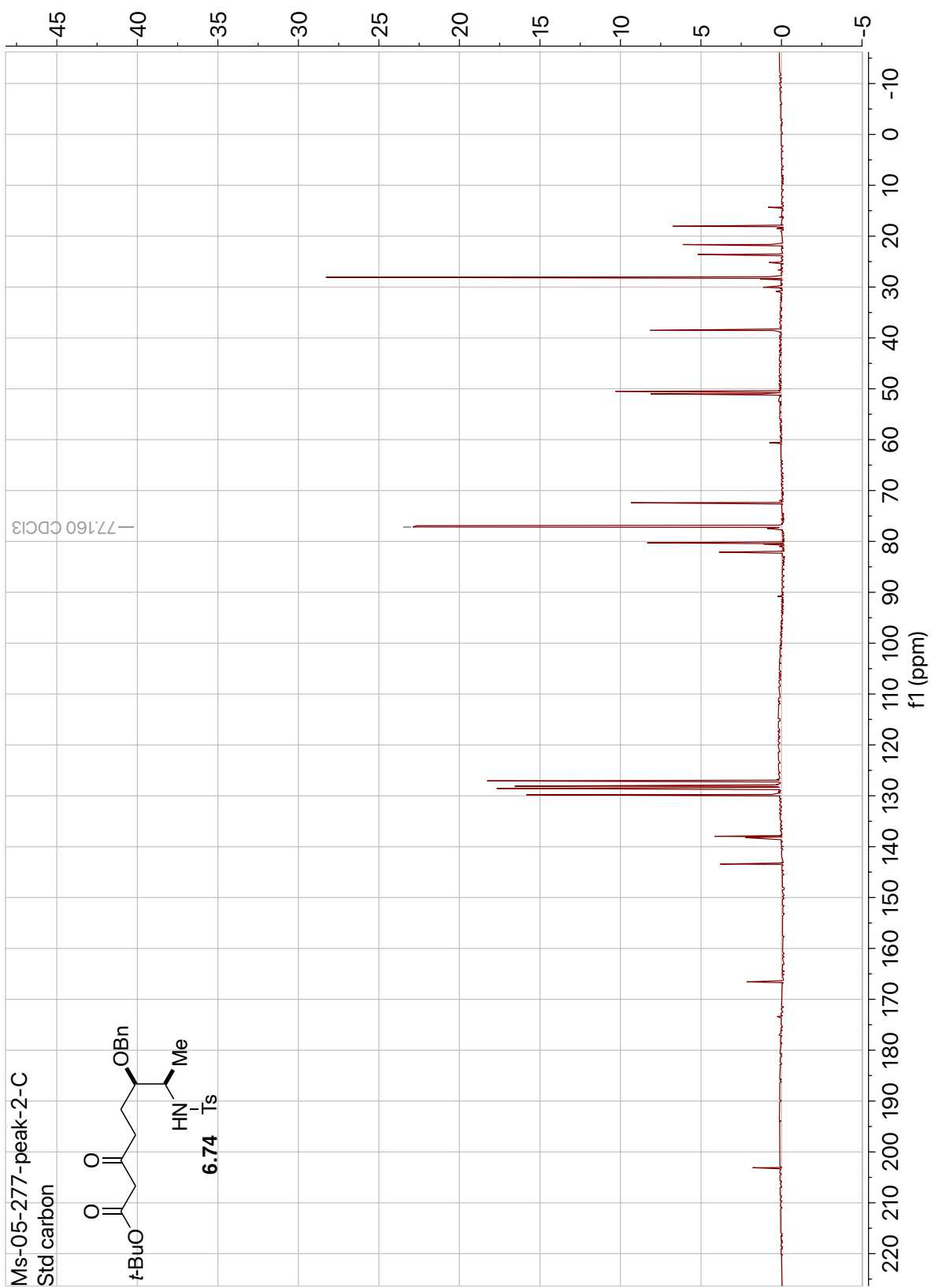


Figure 6.13: ¹³C NMR of Compound 6.74 (125 MHz, CDCl₃).

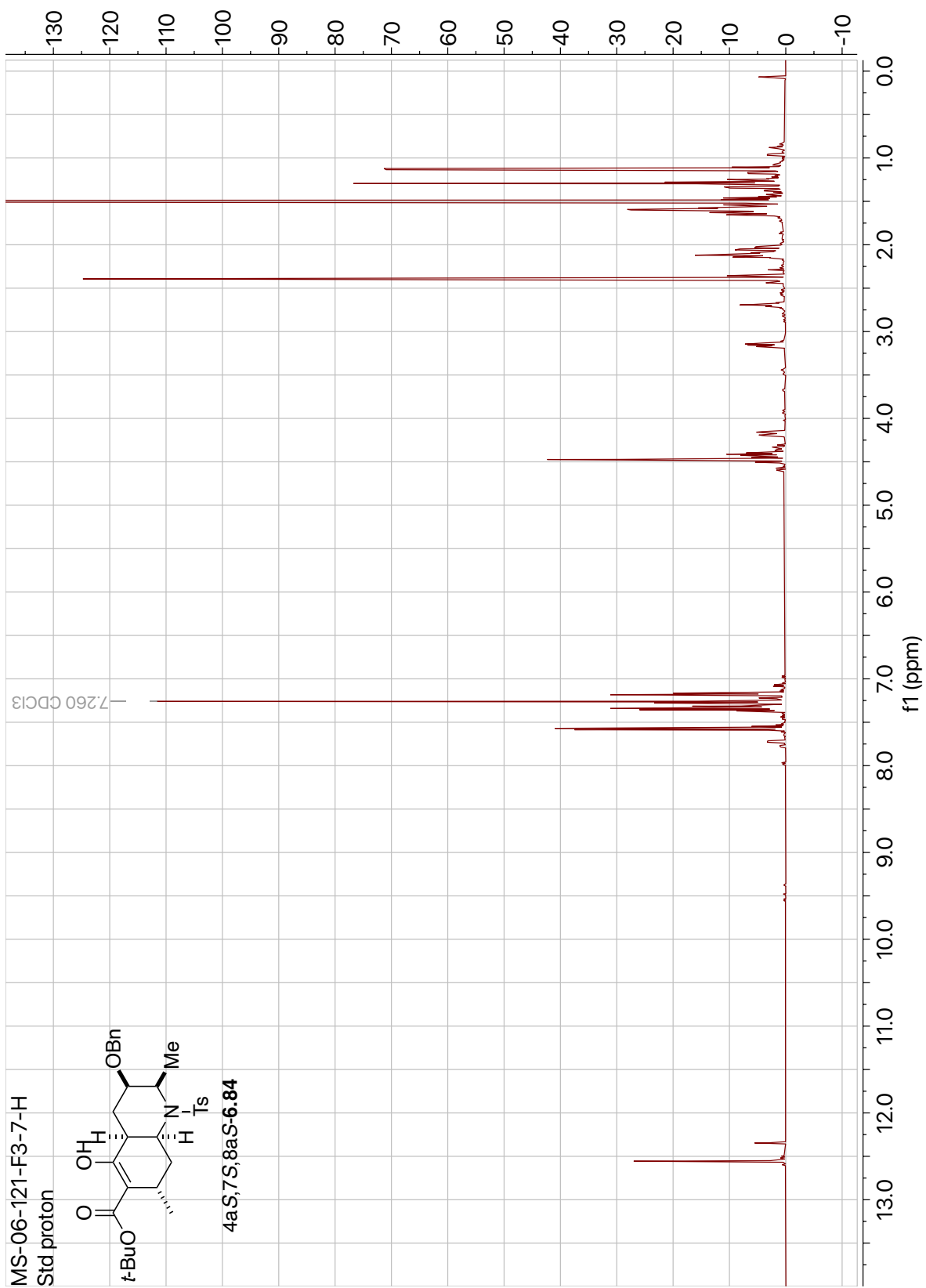


Figure 6.14: ¹H NMR of Compound **6.84** (500 MHz, CDCl₃).

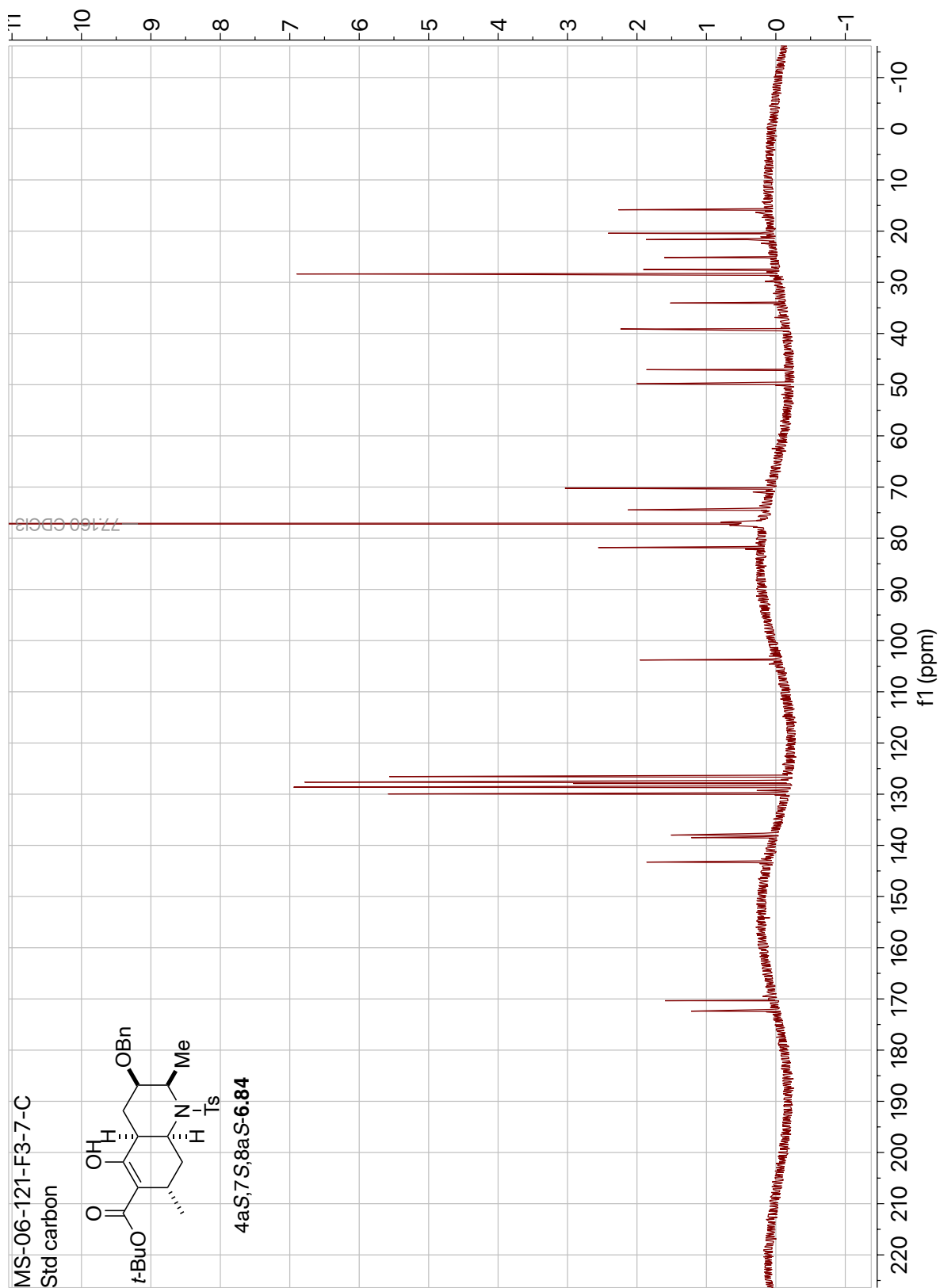


Figure 6.15: ¹³C NMR of Compound **6.84** (125 MHz, CDCl₃).

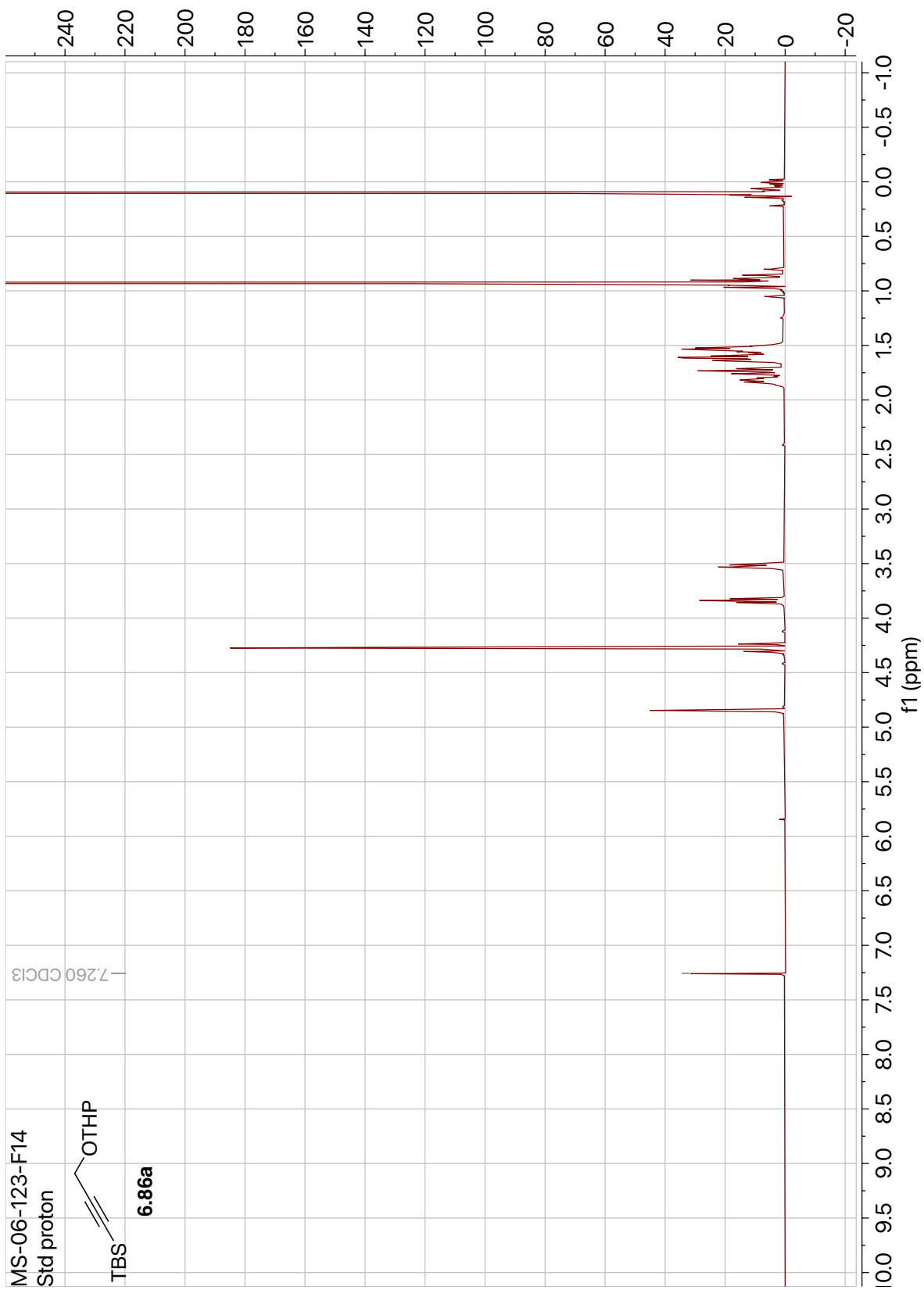


Figure 6.16: ¹H NMR of Compound **6.86a** (500 MHz, CDCl₃).

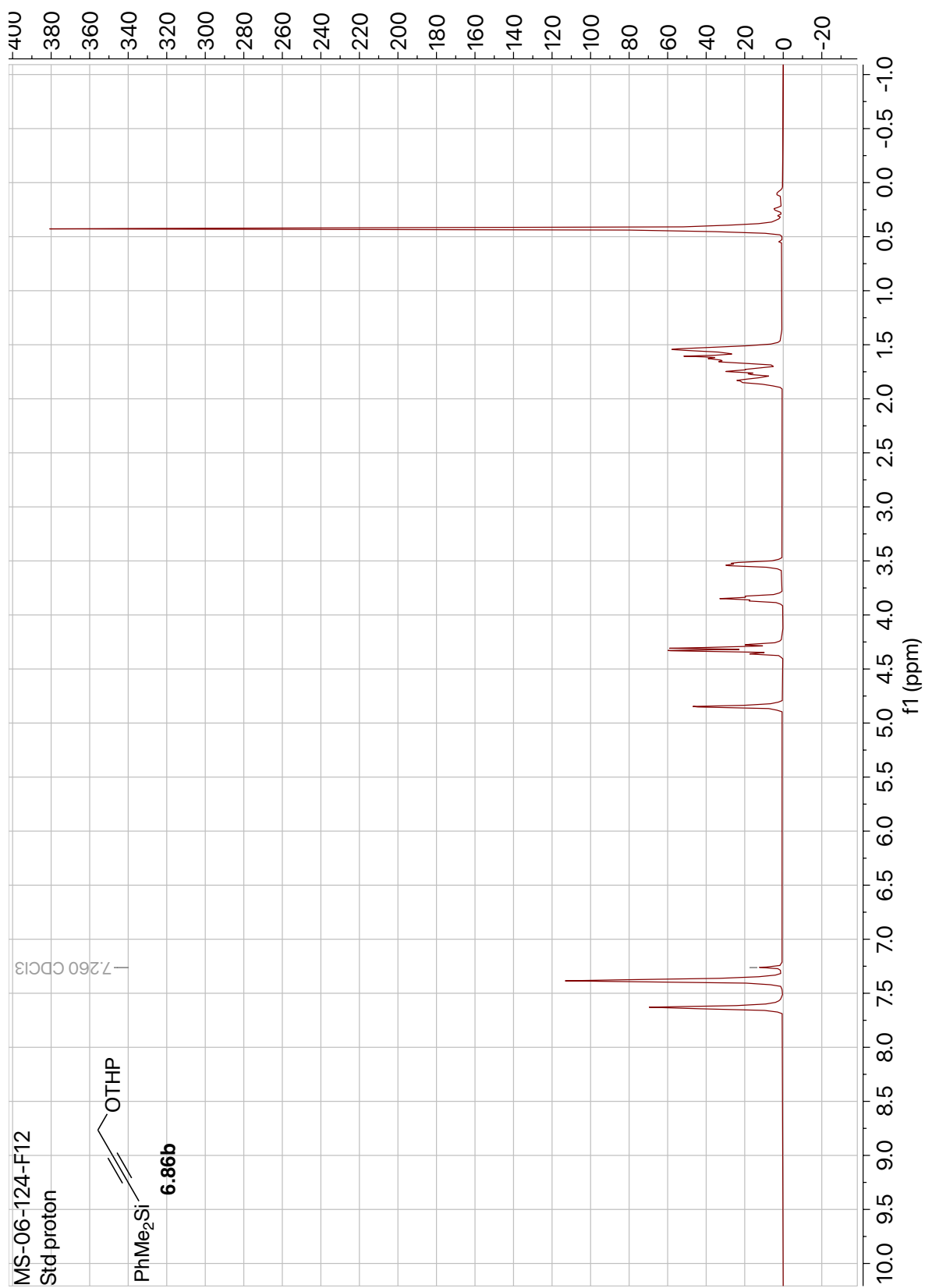


Figure 6.17: ¹H NMR of Compound **6.86b** (500 MHz, CDCl₃).

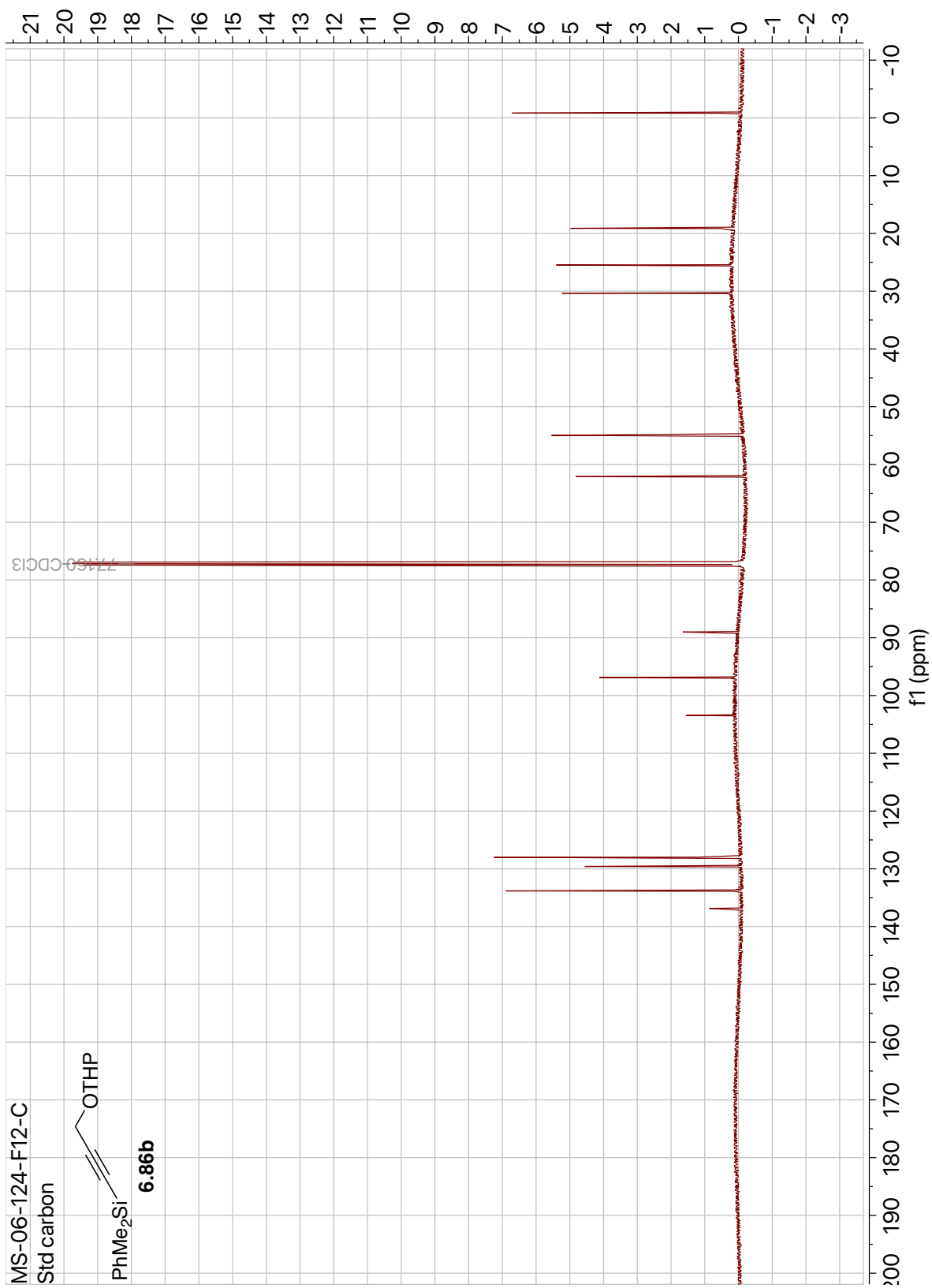


Figure 6.18: ¹³C NMR of Compound **6.86b** (125 MHz, CDCl₃).

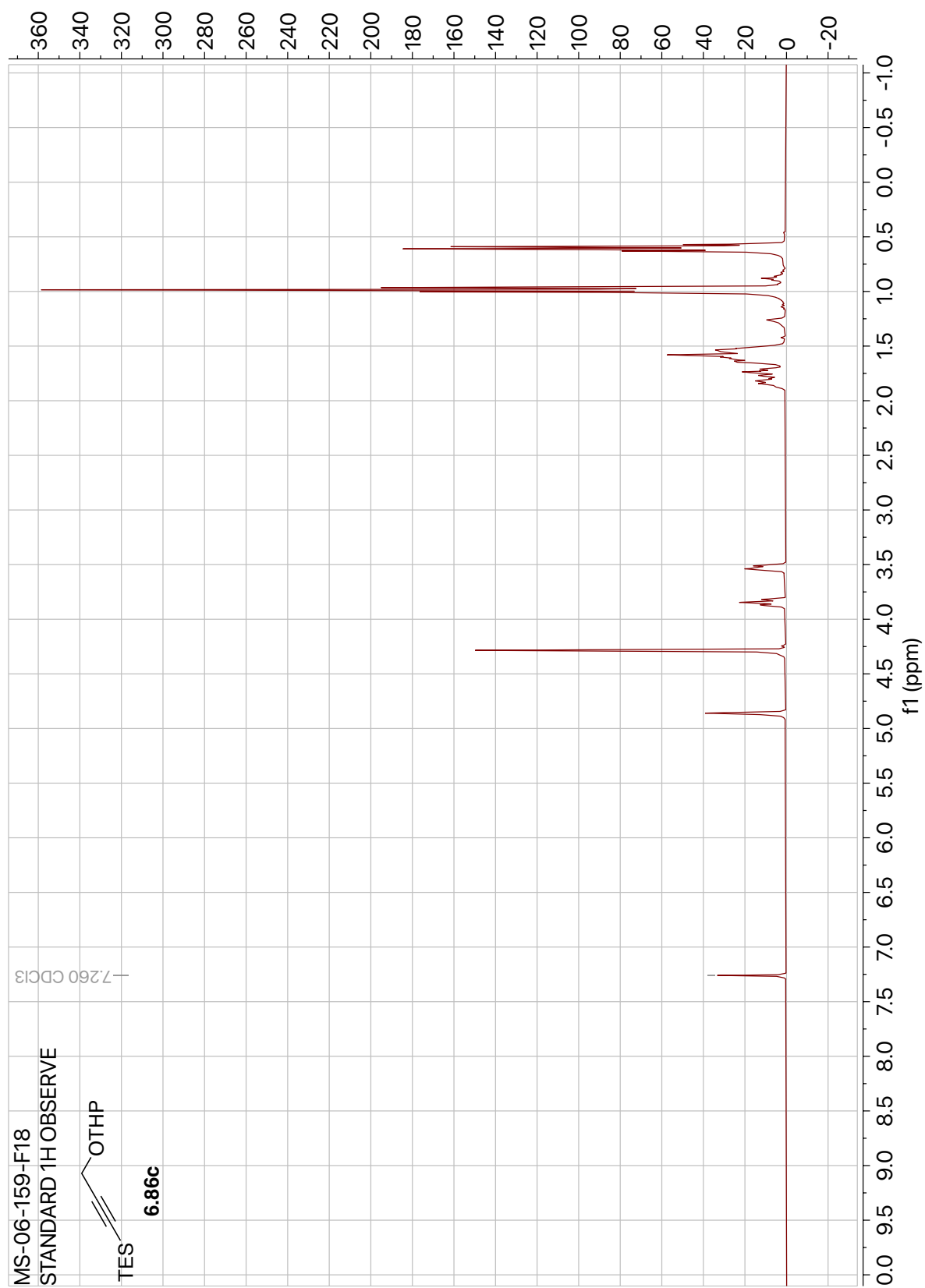


Figure 6.19: ^1H NMR of Compound **6.86c** (400 MHz, CDCl_3).

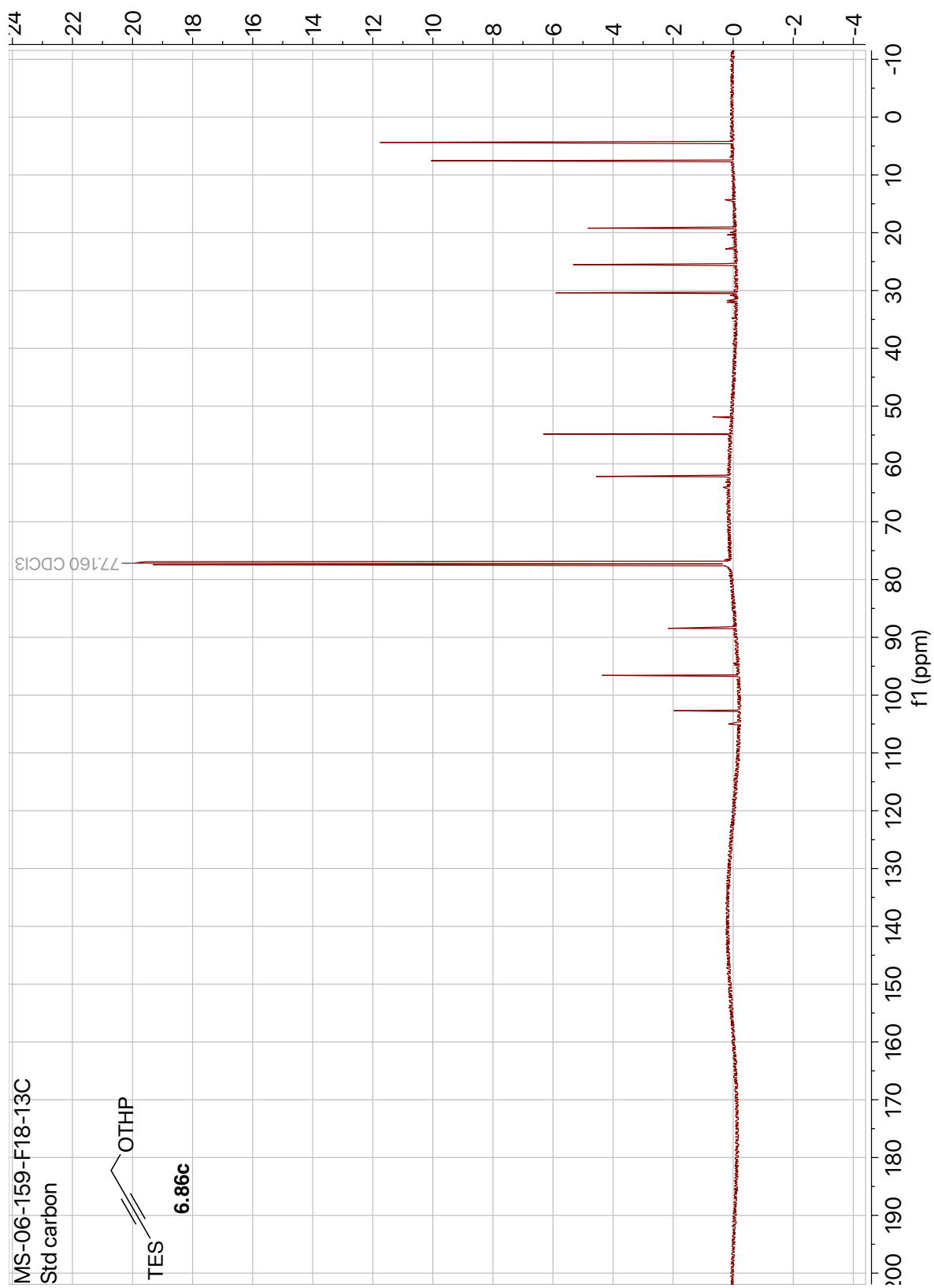


Figure 6.20: ^{13}C NMR of Compound **6.86c** (125 MHz, CDCl_3).

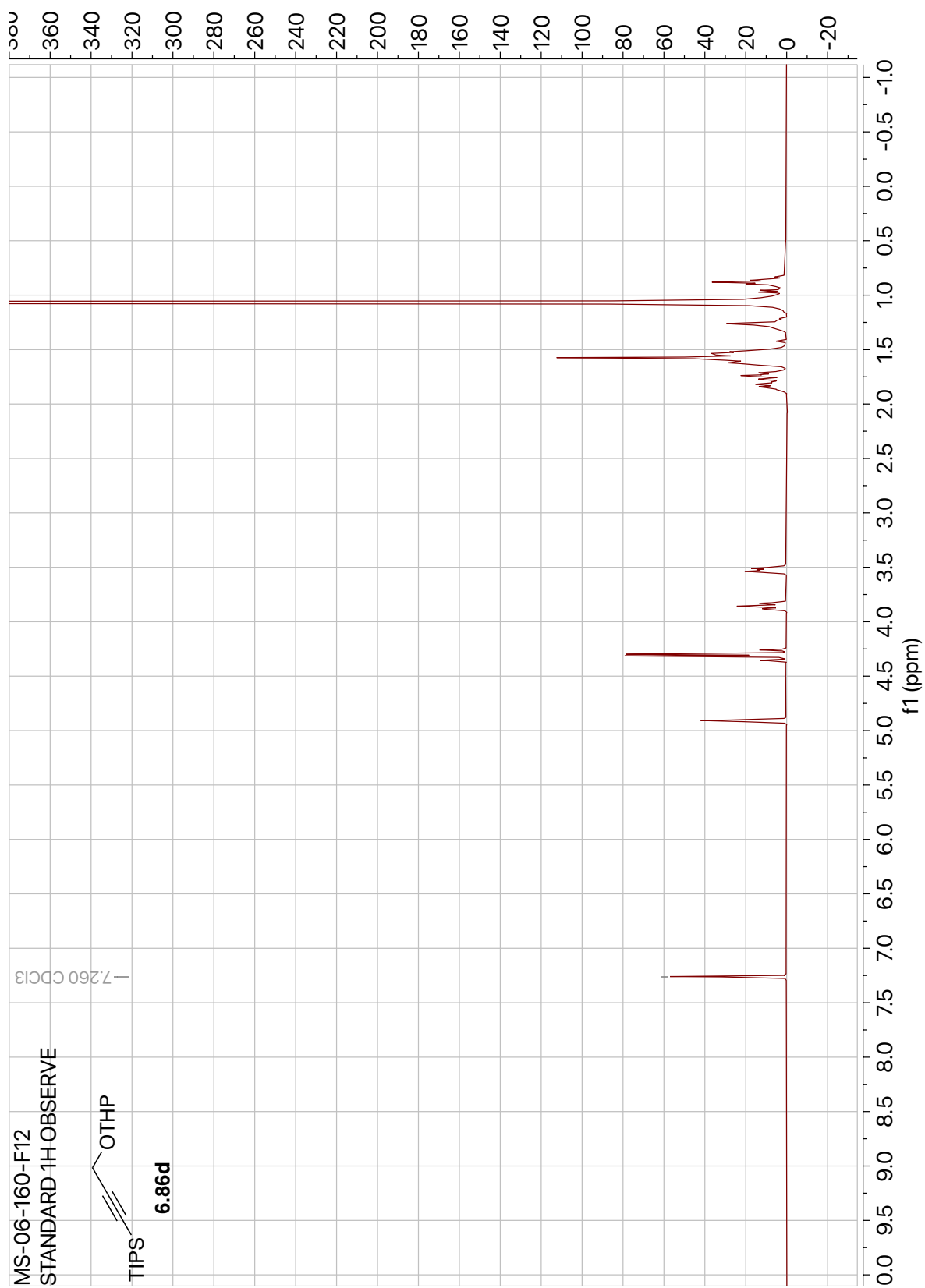


Figure 6.21: ^1H NMR of Compound **6.86d** (500 MHz, CDCl_3).

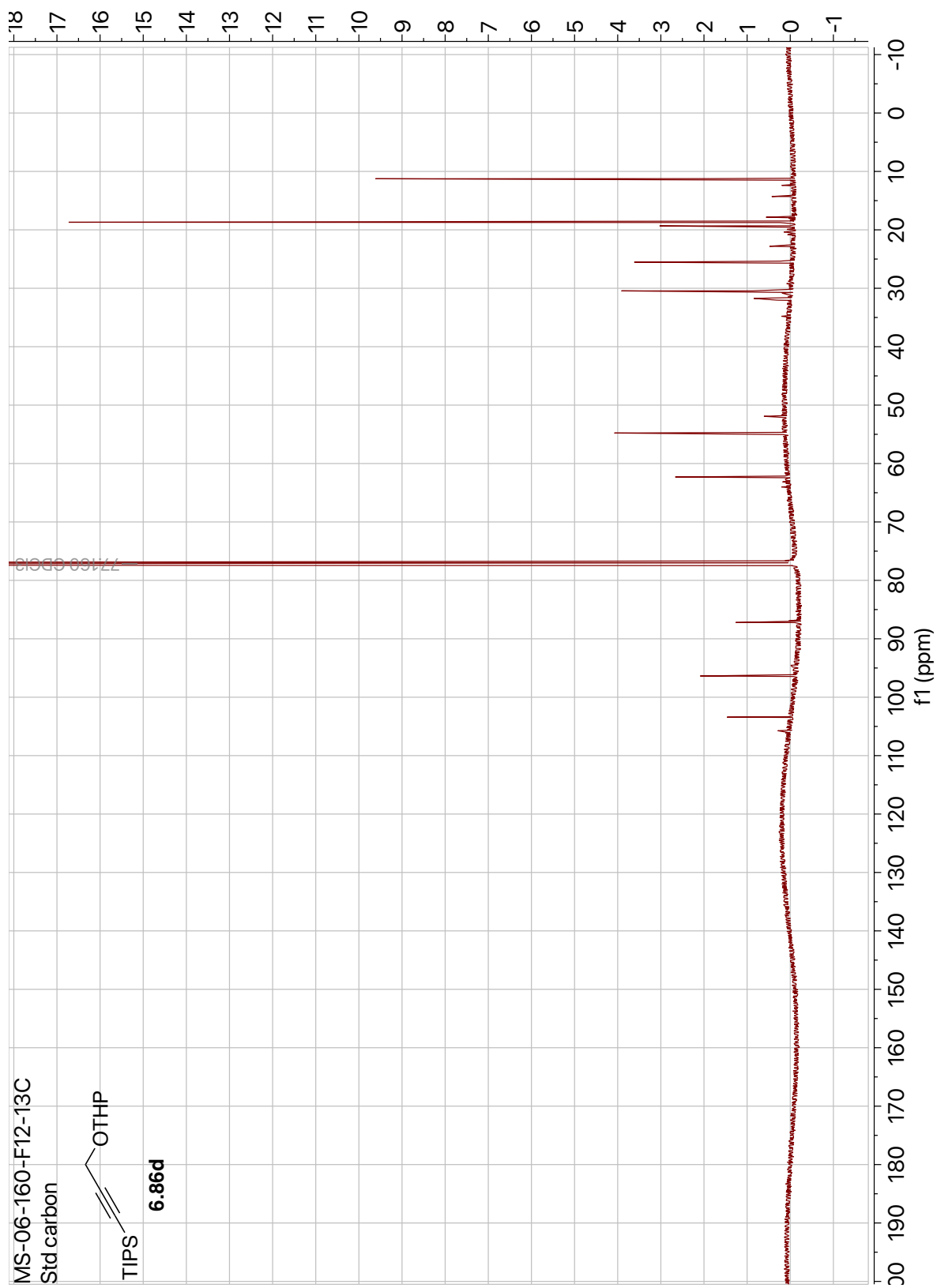


Figure 6.22: ¹³C NMR of Compound **6.86d** (125 MHz, CDCl₃).

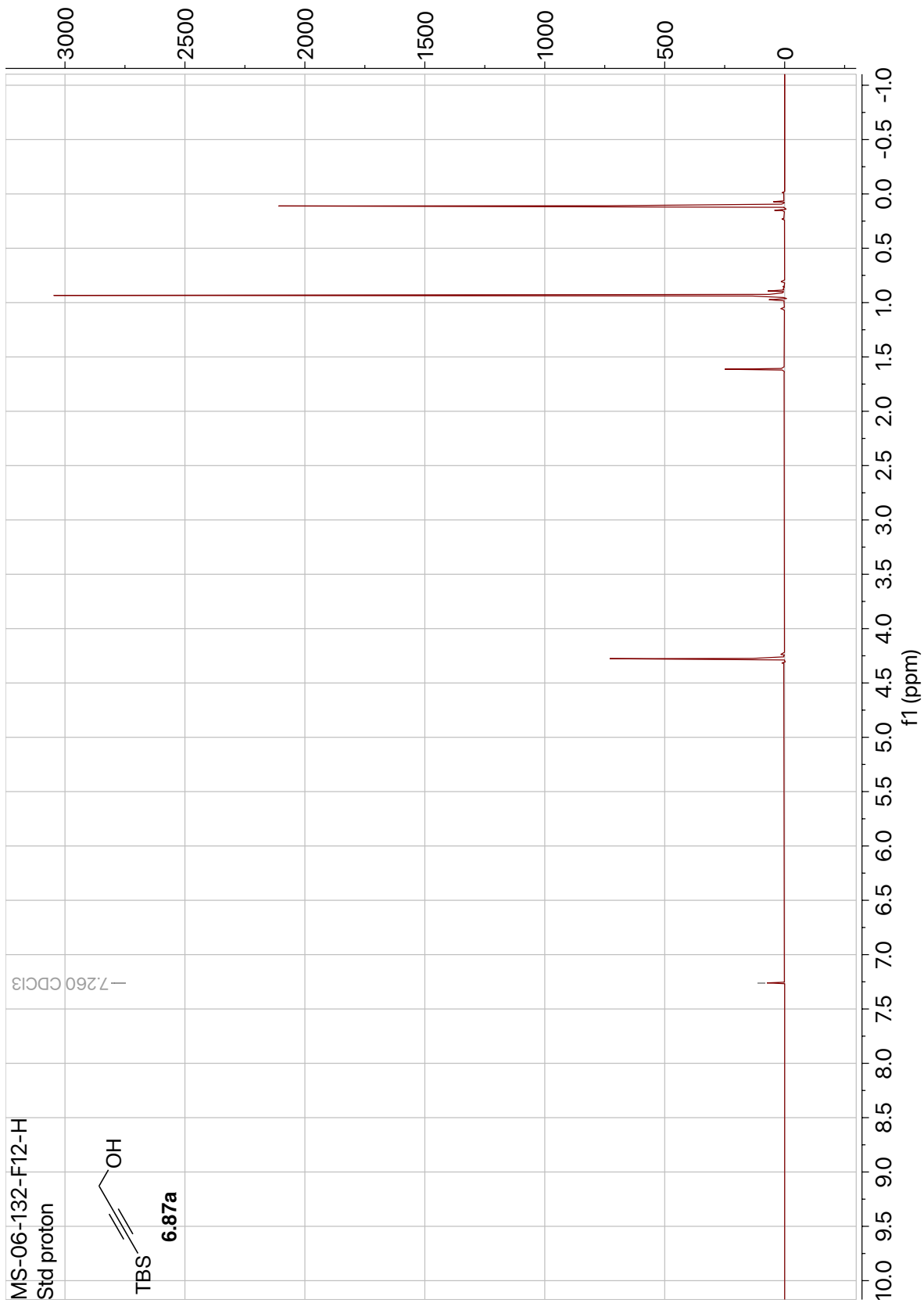


Figure 6.23: ¹H NMR of Compound **6.87a** (500 MHz, CDCl₃).

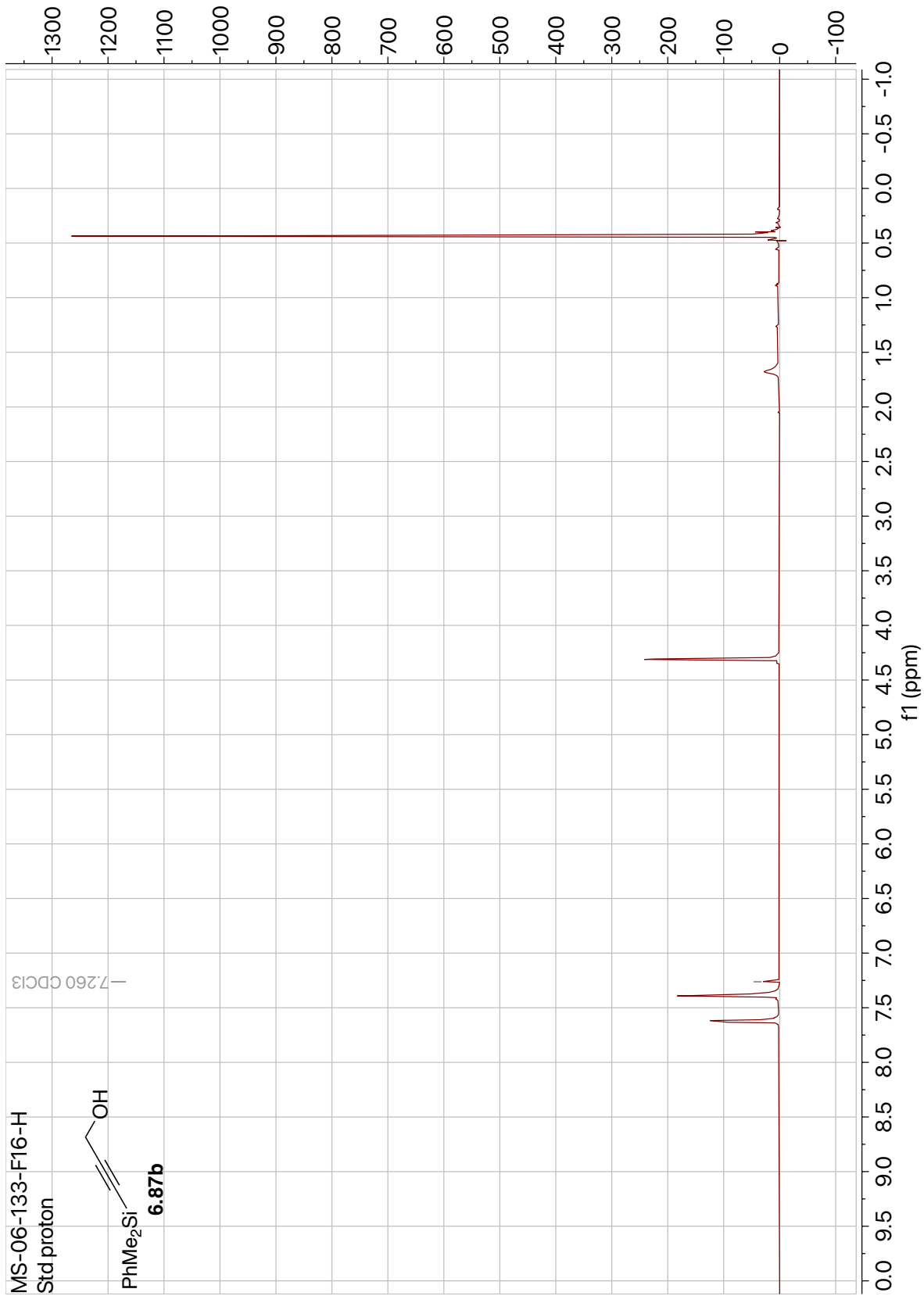


Figure 6.24: ¹H NMR of Compound **6.87b** (500 MHz, CDCl₃).

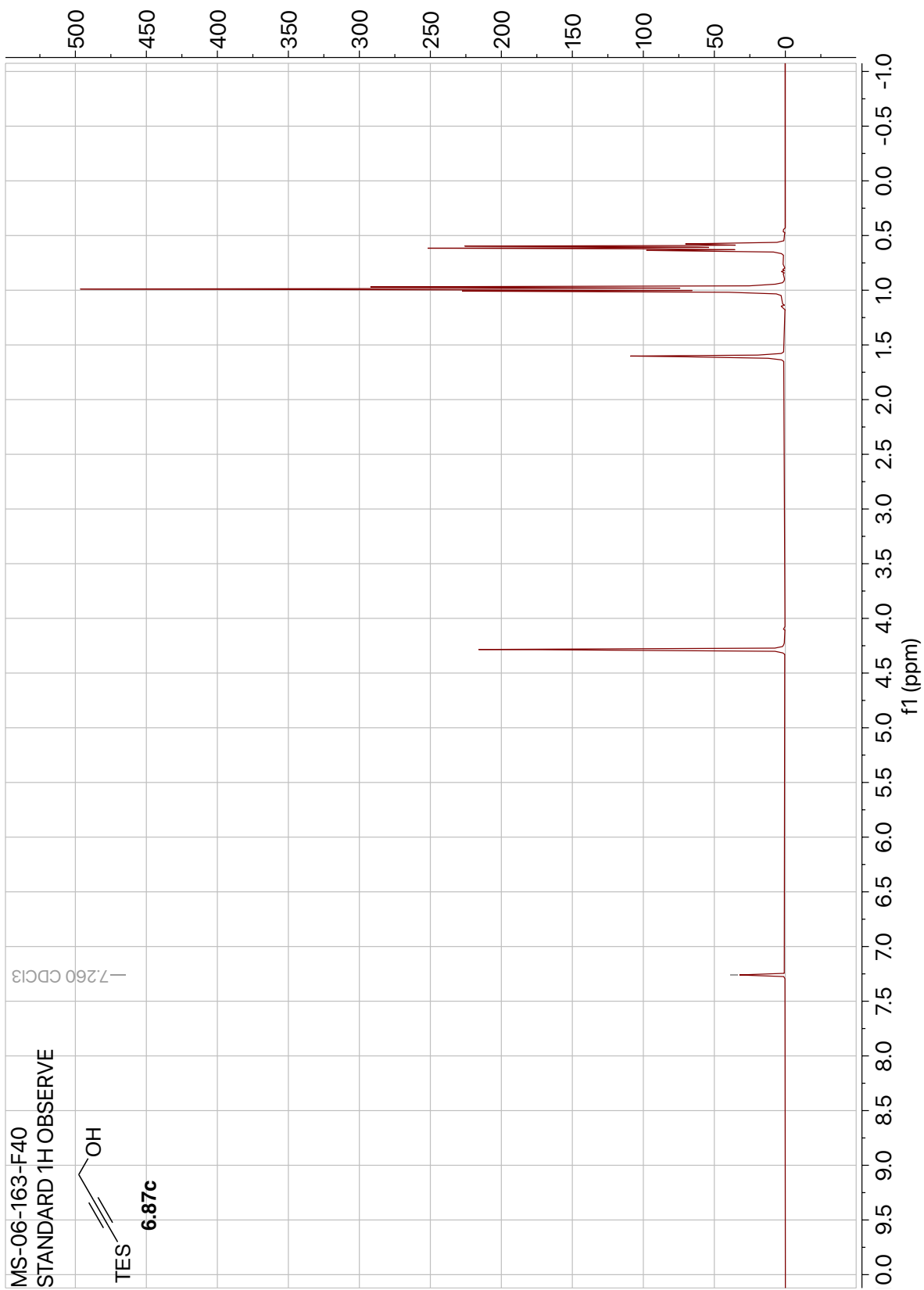


Figure 6.25: ^1H NMR of Compound **6.87c** (400 MHz, CDCl_3).

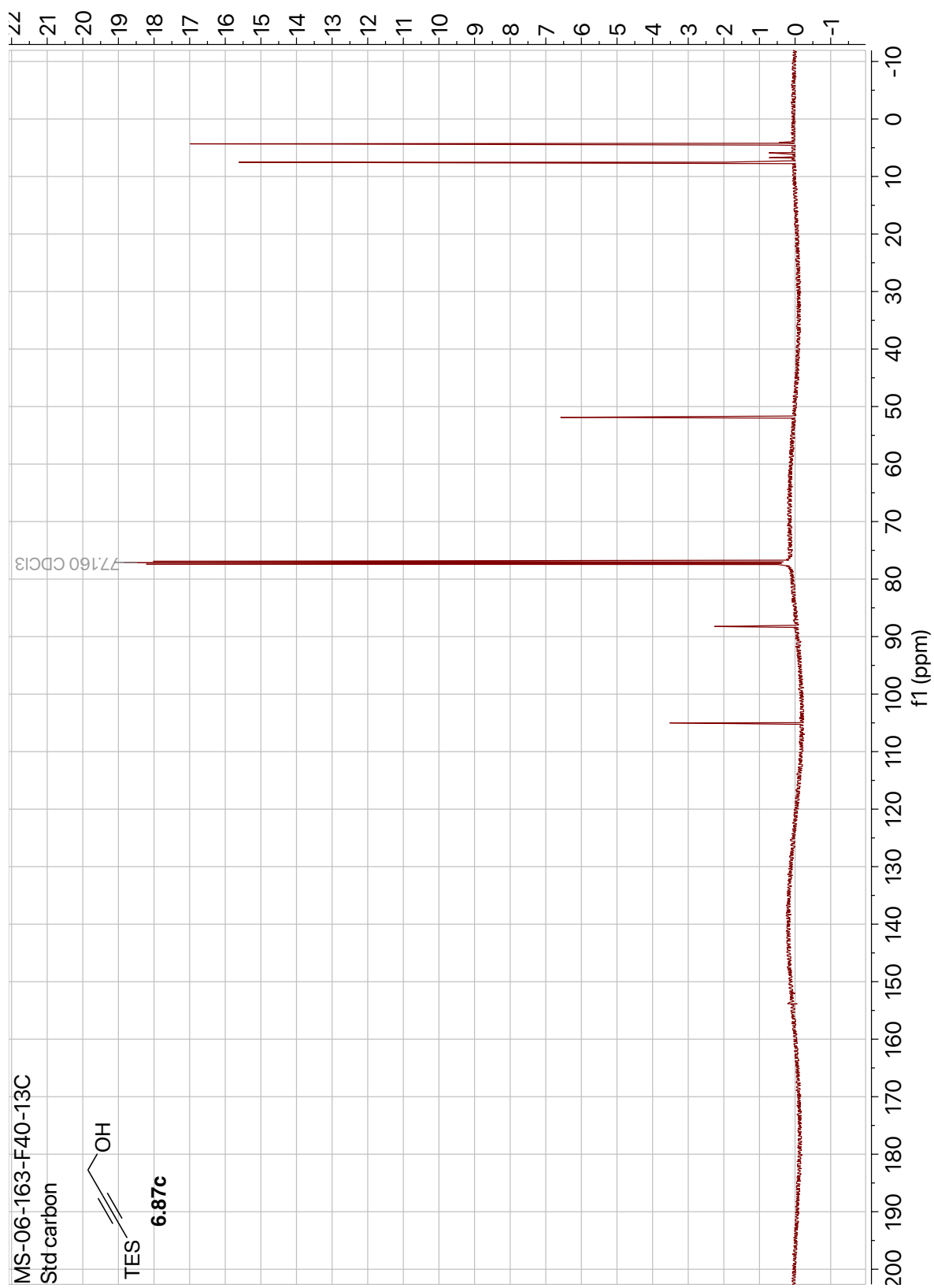


Figure 6.26: ¹³C NMR of Compound **6.87c** (125 MHz, CDCl₃).

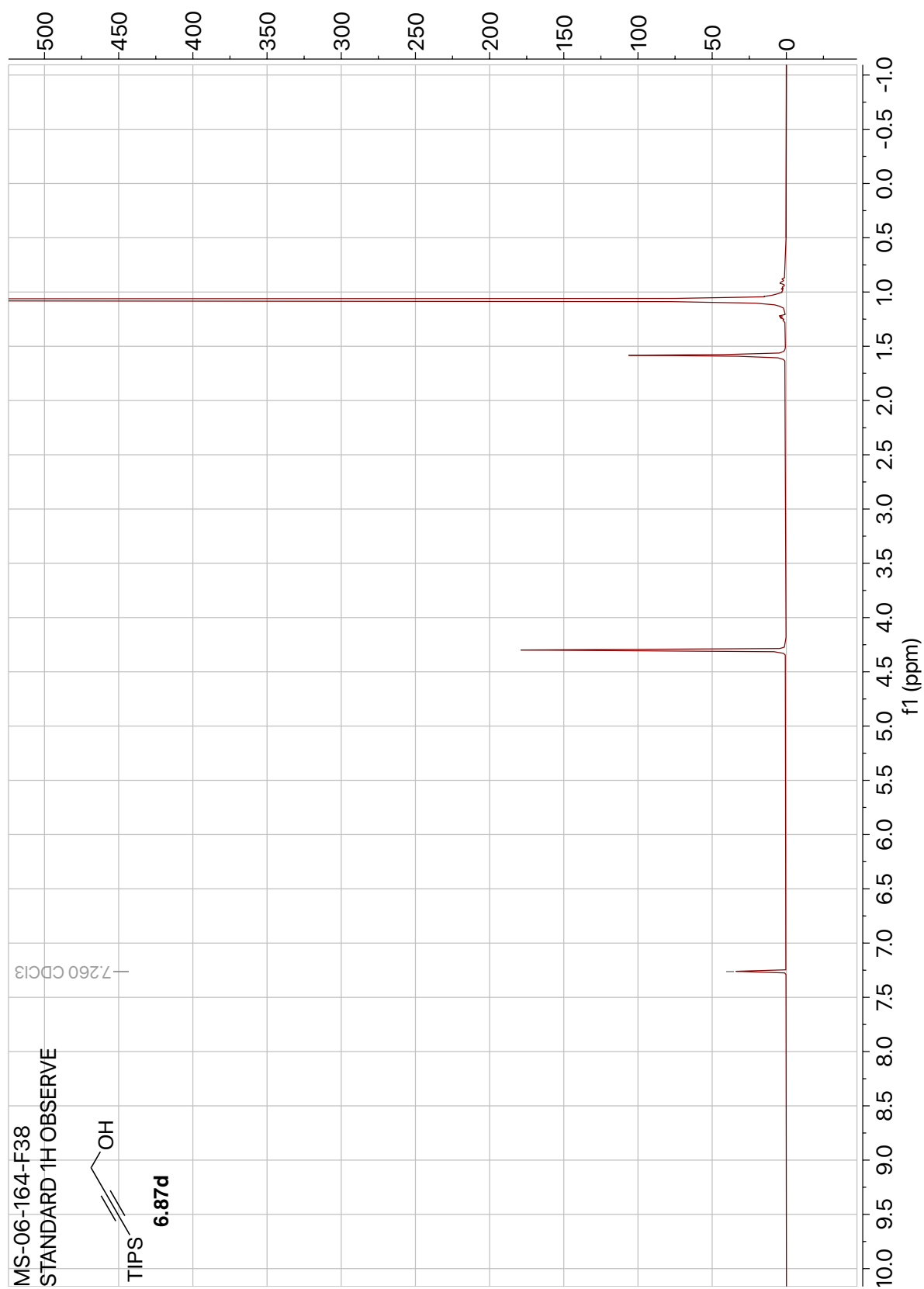


Figure 6.27: ^1H NMR of Compound **6.87d** (400 MHz, CDCl_3).

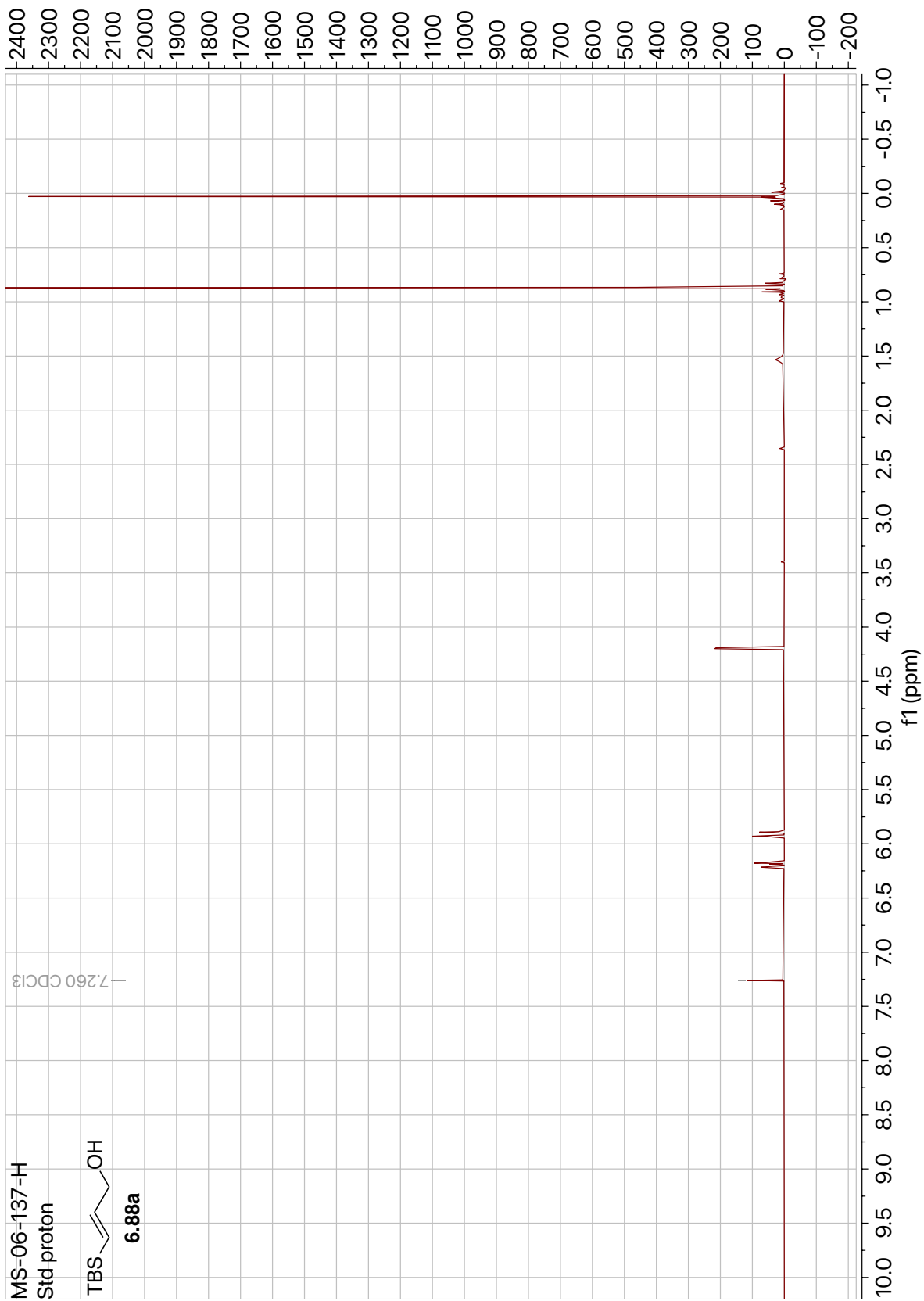


Figure 6.28: ¹H NMR of Compound **6.88a** (500 MHz, CDCl₃).

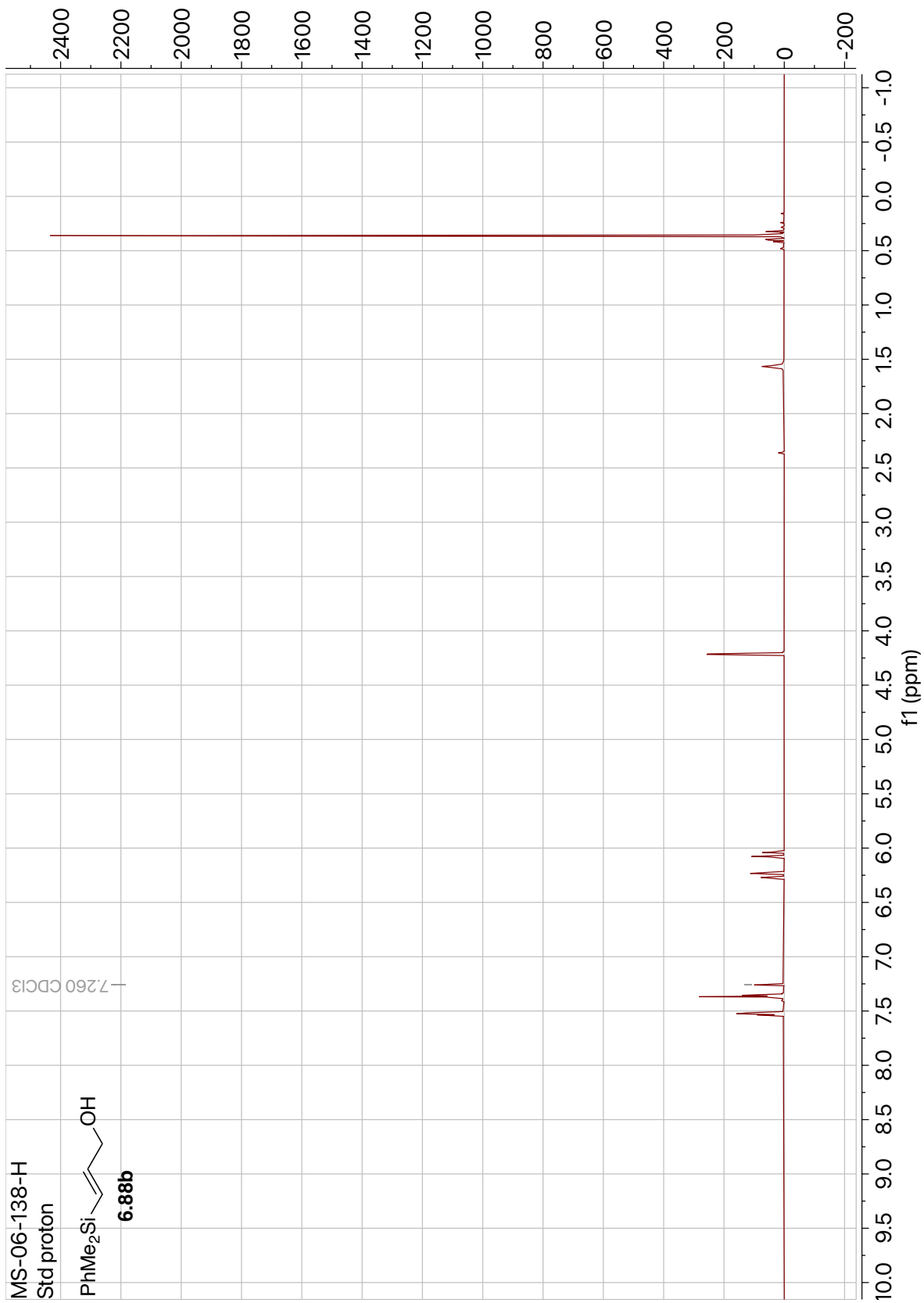


Figure 6.29: ¹H NMR of Compound **6.88b** (500 MHz, CDCl₃).

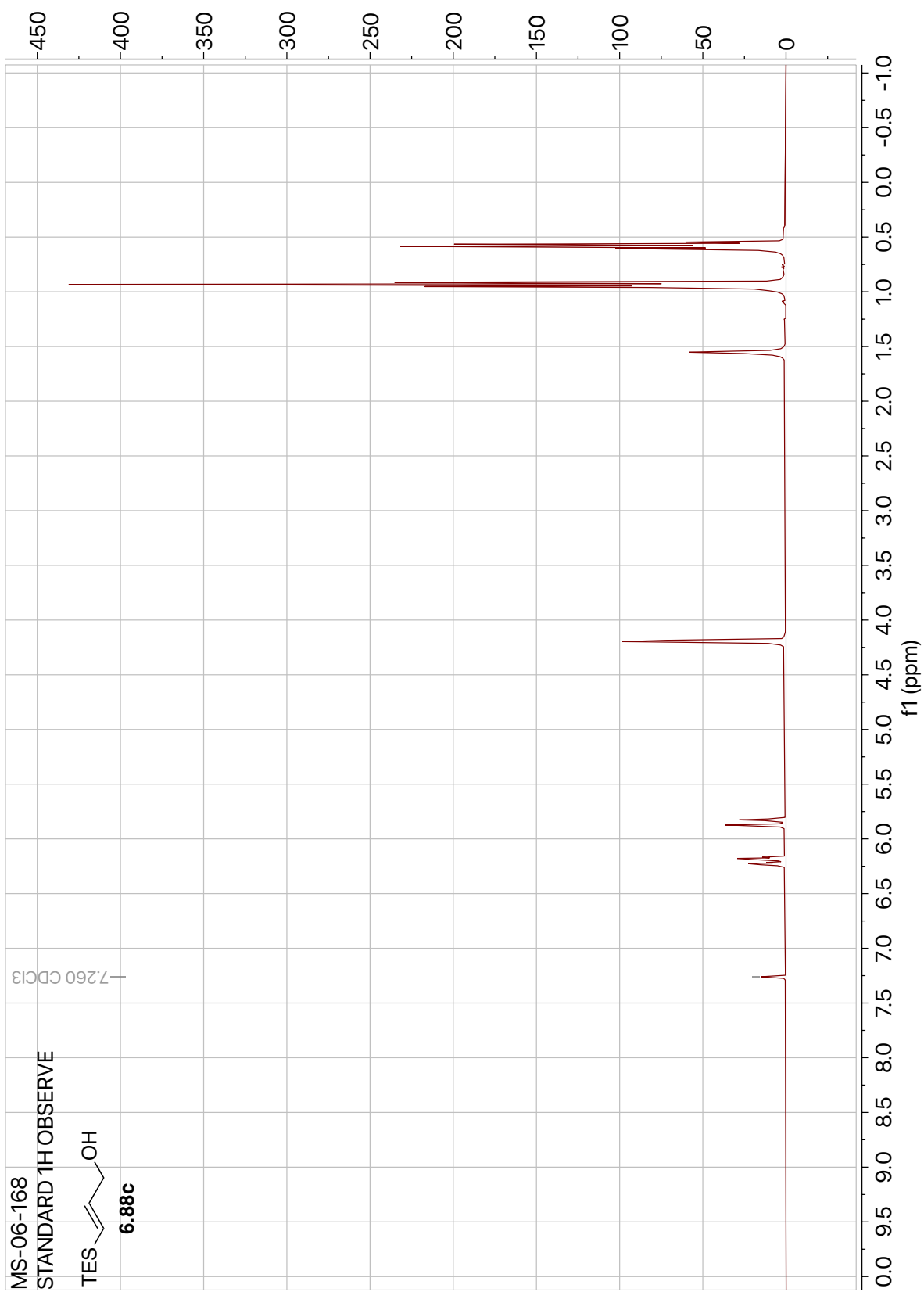


Figure 6.30: ^1H NMR of Compound **6.88c** (400 MHz, CDCl_3).

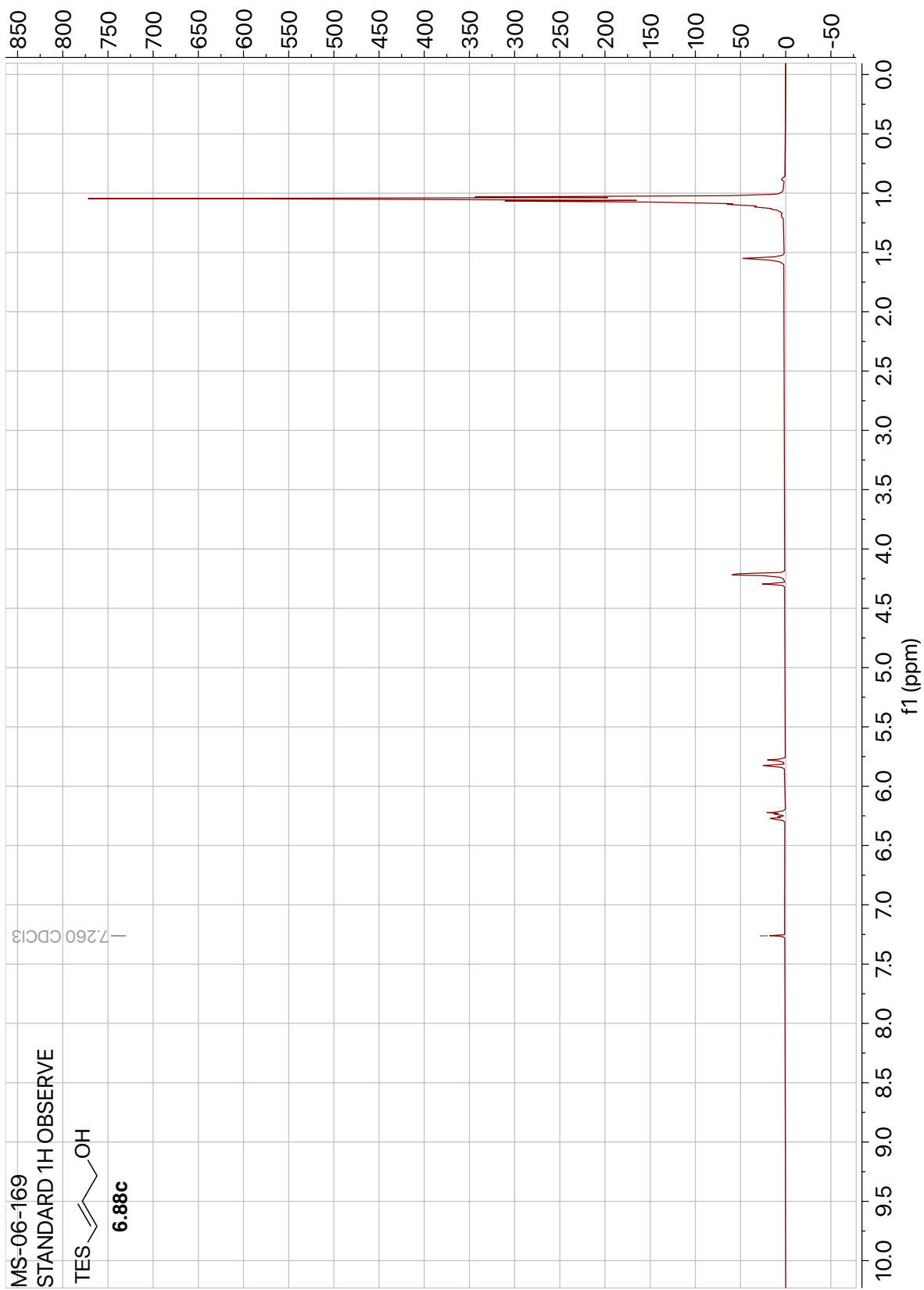


Figure 6.31: ^1H NMR of Compound **6.88d** (400 MHz, CDCl_3).

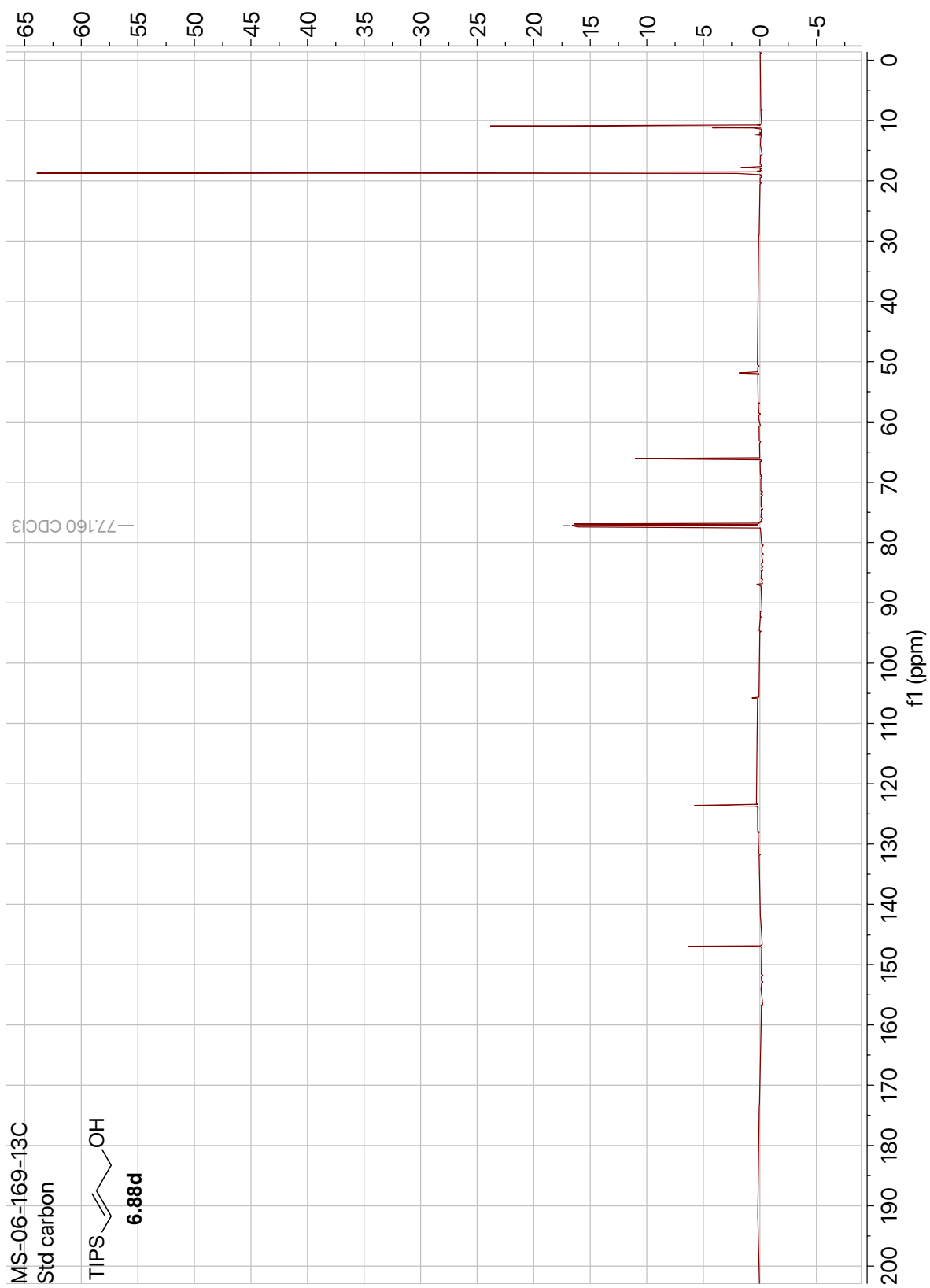


Figure 6.32: ¹³C NMR of Compound **6.88d** (125 MHz, CDCl₃).

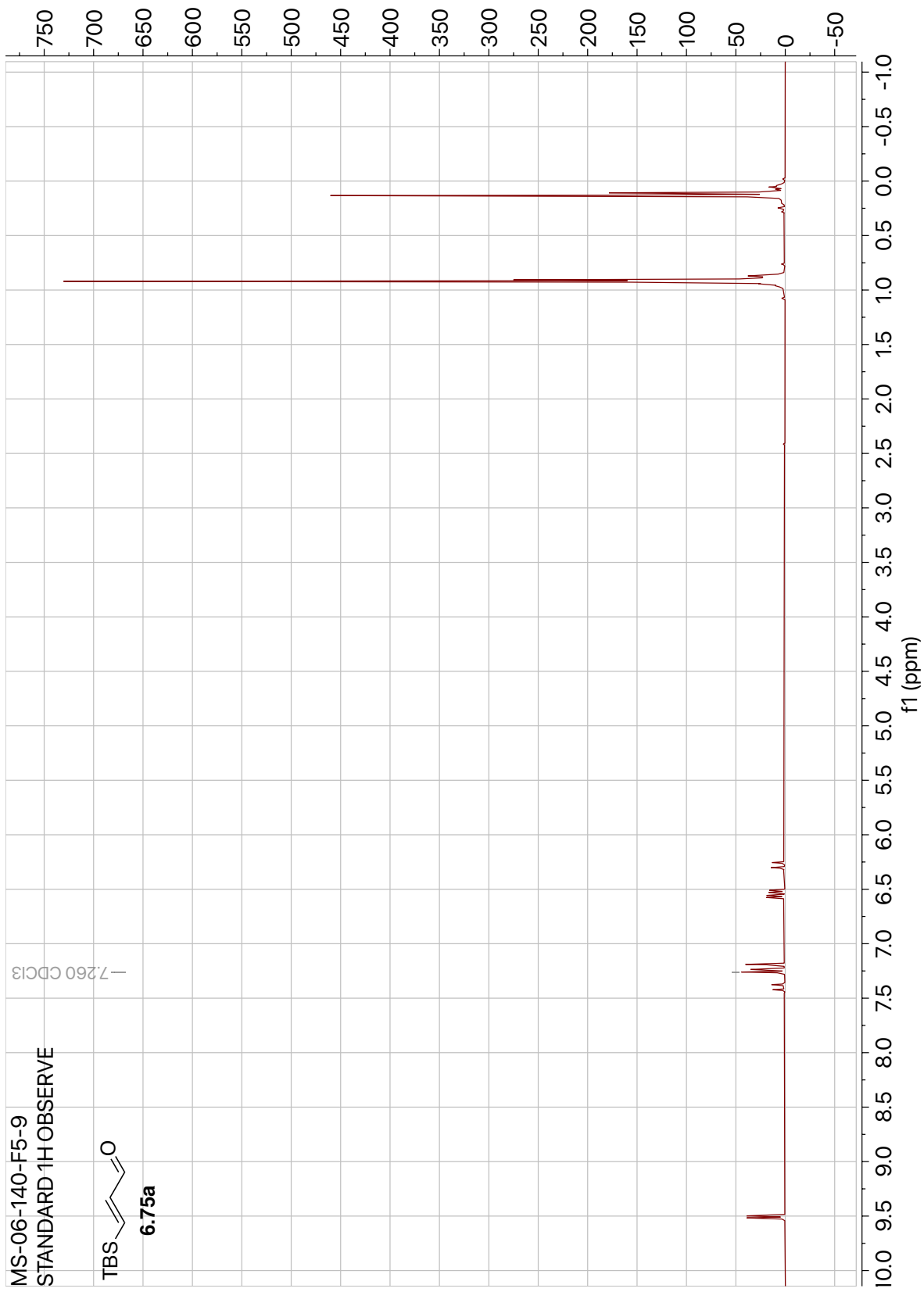


Figure 6.33: ^1H NMR of Compound **6.75a** (400 MHz, CDCl_3).

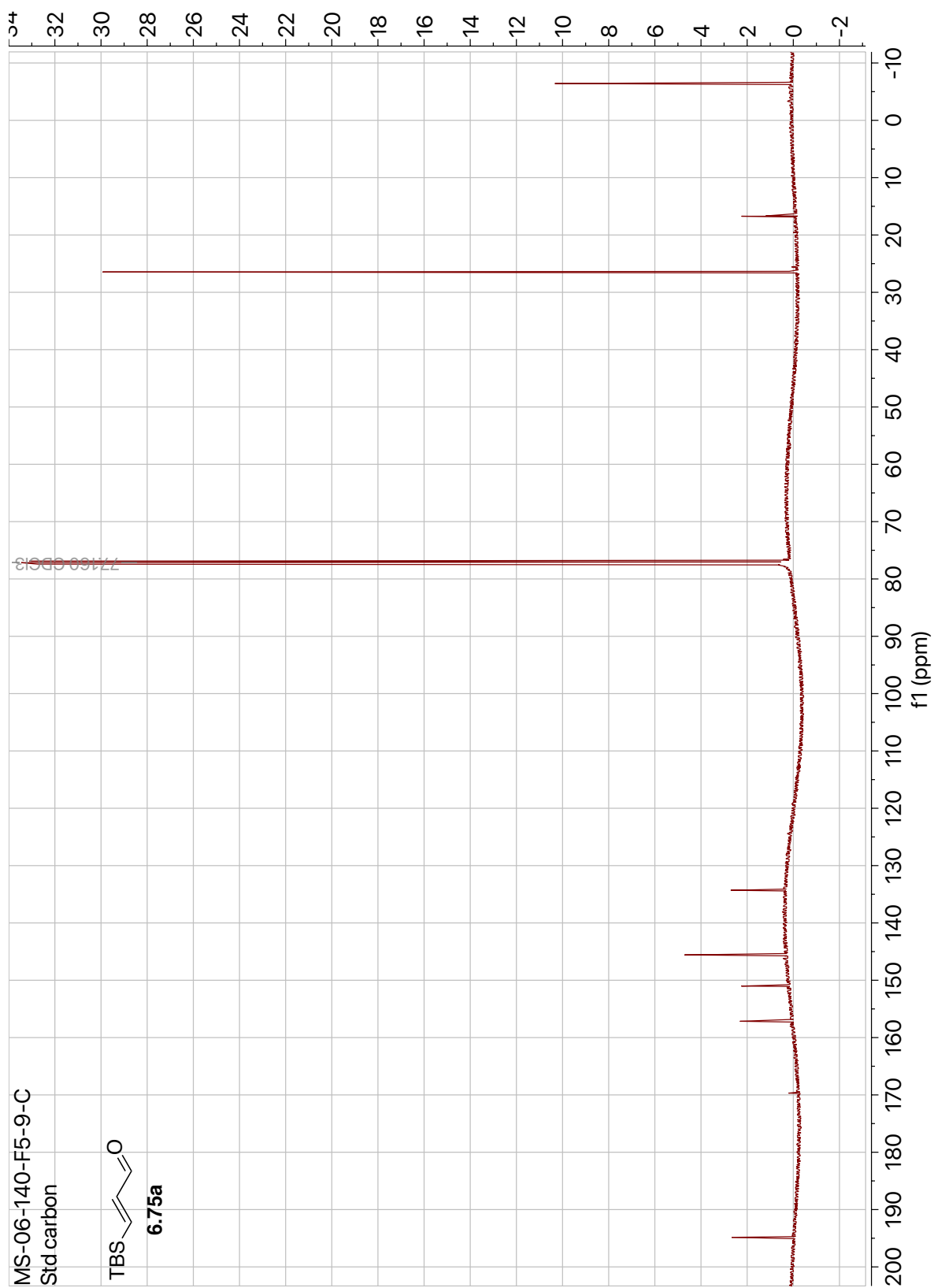


Figure 6.34: ¹³C NMR of Compound **6.75a** (125 MHz, CDCl₃).

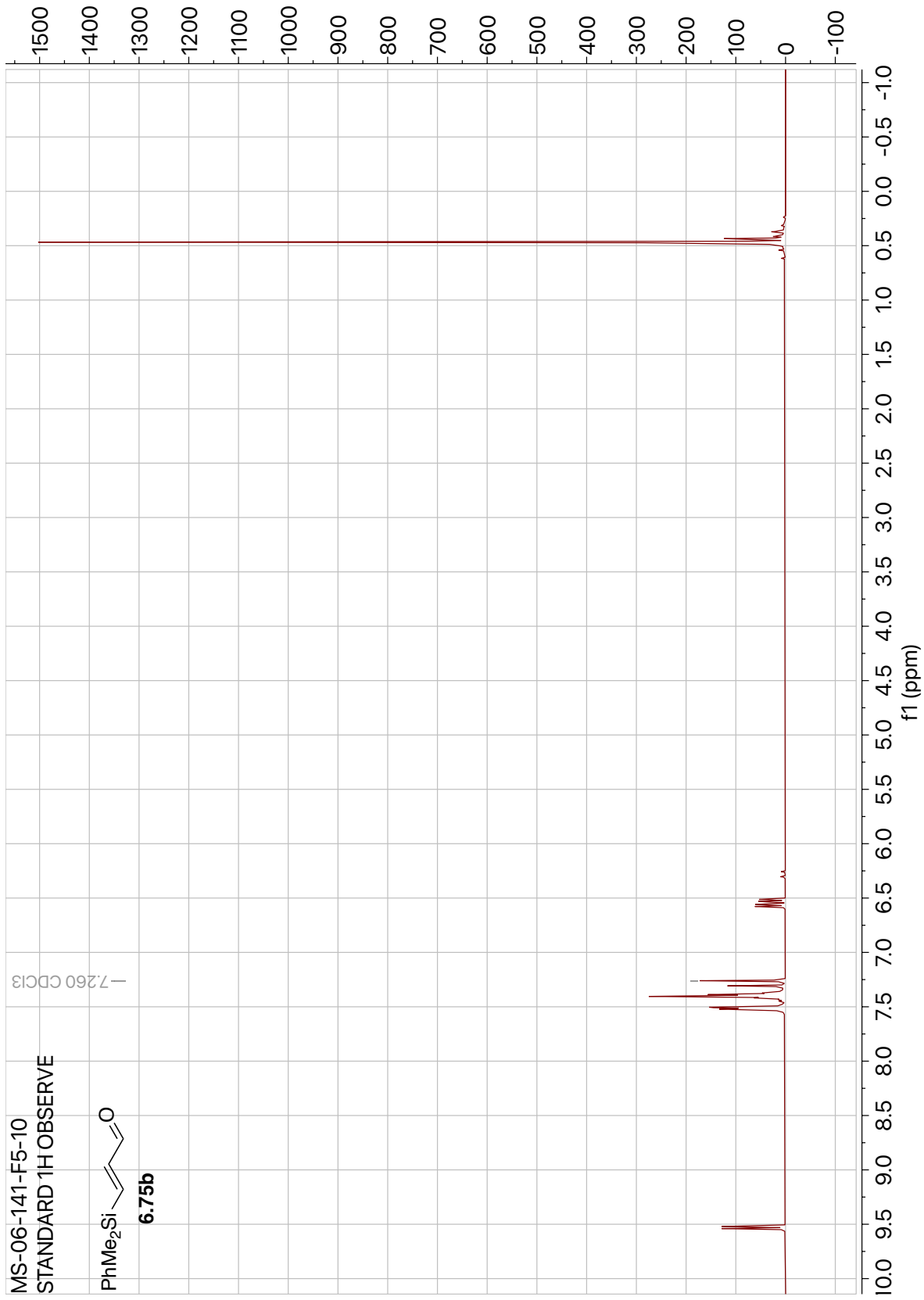


Figure 6.35: ¹H NMR of Compound **6.75b** (400 MHz, CDCl₃).

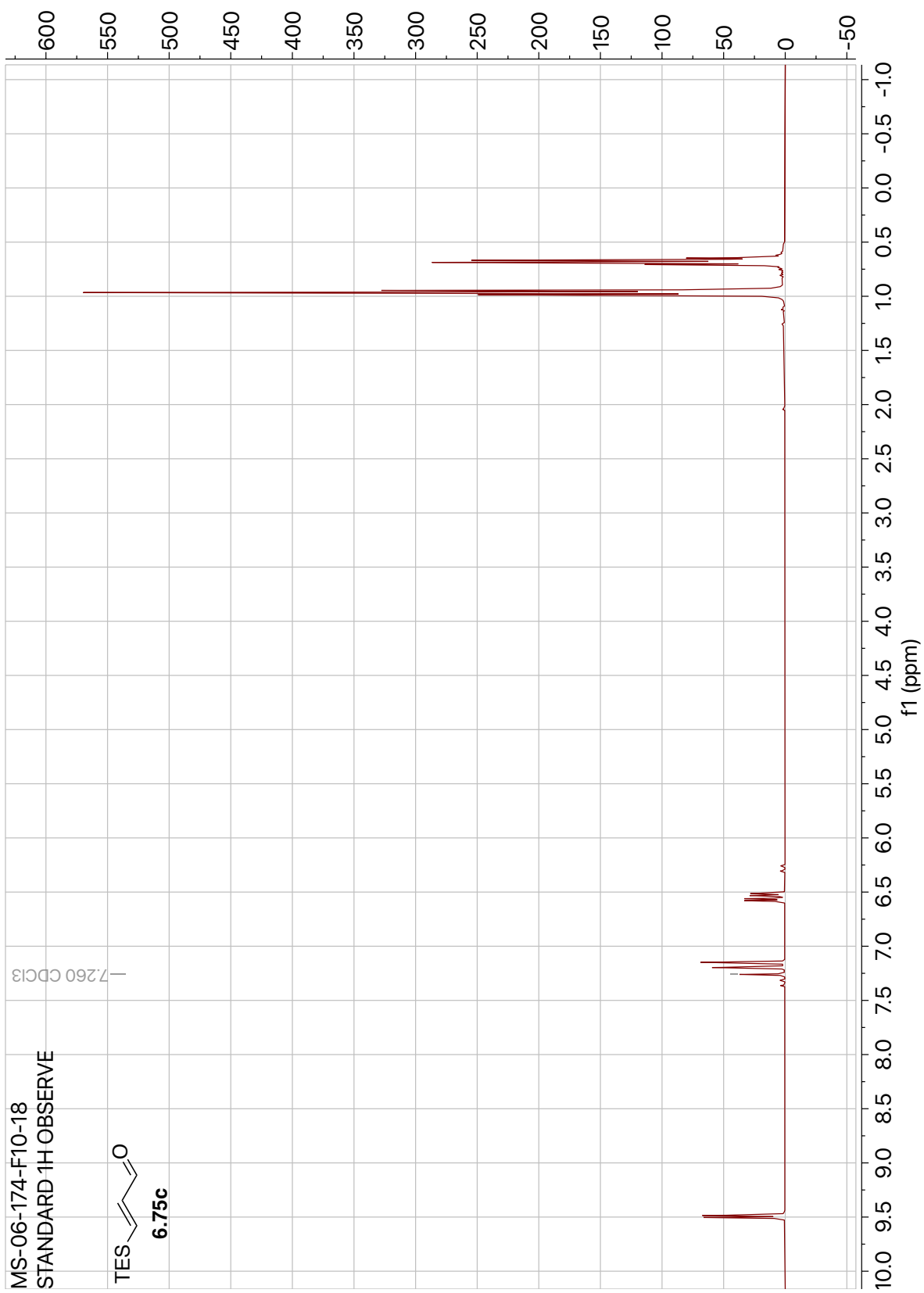


Figure 6.36: ^1H NMR of Compound 6.75c (400 MHz, CDCl_3).

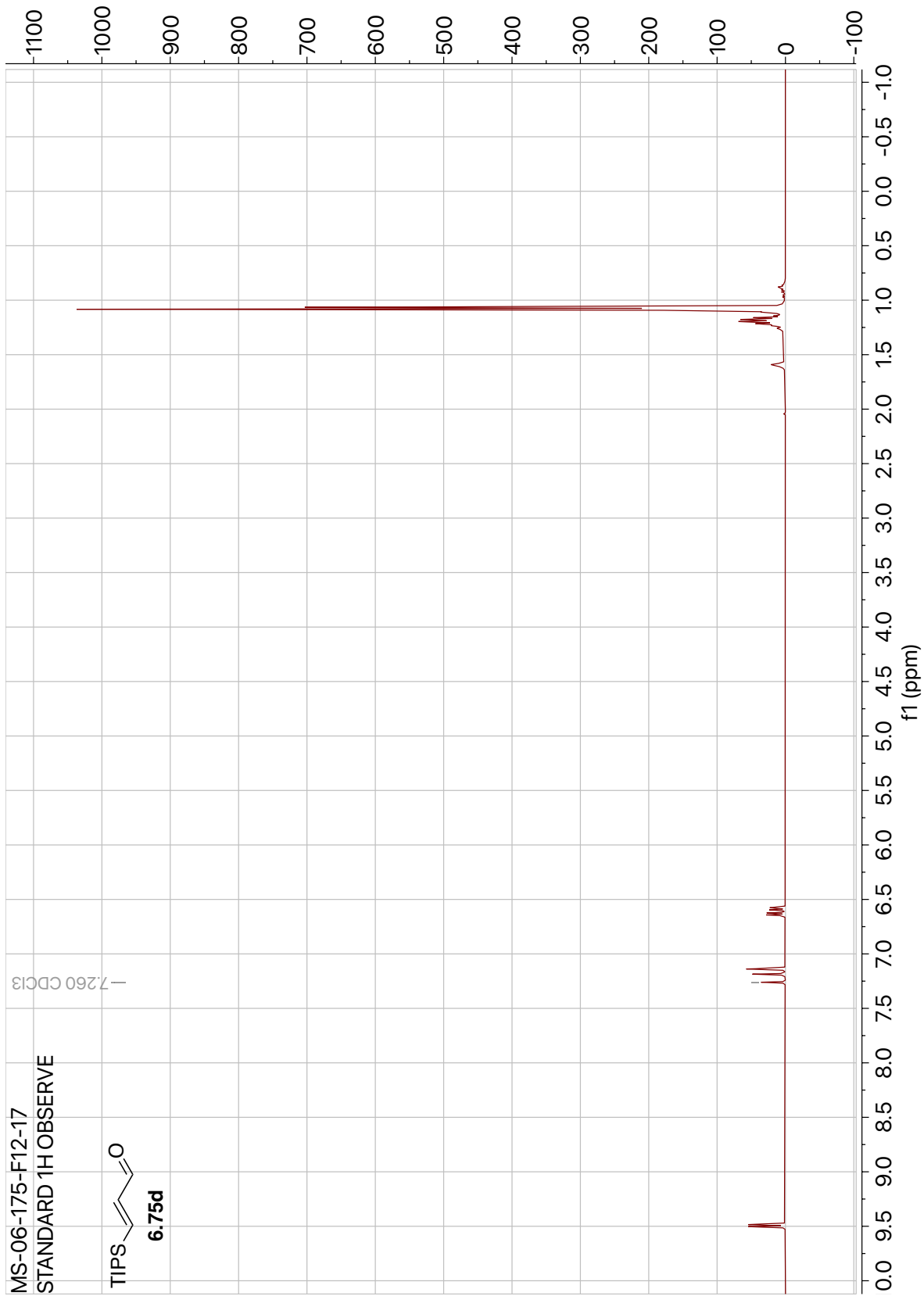


Figure 6.37: ^1H NMR of Compound **6.75d** (400 MHz, CDCl_3).

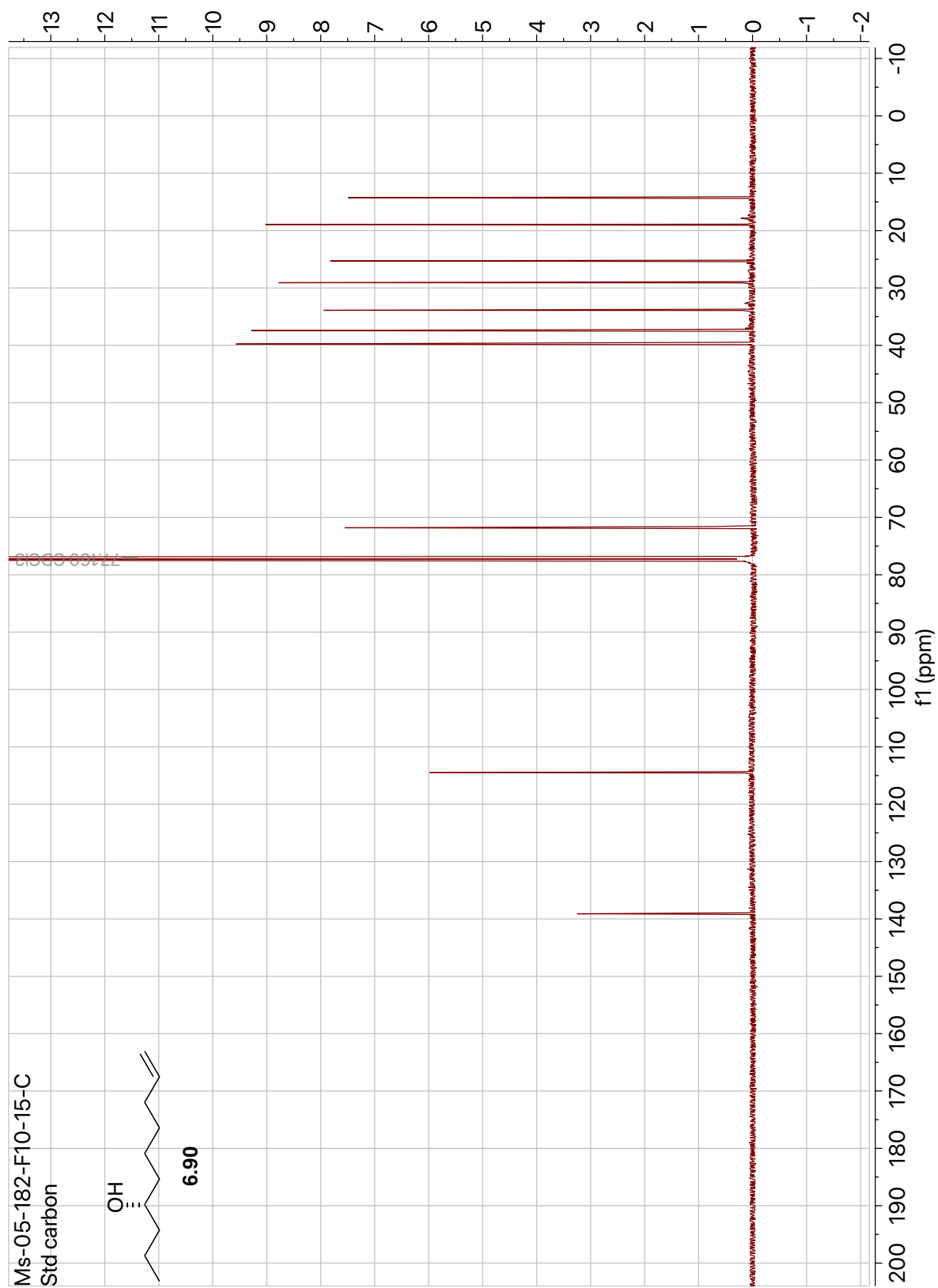


Figure 6.39: ¹³C NMR of Compound **6.90** (125 MHz, CDCl₃).

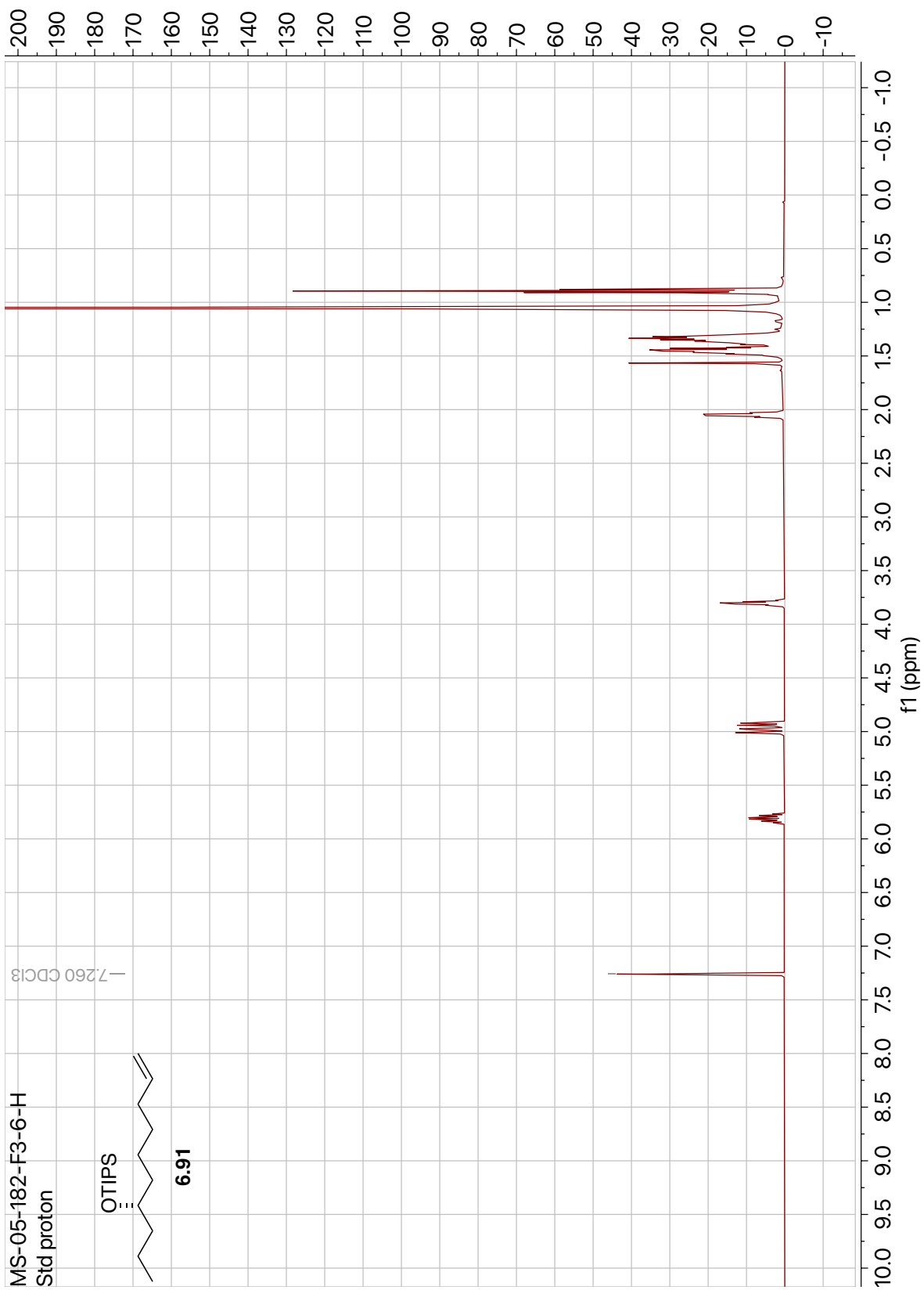


Figure 6.40: ¹H NMR of Compound **6.91** (500 MHz, CDCl₃).

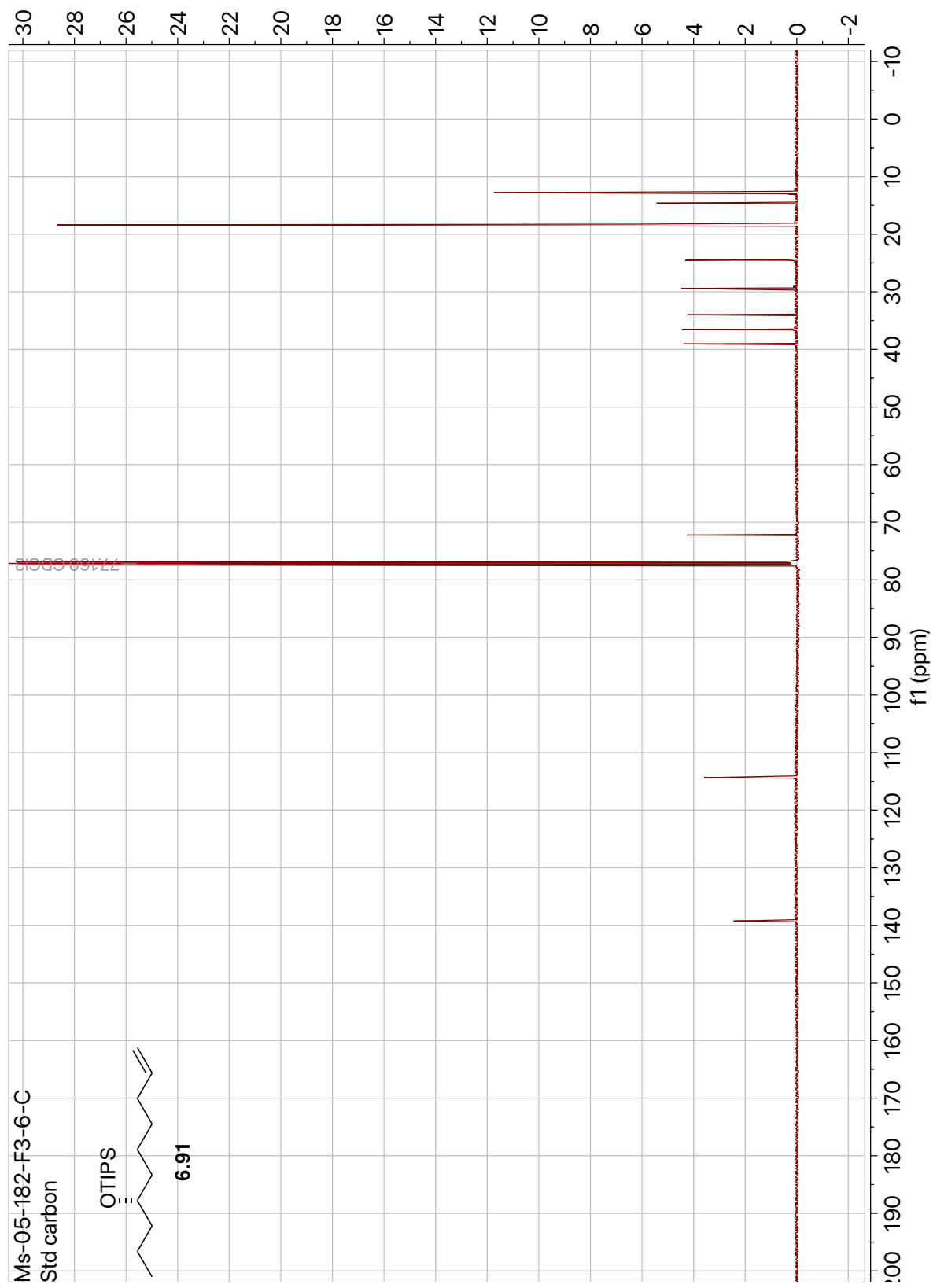


Figure 6.41: ¹³C NMR of Compound **6.91** (125 MHz, CDCl₃).

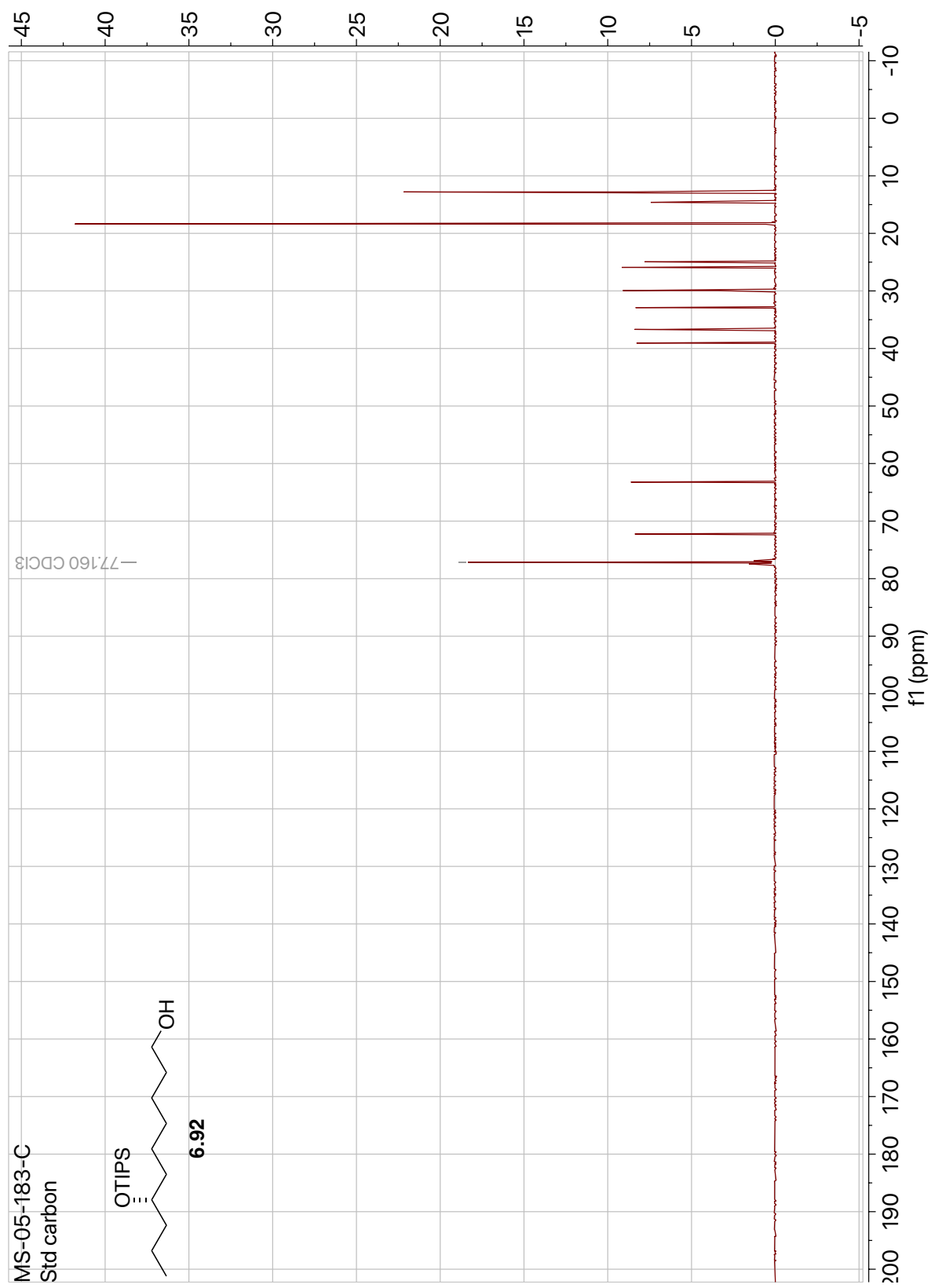


Figure 6.43: ¹³C NMR of Compound **6.92** (125 MHz, CDCl₃).

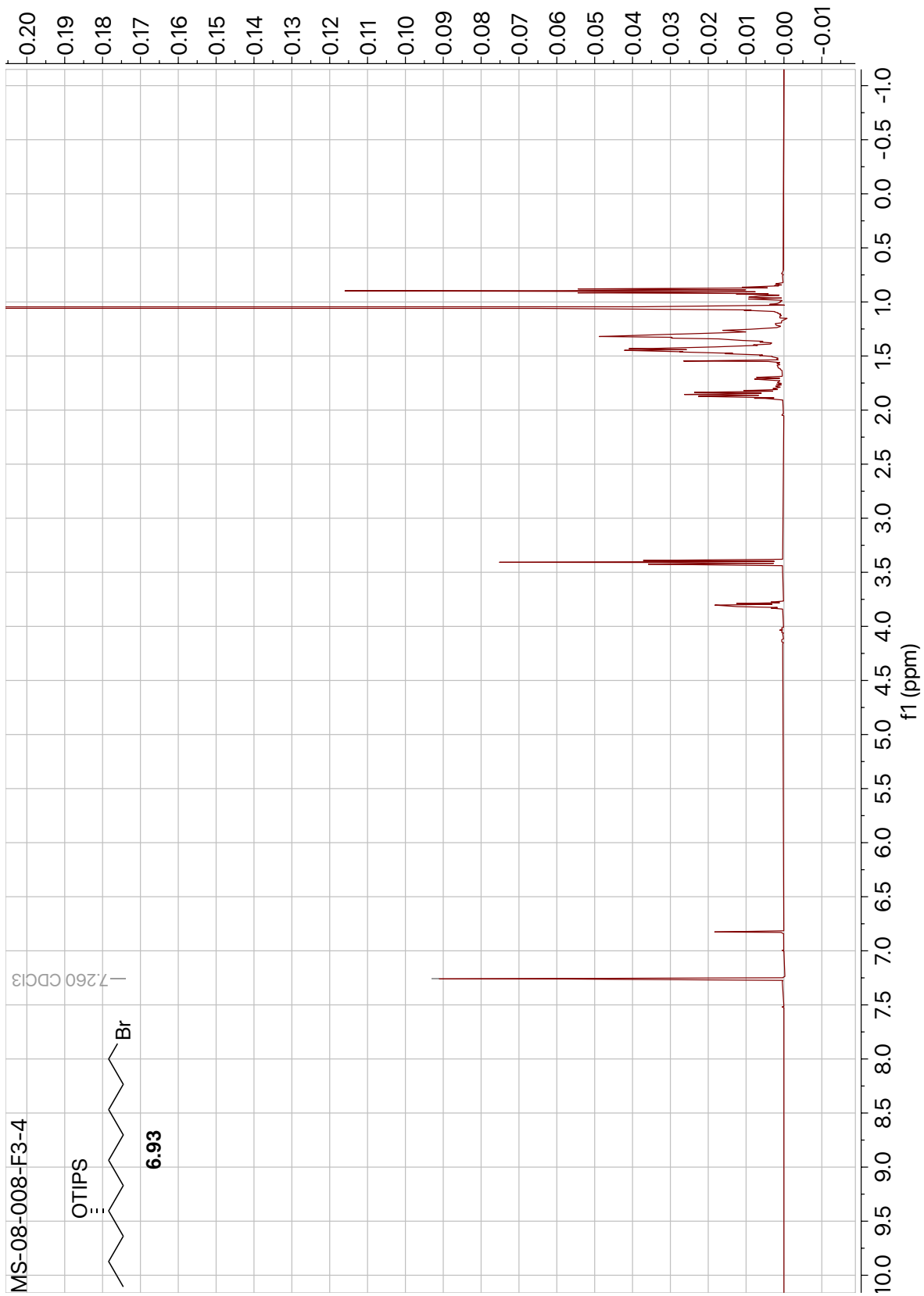


Figure 6.44: ¹H NMR of Compound **6.93** (400 MHz, CDCl₃).

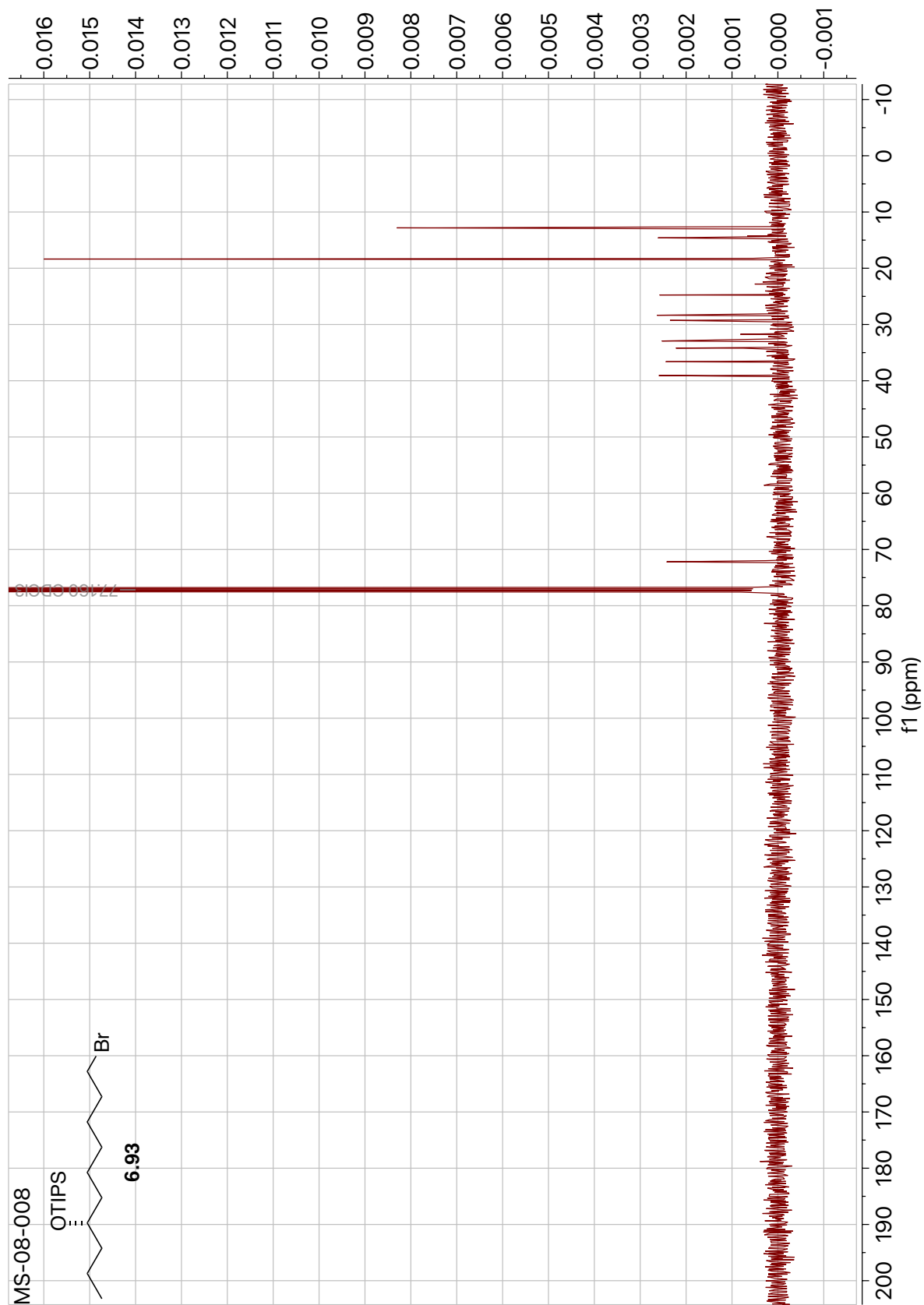


Figure 6.45: ¹³C NMR of Compound **6.93** (100 MHz, CDCl₃).

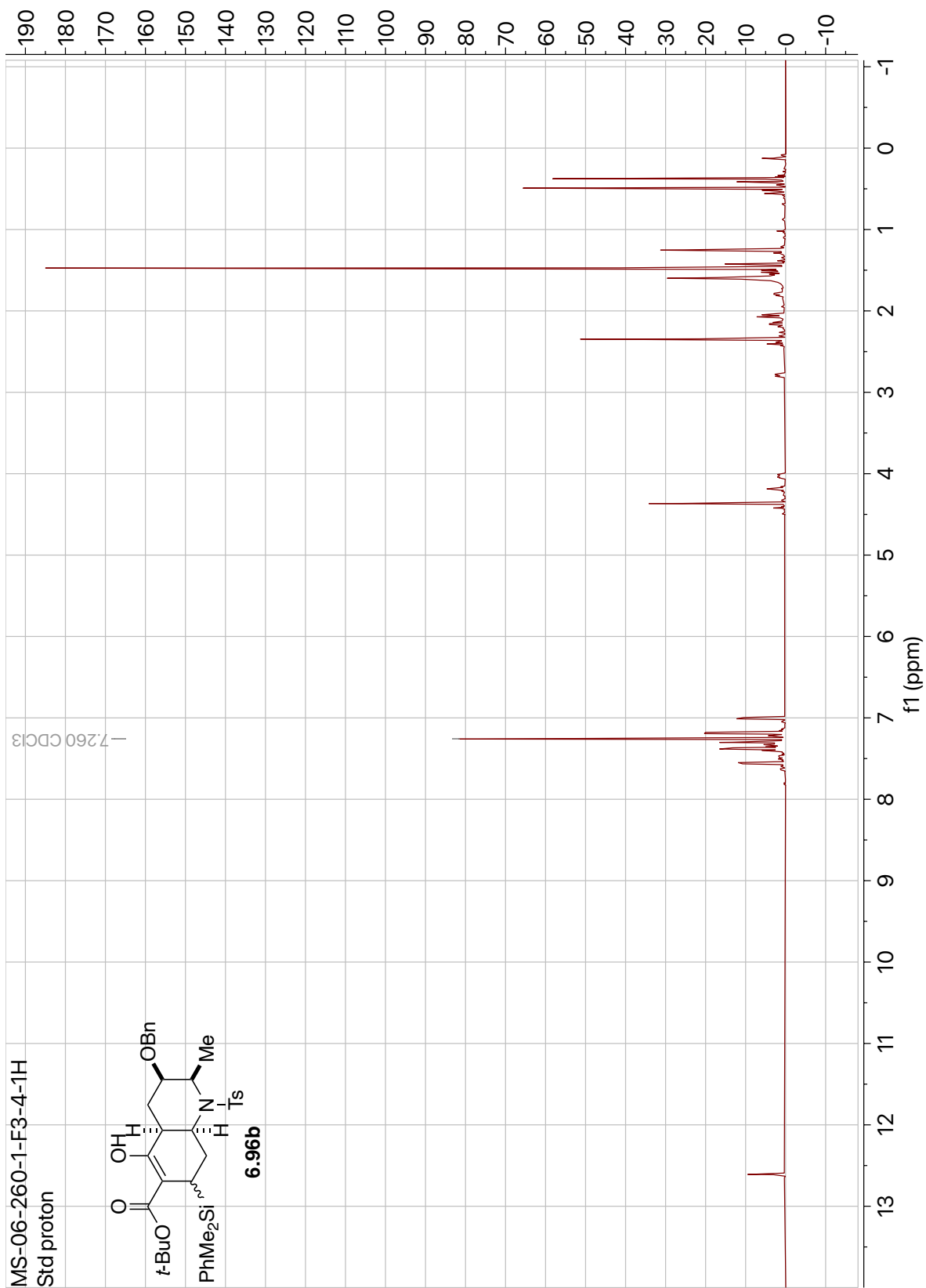


Figure 6.46: ¹H NMR of Compound **6.96b** (500 MHz, CDCl₃).

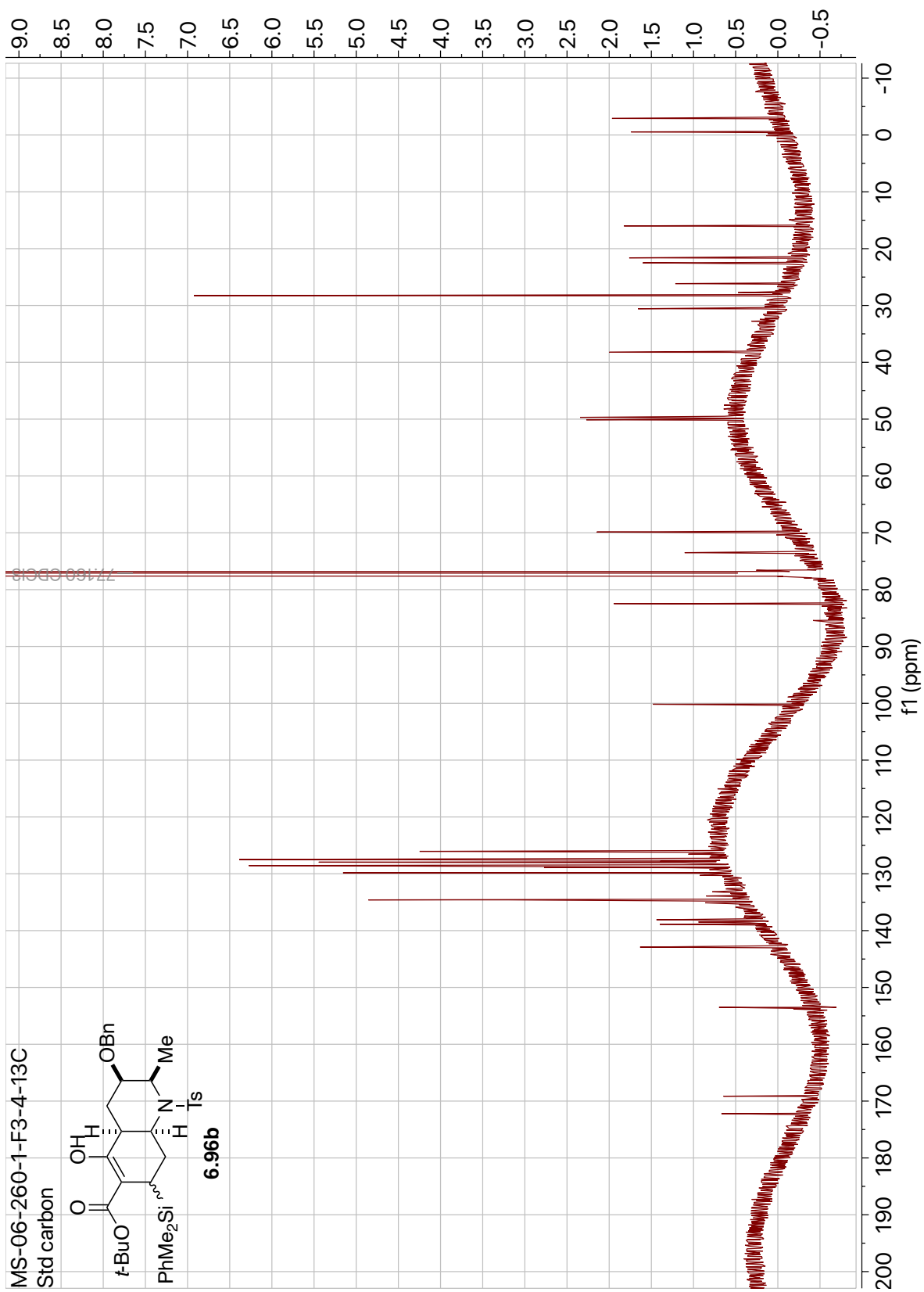


Figure 6.47: ¹³C NMR of Compound **6.96b** (125 MHz, CDCl₃).

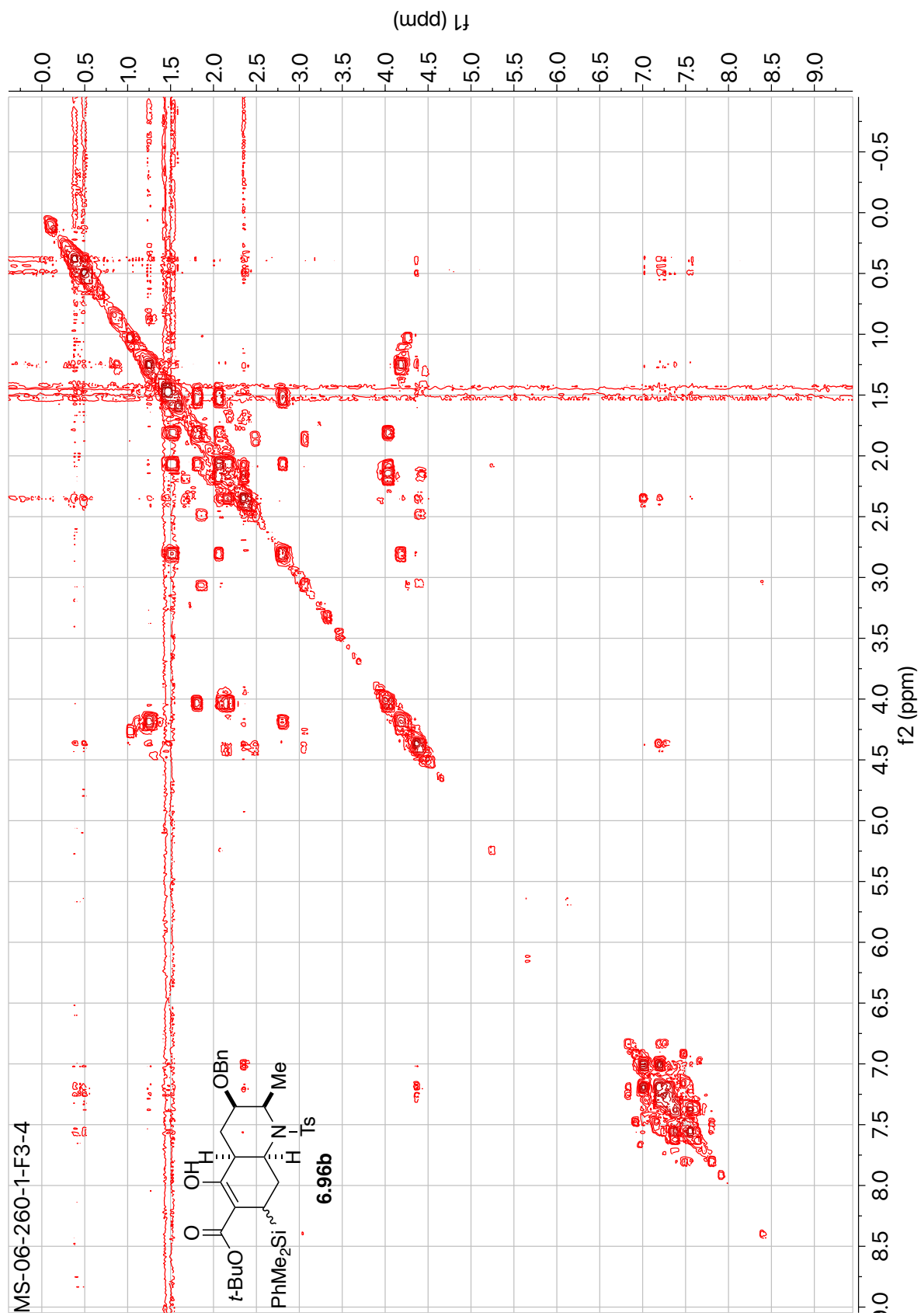


Figure 6.48: COSY of Compound **6.96b** (500 MHz, CDCl₃).

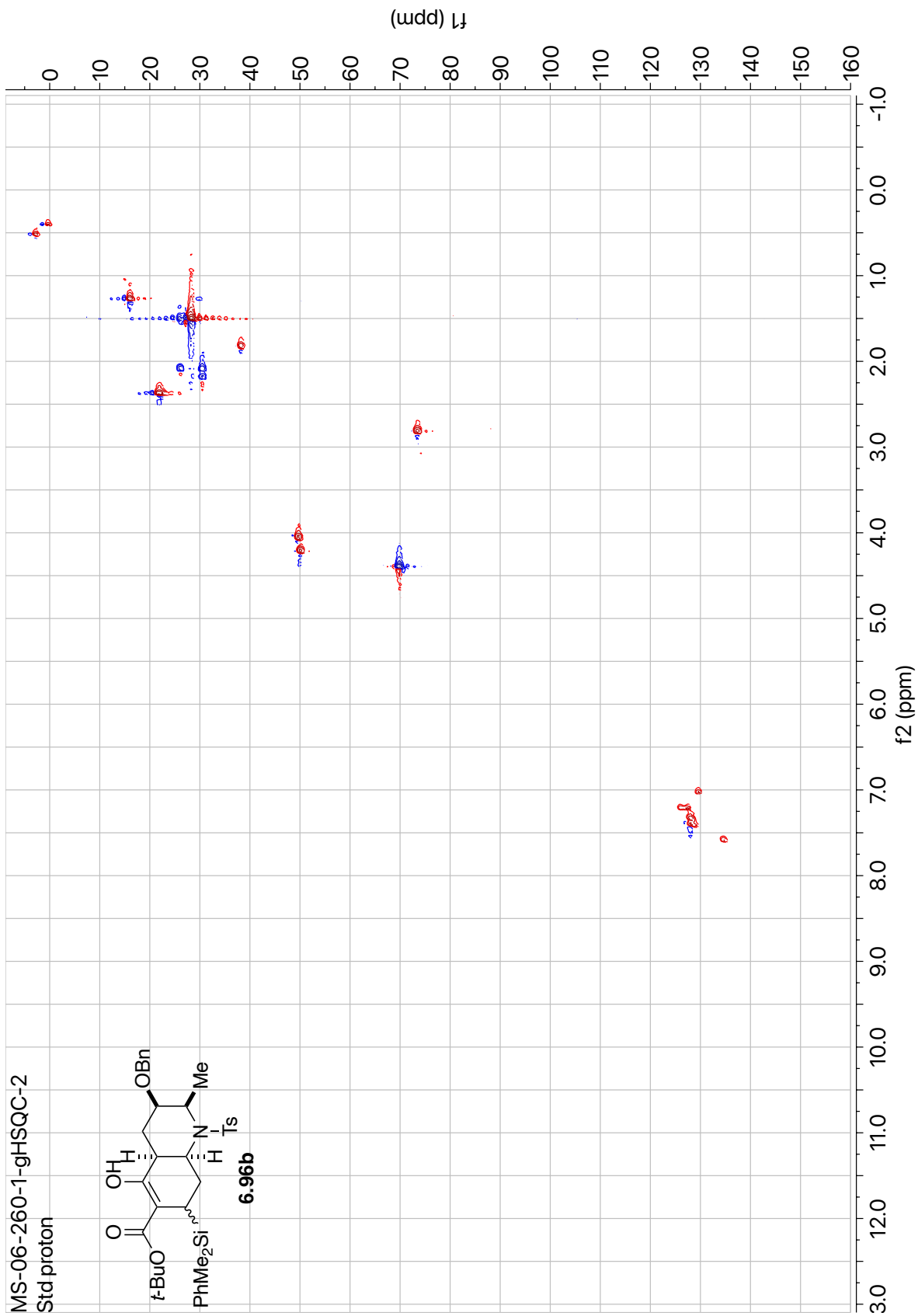


Figure 6.49: gHSQC of Compound **6.96b** (500 MHz, CDCl_3).

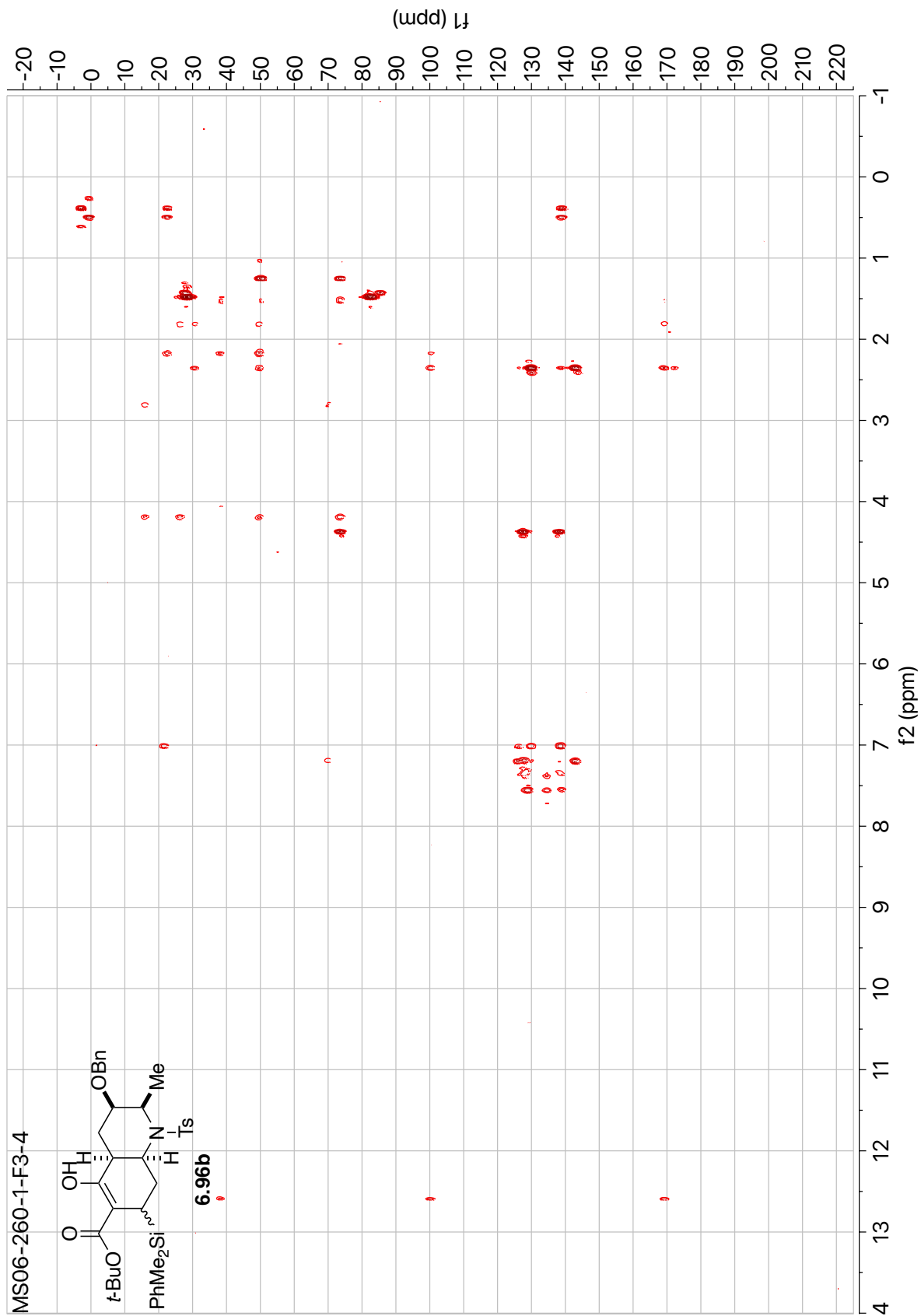


Figure 6.50: HMBC of Compound **6.96b** (500 MHz, CDCl_3).

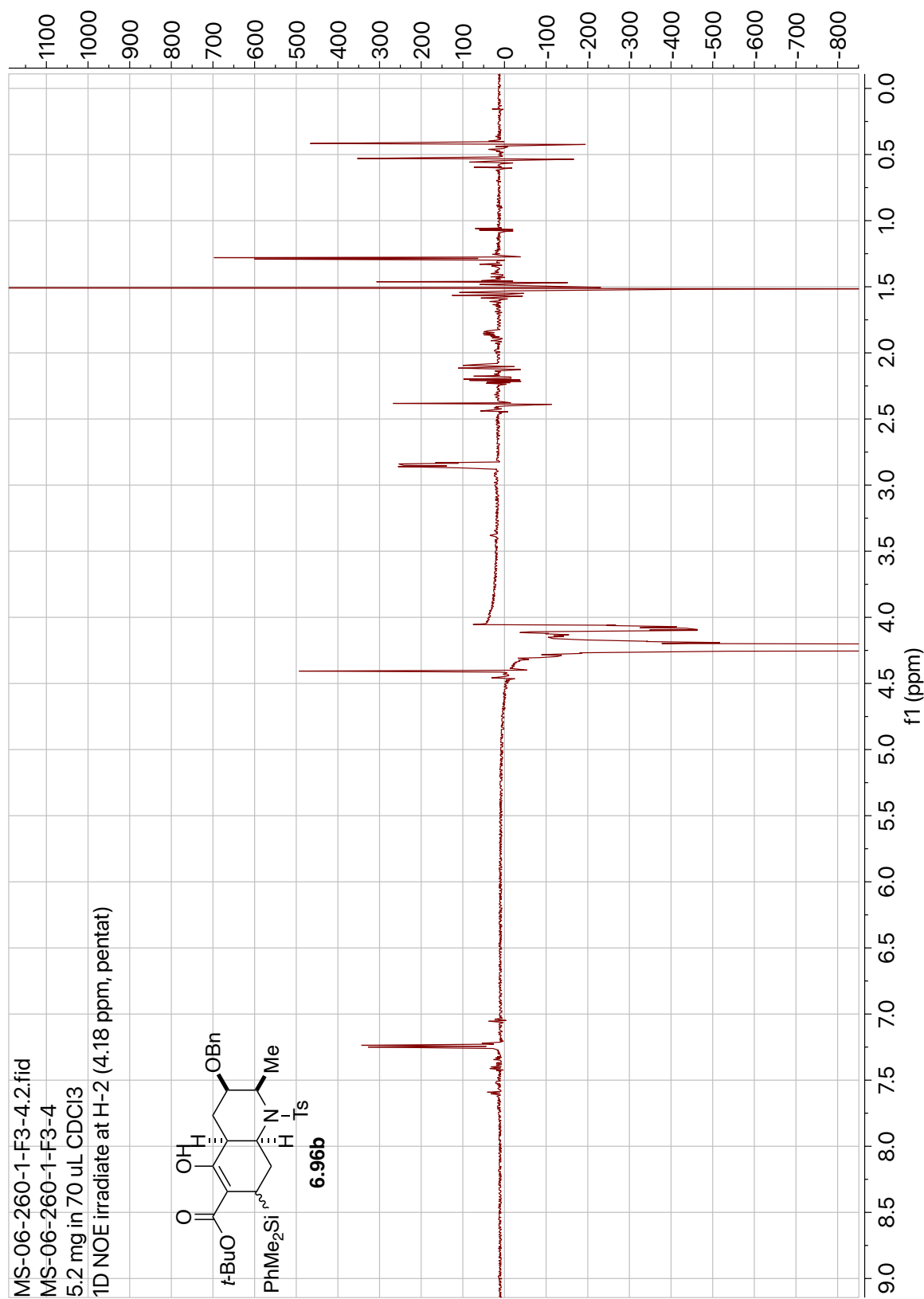


Figure 6.51: 1D NOE of Compound **6.96b**: {H-2} (δ_{H} 4.18, 600 MHz, CDCl₃).

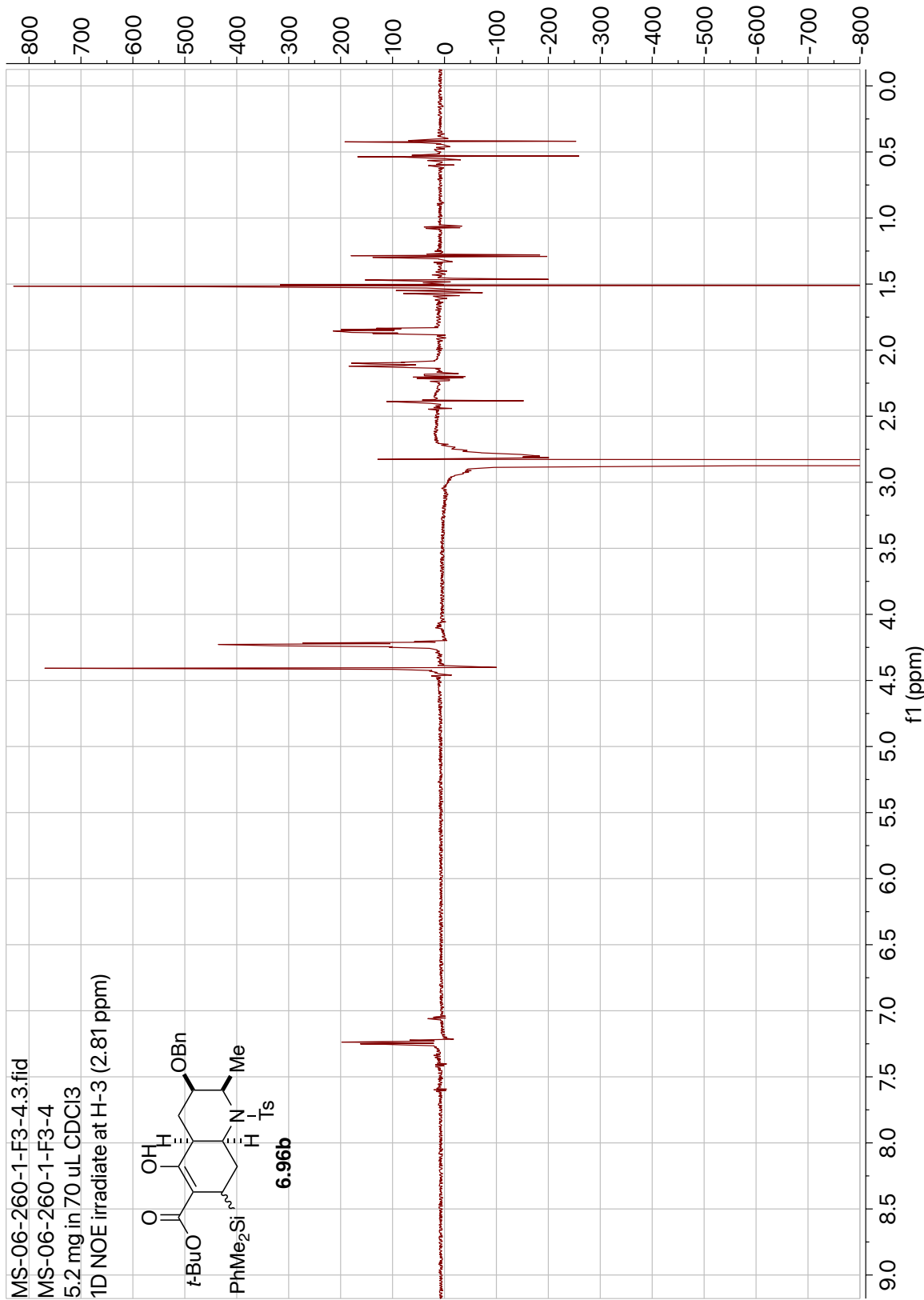


Figure 6.52: 1D NOE of Compound **6.96b**: {H-3} (δ_{H} 2.81, 600 MHz, CDCl₃).

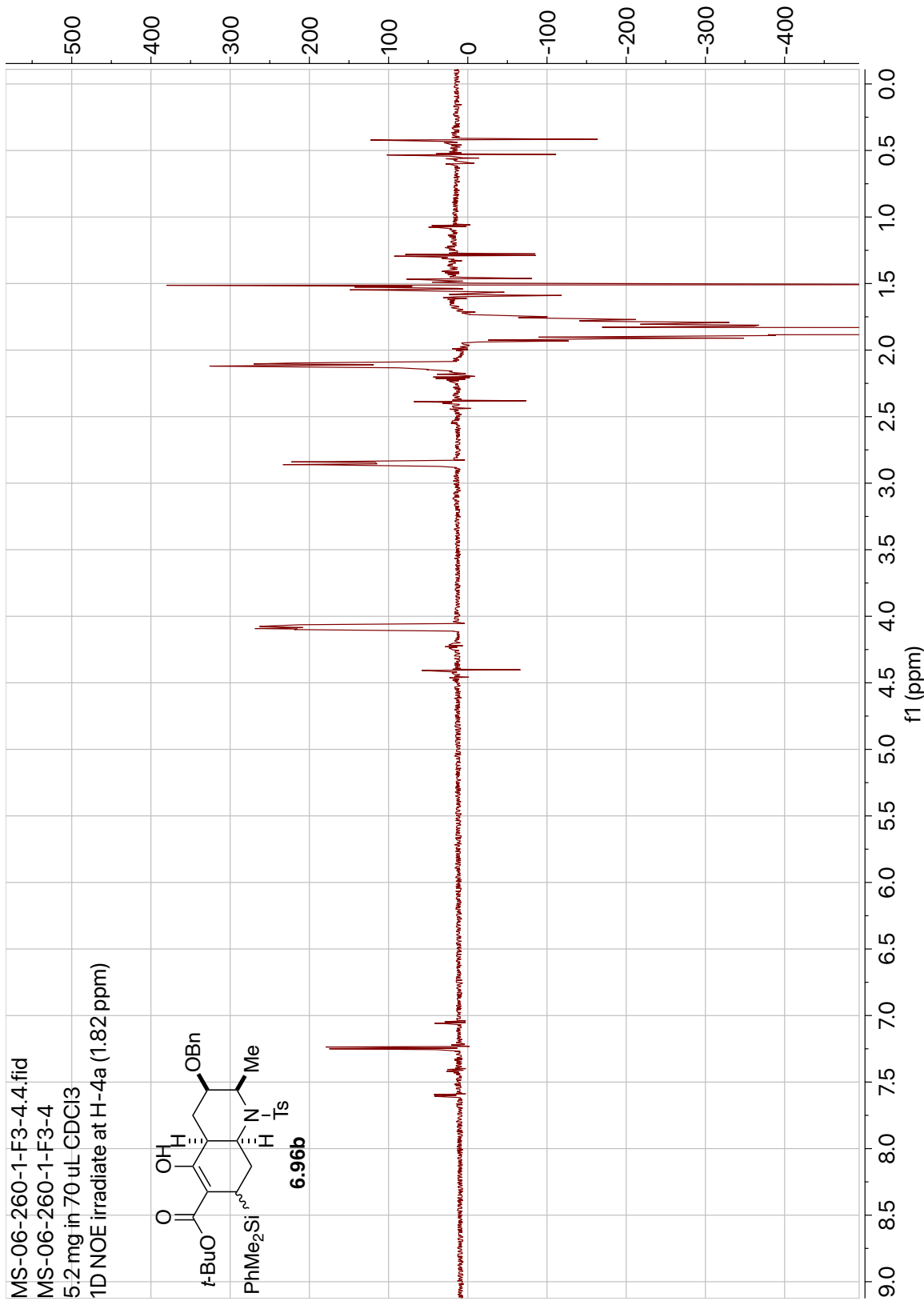


Figure 6.53: 1D NOE of Compound **6.96b**: {H-4a} (δ_{H} 1.82, 600 MHz, CDCl₃).

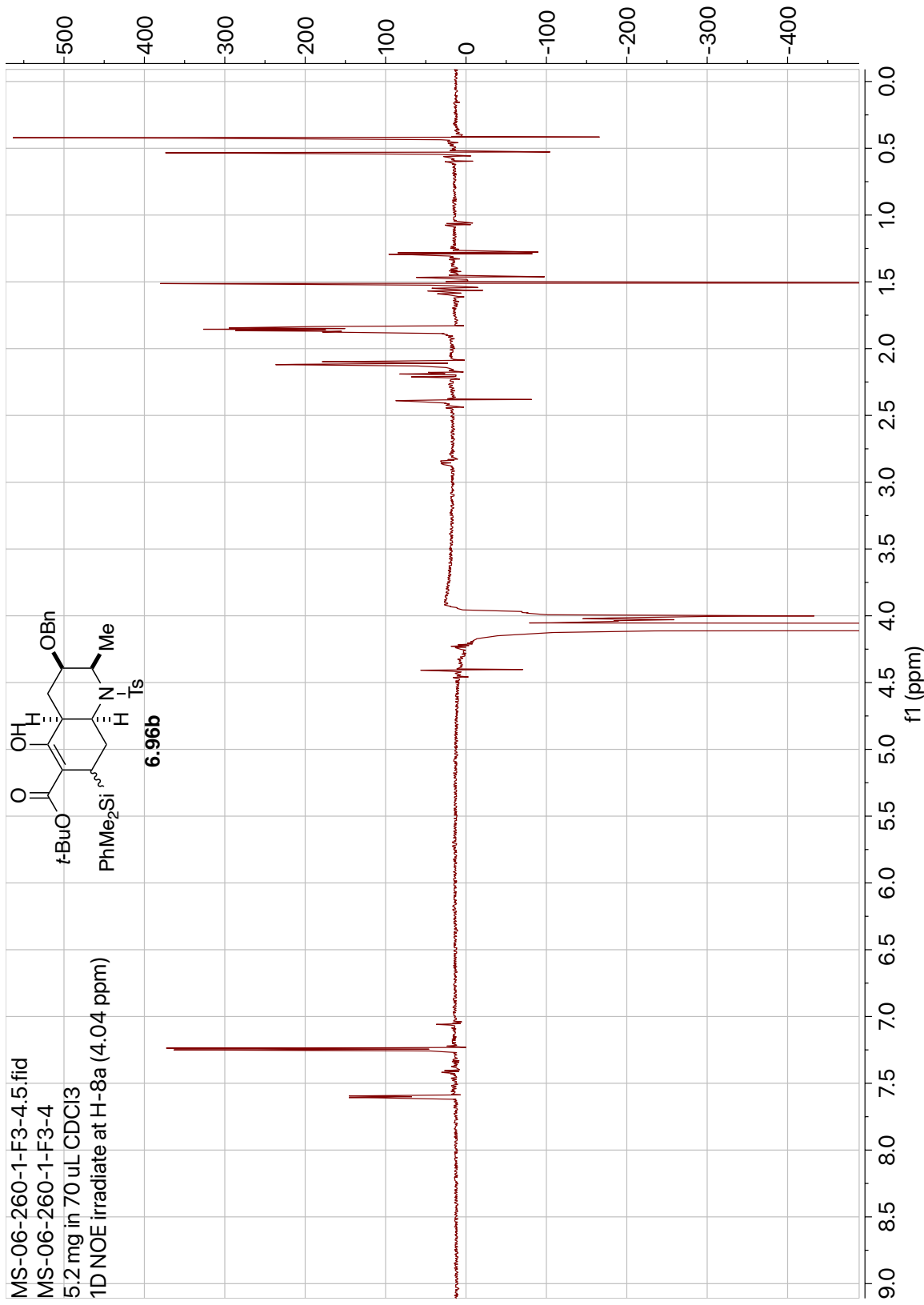


Figure 6.54: 1D NOE of Compound **6.96b**: {H-8a} (δ_{H} 4.04, 600 MHz, CDCl₃).

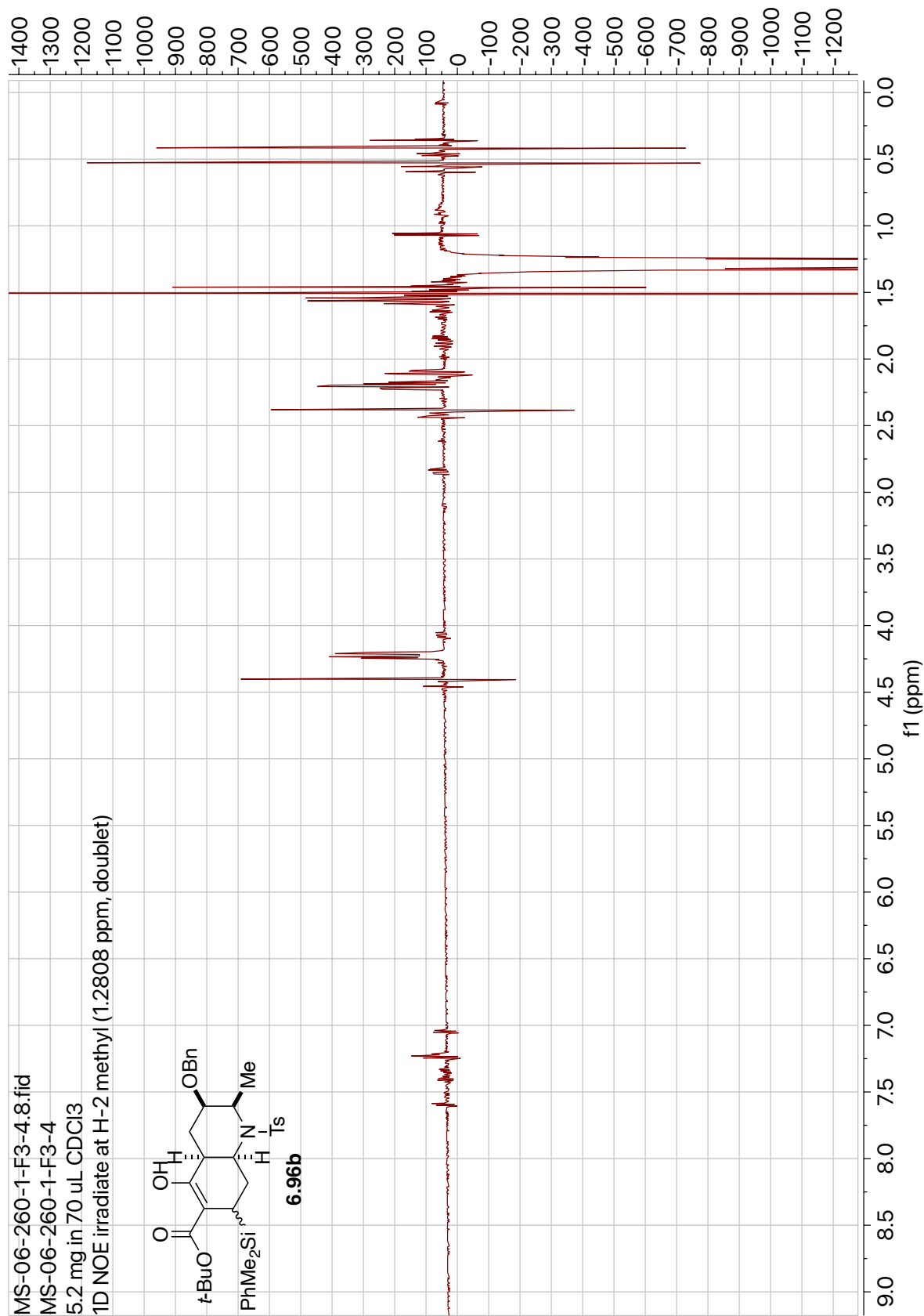


Figure 6.55: 1D NOE of Compound **6.96b**: {H₃-14(Me)} (δ_{H} 1.28, 600 MHz, CDCl₃).

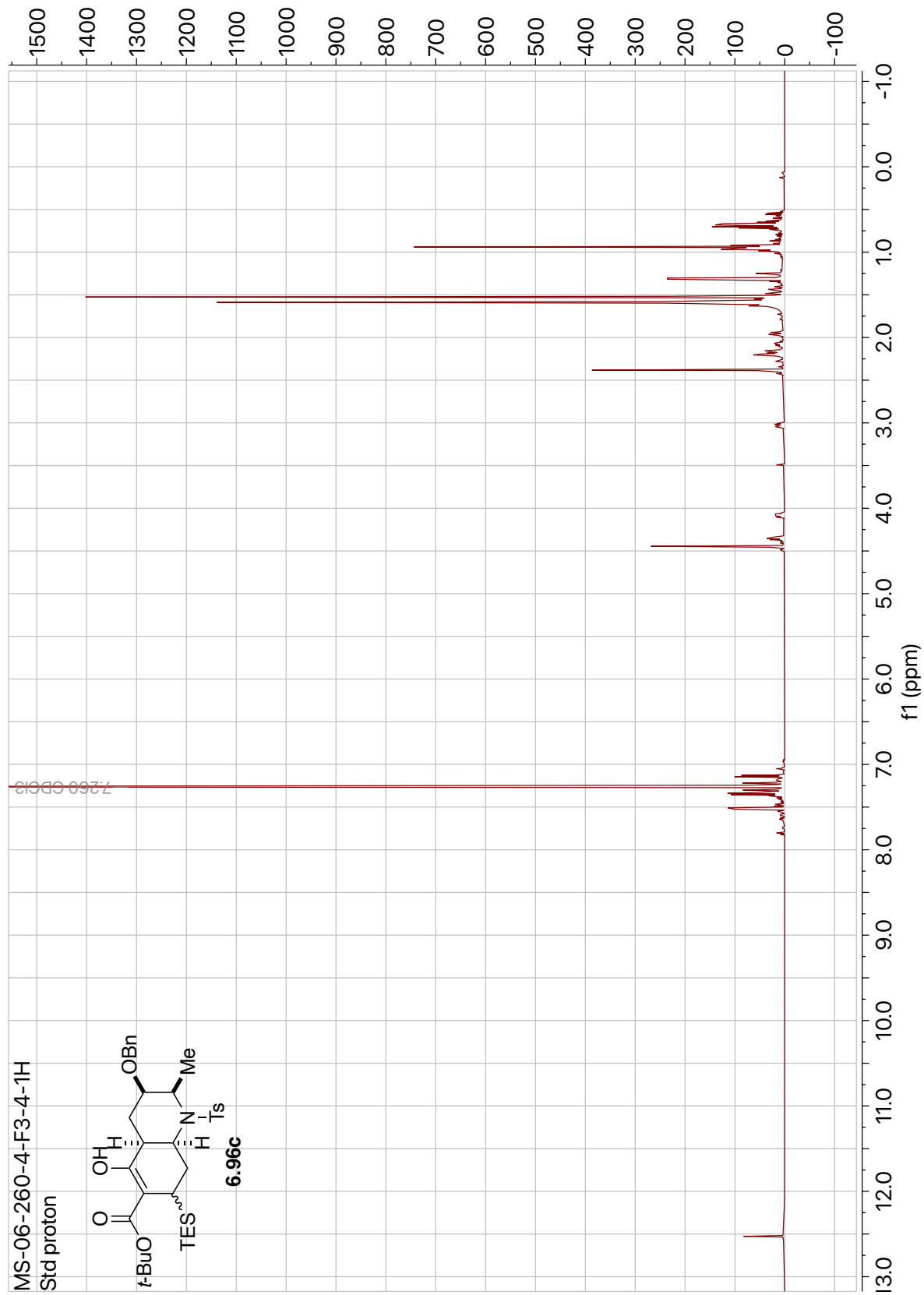


Figure 6.56: ¹H NMR of Compound **6.96c** (500 MHz, CDCl₃).

MS-06-260-4-F3-4-13C

Std carbon

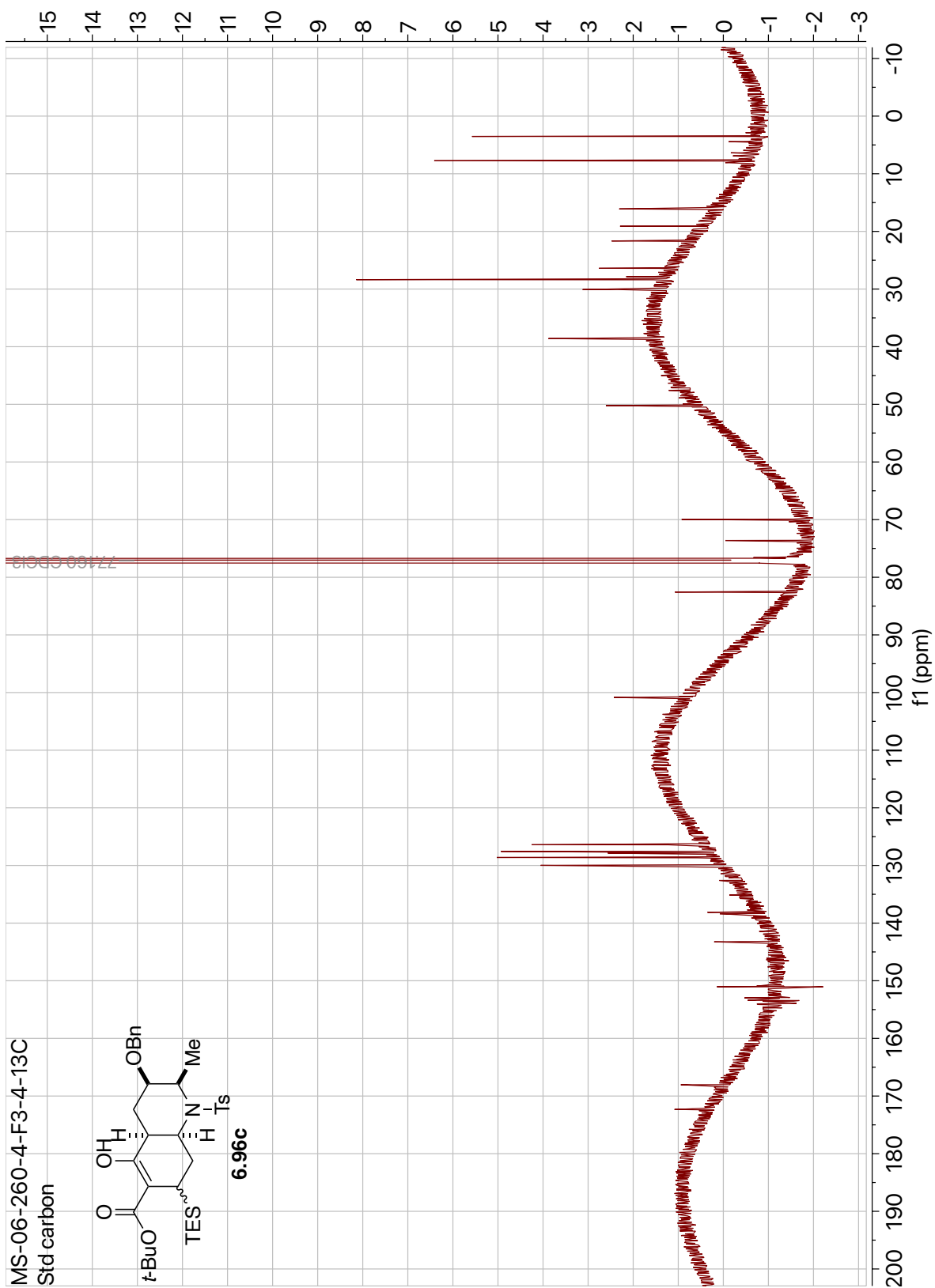
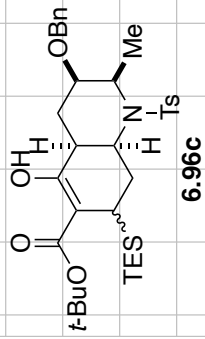


Figure 6.57: ¹³C NMR of Compound 6.96c (125 MHz, CDCl₃).

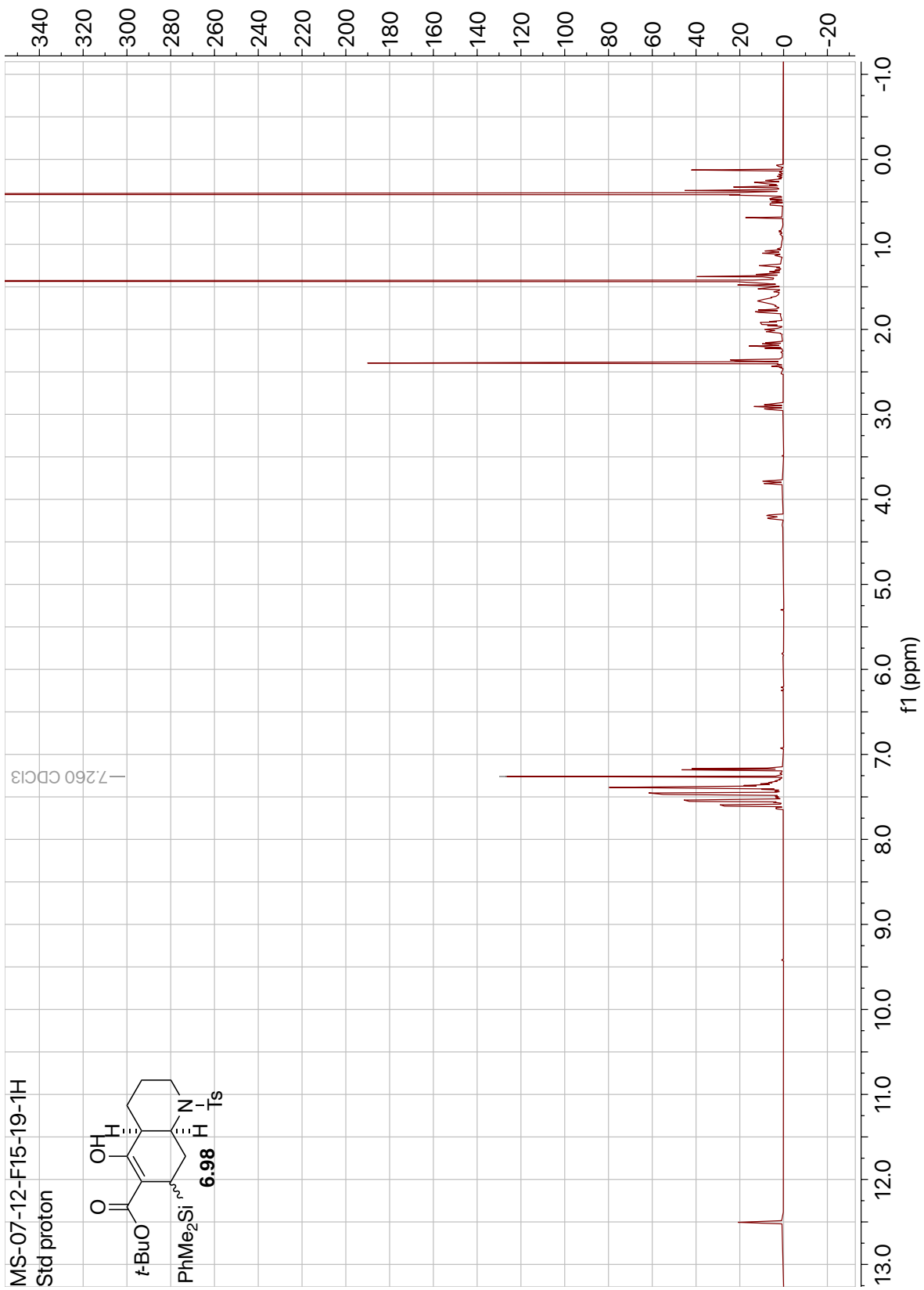
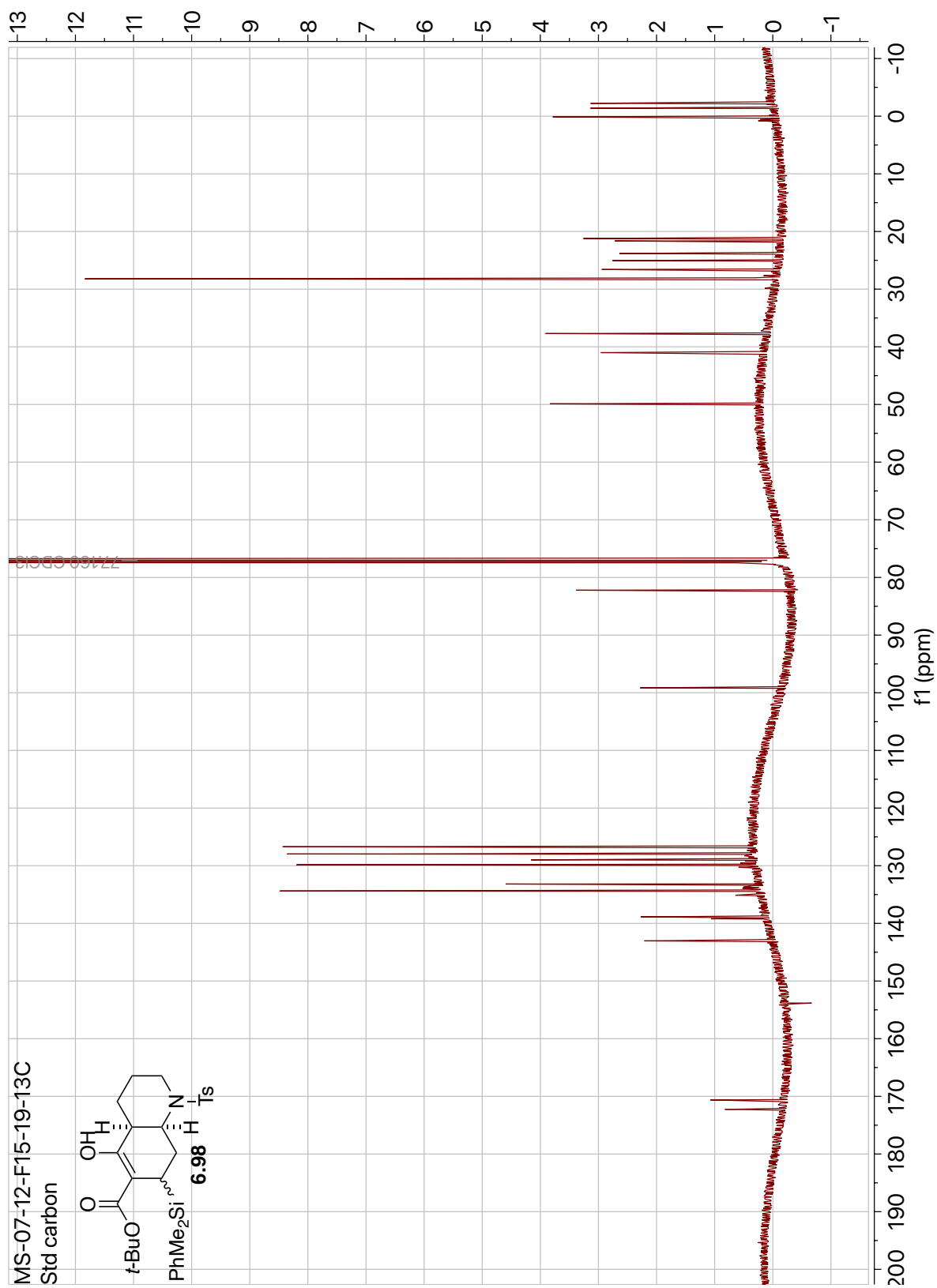


Figure 6.58: ¹H NMR of Compound **6.98** (500 MHz, CDCl₃).



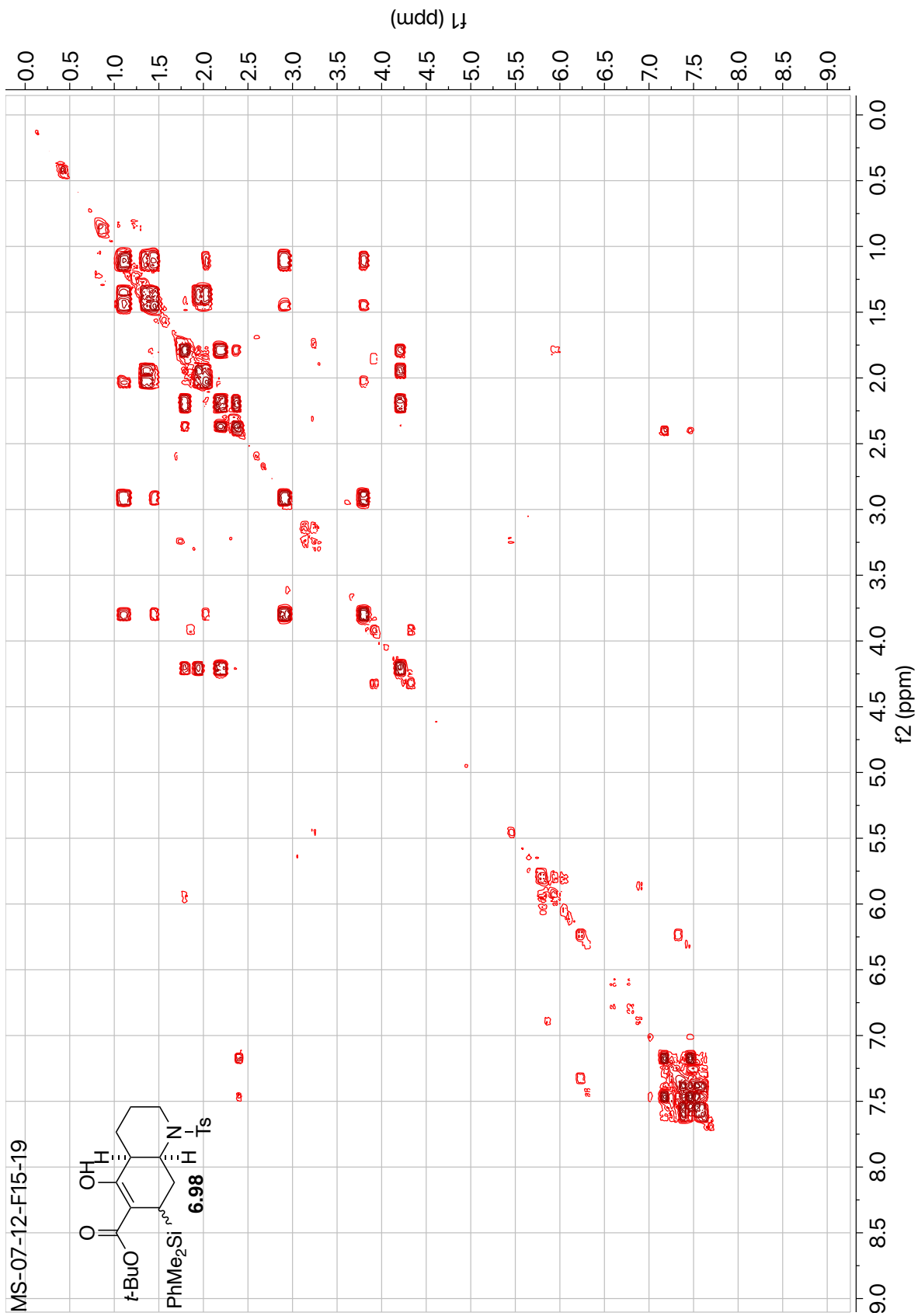


Figure 6.60: DQF-COSY of Compound **6.98** (500 MHz, CDCl₃).

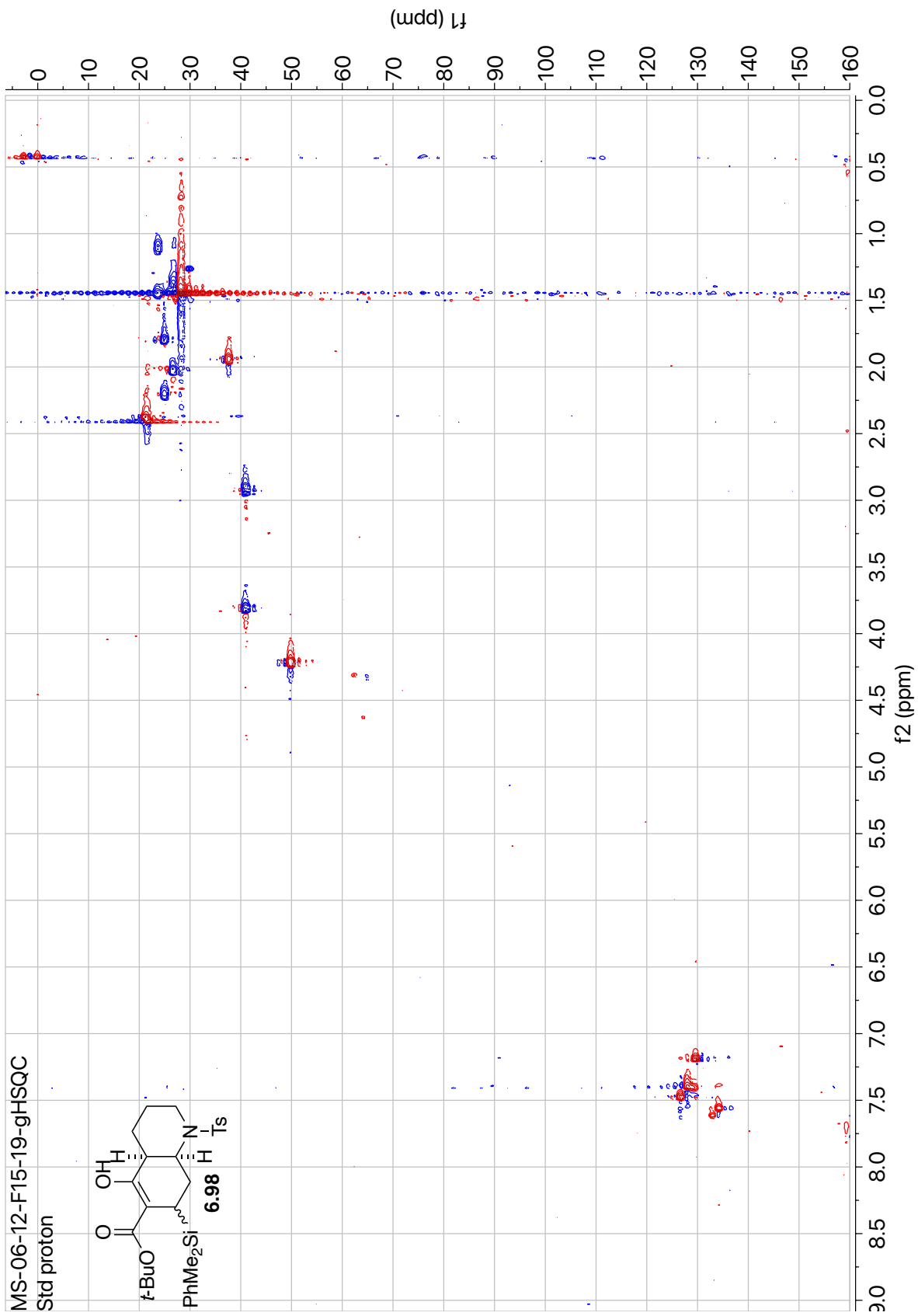


Figure 6.61: gHSQC of Compound **6.98** (500 MHz, CDCl₃).

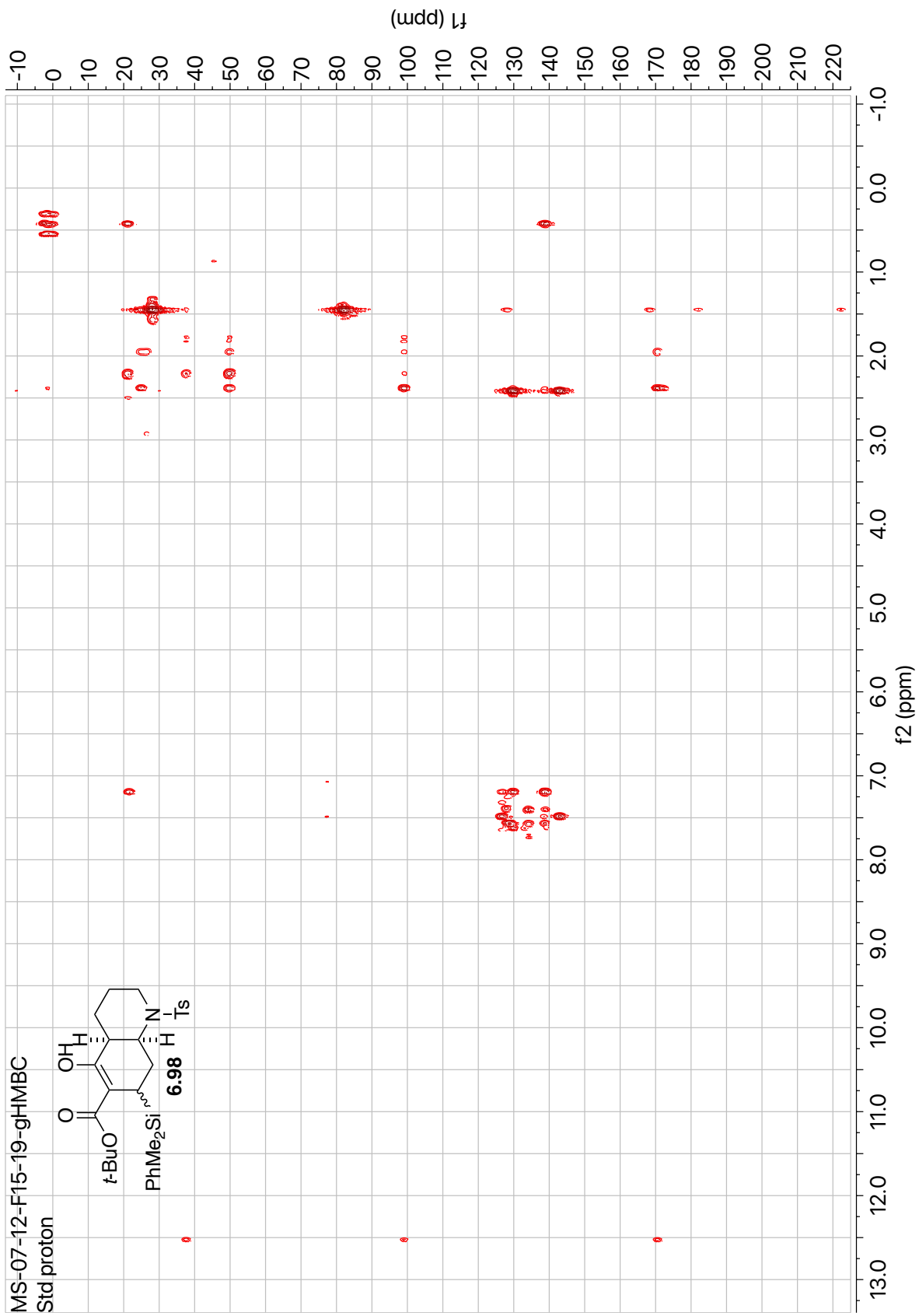


Figure 6.62: gHMBC of Compound 6.98 (500 MHz, CDCl_3).

MS-07-012-F15-19 1D NOESY.2.fid
MS-07-012-F5-19
Sample in 150 uL CDCl3
1D NOESY

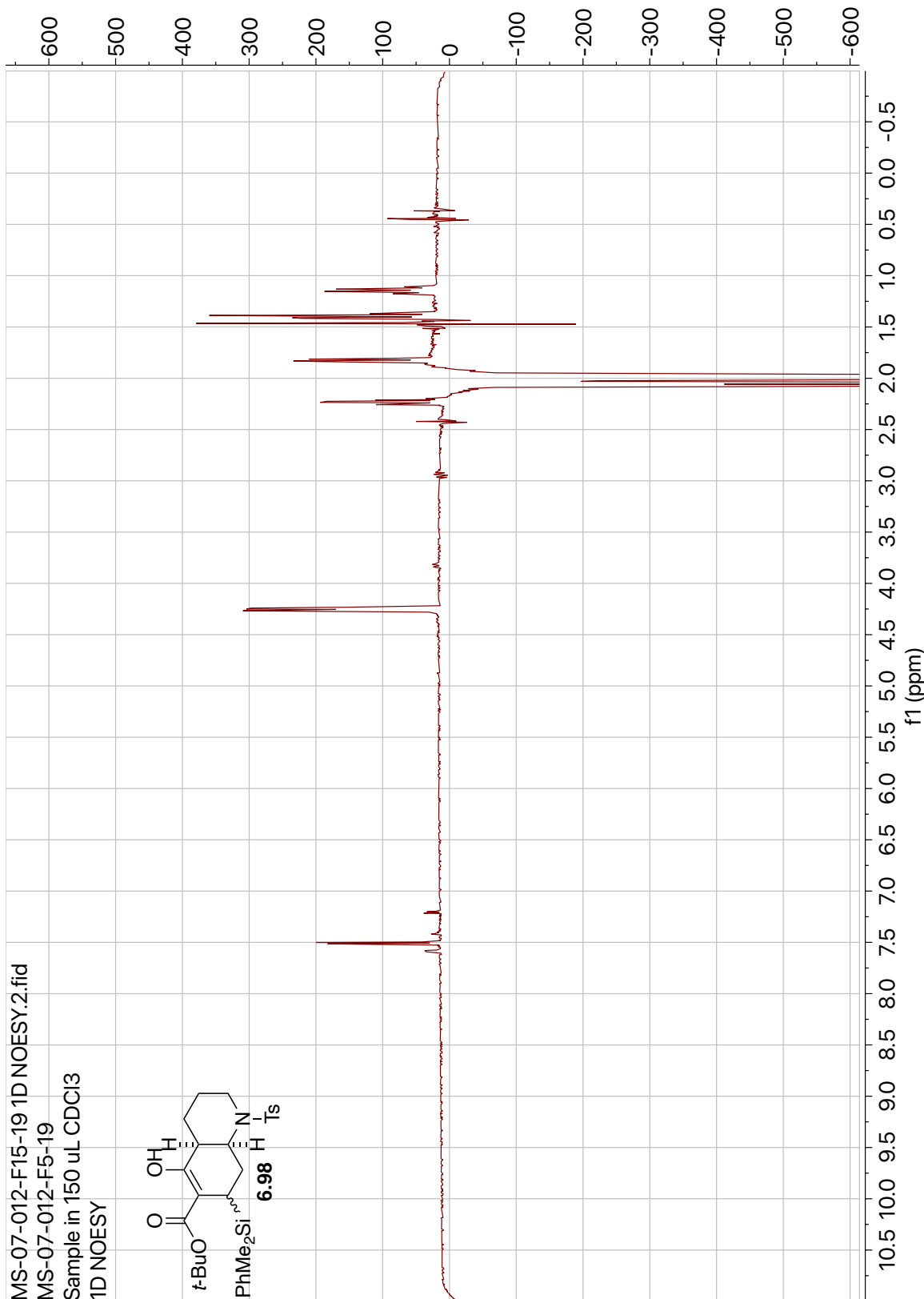
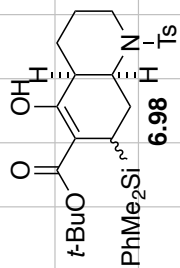


Figure 6.63: 1D NOE of Compound 6.98: {H-4a} (δ_{H} 1.98, 600 MHz, CDCl₃).

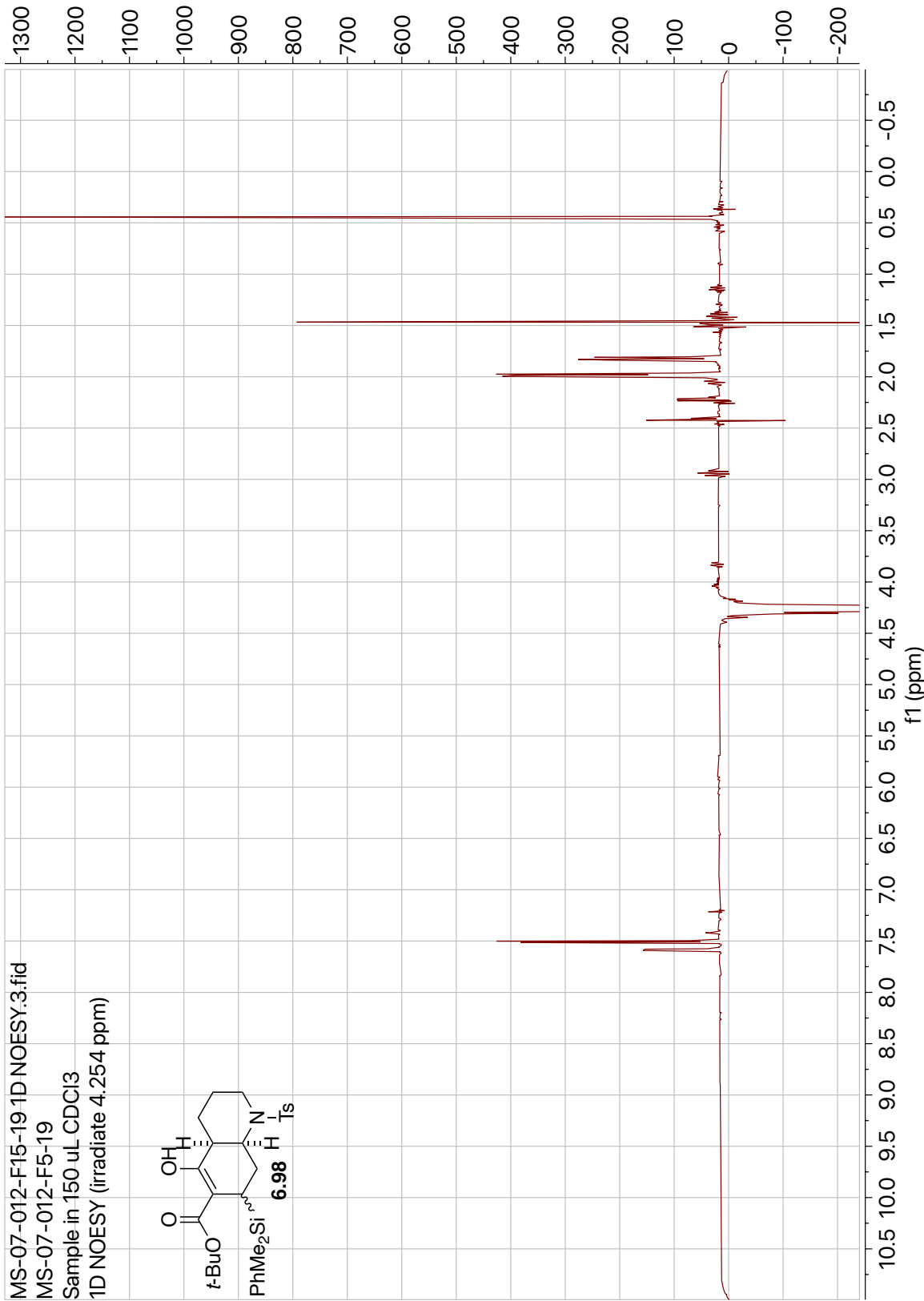


Figure 6.64: 1D NOE of Compound **6.98**: {H-8a} (δ_{H} 4.25, 600 MHz, CDCl₃).

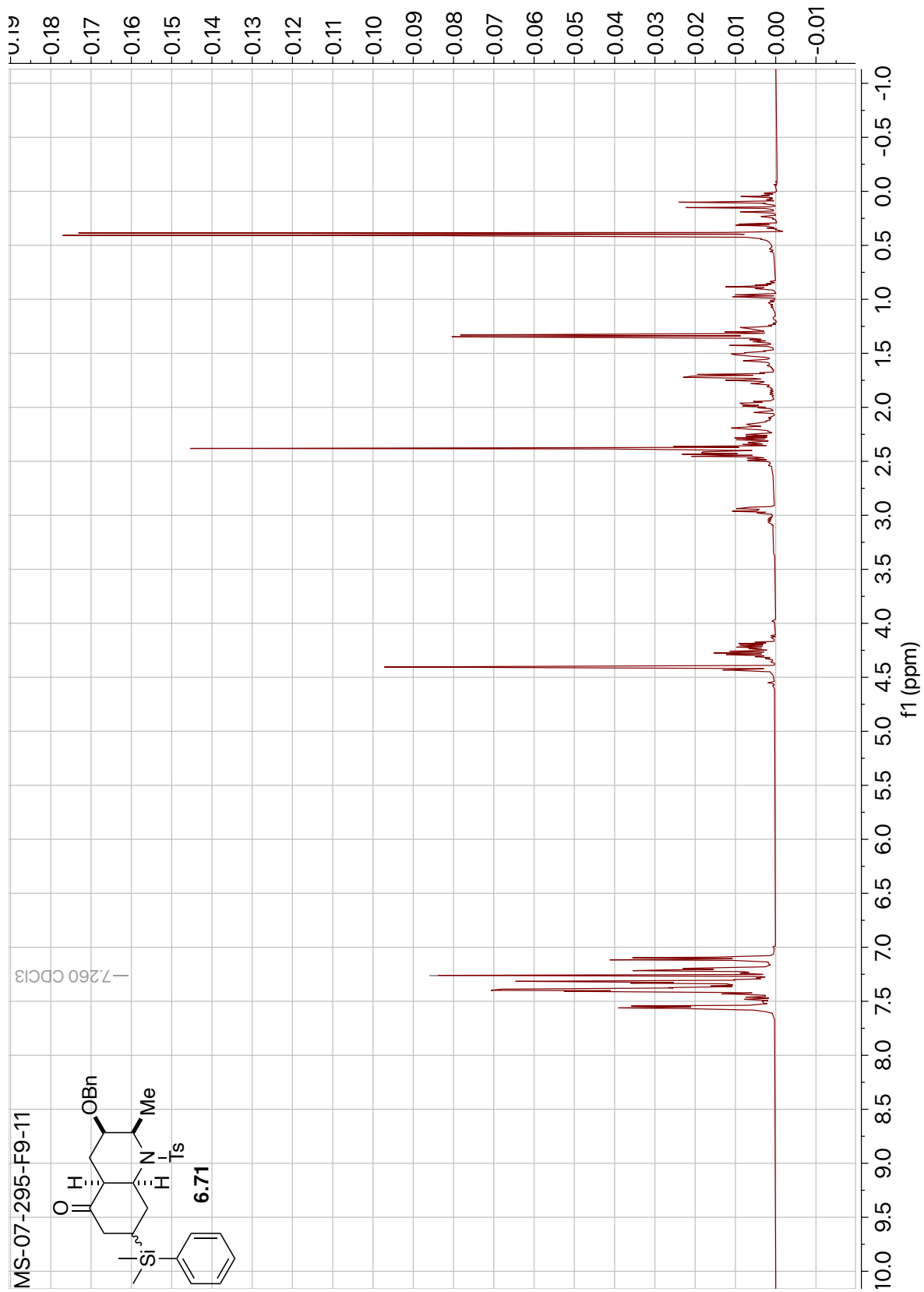


Figure 6.65: ¹H NMR of Compound **6.71** (400 MHz, CDCl₃).

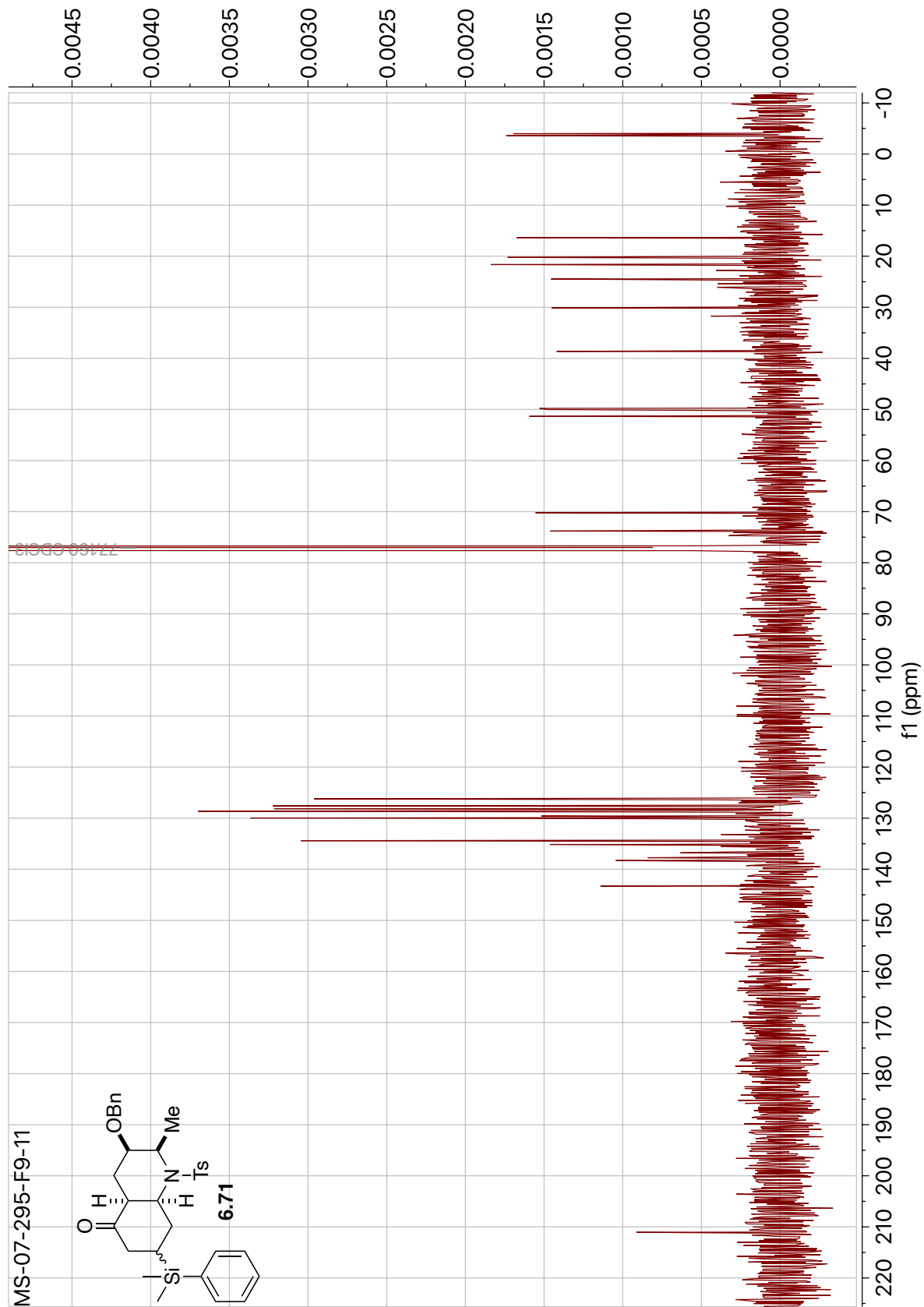


Figure 6.66: ^{13}C NMR of Compound **6.71** (100 MHz, CDCl_3).



Figure 6.67: DQF-COSY of Compound **6.71** (400 MHz, CDCl₃).

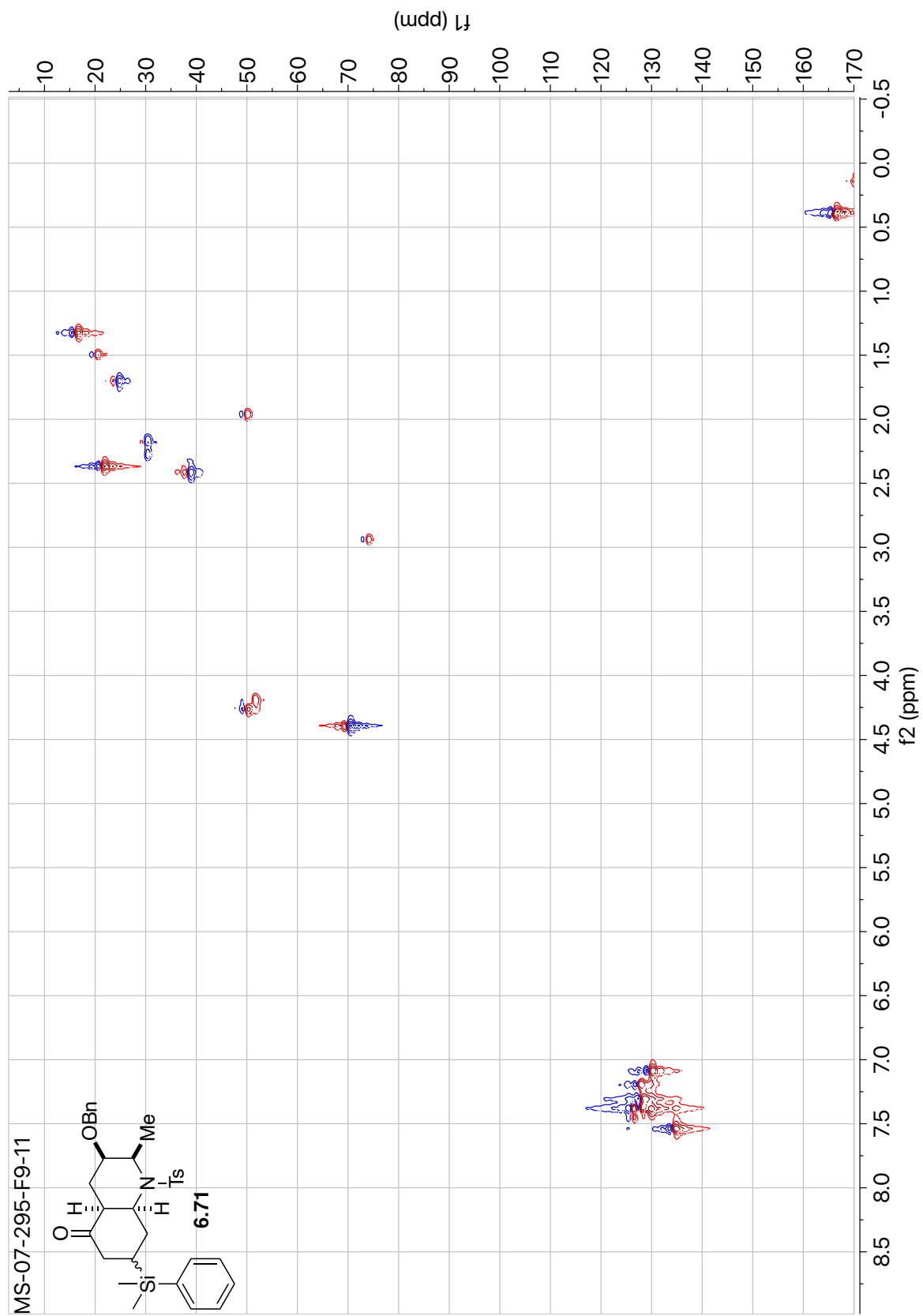


Figure 6.68: HSQC-NUS of Compound **6.71** (400 MHz, CDCl₃).

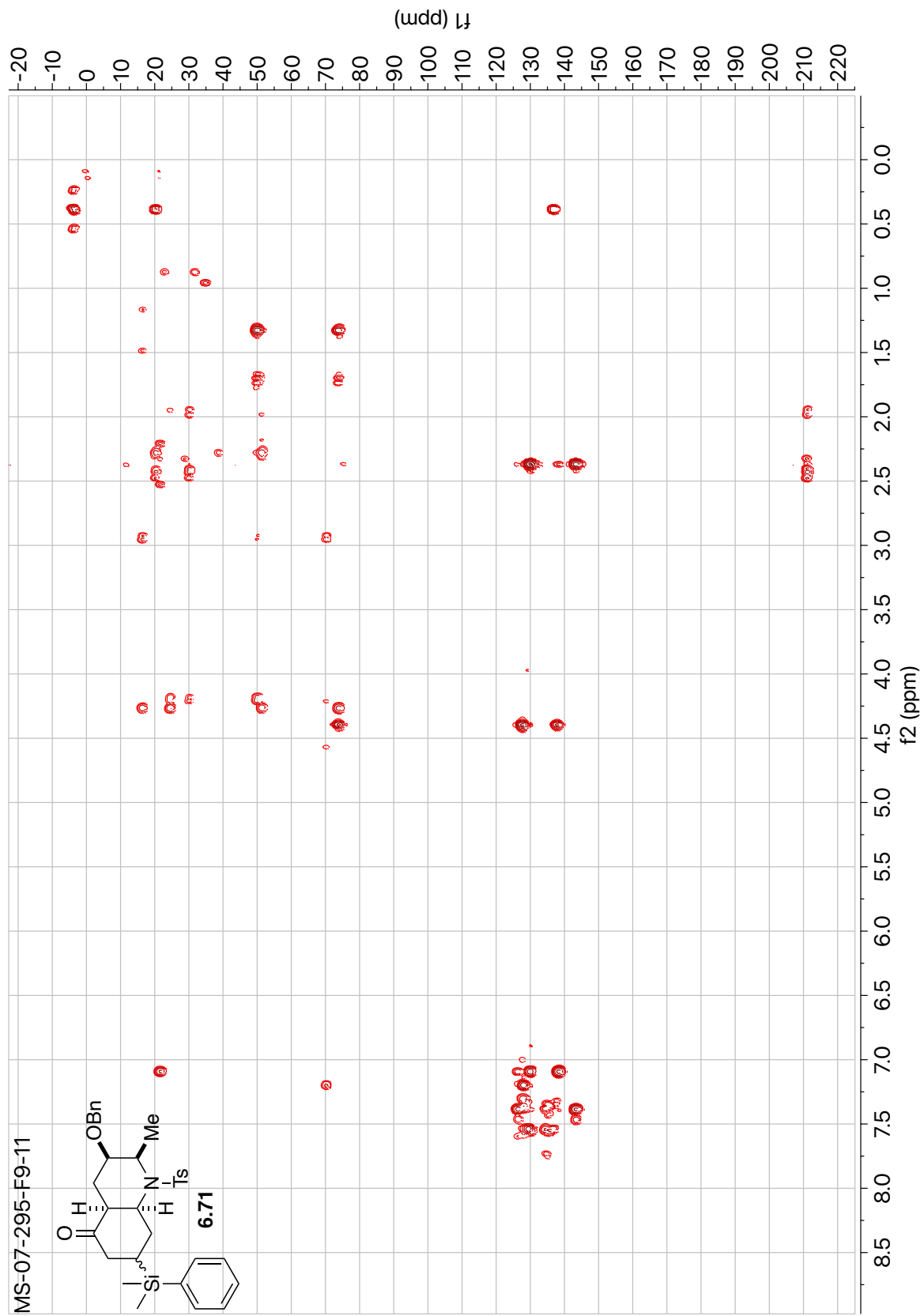
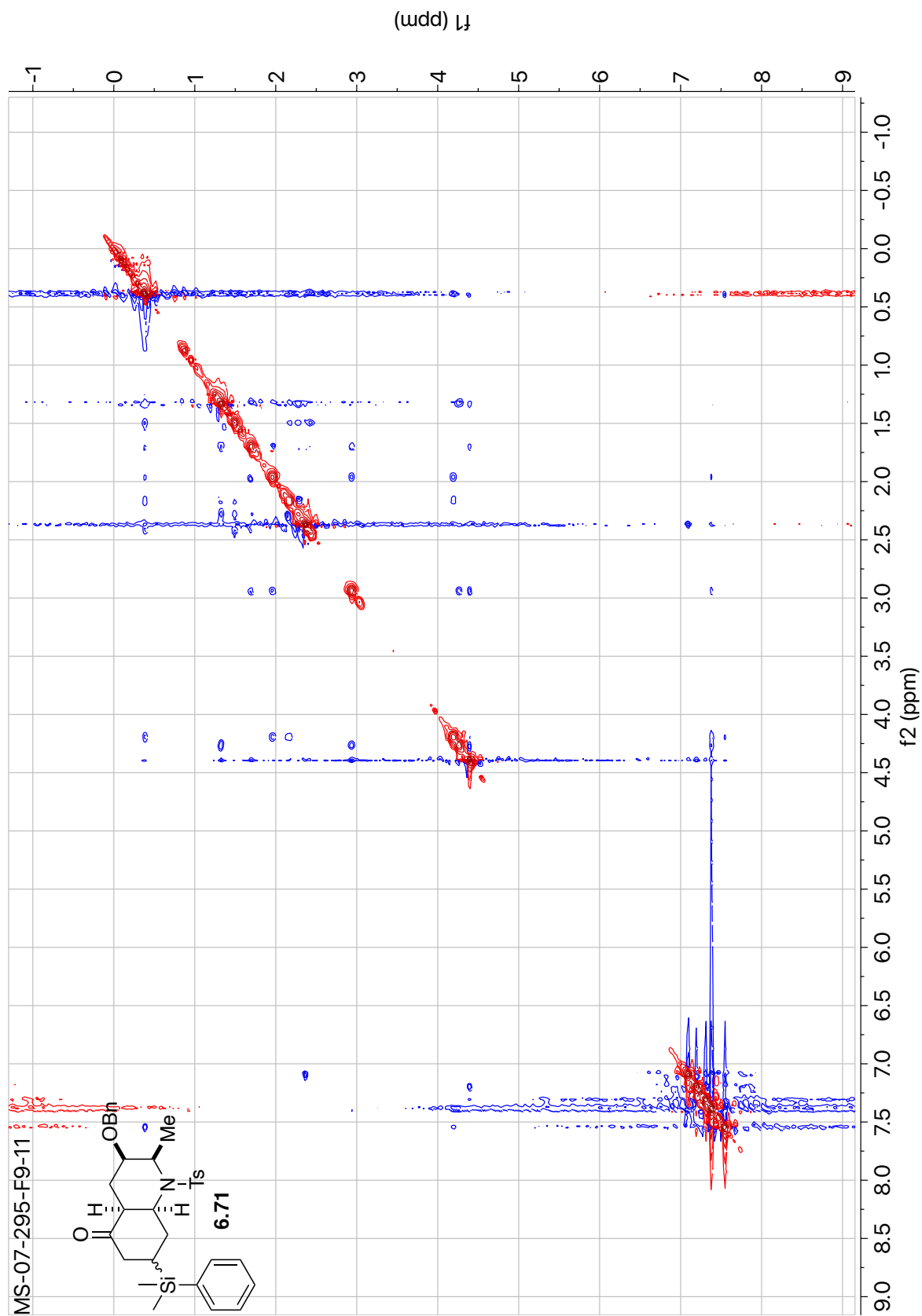


Figure 6.69: HMBC-NUS of Compound **6.71** (400 MHz, CDCl₃).



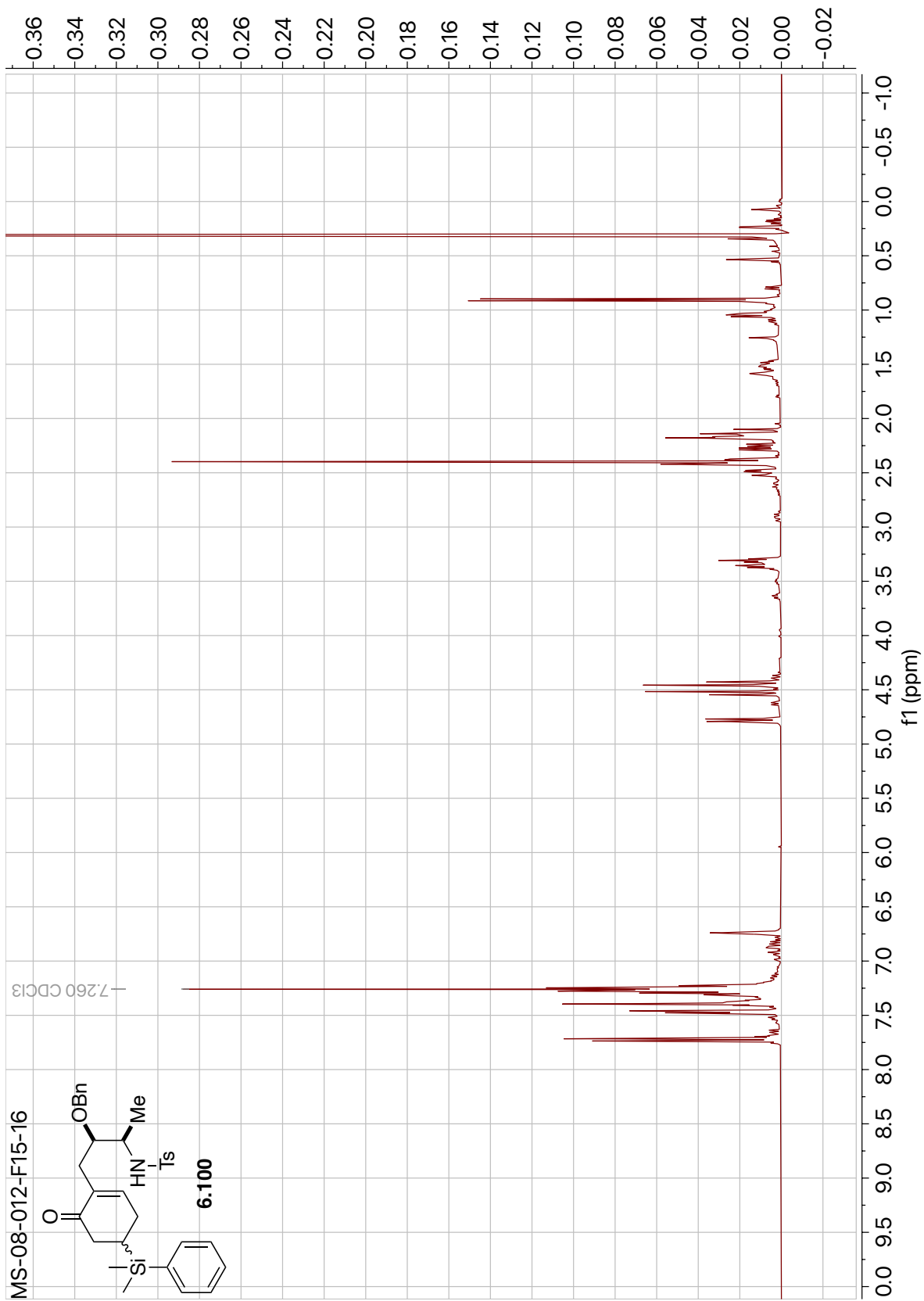


Figure 6.71: ¹H NMR of Compound **6.100** (400 MHz, CDCl₃).

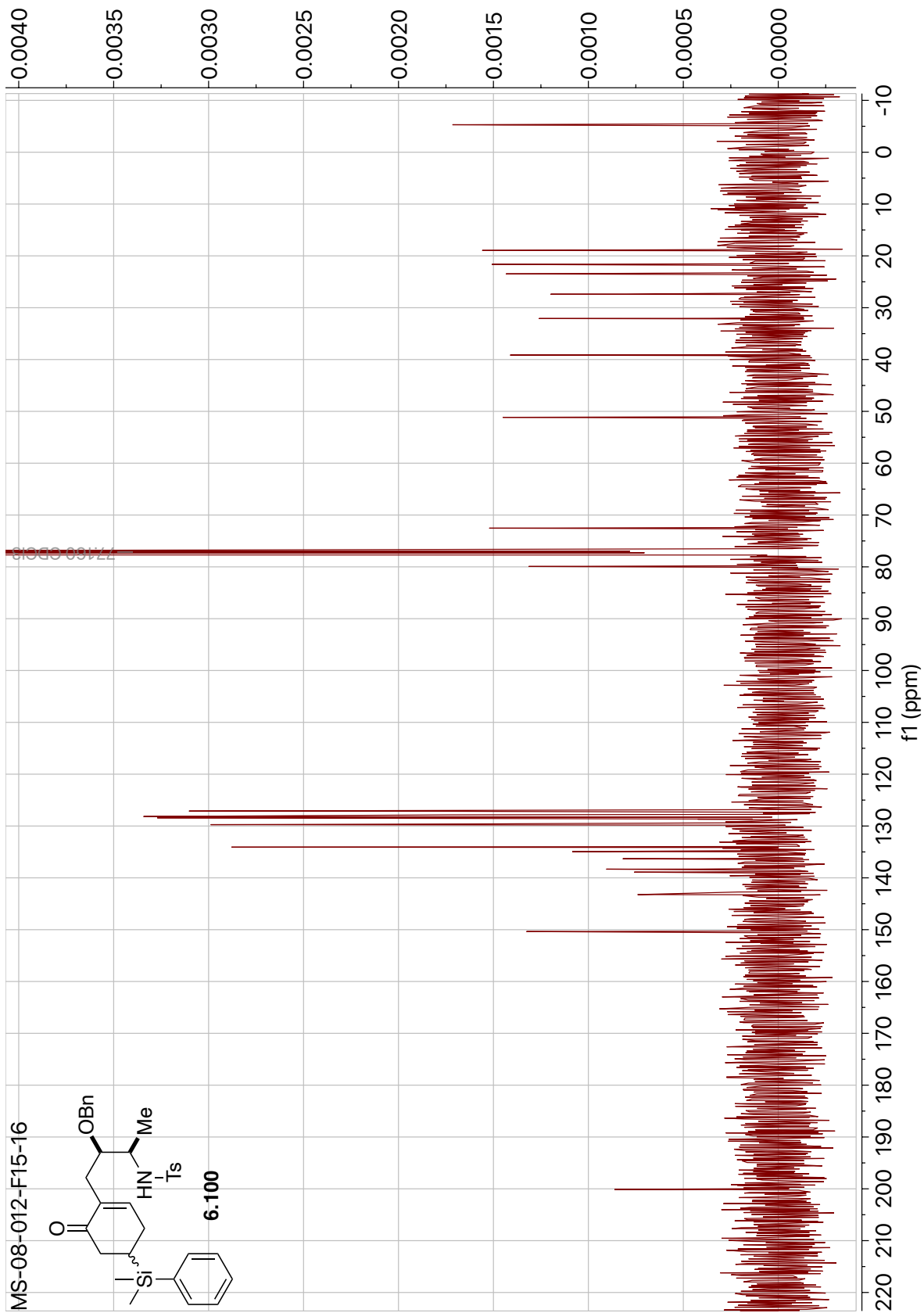


Figure 6.72: ¹³C NMR of Compound **6.100** (100 MHz, CDCl₃).

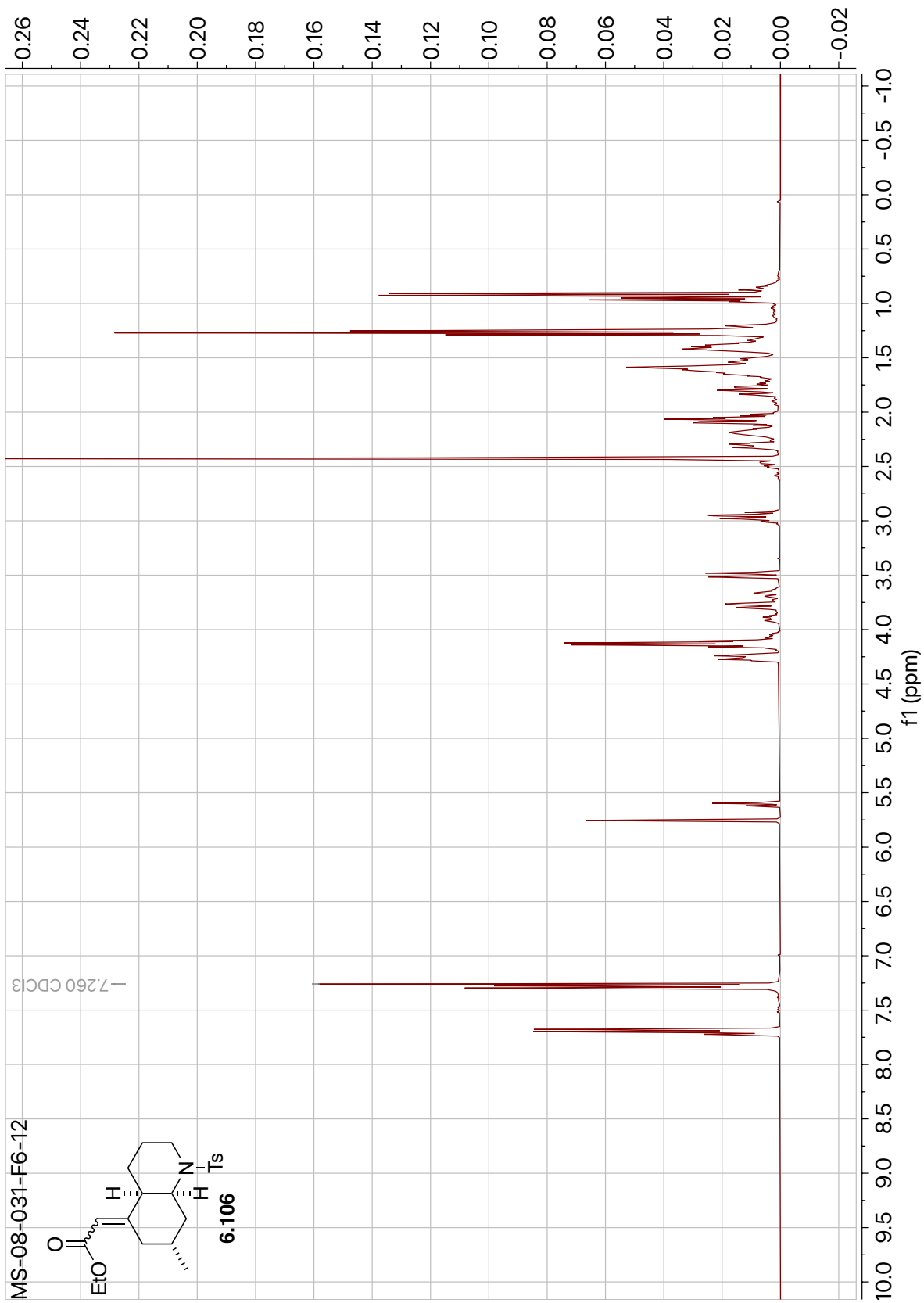
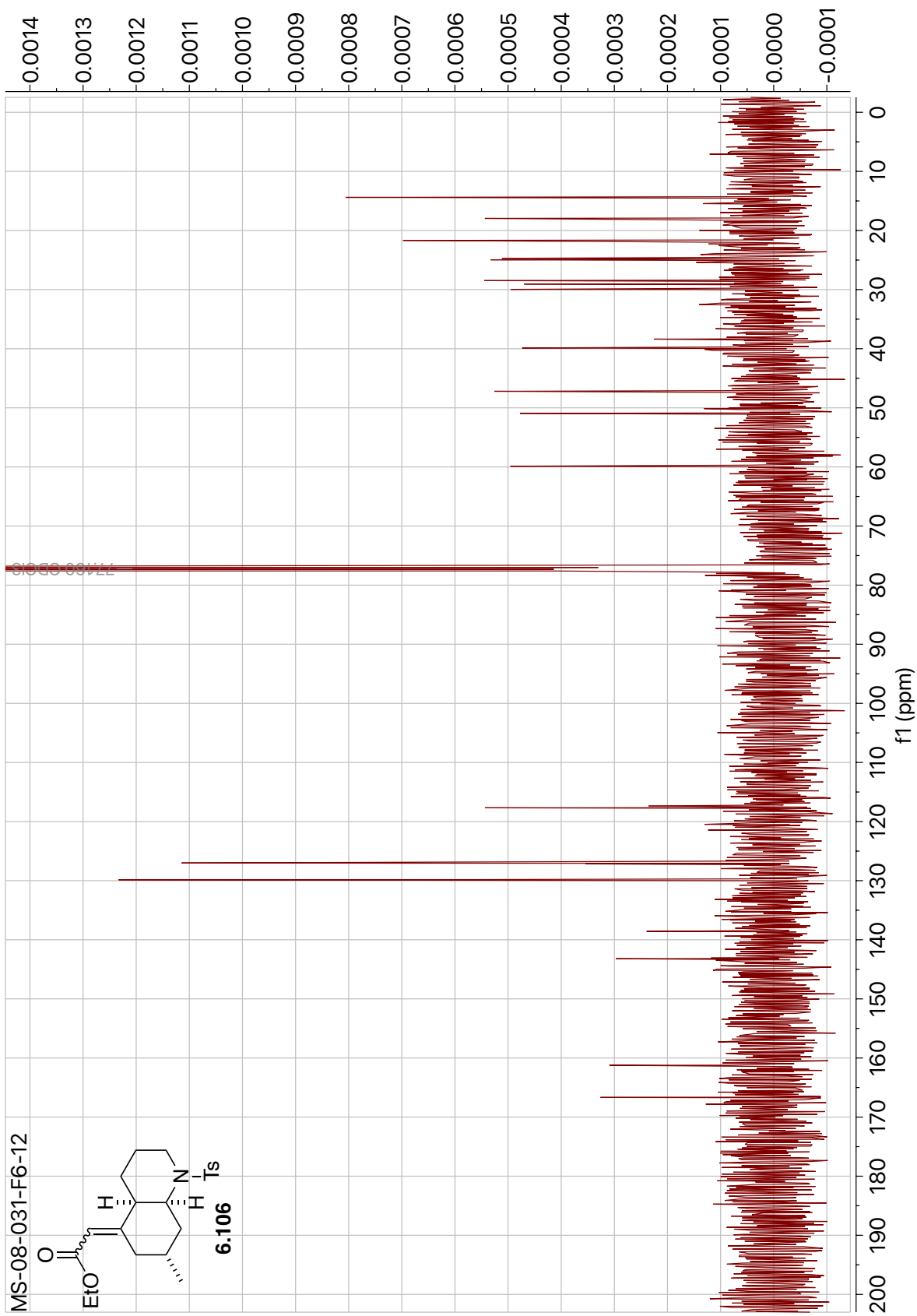


Figure 6.73: ¹H NMR of Compound **6.106** (400 MHz, CDCl₃).



6.8 References

- (1) (a) Steffan, B. *Tetrahedron* **1991**, *47*, 8729-8732. (b) Kubanek, J.; Williams, D. E.; de Silva, D.; Allen, T.; Anderson, R. J. *Tetrahedron Lett.* **1995**, *36*, 6189-6192.
- (2) Casertano, M.; Genovese, M.; Paoli, P.; Santi, A.; Aiello, A.; Menna, M.; Imperatore, C. *Mar. Drugs* **2022**, *20*, 65.
- (3) (a) Wright, A. D.; Goclik, E.; König, G. M.; Kaminsky, R. *J. Med. Chem.* **2002**, *45*, 3067-3072. (b) Davis, R. A.; Carroll, A. R.; Quinn, R. J. *J. Nat. Prod.* **2002**, *65*, 454-457.
- (4) Ómarsdóttir, S.; Wang, X.; Liu, H.-B.; Duggan, B. M.; Molinski, T. F. *J. Org. Chem.* **2018**, *83*, 13670-13677.
- (5) Tsuneki, H.; You, Y.; Toyooka, N.; Sasaoka, T.; Nemoto, H.; Dani, J. A.; Kimura, I. *Biol. Pharm. Bull.* **2005**, *28*, 611-614.
- (6) (a) Toyooka, N.; Okumura, M.; Takahata, H. *J. Org. Chem.* **1999**, *64*, 2182-2183. (b) Toyooka, N.; Okumura, M.; Takahata, H.; Nemoto, H. *Tetrahedron* **1999**, *55*, 10673-10784.
- (7) (a) Ozawa, T.; Aoyagi, S.; Kibayashi, C. *Org. Lett.* **2000**, *2*, 2955-2958. (b) Ozawa, T.; Aoyagi, S.; Kibayashi, C. *J. Org. Chem.* **2001**, *66*, 3338-3347.
- (8) (a) Pu, X.; Ma, D. *Angew. Chem. Int. Ed.* **2004**, *43*, 4222-4225. (b) Pu, X.; Ma, D. *J. Org. Chem.* **2006**, *71*, 6562-6572.
- (9) Niethe, A.; Fischer, D.; Blechert, S. *J. Org. Chem.* **2008**, *73*, 3088-3093.
- (10) Molinski, T. F.; Salib, M. N.; Pearce, A. N.; Copp, B. R. *J. Nat. Prod.* **2019**, *82*, 1183-1189.
- (11) Ma, F.; He, C.; Wang, E.; Tong, R. *Org. Lett.* **2021**, *23*, 6583-6588.
- (12) Barbe, G.; Charette, A. B. *J. Am. Chem. Soc.* **2008**, *130*, 13873-13875.
- (13) Li, G.; Hsung, R. P.; Slafer, B. W.; Sagamanova, I. K. *Org. Lett.* **2008**, *10*, 4991-4994.
- (14) Amat, M.; Pinto, A.; Griera, R.; Bosch, J. *Chem. Eur. J.* **2015**, *21*, 12804-12808.
- (15) (a) Li, X.; Hu, L.; Jia, J.; Gu, H.; Jia, Y.; Chen, X. *Org. Lett.* **2017**, *19*, 5372-5375. (b) Gu, H.; Hu, Y.; Jia, Y.; Zhou, Q.; Luo, G.; Chen, X. *Chem. Eur. J.* **2021**, *27*, 4141-4149.
- (16) Schrey, A.; Osterkamp, F.; Staudi, A.; Rickert, C.; Wagner, H.; Koert, U.; Herrschaft, B.; Harms, K. *Eur. J. Org. Chem.* **1999**, 2977-2990.

-
- (17) Reetz, M. T.; Drewes, M. W.; Lennick, K.; Schmitz, A.; Holdgrun, X. *Tetrahedron: Asymmetry* **1990**, *1*, 375-378.
- (18) (a) Sarkar, D. C.; Das, A. R.; Ranu, B. C. *J. Org. Chem.* **1990**, *55*, 5799-5801. (b) Nakata, T.; Oishi, T. *Tetrahedron Lett.* **1980**, *21*, 1641-1644. (c) Nakata, T.; Kuwabara, T.; Tani, Y.; Oishi, T. *Tetrahedron Lett.* **1982**, *23*, 1015-1016. (d) Ito, Y.; Yamaguchi, M. *Tetrahedron Lett.* **1983**, *24*, 5385-5386.
- (19) Kuhn, R.; Löw, I.; Trischmann, H. *Chem. Ber.* **1957**, *90*, 203-218.
- (20) Widmer, U. *Synth. Commun.* **1987**, 568-570.
- (21) Czernecki, S.; Georgoulis, C.; Provelenghiou, C.; Fusey, G. *Tetrahedron Lett.* **1976**, *17*, 3535-3536.
- (22) Travis, B. R.; Narayan, R. S.; Borhan, B. *J. Am. Chem. Soc.* **2002**, *124*, 3824-3825.
- (23) Demuth, M.; Ritterskamp, P.; Weight, E.; Schaffner, K. *J. Am. Chem. Soc.* **1986**, *108*, 4149-4154.
- (24) (a) Brooks, D. W.; Lu, L. D.-L.; Masamune, S. *Angew. Chem., Int. Ed. Engl.* **1979**, *18*, 72-74. (b) Hodgson, D. M.; Labande, A. L.; Pierard, Y. T. M.; Castro, M. A. *J. Org. Chem.* **2003**, *68*, 6153-6159.
- (25) Bradshaw, B.; Luque-Corredera, C.; Bonjoch, J. *Org. Lett.* **2013**, *15*, 326-329.
- (26) Hazra, C. K.; Irran, E.; Oestreich, M. *Eur. J. Org. Chem.* **2013**, *2013*, 4903-4908.
- (27) Wünsch, S.; Breit, B. *Chem. Eur. J.* **2015**, *21*, 2358-2363.
- (28) Sasaki, M.; Kawanishi, E.; Nakai, Y.; Matsumoto, T.; Yamaguchi, K.; Takada, K. *J. Org. Chem.* **2003**, *68*, 9330-9339.
- (29) Mata, G.; Wölfl, B.; Fürstner, A. *Chem. Eur. J.* **2019**, *25*, 246-254.
- (30) (a) Chong, B.-D.; Ji, Y.-I.; Oh, S.-S.; Yang, J.-D.; Baik, W.; Koo, S. *J. Org. Chem.* **1997**, *62*, 9323-9325. (b) Carlone, A.; Marigo, M.; North, C.; Landa, A.; Jørgensen, K. A. *Chem. Commun.* **2006**, 4928-4930.
- (31) Fustero, S.; Jiménez, D.; Moscardó, J.; Catalán, S.; Pozo, C. d. *Org. Lett.* **2007**, *9*, 5283-5286.
- (32) Wynn, D. A.; Roth, M. M.; Pollard, B. D. "The solubility of alkali-metal fluorides in non-aqueous solvents with and without crown ethers, as determined by flame emission spectrometry." *Talanta* **1984**, *31*, 1036-1040.

-
- (33) Blanchette, M. A.; Choy, W.; Davis, J. T.; Essensfeld, A. P.; Masamune, S.; Roush, W. R.; Sakai, T. *Tetrahedron Lett.* **1984**, *25*, 2183-2186.
- (34) Inanaga, J.; Hirata, K.; Saeki, H.; Katsuki, T.; Yamaguchi, M. *Bull. Chem. Soc. Jpn.* **1979**, *52*, 1989-1993.
- (35) (a) Russ, P. A.; Caress, E. A. *J. Org. Chem.* **1976**, *41*, 149-151. (b) Kanyiva, K. S.; Horiuchi, M.; Shibata, T. *Eur. J. Org. Chem.* **2018**, 1067-1070. (c) Zhang, J.; Li, L.; Wang, L.; Zhang, F.; Li, X. *Eur. J. Med. Chem.* **2010**, *45*, 5337-5344.
- (36) Richers, J.; Pöthig, A.; Herdtweck, E.; Sippel, C.; Hausch, F.; Tiefenbacher, K. *Chem. Eur. J.* **2017**, *23*, 3178-3183.
- (37) Lowe, J. T.; Panek, J. S. *Org. Lett.* **2005**, *7*, 3231-3234.
- (38) Morikawa, S.; Yamazaki, S.; Tsukada, M.; Izuhara, S.; Morimoto, T.; Kakiuchi, K. *J. Org. Chem.* **2007**, *72*, 6459-6463.
- (39) Noichl, B. P.; Durkin, P. M.; Budisa, N. *Biopolymers* **2015**, *104*, 585-600.
- (40) Mukherjee, S.; Kontokosta, D.; Patil, A.; Rallapalli, S.; Lee, D. *J. Org. Chem.* **2009**, *74*, 9206-9209.
- (41) Nakamura, S.; Uchiyama, M.; Ohwada, T. *J. Am. Chem. Soc.* **2004**, *126*, 11146-11147.
- (42) Shore, G.; Organ, M. G.; *Chem. Eur. J.* **2008**, *14*, 9641-9646.
- (43) Kamptmann, S. B.; Brückner, R. *Eur. J. Org. Chem.* **2013**, *2013*, 6584-6600.
- (44) Tanino, K.; Onuki, K.; Asano, K.; Miyashita, M.; Nakamura, T.; Takahashi, Y.; Kuwajima, I. *J. Am. Chem. Soc.* **2003**, *125*, 1498-1500.